

AGARD

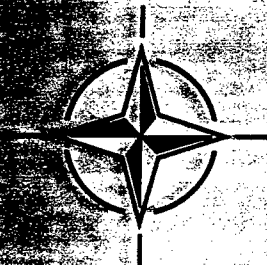
ADVISORY GROUP FOR AEROSPACE RESEARCH & DEVELOPMENT
BP 25, 7 RUE ANCELLE, F-92201 NEUILLY-SUR-SEINE CEDEX, FRANCE

AGARDograph 336

Wind Tunnel Wall Corrections (la Correction des effets de paroi en soufflerie)

This AGARDograph has been produced at the request of the Former Fluid Dynamics Panel of AGARD.

DISTRIBUTION STATEMENT A
Approved for public release;
Distribution Unlimited



NORTH ATLANTIC TREATY ORGANIZATION

DTIC QUALITY INSPECTED 3

DTIC QUALITY INSPECTED 3

Published October 1998

Distribution and Availability on Back Cover

AGARD

ADVISORY GROUP FOR AEROSPACE RESEARCH & DEVELOPMENT
BP 25, 7 RUE ANCELLE, F-92201 NEUILLY-SUR-SEINE CEDEX, FRANCE

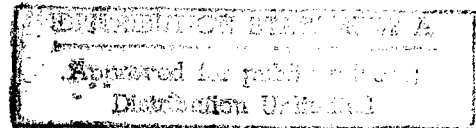
AGARDograph 336

Wind Tunnel Wall Correction

(la Correction des effets de paroi en soufflerie)

by

B.F.R. Ewald (Editor)
Darmstadt University of Technology
Federal Republic of Germany



This AGARDograph has been produced at the request of the Former Fluid Dynamics Panel of AGARD.

19981125 045



North Atlantic Treaty Organization
Organisation du Traité de l'Atlantique Nord

AQ F99-02-0260

The Mission of AGARD*

According to its Charter, the mission of AGARD is to bring together the leading personalities of the NATO nations in the fields of science and technology relating to aerospace for the following purposes:

- Recommending effective ways for the member nations to use their research and development capabilities for the common benefit of the NATO community;
- Providing scientific and technical advice and assistance to the Military Committee in the field of aerospace research and development (with particular regard to its military application);
- Continuously stimulating advances in the aerospace sciences relevant to strengthening the common defence posture;
- Improving the co-operation among member nations in aerospace research and development;
- Exchange of scientific and technical information;
- Providing assistance to member nations for the purpose of increasing their scientific and technical potential;
- Rendering scientific and technical assistance, as requested, to other NATO bodies and to member nations in connection with research and development problems in the aerospace field.

The highest authority within AGARD is the National Delegates Board consisting of officially appointed senior representatives from each member nation. The mission of AGARD is carried out through the Panels which are composed of experts appointed by the National Delegates, the Consultant and Exchange Programme and the Aerospace Applications Studies Programme. The results of AGARD work are reported to the member nations and the NATO Authorities through the AGARD series of publications of which this is one.

Participation in AGARD activities is by invitation only and is normally limited to citizens of the NATO nations.

* AGARD merged with the Defence Research Group of NATO (DRG) on 1 January 1998 to form the Research and Technology Organization (RTO) of NATO. However, both AGARD and DRG will continue to issue publications under their own names in respect of work performed in 1997.

The content of this publication has been reproduced
directly from material supplied by AGARD or the authors.



Printed on recycled paper

Published October 1998

Copyright © RTO/NATO 1998
All Rights Reserved

ISBN 92-836-1076-8



*Printed by Canada Communication Group Inc.
(A St. Joseph Corporation Company)
45 Sacré-Cœur Blvd., Hull (Québec), Canada K1A 0S7*

Wind Tunnel Wall Corrections

(AGARD AG-336)

Executive Summary

This report was compiled by an international team of wind tunnel wall correction experts. It presents the present state of the art in wind tunnel wall corrections with a special emphasis given to the description of modern wall correction methods based on Computational Fluid Dynamics.

This AGARDograph was planned by the AGARD Fluid Dynamics Panel to be a modern sequel of the successful AGARDograph 109 "Subsonic Wind Tunnel Wall Corrections", which was published in 1966. AGARDograph 109 is still valid and continues to be used to provide wall corrections in many wind tunnels. Nevertheless, in the thirty two years since the publication of AGARDograph 109, much work has been done on the subject, and the influence of the new tool of numerical fluid dynamics was so strong, that a sequel to AGARDograph 109 was considered to be necessary.

As the reader will observe, the matter of wind tunnel wall corrections is not completely resolved and further developments are confidently expected. The wind tunnel will continue to play an important role as one of the two main tools of airplane aerodynamic development. In the future, new requirements for wind tunnel testing, new ideas about wind tunnel wall design, new understanding of wind tunnel wall influence and advanced numerical fluid dynamics codes run on more powerful computers will initiate new developments in the field of wind tunnel wall corrections.

La correction des effets de paroi en soufflerie

(AGARD AG-336)

Synthèse

Ce rapport a été rédigé par un groupe de spécialistes internationaux en correction des effets de paroi. Il présente l'état actuel des connaissances dans le domaine de la correction des effets de paroi de soufflerie, et accorde une importance particulière à la description des méthodes modernes de correction des effets de paroi basées sur l'aérodynamique numérique.

Cette AGARDographie a été conçue par le Panel AGARD de la dynamique des fluides comme la suite actualisée de l'AGARDographie 109 sur "La correction des effets de paroi en soufflerie subsonique" qui a reçu un accueil très favorable lors de sa publication en 1966. L'AGARDographie 109 reste valable et continue d'être utilisée pour le calcul de la correction des effets de paroi par bon nombre d'aérodynamiciens. Néanmoins, beaucoup d'efforts ont été consacrés à ce sujet depuis la parution de l'AGARDographie 109 il y a trente deux ans, et l'influence du nouvel outil de la dynamique des fluides numérique a été si marquée qu'il était considéré nécessaire de fournir une suite à cette publication.

Il est évident que la question de la correction des effets de paroi n'est pas totalement résolue encore et il y a tout lieu de croire que d'autres développements suivront. Les souffleries continueront de jouer un rôle important comme l'un des deux principaux outils du développement de l'aérodynamique aéronautique. A l'avenir, de nouveaux développements dans le domaine de la correction des effets de paroi verront le jour sous l'impulsion de nouvelles exigences en matière d'essais en soufflerie, de nouveaux concepts de fabrication des parois, d'une meilleure compréhension de l'influence des parois et de nouveaux codes avancés de dynamique des fluides numérique, exploités sur des ordinateurs plus puissants.

Contents

	Page
Executive Summary	iii
Synthèse	iv
Recent Publications of the Former Fluid Dynamics Panel	xi
Introduction	xiii
Biographies of Authors	B-1
 CHAPTER:	
1. Status of Wind Tunnel Wall Correction Methods	1-1
1.1 The Fundamental Assumption (C.R. Taylor, P.R. Ashill)	1-3
1.2 Tunnel Calibration and Book-Keeping of Corrections (C.R. Taylor, P.R. Ashill)	1-4
1.3 Primary Corrections and Residual Variations (C.R. Taylor, P.R. Ashill)	1-6
1.3.1 Basic Concepts	1-6
1.3.2 Corrections Appropriate to Spatially-Varying Interference Flows	1-8
References for Sections 1.1, 1.2 and 1.3	1-13
1.4 Choice of Correction Method (A. Krynytzky, J.E. Hackett)	1-15
1.4.1 Model Aerodynamics	1-16
1.4.2 Mach Number	1-17
1.4.3 Model Size	1-19
1.4.4 Wind Tunnel Walls	1-20
References for Section 1.4	1-23
2. Conventional Wall Corrections for Closed and Open Test Sections	2-1
2.1 Classical Wall Corrections : Basic Principles, Definitions and Assumptions (A. Krynytzky)	2-4
2.1.1 Co-ordinate System and Governing Equations	2-4
2.1.2 Model Representation	2-6
2.1.3 Tunnel Walls	2-8
2.2 Classical Corrections for Closed Test Sections (A. Krynytzky)	2-12
2.2.1 Classical Corrections for Lift Interference	2-14
2.2.2 Classical Corrections for Blockage Interference	2-22
2.2.3 Wake Blockage Corrections for Separated Flows	2-34
2.3 Panel Methods for Closed-Wall Tunnels (A. Krynytzky)	2-36
2.3.1 General Considerations	2-36
2.3.2 2D Interference	2-40
2.3.3 3D Lift Interference	2-40
2.3.4 3D Blockage Interference	2-43
2.3.5 3D Wing-Body Combinations	2-45
2.3.6 Summary of Panel Methods	2-53
2.4 Classical Corrections for Open Test Sections (B. Ewald)	2-54
2.4.1 Introduction	2-54
2.4.2 Lift Interference	2-55

2.4.3	Blockage Correction	2-60
2.4.4	Wake Correction	2-61
	Nomenclature for Chapter 2	2-62
	References for Chapter 2	2-64
3.	Conventional Corrections in Ventilated Test Sections (A. Krynytzky)	3-1
3.1	Background, Assumptions, and Definitions	3-5
3.2	Wall Boundary Conditions	3-7
3.2.1	Ideal Ventilated Wall Boundary Conditions	3-8
3.2.2	Experimental Investigations of Perforated-Wall Characteristics	3-10
3.2.3	Experimental Investigations of Slotted-Wall Characteristics	3-12
3.3	Interference in 2D Testing	3-14
3.3.1	Interference of Small Models, Uniform Walls	3-14
3.3.2	Interference of Small Models, Non-uniform Walls	3-16
3.4	Interference in 3D Testing, Classical Results	3-18
3.4.1	Slotted Walls	3-19
3.4.2	Porous Walls	3-20
3.5	Computational Approaches to Interference Evaluation	3-22
3.5.1	Point Singularity Model Representation	3-23
3.5.2	Panel Methods, Homogeneous Ventilated Walls	3-24
3.5.3	Panel Methods, Finite-Length and Discrete Slots	3-27
3.6	Conclusion	3-41
	Nomenclature for Chapter 3	3-41
	References for Chapter 3	3-43
4.	Boundary Measurements Methods	4-1
4.1	Fundamental Theories (P.R. Ashill)	4-3
4.1.1	Basic Considerations	4-4
4.1.2	One Variable Methods	4-7
4.1.3	Wall-Signature Methods	4-12
4.1.4	Two-Variable Methods	4-14
	References to Chapter 4.1	4-17
4.2	Closed Test Sections (P.R. Ashill, J.E. Hackett)	4-20
4.2.1	Background	4-20
4.2.2	Boundary Conditions	4-21
4.2.3	Numerical Approximations	4-24
4.2.4	Choice of Method	4-24
4.2.5	Measurements and Analysis of Wall Pressures	4-25
4.2.6	Model and Tunnel Representation when Using the "Matrix" Version of the Wall Pressure Signature Method	4-30
	References to Section 4.2	4-35
4.3	Ventilated Test Sections (M. Mokry, F. Steinle)	4-38
4.3.1	One-Variable Method	4-39
4.3.2	Two-Variable Method	4-48
4.3.3	Alternative Methods	4-55
	Appendix: Rectangular Wall Panel	4-55
	References to Chapter 4.3	4-57

5.	Transonic Wind Tunnel Wall Interference	5-1
	(N.D. Malmuth, R. Crites, J. Everhart, P. Newman, W. Sickles)	
5.1	Background	5-3
5.1.1	Scope and Overview	5-3
5.1.2	Previous Literature and Conferences	5-4
5.1.3	Wall Interference/Reynolds Simulation Trade-Off in Model Sizing	5-4
5.1.4	Correctability	5-5
5.2	Wall Boundary Conditions for Transonic Flows	5-8
5.2.1	Nomenclature for Section 5.2	5-8
5.2.2	Solid Walls	5-10
5.2.3	Porous walls	5-11
5.2.4	Slotted Walls	5-21
5.2.5	Baffled Slotted Walls	5-35
5.3	Computational Approaches	5-37
5.3.1	Tunnel Simulations	5-37
5.3.2	MDA Wall Interference Computations	5-44
5.3.3	AEDC Wall Interference Computations	5-49
5.3.4	NASA Langley WIAC Methods	5-68
5.4	Asymptotic Methods for Transonic Wind Tunnel Wall Interference	5-72
5.4.1	Background	5-72
5.4.2	Overview of Asymptotic Procedures for Small Slender and Large Aspect Ratio Configurations	5-72
5.4.3	Small Slender Configurations	5-73
5.4.4	High Aspect Ratio Theory	5-74
5.4.5	Results - Small Slender Bodies	5-75
5.4.6	Results - Large Aspect Ratio Wings	5-76
5.4.7	Lift Interference and Porous Wall Effects on Slender Wings	5-79
5.4.8	Extension of Large Wall-Height Blockage Interference Theory to Moderate Wall Height Case	5-85
5.4.9	Validations of Theoretical and Computational Simulations for Moderate Wall Height Case	5-86
5.4.10	Non-Circular Wind Tunnel Sections	5-90
5.4.11	Summary, Conclusions and Recommendations	5-94
5.5	Assessment of State of the Art	5-95
5.6	References for Chapter 5	5-98
6.	Bluff-Body Blockage Corrections in Closed- and Open-Test-Section Wind Tunnels	6-1
	(K. Cooper)	
	List of Symbols	6-3
6.1	Introduction	6-5
6.1.1	History and Status	6-5
6.1.2	Closed and Open Test Sections	6-6
6.1.3	Important Test Section Boundaries	6-6
6.1.4	Comparison of Closed and Open Test Sections	6-6
6.2	Methods for Closed Test Sections	6-8
6.2.1	Maskell's Analysis	6-8
6.2.2	Cowdrey's Development	6-11
6.2.3	Hackett's Two-Step Version of Maskell's Analysis	6-11
6.2.4	Commentary on Maskell's Correction	6-13
6.2.5	Wake Buoyancy and the Wake-Induced Drag Increment	6-13
6.2.6	Mercker's Analysis	6-14
6.2.7	Upstream and Downstream Effects	6-16

6.3	Methods for Open Test Sections	6-18
6.3.1	Recent Results from Automotive Testing	6-18
6.3.2	The Primary Effects	6-18
6.3.3	The Method of Mercker and Wiedemann	6-23
6.4	Application to Closed Test Sections	6-29
6.4.1	Aircraft	6-29
6.4.2	Surface Vehicles	6-29
6.4.3	Miscellaneous	6-30
6.5	Application to Open Test Sections	6-30
6.5.1	Surface Vehicles	6-30
6.6	References	6-32
7.	Wall Correction Methods for Powered Models of Conventional Take Off and Landing Aircraft (J.E. Hackett, P.R. Ashill, M. Mokry)	7-1
	List of Symbols for Chapter 7	7-3
7.1	Introduction	7-4
7.2	Determination of Model Power Settings	7-4
7.3	Wall Corrections for Jet-Powered Models	7-5
7.3.1	The Test Environment	7-5
7.3.2	Entrainment Effects for Jet-Powered Models	7-7
7.4	Wall Corrections for Propeller-Powered Models	7-10
7.4.1	Conventional Correction Methods	7-10
7.4.2	Pressure Signature-Based Correction Methods: Propeller Calibration	7-14
7.4.3	Separation of Propeller and Airframe Forces and Moments	7-19
7.4.4	Application of Tunnel Constraint Corrections	7-24
	References for Chapter 7	7-26
	Appendix: glauert.c	7-27
8.	Wall Correction Methods for V/STOL Configurations, Helicopters, Propellers and Windmills (J.E. Hackett)	8-1
	Notation	8-3
8.1	Introduction	8-5
8.1.1	Possible Approaches for Powered Flows	8-5
8.1.2	The V/STOL Testing Environment	8-6
8.2	Flow Modelling-Based Methods	8-11
8.2.1	Heyson's Method	8-11
8.2.2	Panel Methods	8-20
8.3	The Wall Pressure Signature Method	8-22
8.3.1	Theoretical Overview	8-22
8.3.2	Experimental Aspects	8-26
8.3.3	Analysis for the "Source-Source-Sink" Version of the Method	8-27
8.3.4	Analysis for the "Matrix" Version of the Method	8-31
8.3.5	Discussion	8-35
8.4	Tunnel Interference for a Jet-in-Crossflow	8-35
8.4.1	Introduction	8-35
8.4.2	Theoretical Flow Model	8-36
	References for Chapter 8	8-41

9.	Wall Correction Methods for Dynamic Tests (R. Voß)	9-1
9.1	Introduction	9-3
9.2	Physical Basics of Unsteady Wind Tunnel Interference	9-5
9.2.1	Characteristics of Motion-Induced Unsteady Flow Fields	9-5
9.2.2	Wind Tunnel Interference Effects in Unsteady Flow	9-7
9.2.3	Unsteady Wind Tunnel Wall Boundary Conditions	9-9
9.2.4	Acoustic Interference and Tunnel Resonance	9-10
9.3	Wall Adaptation for Dynamic Tests	9-13
9.3.1	Steady Wall Adaptation	9-13
9.3.2	Passive Adaptive Unsteady Walls	9-14
9.3.3	Active Adaptive Unsteady Walls	9-15
9.4	Modelling of Unsteady Wall Interferences as a Basis for Correction Methods	9-16
9.5	Reduction and Correction of Unsteady Wind Tunnel Wall Interferences	9-23
9.5.1	Unsteady Wind Tunnel Wall Corrections by Analytical Methods	9-23
9.5.2	Unsteady Wind Tunnel Wall Corrections Using Measured Tunnel Wall Pressure Values and Numerical Methods	9-24
	References	9-27
10.	Adaptive Wall Techniques (E. Wedemeyer, N.J. Taylor, H. Holst)	10-1
	Lists of Symbols	10-3
10.1	Introduction	10-4
10.2	The Rudiments of Adaptive Wall Techniques	10-5
10.2.1	The Aims of Wall Adaptation	10-5
10.2.2	The Forms of Wall Adaptation	10-6
10.2.3	The Process of Wall Adaptation	10-8
10.2.4	Further Points of Classification	10-11
10.3	Two-Dimensional Testing	10-12
10.3.1	Wall Adaptation by Iteration	10-13
10.3.2	One Step Methods of Wall Adaptation for Group 1 Flows	10-13
10.3.3	Wall Adaptation in Supersonic Flow (Group 5)	10-15
10.3.4	Wall Adaptation in Transonic Flows (Groups 2-4)	10-16
10.4	Three-Dimensional Testing	10-17
10.4.1	Wall Adaptation by Interface Matching	10-17
10.4.2	Target Line Methods: Two-Dimensional Wall Adaptation for Three-Dimensional Flows	10-18
10.4.3	Effects of the Sidewall Boundary Layer	10-25
10.5	Manipulative Algorithms	10-26
10.6	Priorities for the Future	10-28
10.6.1	Data Quality	10-28
10.6.2	Rate of Data Acquisition	10-28
10.6.3	Complexity and Cost	10-29
	Tables	10-31
	Figures	10-31
10.7	References	10-42
	Appendix A	10-45
	Appendix B	10-45

11. Addressing Uncertainties in Wall Corrections (P. Newman, J.L. Everhart)	11-1
11.1 Introduction	11-3
11.2 Fundamental Aspects	11-4
11.2.1 Consequences of the Fundamental Assumption	11-4
11.2.2 Compatibility of Hardware, Software, and Procedures	11-6
11.2.3 Consequences of Physical and Economic Constraints	11-7
11.3 Experimental Aspects	11-7
11.3.1 Traditional Approaches to Determining Interference	11-7
11.3.2 Establishing Data Credibility	11-9
11.3.3 Determining the True Value or "Truth"	11-10
11.3.4 Characterisation of the National Transonic Facility	11-11
11.4 Computational Aspects	11-15
11.4.1 Major Computational Thrusts	11-15
11.4.2 Uncertainty Sources in CFD Based Correction Procedures	11-16
11.4.3 Sensitivity Analysis for Correction Uncertainty Assessment	11-17
11.5 Concluding Remarks	11-18
11.6 References	11-19
12. Future Necessary Work (F. Steinle, R. Crites, A. Krynytzky, T. Binion)	12-1
12.1 Introduction	12-3
12.1.1 Near Term Objectives	12-3
12.1.2 Far-Term Objectives	12-6
12.2 Areas for Emphasis, versus Expectations	12-7
12.2.1 Better Understanding of Application of Wall Interference	12-7
12.2.2 Definition and Measurement of Boundary Conditions	12-11
12.2.3 Computational Methodology, Assessment and Validation	12-14
12.3 Coupling of Wall Interference with other Phenomena	12-19
12.3.1 Compressibility Effects	12-19
12.3.2 Viscous Effects for High Lift and Transonic Interactions	12-19
12.3.3 Support Interference Effects	12-19
12.3.4 Tunnel Non-uniform Flow	12-20
12.4 Reduction of Wall Interference	12-20
12.4.1 Passive Wall Design	12-21
12.4.2 Variable Characteristics Wall Design	12-21
12.4.3 Adaptive Walls	12-21
12.5 Summary of Recommendations	12-22
References to Chapter 12	12-24

Recent Publications of the Former Fluid Dynamics Panel

AGARDOGRAPHS (AG)

Turbulent Boundary Layers in Subsonic and Supersonic Flow
AGARD AG-335, July 1996

Computational Aerodynamics Based on the Euler Equations
AGARD AG-325, September 1994

Scale Effects on Aircraft and Weapon Aerodynamics
AGARD AG-323 (E), July 1994

Design and Testing of High-Performance Parachutes
AGARD AG-319, November 1991

Experimental Techniques in the Field of Low Density Aerodynamics
AGARD AG-318 (E), April 1991

Techniques Expérimentales Liées à l'Aérodynamique à Basse Densité
AGARD AG-318 (FR), April 1990

A Survey of Measurements and Measuring Techniques in Rapidly Distorted Compressible Turbulent Boundary Layers
AGARD AG-315, May 1989

REPORTS (R)

Turbulence in Compressible Flows
AGARD R-819, Special Course Notes, June 1997

Advances in Cryogenic Wind Tunnel Technology
AGARD R-812, Special Course Notes, January 1997

Aerothermodynamics and Propulsion Integration for Hypersonic Vehicles
AGARD R-813, Special Course Notes, October 1996

Parallel Computing in CFD
AGARD R-807, Special Course Notes, October 1995

Optimum Design Methods for Aerodynamics
AGARD R-803, Special Course Notes, November 1994

Missile Aerodynamics
AGARD R-804, Special Course Notes, May 1994

Progress in Transition Modelling
AGARD R-793, Special Course Notes, April 1994

Shock-Wave/Boundary-Layer Interactions in Supersonic and Hypersonic Flows
AGARD R-792, Special Course Notes, August 1993

Unstructured Grid Methods for Advection Dominated Flows
AGARD R-787, Special Course Notes, May 1992

Skin Friction Drag Reduction
AGARD R-786, Special Course Notes, March 1992

Engineering Methods in Aerodynamic Analysis and Design of Aircraft
AGARD R-783, Special Course Notes, January 1992

ADVISORY REPORTS (AR)

A Selection of Test Cases for the Validation of Large-Eddy Simulations of Turbulent Flows
AGARD AR-345, April 1998

Ice Accretion Simulation
AGARD AR-344, Report of WG-20, December 1997

Sonic Nozzles for Mass Flow Measurement and Reference Nozzles for Thrust Verification
AGARD AR-321, Report of WG-19, June 1997

Cooperative Programme on Dynamic Wind Tunnel Experiments for Manoeuvring Aircraft
AGARD AR-305, Report of WG-16, October 1996

Hypersonic Experimental and Computational Capability, Improvement and Validation
AGARD AR-319, Vol. I, Report of WG-18, May 1996

Aerodynamics of 3-D Aircraft Afterbodies
AGARD AR-318, Report of WG-17, September 1995

A Selection of Experimental Test Cases for the Validation of CFD Codes
AGARD AR-303, Vols. I and II, Report of WG-14, August 1994

Quality Assessment for Wind Tunnel Testing

AGARD AR-304, Report of WG-15, July 1994

Air Intakes of High Speed Vehicles

AGARD AR-270, Report of WG-13, September 1991

Appraisal of the Suitability of Turbulence Models in Flow Calculations

AGARD AR-291, Technical Status Review, July 1991

Rotary-Balance Testing for Aircraft Dynamics

AGARD AR-265, Report of WG11, December 1990

Calculation of 3D Separated Turbulent Flows in Boundary Layer Limit

AGARD AR-255, Report of WG10, May 1990

CONFERENCE PROCEEDINGS (CP)

Advanced Aerodynamic Measurement Technology

AGARD CP-601, May 1998

Aerodynamics of Wind Tunnel Circuits and Their Components

AGARD CP-585, June 1997

The Characterization & Modification of Wakes from Lifting Vehicles in Fluids

AGARD CP-584, November 1996

Progress and Challenges in CFD Methods and Algorithms

AGARD CP-578, April 1996

Aerodynamics of Store Integration and Separation

AGARD CP-570, February 1996

Aerodynamics and Aeroacoustics of Rotorcraft

AGARD CP-552, August 1995

Application of Direct and Large Eddy Simulation to Transition and Turbulence

AGARD CP-551, December 1994

Wall Interference, Support Interference, and Flow Field Measurements

AGARD CP-535, July 1994

Computational and Experimental Assessment of Jets in Cross Flow

AGARD CP-534, November 1993

High-Lift System Aerodynamics

AGARD CP-515, September 1993

Theoretical and Experimental Methods in Hypersonic Flows

AGARD CP-514, April 1993

Aerodynamic Engine/Airframe Integration for High Performance Aircraft and Missiles

AGARD CP-498, September 1992

Effects of Adverse Weather on Aerodynamics

AGARD CP-496, December 1991

Manoeuvring Aerodynamics

AGARD CP-497, November 1991

Vortex Flow Aerodynamics

AGARD CP-494, July 1991

Missile Aerodynamics

AGARD CP-493, October 1990

Aerodynamics of Combat Aircraft Controls and of Ground Effects

AGARD CP-465, April 1990

Computational Methods for Aerodynamic Design (Inverse) and Optimization

AGARD CP-463, March 1990

Applications of Mesh Generation to Complex 3-D Configurations

AGARD CP-464, March 1990

Fluid Dynamics of Three-Dimensional Turbulent Shear Flows and Transition

AGARD CP-438, April 1989

INTRODUCTION

In October 1966 the AGARD Fluid Dynamics Panel published the **AGARDograph 109** on the subject of "**WIND TUNNEL WALL CORRECTIONS**". This comprehensive compilation of knowledge of wall corrections available at that time was edited by J. Garner (National Physical Laboratory, England) with contributions from E.W.E. Rogers, W.E.A. Acum also of NPL and E.C. Maskell (Royal Aircraft Establishment, England). Without doubt this AGARDograph 109 has been one of the most successful publications of AGARD and is still today the wind tunnel engineers most authoritative source of wall correction methods and data.

The wall correction methods outlined in AGARDograph 109 are based on subsonic linear and inviscid aerodynamics. In most cases the wall effects are correlated with the measured total aerodynamic forces and simple image methods are used to calculate and correct for the wall effects. Most of these theories were published before 1950 and some appeared as early as the 1920's.

By the time of AGARDograph 109 the computer had not had a significant impact on the calculation of wall interference corrections. Computers had begun to be used for reducing raw wind tunnel data to dimensionless coefficients and for applying simple wall corrections. However, the wall correction methods themselves had not been influenced to any degree by advances in computer technology.

Typical wind tunnel engineers are normally experimentally-minded people who are not really enthusiastic about computational fluid dynamics. A consequence of this is that the adoption of computational methods in practical wall correction schemes has been slow. Routine correction methods, such as those formulated by pioneers such as Prandtl, Glauert, Durand, Goethert, Riegels and Maskell have remained in use even in large high quality wind tunnels in the thirty years since these and other methods were described in AGARDograph 109. Nevertheless, during this period of large amount of theoretical and experimental studies of wind tunnel wall interference were done and these developments have been influenced by the rapid improvements that have been made in computing speed and power. Computer based methods that have been developed include :

1) *Panel Methods*

These methods have made it possible to represent more accurately than linearised theory methods subcritical flows over complex model configurations in the constraining presence of the tunnel walls. Panel methods have also permitted wind tunnels with working sections of relatively small and/or non-standard cross sections (not amenable to treatment by classical image methods) to be modelled. These methods require considerable computing power and for this reason have not yet found wide favour with the wind tunnel testing community. Further discussions of methods of this type will be found in Chapters 2 and 3.

2) *Boundary-measurement methods*

These methods were developed to exploit information available from measurements of the flow at or near the tunnel walls. The general technique is not entirely new, as can be seen in AGARDograph 109, where reference is made to the use of wall pressure measurements to determine the blockage correction in solid-wall wind tunnels. The serious application of these techniques became possible by the development of computers during the '60s and '70s which enabled wall interference velocities to be computed from a large number of flow measurements. Methods of this type can be used to aid the modelling of the flow in the near region of the model for solid wall wind tunnels, for which the wall corrections are critically dependent on the model representation. For perforated or slotted wall wind tunnels, they can be used to provide information on the wall boundary conditions where suitable model representation is available.

Finally, where both normal and streamwise velocity components are measured at the bounding surface, no model representation is needed. These methods and examples of their application are described in Chapter 4.

3) *Computational Fluid Dynamic (CFD) methods*

The current generation of boundary-measurement methods is based on the assumption that the wall-induced flow field satisfies the Prandtl-Glauert equation. However, for many types of transonic flows, particularly those for which the supercritical flow reaches the walls, this assumption is no longer valid. Recognition of this problem led to the use of CFD methods able to model transonic flows and these methods are discussed in Chapter 5.

The increased use of computational methods have arisen from a number of factors including :

1. the growing need for accuracy in wind tunnel testing mainly for commercial transport aircraft development.
2. the recognition that the ability to test at flight Reynolds Numbers in cryogenic wind tunnels, such as the National Transonic Facility at NASA, Langley Research Centre and the European Transonic Wind Tunnel at Cologne, is only valuable if the wall interference corrections can be estimated with sufficient accuracy.
3. the need to perform accurate wind tunnel assessment of CFD methods.

Several times in the past the complete breakthrough of Computational Fluid Dynamics was predicted with the automatic consequence, that the wind tunnel as a scientific tool in fluid dynamics will be obsolete. In this case, further work on wind tunnel wall corrections would be unnecessary.

Today most scientists and engineers working in the field of aerodynamic aeroplane development agree, that the mystery of turbulence guarantees a long life of wind tunnels as an indispensable tool in fluid dynamics. Neither the wind tunnel nor computational methods are able to create progress in aeroplane aerodynamics on their own. Only an intelligent combination of both tools enable the aerodynamicist to create a successful new aerodynamic design.

With these developments in mind the editor on the occasion of the Fluid Dynamics Panel Meeting at Turin in May 1992 proposed that a new AGARDograph on the subject of wind tunnel wall corrections should be produced not to supercede AGARDograph 109 but to complement it. This proposal was approved by AGARD, and during the Fluid Dynamics Symposium in October 1993 at Brussels on the subject of "Wall Interference, Support Interference and Flow Field Measurement" a small group of specialists met for a preliminary discussion. From this group an international team of authors was formed. The aim was to produce an AGARDograph which provides the wind tunnel engineer with a comprehensive review of modern methods, mainly reflecting the new developments in wind tunnel wall corrections since AGARDograph 109.

During the work leading to the AGARDograph 336 there was some controversy over the issue as how to correct data for buoyancy or pressure gradient effects. Chapter 1.2 presents a method due to Taylor. Effectively this method ignores the influence of the wind tunnel walls on the development of the boundary layer on the model and it yields the correction to drag coefficient

$$\delta C_D = - C_D \varepsilon$$

for low speed flow. For thin-wake flows Taylor has argued that the wake blockage component may be ignored so that the equation above may be replaced by :

$$\delta C_D = - C_D \varepsilon_s$$

where suffix S refers to solid blockage. This is in agreement with the classical result for low-speed flow given in AGARDograph 109.

Chapter 6 describes a method recently developed by Hackett [1], which gives a correction to drag coefficient

$$\delta C_D = -C_D \epsilon_w$$

where suffix w refers to wake blockage. Hackett's method, like Taylor's method, is based on concepts valid for inviscid flow, although both can make use of information provided by wall pressures which sense the behaviour of the real flow. Hackett's method has been shown to be more accurate than the classical method or Taylor's method for high blockage, high lift flows. However, neither method has been validated for flows in which viscous effects are significant but not severe enough to cause wholesale separation. Flows of this sort are of particular importance in aeronautical applications. The question of what needs to be done to resolve this issue is dealt with under the heading of "Future necessary work in Wall Corrections" by Steinle in Chapter 12. For more details on this wake drag controversy see also the detailed discussion between J.E. Hackett and several other authors of this AGARDograph in [2].

References

- [1] Hackett, J.E., "Tunnel-Induced Gradients and their Effect on Drag", AIAA Journal, Vol. 34, No. 12, 1996, pp. 2575-2581.
- [2] Discussion on [1] by J.E. Hackett, P.R. Ashill, C.R. Taylor, Kevin R. Cooper and M. Mokry, AIAA Journal, Vol. 36, No. 2, February 1998.

BIOGRAPHIES OF AUTHORS

The compilation of this AGARDograph was possible only by the enthusiastic work of an international group of wind tunnel experts. The editor has to thank each of them for the engagement he invested in this work to the benefit of present and future wind tunnel engineers and aerodynamicists all over the world. We have to testify deepest respect to the authors of AGARDograph 109, who pioneered the subject of wind tunnel wall corrections and with their early effort in the end encouraged us to compile AGARDograph 336. Finally, we have to thank the AGARD Fluid Dynamics Panel who initiated and supported this work.

Patrick Ralph Ashill, PhD

Education :

1956-1959 University of Southampton, B Sc(Eng) Degree awarded June 1959

1960 - 1962 College of Aeronautics, Cranfield, MSc Degree awarded in 1972

1963 - 1968 External student University of Southampton, PhD Degree awarded June 1968

Member AIAA, Fellow of the Royal Aeronautical Society, Silver Medal of the Royal Aeronautical Society, awarded December 1996.

Career :

1962 -1969 : After completing a postgraduate course in aerodynamics at the College of Aeronautics, Cranfield, in 1962, invited to join the staff of the College as a Research Assistant and later as a Senior Research Fellow. Main task was to perform theoretical and experimental (wind tunnel) research on wings in ground effect, but also assisted with teaching.

1969-Present : Joined the Royal Aircraft Establishment (RAE), which became the Defence Evaluation and Research Agency (DERA) in 1997. Have been involved in the study of high-lift wings, wind-tunnel wall interference, boundary-layer transition, active and passive control of shock waves and separation control. Have also performed research into transonic scale effects and methods for calculating viscous transonic flows over aerofoils and wings. Currently, hold the position of DERA Fellow (formerly known as Senior Principal Scientific Officer (Individual Merit)).

Additional information:

Have chaired sessions at ICAS Jerusalem in 1988 on wind-tunnel wall interference, ICAS Anaheim in 1994 on wind tunnel test techniques and laminar flow and at a CEAS (Confederation of European Aeronautical Societies) symposium at Southampton University in 1992.

Was a member of two GARTEur working Groups between 1980 and 1983 concerned with transonic wind-tunnel test techniques and the validation of CFD methods for predicting transonic flows over wings.

Was a member of the AGARD Working Group 14 'Experimental test Cases for CFD Validation', which reported its findings in 1994 (AGARD-AR-303). Was chairman of a sub group concerned with defining requirements for validation experiments.

Travis Binion

Education :

B.S., Mechanical Engineering, Texas Tech University, 1957

M.S., Mechanical engineering, University of Tennessee, 1971

Career :

Mr. Binion has 40 years of experience in engineering/management of research, development, and testing in flight dynamic facilities. He is internationally recognised for his contributions toward understanding the test methodology and wind tunnel environment factors that affect the quality of transonic test data. He has performed and published research over a broad base of technologies including engine/inlet

compatibility, missile base heating and jet/body interactions, wind tunnel wall interference, test section wall configurations, and rocket and turbojet engine simulators for wind tunnel testing. He is presently happily semi-retired where ever he happens to be.

Kevin Russell Cooper

Education:

B.A., General Arts, University of Western Ontario, 1964.

B.Sc., Honours Physics, University of Western Ontario, 1967 (Dean's Honours List).

M.A.Sc., Subsonic Aerodynamics, University of Toronto Institute for Aerospace Studies, 1968.

Career :

1968 - present: Research Officer, Applied Aerodynamics Laboratory, National Research Council of Canada

1983 - 1984: Guest Worker, Cranfield Institute of Technology, U.K.

1987 - 1990: Manager, 9m x 9m Wind Tunnel, National Research Council of Canada

1991-1997 Group Head of General Aerodynamics and Wind Tunnel Facility Manager

Kevin Cooper worked in the field of sub-sonic aerodynamics since 1968. The focus was the steady and the unsteady aerodynamics of bluff bodies and the effects of aerodynamic forces on both the dynamic stability and the response to unsteady wind loads of a broad range of systems from road vehicles to bridges. Since that time he was involved in wind tunnel investigations of almost all types of civil engineering structures and of almost all types of transportation systems. He organised and was involved in international correlation studies of wind tunnel measurements on surface vehicles and buildings that have required me to work in many wind tunnels in Canada, the United States and Europe.

He worked primarily as a consultant for Canadian and foreign Industry on projects that have solved real industrial problems or have developed real products. He also provided technical support for the testing of aircraft models in the 2m x 3m and the 9m wind tunnels of the NRC in the areas of wall corrections and measurement and test technology.

I have served as the manager of the 9m x 9m wind tunnel and of the General Aerodynamics Group of the Aerodynamics Laboratory. In this latter position, I have managed the low-speed wind tunnel facilities at the Montreal Rd site of the NRC.

Currently, I have returned to my research activities and have just completed a major study of an automotive diffuser in ground effect, to better understand the capabilities of diffusers for road and racing applications, and to examine the role of the moving belt in each case. This program will continue as part of the development of novel moving-belt facilities in the model-scale 2m x 3m wind tunnel and in the full-scale 9m x 9m wind tunnel.

Additional Information :

SAE Excellence in Oral Presentation Award, 1990. Gzowski Society Lecture, London, Ont., 1989
Presidents medal for the best Technical paper from the Roads and Transportation Association of Canada, 1977. Member: SAE Road Vehicle Aerodynamics Committee. Member: SAE Wind Tunnel Testing Methods Subcommittee. Chairperson: SAE Wind Tunnel Boundary Corrections Subcommittee
Chairperson: SAE Truck and Bus Aerodynamics Subcommittee. Member: Executive member of the Canadian Wind Engineering Association

Roger Crites

Education :

Bachelor of Aeronautical and Astronautical Engineering from the Ohio State University.
Master of Science in Mechanical Engineering from the University of Missouri-Rolla.

Career :

Mr. Crites is a Research and Engineering Fellow of the Boeing Company (previously McDonnell Douglas Corporation). He is also an Associate Fellow of the AIAA. During thirty years of service, he has published over 30 technical papers, obtained multiple patents, and received many awards and honours for outstanding technical contributions to wind tunnel technology. Mr. Crites directs a high performance research team that is dedicated to providing new technology, enabling major reductions in the cost and cycle time associated with wind tunnel testing. Current activities are focused on wall interference reduction and correction, advanced wind tunnel instrumentation, (such as pressure sensitive paint), and statistical applications to quality, productivity, and optimal test design.

Dr. Joel L. Everhart

Education :

BS (1973) in Aerospace Engineering and MS (1975) in Mechanical Engineering from North Carolina State University. D.Sc. (1988) in Fluid Mechanics from George Washington University.

Career :

Dr. Everhart has been employed at NASA Langley Research Center as a Research Engineer since July 1977. He is a Senior Member of the AIAA and has authored and co-authored over 30 technical publications. His primary research interests are in areas related to wind tunnel wall interference, wind tunnel calibrations, instrumentation accuracy, statistical quality control and data quality, and testing techniques at subsonic and transonic speeds. He has also conducted research in shock/boundary layer interactions and propulsion/airframe integration at hypersonic speeds. He is presently a member of the Research Facilities Branch, Aero- and Gas-Dynamics Division.

Prof. Dipl.-Ing. Bernd F.R. Ewald

Education :

1952-1959 Studied Aeronautical Engineering at the Technical University of Aachen, Germany..

Career :

1960 - 1962	Aeroplane Design Engineer at the Prof. Blume Leichtbau und Flugtechnik Company
1962 - 1965	Experimental Aerodynamicist at Weser-Flugzeugbau, Bremen.
1965 - 1983	Chief of the Experimental Aerodynamics Department at VFW (formed by a merger of Weserflugzeugbau and Focke-Wulf, Bremen. Due to additional mergers the name changed to VFW-Fokker, and finally MBB Bremen). Today the companies name is Daimler Benz DASA Airbus
1968 - 1970	Design and Construction of the VFW Low Speed Wind Tunnel
1970 - 1972	Design of the „GUK“ (German project of a large industrial Low Speed Wind Tunnel, finally resulting in the design of the DNW)
1971 - 1973	Member of the AGARD „Large Wind Tunnels Working Group“ (LaW's)
1972 - 1990	Member of several Advisory Groups of the German Ministry for Research and Technology for the Development of the Large Wind Tunnels DNW and ETW.

- 1974 - 1983 Chief Manager of Airbus Wind Tunnel Programme in Germany.
 1983 - 1998 Professor for Aerodynamics and Measuring Technique at the Darmstadt University of Technology.
- Main Research Fields : Theoretical Aerodynamics, Navier-Stokes-Methods
 Wind Tunnel Design Technology, Wind Tunnel Testing Technology
 Wind Tunnel Balance Design and Fabrication
 Balance Calibration Theory and Calibration Equipment
- 1983 - pres. Consultant of Daimler Benz Aerospace Airbus in the field of Experimental Aerodynamics
 1991 - 1997 Member of the Fluid Dynamics Panel of AGARD. Editor of AGARDograph 336 „Wind Tunnel Wall Corrections“. Member of several Programme Committees.
 Member of DGLR and AIAA

Dr. J. E. Hackett ("Jim")

Education :

5-year apprenticeship with DeHavilland Aircraft Co., working on the Comet, concurrently with first degree studies. 3 years at Imperial College, London leading to Ph.D. and D-I-C. 4 years at The National Physical Laboratory, Teddington, England.

Career :

Since joining Lockheed in 1967, Dr. Hackett has developed and implemented new technology for the Lockheed Low Speed Wind Tunnel. He is the co-inventor of the wall pressure signature correction method, now widely used. His early work included theoretical modelling of powered whole-aircraft configurations with jet-lift, jet-flap or upper-surface blowing installed. This was complemented by experimental work on the jet flap and direct lift including development of tunnel floor boundary layer control for VISTOL and car tests. Dr Hackett received a NASA Certificate of Recognition for his work on eliminating tunnel flow breakdown.

Basic studies of vortex flows included application to the vortex hazard problem and flight simulator work. His research on three dimensional flow measurement includes new analysis methods and improved drag integration. Dr. Hackett holds a patent on a Vortex Diffuser Device for aircraft drag reduction, that has been flight tested successfully.

Dr. Hackett is author of more than two dozen papers and three dozen reports. His contributions to books include "Aerodynamic Testing of Road Vehicles" SAE SP 1 1 76, 1996; "Low Speed Wind Tunnel Testing" by Rae and Pope; "Aerodynamic Drag Mechanisms of Blunt Bodies and Road Vehicles" and "Aircraft Wake Turbulence and its Detection." Collaborative projects have included work with Carleton University, Georgia Tech, the University of Maryland, Texas A & M, Texas Tech., the University of Washington and the University of Western Ontario. Dr. Hackett is a long-time member of the AIAA and SAE and is active in SAE automobile aerodynamics committees. He is currently a Staff Specialist at the Lockheed Martin Low Speed Wind Tunnel in Georgia. His assignments comprise CFDFD testing/correlation for the Ford Motor Company, which includes collaboration with the University of Maryland, and research on wind tunnel test techniques and tunnel interference for Lockheed Martin.

Dr. Hartmut Holst

Education:

- 1965 - 1972 : Study of Aerodynamics and Aerospace at University Carolo-Wilhelmina at Braunschweig, Germany
 1975 - 1976 : Diploma Course at the Von-Karman-Institute for Fluid Dynamics in Brussels, Belgium
 1990 PhD at the University of Clausthal, Germany

Career:

1973 - Present : Research Scientist at the DLR (German Aerospace Research Center), Wind Tunnel Department, and since 1994 at the DLR Institute for Fluid Dynamics at Goettingen.

Research fields:

1973 - 1974 : aeroacoustics

1975 - 1976 : wind tunnel wall interference

1976 - 1985 : low speed aerodynamics, wind tunnel corrections

1986 - 1990 : two-dimensional wall adaptation for 3D flows

1991 - 1994 : transonic flows, wall interference and wall adaptation, modernisation of transonic facility TWG of DLR Goettingen

1994 - Present: wall adaptation, residual wall interferences, productivity, ventilated walls, wall corrections

Additional information:

..... Project support for DNW

..... Involved in modernisation of transonic facility TWG of DLR Goettingen

..... Developing methods for wall adaptation and determination of residuals using measured wall pressures

..... Developing methods for slotted walls (two-step-method)

..... Member of GARTEur group AD AG18 on "Adaptive Wall Wind Tunnels"

Alexander J. Krynytzky

Education :

SB (1971) and SM (1972) from the School of Engineering, Department of Aeronautics and Astronautics, at the Massachusetts Institute of Technology. Two years of additional post-graduate study in aerodynamics at MIT.

Career :

Since 1977 Mr. Krynytzky has worked for the Commercial Aeroplane Group of The Boeing Company in Seattle, Washington, in a variety of assignments in Aerodynamics Technology. Prior to this employment he served two years in the U. S. Army in rotary-wing flight testing at Edwards Air Force Base, California, and as a teaching assistant in graduate school at MIT.

Mr. Krynytzky's work at Boeing has focused on wind tunnel testing techniques, calibration, corrections, and design. He has been involved in numerous wind tunnel configuration studies using both experimental and computational techniques. Notable among these are the Acoustic Test Section for the Boeing Transonic Wind Tunnel, the Low-Speed Aero-Acoustic Facility, the Boeing New Wind Tunnel Complex (design study), and the National Wind Tunnel Complex (industry-government design activity). Mr. Krynytzky has played a key role in joint development activities between the CFD and aerodynamics laboratories that have resulted in increasingly sophisticated applications of panel methods for the evaluation of wall interference in tunnels used by Boeing, especially for ventilated walls.

Interspersed with assignments in the Testing Research and Development Group at the Aerodynamics Laboratories and in the technology development group of Aerodynamics Research, Mr. Krynytzky's career has also included the 737-300 aeroplane, Mod-5 Wind Turbine, and hybrid laminar flow technology.

Dr. Norman D. Malmuth

Education:

BAE, Aeronautical Engineering, University of Cincinnati, 1953

MAE, Aeronautical Engineering, Polytechnic Institute of New York, 1956

Ph.D., Aeronautics, California Institute of Technology, 1962

Career :

1971 - 1972 Lecturer, UCLA

1982 - Present Project Manager - Fluid Dynamics and Senior Scientist, Rockwell International Science Center

1986 - 1989 Consultant - Aerojet General

1980 - 1982 Manager - Fluid Dynamics Group, Rockwell International Science Center

1975 - 1980 Project Manager - Fluid Dynamics Research, Rockwell International Science Center

1968 - 1975 Mathematical Sciences Group, Rockwell International Science Center

1956 - 1968 North American Aviation Division, Los Angeles Division: Preliminary Design Engineer

1961 California Institute of Technology, Teaching Assistant

1953 - 1956 Grumman Aircraft Engineering Corporation, Research Engineer

Dr. Malmuth has been with the Rockwell International Science Center over 30 years; and was with Rockwell International, Los Angeles Division, 12 years. His current activities include basic research in fluid mechanics with emphasis on hypersonic and transonic flow, nonlinear heat transfer and computational fluid dynamics. Dr. Malmuth, who is a specialist in the application of combined asymptotic and numerical (CAN) methods, has applied these tools to Shuttle multibody interference analyses, drag optimisation at transonic speeds, wind tunnel wall interference, hypersonic boundary layer stability and transition with application to the NASP and other hypervelocity vehicles. His hypersonic flow theories and solutions for optimum hypervelocity vehicles are well-documented in the open literature. Another current thrust of his effort is applying his CAN procedures to the development of rapid conceptual design, plasma aeromechanics, store separation methods and flow control. Dr. Malmuth received the Distinguished Alumnus Award at the University of Cincinnati in 1990 and the AIAA Aerodynamics Award in 1991. He is past Chair of the Rockwell Fluid Dynamics Technical Panel, a member of the NASA Numerical Aerodynamic Simulator Committee, AIAA Applied Aerodynamics and Fluid Dynamics Technical Committees, the Society of Industrial and Applied Mathematics, American Physical Society, and is listed in *Who's Who in the World*. He has been a U.S. delegate to AGARD, a Fellow of the AIAA and a Visiting Scientist to Rensselaer Polytechnic Institute. Dr. Malmuth has 80 publications and one patent.

Dr. Miroslav Mokry

Education :

Dipl.-Eng. in Mechanical Engineering from the Technical University of Prague (1960) and Ph.D. from the Czech Academy of Sciences (1967).

Career :

Until 1968 Research Scientist at the Institute for Thermomechanics of the Czech Academy of Sciences, specialising in optical methods of flow measurement in wind tunnels. Since 1969 Research Officer at the Aerodynamics Laboratory of the Institute for Aerospace Research (formerly National Aeronautical Establishment) in Ottawa, Canada. Has been involved in wind tunnel wall interference, CFD and, more recently, vortex dynamics. Sessional lecturer at Carleton University. Co-author of AGARDograph 281, "Two-Dimensional Wind Tunnel Wall Interference", and AGARD-AR-269, "Adaptive Wind Tunnel Walls: Technology & Applications". Professional Engineer of the Province of Ontario, Senior Member of the AIAA, and Member of the CFD Society of Canada.

Dr. Perry A. Newman

Education :

Dr. Newman received BS (1958), MS (1960), and Ph.D. (1970) degrees in Physics from Virginia Polytechnic Institute.

Career :

Dr. Newman has been employed at NASA Langley Research Center since May 1962. His primary research interests since then have been in the calculation of high temperature thermodynamic and transport properties, the computational aspects of transonic flows (CFD), development of non-linear wind-tunnel wall interference assessment and correction (WIAC) procedures, and multidisciplinary analysis and optimisation utilising advanced CFD codes. He has authored or co-authored over 90 technical publications in these research areas. He is presently a Senior Research Scientist in the Multidisciplinary Optimisation Branch of the Research and Technology Group.

William L. Sickles

Education :

Bachelor of Science degree in engineering from the University of Virginia in 1972

Master of Science degree in applied mathematics from the University of Tennessee in 1973

Career :

Bill Sickles is a senior research engineer employed with Sverdrup Technology, Inc., an operating contractor at Arnold Engineering Development Center. For more than a decade he has been involved in computational fluid dynamic development and applications. He has also been involved in investigating and correcting factors that effect wind-tunnel data quality such as wall interference, Reynolds-number scaling effects, tunnel-flow humidity, and tunnel-flow quality. He has authored several papers in these areas. He resides in Tullahoma, Tennessee with his wife, Deirdre, and son, Billy.

Dr. Frank William Steinle, Jr.

Education :

B.S., 1961, Aeronautical Engineering, A&M College of Texas

M.S., 1969, Aeronautics & Astronautics - Gasdynamics, Stanford

University D.E., 1984, Aeronautics & Astronautics, 1984, Texas A&M University

Career :

Officer, USAF, assigned to NASA Ames Research Center, 1962 -1965, as a wind tunnel test engineer. Became a civil servant with NASA in 1965, progressing as Group Leader, Research & Analysis, and then as Assistant Branch Chief of Experimental Investigations Branch in 1983, Project Manager responsible for design of Fluid Mechanics Laboratory. Became Assistant Chief, Aerodynamic Facilities Branch of the Aerodynamics Division in 1984 and Chief of the Branch in 1985, responsible for Ames Unitary, 12-Foot, 14-Foot, 2-Foot, and 6-Foot Wind Tunnels, and Fluid Mechanics, Propulsion Simulation, & Balance Calibration Laboratories. Led project teams for definition of requirements for restoration of the Unitary and 12-Foot Wind Tunnel projects and development of new open-architecture data system for Aerodynamics Division wind tunnels. Retired from NASA in 1994 and relocated to AEDC, Arnold AFB, TN as Executive Engineer for Calspan & Microcraft Technology working as technical consultant to the National Wind Tunnel Complex project. Currently employed by Sverdrup Technology, AEDC, as Senior Engineer Specialist responsible for organising, advocating, planning, and managing advanced wind tunnel facilities and wind tunnel testing technology development projects and by the University of Tennessee as Adjunct Associate Professor teaching in the Engineering Management Department.

Associate Fellow in the AIAA and serves on the Ground Testing Technical Committee. Over 40 publications as either author, or co-author in disciplines of wind tunnel correlation, wind tunnel flow quality, & tunnel wall interference,

Cyril Richard Taylor

Education :

BSo (Hons), Sp. Maths. University of London 1955

Career :

1973-1986 Head of High-Speed Aerodynamics Division and Deputy Chief Superintendent.
Royal Aircraft Establishment, Bedford.

Duties: Manager of

- a) 13 x 9 ft atmospheric, low-speed tunnel
- b) 8 x 8 ft subsonic-supersonic tunnel
(M=0.15 - 0.87 and 1.35 - 2.5, 66 MW, 4 bar.)
- c) 3 x 4 ft high-supersonic-speed tunnel (M=2.5 - 5.0., 66MW, 12 bar.)

Manager for research on aircraft and weapon intakes, wing aerodynamics and for tunnel development.

Technical Advisor on ETW,

Chairman of research advisory groups on powerplant installation aerodynamics and signature reduction.

Chairman of international group on aircraft manoeuvring aerodynamics.

Nigel John Taylor

Education :

B.Sc. (Hons), Aeronautics & Astronautics, University of Southampton, 1987.

Dipl. Eng., University of Southampton, 1987.

Ph.D., Applied Aerodynamics, University of Southampton, 1995.

Career :

1987-1993: University of Southampton, Research Student/Assistant.

1993-date: DERA, Senior Scientist.

Principal research interests lie in the fields of high-lift / manoeuvre aerodynamics and wind tunnel technique development. Has produced technical publications on subjects including parachute design, store carriage on helicopters, wake vortex modelling, high-lift device design and adaptive wall technology.

Additional information:

Member AIAA, 1990.

Member RAeS, 1997.

C. Eng., 1997.

Ralph Voß, PhD

Education :

University Study (Physics) at Hamburg University (1969-1975)

Research Scientist at the Shipbuilding Institute of Hamburg University (1976-1978)

PhD at Göttingen University (1988)

Career :

Since 1979 research Scientist at DLR (German Aerospace Research Center) Institute of Aeroelasticity at Göttingen. Since 1990 Head of „Unsteady Aerodynamics Division“

Research Fields :

Unsteady transonic flow and transonic flutter

Numerical Methods (CFD, Boundary layer coupling, panel methods)

Validation of CFD codes, wind tunnel wall effects

Adaptive wing technology

Elastic flexible aircraft

Dr. Erich Hans Wedemeyer

Education:

1949-1956 Study of Physics at Universities Münster and Göttingen.

1956 Diplom Physicist, University Göttingen.

1969 D. Natural Scis., University Göttingen.

Career:

1956-1961 Research Physicist, Aerodyn. Versuchsanstalt, Göttingen. Research on hydrodynamic stability, wind tunnel techniques. Publications in ZfW, Ing. Archiv.

1962-1966 US Army Ballistic Research Laboratory, Maryland, USA. Development of the theory of confined fluid motion, research on superheated liquids, plasma flows. Publications in Phys. Fluids, J.Fluid Mech., ZfW.

1966-1980 Head of Gasdynamics Department, DLR Göttingen. Research on hydrodynamic stability, vortex flows, adaptive wall wind tunnel techniques. Articles in J.Aircraft, AIAA Journal, Co-Author (with B.G.Karpov) of Engineering Handbook „Liquid-Filled Projectile Design“.

1981-1982 Visiting Professor at the Von Karman Institute, Brussels. Teaching and research on: high angle of attack aerodynamics, vortex breakdown, on adaptive wall wind tunnel techniques. Development of the theory of two-dimensional wall adaptation for three-dimensional flows.

1982-1990 Senior Scientist, DLR, Göttingen. Research on adaptive wall wind tunnel techniques, hydrodynamic stability, transonic flow computation. Articles in J.Aircraft, AIAA Journal, J.Fluid Mech., ZfW, Co-Author of AGARD-AR-269: Adaptive Wind Tunnel Walls. Three patents on adaptive wall wind tunnels.

1990 Retired from DLR Göttingen.

1. STATUS OF WIND TUNNEL WALL CORRECTION METHODS

Authors : C. Taylor }
 P. Ashill } CHAPTERS 1.1 - 1.3
 A. Krynytzky }
 J. Hackett } CHAPTER 1.4

	PAGE
1.1 THE FUNDAMENTAL ASSUMPTION	1-3
1.2 TUNNEL CALIBRATION AND BOOK-KEEPING OF CORRECTIONS	1-4
1.3 PRIMARY CORRECTIONS AND RESIDUAL VARIATIONS	1-6
1.3.1 BASIC CONCEPTS	1-6
1.3.2 CORRECTIONS APPROPRIATE TO SPATIALLY-VARYING INTERFERENCE FLOWS	1-8
1.3.2.1 PRIMARY CORRECTIONS	
1.3.2.2 CORRECTIONS FOR RESIDUAL VARIATIONS	
REFERENCES FOR SECTIONS 1.1, 1.2 AND 1.3	1-13
1.4 CHOICE OF CORRECTION METHOD	1-15
1.4.1 MODEL AERODYNAMICS	1-16
1.4.2 MACH NUMBER	1-17
1.4.3 MODEL SIZE	1-19
1.4.4 WIND TUNNEL WALLS	1-20
REFERENCES FOR SECTION 1.4	1-23

1. STATUS OF WIND TUNNEL WALL CORRECTION METHODS

1.1 THE FUNDAMENTAL ASSUMPTION

In general, the aim of wind-tunnel tests is to make measurements of aerodynamic quantities under strictly controlled and defined conditions in such a way that, despite the presence of the tunnel walls, the data can be applied to unconstrained flow. The existence of a free-air flow which is "equivalent" to that in the tunnel is the fundamental assumption underlying the entire framework of the theory and practice of wind-tunnel wall constraint.

A rigorous definition of equivalence is complicated by the fact that wall interference varies over the model and its wake. If the wall interference were uniform, the equivalent free-air conditions could be defined quite simply as the values of Mach number, incidence and sideslip which, in free air, at the same total pressure and temperature, would give the same forces and moments as those measured in the tunnel.

The existence of spatial variations in the wall-induced velocities means that this equivalence cannot be obtained precisely and some corrections for these variations are needed. The standard approach adopted for tests of aircraft models, described below, is to correct the tunnel Mach number to the equivalent free-air value, and hence obtain the equivalent static and dynamic pressures. If these are used to obtain lift and sideforce coefficients, no further correction is needed, but the angles of incidence and sideslip do need correction. These corrections to Mach number and angles are referred to as "Primary Corrections". The residual variations in the wall-interference velocities can be interpreted as wall-induced distortions of the model and its wake and it is customary to make corrections for these, as discussed in Section 1.3. In most cases these corrections must be based on linearised theory of inviscid flow, as indeed are the corrections to the parameters defining the equivalent free-air flow.

Of course there are errors and uncertainties in the application of these corrections but, if these can be shown to be smaller than the required accuracy, the measured data are, by definition, correctable and the equivalent free-air principle is valid. If not, the data are correctable only to the accuracy determined by the uncertainty in the corrections and, if this is unacceptable, the data must be classified as uncorrectable, though not necessarily without value. The uncertainties in the corrections may be due to approximations in the correction formulae or to factors such as viscous-inviscid interactions in the flows over the model and at the tunnel walls, large model wakes or localised regions of transonic/supersonic flows, and, in general, they are difficult to quantify. The subject of correctability has been addressed by Kemp [12] who outlined a procedure for categorising the wall interference for each test data point and showed how, in principle, the tunnel geometry might be changed to enable correctable data to be obtained for a range of tests which might otherwise be classified as uncorrectable.

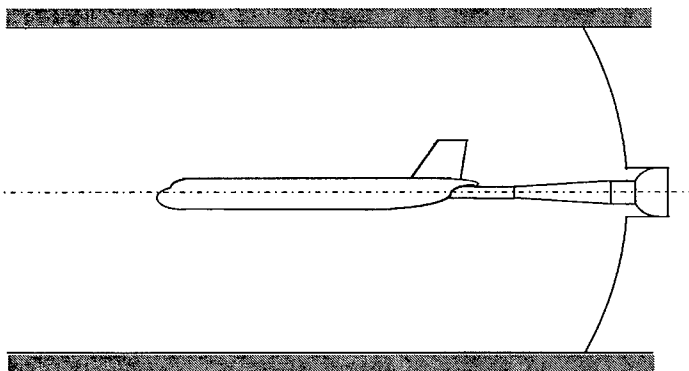
In practice, the issue is usually determined empirically by comparisons with nominally interference-free data, perhaps deduced from tests on models of different sizes or, more satisfactorily, by comparison with results of carefully-controlled experiments in adaptive-wall wind tunnels (Lewis and Goodyer [13], [14] and Ashill, Goodyer and Lewis [3]). Sometimes this can lead to the use of methods of wall correction that are at variance with the classical method outlined above (see, for example, Chapter 6 and Chapter 7) but the classical approach is the most commonly used for aircraft testing, particularly at cruise conditions, where experience suggests that it is valid.

A further element in the process of ensuring accuracy and consistency in the reduction of tunnel measurements to equivalent free-air values is the compatibility between the tunnel calibration and the correction procedure and this is addressed in Section 1.2.

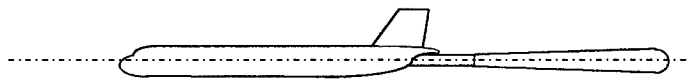
1.2 TUNNEL CALIBRATION AND BOOK-KEEPING OF CORRECTIONS.

Expressed in the most general terms the tunnel calibration establishes quantitative relationships between the flow conditions in the tunnel working section and reference measurements, made at positions in the tunnel which are sufficiently remote from the test volume for them to be unaffected by the presence of the model^{*}. The flow conditions of primary interest are wind speed and direction and variations of these quantities over the space normally occupied by a model. Temperature profiles may also be measured.

The reference measurements which relate to wind speed are usually total and static pressure, together with total temperature and, although in principle, the calibration of the test section might be made using non-intrusive anemometry, it is normal practice to use a static-pressure probe and pressure-sensing yawmeters. Hence the calibration, which is intended to provide 'tunnel-empty' data as a reference base for corrections which allow for the constraining effects of the walls, may not do so unless account is taken of the presence of the probe in the application of constraint corrections.



a) Model on sting support



b) Definition of model

Figure 1.1 Method A

One of two methods must be adopted:

- a) the calibration data is corrected to a truly empty tunnel, or
- b) the calibration data is not corrected for the wall-induced effects of the probe but, for wall constraint analysis, the flow displacement of the model and its sting support is reduced by that of the calibration probe.

With the first approach (method A, Figure 1.1) the "model" must include the sting, terminated at an appropriate point upstream of the quadrant (Figure 1.1b), and the calibration data must be corrected to a tunnel configuration which is consistent with this. This means that the measurements of pressure on the probe should be corrected for the blockage of the probe, including its closure upstream of the quadrant (as

shown for the model in Figure 1.1b) as well as for the direct effects of the nose and flare of the probe (i.e. their influence in unconstrained flow). If the method of constraint correction to be used is based on measurements of pressure changes at the tunnel walls, the wall pressure tapings must be included in the calibration and the datum measurements at these points should also be corrected for the direct and wall-induced effects of the probe.

This method, which is more suited to closed-wall tunnels, for which the corrections are easy to compute with the required accuracy, was adopted for the DRA 8x8 tunnel, and has been reported fully by Isaacs [11].

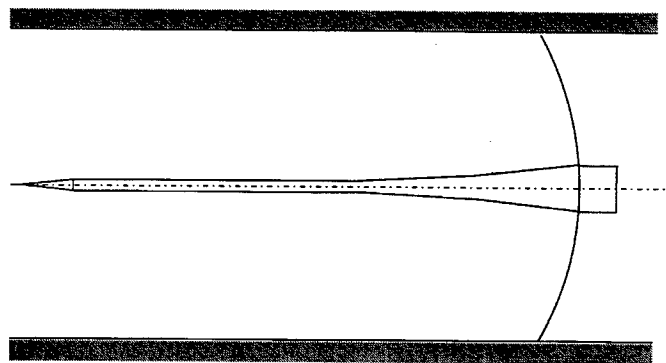
^{*} This restriction does not apply to certain types of boundary-measurement methods which are 'autocorrective' in character. See Chapters 4.1 and 4.3.

If the second approach (method B, Figure 1.2) is adopted, the working section with the probe in place is defined as the empty tunnel (Figure 1.2b). When classical methods are used to calculate the model blockage, the appropriate source distribution should be that for the difference between the displacement flows of the model and the calibration probe, as shown in Figure 1.2c. This is also the case for methods of the one-variable type (see Section 4.1.1). The accurate use of a two-variable method (also defined in Section 4.1.1) will give the correct "model" displacement automatically, however this requires measurements of the differences in both streamwise velocity (or static pressure) and normal velocity at the boundary of the control surface.

Ideally, with method B, the downstream end of the calibration probe should have the same shape as the sting support for models, so that its displacement flow there is close to that for a sting-mounted model (the difference being that due to wake displacement). This limits the length of a "model" and, for ventilated tunnels, ensures that its displacement flow at the walls is mainly in that part of the working section which is likely to be unaffected by the re-entrant flows from the plenum at the downstream end of the working section (e.g. at the re-entry flaps of slotted walls).

Figures 1.1 & 1.2 illustrate the case of sting-mounted models but similar arguments apply when the model is supported on struts i.e. either the struts can be taken as part of the model and the tunnel is calibrated empty or the tunnel is calibrated with the struts in place. Since the balance does not measure the loads on the struts the second approach is probably better but the correct choice may be influenced by the method used to account for strut interference. If this is determined experimentally, consistency must be maintained in the application of constraint corrections, both with the tunnel calibration and the basic test case. The same is true for tests to measure the support interference on sting-mounted models where particular care must be taken to avoid "double accounting" of wall interference associated with the sting.

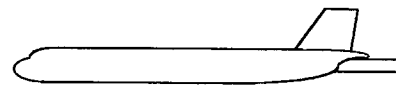
If method B is adopted, tests of wall-mounted models would require a separate tunnel calibration. For this, either method could be used but, for method B, the probe would need to be wall-mounted from the same position as the model.



b) Empty tunnel

Model representation

EQUALS



MINUS

c) Definition of model

Figure 1.2 Method B

1.3 PRIMARY CORRECTIONS AND RESIDUAL VARIATIONS.

1.3.1 BASIC CONCEPTS.

Wall interference is never uniform and the variations over the model and its wake are often significant. There is therefore a choice to be made as to which values of the interference velocities should be used for making corrections. It is here that the concept of primary corrections and residual variations is applied and, as mentioned in Section 1.1, the primary corrections relate the tunnel test parameters to those of an equivalent free air flow.

During wind-tunnel experiments those test parameters which define the test conditions can be regarded as "primary"; basically these are total pressure and temperature, static pressure, together with model incidence and sideslip. These are the parameters to which primary corrections may be applied (normally no correction is needed for total pressure and temperature).

In most model tests the data reduction is made "on-line", using computerised systems. The usual procedure is to correct the measured tunnel reference static pressure to the equivalent free-stream static pressure. This entails using the tunnel calibration to obtain the appropriate "empty-tunnel" condition (as explained in section 1.2) and then to apply the correction for model blockage. The corrected tunnel static is then used to derive corrected Mach number (or velocity) and dynamic pressure, and these are used to compute values of force and moment coefficients. If the primary corrections are based on the proper choice of interference velocities no correction is needed to the measured, balance-axis, force-coefficients, which can then be used to compute the corrected angles of incidence and sideslip. These define the orientation of the free-stream flow vector and hence the directions in which the balance-axis forces should be resolved to obtain aerodynamic-axes forces.

The "residual variations" are the deviations from the freestream flow that is defined by the corrected primary test parameters. They can be thought of as wall-induced distortions of the model and its wake, and correcting the measurements for these distortions can present difficulties, particularly if the main interest is in the pressure distribution.

However, in tests of aircraft models, for which the forces and moments are determined by the Kutta condition at sharp trailing edges, corrections can be made for the effects of the variations of axial velocity and upwash on the measured forces and moments, see section 1.3.2. The difference between the wall-induced upwash at the tailplane and that at the wing is best treated as a change in tail setting.

When tests of models with wings of high aspect ratio are made at high tunnel pressure the aeroelastic distortion of the wing needs to be added to the wall-induced upwash in the determination of both the incidence correction and the residual variation. In cases where allowance has been made for aeroelastic distortion and upwash variation in the design of the model, so that the wing has a datum "effective" shape at a particular test condition, the corrections to incidence, and for residual variations, need to take account of this offset and its variation with tunnel pressure.

Although the bases for the incidence, moment and drag corrections can be derived rigorously for small perturbations in inviscid flow, as shown by Taylor [19], it must be realised that, in cases for which the effects of boundary and shear layers are dominant, this is only a first approximation and, in principle, the uncertainty in these corrections may be a factor in determining the accuracy of the test data. Also, in tests at high subsonic speeds, the residual variation in the streamwise velocity, for which no practicable

method of correction is known, may be a major cause for concern and this, along with the upwash variation, could limit the size of model which should be tested.

The maximum flow deviations that can be accepted will vary with the test objectives but Steinle and Stanewsky [20] have quantified a number of criteria for tests of aircraft-like models aspiring to the standards of high accuracy then current and, although these were formulated for "empty-tunnel" flows, it is logical to apply them to wall-induced variations also. As regards axial velocity, they proposed that the maximum allowable variation over the length of the model (streamwise gradient) should not exceed 0.06% of free-stream but in a later paper Bouis [7] suggested that, for subsonic testing, the maximum peak-to-peak variation in Mach number should be 0.001.

In this context it should be noted that Ashill, Taylor and Simmons [4] have shown that in closed-wall tunnels the effect of the model flow field on the wall boundary layers reduces both the blockage correction and the residual streamwise velocity variation. This effect, which is greater at the higher subsonic Mach numbers, is illustrated in Figure 1.3 (taken from that paper). This shows the residual variations in Mach number, relative to the correction applied at point 'A', for a wing-body model of a transport aircraft when tested in the 8ft closed-wall tunnel at DRA Bedford at a Mach number of 0.90. The contours obtained from calculations which include an allowance for the effect on the boundary layers on the tunnel walls of the wall pressure increments due to the presence of the model are shown in the right side of the Figure; those on the left are for inviscid flow at the walls. It can be seen that, at this high subsonic Mach number, the effect of the wall boundary layers is sufficient to reduce the residual variation over the wing from a value above Bouis' criterion to one which meets it. Although not specifically mentioned by Ashill et al, their calculations also showed that the thickening of the wall boundary layer, due to the presence of the model, was not sufficient to give a significant axial pressure gradient. On the other hand, Hackett (1996) pointed out that gradient effects due to the growth of the wall boundary layers associated with large blockage models in low-speed tests are significant.

It can be expected that, in closed-wall tunnels, the interaction between the model flow field and the wall boundary layers will also reduce the variation in wall-induced upwash. This follows from the work of Adcock and Barnwell [1], who showed that the effects of the wall boundary layers are approximately the same as those of slotted walls. They derived a parameter defining the effective open-area ratio in terms of the thickness and shape parameter of the wall boundary-layer in the empty tunnel and, using the computational approach of Pindzola and Lo [16], gave charts showing the effects of the wall boundary layer on the interference parameters for small models. From these it can be inferred that, in tests of

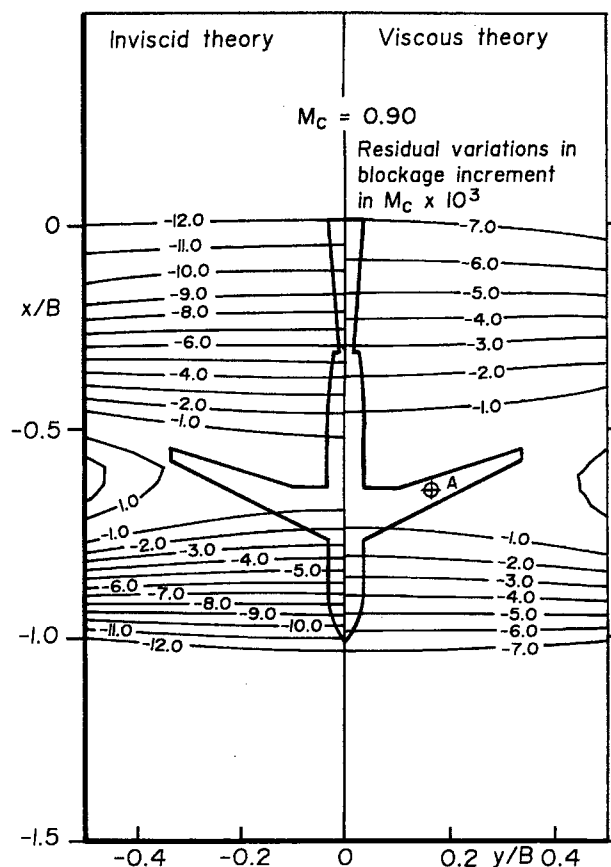


Figure 1.3 Contours of constant residual blockage increment in Mach Number for transport aircraft model in DRA 8ft x 8ft Tunnel

conventionally-sized models, the effect of wall boundary layers on the incidence correction at the model centre of pressure is likely to be negligible but that on the induced camber might be significant.

The calculation of primary corrections and residual variations can only be made when the boundary condition on the flow at the wall is formulated mathematically with sufficient accuracy. The calculations can be based on: a representation of the model (as in classical theory), measurements of pressures at the walls (see section 4) or on a combination of the two, although only the first and last of these may be suitable for "on-line" use.

For solid-wall wind tunnels, the wall boundary condition is well-defined and calculations can be made of wall-induced velocities using model representation methods (subject to allowance for wall boundary layers where necessary). Suitable methods are described in AGARDograph 109 and more recently Freestone of the Engineering Sciences Data Unit [8] has provided charts to allow calculations to be made of wall-induced upwash in solid-wall wind tunnels.

In ventilated tunnels, for which there is generally some uncertainty regarding the wall boundary condition, the primary corrections and residual variations cannot be calculated easily or accurately. Moreover the fact that a ventilated tunnel has low wall-interference (in the sense that the primary corrections are small) does not guarantee that this is also true for the residual variations. This is because all forms of ventilation have viscous losses at the wall and hence, to some degree, are like perforated walls, for which the interference velocities have significant gradients at the model. However the required data can sometimes be obtained experimentally, e.g. from careful comparison of test results with those for closed walls and, when obtained in this way, may be extrapolated to similar model configurations.

1.3.2 CORRECTIONS APPROPRIATE TO SPATIALLY-VARYING INTERFERENCE FLOWS.

AGARDograph 109 covers this topic and gives a number of formulae for aircraft-like models, in some cases offering a number of alternatives. Those for the corrections to angles and moments are based on the extrapolation of two-dimensional relationships and so, for wings of finite aspect ratio, are only approximate. Recently Taylor [19] has reviewed the subject and given formulae which, within the usual assumptions of the theory for small perturbations in subsonic inviscid flow, are exact. These cover the primary correction to incidence, and sideslip and the corrections for the residual variations. His results are given here, without proof, together with any restrictions on their validity which arise from flow conditions at the walls of the working section.

The corrections to incidence and pitching moment are derived from the application of a reverse-flow theorem. For two-dimensional flow, they have been investigated by Lewis and Goodyer [13], [14] and Ashill, Goodyer and Lewis [3], using an adaptive-wall tunnel. Their experiments covered a range of model incidence and Mach number, including cases where there were regions of supercritical flow on the upper surface of the airfoil and, in all instances, the data confirmed the validity of the linear-theory corrections. This suggests that the existence of supercritical flow on the upper surfaces of wings of finite span does not invalidate the results obtained from the theorem and hence they should be accurate for most tests of models at subsonic speeds.

1.3.2.1 PRIMARY CORRECTIONS.

The correction to incidence, at constant lift coefficient, is given by:

$$\delta\alpha = \frac{1}{S(dC_{L_t} / d\alpha)} \iint \bar{\ell}(1)w(x, y)dx dy,$$

where $\bar{\ell}(1)$ is the non-dimensional loading in reverse flow due to unit incidence and $Uw(x,y)$ is the wall-induced upwash. In tests at high dynamic pressure there may be significant aeroelastic distortion of the wing, in which case this should be added to the wall-induced upwash.

In cases where the spanwise variation of the effective upwash is negligible and the chordwise variation is linear, the correction reduces to the simple expression:

$$\delta\alpha = w(\bar{x})$$

where \bar{x} is the chordwise location of the aerodynamic centre in reverse flow. Hence for wings of infinite span, with a linear variation of upwash, the effective incidence is that at the 3/4 chord point, as originally suggested by Pistoletti [17], and, for slender wings with straight trailing edges, and attached flow at the leading edges, it is that at the trailing edge, as shown by Berndt [6].

Analogous expressions apply for the correction to angle of sideslip. In most cases there is little variation of sidewash over the tail fin and the correction to angle of sideslip, at constant sideforce, is then:

$$\delta\beta = v(\bar{x})$$

where $v(\bar{x})$ is the wall-induced sidewash at the position of the aerodynamic centre of the fin.

It is less clear which value of the velocity increment due to blockage should be used to correct the static pressure. Theory gives no guidance for most cases of practical interest and, intuitively, the best value is that which gives the least variation in blockage velocity over the most sensitive region of the flow. For aircraft models in tests at high subsonic speeds this is likely to be at the start of the recompression on the upper surface of the wing, but in cases for which the flow is dominated by a region of separation it is more likely to be that at the separation locus. There is some evidence (Ashill and Keating, [2] and Rueger and Crites, [18]) that the appropriate position for bluff-body flows with separation bubbles is where the blockage is a maximum.

1.3.2.2 Corrections for residual variations.

The corrections for residual variations include that for the variation of wall-induced streamwise velocity on profile drag and those for variations in wall-induced upwash (and aeroelastic distortion) on the lift-dependent drag and on the pitching and rolling moments of the wing. As noted above, the residual variation in sidewash over the fin is usually negligible and the effect of an axial variation in sidewash on the contribution of the body to the yawing moment, if significant, should be estimated by a method which allows for the effect of the boundary layer on the flow over the afterbody.

a) Wall-induced pressure-gradient drag

Wall-induced pressure gradients affect drag in two ways:

- first, in an 'inviscid' way, that is without altering the development of the boundary layers and wake just downstream of the model (i.e. about 10 wake thicknesses), and

- second, in a viscous manner through changes in the development of the boundary layer on the model and of the wake near the model, resulting in changes in skin friction and boundary-layer form (or normal pressure) drag.

Classically, the second of these mechanisms is ignored. Thus, for slender, compact bodies typical of aircraft configurations (for which the virtual volume due to the effective acceleration of the flow may be ignored compared with the actual volume of the model), the contribution of the correction to normal pressure drag is written as:

$$\delta D = V dp / dx \quad (1.1)$$

where V is model volume and dp/dx is the streamwise pressure gradient due to wall interference.

The pressure-gradient term in equation (1.1) could be determined using boundary-measurement methods such as those reviewed in Chapter 4. If such methods are not available one could resort to classical methods as described in AGARDograph 109 and reviewed further in Chapter 2*. Using the latter approach, with the model represented by a doublet and the wake by a point source, Rogers in Chapter 5 of AGARDograph 109, showed that the correction to drag coefficient due to wall-induced pressure gradient in solid-wall wind tunnels may be written as:

$$\delta C_D = -(1 + 0.4M^2)C_D \varepsilon_s, \quad (1.2)$$

where C_D is the drag coefficient excluding the contribution of the trailing-vortex drag and ε_s is the non-dimensional increment in wall-induced streamwise velocity due to solid blockage. This correction is often referred to as the wake buoyancy correction, since it can be interpreted as resulting from the wall-induced pressure gradient due to wake blockage. Note that, while this result is based on the neglect of the second (viscous) effect mentioned above, the effect of viscosity enters the final expression (1.2) through the drag coefficient.

Taylor [19] considered the flow in wind tunnels with solid walls, idealised slotted walls and open jets. Using a different approach to Rogers, he applied the conservation equations (mass, momentum and energy) to the inviscid flow outside the displacement surface of the model and its shear layers. Ignoring the second (viscous) effect above and neglecting second order terms in the energy equation he obtained the result:

$$\delta D = (p_c - p_1)\Delta, \quad (1.3)$$

where p is static pressure, suffix c refers to the (primary) correction at the model reference position and suffix 1 to conditions far downstream of the model. Δ is the displacement area of the wake far downstream. Taylor noted that, for models with 'thin' wakes, the change in static pressure along the working section is small in magnitude compared with the blockage correction to pressure $\delta p = p_c - p_0$, where suffix 0 refers to conditions far upstream of the model. Therefore he replaced equation (1.3) with

$$\delta D = \delta p \Delta. \quad (1.4)$$

In tests of models with simulated engine flows, for which the definition of drag includes pre-entry and post exit components, the correction takes the form:

$$\delta D = \delta p(\delta A + \Delta),$$

* Results for wall-induced pressure gradients in perforated-wall wind tunnels of square cross section as a function of wall porosity can be found from graphs of 'wake blockage factor ratio' in the paper by Pindzola and Lo [16]. See also Chapter 3.

where δA is the change in cross-sectional area of the "engine flow" streamtube between stations far upstream and far downstream.

In the absence of powered engine-flow simulation $\delta A = 0$ and

$$\Delta = \frac{1}{2}(1 + 0.4M^2)SC_D, \quad (1.5)$$

where C_D is the drag coefficient excluding the contribution of the trailing-vortex drag. Thus combining equations (1.4) and (1.5) and noting that, to the order of approximation of linear theory,

$$\delta p = -\rho_0 U_0^2 \varepsilon.$$

it follows that

$$\delta C_D = -(1 + 0.4M^2)C_D \varepsilon. \quad (1.6)$$

Except for high-drag models the contribution of wake blockage to the term ε in equation (1.6) may be ignored to give

$$\delta C_D = -(1 + 0.4M^2)C_D \varepsilon_S$$

which is in agreement with the expression given by Rogers (equation (1.2)).

As observed by Taylor [19], methods for determining the corrections to drag using mass momentum and energy balance between far upstream and downstream, such as that of Taylor, and those given below for lift-dependent drag are only valid in tunnels for which:

- a) the velocity perturbations at the walls, due to the model, do not induce a change in the drag of the walls which is comparable with the required data accuracy and
- b) the tunnel working section is long enough for the perturbation pressures due to model lift and sideforce to be negligible at its ends.

The first condition excludes tunnels with perforated walls and for these there is no simple expression for the correction to profile drag which includes the effect of wall constraint on the wake. In this case, the only solution is to fall back on expressions such as equation (1.1).

Hackett [9] has questioned the validity of the classical model for solid-wall wind tunnels described in AGARDograph 109. He argued that the influence on the drag of the wake source (and its associated images) of the source/sink distribution representing the model is cancelled identically by the influence of the source/sink distribution (and its images) on the drag of the wake source. This leads to the result that the correction to drag for incompressible flow is:

$$\delta C_D = -C_D \varepsilon_w \quad (1.7)$$

where suffix w refers to the wake component of blockage. Further details of this kinematic approach may be found in Chapter 6.

Experience with tests on bluff models and models at high lift suggests that Hackett's flow model is preferable to the classical flow model. Recently, Mokry [15] has derived equation (1.6) from momentum considerations. However, he pointed out that the kinematic approach only allows for one of the effects of the walls on the wake streamwise momentum (due to the difference in streamwise velocity between the flow far upstream of the model and that far downstream outside of the wake) and does not include the

buoyancy effect. The latter would be expected to dominate for attached flows, whereas the evidence of Hackett's studies is that the volume-dependent buoyancy drag is much less important than the correction given by equation (1.6) for bluff models or high-lift models. Ashill and Taylor [5] have shown how it is possible to reconcile Mokry's analysis with the classical formula by allowing for the effect of the walls on the pressure drag of the displacement surface of the model and its shear layers. Hackett [10] has reiterated the reasons for preferring his result.

All these methods rely on inviscid models of the flow in that they do not allow explicitly for the effect on the development of the shear layers on and downstream of the model of the second (viscous) effect described above. This assumption appears justified for models with thin shear layers and attached flows. However, for flows on the point of separation or with regions of separation, the walls may influence the development of the model boundary layers and its wake. Thus consideration needs to be given to the theoretical simulation of real viscous flows in the wind tunnel or systematic wind-tunnel studies of the effect of tunnel walls on the model drag for there to be a complete understanding of this problem.

b) Lift-dependent drag

With these reservations, the correction to lift-dependent drag is determined by the change in the flow at the vortex sheet far downstream of the model, taking into account changes in the loading due to wall-induced upwash (and if necessary aeroelastic distortion of the wing). In general, the correction at zero lift can be ignored and then the correction to drag, at constant lift coefficient, becomes:

$$\delta C_D = C_L^2 \int \{\Gamma(y)\mu(y) - \Gamma'(y)\mu'(y)\} dy.$$

where $\Gamma(y)$ is the normalised spanwise loading on the wing due to unit lift coefficient and $\mu(y)$ is half the downwash induced by the infinite vortex sheet having the same spanwise distribution of vorticity as the wing at unit lift coefficient. The dashed symbols denote in-tunnel values. Here the functions μ and μ' can be regarded as spanwise weighting factors for induced drag.

If the spanwise loading is close to elliptic, and the span of the model (and the aeroelastic distortion) are not excessive, the effects of the change in loading will be small and the change in the weighting factor will be constant across the span. The drag correction is then given by Glauert's formula, i.e. $\delta C_D = \delta\mu C_L^2$, where $\delta\mu$ is simply the wall-induced downwash at infinity downstream.

Strictly this correction is a force directed along the tunnel axis, not along the corrected free-stream axis, but usually this distinction can be ignored and then the correction should be added to the drag force obtained by resolving balance-axis forces onto the corrected free-stream axis.

The difference between the correction given above and that obtained by simply multiplying the lift by the incidence correction, is due to the thrust force at the wing leading edge. As this force only occurs in fully-attached flow it might be expected that, when there is significant flow separation at the leading edge, the drag correction will be closer to the product of the lift force and the induced upwash at the model. This is obviously the case when the measured drag varies roughly as the product of lift and incidence, as for slender wings with sharp leading edges. When, as is often the case, the model is long compared with the height of the working section, there may be a significant wall-induced camber at high lift and since theory gives no guidance on the value of the upwash to use in either the incidence or drag correction, there must be a degree of uncertainty in the correct values for these.

c) Pitching moment and yawing moment

The correction to pitching moment at constant lift, which again is derived using a reverse-flow theorem, is :

$$\delta C_m = -(1/S) \iint \bar{m}(x_1) w(x, y) dx dy,$$

where $\bar{m}(x_1)$ is the loading in reverse flow due to a linearly-varying upwash $U(x-x_1)$, x_1 is the chordwise location of the moment reference axis and $\delta w(x, y)$ is the residual variation of wall-induced upwash (including model aeroelastic distortion).

When the spanwise variation of the residual variation is negligible and the chordwise gradient is linear, the correction becomes:

$$\delta C_m = -\lambda C_{mq}$$

where C_{mq} is the non-dimensional pitching moment derivative for (nose-up) rotation, about the spanwise axis passing through the aerodynamic centre in reverse flow and $\lambda = \bar{c} dw/dx$, with upwash $Uw(x)$.

As mentioned above, the difference between the wall-induced upwash at the tailplane and the correction to incidence is best treated as a change in tail setting.

The correction to the rolling moment of a yawed wing is analogous to that for pitching moment i.e.:

$$\delta C_\ell = -(1/S) \iint \bar{\ell}(x, y) w(x, y) dx dy,$$

where $\bar{\ell}(x, y)$ is the loading in reverse flow due to unit rate of roll and $w(x, y)$ is the wall-induced upwash. In using this equation care needs to be taken that the correction has the correct sign.

When yaw is obtained by a combination of pitch and roll, as may be the case with sting-mounted models, the "upwash" terms in the corrections to incidence, pitching moment and rolling moment must be interpreted as the component of wall-induced velocity normal to the plane of the wing. A similar interpretation also needs to be made for "sidewash" in the correction to angle of yaw. In these cases there may be an additional component to the correction to rolling moment, to account for the change in load on the fin.

References for Sections 1.1, 1.2 and 1.3.

- [1] Adcock J.B. and Barnwell R.W. 1984, "Effects of boundary layers on solid walls in three-dimensional wind tunnels", AIAA Journal Vol 22, No 3.
- [2] Ashill, P.R. and Keating, R.F.A., 1988, "Calculation of tunnel wall interference from wall-pressure measurements." The Aeronautical Journal, Vol. 92, No. 911, pp. 36-53.
- [3] Ashill P.R., Goodyer M.J. and Lewis M.C. 1996, "An experimental investigation into the rationale of the application of wind tunnel wall corrections", ICAS-96-3.4.1, Sorrento, pp 798 - 808.
- [4] Ashill P.R., Taylor C.R. and Simmons M.J. 1995, "Blockage interference at high subsonic speeds in a solid-wall wind tunnel", Proceedings of PICAST 2-AAC 6, Vol 1, pp 81-88, Melbourne 20-23 March 1995.
- [5] Ashill P. R. and Taylor C. R., 1997, "A further contribution to the discussion on 'Tunnel-induced gradients and their effect on drag'", Communicated to AIAA Journal., May 1997.

- [6] Berndt S.B. 1950, "Wind tunnel interference due to lift for delta wings of small aspect ratio", KTH Tech Note Aero TN 19.
- [7] Bouis X. 1984, "ETW Specification and its vindication", Document SC-ETW/D/27.
- [8] Freestone M. M., 1995, "Upwash interference for wings in solid-liner wind tunnels using subsonic linearised-theory", ESDU Data Item 95014.
- [9] Hackett J. E. 1996, "Tunnel-induced gradients and their effect on drag", AIAA Journal, Vol. 34, No. 12, pp 2725 - 2581.
- [10] Hackett J. E., 1997, "Reply to comments by Mokry and Ashill/Taylor on 'Tunnel-induced gradients and their effect on drag'", Communicated to AIAA Journal.
- [11] Isaacs D. 1967, "Calibration of the RAE 8ftx8ft wind tunnel at subsonic speeds, including a discussion of the corrections to the measured pressure distribution to allow for the direct and blockage effects due to the calibration probe", ARC R&M 2777.
- [12] Kemp W. B. Jr. 1976, "Towards the correctable-interference transonic wind tunnel", Proceedings of the AIAA 9th Aerodynamic Testing Conference, 7-9 June 1976, pp 31-38.
- [13] Lewis M.C. and Goodyer M.J., 1995, "Initial results of an experimental investigation into the general application of transonic wind tunnel wall corrections", Second Pacific International Conference on Aerospace Science & Technology, Sixth Australian Aeronautical Conference, Melbourne. Vol. 1, pp 71-80. 20-23 , March 1995.
- [14] Lewis M.C. and Goodyer M.J., 1996, " Further results of an investigation into general applications of wind tunnel wall corrections", Paper 96-0560, AIAA 34th Aerospace Sciences Meeting, Reno, January,.
- [15] Mokry M., 1997, "Comment on 'Tunnel-induced gradients and their effect on drag", Communicated to AIAA Journal., April 1997.
- [16] Pindzola M. and Lo C.F. 1969, "Boundary interference at subsonic speeds in wind tunnels with ventilated walls", AEDC-TR-69-47.
- [17] Pistolesi, E., 1933, "Considerazioni sul problema del bi-plane", Aeronautica, Rome 13, 185
- [18] Rueger, M., Crites, R. And Weirich, R., 1995, "Comparison of conventional and emerging ("measured variable") wall correction techniques for tactical aircraft in subsonic wind tunnels (invited paper) AIAA 95-0108, 1995.
- [19] Taylor C.R. 1996, "Some fundamental concepts in the theory of wind-tunnel wall constraint and its applications", DRA/AS/HWA/TR96055/1.
- [20] Steinle, F. and Stanewsky, E., *Wind Tunnel Flow Quality and Data Accuracy Requirements*, AGARD-AR-184, November 1982.

1.4 CHOICE OF CORRECTION METHOD

(A. Krynytzky & J. Hackett)

"Naturally the precision of calculated interference parameters is far greater than that of any experimental verification of the underlying theory." H. C. Garner, AGARDograph 109

Wall interference prediction, correction and, in some cases, minimisation for a given model and test environment are the objectives of any correction method. Section 1.3 has shown it is both useful and revealing to describe wall interference in terms of primary corrections and residual interference variations. The calculation of primary corrections for a spatially varying interference field (for subsonic inviscid flow) has been discussed, as well as a method for handling residual variations. The main outputs of any wall interference method are thus the primary corrections to freestream velocity (direction and magnitude). However, for large models and for Mach numbers in the high subsonic range, residual interference should be quantified as well. In the adaptive wall case for which the interference goal is zero by definition, residual interference is an appropriate measure of the quality of the adaptation. Intermediate outputs of an adaptive wall method are the wall settings to achieve minimum interference. Wind tunnel model data, corrected for the influence of the walls to equivalent free air conditions, represent the ultimate output of the application of a wall correction method.

The correctability of wind tunnel data to equivalent interference-free conditions may be rigorously evaluated by consideration of interference gradients for linear potential flows or by comparison of in-tunnel to unconstrained-stream flow solutions at corrected flow conditions (virtually mandatory for non-linear flows). Poor correspondence of results of the latter calculations implies a breakdown of the usefulness of wind tunnel test results: there is no interference-free flight condition that corresponds to the wind tunnel flow field in the vicinity of the model. This may occur if interference variations are great enough that simple corrections based on linear theory do not capture the actual integrated interference on the model. The difference in the flow field (in-tunnel to interference-free at nominal corrected conditions corresponding to the tunnel flow) may be due to strictly inviscid loading changes or, more insidiously, fundamental changes in the nature of the flow field around the model. These phenomena include changes in the boundary layer on the model with regard to either onset of separation or change in shock position for compressible flows, modification of separation bubble size or shape, or change in wake trajectory (viscous or vortex).

The choice of a correction method, or whether to bother with wall corrections at all, depends on required data precision and accuracy, and on available resources. Resources include instrumentation, computing hardware and software, qualified staff, and time.

In practice, one is often faced with sizing a model for a given set of test conditions. That is, given a test facility and test envelope, how large a model may be used to generate "valid" wind tunnel data? "Larger" is generally better from the standpoint of aerodynamic simulation for most applications (i.e., closest Reynolds number match, model geometric fidelity, or other model- to full-scale considerations). Permissible magnitudes of wall corrections depend on overall required data accuracies. An error analysis with target data accuracies should be done to establish target maximum levels of wall interference. Steinle and Stanewsky [17] derive permissible flow field variations for a variety of testing requirements. The parameters that relate most directly to wall interference are based on a drag accuracy requirement of $0.0001 \Delta C_D$ (Table 1).

Item	Description	Value
M	Mach number accuracy	0.001
$\alpha, (w/U_\infty)$	Angle of attack (upwash) accuracy	0.01 deg (0.00017)
$[d(w/U_\infty)]/[d(x/c)]$	Flow curvature	≤ 0.03 deg
$[d(w/U_\infty)]/[d\eta]$	Spanwise flow variation	≤ 0.1 deg
$dM/[d(x/L)]$	Streamwise Mach gradient	≤ 0.0006

Table 1 Required Flow Field Accuracies Corresponding to $\Delta C_D=0.0001$
(after Steinle and Stanewsky, [17])

These values provide benchmarks against which the accuracy of primary wall corrections and the spatial variation of the residual wall interference field can be tested. Since the magnitude of primary wall corrections may be small, uncertainties associated with their prediction may be as large as the corrections themselves. The evaluation of data uncertainty may need to take this into account. With a reasonable model size as a starting point, an iterative evaluation of wall interference balanced against accuracy and scaling needs will generate the data for an informed decision.

Four factors govern the aerodynamic interference of wind tunnel walls on a model:

- 1) Nature of the aerodynamic forces generated by the model, including not only lift, drag, and pitching moment, but also the constitution of the total drag (in classical terms, vortex, parasite, and separation drag) and the contributions of simulated power units (including rotors, propellers, fans, and jets).
- 2) Mach number
- 3) Size of the model relative to the dimensions of the test section (length, width, and height).
- 4) Type of test section walls.

1.4.1 MODEL AERODYNAMICS

Model aerodynamics refers to those aspects of the model that require explicit treatment or modelling in the evaluation of wall interference, exclusive of Mach number. These include the displacement (or volume) effect of the model and the customary aerodynamic forces: lift, drag, thrust, and pitching moment. These interference effects are well understood in an attached-flow context and are commonly addressed using classical wall interference concepts. However, the testing of models at high lift, with powered lift (e.g., rotors or lifting fans) can result in large vortex wake deflections within the tunnel that require special modelling attention. Separated wakes present another flow situation requiring additional modelling.

Together with Mach number and model size, model aerodynamics guides the complexity of model representation. For attached flows around small models at low Mach number, use of simple singularities of known strength is adequate (Chapter 2). More complex geometries or large models may require more accurate geometry representation as afforded by panel methods.

Separated wakes behind bluff bodies require special treatment, Chapter 6. In particular, wall pressure measurements can be used to advantage for this case in order to determine the appropriate representation of the separation bubble. Large lift forces may require consideration of wake deflections

in addition to accounting for the separated wakes often associated with configurations near maximum lift. Rotor testing at low speeds introduces additional complexity in that wake trajectories may result in fundamental changes of the in-tunnel flow relative to an interference-free flow. These flows associated with V/STOL configurations are discussed in Chapter 8. Unsteady interference effects largely have to do with cross-stream resonance within the test section walls (Chapter 9).

Boundary measurement methods discussed in Chapter 4 potentially provide advantages with respect to both model and wall representations. Chapter 10 outlines applications of these methods to adaptive wall tunnels, especially for tunnels with two flexible walls for both 2D and 3D testing. Two-variable boundary measurement methods provide the incontestable advantage of not requiring a representation of the model for determination of the interference. This feature is most useful whenever the exact nature of the aerodynamics at the model is not known: small supersonic flow regions near the model, large deflected wing wakes, or separated flow at the model. Though these methods are applicable to any tunnel, the most progress has been made for tunnels with closed walls, largely because of boundary measurement considerations. One-variable boundary measurement methods can be especially helpful for the case of ventilated walls, where sufficient uncertainty exists as to the proper wall boundary condition. Representation of the model is required for this approach.

The modelling of active power simulation (propellers, wind turbines, fans, turbo-powered simulators, blown nacelles or other jet simulation with at most small deflections of the propulsion streamtube) is typically approached by consideration of momentum-streamtube relationships and the use of appropriate source and sink singularities (Chapter 8).

1.4.2 Mach Number

Discussions of the AGARD Fluid Dynamics Panel Working Group 12 [1] used a classification of tunnel flows by speed range from the standpoint of adaptive wall tunnel operation. This classification serves well in a more general wind tunnel testing context because the flow physics are fundamentally the same in all wind tunnels. The first three speed ranges are of particular interest with regard to wall interference (see Chapter 10 for further discussion of these classifications):

- 1) Group 1: subsonic free stream, local embedded supersonic regions may occur near the model; region near the walls is well represented by linearised compressible flow equations.
- 2) Group 2: subsonic free stream; non-linear region (in unconfined flow) extends beyond the walls.
- 3) Group 3: near-sonic and supersonic free stream.

Group 1 flows permit the application of the linearised potential flow equation for the evaluation of wall interference. The effect of compressibility is linearised using the Prandtl-Glauert compressibility factor, $\beta = \sqrt{1 - M^2}$. The governing equation is linear and homogeneous, so that the principle of superposition applies. That is, the interference flow field can be considered an incremental flow field due to the wall potential that can be simply added to the flow due to the model potential. Because a wide variety of practical aerodynamic problems fall into this speed range, and because of the demonstrated success of linearised methods, most of the methods in this publication use the linearised potential equation (which after the Prandtl-Glauert transformation becomes Laplace's equation) as a starting point.

For Group 2 flow the non-linear portion of the flow field, strongest at the model, has grown to include a substantial, if not the entire, region between the model and the wall. In this case, the distortion of the compressible flow field around the model and at the wall location (relative to interference-free conditions)

requires the use of non-linear flow equations for proper characterisation. Wall interference is not easily characterised as an incremental flow field; the calculation of both the in-tunnel and interference-free flow fields may be required. Chapter 5 addresses the estimation of interference for these flows. Chapters 4 (boundary measurement methods) and 10 (adaptive walls) also include discussions of the use of non-linear governing equations. For cases with supersonic flow extending to the walls, the interference of the walls may include the effects of reflected compressible disturbances (compression and expansion waves) on the model. The appearance of reflected disturbances may be considered to be the threshold for classification in the next speed range.

Group 3 flow presents the most difficult situation from the standpoint of correctability in that the flow field between the model and the walls is fully supersonic. In a typical case, the flow around the model is dominated by multiple reflections of expansion and compression disturbances (originating at the model) from the walls, back to the model. Passive ventilated walls have successfully been configured to attenuate isolated shock waves, but a practical method for reducing nonplanar shock reflections for configurations of interest is yet to be demonstrated. An adaptive closed-wall approach to shock reflection attenuation has been demonstrated in 2D testing; the much more difficult 3D problem is beyond the grasp of the current state of the art.

As Mach number is increased into the supersonic range, a point is reached beyond which wall interference ceases to be an issue. This occurs when the flow disturbances from the model, consisting of compression and expansion waves that travel along characteristics, are reflected from the tunnel boundaries and pass downstream of the model. The flow field around the model is therefore interference-free. A first-order estimate of permissible model size in the supersonic speed range is made by simply calculating the Mach diamond based on the upstream Mach number from the model nose (or, if known, the position of the detached nose shock). Thus, for a model positioned at a distance z from the closest tunnel wall, the body length L should be less than $2z / \tan \arcsin(1/M)$. For pointed bodies a more accurate calculation of shock wave trajectory is possible using the exact (Taylor-McColl) solution for conical flows.

For a given model and test section wall, a mapping of flow regimes provides guidance regarding wall interference requirements. A schematic of such a map in the Mach- C_L plane, Figure 1.4, shows the typical progression from Group 1 to Group 3 flow with increasing upstream Mach number at a given lift.

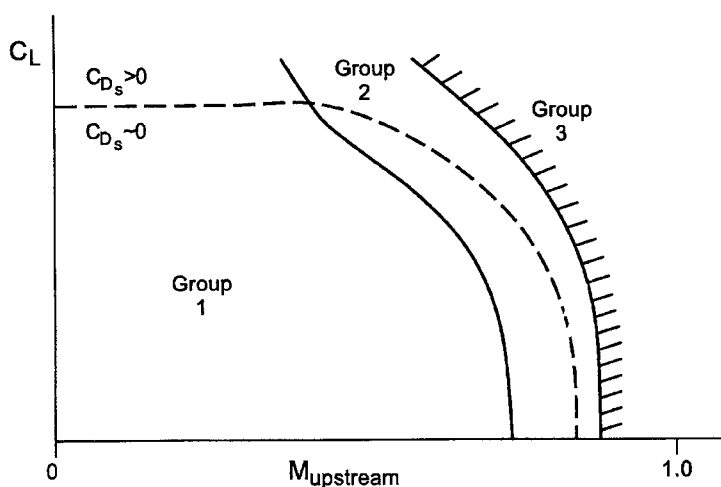


Figure 1.4 : Flow Regime Mapping for a Typical Subsonic Flight Vehicle

With increasing lift the boundaries move to lower Mach numbers. Group 1 flows are amenable to linearised flow analysis. Group 2 flows will generally require non-linear flow analysis, and may not be easily correctable without resorting to an adaptive wall strategy. Group 3 flows are considered uncorrectable except for the case of fully adapted walls. Decreasing model scale (for a given configuration) will move the boundaries toward higher Mach number and lift. In this way, wall correction quality (for a given methodology) can be matched to desired test envelope by the appropriate choice of model size. It is recognised that the boundaries between flow

regimes are not distinct, but represent somewhat arbitrary transition zones between flow classifications. An additional boundary shown in Figure 1.4 delineates the onset of separation at the model. Interference estimates beyond this boundary should include an evaluation of separated wake interference.

1.4.3 MODEL SIZE

Model size relates to wall interference in two basic ways: (1) the gross dimensions of the model are directly proportional to the disturbances generated at the wall, and therefore to the magnitude of the interference felt by the model due to the walls, and (2) the physical extent of the model within the test section determines the severity of wall interference due to the spatial nonuniformity of the interference flow field. It should be noted that aerodynamic size of the model, which depends on the dominant flow phenomena and on the magnitude of the generated aerodynamic forces (see next section), rather than geometric size, is the most relevant characterisation of model size.

In classical wall interference theory (Chapters 2 and 3) models are first considered to be infinitesimal, so that any singularities representing the model's far-field disturbance may be considered to be located at a single point, with the primary interference velocity evaluated at that point and the resulting corrections applied. With regard to the magnitude of the disturbances due to the model, V (volume; for 2D flows, cross-sectional area A) and $C_D S$ (model drag; for 2D flows, $C_d c$) are taken to be the relevant linear scaling parameters representing the symmetric displacement of far-field streamlines, and $C_L S$ (model lift; for 2D flows, $C_l c$) for the asymmetric far-field perturbation due to the model. The strengths of the fundamental singularities used to represent the model are scaled by these model-dependent characteristics.

Model size, as relating to blockage interference, is often described or delimited by the so-called "model blockage" parameter, or A_{max}/C , where A_{max} is the maximum model cross-sectional area (taken normal to the tunnel axis), and C is the test section cross-sectional area. The 2D equivalent is t_{max}/H , where t_{max} is the maximum model thickness and H is the test section height. This parameter has an obvious geometric relationship to the afore-mentioned model volume (for 2D flows, area), depending on the model shape distribution. In the limit of 1D inviscid incompressible flow in a closed-wall tunnel, this area ratio is equal to the increase in effective freestream velocity at the model station. For compressible flow, in the limit of Mach approaching 1.0, this area ratio defines an upstream Mach number for which sonic choking in a closed-wall tunnel will most certainly occur. Thus, in these limiting cases, it is a physically meaningful parameter that bounds the parameters governing blockage interference. For normal model sizes the blockage interference is usually much less than predicted from 1D flow considerations (for example, for unusual shapes "when all is lost", Pope and Harper [14] suggest a factor of 1/4 to account for both solid and wake blockage, with A_{max} taken as the model frontal area). Finite model size and angle of attack contribute to the onset of sonic choking at a lower Mach number than predicted as above.

The first departure from point singularities considers the effect of finite span, both on the magnitude of the interference upwash at the centre of the model and on its spanwise variation. Similarly, model length may give rise to variations of interference from nose to tail, or root to tip for a swept wing. The relevant length scale for these effects are the cross dimensions of the tunnel, so that $2s/B$ (span ratio) and $L/\beta\sqrt{C}$ (body length ratio; for 2D flows, $c/\beta H$) form a logical nondimensionalised set of model dimensions for evaluating effects of the spatial variation of the interference field. In 3D subcritical flow, span and length ratios much less than 1.0 are adequately represented using point singularities at a single model location (as long as the model is either in the centre of the tunnel, or several model dimensions away from a homogeneous wall). This simple approach may prove adequate up to length ratios of one-half or more,

depending on required accuracy. Beyond about one-half, however, spatial nonuniformity of the interference field may become significant, so that multiple-singularity or panel methods should be used. In transonic flow, even very small models may experience unacceptable interference at Mach numbers close to one.

In general, the size of the aerodynamic perturbation due to the model at the wall location is a reasonable indicator of the magnitude of interference (for a given wall geometry). Within each speed range, moreover, there may be criteria for model size defining the validity of various wall interference approaches. This is most clearly demonstrated in the lowest speed range where linear potential flow applies. For linear subsonic flows, the model size criteria can be combined with Mach number using the Prandtl-Glauert factor β to scale physical model size for the first-order effects of compressibility. For example, for a given level of perturbation velocity at the wall, model volume should decrease like β^3 .

1.4.4 WIND TUNNEL WALLS

Concurrent with advances in computational capability, significant developments have occurred with regard to wind tunnel wall geometry since the publication of AGARDograph 109 (Garner et al., [5]). In particular, with the rejuvenation of the adaptive wall concept (Sears, [16]), and subsequent boundary measurement methods, a variety of new approaches for the minimisation and evaluation of wall interference have been developed.

The type of wind tunnel walls spans a range of possibilities. With regard to wall interference methodologies, six approaches may be distinguished:

- 1) Closed parallel walls with no measurements at the boundaries (Chapters 2 and 6).
- 2) Closed parallel walls with boundary pressure measurements (Chapters 4 and 8).
- 3) Closed walls with deflection capability and boundary pressure measurements (Chapters 4 and 10).
- 4) Ventilated walls with no measurements at the boundaries (Chapter 3).
- 5) Ventilated walls with boundary measurements (Chapter 4).
- 6) Active ventilated walls with boundary measurements (Chapter 10).

The majority of existing wind tunnels have passive walls of basically fixed geometry, without adequate instrumentation at the walls for wall interference purposes. Closed-wall test sections of various cross sections are the most numerous for a variety of reasons: historical; relatively low power requirements for a given size and speed of the jet; unambiguous wall boundary condition and therefore well-understood interference characteristics; and potential for superior flow qualities (low spatial and temporal variations of pressure and velocity). Thus, advancements in adaptive wall technology notwithstanding, closed-wall tunnels with aerodynamically parallel walls (for a clear test section) are still the workhorses for most low-speed testing. For small models with attached flow, the use of classical methods (Chapter 2) generally suffices for the calculation of wall interference. Panel methods have proven to be successful extensions of classical techniques, particularly for the investigation of the wall interference of large models (Chapters 2 and 3).

For closed-wall tunnels, significant advances have been made in two areas since the publication of AGARDograph 109 [5]. First, with the development of boundary measurement techniques, the performance envelope of closed-wall tunnels has expanded to include larger models at low speed (both

from the standpoint of blockage and lift, Hackett, [7] and higher subsonic speeds for conventionally sized models (Ashill, Taylor, and Simmons, [4]). Boundary measurement techniques are discussed in Chapter 4 (Sec. 4.2 for closed walls) and adaptive walls, in Chapter 10. Second, the development of the adaptive-wall concept from both theoretical and practical standpoints (see Chapter 10 for a discussion of issues and approaches) has resulted in a deformable-wall test section being a serious candidate for new wind tunnel projects, especially for tunnels using a removable test section configuration.

In particular, practical implementations of the adaptive wall concept have resulted in a number of 2D test sections with deformable floor and ceiling. Theoretically, this is the simplest application of the adaptive wall concept. In principle, the design technology is little different from a flexible supersonic nozzle. Proper adaptation in three dimensions is a much more difficult problem, especially from the constructibility point of view. The rubber test section (Heddergott and Wedemeyer, [8]) and the octagonal deformable test section at the University of Berlin (Ganzer, Igeta, and Ziemann, [6]) are notable examples of deformable 3D closed-wall test sections. Difficulties associated with the desired arbitrary deformations have led to investigations of the use of 2D wall adaptation for 3D testing to minimise certain aspects of the interference (Wedemeyer [19]; Lamarche and Wedemeyer [10]; Wedemeyer and Lamarche [20]). Chapter 10 focuses on this approach as currently the most practical for providing wall interference reduction and control.

Ventilated wind tunnel walls have also undergone significant development in the past 30 years. Though the two basic types of ventilated walls, slotted and perforated, still predominate, a number of advances have been made in their use for the minimisation of wall interference. Experimental investigations of the ventilated wall boundary condition have met with mixed results: perforated walls behave like ideal porous walls over some range of crossflows, with possibly different inflow and outflow characteristics; walls with open slots exhibit a richness of behaviour only approximately captured by the ideal slotted-wall condition with the inclusion of porous-wall pressure-drop terms. Panel methods with the appropriate wall boundary conditions have been successfully applied to ventilated tunnel interference (Chapter 3). With the maturation of boundary measurement techniques, including the development of instrumentation and advances in data acquisition, the analytic forms of the wall boundary conditions can be side-stepped by applying the principles of the one-variable method (Chapter 4).

For perforated walls, a sliding perforated plate backing the primary perforated wall surface provides a means to vary wall openness. This type of wall configuration was pioneered at the Arnold Engineering Development Centre (AEDC) with slanted-hole walls, and is now a common feature of perforated wall retrofits, as well as of new designs. Initial experiments used the variable-porosity feature for global test section porosity variation to optimise clear test flow qualities and to minimise shock reflection at supersonic Mach numbers (Pindzola and Chew, [13]). However, it was realised that streamwise porosity variation could be used to minimise wall interference (Lo, [11]). To date, the TsAGI T-128 Transonic Wind Tunnel is the most ambitious implementation of this approach, the test section wall ventilation consisting of nominally 10% open normal holes, with 128 movable backing plates covering the entire test section (Neyland, [12]). The local porosity can thus be varied independently in each of the 128 zones from 0% (fully closed) to 10% (fully open). Successful adaptation is judged by comparing measured wall pressures to an interference-free prediction of far-field pressures. In general, perforated walls combined with wall pressure instrumentation provide an excellent opportunity for the application of measured boundary condition methods, (Sec. 4.3).

Operational adaptive features for slotted-wall wind tunnels have not yet evolved to the degree that perforated wall adaptation has. The importance of slot shaping has long been known to be important for supersonic flow forming in the low supersonic operating range (Ramaswamy and Cornette, [14]).

Research and development on the use of slot shaping to minimise wall interference has resulted in the calculation of particular slot shapes for minimum interference (Karlsson and Sedin, [9]; Agrell, Petterson, and Sedin, [2]). This work has resulted in a slot flow model that treats the re-entry flow from the plenum into the test section differently from the flow exiting the test section. The FFA T-1500 Transonic Wind Tunnel has manually replaceable contoured slot edges for each of the 16 longitudinal slots based on this work (Torngren, [18]). Various slot shapes were tested to optimise both clear tunnel flow qualities and wall interference. Though remotely actuated variable-geometry slot mechanisms have been proposed for several facilities, none has passed the proof-of-concept stage for wall interference minimisation. Investigations of the wall boundary condition for open slots suggest that the inclusion of a crossflow resistance term in the homogeneous boundary condition describes the actual crossflow boundary condition better than the ideal inviscid slot boundary condition. Real slotted tunnels thus appear to exhibit some of the interference characteristics of perforated-wall tunnels. These observations help bridge the apparent disparity in the fundamental forms of the ideal homogeneous slotted wall boundary condition and the ideal porous wall boundary condition.

A hybrid ventilated wall, consisting of longitudinal openings in the manner of slotted wind tunnels, but with fixed baffles within the slots that provide a D'Arcy-type resistance to crossflow, is used at the Ames 11-ft transonic leg of the Unitary Tunnel. As long as the slot spacing is small relative to the required absence of "graininess" of wall interference, this type of wall may be treated as a homogeneous perforated wall. With regard to shock reflection, Allen [3] shows that the strength of the reflected disturbance from a wall with lines of perforations changes little for more than five or six lines of perforations per wall. Open slots were found to have both a larger reflected disturbance than perforated walls and to require a larger number of slots (compared to lines of perforations) before the reflected disturbance approaches its asymptotic value. Other issues related to local wall non-uniformity include measurement locations and techniques for boundary measurement methods (Chapter 4), and supersonic shock wave cancellation.

An important length scale for these phenomena is the wall boundary layer thickness. It is expected that if the wall opening size and spacing are of the order of the boundary layer or less, then at many boundary layer thicknesses from the wall, the wall ventilation will be perceived as homogeneous. Similar scaling arguments apply to hole size and spacing for perforated walls. Since boundary layers in large wind tunnels are often several inches thick, permissible wall openness length scale may be of this order. Perforated wall openings and spacings are typically less; slot widths may be somewhat larger; but slot spacings are often an order of magnitude greater. The small size of wall openings for perforated wall tunnels and the consequent ability to attenuate impinging shocks and expansions explains their being preferred over slotted walls for low supersonic testing. These general considerations suggest that homogeneous modelling of ventilated walls is appropriate for typical wall configurations, with the notable exception of walls with only several open slots. The non-trivial aspect of this modelling is the value of the crossflow coefficients in the boundary condition. The inclusion of wall boundary layer effects on crossflow characteristics has been investigated, but the uncertainty associated with the estimation of the wall boundary layer on a ventilated wall for a variety of model test conditions presents great difficulty for practical use of this approach. These considerations favour boundary measurement methods for ventilated walls to provide the necessary boundary condition information. For closed-wall tunnels, these methods have also been found to implicitly account for at least part of the effect of the model on the wall boundary layer (see Sec. 4.2).

The test section downstream of the model is an area that gives rise to special problems relating to the interference and modelling of wind tunnel test environments. Difficulties in this area can be attributed to support interference and re-entry/diffuser flow. It is becoming increasingly apparent that careful modelling of these aspects of the test environment is required to evaluate interference in its entirety.

The use of advanced methods is recommended whenever simpler methods fail to satisfy accuracy requirements, which can occur under a variety of conditions:

- 1) Model is not small.
- 2) Large regions of separated flow dominate the flow field due to the model.
- 3) Large regions of supersonic flow exist around the model.
- 4) Supersonic flow extends to any wall surface.
- 5) Pressure perturbations at the wall are large enough to effect changes in the wall boundary layer thickness.
- 6) Streamline deflection due to model-generated forces is significantly modified relative to interference-free conditions.

Advanced methods can (and should) be used whenever they are available (subject to resource constraints), providing that their application for simple attached-flow cases has been validated. Conscientious scrutiny of wall interference results for a range of model geometries and flow conditions can provide valuable clues relative to improved implementations of wall interference methods for specific facilities.

In spite of several decades of research activities aimed at the development of superior wind tunnel wall configurations, no single type of wall has emerged as dominant for 3D testing in the subsonic and transonic speed ranges. Production and research testing facilities around the world now exhibit a wider variety of wall types than ever before. In most cases, testing organisations have large capital and infrastructure investments in their test facilities. Development efforts often target extending the performance envelope (at minimum cost) or understanding the peculiarities of each facility. Wall interference activities are thus proceeding on several fronts, some of which overlap, others which are mutually exclusive. Chapter 12 summarises areas where progress is both needed and anticipated to improve the understanding, evaluation, and control of wind tunnel wall interference.

REFERENCES FOR SECTION 1.4

- [1] AGARD Fluid Dynamics Panel Working Group 12, *Adaptive Wind Tunnel Walls: Technology and Applications*, AGARD-AR-269, April 1990.
- [2] Agrell, N., Petterson, B., and Sedin, Y. C.-J., "Numerical Design Parameter Study for Slotted Walls in Transonic Wind Tunnels", ICAS-86-1.6.2, 1986.
- [3] Allen, H. J., "Transonic Wind Tunnel Development of the National Advisory Committee for Aeronautics", AG 17/P7, 6th Meeting of the Wind Tunnel and Model Testing Panel, November 1954.
- [4] Ashill, P. R., Taylor, C. R., and Simmons, M. J., "Blockage Interference at High Subsonic Speeds in a Solid-Wall Tunnel", *Proceedings of PICAST2-AAC*, Vol. 1, Melbourne, 20-23 March 1995.
- [5] Garner, H. C., Rogers, E. W. E., Acum, W. E. A., and Maskell, E. C., *Subsonic Wind Tunnel Wall Corrections*, AGARDograph 109, October 1966.
- [6] Ganzer, U., Igeta, Y., and Ziemann, J., "Design and Operation of TU-Berlin Wind Tunnel with Adaptable Walls", ICAS-84-2.1.1, 1984.
- [7] Hackett, J. E., "Living with Solid-Walled Wind Tunnels", AIAA-82-0583, March 1982.
- [8] Heddergott, A. and Wedemeyer, E., "Some new test results in the adaptive rubber tube test section of DFVLR Gottingen", ICAS-88-3.8.1, 1988.

- [9] Karlsson, K. R. and Sedin, Y. C.-J., "Numerical Design and Analysis of Optimal Slot Shapes for Transonic Test Sections - Axisymmetric Flows", AIAA-80-0155, January 1980.
- [10] Lamarche, L. and Wedemeyer, E., "Minimisation of Wall Interference for Three-Dimensional Models with Two-Dimensional Wall Adaptation", VKI-TN-149, March 1984.
- [11] Lo, C.-F., "Wind-Tunnel Wall Interference Reduction by Streamwise Porosity Distribution", Technical Note, *AIAA Journal*, Vol. 10, No. 4, April 1972.
- [12] Neyland, V. J., "Review of TsAGI Wind Tunnels", *Proceedings of the International Conference on Wind Tunnels and Wind Tunnel Test Techniques*, Southampton, UK, September 1992.
- [13] Pindzola, M. and Chew, W. L., "A Summary of Perforated Wall Wind Tunnel Studies at the Arnold Engineering Development Centre", AEDC-TR-60-9, August 1960.
- [14] Pope, A. and Harper, J. J., *Low Speed Wind Tunnel Testing*, John Wiley & Sons, Inc., New York, 1966.
- [15] Ramaswamy, M. A. and Cornette, E. S., "Supersonic Flow Development in Slotted Wall Wind Tunnels", AIAA 80-0443, 1980.
- [16] Sears, W. R., *Self-Correcting Wind Tunnels*, *Aeronautical Journal*, February/March 1974.
- [17] Steinle, F. and Stanewsky, E., *Wind Tunnel Flow Quality and Data Accuracy Requirements*, AGARD-AR-184, November 1982.
- [18] Torngren, L., "The FFA T1500 Injection Driven Transonic Wind Tunnel", ICAS-90-6.2.3, 1990.
- [19] Wedemeyer, E., "Wind Tunnel Testing of Three-Dimensional Models in Wind Tunnels with Two Adaptive Walls", VKI-TN-147, October 1982.
- [20] Wedemeyer, E., and Lamarche, L., "The Use of 2-D Adaptive Wall Test Sections for 3-D Flows", AIAA-88-2041, AIAA 15th Aerodynamic Testing Conference, San Diego, CA, May 1988.

2. CONVENTIONAL WALL CORRECTIONS FOR CLOSED AND OPEN TEST SECTIONS

Authors : Alex Krynytzky (Chapter 2.1 - 2.3)
 Bernd Ewald (Chapter 2.4)

	PAGE
2.1 CLASSICAL WALL CORRECTIONS : BASIC PRINCIPLES, DEFINITIONS AND ASSUMPTIONS	2-4
2.1.1 CO-ORDINATE SYSTEM AND GOVERNING EQUATIONS	2-4
2.1.2 MODEL REPRESENTATION	2-6
2.1.3 TUNNEL WALLS	2-8
2.2 CLASSICAL CORRECTIONS FOR CLOSED TEST SECTIONS	2-12
2.2.1 CLASSICAL CORRECTIONS FOR LIFT INTERFERENCE	2-14
2.2.1.1 2D LIFT INTERFERENCE	
2.2.1.2 3D LIFT INTERFERENCE FOR SMALL WINGS	
2.2.1.3 3D LIFT INTERFERENCE FOR WINGS OF FINITE SPAN	
2.2.1.4 APPLICATION OF UPWASH CORRECTIONS	
2.2.2 CLASSICAL CORRECTIONS FOR BLOCKAGE INTERFERENCE	2-22
2.2.2.1 2D SOLID BLOCKAGE FOR SMALL MODELS	
2.2.2.2 2D RANKINE OVALS	
2.2.2.3 2D WAKE BLOCKAGE	
2.2.2.4 3D SOLID BLOCKAGE FOR SMALL MODELS	
2.2.2.5 3D RANKINE BODIES	
2.2.2.6 3D WAKE BLOCKAGE	
2.2.2.7 APPLICATION OF BLOCKAGE CORRECTIONS	
2.2.3 WAKE BLOCKAGE CORRECTIONS FOR SEPARATED FLOWS	2-34
2.3 PANEL METHODS FOR CLOSED-WALL TUNNELS	2-36
2.3.1 GENERAL CONSIDERATIONS	2-36
2.3.2 2D INTERFERENCE	2-40
2.3.3 3D LIFT INTERFERENCE	2-40
2.3.4 3D BLOCKAGE INTERFERENCE	2-43
2.3.5 3D WING-BODY COMBINATIONS	2-45
2.3.6 SUMMARY OF PANEL METHODS	2-53

	PAGE
2.4 CLASSICAL CORRECTIONS FOR OPEN TEST SECTIONS	2-54
2.4.1 INTRODUCTION	2-54
2.4.2 LIFT INTERFERENCE	2-55
2.4.3 BLOCKAGE CORRECTION	2-60
2.4.4 WAKE CORRECTION	2-61
 NOMENCLATURE FOR CHAPTER 2	 2-62
 REFERENCES FOR CHAPTER 2	 2-64

2. CONVENTIONAL WALL CORRECTIONS FOR CLOSED AND OPEN TEST SECTIONS

Investigations of boundary interference in aerodynamic testing date back to the 1920s and 1930s. Glauert's classic monograph on the subject [15] summarises this pioneering work and serves both as a basis for ensuing developments and as a touchstone for evaluating wall interference methods to this day. These early investigations address interference in both closed-wall and open-jet test sections and, to some degree, in test sections whose walls are a combination of these two types. This chapter briefly describes the basic principles of this classical wall interference theory, summarises some fundamental results, and traces several related lines of development since the publication of AGARDograph 109 [13].

The fundamental problem of wall corrections concerns itself with the difference between the flow fields around a body immersed in a uniform oncoming stream of infinite lateral, upstream, and downstream extent, and around the same body in a stream confined or modified by wind tunnel walls. The streamlines around a body in a uniform subsonic onset flow depend on the shape of the body and on the aerodynamic forces acting on the body (which may be considered a result of its shape). In the interference-free case, as distance increases laterally from the body, the streamlines approach the straight and parallel flow of the onset stream. If the wind tunnel's boundaries (the "walls") are far enough away from a model being tested so that the flow perturbation due to the model is negligible, the same uniform parallel flow condition is obtained at the boundary and the flow around the model is therefore not affected by the tunnel boundaries. However, to the extent that the model's influence is perceptible at the boundary, the flow within the tunnel (i.e., around the model) is different from that which would be obtained in an unbounded stream. Classical wall correction theory attempts to account for this difference under a set of simplifying assumptions and corresponding restrictions on the theory's range of applicability. Fundamental to this approach are the concepts of primary corrections and residual variations discussed in Chapter 1.

Elementary interference results for both 2D and 3D models are presented in this chapter. These include the interference of only the tunnel walls remote from the model. So-called sidewall interference, which may be a major source of three-dimensionality in 2D tests, deserves attention as a special interference topic and is beyond the scope of the current discussion. Most of the 3D interference discussion in this chapter addresses a rectangular test section of height, H , and breadth, B , with the test section aspect ratio defined as B/H . Although other test cross sections are in use (e.g., octagonal, circular, elliptical) and interference methods have been developed for these situations, the rectangular section is used as a focus of discussion because of its commonality in practice, and because of the similarity of rectangular section interference to that of other sections of equal area and aspect ratio.

2.1 CLASSICAL WALL CORRECTIONS: BASIC PRINCIPLES, DEFINITIONS, AND ASSUMPTIONS

As used here, the term "classical" refers to the results of the earliest analyses of wind tunnel boundary interference on models in closed-wall and open-jet wind tunnels. The assumptions underlying classical wall interference theory include:

1. Linear potential flow.
2. Perturbation flow at the tunnel boundaries.
3. Model whose dimensions generally are small relative to the tunnel and whose wakes (including both the viscous and vortex wakes) extend straight downstream from the model.
4. Tunnel of constant cross-sectional area extending far upstream and downstream of the model, with boundaries parallel to the direction of the flow far upstream of the model, and whose boundary condition for a given wall is either no flow normal to the wall or a constant pressure at the wall location.

"Conventional" is used as a further classification of wall corrections, which includes the classical. These corrections are based on classical concepts in that the perturbation flow assumptions are used, but model size, wake position, and tunnel boundary conditions are not restricted as above. For present purposes, the tunnel walls are restricted, however, to a fixed geometry with a known pressure-crossflow characteristic. Conventional wall correction methods do not then include specified boundary condition methods or adaptive wall methods. Much of the work reported in AGARDograph 109 [13] satisfies this definition of "conventional", though specified boundary condition methods and adaptive wall methods have appeared in the literature since the 1940s, and are included in AGARDograph 109 [13] as well.

2.1.1 CO-ORDINATE SYSTEM AND GOVERNING EQUATIONS

The co-ordinate system is defined for a conventional wing-body model such that x is the streamwise co-ordinate, y is the lateral or spanwise co-ordinate, and z is the vertical co-ordinate corresponding to the direction of primary lift, Figure 2.1. The origin of the co-ordinate system is typically taken to be on the test section centreline, at the model centre. In 2D flow, the flow field is taken to be invariant with y . Far upstream of the model, the incoming flow is uniform.

Although the definition of classical wall correction methods should properly be restricted to incompressible flows, as mirrored in the early literature, linearised compressibility is included here as a straightforward application of the Goethert transformation (see, for example, Ashley and Landahl, [5]). Thus, the starting point for the development of classical wall interference corrections is the assumption of linearised potential flow between the model and the tunnel boundaries (see Sec. 4.1). Streamline flow is assumed with no allowance for shock waves or separated wakes. The effect of fluid viscosity in the governing equations is ignored. Velocity at any point in the tunnel is the gradient of the potential function in the usual way:

$$\vec{V}(x,y,z) = \nabla\Phi(x,y,z) \quad (2.1)$$

The principle of superposition is a key feature of classical wall interference analysis. This allows the interference flow field to be considered as an incremental flow field to the interference-free flow around

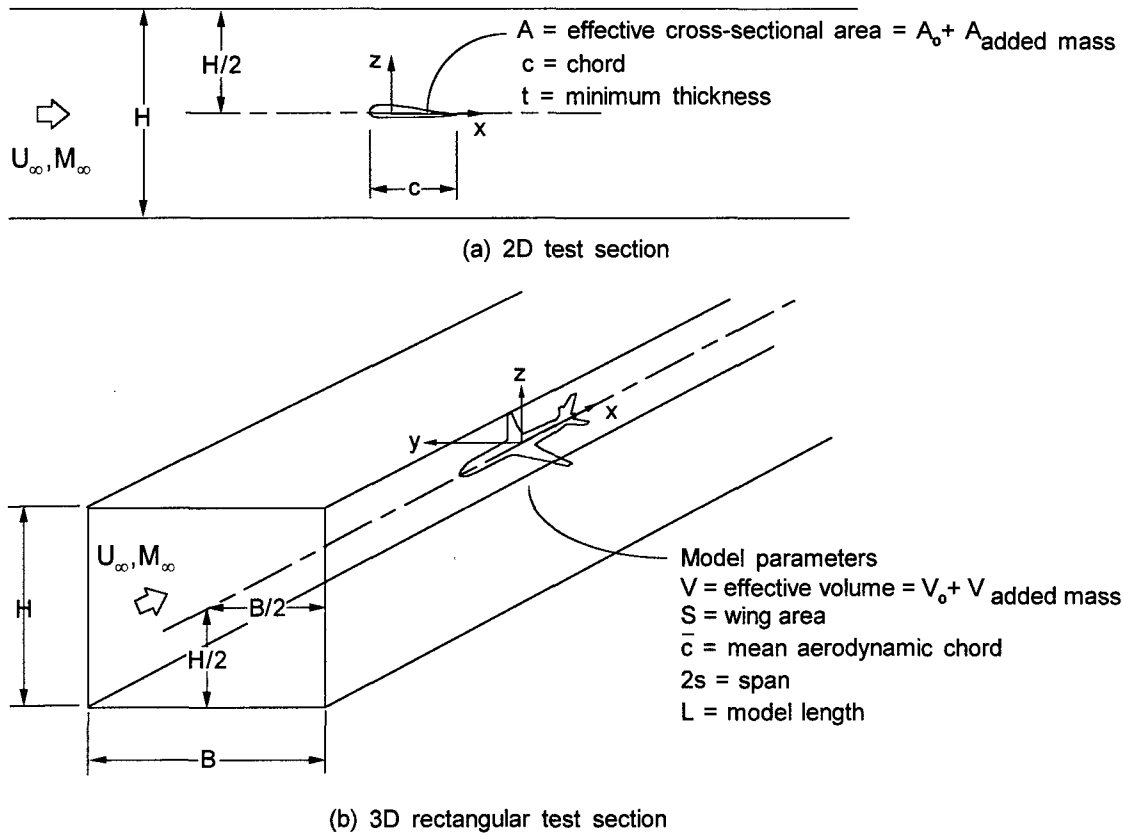


Figure 2.1 : Co-ordinate System and Geometry

the model. Thus, the potential, Φ , is assumed to be expressible as the superposition of a uniform onset stream, the model potential, and the wall potential,

$$\Phi(x, y, z) = -U_{\infty}x + \phi_m(x, y, z) + \phi_w(x, y, z) \quad (2.2)$$

In those regions of the flow away from the model where the flow perturbations to the uniform oncoming stream are small, the model and wall potentials can be considered perturbation velocity potentials. For small deviations from the nominal free stream, the effect of compressibility can be linearised in the full potential equation, resulting in the governing equation for the perturbation velocity potentials,

$$\beta^2 \phi_{xx} + \phi_{yy} + \phi_{zz} = 0 \quad (2.3)$$

where $\beta^2 = 1 - M^2$. That part of the flow field due to the walls, the wall interference velocity field, is the gradient of the wall interference potential,

$$\vec{v}_i(x, y, z) = \frac{\partial \phi_w}{\partial x} \hat{i} + \frac{\partial \phi_w}{\partial y} \hat{j} + \frac{\partial \phi_w}{\partial z} \hat{k} = u_i \hat{i} + v_i \hat{j} + w_i \hat{k} \quad (2.4)$$

The equation for the perturbation velocity potential can be reduced to the Laplace equation ($\nabla^2 \phi = 0$) with the co-ordinate transformation (as developed by Prandtl and Glauert for 2D airfoils and extended to three dimensions by Goethert): $X=x$, $Y=\beta y$, and $Z=\beta z$ (see Sec. 4.1). This transformation relates the linearised compressible flow to an equivalent incompressible flow in stretched co-ordinates.

2.1.2 MODEL REPRESENTATION

The combination of perturbation interference flow at the model and small model size (relative to the tunnel) implies that the variation of the interference velocity throughout the volume proximate to the model is small, so that the interference velocity may be considered a constant throughout the region affecting model aerodynamics. The primary corrections to stream magnitude and direction capture the greater part of the wall influence. The next order of corrections considers the linear streamwise variation of interference velocities (which result in streamwise buoyancy and flow curvature corrections). The interference velocities and gradients are typically evaluated at the model centre which, for simple model representations, is the location of singularities that approximate the flow field far from the model.

Thus, the flow in the immediate vicinity of the model will appear as though the model is immersed in an unbounded uniform onset stream of perturbed magnitude and direction relative to the flow far upstream of the model,

$$\vec{V}_{corrected} = U_{\infty} \hat{i} + \vec{v}_i(0,0,0) = (U_{\infty} + u_i) \hat{i} + v_i \hat{j} + w_i \hat{k} \quad (2.5)$$

This corrected onset velocity is characterised by streamwise and upwash velocity corrections (u_i and w_i), commonly referred to as blockage and upwash interference, respectively. For small models it is sufficient to evaluate the interference velocity and its spatial gradients at the model location. For symmetric models at zero yaw, sidewash interference at the plane of symmetry is identically zero.

The magnitude of the streamwise gradient of u_i ($\partial u_i / \partial x$) is a measure of the convergence (or divergence) of the effective onset stream, resulting in a streamwise buoyancy force on the model. The streamwise gradient of w_i ($\partial w_i / \partial x$) is a measure of the curvature of the effective onset stream, resulting in an additional apparent angle of attack (or equivalently, excess lift at a given angle of attack) and pitching moment.

The restriction on wakes extending straight downstream is in no way fundamental, but simply allows the use of simple, analytic solutions to the Prandtl-Glauert equation to represent the model aerodynamics: line doublet (or horseshoe vortex) for 3D lift and its vortex wake, and a point source for drag (2D and 3D viscous wakes).

The assumptions of a small model and of perturbation velocities at the tunnel boundary mean that only the far-field flow around the model must be properly represented. That is, the details of the model are not important; only the integrated effects at the tunnel boundary of model geometry and loading are important to first order.

The first-order far-field influence of the model arises from three independent features of a model's aerodynamics:

1. Model shape and volume, which causes a displacement or bulging of streamlines around the model, with the streamlines reconverging to unperturbed parallel flow downstream of the model.
2. Model lift, which in three dimensions results in a redirection of momentum of the stream, resulting in a downwash field that persists to downstream infinity.
3. Model parasite drag (i.e., not including induced drag or drag due to separated wakes), which results in an outward displacement of streamlines around the viscous wake that also persists downstream of the model.

For small models, these three characteristics are represented by elementary analytical singularities placed at the model location. The requisite singularities derive from potential flow theory and are summarised in Figure 2.2 : line (or in 2D flow, point) vortex to represent lift, source doublet to represent model volume, and point source to represent the displacement effect of the wake. The far field of virtually any flight vehicle of interest can be represented by an appropriate superposition of these singularities at the model location. The effects of finite model extent may be investigated using multiple singularities of these types, though the main features of model size are illustrated by the finite-span horseshoe vortex for wing span and a source-sink combination for body length. Expressions for the potentials of these singularities are given in subsequent sections.

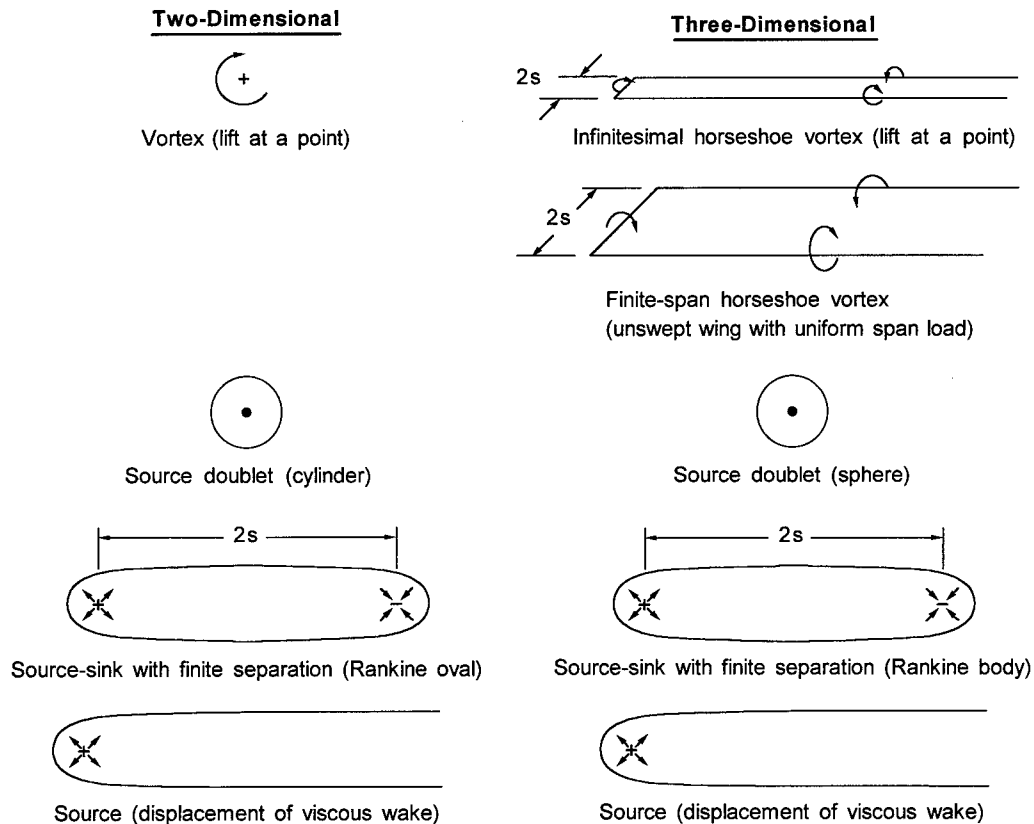


Figure 2.2 Elementary Singularities Used for Model Representation in a Uniform Stream

With the interference velocities at the model location being small, resulting model loading changes (relative to the interference-free case at corrected freestream conditions) are likewise small. This permits the use of singularity strengths taken to be the same as for the interference-free model flow, that is, φ_m is known or specified. For example, a 3D source doublet in a uniform onset flow produces a closed spherical stream surface; thus it represents the potential flow around a sphere. For a sphere in a constrained flow, as in a wind tunnel, this same singularity will produce the same closed spherical stream surface only in the limit of zero model size. Otherwise, the wall potential perturbs the effective closed surface around the doublet; the larger the model size, the greater the deviation. Similarly, use of a specified wing lift distribution (represented by a spanwise distribution of horseshoe vortices) will not fully capture the effect of wall interference on wing loading unless an iterated solution is sought. If model loading changes are not small, due to either model size or sensitivity of the flow to small changes in stream velocity or angle (as at transonic speeds or near stall), classical methods can provide only qualitative guidance, and advanced methods should be considered.

The interference velocities are usually nondimensionalised by the velocity magnitude far upstream of the model,

$$\varepsilon = \frac{u_i}{U_\infty} \quad (2.6)$$

$$\Delta\alpha = \frac{w_i}{U_\infty} \quad (2.7)$$

It is convenient to define an upwash interference parameter (δ) and its streamwise gradient (δ_1),

$$\delta = \frac{w_i}{U_\infty} \frac{C}{SC_L} \quad (2.8)$$

$$\delta_1 = \frac{\partial\delta}{\partial\left(\frac{x}{\beta L}\right)} \quad (2.9)$$

where C is the test section cross-sectional area, and L is a typical length scale (often taken as the height of the test section).

Similarly, the streamwise gradient of blockage interference is of interest because it affects model forces in addition to the change in the effective freestream velocity given by ε . This gradient imposes a streamwise pressure force, or buoyancy drag, on the model that would not be present in the interference-free flow and that must be subtracted from the measured model drag in the tunnel.

As long as there is a region between the tunnel boundaries and the model satisfying the perturbation flow equations described above, the flow at the tunnel boundaries due to only the model is a perturbation flow, even though the model representation may result in large velocity changes (relative to the free stream) close to the model. Conversely, the flow at the model location due to only the walls will likewise be a perturbation flow, even though the flow close to the walls may be subject to large deviations relative to the oncoming free stream, as in the case of flow through longitudinal slots or in the vicinity of holes. If the wall boundary condition is spatially homogeneous, however, the flow at the wall will satisfy Equation 2.2. This is the case for the closed-wall and idealised open-jet test sections.

It should be noted that even for apparently large models, small model results can provide estimates of the adequacy of applying only primary corrections, based on the magnitude of spatial variations of the interference flow field at the location of the model. Such estimates can then guide the decision on the need for more accurate flow modelling.

2.1.3 TUNNEL WALLS

The condition of tunnel walls extending far upstream and downstream (doubly infinite in streamwise extent) permits the application of the method of images with its corresponding set of analytic results. The method of images is a simple yet powerful technique for the evaluation of interference in tunnels with either closed-wall or open-jet boundaries.

The boundary condition for a closed wall is no flow normal to the wall, given exactly in terms of the perturbation potential,

$$\frac{\partial\varphi}{\partial n} = 0 \quad (2.10)$$

where $\varphi = \varphi_m + \varphi_w$.

Allowing the velocity at the tunnel boundaries to differ from the onset stream velocity by only a small amount (the perturbation velocity) also means that these boundary conditions can be linearised if necessary. The boundary condition for an open wall (or free jet) is a constant pressure equal to the static pressure far upstream of the model; in linearised form,

$$\frac{\partial \phi}{\partial x} = 0 \quad (2.11)$$

Finally, the assumption of a tunnel of constant cross section (and constant homogeneous boundary conditions for a given wall) extending to infinity both upstream and downstream of the model provides the simplifications (symmetries and asymptotic boundary conditions) permitting the application of analytic techniques, such as the method of images. Because most wind tunnel tests involve a model located on the centreline of the test section, this symmetry condition can be used to advantage both to simplify the analysis and to permit a convenient decoupling of upwash interference from model volume and wake characteristics, and of blockage interference from model lift.

Consider, for example, a planar closed wall extending to infinity in all directions in proximity to an isolated point singularity whose velocity potential is given by $\phi(x, y, z)$. Figure 2.3 illustrates this situation in two dimensions for the point vortex and source singularities. The desired boundary condition at the wall is $\partial\phi/\partial n = 0$. If the velocity potential of the singularity is such that $\partial\phi/\partial n$ is an odd function of the co-ordinate n normal to the wall (i.e., ϕ is even with respect to n), then by symmetry, the velocity normal to the wall due to this singularity is identically cancelled by placing a so-called image singularity of the same magnitude and strength on the other side of the wall, at the same distance from the wall, on the line normal to the wall and passing through the original singularity. Conversely, if $\partial\phi/\partial n$ for the original singularity is an even function of the co-ordinate n (i.e., ϕ is odd with respect to n), the normal velocity at the wall due to the original singularity is cancelled by an image singularity of equal magnitude and opposite strength. Thus for a planar closed wall, the 2D point vortex requires an image of the opposite sense, while a point source requires an image of the same sense.

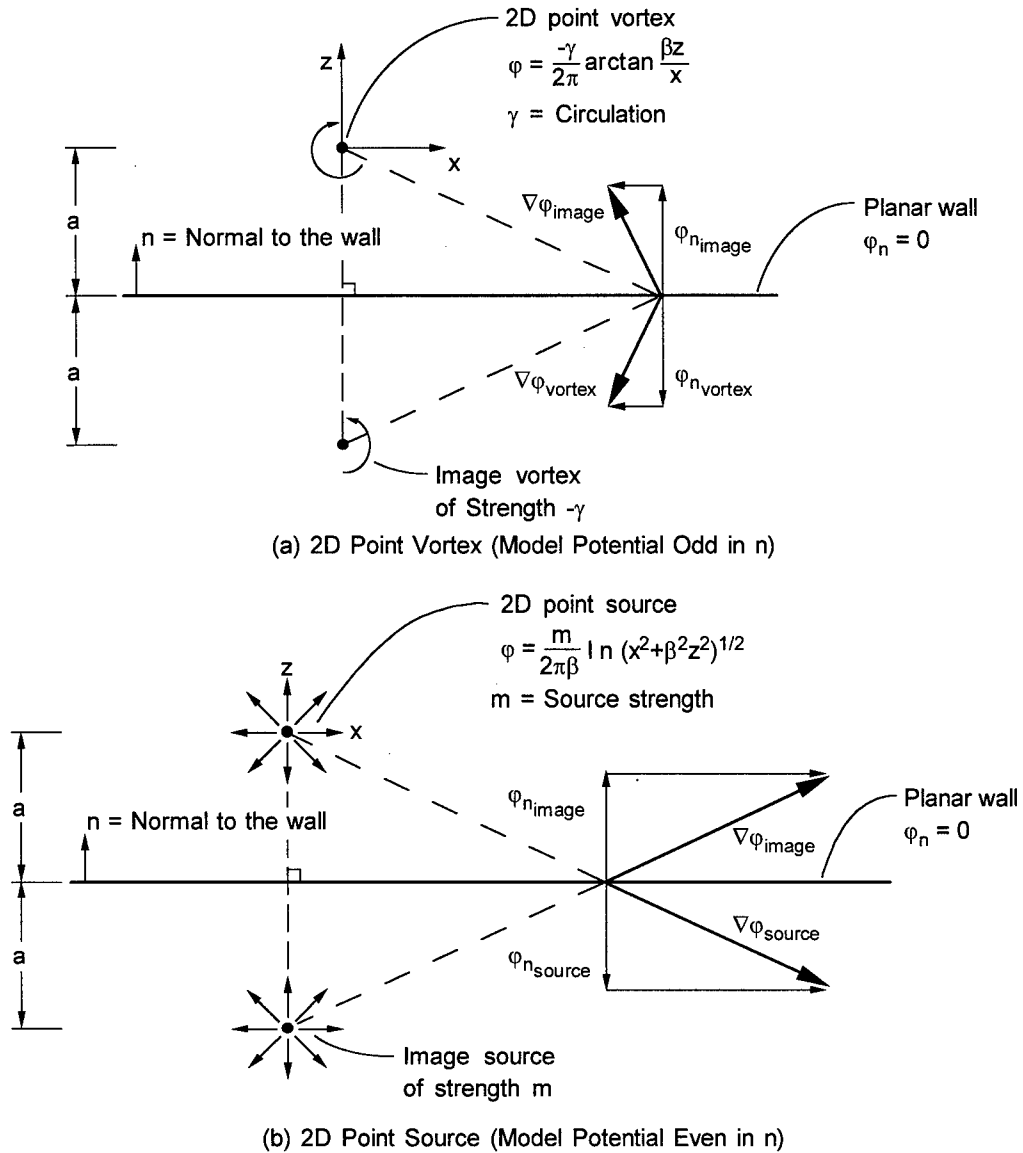
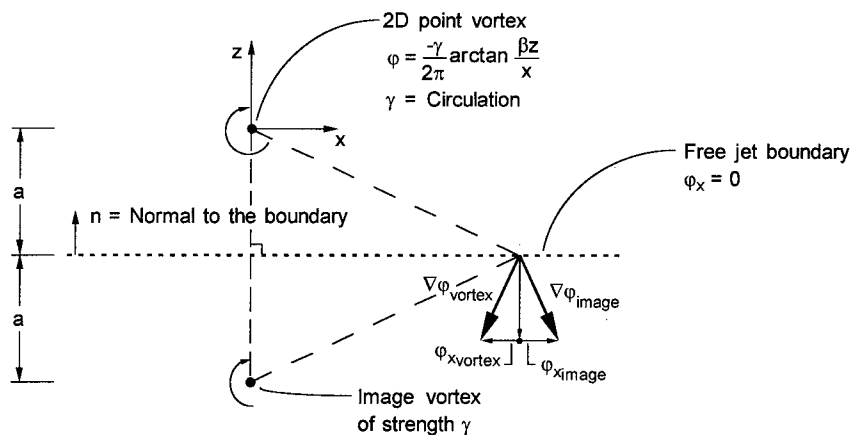


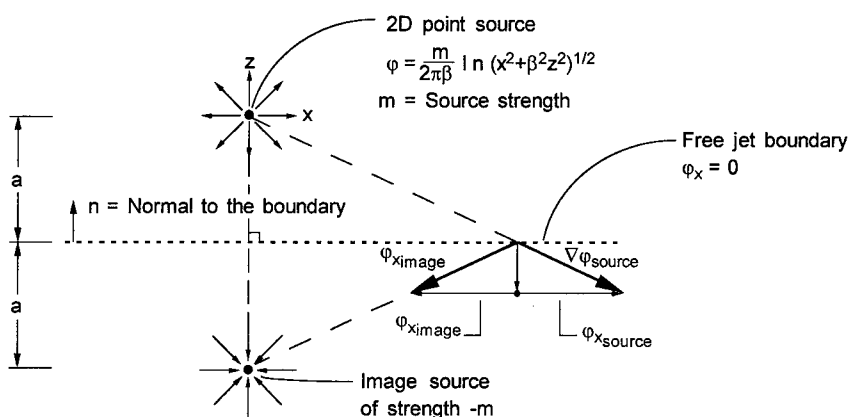
Figure 2.3 Method of Images for a Planar Closed Wall

Similarly, replacing the planar closed wall by a planar free-jet boundary requires satisfying the linearised constant pressure boundary condition. For the streamwise co-ordinate x parallel to the boundary, if $\partial\varphi/\partial x$ of the original singularity is odd in x , then the image singularity must be of the same magnitude and opposite strength. Conversely, if $\partial\varphi/\partial x$ of the original singularity is an even function of x , then the image singularity must be of equal magnitude and strength. Figure 2.4 illustrates the method of images for a planar free-jet boundary.

It is readily apparent that the method of images is not limited to single point singularities, but can be used for any collection of singularities. Nor is it limited to planar wall boundaries; conformal transformations have been used to develop image systems for octagonal and elliptical tunnels as reported in AGARDograph 109 [13]. The objective is merely to cancel a component of velocity (either normal or streamwise) due to the model at the specified boundary by an appropriate choice of image(s) on the other side of the boundary.



(a) 2D point vortex (model potential odd in n)



(b) 2D point source (model potential even in n)

Figure 2.4 Method of Images for a Planar Free-Jet Boundary

The application of the method of images to wall interference involves the development of the set of images required to represent all the wall surfaces of a given test section and summing their effect to determine the interference at the model. Symmetry considerations guide the construction of an image system.

The interference factors for a small model at the centre of a rectangular test section with either all closed or all free-jet boundaries are summarised in Figure 2.5. Circular test section values, indicated for reference, fall very close to square tunnel values.

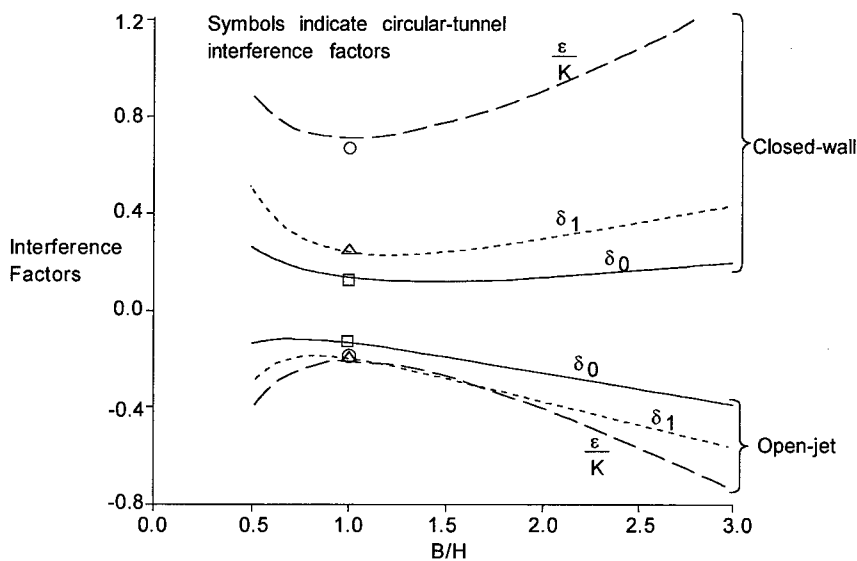


Figure 2.5 Classical Wall Interference Correction Factors for Small Models in Closed-Wall and Open-Jet Rectangular Tunnels

2.2 CLASSICAL CORRECTIONS FOR CLOSED TEST SECTIONS

Test sections with closed, planar, and aerodynamically parallel walls are perhaps the easiest to understand and analyse. The boundary condition for each wall lends itself to treatment by the method of images. The qualitative effects of these walls are predictable based on physical arguments alone, thus providing a common-sense validation of the analytic results. To be sure, the presence of more than one wall requires the use of multiple images. In fact, an infinite array of singularities is required even in the simplest case of two walls. Nonetheless, as has been shown in the literature, the infinite series representing the interference potential for small models in such tunnels converges quickly enough for ready calculation, especially given current computational capabilities.

In two dimensions, the closed-wall boundary condition can be satisfied on the upper and lower walls by using a single row of image singularities both above and below the test section. In constructing the image system each wall initially requires an image outside the test section of the model within the test section. However, the presence of the first-order singularity for the lower wall violates the parallel-flow boundary condition on the upper wall, thus requiring a second singularity above the ceiling, and similarly for the floor. For a model placed midway between the floor and ceiling this results in an infinite set of singularities, all at the same station as the model, equally spaced in z , aligned above and below the test section as indicated in Figure 2.6. A single infinite summation expresses the interference in the test section. This image system is readily generalised to the case of asymmetric model location.

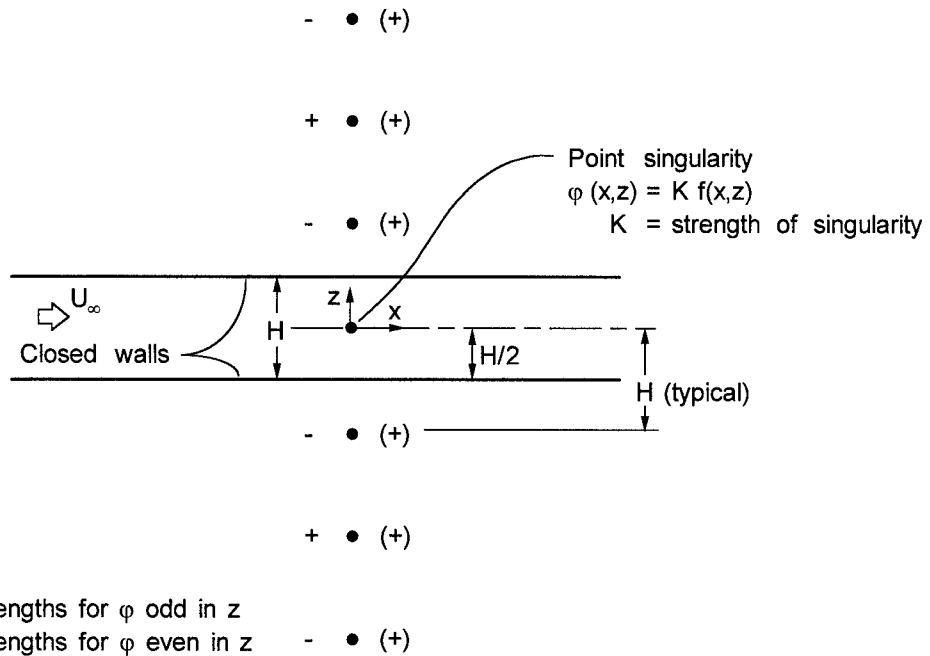


Figure 2.6 Image System for a Singularity at the Centre of a 2D Tunnel with Closed Walls

For the 3D testing situation in rectangular test sections, the image system becomes doubly infinite because of mutual interference of vertical and horizontal walls, which requires images along the diagonals, Figure 2.7. In general, this results in a double summation for the interference in the test section.

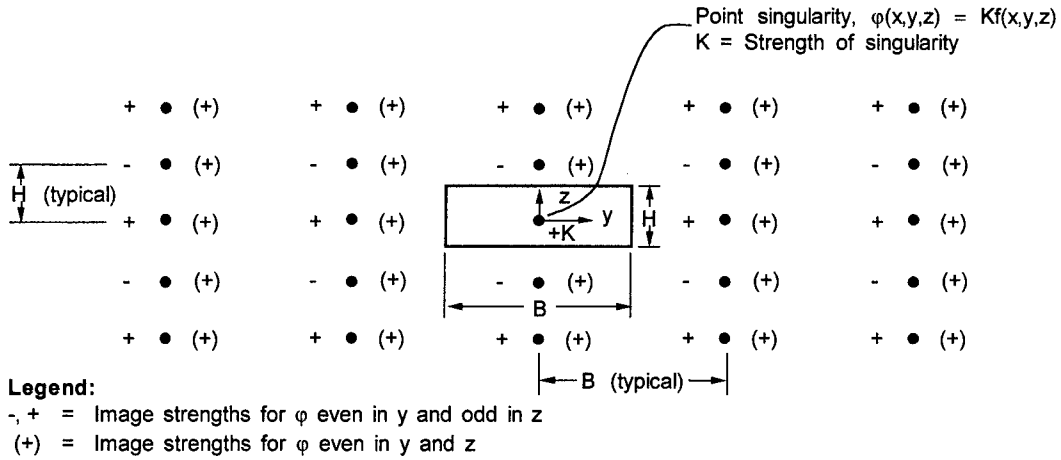


Figure 2.7 : Image System for a Model Singularity in the Centre of a 3D Rectangular Tunnel with Closed Walls

A particularly elegant image system in the crossflow plane far downstream of the bound vortex satisfies the boundary conditions for a closed-wall tunnel of circular cross section, Figure 2.8. This image system has been used to predict the upwash interference at the model, reasoning that the interference at the model location is half the interference value evaluated far downstream.

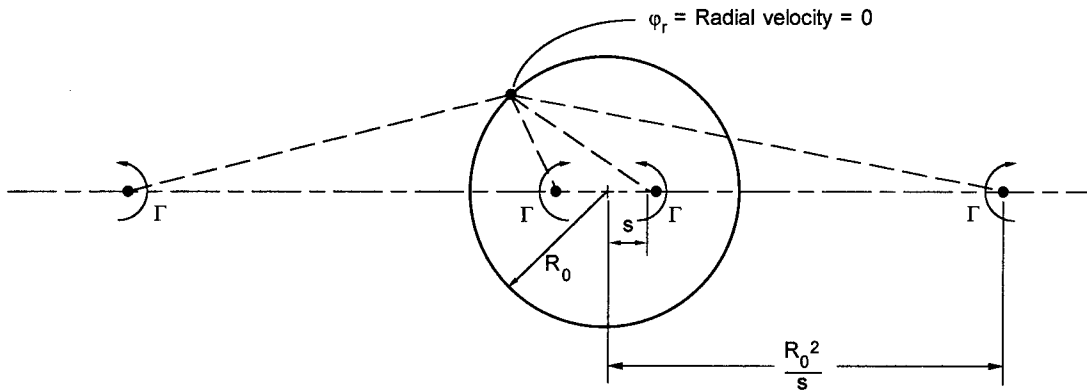


Figure 2.8 Image System for Trailing Vortices in a Tunnel of Circular Cross-Section

Early recognition of the limitations of single-singularity representations of model aerodynamics stimulated the development of multiple-singularity methods and applications, wherein elementary singularities are used as building blocks to represent the finite physical extent of the model. For a closed-wall rectangular tunnel, a complete image system can be specified for each singularity. By superposition, the collection of model singularities along with the corresponding sets of images will satisfy the wall boundary conditions.

All results presented in this section are for model singularities located on the centreline of the test section. Off-centreline model location involves appropriate generalisations of the image systems, resulting in both streamwise and upwash interference at the model location for any single type of singularity. 2D interference results are given throughout the test section, including both streamwise and upwash interference velocity components to highlight the qualitative features of interference variation that a large model at high incidence might experience. These features are mirrored in 3D testing, so that a large 3D model (length and span) may be viewed as immersed in a variable interference flow field. Tunnel users should be alert to the possibility that remote locations of a large model (e.g., outboard wing, body nose, and tail) may experience significantly different interference than predicted at the model

nominal reference location (often taken as the quarter-chord of the mean aerodynamic chord of the wing). 3D interference results presented here are limited to the main results: streamwise interference for the source singularities and upwash interference for the vortex singularities.

2.2.1 CLASSICAL CORRECTIONS FOR LIFT INTERFERENCE

Lift interference is defined to be that part of the wall interference due to circulation (i.e., corresponding to a force normal to the oncoming stream direction) generated by the model. For a small model centrally located in a test section, the model lift results in primarily an upwash interference in the vicinity of the model. Typically, this change in effective freestream direction directly modifies the model aerodynamic angle of attack and requires the resolution of force balance measurements relative to the corrected wind axis direction.

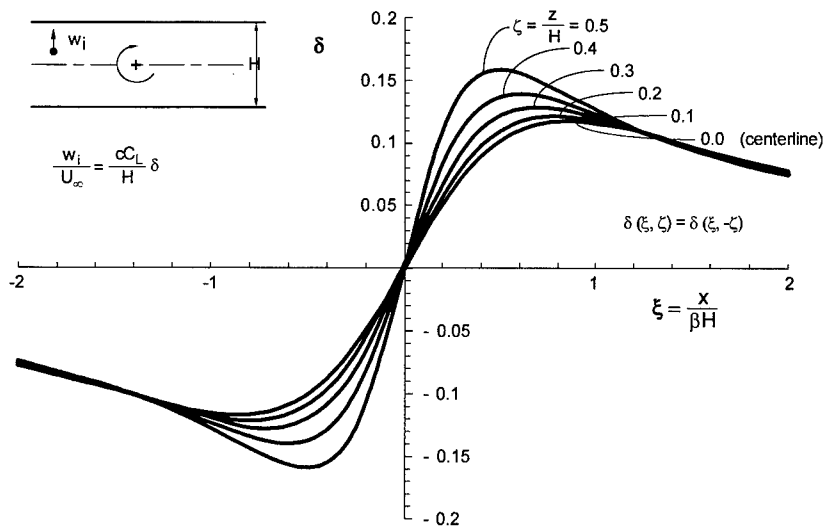
2.2.1.1 2D LIFT INTERFERENCE

In 2D flow, a point vortex singularity is used to represent the lifting effect of an airfoil. The potential for a point vortex located at $x=z=0$ is

$$\phi_m = -\frac{\gamma}{2\pi} \arctan\left(\frac{\beta z}{x}\right) \tag{2.12}$$

where γ , the vortex strength, is $1/2 U_\infty c C_L$ and c is the airfoil chord. Defining nondimensional spatial coordinates $\xi=x/\beta H$ and $\zeta=z/H$, the upwash interference anywhere in the tunnel for a model centrally located between closed upper and lower walls is given by

$$\delta(\xi, \zeta) = \frac{H}{U_\infty c C_L} \frac{\partial \phi_w}{\partial z} = -\frac{1}{4\pi} \sum_{\substack{n=-\infty \\ n \neq 0}}^{n=\infty} (-1)^n \frac{\xi}{\xi^2 + (\zeta - n)^2} \tag{2.13}$$



The upwash interference throughout the test section is shown in Figure 2.9. It is zero at the model station as expected, since the velocity due to each image singularity is in the streamwise direction at this station. The upwash gradient, however, is not zero, so that a model will experience additional lift due to this induced camber relative to the interference-free case. The streamwise curvature interference parameter at the model location ($\xi=\zeta=0$) is

Figure 2.9 Upwash Interference of a 2D Vortex in a Closed-Wall Tunnel

$$\delta_1(0,0) = \left. \frac{\partial \delta}{\partial \xi} \right|_{0,0} = -\frac{1}{4\pi} \sum_{\substack{n=-\infty \\ n \neq 0}}^{\infty} (-1)^n \frac{1}{n^2} = \frac{\pi}{24} \quad (2.14)$$

Since the upwash gradient is proportional to C_L , the uncorrected lift curve will be steeper.

For convenience, a streamwise interference parameter (due to lift) can be defined as

$$\varepsilon_\delta(\xi, \zeta) = \frac{H}{U_\infty c C_L} \frac{\partial \phi_w}{\partial x} = \frac{1}{4\pi\beta} \sum_{\substack{n=-\infty \\ n \neq 0}}^{\infty} (-1)^n \frac{\zeta - n}{\xi^2 + (\zeta - n)^2} \quad (2.15)$$

By symmetry, the streamwise interference is identically zero along the tunnel axis, being positive above the axis and negative below the axis at the model station (for positive lift), Figure 2.10. Far upstream and downstream of the model, both the streamwise and upwash interference velocities approach zero.

Although these results are strictly applicable only to a small model, the implications of finite model size are apparent from consideration of the spatial variations of interference velocities in Figures 2.9 and 2.10. A model centred between the walls at zero incidence may have a chord length that places leading and trailing edges beyond the region of "constant" interference. Further, rotating such a model through a range of incidence angles moves both leading and trailing edges away from the centreline and into regions of variable upwash and streamwise interference. The

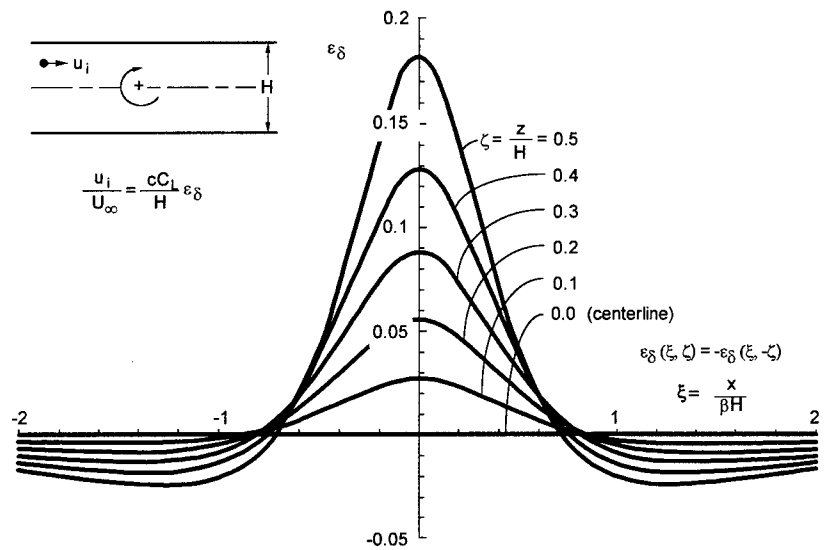


Figure 2.10 Streamwise Interference of a 2D Vortex in a Closed-Wall Tunnel

The limits of linear streamwise upwash along the centreline are no more than about $x/\beta H \leq \pm 0.4$, Figure 2.10. Deviations of both upwash and streamwise interference from the centreline value are small for $z/H \leq \pm 0.2$.

For a small model centrally located between two closed parallel walls, Allen and Vincenti [3] provide the following corrections due to flow curvature. These take account of the actual centre of lift of the model through inclusion of the pitching moment, C_M .

$$\Delta\alpha = \frac{\pi c^2}{96\beta H^2} (C_L + 4C_M) \quad (2.16)$$

$$\Delta C_L = -\frac{\pi^2}{48} \left(\frac{c}{\beta H} \right)^2 C_L \quad (2.17)$$

$$\Delta C_M = \frac{\pi^2}{192} \left(\frac{c}{\beta H} \right)^2 C_L \quad (2.18)$$

These results were derived for an arbitrary chordwise loading (expressed in terms of a Fourier sine series plus a cotangent term to represent the flat plate loading), and are based on the idea of matching suction peaks in the tunnel and in free air. $\Delta\alpha$ is evaluated at the midchord; ΔC_L and ΔC_M represent the linearised loading changes due to the upwash variation over the chord. These corrections are consistent with the classical result of evaluating the angle of incidence correction at the $\frac{3}{4}$ chord for a set of corrections at constant lift (i.e., $\Delta C_L=0$). Alternatively, for no change in pitching moment ($\Delta C_M=0$), the angle of incidence correction should be evaluated at the trailing edge of the airfoil.

The case of off-centre model vortex location is summarised in Chapter II of AGARDograph 109 [13]; quoted results are based on Batchelor [8]. The upwash interference for a vortex located at $x=x_1$ ($\xi=\xi_1$) and $z=d-H/2$ (a distance d from the floor) in a 2D closed-wall tunnel is given as

$$\delta\left(\xi-\xi_1, \frac{d}{H}-\frac{1}{2}\right) = \frac{1}{4\pi} \left\{ \sum_{n=-\infty}^{n=\infty} \frac{\xi-\xi_1}{(\xi-\xi_1)^2 + 4(n-d/H)^2} - 2 \sum_{n=1}^{n=\infty} \frac{\xi-\xi_1}{(\xi-\xi_1)^2 + 4n^2} \right\} \quad (2.19)$$

At a small streamwise distance, $\xi-\xi_1$, from the vortex, ignoring terms of order $(\xi-\xi_1)^3$, this can be approximated as

$$\delta\left(\xi-\xi_1, \frac{d}{H}-\frac{1}{2}\right) = \frac{\pi}{16} (\xi-\xi_1) \left(\frac{2}{3} + \cot^2 \frac{\pi d}{H} \right) \quad (2.20)$$

If the vortex represents the lift of an airfoil acting at the centre of pressure, then for pitching moment defined about the quarter-chord, the centre of pressure is located at a distance downstream of the leading edge,

$$\frac{x_1}{c} = \frac{1}{4} - \frac{C_M}{C_L} \quad (2.21)$$

and the upwash interference can be expressed as

$$\delta\left(\frac{x}{c}, \frac{d}{H}-\frac{1}{2}\right) = \frac{\pi}{16\beta} \frac{c}{H} \left\{ \left(\frac{x}{c} - \frac{1}{4} \right) - \frac{C_M}{C_L} \right\} \left(\frac{2}{3} + \cot^2 \frac{\pi d}{H} \right) \quad (2.22)$$

Batchelor also derives the streamwise interference velocity at the vortex as

$$u\left(\xi=\xi_1, \zeta = \frac{d}{H}-\frac{1}{2}\right) = \frac{u_i}{U_\infty} = -\frac{1}{8\beta} \frac{c}{H} C_L \cot \frac{\pi d}{H} \quad (2.23)$$

Thus, the streamwise interference is identically zero only for a centrally located vortex. Otherwise, it is either positive or negative according to whether the vortex is above or below the test section centreline (as can be inferred from consideration of the incremental effects of the nearest image vortices). These results are analogous to the interference of a centrally located vortex evaluated off-centreline, Figure 2.9.

The above summarises corrections due to lift in a 2D closed-wall tunnel to order $(c/H)^2$. AGARDograph 109 [13] includes a discussion of higher order correction theory (to order $(c/H)^4$), concluding that the lower order results are inaccurate for $c > 0.4\beta H$. For a model centrally located between two closed walls, the following corrections are presented based on Havelock [17], ignoring terms of order $(c/\beta H)^6$,

$$\Delta\alpha = \frac{\pi c^2}{96\beta H^2} (C_L + 4C_M) - \frac{7\pi^3 c^4 C_L}{30720\beta^3 H^4} \quad (2.24)$$

$$\Delta C_L = C_L \left\{ -\frac{\pi^2}{48} \left(\frac{c}{\beta H} \right)^2 + \frac{7\pi^4}{3072} \left(\frac{c}{\beta H} \right)^4 \right\} \quad (2.25)$$

$$\Delta C_M = C_L \left\{ \frac{\pi^2}{192} \left(\frac{c}{\beta H} \right)^2 - \frac{7\pi^4}{15360} \left(\frac{c}{\beta H} \right)^4 \right\} \quad (2.26)$$

The general problem of a thick airfoil has been solved by Goldstein [16] as a power series in (c/H) by transforming the airfoil to a circle, and is summarised in AGARDograph 109 [13]. This solution is consistent with the above results when second-order terms in thickness, camber, and incidence are ignored.

2.2.1.2 3D LIFT INTERFERENCE FOR SMALL WINGS

The lift of a small model can be simulated using an elementary horseshoe vortex of span $2s$ (equivalent to a line doublet), whose potential is given by

$$\varphi_m = \frac{\Gamma s}{2\pi} \left[1 + \frac{x}{(x^2 + \beta^2 r^2)^{\frac{1}{2}}} \right] \left[\frac{z}{y^2 + z^2} \right] \quad (2.27)$$

where the vortex strength (Γs) is $1/4 U_\infty S C_L$, S is the reference area of the wing, and r is the radial cylindrical co-ordinate, $\sqrt{y^2 + z^2}$. The upwash velocity field is then

$$\frac{\partial \varphi_m}{\partial z} = \frac{\Gamma s}{2\pi} \left\{ \left[1 + \frac{x}{(x^2 + \beta^2 y^2 + \beta^2 z^2)^{\frac{1}{2}}} \right] \left[\frac{y^2 - z^2}{(y^2 + z^2)^2} \right] - \frac{\beta^2 x z^2}{(x^2 + \beta^2 y^2 + \beta^2 z^2)^{\frac{3}{2}} (y^2 + z^2)} \right\} \quad (2.28)$$

In the plane of the bound vortex normal to the oncoming stream (that is, for $x=0$) the upwash takes on the simple form

$$w(0, y, z) = \frac{\Gamma s}{2\pi} \left\{ \frac{y^2 - z^2}{(y^2 + z^2)^2} \right\} \quad (2.29)$$

For rectangular tunnels, the image system is a 2D array as discussed in Section 2.1.3. Defining the aspect ratio of the tunnel as $A=B/H$ and evaluating the upwash interference at the model location, $x=y=z=0$, the classical result is recovered:

$$\delta_o = \delta(0,0,0) = \frac{A}{8\pi} \sum_{\substack{n=-\infty \\ \text{excluding} \\ n=m=0}}^{n=\infty} \sum_{m=-\infty}^{m=\infty} (-1)^n \frac{m^2 A^2 - n^2}{[m^2 A^2 + n^2]^2} \quad (2.30)$$

Differentiating (with respect to $x/\beta H$) the expression for upwash interference due to the infinitesimal horseshoe vortex, the analogous expression for upwash gradient at the model location is derived:

$$\delta_1(0,0,0) = \frac{\partial \delta}{\partial(x/\beta H)} \Big|_{0,0,0} = \frac{A}{8\pi} \sum_{\substack{n=-\infty \\ \text{excluding} \\ n=m=0}}^{n=\infty} \sum_{m=-\infty}^{m=\infty} (-1)^n \frac{m^2 A^2 - 2n^2}{[m^2 A^2 + n^2]^{\frac{5}{2}}} \tag{2.31}$$

As developed by Theodorsen [34], similar expressions apply to the upwash interference in rectangular tunnels having all open walls, open sides and closed floor and roof, and closed sides and open floor and roof. Because the image systems for these cases require only appropriate sign changes (see Glauert, Figs. 7 and 8), the factor $(-1)^n$ should be replaced by $(-1)^m$, $(-1)^{m+n}$, and (1) , respectively; see Section 4.1.2.4 (Fig. 4.4).

Along the centreline of rectangular tunnels, the upwash interference asymptotically approaches zero in the upstream direction and a constant positive value in the downstream direction, Figure 2.11. The interference upwash far downstream of the model is due to the image trailing vorticity, which (at this

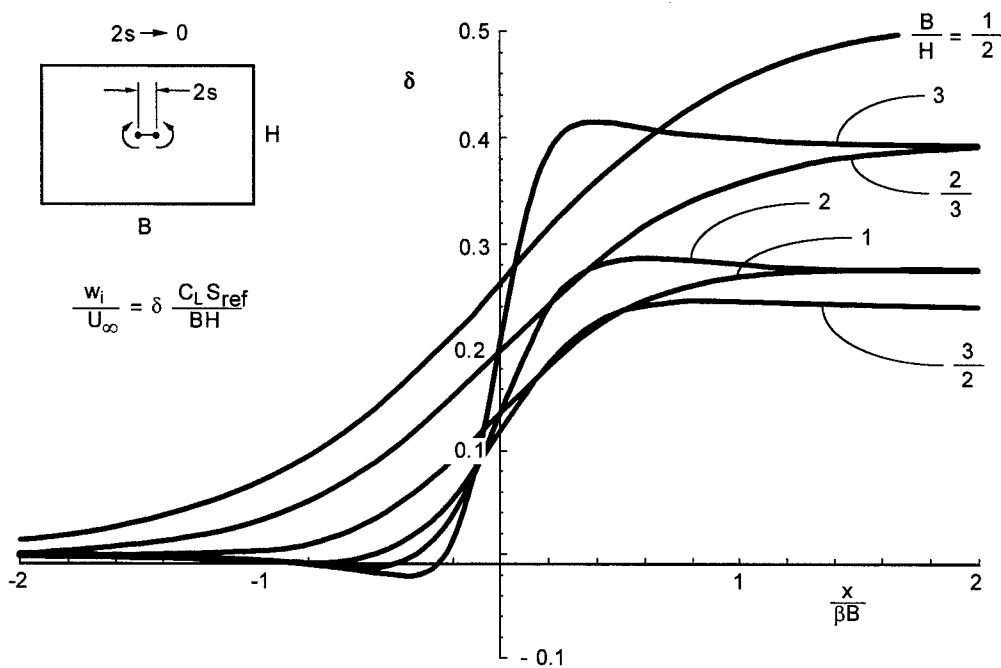


Figure 2.11 Centreline Distribution of Upwash Interference of an Elementary Horseshoe Vortex in Closed-Wall Rectangular Tunnels

location) extends effectively to infinity in both directions. At the model location, the image bound vortex segments do not induce any upwash (as in the 2D case). Because the image trailing vortex segments extend only downstream from the model location, by symmetry the upwash interference at the model is therefore exactly half the value of the downstream asymptotic interference. The spanwise variation of upwash interference, Figure 2.12, is significantly greater for tunnels having $A > 3/2$. The magnitude of interference at the model location increases for $A < 1$. From the standpoint of both small magnitude and minimum spanwise variation, near-optimum upwash interference is obtained for $1 \leq A \leq 3/2$. These small-span results indicate the nature of the interference-gradient problems that will occur for finite-span wings.

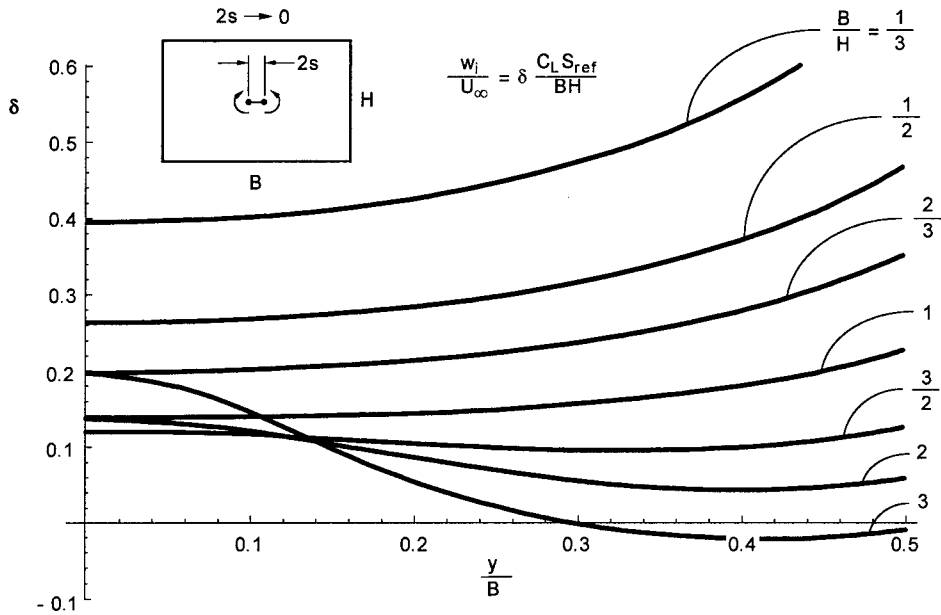


Figure 2.12 Spanwise Distribution of Upwash Interference of an Elementary Horseshoe Vortex in Closed-Wall Rectangular Tunnels

2.2.1.3 3D LIFT INTERFERENCE FOR WINGS OF FINITE SPAN

The effect of finite span of the horseshoe vortex on upwash interference provides the next logical approximation to the interference of a wing. A straight unswept wing having a small chord, finite span and uniform span loading can be represented by a finite-span horseshoe vortex, whose velocity potential is (see Ashley and Landahl, [5])

$$\begin{aligned} \varphi_m &= \frac{1}{4\pi} \int_{-s}^s \frac{\Gamma z}{(y-y_1)^2 + z^2} \left[1 + \frac{x}{R(y-y_1)} \right] dy_1 \\ &= \frac{\Gamma s}{2\pi} \left\{ \arctan\left(\frac{z}{y-s}\right) - \arctan\left(\frac{z}{y+s}\right) - \arctan\left(\frac{x(y-s)}{zR(y-s)}\right) + \arctan\left(\frac{x(y+s)}{zR(y+s)}\right) \right\} \end{aligned} \quad (2.32)$$

where $R(y) = \sqrt{x^2 + \beta^2 y^2 + \beta^2 z^2}$.

Differentiating this expression, the upwash velocity is

$$\frac{\partial \varphi}{\partial z} = \frac{\Gamma s}{2\pi U_\infty} \left\{ \begin{aligned} &\left[\frac{y-s}{(y-s)^2 + z^2} - \frac{y+s}{(y+s)^2 + z^2} \right] \\ &+ \frac{x(y-s)(x^2 + \beta^2(y-s)^2 + 2\beta^2 z^2)}{z^2 (R(y-s))^3 T(y-s)} - \frac{x(y+s)(x^2 + \beta^2(y+s)^2 + 2\beta^2 z^2)}{z^2 (R(y+s))^3 T(y+s)} \end{aligned} \right\} \quad (2.33)$$

where T is defined as

$$T(y) = 1 + \frac{x^2 y^2}{z^2(x^2 + \beta^2 y^2 + \beta^2 z^2)} \quad (2.34)$$

For a finite-span 3D wing it is convenient to define nondimensional co-ordinates using the tunnel breadth: $\xi=x/\beta B$, $\eta=y/B$, and $\zeta=z/B$, and a nondimensional semispan, $\sigma=s/B$. In the plane of the bound vortex, $\xi=\zeta=0$, the upwash interference of a finite-span horseshoe vortex in a rectangular tunnel ($A=B/H$ as before) is given by the double summation of the image system,

$$\delta(0, \eta, 0) = \frac{A}{16\pi\sigma} \sum_{\substack{n=-\infty \\ \text{excluding} \\ n=m=0}}^{\infty} \sum_{m=-\infty}^{\infty} (-1)^n \left\{ \frac{\eta - \sigma - m}{A^2(\eta - \sigma - m)^2 + n^2} - \frac{\eta + \sigma - m}{A^2(\eta + \sigma - m)^2 + n^2} \right\} \quad (2.35)$$

For wings of finite span, upwash interference along the centreline of rectangular tunnels, Figure 2.13, qualitatively mirrors the interference of models of small span. Upwash interference variation along the span of the bound vortex in a square closed-wall tunnel is shown in Figure 2.14. As span increases, the average upwash interference at the centre of the model ($\xi=\eta=\zeta=0$) increases. More important, however, is the increased spanwise variation of interference due to span. This is manifested as increased upwash on the outboard wing with increasing span ratio (due to the increasing proximity of the first set of image trailing vortex segments). The effect of span can be ignored for span ratios less than about 0.5.

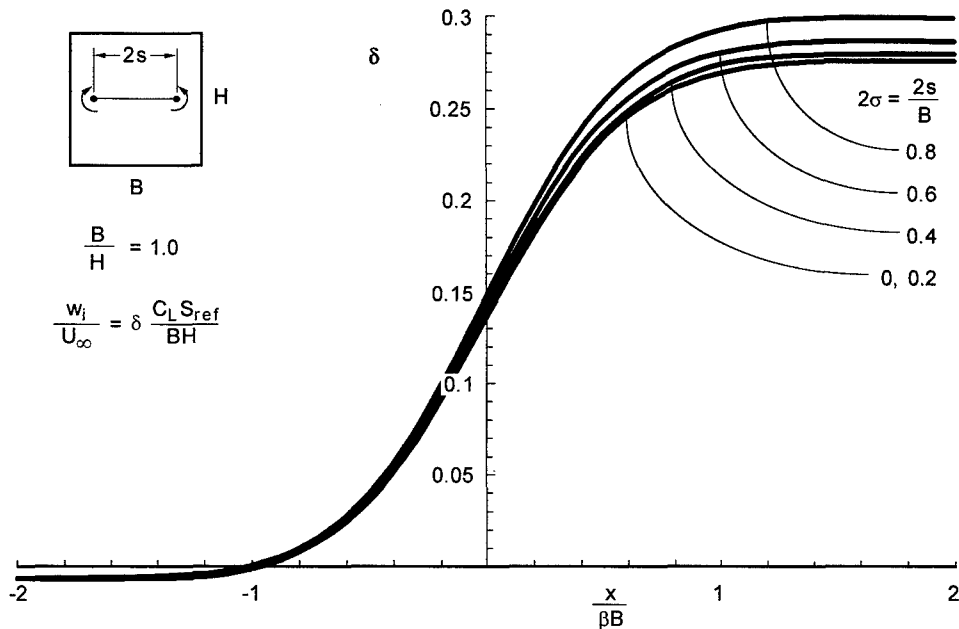


Figure 2.13 Streamwise Interference of a 2D Source Doublet in a Closed-Wall Tunnel

An extensive series of lift interference charts for rectangular and elliptic closed-wall tunnels, including the effects of finite span, uniform versus elliptic span loading, and off-centre wing location, are presented in Pope and Harper [31]. The rapid rollup of trailing vorticity of a finite-span wing into two concentrated trailing vortices duplicates the trailing vortex pattern for uniform loading. The distance between these concentrated trailing vortices, the so-called vortex span, is given as a function of wing aspect and taper ratios. The interference at the wing can be estimated using an effective vortex span smaller than the physical span, but larger than the rollup vortex span. For wings of small span to tunnel width ratio, a

simple average of the physical and rollup vortex span results in negligible error. Large span wings or very exacting correction requirements may demand the consideration of actual spanload.

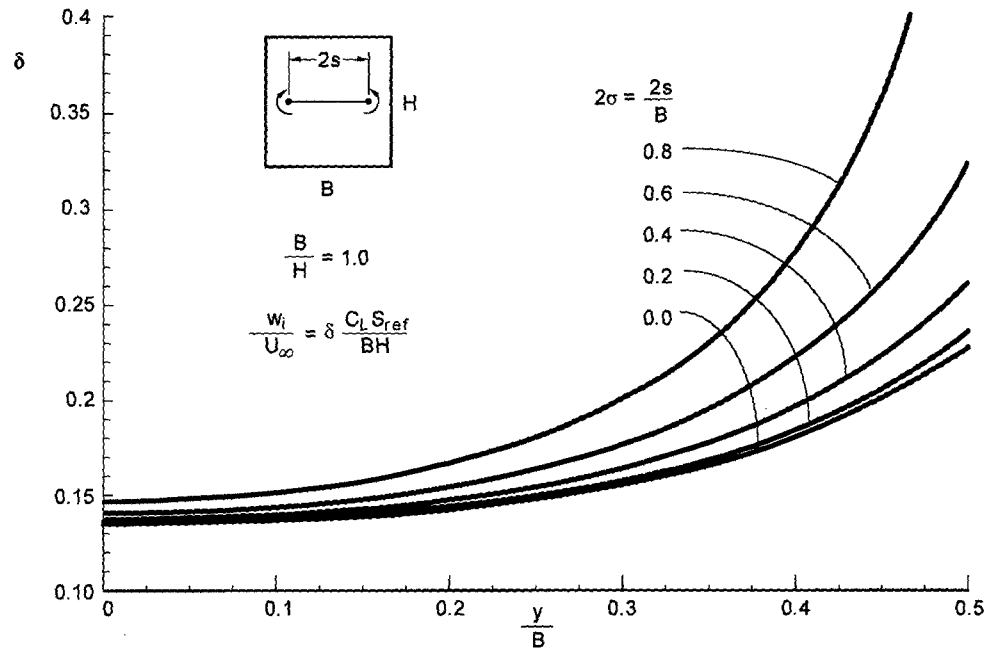


Figure 2.14 Upwash Interference of a 2D Source Doublet in a Closed-Wall Tunnel

2.2.1.4 APPLICATION OF UPWASH CORRECTIONS

Additional upwash at the model location due to the walls requires corrections to angle of attack and drag (due to the change in effective stream direction at the model location, and to pitching moment and lift (or to pitching moment and angle of attack) due to the streamwise gradient of the interference upwash). For a small model and small upwash angle, the corrections to lift and drag due to the former (i.e., rotation of wind axes) are

$$C_{L_{corr}} = C_{L_{unc}} \cos \Delta\alpha - C_{D_{unc}} \sin \Delta\alpha \cong C_{L_{unc}} \quad (2.36)$$

$$C_{D_{corr}} = C_{D_{unc}} \cos \Delta\alpha + C_{L_{unc}} \sin \Delta\alpha \cong C_{D_{unc}} + C_{L_{unc}} \Delta\alpha \quad (2.37)$$

$$\Delta\alpha = \delta_o \frac{S}{C} C_{L_{unc}} \quad (2.38)$$

where $\Delta\alpha$ is evaluated at the model centre of lift (nominally the wing quarter-chord location).

Though the above relationships define a corrected onset stream direction, the model angle of attack must additionally be adjusted for interference stream curvature. Because the wing is immersed in an interference flow field characterised by increasing upwash with x , it appears to have an increased effective camber (in a closed-wall tunnel) compared to an unbounded flow. Corrections for this flow curvature may be applied to pitching moment and to either (or both) lift coefficient or angle of attack. It is perhaps most convenient to consider this flow-induced camber as an additional model incidence (though not to be included in the stream angle change for redefining wind axes) with no adjustment to lift and an additional pitching moment due to this camber that would not occur in an unbounded stream. For a linear longitudinal variation of interference upwash, and relying on linearised airfoil theory results for a

circular-arc airfoil (see Glauert, [15]; or Pope, [31]), the effective increase in incidence is accounted for if the upwash is evaluated at the 3/4-chord location (rather than the quarter-chord, which coincides with the centre of lift in linear theory). In terms of $\Delta\alpha$, δ_o , and δ_1 evaluated at the location of the bound vortex,

$$\alpha_{corr} = \alpha_{unc} + \Delta\alpha + \Delta\alpha_{sc} = \alpha_{unc} + \left(\delta_o + \frac{\bar{c}}{2\beta H} \delta_1 \right) \frac{SC_{Lunc}}{C} \quad (2.39)$$

The pitching moment correction is

$$\Delta C_M = \delta_1 \frac{\bar{c}}{16\beta H} \frac{SC_{Lunc}}{C} \frac{\partial C_L}{\partial \alpha} \quad (2.40)$$

For the 2D case, S and C are replaced by c and H respectively.

For wings of finite span and arbitrary spanwise loading, the average interference upwash (δ_o , in nondimensional terms) can be taken to be the loading-averaged upwash as given in AGARDograph 109,

$$\delta_o = \frac{1}{L} \int_{-s}^s \left(\frac{w_i}{U_\infty} \frac{C}{SC_L} \right) \frac{dL}{dy} dy \quad (2.41)$$

2.2.2 CLASSICAL CORRECTIONS FOR BLOCKAGE INTERFERENCE

Blockage interference is that part of the wall interference due to the displacement of streamlines around a body that carries no lift or side force. Solid blockage represents that part of the blockage due to the volume of the model in the tunnel. This is usually taken to be a closed body, though if the effect of a support sting is sought, under certain circumstances modelling of its volume might take the form of a semi-infinite body which can be represented by a source. A source flow is similarly used to represent the displacement effect of a viscous wake from the model.

2.2.2.1 2D SOLID BLOCKAGE FOR SMALL MODELS

As discussed by Glauert [15], the flow field around any nonlifting body may be represented by a power series in the inverse of the complex spatial co-ordinate. At a large distance from the body, the leading term (of the form of a source doublet) dominates. In 2D flow, the potential of a source doublet is

$$\phi_m = \frac{\mu}{2\pi} \left(\frac{x}{x^2 + \beta^2 z^2} \right) \quad (2.42)$$

In a uniform unconstrained stream, the potential of a source doublet aligned with the oncoming stream represents the flow around a cylinder whose radius (a) is related to the doublet strength,

$$\mu = \left(\frac{2\pi a^2 U_\infty}{\beta} \right) \quad (2.43)$$

The far field of any nonlifting body is approximated by this first-order term if μ is taken as AU_∞/β , where A is the effective cross-sectional area of the model. It is the sum of the model volume (per unit span) and its virtual volume (per unit span) for accelerated flow in the streamwise direction. Using nondimensional

co-ordinates $\xi = x/\beta H$, $\zeta = z/H$, and summing the effect of all the image doublets, the streamwise interference anywhere in the tunnel for a model centrally located between closed upper and lower walls is given by

$$\varepsilon = \frac{u_i}{U_\infty} = -\frac{1}{2\pi\beta^3} \frac{A}{c^2} \left(\frac{c}{H}\right)^2 \sum_{n \neq 0}^{\infty} \frac{\xi^2 - (\zeta - n)^2}{\left[\xi^2 + (\zeta - n)^2\right]^2} \quad (2.44)$$

It should be noted that at any value of ζ , the interference is a maximum at the model location, Figure 2.15, which increases the effective freestream velocity felt by the model. However, due to the streamwise symmetry of the interference, there is no pressure buoyancy force on the model.

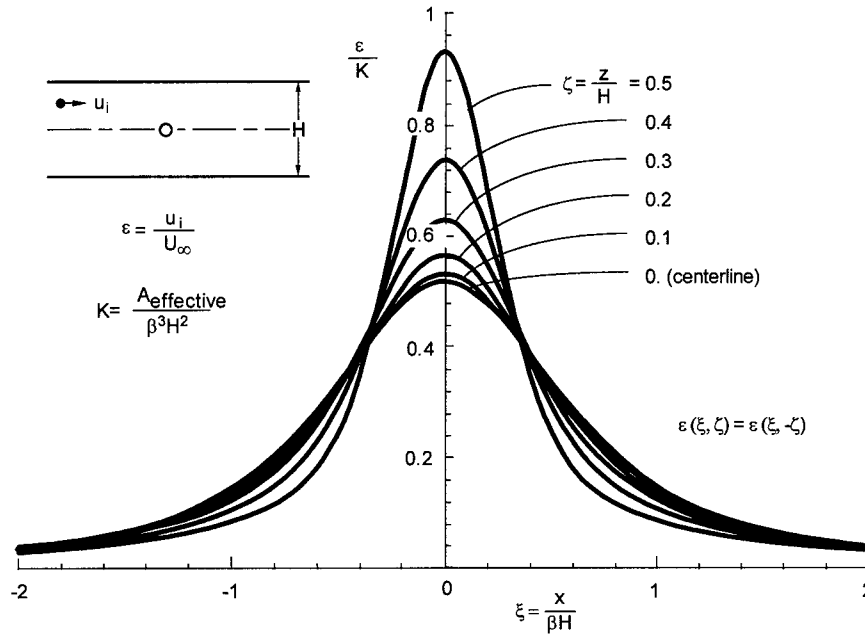


Figure 2.15 Streamwise Interference of a 2D Source Doublet in a Closed-Wall Tunnel

At the model location, $\xi = \zeta = 0$, the interference is given by

$$\varepsilon(0,0) \equiv \varepsilon_0 = \frac{1}{2\pi\beta^3} \frac{A}{c^2} \left(\frac{c}{H}\right)^2 \sum_{\substack{n=-\infty \\ n \neq 0}}^{n=\infty} \frac{1}{n^2} = \frac{\pi}{6} \frac{A}{\beta^3 H^2} \quad (2.45)$$

As for the point vortex, interference at the model station is a minimum on centreline, with interference velocities for $z/H \leq 0.2x/\beta H$ very close to centreline values.

In a manner analogous to the point vortex, an upwash interference parameter for a nonlifting body can be defined :

$$\delta_\varepsilon(\xi, \zeta) = \frac{w_i}{U_\infty} = \frac{1}{U_\infty} \frac{\partial \phi_w}{\partial z} = \frac{1}{2\pi\beta^2} \frac{A}{H^2} \sum_{\substack{n=-\infty \\ n \neq 0}}^{n=\infty} \frac{2\xi(\zeta - n)}{\left[\xi^2 + (\zeta - n)^2\right]^2} \quad (2.46)$$

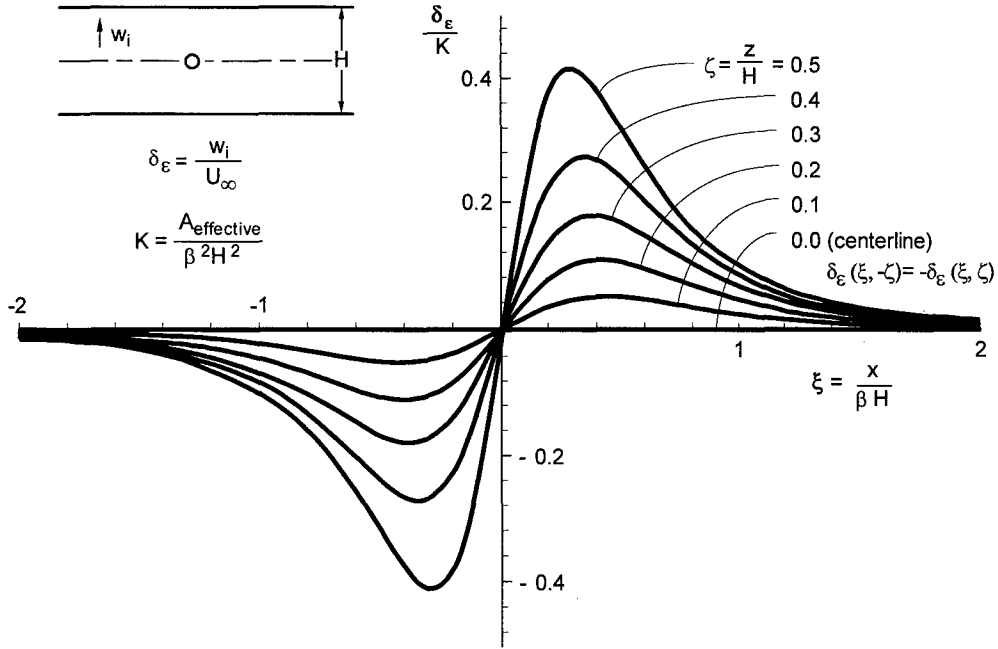


Figure 2.16 Upwash Interference of a 2D Source Doublet in a Closed-Wall Tunnel

By symmetry, the interference upwash due to solid blockage is zero along the axis of the tunnel, Figure 2.16. Off-centreline the interference upwash has a character similar to the upwash interference of a 2D vortex (Fig. 2.9).

Following Glauert [15], the effective cross-sectional area of any 2D body may be written in terms of an equivalent cylinder by defining a body shape factor, λ ,

$$\mu = \frac{\pi}{2} \lambda t^2 U_\infty \quad (2.47)$$

so that the body is represented as an equivalent cylinder of diameter $t\sqrt{\lambda}$. Values of λ as a function of fineness ratio (c/t) are given by Glauert for several shapes: Rankine oval, ellipse, Joukowski section, and a modified Joukowski section. Pope [31] provides shape factors for several NACA airfoil series as well. The shape factor for an ellipse is described by a simple analytic expression,

$$\lambda = \frac{1}{2} \left(1 + \frac{c}{t} \right) \quad (2.48)$$

An alternate body shape factor may be defined by taking the effective cross-sectional area (A) to be $K A_0$, where K is a nondimensional factor depending on body shape and A_0 is the actual cross-sectional area. For an ellipse,

$$K = 1 + \frac{t}{c} \quad (2.49)$$

As fineness ratio increases, K approaches 1 and effective area is essentially the actual cross-sectional area. The more blunt the body, the larger is the effective area. A circle, for example, has an effective area twice its actual cross-sectional area.

In general, the effective cross-sectional area can be calculated for a symmetrical body from the surface velocity distribution, $V(s)$,

$$\lambda = \frac{4}{\pi} \int_{\text{leading edge}}^{\text{trailing edge}} \frac{V(s) z(s)}{U_{\infty} t^2} ds \quad (2.50)$$

Glauert also provides a useful first approximation to λ , for cases when more reliable values are not available,

$$\lambda = \frac{2A_0}{\pi t^2} \quad (2.51)$$

The effect of thickness and angle of attack on blockage interference may be estimated using a general relationship suggested in AGARDograph 109 based on theoretical and empirical investigations,

$$\varepsilon_0 = \frac{\pi}{6} \left[1 + 1.2\beta \left(\frac{t}{c} \right) \right] \left[1 + 1.1 \left(\frac{c}{t} \right) \alpha^2 \right] \frac{A_0}{\beta^3 H^2} \quad (2.52)$$

2.2.2.2 2D RANKINE OVALS

A source and a sink located a finite distance apart ($2s$) on a line parallel to the oncoming stream have a streamline forming a closed body known in 2D flow as a Rankine oval (in 3D the analogous closed stream surface is referred to as a Rankine body). This simple superposition of singularities illustrates the effect of body length on solid blockage. The potential is given by

$$\phi_m = \frac{m}{2\pi\beta} \left[\ln \left((x+s)^2 + \beta^2 z^2 \right)^{\frac{1}{2}} - \ln \left((x-s)^2 + \beta^2 z^2 \right)^{\frac{1}{2}} \right] \quad (2.53)$$

In terms of nondimensional co-ordinates $\xi = x/\beta H$, $\zeta = z/H$, and defining $\sigma = s/\beta H$, the streamwise interference is the sum of all images in the usual way,

$$\varepsilon = \frac{m}{2\pi\beta^2} \frac{c}{H} \sum_{n \neq 0}^{\infty} \left[\frac{\xi + \sigma}{(\xi + \sigma)^2 + (\zeta - n)^2} - \frac{\xi - \sigma}{(\xi - \sigma)^2 + (\zeta - n)^2} \right] \quad (2.54)$$

The streamwise interference of Rankine ovals having a maximum thickness $t/H=0.1$ is shown in Figure 2.17. At small length ratios the interference is indistinguishable from that of a source doublet. Two features characterise the interference as the length of the model increases. First, the interference at the model leading and trailing edges decreases relative to the interference at the model centre. Second, the interference at the centre decreases as the flow in the tunnel approaches the 1D limit for very long models.

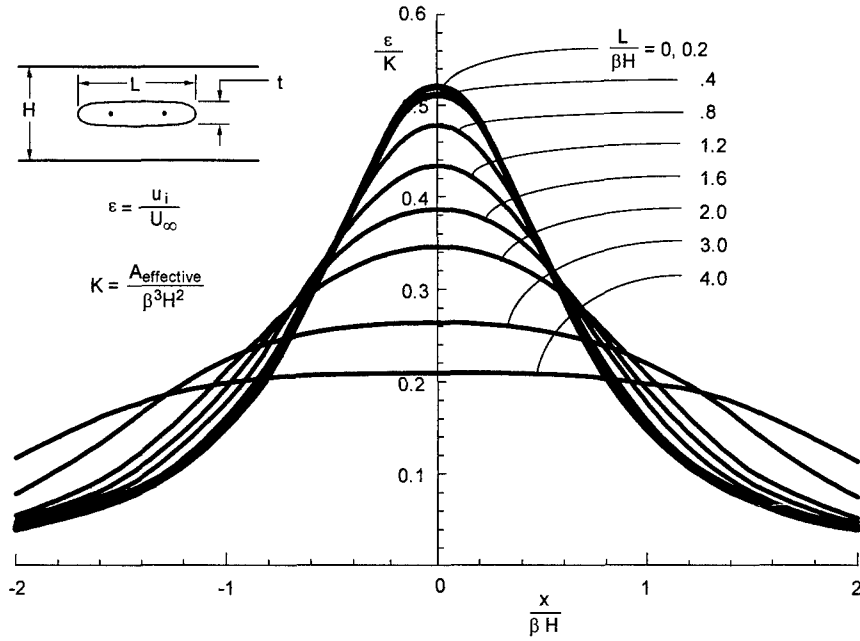


Figure 2.17 Streamwise Interference of Rankine Ovals ($t/H = 0.1$) in a Closed-Wall Tunnel

2.2.2.3 2D WAKE BLOCKAGE

In 2D flow the potential of a point source located at the origin is

$$\phi_m = \frac{m}{2\pi\beta} \ln(x^2 + \beta^2 z^2)^{1/2} \tag{2.55}$$

where m , the source strength, is $1/2 U_\infty c C_D$. In terms of nondimensional co-ordinates $\xi = x/\beta H$ and $\zeta = z/H$, the streamwise interference anywhere in the tunnel for a model centrally located between closed upper and lower walls is given by

$$\varepsilon = \frac{C_D}{4\pi\beta^2} \frac{c}{H} \sum_{n \neq 0}^{\infty} \frac{\xi}{\xi^2 + (\zeta - n)^2} \tag{2.56}$$

The streamwise interference attains its maximum value far downstream of the model location, Figure 2.18. Its magnitude is consistent with 1D streamtube considerations: downstream of the model, the tunnel cross-sectional area is decreased by the equivalent displacement area of the viscous wake plume, so that the flow external to the wake must increase proportionately. In total, the image sources add additional mass to the oncoming stream, so that the uniform velocities far upstream and downstream cannot be equal. An interesting result for this singularity set is the non-zero interference far upstream of the model. Formally, this physical paradox can be alleviated by providing each source with a corresponding sink far downstream of the model, thus closing off each “wake body”. This array of sinks produces an equal and opposite interference flow far upstream that restores the undisturbed onset stream velocity.

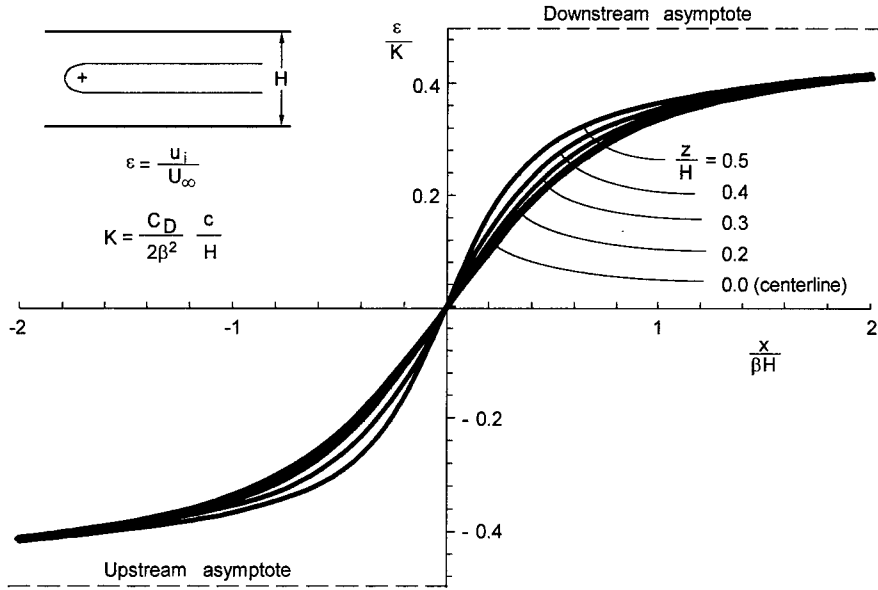


Figure 2.18 Streamwise Interference of a 2D Source in a Closed-Wall Tunnel

A practical approach to wake blockage corrections takes the upstream interference to be zero. Because the setting of tunnel speed commonly relies on a wall static pressure measurement upstream of the test section, the influence of the model at this location is automatically included in the definition of uncorrected tunnel speed. Therefore, the wake blockage interference at the model location should be taken as the difference between the interference at the static pressure reference location and the interference at the model location in Figure 2.18. If the upstream asymptote is used as a reference, the interference at the model is

$$\epsilon_0 = \frac{C_D}{4\beta^2} \frac{c}{H} \quad (2.57)$$

The streamwise gradient of wake blockage interference is a maximum at the model location and results in a buoyancy force on the model. Differentiating the series expression for ϵ due to the source representing the displacement of the wake, the same series appears as for solid blockage of a source doublet, so that

$$\frac{\partial \epsilon_{wake}}{\partial \xi} = \frac{C_D}{2} \frac{\beta H c}{A} \epsilon_{solid} \quad (2.58)$$

At the model location, $\xi = \zeta = 0$,

$$\frac{\partial \epsilon_{wake}}{\partial \xi} = \frac{\pi}{12} \frac{C_D}{\beta^2} \frac{c}{H} \quad (2.59)$$

By symmetry, the interference upwash is zero along the axis of the tunnel and, in the vicinity of the model, the interference upwash is directed from the walls toward the tunnel axis.

2.2.2.4 3D SOLID BLOCKAGE FOR SMALL MODELS

In 3D flow, the potential of a source doublet is

$$\phi_m = \frac{\mu}{4\pi} \frac{x}{(x^2 + \beta^2 r^2)^{\frac{3}{2}}} \quad (2.60)$$

where $r^2 = y^2 + z^2$ and the doublet strength, m , is $U_\infty V$, where V is the effective volume of the model. Analogous to the 2D source doublet, superposition of a 3D source doublet and a uniform oncoming stream represents the flow around a sphere whose radius (a) is related to the doublet strength by

$$\mu = 2\pi a^3 U_\infty \quad (2.61)$$

The streamwise velocity due to this singularity is

$$\frac{\partial \phi}{\partial x} = -\frac{\mu}{4\pi} \left\{ \frac{2x^2 - \beta^2 r^2}{(x^2 + \beta^2 r^2)^{\frac{5}{2}}} \right\} \quad (2.62)$$

For a rectangular tunnel, an array of image doublets placed as for the lifting case (but, unlike the lifting case, all having the same sign) satisfies the closed-wall boundary condition at the walls. Using $L_{ref} = \sqrt{BH}$ as the reference length for nondimensional co-ordinates ($\xi = x/\beta L_{ref}$, $\eta = y/L_{ref}$, $\zeta = z/L_{ref}$), the streamwise interference anywhere in the tunnel for a model located in the centre of a rectangular test section is given by

$$\varepsilon = \frac{u_i}{U_\infty} = -\frac{A^{\frac{3}{2}}}{4\pi\beta^3} \frac{V}{(BH)^{3/2}} \sum_{\substack{n=-\infty \\ \text{excluding} \\ n=m=0}}^{n=\infty} \sum_{n=-\infty}^{m=\infty} \left\{ \frac{2\xi^2 - (\eta\sqrt{A} - mA)^2 - (\zeta\sqrt{A} - n)^2}{\left[\xi^2 + (\eta\sqrt{A} - mA)^2 + (\zeta\sqrt{A} - n)^2 \right]^{\frac{5}{2}}} \right\} \quad (2.63)$$

As for the 2D case (Fig. 2.15) the streamwise interference is a maximum at the model location, Figure 2.19, which increases the effective free stream, but with no consequent pressure buoyancy effect on the model. By symmetry, the interference upwash is zero along the axis of the tunnel.

Evaluating the interference at the model location, $\xi=\eta=\zeta=0$, the classical result is recovered,

$$\varepsilon_0 \equiv \varepsilon(0,0,0) = \frac{A^{\frac{3}{2}}}{4\pi} \frac{V}{\beta^3 (BH)^{3/2}} \sum_{\substack{n=-\infty \\ \text{excluding} \\ n=m=0}}^{n=\infty} \sum_{m=-\infty}^{m=\infty} \frac{1}{\left[m^2 A^2 + n^2 \right]^{\frac{3}{2}}} \quad (2.64)$$

For an arbitrary axisymmetric body, a body shape factor, λ , is defined (per Lock [22]; also Glauert [15]) so that the blockage velocity is

$$\varepsilon_0 = \tau \lambda \left(\frac{A_{\text{maximum}}}{C} \right)^{3/2} \quad (2.65)$$

where $C =$ tunnel area ($= BH$ for a rectangular section), τ depends on the shape of the tunnel and λ on the shape of the body. Using this definition of λ , the far field is approximated by the flow around an equivalent sphere of diameter $t\lambda^{1/3}$, where t is the maximum body thickness.

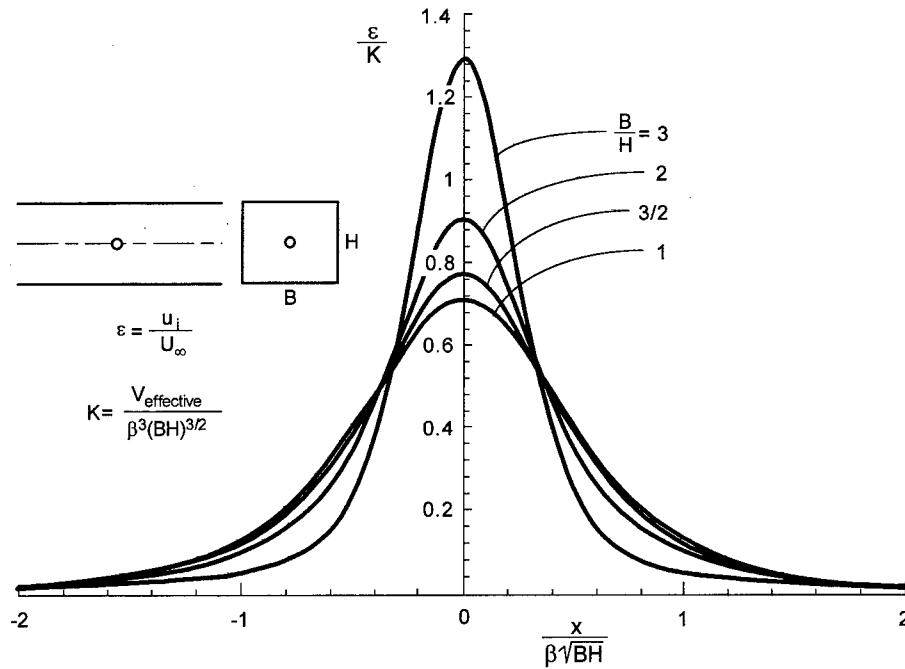


Figure 2.19 Centreline Distribution of Streamwise Interference of a 3D Source Doublet in Closed-Wall Rectangular Wind Tunnels

The effective volume can be calculated from the surface velocity distribution, $V(s)$, using

$$\lambda = 4 \int_{\text{leading edge}}^{\text{trailing edge}} \frac{V(s) [z(s)]^2}{U_{\infty} t^3} ds \quad (2.66)$$

Glauert provides an approximation for the 3D case corresponding to Equation 2.51 in two dimensions,

$$\lambda = \frac{4V_0}{\pi t^3} \quad (2.67)$$

where V_0 is the body volume.

2.2.2.5 3D RANKINE BODIES

The effect of body length is illustrated by results for the Rankine body, which is formed by the superposition of an upstream source and downstream sink (of equal strengths) located colinearly with the oncoming free stream. As in 2D flow, the source doublet is the limiting case as the source-sink separation distance ($2s$) approaches zero. Keeping source strength constant, a closed body of increasing fineness ratio results with increasing separation distance. The velocity potential of a source and sink located on the x -axis at $x=\pm s$ is

$$\varphi_m = \frac{m}{4\pi} \left\{ \frac{-1}{\left((x+s)^2 + \beta^2 r^2 \right)^{\frac{1}{2}}} + \frac{1}{\left((x-s)^2 + \beta^2 r^2 \right)^{\frac{1}{2}}} \right\} \quad (2.68)$$

where $r^2 = y^2 + z^2$. The streamwise velocity due to these singularities is given by

$$\frac{\partial \varphi}{\partial x} = \frac{m}{4\pi} \left\{ \frac{x}{\left[(x+s)^2 + \beta^2 r^2 \right]^{\frac{3}{2}}} - \frac{x}{\left[(x-s)^2 + \beta^2 r^2 \right]^{\frac{3}{2}}} \right\} \quad (2.69)$$

Using $L_{ref} = \sqrt{BH}$ as the reference length for nondimensional co-ordinates ($\xi = x/\beta L_{ref}$, $\eta = y/L_{ref}$, $\zeta = z/L_{ref}$) and for the singularity half-distance ($\sigma = s/\beta L_{ref}$), the streamwise wall interference for a Rankine body of revolution on the centreline of a closed-wall rectangular test section is found by summing all the image potentials,

$$\varepsilon = \frac{A^{\frac{3}{2}}}{4\pi\beta^2} \frac{m}{U_{\infty} BH} \sum_{\substack{n=-\infty \\ \text{excluding} \\ n=m=0}}^{\infty} \sum_{m=-\infty}^{\infty} \left\{ \frac{\left[\frac{\xi + \sigma}{\left[(\xi + \sigma)^2 + (\eta\sqrt{A} - mA)^2 + (\zeta\sqrt{A} - n)^2 \right]^{\frac{3}{2}}} \right]}{x - \sigma} - \frac{\left[\frac{\xi - \sigma}{\left[(\xi - \sigma)^2 + (\eta\sqrt{A} - mA)^2 + (\zeta\sqrt{A} - n)^2 \right]^{\frac{3}{2}}} \right]}{x - \sigma} \right\} \quad (2.70)$$

The longitudinal distribution of blockage interference along the centreline of the tunnel for several Rankine bodies having a maximum diameter ratio $t/L_{ref} = 0.1$ is shown in Figure 2.20.

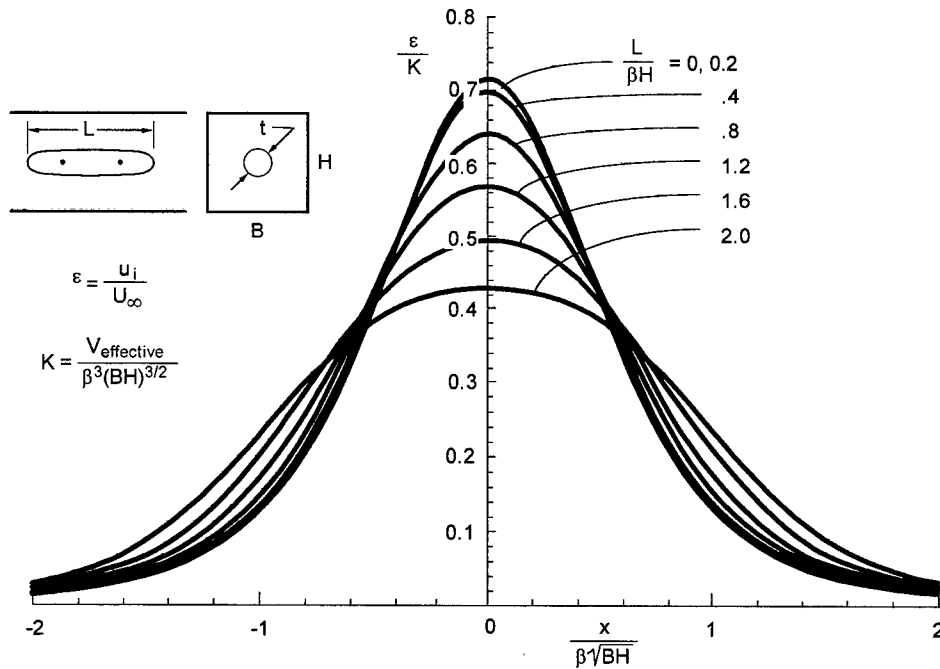


Figure 2.20 Streamwise Interference of Rankine Bodies ($t/\sqrt{BH} = 0.1$) in a Closed-Wall Square Tunnel

The effect of large body length may be understood by considering the limiting case of a very long body. The flow between such a model and the walls is effectively 1D so that the interference at any station is approximately the velocity corresponding to the decrease in flow area due to the model cross section. By continuity,

$$(\rho UC)_{upstream} = \rho(x) (U_{upstream} + u_i(x)) (C - A_{model}(x)) \quad (2.71)$$

For small ε and A_{model}/C the blockage (to first order) at the centre (assuming the maximum body diameter occurs here) of a very long body is

$$\varepsilon = \left(\frac{A_{\text{maximum}}}{\beta^2 C} \right) \quad (2.72)$$

In AGARDograph 109 the effect of body length on peak interference is given for a Rankine body in a circular tunnel in terms of a modified tunnel shape factor. Figure 2.21 compares those results with similar calculations for Rankine bodies in a square tunnel. The square and circular tunnel results correspond very closely. The peak interference decreases significantly for model length ratios of practical interest. Typical large models may approach and even exceed length ratios of 1. Reflection plane models (so-called half-models) may approach length ratios of 2. The one-dimensional flow approximation is the interference asymptote for large model length and corresponds very closely to the 3D interference results for body length ratios above about 3. Results for a family of 2D Rankine ovals ($t/H=0.1$) are shown in Figure 2.21 for reference.

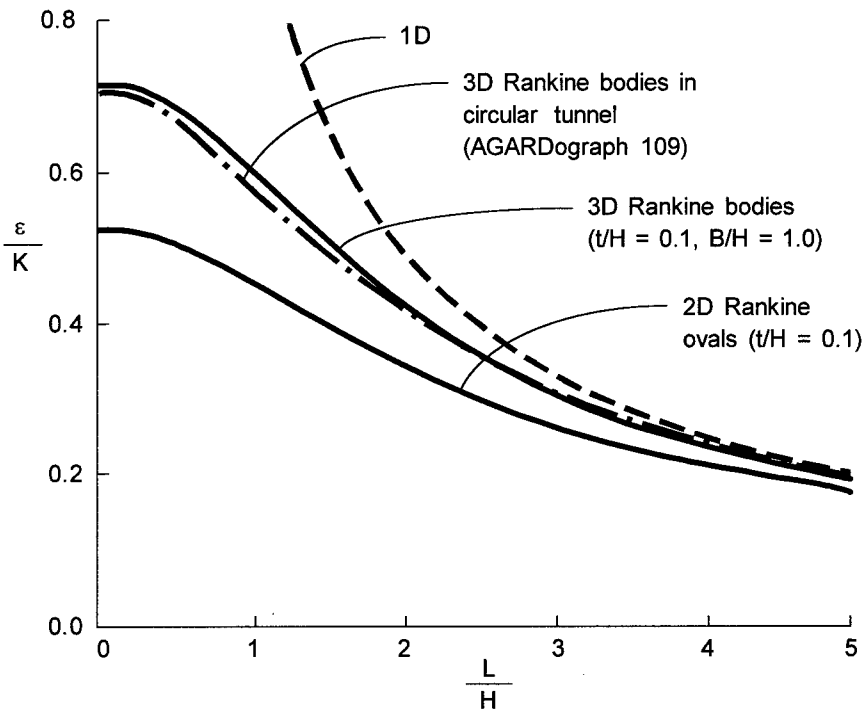


Figure 2.21 Effects of Body Length on Streamwise Interference

2.2.2.6 3D WAKE BLOCKAGE

In 3D flow, the potential of a point source is

$$\phi_m = -\frac{m}{4\pi} \frac{1}{(x^2 + \beta^2 r^2)^{\frac{1}{2}}} \quad (2.73)$$

where m , the source strength, is $1/2 U_\infty S C_D$. The streamwise velocity due to this singularity is

$$u = \frac{\partial \phi}{\partial x} = \frac{m}{4\pi} \frac{x}{(x^2 + \beta^2 r^2)^{\frac{3}{2}}} \quad (2.74)$$

As in the previous section, a 2D doubly infinite array of image singularities (see Fig. 2.7) satisfies the boundary conditions for a rectangular closed-wall tunnel. Using $L_{ref} = \sqrt{BH}$ as the reference length for nondimensional co-ordinates ($\xi = x/\beta L_{ref}$, $\eta = y/L_{ref}$, $\zeta = z/L_{ref}$) as before, the nondimensionalised streamwise interference anywhere in the tunnel for a model located on the centreline of a rectangular tunnel is then given by

$$\varepsilon = \frac{A^{\frac{3}{2}}}{8\pi\beta^2} \frac{C_D S}{BH} \sum_{\substack{n=-\infty \\ \text{excluding} \\ n=m=0}}^{n=\infty} \sum_{m=-\infty}^{m=\infty} \frac{\xi}{\left[\xi^2 + (\eta\sqrt{A} - mA)^2 + (\zeta\sqrt{A} - n)^2 \right]^{\frac{3}{2}}} \quad (2.75)$$

As for the 2D case, this formulation results in $\varepsilon=0$ at the model location and a finite (negative) blockage far upstream of the model, Figure 2.22. The interference at the model location relative to the velocity far upstream is

$$\varepsilon_0 = \frac{C_D S}{4\beta^2 BH} \quad (2.76)$$

Along tunnel centreline ($\eta=\zeta=0$) the buoyancy due to the longitudinal gradient of wake blockage is found (as for the 2D case) to be related to the solid blockage distribution,

$$\frac{\partial \varepsilon_{wake}}{\partial \xi} = \frac{C_D}{2} \frac{S(BH)^{1/2}}{V} \beta \varepsilon_{solid} \quad (2.77)$$

The relationship between the longitudinal gradient of wake blockage and the value of solid blockage is to be expected considering that the source doublet point singularity is the x -derivative of the velocity potential of a point source. Thus, the second derivative (with respect to x) of the velocity potential of a point source is the same as the first derivative (with respect to x) of a source doublet, except for the ratio of the respective singularity strengths. Because the image systems are identical for the wake and solid blockage cases, the interference flow fields will be related in this way.

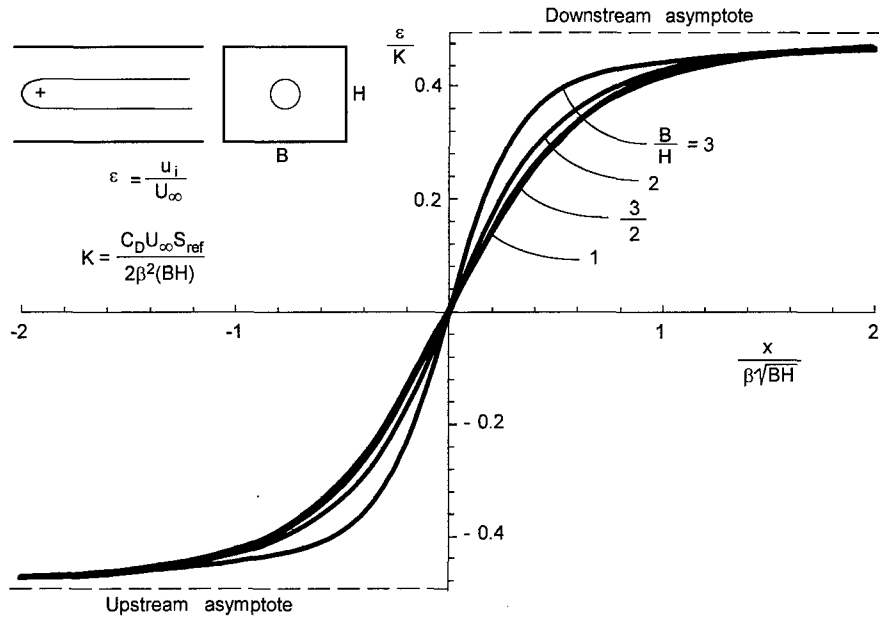


Figure 2.22 : Centreline Distribution of Streamwise Interference of a 3D Source in Closed-Wall Rectangular Tunnels

2.2.2.7 APPLICATION OF BLOCKAGE CORRECTIONS

The change of effective freestream magnitude at the model location necessitates correction of flow reference quantities: velocity, Mach number, dynamic pressure, static pressure, temperature, density, and Reynolds number. For small ϵ (taken to be the sum of all model elements contributing to blockage) and γ =ratio of specific heats=1.4, linearised corrections are as follows:

$$U_{corr} = U_{unc} (1 + \epsilon) \quad (2.78)$$

$$M_{corr} = M_{unc} \left[1 + (1 + 0.2 M_{unc}^2) \epsilon \right] \quad (2.79)$$

$$q_{corr} = q_{unc} \left[1 + (2 - M_{unc}^2) \epsilon \right] \quad (2.80)$$

$$p_{corr} = p_{unc} (1 - 1.4 M_{unc}^2 \epsilon) \quad (2.81)$$

$$T_{corr} = T_{unc} (1 - 0.4 M_{unc}^2 \epsilon) \quad (2.82)$$

$$\rho_{corr} = \rho_{unc} (1 - M_{unc}^2 \epsilon) \quad (2.83)$$

$$Re_{corr} = Re_{unc} \left[1 + (1 - 0.7 M_{unc}^2) \epsilon \right] \quad (2.84)$$

where the uncorrected flow parameters (subscript "unc") are identified with the remote upstream parameters (subscript " ∞ ") in the tunnel.

For small models in a linear streamwise static pressure gradient, the pressure buoyancy force acting on the model in the tunnel is simply the product of the effective model volume and the gradient,

$$\Delta C_D = -\frac{V}{S\bar{c}} \frac{dC_p}{d\left(\frac{x}{\bar{c}}\right)} \cong \frac{2V}{S\bar{c}} \frac{\bar{c}}{\beta L_{ref}} \frac{\partial \epsilon}{\partial \xi} \quad (2.85)$$

where $\xi = x/\beta L_{ref}$ and dC_p/dx is the externally imposed streamwise pressure gradient at the model location and, consistent with the perturbation assumptions, C_p is expressed as $-2u/U_\infty$. For a closed-wall tunnel, the measured drag of the model is increased, so that the necessary correction to drag is the negative of the above incremental buoyancy force.

For the 2D situation, the corresponding buoyancy drag force per unit span is

$$\Delta C_D = -\frac{A}{c^2} \frac{dC_p}{d\left(\frac{x}{c}\right)} \cong \frac{2A}{c^2} \frac{c}{\beta H} \frac{\partial \epsilon}{\partial \xi} \quad (2.86)$$

where $\xi = x/\beta H$ and A is the effective cross-sectional area of the model.

2.2.3 WAKE BLOCKAGE CORRECTIONS FOR SEPARATED FLOWS

The problem of separated wakes, characterised by a free shear layer surface bounding a separation "bubble" behind the model, was recognised by Glauert [15], who accounted for the increased drag (attributed to blockage interference) due to separated wakes using an empirical factor η , which represents the size of the separated wake. Investigation of the effect of separated wakes was stimulated by the observed failure of classical interference theory for predicting tunnel constraints for flat plates at large incidence. The model that forms the theoretical basis for this correction is shown in Figure 2.23 (for 2D flow). For incompressible flow, Glauert's corrected dynamic pressure is

$$q_{corr} = q_{unc} \left[1 - \eta \frac{t}{H} \right]^{-2} \quad (2.87)$$

where t is the thickness of the blunt base. In three dimensions, t and H are replaced by the size of the separated wake at the body and C . For this case, Glauert quotes values of η as a function of t/c based on experiments with three Joukowski sections, a Rankine oval, ellipse, circle, and a flat plate.

Maskell [25] revisited the problem in trying to resolve differences in high-lift characteristics of delta wing models tested in different wind tunnels, especially beyond the onset of stall. For a flat plate normal to the

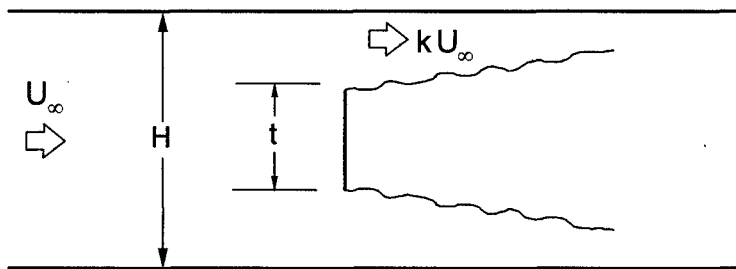


Figure 2.23 Model of Separated Wake Flow in a 2D Closed-Wall Tunnel

flow (similar to the situation of Fig. 2.23), the corrected dynamic pressure is derived as

$$q_{corr} = q_{unc} \left[1 + \theta \frac{C_D S}{C} \right] \quad (2.88)$$

where θ , the blockage factor for bluff-body flow, is given by

$$\theta = \frac{1}{k_c^2 - 1} \quad (2.89)$$

The parameter k is related to the base pressure coefficient, C_{pb} ,

$$k^2 = 1 - C_{pb} \cong k_c^2 \left[1 + \frac{C_D S}{(k_c^2 - 1) C} \right] \quad (2.90)$$

and the subscript "c" refers to corrected quantities. Maskell suggests use of the iterative formula

$$(k_c^2)_n = k^2 \left\{ 1 + \frac{1}{[(k_c^2)_{n-1} - 1]} \frac{C_D S}{C} \right\}^{-1} \quad (2.91)$$

to determine k_c , where subscript "n" denotes the nth estimate of k_c . For flat plates of aspect ratio between 1 and 10, a value of $\theta \cong 5/2$ is given as unlikely to result in serious error. This appears to be a consequence of the observed tendency of separated wakes behind rectangular flat plates toward axial symmetry. For this value of θ , the resulting blockage interference is five times greater (in terms of dynamic pressure correction) than if classical source-derived interference corrections were applied.

The extension of the above theory to a wing relies on the principle of superposition: it is supposed that the effect of the separated wake of the wing can be treated incrementally in a manner analogous to the normal flat plate. The most difficult part of determining this correction is evaluating the separated wake drag contribution. That is, the model drag can be considered to be the sum of three contributions,

$$C_{Dtotal} = C_{Dvortex} + C_{Dprofile} + C_{Dseparated} \quad (2.92)$$

where the first term is the inviscid induced drag due to lift, the second is the attached boundary layer profile drag, and only the third term is to be used in estimating the dynamic pressure correction due to separated wake blockage. Determination of the separated wake term requires determination of the onset of stall and a bookkeeping of profile drag and drag due to lift beyond stall.

2.3 PANEL METHODS FOR CLOSED-WALL TUNNELS

Advances in computational fluid dynamics (CFD) have paralleled the phenomenal increases in computational capability over the past 30 years. Even for simple model configurations in rectangular tunnels, it may be argued that solution of the boundary value problem with specified normal flow at control points at the wind tunnel wall is quicker and easier than calculation of the double summations of the previous sections. Continuing advances in computing power have put simple panel solutions within the capability of low-end engineering workstations and even personal computers.

With the maturation of production CFD codes and the development of custom wall interference codes, the calculation of wall interference for large models within test sections of arbitrary shape (including the effects of finite length) and with increasing accuracy with regard to the accounting of compressibility and viscous effects has been made possible and, in many applications, routine. Further, it is but a short step from the closed-wall boundary value problem to the ideal ventilated-wall boundary conditions (Sec. 3.2.3) and next, to use of measured wall boundary conditions (Chapter 4).

This section is limited to the application of CFD to wall interference for inviscid, linear compressible flows in closed-wall tunnels. As intended here, a "panel method" is any method in which the tunnel walls and, in many cases, the model are represented by singularity distributions on their surfaces. The singularities are fundamental solutions of Laplace's equation. Commonly used singularities include vortex lines for vortex lattice codes, constant strength source or doublet panels for simple panel codes, and higher order source or doublet panels for higher order panel codes.

The multitude of panel code applications to problems of wind tunnel interference precludes any attempt of an exhaustive review. In this regard AGARD R-692 [1] contains comprehensive review articles describing the wide range of interference problems and approaches in both Europe and North America. Although dated, this reference accurately reflects accomplishments and future directions of interference study in the premier aerospace laboratories of the participating countries. The problems identified at that time have since been pursued with ever more powerful computational tools. This section reviews some general principles of current CFD approaches, and provides a few examples that are indicative of typical results.

2.3.1 GENERAL CONSIDERATIONS

Evaluation of wind tunnel wall interference using a panel method provides advantages over classical methods based on the method of images with regard to both model and tunnel representation. First, the analysis of large and complex models is possible, though calculation of vortex wake trajectories and modelling of large separated wakes remain as areas of difficulty. Second, a panel approach to modelling the wind tunnel can directly address arbitrary cross-sectional shapes, streamwise variations of tunnel area, arbitrary wall boundary conditions (both in form and spatial variations), and the presence of support systems. The two main disadvantages (relative to simpler methods) are an increased complexity of analysis, involving more effort for preparation of analysis inputs, and the requirement for perhaps substantial computational resources.

A secondary disadvantage of panel solutions is the particular nature of each solution. That is, each flow condition (i.e., model configuration, position, attitude, and onset Mach number) requires separate analysis; generalisation of results is not immediately possible from a single analysis. Although in many cases linear theory may be used to establish typical parametric variations from the results of a single

solution for small changes of configuration or flow condition, a number of analysis cases may be needed both to verify classical trends and to capture variations of wall interference over the range of desired test variables (angle of attack, lift coefficient, Mach number).

The basic principles regarding the use of panel methods for interference calculation parallel those for the method of images. That is, the potential at any point in the flow is the sum of the potentials of all the panel singularities. The panel code solves for the strengths of all these singularities, subject to boundary conditions at each panel control point. The interference velocity potential of the walls is the sum of all the wall panel potentials. The wall panels thus produce the same incremental flow field as the entire collection of image singularities in the method of images. Zero interference around the model is obtained in the degenerate case of zero panel strengths everywhere on the wall. This will occur if closed-wall panels (with a $\partial\phi/\partial n=0$ boundary condition) are disposed on an interference-free streamtube around the model. Alternatively, zero interference is obtained if the boundary conditions at each panel provide the interference-free velocity vector (i.e., due to the model alone), or simply if the walls are "far enough" away so that disturbances at the model due to the wall are negligible.

Figure 2.24, Vaucheret [35], provides model representation requirements in terms of wing geometry for a given error (0.03 deg/ C_L) in interference upwash prediction for a square test section with closed sidewalls and porous floor and ceiling. This work indicates that a large range of sweep and span ratios are adequately represented by an infinitesimal horseshoe vortex ($2s/B=0$, $\Lambda=0$). Representation of finite wingspan captures a significant additional portion of the model wing design space, with wing sweep modelling required only for very large sweep or span ratio. Boundaries excluding models of large blockage and span ratios are also indicated.

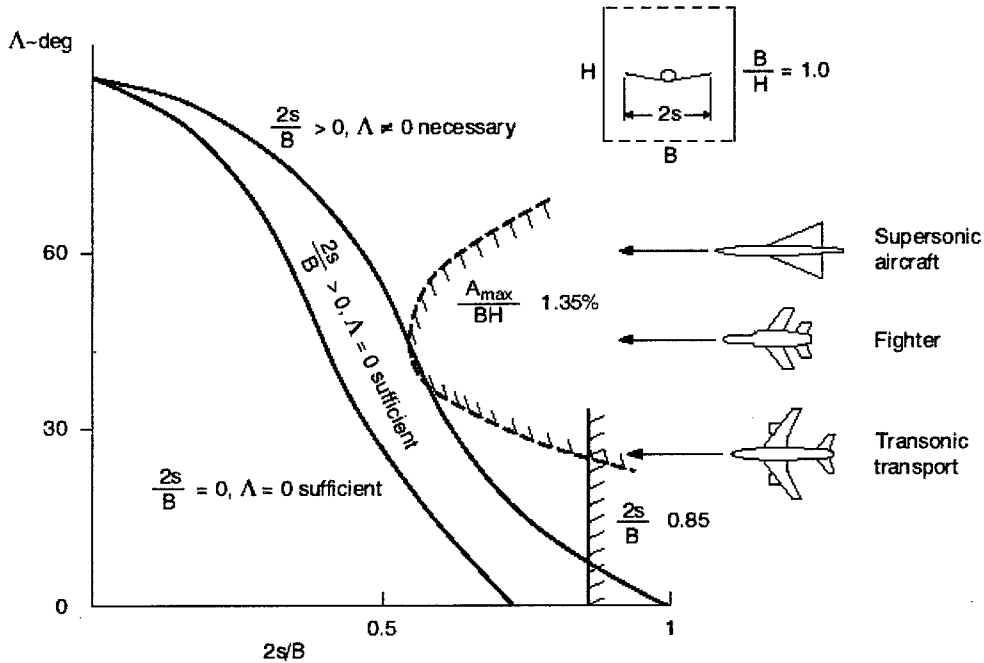


Figure 2.24 Modelling Requirements for Wings (Vaucheret [35])

Representations of the test model have increased in complexity concurrently with computational capability. The effects of finite model size can be represented by distributions of the fundamental model singularities within the test section. In general, any body shape can be generated by a distribution of source singularities. Similarly, any lift distribution can be approximated by a distribution of horseshoe vortex singularities. The strengths of these singularities are specified for a given flight condition.

Alternatively, model singularity strengths may be left as unknowns (requiring a corresponding set of boundary conditions or constraints), so that the effect of wall interference on model loading is explicitly calculated along with the interference field itself. Hybrid approaches are possible as well, wherein part of the model aerodynamics may be specified, such as the net source strength corresponding to skin friction drag.

For specified singularity methods, the model may be represented by a lumped parameter collection of singularities or singularity distributions that mimic the theoretical far-field interference-free flow around the model. To the extent that the distribution of singularity strengths represents the salient characteristics of the test article in the tunnel (volume distribution, lift, drag, pitching moment, span loading, etc.), this approach can be used to predict the interference of models that are not small. Complete image systems are usually not used explicitly. Rather, the tunnel walls are represented by a distribution of singularities located at the walls: source or doublet panels, or vortex lines, depending on the method. The closed-wall boundary condition ($\partial\phi/\partial n=0$) is enforced at control points at the wall, resulting in a set of linear equations for the wall singularity strengths. The wall interference flow field is that part of the flow field due to the wall singularities only.

If the model is panelled, model panel strengths add to the number of unknowns subject to satisfying boundary conditions at the model surface. Leaving model aerodynamic loading as unknown is more exact than a priori specification of model aerodynamics, because satisfaction of the boundary conditions at the model includes the effect of the tunnel walls. In principle, this influence can include a change in separated wake shape if an appropriate wake model is implemented (Chapter 6). If model panelling is sufficiently dense, leaving model singularities as unknowns also permits the evaluation of interference from integrated model characteristics calculated both in the tunnel and in free air. Panel generation for straight, closed-wall tunnels with parallel walls is straightforward; panelling of the model, a variable-section tunnel, or a support system may require significant effort.

The issues facing an analyst using a panel method for wall interference prediction may be categorised as relating to:

- 1) Problem formulation: specification of boundary conditions may put the existence or uniqueness of a solution in jeopardy.
- 2) Tunnel panelling: tunnel length, circumferential and longitudinal panel density.
- 3) Model representation: number and distribution of singularities; panel density.

The computational approaches to wall interference calculation described here are in large part based on the use of flow codes developed for the analysis of so-called external flows. Their application to internal flows, such as the wall interference problem, usually involves embedding the tunnel in a uniform onset stream. As discussed by Holt and Hunt [19], using these methods to solve for the flow with both internal (the model) and external (the walls) boundaries cannot be done with impunity. Indiscriminate application of boundary conditions can result in uniqueness and existence problems for the sought-after solution. For example, a tunnel having closed and parallel walls may be modelled as a panelled prism with upstream and downstream faces normal to the tunnel axis. However, the normal flow on each of these faces cannot be independently specified. The panels representing the tunnel walls have a specified zero normal flow, so continuity of mass requires that integrated inflow to the tunnel must equal integrated outflow. Holt and Hunt address this problem by placing the wind tunnel, modelled as a long open-ended tube, in an external uniform flow field and parallel to it. Other variations on this approach may be code-dependent, but typically involve specification of flow at one end of the tunnel, either explicitly or implicitly.

Figure 2.25 summarises the boundary conditions for a wind tunnel analysis using a panel code similar to PANAIR (Magnus and Epton [24]).

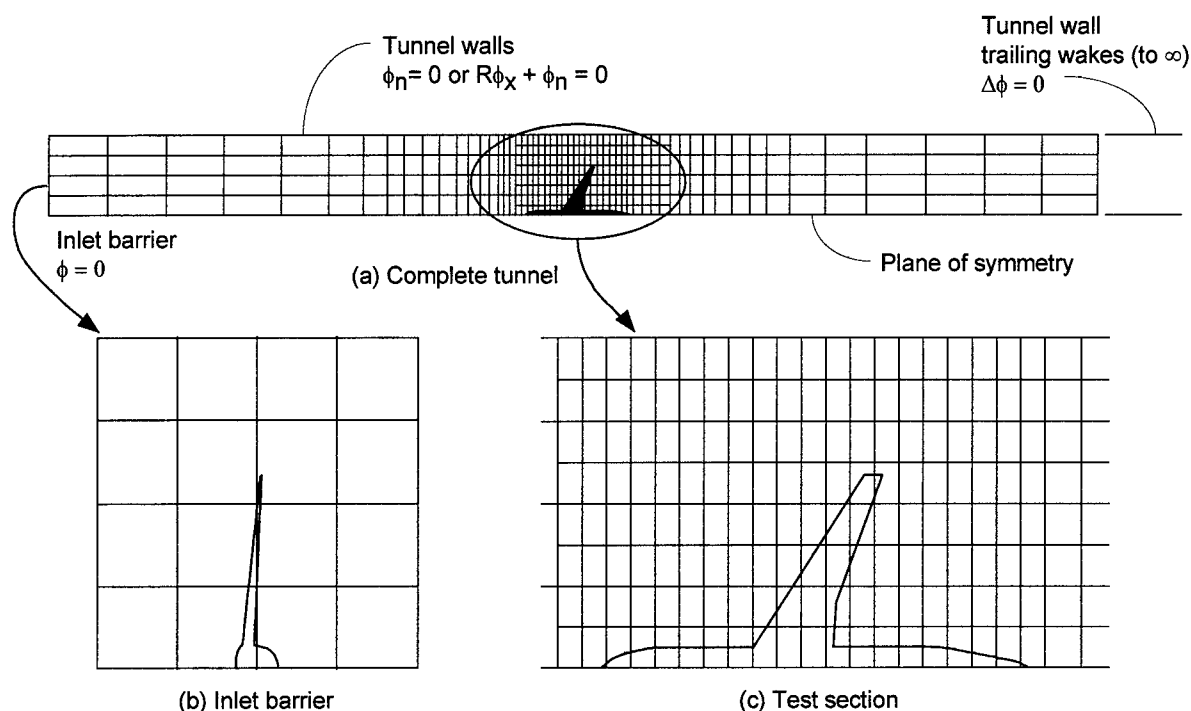


Figure 2.25 Boundary Conditions for a Tunnel Analysis Using PANAIR

Tunnel panelling should be guided by the usual common-sense panelling rules. Panelling should be dense enough to capture the flow features of interest. A simple check consists of increasing panel density until the solution stops changing. To represent the theoretical infinitely long tunnel, a panelled tunnel must be long enough that flow perturbations due to the model are negligible at the upstream end. Inspection of wall panel strengths and verification that they approach the desired zero upstream asymptote of the ideal long tunnel are recommended checks of any new solution. Evaluation of the uniformity of the incoming flow field at the upstream end of the tunnel is an additional check of the adequacy of upstream tunnel length. Downstream of the model similar considerations apply, though flow perturbations due to the model cannot be expected to disappear because of the convected model wakes (both vortex and viscous). However, the flow should approach an asymptotic state in the downstream direction as well. Again, inspection of wall singularity strengths or the flow field can indicate the adequacy of downstream tunnel length.

Similar considerations govern the specification of model singularities or panels. The safest approach is to increase model singularities (panels) until the calculated interference stops changing. If details such as changes in spanwise or chordwise wing loading are desired, model panelling must be as detailed as would be required of a free-air analysis.

Besides comparison of interference results from a panel method to classical results, other common-sense checks can lend credence to a particular panel solution. For closed-wall tunnels the walls should not leak: the massflow entering the tunnel at the upstream face plus any flow added at the model location should equal the massflow leaving the tunnel at its downstream end. Loss (or gain) of mass through the tunnel walls may be due to insufficient wall panel density, an error in panelling such as a reversed specification of panel normal vectors (conventionally, positive normal vectors point into the flow of

interest), or an improperly specified wall boundary condition. Another global "reasonableness" check of a closed-wall solution is the expected relationship of model lift to integrated pressure force on the walls: these should be equal and opposite. For ventilated walls similar considerations apply, but the momentum flux of the flow through the walls must also be included.

2.3.2 2D INTERFERENCE

Many advancements in wall interference technology were pioneered in the 2D domain due to its relative simplicity before similar techniques and approaches were applied to 3D flows. Analytic methods for 2D flows are more tractable; for example, complex variable techniques may be applied. For panel methods, the main advantage of 2D flows is computational simplicity due to greatly reduced problem size (i.e., number of unknowns). From the experimental standpoint, the primary advantage (for wall interference purposes) of the ideal 2D test set-up compared to a 3D test set-up derives from the fact that measurements and wall boundary adaptations are functions of only the streamwise co-ordinate. Thus both the number of measurements and the computational requirements to assess and reduce interference are typically at least an order of magnitude smaller than for a 3D test set-up.

Unfortunately, two factors conspire against the apparent simplicity of a 2D test: two-dimensionality of model disturbances and the model interaction with tunnel sidewall boundary layers. In two dimensions, flow disturbances due to a source doublet, for example, decrease as the square of the lateral distance from the model, compared to the cube of the lateral distance for a 3D doublet (see Sec. 2.2). Thus, the flow perturbations at the walls are larger for typical 2D cases than typical 3D cases, resulting in larger interference, and requiring the use of non-linear flow equations at much lower upstream Mach numbers. The sidewall boundary layer is more insidious because its response to the model pressure distribution can result in effectively a wavy sidewall, thus violating the required symmetry condition for planar flow. This issue is discussed in GARTEUR [14] and Mokry et al. [26]. Barnwell [6], Barnwell and Sewall [7] and Murthy [27], [28], [29] and [30] describe flow models for estimating the interference effects of the sidewall boundary layer.

Holt and Hunt [19] describe several applications of panel methods to wind tunnel interference problems. For 2D flows, a direct panelling approach was abandoned (due to "leakage" problems, unless a very dense panelling was used) in favour of a panel method using a standard Schwartz-Christoffel transformation. The airfoil has a 2-ft chord, a thickness ratio of 7%, and a chord-height ratio of 2/7. For 2D high-lift testing, it is shown that the lift curve of a clean airfoil is adequately corrected to interference-free conditions using classical corrections. With flaps deflected, however, classical corrections are shown to result in lift corrections 2-5 times greater than corrections deduced using a panel technique. In these calculations, leading-edge flap incidence was explicitly varied to match leading-edge pressure peaks to free-air calculations in order to produce an incidence scan at fixed flap angle.

2.3.3 3D LIFT INTERFERENCE

Joppa [20] describes a vortex lattice method for the calculation of upwash interference in closed-wall tunnels of arbitrary cross section, Figure 2.26. The walls are represented by a tubular vortex sheet composed of a network of square vortex rings. Results are shown for a uniformly loaded, finite-span horseshoe vortex centrally located in circular, square, and rectangular ($B/H=5/3$) tunnels. The longitudinal variation of interference essentially duplicates the result from the method of images for the square tunnel.

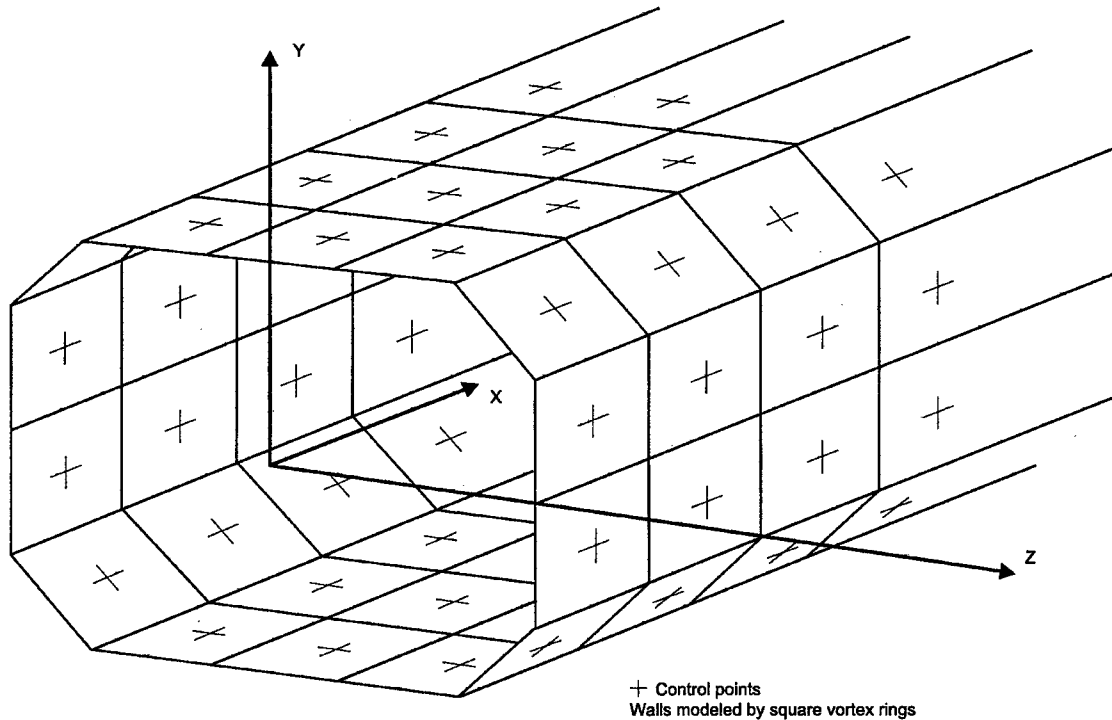


Figure 2.26 Vortex Lattice Representation of a Rectangular Tunnel with Corner Fillets (Joppa [20])

A panelling density consisting of 16 segments to represent the tunnel cross section was found to be adequate. Consideration of the longitudinal variation of calculated vortex strength at the walls suggests that the presence or absence of tunnel walls more than about a diameter upstream or downstream of the wing contributes little to the solution at the model. It is concluded that a length to diameter ratio of 3 to 4 is ample (for a vortex span ratio, $2s/B=0.4$). The method is used to calculate the upwash wall interference downstream of the wing, with stations above and below tunnel centreline representing typical tail locations (Joppa [21]). The effect of wake displacement was investigated and found to be significant with regard to upwash at the tail. It is concluded that wall-induced velocities cause the vortex wake to be deflected less than in free air, with the direct result that the upwash change at the tail due to the in-tunnel wake position may be of the same order as the usual wall interference upwash. This effect may be either positive or negative depending on tail location.

Holst [18] presents results comparing upwash variation as a function of wing sweep angle for constant and elliptic lift distributions using the method of Joppa [20]. Increasing root-to-tip upwash variation with increasing sweep angle, Figure 2.27, is expected given the longitudinal variation of upwash interference in closed-wall tunnels.

Holt and Hunt [19] give an example of a typical panel analysis of a tapered swept wing at 15 deg incidence of span ratio $2/3$ in a rectangular tunnel. Their results illustrate both the effect of wall interference and of wake relaxation on span loading. The suppression of wake downward drift by closed wind tunnel walls is recognised as a potentially significant source of interference, especially for close-coupled configurations (e.g., canard-wing). It is noted that proper comparison of in-tunnel and free-air panel solutions to extract wall interference depends on consistent assumptions for the wake modelling. This work also illustrates a logical extension of the use of panel methods for wall interference evaluation: analysis of the complete testing environment including model supports.

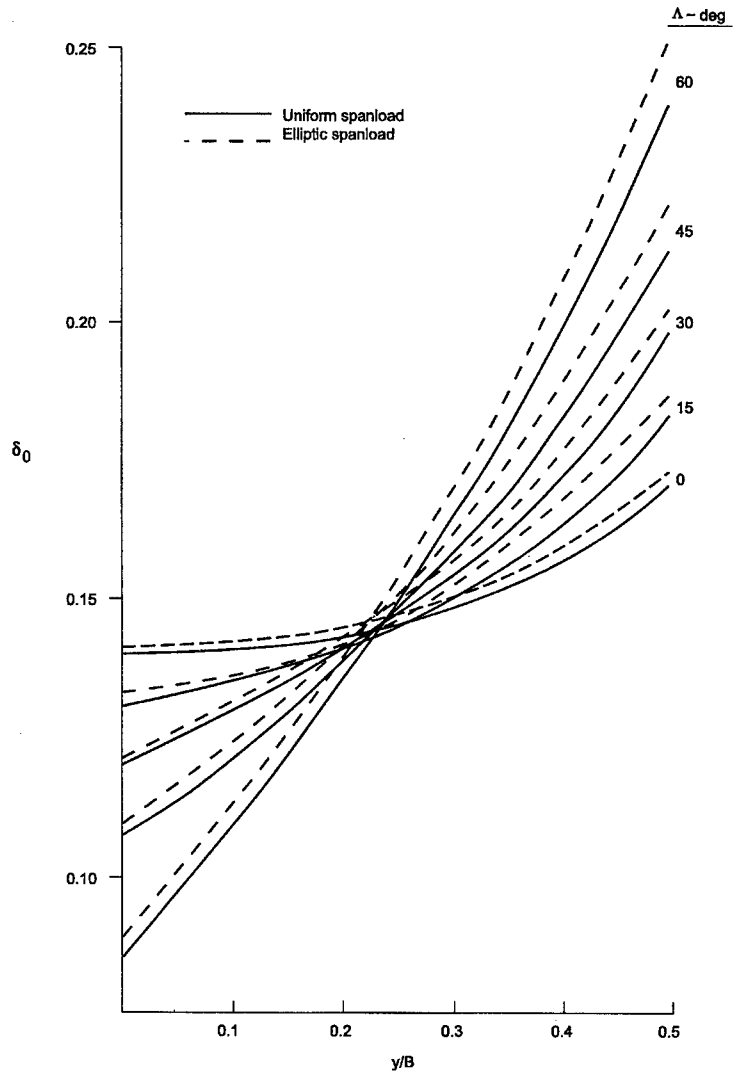


Figure 2.27 : Spanwise Variation of Upwash Interference for Swept Wing in a Closed-Wall Tunnel; $2s/B = 0,6$, $B/H = 1.0$ (Holst [18])

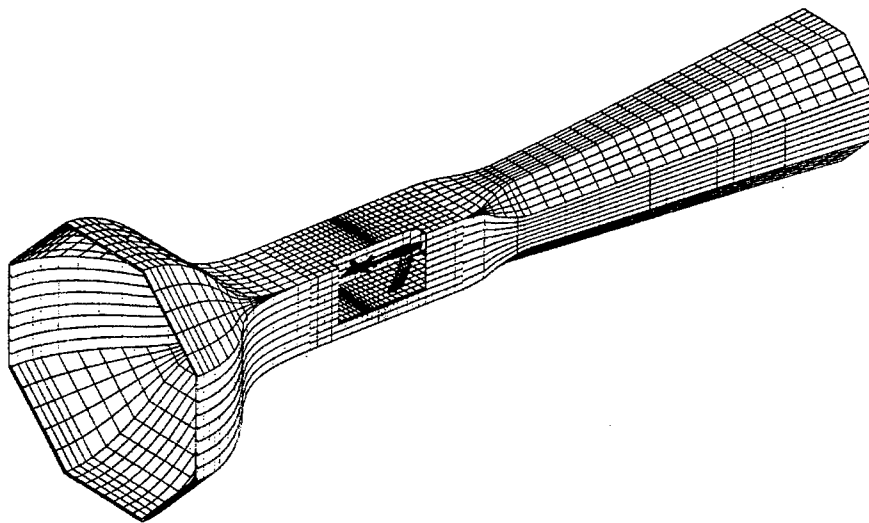


Figure 2.28 Complete KKK Wind Tunnel Panelling (Steinbach [33])

Steinbach [33] reports results of a panel analysis that further extends this approach in representing a complex test environment: the entire test leg, including aeroplane model and the sting support system, is panelled, Figure 2.28. The interference contributions of individual tunnel elements are compared. Calculated lift, drag, and pitching moment corrections due to the support system for a fighter model are found to be larger than corrections due to the walls.

With regard to experimental validation of a panel method for lift interference prediction, Vaucheret [36] compares incremental wall pressures due to model lift for the ONERA M2 model and demonstrates good agreement with predictions at an upstream Mach number of 0.81.

The interference of delta wings has been calculated using a free vortex sheet code (Frink [12]). The effects of span ratio and angle of attack are investigated. A dependence of lift interference on angle of attack is found and shown to be the result of the nonplanar vortex wake. The effects of tunnel walls on vortex sheet position and on upper surface pressures are also calculated.

A method exemplifying a hybrid of the method of images and panel methods is reported by Fiddes and Gaydon [11]. The test model and its first few images are panelled explicitly, permitting a relatively coarse wall panelling (Fig. 2.29). Engineering Sciences Data Unit Item 95014 provides upwash interference factors calculated using this method for a wide variety of wing planforms and span ratios in closed-wall rectangular tunnels. Chordwise and spanwise variation of the upwash interference factors, as well as average values, are given for wings of zero thickness centrally located in the tunnel. Cases include span ratios, $2s/B=0.4, 0.6, \text{ and } 0.8$, for tunnel aspect ratios, $B/H=10/7, 1, \text{ and } 0.7$.

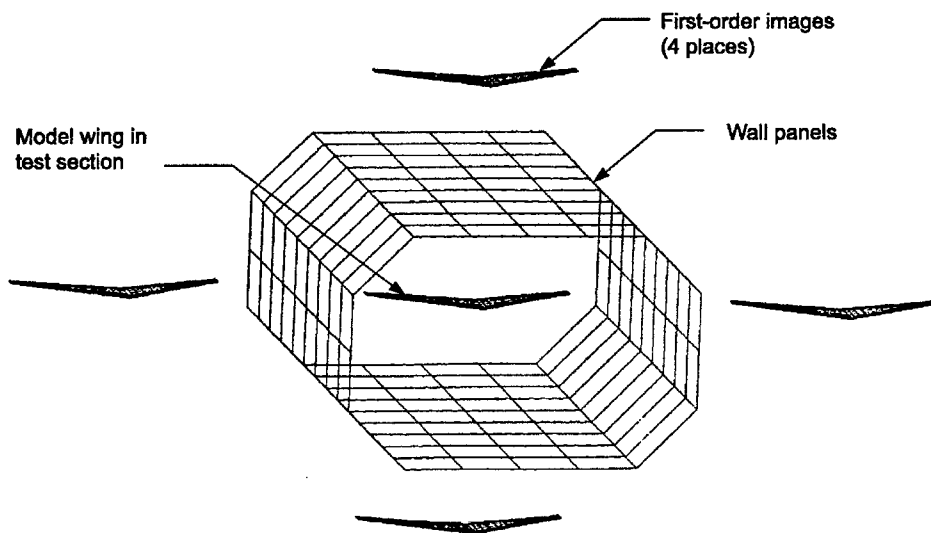


Figure 2.29 Hybrid Panel/Image Method (Fiddes and Gaydon [11])

2.3.4 3D BLOCKAGE INTERFERENCE

Vaucheret [36] presents interference results using a multiple-singularity method whereby the adequacy of model representation is evaluated by inspection of wall pressures. A rule of thumb is proposed for ellipsoids: the number of source doublets should be at least twice the fineness ratio. Good correspondence of measured and predicted Mach number at the wall is shown for a missile configuration represented by 30 doublets. The effect of the model support sting is evaluated by additional doublets.

The adequacy of modelling is validated by comparison of experimental and predicted wall pressures (Fig. 2.30).

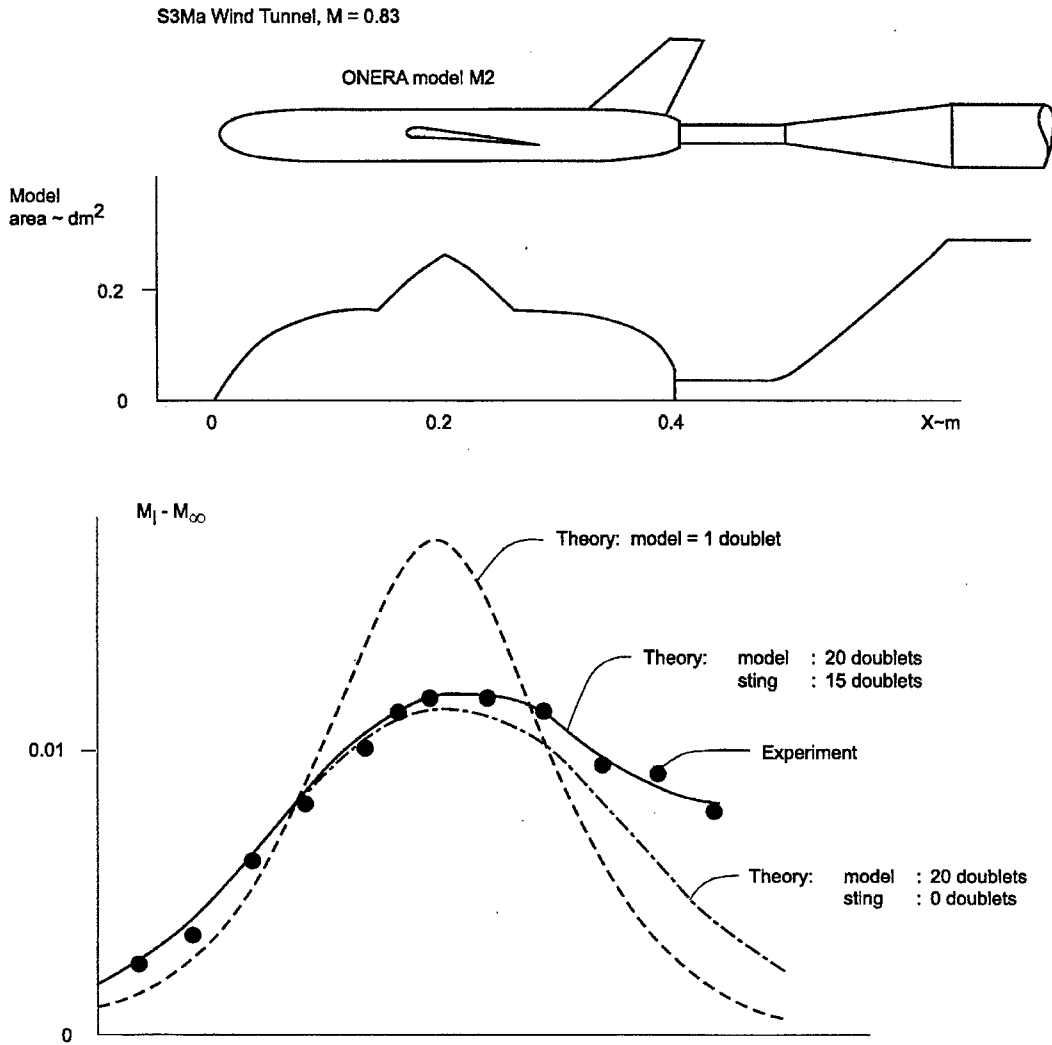


Figure 2.30 Wall Pressures due to Model and Sting in a Closed-Wall Tunnel (Vaucheret, [36])

Figure 2.31 shows the panelling of several axisymmetric bodies used as validation cases of a panel code calculation of wall interference. The maximum diameter of the bodies is about one-fifth the height of the tunnel. Figure 2.32 compares the results of blockage calculations for a Rankine body in rectangular closed-wall tunnels using a higher order panel code (Magnus and Epton [24]) to the method-of-images

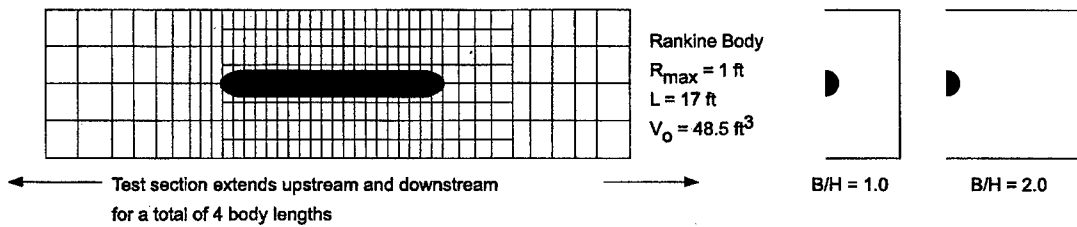


Figure 2.31 Rankine Body in Closed-Wall Rectangular Tunnels

calculations. Both the maximum value of interference and the distribution along tunnel centreline are essentially identical for these two methods. Interference predicted by classical methods for small models (Glauert, [15]) also agrees with these predictions if the finite-length body correction (Fig. 2.21) is applied to the Rankine body.

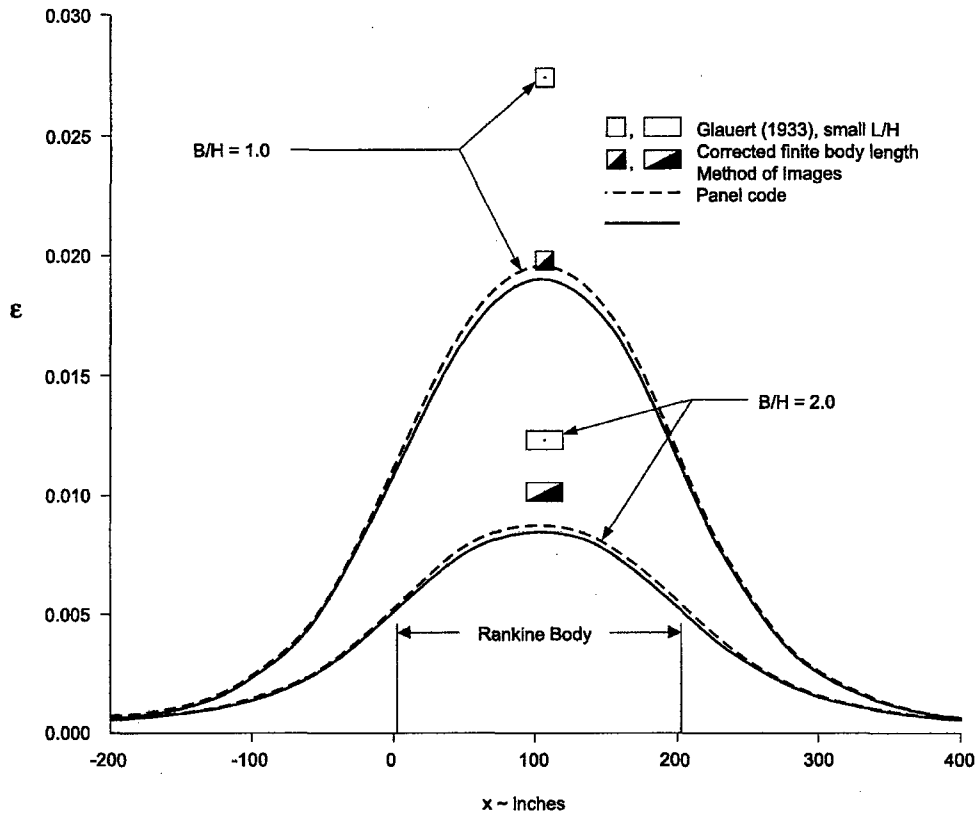


Figure 2.32 Blockage Interference of a Rankine Body in Rectangular Wind Tunnels, $L/H = 1.5$, $M = 0$

2.3.5 3D Wing-Body Combinations

The magnitude and importance of upwash wall corrections have served to focus many analysis efforts on the lift interference problem in isolation. Thus, factors bearing on upwash interference, span ratio, span loading, wing planform, and wake trajectory, have been reported extensively. The examples discussed in previous sections are representative but by no means exhaustive. Several citations also address lifting systems in combination with a blockage body and wake or sting system (e.g., Vaucheret and Vayssaire [35], and Vaucheret [36], are exemplary in discussing the spectrum of wall interference corrections in both closed-wall and ideal ventilated-wall tunnels).

High-lift testing of transport configurations is crucial for the development of multi-element high-lift systems. Lynch [23] gives an example of panel-code predictions of leading-edge slat pressure reductions due to the influence of closed wind tunnel walls. Because of the sensitivity of flow breakdown on the slat to this pressure minimum, wall interference can have a significant effect on maximum attainable lift.

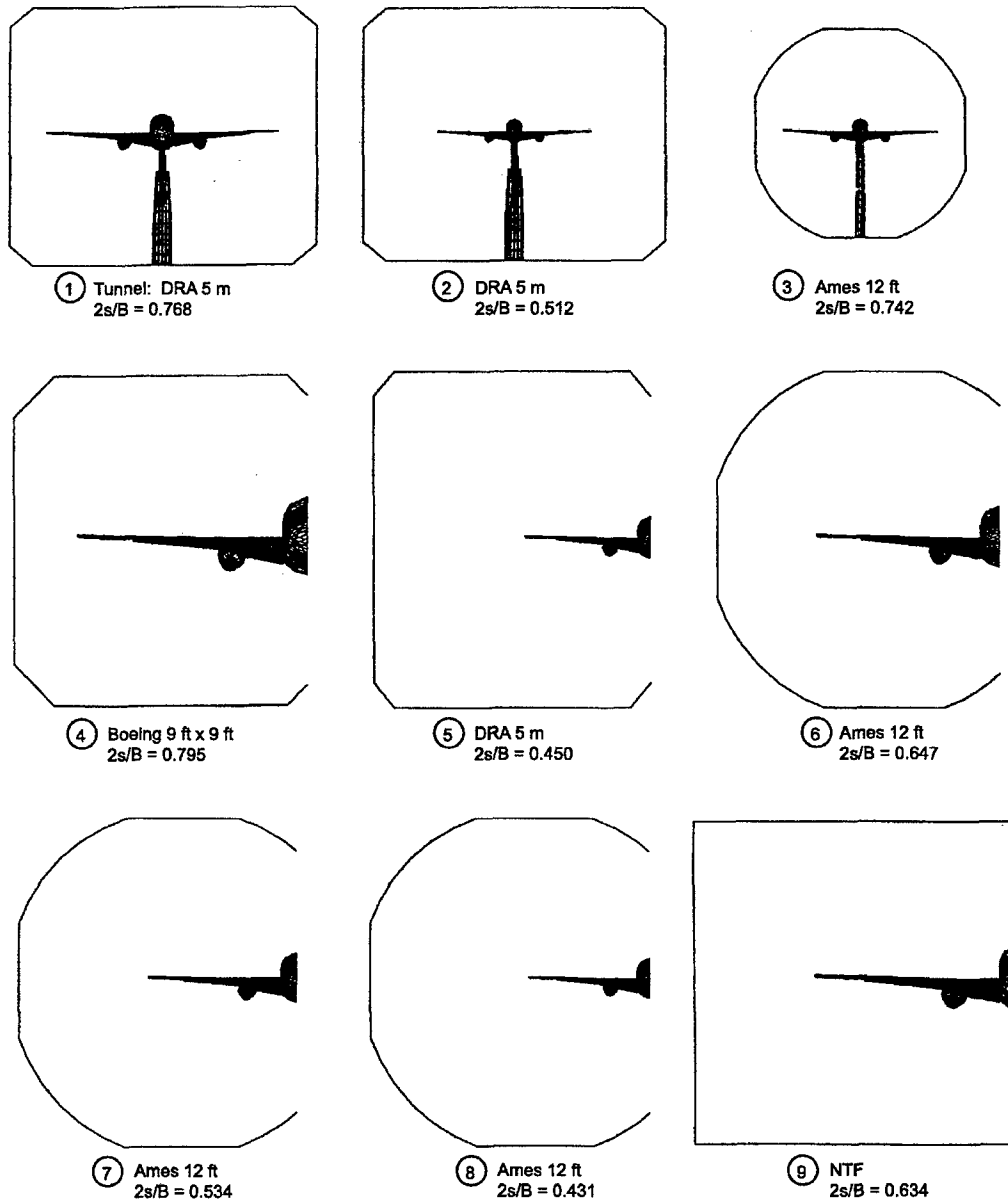


Figure 2.33 : Panel Study of Interference in Closed-Wall Tunnels (Amonlirdviman [4])

A similar computational study of high-lift transport configurations in closed-wall tunnels (Amonlirdviman [4]) Figure 2.33, quantified the spanwise interference variation at the wing for a variety of model-tunnel combinations. Both full and half-models were analysed. Full models were analysed with and without support strut fairings (shown in Fig. 2.33). Increased upwash and blockage interferences on the outboard wing are indicated for span ratios greater than 0.7, Figure 2.34.

A CFD study of a transport high-lift model in the Defence Research Agency (DRA) 5-meter, high-Reynolds-number wind tunnel was performed to validate the basic wall corrections used to reduce the wind tunnel data, to examine the spatial variation of the interference field, and to evaluate mounting system interference effects (Curtin [9]). The model is mounted at the tunnel centreline using a floor-mounted strut system and was analysed at two angles of attack, 6 and 15 deg. A side view of the panelling, Figure 2.35, shows the wing-body-nacelle model at 15 deg, the support strut, strut windshield,

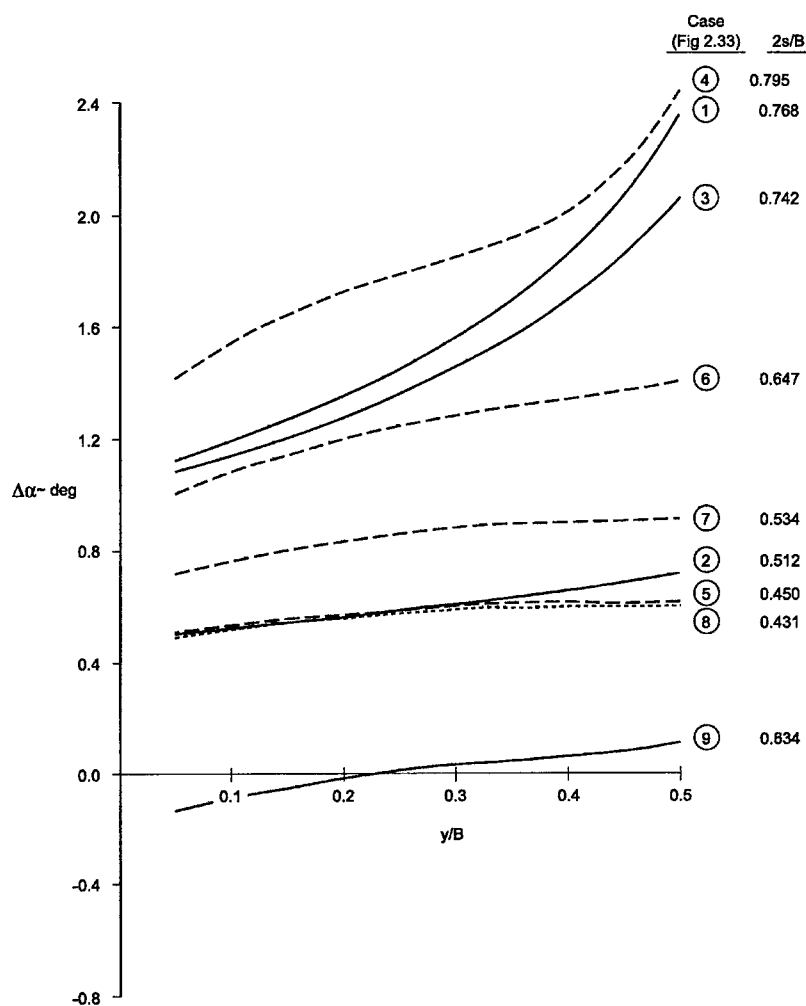


Figure 2.34 : Spanwise Variation of Upwash Interference (Amonlirdviman [4])

and floor and ceiling locations. The pitch link was not included in the panelling. The interference upwash angle and dynamic pressure ratio for a case with no mounting system, Figure 2.36, exhibit considerable variation over the wing planform. Upwash spans a range of over 1 deg from the leading edge of the wing root to the wingtip, with the tip at a higher angle of attack (therefore prone to premature stall in the tunnel relative to free air). The spanwise variation of blockage interference likewise increases the effective tip loading relative to free air. The span load in the tunnel reflects these effects, Figure 2.37. The interference velocity components, both streamwise and upwash, were evaluated at the 3/4 mean aerodynamic chord location. The streamwise interference velocity at this point was found to be different for the two angles of attack, with dynamic pressure ratios of 1.0093 and 1.0121, respectively. Using these values to compute model lift coefficient at each condition, the resulting lift interference parameter is $\delta_0=0.1394$. These estimates compare to values of $\delta_0=0.1463$ and dynamic pressure ratio=1.0147 (independent of angle of attack) derived by classical means.

An example of the use of CFD to evaluate test section design concerns the effect of corner fillets on wall interference. The interference of a transport half-model in a proposed large low-speed tunnel was evaluated using a panel code, Figure 2.38. Interference at the model centre is reasonably represented by classical methods, Figure 2.39; even the incremental differences due to fillet size are qualitatively captured. Interference at the wing, Figure 2.40, shows significant deviation of interference from

centreline values, especially for the wingtip tip. Interference along an axial line through the mean aerodynamic chord is very similar to centreline values. Interference along an axial line near the wingtip reflects the calculated spanwise variation of interference.

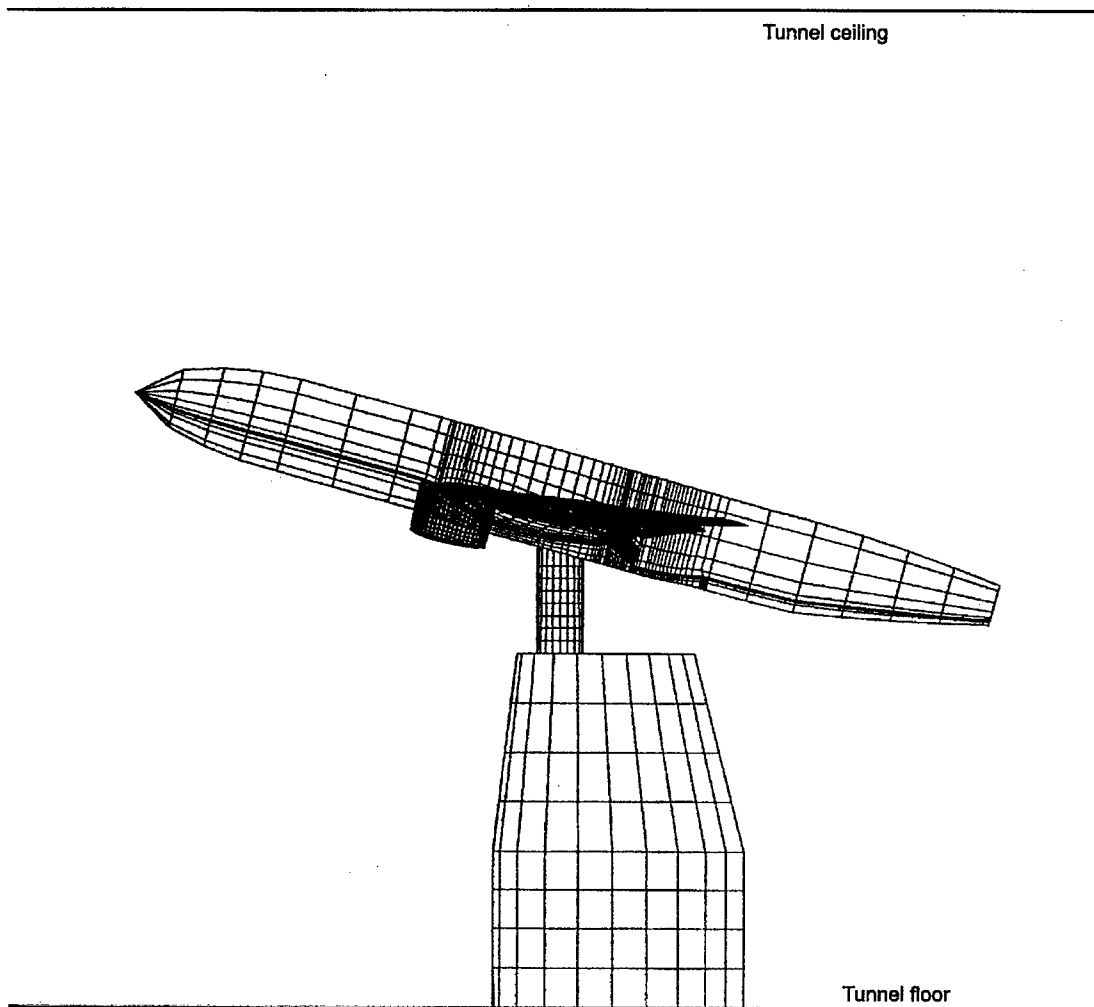
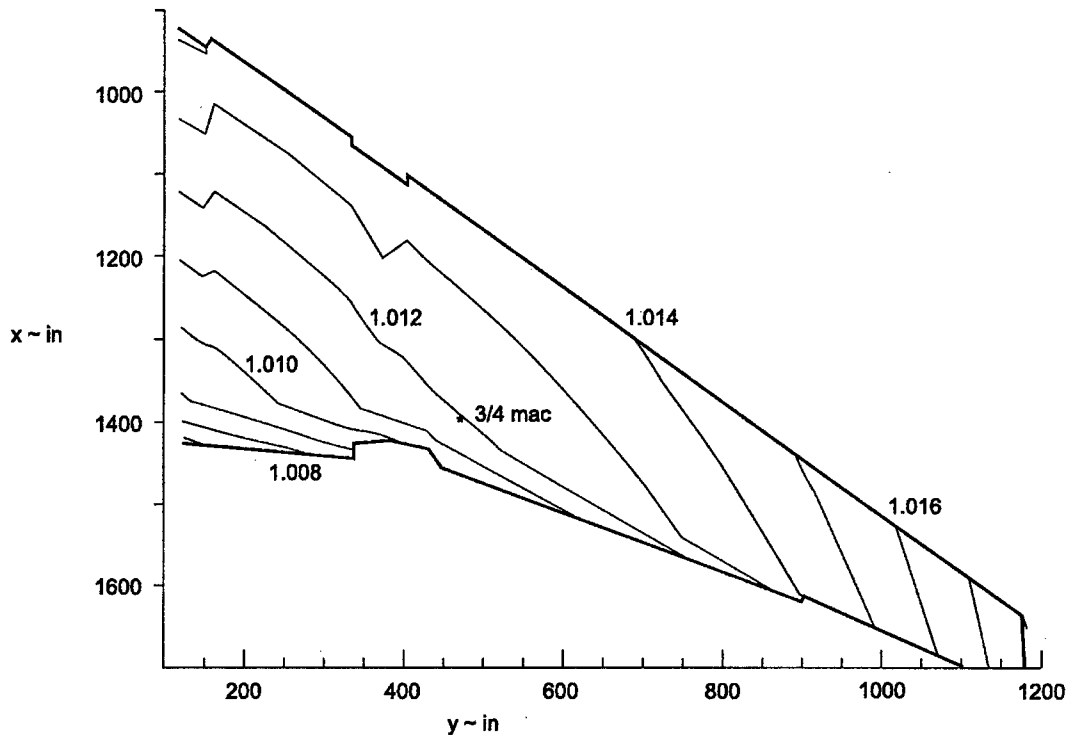
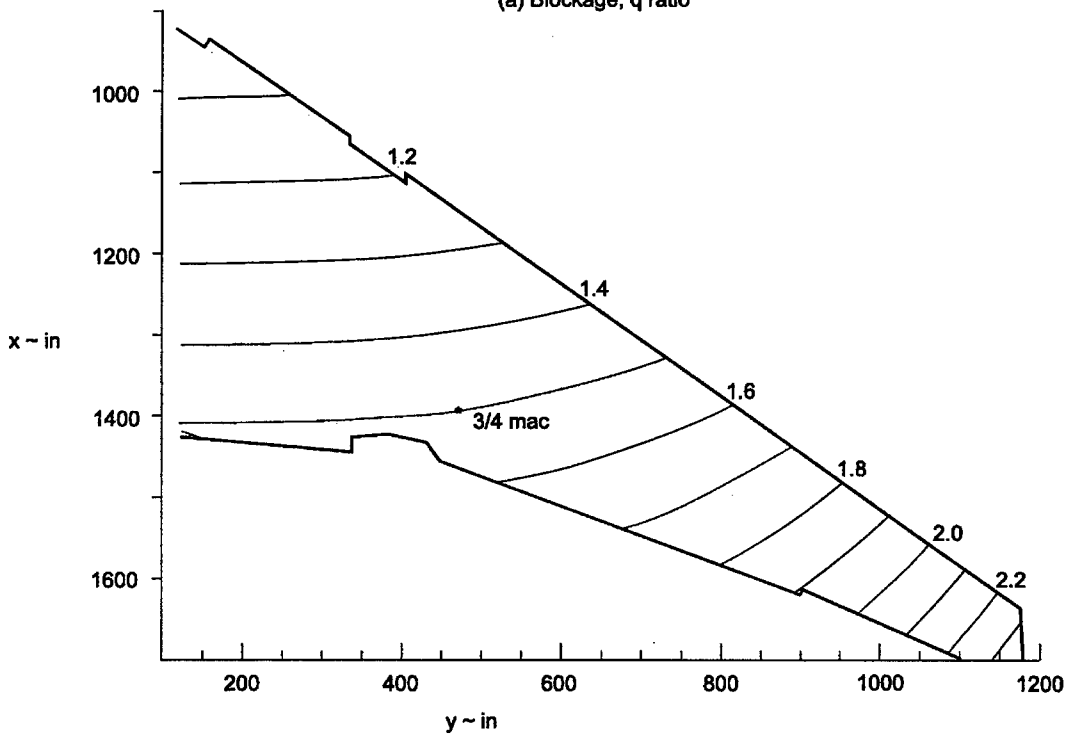


Figure 2.35 Panelling of Transport Model in DRA 5-m Wind Tunnel with Support Strut and Windshield (Curtin [9])

(a) Blockage, q ratio

(b) Upwash, degrees

Figure 2.36 : Interference of Transport Model in DRA 5-m Wind Tunnel;
 $C_L \approx 2.3$, $M=0.25$, $2s/B=0.76$ (Curtin [9])

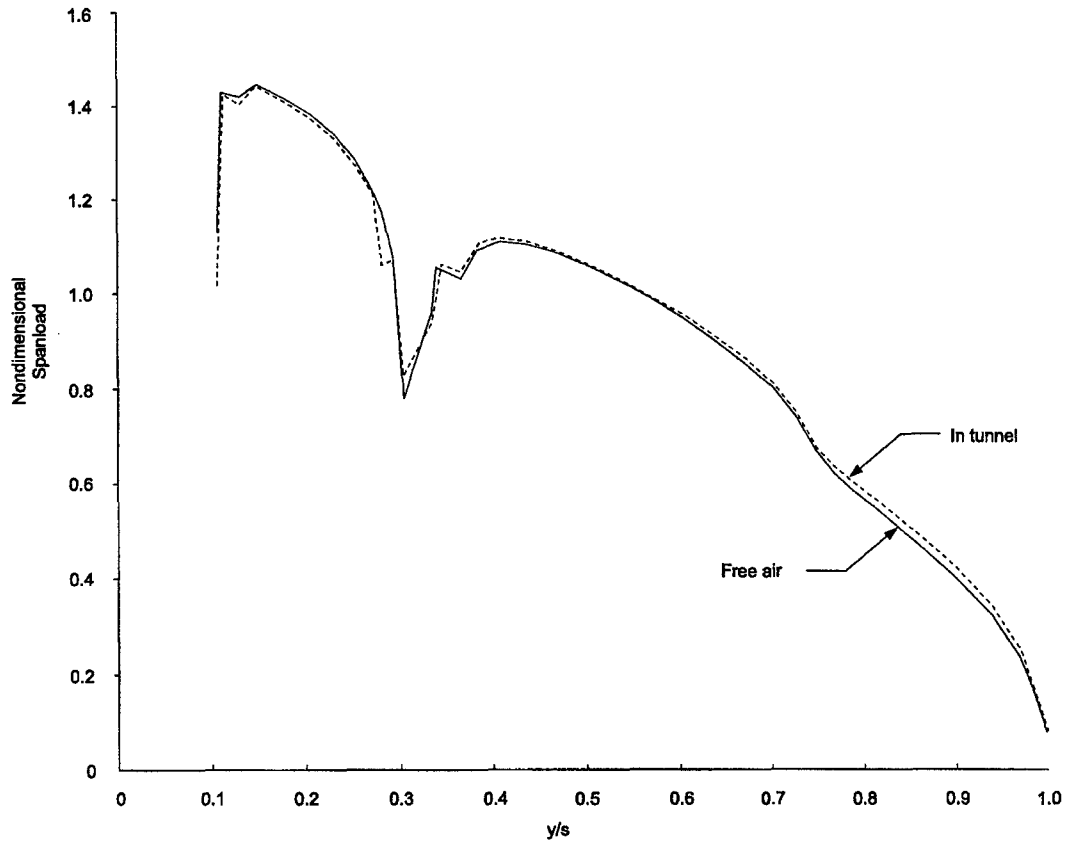


Figure 2.37 Span Load of Transport Model in DRA 5-m Wind Tunnel; $C_L \approx 2.3$, $M=0.25$, $2s/B=0.76$ (Curtin [9])

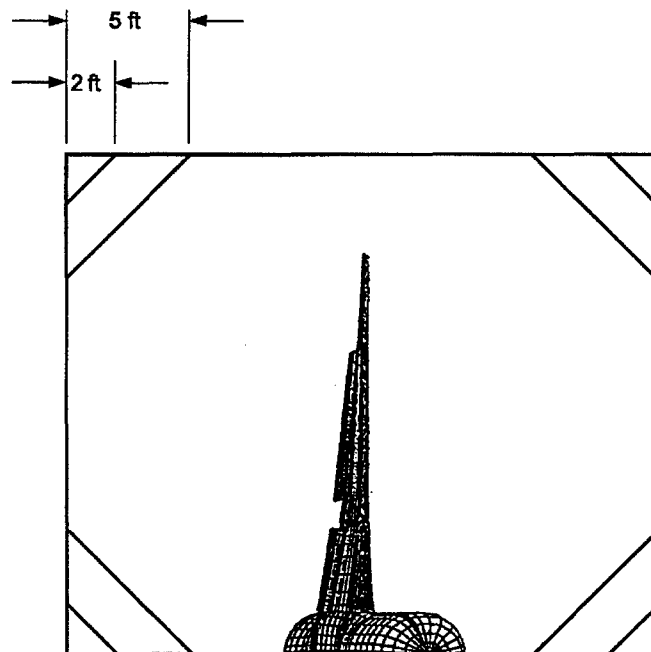


Figure 2.38 Low-Speed Wind Tunnel Corner Fillet Study; $B = 40$ ft, $H = 24$ ft

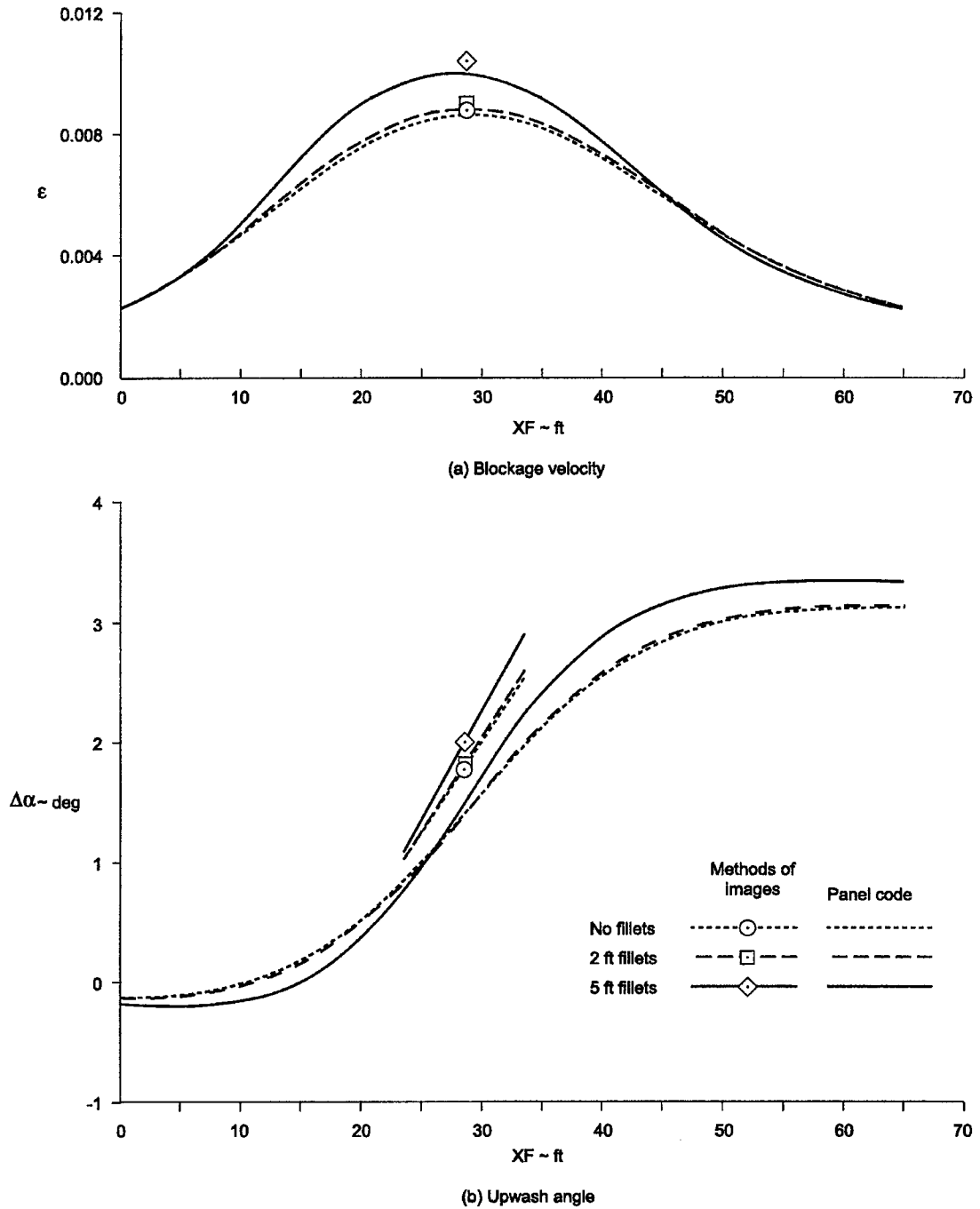
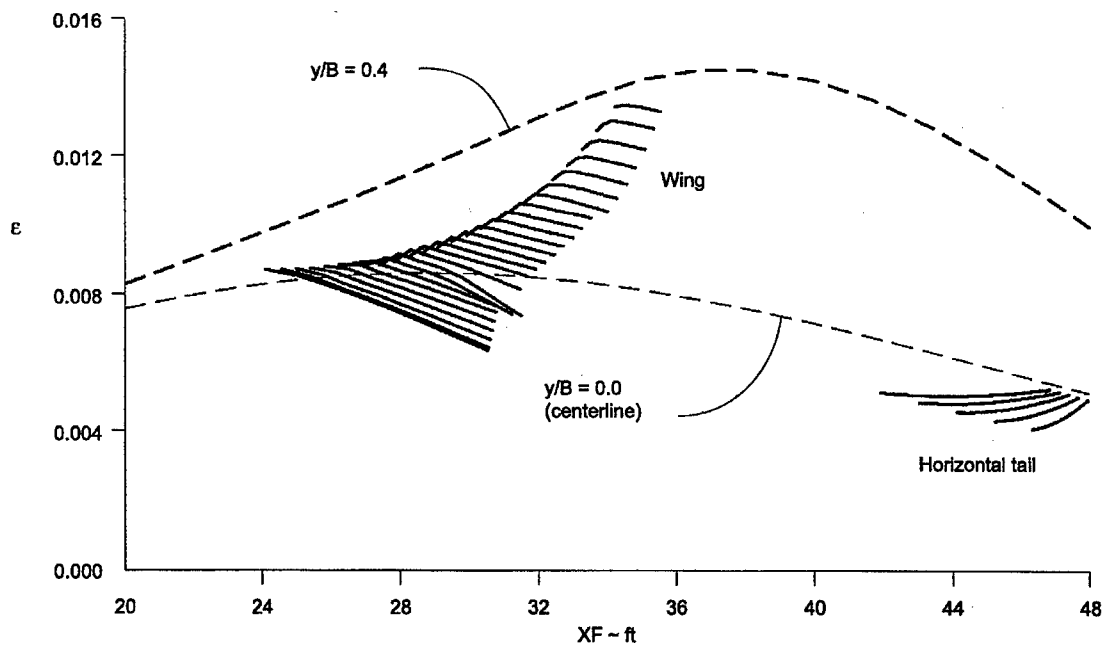
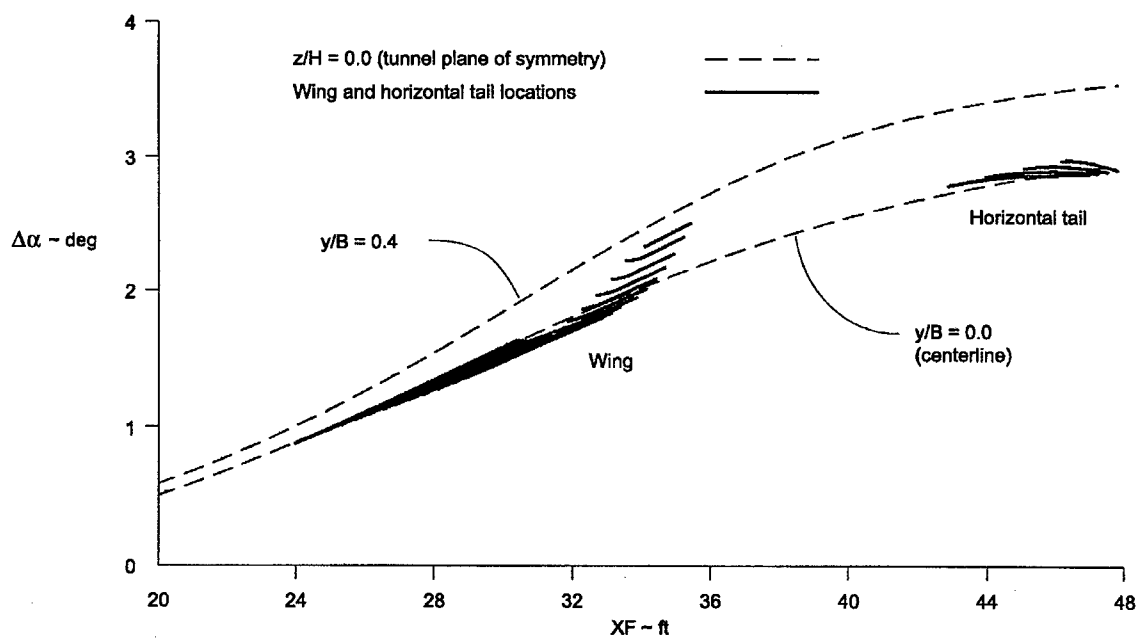


Figure 2.39 : Effect of Corner Fillets on Centreline Interference of a Subsonic Transport Model in a Closed-Wall Tunnel; $B/H = 5/3$, $S = 129.43 \text{ ft}^2$, $2s/B = 0.8$, $C_L = 1.86$



(a) Blockage Interference



(b) Upwash Interference

Figure 2.40 Wall Interference Variation at the Wing of a Subsonic Transport in a Closed-Wall Tunnel (No Corner Fillets); $B/H = 5/3$, $S = 129.43 \text{ ft}^2$, $2s/B = 0.8$, $C_L = 1.86$

2.3.6 SUMMARY OF PANEL METHODS

Panel methods for closed-wall tunnels have been used in a broad range of applications. Correspondence of wall interference from panel methods and classical methods has been demonstrated for small models. Unless extreme accuracy is required, classical methods are adequate for small models. The distribution of interference for large models (with no substantial separated flow) is credibly represented by panel methods at low subsonic Mach numbers, though in extreme cases the correctness of the flow field may be in question. The degree of correctness may be assessed by examination of the interference flow field. A computational approach for dealing with such issues has emerged as a force-correction method (Rueger et al. [32]) whereby CFD produces incremental corrections to model integrated forces and moments. To the extent that both the flow physics and the wall boundary conditions are accurately modelled, this approach can extend the correctness of model data beyond the boundaries of linear theory.

The use of panel methods to predict wall interference has in many cases supplanted classical techniques for closed-wall tunnels. The use of CFD for wall interference evaluation has further evolved along two parallel and complementary lines: more accurate specification of the wall boundary conditions and more accurate representation of the fluid physics. Wall boundary condition descriptions have moved toward one- and two-variable methods described in Chapter 4. Improved flow physics modelling includes the treatment of separated wakes (Chapter 6), vortex wake relaxation techniques, and the inclusion of compressibility in the flow equations for high-speed flows (Chapter 5). Such advanced methods are required for accurate interference predictions when these flow phenomena dominate the flow near a model that is "not small" relative to the tunnel. These methods are characterised by increased computational complexity and the requirement of measurements at the walls. Their use may also surrender the simplicity of the principle of superposition, a significant feature of linear potential flow. The success of panel methods over a wide range of subcritical flow conditions suggests their use not only in routine testing applications within their accepted range of validity, but also as a touchstone against which advanced methods may be tested.

2.4 CLASSICAL CORRECTIONS FOR OPEN TEST SECTIONS

2.4.1 INTRODUCTION

When Ludwig Prandtl started scientific aerodynamic work in wind tunnels about in 1915 at Göttingen, he designed his first wind tunnel with an open test section and a circular nozzle with 2.24 m exit diameter. Without doubt the open test section offers some advantages to the wind tunnel engineer. He enjoys the free accessibility to the test section flow, the easy installation of model suspensions and the simple installation of flow survey probes.

Nevertheless some twenty years later a different and more modern wind tunnel design standard was set mainly by Frank Wattendorf in the United States, which heavily influenced wind tunnel design all over the world. The closed test section was introduced. The advantage of a reduced power consumption, improved flow quality due to the smooth flow at the walls and a more precisely defined boundary condition of the test section flow, which made more precise wall corrections possible, outweighed the disadvantage of less comfortable accessibility. So today the closed wall test section dominates at least the aviation wind tunnel design. For a long time in Germany this was not the case. The authority of Ludwig Prandtl was so strong, that even the first low speed tunnels built in Germany after the war (and after the death of Ludwig Prandtl !) in about 1955 still were designed with open test sections.

For identical model dimensions generally the wall corrections are smaller (and have opposite sign) for open test sections than for closed wall test sections. Nevertheless the closed wall offers more precise wall corrections because of the more precise definition of the wall boundary condition.

Open test sections are still widely used in the automotive industry. The simple reason for the preference of the open test section is that automotive engineers prefer to test full scale cars instead of down-scaled models. Nevertheless for financial reasons these automotive tunnels are built too small at least according to the standards of aeronautical aerodynamicists. In a closed test section this size of „models“ would result in severe flow field disturbance or even flow breakdown. The open test section is more forgiving and allows meaningful measurements even with blockage ratios, which are never used for aeronautical testing. In consequence the automotive engineers have a lot of trouble with wall corrections for large blockage ratios with bluff bodies, but this is not the general subject of this AGARDograph. For a more detailed analysis of bluff body corrections see chapter 6 of this AGARDograph.

In the recent past a new challenge in the wind tunnel technology brought the open test section back into the wind tunnel engineers' field of vision. Aeroacoustic testing becomes a more and more important part of low speed wind tunnels work load. At least at the moment the open test section, which shows no reflection of acoustic waves from the test section walls, is superior for aeroacoustic testing. It is easy, to equip the plenum around the open test section with sound-absorbing walls, which results in a very quite wind tunnel. Fortunately these aeroacoustic tests do not require ultra-precise wall corrections.

So the open test section wall corrections are less important at least for the aeronautical wind tunnel work and in this AGARDograph only a simple overview is given, which is more or less a condensed version of the open test section comments in the AGARDograph 109 [13].

In the wind tunnel literature sometimes the „¾ open wind tunnel“ is mentioned. In most cases this term is used for automotive tests in open test sections with a closed floor, which represents the road. With respect to wall corrections the term „¾ open test section“ is misleading. The closed floor of the test section is not a wall, which produces wall interference, but is part of the model configuration. So this test set-up is nothing else than an open test section. All formulas or methods for wall corrections can be

applied to this test set-up, if the total arrangement is reflected against the floor. The resulting test section with twice the height and two cars and a horizontal symmetry plane in the middle of the test section can be treated with normal open test section correction methods.

The basic principles of the classical wall corrections outlined in chapter 2.1 are valid for the closed test section and for the open test section as well. As mentioned already in chapter 2.1.3 the only difference is the wall boundary condition. The boundary condition of the closed wall is the non-existence of velocity components normal to the wall, which results in

$$\frac{\partial \varphi}{\partial n} = 0 \quad (2.93)$$

The boundary condition of the open test section is a constant pressure at the jet boundary, which corresponds to the static pressure of the plenum surrounding the test section. This boundary condition results in

$$\frac{\partial \varphi}{\partial x} = 0 \quad (2.94)$$

In the AGARDograph 109 some remarks and formulas are given for the corrections of two dimensional wings spanning open test jets. Since test set-ups like this totally disappeared from the aeronautical wind tunnel testing practice, this case is not mentioned here.

2.4.2 LIFT INTERFERENCE

The equations 2.27, 2.28 and 2.29 are valid for open test sections as well. According to the work of Theodorsen (1931) the result for the upwash interference is

$$\delta_o = \delta(0,0,0) = \frac{A}{8\pi} \sum_{\substack{n=-\infty \\ \text{excluding} \\ n=m=0}}^{n=\infty} \sum_{m=-\infty}^{m=\infty} (-1)^m \frac{m^2 A^2 - n^2}{[m^2 A^2 + n^2]^2} \quad (2.95)$$

The analogous expression for the upwash gradient at the model location becomes :

$$\delta_1(0,0,0) = \left. \frac{\partial \delta}{\partial(x / \beta H)} \right|_{0,0,0} = \frac{A}{8\pi} \sum_{\substack{n=-\infty \\ \text{excluding} \\ n=m=0}}^{n=\infty} \sum_{m=-\infty}^{m=\infty} (-1)^m \frac{m^2 A^2 - 2n^2}{[m^2 A^2 + n^2]^{\frac{5}{2}}} \quad (2.96)$$

The application of upwash corrections is described in section 2.2.1.4. The correction formulas are :

$$C_{Lcorr} = C_{Lunc} \cos \Delta\alpha - C_{Dunc} \sin \Delta\alpha \cong C_{Lunc} \quad (2.1)$$

$$C_{Dcorr} = C_{Dunc} \cos \Delta\alpha + C_{Lunc} \sin \Delta\alpha \cong C_{Dunc} + C_{Lunc} \Delta\alpha \quad (2.2)$$

$$\Delta\alpha = \delta_o \frac{S}{C} C_{Lunc} \quad (2.3)$$

The additional correction for the streamline curvature is given by equation 2.39 for the angle of attack :

$$\alpha_{corr} = \alpha_{unc} + \Delta\alpha + \Delta\alpha_{sc} = \alpha_{unc} + \left(\delta_o + \frac{\bar{c}}{2\beta H} \delta_1 \right) \frac{SC_{Lunc}}{C} \quad (2.4)$$

and by equation 2.40 for the pitching moment :

$$\Delta C_M = \delta_1 \frac{\bar{c}}{16\beta H} \frac{SC_{Lunc}}{C} \frac{\partial C_L}{\partial \alpha} \tag{2.5}$$

Figure 2.41 [13] shows the lift interference on small wings in open and closed rectangular tunnels for comparison. In this figure the lift interference parameter is shown also for test sections with top and bottom wall only (type 3) and for test sections with side walls only (type 4). Such test sections are no longer used in wind tunnel practice.

For wings with finite span the lift interference parameter δ is given in Figure 2.42 ¹. These data are valid for uniform spanwise loading of the wings. The lift interference parameter is plotted against the „Effective span/Tunnel width“ ratio; the parameter λ is the „height/width“ ratio of the open test section.

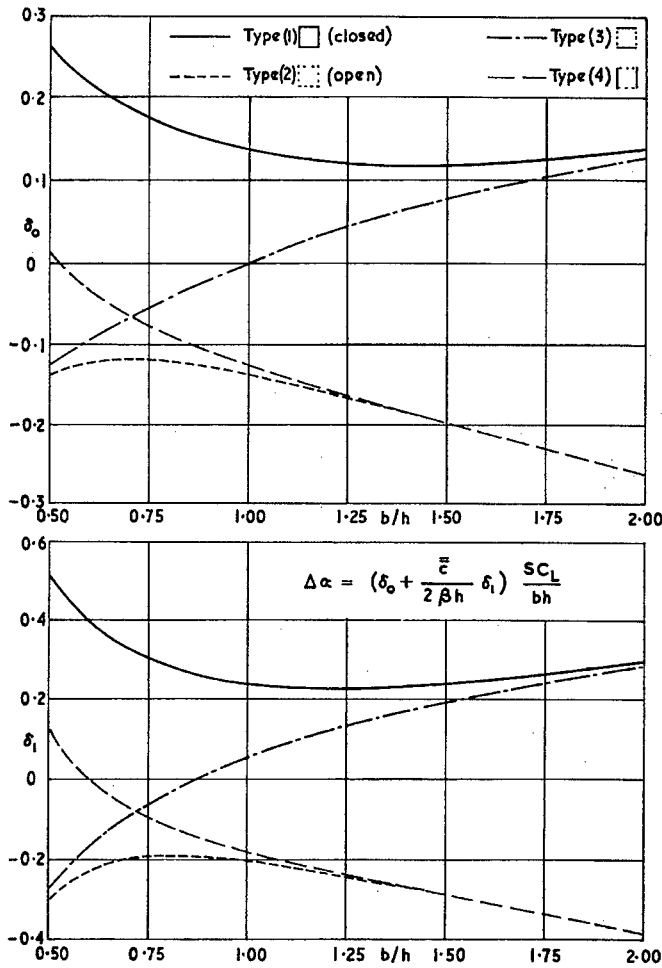


Figure 2.41 : Lift interference on small wings in rectangular tunnels

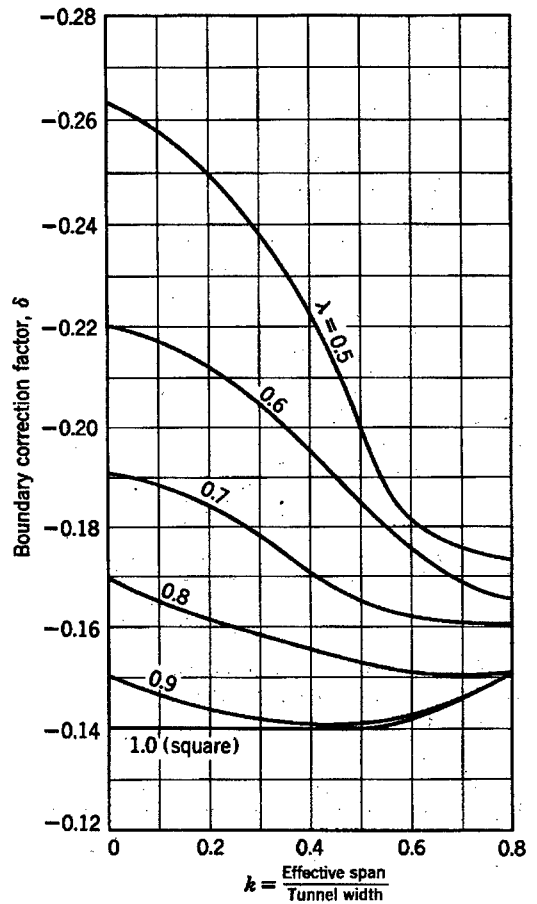


Figure 2.42 : Values for δ for a wing with uniform loading in an open rectangular jet

If the wing is displaced above or below the centreline of an open test section, the lift interference parameter may be taken from Figures 2.43 and 2.44. Figure 2.43 is valid for a square jet. Figure 2.44 gives the lift interference parameter for an open test section with a height to width ratio of 0.5.

¹ The Figures 2.42 to 2.50 were taken from [31]

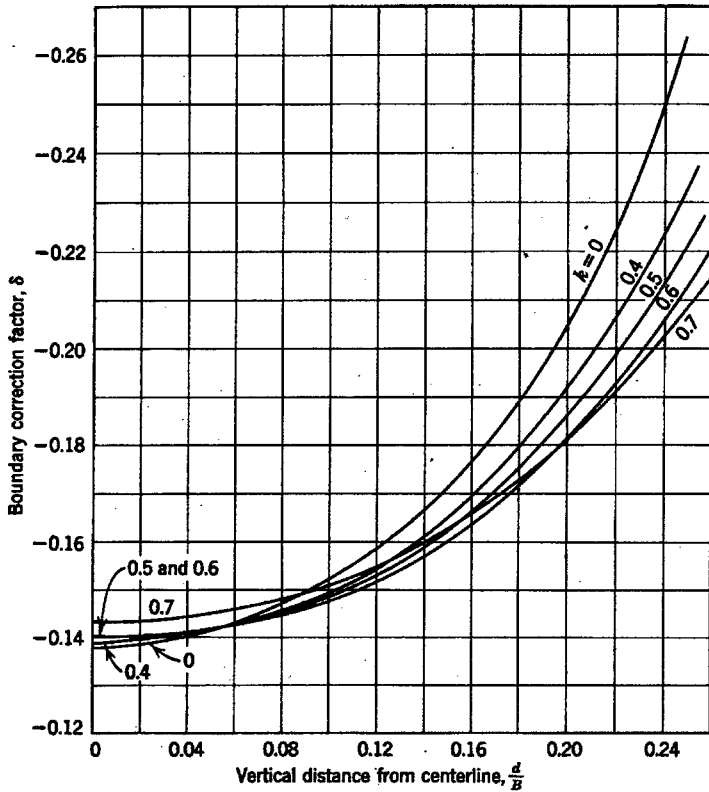


Figure 2.43 : Lift interference parameter for wings displaced above or below the test section centreline. (Square jet)

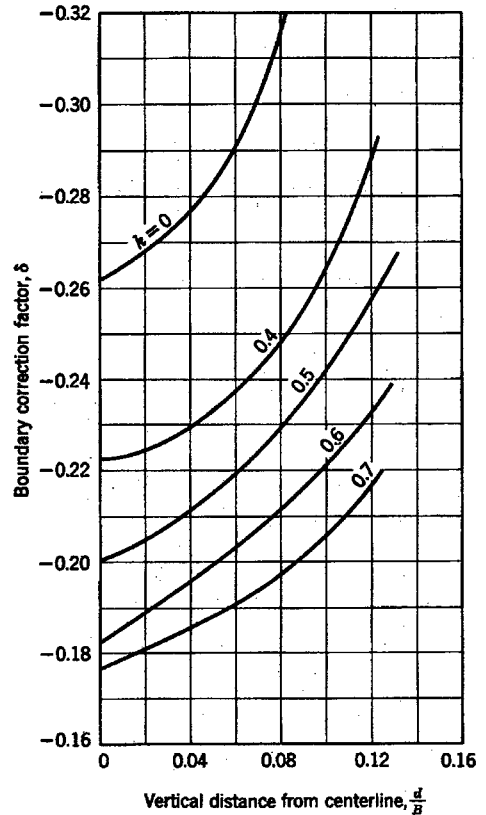


Figure 2.44 : Lift interference parameter for wings displaced above or below the tunnel centreline. Rectangular jet, $\lambda = 0.5$

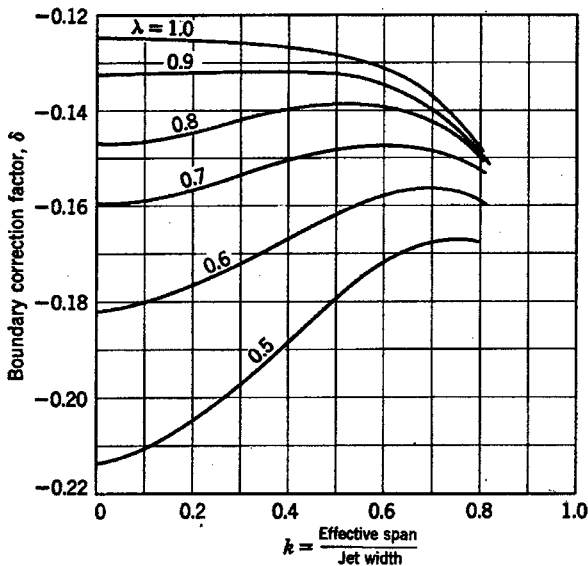


Figure 2.45 : Lift interference parameter for a wing with uniform loading in an open elliptical test section

A limited number of old wind tunnels with open circular or elliptic test sections are still in operation. For wings on the tunnel centreline with uniform loading Figure 2.45 gives the lift interference parameter for this test section configuration. In this figure the parameter $\lambda = 1.0$ designates a circular jet.

Figure 2.46 gives the lift interference parameter for elliptic open test sections with a width/height ratio of 2 : 1 for wings with uniform loading displaced from the centreline of the test section. Finally Figure 2.47 gives the lift interference parameter for wings with elliptic loading in circular and elliptic open test sections.

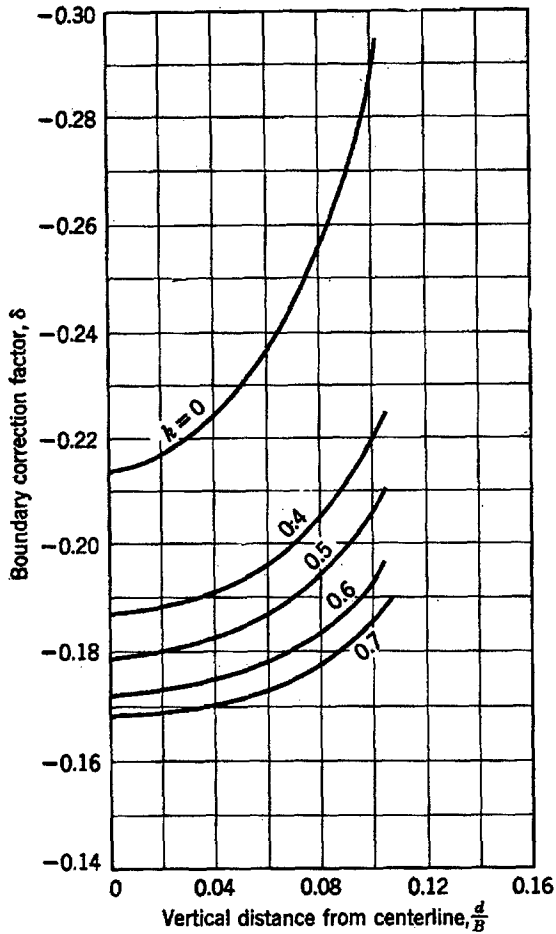


Figure 2.46 : Lift interference parameter for a wing with uniform loading displaced from the centreline of an open 2 : 1 elliptic test section.

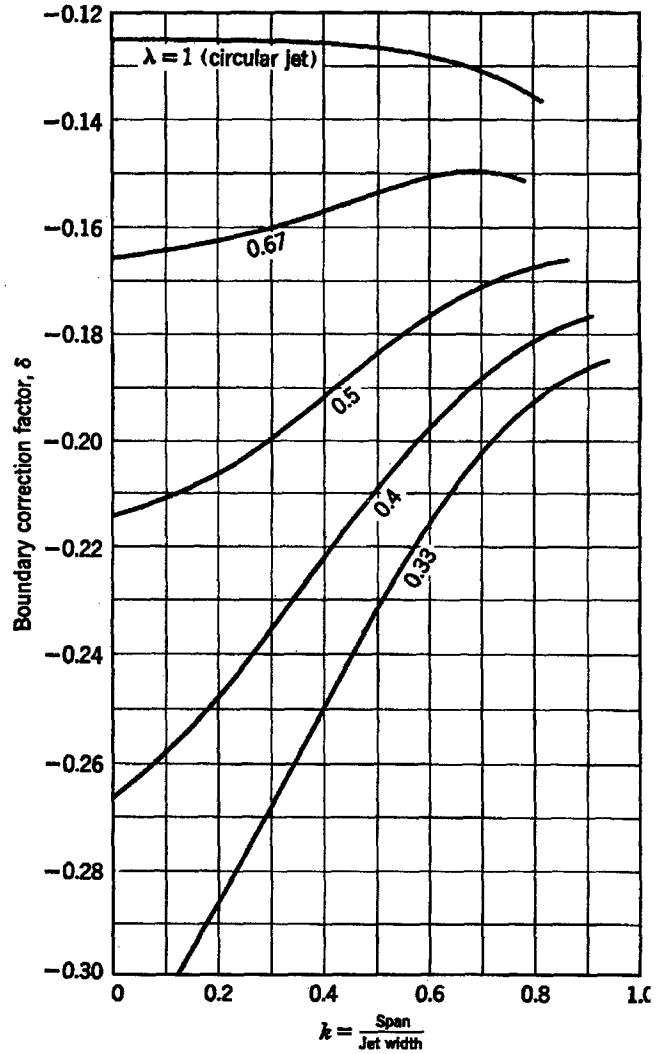


Figure 2.47 : Lift interference parameter for wings with elliptic loading in open circular/elliptic test sections

For the downwash correction at the tail of a model an additional correction factor τ_2 can be defined. At a distance l_1 behind the quarter-chord line of the wing the boundary induced downwash w_k is :

$$w_k = \delta \frac{S}{C} C_{LW} (1 + \tau_2) V \tag{2.97}$$

For open test sections, some doubts exist about the validity of this correction if the tail length of the model is more than 40 % of the test section width.

Values for the downwash correction factor τ_2 are given in the Figures 2.48 to 2.51.

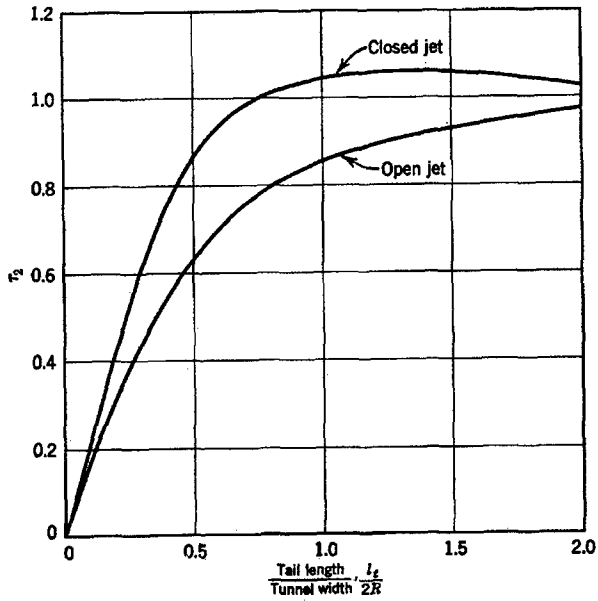


Figure 2.48 : Correction factor τ_2 for open and closed circular test sections

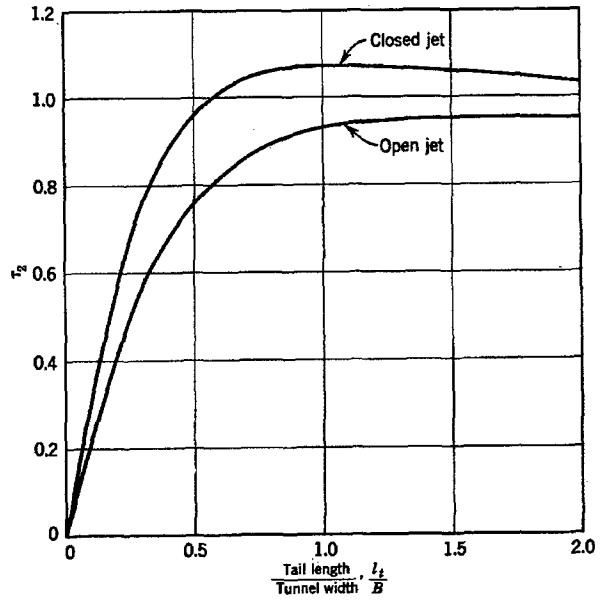


Figure 2.49 : Correction factor τ_2 for open and closed elliptic test sections

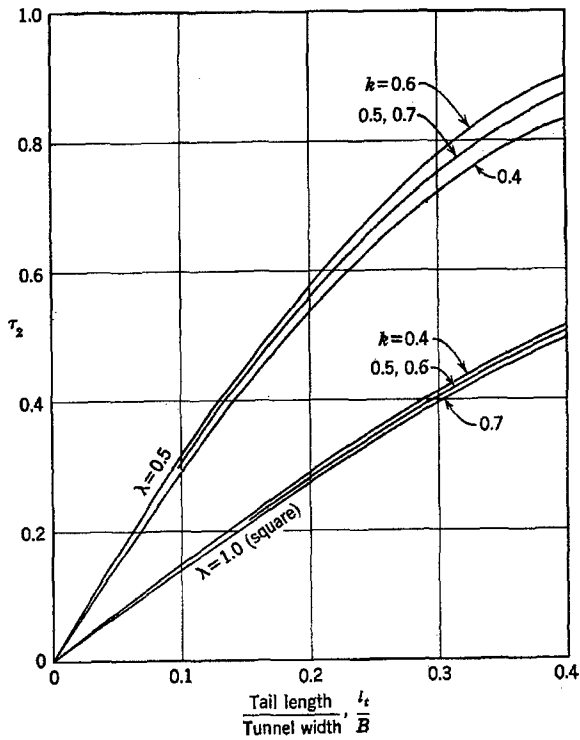


Figure 2.50 : Correction factor τ_2 for two open rectangular test sections, wing on centreline, tail on centreline

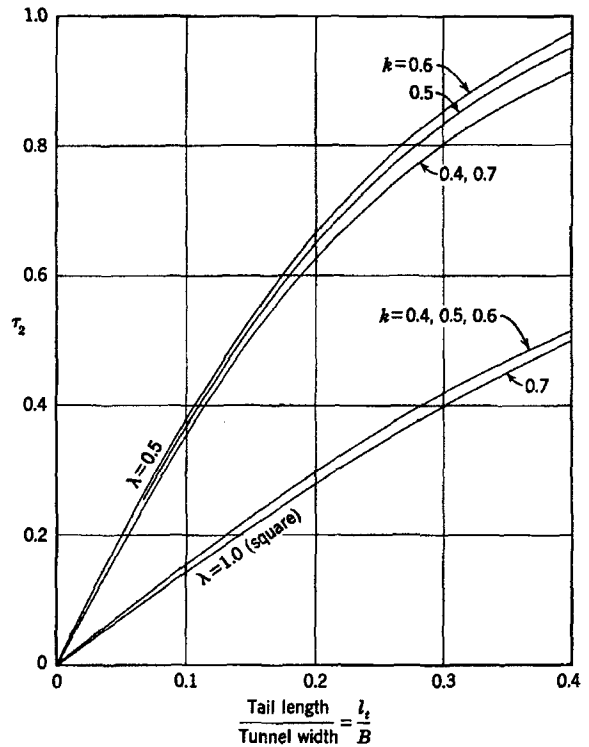


Figure 2.51 : Correction factor τ_2 for two open rectangular test sections, wing on centreline, but tail 0.1 b above or below centreline

2.4.3 BLOCKAGE CORRECTION

As for a closed tunnel, the boundary condition of a small model at the centre of a square open jet can be represented by an infinite set of images. In this case the signs of the doublets alternate, so the interference velocity at the models position is smaller than in the case of closed walls and of opposite sign. For the square open test section case in [13] (after Lock [23]) equation (2.98) is given, which in terms of model volume and with allowance for compressibility effects results in the simple equation (2.99).

$$\varepsilon_s = \tau \left(\frac{A_m}{h^2} \right)^{3/2} \lambda_3 \quad (2.98)$$

$$\varepsilon_s = -0.211 \frac{V}{\beta^3 h^3} \quad (2.99)$$

For rectangular open test sections Wuest [37] evaluated values for τ :

$$\tau = \frac{1}{2\pi^{3/2}} \sum_{-\infty}^{\infty} \sum_{-\infty}^{\infty} (-1)^{m+n} \left(\frac{bh}{m^2 b^2 + n^2 h^2} \right)^{3/2} \quad (2.100)$$

The results are plotted in Figure 2.52¹.

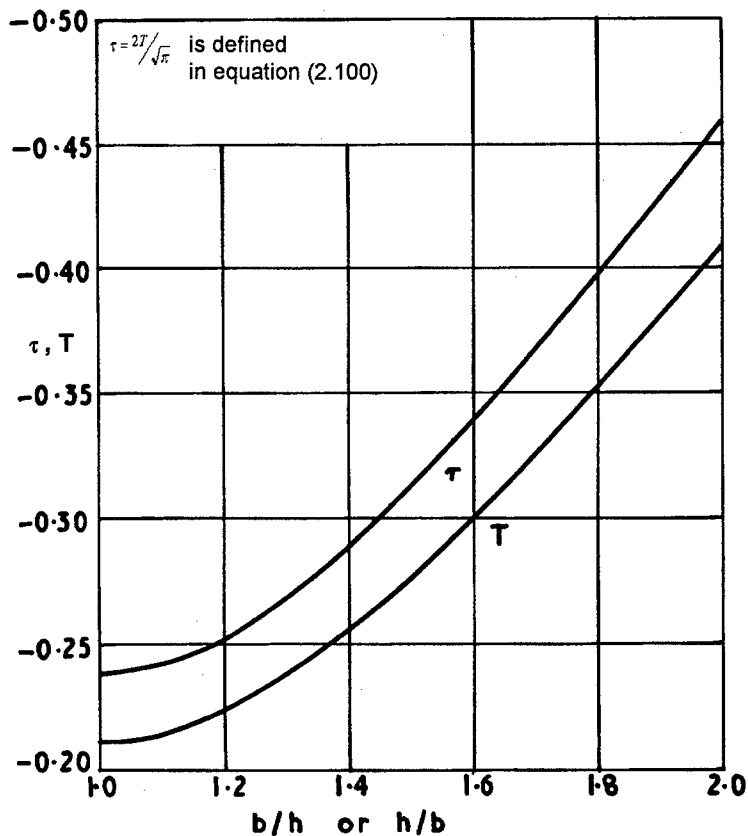


Figure 2.52 : Tunnel-shape parameters for small models in open rectangular tunnels

¹ The Figures 2.52 and 2.53 are taken from [13]

For circular open test sections Lock [22] gave an equation

$$\varepsilon_S = -0.206 \left(\frac{A_m}{C} \right)^{3/2} \lambda_3 \quad (2.101)$$

where λ_3 is given in Figure 2.53.

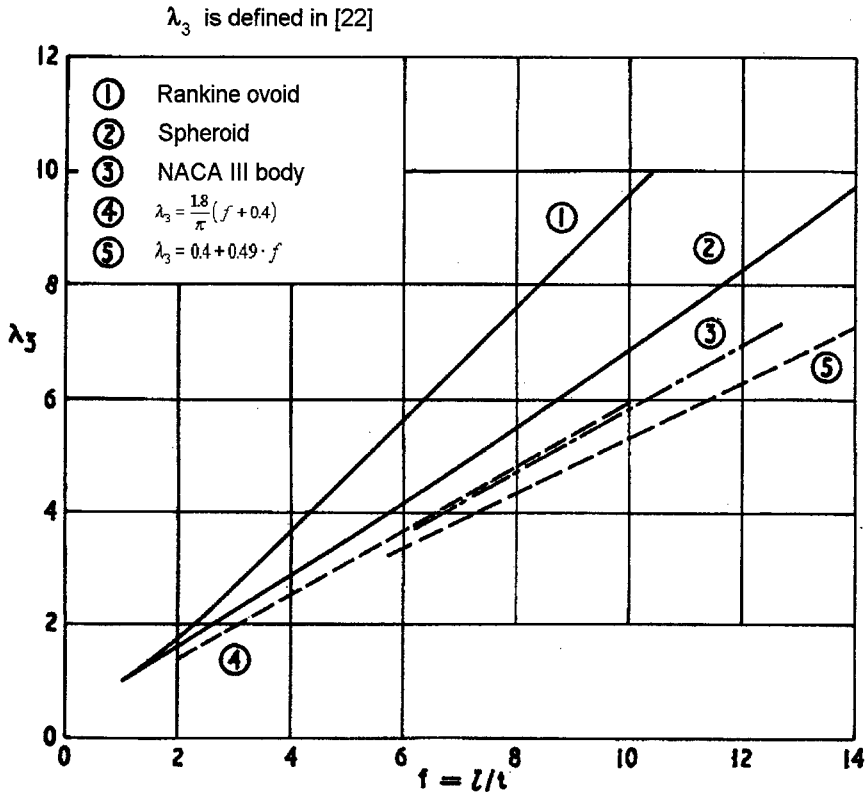


Figure 2.53 : Body-shape parameter

A more simple equation for circular open test sections in terms of Mach number, tunnel diameter and model volume is

$$\varepsilon_S = -0.0333 \frac{V}{R^3} \cdot \frac{1}{\beta^3} \quad (2.102)$$

For the few tunnels with elliptical open test sections still in operation one may use the equation

$$\varepsilon_S = (T_R + 0.029) \left(\frac{1}{C} \right)^{3/2} \frac{V}{\beta^3} \quad (2.103)$$

where T_R can be taken from Figure 2.52 for a rectangular open jet with breadth/ height ratio equal to m/n and $C = \frac{1}{4} \pi m n$.

2.4.4 WAKE CORRECTION

Little is known about wake blockage effects in open test sections; in most cases they are considered to be negligible. A sophisticated theoretical investigation is hardly worthwhile, since in any case the wake blockage effects will be disturbed by the wind tunnels individual collector inlet effects.

NOMENCLATURE FOR CHAPTER 2

A	=	effective cross-sectional area of 2D model = A_0 + added-mass area
A	=	rectangular tunnel aspect ratio = B/H
A_0	=	dimensional cross-sectional area of 2D model
A_m	=	maximum transverse cross-section of model
a	=	body radius
B	=	tunnel breadth
C	=	cross-sectional area of test section
C_D	=	drag coefficient
C_d	=	drag coefficient for 2D model
C_L	=	lift coefficient
C_{LW}	=	lift coefficient of wing
C_l	=	lift coefficient for 2D model
C_M	=	pitching moment coefficient
C_p	=	pressure coefficient
c	=	airfoil chord
\bar{c}	=	mean aerodynamic chord
d	=	distance of 2D vortex from the floor
f	=	body fineness ratio
H	=	tunnel height
K	=	nondimensional body shape factor; nondimensional factor for interference parameters; singularity strength
k	=	base pressure parameter
k	=	model span ratio $\left(\frac{\text{Effective span}}{\text{Tunnel width}}\right)$
L	=	length; wing lift
M	=	Mach number
m	=	source strength
m	=	major axis of elliptical tunnel
n	=	spatial co-ordinate normal to the test section wall
n	=	minor axis of elliptical tunnel
p	=	static pressure
q	=	dynamic pressure
Re	=	Reynolds number
R_{max}	=	maximum body radius
r	=	cylindrical co-ordinate = $(y^2 + z^2)^{1/2}$
S	=	wing reference area
s	=	wing or vortex semi-span
s	=	source-sink separation distance for Rankine ovals and bodies

T	=	static temperature
t	=	maximum thickness
U	=	streamwise velocity
U_{∞}	=	upstream reference velocity
u	=	perturbation x-velocity
\mathbf{V}	=	total velocity vector = $\nabla\Phi$ for potential flow
V	=	velocity magnitude
V	=	effective model volume in 3D = V_0 + added-mass volume
V_0	=	dimensional volume of 3D model
v	=	perturbation y-velocity
w	=	perturbation z-velocity
w_k	=	downwash correction at tail position
x	=	streamwise spatial co-ordinate
y	=	spanwise (or lateral) spatial co-ordinate
z	=	vertical spatial co-ordinate

Greek Symbols

α	=	angle of attack
β	=	Prandtl-Glauert compressibility factor = $(1 - M^2)^{1/2}$
γ	=	vortex strength in 2D = $1/2 U_{\infty} c C_L$
Γ_s	=	vortex strength in 3D = $1/4 U_{\infty} S C_L$
δ	=	lift interference parameter
δ_0	=	lift interference parameter evaluated at the model centre
δ_e	=	upwash interference due to blockage
δ_1	=	streamwise curvature interference parameter
ε	=	blockage interference ratio = u_i / U_{∞}
ε_{δ}	=	streamwise interference due to lift
ζ	=	nondimensional vertical co-ordinate = z / L_{ref}
θ	=	blockage factor for bluff-body flow
Λ	=	wing sweep angle
λ	=	body shape factor
λ	=	test section height/width ratio
μ	=	doublet strength
η	=	nondimensional spanwise co-ordinate = y / L_{ref}
η	=	empirical factor for separated wake interference
ξ	=	nondimensional streamwise co-ordinate = $x / \beta L_{ref}$
ρ	=	fluid density
σ	=	nondimensional wing or vortex semi-span
τ	=	tunnel shape factor
Φ	=	total velocity potential

ϕ	=	perturbation potential
ϕ_m	=	perturbation potential due to the model
ϕ_w, ϕ_i	=	perturbation potential due to the walls (= interference potential)

Subscripts

b	=	base
c	=	corrected
$corr$	=	corrected
i	=	interference
m	=	model
n	=	normal
ref	=	reference
unc	=	uncorrected
w	=	walls

REFERENCES FOR CHAPTER 2

- [1] AGARD, *Wind Tunnel Corrections for High Angle of Attack Models*, papers presented in Munich, Germany, May 1980, AGARD R-692, February 1981.
- [2] AGARD, *Wall Interference in Wind Tunnels*, papers presented in London, UK, May 1982, AGARD CP-335, September 1982.
- [3] Allen, H. J. and Vincenti, W. G., *Wall Interference in a Two-Dimensional-Flow Wind Tunnel with Consideration of the Effect of Compressibility*, NACA Report 782, 1944.
- [4] Amonlirdviman, K., "Wind Tunnel Wall Interference Study Using A502 and Heyson's Wall Interference Code", unpublished analysis, August 1997.
- [5] Ashley, H. and Landahl, M., *Aerodynamics of Wings and Bodies*, Addison-Wesley Publishing Co., 1965.
- [6] Barnwell, R. W., "Similarity for Sidewall Boundary-Layer Effect in Two-Dimensional Wind Tunnels", *AIAA Journal*, Vol. 18, September 1980.
- [7] Barnwell, R. W. and Sewall, W. G., "Similarity Rules for Effects of Sidewall Boundary Layer in Two-Dimensional Wind Tunnels", paper 3 in AGARD CP-335, 1982.
- [8] Batchelor, G. K., "Interference on Wings, Bodies and Airscrews in a Closed Wind Tunnel of Octagonal Section", Report ACA-5 (Australia), 1944.
- [9] Curtin, M. M., "DRA Wall Effects on High Lift Model", unpublished analysis, April 1994.
- [10] Engineering Data Sciences Unit, "Upwash Interference for Wings in Solid-Liner Wind Tunnels Using Subsonic Linearised-Theory", ESDU 95014, October 1995.
- [11] Fiddes, S. P. and Gaydon, J. H., "A Hybrid Panel/Image Method for Calculating Wall Constraint Effects in Subsonic Wind Tunnels", ICAS-94-3.3.2, 1994.
- [12] Frink, N. T., "Computational Study of Wind-Tunnel Wall Effects in Flow Field around Delta Wings", AIAA 87-2420, August 1987.
- [13] Garner, H. C., Rogers, E.W. E., Acum, W. E. A., and Maskell, E. C., "Subsonic Wind Tunnel Wall Corrections", AGARDograph 109, October 1966.

- [14] GARTEUR Action Group AD (AG-02), "Two-Dimensional Transonic Testing Methods", GARTEUR TP-011, NLR TR 83086 U, July 1981.
- [15] Glauert, H., "Wind Tunnel Interference on Wings, Bodies, and Airscrews", ARC R&M No. 1566, 1933.
- [16] Goldstein, S., "Two-Dimensional Wind-Tunnel Interference", ARC R&M 1902, 1942.
- [17] Havelock, T. H., "The Lift and Moment on a Flat Plate in a Stream of Finite Width", Proc. Roy. Soc., Series A, Vol. 166, 1938.
- [18] Holst, H., "German Activities on Wind Tunnel Corrections," paper 4 in AGARD R-692, May 1980.
- [19] Holt, D. R. and Hunt, B., "The Use of Panel Methods for the Evaluation of Subsonic Wall Interference", paper 2 in AGARD CP-335, September 1982.
- [20] Joppa, R. G., *A Method of Calculating Wind Tunnel Interference Factors for Tunnels of Arbitrary Cross-Section*, NASA CR-845, July 1967.
- [21] Joppa, R. G., *Wind Tunnel Interference Factors for High-Lift Wings in Closed Wind Tunnels*, NASA CR-2191, February 1973.
- [22] Lock, C. N. H., "The Interference of a Wind Tunnel on a Symmetrical Body", ARC R&M 1275, 1929.
- [23] Lynch, F. T., Crites, R. C., and Spaid, F. W., "The Crucial Role of Wall Interference, Support Interference, and Flow Field Measurements in the Development of Advanced Aircraft Configurations", paper 1 in AGARD CP-535, October, 1993.
- [24] Magnus, A. E. and Epton, M. A., *PAN AIR - Computer Program for Predicting Subsonic or Supersonic Linear Potential Flow About Arbitrary Configurations Using a Higher Order Panel Method, Volume I, Theory Document (Version 1.0)*, NASA CR-3251, 1980.
- [25] Maskell, E. C., "A Theory of the Blockage Effects on Bluff Bodies and Stalled Wings in a Closed Wind Tunnel", ARC R&M No. 3400, November 1963.
- [26] Mokry, M., Chan, Y. Y., and Jones, D. J., edited by Ohman, L. H., "Two-Dimensional Wind Tunnel Wall Interference", AGARD AG-281, November, 1983.
- [27] Murthy, A. V., *Corrections for Attached Sidewall Boundary-Layer Effects in Two-Dimensional Airfoil Testing*, NASA CR-3873, February, 1985.
- [28] Murthy, A. V., *Effect of Aspect Ratio on Sidewall Boundary-Layer Influence in Two-Dimensional Airfoil Testing*, NASA CR-4008, September 1986.
- [29] Murthy, A. V., *A Simplified Fourwall Interference Assessment Procedure for Airfoil Data Obtained in the Langley 0.3-Meter Transonic Cryogenic Tunnel*, NASA CR-4042, January, 1987.
- [30] Murthy, A. V., "Correction for Aspect Ratio Effects in Airfoil Testing", DLR Report IB 222-90A15, March, 1990.
- [31] Pope, A. and Harper, J. J., *Low-Speed Wind Tunnel Testing*, John Wiley & Sons, Inc., New York, 1966.
- [32] Rueger, M. L., Crites, R. C., Weirich, R. F., Creasman, F., Agarwal, R. K., and Deese, J. E., "Transonic Wind Tunnel Boundary Interference Correction", paper 21 in AGARD CP-535, July 1994.
- [33] Steinbach, D., *Calculation of wall and model support interferences in subsonic wind tunnel flows*, ZFW, Vol. 17, pp. 370-378, 1993.
- [34] Theodorsen, T., *The Theory of Wind Tunnel Wall Interference*, NACA Report 410, 1931.
- [35] Vaucheret, X. and Vayssaire, J. C., "Corrections de parois en écoulement tridimensionnel transsonique dans des veines a parois ventilées", paper 16 in *Wind Tunnel Design and Testing Techniques*, AGARD CP-174, London, 1976.

- [36] Vaucheret, X., "Améliorations des calculs des effets de parois dans les souffleries industrielles de l'ONERA", paper 11 in AGARD CP-335, May 1982.
- [37] Wuest, W., „Verdrängungskorrekturen für rechteckige Windkanäle bei verschiedenen Strahlbegrenzungen und bei exzentrischer Lage des Modells.“ Z. Flugwiss, Vol. 9, pp 15-19 and Errata p. 362.

3. CONVENTIONAL CORRECTIONS IN VENTILATED TEST SECTIONS

AUTHOR: ALEX KRYNYTZKY

	PAGE
3.1 BACKGROUND, ASSUMPTIONS, AND DEFINITIONS	3-5
3.2 WALL BOUNDARY CONDITIONS	3-7
3.2.1 IDEAL VENTILATED WALL BOUNDARY CONDITIONS	3-8
3.2.2 EXPERIMENTAL INVESTIGATIONS OF PERFORATED-WALL CHARACTERISTICS	3-10
3.2.3 EXPERIMENTAL INVESTIGATIONS OF SLOTTED-WALL CHARACTERISTICS	3-12
3.3 INTERFERENCE IN 2D TESTING	3-14
3.3.1 INTERFERENCE OF SMALL MODELS, UNIFORM WALLS	3-14
3.3.2 INTERFERENCE OF SMALL MODELS, NON-UNIFORM WALLS	3-16
3.4 INTERFERENCE IN 3D TESTING, CLASSICAL RESULTS	3-18
3.4.1 SLOTTED WALLS	3-19
3.4.2 POROUS WALLS	3-20
3.5 COMPUTATIONAL APPROACHES TO INTERFERENCE EVALUATION	3-22
3.5.1 POINT SINGULARITY MODEL REPRESENTATION	3-23
3.5.2 PANEL METHODS, HOMOGENEOUS VENTILATED WALLS	3-24
3.5.3 PANEL METHODS, FINITE-LENGTH AND DISCRETE SLOTS	3-27
3.6 CONCLUSION	3-41
NOMENCLATURE FOR CHAPTER 3	3-41
REFERENCES FOR CHAPTER 3	3-43

3. CONVENTIONAL CORRECTIONS IN VENTILATED TEST SECTIONS

Prior to the 1940s, closed-wall wind tunnels, and to a somewhat lesser extent, open-jet facilities, were the standard types of ground-based aerodynamic testing facilities. As described in Chapter 2, the fundamental characteristics of wall interference of small models in incompressible flow in these types of tunnel were established by the mid-1930s, e.g. Glauert [25]; Theodorsen, [62]). These analyses of lift and blockage interference in closed-wall and open-jet test sections predicted corrections of opposite sign. Reasoning that walls of some intermediate geometry would therefore minimise the interference, testing with walls having a mix of open and closed elements was undertaken.

Concurrent with these developments in testing methodology, the maturation of the applied aeronautical sciences (aerodynamics, structures, propulsion) was enabling flight speeds approaching the speed of sound. Investigation of aerodynamic characteristics of flight vehicles in closed-wall tunnels encounters serious difficulties in this speed range. Extremely small model sizes are required to avoid sonic choking of the flow around the model in a closed-wall test section. One-dimensional compressible flow relationships provide the limiting case of maximum model cross-sectional area for choked flow: for example, a model with an area blockage ratio of 0.01 permits a maximum upstream Mach number of only about 0.89. This problem is manifested even in linearised compressible flow, for which the Prandtl-Glauert compressibility transformation results in blockage interference velocities increasing like $1/\beta^3$ (Goethert [26]). The theoretical singularity at Mach = 1.0 (due to linearisation of the compressibility effect) is consistent with experimental difficulties experienced at high-subsonic test Mach numbers.

An unexpected consequence of testing with walls comprising both open and closed elements was a substantial increase in achievable upstream Mach number before the onset of sonic choking around the model. This discovery led to a new paradigm for wind tunnel testing at speeds where compressibility is no longer negligible: the ventilated wall. Two basic wall geometries have emerged as preferred ventilated wall types: slotted walls, comprising solid wall areas (slats) alternating with longitudinal slots, and perforated walls, which are characterised by a pattern of holes in an otherwise solid wall surface. Most commonly, the test section is surrounded by a single large open plenum chamber assumed to be at a constant static pressure that is usually used as the tunnel Mach number reference pressure, Figure 3.1. This plenum chamber may be vented at its downstream end to the test section diffuser through a variable-geometry re-entry flap system, or may be actively pumped by a plenum evacuation system (PES) which typically can remove up to several percent of the tunnel mass flow from the plenum, usually to be reinjected elsewhere into the tunnel circuit. Use of a PES is especially advantageous in the transonic speed range to maximise clear tunnel flow uniformity, to assist expansion of the upstream flow to supersonic test Mach numbers, and to help offset the adverse effects of wake blockage in the downstream part of the test section.

Experience with slotted walls has led to their use primarily for subsonic testing. Perforated walls are preferred in the near-sonic and low-supersonic speed range, due to their ability to attenuate shock (and

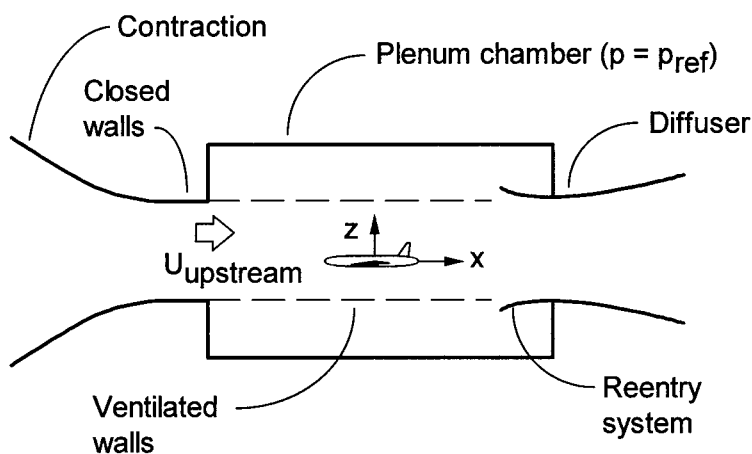


Figure 3.1 : Ventilating Wall Wind Tunnel, General Arrangement

expansion) wave reflections with the right choice of openness ratio (Estabrooks [17]; Jacocks [33]; Neiland [51]). Ventilated walls of one type or the other (or, in some cases, of a hybrid type), whose geometry remains fixed (or at most varies uniformly with Mach number) have been the mainstay of aerodynamic testing at Mach numbers from approximately 0.6 to 1.2 since their introduction in the 1940s and early 1950s (Goethert [27]).

With the maturation of aerodynamic testing technology, data accuracy needs have become more stringent (Steinle and Stanewsky [61]), with parallel accuracy requirements with regard to interference corrections. The continuing expansion of high Reynolds number testing (Goldhammer and Steinle [28]) has stimulated an increased appreciation of Reynolds number effects, which in turn has increased the pressure on model size in order to simulate flight Reynolds numbers more closely. Model size (relative to test section dimensions) thus continues to play a key role in interference calculations. Similarly, there is a continuing demand for more comprehensive predictions of flight characteristics, including increased emphasis on flight regimes where the effects of compressibility are strong (both on the flight characteristics themselves and on the wall interference as well). For subsonic flight vehicles whose design point is close to drag rise or beyond, this includes flight conditions at Mach numbers approaching 1.0, with substantial regions of supersonic flow, and possibly with large areas of separated flow. Supersonic flight vehicles require testing through their entire flight envelope, typically including Mach numbers as close to 1.0 as possible. Each of these factors increases the magnitude of the wall interference, consequently maintaining pressure on improving wall interference methods for ventilated wall tunnels.

Even though the theory of ventilated-wall wind tunnels is less soundly based than for closed-wall tunnels, conventional ventilated-wall tunnels offer several practical advantages: demonstrated small interference effects in subsonic flow (compared to closed-wall tunnels), the ability to operate at high-subsonic Mach number and through the sonic and low-supersonic speed range, and the operational simplicity of fixed-geometry ventilated walls. These advantages, coupled with both a substantial capital investment in existing test facilities and continuing competitive pressure to improve wind tunnel data accuracy, provide the motivation to understand ventilated wall behaviour.

Perhaps the greatest difficulty in the application of the methodology and results of ventilated-wall interference theory is the approximate nature of the ideal ventilated-wall boundary conditions and the unknown relationship between physical wall geometry and wall crossflow parameters. This weakness has motivated investigations of crossflow characteristics of particular wall geometries, the use of measured boundary conditions to determine wall characteristics (e.g., Mokry et al. [47]), development of alternate wall crossflow models, and finally, the direct use of measurements near the wall as boundary conditions in the computation of interference (see Chapter 4). The application of boundary measurement techniques for interference estimation of ventilated walls appears to be a viable approach, particularly for perforated walls (e.g., in 2D, Mokry and Ohman [48]; in 3D, Mokry, Digney, and Poole [50], Beutner, Celik, and Roberts [9], and even for slotted walls (Freestone and Mohan [22]). Nonetheless, because of the additional instrumentation, measurement, and computational requirements of such methods, testing with passive, nonadaptive, ventilated walls and the use of classically based corrections predominates in practice, especially for 3D tunnels.

The impact of improvements in high-speed computing cannot be overemphasised. The CFD codes and techniques developed over the past three decades for analysis of flight vehicles in an unconstrained flow are now being applied to the analysis of models within wind tunnels. More complex and larger test configurations, asymmetric installations in the test section, general tunnel cross sections, and a variety of

wall boundary conditions can now readily be analysed. The influences of finite test section length and model supports can also be evaluated.

3.1 BACKGROUND, ASSUMPTIONS, AND DEFINITIONS

“Conventional” wall corrections are taken to be those that apply to tunnel flows where the influence of the walls is approximated as an incremental flow field in the vicinity of the model that is calculable using linearised potential flow theory, and where the walls are basically of fixed geometry with known crossflow characteristics. Thus it is assumed that the flow around the model in the wind tunnel is governed by Equation 2.3, subject to the limitations described in Section 2.1. The potential at any point in the tunnel is expressed as the superposition of the separate potentials representing a uniform onset free stream, the model, and the walls (see Chapter 2):

$$\Phi(x, y, z) = -U_\infty x + \phi_m(x, y, z) + \phi_w(x, y, z) \quad (3.1)$$

Compressibility is taken into account through the Prandtl-Glauert compressibility factor β . The interference flow field is due to simply the wall potential. The test section is usually taken to be of constant section throughout its length, with flow through the walls satisfying a boundary condition relating the crossflow velocity and the pressure difference across the walls, Figure 3.2. For analytic solutions the tunnel is typically taken to be doubly infinite in length. When computational approaches such as panel methods are used, tunnel length is necessarily finite, but (usually) long. Model flows with substantial embedded supersonic regions, at high lift coefficients so that wake position or separated wake effects become important, and in the transonic, near-sonic, and low-supersonic speed regimes are beyond the scope of this chapter.

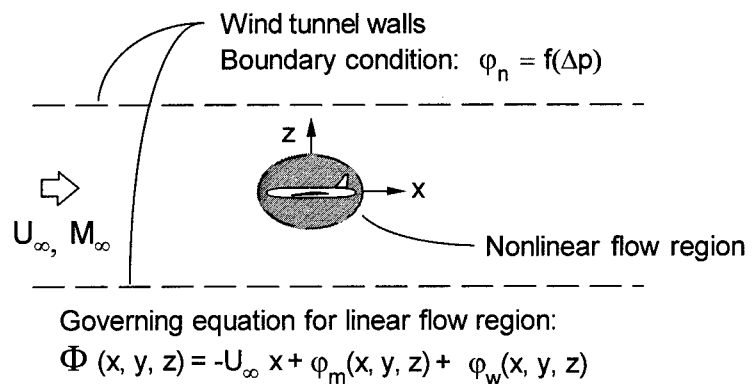


Figure 3.2 : Potential Flow in an Ideal Wind Tunnel
With Ventilated Walls

“Conventional” ventilated walls are taken to be either longitudinally slotted walls, perforated walls, or a combination of these two wall types, whose behaviour is described locally by a simple pressure-crossflow relationship (see Sec. 3.2.1) and whose geometry remains fixed over a given range of test conditions. It is assumed that these walls are vented to a single large plenum chamber, whose pressure is constant and is taken to be the reference static pressure for the calculation of the onset Mach number in the tunnel. Note that for a plenum of finite longitudinal extent, the Mach number far upstream does not necessarily correspond to this plenum reference Mach number.

AGARDograph 109 [24]) provides a comprehensive review of a wide variety of wall configurations and their interference. In general, the interference of ventilated walls had not been investigated to the same level of detail as corresponding closed-wall configurations. Admittedly, contributing factors to this state of affairs include the additional wall parameters (which increase the number of cases of interest), the additional analytic and computational complexities associated with ventilated-wall boundary conditions, and the recognised approximate nature of these boundary conditions. In particular, only limited or no

interference information is given for rectangular tunnels with all four walls slotted or perforated (see Table 6.1 of AGARDograph 109). Interference calculations for some of these cases have since been published (Pindzola and Lo [53]; Lo and Oliver [43]; Keller and Wright [38]).

The wall interference corrections in AGARDograph 109 for steady flows are discussed in terms of interference velocity components: longitudinal (or streamwise, u_i) and cross-stream (typically upwash, w_i). Because of their one-to-one correspondence to simple representations of model volume and lift for a model at the centre of a tunnel with uniform walls, these interferences are commonly referred to as blockage and lift interference, respectively. The separate interference velocity components are assumed to be independent and superposable. Independence can be obtained by suitable symmetry restrictions: a small model located at the centre of a tunnel of symmetric cross section and having uniform walls. Cross-coupling of interference velocity components and model characteristics (blockage interference due to lift, for example) will occur for models asymmetrically located relative to the walls and for non-linear wall crossflow characteristics. Non-linear wall ventilation can be the result of actual geometric differences among the walls, but is usually attributed to the action of viscosity at the walls. Superposition is valid provided the magnitudes of the corrections remain small and the Mach number is not too close to 1.0.

Interference corrections for ventilated walls are further classified in AGARDograph 109 according to wall type and test section cross section. The wall type refers to the boundary condition to be satisfied at the wall, mainly: closed-wall, open-jet, ideal slotted, or ideal porous, though there is some discussion of the hybrid slotted wall (slots with crossflow resistance). The test sections considered are the 2D tunnel (planar flow), circular (or by co-ordinate transformation, elliptical), rectangular and, less comprehensively, octagonal (or rectangular with corner fillets). Most of the results given are for walls whose geometry does not vary streamwise and that extend far upstream and downstream of the model.

As suggested in Chapter 2, the interference results for small models in 2D and rectangular test sections are considered suitably representative of many interference situations encountered in practice (the major exclusions include sidewall interference in 2D testing, "large" models, and models "too close" to the walls). Rectangular sections with corner fillets or elliptical cross sections may be approximated by rectangular tunnels of equal cross-sectional area and equivalent aspect ratio (width to height ratio). This approximation is supported by the close correspondence of interference characteristics of square and circular ventilated test sections.

For a small model, a subsonic onset Mach number not too close to 1.0, and for attached flow over the model, the variation of the interference flow field is negligible throughout the model volume, so that primary corrections to the freestream magnitude and direction are adequate. As discussed in Chapter 4, small embedded regions of supersonic flow around the model may be permitted. For larger models, or for more accurate correction, consideration of linear streamwise variations of interference velocities may be necessary. These result in buoyancy corrections to model drag and additional corrections to angle of attack (or lift) and pitching moment due to streamwise curvature. Non-linear streamwise or significant spanwise variation of interference may be addressed using the methods for residual interference corrections outlined in Section 1.3. The flow field around very large models may ultimately not be easily correctable to equivalent freestream conditions.

The interference flow field is commonly described in nondimensional terms as defined in Equations 2.6 and 2.8 for streamwise and cross-stream (upwash) interference velocity perturbations:

$$\varepsilon = \frac{u_i}{U_\infty} \quad (3.2)$$

$$\delta = \frac{w_i}{U_\infty} \frac{C}{SC_L} \quad (3.3)$$

Solid blockage interference for small models in ventilated-wall tunnels is conveniently expressed in terms of the blockage parameter Ω_S , the ratio of solid blockage in the ventilated test section to that in a closed-wall test section of the same cross section:

$$\Omega_S = \frac{\varepsilon_{ventilated}}{\varepsilon_{closed}} \quad (3.4)$$

Thus, $\Omega_S=1$ for a closed-wall test section. Some basic classical results for ε_{closed} for small models in 2D and rectangular test sections are given in Chapter 2.

The streamwise gradient of ε , $\partial\varepsilon/\partial x$, results in a pressure force on the model (buoyancy drag), whose magnitude is proportional to the effective volume of the model (for small models in linear gradients). The streamwise gradient of upwash, or flow curvature, characterised by

$$\delta_1 = \frac{\partial\delta}{\partial\left(\frac{x}{\beta L}\right)} \quad (3.5)$$

results in additional angle-of-attack and pitching moment corrections for even small models.

For models of large size, applying only primary corrections to the free stream is at best approximate. Residual corrections may be adequate for many cases but large variations of blockage and/or upwash interference over the region occupied by the model may ultimately not be correctable. That is, there is no equivalent unconstrained flow (with a uniform onset velocity) for the model geometry being tested. This situation is particularly acute in transonic flow fields because of their extreme sensitivity to small variations in onset flow conditions. The adequacy of corrections can be tested by careful comparison of computed model aerodynamic characteristics from in-tunnel and unconstrained-stream solutions (at flight conditions that include primary interference corrections). Such a test requires a higher degree of sophistication of model representation than for the calculation of simple linearised corrections. Paneling or gridding requirements for this type of analysis are the same as for typical high-resolution free-air analyses.

3.2 WALL BOUNDARY CONDITIONS

The wall boundary condition distinguishes ventilated walls from closed-wall or free-jet boundaries. A useful simplification of the actual wall boundary condition is to treat the walls as homogeneous, wherein the open- and closed-wall areas are not represented separately, but as an equivalent permeable surface (Davis and Moore [14]; Goethert [27]). The normal velocity through the walls thus is a local average, varying smoothly and in a continuous manner as a function of the (similarly spatially averaged) pressure distribution on the walls. Walls with perforations are thus idealised as permeable porous surfaces with infinitesimally small holes. Slotted tunnels are idealised as having an infinite number of very small slots distributed around the tunnel boundaries.

The validity of the assumption of homogeneous walls depends on the length scale of the wall openness and the Mach number. It is expected that the effect of wall "graininess" will be felt out into the tunnel stream a distance on the order of L/β , where L is the length scale associated with the wall openings. As long as L/β is small compared to the tunnel dimension (or more directly, to the distance from the wall to the closest model part, such as a wing tip), the interference felt by the model will be the same for homogeneous walls as for discretely ventilated walls having equivalent crossflow properties. There are often two distinct geometric length scales associated with a given ventilated wall: the typical size of the discrete openings and their spacing. A third length scale may also be involved: the wall boundary layer thickness, whose properties have been found to influence the wall crossflow characteristics.

For perforated walls, the openness length scales are the hole diameter and spacing. For slotted walls, they are the slot width and circumferential slot spacing. Consideration of typical perforated wall arrangements suggests that treating perforated walls as homogeneous (for wall interference purposes) is a valid assumption given the typical small scale of perforations. Slotted-wall openness length scales, on the other hand, are often at least an order of magnitude larger. For some tunnels, the slot spacing approaches a substantial fraction of a test section dimension. The assumption of homogeneous walls is more tenuous in this case, especially for models whose components are on the order of an openness length from a wall surface (e.g., wing tips of large-span models, body tail or nose for long models at high angles of attack).

For cases where the walls cannot be treated as homogeneous, the alternating open- and closed-wall areas (slots and slats) can be modelled separately, for example, by an appropriate mix of closed-wall and open-jet boundary conditions. In such situations, simplicity and computational efficiency are sacrificed for higher fidelity of the simulation.

Measured boundary condition methods with ventilated walls may be strongly influenced by wall inhomogeneities (closed and open elements). The resulting local flow gradients are not representative of the far-field homogeneous boundary condition. Correction methods for individual measurements, alternate measurement strategies, or explicit computational modelling of wall elements may be required.

3.2.1 IDEAL VENTILATED WALL BOUNDARY CONDITIONS

The boundary conditions of ventilated walls are motivated by physical considerations (see, for example, Davis and Moore [14]; Baldwin et al. [3]; Goethert [27]). The so-called ideal porous wall boundary condition can be derived by consideration of porous walls as a lattice of lifting elements. The pressure difference across the wall is then proportional to the flow inclination (θ) at the wall,

$$C_{p_{wall}} = \frac{P_{wall} - P_{plenum}}{q_{\infty}} = \frac{2 v_{normal}}{R U_{\infty}} = \frac{2}{R} \theta \quad (3.6)$$

In linearised perturbation form, with the plenum pressure taken to be the same as the pressure far upstream,

$$\varphi_n = -R\varphi_x \quad (3.7)$$

where R is an experimentally determined constant of proportionality. Note that the limits $R=0$ and $R \rightarrow \infty$ correspond to the standard closed-wall and free-jet boundary conditions, respectively. It is convenient to define an alternate perforated wall parameter,

$$Q = \frac{1}{\left(1 + \frac{\beta}{R}\right)} \quad (3.8)$$

so that $Q=0$ corresponds to a closed wall, and $Q=1$ to a free jet.

The ideal homogeneous slotted-wall boundary condition is developed by consideration of the balance of pressure difference across the slots and streamwise flow curvature in the vicinity of the slots,

$$\varphi_x + K\varphi_{xn} + \frac{\varphi_n}{R} = 0 \quad (3.9)$$

where the third term represents a viscous pressure drop across the slot and K , the slot parameter, is related to slot geometry, including the approximate effect of slot depth (t/a), according to

$$K = d \left[\frac{1}{\pi} \log_e \left(\operatorname{cosec} \frac{\pi a}{2d} \right) + \frac{t}{a} \right] \quad (3.10)$$

Slotted-wall geometry definitions are summarised in Figure 3.3. For an ideal inviscid slotted wall (i.e., $R \rightarrow \infty$), closed-wall and free-jet boundary conditions correspond to $K \rightarrow \infty$ and $K=0$, respectively. As for the ideal porous wall, a convenient alternate slot parameter is defined,

$$P = \frac{1}{1 + F} \quad (3.11)$$

where F is proportional to K according to

$$\begin{aligned} F &= 2K/H && \text{for a 2D test section.} \\ F &= K/r_0 && \text{for a circular test section.} \\ F &= K/H && \text{for a rectangular test section.} \end{aligned}$$

$P=0$ and $P=1$ correspond to closed-wall and free jet boundary conditions respectively.

The boundary conditions for walls with discrete slots comprise

$$\begin{aligned} \varphi_n &= 0 && \text{on the slats (i.e., the closed-wall segments between slots).} \\ \varphi_x + \varphi_n/R &= 0 && \text{for slots with crossflow resistance.} \\ \varphi_x &= 0 && \text{for open slots.} \end{aligned}$$

The ideal ventilated-wall boundary conditions may be viewed as first-order approximations to ventilated-wall crossflow characteristics. These simple analytic expressions are intended to capture the dominant flow physics at the wall, as perceived at some distance from the wall (i.e., at the model location). Improvements in ventilated wall modelling have focused on more accurate descriptions of the flow near the wall, including:

- 1) Effect of boundary layer thickness on the wall crossflow characteristics.
- 2) Non-linear pressure-drop terms (e.g. proportional to square of crossflow velocity).
- 3) Entry of stagnant plenum air into the test section.

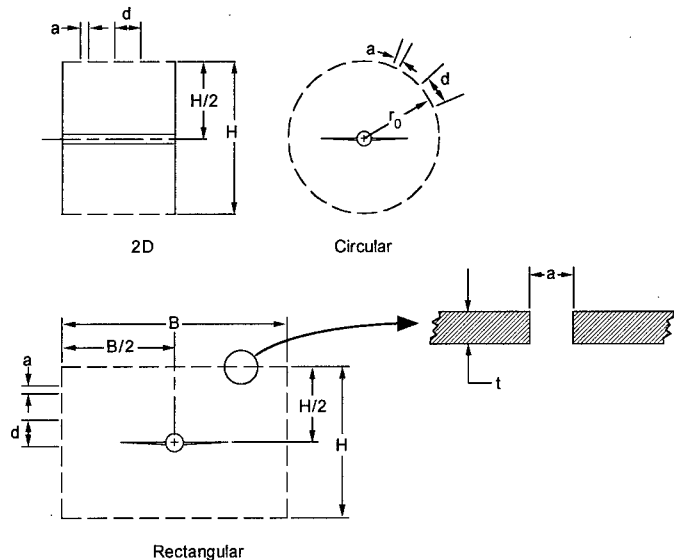


Figure 3.3 : Slotted Tunnel Geometry

3.2.2 EXPERIMENTAL INVESTIGATIONS OF PERFORATED-WALL CHARACTERISTICS

Many investigations, both theoretical and experimental, have been undertaken to capture the behaviour of various perforated-wall geometries. Perforated walls are taken to be any wall with a pattern of small openings, usually round holes drilled either normal to the wall surface or at a fixed angle to the normal. Variable porosity features have been implemented in several facilities using a sliding backing plate.

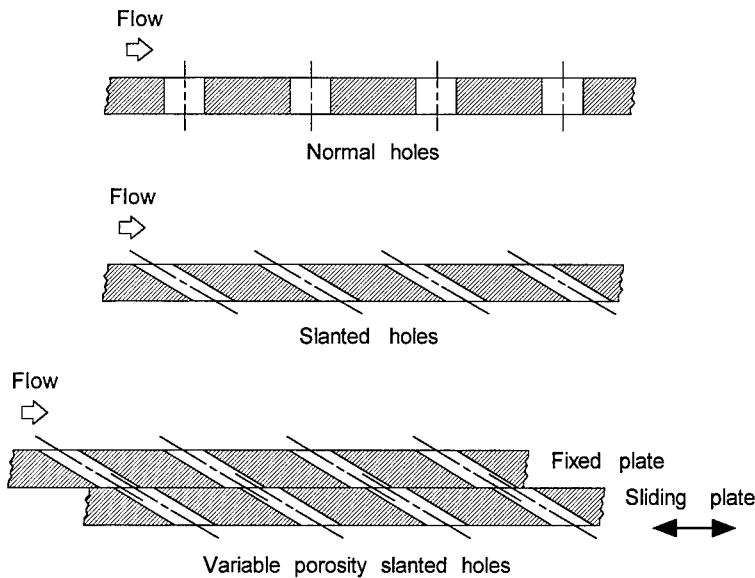


Figure 3.4 Perforated Wall Configurations

Methods for determination of the velocity normal to the wall include direct velocity measurements near the wall, massflow measurement through a portion of wall vented to an otherwise sealed and pumped plenum, and a hybrid theoretical-experimental method for the calculation of crossflow at the wall. Pressure differences across the wall may be applied either by a model in the test section, or by active plenum pumping with a "clear" test section. The second approach uses measured wall pressure differences, but avoids the direct measurement or calculation of crossflow velocity at the wall. The necessary information for determining wall characteristics may come from wall pressure correlations (test-theory), from tests of a model in several facilities, or tests of geometrically similar models in the same facility. The starting point for the latter two approaches is a set of interference-free data (e.g., small model in a very large tunnel) and a methodology for extracting lift and blockage interference from comparisons of model data.

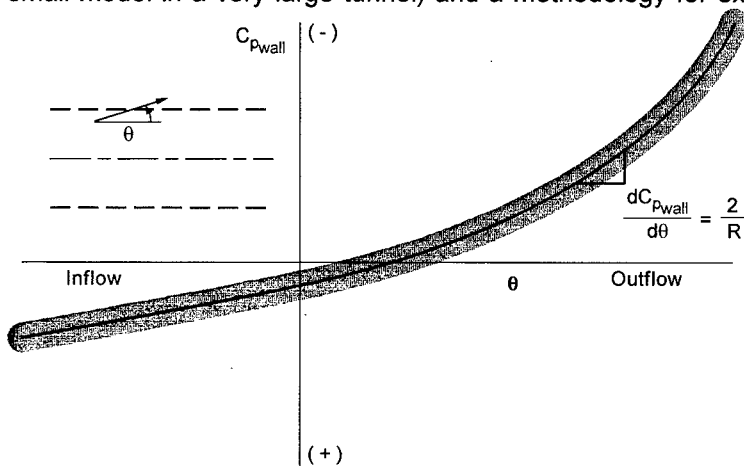


Figure 3.5 Non-linear Porous-Wall Crossflow Characteristics

Figure 3.4 illustrates some typical perforated wall configurations. Slanted hole walls were developed to offset the observed lower resistance to inflow compared to outflow. A large number of configuration variations have been tested, including splitter plates and screens in the openings to attenuate discrete noise tone production, various hole patterns, openness ratios, and hole angles.

Two general approaches for the determination of a pressure-crossflow relationship may be distinguished. The first relies on explicit measurement (or calculation) of both pressure difference and crossflow at the wall.

Some of the deviations from linear crossflow behaviour that have been experimentally observed are illustrated in Figure 3.5. These include non-zero crossflow at zero pressure difference across the walls, different initial slopes for inflow and outflow, and non-linear behaviour as crossflow velocities increase. These behaviours are attributed to the effect of the wall boundary layer. Several experimental investigations have therefore focused on

correlations of these additional parameters with wall boundary layer thickness.

A first step toward characterising the interference of walls with non-linear wall resistance would be simply to model different wall resistance for inflow and outflow. Mokry, Peake, and Bowker [47] allow opposing perforated walls (20.5 percent openness normal holes in 2D testing) to have different resistance, based on the observation that for an airfoil with lift, measured wall pressures on opposite walls are of opposite sign relative to the plenum, so that the floor would experience primarily outflow, and the ceiling, inflow to the test section. This approach results in much better correspondence of predicted wall pressures to measurements than use of the same resistance for both floor and ceiling. For cases shown, the ceiling R value (inflow) is about three times larger than the floor R value (outflow). Chan [11] establishes a correlation of wall crossflow characteristics for inflow to the test section that depends explicitly on the wall boundary layer displacement thickness. Two correlations are given: a quadratic relationship of wall mass flux as a function of $C_p \delta^*/d$ for $\delta^*/d \leq 0.25$ and a linear relationship between wall mass flux and wall C_p for $\delta^*/d > 0.25$.

Jacocks [34] presents wall crossflow characteristics for slanted-hole perforated walls (holes drilled at 60 deg from the normal), including variable porosity configurations and the effects of screens and splitter plates for edge-tone noise suppression. Test Mach numbers ranged from 0.5 to 0.85 with limited results at 0.9 and 1.2. A combined experimental-theoretical approach is used to calculate the crossflow at the wall, thus sidestepping the direct measurement of mass flux through the wall (limited crossflow measurements were made in order to validate the method). Some configurations tested clearly exhibit differential resistance of inflow and outflow. Decreased wall resistance resulted from increasing porosity and also from increased boundary layer thickness. The value of R increased by factors of 2 to 3 (depending on wall configuration) for δ^*/d varying between about 0.1 to almost 1.0. It is suggested that the results of Mokry et al. [47] are the result of a thicker boundary on the inflow wall. The addition of screens improved crossflow linearity. It is concluded that most, but not all, perforated walls can be assumed linear for purposes of calculating subsonic wall interference. However, each wall of a given wind tunnel may require a different characterisation to capture differences in mean wall boundary-layer thicknesses.

Matyk and Kobayashi [44] report direct measurements of wall crossflow as a function of pressure across the wall for wall samples with baffled slots representing the wall configurations of the Ames 2-ft by 2-ft and 11-ft by 11-ft transonic wind tunnels. Data for only outflow were acquired over a range of $\Delta p/q_\infty$ from 0 to 0.5 and higher. Significant non-linear behaviour was observed for wall normal massflow ratios above approximately 0.04. Wall characteristics were consistent across the tested Mach number range ($0.5 < M < 1.2$).

Ivanov [32] reports very good linear crossflow behaviour of wall samples with normal holes in a wind tunnel with a relatively thick wall boundary layer (displacement thickness to hole diameter ratios greater than 1). Characteristic slopes differing by more than a factor of 2 were determined for inflow and outflow with no discernible trend with Mach number ($0.4 < M < 0.98$).

Vayssaire [67] summarises values of R deduced from experiments comparing model measurements with different walls. This method relies on model data from a closed-wall tunnel for which corrections are nominally known. For example, mapping of a model characteristic (such as shock position) from ventilated wall tests to corrected closed-wall data provides the ventilated-wall blockage correction, from which an average effective wall characteristic can be inferred using theoretical curves. Other corrections are then calculated using this inferred wall resistance. Pounds and Walker [54] similarly deduce global R

values for variable-porosity walls from measured lift curves of a semispan wing-body model using data from a large tunnel as the interference-free baseline.

Starr [58] used pressure distributions on a cone-cylinder model in a Ludwig tube at Mach numbers between 0.95 and 1.2 to assess effective wall porosity sensitivity (for slanted holes at 60 deg from the normal) to wall boundary layer changes. For δ^*/d varying from about 0.13 to 0.28 the equivalent wall porosity change was found to be about 1 percent.

Crites and Rueger [13] provide a wall crossflow correlation for a set of five perforated wall samples of various geometries. Their results are similar to Chan [11] in that the quadratic dependence of crossflow on wall pressure is much greater for inflow to the test section than for outflow.

In summary, R values estimated for different tunnels exhibit a large degree of variability, even for similar nominal openness. Wall boundary layer thickness, especially in regions of inflow to the test section, appears to play a dominant role in wall resistance. The observed linearity of the wall pressure-crossflow relationship under many conditions leaves open the possibility of adequate wall corrections using locally linear approximations. However, allowance for variation of the wall resistance factor with inflow and outflow or with wall boundary layer thickness is likely required for high-quality wall interference predictions. The inclusion of a quadratic crossflow term is recommended by some investigators, though simple linear characterisations appear to work well for small wall crossflow. Because of the dependence of wall performance on wall boundary layer (which may in turn depend on plenum suction), it is recommended that wall resistance values or curves (R or $dC_p/d\theta$ vs. wall openness) be determined for each facility under typical operating conditions according to desired accuracy requirements.

3.2.3 EXPERIMENTAL INVESTIGATIONS OF SLOTTED-WALL CHARACTERISTICS

The investigation of flow through open slots has advanced on several fronts. The effect of wall thickness has been explored using inviscid slot flow models. Experimental measurements aimed at establishing the slotted-wall boundary condition have successfully documented the richness of flow phenomena through slots and have been instrumental in guiding the development of slot models.

The effect of wall thickness on slot parameter K has been investigated by Chen and Mears [12] for ideal slots without crossflow resistance using a potential-flow doublet-rod wall model. Barnwell [4], as well as correcting an error in the preceding analysis, generalises the flat-slat boundary condition to a slot with sidewalls or separation in the plenum. He concludes that for the sidewall case (i.e., deep slots of constant width),

$$K_{\text{sidewalls}} = \frac{1}{\pi} \log_e \frac{d}{2a} \quad (3.12)$$

For the case of separation on the plenum side,

$$K_{\text{separated}} = \frac{1}{\pi} \log_e \left[\frac{2 + \pi d}{4\pi a} \right] \quad (3.13)$$

For small a/d , Equations 3.10, 3.12, and 3.13 provide only slightly different values of K . A greater cause for concern involves the experimental determination of K . Continuing research at NASA Langley aimed at validating a slot-flow model (Barnwell [5], Everhart and Barnwell [18]) included evaluation of K from measurements near a slotted wall in a 2D tunnel. Figure 3.6, from Everhart [19]), summarises some of

these results. Everhart's results for a four-slot wall configuration compare favourably with other published experimental values, which all deviate significantly from the inviscid slotted-wall theoretical predictions.

Experimental confirmation of pressure drop proportional to crossflow velocity in the slotted-wall boundary conditions, as suggested by Baldwin et al. [3], is given by Goethert [27] for a single open slot, with a quadratic dependence (for outflow) becoming apparent above a wall pressure coefficient of about 0.04. Everhart [19] confirms a quadratic pressure-crossflow relationship for large crossflows in the absence of flow curvature. Nevertheless, it is concluded that the ideal form of the slotted-wall boundary condition (Eq. 3.9 with $R \rightarrow \infty$) describes the wall pressure drop upstream of the maximum model thickness if a reference pressure zero-shift is included. Downstream of this point wall pressures are only qualitatively predicted.

The above investigations have benefited from parallel theoretical and experimental developments (Berndt and Sorensen [8]; Berndt [6]; Nyberg [52]; Berndt [7]), which have resulted in a slot-flow model motivated by observed slot-flow physics. The boundary between high-velocity air originating in the test section and quiescent air from the plenum is tracked, and empirical coefficients are used to account for flow separation at the slot edges and for viscous flow within the slot, Figure 3.7. This method has shown good correlation (using the non-linear perturbation potential flow equation) with measured wall pressures at Mach numbers up to 0.98 and has been used to design the contoured slots for the FFA T1500 Transonic Wind Tunnel (Karlsson and Sedin [36]; Sedin and Sorensen [56]; Agrell, Pettersson, and Sedin [1]; Agrell [2]). Firmin and Cook [21] provide independent experimental confirmation (from pitot-static probe measurements and oil flow visualisation near the slots) of the penetration of low-energy plenum air into a slotted test section downstream of an airfoil model. This penetration is cited as a serious obstacle for determination of an equivalent homogeneous

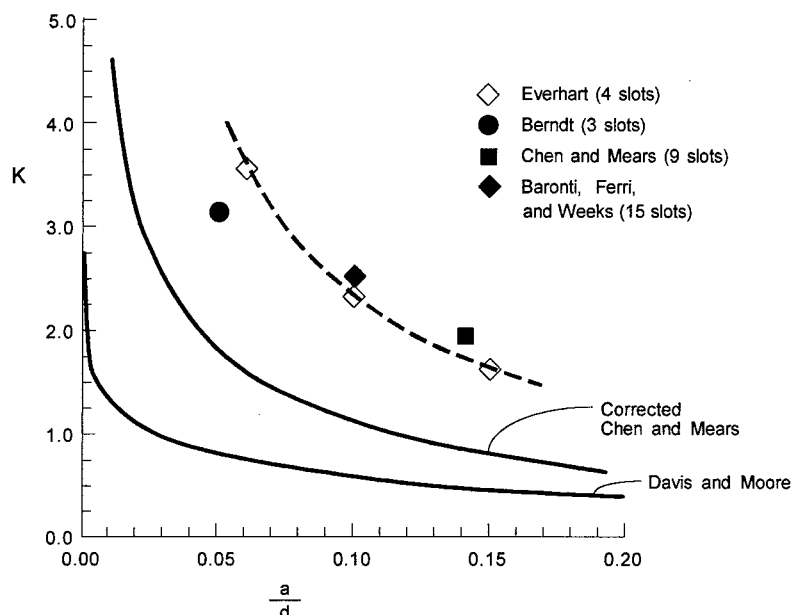


Figure 3.6 Experimental Values of Ideal Slot Coefficient, $M = 0.7$ (after Everhart [18])

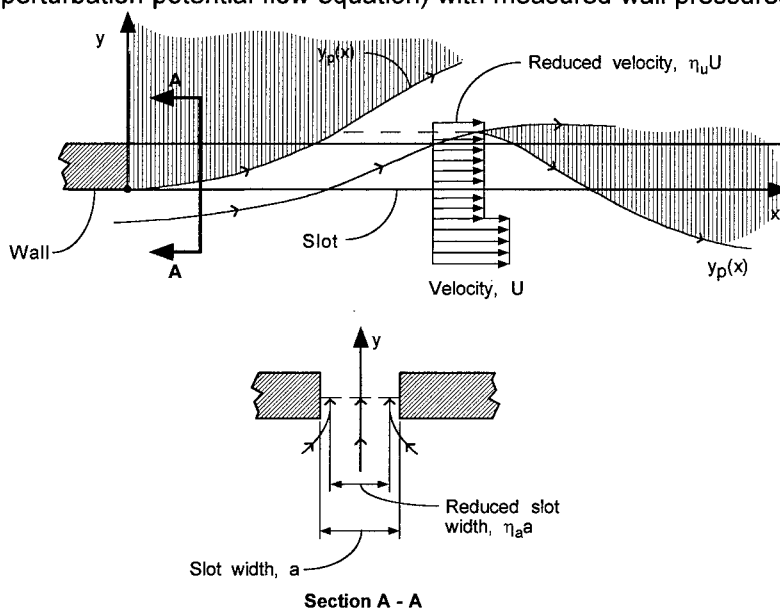


Figure 3.7 : Slot Flow Model (after Sedin and Sorensen [54])

boundary condition for slotted walls. It is suggested that porous walls behave similarly with regard to low-energy re-entry flow, but wall homogeneity would not be an issue due to the smaller length scales of the wall ventilation.

In addition to the work reported above, other investigators have reported the results of flowfield measurements in the vicinity of slots. Wu, Collins, and Bhat [68] document the 3D character of the flow near a single baffled slot with varying suction through the slot. They measured a vortex-like secondary flow in the crossflow plane whose effect extended beyond the edge of the boundary layer at low suction rate. Suction was found to have a large effect on boundary layer displacement thickness on the slot. A non-linear relationship between crossflow velocity at the slot and at the edge of the boundary layer (the equivalent inviscid crossflow) was measured. Everhart, Igoe, and Flechner [20] provide a database of flowfield measurements near and within an open slot, including the effects of plenum suction and the presence of a model (NACA 0012-64 2D airfoil). In the course of the development of a "two-variable" boundary interference approach for slotted walls, Freestone and Mohan [22] show good agreement between measured and predicted slot flows in a low-speed test of a large 2D airfoil. Slot flows are measured using a traversing flow-angle probe; predictions are from the slot-flow model of Berndt and Sorensen [8] with the addition of a linear resistance term for flow into the test section.

3.3 INTERFERENCE IN 2D TESTING

Some of the principal results given in AGARDograph 109 and Pindzola and Lo [53] for small models are repeated here as benchmarks. These results were calculated using a Fourier transform method.

Engineering Sciences Data [15] has published comprehensive summary carpet plots of lift and blockage interference and gradient factors for 2D point singularities in ideal porous and slotted test sections.

3.3.1 INTERFERENCE OF SMALL MODELS, UNIFORM WALLS

Interference parameters for a small model in the centre of a 2D test section with (homogeneous) slotted and porous walls are shown in Figure 3.8 as functions of slotted wall parameter P , and porous wall parameter Q , respectively. The model is represented as the superposition of a point vortex whose strength is proportional to lift, and by a point source doublet whose strength is proportional to the model effective cross-sectional area. It is recalled (Eq. 2.45, Sec. 2.2.1.1) that the blockage of a small model in a 2D closed-wall test section is given by

$$\varepsilon_{closed} = \frac{\pi}{6} \frac{A}{\beta^3 H^2} \quad (3.14)$$

where A is the effective cross-sectional area of the model and H is the height of the test section.

Although the closed-wall and open-jet limits of P and Q (0 and 1, respectively) are the same for these two types of walls, the interference characteristics at intermediate values of P and Q are fundamentally distinct (except when consideration is given to slots with crossflow resistance). From Figure 3.8 it can be seen that it is not possible to obtain zero blockage and zero upwash interference simultaneously with any uniform porous wall or uniform inviscid slot geometry.

The longitudinal distribution of blockage interference midway between the walls (for a model likewise located) is shown in Figure 3.9. For ideal slotted walls with no viscous pressure-drop term ($Q=0$), the

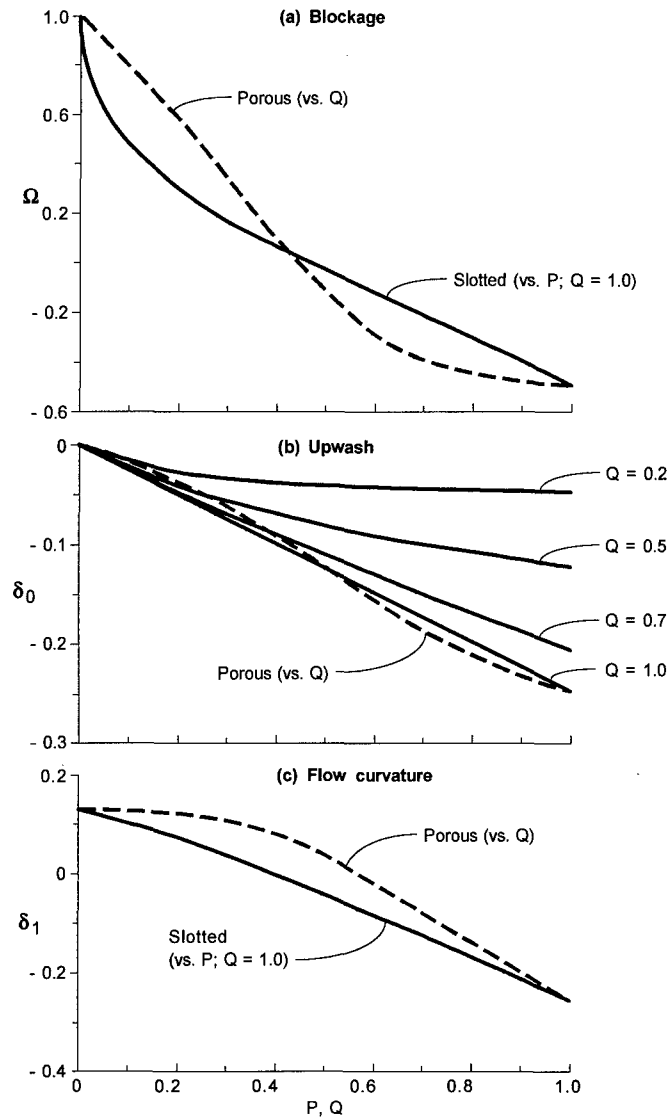


Figure 3.8 2D Interference in Ideal Slotted and Porous Tunnels

interference velocity along the tunnel centreline is symmetric fore and aft of the model. Consequently, there is no interference buoyancy force on the model. In contrast, porous walls (except for the limiting cases of closed and open jets) exhibit a longitudinal interference gradient, producing a buoyancy force on the model. The gradient is very nearly a maximum for the value of porosity for zero blockage interference (Pindzola and Lo [53], Figure 3.5). Similar interference distributions can be expected for slots with non-zero Q .

The longitudinal variation of upwash interference is shown in Figure 3.10 for ideal slotted and porous walls (Pindzola and Lo [53]). Zero upwash at the model location is obtained for closed walls only. Zero upwash gradient is obtained for intermediate values of P and Q (for slotted and porous walls, respectively), but the upwash is non-zero for these cases.

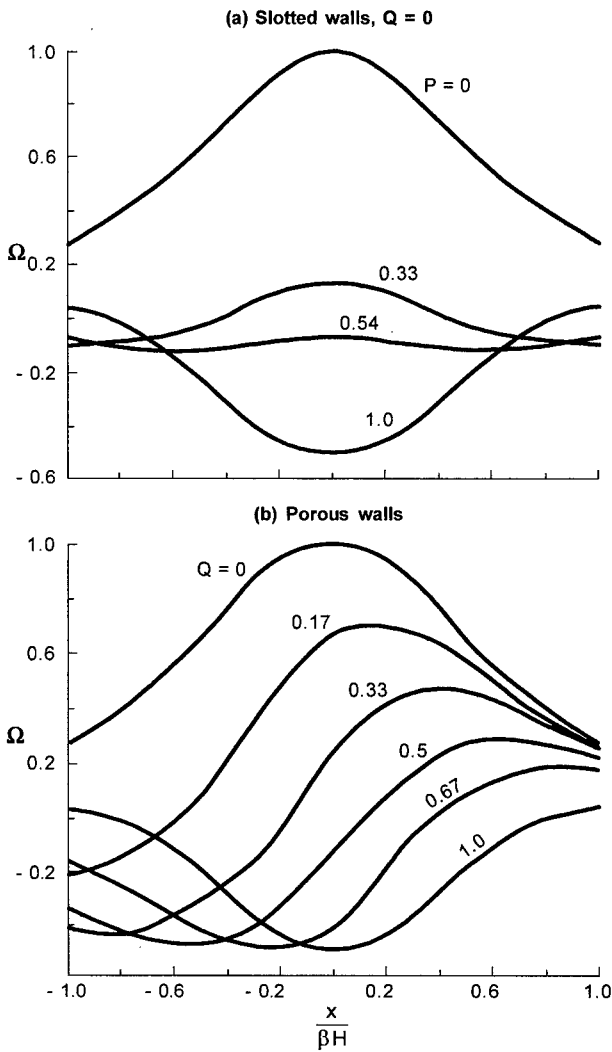


Figure 3.9 Longitudinal Variation of Blockage Interference in 2D Slotted and Porous Tunnels

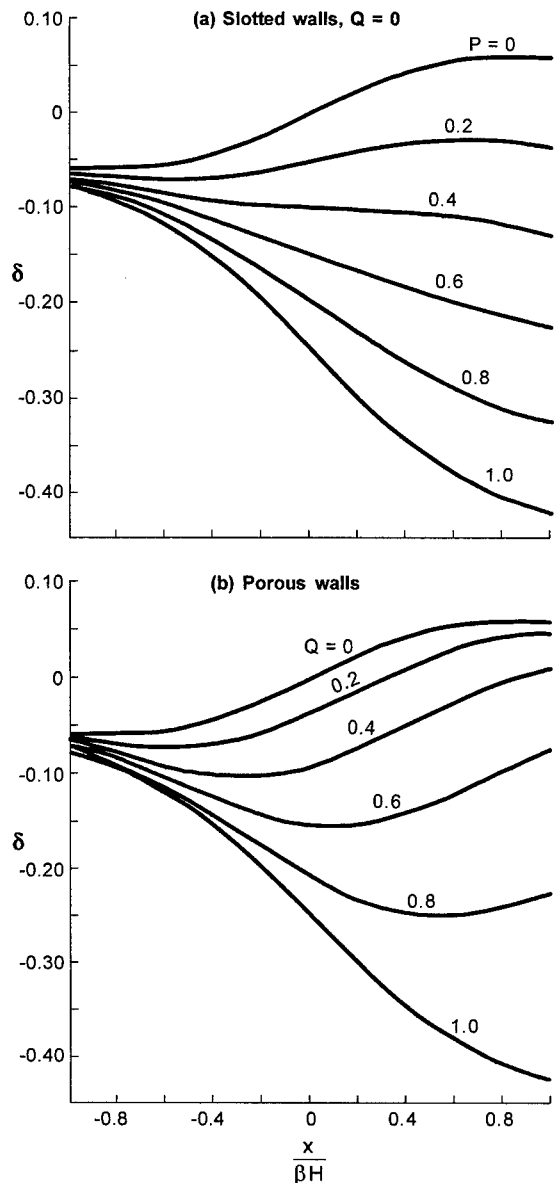


Figure 3.10 Longitudinal Variation of Upwash Interference in 2D Slotted and Porous Tunnels

3.3.2 INTERFERENCE OF SMALL MODELS, NONUNIFORM WALLS

The shortcomings of the ideal porous-wall boundary condition have long been recognised (see discussion in Sec. 3.2.2): the approximate nature of a linear crossflow boundary condition, the empiricism required to determine the crossflow resistance factor R for a given wall geometry, and the non-linear crossflow behaviour of real walls. The distinct flow physics of high total pressure flow out of the test section relative to low total pressure flow from the plenum into the test section suggests, at the minimum, a distinction between these flow regimes. The development of slanted-hole porous walls was instigated in part to balance inflow and outflow wall performance. Parallel developments in modelling walls with open slots explicitly recognised the different nature of re-entry flow from the plenum into the test section (Berndt [6]).

Such an approach has been applied, in an approximate way, to the NAE 15-in by 60-in 2D test section of the 5-ft by 5-ft Transonic Wind Tunnel (Mokry, Peake, and Bowker, [47]). For a lifting airfoil, it is proposed that the ceiling, or wall surface above the model, experiences predominantly inflow from the surrounding plenum because most of its extent will experience a pressure due to the model less than freestream static pressure (identified with the uniform plenum pressure). Conversely, the floor, with an imposed model pressure greater than plenum pressure (for the most part), will experience primarily outflow. Permitting each wall to have its own characteristic R may thus be expected to more accurately reflect the actual interference from these walls. Closed-form expressions are developed for interference quantities at the location of a small model (represented by a source doublet for volume and a point vortex for lift of an airfoil model at the centre of the tunnel). For equal upper and lower wall characteristics (and for a model centrally located), streamwise interference velocity at the model location is proportional to only the displacement effect of the model (doublet strength). Upwash interference velocity at the model is similarly dependent only on model lift (circulation). Allowing upper and lower walls to have different crossflow resistance factors (R_U and R_L) results in loss of this separability. For this more general case, streamwise interference velocity depends on both volume and lift, as does upwash. Interference factors are defined so that

$$\varepsilon = \frac{u_i}{U_\infty} = \Omega_s \frac{\pi}{6\beta^3} \left(\frac{c}{H}\right)^2 \frac{A}{c^2} + \Omega_\delta \frac{c}{H} C_L \quad (3.15)$$

$$\frac{w_i}{U_\infty} = \delta_0 \frac{c}{H} C_L + \delta_\Omega \frac{\pi}{6\beta^3} \left(\frac{c}{H}\right)^2 \frac{A}{c^2} \quad (3.16)$$

where Ω_s , Ω_δ , δ_0 , and δ_Ω are analytic functions of R_U and R_L :

$$\Omega_s = 1 - \frac{3(t_U + t_L)}{2} + \frac{3}{2} \left(\frac{t_U + t_L}{2}\right)^2 - \frac{3(t_U + t_L - 1)}{4} \left[\cos\left(\frac{\pi(t_U + t_L)}{2}\right) - 1 \right] \quad (3.17)$$

$$\Omega_\delta = -\frac{1}{8\beta} \sin\left(\frac{\pi(t_U - t_L)}{2}\right) \quad (3.18)$$

$$\delta_0 = -\frac{1}{4} \left\{ \frac{t_U + t_L}{2} + \frac{1}{2} \left[\cos\left(\frac{\pi(t_U - t_L)}{2}\right) - 1 \right] \right\} \quad (3.19)$$

$$\delta_\Omega = \frac{3}{2} \beta \left(\frac{t_U + t_L - 1}{2}\right) \sin\left(\frac{\pi(t_U - t_L)}{2}\right) \quad (3.20)$$

where t_U and t_L are defined as

$$t_{U,L} = \frac{2}{\pi} \arctan\left(\frac{R_{U,L}}{\beta}\right) \quad (3.21)$$

These interference factors are shown in Figure 3.11 as functions of Q_U and Q_L . For $Q_U=Q_L$ the cross-coupling factors Ω_δ and δ_Ω are identically zero. Mokry et al. [47] report much better correspondence of measured wall pressures with predicted pressures for the best choice of distinct floor and ceiling porosity factors than is possible with equal wall crossflow factors.

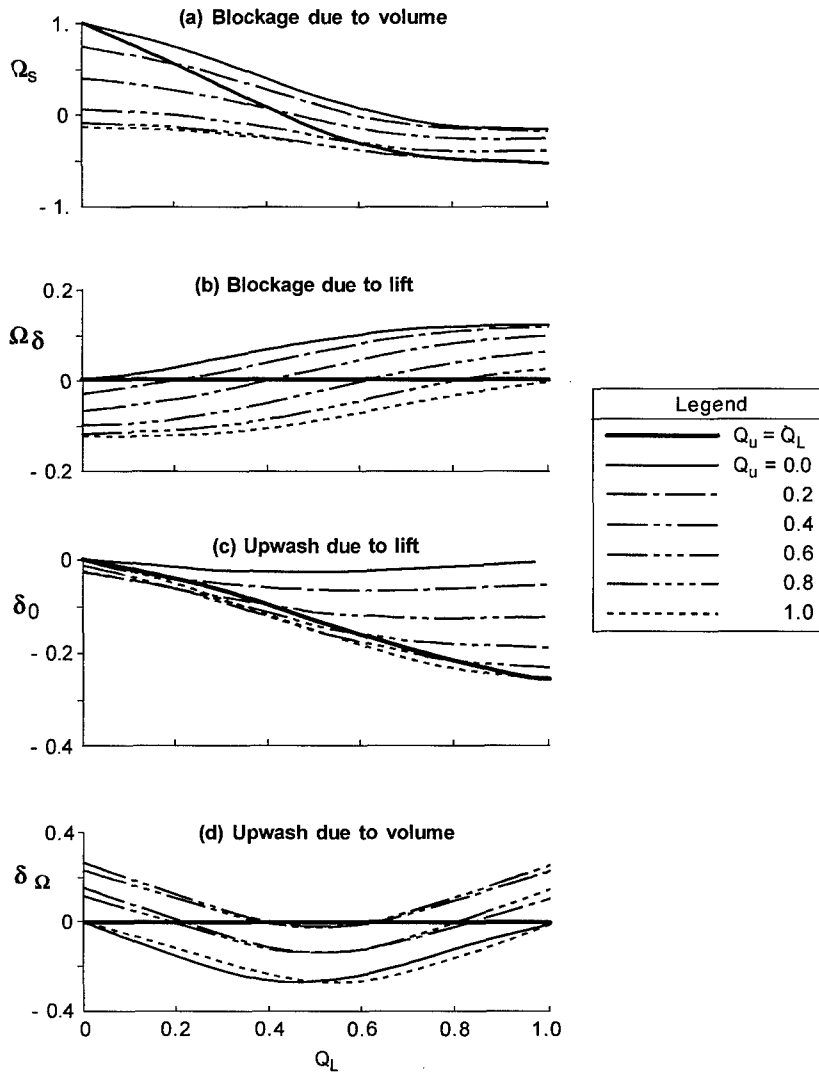


Figure 3.11 Interference in 2D Porous-Wall Tunnels With Different Floor and Ceiling Characteristics

3.4 INTERFERENCE IN 3D TESTING, CLASSICAL RESULTS

Techniques and methods for predicting the interference of a 3D model in a ventilated-wall test section parallel those used in two dimensions (with the obvious exception of complex variable methods).

The interference in ventilated-wall tunnels is characterised by the parameters defined by Equations 3.2 through 3.5: ε , δ , Ω_s , and δ_1 . In 3D flow the blockage interference velocity ratio in a ventilated tunnel is thus given by

$$\varepsilon = \frac{\tau V \Omega_s}{\beta^3 C^{3/2}} \quad (3.22)$$

where Ω_s is a function of ventilated wall characteristics, τ is the tunnel shape factor, V is the effective model volume, and C is the area of the tunnel cross section. The wake blockage interference ratio, Ω_w , is similarly defined,

$$\varepsilon_w = \frac{\tau V \Omega_w}{\beta^3 C^{3/2}} \quad (3.23)$$

For small models centrally located in a test section with walls of uniform properties (i.e., constant coefficients in the ideal ventilated-wall boundary condition, Eq. 3.9) and with viscous and vortex wakes trailing straight downstream, symmetry considerations analogous to the 2D case confirm the decoupling of blockage and lift interference. That is, the streamwise interference velocity is due only to model volume and drag (the source singularities) and the cross-stream interference velocity (upwash) is due only to model lift. It can be expected that, just as for closed walls (Sec. 2.2) and for 2D porous walls (Sec. 3.3.2), this independence applies specifically to the model location. Interference velocity components at off-centreline locations, for models not centrally located, and for arbitrary distributions of wall properties may be due to both lift and blockage effects.

3.4.1 SLOTTED WALLS

Figure 3.12 shows the interference factors at the model location for small models in circular and rectangular wind tunnels with uniform homogeneous slotted walls. These data are compiled from AGARDograph 109 [24], Pindzola and Lo [53], and Holst [29]. The close correspondence of interference in circular and square test sections is expected.

A particularly simple analytic form approximates the lift interference of a small model in a circular slotted tunnel,

$$\delta_0 = \frac{1}{8} \frac{(F-1)}{(F+1)} \quad (3.24)$$

It is noted in AGARDograph 109 that this result is obtained both from the method of Baldwin et al. [3], whose solution for an infinitesimal span horseshoe vortex is obtained by a Fourier transform method, and Davis and Moore [14], who give a solution for a finite-span horseshoe vortex (i.e., a uniformly loaded wing of zero sweep).

The solid blockage factor (Ω_s) changes only slightly with tunnel cross section because the closed tunnel reference blockage (through the tunnel shape factor τ) captures most of this influence.

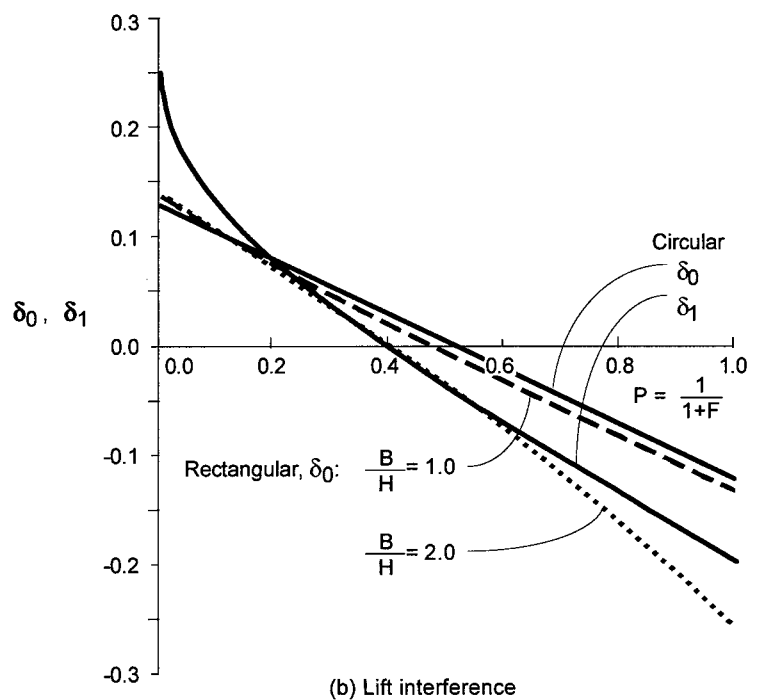
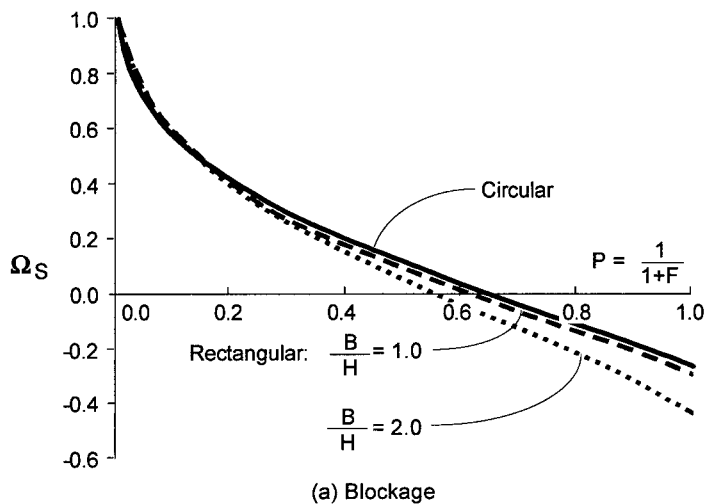


Figure 3.12 Interference of Small 3D Models in Ideal Slotted Tunnels

Lift interference, characterised by the interference factor δ , exhibits a larger variation with tunnel cross section. As discussed in Pindzola and Lo [53], for an ideal slotted tunnel the wake blockage interference is zero at the model (as well as far upstream) and the streamwise gradient due to solid blockage is zero (due to upstream and downstream symmetry of the blockage distribution). However, the streamwise gradient of wake blockage is not zero, resulting in a pressure gradient acting on the model, producing a force proportional to model effective volume. It is shown that for ideal slotted walls this gradient is identified with the magnitude of the solid blockage,

$$\frac{\partial \epsilon_{wake}}{\partial x} = -\frac{C_D S}{2V} \epsilon_{solid, closed} \Omega_s \quad (3.25)$$

Interference values for tunnels with just two slotted walls (typically the floor and ceiling) and two closed walls (sidewalls) are given by Pindzola and Lo [53], as well as for slotted tunnels with sidewalls having different slot parameters than the floor and ceiling.

3.4.2 POROUS WALLS

Figure 3.13 summarises the interference factors at the model location for small models in circular and rectangular wind tunnels with uniform ideal porous walls. These data are compiled from AGARDograph 109 (circular tunnel), Pindzola and Lo [53], and Lo and Oliver [43]. Just as for ideal slotted walls, the wake blockage gradient for ideal porous walls is given by Equation 3.25. Unlike slotted walls, however, ideal porous walls result in a non-zero streamwise gradient of solid blockage and in a non-zero wake blockage level. As discussed in AGARDograph 109 and elsewhere, wake blockage does not approach the classical closed wall result as porosity approaches zero. Mokry [46] explains this paradox as arising from the assumption that the walls are of infinite streamwise extent which results in discontinuous behaviour for the closed-wall case at upstream infinity. The importance of accounting for the proximity of the reference pressure measurement station to the model is emphasised, so that wake blockage is properly evaluated relative to the tunnel reference pressure location. Mokry [46] provides plots of streamwise variation of wake blockage for the 2D porous wall case. Lo and Oliver [43] provide similar distributions for 3D porous wall tunnels.

Pindzola and Lo [53] provide plotted interference parameters including streamwise distributions for porous wall tunnels having sidewalls of different characteristics than the floor and ceiling. Vaucheret [63] presents interference results for a test section with closed sidewalls and porous floor and ceiling. Appendices (in Vaucheret, [63]) document the equations used for application of the analytic Fourier transform method for 3D porous-wall tunnels with closed sidewalls and for a 2D porous-wall tunnel with different floor and ceiling characteristics.

Schilling and Wright [55] have calculated the upwash interference of finite-span horseshoe vortices (i.e., uniform wing loading) with span ratios of 0.3 and 0.7 in rectangular test sections with B/H from 0.5 to 2.0. Figure 3.14 summarises their results for the smaller span ratio. Closed-wall and open-jet results from Figure 2.5 (method of images) are shown for reference. Spanwise variation of interference is very small for the smaller span ratio; the larger span has substantially increased interference on the outboard wing.

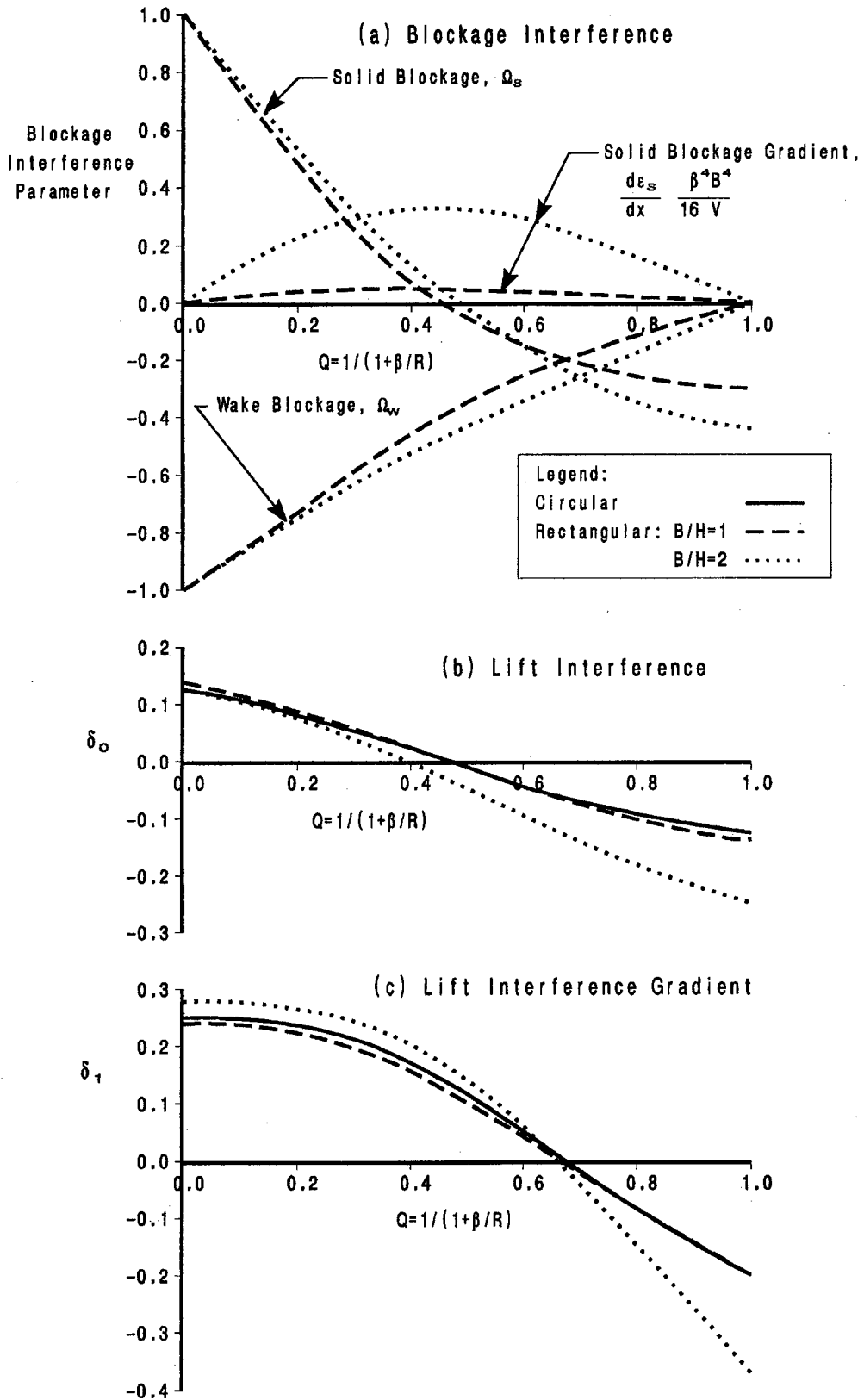


Figure 3.13 Interference of Small 3D Models in Ideal Porous Tunnels

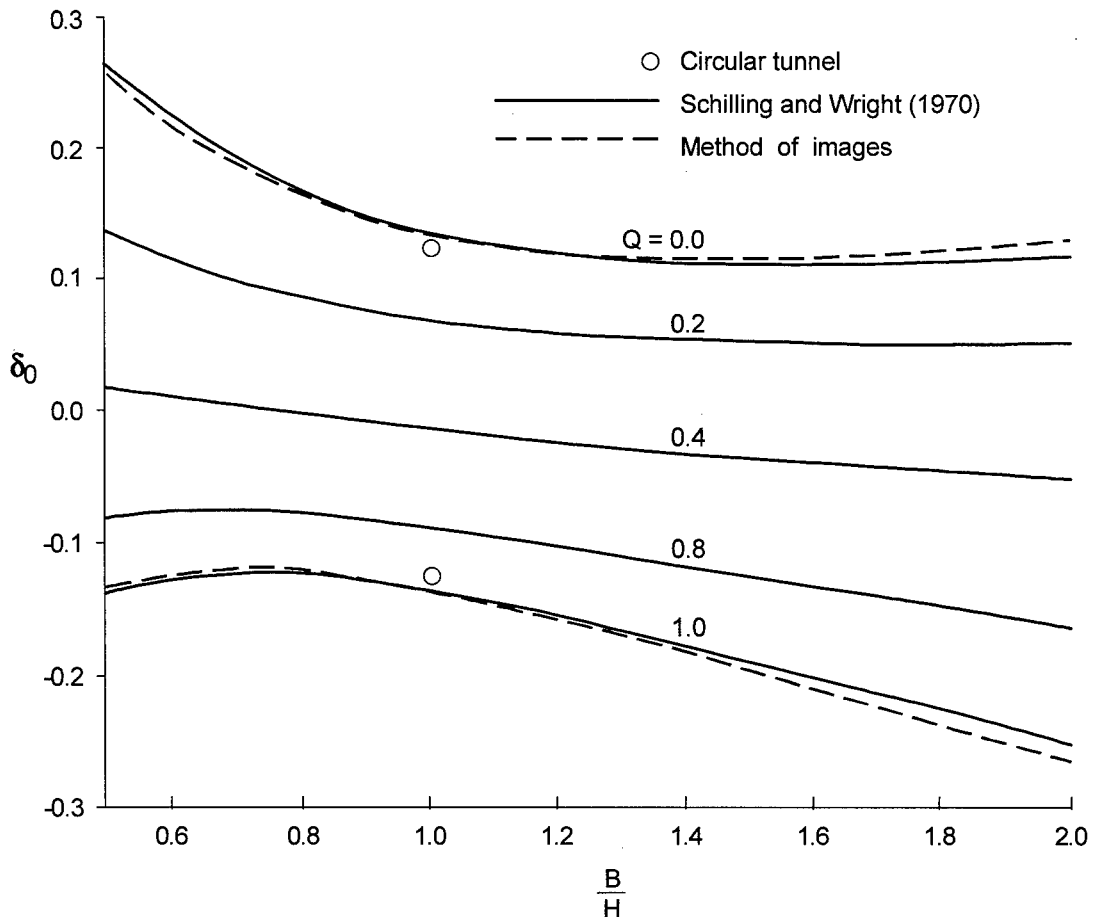


Figure 3.14 Lift Interference of Small 3D Wings in Ideal Porous Rectangular Tunnels

3.5 COMPUTATIONAL APPROACHES TO INTERFERENCE EVALUATION

The evolution of applied methods since the publication of AGARDograph 109 has generally followed the path from Fourier transform methodology (which forms the basis of results in Sec. 3.4), to panel methods with general analytic boundary conditions, and finally stepping to direct use of measured boundary conditions (see Chap. 4). An example of the latter approach is reported by Mokry, Digney, and Poole [50], who use measured wall pressures from a porous-wall transonic wind tunnel as specified boundary conditions in a panel code to assess wall interference. In general, the test article may be represented by either known or unknown singularity distributions, depending on model size, complexity, and accuracy requirements.

The principle of superposition states that the interference of collections of singularities is the sum of the separate contributions of each singularity. For a small model centrally located in a tunnel with uniform walls, this involves the solid blockage of the model volume distribution, lift interference from consideration of the model's lift (independent of volume distribution), and wake blockage from consideration of the viscous and separated wake drags. Use of singularities with strengths derived from gross model aerodynamics (volume, lift, drag) has the practical advantages of ease of use and bookkeeping simplicity. At the other extreme of model representation complexity, with a complex model geometry with many

unknowns, the analysis of a given configuration often proceeds by modelling the entire configuration and then extracting interference velocities and gradients (streamwise interference and upwash) without explicit identification with their separate origins in the classical sense.

3.5.1 POINT SINGULARITY MODEL REPRESENTATION

Keller and Wright [38] describe a panel approach for calculating the interference of lifting elements at arbitrary positions in ideal slotted (homogeneous) and porous rectangular test sections. A lifting wing is represented by a distribution of horseshoe vortices that can be located anywhere in the tunnel. Finite span, sweep, and arbitrary (specified) span loading can thus be modelled. Sample FORTRAN code is included both by Keller and Wright [38] and Keller [37]. The latter generalises the panel method to permit boundary conditions of the form

$$c_1\varphi + c_2\varphi_x + c_3\varphi_n + c_4\varphi_{xn} = 0 \quad (3.26)$$

This permits investigation of slots with crossflow resistance, or so-called "viscous" slots, as well as ideal homogeneous slotted walls and ideal porous walls. The first term was used to investigate the integral form of the ideal slotted-wall boundary condition, leading to an understanding of the effect of finite tunnel length in the analysis: interference at the model stabilises to expected values when the tunnel starts about three tunnel widths upstream of the model. The effect of porosity in the slots is found to be large, as might be expected because the walls would behave like porous walls of equivalent $R = \tau R_{slot}$, where τ is the openness ratio of the slots, as long as the number of slots is not too small.

Parametric studies of interference in perforated wall tunnels (with closed sidewalls) are reported by Vaucheret [63]. Test section height to width ratio, wing span to width ratio, wing sweep, and horizontal wall porosity were investigated. Model representation and size limits are presented for keeping corrections below specified thresholds. Tunnel configurations for minimum interference are investigated in terms of horizontal wall characteristics, tunnel aspect ratio, and wing span. A similar set of results is given for a 2D porous test section with different floor and ceiling characteristics. An optimum 2D wall configuration for minimum interference is suggested as a closed floor ($Q=0$) and ceiling having $Q=0.22$.

The need for multiple singularities to represent the volume distribution of a typical model is demonstrated by Vaucheret [65] by consideration of wall pressure signatures, showing that 12 doublets adequately represent an ellipsoid ($L/D=6$) of 1% blockage in a square closed-wall tunnel, and that use of 30 doublets for a missile configuration provides a reasonable prediction of experimental pressures in a circular closed-wall tunnel. Similar calculated results for a single-doublet and a 20-doublet representation of the above ellipsoid are given for a square test section with porous walls, with significant differences in both blockage interference and blockage gradient, Figure 3.15. The method is extended to include wake blockage and support interference. Lift is represented by a flat vortex sheet, taking into account span, sweep, and span loading. Calculated wall pressures (at zero lift and increments due to lift) matched measured pressures best for a porosity factor of $Q=0.2$ (S3Ma wind tunnel). Sample calculations are also given for models mounted above or below tunnel centreline, highlighting the coupling of streamwise and upwash interference velocities with both model volume and lift.

WALINT, a wall interference code developed at the NASA Ames Research Centre (Steinle and Pejack [60]), uses point singularities to represent the model in rectangular slotted or porous test sections. Excellent agreement of upwash interference from WALINT and from the method of images for closed-wall and open-jet wall boundary conditions is shown. For the baffled slots of the Ames 11-ft Transonic

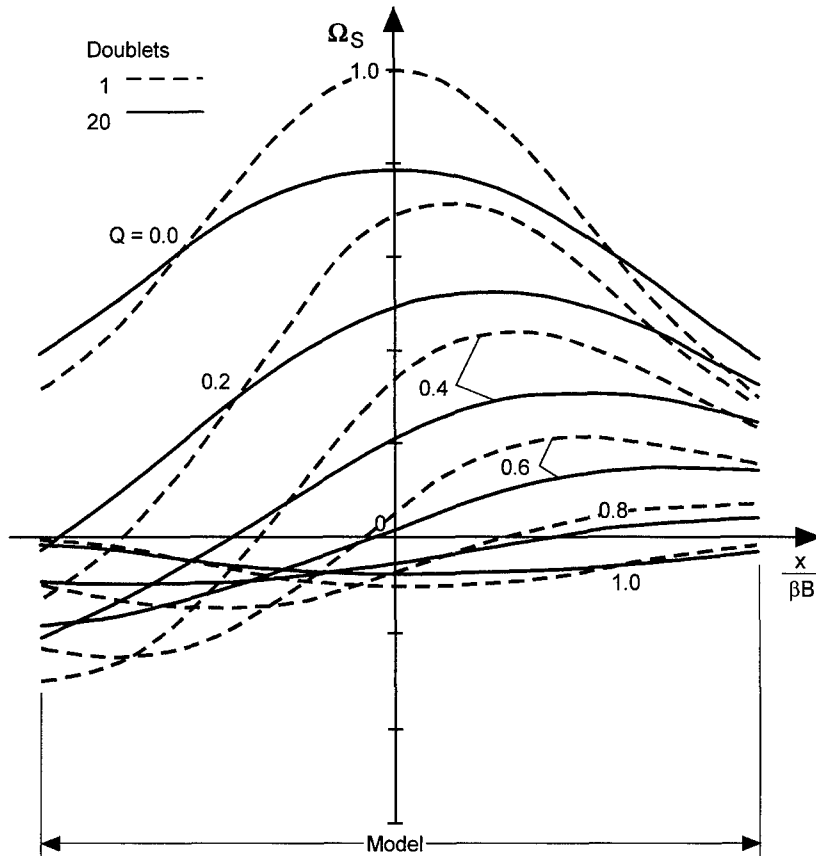


Figure 3.15 Effect of Model Representation on Solid Blockage of an Ellipsoid ($L/D = 6$, blockage = 1%) in a Square Ideal Porous Tunnel with Closed Sidewalls (Vaucheret [65])

Wind Tunnel, a value of $R=19$ is quoted. Because there are many slots (54 total on four walls), in the limit of large R (no crossflow resistance) the calculated interference of the walls with discrete slots should be very similar to that of ideal homogeneous slotted walls. The ideal inviscid slot results for a rectangular tunnel with closed sidewalls are essentially duplicated by WALINT using $R/\beta=10,000$. The interference equivalence of homogeneous porosity and porous strips is demonstrated, with identical upwash interference for a lifting element located within the central region of the test section ($|y/B|<0.3$). Steinle and Mabey [59] report computed interference results from WALINT using 20 singularities to represent an elliptically loaded wing with a span to tunnel width ratio of 0.7. Twelve source doublets were used to represent a model body whose length equals the wing span. For the cases analysed the spanwise variation of interference upwash was much less for slots with resistance than for ideal slots.

3.5.2 PANEL METHODS, HOMOGENEOUS VENTILATED WALLS

Most recent computations of wall interference rely on panel or vortex lattice computational methods. Vaucheret [66] reports results from a vortex lattice code used to overcome restrictions of classical analytical methods regarding geometry of the test section (both in cross-section and streamwise extent), model and sting incidence, and wall boundary conditions. A model and its support system may be represented by either a collection of singularities of strengths determined by the known geometry and loading, or by panels with unknown strengths. For a closed-wall case, inlet conditions were uniform to within $C_p < 10^{-5}$ when the test section length was at least seven times the tunnel height. Use of a non-

linear porous-wall boundary condition is compared to results with a linear crossflow wall characteristic. The addition of perforated window inserts in the closed sidewalls of a test section with perforated floor and ceiling (S2 tunnel) is shown to decrease both the spanwise and chordwise variation of upwash interference for a transport model. The effects of model proximity to reference static pressure taps are shown for the S1Ma tunnel. It is suggested that not more than 6000 mesh cells be used per half-configuration (i.e., for problems with one plane of symmetry and including a support that requires panelling). For a simple case, however, it is reported that the upwash correction in a cylindrical test section is essentially the same for solutions with 270 and up to 5600 panels.

PAN AIR, a higher order panel code for linearised potential flow analysis (Magnus and Epton [45]) as well as TRANAIR, which solves the full potential equations (Johnson et al. [35]), have been used to investigate interference in the Ames 11-ft Transonic Wind Tunnel. Tunnel modelling has mainly been limited to long tunnels with constant wall properties. Computational tunnels typically extend two or more model lengths upstream and downstream of the model. The model in the test section is a part of the input geometry; the singularity strengths associated with its panelling are unknowns along with the wall panel strengths. The effect of the walls on model loading is thus an explicit part of the solution. The walls were modelled as homogeneous ideal porous walls with $R=1.14$, corresponding to $R=19$ for the baffled slots (at 6% openness) as recommended by Steinle and Pejack [60].

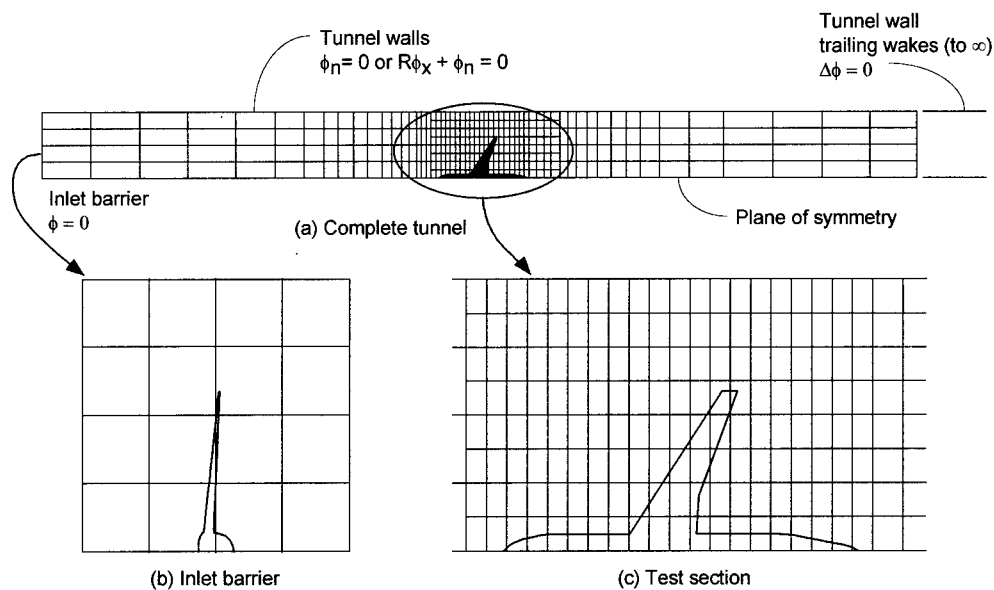


Figure 3.16 Typical Panelling with Boundary Conditions

Figure 3.16 depicts a typical panelling and associated boundary conditions for the analysis of a floor-mounted half-model with ideal homogeneous porous walls. The floor is not panelled because it is treated as a plane of symmetry in the analysis. Approximately 2000 panels are used: about 1000 for the wind tunnel walls, the remainder for the model. It was found that doubling the panelling had a negligible effect on the interference. This panelling exhibits several features characteristic of this type of analysis. The tunnel is very long so that flow perturbations due to the model are negligible before the ends of the computational tunnel are encountered (except for the trailing vortex wake at the downstream end; no viscous wake was included in this analysis). Wall panel size is varied to adequately capture streamwise and circumferential variations of the pressure field due to the model. Far upstream where pressure gradients are small, large panels are sufficient. In the region around the model, streamwise panel

spacing is decreased significantly and circumferential panel density is doubled. No leakage problems have been encountered. Inflow through the upstream face equals outflow at the downstream end of the tunnel as long as the walls are long and have constant ideal characteristics.

Good agreement with wall pressures measured between the slots have been obtained. Calculated interference for several transport models, Figure 3.17 (Goldhammer and Steinle [28]) exhibits differences in lift interference attributable to differences in both wing span and sweep. Blockage interference is small and essentially the same for these models. The spatial variation of interference for the largest of these wings at a cruise condition is illustrated in Figure 3.18. A root-to-tip Mach increase of 0.005 represents the streamwise gradient of blockage due to porous-wall crossflow characteristics. Upwash interference variation over the wing planform is only slightly larger than 0.02 degree.

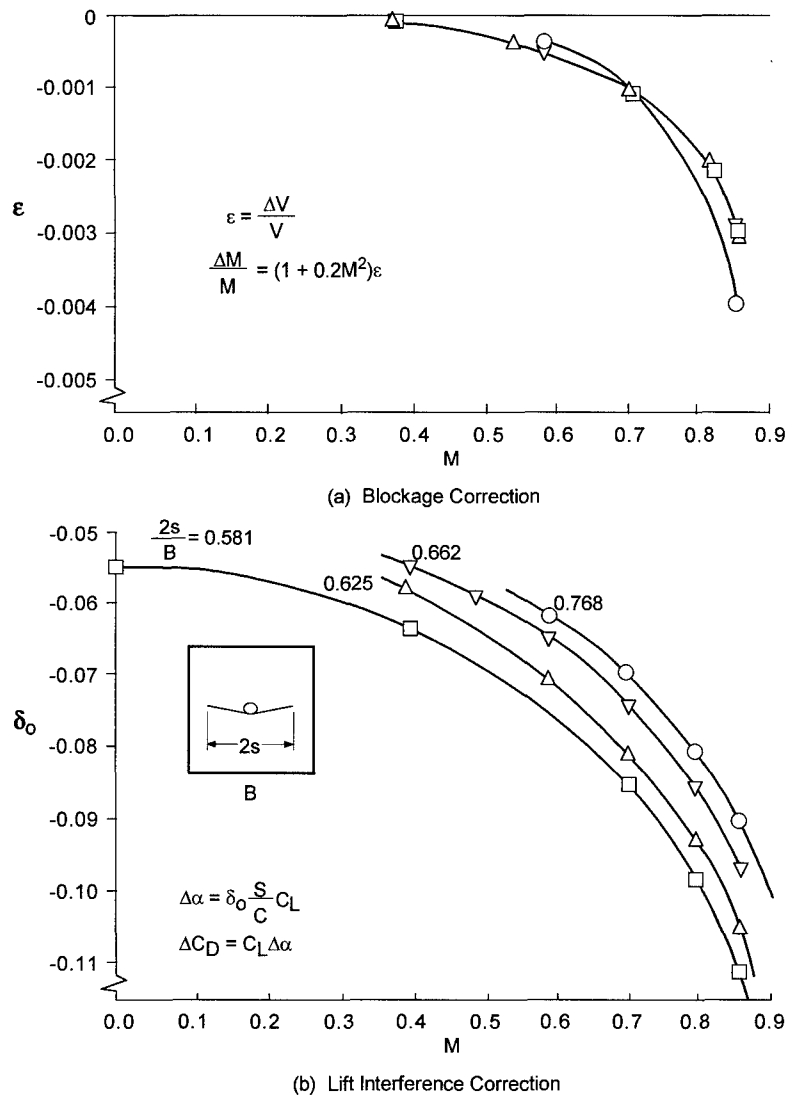


Figure 3.17 Interference at the Wing Reference Location for Transport Half-Models in an Ideal Porous-Wall Tunnel; $R=1.14$, $B/H=2.0$, $M = 0.80$, $C_L \cong 0.45$ (Goldhammer and Steinle [28])

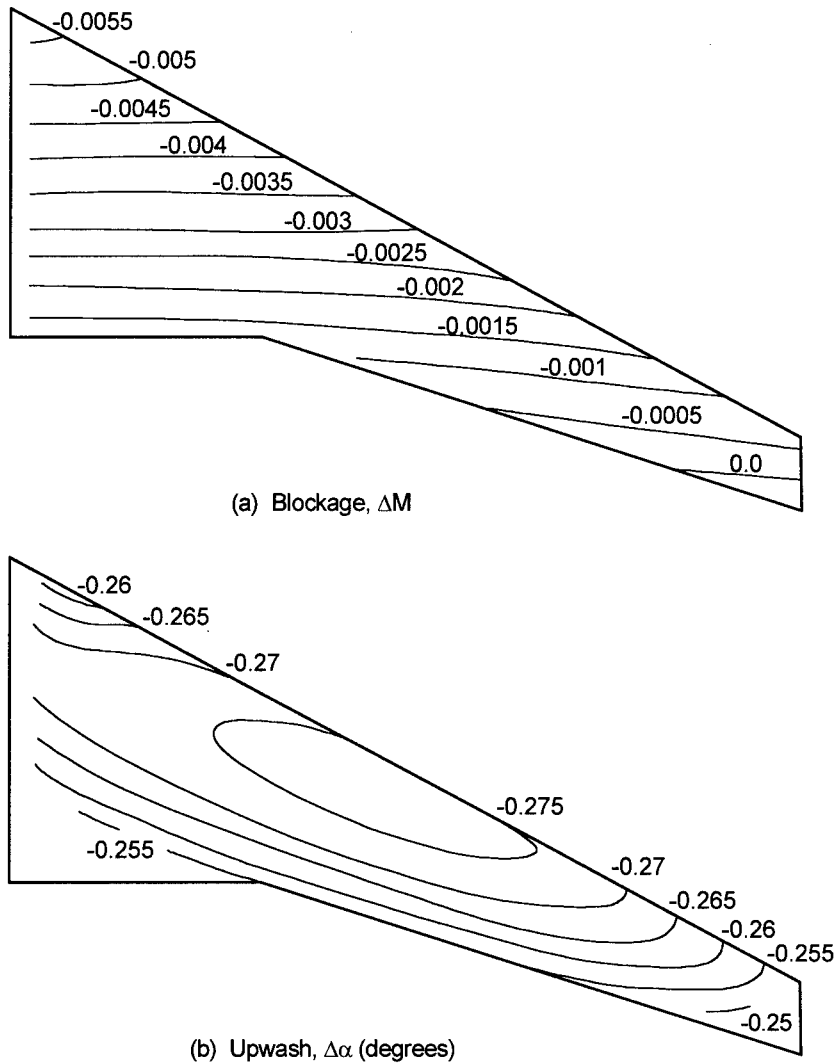


Figure 3.18 Interference Distribution at the Wing in an Ideal Porous-Wall Tunnel: $R = 1.14$, $B/H = 2.0$, $M = 0.8$, $C_L \cong 0.45$, $2s/B = 0.768$ (Goldhammer and Steinle [28])

3.5.3 PANEL METHODS, FINITE-LENGTH AND DISCRETE SLOTS

Two geometric features that differentiate all real test sections from the idealised tunnels of the preceding sections are discreteness of wall ventilation and finite upstream and downstream extent of wall ventilation. Related to the latter are the further considerations of model support struts and test section diffuser interference at the downstream end of the test section, as well as possible entrance effects due to proximity of the contraction at the upstream end of the test section.

Generally the importance of these elements may be discounted as distance from the disturbance source (in hydraulic diameters) increases beyond one. This is hardly ever the case at the downstream end of the test section where a combination of a closed-wall diffuser, a large support strut, and possibly re-entry plenum flow often occurs within a hydraulic diameter from the end of the model. The issue of discreteness of wall openings arises in two general contexts: interference of walls with a small number of slots and the implications of wall flow details on measurement methods (Chap. 4).

Kemp [39] [40] has developed a numerical method of a slotted wind tunnel test section using a general-purpose panel program as a starting point. Model lift and volume distribution can be represented by singularities with specified strengths. Walls are modelled using superposed source and doublet panels, Figure 3.19. The homogeneous ideal slot boundary condition (in integral form) may be specified for the

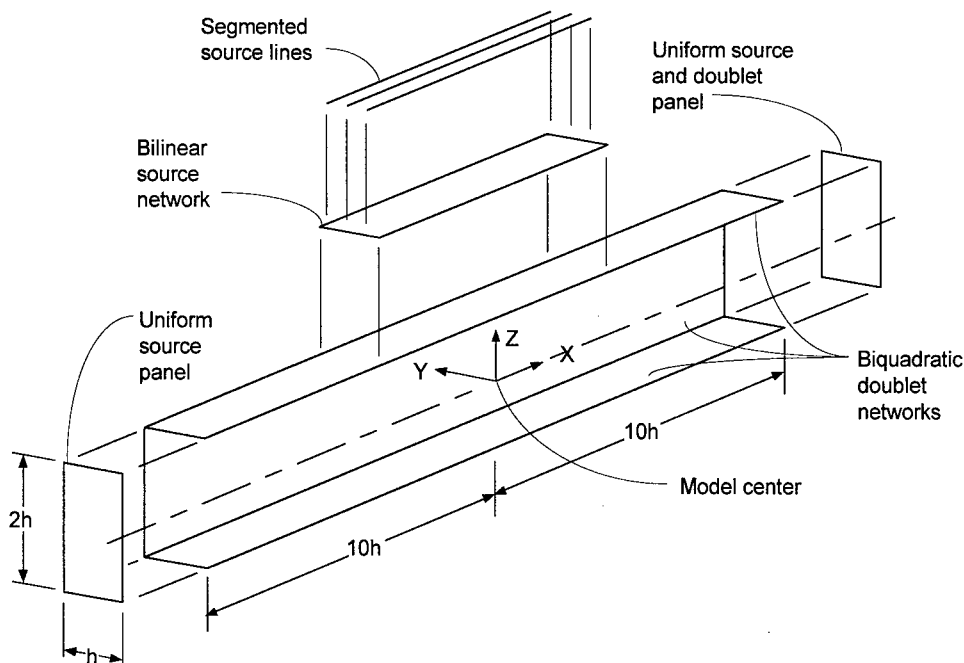


Figure 3.19 Tunnel Modelling (Kemp [40])

walls. Discrete slots are modelled by the addition of source lines to gather the distributed mass flux through the wall. Consideration of flow in the crossflow plane toward a single slot suggests that within a slot spacing from the wall the flow is the same as for the equivalent homogeneous slotted wall. Investigation of non-linear slot boundary conditions (including a quadratic crossflow term and an approximation to the slot inflow model developed by Berndt and Sorensen [8]) found significant streamwise interference due to lift for a model in the centre of the tunnel. Calculation of interference for slots of finite length ($-1.58 < x/H < 1.46$) resulted in unbalanced massflow through the tunnel. The walls were initially found to provide a net inflow to the tunnel. Balanced inflow and outflow was achieved by letting the plenum pressure in the slotted-wall boundary condition be different from the upstream reference pressure. In effect, the plenum is numerically depressurised until it no longer pushes a net inflow into the test section.

For tunnels of infinite upstream and downstream extent and with constant coefficients in the ideal boundary condition, integration of Equation 3.9 in x from far upstream to far downstream results in zero net mass flux through the walls (as long as ϕ , the perturbation potential of the model, goes to zero at these limits). Any other streamwise distribution of wall properties, R and K , or nonlinearity of the boundary condition (as noted by Kemp, see above) can be expected to result in a tunnel exit flow which does not equal the entrance flow. The walls may either add or extract flow from the tunnel. The strategy of adjusting plenum pressure in the ventilated-wall boundary condition must be applied for each particular flow condition for a given model. Pressure and force coefficients computed using upstream flow conditions must be recalculated to reflect the plenum static pressure and its associated Mach number as the proper reference conditions. This parallels the common operating primacy of plenum static pressure in real ventilated-wall tunnels.

The effect of finite slot length on the interference of the three basic point singularities is shown in Figure 3.20 (from Kemp [40]). Closed-wall interference is shown for reference. For solid blockage, Figure 20a, blockage at the model location for the two slotted-wall cases is in agreement if the reference static pressure is taken as plenum pressure (represented by the parameter u_p) for the finite-length slot case. In Figure 20b, the case with plenum suction (for offsetting wake blockage) demonstrates decreases in both wake blockage and wake blockage gradient at the model location. Lift interference at the model location is affected very little by the finite extent of the slots or by the numerical simulation of a re-entry flap at the trailing edge of the test section, Figure 20c. Depending on the size of the model, however, upwash at the tail may be affected.

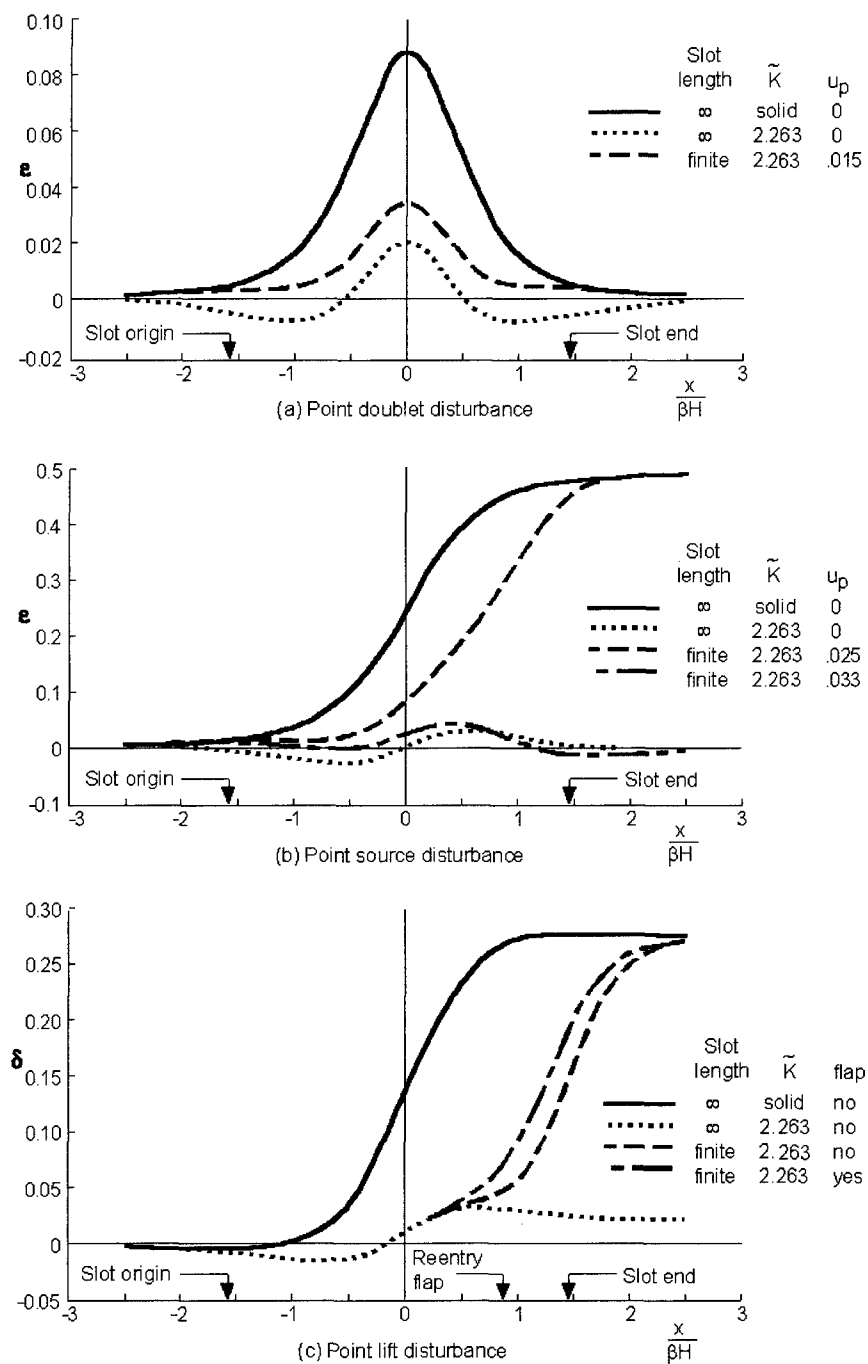
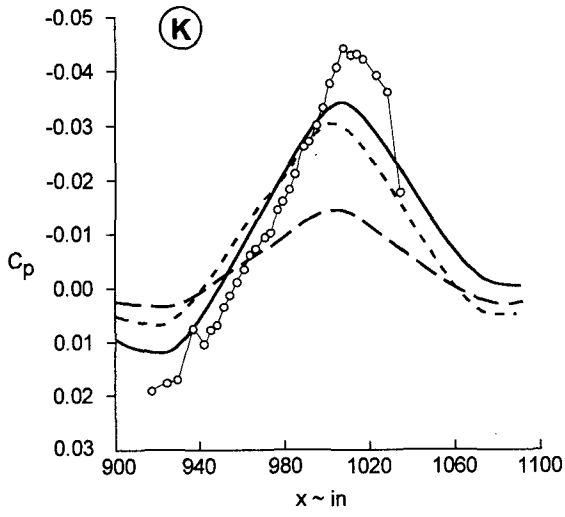


Figure 3.20 Effect of Finite Length of Slots on Interference (Kemp [40])

The evolution of wall correction methodology as applied to a production transonic wind tunnel is exemplified by developments at the Boeing Transonic Wind Tunnel (BTWT). Operation as a high-subsonic wind tunnel began in 1944 with conversion to transonic capability in 1953, including the installation of slotted walls. The test section has an 8-ft by 12-ft rectangular cross section with 2-ft corner fillets. The walls have 16 longitudinal slots at a nominal openness of 11%. Panel code interference calculations (Lee [42]) using the ideal homogeneous slotted-wall boundary condition (Eq. 3.9 without the viscous term) for a moderately sized model ($2s/B < 0.6$) corresponded very closely to the classical value, $\delta_0 = -0.11$ (Davis and Moore [14]) for lift interference. Calculated blockage corrections were so small as to be considered unverifiable.

An example where discrete slot modelling was found necessary is shown in Figure 3.21. The closed-wall corner fillets at the BTWT floor intrude into the flow field of a floor-mounted half-model at its plane of symmetry. Although details of the flow through the slots are not expected to be well represented in this inviscid calculation, comparison of calculated wall pressures to measurements provides some clues regarding slotted-wall behaviour for this tunnel. Increasing magnitude of the pressure peak due to wing lift (section K in Fig. 3.21) is expected with increasing wall resistance (R decreasing). Movement of the pressure peak (due to lift) downstream is also associated with decreasing R . Decreasing the slot width, consistent with the slot-flow model of Berndt and Sorensen [8] would be expected to improve this aspect of the correlation. The resistance of the slots improves the wall pressure correlation on the pressure side of the wing as well, though the more meaningful metric is the pressure difference between opposite walls (an error or bias in reference Mach number or static pressure would be manifested as a C_p zero shift). Although the longitudinal extent of pressures is limited, upstream values suggest an asymptotic approach to a non-zero C_p . This is consistent with the previous discussion relating to plenum pressure lower than upstream static pressure for finite-length wall ventilation. Finally, even though the downstream range of pressure measurements is very limited, there is some indication of a longitudinal gradient in the measurements that is not present in the theoretical models. This is thought to be related to non-ideal slot behaviour. The proximity of the unventilated fillets has the effect of shifting the interference toward more closed-wall values relative to the equivalent homogeneous-wall tunnel, Figures 3.22 and 3.23.



- Test
- - - Homogeneous slotted walls
- · - Discrete open slots
- Discrete porous slots, R = 19

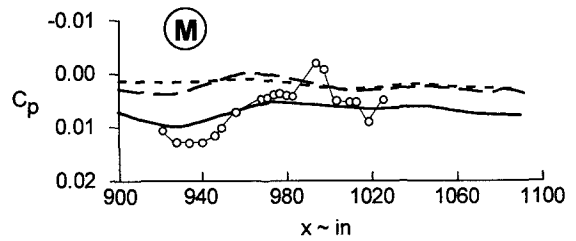
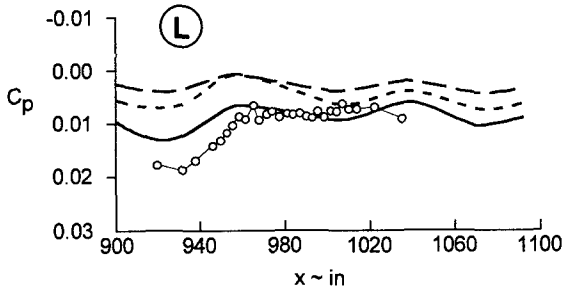
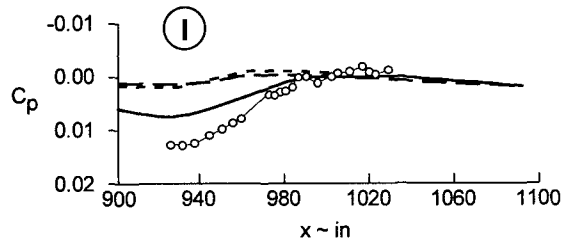
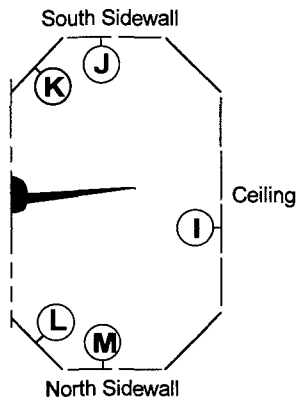
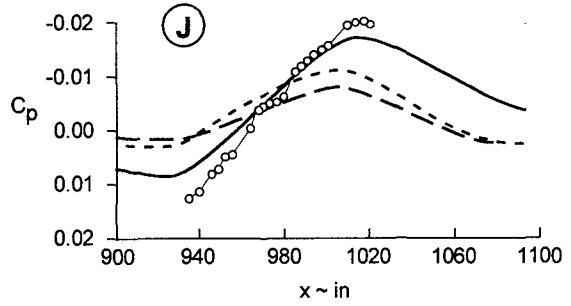


Figure 3.21 Wall Pressures in a Slotted-Wall Tunnel with a Transport Wing-Body Half-Model, $M = 0.8$, $C_L \cong 0.45$

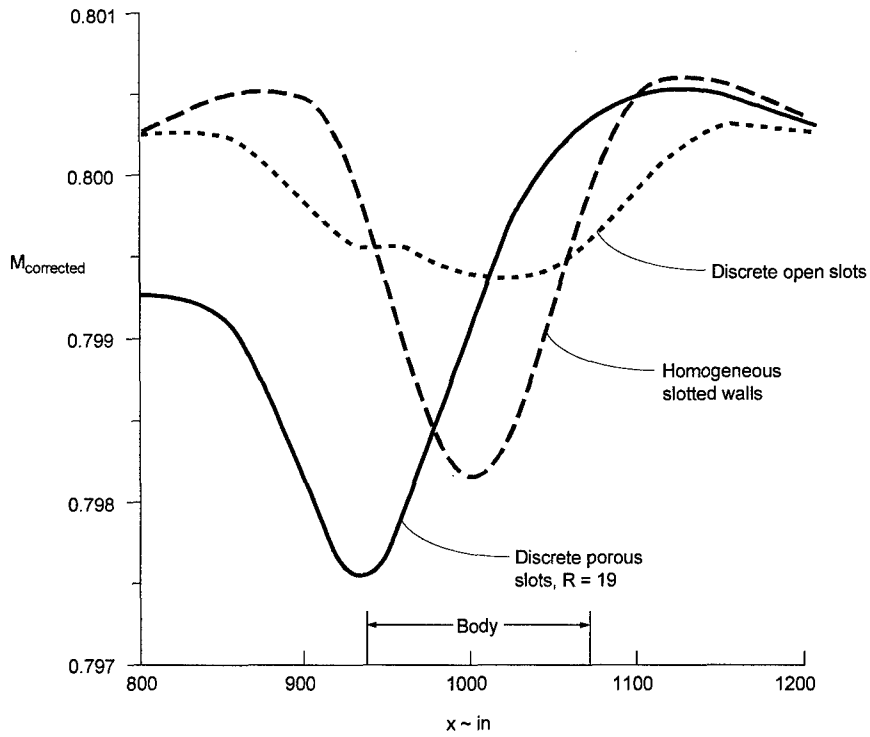


Figure 3.22 Longitudinal Distribution of Blockage Interference of a Transport Half-Model in a Slotted-Wall Tunnel, $M = 0.8$, $C_L \cong 0.45$

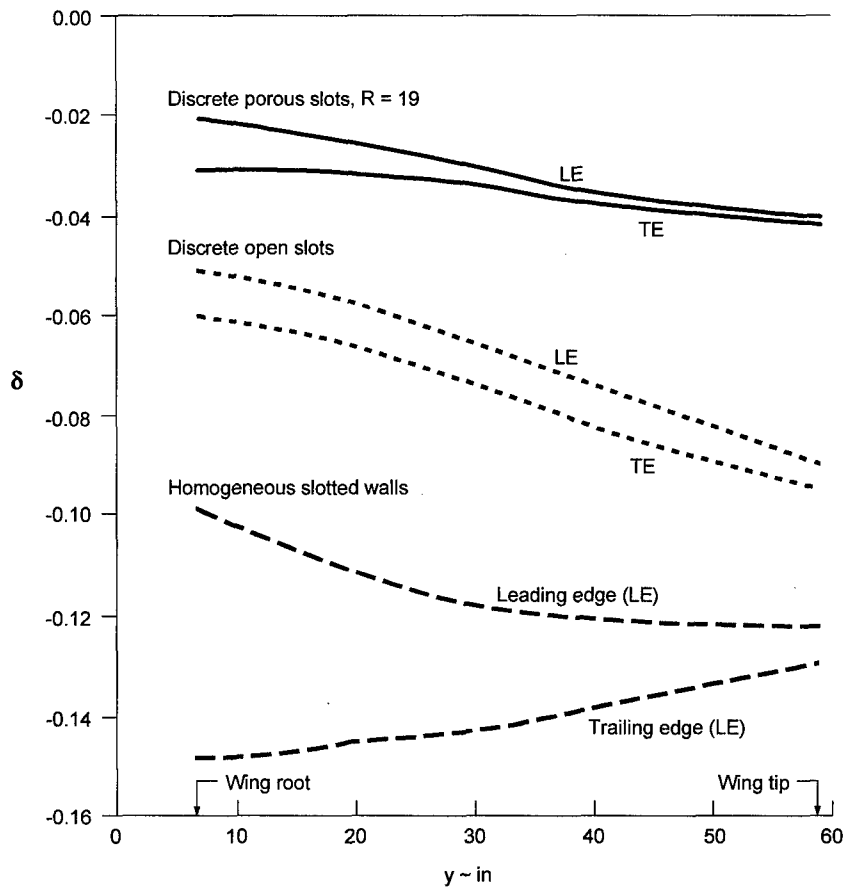


Figure 3.23 Spanwise Variation of Upwash Interference of a Transport Half-Model in a Slotted-Wall Tunnel, $M = 0.8$, $C_L \cong 0.45$

Continuing concern over the proper slotted-wall boundary condition has been addressed by a series of wall interference investigations in which typical sting-mounted transport wing-body models have been tested and analysed in BTWT with two different wall configurations: closed walls and 11% open slots. Code predictions of the interference in the closed-wall test section were used to correct the measured force data. These interference-free data were used to deduce lift interference of the slotted walls. Assuming that blockage and flow curvature corrections are small in the slotted test section, the lift interference factor for slotted walls is calculated from the interference-free (closed-wall measurements, corrected using CFD upwash and blockage) and uncorrected (slotted-wall measurements) lift-curve slopes,

$$\delta_0 = \frac{C}{S} \left[\frac{1}{a_{corr}} - \frac{1}{a_{unc}} \right] \quad (3.27)$$

In parallel to the experimental efforts, the wall boundary conditions were varied computationally with the goal of matching wall pressures measured midway between wall slots both above and below the model. The wall pressure data quality is considerably improved by first subtracting clear-tunnel distributions. The resulting pressures are then interpreted as being due to only the model and its sting support. Further conditioning of the wall data is done by fitting each wall pressure measurement (the i -th tap) in a least-squares sense in C_L (up to 0.45) at each Mach number:

$$C_{p_i} = CP0_i + CP1_i \times C_L \quad (3.28)$$

where $CP0$ is the model signature at zero lift and $CP1$ represents the incremental effect of model angle of attack. Figure 3.24 compares the experimentally determined coefficients to CFD predictions for the closed-wall configuration. The better correlation of the full potential code with experiment reflects the role of non-linear compressibility in the flow. For the slotted-wall configuration, various ventilated-wall boundary conditions have been investigated: ideal homogeneous slots, discrete slots with an open-jet (constant pressure) boundary condition, constant ideal porosity applied at the slots, and several combinations of variable porosity. The variable-porosity wall models are motivated by physical considerations: the volume of the pressure plenum below the floor is restricted by a large external force balance and its associated enclosure. Figure 3.25 compares measured wall pressure for the slotted walls to CFD calculations for walls with $R=10$ for the floor slots and $R=18$ for the remaining slots.

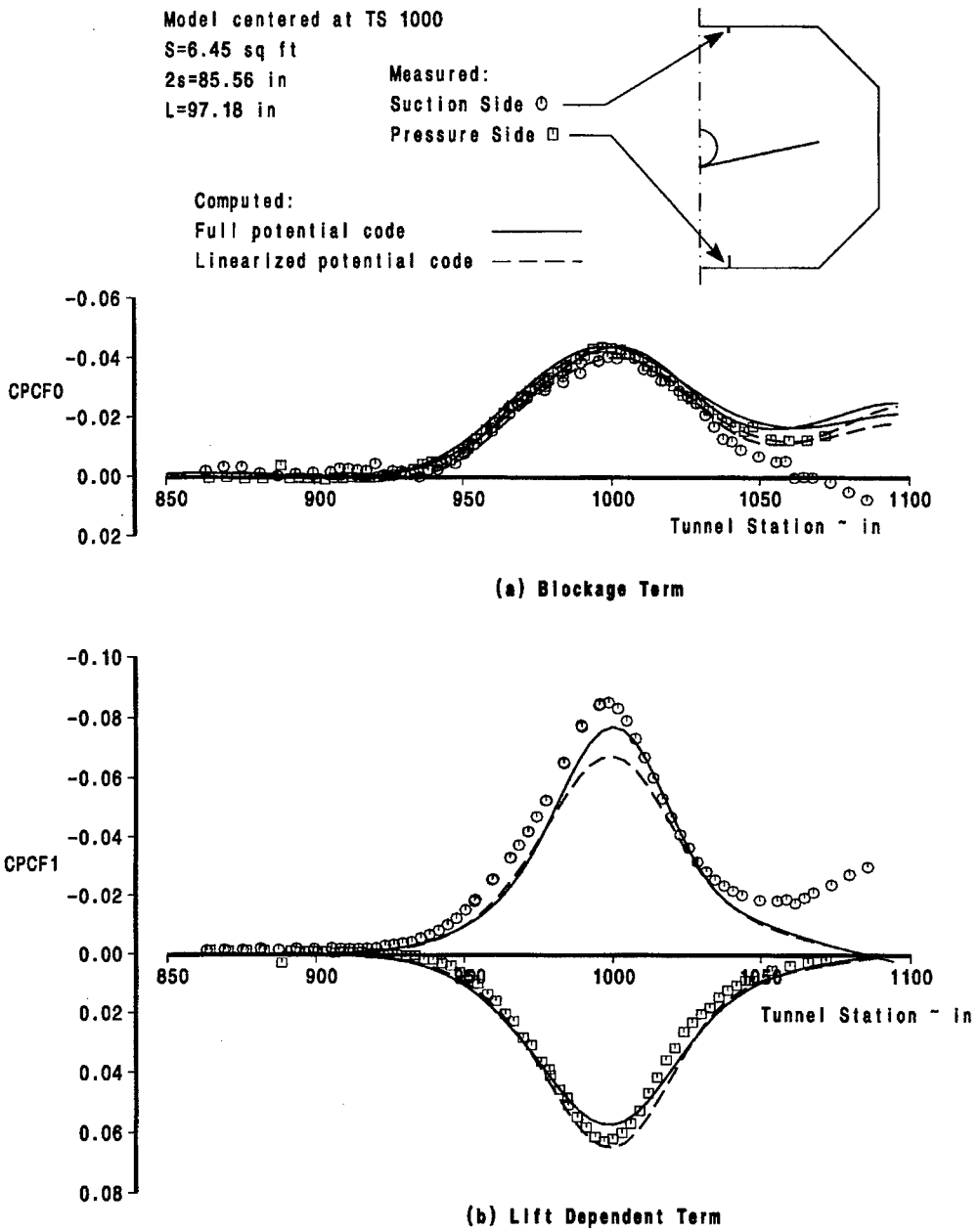


Figure 3.24 Computed and Measured Wall Pressures with Closed Walls
 767-300 Wing-Body at $M = 0.80$

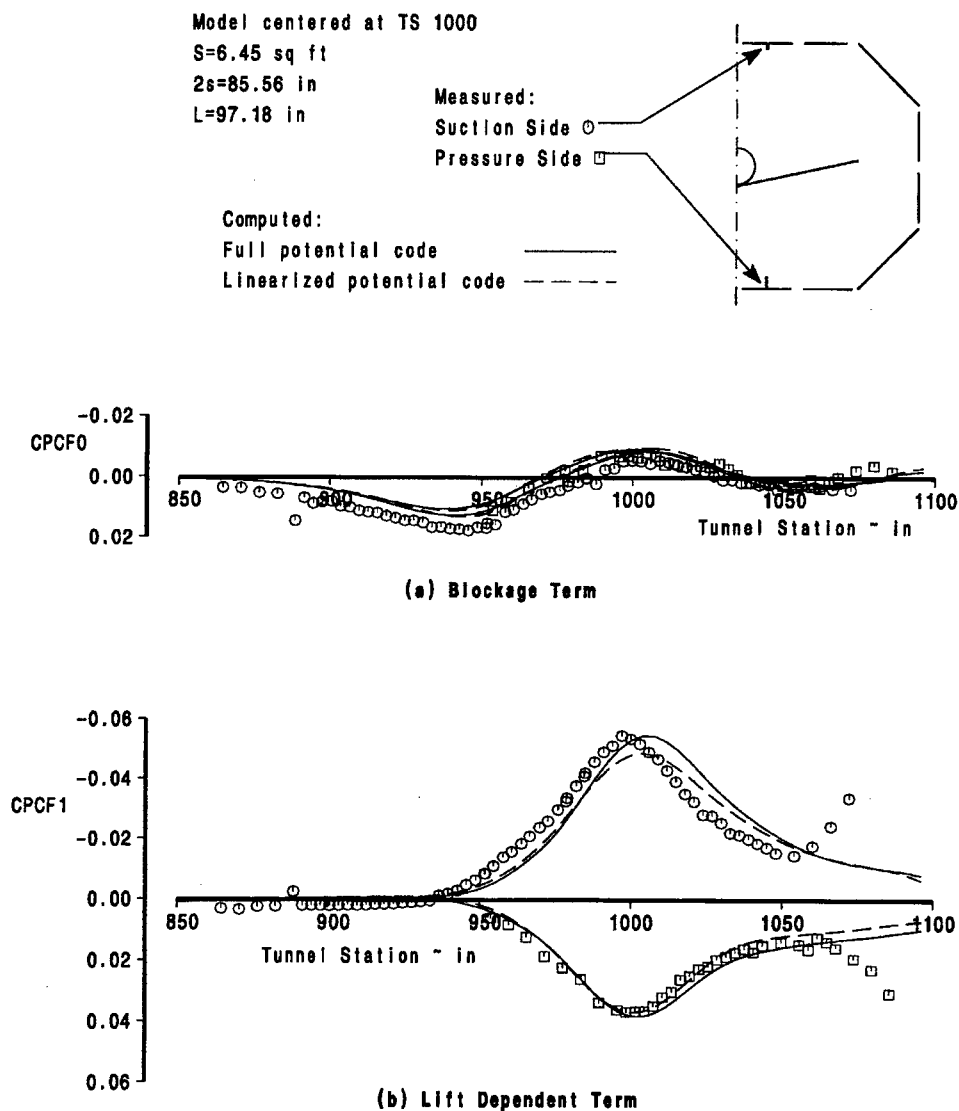


Figure 3.25 Computed and Measured Wall Pressures with Slotted Walls 767-300 Wing-Body at $M = 0.80$

The interference factors deduced from these studies are shown in Figure 3.26. The Mach number correction for closed walls from the linear potential code shows no variation of blockage interference with model attitude. The full potential code indicates similar interference at zero lift ($\alpha = -2$ deg), but slightly increased blockage with angle of attack. The variation of δ_0 with Mach number for the experimental data suggests that the slot characteristics include some measure of porous-wall behaviour (for which interference factors depend on R/β). The irregularity for $M > 0.80$ is thought to be due to uncertainty in the blockage correction used to correct the closed

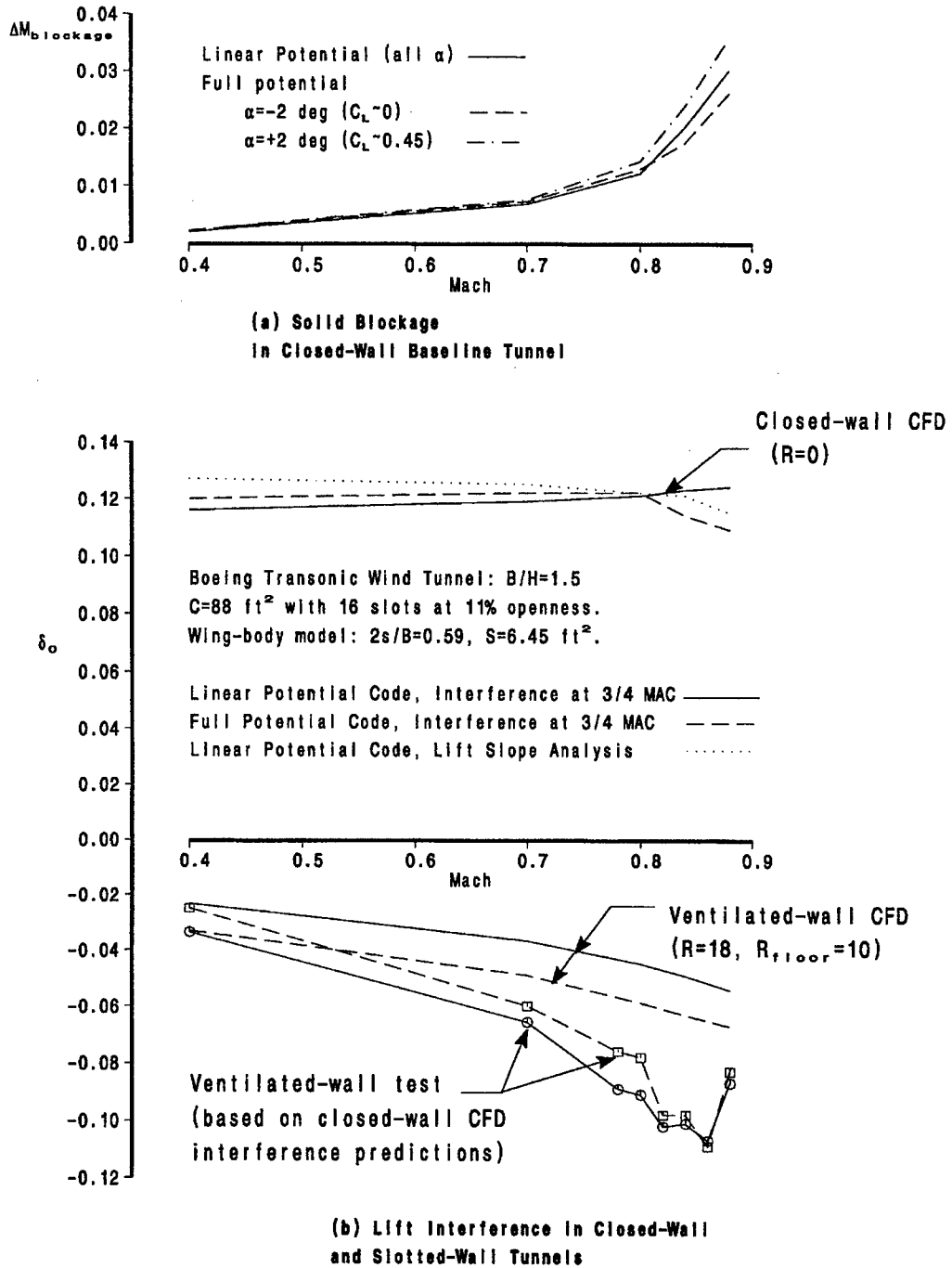


Figure 3.26 Interference of a Subsonic Transport Model in a Slotted-Wall Tunnel

wall data at high-subsonic Mach numbers. An error in the blockage correction factor (ϵ) for closed walls of 0.001 corresponds to a dynamic pressure correction ratio of 1.002, which directly scales the measured lift curve slope. At $M=0$, this corresponds to a numerically equivalent change in δ_0 of approximately 0.01. An error of this magnitude for incompressible solid blockage is magnified fourfold at $M=0.84$. This source of uncertainty is present in both the closed-wall interference value and in the assumption of negligible slotted-wall interference. Uncertainties in δ_0 are due to both sources. This interdependence of extracting two or more interference components from a single set of data having unknown interference suggests that increasing accuracy requirements on one component be matched by corresponding accuracy for the others, including the accuracy of the "interference-free" data set.

The distribution of blockage and upwash interference at the wing at $M=0.80$ for closed walls and the differential resistance wall model is shown in Figure 3.27. These results support the initial assumption of negligible blockage interference and demonstrate a significantly smaller variation of upwash interference over the wing planform for slotted walls compared to closed walls.

An investigation of wall and slot geometry in support of slotted transonic tunnel development efforts considered the effect of slot number on interference. The slotted-wall boundary conditions for this study combine adjacent columns of panels with either an open-jet or closed-wall boundary condition. Figures 3.28 and 3.29 compare interference at the model station ($x=2000$ in) for two cases of equivalent total slot openness (10%): 4 slots (2 on each of the floor and ceiling) and 24 slots (6 on each of the floor and ceiling, 4 on each sidewall). Larger spanwise gradients of both blockage and lift interference are evidently due to the closed sidewall. Longitudinal gradients of interference at the tunnel centreline are very similar, Figure 3.29. Another tunnel development study using a porous-slot boundary condition (Bussoletti et al. [10]) indicates that interferences at the model for a large number of slots and for equivalent homogeneous walls are very similar, Figure 3.30.

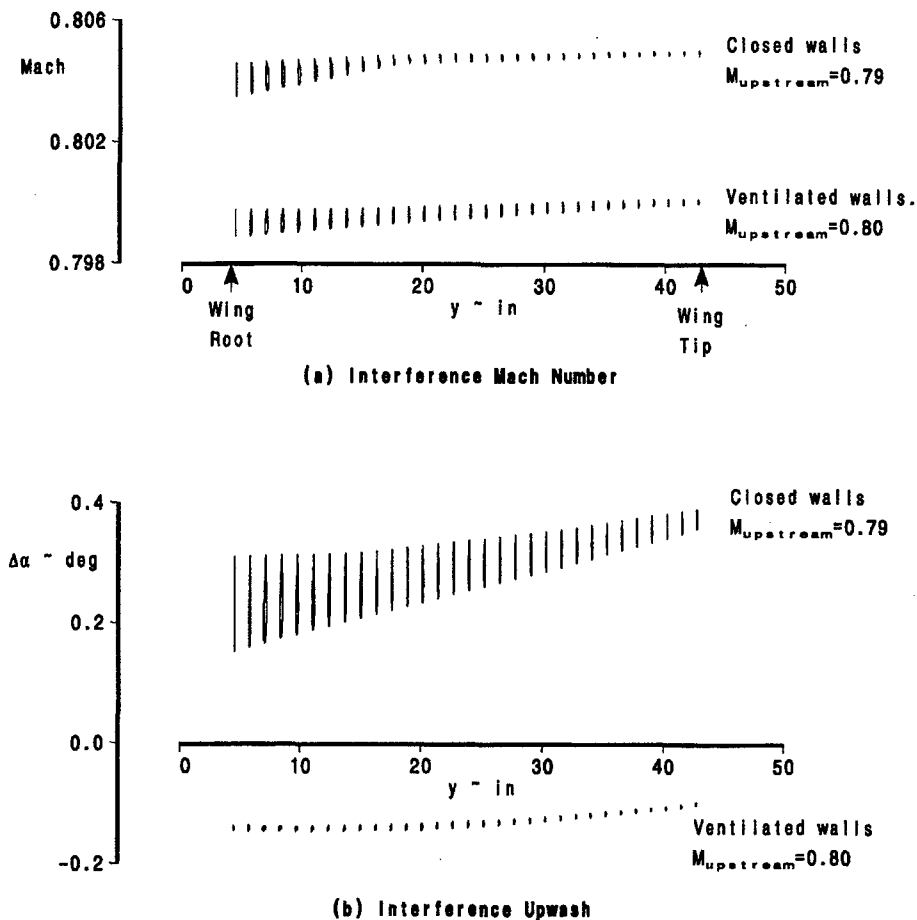


Figure 3.27 Interference at the Wing of a Transport Model in Tunnels with Closed and Ventilated Walls, $2s/B = 0.594$, $C_L \approx 0.45$, $B/H = 1.5$

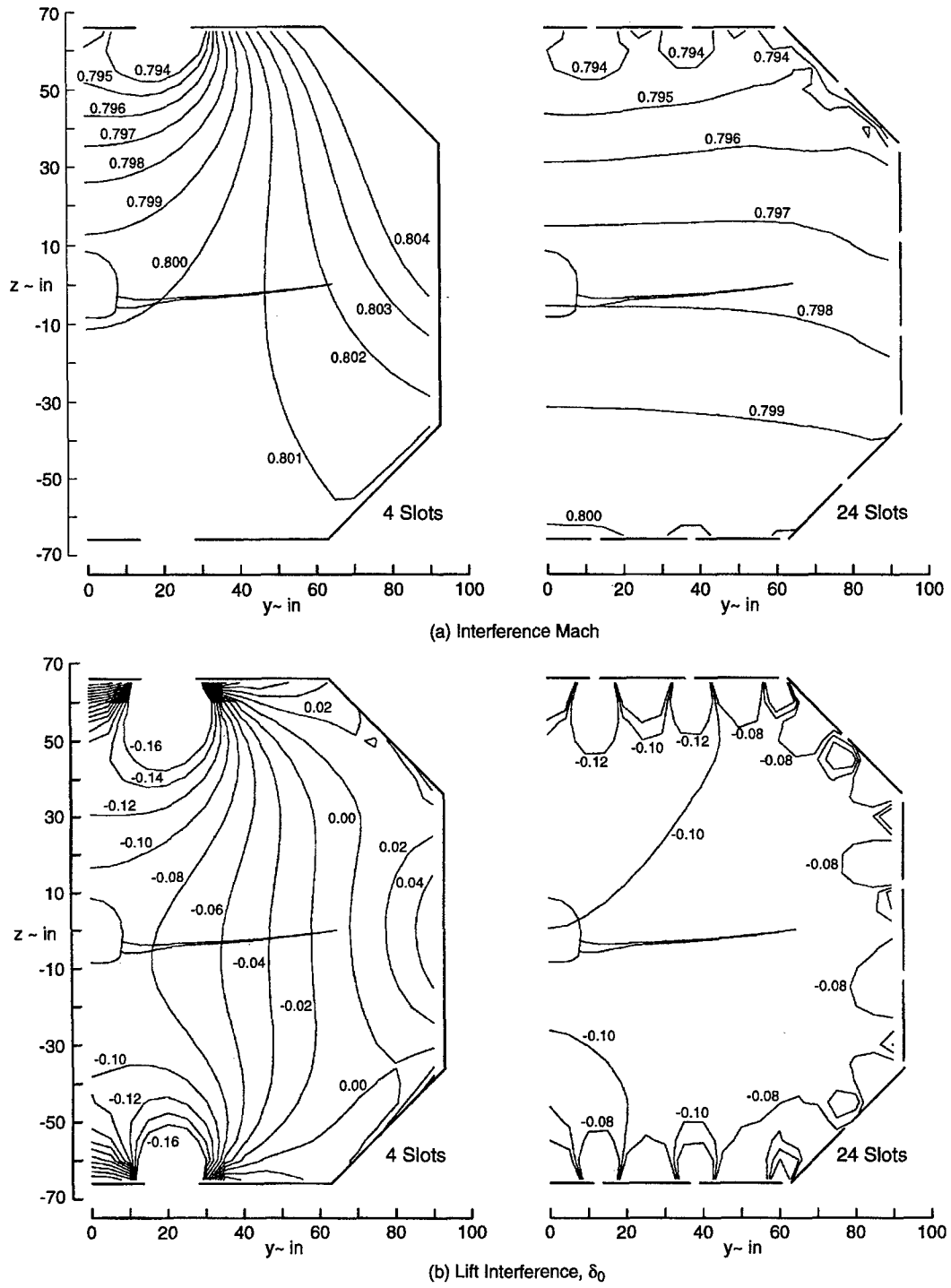
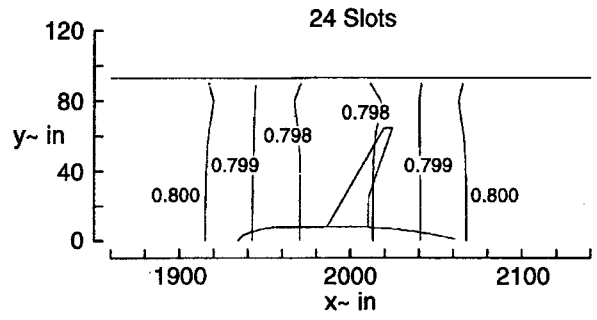
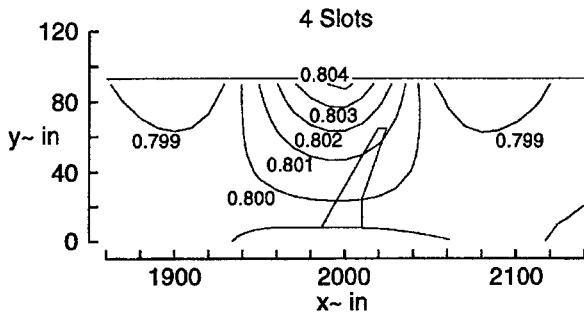
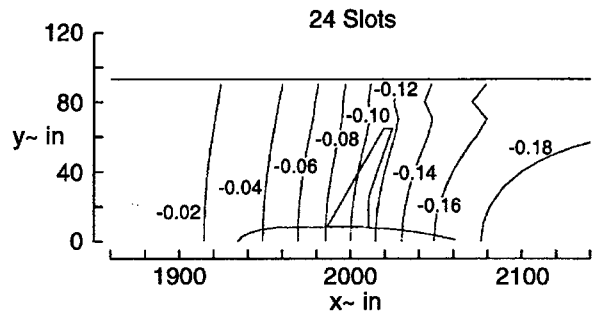
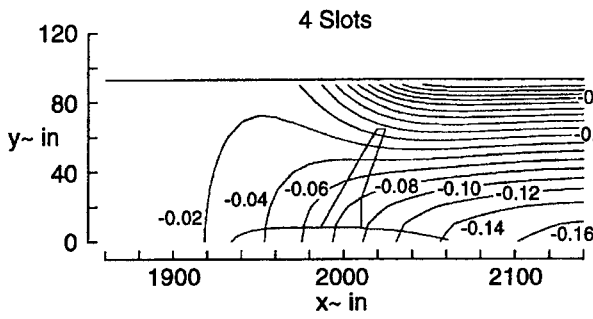


Figure 3.28 : Effect of Number of Slots on Interference in the Vertical Cross-Plane at the Model Centre



(a) Interference Mach



(b) Lift Interference, δ_0

Figure 3.29 : Effect of Number of Slots on Interference in the Horizontal Streamwise Plane through the Model Centre

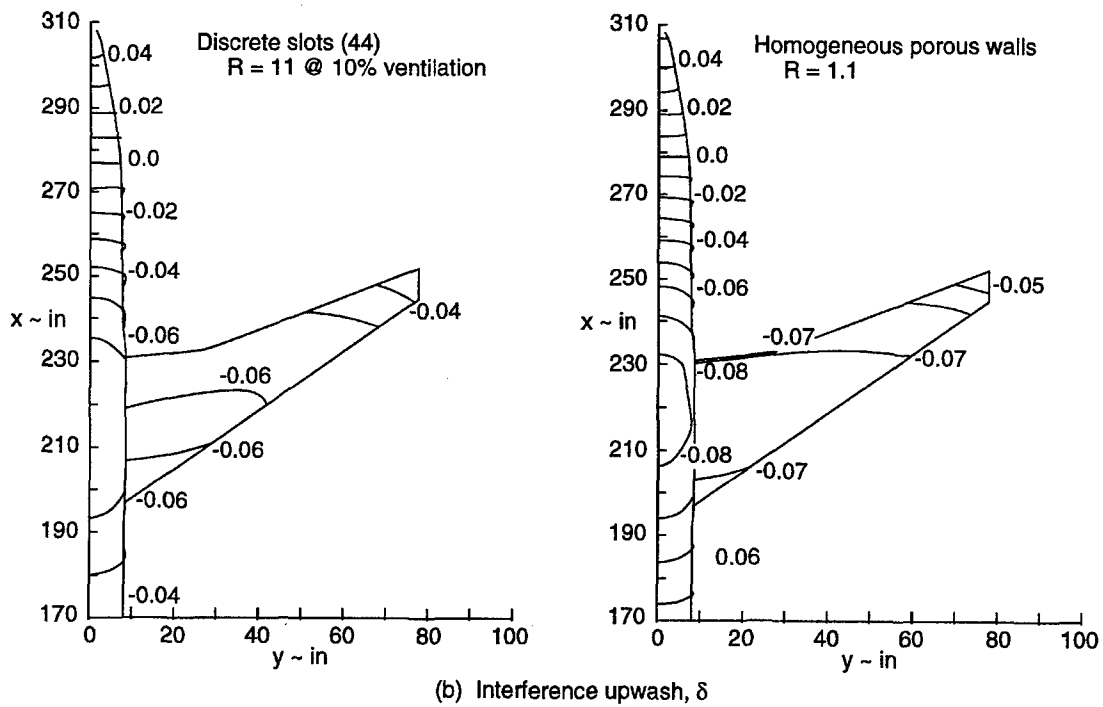
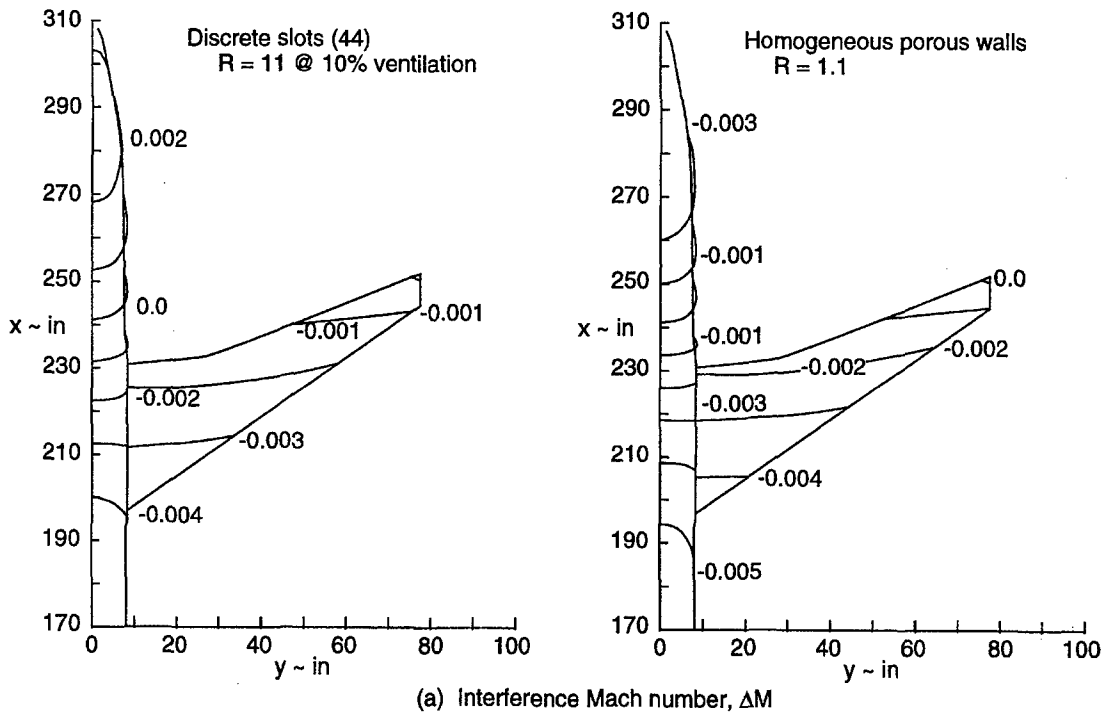


Figure 3.30 Interference at the Model, Homogeneous Porous Walls and Discrete Slots;
 $M = 0.80$, $C_L \cong 0.5$, $2 s/B = 0.83$, $B/H = 1.41$

3.6 CONCLUSION

The validation required of a computational model of a ventilated-wall tunnel depends on required accuracy of the wall correction quantities. Closed-wall and open-jet interference bound interference magnitudes for ideal ventilated walls with uniform characteristics. However, walls that have variable properties or flow fields with significant asymmetry may produce an interference field with strong coupling among the components. Refinement of interference predictions in several large ventilated wind tunnels has led to computational models with modified ideal-wall boundary conditions. These are verified mainly empirically; the deviation of experimental results from ideal wall predictions are usually attributed to non-ideal crossflow characteristics of the walls. Difficulties remain in modelling the downstream portion of a real test section, including the effects of plenum re-entry flow, model support systems, and wall divergence into the test section diffuser. These can especially affect pressure buoyancy forces on the test article. Nevertheless, computational models serve both as a predictive tool and as a stepping stone to boundary measurement methods. Predicted gradients of wall interference, although difficult to validate, are indicators of test situations that may require more sophisticated correction techniques than afforded by linear theory or that may be uncorrectable.

Wall characterisation efforts to date have focused either on direct measurement of wall crossflow characteristics or on correlation of measured pressures "at the wall" with computed pressures. Non-ideal wall behaviour and persistent upward pressure on test model size relative to the test section suggest that customised computational models will continue to be developed for specific ventilated-wall tunnels. As wall validation efforts mature, the decision to shift to boundary measurement methods will depend on a balance of required boundary measurement effort, computational requirements, and the accuracy of alternate methods relative to test objectives.

NOMENCLATURE FOR CHAPTER 3

A	=	effective cross-sectional area of a 2D model
a	=	slot width
B	=	tunnel breadth
b	=	tunnel half-breadth
C	=	cross-sectional area of a test section
C_D	=	drag coefficient
C_L	=	lift coefficient
C_p	=	pressure coefficient
c	=	airfoil chord
D	=	body diameter
d	=	slot spacing
F	=	slotted wall parameter
		$= 2 K / H$ for a 2D test section
		$= K / r_0$ for a circular test section
		$= 2 K / H$ for a rectangular test section

H	=	tunnel height
h	=	tunnel half-height
K	=	ideal slot parameter = $d / \pi \log_e (\operatorname{cosec} \pi a / (2d))$
L	=	reference length
M	=	Mach number
m	=	source strength = $\frac{1}{2} U_\infty S C_D$
P	=	slotted wall parameter = $1 / (1 + F)$
p	=	static pressure
Q	=	porous wall parameter = $1 / (1 + \beta / R)$
q	=	dynamic pressure = $\frac{1}{2} \rho U^2$
R	=	porous wall resistance factor
r	=	cylindrical co-ordinate = $(y^2 + z^2)^{1/2}$
r_0	=	radius of circular test section
S	=	wing reference area
s	=	wing semi-span
T	=	blockage shape factor for rectangular tunnels = $\varepsilon \beta^3 (BH)^{3/2} / V$
t	=	slot depth (= wall thickness)
t	=	porous wall parameter = $2/\pi \arctan(R/\beta)$
U_∞	=	upstream reference velocity
u	=	perturbation velocity in the streamwise (x) direction = $\partial\phi/\partial x$
V	=	model effective volume
v	=	perturbation velocity in the lateral (y) direction = $\partial\phi/\partial y$
v_{normal}	=	velocity component normal to the wall
w	=	perturbation velocity in the vertical (z) direction = $\partial\phi/\partial z$
x	=	streamwise spatial co-ordinate
y	=	spanwise (or lateral) spatial co-ordinate
z	=	vertical spatial co-ordinate

Greek Symbols

α	=	angle of attack
β	=	Prandtl-Glauert compressibility factor = $(1 - M^2)^{1/2}$
δ	=	lift interference parameter = $(w_i / U_\infty) A / (S C_L)$
δ_0	=	lift interference parameter evaluated at model centre
δ_1	=	streamwise curvature interference parameter
δ_Ω	=	upwash interference due to solid blockage
Γs	=	vortex strength = $1/4 U_\infty S C_L$
ε	=	blockage interference ratio = u_i / U_∞
θ	=	flow inclination

μ	=	doublet strength = $U_\infty V$
τ	=	tunnel shape factor, or slotted wall openness ratio
Φ	=	total velocity potential
ϕ	=	perturbation velocity potential
Ω_s	=	streamwise interference parameter due to solid blockage
Ω_w	=	wake blockage interference ratio
Ω_d	=	upwash interference parameter due to solid blockage

Subscripts

i	=	interference
L	=	lower wall
m	=	model
n	=	normal
p	=	plenum (i.e., corresponding to plenum pressure)
S	=	solid (i.e., due to model volume)
U	=	upper wall
W	=	wake (i.e., due to the displacement effect of the model's wake)
w	=	walls

REFERENCES FOR CHAPTER 3

- [1] Agrell, N., Pettersson, B., and Sedin, Y. C.-J., "Numerical Computations and Measurements of Transonic Flow in a Slotted-Wall Wind Tunnel", AIAA 87-2610, August 1987.
- [2] Agrell, N., "Computational Simulations for Some Tests in Transonic Wind Tunnels", paper 14 in AGARD CP-535, October, 1993.
- [3] Baldwin, B. S., Turner, J. B., and Knechtel, E. D., *Wall Interference in Wind Tunnels with Slotted and Porous Boundaries at Subsonic Speeds*, NACA TN 3176, May 1954.
- [4] Barnwell, R. W., "Improvements in the Slotted-Wall Boundary Condition", Proceedings of the AIAA 9th Aerodynamic Testing Conference, June 1976.
- [5] Barnwell, R. W., "Design and Performance Evaluation of Slotted Walls for Two-Dimensional Wind Tunnels", NASA TM 78648, February 1978.
- [6] Berndt, S. B., "Inviscid Theory of Wall Interference in Slotted Test Sections", *AIAA Journal*, Vol. 15, September 1977.
- [7] Berndt, S. B., "Flow Properties of Slotted-Wall Test Sections", paper 6 in AGARD CP-335, May 1982.
- [8] Berndt, S. B. and Sorensen, H., "Flow Properties of Slotted Walls for Transonic Test Sections", paper 17 in AGARD CP-174, October 1975.
- [9] Beutner, T. J., Celik, Z. Z., and Roberts, L., "Determination of Solid/Porous Wall Boundary Conditions from Wind Tunnel Data for Computational Fluid Dynamics Codes", paper 16 in AGARD CP-535, July 1994.

- [10] Bussoletti, J. E., Huffington, J. R., Krynytzky, A. J., and Saaris, G. R., "CFD Studies in Support of NWTC Test Section Design", AIAA 97-0096, January 1997.
- [11] Chan, Y. Y., "Wall Boundary-Layer Effects in Transonic Wind Tunnels", paper 7 in AGARD CP-335, May 1982.
- [12] Chen, C. F. and Mears, J. W., "Experimental and Theoretical Study of Mean Boundary Conditions at Perforated and Longitudinally Slotted Wind Tunnel Walls", AEDC TR-57-20, December 1957.
- [13] Crites, R. and Rueger, M., "Modelling the Ventilated Wind Tunnel Wall", AIAA 92-0035, January 1992.
- [14] Davis, D. D., Jr., and Moore, D., *Analytical Study of Blockage and Lift-Interference Corrections for Slotted Tunnels Obtained by Substitution of an Equivalent Homogeneous Boundary for the Discrete Slots*, NACA RM L53E07b, June 1953.
- [15] Engineering Sciences Data Unit, "Lift-interference and blockage corrections for two-dimensional subsonic flow in ventilated and closed wind tunnels.", Item 76028, November 1976; Amend. A, October 1995.
- [16] Epton, M. A., "Model Formulation in WALINT", private communication, 1988.
- [17] Estabrooks, B. B., "Wall-Interference Effects on Axisymmetric Bodies in Transonic Wind Tunnels with Perforated Wall Test Sections", AEDC TR-59-12, June 1959.
- [18] Everhart, J. L., and Barnwell, R. W., "A Parametric Experimental Study of the Interference Effects and the Boundary-Condition Coefficient of Slotted Wind Tunnel Walls", AIAA 78-805, April 1978.
- [19] Everhart, J. L., "Theoretical and Experimental Analysis of the Slotted-Wall Flow Field in a Transonic Wind Tunnel", SAE 871757, 1987.
- [20] Everhart, J.L., Igoe, W.B. and Flechner, S.G., "Slotted-Wall Flow-Field Measurements in a Transonic Wind Tunnel", NASA TM 4280, August 1991.
- [21] Firmin, M. C. P., and Cook, P. H., "Disturbances from Ventilated Tunnel Walls in Aerofoil Testing", RAE Technical Memo AERO 1971, 1983.
- [22] Freestone, M. M., and Mohan, S. R., "Interference Determination for Wind Tunnels With Slotted Walls", paper 19 in AGARD-CP-535, July 1994.
- [23] Freestone, M. M., Mohan, S. R., and Lock, R.C., "Interference Corrections in Wind Tunnels with Slotted Walls", Paper 16, Proceedings of Conference on "Wind Tunnels and Wind Tunnel Test Techniques", Royal Aeronautical Society, 1992.
- [24] Garner, H. C., Rogers, E. W. E., Acum, W. E. A., and Maskell, E. C., "Subsonic Wind Tunnel Wall Corrections", AGARDograph 109, October 1966.
- [25] Glauert, H., "Wind Tunnel Interference on Wings, Bodies, and Airscrews", ARC R&M No. 1566, 1933.
- [26] Goethert, B. H., *Wind Tunnel Corrections at High Subsonic Speeds Particularly for an Enclosed Circular Tunnel*, NACA TM 1300, 1952.
- [27] Goethert, B. H., *Transonic Wind Tunnel Testing*, Pergamon Press, New York, 1961.
- [28] Goldhammer, M. E., and Steinle, F. W., Jr., "Design and Validation of Advanced Transonic Wings Using CFD and Very High Reynolds Number Wind Tunnel Testing", 17th ICAS Congress, September 1990.
- [29] Holst, H., "German Activities on Wind Tunnel Corrections", paper 4 in AGARD R-692, May 1980.
- [30] Holst, H., "Three Dimensional Wall Corrections for Ventilated Wind Tunnels", paper 8 in AGARD CP-335, May 1982.
- [31] Holt, D. R. and Hunt, B., "The Use of Panel Methods for the Evaluation of Subsonic Wall Interference", paper 2 in AGARD CP-335, May 1982.

- [32] Ivanov, A. I., "An Experimental Study of Gas Flow Near the Perforated Walls of a Transonic Wind Tunnel", *Fluid Mechanics - Soviet Research*, Vol. 17, No. 4, July-August 1988.
- [33] Jacocks, J. L., "Determination of Optimum Operating Parameters for the AEDC-PWT 4-Ft Transonic Tunnel with Variable Porosity Test Section Walls", AEDC TR-69-164, August 1969.
- [34] Jacocks, J. L., "Aerodynamic Characteristics of Perforated Walls for Transonic Wind Tunnels", AEDC TR-77-61, June 1977.
- [35] Johnson, F. T., Samant, S. S., Bieterman, M. B., Melvin, R. G., Young, D. P., Bussoletti, J. E., and Hilmes, C. G., *Tranair: A Full-Potential, Solution-Adaptive, Rectangular Grid Code for Predicting Subsonic, Transonic, and Supersonic Flows About Arbitrary Configurations*, NASA CR 4348, December 1992.
- [36] Karlsson, K. R. and Sedin, Y. C.-J., "Numerical Design and Analysis of Optimal Slot Shapes for Transonic Test Sections - Axisymmetric Flows", *Journal of Aircraft*, Vol. 18, March 1981.
- [37] Keller, J. D., *Numerical Calculation of Boundary-Induced Interference in Slotted or Perforated Wind Tunnels Including Viscous Effects in Slots*, NASA TN D-6871, August 1972.
- [38] Keller, J. D., and Wright, R. H., *A Numerical Method of Calculating the Boundary-Induced Interference in Slotted or Perforated Wind Tunnels of Rectangular Cross Section*, NASA TR R-379, November 1971.
- [39] Kemp, W. B., Jr., "A Slotted Test Section Numerical Model for Interference Assessment", *Journal of Aircraft*, Vol. 22, March 1985.
- [40] Kemp, W. B., Jr., *Computer Simulation of Wind Tunnel Test Section With Discrete Finite-Length Wall Slots*, NASA CR 3948, April 1986.
- [41] Kemp, W. B., Jr., *Description and Evaluation of an Interference Assessment Method for a Slotted-Wall Wind Tunnel*, NASA CR 4352, April 1991.
- [42] Lee, K. D., "Numerical Simulation of the Wind Tunnel Environment by a Panel Method", AIAA 80-0419, March 1980.
- [43] Lo, C. F. and Oliver, R. H., "Boundary Interference in a Rectangular Wind Tunnel with Perforated Walls", AEDC TR-70-67, April 1970.
- [44] Matyk, G. E. and Kobayashi, Y., "An Experimental Investigation of Boundary Layer and Crossflow Characteristics of the Ames 2- by 2-Foot and 11- by 11-Foot Transonic Wind-Tunnel Walls", NASA TM 73257, December 1977.
- [45] Magnus, A. E. and Epton, M. A., *PAN AIR - Computer Program for Predicting Subsonic or Supersonic Linear Potential Flow About Arbitrary Configurations Using a Higher Order Panel Method, Volume I, Theory Document (Version 1.0)*, NASA CR-3251, 1980.
- [46] Mokry, M., "A Wake Blockage Paradox in a Perforated Wall Wind Tunnel", *AIAA Journal*, Vol. 9, No. 12, Dec 1971.
- [47] Mokry, M., Peake, D. J., and Bowker, A. J., "Wall Interference on Two-Dimensional Supercritical Airfoils, Using Wall Pressure Measurements to Determine the Porosity Factors for Tunnel Floor and Ceiling", National Aeronautical Establishment Report LR-575, February 1974.
- [48] Mokry, M., and Ohman, L., "Application of the Fast Fourier Transform to Two-Dimensional Wind Tunnel Wall Interference", *Journal of Aircraft*, Vol. 17, June 1980, pp. 402-408.
- [49] Mokry, M., "Evaluation of Three-Dimensional Wall Interference Corrections from Boundary Pressure Measurements", National Research Council of Canada LTR-HA-51, November 1980.
- [50] Mokry, M., Digney, J. R., and Poole, R. J. D., "Doublet-Panel Method for Half-Model Wind-Tunnel Corrections", *Journal of Aircraft*, Vol. 24, May 1987.

- [51] Neiland, V. M., "Optimum Porosity of Wind Tunnel Walls at Low Supersonic Velocities", *Izvestiya Akademii Nauk SSSR, Mekhanika Zhidkosti i Gaza*, No. 4, July-August 1989.
- [52] Nyberg, S-E., "Review of Some Investigations on Wind Tunnel Wall Interference Performed in Sweden in Recent Years", paper 6 in AGARD R-692, May 1980.
- [53] Pindzola, M., and Lo, C. F., "Boundary Interference at Subsonic Speeds in Wind Tunnels with Ventilated Walls", AEDC TR-69-47, May 1969.
- [54] Pounds, G. A., and Walker, J., "Semispan Model Testing in a Variable Porosity Transonic Wind Tunnel", AIAA 80-0461, March 1980.
- [55] Schilling, B. L., and Wright, R. H., *Calculated Wind-Tunnel-Boundary Lift-Interference Factors for Rectangular Perforated Test Sections*, NASA TN D-5635, February 1970.
- [56] Sedin, Y. C-J., and Sorensen, H., "Computed and Measured Wall Interference in a Slotted Transonic Test Section", *AIAA Journal*, Vol. 24, March 1986.
- [57] Sloof, J. W., and Piers, W. J., "The Effect of Finite Test Section Length on Wall Interference in 2-D Ventilated Wind Tunnels", paper 14 in AGARD CP-174, October 1975.
- [58] Starr, R. F., "Experiments to Assess the Influence of Changes in the Tunnel Wall Boundary Layer on Transonic Wall Crossflow Characteristics", paper 18 in AGARD CP-174, October 1975.
- [59] Steinle, F. W., Jr., and Mabey, "Computer Studies of Hybrid-Slotted Working Sections with Minimum Interference at Subsonic Speeds", NASA TM 86002, August 1984.
- [60] Steinle, F. W., Jr., and Pejack, E. R., "Toward an Improved Transonic Wind-Tunnel-Wall Geometry - A Numerical Study", AIAA 80-0442, March 1980.
- [61] Steinle, F. W., Jr., and Stanewsky, E., "Wind Tunnel Flow Quality and Data Accuracy Requirements", AGARD AR-184, November 1982.
- [62] Theodorsen, T., *The Theory of Wind Tunnel Wall Interference*, NACA Report 410, 1931.
- [63] Vaucheret, X., "Reduction des corrections de parois en veines d'essais transsoniques classiques a l'aide d'etudes parametriques sur ordinateur", ONERA TP 1976-60, June 1976.
- [64] Vaucheret, X. and Vayssaire, J. C., "Corrections de parois en ecoulement tridimensionnel transsonique dans des veines a parois ventilees", paper 16 in AGARD CP-174, October 1975.
- [65] Vaucheret, X., "Ameliorations des calculs des effets de parois dans les souffleries industrielles de l'ONERA", paper 11 in AGARD-CP-335, May 1982.
- [66] Vaucheret, X., "Vortex Lattice Code for Computation of Wind Tunnel and Support Effects on Models", *La Recherche Aerospatiale* (English edition), No. 1991-2, pp. 39-51.
- [67] Vayssaire, J. C., "Survey of Methods for Correcting Wall Constraints in Transonic Wind Tunnels", AGARD R-601, April 1973.
- [68] Wu, J. M., Collins, F. G., and Bhat, M. K., "Three-Dimensional Flow Studies on a Slotted Transonic Wind Tunnel Wall", AIAA 82-0230, January 1982.

4. BOUNDARY MEASUREMENTS METHODS

Authors	:	P.Ashill	(Chapter 4.1, 4.2)
		J.E. Hackett	(Chapter 4.2)
		M. Mokry	(Chapter 4.3)
		F. Steinle	(Chapter 4.3)

	PAGE
4.1 FUNDAMENTAL THEORIES	4-3
4.1.1 BASIC CONSIDERATIONS	4-4
4.1.2 ONE VARIABLE METHODS	4-7
4.1.2.1 DIRICHLET PROBLEM	
4.1.2.2 NEUMANN PROBLEM	
4.1.2.3 MIXED PROBLEM	
4.1.2.4 MODEL REPRESENTATION ERRORS	
4.1.3 WALL-SIGNATURE METHODS	4-12
4.1.4 TWO-VARIABLE METHODS	4-14
REFERENCES TO CHAPTER 4.1	4-17
4.2 CLOSED TEST SECTIONS	4-20
4.2.1 BACKGROUND	4-20
4.2.2 BOUNDARY CONDITIONS	4-21
4.2.3 NUMERICAL APPROXIMATIONS	4-24
4.2.4 CHOICE OF METHOD	4-24
4.2.5 MEASUREMENTS AND ANALYSIS OF WALL PRESSURES	4-25
4.2.5.1 WALL PRESSURE-SIGNATURE METHODS	
4.2.5.2 TWO VARIABLE METHODS	
4.2.6 MODEL AND TUNNEL REPRESENTATION WHEN USING THE	4-30
"MATRIX" VERSION OF THE WALL PRESSURE	
SIGNATURE METHOD	
4.2.6.1 INTRODUCTION	
4.2.6.2 BASIC APPROACH	
4.2.6.3 MODEL GEOMETRY AND ITS REPRESENTATION	
4.2.6.4 REFERENCE CASE	
4.2.6.5 THE SOLVER	
4.2.6.6 WALL ORIFICE CONFIGURATIONS	
4.2.6.7 CASES WITH NO ELEMENT OPTIMISATION (TOLC = 0)	
4.2.6.8 CASES WITH ELEMENT OPTIMISATION	
4.2.6.9 REVIEW	
4.2.6.10 OTHER MODEL CONFIGURATIONS	
4.2.6.11 THREE-WAY INTERACTIONS	
REFERENCES TO CHAPTER 4.2	4-35

	PAGE
4.3 VENTILATED TEST SECTIONS	4-38
4.3.1 ONE-VARIABLE METHOD	4-39
4.3.2 TWO-VARIABLE METHOD	4-48
4.3.3 ALTERNATIVE METHODS	4-55
APPENDIX: RECTANGULAR WALL PANEL	4-55
REFERENCES TO CHAPTER 4.3	4-57

4. BOUNDARY MEASUREMENTS METHODS

The importance of measuring flow conditions at outer boundaries has been known for some time, particularly for solid-wall wind tunnels. However, it has only been in recent years that sufficient computing power has become available to make use of this information. Thus it is no coincidence that the increase in interest in boundary-measurement methods has occurred during the last decade or so when the rate of development in computing technology has been so rapid. This Chapter begins with a review of fundamental theories of boundary-measurement methods (Chapter 4.1) and then describes the application of the methods to closed-wall tunnels in Chapter 4.2 and to ventilated test sections in Chapter 4.3.

4.1 FUNDAMENTAL THEORIES

After basic issues are considered, the various classes of methods are reviewed, and the relative advantages and disadvantages of the methods are discussed.

LIST OF SYMBOLS for chapter 4.1

B	breadth of working section of equivalent wind tunnel of rectangular section
C_p	static-pressure coefficient
G, G_D, G_F	Green's functions
G_N, G_{DN}	
H	height of working section of equivalent wind tunnel of rectangular section
M	Mach number
n	normal inward towards working section in transformed (Prandtl-Glauert) space
P	point within region bounded by S
R	fictitious region outside the region bounded by S
S	measurement surface in transformed space
T	wall shape factor for doublet
u	streamwise velocity perturbation
U	stream speed
V	model volume
x,y,z	cartesian co-ordinate system (Fig 4.1)
X,Y,Z	transformed co-ordinates, = (x, βy , βz)
α	angle of incidence
β	Prandtl-Glauert factor, = $\sqrt{1 - M_F^2}$
δ_0, δ_1	lift interference parameters
Δ	increment due to wall effect
∇^2	Laplace operator
Φ	velocity potential
ϕ	perturbation velocity potential

SUFFIXES

F	equivalent free-air flow
l	wall-induced flow
i,j	differentiation with respect to either x,y or z in either case
R	fictitious region outside region contained within S
S	measurement surface
T	adjacent to wind-tunnel walls
U, D	upstream and downstream faces
V_0	volume integration in the fictitious region R
∞	conditions far upstream

4.1.1 BASIC CONSIDERATIONS

Consider the flow about a model of an aircraft in a wind tunnel (Figure 4.1) with sub-sonic conditions far upstream. Suppose, initially, that the flow everywhere in the working section is irrotational, implying that any shock waves are weak and that the turbulent shear layers are thin. The flow may therefore be defined uniquely by the velocity potential Φ or the perturbation velocity potential $\varphi = \Phi - U_\infty x$, where U_∞ is the speed

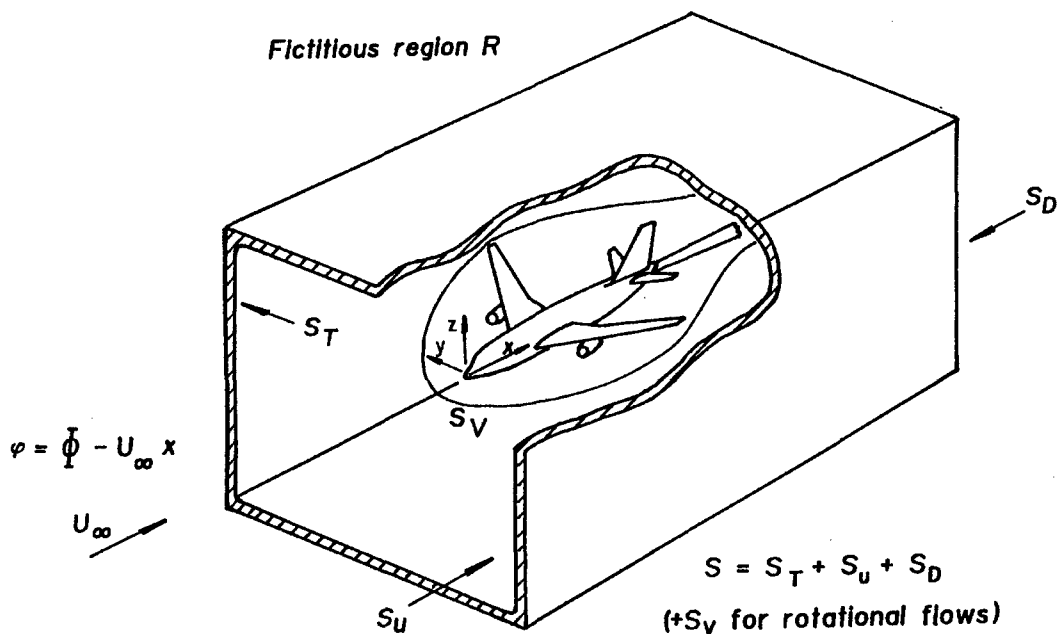


Figure 4.1 : Wind Tunnel Test Section with Model

of the notional flow far upstream, usually determined by calibration of the empty test section. This flow satisfies the exact potential equation (Küchemann, [27]), which may be written in the form :

$$\beta^2 \varphi_{xx} + \varphi_{yy} + \varphi_{zz} = f(\Phi_i, \Phi_{ij}, U_F; M_F), \quad (4.1)$$

where $\beta^2 = 1 - M_F^2$ and M_F is the Mach number corrected for blockage, i.e. the free-stream Mach number of an equivalent 'free-air' flow. The corrected Mach number and the corresponding corrected free-stream speed, U_F , are preferred in Equation (4.1) to the corresponding conditions far upstream because the former quantities

determine the character of the flow in the near field of the model. Suffixes i and j , respectively, refer to differentiation with respect to either x , y or z . The function f is a term that is non-linear in the derivatives of Φ and which becomes significant in transonic-flow regions near the model.

The Prandtl-Glauert transformation may be used to replace Equation (4.1) by

$$\nabla^2 \varphi = f(\Phi_i, \Phi_{ij}, U_F, M_F) / \beta^2 \quad (4.2)$$

where

$$\nabla^2 \varphi = \varphi_{xx} + \varphi_{yy} + \varphi_{zz}$$

and

$$(X, Y, Z) = (x, \beta y, \beta z).$$

Consider now the 'free-air' flow about the same model at the free-stream speed U_F and at an angle of attack differing from the geometric angle of attack of the model in the tunnel by $\Delta\alpha$ (Figure 4.2). For flows and models with a vertical plane of symmetry this flow is characterised by the perturbation potential

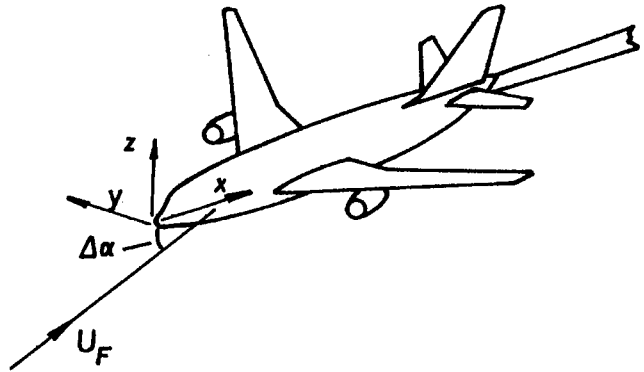


Fig 4.2 Free-air flow about same model

$$\varphi_F = \Phi_F - U_F x - U_F \Delta\alpha z$$

and satisfies the equation

$$\Delta^2 \varphi_F = f[(\Phi_F)_i, (\Phi_F)_{ij}, U_F; M_F] / \beta^2 \quad (4.3)$$

If either

- a) the two flows are identical ($\Phi = \Phi_F$) in the region near the model, so that the tunnel flow may be corrected to an equivalent 'free-air' flow,
- or b) the perturbations in the flow induced by the model are 'small' everywhere,
- or c) the Mach number of the flow is everywhere close to zero, i.e. the two flows are essentially incompressible, then the right-hand sides of Equations (4.2) and (4.3) are either identical but non-zero, or negligible. This being the case, subtraction of Equation (4.3) from Equation (4.2) leads to the expression

$$\nabla^2 \varphi = 0 \quad (4.4)$$

where

$$\varphi_I = \varphi - \varphi_F$$

is the wall-interference potential. Since, by Equation (4.4), this potential is harmonic within the working section, it is possible to use Green's formula (Weatherburn, [51]) to write for the point P in the (transformed) working section

$$4\pi \varphi_I(P) = - \int_S \left[\frac{\partial \varphi_I}{\partial n} G - \varphi_I \frac{\partial G}{\partial n} \right] dS, = - \int_S \left(\left[\frac{\partial \varphi}{\partial n} - \frac{\partial \varphi_F}{\partial n} \right] G - (\varphi - \varphi_F) \frac{\partial G}{\partial n} \right) dS. \quad (4.5)$$

Here n is the normal inward towards the working section and the integration is performed over the measurement or boundary surface S , comprising a surface at or close to the walls, S_T , with faces at the upstream and downstream extremities of the working section, S_U and S_D , (Figure 4.1). G is a Green's function that is harmonic everywhere within the measurement region except at the point P . Near this point G behaves like $1/r$, where r is the distance between the point P and a variable point in the region.

For the wall interference potential to be harmonic everywhere within the volume bounded by S the quantity $(\varphi - \varphi_F)$ must be single-valued there. This means that the difference in circulation between the two flows around any circuit within the working section must be zero and, also,

$$\int_S \left(\frac{\partial \varphi}{\partial n} - \frac{\partial \varphi_F}{\partial n} \right) dS = 0,$$

i.e., to the accuracy of linear theory, the net flux of the wall-induced flow across S must be zero. These conditions need to be borne in mind in any numerical method for determining wall interference based on Equation (4.5).

The analysis above may, with certain restrictions, be extended to rotational flows. The first restriction is that the vorticity is confined to a region surrounding the model, as illustrated in Figure 4.1, where it is shown to be bounded by the surface S_v . The surface S in Equation (4.5) then has to include the surface S_v . However, if it is possible to correct the wind tunnel flow to an equivalent free-air flow, the analytical continuation of the wall-interference potential is harmonic within the rotational-flow region. Hence, by Green's theorem (Weatherburn, [51]), the contribution of the extra term vanishes. Thus, in this circumstance, Equation (4.5) applies to rotational flows as well.

To determine the wall-interference potential at a point in the working section by using Equation (4.5), it is necessary to know both the wall interference potential itself and its normal gradient at the measurement surface. This, in turn, means that perturbation potential of the wind-tunnel flow and its normal gradient have to be determined at the surface; furthermore, a satisfactory representation of the free-air flow around the model has to be derived. This implies that three independent variables are required, two from flow measurements at the surface S and a third, defining the model free-air flow, by calculation. However, the number of variables needed can be reduced to two by using the freedom to choose an appropriate Green's function for the boundary-value problem. Depending on the choice of Green's function, the two variables can either comprise one defining the flow at any one part of the measurement surface and another specifying the free-air flow or two defining the conditions at the measurement surface. Kraft [25] suggested that a measure of merit of any technique is how well the two independent quantities are evaluated. Kraft proposed that the two classes of method should be, respectively, called 'one-variable' and 'two-variable' methods. As its name implies, the former class needs the measurement of only one flow variable at the measurement surface, but it does require a representation of the model free-air flow. The second class, on the other hand, requires two variables to be measured, but it does not need a simulation of the model flow. A third, hybrid class uses a) a complete knowledge of one flow variable, or an assumed relationship between the two flow variables, at the measurement surface, and b) limited measurements of a second flow variable on the same surface. In these 'wall-signature' methods, a model representation is used, and the 'signature' of the second variable is used to define either the strengths of the singularities representing the model or the values of a parameter linking the two flow variables. In the remainder of this Chapter the three types of methods are reviewed. Discussion of one-variable methods (Chapter 4.1.2) is followed by a review of 'wall-signature' methods (Chapter 4.1.3). Finally, two-variable methods are discussed in Chapter 4.1.4.

4.1.2 ONE VARIABLE METHODS

4.1.2.1 DIRICHLET PROBLEM

For the Dirichlet problem, where the interference potential is specified on S , the appropriate Green's function is one that vanishes on the measurement surface leaving

$$4\pi \phi_I(P) = \int_S (\phi - \phi_F) \frac{\partial G_D}{\partial n} dS. \quad (4.6)$$

With the appropriate Green's function, G_D , defined, the integral can, in principle, be evaluated once the perturbation potentials ϕ and ϕ_F are known on S . The perturbation potential ϕ can, in principle, be inferred from

i) measurements of static pressure at the outside surface S_T by appropriate integration of the linearised version of Bernoulli's equation,

$$\frac{\partial \phi}{\partial x} = - \frac{U_\infty C_p}{2}, \quad (4.7)$$

provided that the pressure coefficient C_p is of sufficiently small magnitude for second order terms in Bernoulli's equation to be ignored¹, and

ii) a knowledge of the way the perturbation velocity potential varies across the upstream and downstream faces S_U and S_D . If these surfaces are perpendicular to the tunnel axis this variation can be determined by measurement of the upwash component of velocity at these faces. However, for sufficiently long working sections, where the two faces are far removed from the model, this is probably unnecessary because the contributions of the integrals over these faces can reasonably be ignored.

The integration of Equation (4.7) has been avoided in existing methods of the 'Dirichlet' type, which are based on the streamwise velocity increment $u = \partial\phi/\partial x$ instead of the perturbation velocity potential ϕ . However, in these methods, a further integration is needed to determine the wall-induced upwash, and the constant of integration is determined from a measurement of the upwash at the upstream measurement station. The alternative expressions have been derived for cylindrical boundary surfaces. For these types of surfaces, a comparable expression may be derived from Equation (4.6) by differentiating each side of this equation by X . Mokry and Ohman [36], in two dimensions, and Mokry [38], in three dimensions, used Fourier transform techniques, in effect, to determine the required Green's function. Later, Mokry et al [40] used a doublet-panel method, in which the doublet distribution on the measurement surface is determined satisfying the boundary condition for the wall-induced increment in streamwise velocity. In all these methods, the influence of the upstream and downstream faces can, in principle, be accommodated provided information about the variation of the streamwise increment in velocity across them is available. In an analysis of the two-dimensional problem in a working section of infinite length, Capelier et al [7] used complex-variable theory to solve the equivalent Schwarz problem (Mokry et al [39]). An extension of this method to the case of a semi-infinite working section was later developed by Paquet [43], who specified boundary conditions for the streamwise velocity increment on an upstream measurement face.

¹ If these terms cannot be neglected then it will, in general, be necessary to determine the streamwise velocity increment and hence the perturbation potential at the measurement surface by integrating the Euler equations in the direction of the tunnel axis (Ashill and Keating [2] and Maarsingh et al [34]).

Methods using either the wall interference potential or the streamwise velocity increment are 'autocorrective'. This means that calculations by them of corrected stream speed are automatically compensated for errors in the reference-pressure measurement (Capelier et al [7] and Paquet [43]).

4.1.2.2 NEUMANN PROBLEM

For the Neumann problem the normal gradient of the interference potential, or the normal component of the wall-induced velocity, is given on the boundary. The required Green's function, G_N , is one with vanishing normal gradient on S giving

$$4\pi \phi_I(P) = - \int_S \left(\frac{\partial \phi}{\partial n} - \frac{\partial \phi_F}{\partial n} \right) G_N dS. \quad (4.8)$$

The term $\partial\phi/\partial n$ in Equation (4.8), implies that the normal component of velocity or the flow angle has to be specified on S . The measurement of flow angle causes no significant problems for wind tunnels with solid, though possibly, flexible walls, since the flow angle is essentially defined by the condition of no flow through the walls². On the other hand, for porous or slotted walls, flow angle needs either to be measured or to be deduced from wall and plenum pressure measurements by using elaborate theoretical models. Measurement of flow angle with the required accuracy is extremely difficult. For this reason, methods of the 'Neumann' type are not favoured for porous or slotted-wall wind tunnels. Indeed, the use of the wall-induced streamwise velocity as a boundary condition, was originally proposed by Capelier et al [7] with just this problem in mind.

Where the difference in normal velocity is used as the boundary condition, as for Equation (4.8), the technique is autocorrective in that errors in measurements of normal velocity or flow angle far upstream of the model are compensated for by the method.

4.1.2.3 MIXED PROBLEM

In some cases, where the normal velocity is well defined on parts of the boundary and the streamwise velocity increment or the perturbation potential on other parts, a mixture of types of boundary condition may be appropriate. An example of where such a treatment might be used is for a case with solid sidewalls and upper and lower walls that are either perforated, slotted or flexible. In such cases, the boundary S_T may be divided into S_1 and S_2 , on which conditions of the 'Dirichlet' and 'Neumann' types are, respectively, applied. If, for example, the upstream and downstream faces are sufficiently remote from the model for their effects to be ignored, the solution for the interference potential may be expressed as:

$$4\pi \phi_I(P) = \int_{S_1} (\phi - \phi_F) \frac{\partial G_{DN}}{\partial n} dS - \int_{S_2} \left(\frac{\partial \phi}{\partial n} - \frac{\partial \phi_F}{\partial n} \right) G_{DN} dS, \quad (4.9)$$

to be cylindrical and of infinite length; the wall-interference potential, ϕ_I , was expressed as the sum of contributions due, respectively, to the model, an infinite array of images of the model simulating the solid sidewalls and a remainder to allow for the flexible roof and floor. The last contribution was determined by separation of variables and Fourier transforms of the resulting set of two-dimensional, partial-differential equations. Smith [47],[49] used mixed boundary conditions in his treatment, by a panel method, of wall

² It may be necessary to allow for the effect on normal velocity at the measurement surface of the change in wall boundary layer displacement thickness between the empty tunnel and the model-in-tunnel cases (see Chapter 4.2).

interference on the flow over two-dimensional aerofoils in a working section that was slotted in one part and solid upstream and downstream of it. Boundary pressures were measured only over a part of the working section, which extended beyond the slotted region. He applied conditions of the 'Dirichlet' type to this part (S_1) and 'Neumann' type conditions to the solid regions upstream and downstream of it (S_2).

Mokry et al [39] noted that some care needs to be taken with mixed boundary conditions at any line or point where the conditions change from one sort to another. They also raised concerns about the uniqueness of the solution which, in the case considered by Smith [47], is presumably ensured by satisfying the condition of smooth flow at the two joins.

4.1.2.4 MODEL REPRESENTATION ERRORS

As noted in Section 2.1 one-variable methods require some form of model representation. In principle, the simulation may be achieved with suitable distributions of potential singularities so long as the flow is subcritical at the tunnel walls. The problem is to determine the strengths of the singularities. Smith [47] noted the importance of accurate model representation, arguing that errors caused by inaccurate modelling could be as large as the interference quantity itself. For subcritical flows over wings or bodies at low angles of incidence, linear theory can be used with allowance for model thickness or cross-sectional area (Garner et al [15]) and with other modifications, as described below. However, for transonic flows or for flows with large regions of separation, the problem is much less easily solved owing to the non-linear character of the flow in the near field of the model. Numerical methods have been developed, in which various approximations to the Navier-Stokes equations have been solved for aerofoils and wing-body configurations (Kemp [23], Newman et al [42] and Rizk and Smithmeyer [45]). These methods require both the wind tunnel and 'free-air' flows to be calculated and are expected to be of particular value when there are supercritical-flow patches at the wall, but it is unlikely that it will be possible to correct such flows to 'free-air' conditions except in adaptive-wall tunnels (see Chapter 4.1.4). It would appear that these methods have not been used to calculate the strengths of the equivalent potential-flow singularities. However, Mokry [41], applying a suitable contour integration to numerical coupled solutions of the Euler and boundary-layer equations, has determined doublet strength for transonic flows over aerofoils with supercritical flows contained within the working section.

If numerical calculations of transonic flows, or, indeed, any other complex flows, are to be avoided, three possible approaches may be used to minimise errors due to model representation:

- i) **Exploit an observed tendency for different types of boundary condition to have different levels of sensitivity to model representation errors.**

It may be noted that the contribution of the model representation term to the wall interference potential can be determined for each type of boundary condition by setting $\phi = 0$ in Equation (4.6) and $\partial\phi/\partial n = 0$ in Equation (4.8), while, for Equation (4.9), it follows by setting $\phi = 0$ on S_1 and $\partial\phi/\partial n = 0$ on S_2 . This implies that, for wind tunnels with long, cylindrical working sections, the respective contributions due to model representation in methods of the 'Dirichlet' and 'Neumann' type can be inferred from classical results for tunnels with open-jet and solid walls and, for mixed boundary conditions, by a combination of wall types. In this respect, it is useful to think of a wind tunnel having a working section with the same cross section as the measurement surface and with classical wall boundary conditions, hereafter referred to as the 'equivalent wind tunnel'.

The observations in the last paragraph are not merely of academic interest, since they allow extensive experience with classical wall-interference methods to be used to assess the contribution to wall-induced velocities from imperfect model representation. In the past, particular emphasis has been placed on determining the strength of the doublet representing the volume effect of the model and its associated supercritical flow in the far field. The reason for this is that non-linear effects of compressibility affect doublet

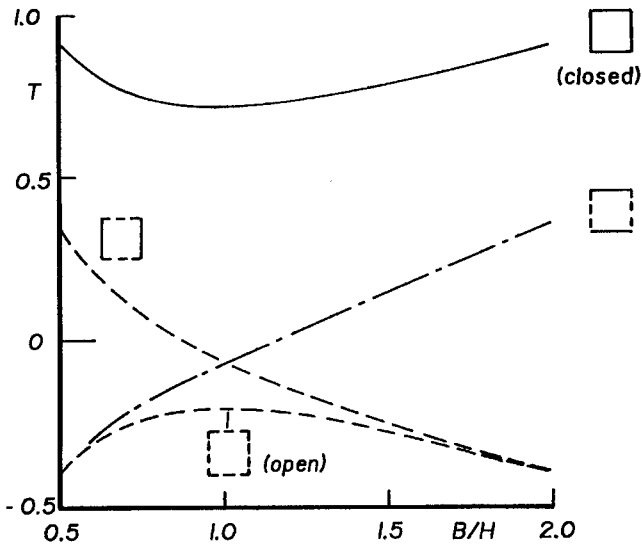


Fig 4.3 Wall shape factor T

strength in a way that is not represented in linear theory, and, consequently, this is a possible source of error. It is therefore interesting to compare the wall corrections associated with a source-sink doublet placed on the tunnel axis in various equivalent wind tunnels of rectangular cross section. Results for the wall shape factor for the doublet

$$T = \frac{(BH)^{\frac{3}{2}} u_I^m}{V U_F}$$

are plotted in Figure 4.3 against (effective) working section breadth to height ratio B/H , where u_I^m is the wall-induced or blockage increment in streamwise velocity at the model for incompressible-flow conditions and V is model volume.

Shown in the figure are cases with working sections that are **i**) fully-closed (Neumann), **ii**) fully-open (Dirichlet), **iii**) mixed, open sidewall and closed roof and floor and **iv**) mixed, open roof and floor and closed sidewalls. Results for the fully-closed and fully-open cases have been gleaned from information given by Garner et al [15], while the results for the two 'mixed' cases have been calculated for this study. For values of B/H close to unity, the 'Dirichlet' case gives a wall shape factor that is only 28% of the magnitude of that of the 'Neumann' approach, indicating that the 'Dirichlet' approach is to be preferred to the 'Neumann' approach from the point of view of minimising model-representation errors. For $B/H = 1$ the 'mixed' approach gives an even lower value, with a magnitude of only 10% of that of the 'Neumann' value. The 'mixed' approach also yields zero blockage (due to model representation) for mixed conditions of type **iii**) above with $B/H = 1.17$ or of type **iv**) with $B/H = 1/1.17 = 0.85$. These are significant results which could have an important bearing on where and how to apply wall boundary conditions with one-variable methods and possibly also on the design of any future wind tunnels.

Similar conclusions have been reached in calculations performed for 'long' bodies simulated by an axial distribution of sources or sinks, results of which are given by Ashill (1994), who presents a fuller account of a study of effects of types of boundary conditions on model representation errors.

It should be remembered that the porous or slotted region does not necessarily occupy the whole length of the working section. It may, therefore, be possible to exploit this feature by using, as Smith [47],[49] has done, boundary conditions which differ from one part of the working section length to another. It may be possible to decrease the open-area ratio of the equivalent wind tunnel by applying 'Neumann' type conditions where the wall is solid upstream (and downstream) of the slotted or perforated region. For slotted-wall tunnels, it may be possible to apply the solid-wall condition on parts of the slats between the slots to reduce the sensitivity to model representation errors. Kemp [22] applied boundary conditions in this way in his method for

three-dimensional models in a slotted-wall tunnel, but for the different reason that he was limited by the number of slat pressure measurements that were available.

Results for lift-interference parameters of a 'small' wing are shown in Figure 4.4 for various types of classical boundary conditions (Garner et al [15]). For a square tunnel the smallest values of the classical parameters δ_0 and δ_1 are obtained with the walls of the equivalent wind tunnel open at the sides and closed in the roof and floor, for which $\delta_0 = 0$. This means that, if an accurate estimate of lift interference is the overriding consideration and there are doubts about the accuracy of the representation of the model lift distribution, 'Dirichlet' type conditions should be applied at the sidewalls and 'Neumann' type conditions at the roof and floor. Plainly, this is an unattractive option for tunnels with a slotted roof and floor such as ETW and NTF. Fortunately, the lift distribution of models is usually determined from measurement or can be estimated with some confidence. Consequently, errors from this source are unlikely to be serious.

Basing his ideas on the earlier work of Davis [11],

Schairer [46] developed a method for two-dimensional tests in which the influence of model representation was eliminated altogether by using measurements of one flow variable, normal velocity, at two separate surfaces. Schairer found that he was unable to obtain wall-induced velocities of adequate accuracy owing to the limited range of the measurements along the working section. The method does not seem to have been adapted to three-dimensions, but studies by Davis [11] suggest that the method is much more complicated for three-dimensional flows.

ii) Make use of experience from testing in solid-wall wind tunnels.

Evans [12] was able to make significant progress using measurements of wall pressures. As well as drawing attention to the importance of representing body length for typical models, he showed the significance of using the corrected Mach number in the Prandtl-Glauert factor when determining the strengths of the sources and sinks representing a body. This important point, which does not appear to have been fully grasped in some later work, is illustrated in Figure 4.5 showing comparisons between calculation and measurement of wall pressure measurements in the RAE 10ft x 7ft Tunnel for a series of bodies. Since the correction is not known *a priori*, this implies an iteration process. However, if, as is often the case, the corrections are calculated 'on line' during the test, the nominal Mach number can be adjusted until the corrected Mach number corresponds with the desired value. Evans concluded that an error in the solid blockage at drag-rise conditions could be reconciled with an increase in the effective volume of the model, and he suggested that this error is directly proportional to the rise in drag coefficient. Although plausible and based on comparisons with wall pressure measurements, this result does not have a rigorous theoretical basis.

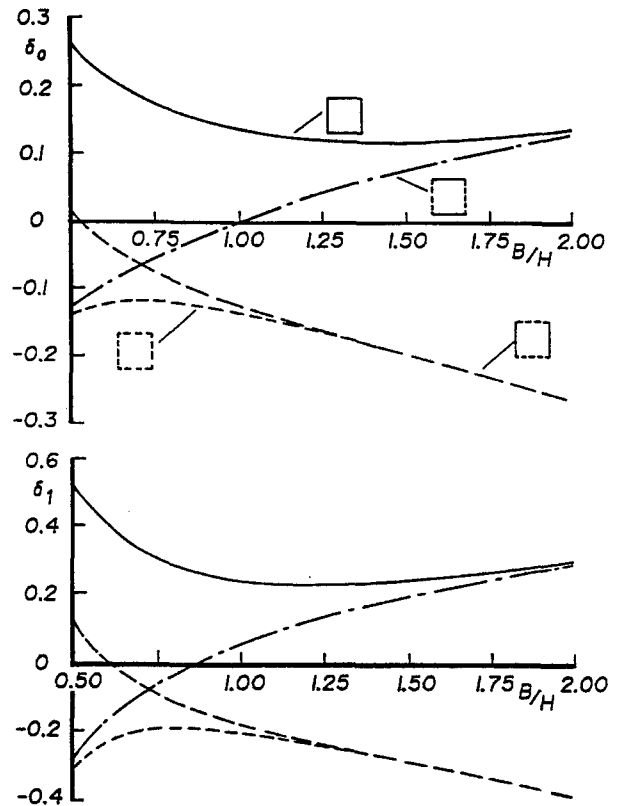


Fig 4.4 Lift interference for 'small' wings on axis of equivalent wind tunnel of rectangular cross section

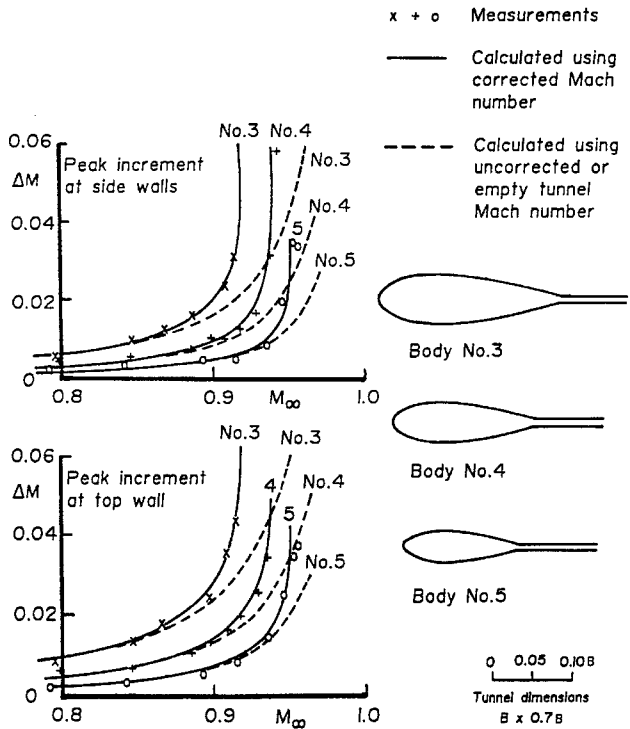


Fig. 4.5 Comparison of measured and calculated peak increments in wall Mach numbers for three bodies after Evans (1949)

iii) Obtain more accurate estimates of singularity strengths using asymptotic expansion or other approximate methods.

Using the method of matched asymptotic expansions, Chan [8],[9] established a correction for compressible non-linear effects to doublet strength for two-dimensional aerofoils. For the same problem, Smith [48] used Green's formula to obtain an estimate of the doublet strength. Mokry [41] showed that doublet strength depends on aerofoil camber and angle of incidence as well as thickness. It would appear that these approaches have not yet been extended to three dimensions. No correction is needed to vortex strength for compressibility if the spanwise distribution of local lift coefficient of a wing is known either from pressure measurements or can be inferred from overall-force measurements.

4.1.3 WALL-SIGNATURE METHODS

As noted earlier, there are two variants of the wall-signature method. In the first, one component of velocity is known and the other is measured at a limited number of points on the measurement boundary. By matching calculation to measurement at this boundary it is then possible to determine the strengths of the singularities representing the model. The best known application of this type of method is to solid-wall wind tunnels, for which the normal-velocity component may be taken to be zero at the walls. Therefore, with the measurement boundary taken to coincide with the walls, the solution to the Neumann problem, Equation (4.8), may be used to obtain:

$$4\pi\phi_I(P) = - \int_S \frac{\partial\phi_F}{\partial n} G_N dS. \tag{4.10}$$

After differentiation by X, Equation (4.10) may be re-expressed as:

$$4\pi[u(P) - u_F(P)] = - \int_S \frac{\partial\phi_F}{\partial n} \frac{\partial G_N}{\partial X} dS,$$

or as

$$u(P) = u_F(P) - \frac{1}{4\pi} \int_S \frac{\partial\phi_F}{\partial n} \frac{\partial G_N}{\partial X} dS. \tag{4.11}$$

Here the differentiation with respect to X has been taken under the integral sign because G_N is smooth and continuous within the region of integration. If the point P is taken to be limitingly close to the walls, the left-hand side of Equation (4.11) may then be defined by static-pressure measurements at the walls, together

with the linear Bernoulli Equation (4.6), at N points. Thus, if the model is represented by a distribution of N singularities, Equation (4.11) may be regarded as a linear (integral) equation for the unknown singularity strengths. For a wind tunnel with a cylindrical working section of length that is sufficiently large to be assumed infinite, the integral in Equation (4.11) may be replaced by a doubly-infinite sum for each singularity, representing the image effect of the tunnel walls.

The idea behind this approach, which is illustrated in Figure 4.6, goes back to the 1940's when the problems of testing at high subsonic speed in solid-wall tunnels were first addressed. Mokry et al [39], reviewing various early methods for two-dimensional flows, described a simple procedure to determine the strengths of a doublet, vortex and source representing a lifting aerofoil from static-pressure measurements at three points on both the roof and floor of the working section. They argued that methods of this type are superseded by two-variable methods, to be described later, which need no model representation. A contrary view is that wall-signature methods are to be preferred in some applications because

they need relatively-few measurement points compared with two-variable methods. Smith [47], using a method similar to that described by Mokry [37], suggested that an aerofoil with a chord to working section height ratio of about 0.2 could probably be represented adequately in the far field by about ten singularities placed at a single point, requiring ten measurement points. Evans [12] found that it was possible to represent a body of revolution by a point source and point sink, in each case placed at a fixed distance from the centre of volume of the body on its axis, indicating the need for two measurement points. These numbers of measurement points would be considered much too low for a two-variable method. However, where the model flow field is complex and not easily represented by singularities, two variable methods are probably to be preferred (see Section 4.2.4). Nevertheless, the wall-signature strategy has been used to determine wall corrections for models with separated flows (Hackett and Wilsden [18], [19] and Hackett et al [20]) and jets in cross flow (Wilsden and Hackett [52]).

Le Sant and Bouvier [29] found that the matrix inversion needed to solve equation (4.11) is ill-conditioned owing to the insensitivity of the flow at the walls to details of the model. They suggested that this problem could be overcome by gathering singularities into groups with fixed relative strengths. A method similar to this is routinely used to determine the blockage for tests at subsonic speeds in the 8ft x 8ft (solid-wall) Wind Tunnel at the Defence Evaluation and Research Agency (DERA), Bedford (Isaacs [21]). The axial source distribution representing model volume is assumed to be represented adequately by linear theory and the theory is used merely to determine the ratio between the mean value of the streamwise velocity increment at four points on the walls (two on the roof and two corresponding ones on the floor) and the blockage increment at a reference point on the model. Measurements of the change in static pressure coefficient between the empty tunnel case and the case with the model in the wind tunnel at these same points provide sufficient

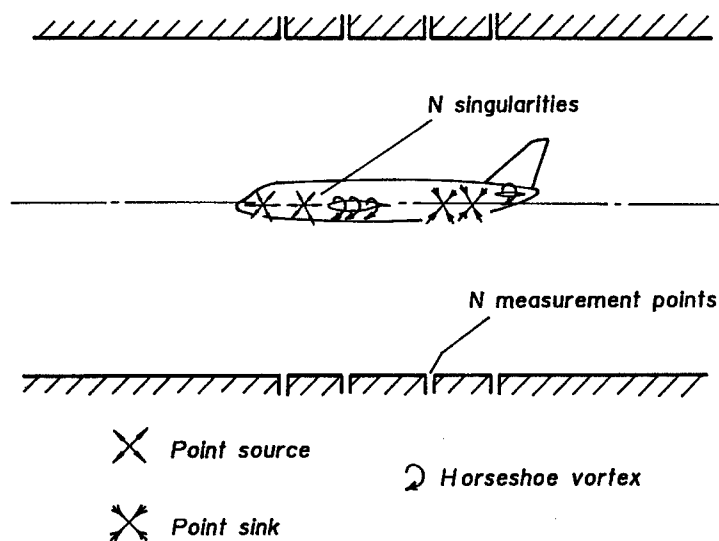


Fig 4.6 Sketch illustrating 'Wall signature method' for solid wall wind tunnels

information to determine the blockage at the model reference point. Experience has suggested that the method is reliable (Isaacs [21]).

If comprehensive measurements could be made of static pressures at the measurement boundary, a similar procedure to that described above could, in principle, be developed using, instead, the 'Dirichlet' approach, together with limited measurements of flow angle to give normal velocity at the boundary. This approach may be useful for wind tunnels with perforated or slotted walls but it has not yet been tried as far as is known.

The second variant of the method uses a 'wall' pressure signature to establish or check the value or values of a parameter linking the flow variables at the measurement surface. This approach has been used by Vaucheret [50], who combined a validated model representation with wall pressure measurements, to infer the porosity of the roof and floor liners of the ONERA S2Ma Tunnel. In a similar way, Goldhammer and Steinle [16] made static pressure measurements on four rails to verify the porosity factor used in a simulation of slotted walls. As with Vaucheret's method, a model representation is used.

4.1.4 TWO-VARIABLE METHODS

In section 4.1.2.4 it was shown that the contribution of the model representation term to a particular component of wall-induced velocity at a point on the model could be eliminated by a suitable mixture of types of boundary condition on S . Equation (4.5) indicates that the contribution of model representation terms vanishes identically when

$$0 = \int_S \left(\frac{\partial \varphi_F}{\partial n} G - \varphi_F \frac{\partial G}{\partial n} \right) dS. \quad (4.12)$$

This suggests that the Green's function satisfying this condition is that for an interference-free, equivalent wind tunnel. In turn, this suggests that the appropriate Green's function is:

$$G = G_F = \frac{1}{r},$$

the free-space Green's function (Mokry et al, [39]), which, in aerodynamic terms, may perhaps be called the 'free-air' Green's function. For this Green's function, Green's formula gives

$$\int_S \left(\frac{\partial \varphi_F}{\partial n} \frac{1}{r} - \varphi_F \frac{\partial}{\partial n} \left(\frac{1}{r} \right) \right) dS - \int_{V_0} \frac{1}{r} \Delta^2 \varphi_F dV = 0, \quad (4.13)$$

where V_0 refers to volume integration in the fictitious region, R , outside the measurement region (Fig 4.1). Thus, provided that the perturbations in the free-air flow outside the working section are 'small', the perturbation potential φ_F may be considered harmonic in this region with the consequence that

$$\int_S \left(\frac{\partial \varphi_F}{\partial n} \frac{1}{r} - \varphi_F \frac{\partial}{\partial n} \left(\frac{1}{r} \right) \right) dS = 0.$$

Thus, for flows of this type, the Green's function G_F satisfies equation (4.12) to give, in place of equation (4.5), an expression no longer containing model-related terms

$$4\pi \varphi_I(P) = - \int_S \left(\frac{\partial \varphi}{\partial n} \frac{1}{r} - \varphi \frac{\partial}{\partial n} \left(\frac{1}{r} \right) \right) dS. \quad (4.14)$$

This expression was derived by Ashill and Weeks [4] in a somewhat different way to the way presented here and it appears in a number of references (Kraft [25], Mokry [35] and Labrujere [28]) giving a particularly elegant derivation. Corresponding expressions have been obtained for plane, two-dimensional flows, using, variously, Fourier transforms (Lo [33]), Green's formula in the plane (Ashill and Weeks [5] and Labrujere [28]) and Cauchy's integral formula (Ashill and Weeks [5], Kraft and Dahm [26] and Smith [49]).

A consequence of not having to know anything about the flow around the model is that it is necessary to measure both components of velocity at all parts of the measurement boundary. The first term under the integral sign in equation (4.14), recognised as the contribution of sources of strength $\partial\phi/\partial n$, requires the normal component to be known at S, while, for the second term, which is the contribution of source doublets, the streamwise velocity increment on S is needed. For solid-wall tunnels, including certain types of adaptive-wall wind tunnels with flexible liners, this poses no significant problems, since the normal component is effectively defined by the condition of no flow through the walls³. For other types of walls, however, the measurement of normal velocity over the whole measurement boundary is much more difficult. As a result, the method has largely been restricted, up to now, to solid-wall tunnels (Ashill and Weeks [4] and Ashill and Keating [2], [3]), although some progress is being made in determining the normal component in perforated and slotted wall tunnels (Freestone and Mohan [13] and Mohan and Freestone [14]).

A major enhancement that became possible with two-variable methods is the calculation of wall interference for complex flows in solid-wall tunnels, e.g. those for high-lift configurations, helicopters and other V/STOL aircraft. The facility to ignore the flow around the model is an important advantage. One area which has been known to cause difficulties in the past is the calculation of blockage for aircraft configurations at high angles of attack, where the flow over the lifting surface is partially separated. In particular, experience in various establishments with the semi-empirical method due to Maskell for calculating blockage was not entirely favourable. However, it was found that, in many cases, Maskell's method gives an overestimate for blockage correction with a consequential underestimate in maximum lift coefficient. This view was confirmed for a combat-aircraft configuration (Ashill and Keating [2], [3]) and for a civil transport model (Kirkpatrick and Woodward [24]) by comparisons between results from Maskell's method and of calculations using a two-variable method. A careful and thorough assessment of a two-variable method for tests at low speed and high lift has been made by Maarsingh et al [34].

Another area where two-variable methods have been used is in the calculation of residual wall interference in adaptive-wall tunnels (Lewis et al [32] and Lewis [31]), where, as noted before, it is routinely necessary to measure both flow angle and static pressure at the measurement boundary. Mokry [35] showed how equation (4.14) may be manipulated to give a convergence formula to allow the shape of the walls of an adaptive-wall wind tunnel to be altered in one step to give nominally interference-free flow. He also showed that two-variable methods are autocorrective in character.

Since the Green's function in equation (4.14) is known, special techniques for determining the function, or equivalent techniques, are unnecessary in two-variable methods. Methods of this type can, therefore, be applied to measurement boundaries of irregular shape with relative ease. In this respect, two-variable methods may be favourably contrasted with one-variable methods.

If the free-air perturbation potential in the fictitious region R is not harmonic, then the volume integral in equation (4.13) can no longer be ignored and equation (4.14) is replaced by

³ As noted before, allowance may need to be made for the change in wall boundary-layer thickness between the tunnel empty and model-in-tunnel cases, further information being given in Chapter 4.2.

$$4\pi \varphi_I(P) = - \int_S \left(\frac{\partial \varphi}{\partial n} \frac{1}{r} - \varphi \frac{\partial}{\partial n} \left(\frac{1}{r} \right) \right) dS + \int_{V_o} \left(\frac{1}{r} \right) \Delta^2 \varphi dV. \quad (4.15)$$

It may be thought that this is an extreme situation and, as mentioned before, that it would not be possible to correct such flows to equivalent free-air conditions. However, flows of this type are found in adaptive-wall tunnels at high subsonic speeds (Lewis et al [32] and Lewis [30]), and it has therefore been necessary to establish the magnitude of the residual corrections for wall constraint (Lewis [30]). For practical reasons, it might be convenient to avoid eliminating tunnel-wall interference altogether in adaptive-wall wind tunnels, concentrating, instead, on ensuring that the wind-tunnel flow may be corrected to equivalent free-air conditions.

A problem with equation (4.15) is that it requires the source term or volume integral in the fictitious region R outside the measurement region to be calculated. This requires a (transonic) flow-field calculation as well as the evaluation of the integral. To avoid the latter difficulty it is useful to think of a flow in the fictitious region R with a velocity potential φ_R that is identical to the free-air flow velocity potential in the near field of the model. This implies that the difference in perturbation potentials ($\varphi_F - \varphi_R$) is harmonic in this region. Thus, if Green's formula is applied to the perturbation potential φ_R in the same way as was done to obtain equation (4.13) and the resulting expression is combined with equation (4.15), it is found that

$$\begin{aligned} 4\pi \varphi_I(P) &= - \int_S \left(\left(\frac{\partial \varphi}{\partial n} - \frac{\partial \varphi_R}{\partial n} \right) - (\varphi - \varphi_R) \frac{\partial}{\partial n} \left(\frac{1}{r} \right) \right) dS + \int_{V_o} \left(\frac{1}{r} \right) \Delta^2 (\varphi_F - \varphi_R) dV, \\ &= - \int_S \left(\left(\frac{\partial \varphi}{\partial n} - \frac{\partial \varphi_R}{\partial n} \right) \frac{1}{r} - (\varphi - \varphi_R) \frac{\partial}{\partial n} \left(\frac{1}{r} \right) \right) dS. \end{aligned} \quad (4.16)$$

Mokry [35] refers to this variant of the two-variable approach as an 'interface - discontinuity method', expressing the fact that the equation contains discontinuities in the normal velocity and perturbation potential across the measurement boundary.

For a solid-wall tunnel

$$\frac{\partial \varphi_R}{\partial n} = \frac{\partial \varphi}{\partial n},$$

and thus equation (4.16) reduces to

$$\varphi_I(P) = \frac{1}{4\pi} \int_S (\varphi - \varphi_R) \frac{\partial}{\partial n} \left(\frac{1}{r} \right) dS.$$

This expression is recognised as the potential at P due to a distribution of source doublets of strength $(\varphi - \varphi_R)$ on S, and, for a cylindrical measurement surface, the integral may be rewritten in terms of a distribution of horseshoe vortices (Ashill and Keating [3] and Mokry [35]). The strength of each of these vortices is directly proportional to the local wall loading. Judd (unpublished research, Southampton University) derived the corresponding expression for two-dimensional flows which was used by Goodyer and Wolf [17] to determine residual corrections in the flexible-wall tunnel at Southampton University. This method was later extended to three dimensions by the Southampton-University group (Lewis [31]). For the study of aerofoils at transonic speeds in the same wind tunnel, Lewis [30] performed calculations of the fictitious flow (effectively to determine either φ_R or $\partial \varphi_R / \partial x$) using a transonic small-perturbation method. Since the boundaries of the fictitious flow are cylindrical or planar, this calculation is less demanding than that for the free-air flow about the model at transonic speeds, particularly in three dimensions.

If the external flow is solved as a Dirichlet problem so that

$$\varphi_R = \varphi$$

at the measurement surface, equation (4.16) reduces to

$$\varphi_I(P) = - \frac{1}{4\pi} \int_S \left(\frac{\partial \varphi}{\partial n} - \frac{\partial \varphi_R}{\partial n} \right) \frac{1}{r} dS,$$

which is the potential due to a distribution of sources of strength $(\partial\varphi/\partial n - \partial\varphi_R/\partial n)$. This approach was suggested by Rebstock and Lee [44].

REFERENCES to Chapter 4.1

- [1] Ashill, P. R., 1993, "Boundary-flow measurement methods for wall interference assessment and correction - classification and review." AGARD-CP-335, pp 1.1 - 1.12.
- [2] Ashill, P.R. and Keating, R.F.A., 1985, "Calculation of tunnel wall interference from wall-pressure measurements." RAE TR 85086,. (This report provides a more detailed account of the work referred to in the following reference).
- [3] Ashill, P.R. and Keating, R.F.A., 1988, "Calculation of tunnel wall interference from wall-pressure measurements." *Aeronautical Journal*, Vol. 92, No.911, pp.36-53.
- [4] Ashill, P.R. and Weeks, D.J., 1982, "A method for determining wall-interference corrections in solid-wall tunnels from measurements of static pressure at the walls." AGARD-CP-335, pp.1.1-1.12.
- [5] Ashill, P.R. and Weeks, D.J., 1978 , "An experimental investigation of the drag of thick supercritical aerofoils - a progress report." RAE TM Aero 1765.
- [6] Ashill, P.R. and Weeks, D.J., 1981, "Techniques developed in Europe for tunnel-wall corrections using measured boundary conditions." Unpublished Proceedings of the 1981 AGARD FDP Subcommittee on Wind Tunnels and Testing Techniques Meeting on 'Integration of Computers and Wind Tunnel Testing', RAE Bedford UK, 18-19 February. 1981
- [7] Capelier, C., Chevallier, J.P. and Bouniol, F., 1978, "Nouvelle methode de correction des effets de parois en courant plan." *La Recherche Aerospaciale*, 1978-1.
- [8] Chan, Y.Y., 1980, "A singular perturbation analysis of two-dimensional wind tunnel interferences." *Journal of Applied Mathematics & Physics*, Vol. 31, pp.605-619.
- [9] Chan, Y.Y., 1980, "Lift effect on transonic wind tunnel blockage." *Journal of Aircraft*, Vol. 17, No.12, pp.915-916.
- [10] Chevallier, J.P., 1983, "Survey of ONERA activities on adaptive-wall applications and computation of residual corrections." NASA CP-2319, pp.43-58.
- [11] Davis, S.S., 1981, "A compatibility assessment method for adaptive-wall wind tunnels." *AIAA Journal*, Vol. 19, No. 9, pp.1169-1173.
- [12] Evans, J.Y.G., 1949, "Corrections to velocity for wall constraint in any 10 x 7 rectangular subsonic wind tunnel." ARC R&M 2662.
- [13] Freestone, M. M. and Mohan, S. R., 1994, „Interference determination for wind tunnels with slotted walls.“, AGARD-CP-535, pp 19-1 - 19-12.

- [14] Mohan, S. R. and Freestone, M. M., 1994, „Interference determination for three dimensional flows in slotted liner wind tunnels.“ ICAS-94-3.3.1, Anaheim, California, USA, 18-23 Sept. 1994
- [15] Garner, H.C., Rogers, E.W.E., Acum, W.E.A. and Maskell, E.C., 1966, "Subsonic wind tunnel wall corrections.", AGARD-AG-109.
- [16] Goldhammer, M.I. and Steinle, F.W., 1990, "Design and validation of advanced transonic wings using CFD and very high Reynolds number wind tunnel testing." ICAS 90-26.2.
- [17] Goodyer, M.J. and Wolf, S.W.D., 1980, "The development of a self-streamlining flexible walled transonic test section." USA AIAA-80-440-CP.
- [18] Hackett, J.E. and Wilsden, D.J., 1975, "Determination of low speed wake-blockage corrections via tunnel-wall static pressure measurements." AGARD-CP-174, pp.22.1-22.9.
- [19] Hackett, J.E. and Wilsden, D.J., 1979, "Estimation of tunnel blockage from wall pressure signatures: a review and data correlation." NASA CR-152241.
- [20] Hackett, J.E., Wilsden, D.J., and Stevens, W.A., 1981, "A review of the wall pressure signature and other tunnel constraint correction methods for high angle-of-attack tests." AGARD-R-692.
- [21] Isaacs, D., 1969, "Calibration of the RAE Bedford 8ft x 8ft wind tunnel at subsonic speeds, including a discussion of the correction to the measured pressure distribution to allow for the direct and blockage effects due to the calibration probe." ARC R&M 2777.
- [22] Kemp, W.B. Jr., 1988, "A panel method procedure for interference assessment in slotted-wall wind tunnels." USA AIAA-88-2537.
- [23] Kemp, W.B. Jr., 1976, "Towards the correctable-interference transonic wind tunnel." Proceedings of the AIAA 9th Aerodynamic Testing Conference, 7-9 June 1976, pp.31-38.
- [24] Kirkpatrick, D.L.I. and Woodward, D.S., 1990, "Priorities for high-lift testing in the 1990s." AIAA-90-1413.
- [25] Kraft, E.M., 1983, "An overview of approaches and issues for wall interference assessment/correction." NASA CP-2319, pp.3-20.
- [26] Kraft, E.M. and Dahm, W.J.A., 1982, "Direct assessment of wall interference in a two-dimensional subsonic wind tunnel." USA AIAA-82-0187.
- [27] Küchemann, D., 1978, "The aerodynamic design of aircraft." London, Pergamon Press.
- [28] Labrujere, Th. E., 1984, "Correction for wall interference by means of a measured-boundary-condition method." Holland NLR TR 84114 U.
- [29] Le Sant, Y., and Bouvier, F., 1992, "A new adaptive test section at ONERA Chalais-Meudon." Proceedings of European Forum on Wind Tunnels and Wind Tunnel Test Techniques, Southampton University, 14-17 September 1992, Paper 41.
- [30] Lewis, M.C., 1988, "Aerofoil testing in a self-streamlining flexible walled wind tunnel." NASA CR-4128.
- [31] Lewis, M. C., 1991, "Two-dimensional wall adaptation for three-dimensional flows." Proceedings of the International Conference on Adaptive Wall Wind Tunnel Research and Wall-Interference Correction (ICAW), June, 1991, Paper A2.
- [32] Lewis, M. C., Taylor N. J. and Goodyer, M. J., 1992, "Adaptive wall technology for three-dimensional models at high subsonic speeds and aerofoil testing through the speed of sound." Proceedings of the Royal Aeronautical Society Symposium 'Wind Tunnels & Wind Tunnel Test Techniques', Southampton University, 14-17 October 1992, Paper 32.

- [33] Lo, C.F., 1978, "Tunnel interference assessment by boundary measurements." *AIAA Journal*, Vol. 16, No.4, pp.411-413.
- [34] Maarsingh, R. A., Labrujere, Th. E., and Smith, J., 1988, "Accuracy of various wall-correction methods for 3D subsonic wind-tunnel testing." AGARD-CP-429, pp.17.1-17.13.
- [35] Mokry, M., 1989, "Residual interference and wind tunnel wall adaptation." USA AIAA-89-0147.
- [36] Mokry, M. and Ohman, L. H., 1980, "Application of the Fast Fourier Transform to two-dimensional wind tunnel wall interference." *Journal of Aircraft*, Vol. 17, No. 6, pp.402-408.
- [37] Mokry, M., 1971, "Higher order theory of two-dimensional wall interference in a perforated wall wind tunnel." Canada NRC LR-853.
- [38] Mokry, M., 1982, "Subsonic wall interference corrections for finite-length test sections using boundary pressure measurements." AGARD-CP-335, pp.10.1-10.15.
- [39] Mokry, M., Chan, Y. Y., Jones, D.J. and Ohman, L. H. (ed.), 1983, "Two-dimensional wind tunnel wall interference." AGARD-AG-281.
- [40] Mokry, M., Digney, J. R. and Poole, R. J. D., 1987, "Doublet-panel method for half-model wind-tunnel corrections." *Journal of Aircraft*, Vol. 24, No. 5, pp. 322-327.
- [41] Mokry, M., 1995, "On the subsonic and transsonic doublet in the farfield representation of an airfoil", AIAA-95-1879
- [42] Newman, P.A. Kemp, W. B. Jr. and Garriz, J. A., 1988, "Emerging technology for transonic wind-tunnel-wall interference assessment and corrections." USA SAE Paper 881454.
- [43] Paquet, J. B., 1979, "Perturbations induites par les parois d'une soufflerie, methods integrals." These Doc.Ing., Universite de Lille.
- [44] Rebstock, R. and Lee, E. E. Jr., 1988, "Capabilities of wind tunnels with two adaptive walls to minimize boundary interference in 3D model testing." *Transonic Symposium: theory, application, and experiment*, NASA Langley, April 1988, NASA CP-3020 Vol. 1, Part 1, pp.891-910, March 1989.
- [45] Rizk, M.H. and Smithmeyer, M. G., 1982, "Wind tunnel wall interference corrections for three-dimensional flows." *Journal of Aircraft*, Vol. 19, No.6, pp.465-472.
- [46] Schairer, E. T., 1984, "Two-dimensional wind-tunnel interference from measurements on two contours." *Journal of Aircraft*, Vol. 21, No.6, pp.414-419.
- [47] Smith, J., 1981, "A method for determining 2D wall interference on an aerofoil from measured pressure distributions near the walls and on the model." Holland NLR TR 81816 U.
- [48] Smith, J., 1986, "A transonic model representation for two-dimensional wall interference assessment." Holland NLR TR 86026 U.
- [49] Smith, J., 1982, "Measured boundary condition methods for 2D flows." AGARD-CP-335, pp.9.1-9.15.
- [50] Vaucheret, X., 1982, "Amelioration des calculs des effets de parois dans les souffleries industrielles de l'ONERA." AGARD-CP-335, pp.11.1-11.12, (English translation in NASA TM-76971).
- [51] Weatherburn, C. E., 1978, "Advanced vector analysis." London, G.Bell & Sons Ltd.
- [52] Wilsden, D. J. and Hackett, J. E., 1983, "Tunnel constraint for a jet in crossflow." NASA CP-2319, pp.273-290.

4.2 CLOSED TEST SECTIONS

LIST OF SYMBOLS for chapter 4.2

B	working section breadth
C	Working section cross-sectional area
D	Hydraulic diameter
H	working section height
M	free-stream Mach number
N	parameter defined by Adcock and Barnwell (1984)
S	Model reference area
TOLC	<u>T</u> OLerance for <u>C</u> olumns
β	Prandtl-Glauert factor, $\beta = \sqrt{1 - M^2}$
Δ	Increment due to presence of model
δ	Lift interference parameter
δ^*	Wall boundary layer displacement thickness in empty tunnel at model station
θ	Wall boundary layer momentum thickness in empty tunnel at model station
Ω	Ratio of solid blockage in a wind tunnel of given height to breadth ratio with wall boundary layers to the maximum value of solid blockage in the same wind tunnel without boundary layers

4.2.1 BACKGROUND

The possible benefits of using measurements of wall pressures to calculate wall-interference corrections in closed-wall test sections were realised in the early 1940's when compressibility effects on the flows over wings and bodies were first observed (Göthert [13], Thom [32]). A review of this early work is given in Section 5 of AGARDograph 109 by Garner et al [11]. It was appreciated early on that linear-theory descriptions of the near-field flow around the model are increasingly inadequate as free-stream Mach number increases towards unity. This led to the idea of using wall pressures to determine the strengths of the singularities representing the model. This was justified on the grounds that the flow satisfies the linearised potential equation in the far field. Methods of this type are known as wall-signature or wall pressure signature methods, the underlying theory for which has been described in Section 4.1.3.

In the 1970's an analogous problem was discovered with the representation of wind-tunnel models at high lift, in which flow separation may occur on part of the model (Hackett and Wilsden [14], [16], and Hackett, Wilsden and Stevens [17]). For flows of this type linear theory is totally inadequate for modelling the near field. Hackett and his colleagues used wall pressures to determine the strengths of singularities representing the model flow in the far field. This aspect is considered in more detail in Sections 4.2.5 and 4.2.6, and in Section 8.3. The usual Neumann condition of zero normal velocity at the walls was applied by using the classical method of images. Hackett's group was able to demonstrate the application of the wall signature method to a wide range of flows, including wings with jet flaps. A related approach has been adopted by Ulbrich, Lo and Steinle [33], Ulbrich and Steinle [34], [35].

The development of the two-variable method in the late 1970's provided a further technique for calculating wall interference in closed-wall tunnels. The derivation of this method has been given in Section 4.1.4

and in this approach wall interference is defined by the distributions of two flow variables on a surface surrounding the model - the streamwise and normal components of velocity. No model representation is needed. If the surface is taken to coincide with the wind-tunnel walls, the normal component is usually set to zero to satisfy the condition of no flow through the walls, as with the wall signature method. However, where there are significant interactions between the constrained flow over the model and the wall boundary layers, allowance may need to be made for the change in displacement effect of the wall boundary layers. This aspect is discussed further in Section 4.2.2. This leaves only one variable to be determined - the streamwise velocity - and this can be inferred from Bernoulli's equation so long as the velocity perturbations at the wall are small compared with free-stream speed. This question is considered further in Section 4.2.4.

4.2.2 BOUNDARY CONDITIONS

The assumption usually used in both the wall signature and two-variable methods that the normal component of velocity is zero at the walls is equivalent to neglecting the interaction between the inviscid flow-field and the wall boundary layers. The validity of this assumption needs to be carefully assessed in each case. At one extreme where the flow perturbations are small, as for example in low-speed flows over a model at low lift, the effect on the wall boundary layers can be demonstrated to be negligible by simple one-dimensional considerations. At the other extreme, where flow perturbations are 'large', the interaction cannot be ignored. Examples of the latter type include flows where shock waves reach the wall (Lewis, 1988) and where the wall boundary layer separates as a result of large adverse pressure gradients induced by high-lift models (see Section 8).

Berndt [7] appears to have been the first to draw attention to the effect on blockage and the choking Mach number of the interaction between the inviscid flow-field associated with the model and wall interference and the wall boundary layers. He used a simplified method to calculate the effect. More recently a theoretical method with some simplifications has been presented by Adcock and Barnwell [2] for tunnels of rectangular cross section. This method is based on approach of Pindzola and Lo [26] for slotted-wall tunnels to solve the boundary-value problem for the perturbation potential. The simplifications made include the neglect of the change in wall shear stress due to the presence of the model and the assumption that the transformed shape factor is unity. Both these assumptions are justified for the high Reynolds number conditions of wind tunnels. In addition it is assumed that, in the empty tunnel, δ^* and θ , the wall boundary-layer displacement and momentum thicknesses may both be taken constant and equal to the values at the model station. It is further supposed that the wall boundary layer is two-dimensional in character so that its development when the model is in the working section can be described by the Von Karman momentum integral equation. As well as studying the effect on blockage, Adcock and Barnwell also considered the extent to which lift interference is influenced. For this purpose they represented model volume by a source doublet and the lifting effect by a vortex doublet. For the analysis they found it convenient to define a parameter

$$N = \frac{1}{1 + \frac{2\delta^*}{B} \left(1 + \frac{\delta^* + \theta}{\beta^2 \delta^*} \right)} \quad (4.17)$$

Results for the ratio of the solid blockage in a wind tunnel of given height to breadth ratio with wall boundary layers to the maximum value of solid blockage in the same wind tunnel without wall boundary layers, Ω , and the lift interference factor δ are shown in Figure 4.7 and 4.8 for working sections with $H/B = 1$. Charts such as these and others given by Adcock and Barnwell provide a useful guide as to the likely magnitude of the effect both on blockage and on angle of incidence in the absence of wall-pressure

measurements (see below). Adcock and Barnwell observed that, owing to linearisations in the method, results obtained with it should only be used for values of N down to about $2/3$. For the typical values $2\delta^*/B = 0.01$, $\delta^*/\theta = 1.4$ and $M = 0.8$, $N = 0.95$ and, it may be inferred from Figure 4.7, that the maximum value of Ω is 0.85. In other words, for this case, the maximum blockage is 85% of the value predicted by classical inviscid theory. Regarding the effect on lift interference, Figure 4.8 shows that, at the position of the doublet, the wall boundary layers only affect the streamwise gradient of wall-induced upwash, the gradient becoming less as the parameter N decreases.

A combined experimental-theoretical study has been made of the effect of wall boundary layers on the blockage of bodies at high subsonic speeds (Ashill, Taylor and Simmons [5]). Results for measured values of the mean of the increment in pressure coefficient, relative to empty-tunnel conditions, at the roof and floor of the working section for an axisymmetric body at zero angle of incidence are shown in Figure

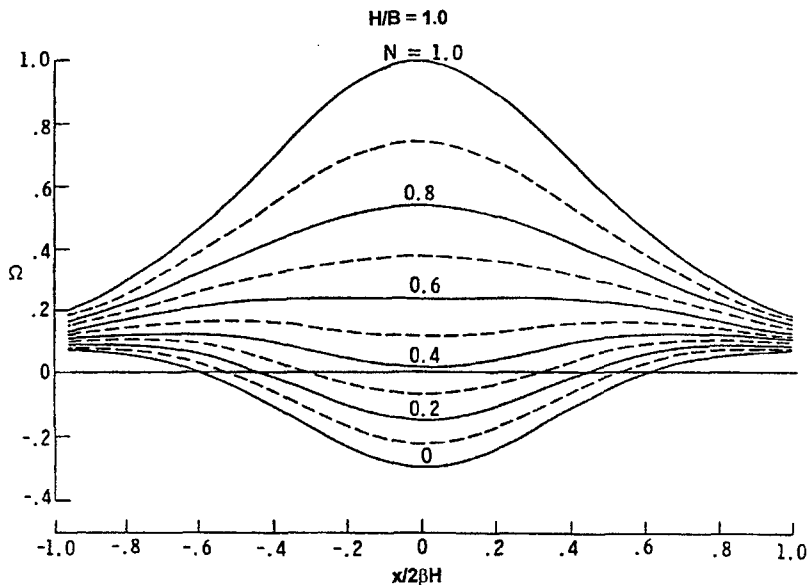


Figure 4.7 Calculated effect of wall boundary layers on blockage (after Adcock and Barnwell [2])

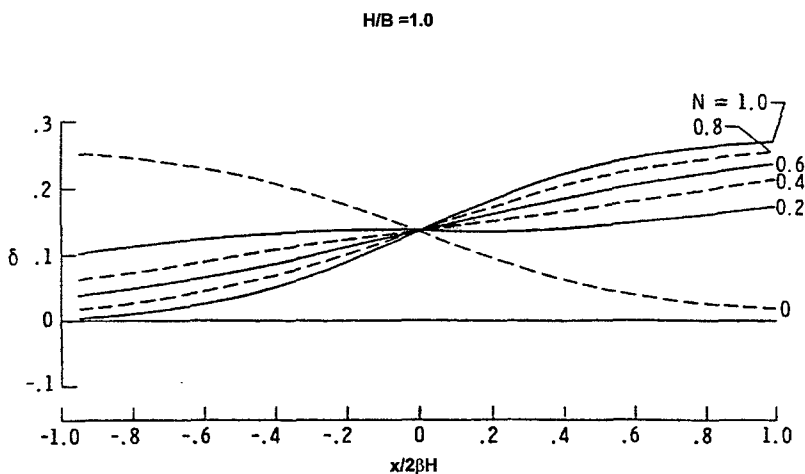


Figure 4.8 Calculated effect of wall boundary layers on lift interference (after Adcock and Barnwell, 1983)

4.9. In this figure the measured data are compared with results of a classical inviscid theory and those of the same theory but including allowance for the wall boundary-layer effect. The viscous theory gives improved agreement with measurement, particularly at the highest Mach number shown, $M = 0.93$. This theory differs from that due to Adcock and Barnwell in that a viscous-inviscid iteration process and a more-accurate form of the normal-velocity condition are used. As in the treatment of Adcock and Barnwell, Ashill et al solved the Von Karman momentum equation and, to simplify the boundary-value

problem, took the normal velocity to be constant around the working section at a fixed streamwise or axial station¹. Furthermore, based on assessments of calculations of two-dimensional boundary layers by the method of Green, Weeks and Brooman (1973), they took the boundary-layer shape parameter to be a constant. With these assumptions the expression corresponding to equation (4.17) is:

$$N = \frac{1}{1 + \frac{2\delta^*}{B} \left(\frac{\delta^* + \theta}{\beta^2 \theta} \right)} \quad (4.18)$$

Equations (4.17) and (4.18) give results for N that become increasingly close as Mach number and shape parameter δ^*/θ both tend to unity.

Similar values for the change in blockage due to the wall boundary layers are obtained by the two methods. Figure 4.9 shows that the effect of the interaction is significant. Fortunately, methods that make use of wall-pressure measurements, such as those referred to above, account for a major part of the effect. This remark is supported by the results of calculations by a two-variable method for transonic flows over an aerofoil where the wall pressure gradients were mild (i.e. the supercritical region was contained within the working section). These calculations (Ashill and Weeks [6], Rueger et al [26]) indicate that, when use is made of wall-pressure measurements in a two-variable method, the boundary-layer effect is not significant. The reason for this is that the wall pressures contain some information on the effect of the wall boundary layer on the flowfield. However, more recent work by Ashill et al [5] suggests that the effect needs to be allowed for with wall-pressure methods as Mach number approaches unity when the pressure gradients at the wall induce larger changes in boundary-layer thickness than at lower speeds. Similarly, the effect may well need to be represented for flows over high lift wings at low speeds where the pressure gradients induced at the walls can be relatively large.

In summary, for models at cruise conditions, the effect on calculated wall-induced velocities of the interaction between the inviscid flowfield and the wall boundary layers is likely to be insignificant except at high subsonic speeds, provided that a method based on wall-pressure measurement is used. More generally, the effect is likely to be important when the wall boundary layer is close to separation and may therefore be important for high-lift models at low speeds. Care should therefore be taken to monitor wall

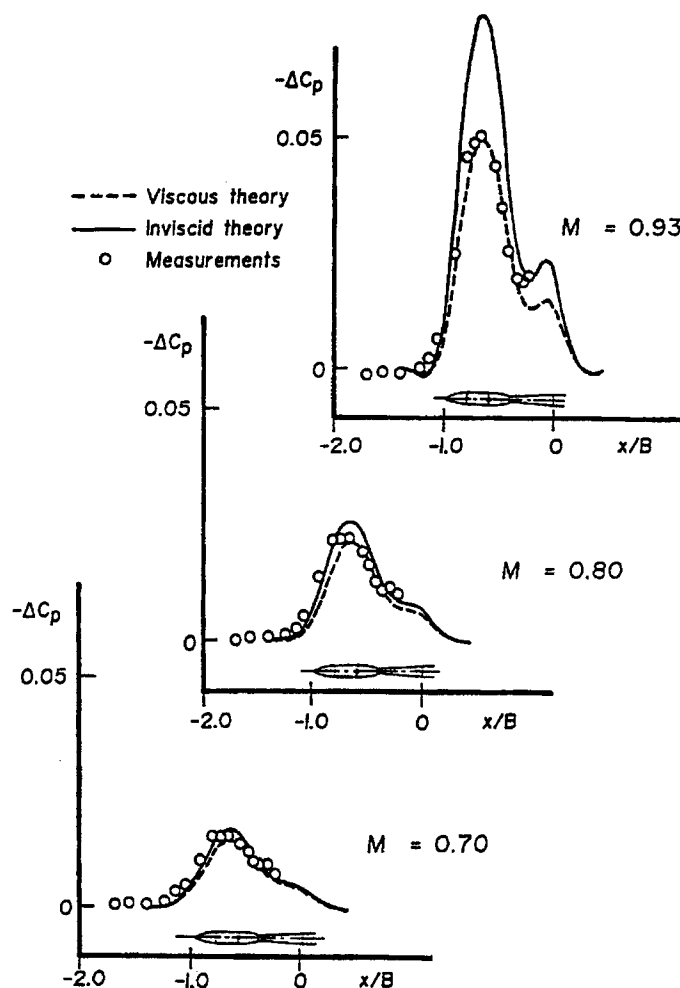


Figure 4.9 : Axial distributions of increment in wall static pressure coefficient due to the presence of the model : comparison between measurement and viscous and inviscid theories

¹ This approach would need to be modified for the lifting case where significant variations in boundary-layer thickness would be expected around the working section.

pressure distributions so that, if in doubt, calculations can be made of wall boundary layer development relative to empty-tunnel conditions.

4.2.3 NUMERICAL APPROXIMATIONS

Provided that the effect of the wall boundary layers can be ignored the effect of the walls may either be represented by the classical method of images (as in the wall pressure signature method) or by a distribution over the walls of elementary source doublets or horseshoe vortices (as in the two-variable method). In the former case consideration needs to be given to the numerical convergence of the doubly-infinite series and methods of accelerating convergence may need to be considered. One such, which has been applied by Isaacs [19] to the case of sources within wind tunnels of rectangular cross section, involves replacing the source images far from the walls by a source sheet. Analytical relationships may be used to replace double summations by rapidly convergent single series (Glauert [12], Garner et al [11]).

A method of representing the elementary source doublets by constant-density panels in the two-variable method is described in Section 4.3. An approximation to the alternative horseshoe-vortex approach is described by Ashill and Weeks [6]. So long as wall interference is not required close to the wind-tunnel walls a simple numerical integration procedure may be used to evaluate the integrals (e.g. Simpson's rule). However, if this is not the case special treatment of the singular integrals will be required. This may be done by using a panel method analogous to that described in Section 4.3.

4.2.4 CHOICE OF METHOD

Faced with the choice of the two wall-pressure methods, the wind-tunnel engineer needs to know their relative advantages or disadvantages. For attached flows typical of transport aircraft models at cruise conditions the wall-signature method is easy to apply and requires only a small number of wall-pressure measurements (Isaacs [19]). The model may be represented without difficulty by distributed singularities. The two-variable method, on the other hand, needs no model representation, as noted before, but requires many wall pressure measurements, typically of the order of 100 (Ashill and Weeks [6]). For this reason, a wall-signature method has been favoured for correcting data for blockage in tests on conventional aircraft models at high subsonic-speed cruise conditions in the 8ft x 8ft Tunnel at DRA Bedford.

For flows over aircraft models at high lift, the problem of model representation is more difficult and requires some experience in determining suitable distributions (see Section 4.2.6 and Section 8). However, as for high-speed testing, only a small number of wall-pressure measurements is needed. This contrasts with the two-variable method, which, as at high speed, needs a large number of wall-pressure measurements (Ashill and Keating [4]). On the other hand, for complex flows, such as those as studied by Ashill and Keating over a combat-aircraft model at high lift, the ability to obtain wall-interference without the need to know anything about the flow over the model is a clear advantage of the two-variable approach.

Wall boundary condition methods need only be used where classical methods, based on linear theory, cannot be applied or are expected to fail. However, where possible, calculations should be performed by a classical image method, if only as a check that the results obtained from a wall boundary condition method are sensible. As a general rule, it is recommended that wall-induced velocities should be calculated by more than one method.

4.2.5 MEASUREMENTS AND ANALYSIS OF WALL PRESSURES

4.2.5.1 WALL PRESSURE-SIGNATURE METHODS

It is self evident that success in using the wall pressure signature approach rests in measuring the signatures properly. The signal level can be small for small or low-drag models and imperfections in the tunnel, its instrumentation and its operation can easily compromise the pressure-signature measurements.

An ideal pressure signature requires:

- A test section length of 2.5 to 3.0 hydraulic diameters. This is rarely achieved in existing general purpose tunnels. The pressure signature peak, which typically lies aft of the model, should be between 35% and 40% of the test section length from the start of the test section.
- Smooth data with local inconsistencies and errors due to orifice and test section surface characteristics removed. This involves referencing all signatures to the appropriate 'empty-tunnel' condition, which might include model supports (sting, mounting struts, etc., as discussed in section 1.2, see also section 8.3.2).
- High quality pressure instrumentation and proper transducer ranging.
- Well-defined asymptotes at the upstream and downstream ends of the signature. The front of the signature should asymptote to the test section reference pressure. An offset asymptote can be handled successfully provided that it is well defined.

Figure 4.10 shows three pressure orifice distributions used in the Lockheed wind tunnels and a suggested distribution that will be discussed below. All four examples involve tunnels with $B/H = \sqrt{2}$. The orifice X-locations are normalised on working-section width, B, and a sub-scale based on hydraulic

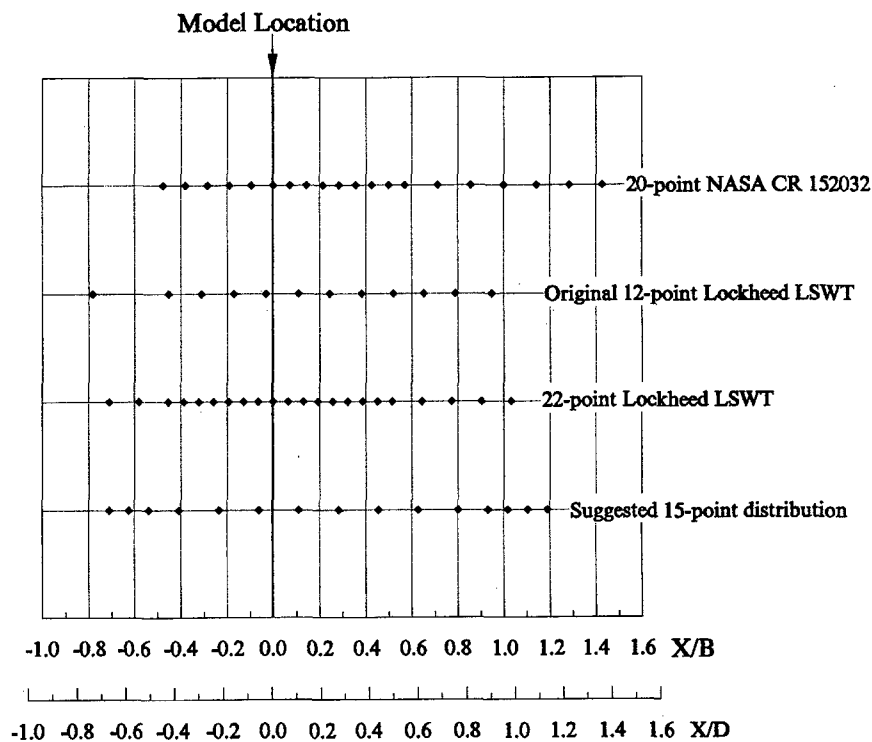


Figure 4.10 Typical orifice locations for the pressure signature method

diameter, D , is provided. Four-wall application is preferred but practical considerations may preclude floor-mounted orifices, particularly in large tunnels. This is discussed further in Section 8.3.2. The first distribution (the upper set) was employed in the (previously) Lockheed 30" x 43" MTF Wind Tunnel during the development of the wall pressure signature method for powered models (see for example Hackett and Boles [15]). To provide sufficient length for large wakes to develop, the test section length was doubled, leaving the model in its original position. This placed the model at approximately a quarter of the test section length from the entry point. The second example shows the system originally installed in the Lockheed 23 $\frac{1}{4}$ ft x 16 $\frac{1}{4}$ ft Low Speed Wind Tunnel. There are too few orifices and the signature is too short for general purpose testing but, with care, the system can be used for car testing. The greatest difficulty with this particular arrangement lies in obtaining sufficiently accurate wake source values and there is likely to be an adverse impact on calculations of the wake-induced drag increment (see Section 6.2.6 and 8.3.1.5). The third example shows a preferred arrangement for this tunnel. The last example is a further orifice arrangement suggested for test sections of insufficient length. Point concentration has been increased towards the end of the signature in an attempt to capture the asymptotes more successfully. The added points should be used as part of a larger array when fitting the asymptotes.

When setting up a tunnel system to measure pressure signatures, the following additional sources of trouble should be borne in mind:

- i) bad readings from failed or failing pressure transducers.
- ii) influence of the model and its images beyond the walls on the reading of the tunnel reference pressure. This problem can sometimes be corrected by regarding the reference pressure reading as part of the wall pressure signature.
- iii) interference from model-induced distortions (relative to empty test section conditions) of the wall boundary layers. In extreme cases, where a high energy jet hits a tunnel wall, for example, flow control may be needed at that wall (see Section 8.3.1).
- iv) insufficient sensitivity and/or accuracy of the pressure instrumentation.
- v) an insufficient number or poorly selected distribution of pressure orifices.

Human monitoring of each pressure signature is an unrealistic and costly burden, and computer monitoring has not been used, as far as is known, because of the difficulty of doing so. This is a fertile area for the use of intelligent systems.

4.2.5.2 TWO VARIABLE METHODS

Most of the points made above in connection with the measurement of wall pressure signatures apply to two variable methods. However, there are considerations special to two variable methods which need to be borne in mind, as discussed below.

As noted before the streamwise velocity required as a boundary condition is usually determined from wall pressure measurements using the linear form of Bernoulli's equation. This may be justified if the perturbations in streamwise velocity at the walls are small compared with free-stream speed. If these perturbations are not 'small', it may be necessary to solve Euler's equation for the flow at the measurement surface given the pressure distribution (Ashill and Keating [3] and Maarsingh et al [23]). The use of a non-linear relationship to determine streamwise velocity can only be justified at low speeds when the governing equation for the inviscid flow, Laplace's equation, is 'exact'. At high subsonic speeds, where the linearised potential equation is solved, no increase in accuracy can be expected from refining the

estimate of wall streamwise velocity.

For the application of the two variable method it is recommended that the choice of wall orifice locations should be determined and perhaps optimised² by prior calculation using 'exact' solutions from classical linear theory. In these calculations an effort should be made to simulate as closely as possible the flow around the models, bearing in mind the different types of flows likely to be studied. Such a procedure was described by Ashill and Weeks [6] for a wind tunnel of square cross section and later applied to a low-speed wind tunnel of rectangular ($b = 4\text{m} \times h = 2.7\text{m}$) cross section by Ashill and Keating [4].

Results of such assessments are shown as test cases in Figures 4.11, 4.12 and 4.13 for a floor mounted half model in the rectangular working section noted above. In the first test case the model wake is represented by a point source (Figure 4.11): in the second test case model volume is simulated by a source and sink (Figure 4.12) while, in the third test case, the lift is simulated by a horseshoe vortex (Figure 4.13). Linear theory is used to supply values of streamwise velocity at the positions of the wall orifices and this information is then used in calculations of wall-induced velocities at and along the model axis by the two-variable method. These comparisons confirmed the suitability of the choice of orifice number which, as noted in Section 4.2.1, was about 100, the orifices being placed about one tunnel breadth upstream and downstream of the model centre-line. However, these studies and others described by Rueger et al [28] suggest that the two-variable method is 'robust' in that pressure orifices can be removed without significantly affecting the accuracy of the method. Sensitivity studies such as these should be performed before any test and should form the basis for the assessment of the requirements for new wind tunnels. For existing wind tunnels, any shortfall in the number of wall holes can be made good with static tubes or static rails attached to the tunnel walls.

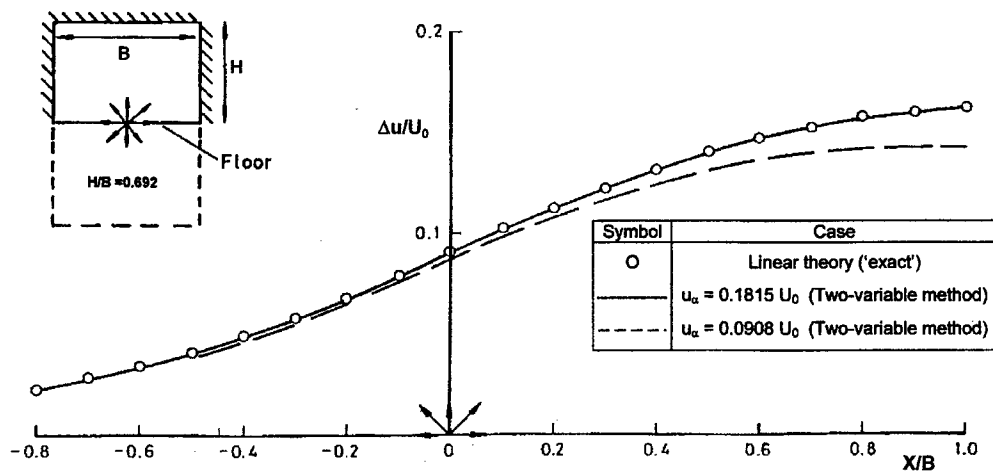


Figure 4.11 Test case 1. Point source. Blockage at 'floor' line

² Here 'optimised' is used in the sense of meaning minimising the number of orifices for a certain level of accuracy.

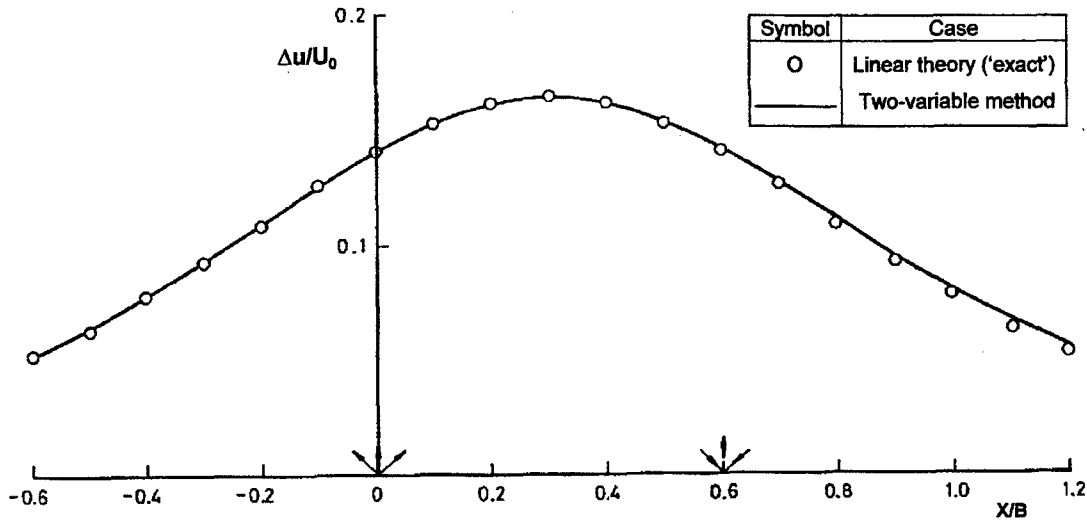


Figure 4.12 : Test case 2. Point source and sink. Blockage increment of velocity at 'floor' centre line

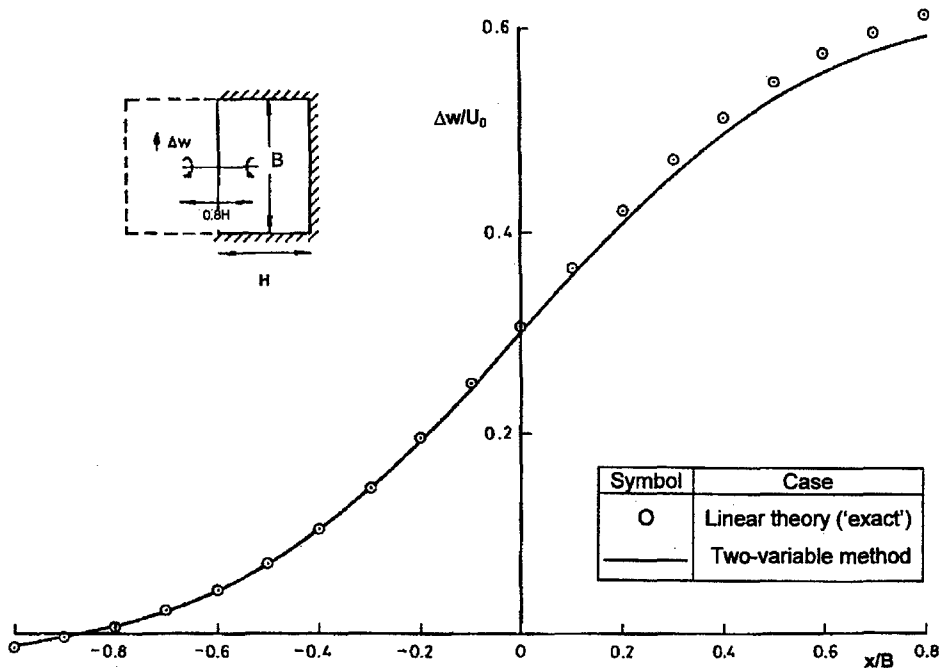


Figure 4.13 Test case 3. Horseshoe vortex. Wall-induced upwash at centre-span of vortex

An alternative approach, used by Ashill and Weeks [6], Ashill and Keating [4] and more recently by Rueger et al [28], assumes the working section to be of infinite length. The effects on the induced velocities in the region of the model of the singularities on the upstream and downstream faces are then ignored. The upstream value of the pressure increment is taken to be zero while the downstream value can be determined from momentum considerations (Ashill and Keating [4]). The blockage in the region of the model ($0 < x/B < 0.6$) is not sensitive to errors in the far-downstream value of the increment in pressure coefficient or velocity increment, u_∞ , as may be inferred from Figure 4.11. Here an error of as high as 50% in this value causes errors of only about 5% in the blockage increment in the vicinity of the model. The pressure increments between either the most upstream or most downstream orifices and the limiting

values are obtained by interpolation assuming an exponential variation as expected from classical linear theory of wall interference for solid-wall wind tunnels. Calculations using classical linear theory (Ashill and Keating [3]) suggested that the length upstream and downstream of the model where wall pressures are measured should be approximately one working section breadth. Again, however, the suitability of the choice should be checked for individual cases.

The measurements of wall pressures should be referred to empty-tunnel conditions³. This needs to be done to allow for:

- a) the likely non-cylindrical nature of the tunnel walls and the growth of the wall boundary layers in the empty tunnel;
- b) imperfections in the wall holes; and
- c) static-pressure errors due to hole size (Shaw [29] and Franklin and Wallace [9]).

Wind-tunnel users should not be surprised to find that, before being referred to empty-tunnel conditions, wall pressure distributions contain a significant degree of scatter, due mainly to effect b). However, when 'tared' to empty-tunnel conditions, smooth distributions may be expected. Where a two-variable method is used, the pressures should be checked for any faulty readings and removed prior to interpolation of the pressure data.

Consideration needs to be given to the interaction between the model supports and the tunnel walls. In some cases, the supports may intersect the tunnel walls. This poses problems because of the need then to measure a large number of pressures in the region of the supports where pressure changes rapidly. One possible way of avoiding this difficulty is to define the 'empty tunnel' as the wind tunnel including the supports but excluding the model, as previously suggested in Section 1.2. This glosses over the problem of allowing for any interaction between the model and support flowfields which has to be considered separately.

Ideally, the reference pressure should be measured sufficiently far upstream not to be affected by the presence of the model. Fortunately, for solid-wall tunnels, the combined direct and wall interference effect decays exponentially with distance, as implied before, so that the effect on the reference static pressure is likely to be negligible, at least for a wind tunnel with a working section of reasonable length. If, for any reason, the reference wall hole is affected by the presence of the model, it may be possible to invoke the auto-corrective character of the two-variable method (Mokry [25], see also Section 4.3). What this means is that the method substantially corrects for any error in reference pressure, a small residual error remaining owing to extrapolation to a 'false' zero far upstream.

Owing to the fact that the two variable method involves integration's, wall-induced velocities determined by this method tend to be insensitive to random errors in wall pressures. Nevertheless, wall-pressure distributions should be carefully monitored to ensure that the calculations of wall-induced velocities are not corrupted by erroneous pressure measurements. As mentioned in Section 4.2.5.1, this suggests the need for intelligent systems to remove such data before the calculations are performed.

Systematic errors will arise from inaccuracies in transducer calibrations, but these can be estimated by applying the errors as small perturbations to the pressure or streamwise velocity distributions in the method. Such studies are an important prerequisite for establishing the errors in the method.

³ Empty-tunnel wall-pressure data will normally be taken during the calibration of the wind tunnel. Details of the calibration procedure for testing at high subsonic speeds in a solid-wall tunnel are given by Isaacs [19]. He demonstrated the importance of allowing for the direct and blockage effects of the calibration probe when determining 'empty-tunnel' static pressures at high subsonic speeds.

4.2.6 MODEL AND TUNNEL REPRESENTATION WHEN USING THE „MATRIX“ VERSION OF THE WALL PRESSURE SIGNATURE METHOD.

4.2.6.1 INTRODUCTION

Section 4.2.5.1 gave general guidance on the installation and use of wall pressure orifices and their application to pressure-based wind tunnel correction methods. The recommended geometries were based largely on ad hoc experience, extending in some cases over a decade or more. However there was no reference to the relationship of the orifice configuration to the model under test and no indication of how an orifice system might be optimised for a given model. The present section will address these and other practical issues in a systematic way, including reviews of which walls should be instrumented, length of orifice rows and orifice spacing.

4.2.6.2 BASIC APPROACH

The 'matrix' version of the pressure signature method employs vortex, source and doublet singularities on the model at fixed locations that correspond to matrix columns (see Hackett et al [18]). Sensing locations on the tunnel walls (pressure orifices) correspond to the matrix rows. The form of the equation is shown below:

$$\left| \begin{array}{c} \text{Influence} \\ \text{Coefficients for} \\ \text{U-component} \\ \text{at walls} \end{array} \right| \cdot \left| \begin{array}{c} \text{Singularity} \\ \text{strengths} \end{array} \right| = \left| \begin{array}{c} \text{Measured or} \\ \text{reference} \\ \text{U-components} \\ \text{at walls} \end{array} \right|$$

The matrix elements are the U-component interference coefficients for the model singularities, with their tunnel images, at the orifice locations on the tunnel surfaces (see Equation 4.11 and the subsequent discussion). In practice it is found that matrix conditioning is poor and solution oscillations that propagate into the interference field are not unusual. Since matrix conditioning depends on the particulars of both rows and columns, it is difficult to make recommendations concerning orifice spacing, for example, without reference to what the model is and how it is represented. Model representation and orifice geometry will therefore be addressed using an example derived from an actual test. The approach that will be described below may be applied to other geometry's, as needed.

The example cases will be limited to axial velocity interference, which is found to be more challenging than upwash interference in problems of the present type. Experience shows that, when the axial flow interference is calculated correctly, the upwash interference is reliable.

4.2.6.3 MODEL GEOMETRY AND ITS REPRESENTATION

The test example involves a flat plate model that represents the plan view of a modern fighter aircraft. Such a model was tested and wall pressure data and analyses are available, though they will not be employed directly here. Figure 4.14 shows the model and tunnel details. The model was mounted with its trailing edge 0.99 ft above the tunnel centre plane and its nose 3.45 ft below the tunnel roof. The cross-effects between lift and blockage were therefore very significant. The program is fully three dimensional and off-centre effects are included in all analyses. The model angle-of-attack was near stall and the measured wind-axis C_L and C_D were 1.17 and 0.91 respectively.

Figure 4.14 includes a sketch of the model with line singularities at seven locations along the chord. A horseshoe vortex, a line source, and a forward-directed line doublet were placed at each location, giving a total of twenty-one elements for the case shown. Line doublets, which were not used in previous solutions of this type, have been included to improve the representation of flow closure.

4.2.6.4 REFERENCE CASE

To provide a well-controlled example, a reference case was generated using a theoretical, uniformly loaded model with the C_L and C_D values quoted above. The lift and drag loads were distributed uniformly, using the seven vortex and seven source elements shown in Figure 4.14. Line doublet strength was selected by subtracting the calculated vortex-plus-source signature from measured data and matching the residue.

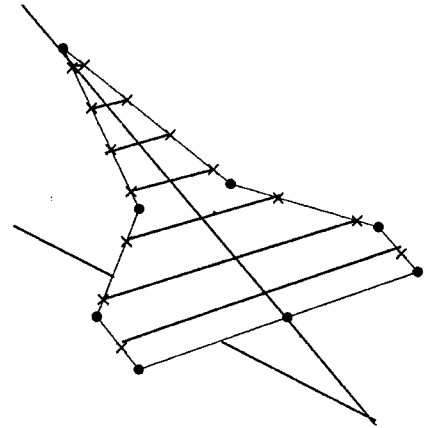
For the studies below, a reference wall signature was calculated using the reference singularity strengths just described. This becomes the column vector on the right-hand side. A corresponding reference interference curve was calculated at positions along the model centreline. As a first check, the solution singularity values are compared with the reference values. Exact agreement is desirable but not essential for good interference solutions. However, excessive oscillations in singularity strength lead to incorrect interference. The obvious second check is to ensure that interference distribution calculated using the returned singularities agrees with the reference interference curve.

4.2.6.5 THE SOLVER

A solver is used that employs a proprietary orthonormalisation scheme. Its major advantage is that it detects near linear dependence between columns and rejects the appropriate column. This process is controlled by a user-defined variable 'TOLC' (TOLerance for Columns). A zero value of TOLC leaves the original matrix intact. Least-squares solutions are obtained when the row and column counts differ.

4.2.6.6 WALL ORIFICE CONFIGURATIONS

The left-hand side of Figure 4.15 defines orifice configurations evaluated in the present study. Case 1, the baseline, has orifices on the centrelines of the roof, floor and left wall of the tunnel. The right wall data is redundant for the present unyawed cases. For Case 1, some twenty orifices per wall extend from about one tunnel diameter ahead of the model to one diameter behind it. Cases 2 and 3 explore the effects of shortening all signatures. Cases 4 and 5 investigate the effects of doubling the orifice spacing, while



TUNNEL :

$B = 23.25$ ft, $H = 16.25$ ft

Orifices from -18 to $+20$ ft, 2 ft spacing

Model TE 0.99 ft above tunnel centerline

Model nose 3.45 ft below tunnel roof

MODEL :

Double-delta planform

Span = 5.56 ft, Length = 6.38 ft

$\alpha = 35.34$ DEG $C_L = 1.17$, $C_D = 0.913$

Ref Area = 15.63 sq ft, S/C = 0.0414

7 Horseshoe vortices

7 Line sources

7 x-directed Line doublets

Figure 4.14 Model and tunnel details for baseline case

Case no.	Orifice Configuration	Matrix R x C		Sig RMS Error		Interfer. RMS Error	
		BASIC R x C	OPT R x C	BASIC x 10 ³	OPT x 10 ³	BASIC x 10 ³	OPT x 10 ³
1	Baseline: roof, left wall & floor, X = - 18.0 to + 20.0 ft by 2.0 ft	60 x 21	60 x 14	0.368	0.015	0.0082	0.0466
2	X = - 10.0 to + 10.0	33 x 21	33 x 14	2.792	0.012	4.7418	0.0497
3	X = - 4.0 to + 4.0	15 x 21	15 x 10	0.719	0.015	13.8500	0.0147
4	Baseline with odd points only	30 x 21	30 x 11	0.122	0.019	0.2773	0.0542
5	Baseline with even points only	30 x 21	30 x 12	2.134	0.015	4.6750	0.0465
6	All four walls	78 x 21	78 x 14	1.291	0.014	1.5135	0.0486
7	Roof and left wall	40 x 21	40 x 13	0.125	0.009	0.0960	0.0512
8	Roof only (C>R)	20 x 21	20 x 10	0.018	0.004	1.0690	0.1537

Fig 4.15 Effect of column optimisation for 7+7+7 initial elements and various wall orifice configurations.

retaining the baseline total length. The effect of adding back the right-hand wall is explored in Case 6. Cases 7 and 8 investigate roof-and-left wall and roof-only cases.

4.2.6.7 CASES WITH NO ELEMENT OPTIMISATION (TOLC = 0)

The "7 + 7 + 7" case reproduces the reference solution only for the baseline orifice configuration. Earlier studies, employing a similar "5 + 5 + 5" element arrangement closely followed the original input for all cases except the very short signature, Case 3. The singularity strengths in the 5 + 5 + 5 Case 3 oscillated strongly and the interference results were useless. This is probably attributable to the shortness of the signatures.

Repeating the same exercise for the 7+7+7 geometry gave noticeable RMS errors for the signature fit (Figure 4.15, column 5) and mainly oscillating singularity solutions. Case 1, the baseline, gave good interference results (Figure 4.16, upper plot) and Case 7 (roof and left wall) was probably acceptable. Of the remaining solutions, only Case 4 (doubled orifice spacing, "odd" points) was "on the page." However Case 5 ("even" points) displayed matrix instability and, like the remaining orifice configurations, gave interference values that were several times too high. Many of these curves oscillated and were obviously wrong, but those that were smooth could have been misleading had the reference curve not been available.

4.2.6.8 CASES WITH ELEMENT OPTIMISATION

On increasing the control parameter, TOLC, the column count for the baseline wall orifice configuration decreased monotonically from 21 to 12 over the range considered. The amount of column reduction depends upon the orifice configuration. As TOLC was increased, two minima occurred in the RMS error of

the fitted wall signature: experience has shown that the second gives superior results. The right half of Figure 4.15 summarises the RMS errors in the wall signature and interference curve fits. The column count at the optimum varies between ten and fourteen elements depending upon the orifice configuration. The optimised results show a very significant improvement in the signature fitting errors compared with the basic solution with the full 7 + 7 + 7 element count.

The lower plot of Figure 4.16 shows U-component interference curves at the model centreline for the optimised cases. The corresponding RMS errors are given in Figure 4.15. Most of the interference solutions are bunched at a level approximately 0.0002 higher than the reference curve. This represents acceptable accuracy and the fact that the curves are tightly grouped is probably the more important. Case 8, with only roof orifices, gave the only unsatisfactory solution. Case 3 was in close agreement with the reference curve but this is considered coincidental.

The fact that the unoptimised Case 8 gave a low RMS error for the signature fit yet a high interference RMS error requires comment. If the influence matrix is square and is solved successfully, the signature fit RMS error will be near-zero (by definition) whether or not the reference singularity values are returned. In fact, the singularity strengths may oscillate and produce an unacceptable interference result. This is what happened for the unoptimised Case 8, for which the influence matrix is nearly square. Obtaining a good signature fit does not guarantee good interference values, particularly if the matrix is near-square.

Figure 4.17 identifies the singularities retained for the various 7 + 7 + 7 solutions. Most of the vortex elements were usually retained and most of the doublet elements were usually rejected. The sources and doublets just ahead of the trailing edge were always retained, as were the sources near the apex of the delta. The consistent pattern of singularity locations in Figure 4.17 suggests that such a pattern might be used successfully without an optimiser for this configuration and angle of attack.

Increasing the column count first to 10 + 10 + 10 and then to 15 + 15 + 15 was beneficial. The eight cases were increasingly tightly grouped and the groups lay increasingly close to the reference curve. Evidently, with a larger choice of element locations afforded by the larger element counts, the optimiser can choose a better element arrangement.

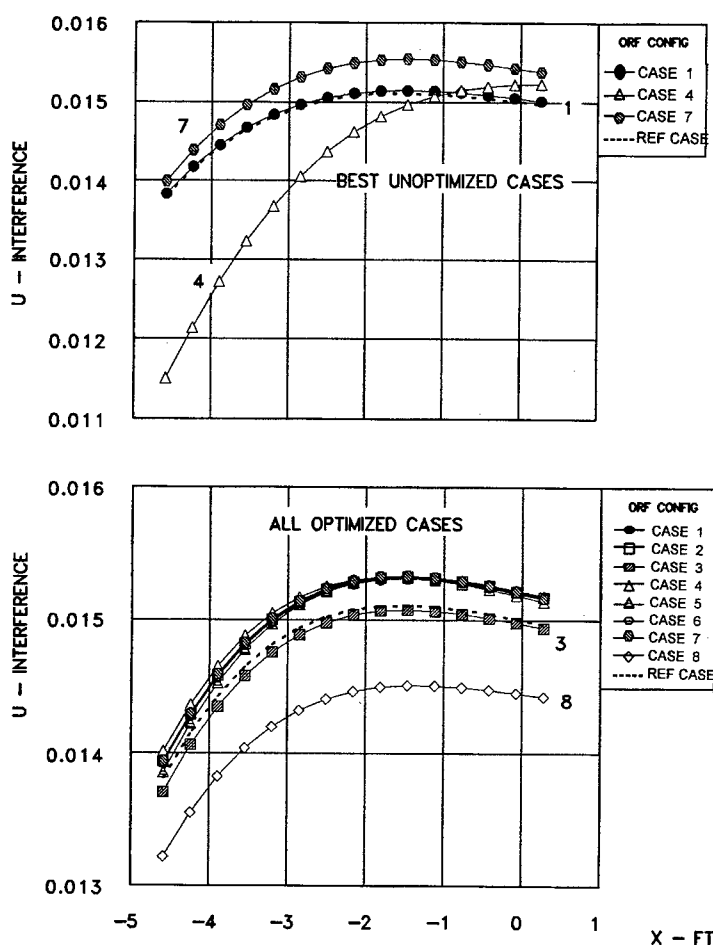


Figure 4.16 Interference for unoptimised and optimised cases (7 + 7 + 7 initial elements)

Wall config		1	2	3	4	5	6	7	8
Vortex elements	1	*	*	*	*	*	*	*	*
	2	*	*	*	*	*	*	*	*
	3	*	*	*	*	*	*	*	*
	4	*	*	*	*		*	*	*
	5	*	*			*	*	*	*
	6	*	*	*	*	*	*	*	*
	7	*	*	*	*	*	*	*	
Source elements	8	*	*	*	*	*	*	*	*
	9	*	*			*	*	*	*
	10				*				
	11	*	*			*	*	*	
	12	*	*				*		
	13								
	14	*	*	*	*	*	*	*	*
Doublet elements	15								
	16								
	17								
	18								
	19			*	*				
	20	*	*			*	*	*	
	21	*	*	*	*	*	*	*	*
TOTAL	21	14	14	10	11	12	14	13	10

* Filled squares denote retained matrix columns

Fig 4.17 Element disposition for optimised cases

4.2.6.9 REVIEW

It was shown above that there are two practical approaches to configuring the model elements. If "straight" solutions are to be used, with no column optimisation, then the element count must be kept low (5 + 5 + 5 in the case above) and the singularity solutions must be watched carefully for undue oscillation. In cases of doubt, the element count should be reduced. If an optimisation scheme is used the number of elements can be increased significantly (to 15 + 15 + 15, say). An increase is not essential when using an optimiser but, as was shown above, a better fit to the reference solution is obtained. Whichever strategy is adopted, it is important to ensure that the elements are placed appropriately to capture the model's loads. It is also beneficial to employ "over square" matrices with significantly more rows (orifices) than columns (model elements). This makes the RMS errors in fitting the wall signatures more meaningful.

The baseline case, above, is a good orifice arrangement for the model configuration employed here. Having a lift coefficient that is close to the maximum, it is one of the most important low speed cases and may also be among the most demanding. The first optimum for the 7 + 7 + 7 configuration (not shown) was helpful in identifying marginal wall configurations. Cases 2 and 3 showed that it is inadvisable to shorten the signatures below the Case 1 value. Cases 4 and 5 showed that orifice spacing should not be reduced. Omission of the orifices on the floor centreline (Case 7) gave surprisingly good results, which is helpful because of the vulnerability of instrumentation placed there, particularly in a large tunnel. The fact that Case 8, with roof-only data, was the weakest (Figure 4.16) comes as no surprise, since the program is being asked to distinguish between lift and blockage effects using a single signature.

4.2.6.10 Other Model Configurations

Various pressure orifice geometry's have been reviewed for an unyawed model at a single angle-of-attack and one height in the tunnel. The present study does not address the needs of other data points or other configurations. However, the baseline orifice configuration selected above is generally similar to a layout that has been used successfully in the Lockheed Low Speed Wind Tunnel for many years. In that tunnel, the wall orifices are above the centreline, to avoid windows, there are extra orifices opposite the model, and there are no floor orifices.

Despite the above, there will be occasions when more assurance is required. In such cases, a study similar to the one described in the main body of this section should be carried out. This would involve a simple theoretical model, placed at the appropriate position and attitude in the tunnel and carrying the correct loads. Wall signatures and reference interference curves should be calculated, as described above, and trial runs performed to find the best orifice and model element configurations. In facilities with an existing orifice system, its suitability can be assessed in a similar way and any additional orifices that are needed can be identified.

4.2.6.11 Three-way Interactions

Tunnel Interference is usually thought of in terms of the classical vortex, source and doublet theoretical representation of the model and its tunnel image system. Not a lot of attention has been paid, until recently, to the possibility that the model support system may also become involved in the interference process. Two examples of this surfaced during the tests upon which the above example is based. Both involved the sting support system and both represent ongoing work. The comments below should therefore be considered provisional.

In the first example, a study of model absent (sting present) and model-present pressure signatures suggested that the sting immediately aft of the model was experiencing model-induced download. Extra model elements were therefore added to those shown here to represent the forward part of the sting.

The second example involves a large floor-to-roof tower that supports the base of the sting and carries a carriage that moves vertically as the sting pitches. Being in the wake of the model, it was found that the loads on the tower, too, changed with the model present. Analyses based solely on model out datum corrections were inadequate, even though the tower was present for the datum measurements and the sting pitch setting was appropriate. In fact, the tower appeared to the flow as a vertical line source whose presence destabilised the pressure signature solutions. Adding a floor-to-roof line source, of unknown strength, improved the solutions. The lesson learned was that, if the model flow interferes with tunnel components and/or the model supports and the wall signatures are affected, then it is essential to represent those components in the influence matrix.

REFERENCES TO SECTION 4.2.

- [1] Acum, W. E. A., 1953, "Corrections for symmetrical and swept and tapered wings in rectangular wind tunnels", ARC R&M 2777.
- [2] Adcock, J. B., and Barnwell, R. W., 1984, "Effects of boundary layers on solid walls in three-dimensional wind tunnels", AIAA Journal Vol 22, No 3.

- [3] Ashill, P.R. and Keating, R.F.A., 1985, RAE unpublished report.
- [4] Ashill, P.R. and Keating, R.F.A., 1988, "Calculation of tunnel wall interference from wall-pressure measurements." *The Aeronautical Journal*, Vol. 92, No. 911, pp. 36-53.
- [5] Ashill, P. R., Taylor, C. R. And Simmons, M. J., 1995, "Blockage Interference at High Subsonic Speeds in a Solid-Wall Wind Tunnel.", *Proceedings of PICAST 2 - AAC 6*, Vol 1, pp 81-88, Melbourne 20 -23 March 1995.
- [6] Ashill, P.R. and Weeks, D.J., 1982, "A method for determining wall-interference corrections in solid-wall tunnels from measurements of static pressure at the walls." AGARD-CP-335, pp.1.1-1.12.
- [7] Berndt, S. B., 1952, „Approximate calculation of the influence of wall boundary layers on solid walls in three dimensional subsonic wind tunnels.“, FFA (Sweden) Report No. 45
- [8] Bouis, X., 1984, "ETW specification and its vindication." Document SC-ETW/D/27 (Revision 4).
- [9] Franklin, R. E, and Wallace, J. M., 1970, "Absolute measurements of static-hole error using flush transducers." *J. Fluid Mech.*, 42, 33.
- [10] Freestone, M. M., 1995, "Upwash interference for wings in solid-liner wind tunnels using subsonic linearised-theory." ESDU Data Item 95014.
- [11] Garner, H.C., Rogers, E.W.E., Acum, W.E.A. and Maskell, E.C., 1966, "Subsonic wind tunnel wall corrections.", AGARD-AG-109.
- [12] Glauert, H., 1942, "The elements of aerofoil and airscrew theory", Cambridge University Press, Fourth Impression.
- [13] Göthert, B., 1940 "Windkanalkorrekturen bei hohen Unterschallgeschwindigkeiten unter besonderer Berücksichtigung des geschlossenen Kreiskanals. Deutsche Luftfahrtforschung Forschungsbericht 1216 (translated as NACA Tech Memo 1300).
- [14] Hackett, J.E. and Wilsden, D.J., 1975, "Determination of low speed wake-blockage corrections via tunnel-wall static pressure measurements." AGARD-CP-174, pp. 22.1-22.9.
- [15] Hackett, J. E., and Boles, R. A., 1977, „Ground simulation and Wind tunnel blockage for a swept jet-flapped wing tested to very high lift coefficients.“ NASA CR 152,032 (also AIAA 74-641)
- [16] Hackett, J.E. and Wilsden, D.J., 1979, "Estimation of tunnel blockage from wall pressure signatures: a review and data correlation." NASA CR-152241.
- [17] Hackett, J.E., Wilsden, D.J., and Stevens, W.A., 1980, "A review of the wall pressure signature and other tunnel constraint correction methods for high angle-of-attack tests." AGARD-R-692.
- [18] Hackett, J. E., Sampath, S., and Philips, C. G., 1981, "Determination of wind tunnel constraint effects by a unified wall pressure signature method: Part I, Applicationa to winged configurations." NASA CR 166,186.
- [19] Isaacs, D., 1969, "Calibration of the RAE Bedford 8ft x 8ft wind tunnel at subsonic speeds, including a discussion of the correction to the measured pressure distribution to allow for the direct and blockage effects due to the calibration probe." ARC R&M 2777.
- [20] Jones, R. T. And Cohen, D., "High speed wing theory." Princeton Aeronautical Paperbacks (No. 6), Princeton University Press, 1960.

- [21] Lewis, M. C. And Goodyer, M. J., 1995, "Initial Results of an Experimental Investigation into the General Application of Transonic wind Tunnel Wall Corrections." Proceedings of PICAST2 - AAC 6, Vol 1, pp 71-79, Melbourne 20-23 March 1995.
- [22] Lewis, M.C., 1988, "Aerofoil testing in a self-streamlining flexible walled wind tunnel." NASA CR-4128.
- [23] Maarsingh, R.A., Labrujere, Th.E., and Smith, J., 1988, "Accuracy of various wall-correction methods for 3D subsonic wind-tunnel testing." AGARD-CP-429, pp.17.1-17.13.
- [24] Mokry, M. and Ohman, L. H., 1980, "Application of the Fast Fourier Transform to two-dimensional wind tunnel wall interference." Journal of Aircraft, Vol. 17, No. 6, pp 402-408
- [25] Mokry, M., 1989, "Residual interference and wind tunnel wall adaptation." USA AIAA-89-0147.
- [26] Pindzola, M. and Lo, C. F., 1969, "Boundary interference at subsonic speeds in wind tunnels with ventilated walls" AEDC-TR-69-47.
- [27] Pistolesi, E., 1933, Considerazioni sul problema del bi-plane, Aeronautica, Rome 13, 185
- [28] Rueger, M., Crites, R. And Weirich, R., 1995, "Comparison of conventional and emerging ("measured variable") wall correction techniques for tactical aircraft in subsonic wind tunnels (invited paper) AIAA 95-0108, 1995.
- [29] Shaw, R., 1960. "The influence of hole dimensions on static pressure measurements". J. Fluid Mech., 7 , 550.
- [30] Steinle, F. and Stanewsky. E., 1982, "Wind tunnel flow quality and data accuracy requirements", AGARD-AR-184.
- [31] Taylor, C. R., 1996, "A note on some fundamental concepts in the theory of wind-tunnel wall constraint and its application", DRA/AS/HWA/TR96055/1
- [32] Thom, A., 1943, "Blockage corrections in a closed high-speed tunnel." ARC R&M 2033.
- [33] Ulbrich, N., Lo C. F. and Steinle F. W., Jr., 1992, "Blockage correction in three-dimensional wind tunnel testing based on the wall signature method" AIAA 92-3925 .
- [34] Ulbrich, N. and Steinle, F.W., Jr., 1994 "Real-time wall interference calculation in three-dimensional subsonic wind tunnel testing", AIAA 94-0771.
- [35] Ulbrich, N. And Steinle, F. W., Jr., 1995 "Semi-span model wall interference prediction based on the wall signature method", AIAA 95-0793.

4.3 VENTILATED TEST SECTIONS

Contemporary developments in wall correction methods for ventilated wall test sections have shown an increasing reliance on measurements of wall boundary data. An excellent work recognising these new trends in two-dimensional testing has been produced by the Group for Aeronautical Research and Technology in Europe (GARTEur [26]).

Although it has been demonstrated both experimentally (Chen and Mears [12], Jacocks [33], Matyk and Kobayashi [45], and Crites and Rueger [15]) and computationally (Chan [11]) that the cross-flow properties of ventilated walls are non-linear (even strongly) and dependent on the wall boundary layer development, the correction techniques based on idealised, linear boundary conditions have retained a great deal of appeal. The main reason is that the parameters in the empirical boundary conditions (porosity or slot parameters) can usually be tuned so as to provide correlation of key aerodynamic quantities for two or more different-scale calibration models in the same facility (Firmin and Cook [20]). An approach less sensitive to wall Reynolds number effects (Aulehla [6]), is to adjust the boundary condition parameters in such a way that the corrected data agree with those measured on the same model in a very large facility, assumed to be interference free (Binion and Lo [8], Starr [72], and Sickles and Erickson [66]). The obtained values of these parameters may then be used to correct the wind tunnel data of other models which are similar to the calibration models in shape and size. Besides simplicity of application, the most appealing aspect of this (classical) approach is that it generates consistent, smooth corrections: if the measured dependence of C_L on α or C_D on C_L is smooth, so will be the corrected one. The corrections are predictive, which means that if we can estimate what the measured forces will be, we will also be in position to predict the corrections, in advance of a wind tunnel test, see Chapter 3.

A practical advantage of the classical methods is also that there is no need to measure quantities other than those directly related to the test model. However, if the static pressures at the test section walls happen to be measured and compared with those predicted using the idealised boundary conditions, substantial differences are likely to be uncovered. One of the possibilities to reduce this inconsistency in wall interference evaluation is to locally modify the wall boundary conditions in such a way that they provide the best possible agreement with the measured wall data (Mokry et al. [47], Jones, D.J. [34], Vaucheret [77], and Piat [58]). The values of the parameters in the boundary conditions will of course differ from test to test. Using this approach, the modified boundary conditions, regardless of their possible physical significance, provide no more than a fit of the measured boundary data. From here on it is only a small step to realise (Capelier et al. [10]) that the measured boundary data can directly be used as input. One is not limited to measuring data from the boundary. Pressure measurements on the model can be used similarly in conjunction with calibration of selected pressures for Mach and angle of attack effects and then employing closed wall and open wall settings. The closed wall settings in conjunction with a suitable means of estimating displacement thickness and any wall divergence effects then represent a boundary condition that is sufficiently known. Corrections to the closed wall case then form a reference to the open wall case. Variation of parameters in the boundary condition for the open wall case will permit finding the parameters that produce corrections which will best satisfy the corrected closed wall results in say, a least squares sense. These results can then be compared with those determined from matching measured wall data, or vice-versa for improved confidence.

In spite of the fact that much of the empiricism of the classical correction methods is eliminated by the boundary measurement methods, it is the latter ones that are under steady scrutiny. Their general acceptance is hindered by the fact that making the required flow measurement in ventilated test sections can be a very complex task and evaluation of corrections from a larger boundary input requires a small-

scale numerical code rather than a simple formula or chart. In addition, the corrections can only be used in the "post-test assessment" mode. It is no longer possible to predict the corrections by specifying the aerodynamic forces: a wind tunnel experiment with actual wall pressure measurements needs to be performed first; and only then the corrections can be evaluated. Also, a larger experimental data input produces corrections which are "scattered" in comparison with the classical ones (Labrujère et al. [40]). This is not to say that global corrections to tunnel reference conditions can't be determined in advance. Any prior post-test corrections are candidates for developing a library of corrections with a suitable empirical analysis. In many cases, global corrections are sufficient (e.g., Goldhammer and Steinle [28])

4.3.1 ONE-VARIABLE METHOD

The method proposed by Capelier et al. [10], and in a simpler form also by Blackwell [9], is the most popular technique for the post-test assessment of subsonic wall interference from boundary pressure measurements in wind tunnels with ventilated walls. It is assumed that the velocity disturbance potential near the walls is governed by the linear Prandtl-Glauert equation,

$$\beta^2 \frac{\partial^2 \phi}{\partial x^2} + \frac{\partial^2 \phi}{\partial y^2} + \frac{\partial^2 \phi}{\partial z^2} = 0 \quad (4.3.1)$$

and that it may be split into the free air and wall interference parts,

$$\phi = \phi_F + \phi_I. \quad (4.3.2)$$

The only difference from the classical wall interference approach is in replacing the idealised wall boundary condition by the "measured" one, namely by

$$\frac{\partial \phi}{\partial x} = u \quad (4.3.3)$$

where

$$u = \frac{U - U_\infty}{U_\infty}$$

is the measured streamwise component of perturbation velocity.

Unlike flow near the model, where stagnation and locally supersonic regions may exist, flow near the walls is significantly less perturbed so that linearisation may apply up to quite high subsonic Mach numbers. If the model is small relative to the test section and sufficiently remote from the walls, it is only when free stream Mach number is close to unity that portions of the walls become near critical or supercritical, making the assumptions of Eqs.(4.3.1)-(4.3.2) invalid.

The way Eq.(4.3.2) is usually interpreted is that ϕ_F is a disturbance velocity potential that would be generated by the model if loaded by the same aerodynamic forces in free air, and ϕ_I is the wall interference potential induced by the walls. In other words, ϕ_I is an increment to ϕ_F that makes the total satisfy the (measured) wall boundary conditions.

Provided that ϕ_F satisfies Eq.(4.3.1) near the walls, it can be represented there (and in the infinite exterior region) by internal singularities. In contrast, ϕ_I can be represented by external singularities (images). An equally justifiable assumption is that ϕ_I be non-singular, but discontinuous across the

interface between the interior and exterior flow. This latter approach is used when evaluating ϕ_I by a panel method. Regardless of the representation of the exterior fictitious flow, the key premise of subsonic wall interference theory is that ϕ_I is non-singular in the interior (including the volume occupied by the model), allowing to evaluate the velocity corrections to (uniform) wind tunnel stream as the components of $\text{grad}\phi_I$. Although an application of this concept is almost axiomatic in both the classical and the boundary measurement methods, one should remember that it is merely an engineering approximation, even for low-speed (incompressible) flows.

The assumptions upon which the one-variable method is based are thus the following: the axial component of wall interference velocity

$$u_I = \frac{\partial\phi_I}{\partial x} \quad (4.3.4)$$

satisfies the differentiated Eq.(4.3.1), that is

$$\beta^2 \frac{\partial^2 u_I}{\partial x^2} + \frac{\partial^2 u_I}{\partial y^2} + \frac{\partial^2 u_I}{\partial z^2} = 0 \quad (4.3.5)$$

in the entire test section interior (including the volume occupied by the model).

Using Eq.(4.3.2), the boundary values of u_I are evaluated on the measurement surface as

$$u_I = u - u_F \quad (4.3.6)$$

Here u_F is the axial component of disturbance velocity that would be induced at the location of the measurement surface by the same model in free air, at the same stream velocity, U_∞ , and the same aerodynamic forces. Provided that the measurement surface is sufficiently remote from the model, we only need to know the far-field approximation of u_F .

Equations (4.3.5) and (4.3.6) specify an interior Dirichlet problem and there are a large number of methods available to solve it analytically or numerically. For simpler geometry's, closed-form solutions are obtainable using integral transforms (Capelier et al. [10]) or the Fourier method (Mokry and Ohman [49], Mokry [50], and Rizk and Smithmeyer [61]). A detailed description and coding of two of these techniques in Fortran are given by Gopinath [29].

The Dirichlet problem for Laplace's equation, to which Eq.(4.3.5) is reducible (by a co-ordinate transformation) is known to have a unique solution inside a region, provided that the boundary values are specified everywhere on its bounding surface. This guarantees that there is only one solution to u_I for the given prescribed values of u_I on the boundary. As we shall see below, the same cannot be said of the interference velocity components v_I and w_I , evaluated from the same boundary values of u_I .

A natural approach (e.g. Stakgold [71]) to solving the Dirichlet problem for Laplace's equation is to represent u_I by the double layer potential :

$$u_I = \frac{1}{4\pi} \int_S f \frac{\partial}{\partial n} \left(\frac{1}{r} \right) dS, \quad (4.3.7)$$

where f is the doublet density and r is the distance between the fixed observation point x_0, y_0, z_0 (where u_I is being evaluated) and point x, y, z , which runs over the surface S in the course of integration. The derivative $\partial/\partial n$ is taken in the direction of the inward normal, that is pointing into the test section interior.

If the observation point is on surface S , the integrand becomes singular, because r appearing in the denominator will be zero when the running point reaches the observation point. Nevertheless integral (4.3.7) exists; but, because of its singular nature, its value depends on which side of the integration surface the observation point lies. In other words, u_j is discontinuous across S . Taking the limit as the observation point becomes a point on the inner (flowfield) side of surface S , we obtain

$$u_j = \frac{f}{2} + \frac{1}{4\pi} \int_S f \frac{\partial}{\partial n} \left(\frac{1}{r} \right) dS, \quad (4.3.8)$$

where a small circular neighbourhood of the observation point (where $r = 0$) is considered removed from the surface integration; its contribution has already been accounted for by the isolated term $f/2$.

With respect to the unknown density f , Eq.(4.3.8) can be interpreted as a Fredholm integral equation of the second kind. The solution can be obtained numerically by dividing S into panels of (piecewise) constant density f , applying Eq.(4.3.8) at panel centroids and solving the resulting system of linear algebraic equations (Mokry et al. [52]). If the walls are straight, the matrix is easily assembled using the contribution of a rectangular panel of unit doublet density, elaborated in the Appendix. The isolated term $f/2$ in Eq.(4.3.8) provides the diagonal element, or contribution of the panel to its own centroid.

The major source of inaccuracy, which is common to all wall interference methods based on boundary measurements, is incompleteness or sparseness of the experimental pressure data. The boundary values of u_j have to be interpolated or extrapolated over a complete boundary (finite or infinite), in order to make the Dirichlet problem fully defined. More specifically, the panel method will require the knowledge of u_j at all panel centroids, as shown schematically in Figure 4.18. The crosses indicate the measurement points and the solid and open circles are the panel centroids on measurement and non-measurement surfaces respectively. A variant of the panel method which does not require extensive pressure measurements or interpolation has been reported by Ulbrich and Steinle [75], [76] for full-span and half-span models with an image plate. The method employs precalculated influence coefficients for both wall panels and singularities used to represent the model at a few control points on the tunnel boundary. Known strengths of singularities from measured force and moment data and assumed distribution of loading are taken into account in determining the strength of the remaining singularities (equivalent to two unknowns) by satisfying the measured pressures in a least squares sense. The method is designed to compute global blockage and angle-of-attack corrections in near real-time. In effect, it combines the features of a direct method and a one-variable method. The application reported is for a solid wall tunnel. However, the influence method is more general and can be applied to either a porous or a slotted wall, providing that a reliable measurement of pressure at the boundary is obtained.

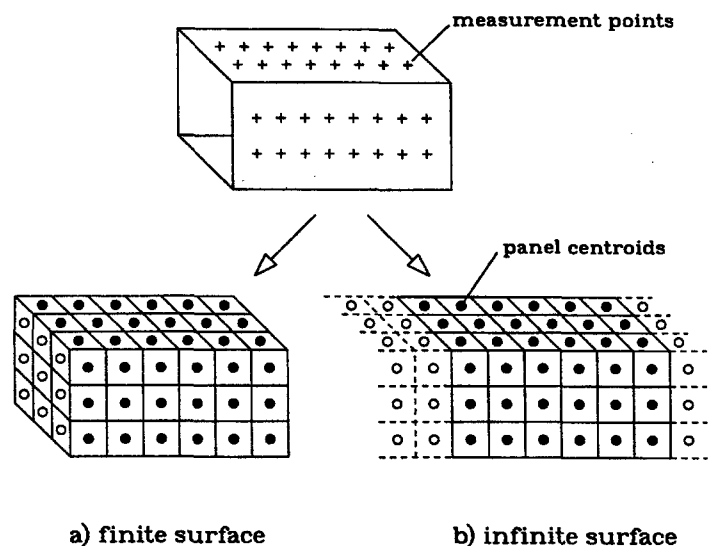


Figure 4.18 Illustrating measurement and input of boundary data

The simplest way to tell how well a proposed interpolation scheme works is to test it on a theoretical example: generate u_f by external singularities or images (Holst [32]) and check how faithfully the method reproduces u_f inside the test section from the known boundary values at the measurement points.

By nature of the solutions to elliptic equations, such as Laplace's or Prandtl-Glauert's, the evaluation of subsonic wall interference corrections from the boundary data is a smoothing operation. Unless the corrections are required to be known in the vicinity of the walls, pre-smoothing of the boundary data is unnecessary. Elimination of grossly erroneous boundary input points is an entirely different matter: although an individual disturbance will smooth out and will not likely be detectable as a localised perturbation at the model, it will influence the overall level of calculated wall interference. Another characteristic of linear subsonic wall interference, following from the so-called "max-min" property, is that the corrections at the tested model can neither be greater nor smaller than their respective maxima or minima attained at the walls

Compensation for errors of the reference velocity or pressure is another important feature of the method. An uninitiated experimenter may find it quite amazing that if we change the reference pressure on which the stream Mach number M is based slightly, then recalculate the wall C_p 's and evaluate a new ΔM , the same corrected Mach number, $M + \Delta M$, is found. Actually, the principle is nearly self-evident: if the error of the (upstream) reference velocity U_∞ is δU_∞ , then the boundary perturbation velocities $U - (U_\infty + \delta U_\infty)$ will be offset by $-\delta U_\infty$ from their true value $U - U_\infty$. However, since $-\delta U_\infty = \text{constant}$ is also a solution of Eq.(4.3.5), the incremental correction, being of equal magnitude but opposite sign to the reference velocity error, restores U_∞ as the true reference velocity. Naturally, the relationship between pressure and velocity requires linearisation, so that the principle is restricted to small errors (Paquet [56]). The principle may also be compromised if extrapolation of U towards the "false" upstream reference $U_\infty + \delta U_\infty$ is used (GARTEur [26]).

Similarly, in ventilated test sections the autocorrection principle establishes the correspondence between the velocity based on plenum pressure, $U_\infty + \delta U_\infty$, and the actual stream velocity U_∞ . In this context each wind tunnel test with wall pressure measurements in effect is also a calibration test. Empty wind tunnel calibration, as used in the classical wall interference approach, is a poor substitute since the model influences not only the wall pressure, but also the plenum pressure (Smith [67], Aulehla [6], and Everhart and Bobbitt [18]).

A related question often asked is: if small errors of the reference Mach number don't matter is it also true that small errors of C_L and C_D don't? Unfortunately they do. Accuracy of the one-variable method is greatly dependent on accuracy with which the free air potential ϕ_F can be predicted along the boundary surfaces (GARTEur [26], Chevallier [13]). At low subsonic flow conditions, the far-field can be generated fairly well by internal singularities, determined from the model geometry and measured loading (Binion and Lo [8], Rizk and Smithmeyer [61], Vaucheret [77] and Mokry [51]). This approach becomes less reliable at high incidence cases, where the extent of separated flow regions is generally unknown. Model representation by subsonic-flow singularities needs also to be modified near critical flow conditions, see Cole and Cook [14], Kemp [37] and Al-Saadi [2]. However, when the supersonic flow regions become extensive, perhaps even reaching the wind tunnel walls, the superposition principle, on which Eq.(4.3.6) is based, will no longer apply. The linear correction method may even then go on producing numbers; nevertheless, alternative wall correction methods which respect the true, non-linear nature of transonic flow should be applied (see Chapter 5.)

In the one-variable method the transverse velocity components

$$v_I = \frac{\partial \phi_I}{\partial y} \quad \text{and}$$

$$w_I = \frac{\partial \phi_I}{\partial z} \quad (4.3.9)$$

are obtained from u_I by integrating the irrotational-flow conditions

$$\frac{\partial v_I}{\partial x} = \frac{\partial u_I}{\partial y} \quad \text{and}$$

$$\frac{\partial w_I}{\partial x} = \frac{\partial u_I}{\partial z} \quad (4.3.10)$$

The flow angle corrections are thus determined up to (unknown) integration constants. This is somewhat disappointing; however, the variations of wall induced angularity over the model can still be evaluated and a case made whether the wind tunnel test is correctable or not (Steinle and Stanewsky [73]).

In Figure 4.19 an example of corrections evaluated by the one-variable method is given for the Canadair Challenger half-model tested in the IAR Blowdown Wind Tunnel. The boundary pressures were measured by 6 static pressure tubes (2 on top, 2 on bottom and 2 on the sidewall) and the division of the test section boundary box in the x, y, z directions was $11 \times 5 \times 5$, giving a total of 215 panels. The ΔM and $\Delta \alpha$ correction contours were plotted in the horizontal plane (wing planform). There is no ambiguity in the interpretation of the ΔM correction but, as we have indicated above, the absolute level of the $\Delta \alpha$ correction is not known with certainty.

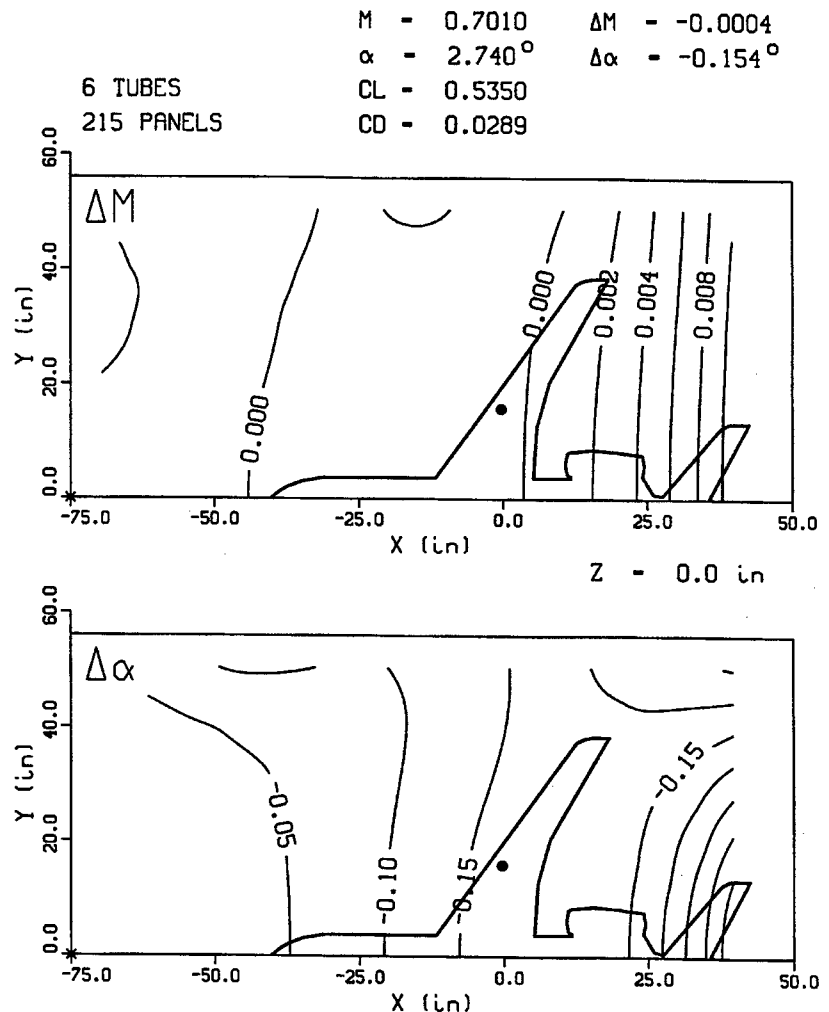


Figure 4.19 Wall corrections for a Canadair Challenger half model test in the IAR Blowdown Wind Tunnel, produced by the one-variable method

Values to the unknown angular constants can be assigned (as has been done in Figure 4.19) by assuming that flow enters the test section parallel to its axis. This is accomplished by imposing the conditions

$$v_I + v_F = 0 \quad \text{and} \quad w_I + w_F = 0 \quad (4.3.11)$$

at an upstream axial point. If we instead imposed a condition that v_I and w_I vanish there, we would in effect assume that far upstream flow angles are the same as they would be in free air. Simple theoretical analyses contradict the latter assumption by showing that under the confinement of a constant cross-section channel the flow angles upstream of the model decay much faster with the distance from the model than they would in free air.

We can illustrate this on a simple example, which is of some relevance to testing of high-aspect ratio wings. Consider a two-dimensional vortex placed midway between two walls, as shown in Figure 4.20.

The free-air potential of the vortex is

$$\phi_F = \frac{-\gamma}{2\pi} \arctan \frac{z}{x}$$

compare Eq. (2.12). The vortex induces along the x -axis the normal velocity

$$v_F = \frac{\partial \phi_F}{\partial z} = \frac{-\gamma}{2\pi x} = \frac{-\gamma}{2h \left(\frac{\pi x}{h} \right)}$$

The normal velocity along the axis of a closed-wall wind tunnel, as obtained by the method of images (Theodorsen, 1931), is

$$v = v_F + v_I = \frac{-\gamma}{2h \sinh \left(\frac{\pi x}{h} \right)}$$

Evidently, the test section height h plays a key role here: if $h \rightarrow \infty$, then $v \rightarrow v_F$. However, if h is finite, then according to the l'Hospital rule

$$\lim_{x \rightarrow -\infty} \frac{v}{v_F} = 0,$$

which says that with increasing the upstream distance, v tends to zero much faster than v_F . This is also well apparent in Figure 4.20a, where both velocities are plotted as functions of axial distance.

The question what happens if a portion of the wall is ventilated is more difficult to answer since, as we have pointed out before, the ventilated wall boundary conditions are generally unknown. It seems that the principle still holds, at least for "passive" wind tunnel walls where no

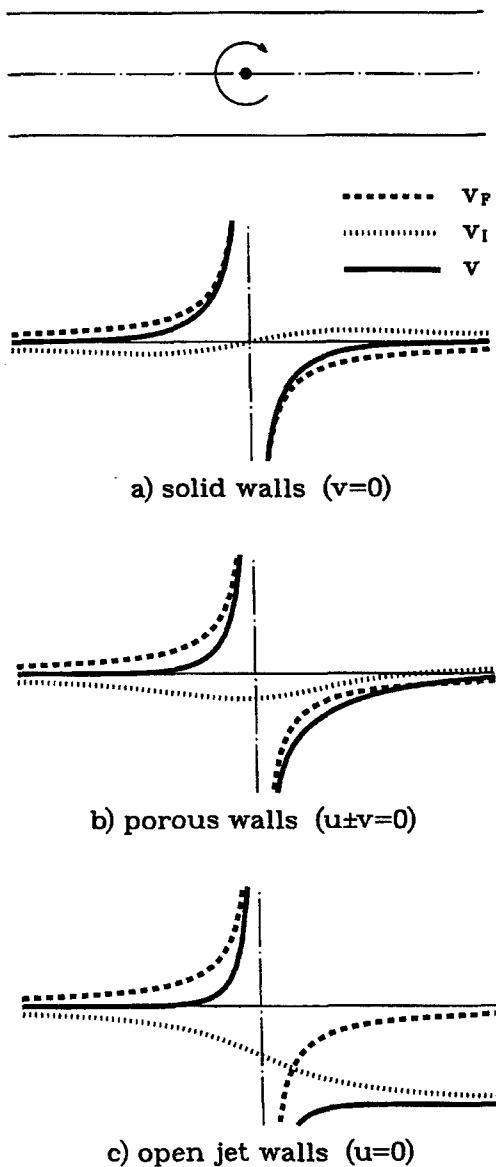


Figure 4.20 Upwash velocity along the axis of a test section induced by a point vortex

forced blowing or sucking is employed. In Figure 4.20b the same v_F as before is compared with v calculated using an assumption that $v = -u$ on the upper wall and $v = u$ on the lower wall. This relationship is a special case of the ideal porous-wall boundary condition $v \pm Pu = 0$ with porosity (permeability) parameter $P = 1$. The formula which was used to generate the axial values of v was again obtained using the method of images (Ebihara [17]). We see that porosity $P > 0$ makes convergence upstream of the vortex more rapid and downstream slow. If $P \rightarrow \infty$, corresponding to approaching the open jet condition $u = 0$, the convergence of v upstream of the vortex improves further, but downstream of the vortex the flow becomes permanently deflected, see Figure 4.20c. Based on these and similar observations, the upstream conditions described by Eqs.(4.3.11) appear to be quite acceptable. It is of course realised that these conditions may lead to serious errors if imposed too close to the model (Akai and Piomelli, 1984). A more rigorous approach (at least on paper) is to actually measure the flow angles at some point, preferably non-intrusively.

As a point of interest, we may also mention that the complex-variable treatment of the 2D problem leads to the Schwarz problem (Smith [69]), consisting of determining an analytic function inside a domain from its defined real part on the boundary. Theory (e.g. Gakhov [24]) shows that the integration of the Cauchy-Riemann equations introduces an unknown imaginary constant that needs to be specified in order to make the solution unique. Translated into the language of aerodynamics: the flow angle constant is again unknown.

Last but not least in order of importance are the methods of measuring the perturbation u -velocity along the test section boundary. Since the wall correction method is based on potential-flow theory, the measurement should not be made on the wall itself, but at a distance where the effect of the wall boundary layer on static pressure is negligible. The simplest way to obtain u is by measuring static pressure on a plate (rail) instrumented with pressure orifices, as illustrated in Figure 4.21a. The plate is mounted on the wall in the direction parallel to mainstream. For isentropic flow in the x, z -plane it follows

$$C_p = \frac{2}{\gamma M_\infty^2} \left\{ \left[1 - \frac{\gamma-1}{2} M_\infty^2 \left(\frac{U^2 + W^2}{U_\infty^2} \right) \right]^{\frac{\gamma}{\gamma-1}} - 1 \right\} = -2u - u^2 - w^2 + \dots$$

where C_p is the measured pressure coefficient and $u = (U - U_\infty)/U_\infty$ and $w = W/U_\infty$ are the components of the disturbance velocity in the x and z directions. the first-order approximation, valid throughout the whole subsonic-supersonic regime, is :

$$u = -\frac{1}{2} C_p \quad (4.3.12)$$

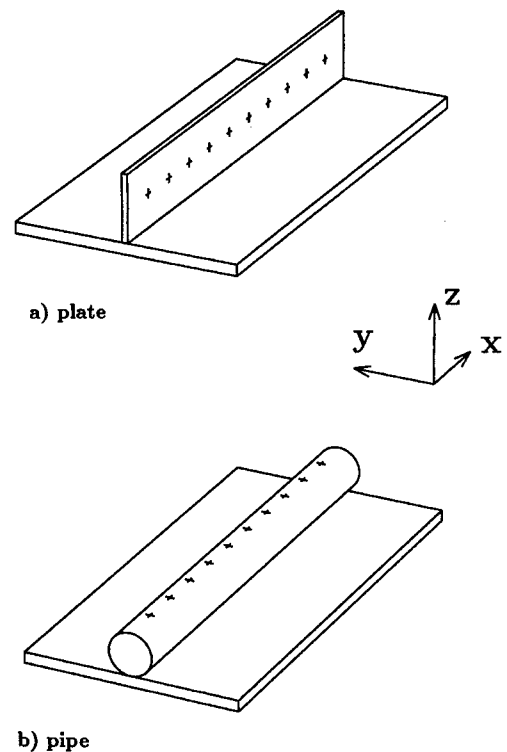


Figure 4.21 Schematic of devices with a single row of pressure orifices

If there is a lateral component of velocity (in the y -direction), the plate interacts with the flow and the measured pressure may no longer represent the local stream static pressure. For three-dimensional flows, a more suitable device is a pipe with a row of pressure orifices facing the test section interior, Figure 4.21b. The pipe also interacts with the ambient flow, but in a more predictable manner. Using slender body theory, Nenni et al. (1982) derived for a pressure coefficient on a circular cross-section pipe

$$C_p = -2u - \beta^2 u^2 + 2d \left(\frac{\partial v}{\partial x} \cos \omega + \frac{\partial w}{\partial x} \sin \omega \right) - 4(v \sin \omega - w \cos \omega)^2 \quad (4.3.13)$$

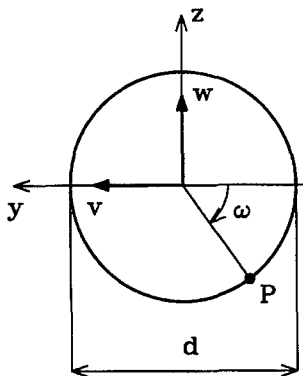


Figure 4.22 : Cross-flow plane of a circular pipe

where u, v, w are the components of disturbance velocity, d is the pipe diameter, and ω is the azimuthal angle of the pressure orifice P , as defined in Figure 4.22. For the orifices shown in Figure 4.21b the corresponding azimuthal angle is $\omega = 3\pi/2$. However, regardless of the azimuthal location of the pressure orifices, the transverse components of velocity v and w need to be known, in order to retrieve u from Eq.(4.3.13). This may be possible if the wall interference evaluation is arranged in an iterative fashion. The contributions of v and w and their derivatives can of course be eliminated by using several rows of pressure orifices (Nenni et al. [53]). A more serious objection to using Eq.(4.3.13) is that it has been derived for inviscid flow and would not apply should the pipe be immersed, partly or totally, in the wall boundary layer. In contrast,

the linear approximation, as described by Eq.(4.3.12), may hold even then. Assuming that C_p is constant across the boundary layer in the direction normal to the wall, then the evaluated u represents the perturbation velocity on the outer edge of the boundary layer. Provided that the boundary displacement is small compared to the dimensions of the test section, the displacement may be neglected in routine wall interference computations.

A practical implementation of these static pressure devices is illustrated in Figure 4.23. The "rail" was the initial design used in early two-dimensional measurements in the High Speed Wind Tunnel in Ottawa (Peake et al. [57]). The impetus for its development came from an idea to supply the CFD method by Magnus and Yoshihara [44] by a pressure boundary condition, in an attempt to simulate computationally flow past an airfoil under the constraint of wind tunnel walls. Similar rails were subsequently built in a number of other facilities (Blackwell [9], Sawada [63], and Smith [68]) and used even for half-model (Pounds and Walker [59] and Hinson and Burdges [31], Goldhammer and Steinle [28]) and

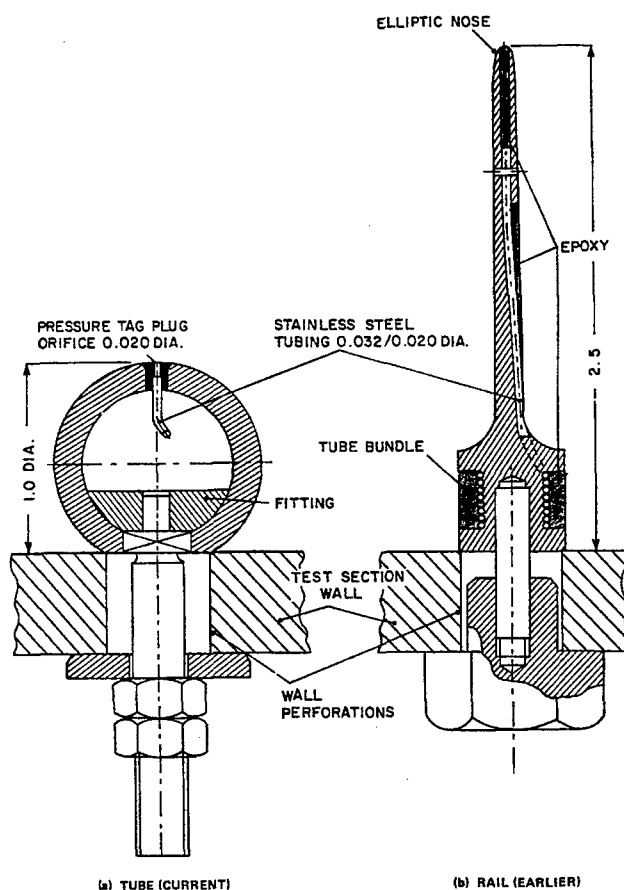


Figure 4.23 IAR Static pressure devices

full-model testing (Mokry and Galway [48]). Later, the rails were superseded by pipes (tubes), as they were easier to manufacture and also more suitable for three-dimensional testing. As discussed by Galway [25], the number and location of these pressure pipes depend upon the test section and model configuration, so that adequate definition of the pressure at the boundary surface through interpolation and extrapolation is possible. In the examples shown in Figure 4.24, a slightly irregular placement of the pipes was enforced by wall structural supports on the plenum side of the test section.

For slotted walls, where the mean-flow boundary conditions are established at greater distances from the walls, installation of pressure tubes or rails becomes less practical, although still feasible (Smith [69]). The inviscid slot flow analyses suggest that the pressure orifices need to be located at least one slot spacing distance from the wall, in order not to be adversely affected by the rapidly varying flow in the slot (Smith [69], Kemp [36] and Steinle [73]). This hypothesis was verified experimentally by Everhart and Bobbitt [18]. For longitudinally slotted walls it is often more convenient to measure the boundary pressures using orifices installed directly in the slats, usually along or close to their centerlines (Sewall [64]). In determining the

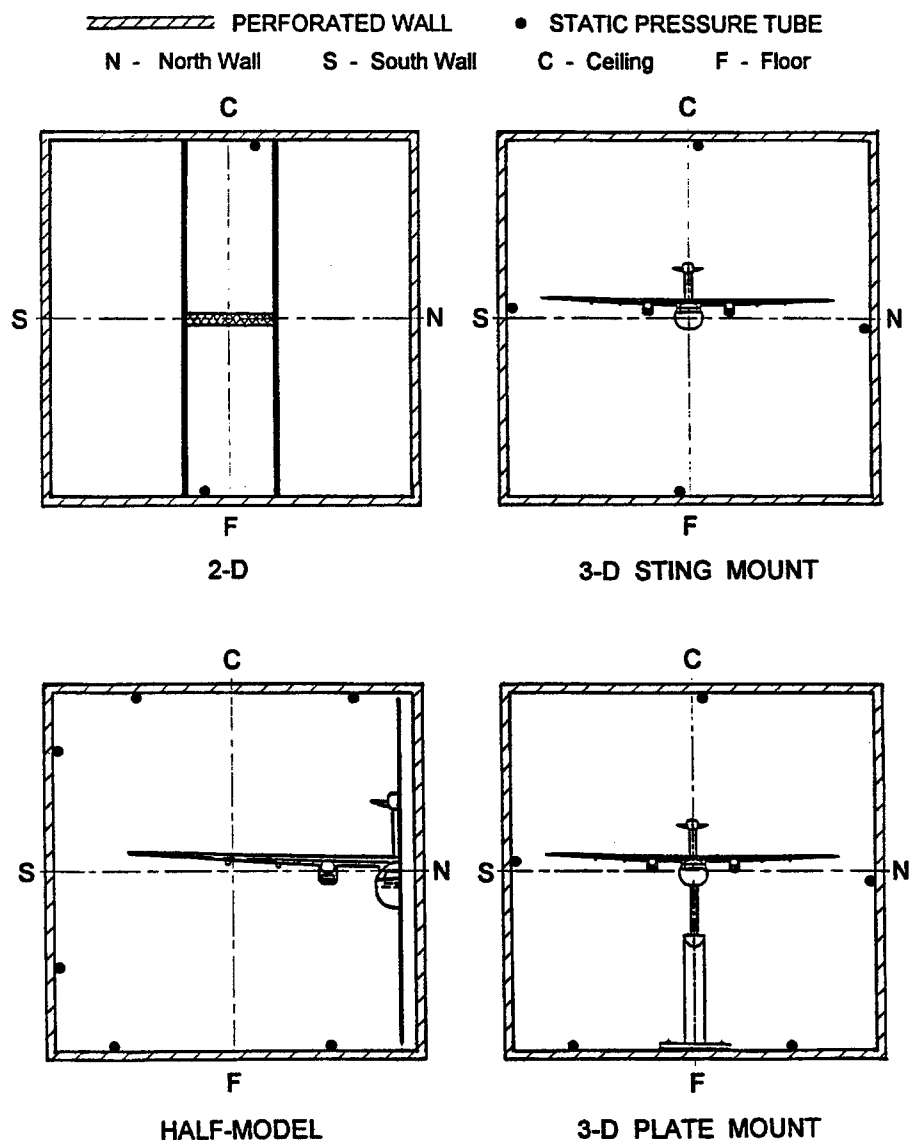


Figure 4.24 Location of static pressure tubes (pipes) for different modes of testing

streamwise component of perturbation velocity, u , it is necessary, in principle, to apply a correction to the value obtained from Eq.(4.3.12) when slat pressure coefficient is used as input. Based on the inviscid slot flow analysis by Berndt [7], Freestone et al. [22] deduced that for typical slotted wall geometry's the error of the mean value of u would not exceed 0.004 (0.4% of freestream velocity). This error estimate is consistent with earlier findings of Smith [69] and Firmin and Cook [20], implying that the pressure measurement made over the centre of the slat may be used as a reasonable approximate to the local mean static pressure at subsonic speeds. Unfortunately, there is also contradicting experimental evidence (GARTEur [26], and Everhart and Bobbitt [18]) that, depending on slot geometry and orifice locations, the differences between the slat pressures and mean static pressures can be more substantial. The conclusion to be drawn from this discussion is that, unless supported by supplementary flow measurements, pressure measured on the slats should not be presumed equal to the mean static pressure at the wall. A positive aspect of slat pressure measurement is that it is non-intrusive, in contrast to that provided by a static pressure pipe. Unfortunately, the effects of viscosity and vorticity in the immediate vicinity of the slotted wall generate very complex cross-flow patterns (Wu et al. [79]) that make a rigorous interpretation of the measured pressure data difficult.

Concerning the perforated walls, the measurement of pressure by orifices installed directly in the walls is even more problematic. For closely-spaced perforation holes the measured pressure suffers from a great deal of scatter even when the pressure orifices are positioned exactly at the same locations with respect to the surrounding perforation holes (Ohman and Brown [54]). This poses a problem especially for three-dimensional testing, where the pressure disturbances generated by the model are generally weak and hidden in the scatter generated by the holes. Since the scatter is spatially fixed, a partial remedy is in calculating the wall interference correction as an incremental one, using the differences of boundary pressures measured with model in and model out. Another possibility is to plug the perforation holes surrounding the pressure orifice, but this of course changes the local permeability of the wall. A variant of the perforated wall which avoids this problem is a porous-slotted wall comprised of a sufficient number of lines of porosity as to behave closely as a uniform porous wall such as the NASA Ames 11-by 11-Foot Transonic Tunnel. In this case, static pressure measurements can be made without affecting local porosity.

4.3.2 TWO-VARIABLE METHOD

The first successful evaluation of the 2-D interference flow field from two flow variables measured at the control surface was reported by Lo [42]. Both numerical demonstration and experimental verification are given in the same paper. The method uses the Fourier transform solution (Lo and Kraft [43]) for linearised subsonic flow past a nonlifting airfoil. A more straightforward Cauchy's integral approach to the two-variable method was subsequently described by Kraft and Dahm [38], Smith [69], and Amecke [3]. The general formulation of the method for 3-D flows, based on Green's identity, is due to Ashill and Weeks [4]; for more discussion see also Ashill and Keating [5]. A Fourier transform solution for the blockage interference, obtained as a function of two velocity components measured at a circular-cylinder surface, has recently been given by Qian and Lo [60].

The two-variable method for the ventilated-wall test sections is essentially the same as for the closed-wall test section described in Chapter 4.1.4 and 4.2.5.2. The only difference lies in the fact that the normal velocity at the solid wall is known, whereas for the ventilated walls it needs to be measured.

The wall interference potential obtained from Eq.(4.14) is

$$\phi_I = -\frac{1}{4\pi} \int_S \left[\frac{\partial\phi}{\partial n} \frac{1}{r} - \phi \frac{\partial}{\partial n} \left(\frac{1}{r} \right) \right] dS \quad (4.3.14)$$

where ϕ_I is to be evaluated at an interior point $P(x_0, y_0, z_0)$ and r is a distance between this point and point $Q(x, y, z)$ that identifies the location of the surface element dS . The "observation" point P is held fixed, whereas Q is a "running" or "dummy" point in the integration's on the right-hand side of Eq.(4.3.14). As in Chapter 4.1, the normal derivatives are taken inward towards the working section. Physically, Eq.(4.3.14) can be interpreted as a surface distribution of sources of density $\partial\phi/\partial n$ and a surface distribution of doublets of density $(-\phi)$.

The two-dimensional analogue of Eq.(4.3.14) is (Labrujère et al., 1986)

$$\phi_I = -\frac{1}{2\pi} \int_C \left[\frac{\partial\phi}{\partial n} \ln\left(\frac{1}{r}\right) - \phi \frac{\partial}{\partial n} \ln\left(\frac{1}{r}\right) \right] ds \quad (4.3.15)$$

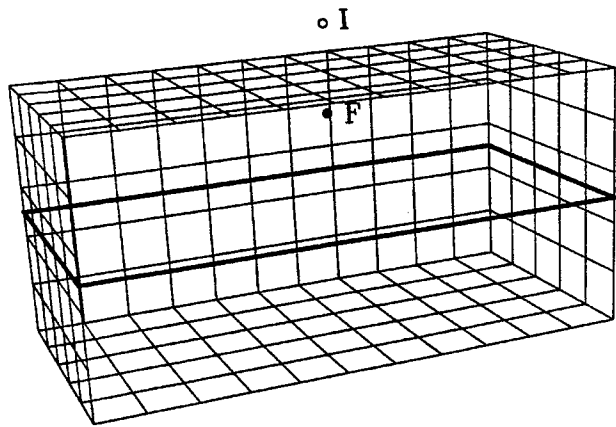
where ds is the element of arc length of the boundary contour C . In two dimensions, ϕ can be differentiated in the direction tangent to the contour, so that the specification of ϕ is equivalent to specifying the tangential component of disturbance velocity, $\partial\phi/\partial s$. An alternative Cauchy-integral formulation of the two-variable method (Smith [69]) uses the complex disturbance velocity $u - iv$.

The number of velocity components needed to be measured in order to implement the two-variable method in three dimensions is again as the name of the method suggests: two. From ϕ defined on the bounding surface two components of tangential velocity can be derived; yet, if one of them is measured, the other is determined by integrating the irrotational-flow conditions. The second velocity component that needs to be measured is the normal one, $\partial\phi/\partial n$.

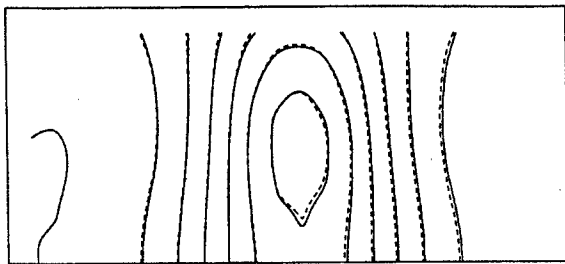
As discussed in Chapter 4.2, the two-variable method is most easily applied to solid wall test sections, where the normal velocity component, $\partial\phi/\partial n$, can be determined from the local slope of the boundary-layer displaced wall surface. If the test section walls are straight and the boundary layer growth is neglected, $\partial\phi/\partial n = 0$. In that case the source distribution drops out of Eq.(4.3.14) and the implementation of the method is particularly simple.

Before discussing the techniques for measuring $\partial\phi/\partial n$ in ventilated-wall wind tunnels, we shall set up a simple numerical model to illustrate how the method is supposed to work when both ϕ and $\partial\phi/\partial n$ participate. Integral (4.3.14) and its derivatives will be approximated as sums of contributions of constant-density panels, into which the boundary surface S is divided. The closed-form solutions for the contributions of a rectangular, unit-density source or doublet panel are given in the Appendix. What remains to be done is to change the co-ordinates from the local (panel) co-ordinate system to the global (test section) co-ordinate system, multiply the contributions by the local source and doublet densities, and then sum up all panel contributions. There is no system of equations as such to be solved in the two-variable method.

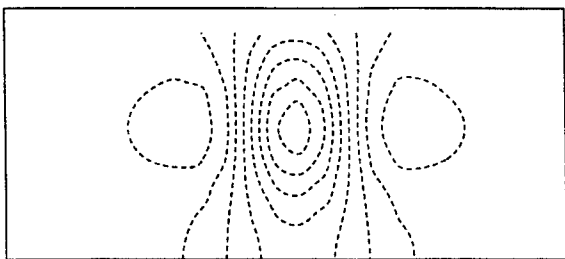
In the example shown in Figure 4.25a the test section is a simple right-angled box. The panels cover the top, bottom and side walls, and also the upstream and downstream faces. The plane $y = 0$ is assumed to be a plane of symmetry (a solid reflection plate in the half-model test arrangement). The division of



a) Paneling of the test section;
singular points and observation plane



b) u-velocities induced by a doublet at point I



c) u-velocities induced by a doublet at point F

Figure 4.25 Processing of external and internal singularities by the two-variable method

$\phi = \phi_I$, then the value of the integral will again be ϕ_I because ϕ_I is non-singular in the test section interior. However, if we set $\phi = \phi_F$, then the integral vanishes since ϕ_F is non-singular in the test section exterior. Accordingly, if the model is represented by internal singularities and the wind tunnel walls by the external singularities, the method will automatically account only for the external ones. This is exactly what is done when evaluating wall interference using the method of images: the summation is carried out over the whole infinite array of singularities and then the internal ones are subtracted. An interesting point is that the two-variable method does it by processing the measured boundary values of ϕ and $\partial\phi/\partial n$, regardless of whether or not the internal and external singularities can be reconstructed from them.

the box in the x, y, z directions is $11 \times 5 \times 5$, making a total of 215 panels. Symmetry is built into the scheme by supplementing the contribution of each panel by its reflected counterpart.

Figure 4.25b shows the effect of a point doublet in the x -direction, located at point I outside the box. Superimposed with the uniform stream, the singularity is known to model incompressible flow past a sphere. The broken lines are the u -velocity contours induced by the doublet at the interior plane $z = 0$. The solid lines are the contours produced by the two-variable method from the values of ϕ and $\partial\phi/\partial n$ generated by the doublet at the panel centroids. Apart from small numerical inaccuracies, the method is seen to have produced the effect of an external singularity $\phi = \phi_I$.

Figure 4.25c shows the effect of the same doublet placed the same distance from the wall at point F inside the box. The broken lines are still present, except that they are more dense because the doublet is now much closer to the observation plane than before. However, the solid lines have all disappeared. (Actually, there would still be numerical error contours; but the selected contour step was too large to capture them.) The two-variable method has thus eliminated the effect of an internal singularity, $\phi = \phi_F$.

A question arises whether the same also applies to potential-flow singularities other than doublets. The answer, which follows from Green's (third) identity, is affirmative. If we

substitute in the integrand of Eq.(4.3.14)

It is now also apparent that the above conclusions could have been obtained by examining Eq.(4.3.14) in the first place without resorting to any kind of numerical experimentation. However, the simple numerical box just described is in fact a prototype of a wall interference code that would, apart from minor geometrical modification, be used to correct measurements in an actual test section of a wind tunnel. The easiest way to check the code for errors and inaccuracies is by processing some well-defined singularities, exactly the same way as has been demonstrated. By further modifying this numerical experiment one can also determine how many panels are needed to represent the walls adequately, how many measurement points are required and where they should preferably be located, how the interpolations should be set up, whether the integrals over the upstream and downstream ends could possibly be dropped (Labrujère et al. [41]), and so on. As we have already mentioned, the method is simple in principle, but there are many possibilities of how it could be implemented, each of them giving somewhat different answers.

The simplest device for measuring two components of velocity is a plate with two rows of pressure orifices, aligned with the direction of mainstream, as shown schematically in Figure 4.26a. Assuming that the plate is in the x, y -plane where the x -axis is parallel with the orifice rows, we obtain (for small pressure perturbations) midway between the orifices

$$u = \frac{1}{2}(u_1 + u_2) = -\frac{1}{4}(C_{P1} + C_{P2}) \quad (4.3.16)$$

and, from the irrotational-flow condition,

$$\frac{\partial w}{\partial x} = \frac{\partial u}{\partial z} = \frac{u_2 - u_1}{d} = \frac{C_{P1} - C_{P2}}{2d}, \quad (4.3.17)$$

where d is the distance of the orifice rows.

A better device, especially for three-dimensional testing, is the double-orifice tube, also known as the Calspan pipe (Nenni et al. [53], Smith [70]), see Figure 4.26b. The pipe is equipped with two diametrically opposing rows of orifices, one facing the test section interior and the other one the wall. Substituting $\omega = \pi/2$ and $\omega = 3\pi/2$ in Eq.(4.3.13), we obtain respectively

$$C_{P1} = -2u - \beta^2 u^2 + 2d \frac{\partial w}{\partial x} - 4v^2$$

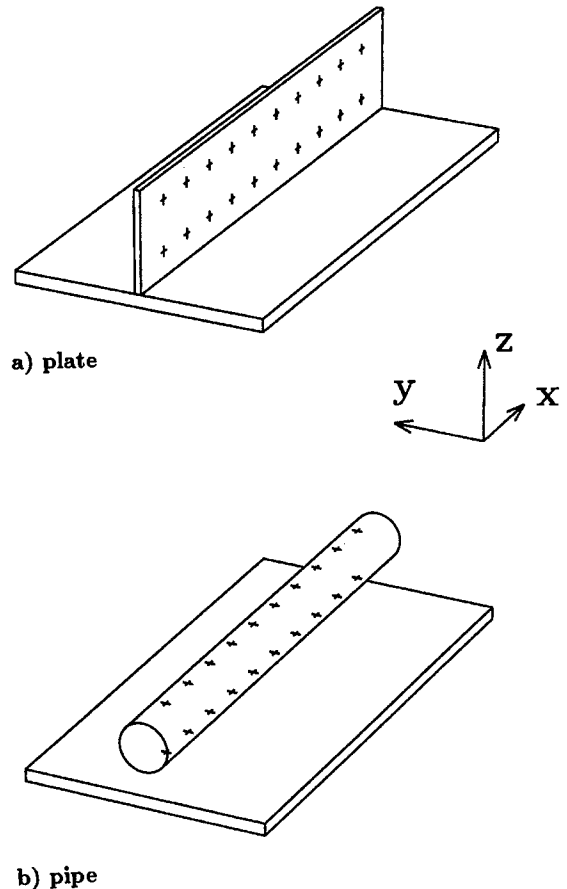


Figure 4.26 Schematic of devices with two rows of pressure orifices

$$C_{p2} = -2u - \beta^2 u^2 - 2d \frac{\partial w}{\partial x} - 4v^2$$

Adding and subtracting these expressions and retaining only the highest-order terms, we find that u is again approximated by Eq.(4.3.16); but, for the streamwise derivative of the normal velocity it follows:

$$\frac{\partial w}{\partial x} = \frac{C_{p1} - C_{p2}}{4d} \quad (4.3.18)$$

where d is the tube diameter. Comparing Eqs.(4.3.17) and (4.3.18) we see that for the same $\partial w/\partial x$ and distances, d , of the orifices, the Calspan pipe doubles the pressure difference which otherwise would be measured by the dual-orifice plate. This amplification is especially welcome when the measured pressure differences are of the same magnitude as the discrete perturbations emanating at the ventilated walls (Smith [70]), or in low speed wind tunnels, where the pressure differences are weak in general (Fernkrans [19]).

In either case, the w -velocity has to be obtained from its derivative by integration, and there re-appears again the familiar problem of determination of an unknown integration constant. Nenni et al. (1982) describe the steps to be taken as follows: assuming that w is known at a reference station x_R , then $\partial w/\partial x$ can be integrated to give

$$w(x) = w(x_R) + \int_{x_R}^x \frac{\partial w}{\partial x} dx \quad (4.3.19)$$

If w can be measured at a suitable reference point, the pressure distributions along the top and bottom of the pipe can also be used to determine w , in addition to u . This supplementary measurement of $w(x_R)$ has to be made by an alternative measuring technique, or else x_R has to be chosen where $w(x_R)$ is expected to be zero. As the major shortcomings of measuring flow direction by the Calspan pipe identified were: weak pressure differences and reliance on slender-body theory, which ignores the possible effects of viscosity and flow non-uniformity in the vicinity of the walls (Smith [70]).

Because half the (diametrically opposing) orifices face the wall, the pipe has to be positioned some distance from the wall. A typical example is in Figure 4.27, showing an installation of a Calspan pipe in the NLR Pilot Tunnel (GARTEur [26]). An interesting concept for three-dimensional testing is the AEDC rotating pipe system (Parker and Erickson [55] and Sickles [65]), shown in Figure 4.28. The system consists of two pipes and a mechanism that can rotate them about the centreline of the perforated-wall test section (AEDC Tunnel 4T). The pipes sweep out a cylindrical measurement surface, approximately one inch from the wall at the closest point. Each 5/8-inch diameter pipe is equipped with 40 pairs of diametrically opposing orifices, distributed more densely where large pressure gradients are expected. The pressure and the difference in the pressures for each pair are used to determine the components of velocity in the streamwise and radial directions. The integration to determine the longitudinal distribution of the radial component of velocity is performed over two intervals: from upstream to peak suction pressure, and (backward) from downstream to peak suction pressure. The integration constants for the two regions are measured by upstream and downstream flow angle probes, also visible in Figure 4.28. A more detailed discussion of the apparatus and sample measurements can be found in Kraft et al. [39].

For slotted walls, it has also been suggested to measure or establish the mean flow boundary conditions from velocities measured by probes traversed inside the slots (Freestone and Mohan [23]). Provided that the streamwise variations of the mean normal velocity are relatively slow, as most experiments confirm, a

probe traverse could be substituted by a number of fixed flow angle probes (Mohan and Freestone, [46]), making the technique suitable even for production wind-tunnel testing.

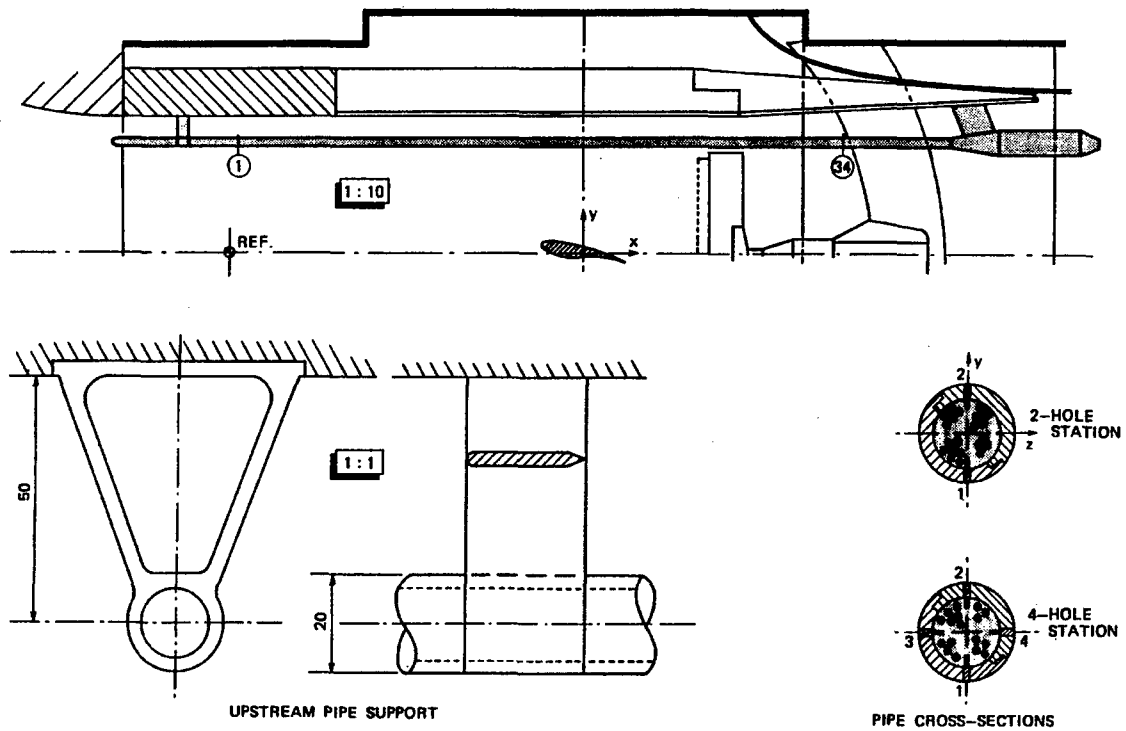


Figure 4.27 Calspan pipe and its mounting in the NLR Pilot Tunnel

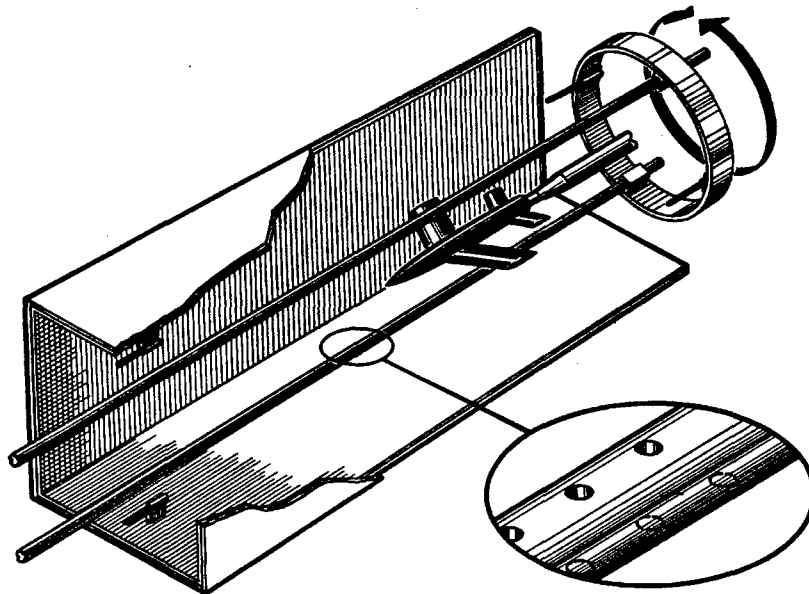


Figure 4.28 AEDC Two-Variable Measuring System

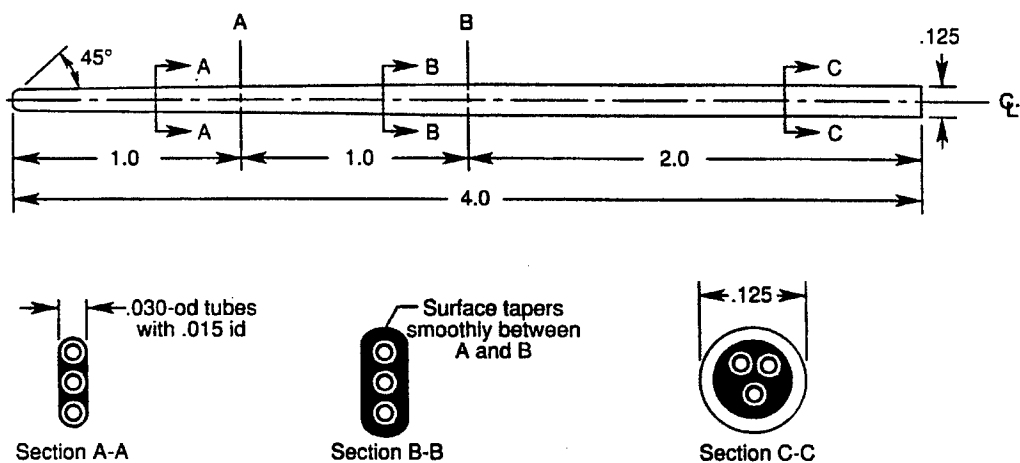


Figure 4.29 NASA/United Sensor flow angle probe

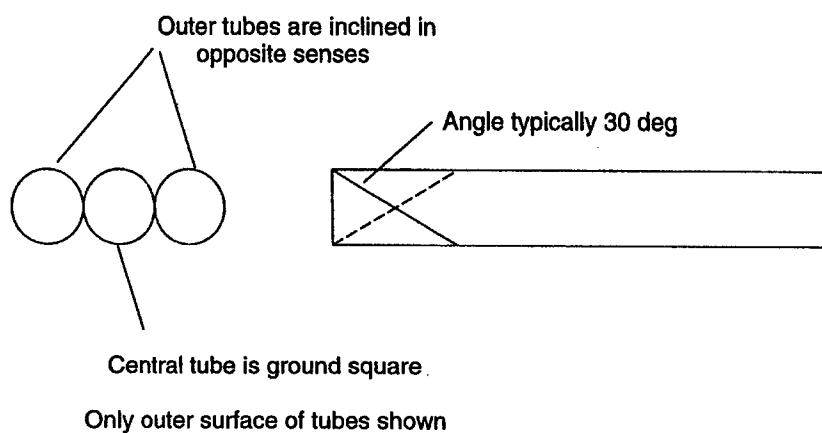


Figure 4.30 Sketch of in-line probe to measure flow angle in presence of shear (Courtesy of M.M. Freestone)

A typical three-tube flow angle probe, used by Everhart and Bobbitt [18] for slot flow measurements in the NASA Langley 6 × 19 Inch Transonic Tunnel, is shown schematically in Figure 4.29. In an effort to eliminate the error when crossing the shear layer, Freestone has recently developed a flow angle probe, whose pressure-measuring tubes are positioned parallel to the wall, see Figure 4.30.

The velocity component normal to the wall normal is quite substantial inside the slot and all indications are that it can be measured very accurately. A difficulty arises when one wishes to establish correspondence between the velocity inside the slot and the mean or "homogeneous" normal velocity at the wall that enters Eq.(4.3.14) or (4.3.15). In theory, the latter can be evaluated by laterally averaging the mass flux using the slender-body theory (Everhart and Bobbitt [18]). Unfortunately, viscous effects in the slots do not just manifest themselves by narrowing the effective slot width (vena contracta). Experimental data show that along the slot segments where air is flowing into the test section, rather than out of it, the crossflow is causing a rapid thickening of the wall boundary layer. This effective amplification of the mean normal velocity over the inflow regions of the walls was found to be of up to about 4.0 (Freestone and Mohan [23]). Quantitative observations of similar kind, both in slotted and perforated walls, have also been made by Vidal et al. [78], Chan [11], Firmin and Cook [20], and Crites and Rueger [15]. Freestone (private communication, 1995) suggests: "It is possible in principle to make a series of measurements in the test section of interest, specially designed to provide the amplification factor in sufficient detail for subsequent application. Whether or not it would be feasible or practical undertaking is not so clear. Much may depend on first demonstrating that it is not necessary to know the streamwise variations in boundary layer thickness very precisely in order to achieve the desired accuracy of wall interference. Perhaps it would be adequate to know the overall increase in thickness over the length of the inflow region, but even this, in a three-dimensional test, is no small task." Another possibility

is keeping the amplification factor close to unity by enforcing outflow above and below the model and returning the drawn air to the wind-tunnel circuit some distance downstream (Mohan and Freestone [46]). Of course, the corresponding pressure gradient can make the measured model data difficult to correct to free stream conditions.

In spite of the current difficulties in measuring the normal component of velocity at the wind tunnel boundary, the uncertainty of the model representation inherent in the one-variable method is a far more serious problem, especially in transonic or separated flow regimes. As spelled out by Rubbert [62] and the GARTEur Report [26], attention will undoubtedly turn more and more to the two-variable method, which is capable of producing corrections from two components of boundary velocity, without knowing anything about the flow in the neighbourhood of the model. Since the relative accuracy or dependability of the two-variable method is a function of measurement accuracy's inherent in producing the two components of velocity near the walls, it is predominantly in improving the measurement techniques where progress can be made.

4.3.3 ALTERNATIVE METHODS

There are other methods of utilising boundary measurements in the evaluation of subsonic wall interference besides those discussed in this Chapter, but most of them are not as direct as those described above. An attractive approach, at least from the production-testing viewpoint, is to use the two-variable method with the measurement of one variable. This is of course possible only if the wall boundary condition is known, so that the unknown variable (normal velocity) can be derived from the measured one (pressure). An example of this approach is discussed by Rueger and Crites, et. al. (1994.) In this approach the uncertainty of model representation, inherent in the one-variable method, is traded for the uncertainty in the wall boundary condition. The boundary condition at a given wall location can be established, for example, by applying the one-variable method in instances when the model far field can be well predicted (subcritical, low incidence flow). In essence, the evaluation of the transverse velocity components v_I and w_I consists of streamwise integrating Eqs.(4.3.10), where the derivatives of u_I have been obtained by the one-variable method. The subsequent two-variable evaluation is used in flow situations where the far-field of the model cannot be predicted as reliably (high incidence or supercritical flow).

APPENDIX: RECTANGULAR WALL PANEL

Considered is a rectangular panel

$$R = \{(x, y, z): x_1 \leq x \leq x_2, y_1 \leq y \leq y_2, z = 0\},$$

whose normal is oriented along the positive z -axis and whose source or doublet density is unity. The distance of the observation point x_0, y_0, z_0 from the panel point x, y, z is

$$r = \sqrt{(x_0 - x)^2 + (y_0 - y)^2 + (z_0 - z)^2}.$$

Evaluation of the potential and its derivatives induced by the panel at the observation point can be quite tedious (Hess and Smith [30], Holst [32], Katz and Plotkin [35]) but the results can be manipulated into neat, Biot-Savart-type formulae.

For the source panel, we obtain

$$\begin{aligned}
 -\int_R \frac{1}{r} dS &= (x_0 - x_2)(u_{22}^s - u_{21}^s) + (x_0 - x_1)(u_{11}^s - u_{12}^s) + (y_0 - y_2)(v_{22}^s - v_{12}^s) + \\
 &\quad + (y_0 - y_1)(v_{11}^s - v_{21}^s) + z_0(w_{11}^s - w_{21}^s + w_{22}^s - w_{12}^s) \\
 -\frac{\partial}{\partial x_0} \int_R \frac{1}{r} dS &= u_{11}^s - u_{21}^s + u_{22}^s - u_{12}^s \\
 -\frac{\partial}{\partial y_0} \int_R \frac{1}{r} dS &= v_{11}^s - v_{21}^s + v_{22}^s - v_{12}^s \\
 -\frac{\partial}{\partial z_0} \int_R \frac{1}{r} dS &= w_{11}^s - w_{21}^s + w_{22}^s - w_{12}^s
 \end{aligned}$$

where

$$\begin{aligned}
 u_{ij}^s &= \ln[r_{ij} - (y_0 - y_j)] \\
 v_{ij}^s &= \ln[r_{ij} - (x_0 - x_i)] \\
 w_{ij}^s &= \arctan \frac{(x_0 - x_i)(y_0 - y_j)}{z_0 r_{ij}}
 \end{aligned}$$

and

$$r_{ij} = \sqrt{(x_0 - x_i)^2 + (y_0 - y_j)^2 + z_0^2}.$$

The normal velocity induced by a source panel has a jump discontinuity across the panel: if $x_1 < x_0 < x_2$, $y_1 < y_0 < y_2$ and $z_0 \rightarrow 0^\pm$,

$$-\frac{\partial}{\partial z_0} \int_R \frac{1}{r} dS \rightarrow \pm 2\pi.$$

The tangential velocities and the potential itself are continuous across the panel.

For the doublet panel, similarly,

$$\begin{aligned}
 \int_R \frac{\partial}{\partial z} \left(\frac{1}{r} \right) dS &= -\frac{\partial}{\partial z_0} \int_R \frac{1}{r} dS = w_{11}^s - w_{21}^s + w_{22}^s - w_{12}^s \\
 \frac{\partial}{\partial x_0} \int_R \frac{\partial}{\partial z} \left(\frac{1}{r} \right) dS &= u_{11}^d - u_{21}^d + u_{22}^d - u_{12}^d
 \end{aligned}$$

$$\frac{\partial}{\partial y_0} \int_R \frac{\partial}{\partial z} \left(\frac{1}{r} \right) dS = v_{11}^d - v_{21}^d + v_{22}^d - v_{12}^d$$

$$\frac{\partial}{\partial z_0} \int_R \frac{\partial}{\partial z} \left(\frac{1}{r} \right) dS = w_{11}^d - w_{21}^d + w_{22}^d - w_{12}^d$$

where

$$u_{ij}^d = \frac{z_0(y_0 - y_j)}{[(x_0 - x_i)^2 + z_0^2] r_{ij}}$$

$$v_{ij}^d = \frac{z_0(x_0 - x_i)}{[(y_0 - y_j)^2 + z_0^2] r_{ij}}$$

$$w_{ij}^d = - \frac{(x_0 - x_i)(y_0 - y_j)}{(x_0 - x_i)^2 (y_0 - y_j)^2 + z_0^2 r_{ij}^2} \left(r_{ij} + \frac{z_0^2}{r_{ij}} \right)$$

The potential of the doublet panel has a jump discontinuity across the panel: if $x_1 < x_0 < x_2$, $y_1 < y_0 < y_2$ and $z_0 \rightarrow 0 \pm$,

$$\int_R \frac{\partial}{\partial z} \left(\frac{1}{r} \right) dS \rightarrow \pm 2\pi$$

The velocity components are continuous.

REFERENCES TO CHAPTER 4.3

- [1] Akai, T.J and Piomelli, U., 1984, "Effect of Upstream Parallel Flow on Two-Dimensional Wind-Tunnel Tests," AIAA-84-2153.
- [2] Al-Saadi, J.A., 1991, "Model Representation in the PANCOR Wall Interference Assessment Code," NASA TM-104152.
- [3] Amecke, J., 1985, " Direkte Berechnung von Wandinterferenzen und Wandadaptation bei zweidimensionaler Strömung in Windkanälen mit geschlossenen Wänden," DFVLR-FB 85-62; also translated as NASA TM-88523, 1986.
- [4] Ashill, P.R. and Weeks, D.J., 1982, "A Method for Determining Wall-Interference Corrections in Solid-Wall Tunnels from Measurements of Static Pressure at the Walls," AGARD-CP-335, pp.1.1 - 1.12.
- [5] Ashill, P.R. and Keating, R.F.A., 1988, "Calculation of Tunnel Wall Interference from Wall-Pressure Measurements," The Aeronautical Journal of the Royal Aeronautical Society, pp.36-53.
- [6] Aulehla, F., 1977, "Drag Measurement in Transonic Wind Tunnels," AGARD-CP-242, pp.7.1-7.18

- [7] Berndt, S.B., 1982, "Measuring the Flow Properties of Slotted Test-Section Walls," FFA 135, The Aeronautical Research Institute of Sweden.
- [8] Binion, T.W. and Lo, C.F., 1972, "Application of Wall Corrections to Transonic Wind Tunnel Data," AIAA-72-1009.
- [9] Blackwell, J.A., 1979, "Wind-Tunnel Blockage Correction for Two-Dimensional Transonic Flow," Journal of Aircraft, Vol.16, No.4, pp.256-263.
- [10] Capelier, C., Chevallier, J.P., and Bouniol, F., 1978, "Nouvelle méthode de correction des effets de parois en courant plan," La recherche aérospatiale, Jan.-Feb. 1978, pp.1-11; also translated as ESA-TT-491, 1978.
- [11] Chan, Y.Y., 1981, "Analysis of Boundary Layers on Perforated Walls of Transonic Wind Tunnels," Journal of Aircraft, Vol.18, pp.469-473.
- [12] Chen, C.F. and Mears, J.W., 1957, "Experimental and Theoretical Study of Mean Boundary Conditions at Perforated and Longitudinally Slotted Walls," Tech. Rep. WT-23, Brown University.
- [13] Chevallier, J.P., 1984, "Survey of ONERA Activities on Adaptive-Wall Applications and Computation of Residual Corrections," Wind Tunnel Wall Interference Assessment/Correction 1983, NASA CP 2319, pp.43-58.
- [14] Cole, J.D. and Cook, L.P., 1986, "Transonic Aerodynamics," North-Holland, pp.259-272.
- [15] Crites, R. and Rueger, M., 1992, "Modeling the Ventilated Wind Tunnel Wall, AIAA 92-0035.
- [16] Crites, R. and Steinle, F.W., Jr., 1995, "Wall Interference Reduction Methods for Subsonic Wind Tunnels", AIAA 95-0107.
- [17] Ebihara, M., 1972, "A Study of Subsonic Two-Dimensional Wall-Interference Effect in a Perforated Wind Tunnel with Particular Reference to the NAL 2m x 2m Transonic Wind Tunnel," TR-252T, National Aerospace Laboratory, Tokyo.
- [18] Everhart, J.L. and Bobbitt, P.J., 1994, "Experimental Studies of Transonic Flow Field Near a Longitudinally Slotted Wind Tunnel Wall," NASA Technical Paper 3392.
- [19] Fernkrans, L., 1993, "Calculation of Low Speed Wind Tunnel Wall Interference from Static Pressure Pipe Measurements," AGARD-CP-535, pp.23.1-23.7.
- [20] Firmin, M.C.P. and Cook, T.A., 1968, "Detailed Exploration of the Compressible Viscous Flow over Two-Dimensional Aerofoils at High Reynolds Numbers," ICAS Paper 68-09.
- [21] Firmin, M.C.P. and Cook, P.H., 1983, "Disturbances from Ventilated Tunnel Walls in Aerofoil Testing," AGARD-CP-348, pp. 8.1-8.15.
- [22] Freestone, M.M., Lock, R.C., and Mohan, S.R., 1991, "Determination of Wind Tunnel Interference Due to Slotted Wall Liners," MED/AERO Rept. No.179, City University, London.
- [23] Freestone, M.M. and Mohan, S.R., 1993, "Interference Determination for Wind Tunnels With Slotted Walls," AGARD-CP-535, pp.19.1-19.12.
- [24] Gakhov, F.D., 1966, "Boundary Value Problems," Pergamon Press.
- [25] Galway, R.D., 1994, "Measurement of Low Level Pressure Disturbances in Proximity to a Perforated Wall in a Blowdown Wind Tunnel," presented at the 81st. Semi-annual Meeting of the Supersonic Tunnel Association, Buffalo, N.Y.
- [26] GARTEur Action Group AD(AG-23), 1983,
- [27] "Two-Dimensional Transonic Testing Methods," NLR TR 83086 U.

- [28] Goldhammer, M.I. and Steinle, F.W., Jr., 1990, "Design and Validation of Advanced Transonic Wings Using CFD and Very High Reynolds Number Wind Tunnel Testing," ICAS 90-26.2.
- [29] Gopinath, R., 1985, "Wall Interference Studies in 3-D Flows," TM-AE-8508, National Aeronautical Laboratory, India.
- [30] Hess, J.L. and Smith, A.M.O., 1966, "Calculation of Potential Flow About Arbitrary Bodies," Progress in Aeronautical Sciences, Vol.8, pp.1-138.
- [31] Hinson, B.L. and Burdges, K.P., 1981, "Evaluation of Three-Dimensional Transonic Codes Using New Correlation-Tailored Test Data," Journal of Aircraft, Vol.18, No.10, pp.855-861.
- [32] Holst, H., 1990, "Verfahren zur Bestimmung von dreidimensionalen Windkanalwandinterferenzen und Wandadaptionen mit Hilfe gemessener Wanddrücke bei kompressibler Unterschallströmung," DLR-FB 0-46.
- [33] Jacocks, J.L., 1976, "An Investigation of the Aerodynamic Characteristics of Ventilated Test Section Walls for Transonic Wind Tunnels," Doctoral Thesis, The University of Tennessee.
- [34] Jones, D.J., 1979, "A Method for Computing 2-D Wind Tunnel Wall Interference Effects Allowing for Variable Porosity along Floor and Ceiling," LTR-HA-37, National Aeronautical Establishment, National Research Council Canada.
- [35] Katz, J. and Plotkin, A., 1991, "Low-Speed Aerodynamics," McGraw-Hill, pp.282-288.
- [36] Kemp, W.B., 1985, "A Slotted Test Section Numerical Model for Interference Assessment," Journal of Aircraft, Vol.22, No.3, pp.216-222.
- [37] Kemp, W.B., 1990, "User's Guide to PANCOR: A Panel Method for Interference Assessment Method for a Slotted-Wall Wind Tunnel," NASA CR-4352.
- [38] Kraft, E.M. and Dahm, W.J.A., 1982, "Direct Assessment of Wall Interference in a Two-Dimensional Subsonic Wind Tunnel," AIAA-82-0187.
- [39] Kraft, E.M., Ritter, A., and Laster, M.L., 1986, "Advances at AEDC in Treating Transonic Wind Tunnel Wall Interference," ICAS-86-1.6.1.
- [40] Labrujère, T.E., Maarsingh, R.A., and Smith, J., 1986, "Wind Tunnel Wall Influence Considering Two-Dimensional High-Lift Configurations," Journal of Aircraft, Vol.23, pp.118-125.
- [41] Labrujère, T.E., Maarsingh, R.A., and Smith, J., 1988, "Evaluation of Measured-Boundary-Condition Methods for 3D Subsonic Wall Interference," NLR TR 88072 U.
- [42] Lo, C.F., 1978, "Tunnel Interference Assessment by Boundary Measurements," AIAA Journal, Vol.16, No.4, pp.411-413.
- [43] Lo, C.F. and Kraft, E.M., 1978, "Convergence of the Adaptive-Wall Wind Tunnel," AIAA Journal, Vol. 16, pp.67-72.
- [44] Magnus, R. and Yoshihara, H., 1972, "Steady Inviscid Transonic Flows over Planar Airfoils - A Search for a Simplified Procedure," NASA CR-2186.
- [45] Matyk, G.E. and Kobayashi, Y., 1977, "An experimental Investigation of Boundary Layer and Crossflow Characteristics of the Ames 2-by 2-Foot and 11- by 11-Foot Transonic Wind-Tunnel Walls," NASA T.M. 73257.
- [46] Mohan, S.R. and Freestone, M.M., 1994, "Interference Determination for Three-Dimensional Flows in Slotted-Liner Wind Tunnels," ICAS-94-3.3.1.

- [47] Mokry, M., Peake, D.J., and Bowker, A.J., 1974, "Wall Interference on Two-Dimensional Supercritical Airfoils, Using Wall Pressure Measurements to Determine the Porosity Factors for Tunnel Floor and Ceiling," LR-575, National Aeronautical Establishment, National Research Council Canada.
- [48] Mokry, M. and Galway, R.D., 1977, "Analysis of Wall Interference Effects on ONERA Calibration Models in the NAE 5-ft. x 5-ft, Wind Tunnel," LR-594, National Aeronautical Establishment, National Research Council Canada.
- [49] Mokry, M. and Ohman, L.H., 1980, "Application of the Fast Fourier Transform to Two-Dimensional Wind Tunnel Wall Interference," *Journal of Aircraft*, Vol.17, pp.402-408.
- [50] Mokry, M., 1982, "Subsonic Wall Interference Corrections for Finite-Length Test Sections Using Boundary Pressure Measurements," AGARD-CP-335, pp.10.1 - 10.15.
- [51] Mokry, M., 1985, "Subsonic Wall Interference Corrections for Half-Model Tests Using Sparse Wall Pressure Data," LR-616, National Aeronautical Establishment, National Research Council Canada.
- [52] Mokry, M., Digney, J.R., and Poole, R.J.D., 1987, "Doublet-Panel Method for Half-Model Wind-Tunnel Corrections," *Journal of Aircraft*, Vol.24, pp.322-327.
- [53] Nenni, J.P., Erickson, J.C., and Wittliff, C.E., 1982, "Measurement of Small Normal Velocity Components in Subsonic Flows by Use of Static Pipe," *AIAA Journal*, Vol.20, pp.1077-1083.
- [54] Ohman, L.H. and Brown, D., 1990, "Performance of the New Roll-In Roll-Out Transonic Test Sections of the NAE 1.5m x 1.5m Blowdown Wind Tunnel," ICAS-90-6.2.2.
- [55] Parker, R.L. and Erickson, J.C., 1982, "Development of a Three-Dimensional Adaptive Wall Test Section with Perforated Walls," AGARD-CP-335, pp.17.1-17.14.
- [56] Paquet, J.B., 1979, "Perturbations induites par les parois d'une soufflerie - méthodes intégrales," Thèse Ing. Doc., Université de Lille, 1979.
- [57] Peake, D.J., Bowker, A.J., Mokry, M., Yoshihara, H., and Magnus, R., 1974, "Transonic Lift Augmentation of Two-Dimensional Supercritical Aerofoils by Means of Aft Camber, Slot Blowing and Jet Flaps, in High Reynolds Number Flow," ICAS Paper No.74-11.
- [58] Piat, J.F., 1994, "Calculs des effets de parois dans des veines à parois perforées avec un code de singularités surfaciques," AGARD-CP-535, pp.27.1-27.12.
- [59] Pounds, G.A. and Walker, J., 1980, "Semispan Model Testing in a Variable Porosity Transonic Wind Tunnel," AIAA-80-0461.
- [60] Qian, X. and Lo, C.F., 1994, "Two-Variable Method for Blockage Wall Interference in a Circular Tunnel," *Journal of Aircraft*, Vol.31, No.5, pp.1130-1134.
- [61] Rizk, M.H. and Smithmeyer, M.G., 1982, "Wind-Tunnel Interference Corrections for Three-Dimensional Flows," *Journal of Aircraft*, Vol.19, pp.465-472.
- [62] Rubbert, P.E., 1981, "Some Ideas and Opportunities Concerning Three-Dimensional Wind-Tunnel Wall Corrections," *Wind-Tunnel / Flight Correlation - 1981*, NASA Conference Publication 2225, pp.217-229.
- [63] Sawada, H., 1980, "A New Method of Calculating Corrections for Blockage Effects in Two-Dimensional Wind Tunnel with Ventilated Walls, Using Wall Pressure Measurements," *Transactions of the Japan Society for Aeronautical And Space Sciences*, Vol.22, No.61, pp.155-168.
- [64] Sewall, W.G., 1984, "Wall Pressure Measurements for Three-Dimensional Transonic Tests," AIAA-84-0599.

- [65] Sickles, W.L., 1983, "A Data Base for Three-Dimensional Wall Interference Code Evaluation," NASA CP-2319, pp.101-115.
- [66] Sickles, W.L. and Erickson, J.C., 1990, "Wall Interference Corrections for Three-Dimensional Transonic Flows," AIAA 90-1408.
- [67] Smith, J., 1976, "Results of a Preliminary Investigation on 2-Dimensional Ventilated-Wall Interference, Based on an Analysis of Plenum Pressure Behaviour," Memorandum AC-76-012, National Aerospace Laboratory NLR.
- [68] Smith, J., 1981, "A Method for Determining 2D Wall Interference on an Aerofoil from Measured Pressure Distributions near the Walls and on the Model," NLR TR 81016 U.
- [69] Smith, J., 1982, "Measured Boundary Conditions Methods for 2D Flow," AGARD-CP-335, pp.9.1 - 9.15.
- [70] Smith, J., 1985, "2D Wall Interference Assessment Using Calspan Pipes," NLR TR 85065 U.
- [71] Stakgold, I., 1968, "Boundary Value Problems of Mathematical Physics," Vol.II, Macmillan.
- [72] Starr, R.F., 1978, "Experimental Observations of Wall Interference at Transonic Speeds," AIAA 78-164.
- [73] Steinle, F.W., Jr. and Stanewsky, E., 1982, "Wind Tunnel Flow Quality and Data Accuracy Requirements," AGARD-AR-184.
- [74] Theodorsen, T., 1931, "The Theory of Wind-Tunnel Wall Interference," NACA Rept.410.
- [75] Ulbrich, N. and Steinle, F.W., Jr., 1994, "Real-Time Wall Interference Calculations in three-dimensional Subsonic Wind Tunnel Testing," AIAA 94-0771.
- [76] Ulbrich, N. and Steinle, F.W., Jr., 1995, "Semispan Model Wall Interference Prediction Based on the Wall Signature Method," AIAA 95-0793.
- [77] Vaucheret, X., 1982, "Améliorations des calculs des effets de parois dans les souffleries industrielles de l'ONERA," AGARD-CP-335, pp.11.1-11.12.
- [78] Vidal, R.J., Erickson, J.C., and Catlin, P.A., 1975, "Experiments with Self-Correcting Wind Tunnel," AGARD-CP-174, pp.11.1-11.13.
- [79] Wu, J.M., Collins, F.G., and Bhat, M.K., 1983, "Three-Dimensional Flow Studies on a Slotted Transonic Wind Tunnel Wall," AIAA Journal, Vol.21, pp.999-1005.
- [80] Steinle, F.W., Jr., "Development of the Porous-Slot Geometry of the NWTC Test Section", AIAA 07-0097

5. TRANSONIC WIND TUNNEL WALL INTERFERENCE

Authors N. Malmuth,
 R. Crites
 J. Everhart,
 P. Newman
 W. Sickles

	PAGE
5.1 BACKGROUND	5-3
5.1.1 SCOPE AND OVERVIEW	5-3
5.1.2 PREVIOUS LITERATURE AND CONFERENCES	5-4
5.1.3 WALL INTERFERENCE/REYNOLDS SIMULATION TRADE-OFF IN MODEL SIZING	5-4
5.1.4 CORRECTABILITY	5-5
5.2 WALL BOUNDARY CONDITIONS FOR TRANSONIC FLOWS	5-8
5.2.1 NOMENCLATURE FOR SECTION 5.2	5-8
5.2.2 SOLID WALLS	5-10
5.2.3 POROUS WALLS	5-11
5.2.3.1 McDONNELL-DOUGLAS POROUS WALL BOUNDARY CONDITION	5-11
5.2.3.1.1 EXPERIMENTAL SET-UP	
5.2.3.1.2 EXPERIMENTAL PROCEDURE	
5.2.3.1.3 AIR-OFF RESULTS	
5.2.3.1.4 AIR-ON RESULTS	
5.2.3.2 AEDC PERFORATED-WALL BOUNDARY CONDITION	5-17
5.2.3.3 FREESTONE POROUS WALL STUDIES	5-20
5.2.4 SLOTTED WALLS	5-21
5.2.4.1 FREESTONE SLOTTED WALL STUDIES	5-21
5.2.4.2 BERNDT BOUNDARY CONDITION AND IMPLEMENTATION	5-22
5.2.4.3 LARC BOUNDARY-CONDITION MEASUREMENTS AND CORRELATIONS	5-24
5.2.4.3.1 OVERVIEW	
5.2.4.3.2 NASA LANGLEY SLOTTED-WALL EXPERIMENTS	
5.2.4.3.3 CORRELATION OF COEFFICIENTS FOR IDEAL SLOTTED-WALL BOUNDARY CONDITION	
5.2.4.3.4 LINEARISATION OF THE SLOTTED-WALL BOUNDARY CONDITION	
5.2.4.3.5 EFFECT OF AIRFOIL MODEL ON PLENUM PRESSURE	
5.2.4.3.6 CORRELATION OF BOUNDARY PRESSURE MEASUREMENTS WITH THEORY	
5.2.4.3.7 VARIATION OF BOUNDARY-CONDITION COEFFICIENTS	
5.2.4.3.8 COMPARISON OF COEFFICIENTS WITH BERNDT'S SLOT-DEPTH HYPOTHESIS	
5.2.4.3.9 IMPLEMENTING EVERHART'S BOUNDARY CONDITION EQUATION	
5.2.4.4 TRANSONIC SLOT DESIGN	5-33
5.2.4.4.1 DESIGN METHOD FOR TWO-DIMENSIONAL SLOTTED WALLS	
5.2.4.4.2 NTF SLOT DESIGN	
5.2.4.4.3 SUPERSONIC SLOT DESIGN - METHOD OF RAMASWAMY AND CORNETTE	
5.2.5 BAFFLED SLOTTED WALLS	5-35
5.2.5.1 BACKGROUND	5-35
5.2.5.2 BOUNDARY CONDITION FOR AMES 11-Ft TRANSONIC TUNNEL	5-35

	PAGE
5.3 COMPUTATIONAL APPROACHES	5-37
5.3.1 TUNNEL SIMULATIONS	5-37
5.3.1.1 LINEAR THEORY	5-37
5.3.1.2 TRANSONIC SMALL DISTURBANCE EQUATION (TDSE) METHODS	5-39
5.3.1.3 FULL-POTENTIAL EQUATION (FPE) METHODS	5-41
5.3.1.4 EULER EQUATION METHODS	5-42
5.3.1.5 NAVIER STOKES EQUATION METHODS	5-43
5.3.2 MDA WALL INTERFERENCE COMPUTATIONS	5-44
5.3.2.1 BACKGROUND	5-44
5.3.2.2 EMPIRICAL CORRECTIONS	5-45
5.3.2.3 TWO POINTS OF VIEW	5-47
5.3.2.4 APPLICATION OF THE MDA WALL FLOW MODEL	5-48
5.3.3 AEDC WALL INTERFERENCE COMPUTATIONS	5-49
5.3.3.1 INTRODUCTION	5-49
5.3.3.2 WALL INTERFERENCE PROCEDURE	5-50
5.3.3.3 WALL INTERFERENCE RESULTS	5-51
5.3.3.4 MODEL DESCRIPTIONS	5-51
5.3.3.5 WIM1T AND WIM4T WALL-INTERFERENCE COMPUTATIONS	5-53
5.3.3.6 SSLV WALL-INTERFERENCE COMPUTATIONS	5-57
5.3.3.7 TST WALL-INTERFERENCE COMPUTATIONS	5-58
5.3.3.8 CONCLUSION	5-68
5.3.4 NASA LANGLEY WIAC METHODS	5-68
5.3.4.1 NON-LINEAR AIRFOIL TUNNEL WIAC CODES	5-69
5.3.4.2 LINEAR AND NON-LINEAR 3D WIAC CODES	5-70
5.4 ASYMPTOTIC METHODS FOR TRANSONIC WIND TUNNEL WALL INTERFERENCE	5-72
5.4.1 BACKGROUND	5-72
5.4.2 OVERVIEW OF ASYMPTOTIC PROCEDURES FOR SMALL SLENDER AND LARGE ASPECT RATIO CONFIGURATIONS	5-72
5.4.3 SMALL SLENDER CONFIGURATIONS	5-73
5.4.4 HIGH ASPECT RATIO THEORY	5-74
5.4.5 RESULTS - SMALL SLENDER BODIES	5-75
5.4.6 RESULTS - LARGE ASPECT RATIO WINGS	5-76
5.4.7 LIFT INTERFERENCE AND POROUS WALL EFFECTS ON SLENDER WINGS	5-79
5.4.8 EXTENSION OF LARGE WALL-HEIGHT BLOCKAGE INTERFERENCE THEORY TO MODERATE WALL HEIGHT CASE	5-85
5.4.9 VALIDATIONS OF THEORETICAL AND COMPUTATIONAL SIMULATIONS FOR MODERATE WALL HEIGHT CASE	5-86
5.4.10 NON-CIRCULAR WIND TUNNEL SECTIONS	5-90
5.4.11 SUMMARY, CONCLUSIONS AND RECOMMENDATIONS	5-94
5.5 ASSESSMENT OF STATE OF THE ART	5-95
5.6 REFERENCES FOR CHAPTER 5	5-98

5. TRANSONIC WIND TUNNEL WALL INTERFERENCE

5.1 BACKGROUND

5.1.1 SCOPE AND OVERVIEW

Transonic wind tunnel corrections pose unique and difficult challenges. Because of their technical importance, they have been the subject of active research since World War II. The subject is vast; and adequate treatment demands a separate treatise such as an update of Goethert [71]. Although much progress has been made, significant effort is still needed to cope with current needs and issues, since large gaps remain in our knowledge. Because significant developments have occurred since the last AGARD review of this topic [67], an updated assessment is appropriate. Although not an exhaustive survey, this chapter is intended to provide a current glimpse of some activities in transonic wall interference. It contains different perspectives from Arnold Engineering Development Center (AEDC), McDonnell Douglas, NASA Langley and Rockwell Science Center. It makes no attempt to discuss the important area of experimental and instrumentation methods exemplified by the continuing challenges of making accurate static pressure measurements near ventilated walls, and non-invasive optical diagnostics for three-dimensional transonic wind tunnel flow mapping and visualisation. Rather, it emphasises the related topics of wall simulation and correction prediction procedures. These are especially difficult because of the nonlinearity of the flow as well as shock wave interactions with the walls and their consequences for extrapolation from ground tests to flight.

As compared to low and moderate supersonic speeds, the corrections can be large. Except for weak supercriticality (WS), which is defined by a high subsonic flow containing only small supersonic pockets, compressible corrections based on the imaging, and superposition methodology such as panel methods used extensively for low Mach number wind tunnel flows are not applicable since the flow is highly non-linear with shocks. In the wind tunnel, WS implies that the far upstream and downstream regions are subsonic, without non-linear mixed flow effects. WS frequently occurs over commercial transport aircraft at cruise conditions. Because of such practicality, some of this chapter relates to this situation. In the wind tunnel, WS is also associated with supersonic bubbles whose height is small compared to the wall height. When these two dimensions are comparable, and the freestream is slightly subsonic, the flow has been classified by Hornung and Stanewsky [85] as Group 1. Group 2 flows are also associated with subsonic freestreams but with free field sonic bubbles penetrating the walls. Sonic Mach number and choked flow are special subcases of Group 2 flows. Slightly supersonic freestreams are classified as Group 3. We will be concerned with all three groups in this chapter. Adaptive walls in which the wind tunnel walls or near-wall regions are configured to replicate free field conditions will be mentioned only in passing, as these are discussed in Chapter 10.

5.1.2 PREVIOUS LITERATURE AND CONFERENCES

Since Garner, *et al.* [67] as well as Pindzola and Lo [151], a number of conferences and summary papers dealing with wind tunnel wall interference have been published. Although much of this work was not exclusively for the transonic flow regime (see the subsonic material discussed in the previous chapters herein), many of the ideas and procedures are applicable to this speed range (albeit, frequently, with the restriction of weak supercriticality and subsonic far fields).

Several conference proceedings devoted to wall interference are:

- a) Wall Interference in Wind Tunnels; AGARD [3]
- b) Wind Tunnel Wall Interference Assessment/Correction—1983; Newman and Barnwell, editors [139]
- c) Adaptive Wall Wind Tunnels and Wall Interference Correction Methods; Hornung and Stanewsky, editors [85]
- d) International Conference on Adaptive Wall Wind Tunnel Research and Wall Interference Correction; He, editor [83]
- e) Wall Interference, Support Interference, and Flow Field Measurements; AGARD [5]

In addition, since 1970, a number of other AGARD Symposia and AIAA Meetings related to wind tunnel and testing techniques, have included sessions devoted to wall interference. Noteworthy summary papers in addition to those appearing in the previously cited conference proceedings are:

- a) Two-Dimensional Transonic Testing Methods; Elsenaar, editor [49]
- b) Two-Dimensional Wind Tunnel Wall Interference; Mokry, *et al.* [133],
- c) Wind Tunnel Wall Interference; Newman, *et al.* [138],
- d) Advances at AEDC in Treating Transonic Wind Tunnel Wall Interference; Kraft, *et al.* [109],
- e) Calculation of Transonic Wall Interference; Donegan, *et al.* [47],
- f) Emerging Technology for Transonic Wind-Tunnel Wall Interference Assessment and Corrections; Newman, *et al.* [142],
- g) Wall Interference Assessment and Corrections; Newman, *et al.* [143].

Lynch, *et al.* [117] and Ashill [12], which appear in AGARD [5], review and summarise recent wall interference correction status and needs. Adaptive wind tunnel wall technology and applications have been reviewed recently in AGARD [4]. Also, a bibliography of wall interference work in the 1980's by Tuttle and Cole [178] cites many papers.

5.1.3 WALL INTERFERENCE/REYNOLDS SIMULATION TRADE-OFF IN MODEL SIZING

Currently, the issue of US wind tunnel modernisation is being addressed. A major thrust is attainment of near-flight Reynolds numbers. If large models are used, wall and sting interference are limiting factors in obtaining a tunnel flow even qualitatively resembling that of flight. In particular, testing at transonic speeds can produce steep wave fronts that reflect back on the model. Ventilated walls, porous and slotted, were developed to cancel blockage and allow testing through the transonic range, while porous walls, specifically, have been developed with the aim of cancelling these reflections. In spite of the

advances made in this technology as well as computational simulations, much still needs to be done to understand the trade-offs in sizing wind tunnel models and test sections to minimise wall and sting effects while maximising model Reynolds numbers. Key factors in this balance are shock-boundary layer interactions, and coupling of separation with laminar-turbulent transition. These as well as other highly Reynolds number-dependent phenomena affect whether the wind tunnel and the free flight flow resemble each other.

An extreme example of trade-offs between wall interference and required physical flow simulation was posed by the special requirements of the NASA supercritical, laminar flow control (LFC), swept-wing experiment (Harris, *et al.* [82]) conducted in the 8-Ft Transonic Pressure Tunnel (8-Ft TPT) at the Langley Research Center. Specifically, a proper simulation of an unbounded supercritical-flow condition about an infinite-span yawed wing of large chord at low noise and turbulence levels was desired. A transonic test condition was needed in order to establish the compatibility of an active LFC wing-suction system with the current high-performance, supercritical-airfoil technology. The LFC experiment had to be done in a wind tunnel that had levels of stream turbulence and acoustic noise approaching those of flight conditions so that the suction required to maintain laminar flow on the model was realistic. Conventional slotted or porous-walled transonic tunnels were inadequate in this regard; however, installation of screens and honeycomb, as well as closing the slots and choking the flow at the downstream end of the test section significantly reduced pressure fluctuations in the test section. Since transport aircraft envisioned for LFC applications have moderately swept wings of high aspect ratio where crossflow instability is the dominant transition mechanism, this instability must be investigated at appropriate flight crossflow Reynolds numbers. This requirement, together with the physical-size limitations set by slot-duct construction in the test panel and the required limitations on roughness-height Reynolds number for laminar flow, resulted in a large-chord swept-wing panel. In the 8-ft TPT, both the resulting ratio of tunnel height to model chord and the wing-panel aspect ratio are somewhat less than unity.

The liner designed by Newman, *et al.* [141] and constructed for the LFC experiment is characterised by its contoured shape of nonporous materials which produces a specified flow at the fixed transonic design or test condition. To produce a transonic wind-tunnel flow that simulates free-air flow about an infinite-span yawed wing, all bounding test-section walls had to be contoured. This contouring extended well into the existing tunnel contraction and diffuser in order to establish the flow and minimise loss of tunnel performance. The sensitivity of high-speed channel flows to the effective cross-sectional area-ratio distribution required viscous boundary-layer displacement corrections be made. This example illustrates the complex trade-offs that are needed in a useful wind tunnel simulation that can attempt to replicate flight conditions.

5.1.4 CORRECTABILITY

If the essential physics of the free field flow can be closely approximated by the wind tunnel, and if the fluid-dynamic phenomena on and near both the aerodynamic model and the tunnel walls are properly captured and described by the mathematical formulation, the test data are defined to be **correctable**. Determining the correctability envelope remains elusive due to our limited knowledge (particularly in the transonic regime) of separation, turbulence, transition, shock wave phenomena and non-linear flow physics. Kemp [104] introduced the concept of a correctable-interference transonic wind tunnel combining a capability for wall-interference assessment with a limited capability for wall control. In that paper, he demonstrated the feasibility of using experimentally measured data directly as boundary values for the assessment in lieu of more generally formulated but less accurate wall boundary conditions. He

anticipated that such principles, used in non-linear flow codes, would lead to an accurate assessment of the wall interference for transonic tunnels.

Quoting from Kemp [104], "This capability alone [accurate assessment], however, will not produce the desired result of eliminating wall interference as an error source in transonic wind-tunnel testing. The concept of the self-correcting wind tunnel (Goodyer [73]; Sears [162]; and, Ferri and Baronti [59]) which would exercise iteratively some form of controllable walls and the associated control logic to satisfy an interference-free criterion has been proposed by others. The difficulties envisioned in implementing and operating the self-correcting wind tunnel are significant. An alternate approach to the minimisation of testing errors due to wall interference, designated as the correctable-interference transonic wind tunnel, is offered here."

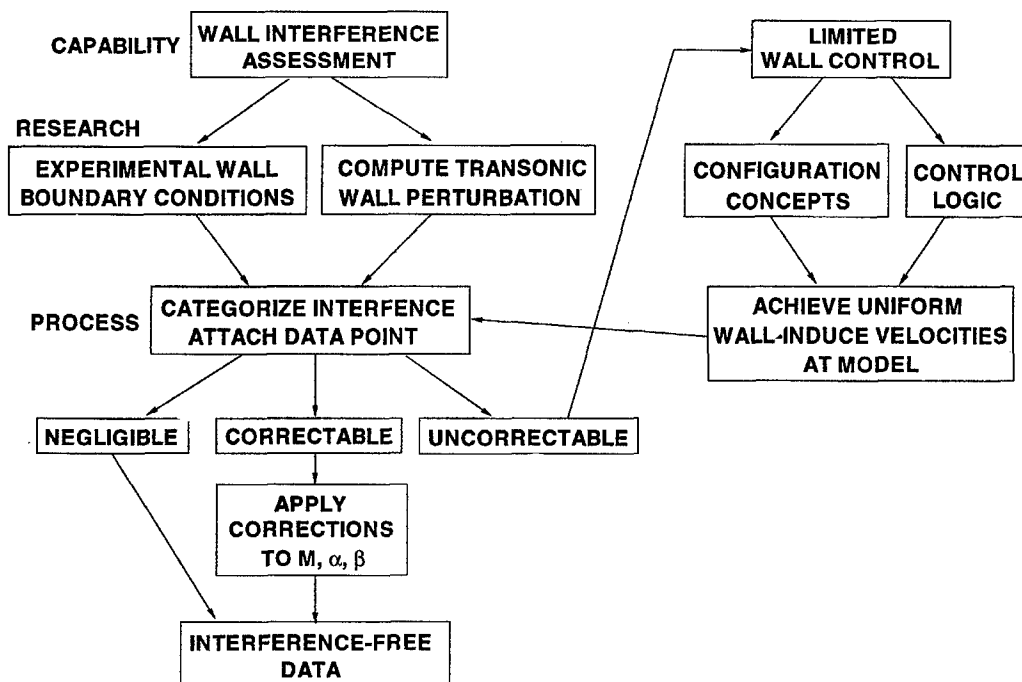


Figure 5.1 : The correctable interference transonic wind tunnel concept

"The correctable-interference transonic wind tunnel would combine the capability for assessment of wall interference with a limited capability for wall control. Four primary areas in which research is needed to achieve these capabilities are noted on Figure 5.1. The interference assessment capability would be used to categorise the interference existing at each test condition as negligible, correctable, or uncorrectable using criteria which could be adjusted according to the data accuracy required for the test. Wall control would be used only for those conditions assessed as uncorrectable and only to the extent necessary to achieve a correctable condition, thus the wall-control requirements are less restrictive than those for a self-correcting tunnel and possibly could be achieved with a simpler wall mechanism. The assessment and control capabilities would be combined to search out a test section configuration which maximises the range of test conditions falling in the negligible or correctable interference categories. This configuration would then become the standard fixed geometry test section used for the bulk of the wind-tunnel tests, thereby providing a high productivity rate. The results discussed in the preceding sections imply that the interference assessment and correction capability can be achieved using the data normally measured on a wind-tunnel model, supplemented by the survey over a control surface near the walls of

only a single flow parameter rather than the two independent parameters required for the self-correcting tunnel.”

Beyond the foregoing, correctability, which is a major issue for transonic testing will be not be discussed extensively here, except for Section 5.3.2.3.

This chapter will give some perspectives on transonic wind tunnel wall correction methodology. Modern computational fluid dynamics (CFD) methods will be reviewed, including augmentation of the interference prediction techniques with experimental measurements. An update of treatment of wall boundary conditions will be provided. These two topics will be addressed from the viewpoints of Arnold Engineering Development Center (AEDC), McDonnell Douglas and NASA Langley. It should be noted that wall boundary conditions remain the central issue in modelling transonic wind tunnel flows. To complement the CFD discussion, an overview of combined asymptotic and numerical (CAN, Combined **A**symptotic and **N**umerical) procedures will be provided. Finally, prospects for the future will be briefly indicated.

5.2 WALL BOUNDARY CONDITIONS FOR TRANSONIC FLOWS

To predict wall interference at transonic speeds, some sort of non-linear boundary value problem involving the gasdynamic equations of motion needs to be solved. For this problem to be properly posed, appropriate boundary conditions are crucial. Obtaining these conditions for the variety of ventilated walls used to mitigate shock reflections in transonic testing is challenging, and in some cases overwhelming, since the small-scale fluid-mechanical interactions can be quite complex, involving the effect of injection and suction in wall boundary layers leading to complex flow patterns. These are exemplified by return jets and vortical structures in perforated, slotted, and baffled slotted wind tunnels. The specification of boundary conditions is further complicated by the possibility of turbulence and coupling of flow and tunnel-wall boundary vibrations.

Obviously, a detailed solution of these small-scale flows may be impractical and not warranted in obtaining rapid assessments of interference by the test engineer. This view is clarified by formulating the wall interference problem as a multi-scale asymptotic problem in which one scale is the local flow near the wall ventilations, with a length comparable to wall openings; another is the main flow for a length scale comparable to the wall height, or characteristic model dimension. This approach is exemplified by matched asymptotic procedures used by Berndt [24] and others. In these models, only the far field boundary conditions of the ventilated wall boundary layer flow are important for the interference problem. Empirical methods and other techniques such as those developed by Mokry, *et al.* [133] which require pressure measurements near the walls have been proposed instead of these conditions. The latter are associated with the previously mentioned Wall Interference Assessment and Correction (WIAC) approaches. For large blockage situations associated with achieving high unit Reynolds near flight conditions, the nonlinearities and complexities of the wall and model viscous flows become important. Current integral and empirical methods of handling these cases will be subsequently covered.

The discussion that follows gives an overview of some procedures that are currently in use to formulate wall boundary conditions. Solid wall tunnels are discussed first, followed by the traditional porous and slotted wall geometries, and ending with the more recently developed baffled slot geometry. Related work on slotted wall design to minimise transonic interference and choking is also discussed.

5.2.1 NOMENCLATURE FOR SECTION 5.2

A	Area, also slotted-wall boundary condition coefficient (see equations 5-9 and 5-16)
B, B'	Slotted-wall boundary condition viscous coefficients
C_D	Discharge coefficient
C_L	Lift coefficient
C_M	Pitching moment coefficient
C_p	Local pressure coefficient
C_{ps}	Slot pressure coefficient
C_{pw}	Wall pressure coefficient
D	Measured (known) terms in boundary condition evaluation
D_F	Unknown (least-squares-fit) terms in boundary condition evaluation

d	Porous wall hole diameter or slot spacing
H	Tunnel height
h	Tunnel semi-height
K	Slotted-wall streamline curvature coefficient
k	Nondimensional slotted-wall streamline curvature coefficient, $= K \frac{d}{h}$
k_1, k_2, k_3	Interference factors
L	Wall hole length
m	mass flow rate
P	Local static pressure
q_∞	Freestream dynamic pressure
R	Classical wall porosity factor
T	Total temperature
t	Depth (thickness) of slotted wall
U	Inviscid edge velocity
V_n	Equivalent inviscid normal velocity
V_w	Wall crossflow velocity
u, v, w	Perturbation velocity components
α	Angle of attack
ΔP_w	Pressure drop across the wall
δ^*	Local boundary layer displacement thickness
ε	Orifice coefficient
η	Wall porosity
θ_s	Flow angle in slot
θ_w	Flow angle at wall
λ	Wall mass flux
ν	Prandtl-Meyer angle
ρ	Density
τ	Wall openness ratio, percent
ϕ_x, ϕ_y	Potential gradients
χ	Hole inclination angle

Subscripts:

ff	Far field
n	Normal to tunnel wall
te	Tunnel empty
w	At the wall
∞	At infinity or in the free stream

Abbreviations:

AEDC	Arnold Engineering Development Center
LaRC	Langley Research Center
MDA	McDonnell-Douglas Aerospace
NASA	National Aeronautics and Space Administration
NTF	National Transonic Facility
NWTC	National Wind Tunnel Complex
PSWT	Poly Sonic Wind Tunnel
TWT	Trisonic Wind Tunnel
WIAC	Wall Interference Assessment and Correction
WS	Weak supercriticality

5.2.2 SOLID WALLS

Transonic testing in solid wall wind tunnel facilities presents significant challenges to the engineer wishing to acquire quality aerodynamic data. In particular, as the test Mach number exceeds 0.87-0.90 for three-dimensional flows, and even much lower speeds for two-dimensional airfoils (depending on the thickness and lift), the effects of solid blockage due to an improperly sized model and its support system may severely limit or even prevent testing. For models sized in the 0.5-percent range, experience has shown that drag divergence may be significantly different than that obtained for a 0.25-percent blockage model. Furthermore, the wall-induced interference may be of such magnitude that the data are uncorrectable (i.e., no free air condition exists to which the data may be corrected).

In transonic flow with solid walls, wall viscous effects **must** be considered. At high transonic Mach number, interactions with the tunnel wall may be unstable due to shock wave impingement on the wall boundary layer. This interaction may cause the wall boundary layer to cyclically thicken and thin, and/or separate and reattach, yielding unsteady interference corrections to the supposedly steady aerodynamic data. Even when the shock does not impinge directly on the wall, the sensitivity of high Mach number flows to effective tunnel cross-sectional area changes requires that the wall-normal velocity be determined from the rate of change of the wall boundary layer displacement thickness. Typically, this normal-velocity boundary condition is zero for inviscid, flat solid walls and is approximated as such for low speed, incompressible flows. Wall viscous blockage due to the stagnation point near the model leading edge responds to the local model pressure field, appearing first as a thickening and then as a thinning of the wall boundary layer as the flow traverses the region. This phenomena effectively creates a nozzle which can reverse the normal effect of the pressure gradient on flat or mildly diverged walls. In other words, the corrections are opposite in sign to those normally obtained.

Several approximate treatments of the interaction of the model pressure field with the boundary layers on the solid sidewalls in an airfoil tunnel have been developed and used to obtain wall interference correction contributions. Basically, the effective-inviscid shape of the sidewall is no longer a flat reflection plane; the large pressure gradients due to the model are imposed directly upon the sidewall boundary layers resulting in appreciable nonplanar, effective-inviscid distortions and adversely impacting the desired 2-D symmetry. At low subsonic Mach numbers and for wide tunnels, this distortion is limited to a small region at the sidewalls. However, as the Mach number increases, this distortion can destroy the 2-D symmetry. At

places where the flow becomes mildly supersonic, generally a bubble between the forward sonic locus and the terminating shockwave, the flow characteristics are nearly perpendicular to the streamlines, permitting propagation of pressure disturbances directly across the tunnel from the sidewalls.

In a series of papers, Barnwell [18], Barnwell and Sewall [19], and Sewall [166] showed that a similarity rule can be derived and used, in lieu of a boundary condition, to approximate this sidewall influence. In this rule, a Mach number shift, which depends on the nominal test Mach number and tunnel-empty sidewall boundary-layer parameters at the model location, can be identified as a Mach number correction. This correction is generally of opposite sign to that normally expected in a solid wall tunnel. It was subsequently shown by Ashill [11] and Murthy [137] that this sidewall boundary-layer correction to the Mach number also depends on the model aspect (or tunnel width to model chord) ratio. These approximations are based on subsonic flow ideas and have been incorporated in a number of airfoil tunnel correction codes, even for mixed (transonic) flow. However, at high subsonic flow on modern blunt airfoils, the approximations may become invalid when the forward sonic point is very near the airfoil leading edge (see, for example, Gumbert, *et al.* [81]).

The interaction of the model pressure field with the boundary layers on solid walls in 3-D has been similarly approximated by Adcock and Barnwell [2] where it was found that the Mach number correction is relatively less than in 2-D, but still appears to be of opposite sign than that expected for solid walls. That is, the tunnel appears to be more open around the model than what is indicated by the conventional solid (closed) wall correction. The phenomena is also very important in semi-span model testing at high subsonic and transonic Mach numbers; however, it appears that these sidewall boundary-layer approximations have not been used. Instead, one attempts a more rigorous CFD solution for the interaction as will be discussed in section 5.3.1.5.

Ashill's method applied to a three-dimensional, high-transonic Mach number experiment (Ashill *et al.* [14]) necessarily included the wall-normal velocity computed from the tunnel wall boundary layer to extend the method to a freestream Mach number of about 0.9. This application represents the extreme upper limit for linear methods applied to weakly supercritical (Group 1) flows; while the transonic Laminar Flow Control Experiment (Harris, *et al.* [82]) with a completely three-dimensional aerodynamically- and viscous-contoured tunnel liner (Newman, *et al.* [141]) represents a case for highly supercritical (Group 2) flows.

Because transonic open jet tunnels are unsteady and have large power requirements; because solid wall tunnels are very sensitive to area change at high Mach number; and, because the flow in both open jet and solid wall tunnels yield physically inappropriate flow solutions which have corrections of opposite sign, the aerodynamicist must resort to wind tunnels with either ventilated walls or those which have an adaptive capability. A discussion of adaptive wall boundary conditions and technologies is presented in detail in Chapter 10. The remainder of Section 5.2 will discuss boundary conditions applicable to porous wall, slotted wall, and baffled-slotted wall wind tunnels.

5.2.3 POROUS WALLS

5.2.3.1 McDONNELL-DOUGLAS POROUS WALL BOUNDARY CONDITION

Numerical simulation of wind tunnel flow fields in a ventilated transonic test section requires proper modelling of the walls. This is particularly true for transonic wind tunnel wall interference correction. Several current concepts for predicting or correcting ventilated test section data for wall interference

involve the numerical simulation of an aircraft model in the wind tunnel, and in free-flight (Crites [41]; Rueger and Crites [160]; and, Sickles and Erickson [168]).

As pointed out in the literature (Kraft [107]; and, Rueger and Crites [160]) precise agreement between computed model pressure distribution (or forces) and measured values is not necessary in order to obtain accurate corrections. The corrections are based on the difference between two solutions, with the simulation of the aircraft model common to both. Significant error in the simulation of the model will be minimised.

The same is not true for simulation of the tunnel wall. The effect of the wall is precisely the object of the exercise. Errors in modelling its interaction with the main flow are reflected as errors in the correction. The degree of fidelity required in modelling the ventilated wall depends on the type of wall, and how strongly the aircraft model flow field interacts with it. There is evidence that for a relatively large tunnel with a relatively small model, the classical linear wall boundary condition

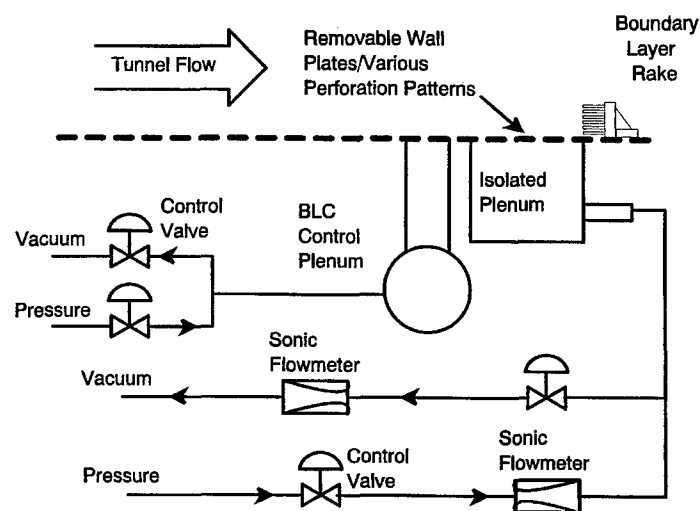
$$R\phi_x + \phi_y = 0$$

is adequate (Kraft [107]; Phillips and Waggoner [149]; and, Steinle [174]). In such cases all that is necessary is the determination of R at the wall pressure ratio characteristic of normal operation (Matyk and Kobayashi [127]).

Smaller transonic tunnels (such as the McDonnell Douglas Aerospace 4-foot x 4-foot PSWT) use relatively large models to reduce model infidelity and improve Reynolds number simulation. As a result the model flow field interacts more strongly with the wall. The linearised wall flow boundary conditions fail to provide useful interference corrections. It seems likely that this is also true for larger tunnels when testing very large models.

5.2.3.1.1 EXPERIMENTAL SET-UP

The wall flow boundary condition was determined from experimental data taken on a set of ventilated plates simulating various transonic walls. This effort was conducted in the 1x1-ft. transonic test section of the MDA Trisonic Wind Tunnel (TWT). (Note: Similar experiments were conducted by Freestone and Henington [61].) Figure 5.2 illustrates the basic set-up. A can (isolated plenum) within the transonic



plenum is attached such that various test plates (ventilated wall samples) can be mounted flush with the transonic wall. The flow into or out of the can is controlled and measured by sonic flowmeters. A dozen taps are located over the face of the test plate to record the static pressure distribution. Just upstream of the test plate, several rows of perforated holes in the tunnel wall were connected to a manifold and used to apply suction or blowing to alter the approaching boundary layer.

Figure 5.2 : Wall Cross-Flow Test Set-Up

Figure 5.3 defines the geometry of the five test plates evaluated. The first of these is the same 22.5% perforated wall used in the 1-ft. tunnel. The second represents the wall of a 4x4-ft. blow down tunnel scaled according to boundary layer displacement thickness typical in the two tunnels. Plates 3 and 4 are also 22.5% porosity, but hole diameter and plate thickness differ. Plates 1 through 4 are typical of the design previously investigated by Chew [36]. Plate 5 is a 6% porous, 60-degree inclined hole design typical of the transonic walls investigated by Jacocks [88].

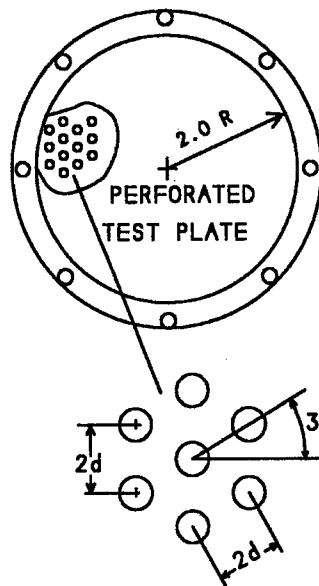


PLATE	d	L	η	θ
1	.125	.125	.225	0
2	.150	.300	.225	0
3	.062	.125	.225	0
4	.062	.300	.225	0
5	.125	.250	.060	60

NOTES: L IS HOLE LENGTH WHICH IS PLATE THICKNESS, EXCEPT FOR PLATE NO. 5.

PLATE 5 HAS 60 DEG. INCLINED HOLES.

HOLE PATTERN FOR PLATES 1 - 4

Figure 5.3 : Wall Cross-Flow Test Plates

5.2.3.1.2 EXPERIMENTAL PROCEDURE

The test was designed to measure wall crossflow as a function of wall pressure. Variables were Mach number, Reynolds number, boundary layer thickness, hole diameter, wall thickness, and hole inclination angle. Admittedly, some of these variables were not exercised very extensively. For instance, there were only two hole inclination angles tested, and the inclined hole data were for only one hole diameter and wall thickness.

There were two parts to the test. The first involved determining the boundary layer characteristics of the flow at the upstream edge of the test plate. This was done by mounting a boundary layer rake (of total pressure tubes) at the leading edge of the test plate and exercising total pressure and Mach number to cover the test range. Some measurements were taken with typical levels of blowing from the test plate to see if the effects would propagate forward and invalidate the rake data. During this portion of the test, crossflow data were not taken due to interference from the boundary layer rake. During the second portion of the test the boundary layer rake was moved downstream and used to measure boundary layer characteristics of the flow at the downstream edge of the test plate. Wall crossflow data were acquired during this portion of the test.

A full discussion of this effort, including the development of a mathematical model of the wall crossflow process was reported in the literature (Crites and Rueger [42]). Only highlights of this effort are included here.

5.2.3.1.3 AIR-OFF RESULTS

Wall crossflow was measured for blowing and suction with no primary tunnel flow. The results for the various plates were correlated according to the relation

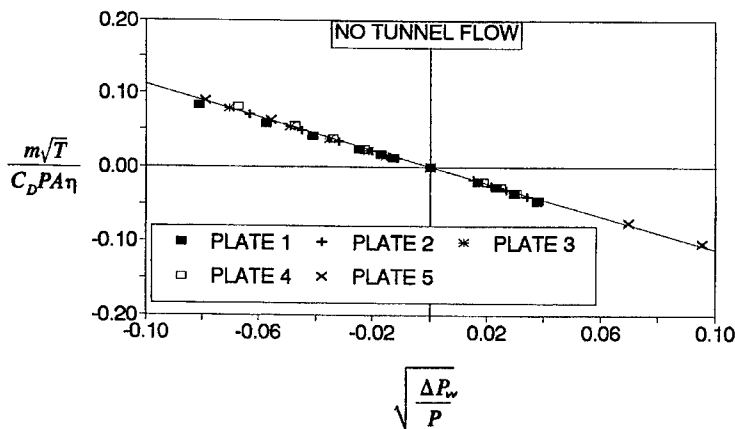


Figure 5.4 : Cross-Flow Characteristic (No Tunnel Flow)

$$\frac{m\sqrt{T}}{C_D P A \eta} = K \sqrt{\frac{\Delta P}{P}}$$

The theoretical value of K is -1.098 for the chosen sign conventions. The value providing the best fit to the data for all five plates is -1.112 . The results are shown in Figure 5.4. The discharge coefficient, C_D , values for each plate were experimentally determined and range from about 0.7 to 0.8.

5.2.3.1.4 AIR-ON RESULTS

For air on, it is common to normalise the crossflow by the freestream condition. The normalised crossflow velocity is defined as

$$V_w = \frac{(\rho v)_w}{(\rho U)_\infty}$$

and the wall pressure coefficient is given by

$$C_{pw} = \frac{\Delta P_w}{q_\infty}$$

When comparing different wall configurations, it becomes obvious that C_{pw} is not adequate to correlate the crossflow characteristics. Figure 5.5 shows the crossflow characteristics of all five test plates at Mach 0.6. Although the characteristics are well defined, there is not a high degree of correlation.

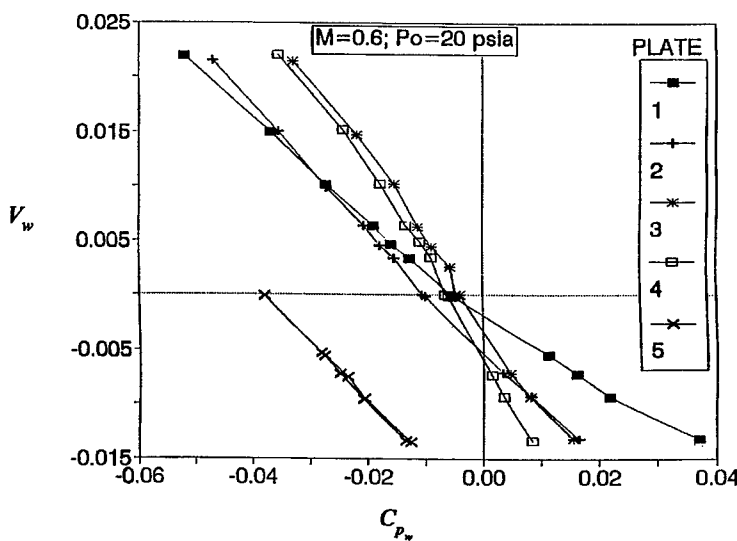


Figure 5.5 : Cross-Flow with Tunnel Flow

Figure 5.5 shows the crossflow characteristics of all five test plates at Mach 0.6. Although the characteristics are well defined, there is not a high degree of correlation.

Based on physical reasoning, a new independent variable was defined. Specifically

$$C_{p'} = C_{pw} \sqrt{\frac{\delta^*}{d}}$$

Further investigation revealed that the physical process in the individual holes is different for outflow (suction) than inflow (blowing). In suction, the flow

pulled into the holes carries considerable x -momentum. This leads to an impact pressure on the downstream side of the holes that is considerably above local static pressure. This forces some flow through the holes, but also creates a circumferential flow that results in a fountain near the upstream edge of the holes — ejecting air back into the freestream. In the absence of a pressure drop across the wall, viscous entrainment of the air in the holes causes an offset in the crossflow characteristic. That is, $V_w < 0$ when $\Delta P_w = 0$.

In blowing, plenum air with very little momentum is ejected into the freestream. Since the velocity in the plenum is very small, no x -directed momentum is carried into the hole, and the crossflow characteristic is changed. In addition, it is necessary to account for the differences in relative edge sharpness due to the hole size and fabrication method. This was done by including the discharge coefficient, C_D , obtained for the no-tunnel flow condition.

Other factors considered were, the effects of hole inclination, and the offset in V_w at $C_{pw} = 0$. The final result was a correlation which collapses the data for all five perforated plate geometries. For $V_w > 0$, this correlation is

$$\frac{V_w}{\eta C_D \cos^2(\theta)} = a_1 \Delta C_p + b_1 \sqrt{\Delta C_p}$$

with $a_1 = -1.557$, $b_1 = -0.2242$. For $V_w < 0$, the correlation is

$$\frac{V_w}{\eta C_D \sqrt{\frac{L}{d}} \cos^2(\theta)} = a_2 \Delta C_p + b_2 \sqrt{\Delta C_p}$$

with $a_2 = -2.047$, $b_2 = -0.0304$, and

$$\Delta C_p = C_{p'} - C_{p'}|_{V_w=0}$$

Note that for blowing, $V_w > 0$, the quadratic dependence on pressure is much greater than for suction, $V_w < 0$.

Figure 5.6 shows data from all five perforated wall designs for Mach 0.6. The correlation given successfully collapses the entire data set.

V_w , the wall crossflow, is not the correct boundary condition for an inviscid flow solver. The displacement effect of the boundary layer must be included. The equivalent normal velocity (flow angle) at the wall surface, V_n , is needed. Conservation of mass for an elemental control volume at the wall surface requires that

$$V_n = V_w + \frac{1}{(\rho U_\infty)} \frac{d(\rho U \delta^*)}{dx}$$

where density variations are ignored because, typically, they are small, except for strong shocks at the wall.

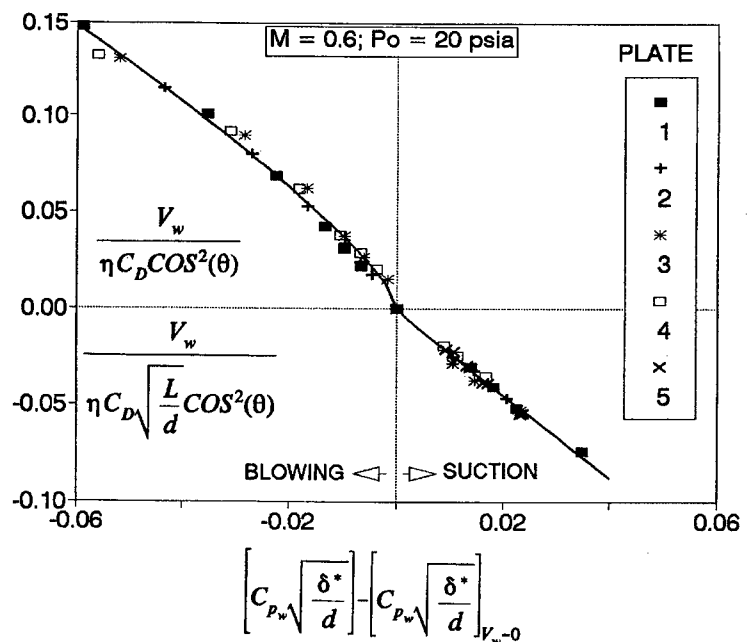


Figure 5.6 : Cross-Flow Characteristic Correlation

The well known incompressible relation,

$$C_p = -2\phi_x$$

can be used with good accuracy for typical transonic wall region flows to eliminate U in favour of C_p . The result is

$$V_n = V_w + \frac{d\delta^*}{dx} - \frac{\delta^*}{2} \frac{dC_p}{dx}$$

V_w is known from the measured mass flow through the wall. The gradients in δ^* and C_p are computed from measured boundary layer and wall pressure data.

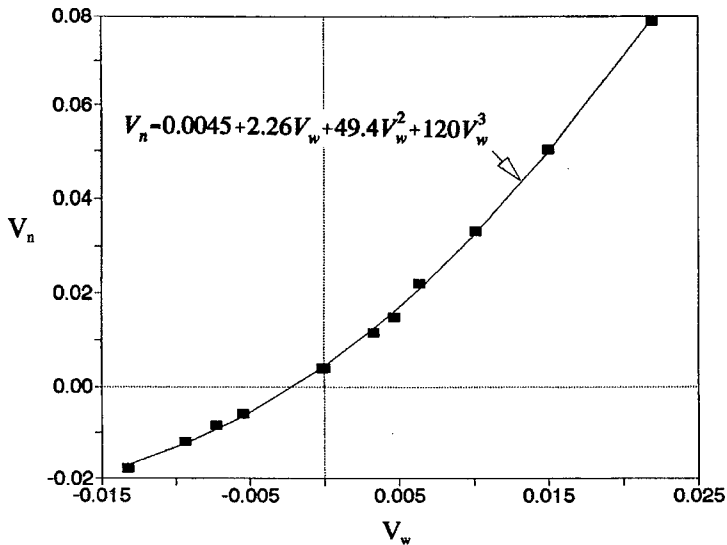


Figure 5.7 : Effective Normal Velocity versus Cross-Flow

The result allows the calculation of V_n corresponding to the crossflow, V_w , mean pressure coefficient, C_{pw} , and mean boundary layer thickness, $(\delta^* + \delta_1^*)/2$. As shown in Figure 5.7, V_n correlates directly with V_w . Specifically,

$$V_n = a_0 + a_1 V_w + a_2 V_w^2 + a_3 V_w^3.$$

This direct dependence of V_n on V_w has been noted by others (Agrell [6]; and, Barnwell [20]). The relationship seems very robust. In fact the same dependence can be deduced from published data (Baronti, *et al.* [22]) for laminar boundary layers with transpiration at the wall.

Note that

$$\frac{d\delta^*}{dx} = V_n - V_w + \frac{\delta^*}{2} \frac{dC_p}{dx},$$

completes a set of equations that can be solved numerically for the unknown values V_w , δ^* , and $V_n(x)$.

Solution presumes that values of measured, or interpolated wall pressures are available on two-dimensional strips running the length of the test section. The number of strips depends on the CFD grid, or panel distribution simulating the wall. In addition, starting values of displacement thickness at the test section inlet, δ_0^* , must be known. With these starting conditions any of a number of numerical techniques can be used to march the solution downstream. A conventional Runge-Kutta integration scheme is used to obtain solutions.

Figure 5.8 shows typical results for the ceiling centreline for a recent wind tunnel test. Note that the desired boundary condition, V_n , is different than the crossflow V_w .

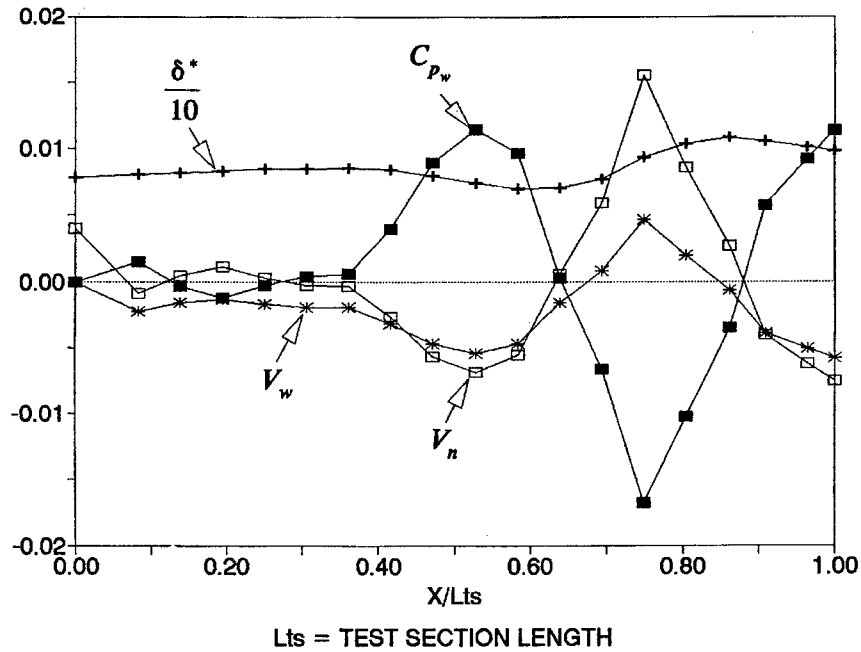


Figure 5.8 : Typical wall boundary solution computed on centreline

5.2.3.2 AEDC PERFORATED-WALL BOUNDARY CONDITION

Perforated walls have been shown to be effective in minimising wall interference and have allowed testing through the transonic regime. On the other hand, they have introduced the enormous challenge of characterising the wall behaviour and correcting the test article data for the remaining wall interference. Requirements for larger test articles and higher quality data make the challenge more difficult and more critical. To precisely compute the wall interference effects using modern CFD techniques, an accurate model of the wall behaviour is essential. In addition, the wall model must provide stable and robust results when incorporated as a boundary condition in a numerical algorithm. The challenge of developing an accurate wall model is particularly difficult at transonic conditions where the wall behaviour is dependent on a complex relationship of local flow conditions. Classical definitions of the wall behaviour for perforated walls (Garner, *et al.* [67], Pindzola and Lo [151]) have been shown to be inadequate at transonic speeds for the aforementioned requirements.

Classical perforated wall boundary conditions assume a fixed global and homogeneous description of the wall characteristic, which is defined as the ratio of the pressure coefficient difference across the wall to the flow angle at the wall. Because the hole diameter of the perforations is small compared to the tunnel dimensions, the local effect of the discrete holes diminishes rapidly, and homogeneity is a reasonable assumption. However, the measurements made by Jacocks [88] of the local flow properties in the vicinity of perforated walls indicate that a fixed global specification of the wall characteristics is not adequate and that local specification is necessary. This is particularly important at transonic conditions and for large test articles where the wall gradients are large and the local flow properties change drastically. The data in Jacocks [88] show that the boundary-layer displacement thickness is one of the most important parameters to consider when quantifying the wall characteristic. Because of the large gradients at the wall generated by the test article, there is significant spatial variation in the boundary layer displacement

thickness within a perforated wall test section. Therefore, the challenge reduces to defining a wall characteristic in terms of the pertinent local variables.

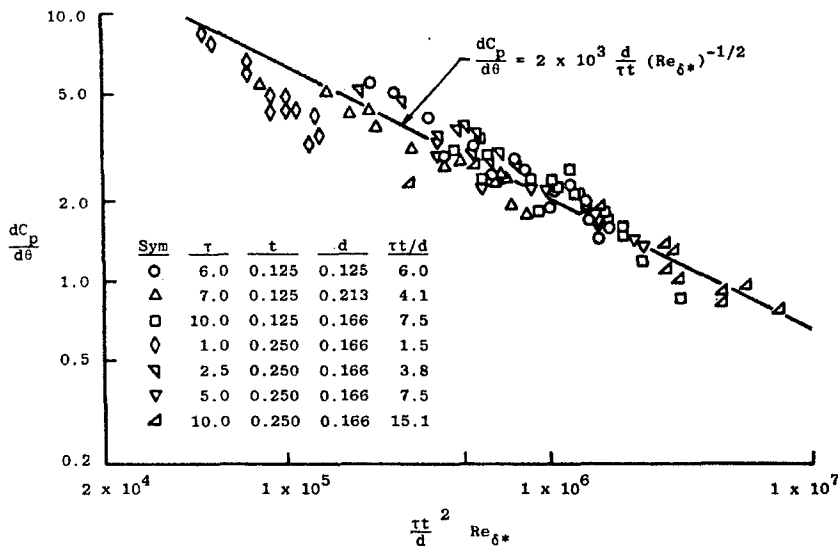


Figure 5.9 : AEDC perforated-wall displacement thickness correlation

For the AEDC perforated walls, having perforation holes inclined 60° from wall-normal direction, Jacocks [88] has found an empirical crossflow characteristic illustrated in Figure 5.9. The homogeneous pressure coefficient at the wall, expressed as a function of the local flow angle has the approximate slope

$$\frac{dC_p}{d\theta} = 2000 \frac{d}{\tau t} Re_{\delta^*}^{-1/2} \quad (5-1)$$

where t is the wall thickness, d is the hole diameter, τ is the wall open area ratio in

percent, C_p is the pressure coefficient difference across the wall and Re_{δ^*} is the unit Reynolds number based on δ^* , the boundary-layer displacement thickness. It should be mentioned that Reynolds number was not an independent variable in the experiments discussed in Jacocks [88]. Therefore, the correlation may not be universal. However, the correlation is descriptive of the observed behaviour for AEDC perforated walls as Reynolds number is changed, *i.e.*, as Reynolds number increases, the perforated wall behaves as if it were more open (Jacocks [88]).

In order to incorporate this empirical correlation into the solution of the tunnel flow field, the boundary-layer displacement thickness on the wall must be calculated. To compute the boundary-layer displacement thickness on the perforated wall in an inviscid flow-field calculation, an approximate technique has been devised using insight gained from previous computations with a more exact method (Whitfield [182]). The continuity equation in integral form may be written as

$$\frac{1}{\rho u} \frac{d}{dx} (\rho u \delta^*) + \theta - \lambda = 0 \quad (5-2)$$

where λ is the wall mass flux defined such that outflow from the test section is considered positive, ρ is the density and u is the component of the velocity in the freestream direction. In principle, to solve (5-2), a streamwise momentum equation is needed. However, previous computations of permeable wall turbulent boundary layers in Jacocks [88] and Erickson and Homicz [52] indicate that the flow angle and wall mass flux are nonlinearly related and can be expressed as

$$\theta - \lambda = 0.125 \theta [4 - \theta (55 + 250 \theta)] - 0.002 \quad (5-3)$$

The correlation of (5-3) can then be used to integrate (5-2) and determine the distribution of δ^* . Initial upstream conditions for the boundary-layer calculations are provided by a correlation of data from three transonic wind tunnels at AEDC. The correlation, shown in Figure 5.10, relates the displacement thickness at the test section entrance to Reynolds number and tunnel size as

$$Re_{\delta^*} = 0.11 Re_H^{4/5} \quad (5-4)$$

where H is the tunnel height.

This wall model has been successfully incorporated as a boundary condition into several flow solvers. The boundary condition has been shown to be both stable and robust. It should be emphasised that the far-field tunnel flow field is solved inviscidly using Euler equations while the test-article near field can be solved using either Euler or Navier-Stokes equations depending on the importance of near-field viscous effects. This boundary condition has been successfully applied at AEDC for steady subcritical and supersonic flows at subsonic freestream Mach numbers (Donegan, *et al.* [47], and Sickles and Erickson [167], [168]) and for low supersonic freestream Mach numbers (Martin [126]).

The wall model is incorporated in a time marching algorithm as follows. Using the distributions of ρu and θ at the walls, which are supplied by the inviscid numerical solution, the boundary-layer displacement thickness δ^* is calculated, the local wall characteristic is determined from (5-1), and the wall pressure P_w is computed as

$$P_w = P_\infty + q_\infty \theta \frac{dC_p}{d\theta} \quad (5-5)$$

where q is the dynamic pressure, C_p is the pressure coefficient and ∞ subscripts refer to freestream conditions. The wall pressure is then incorporated into a CFD flow solver as a boundary condition by specifying the internal energy e at the walls to be

$$e = \frac{P_w}{(\gamma - 1)} + \frac{1}{2} \rho (u^2 + v^2 + w^2) \quad (5-6)$$

where v and w are velocity components perpendicular to u , and γ is the specific heat ratio.

The wall boundary condition is updated at each iteration in the numerical solution based on the most recent calculation of the flow parameters.

The conclusions drawn from the work of Jacocks are confirmed by the results of Crites and Rueger [42]. They, through separate experiments, developed a similar wall model. Figure 5.11 shows a comparison between the boundary-layer amplification factors λ from (5-3) for the two correlations. The agreement is excellent within correlation range ($-0.02 < \theta < 0.02$ radians) but differ at larger flow angles. For large models, the flow angles may extend beyond the correlation range and additional effort and data must be obtained to extend the correlation with confidence.

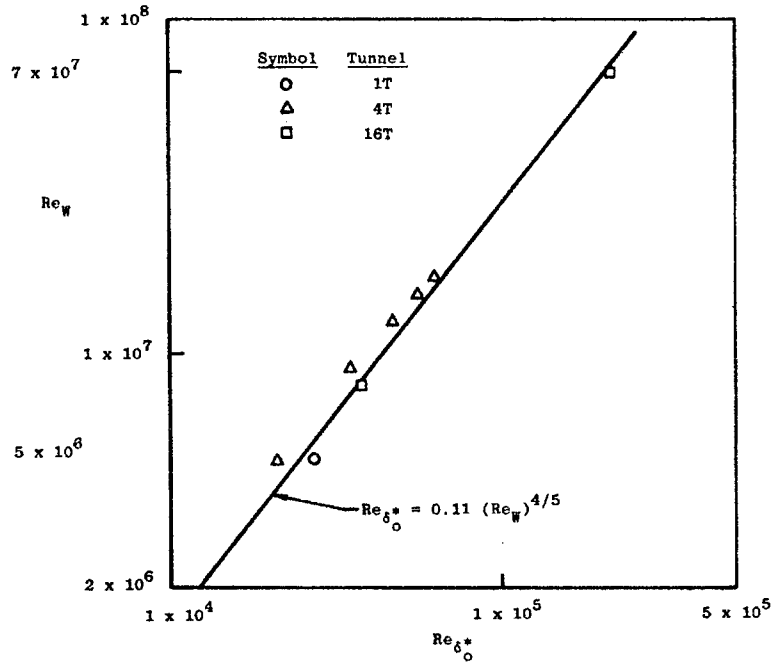


Figure 5.10 : Test section entrance characteristic correlation data

(Donegan, *et al.* [47], and Sickles and Erickson [167], [168]) and for low supersonic freestream Mach numbers (Martin [126]).

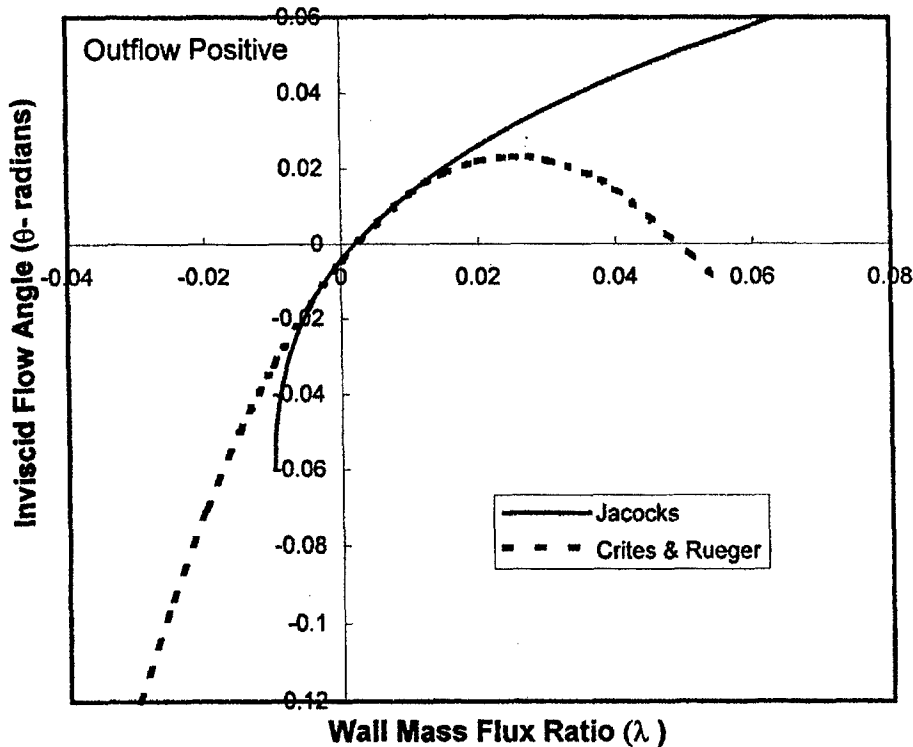


Figure 5.11 : Inviscid flow angle versus wall mass flux ratio

5.2.3.3 FREESTONE POROUS WALL STUDIES

In solid wall tunnels, measured boundary flow variables are relatively easy to obtain, with longitudinal velocities determined from pressure measurements and normal velocities prescribed as zero. A higher-order specification of the normal velocity may be obtained, if required, by computing the effect of the wall boundary layer. However, significant challenges arise when making boundary measurements along ventilated, transonic walls because the wall pressure there is, typically, not a good, average (or homogeneous) representation of the rapidly varying flow near and through the wall, and devices such as rails or pipes must be used to obtain pressures which are unaffected by the localised effects of the wall geometry (see Chapter 4). Additionally, the normal velocity measured in open regions near the wall is highly dependent on the details of the wall-ventilation geometry and the wall viscous effects, and it must somehow be related to the far field average of the close-wall neighbourhood. In spite of these and other difficulties, the success of the two variable, boundary-measurement method of Ashill and Weeks [13]; (see, also, Chapter 4 in AG-336) for interference correction in solid wall wind tunnels prompted Freestone, Gascoigne, and Lock [63] to investigate its transonic extension to a tunnel with a single 6-percent-open wall with uniformly-distributed, 60-degree inclined perforations. A NACA 0012 airfoil at zero lift was used as the disturbance model. Static pressure measured along lines on the walls were assumed *sufficiently* close to the far field average to yield accurate values of the streamwise velocity—no further accuracy assessment was given. Correlation experiments (Freestone and Henington [61]) were conducted to characterise the normal velocity variation with wall pressure drop (wall pressure minus plenum pressure) and boundary layer displacement thickness. Consistency checks between the measured and calculated values of boundary-layer displacement thickness revealed significant discrepancies for the blown boundary layer which occurs for tunnel inflow conditions. For these regions,

predictions underestimated the measured growth rate by a factor of two to three, requiring an empirical velocity correction for these effects. The corrected boundary data were then used as input to Ashill's method to obtain Mach number and upwash distributions on the tunnel centreline which, then, were used to correct the airfoil test data. Comparisons between the tunnel data and free-air computations and comparisons with that acquired in a large tunnel were generally good, implying that the application of the correction technique in ventilated tunnels is feasible.

5.2.4 SLOTTED WALLS

The reader is referred to Chapter 3.2 and Figure 3.3 for a general discussion of the slotted wall and its geometry. For slotted walls, the associated geometric length scales are the slot width, a , the slot spacing, d , and the tunnel semi-height, $h=H/2$. Historically, an infinite number of longitudinal slots are assumed when developing the wall geometry model, while inviscid flow is assumed for the fluid-dynamic model. This leads to the relatively simple forms of the boundary condition given by equation (3.9), and classical solutions have been developed accordingly (for example, Davis and Moore [46]). The inability of the classical boundary condition to properly account for wall effects at transonic Mach numbers, under high-lift test conditions, and for large wind tunnel models has been particularly evident since the advent of computational fluid dynamics where significant discrepancies were revealed between computation and experiment. As with porous wall boundary conditions, the impact of wall viscous effects have been recognised as significant and an area where much research needs to be conducted. The importance of the boundary-layer displacement thickness, δ^* , as a viscous length scale, has become increasingly apparent, and other scales may exist for the low-energy flow re-entering the test section downstream of the model. This section summarises recent slotted-wall boundary condition research beyond the classical approach presented in Chapter 3, particularly, as applied to wind tunnel testing at transonic Mach numbers.

5.2.4.1 FREESTONE SLOTTED WALL STUDIES

Freestone successfully applied Ashill's method (see Chapter 4) to porous wall tunnels (see section 5.2.3.3) and, then, investigated its application to tunnels with slotted walls. In ventilated-wall tunnels, the experimentalist has the difficult task of measuring the two flow variables directly, such as u and v (via pressure and flow direction, respectively), or measuring a single flow variable and obtaining the other using a theoretical representation of the boundary condition—both methods were evaluated by Freestone, Mohan, and Lock. Their initial, verification study (Mohan, *et al.* [132]) was in a low-speed, two-dimensional tunnel where they chose the latter approach. Longitudinal velocities at the boundary were determined from the wall pressures measured on the slot centreline, and normal velocities were determined from the pressure drop across the tunnel wall using the wall boundary condition developed by (Berndt [24], see section 5.2.4.2). They extended the validation in Freestone *et al.* [64] to two-dimensional flow about an airfoil in the Mach number region covering 0.5 to 0.85. The tunnel was equipped with four 20-percent-open slots each in the top and bottom walls. As in the earlier study, they obtained values of normal mass flux through the slot from Berndt's theory; however, they also evaluated the use of measured normal slot mass flux obtained using flow angle probes. Two significant conclusions were that accurate tunnel-centreline interference distributions may only require normal slot velocity measurements to within 10-percent of their maximum, and that slot velocity distributions may adequately be determined with only a limited number of measurements in each slot. Further two-dimensional work

presented by Freestone and Mohan [62] indicates that, in some situations, wall-interference corrections determined by averaging slot flow measurements can be significantly different from those determined using the Berndt theory. These differences are the result of an incomplete understanding and modelling of the wall viscous effects in regions of low-energy inflow from the plenum; they are not unlike those effects noted at a perforated wall where inflow, also, amplifies the boundary-layer growth rate. Wall velocity magnification factors of 4 to 5 in the inflow regions were required to produce agreement between predicted and observed model pressure distributions. Finally, Mohan and Freestone [131] extended the Ashill method to three-dimensional, low-speed flow in a slotted-wall tunnel about a 25-degree swept, sidewall-mounted wing. The tunnel was equipped with four, 15-percent-open slots each on the top and bottom walls. Slot flow measurements were obtained with a pitch/yaw probe traversed along each slot centreline, while pressure measurements were obtained on the slat centres. Comparing their results with data on the same model acquired with solid walls (also corrected by Ashill's method) allowed them to report correction accuracies of the order 0.05° in upwash and 0.002 in blockage. However, these levels of accuracy were achieved in experiments where low-energy inflow was avoided.

5.2.4.2 BERNDT BOUNDARY CONDITION AND IMPLEMENTATION

Berndt and Sørensen [26] derived the two-dimensional, homogeneous-wall boundary condition

$$C_{pw} - C_{ps} = 2 \frac{\rho U}{\rho_\infty U_\infty} dK \frac{\partial \theta_s}{\partial x} + \frac{\rho}{\rho_\infty} \theta_s^2 \quad (5-7)$$

by integrating the pressure along a two-dimensional spanwise path from the centre of the slat to and through the slot and into the plenum. The analysis neglected shear stress contributions and estimated the value of the slotted-wall performance coefficient K from an inviscid analysis similar to that of the classical Davis and Moore theory [46] but with allowances for the effect of slot depth (wall thickness). The resulting equation essentially combines the functional forms of Davis and Moore with that of Wood [185] who described the wall pressure-drop condition using only a quadratic crossflow term. Transonic validation experiments were conducted at $M=0.903$ with a circular arc airfoil and oil flow visualisations,

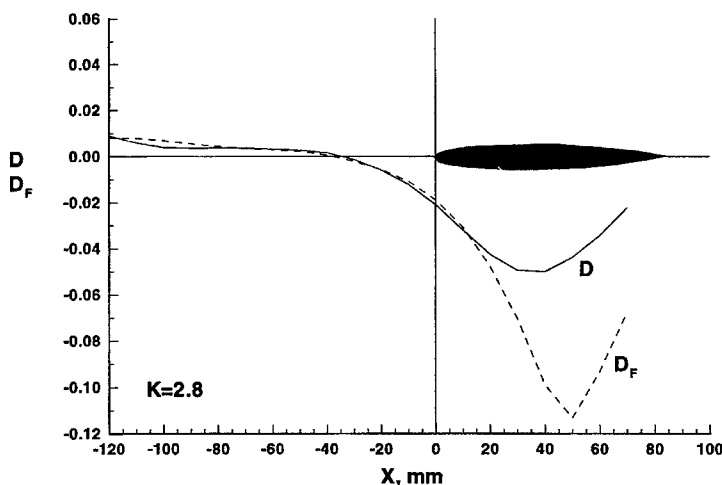


Figure 5.12 : Comparison of Berndt's theoretical two-dimensional, slotted-wall boundary condition with his experimental results for $M=0.903$. D is the measured wall pressure drop (see equation (5-8a)) and D_F is the theoretical fit of the wall pressure drop (see Equation (5-8b)).

flow angles, and pressure measurements were obtained in the slot region. A comparison between theory and experiment using data obtained from Berndt and Sørensen [26] is presented in Figure 5.12 where D and D_F are given by

$$D_F = 2 \frac{\rho U}{\rho_\infty U_\infty} dK \frac{\partial \theta_s}{\partial x} \quad (5-8a)$$

and

$$D = C_{pw} - C_{ps} - \frac{\rho}{\rho_\infty} \theta_s^2 \quad (5-8b)$$

The theoretically-determined value of K used in the comparison is 2.8. The airfoil model extends from tunnel station 0 mm to station 90 mm. For outflow through the slots to the plenum

chamber, reasonable agreement between the theory and experiment was achieved upstream of the maximum model-thickness position; however, downstream of this position where the flow returned to the tunnel through the slots and where the effects of viscosity are large, only a few measurements with large uncertainties were obtained and the agreement is poor.

Based on the success of the upstream comparisons and the insight developed from the experimental data, Berndt [24] extended his inviscid theory to three-dimensional walls with a few, narrow slots. The extension used matched asymptotic expansion theory combined with slender-body crossflow theory to develop inner (or near field) and outer representations of the slotted-wall flow field. The resulting family of boundary conditions are local in the sense that variations in slot geometry and plenum pressure are captured in the inner flow representation. The original formulation was developed for axisymmetric flows which are homogeneous in the sense that the slot outer representations are averaged to yield a much simplified wall boundary condition. This simplified boundary condition yields nearly the same result in the vicinity of the model as would be obtained with a full, detailed representation of the wall.

In 1979 Karlsson and Sedin implemented Berndt's boundary condition in a transonic small disturbance code for constant width slots, and then extended this in 1980 to slots with varying width. Their goals were 1) to use the boundary condition to examine the slotted wall interference on axisymmetric models in axisymmetric tunnels at high Mach numbers ($M=0.96-0.98$) and 2) to design minimum interference slot geometries using an inverse design method. For these flow conditions, the slot geometry and the magnitude of the interference was very sensitive to body geometry and Mach number. Added slot mass flux due to the growth of the wall boundary layers was approximated assuming a turbulent flat plate boundary layer on the slats and these effects were found particularly important and large on the downstream, inflow region, as was observed in the two-dimensional studies. In the downstream region the predicted slot openness was significantly increased over the inviscid, geometric value. The computations were further extended in 1982 by Sedin and Karlsson [164] to asymmetric flow conditions for slender, lifting, delta wings in wind tunnels with constant width slots. The computations showed that negligible pressure interference was difficult to obtain when models were sized to achieve acceptable model Reynolds numbers. Predictions of linear theory were verified in that lift and drag interference were separately minimised for different slotted wall geometries, and that lift interference was reduced when the top-wall slots were opened to larger values than those on the bottom wall. More detailed, but still simple, approximations of the slot viscous effects were included by Sedin and Karlsson [165] via the use of two slot reduction coefficients for the stream-wise slot velocity and the narrowing of the slot width. Rational selection of the coefficient values was based on experimental data and very promising comparisons between computations and measured wall pressure data were presented for freestream Mach numbers of 0.90, 0.95, and 0.98 for 2.23% blockage, axisymmetric models tested in octagonal tunnels, for both shallow (19 mm) and deep (52 mm) slot configurations. As a measure of efficiency, the deep slots were able to maintain a larger pressure difference across the wall than the

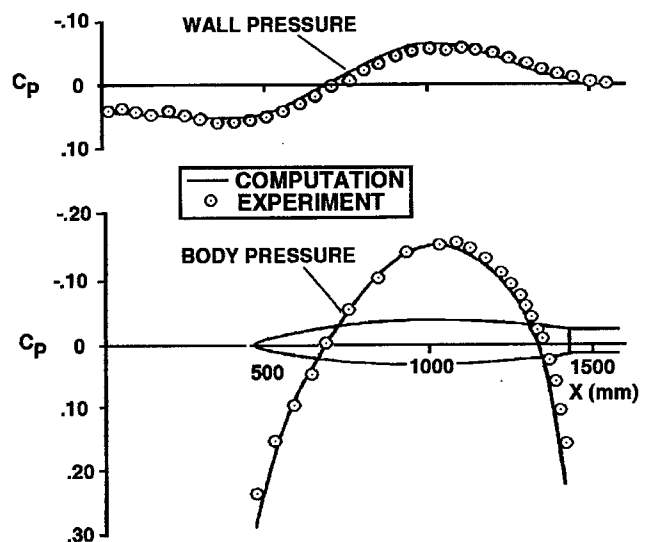


Figure 5.13 : Comparisons of Berndt's three-dimensional slotted-wall boundary condition including viscous slot flow losses with experiment for $M=0.9$. Deep slot configuration.

shallow slots. Comparison results between the experiment and the computationally determined pressures on the walls and model are presented in Figure 5.13.

Berndt's boundary condition was extended to nonaxisymmetric tunnel geometries by Sedin, *et al.* [163]. Significantly, it loses the property of homogeneity but remains much simpler than solutions which model the details of the slot geometry. Agrell, *et al.* [7] applied the boundary condition to large blockage (1.5%), lifting models in rectangular wind tunnels where they were able to demonstrate the design of slotted walls allowing closely matched aerodynamic test results with freestream conditions. Agrell [6] further applied this code to predict wall interference in measurements obtained on two different models tested in two similar transonic tunnels (one large and one small) at Mach numbers of 0.90 and 0.95 at 0° and 10° incidence. Five different slotted wall geometries were considered for the smaller facility, including one geometry which matched that of the larger facility. Although good results were generally obtained, significant differences were, again, present between computed and measured results which can be directly traced to the inability of the Berndt boundary condition to properly model inflow to the test section where viscous effects become prominent. The solution uncertainty which exists for tunnel inflow conditions where viscous effects are strong is a particular weakness for all forms of the slotted-wall boundary condition. Here, few data exist for either modelling the physics or for validation.

5.2.4.3 LARC BOUNDARY-CONDITION MEASUREMENTS AND CORRELATIONS

5.2.4.3.1 OVERVIEW

The requirement by industry and the research community for high-Reynolds-number transonic aerodynamic data and the maturation of cryogenic-testing technology spurred the development of the National Transonic Facility at the NASA Langley Research Center in the United States (Foster and Adcock [60]). Additional convergent technologies, such as high-accuracy instrumentation with high-data rates, offered the possibility of improved test results with significantly reduced measurement uncertainty. Included in these technologies were the development of mathematical algorithms and computer hardware capabilities suitable for solving complex transonic flow equations for simulations in both free air and in wind tunnels. With these new capabilities wind tunnels could be designed for improved performance, specifically in the region extending from the nozzle to the diffuser, and the test section could be tailored for reduced interference due to the slotted walls (Barnwell [20]; Ramaswamy and Cornette [154]; Newman, *et al.* [143]). However, comparisons of transonic test results with computational wind tunnel solutions revealed significant discrepancies which were traceable to the modelling of the slotted-wall boundary condition. These discrepancies appeared in both the form of the boundary condition and in the value of its associated coefficients. As an example, a modified form of the Ideal slotted-wall boundary condition

$$C_{pw} - C_{ps} = A + 2dK \frac{\partial \theta_w}{\partial x} = A - dK \frac{\partial C_{pw}}{\partial y} \quad (5-9)$$

relating the pressure drop across the wall to the streamline curvature ignores all slot viscous effects and assumes small, negligible flow angles at the wall, conditions which are, generally, incompatible with reality. The A coefficient is a necessary, first-order addition to the Ideal slot condition which accounts for the large outflow through the slotted wall due to the growth of the tunnel-empty boundary layer and other effects of tunnel geometry. Tunnel wall boundary layer effects may have a pronounced effect on the wall flow characteristics, particularly for flow returning to the test section from the plenum. In this region, the tunnel wall boundary layers may separate or form a bubble of quiescent air over the slot (Berndt and

Sørensen [26]). Magnification factors of two to four times the local velocity have been used (Freestone and Mohan [62]) to account for this effect on computed interference velocities. The geometry-dependent slotted-wall performance coefficient, K , is the value of the potential evaluated in the slot, and must be obtained from appropriate theory (Davis and Moore [46]; Chen and Mears [35]; Berndt and Sørensen [26]; Barnwell [20]) or experiment (Chen and Mears [35]; Baronti, *et al.* [22]; Berndt and Sørensen [26]; Everhart and Barnwell [54]).

The classical values of K are typically obtained by assuming a two-dimensional, inviscid cross flow over a wall with a spanwise-infinite number of identical, infinitely-long longitudinal slots. The Davis and Moore theoretical model [46] for this cross flow assumes a zero-thickness slat, while the Chen and Mears theory [35], as corrected by Barnwell [20], attempts to model the slat thickness. Chen and Mears predictions for K are a factor of two larger than those of Davis and Moore. Experiments to determine the value of K are difficult to conduct, time consuming, and, typically, have been single point experiments with no variation in wall geometry or test conditions, resulting in an inconsistent evaluation database. Early experimental values of K (Chen and Mears [35]; Berndt and Sørensen [26]; Baronti, *et al.* [22]; Binion [28]) are a factor of two to four times larger than the theoretical models, and are parametrically inconsistent in that they were obtained at different test conditions and with various combinations of wall geometries. A comparison of the K values obtained by these methods (Barnwell [21]) is summarised in Figure 5.14.

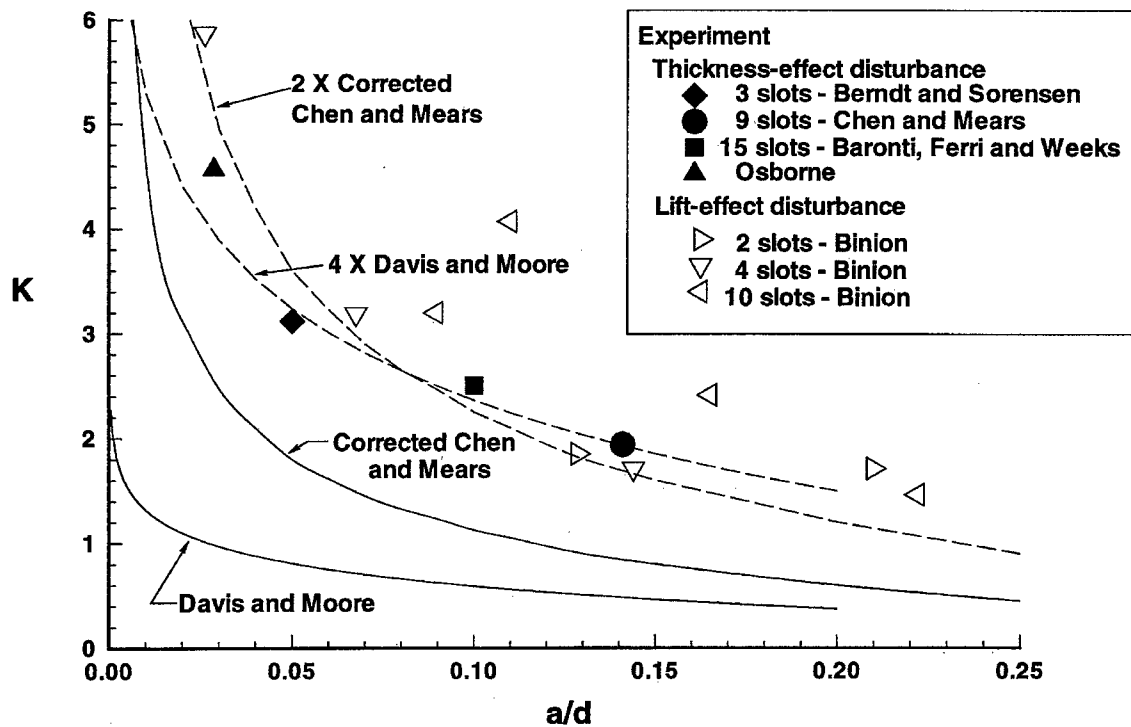


Figure 5.14 : Barnwell correlation for parameter K for slotted-wall boundary condition

5.2.4.3.2 NASA LANGLEY SLOTTED-WALL EXPERIMENTS

An experimental slotted-wall database was developed by Everhart and Barnwell [54], Everhart [53], [58] and Everhart and Bobbitt [55] to resolve some of the coefficient inconsistencies in the slotted-wall boundary condition. The experiments were conducted in the NASA Langley Research Center 6-By 19-Inch Transonic Tunnel (Ladson [112]) using a symmetrical, 6-inch chord NACA 0012 as the reference airfoil model. In these studies, a consistent, two-dimensional database, including (1) pressures measured along three parallel rows of orifices on the tunnel sidewall above and near the slots, (2) limited slot flow angles, and (3) airfoil pressure distributions and lift and moment coefficients was obtained for a parametrically-varied set of slotted-wall geometries and test conditions. The constant-width slot geometries had 1, 2, and 4 slots with openness ratios varying from 3.75 percent to 15 percent. Airfoil model pitch was varied over a range of -4° to 4° , while freestream Mach number was varied from 0.2 to 0.90. Additional, limited, slot flow-angle survey studies were also reported by Everhart, *et al.* [57] and Everhart and Goradia [56] for data acquired in the NASA Langley Diffuser Flow Apparatus (Gentry, *et al.* [70]).

5.2.4.3.3 CORRELATION OF COEFFICIENTS FOR IDEAL SLOTTED-WALL BOUNDARY CONDITION

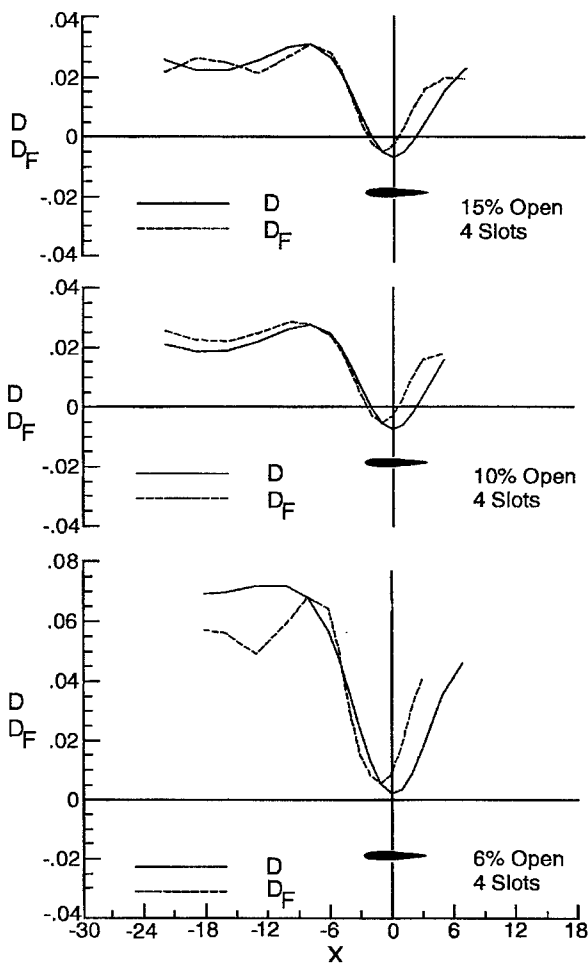


Figure 5.15 : Comparison of ideal form of slotted-wall boundary condition with experiment using 6-by 19 inch Transonic Tunnel data. $M=0.7$, $\alpha=0^\circ$.

The Langley slotted-wall database was used to obtain consistent estimates of the A and K coefficients in the Ideal slotted-wall boundary condition (5-9). Using a two-point evaluation method the K coefficient is determined by scaling the streamline-curvature gradient upstream of the maximum thickness point of the airfoil to match the wall-pressure-drop distribution. The A coefficient is facility dependent and defined to match the upstream pressure-drop distribution where the streamline curvature is negligible. Comparisons of the measured and computed pressure-drop distributions versus longitudinal tunnel station for several wall openness ratios at Mach 0.70 are shown in Figure 5.15 where the measured (or left) side of equation 5-9 is denoted by D and the computed (or right) side of equation 5-9 is denoted by D_F . The pressure-distribution match is generally reasonable upstream of maximum model thickness (minimum pressure). As with the Berndt boundary condition (see Section 5.2.4.2) considerable differences exist downstream of this position where inflow to the test section occurs. Furthermore, the curves are skewed and in no observed case did the computed minimum pressure align with the measured minimum pressure. The K coefficients determined for the Ideal boundary condition for all wall geometries are shown in Figure 5.16 for a freestream Mach

number of 0.7. The dashed-line fairings show very consistent variations with both openness ratio and number of slots. The agreement of the one-slot and two-slot results with theory is fortuitous in that these two theories were derived assuming an infinite number of slots of uniform openness. The three-slot results (filled circle) computed using the Berndt and Sørensen [26] data correlate well with the Langley results in that it lies between the two-

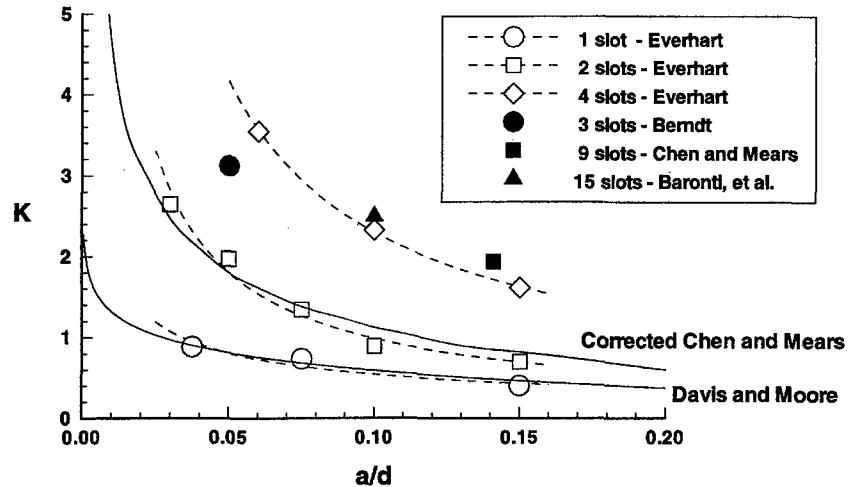


Figure 5.16 : Variation of K with openness ratio for the ideal form of the slotted-wall boundary condition. $M=0.7$, $\alpha=0^\circ$

and four-slot results. The experimental results for 9 slots (filled square, Chen and Mears [35]) and for 15 slots (filled triangle, Baronti, *et al.* [22]) have the right magnitude relative to the Langley four-slot results. Even though the infinite-slot theoretical trends are similar to the experimental results, quantitatively they give K values which are much smaller than those for the four-slot configuration when, in fact, they should be larger. On this basis, it would seem that the homogeneous-wall condition is rapidly approached for walls with four or more slots and that a valid, limited use of the Ideal boundary condition can be made for some conditions, as long as an experimentally-determined value of K is used.

5.2.4.3.4 LINEARISATION OF THE SLOTTED-WALL BOUNDARY CONDITION

An experimental and analytical examination of the Langley databases resulted in the boundary condition

$$C_{pw} - C_{ps} = 2dK \frac{\partial \theta_w}{\partial x} + B\theta_s + \theta_s^2 = -dK \frac{\partial C_{pw}}{\partial y} + B\theta_s + \theta_s^2 \quad (5-10)$$

which relates the pressure drop across the wall to the streamline curvature near the wall, and to a linear and quadratic variation of the flow angle in the slot. Based on available information, the flow angle in the slot, θ_s , should be taken at the *vena contracta*, where it maximises. The value of C_{pw} is that achieved in the tunnel in the far field of the slot where the flow is unaffected by the local geometry of the slot. The pressure coefficient C_{ps} is the pressure imposed on the slot by the plenum. Equation (5-10) will reduce to

$$C_{pw} - C_{ps} = B\theta_s + \theta_s^2 \quad (5-11)$$

for an empty tunnel with no streamline curvature near the wall. For large outflow through the slots, usually caused by the build-up of the tunnel wall boundary layer or by converged walls, the quadratic term dominates and the equation (5-11) will further reduce to

$$C_{pw} - C_{ps} = \theta_s^2 \quad (5-12)$$

Limited slot flow measurements obtained by Gardenier and Chew (Goethert [71]), Berndt and Sørensen [26], and Everhart [58] validate equations (5-11) and (5-12). The coefficient B is dependent on the details of the slot geometry and the boundary layer growth, and, to date, specific experiments to generate variational correlations have not been conducted.

Equation (5-10) can be linearised as follows. First, subtract equation (5-11) from (5-10), to obtain

$$(C_{pw} - C_{pw,te}) - (C_{ps} - C_{ps,te}) = -dK \frac{\partial C_{pw}}{\partial y} + B(\theta_s - \theta_{s,te}) + (\theta_s^2 - \theta_{s,te}^2) \quad (5-13)$$

Letting

$$\Delta\theta = \theta_s - \theta_{s,te} \quad (5-14)$$

be the increment between the flow angle in the slot with the model installed and the undisturbed flow angle in the slot in the empty tunnel will yield

$$\theta_s^2 - \theta_{s,te}^2 = 2(\Delta\theta)\theta_{s,te} + (\Delta\theta)^2 \approx 2(\theta_s - \theta_{s,te})\theta_{s,te} = A + B'\theta_s \quad (5-15)$$

if $\Delta\theta$ is small. Implicit in (5-15) is the assumption that $\theta_{s,te}$ is approximately constant in the vicinity of the model (Everhart [58]). Substitution of (5-14) and (5-15) into (5-13) yields

$$(C_{pw} - C_{pw,te}) - (C_{ps} - C_{ps,te}) = A - dK \frac{\partial C_{pw}}{\partial y} + B\theta_s \quad (5-16)$$

where B is a reformulated viscous coefficient. Far upstream, the model-induced streamline curvature is very small and, for large outflow, the B coefficient is negligible. The A coefficient can then be thought of as a measure of the difference between the empty-tunnel plenum pressure and that measured with the model installed at the same freestream Mach number.

Values of the slotted-wall boundary condition coefficients A , K , and B were determined in Everhart [58] from experimental data using the method of least squares. Representative correlations are presented in Section 5.2.4.3.7.

5.2.4.3.5 EFFECT OF AIRFOIL MODEL ON PLENUM PRESSURE

Many transonic wind tunnels use the plenum pressure as the tunnel reference pressure for calibration and Mach number control. An unstable reference condition exists if the plenum pressure is sensitive to the presence of the model and its test environment. Under these conditions the facility is not operating at the required test conditions, and the resulting aerodynamic data must be corrected accordingly. However, in general, the magnitude of the correction is an unknown because the model effect is unknown. Everhart and Bobbitt [55] quantified this effect for a NACA 0012 airfoil model tested in the NASA Langley 6-By 19-Inch Transonic Tunnel at zero lift by examining the far-field pressure drop coefficient, $\Delta C_{p,ff}$. This coefficient is defined as the plenum pressure coefficient subtracted from the freestream pressure coefficient measured upstream of the slot origin in a location which is undisturbed when the model is present. (This upstream pressure is used to calibrate and operate the wind tunnel.) Pressure drop coefficient results plotted versus wall openness ratio obtained with and without the model installed for a freestream Mach number of 0.7 are presented in Figure 5.17. For matched freestream Mach numbers, the airfoil presence causes the plenum pressure to drop globally relative to the corresponding tunnel-empty case. This effect is present for all slot geometries tested; however, the difference decreases with increasing openness ratio. For openness values greater than 10 percent, the difference in the measurements is small, an indication that the tunnel is approaching open-jet conditions in which the freestream static pressure is equal to that of the surrounding plenum. The fact that the plenum pressure is lower than the average pressure in the tunnel is a result of a jet pumping effect exerted on the plenum by the tunnel. These observations are consistent with other transonic data published by Berndt and Sørensen [26] and, also, at low speed with high model-induced blockage results obtained by Kuentner,

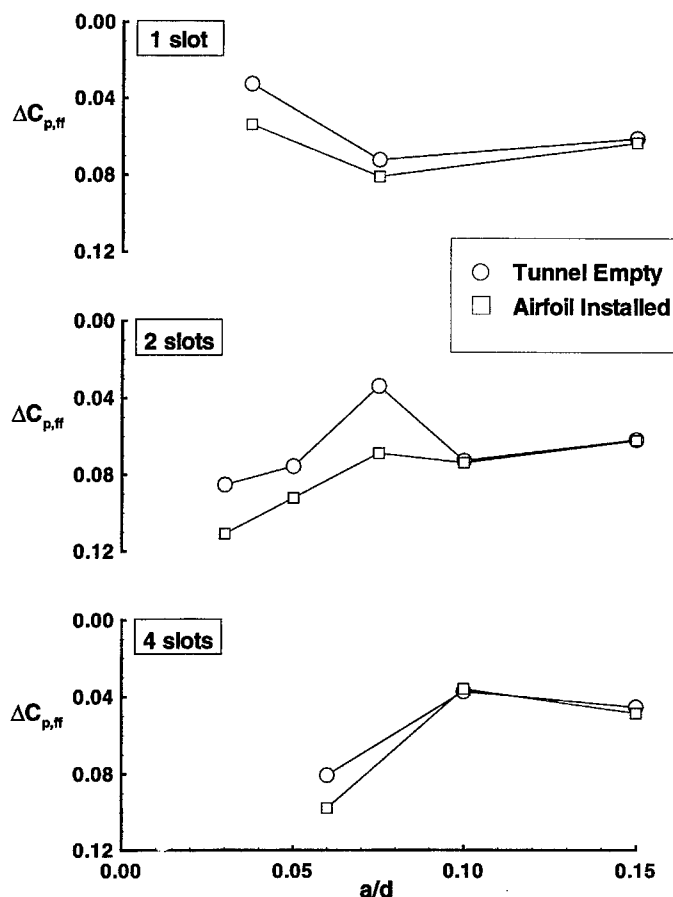


Figure 5.17 : Effect of two-dimensional model on slotted-wall wind tunnel plenum pressure. $M=0.7$, $\alpha=0^\circ$

et al. [111] in an open-jet automotive wind tunnel. These results warrant caution when calibrating ventilated wind tunnels, and, particularly, for models tested at high speed or under high loading conditions where the plenum pressure is used as the reference condition.

5.2.4.3.6 CORRELATION OF BOUNDARY PRESSURE MEASUREMENTS WITH THEORY

Experimental and mathematical procedures for obtaining best-fit correlations of the unknown coefficients given by equation (5-16), the linearised version of (5-10), are presented in Everhart [58]. The goodness of the agreement is demonstrated in Figure 5.18 by plotting the measured (or left) side of (5-16) defined as

$$D = (C_{pw} - C_{pw,te}) - (C_{ps} - C_{ps,te}) \quad (5-17a)$$

and the fitted (or right) side of (5-16) defined as

$$D_F = A - dK \frac{\partial C_{pw}}{\partial y} + B\theta_s \quad (5-17b)$$

versus longitudinal distance along the slotted wall. The comparisons obtained at Mach 0.70 are for three different four-slot wall configurations for openness ratios of 15-, 10-, and 6-percent. Airfoil incidence is zero degrees. The slots begin at station -23 inch, open linearly to station -19 inch, and extend with constant width to station 19.5 inch. The sharp slope discontinuity in the D_F curve at station 3 inch is the

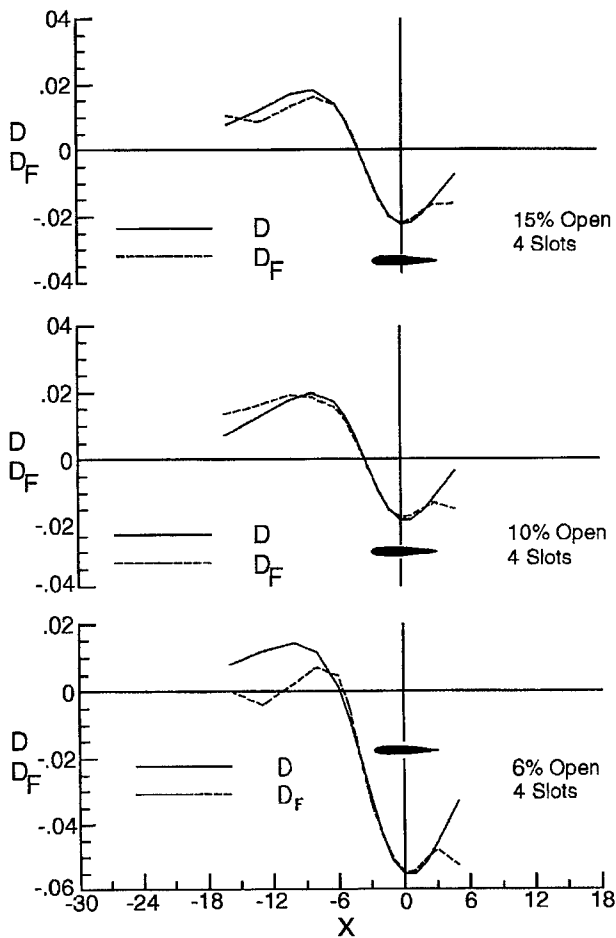


Figure 5.18 : Comparison of Everhart's slotted-wall boundary condition with experiment using 6- by 19-inch Transonic Tunnel data. $M=0.7$, $\alpha=0^\circ$.

5.2.4.3.7 VARIATION OF BOUNDARY-CONDITION COEFFICIENTS

Figure 5.20 shows the variation of the K coefficient with openness ratio for a freestream Mach number of 0.7 and zero angle-of-attack. The dashed lines are fairings which indicate trends of those walls with the same number of slots. Sufficient information exists to obtain a K value from the Berndt and Sørensen [26] data which is shown as the filled symbol. The addition of the $B\theta_s$ term absorbs part of the contribution to wall-pressure drop originally assumed in total by the streamline-curvature term and, as a result, reduces the K coefficient values compared to the "ideal" values (see Figure 5.16) determined from equation (5-9). The variation with the number of slots is consistent in that increased values of K are obtained with larger numbers of slots. However, the results for three and four slots are very nearly the same which indicates, as expected, that the assumption of a homogeneous boundary condition is more closely modelled by the walls with the larger number of slots.

The corresponding B coefficients are also shown in Figure 5.20. The variations of the one- and two-slot results are very similar; however, the results change slope for the walls with four slots. This behaviour is not too surprising since one of the greatest uncertainties is the behaviour of the boundary layer over the slotted wall and how it interacts with the flow through the slot. The larger the number of slots the smaller the ratio of slot width to wall boundary layer displacement thickness, yielding a more uniform variation of

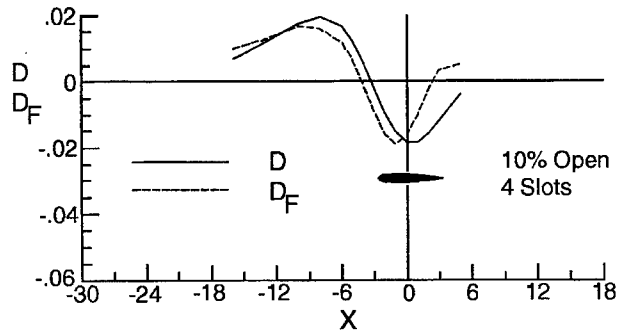


Figure 5.19 : Effect of excluding the linear flow angle contribution from Everhart's form of slotted wall boundary condition. $M=0.7$, $\alpha=0^\circ$

result of flow-angle probe support contamination. These same data are used again in Figure 5.19 to, again, demonstrate the effect of excluding the linear contribution of the flow angle. This, in effect, reduces the equation to the Ideal form of the boundary condition given by equation (5-9). In all cases, a mismatch or skewing of the curves exists which can only be removed if the linear contribution to flow angle is retained as previously shown in Figure 5.18.

the wall flow-field properties. It is clear, based on these results that a linear flow-angle contribution is required in the boundary condition equation to properly model the pressure drop through a longitudinally-slotted wind-tunnel wall. The actual numerical value of the coefficient must be determined for the given slotted-wall configuration.

The A coefficients presented in Figure 5.20 reveal scatter which appears to be related to uncertainty in the flow angle. If A is assumed to result exclusively from the decrease in the plenum pressure coefficient due to the presence of the model, then, for this Mach number, an A value of 0.02 will yield a Mach number increment of 0.008.

Additional variations with Mach number and model lift may be found in Everhart [53], [58]. In general, the following statements can be made for these test conditions.

(1) At fixed lift, a regular, monotonic increase in the values of A , K , and B occurred with increasing Mach number; however, it is possible that this effect is the result of viscous narrowing of the slot.

(2) At fixed Mach number, only slight (if any) coefficient variation occurred with changes in lift coefficient.

Because the 6- by 19-inch Transonic Tunnel is an atmospheric wind tunnel, variations in the ratio of wall boundary-layer thickness to slot width are only those which would occur as a result of changing unit Reynolds number by a factor of about 2. Additionally, this variation cannot be made independent of changes in Mach number. As a result, the parametrically-varying effects of slot Reynolds were not independently examined.

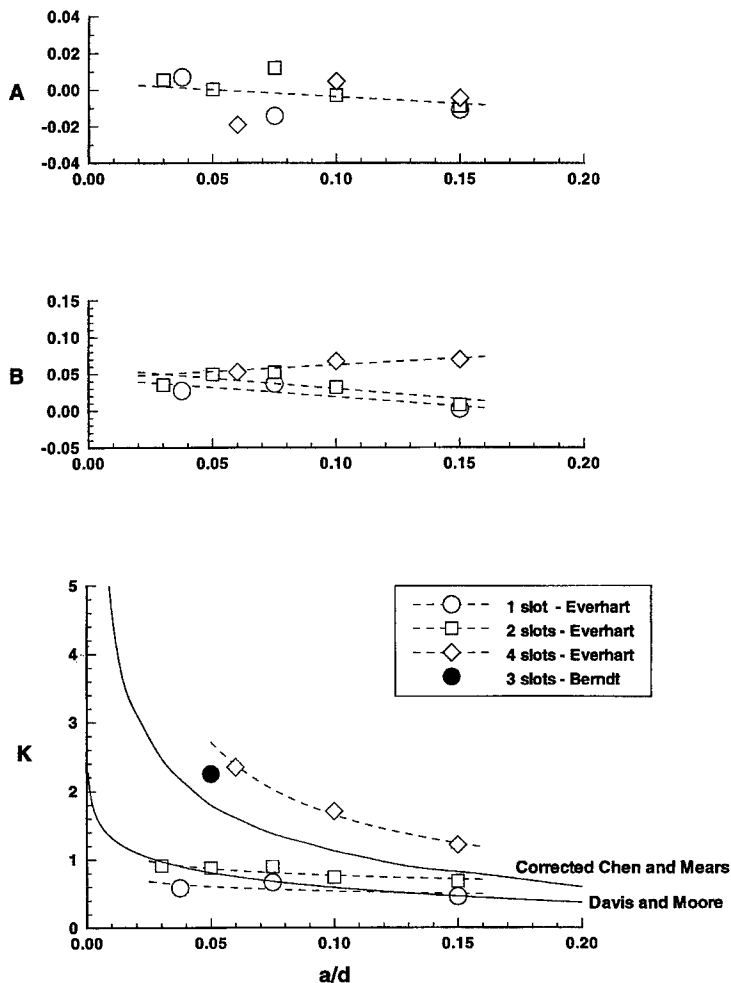


Figure 5.20 : Variation of coefficients with openness ratio for Everhart's form of slotted-wall boundary condition. $M=0.7$, $\alpha=0^\circ$.

5.2.4.3.8 COMPARISON OF COEFFICIENTS WITH BERNDT'S SLOT-DEPTH HYPOTHESIS

Berndt [24] developed a second-order approximation for the K coefficient which isolated an effect due to slot depth (see, also, Goethert [71]). His result is expressed as

$$K = -\frac{1}{\pi} \ln \left[\sin \left(\frac{\pi a}{2d} \right) \right] + 0.462 + \frac{t}{a} = K_{DM} + 0.462 + \frac{t}{a} \tag{5-18}$$

where K_{DM} is the theoretical Davis and Moore [46] form of the slotted-wall K coefficient for a zero-thickness wall. In 1982 Berndt [25] further proposed highlighting the thickness parameter t/a by writing

$$\Delta K = K - K_{DM} = 0.462 + \frac{t}{a} \tag{5-19}$$

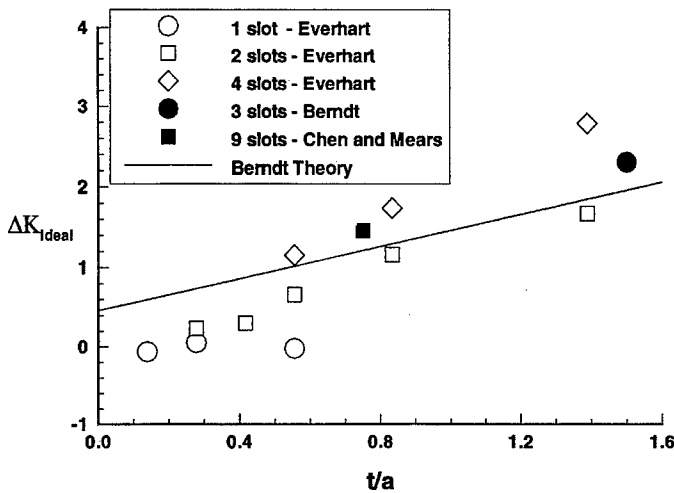


Figure 5.21 : Influence of slot depth on Ideal form of slotted-wall boundary condition efficient K . $M=0.7, \alpha=0^\circ$.

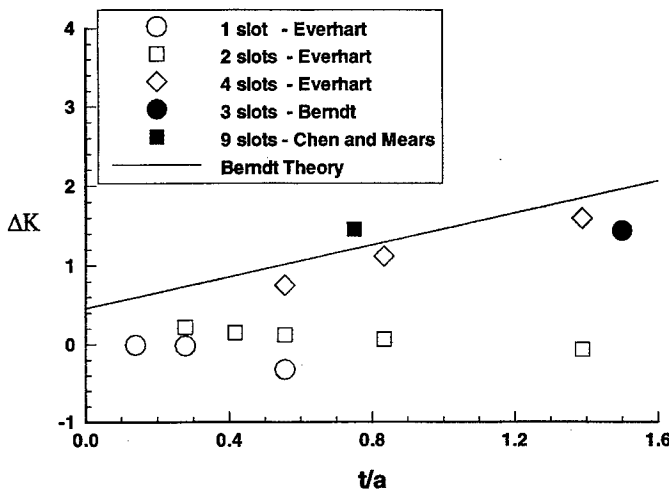


Figure 5.22 : Influence of slot depth on Everhart form of slotted-wall boundary condition coefficient K . $M=0.7, \alpha=0^\circ$.

Applying this expression to the Ideal boundary-condition values of Figure 5.16 yields the results presented in Figure 5.21. It appears that ΔK values do correlate with slot thickness; however, this trend has a different slope and intercept than that of the theoretical prediction.

Comparable results for the Everhart boundary condition given on Figure 5.20 are shown in Figure 5.22. Based on previous discussions, the one- and two-slot results should not match the theoretical prediction, which is indeed the case as exhibited by their flat distribution with slot depth. The Everhart four-slot, Berndt three-slot, and Chen and Mears nine-slot values closely approximate the Berndt hypothesis of (5-19). These results support the earlier observation that they are close to representing a homogeneous slotted wall (see section 3.2) and lend further credence to the Berndt slot-depth hypothesis as represented by equation (5-19).

5.2.4.3.9 IMPLEMENTING EVERHART'S BOUNDARY CONDITION EQUATION (5-10)

Presently, no known utilisation of equation (5-10) exists in any computational formulation. However, because of its nonlinearity, implementation of equation (5-10) will require iterative numerical procedures similar to the slotted wall

boundary condition of Berndt (section 5.2.4.2) and porous wall boundary conditions of MDA (sections 5.2.3.1 and 5.3.1) or the AEDC (sections 5.2.3.2 and 5.3.2).

5.2.4.4 TRANSONIC SLOT DESIGN

5.2.4.4.1 DESIGN METHOD FOR TWO-DIMENSIONAL SLOTTED WALLS

Barnwell [21] developed improved procedures for designing slotted walls for two-dimensional transonic wind tunnels which were then applied to the NASA Langley 6- by 28-Inch Transonic Tunnel and to the 8-inch by 24-inch slotted test section of the 0.3-Meter Transonic Cryogenic Tunnel. The procedure emphasises the maintenance of small disturbances at the wall and small crossflow velocities in the slot which, accordingly, allows the use of the small-disturbance form of the slotted-wall boundary condition given by

$$C_{pw} = 2K \frac{d}{h} \frac{\partial \theta_w}{\partial (x/h)} = 2k \frac{\partial \theta_w}{\partial (x/h)} \quad \text{where} \quad k = K \frac{d}{h}$$

and, where C_{pw} is the ambient pressure coefficient near the tunnel wall, θ_w is the flow angle near the tunnel wall, d is the slot spacing, h is the tunnel semi-height, K is the slotted-wall performance coefficient, and k is the slotted-wall boundary-condition coefficient.

An examination of Pindzola and Lo [151] for ideal slotted-wall tunnels shows that model blockage vanishes at the value $k=1.18$, that wake blockage at the model is zero, that the gradient in the wake blockage vanishes at zero model blockage, that downwash is nearly constant in the vicinity of the model for zero blockage (it can only be eliminated in a closed tunnel), and, that the streamline curvature vanishes at $k=1.58$. Therefore, in the classical sense it is obvious that that no single, fixed-wall geometry can eliminate all interference effects, and that compromises in wall geometry must be made. According to linear theory, it can also be shown that the blockage increment at the model position induced by a wake survey rake is negative, and, since blockage interference is positive for closed walls and negative for open walls, it is possible to reduce blockage interference at the model position by controlling the wall openness at the rake position.

With these facts in mind and because computational predictions using classical boundary conditions are significantly different from experiment, Barnwell next examined the variation of K with slotted-wall openness ratio, a/d . A summary of his analysis is presented in Figure 5.14. Theoretical, homogeneous-boundary representations of the slotted wall developed by Davis and Moore [46] for an infinitely thin slotted wall and by Chen and Mears [35], corrected by Barnwell [20], for a wall with finite thickness have functionally different variations for small a/d and yield differences in K which vary by a least a factor of two. Direct experimental measurements of K by Chen and Mears [35], Baronti, *et al.* [22], Berndt and Sørensen [26], and K values inferred from experimental measurements by Osborne [146] and Binion [28] were found to be in disagreement with both theories. An experimental correlation band given by 4 times the Davis and Moore theory and 2 times the corrected Chen and Moore theory bounds the thickness-effect only data. (Experimental values determined later by Everhart [53], [58] also lie within this correlation band (see Figure (5.16)).

The minimum blockage value of K may now be determined for a tunnel of height $2h$ with a specified number of slots (giving the slot spacing, d). The required openness ratio is determined from the correlation which allows the slot width to be specified. For the Langley 6- by 28-Inch Transonic Tunnel, this procedure yields one 6-percent open slot, two 2-percent open slots, or four very narrow slots. Because of the potential for large (possibly sonic) crossflow velocities with a 2-percent-open (or less) wall, a single-slot configuration with a 5-percent open area was selected. Theoretically, this wall geometry creates a slightly positive blockage to cancel the negative blockage imposed by the wake rake and it

reduces the streamline curvature correction. A similar evaluation was made for the 8-inch-wide by 24-inch-high slotted test section of the Langley 0.3-Meter Transonic Cryogenic Tunnel, resulting in a minimum blockage geometry with two 5-percent-open slots each on the top and bottom walls.

5.2.4.4.2 NTF SLOT DESIGN

Slotted-wall design criteria for the National Transonic Facility noted by Newman, *et al.* [143] were

- 1) zero lift interference with four walls slotted, and
- 2) smooth Mach number distributions at supersonic test conditions.

The first design criterion was met by extending the two-dimensional procedures described in Section 5.2.4.4.1. The second criterion was satisfied by using the method of Ramaswamy and Cornette [154] to provide a suitable supersonic slot entry region (see Section 5.2.4.4.3). Slightly closing the walls at the model station accounted for the negative blockage effect of the model support. Sidewall slots, though included in the original design, were not installed; however, provisions exist for the installation of 2 such slots in each sidewall. The resulting model region of the NTF test section has 5-percent open transonic walls with six uniformly-spaced slots each on the top and bottom walls, and solid sidewalls.

5.2.4.4.3 SUPERSONIC SLOT DESIGN—METHOD OF RAMASWAMY AND CORNETTE

Methods to design supersonic slotted walls and evaluate supersonic flow in a slotted wall wind tunnel were developed by Ramaswamy and Cornette [154]. Fundamentally, the method of characteristics is combined with a wall boundary condition which relates the local value of the Prandtl-Meyer angle, ν_w , to the local flow angle, θ_w . In analysis mode $(\nu - \theta)_w$ is prescribed along characteristics striking the wall. The angle ν_w is determined using the Mach number computed from local wall pressures. By assuming homogenous flow near the wall, large crossflow through the slot, and no streamline curvature, the angle θ_w is obtained from

$$\theta_w = \varepsilon \frac{a}{d} \sqrt{C_{pw}}$$

The slot orifice coefficient, ε , is used to account for the *vena contracta* effect of the crossflow jet and the wall boundary layer effects. Wind tunnel calibration data obtained in the Langley 8-Foot Transonic Pressure Tunnel (Harris, *et al.* [82]) and in the Langley Diffuser Flow Apparatus (Gentry, *et al.* [70]) were used to validate the method, and extremely good correlations between theory and experiment were obtained using slot orifice coefficients in the range of 0.8 to 0.9. In the design method, smooth longitudinal distributions of test section centreline Mach number and $(\nu + \theta)_w$ along characteristics leaving the wall are prescribed. Since θ is zero on the tunnel centreline, the value of $\nu_w = \nu_{cl}$ is determined and, hence, θ_w . The wall pressure drop is obtained from the wall Mach number which, upon specification of an appropriate orifice coefficient, allows the required wall openness ratio, a/d , to be determined. To avoid overexpansion and for smooth supersonic flow to exist in the test region, the required distribution of slot openness ratio was found to increase to a maximum and then decrease to zero. However, because the wind tunnel must also operate at transonic speeds, the slot openness is only allowed to decrease to that value required to minimise wall effects at transonic speeds.

5.2.5 BAFFLED SLOTTED WALLS

5.2.5.1 Background

Baffled slotted wind tunnel walls were originally developed for the NASA Ames Research Center 11-Ft. Transonic Tunnel where a full-scale 1981 demonstration of the concept validated its feasibility. Additionally, this geometry was proposed for the recently cancelled NWTC Subsonic and Transonic Wind Tunnels initiative (Sickles and Steinle [170]). Baffled slotted walls are created by filling longitudinal slots with nominally spanwise-oriented baffles. The baffles remove the dependency on streamline curvature, a characteristic of the flow through the more traditional slots, and create strips of porosity described by Darcy's Law for pressure drop through a porous medium. Baffled slotted walls combine several important attributes of porous walls and slotted walls. First, early acoustic studies by Daugherty and Steinle [44], Jacocks [88], and Daugherty, *et al.* [45] verified that properly-designed baffles were quieter than the uniformly-distributed discrete holes in porous walls. These and other unpublished studies have led to recently-developed methods of reducing ventilated-wall noise to levels comparable with that of a solid wall tunnel (Steinle [175]). Next, good optical accessibility is a must for modern, nonintrusive measurement methods and slots allow significantly improved access compared to porous walls. Finally, supersonic wave attenuation by a porous wall is superior to that offered by a slotted wall. Sickles and Steinle computationally demonstrated good attenuation properties which rapidly approach homogeneity and match porous wall characteristics for eight or more baffled slots (Steinle [175]).

Flow field survey data which characterise the flow over a baffled slotted wall with a segmented plenum chamber were obtained by Wu, *et al.* [187] and by Bhat [27]. These data were obtained for flows into and out of the plenum (i.e. under suction and blowing conditions) and reveal the complex flow character associated with ventilated walls. For flow into the plenum, large streamwise counter-rotating vortices co-exist in the test section along each side of the baffled slot. These vortices were removed with increasing pressure drop (decreasing plenum pressure) across the wall. Conversely, the strength of the vortices was increased with decreasing pressure drop (increasing plenum pressure). For outflow conditions, the test-section-side behaviour of the wall flow field should be similar to that over the slotted wall. Therefore, these data offer insight into the flow behaviour over the more traditional transonic slotted wall geometry. Though not specifically addressed in their reports, the data of Wu, *et al.* [187] and Bhat [27] allow one imagine how flow into the tunnel through both slotted and porous walls could conceivably energise these vortices to the point of ultimately separating them and the tunnel-wall boundary layer from the tunnel wall surface. Obviously, significant viscous-interaction research remains before ventilated tunnel-wall boundary conditions are fully understood.

5.2.5.2 BOUNDARY CONDITION FOR AMES 11-FT TRANSONIC TUNNEL

Unpublished semispan data acquired while testing a large RAE model 864 were used to determine the boundary condition of the baffled slotted walls of the Ames 11-Ft. Transonic Tunnel (Steinle [175]). The basic tunnel geometry has 5.6-percent-open baffled slots on all four walls. For this test, the tunnel floor was sealed and used as the semispan reflection plane while the other three walls were tested in three configurations with (1) completely open slots, (2) completely closed walls, and (3) with the top tunnel wall closed and tunnel sidewall slots open. The model was spanwise instrumented with six longitudinal rows of pressure orifices, and data were acquired over a range of model pitch and freestream Mach number. For the closed-wall tunnel, configuration (2), the spanwise distribution of the angle-of-attack correction was computed by simulating the wing with 10 horseshoe vortices and by using the method of images for

compressible flow. For tunnel configuration (3) (top wall closed), the spanwise angle of attack correction for the baffled slotted wall was determined using the method of Kraft and Lo [108] for a family of resistive values, R , and streamline-curvature coefficients, K , for a freestream Mach number of 0.7. The envelope of these R - K pairs which gave the best overall comparison with the closed-wall results was extrapolated to that corresponding to a uniformly-distributed porous wall. Because the Kraft and Lo theory is for a uniformly-distributed porous wall, dividing the extrapolated resistive value by the baffled-slotted-wall openness ratio will accumulate all resistivity into discrete slots, yielding a resistivity value of approximately 19 for the 11-Ft Tunnel. Results obtained in the Ames 2- by 2-Ft Tunnel by Matyk and Yasunori [127] unsurprisingly gave a significantly different resistivity value due to non-amplification by a much thinner tunnel-wall boundary layer; however, as expected, their results showed a general independence with Mach number due to the low-speed flow through the baffled slot. Calculations of the spanwise variation in lift interference for these data in the 11-Foot tunnel and other case studies are shown in Steinle and Pejack [176]. Additional wall-interference calculations which characterise the baffled-slotted wall are presented by Crites and Steinle [43].

5.3 COMPUTATIONAL APPROACHES

In this section a brief overview of computational or CFD approaches used to simulate transonic wind-tunnel test-section flows is given by means of a few sample numerical implementations and results. This is not intended to be a thorough review of CFD methods or simulations of wind-tunnel flows, all of which have become possible since the publication of AGARDograph 109 [67]. The methods discussed in this section use a wide range of mathematical boundary conditions from the classical-like, where the boundary condition is known and prescribed *a priori*, to the non-linear, where the boundary condition simulating the tunnel-wall flow must be iteratively solved as a part of the entire solution process. Modern boundary measurement methods incorporating near-wall flow data as a boundary condition are also presented. These boundary conditions are used in WIAC techniques which are becoming increasingly attractive as measurement accuracy improves and instrumentation costs per channel rapidly decrease (for example, multi-channel electronically-scanned pressure transducers or pressure-sensitive paint techniques), and as computational power soars and moves to the desktop.

5.3.1 TUNNEL SIMULATIONS

The division of the subsections herein is based upon the flow equation approximation used in the wind-tunnel simulations.

5.3.1.1 LINEAR THEORY

A number of linear theory flow codes have been modified to include homogeneous classical-like wind-tunnel wall boundary conditions on the outer or far-field boundary. Keller and Wright [94] is a sample implementation which includes a variety of such wall conditions. There, they developed a numerical method to examine incompressible boundary-induced interference in rectangular wind tunnels with slotted or perforated walls which Keller [93] later modified and extended to include slot viscous effects. The walls were modelled with source panels on which a general boundary condition of the form

$$c_1\varphi + c_2 \frac{\partial\varphi}{\partial x} + c_3 \frac{\partial\varphi}{\partial n} + c_4 \frac{\partial^2\varphi}{\partial x\partial n} = 0$$

was applied. The coefficients were specified according to the type of tunnel wall and boundary condition being evaluated as specified in the following table:

TYPE OF BOUNDARY CONDITION	c_1	c_2	c_3	c_4
Closed wall	0	0	1	0
Open jet	0	1	0	0
Perforated wall	0	1	$\frac{1}{R}$	0
Ideal slotted wall: integrated form	1	0	K	0
Ideal slotted wall: differentiated form	0	1	$\frac{\partial K}{\partial x}$	K
Slotted wall with viscosity in slots	0	1	$\frac{\partial K}{\partial x} + \frac{1}{R}$	K

Besides presenting a simple method for evaluating interference, the method computationally revealed the very significant effect of viscosity on the wall-induced interference. For a square tunnel with four 6-percent open slots each in the top and bottom walls, the lift interference factor, δ_0 , was found to vary from 0.078 to -0.012 as R varied from 0.333 to 3, respectively. Pearcey, *et al.* [148] showed typical values of R of the order of 1.

Other linear theory codes have been modified or developed to model various discrete aspects of wind-tunnel geometry, including the walls. For example, Lee [114] simulated the testing environment of practical 3-D, subsonic, rectangular cross-section wind tunnels using a higher-order panel method. A homogeneous slotted wall boundary condition was used to represent the effects of slot openness in a finite length test section which included corner fillets. In addition, the test model size, shape, location and mounting system were also simulated, thus, providing both a diagnostic tool for interpreting experimental data as well as a design tool for the test environment. As another example, Kemp [103], [96], [97], developed STIPAN, a high-order panel code which simulates a slotted wind tunnel test section with discrete, finite-length wall slots subject to plenum chamber constraints and terminated by a re-entry region to smooth the flow transition to the solid wall diffuser. Both non-linear effects of the dynamic pressure of the slot outflow jet and of the low energy of the slot inflow are considered; the test model and sting support are also represented. These simulation features were selected to be those appropriate for the subsequent intended use of this simulation in a wall interference assessment and correction (WIAC) procedure, PANCOR, using a modified wall model making use of sparsely located wall pressure measurements (Kemp [98],[95]). Figures 5.23 and 5.24, taken from this latter reference, illustrates the STIPAN/PANCOR slotted-wall model. Simulation results demonstrated that accounting for the discrete slots is important in interpreting wall pressures measured between the slots, and that accounting for non-linear slot flow effects produces significant changes in tunnel-induced velocity distributions; in particular, a longitudinal component of tunnel-induced velocity due to model lift is produced. A characteristic mode of tunnel flow interaction with constraints imposed by the plenum chamber and diffuser entrance is apparent in the results.

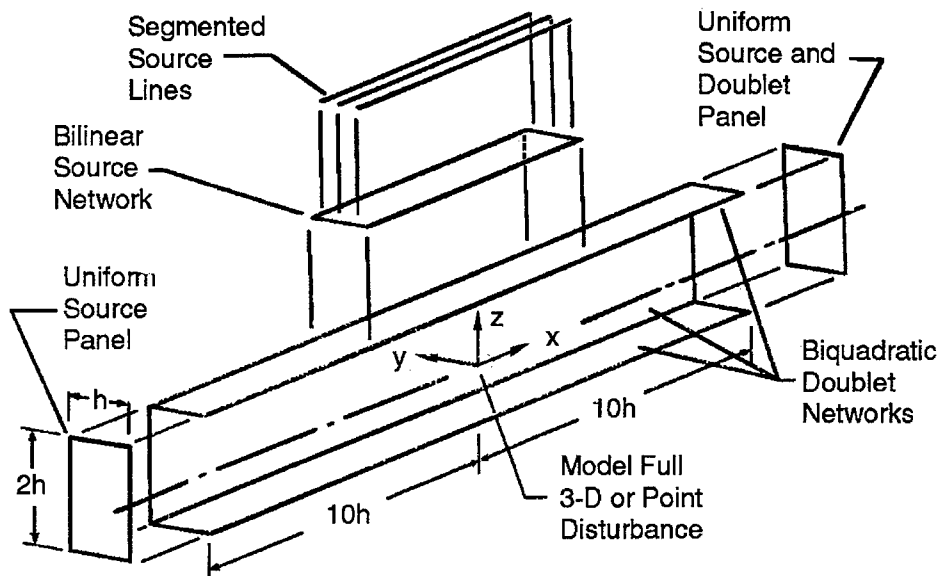


Figure 5.23 : STIPAN/PANCOR slotted wall model
Singularities used on tunnel flow domain

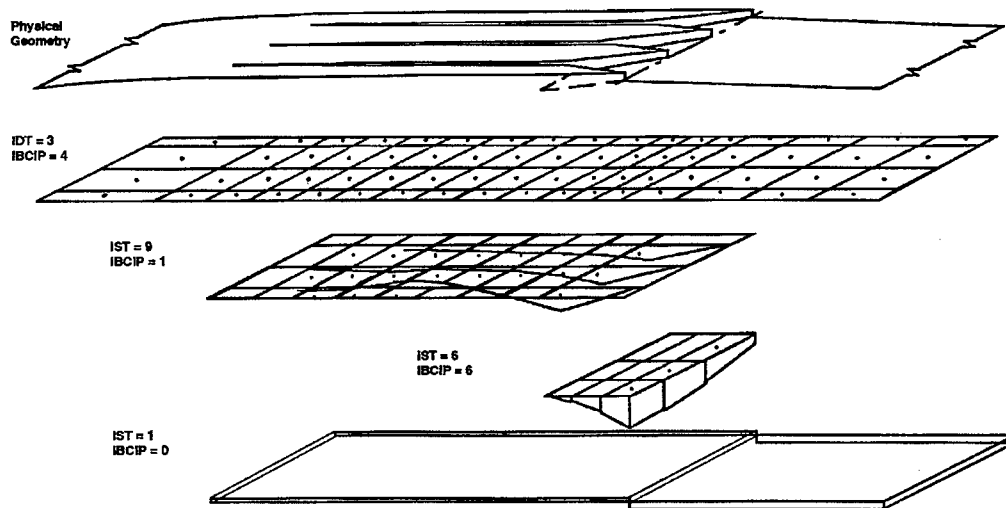


Figure 5.24 : STIPAN/PANCOR slotted wall model.
Panel network superposition used to represent a slotted tunnel wall

5.3.1.2 TRANSONIC SMALL DISTURBANCE EQUATION (TSDE) METHODS

The non-linear TSDE considered here is generally of the form

$$(1 - M^2)\phi_{xx} + \phi_{yy} + \phi_{zz} = 0$$

where M is the local Mach number and ϕ is the small disturbance perturbation velocity potential. Various approximations are made to calculate M , but all contain at least one non-linear term of the form $A\phi_x\phi_{xx}$. Axisymmetric, slender lifting body, and 2-D versions of the TSDE all retain this term while appropriately dropping others. However, more non-linear terms and those involving cross-derivatives must be added to adequately approximate swept shock waves on swept wings.

The advent of practical transonic computational fluid dynamic calculations around 1970 (Murman and Cole [136]) allowed one to perform numerical experiments related to tunnel-wall effects. General conclusions were: (1) somewhere in the transonic regime linear superposition does break down (Murman [135]) and (2) wall characteristics can be very non-linear at transonic conditions (Kacprzynski [90]) and dependent upon the model pressure field through its influence on the wall boundary layers, especially those on the mounting walls in 2-D airfoil and semi-span wing tests, as mentioned in section 5.2.2. The latter two references were early discussions of 2-D (airfoil) TSDE applications utilising ventilated wall boundary conditions; Murman, *et al.* [134] discusses the TSFOIL code resulting from Murman's earlier work.

Early TSDE results for circular tunnel geometries were presented for axisymmetric bodies by Bailey [15] and for slender lifting wing-body combinations by Barnwell [17]. Simulations have also been used in conjunction with deriving/assessing approximate ventilated wall boundary conditions. A series of papers by Karlsson and Sedin [91], [92], [164], [165], discussed in section 5.2.4.2, used an axisymmetric TSDE in assessing various slotted tunnel wall boundary condition approximations.

Extension to TSDE simulation of a 3-D wing in a rectangular cross-section wind tunnel with rather arbitrary boundary conditions was presented by Newman and Klunker [140]. The boundary condition used to model the tunnel walls was the integrated form of the generalised linear homogeneous condition as given by Keller [93] and discussed in section 5.3.1.1. However, an inhomogeneous term must be

added to account for integration constants; it also accounts for physical effects such as non-zero C_p in the plenum or contoured walls. This condition is:

$$A\phi_n + B\phi_x + C\phi + D = 0$$

Conventional linear wall conditions are obtained as

Open jet	$A=C=D=0$	$B \neq 0$
Straight solid	$B=C=D=0$	$A \neq 0$
Contoured solid	$B=C=0$	$-D/A = \text{wall slope}$
Porous	$C=D=0$	$B/A = \text{porosity or restriction parameter}$
Slotted	$B=D=0$	$C/A = \text{slot geometry parameter}$

Also note that the addition of a term $E\phi_{xx}$ would allow one to model the Adcock and Barnwell [2] approximation of viscous effects on solid tunnel walls as discussed in Section 5.2.2.

As pointed out by Newman and Klunker [140], "Several points should be made concerning the tunnel-wall boundary condition. First, it is considered to be an average relationship between various local inviscid flow properties which applies near the wall rather than on it. Second, in an iterative finite-difference calculation there is a great deal of flexibility regarding the form of the boundary condition itself since (a) it need not even have a functional form (i.e., could be measured flow properties) much less be linear; (b) the parameters in it can vary with local tunnel geometry or local flow conditions; and (c) it is restricted, however, in that the relaxation calculation must be stable. Third, the porosity and slot geometry parameters must be determined experimentally." However, "these parameters are dependent on local flow conditions near the tunnel wall which for transonic flows are influenced not only by the tunnel operating conditions but also by the test configuration." Nevertheless, they concluded that "the results for tunnel-wall modelling demonstrate that various conventional tunnel-wall boundary conditions can be incorporated in numerical computations. Such modelling should be useful in assessing interference effects and as an aid in the design of wind tunnels." These 3-D TSDE calculations for a wing in a simulated NTF tunnel indicated a need for some sidewall relief. The two slots incorporated in each sidewall design provide this relief and are compatible with the mechanical and optical requirements on the NTF test section.

Indeed, later uses of the 3-D TSDE in approximate boundary condition and ventilated wall design assessment, as well as for wall interference prediction have been reported by others. For example, Sedin, *et al.* [163] and Agrell, *et al.* [6], [7] used it for slotted wall studies as discussed in Section 5.2.4.2. Phillips and Waggoner [149], [150] implemented the classical boundary condition formulations in a nonconservative, transonic small disturbance code (Boppe [30]). The boundary conditions (including solid walls, open jets, porous and slotted walls, and solid and slotted walls with viscous effects) were applied independently on the different tunnel walls to obtain a pre-test estimate of wall interference effects on the aerodynamic test data. Comparisons between predictions and measured reference data (Lockman and Seegmiller [116]) revealed discrepancies in wing shock locations of about 5 percent. These discrepancies were attributable to the numerical differences in nonconservative versus conservative finite difference formulations and other not-modelled details of the shock-wave/boundary-layer interaction. Al-Saadi [8], [9], [10] computed the transonic flow over two different transport configurations tested in the National Transonic Facility using a nonconservative, transonic small disturbance code in which several, usually-neglected, higher-order terms were retained to improve shock-wave and wing-sweep simulations (Boppe [30]). Tunnel-wall boundaries were modelled using the Berndt discrete-slot boundary condition

and comparisons with measured wall pressures were used to assess the quality of the simulation. Though good comparisons were generated for some cases, uncertainties in the wall pressure measurements and in the viscous boundary-condition modelling require a more detailed analysis to be performed when appropriate data become available, particularly at the higher Reynolds numbers where good data are non-existent.

5.3.1.3 FULL-POTENTIAL EQUATION (FPE) METHODS

For steady, inviscid, irrotational flow ($\nabla \times V = 0$), a velocity potential ϕ can be defined ($V = \nabla \phi$) which satisfies the non-linear FPE, written here in Cartesian co-ordinates as

$$(a^2 - \phi_x \phi_x) \phi_{xx} + (a^2 - \phi_y \phi_y) \phi_{yy} + (a^2 - \phi_z \phi_z) \phi_{zz} - 2(\phi_x \phi_y \phi_{xy} + \phi_y \phi_z \phi_{yz} + \phi_z \phi_x \phi_{xz}) = 0$$

where a is the speed of sound which depends on the velocity components ϕ_x , ϕ_y , and ϕ_z . However, unlike the TSDE, this FPE equation (or its equivalent for a stream function) is generally solved in a "body-oriented" or mapped co-ordinate system in order to obtain sufficient resolution and near orthogonality in high gradient and curvature regions of the flow. Thus, a non-trivial issue for simulation of tunnel flows using a structured grid is to find an appropriate simultaneous mapping for both test model and tunnel walls. This should be no problem, however, for an unstructured grid approach.

The classic transonic relaxation solutions obtained by Emmons [50] were for an airfoil (the NACA 0012) in a solid wall wind tunnel and in free-air. It is interesting to note that he stated then:

"Theoretical predictions of the effect of wind-tunnel walls for incompressible fluids have been successful with the required accuracy. For increasing Mach numbers, however, the corrections increase very rapidly and have a very profound effect on the flow as shock waves appear. Thus, the best experimental method in aerodynamics is seriously handicapped by the lack of knowledge of what wind-tunnel-wall corrections should be made to wind-tunnel test results."

He concluded:

"Although the relaxation method appears to be adequate to solve the very involved differential equations and boundary conditions describing the flow of a compressible fluid, the calculations are too involved to permit the investigation of a very wide range of interesting cases without the use of high-speed calculating machines."

His calculations were done by hand; it would be another twenty-five years before such high-speed calculations would even be demonstrated!

In 1975, transonic flow solutions obtained by relaxation of the FPE for both 2-D and axisymmetric models inside wind tunnel walls appeared. Kacprzyński [90] presented results for an airfoil in a porous wind tunnel with non-linear wall behaviour. He mapped the region exterior to the airfoil, including the walls, into the interior of a circle and found the solution method to be extremely efficient numerically. However, he concluded that the inclusion of viscous effects would require costly updating of the mapping function. Another analysis of this problem is given by Catherall [32] for flow past airfoils in solid, porous or slotted wind tunnels. South and Keller [172] considered transonic flow past axisymmetric bodies in a wind tunnel where the region between the body and tunnel wall is mapped onto a rectangular plane. A general linearised homogeneous wall boundary condition, essentially that given and discussed in Section 5.3.1.2, was enforced to model solid, open-jet, and idealised porous and slotted walls. They addressed the computational mapping, numerical implementation of boundary conditions, stability, and convergence

issues for the FPE in such applications. Results were also presented for nonlifting 2-D tunnel flow simulations.

In the early 1980's FPE applications related to simulating wind tunnel flows for 2-D, axisymmetric, and 3-D configurations continued to address the required co-ordinate mappings. Doria and South [48] developed a nearly orthogonal mesh by a sequence of Schwarz-Christoffel transformations and shearings appropriate to 2-D lifting airfoils and axisymmetric bodies in a wind tunnel. The finite-volume relaxation process was investigated using several different iterative schemes; solution convergence of nearly choked channels was found to be slower than that for other transonic flows. Mercer, *et al.* [128] and Mercer and Murman [129] developed a fully-conservative, finite-volume FPE computer program to simulate transonic flow past a swept wing in a wind tunnel with specified normal flow at the walls. They obtained an approximately orthogonal mesh conforming to both the wing and the tunnel walls. This code was intended to simulate the wind tunnel in preliminary studies of 3-D adaptive wall concepts; some 2-D airfoil example calculations, used in the code verification, were given and a 3-D sample result was demonstrated.

5.3.1.4 EULER EQUATION METHODS

The Euler equations express the conservation of mass, momentum and energy for inviscid rotational flow and are written in 3-D Cartesian co-ordinates (x_i), with corresponding velocity components (u_i), as

$$\frac{\partial w}{\partial t} + \sum_i \frac{\partial f_i(w)}{\partial x_i} = 0$$

The vectors w and f_i are functions of the velocities (u_i), pressure (p), density (ρ), total energy (E), and total enthalpy (H) given by

$$w = \begin{bmatrix} \rho \\ \rho u_1 \\ \rho u_2 \\ \rho u_3 \\ \rho E \end{bmatrix} \quad \text{and} \quad f_i = \begin{bmatrix} \rho u_i \\ \rho u_1 u_i + p \delta_{1i} \\ \rho u_2 u_i + p \delta_{2i} \\ \rho u_3 u_i + p \delta_{3i} \\ \rho H u_i \end{bmatrix}$$

where $p = (\gamma - 1) \rho \left[E - \frac{1}{2} \sum_i u_i^2 \right]$, $\rho H = \rho E + p$, and $\delta_{ij} = 1$ for $i=j$, 0 otherwise.

The early numerical solutions of these equations were also generally done in body-fitted co-ordinates; i.e., on mapped structured grids, similar to those used for FPE solutions, or on embedded grids (Benek, *et al.* [23]) and first for 2-D airfoils. An interesting example by Gaffney, *et al.* [66], who solved the Euler equations on Cartesian co-ordinates for a multielement airfoil, pointed out the more serious problem associated with inviscid CFD solutions for realistic configurations tested in wind tunnels at supercritical Mach numbers. They conclude that their

"calculations...illustrate the importance of taking into consideration wall interference effects when comparing the predictions of theory with experiment. With the exceptions of regions where viscous-inviscid" interactions "are strong," (i.e., regions at trailing edge of main airfoil and leading edge of flap) "calculations based on the Euler equations, when coupled with wall corrections, based on shifts in Mach number" (i.e., the Sewall [166] sidewall boundary-layer contribution discussed in 5.2.2) "and angle of

attack" (i.e., data of Stanewsky and Thibert [173]) "yield remarkable agreement with experiment. However, without proper considerations of viscous-inviscid interactions, simple shifts of angle of attack and Mach number will not bring the predictions of free air calculations in line with those of wind tunnel measurements."

Many uses of 3-D Euler equation CFD solvers in supercritical or transonic wind tunnel applications have been made in the last decade; however, either the configuration or test results tend to be proprietary or sensitive, so that information has not been openly reported. Applications are also mentioned in sections 5.3.2, 5.3.3, and 5.3.4 so little more than a few generalities will be mentioned here. For complex configurations, the body-fitted grids used are block-structured, embedded, or unstructured. These equations are frequently coupled with an approximate boundary layer solver to account for some of the viscous interactions. Tunnel wall boundary conditions, if used, are generally still modelled, due to the flow complexities at the ventilated walls that are required for transonic testing. However, the inability of the Euler equations to properly capture important viscous-inviscid interactions tends to limit their use.

5.3.1.5 NAVIER STOKES EQUATION METHODS

The specific form of the terms in a compressible, turbulent Navier-Stokes equation set depends upon the velocity decomposition and averaging, as well as the turbulence modelling that is used (see, for example, Vandromme and Haminh [179] or Wilcox [184]). In the transonic and high-speed flows of interest here, typically those for aerospace configurations as tested in wind tunnels, both compressible and pressure-gradient effects are important for the shock-wave/boundary-layer interactions which occur. Usually, a thin-layer approximation of the Reynolds' Averaged Navier-Stokes (RANS) equations, written in body-oriented co-ordinates, is employed in the numerical codes. Turbulence modelling utilised over the last decade or so has been primarily algebraic or for one- or two-equation models. Since it is not our purpose to discuss the elaborate equations nor details here, the reader is referred to the cited literature for such information.

Some times, the verification or validation studies for RANS algorithms and turbulence models is attempted by comparing and/or correlating code predictions with measured data on simple configurations where the wind tunnel walls must be considered. The early 3-D study reported by Kordulla [106] is an example; it illustrates the magnitude of the complexities, both experimental and computational, involved in a seemingly simple case. There, results from six different RANS codes, all using the Baldwin-Lomax algebraic turbulence model, were compared with transonic (supercritical) data on a swept semi-span wing mounted on a splitter plate in a solid wall wind tunnel. The tunnel wall interference effects were noted in the pressure distributions, streamline patterns, and integrated forces. However, there were also noticeable effects due to variations in transition location, juncture region modelling, inviscid-viscous wall boundary conditions, and computational gridding. This was for a solid tunnel wall case; the detailed resolution required for a direct simulation of the viscous flow at the ventilated walls normally used in transonic testing is not now feasible. Therefore, one must resort to approximate wall boundary conditions or descriptions as discussed in section 5.2. Use of two perforated wall boundary conditions with Navier-Stokes codes for tunnel flow simulation is indicated in 5.3.2 and 5.3.3.

Simulation of the shock-wave/boundary-layer interactions at the sidewalls in airfoil tunnels and on the mounting wall in semispan wing tests using RANS codes has been done. For example, airfoil tunnel simulations using 3-D codes with viscous sidewall boundary conditions were reported by Obayashi and Kuwahara [145], Swanson, *et al.* [177], and Radespiel [153]. Their results show the loss of 2-D symmetry due to the sidewall boundary layer separation upon its interaction with the shock on the model.

Simulation of the mounting wall viscous layer in a semispan wing test was reported, for example, by Vatsa and Wedan [180]. It is seen that the mounting wall boundary layer interacts with the shock on the model and separates, thus altering the shock strength and position, the streamline pattern, and the separation over an appreciable part of the model span. Milholen and Chokani [130] used a RANS code to calculate the interaction between a wind tunnel sidewall boundary layer and the transonic flow at flight Reynolds number about a thin, low-aspect-ratio wing mounted on that wall. The sidewall boundary layer was seen to have a strong influence on the flow about the wing; the computed wing pressures were in excellent agreement with the data, showing vast improvement over previous free-air computations.

As with the Euler equation CFD codes, applications of the RANS codes are being made to design wind tunnel tests and aid in the interpretation of test results (again, see 5.3.3). As the computational power (speed, memory, and communication bandwidth) of the computer hardware available at the engineer's desk and tunnel continues to increase, so too will the computational fidelity of his computer software. Of the computational gains made in CFD, about half can be attributed to hardware improvements, with the other half coming from algorithm improvements. When Garner, *et al.* [67] was published, CFD did not exist.

5.3.2 MDA WALL INTERFERENCE COMPUTATIONS

5.3.2.1 BACKGROUND

Although McDonnell Douglas Aerospace (MDA), currently part of the Boeing Company, tests its advanced fighter configurations in wind tunnel facilities around the world, they own and operate a small 4-foot x 4-foot tunnel. This tunnel is very busy with advanced design, missile, and diagnostic tests. The MDA approach to correcting transonic wind tunnel data for wall interference has been strongly influenced by the need to provide viable wall corrections for this small facility — often with oversized models designed to test in a larger tunnel. Furthermore, the need to provide timely corrections for “production” mode testing has resulted in a pragmatic (if not always rigorous) approach that has been demonstrated to provide good quality corrections quickly and economically for many different advanced fighter configurations. A typical “large” model for which validated corrections have been provided would be a 6% F-18 in the 4x4 foot test section.

Two types of corrections can be provided, depending on model size and allowable uncertainty in results. The most economical is an empirical approach obtained from an experimental wall interference database developed by testing a set of four geometrically similar models of different scale in several different size wind tunnels. The more rigorous (and more expensive) method uses numerical simulation of the model in the wind tunnel and in free flight -- taking the difference between the two solutions as an incremental correction for the wind tunnel data. ***The key to the success of this approach is the fidelity of the tunnel wall boundary conditions.***

These two approaches will be briefly described. The development of the wall boundary condition was previously described in section 5.2.3.1. A more complete discussion may be found in the literature.

5.3.2.2 EMPIRICAL CORRECTIONS

As previously noted, the empirical approach was developed from an experimental wall interference database. A set of four models was used to generate this database. In determining the basic design of the "boundary interference" models, the need for simplicity and accuracy in fabrication was balanced against the desire to have a realistic flight configuration. In the end, a simple cylindrical body with a delta wing was used. An ellipsoidal nose was faired into the body at the wing apex location, and a boat tail was added to reduce drag. A NACA 0006 wing section was used, with thickness scaled according to local chord.

A total of four geometrically similar models were constructed, two for use in each facility. Model #2 was sized to have the same relative blockage in the 4x4 foot Poly Sonic Wind Tunnel facility (PSWT) as a typical flight configuration model. Relative blockage is defined here as the maximum cross-sectional area of the model at zero degrees angle of attack, divided by the cross-sectional area of the wind tunnel test section. Model #1 has a relative blockage twice as great as model #2. The smaller two models were designed to significantly exceed standard rules of thumb for model sizing, when tested in the 1x1 foot Transonic Wind Tunnel facility (TWT). Figure 5.25 shows dimensions for the configuration based on reference chord length and the value of reference chord length for each of the four models.

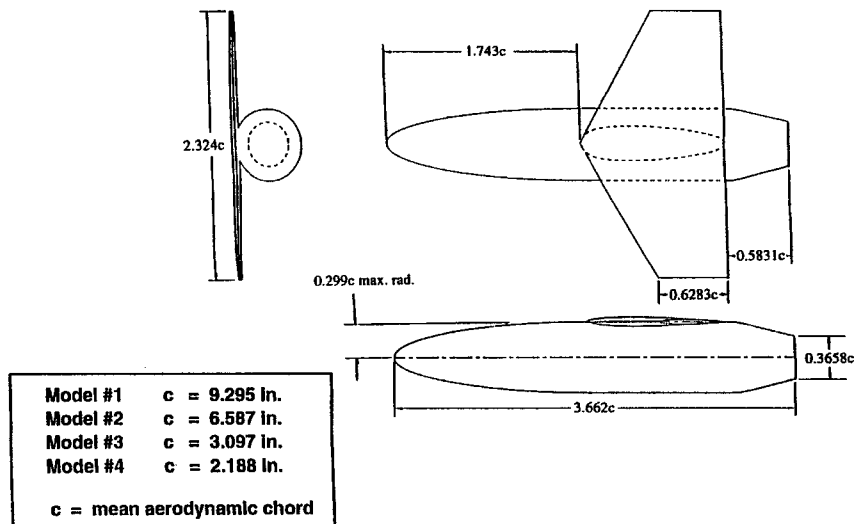


Figure 5.25 : Interference Model Set Dimensions

The models were designed for use with an internal six component strain gage balance. The larger two models (models #1 and #2) use a 1.5 inch diameter balance, while models #3 and #4 use a 0.75 inch diameter balance. Each balance had a separate sting support. Boundary layer transition strips were placed on the nose and both wing surfaces at approximately the 5% chord. Four base pressure taps were provided on the largest two models, on the other models the base area was negligible. As a cost saving measure, no additional pressure instrumentation was provided on any of the four models.

The models were designed for use with an internal six component strain gage balance. The larger two models (models #1 and #2) use a 1.5 inch diameter balance, while models #3 and #4 use a 0.75 inch diameter balance. Each balance had a separate sting support. Boundary layer transition strips were placed on the nose and both wing surfaces at approximately the 5% chord. Four base pressure taps were provided on the largest two models, on the other models the base area was negligible. As a cost saving measure, no additional pressure instrumentation was provided on any of the four models.

Models #1 and #2 were tested in the PSWT. Models #3 and #4 were tested in both the TWT and PSWT. In addition, data were obtained for model #1 in the Ames 11 ft. Transonic Tunnel. Figure 5.26 shows a summary of the 4 models

$$\text{Blockage} = \frac{\text{Model Reference Area}}{\text{Tunnel Cross-Section}}$$

	Model #1	Model #2	Model #3	Model #4
NASA Ames (11ft. x 11 ft.)	.01108	-	-	-
MDA PSWT (4 ft. x 4 ft.)	.08381	.04191	.009306	.004651
MDA TWT (1 ft. x 1 ft.)	-	-	.1489	.07442

Figure 5.26 : Interference Model Tests

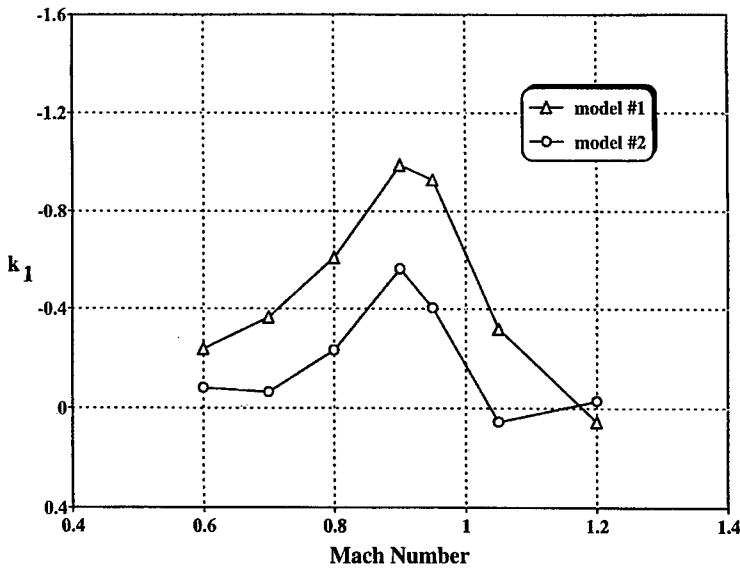


Figure 5-27 : Angle of Attack Interference factor in PSWT

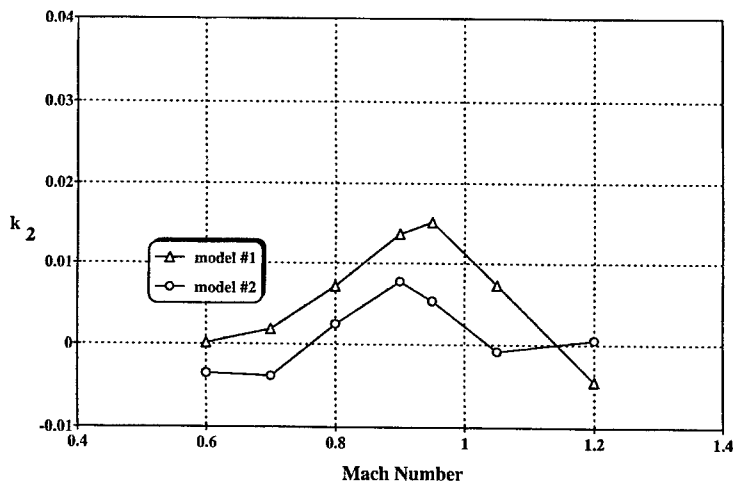


Figure 5.28 : Induced Drag Interference Factor in PSWT

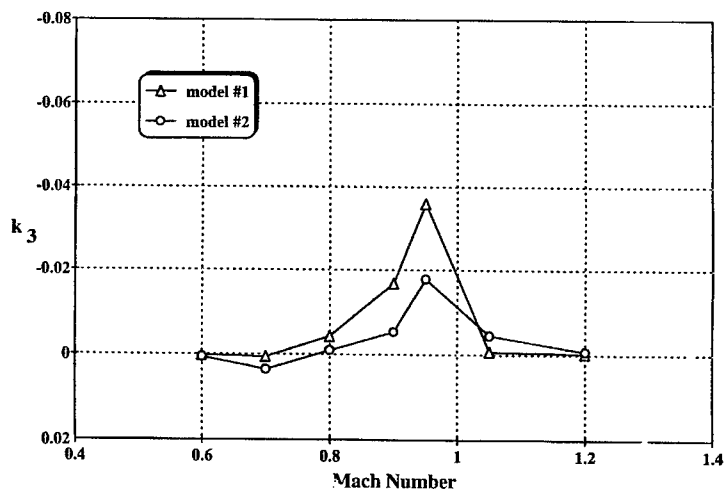


Figure 5.29 : Pitching Moment Interference Factor in PWST

with relative blockages in each facility where they were tested. An overview of experimental results and discussion of treatment of the data to remove Reynolds number effects is given in Rueger and Crites [160].

After examination of the extensive database created by testing these models over a period of two years, it was determined that a relatively simple form was suitable for expressing first order interference induced increments. From Rueger, *et al.* [161]

$$\Delta\alpha = k_1 C_L$$

$$\Delta C_D = k_2 C_L^2 + \frac{\Delta\alpha}{57.3} C_L$$

$$\Delta C_M = k_3 C_L$$

The constants k_1 , k_2 , k_3 are termed interference factors and are determined by curve fitting interference increments from the database. It should be noted that these expressions are not unique. Other forms may be equally valid.

Figures 5.27, 5.28, and 5.29 show typical variation in wall interference for the two largest models in the set for the 4-foot PSWT tunnel. Note that the interference effect increases sharply (as expected) in the vicinity of Mach 1, and then decreases toward zero as Mach 1.2 is approached.

First order corrections are obtained quickly and simply by scaling the experimental interference by appropriate factors such as reference area, tail length, etc. This gives good first order corrections. Where greater accuracy is required, the interference factors are computed at a couple of points and then curve fit, using the method defined below.

5.3.2.3 TWO POINTS OF VIEW

In transonic wind tunnels with relatively small models, a linear wall boundary condition is usually assumed. The wall interference question is: What angle-of-attack and Mach number would be required for the same model in free-flight to develop the same lift measured in the wind tunnel? Corrections are sought for Mach number and angle-of-attack. This approach is a descendant of the method of images (Pope [152]) used to obtain wall interference corrections for low speed solid wall, or open jet, test sections. Extension of this approach to ventilated transonic test sections in Pindzola and Lo [151] and Rizk and Murman [159] naturally retained the initial point of view; i.e., wall interference is seen as an error in Mach number and angle-of-attack. As previously mentioned in Section 5.1.1, a sufficient condition for this approach is WS. However, some of the concepts can be formalised within the framework of asymptotic expansions for Group 1 and possibly Group 2 and 3 flows. The application to Group 1 flows is given in Section 5.4.

In tunnels with relatively large models, the classical approach often fails for two reasons. First, the model is closer to the wall, interactions are stronger, and significant interference gradients develop about the model. In this case there is no single value of Mach number and angle-of-attack that is equivalent to the free-flight condition for the measured forces. The condition is said to be "uncorrectable". Second, the linear wall boundary condition usually used in this type of analysis breaks down and does not apply.

In tunnels with small models, the model-impressed pressure signature is weak at the wall. Also, the boundary layer thickness tends to establish a relatively constant distribution over the walls. In this case, the assumption that crossflow is governed by local wall pressure may be warranted. However, in smaller tunnels the wall signature becomes significant, and, as shown by Jacocks [88], the local crossflow through the wall depends on local pressure and on local boundary layer displacement thickness. Local displacement thickness is strongly dependent on the upstream distribution of pressure and crossflow (transpiration). Therefore, crossflow is really a complex non-linear phenomenon depending not just on the local pressure (classical assumption), but also on the local boundary layer, and therefore on upstream pressure and crossflow distributions. In smaller tunnels (or large tunnels with very large models) the true non-linear nature of the crossflow and boundary layer displacement effect must be considered.

An alternate point of view discards the paradigm that wall interference should be viewed as error in test Mach number and pitch angle. Instead of considering the lift developed on the model as invariant, the test conditions of Mach number and model incidence angle are taken as constant. The question asked is:

If the walls (and model support) are removed while maintaining constant Mach number and angle-of-attack, how will the forces developed on the model (pressure distribution over the model) change? From this point of view, interference gradients about the model are automatically taken into account.

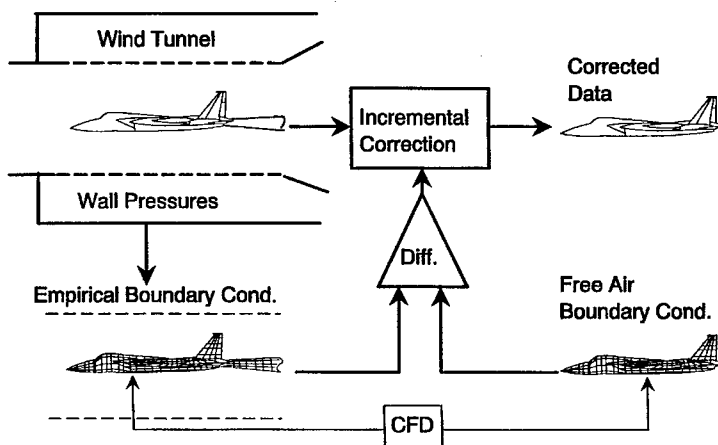


Figure 5.30 : Boundary Interference Correction Method

As shown in Figure 5.30, the correction procedure involves three steps. First, an appropriate numerical flow solver is used to simulate the aircraft model, model support structure, and wind tunnel walls. Measured wall pressures are used

with an empirical procedure to compute the equivalent inviscid boundary conditions simulating the non-linear viscous wall interaction. Second, numerical solutions are obtained with the walls and model support removed (free-flight boundary conditions). Third, the incremental differences in the computed forces and moments are applied to the experimental data as a correction.

5.3.2.4 APPLICATION OF THE MDA WALL FLOW MODEL

The wall flow model of Section 5.2.3.1.4 has been used successfully with flow solvers ranging from panel codes to Navier-Stokes codes. For Mach numbers producing only weak shocks, high order panel codes or full potential methods are useful. For higher Mach numbers, Euler solvers are required. Figure 5.31 shows typical application of the wall flow model. Generally three or four iterations of the wall flow model, separated by a few hundred solver iterations is adequate. Figures 5.32, 5.33, and 5.34, compare computed interference factors using panel and Euler solvers with the empirical interference factors discussed in Section 5.2.3.2. Figures 5.35 and 5.36 show typical corrections of PSWT data for MCM (a super cruise variant), and a 6% scale F-18. The MCM was tested in the PSWT (4x4-foot tunnel) and the NASA Ames 11-Ft Transonic Tunnel. The F-18 was tested in the PSWT and the NASA Langley 7x10-Ft Transonic Tunnel. The PSWT wall, with 22.5% porosity produces open-jet type interference effects. The corrections applied make a considerable improvement.

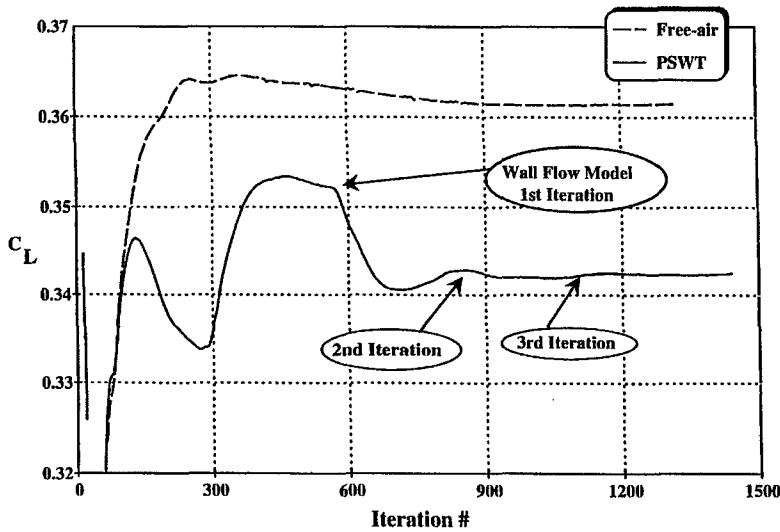


Figure 5.31 : Lift Iteration History

The MCM was tested in the PSWT (4x4-foot tunnel) and the NASA Ames 11-Ft Transonic Tunnel. The F-18 was tested in the PSWT and the NASA Langley 7x10-Ft Transonic Tunnel. The PSWT wall, with 22.5% porosity produces open-jet type interference effects. The corrections applied make a considerable improvement.

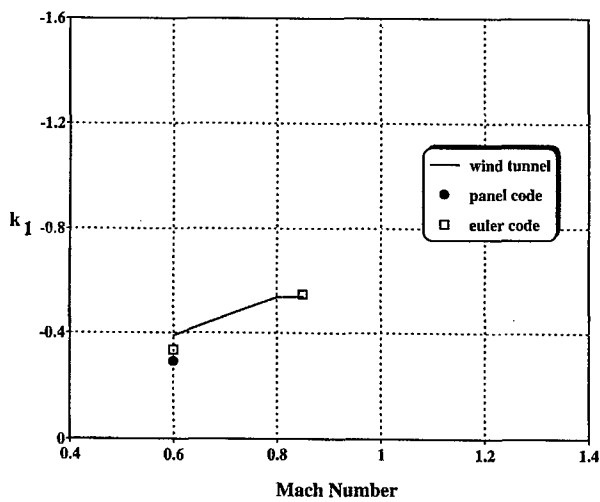


Figure 5.32 : Angle of Attack Interference Factor in the PSWT

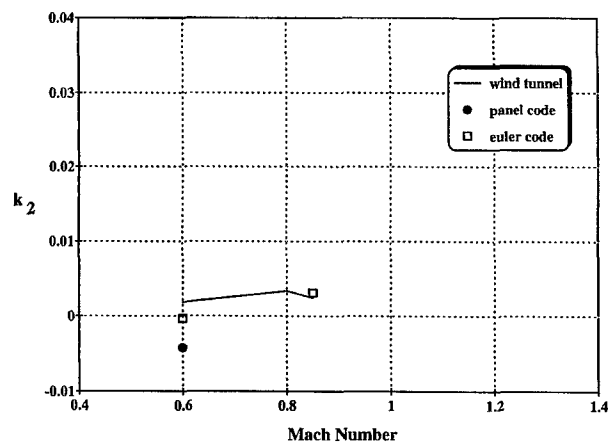


Figure 5.33 : Induced Drag Interference Factor in the PSWT

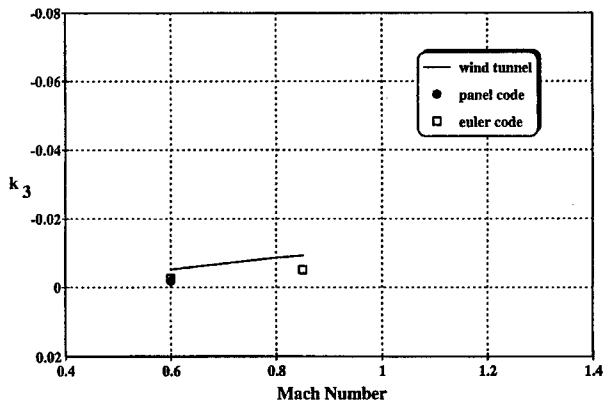


Figure 5.34 : Pitching Moment Correction Factor in the PSWT

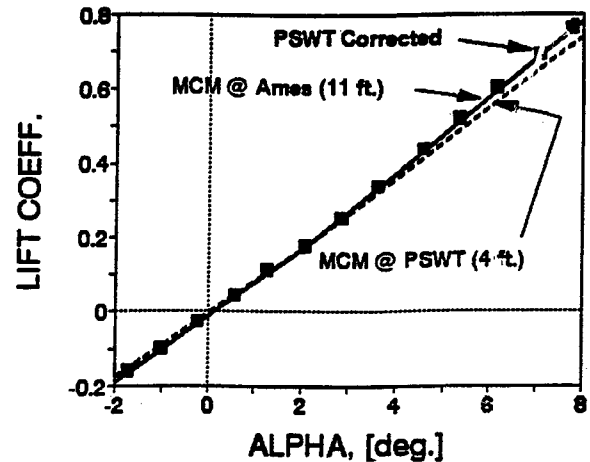


Figure 5.35 : Correction of MCM Lift

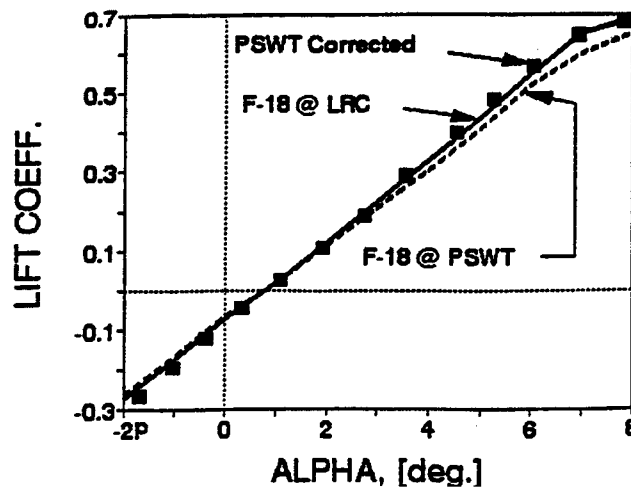


Figure 5.36 : Correction of F-18 Lift

5.3.3 AEDC WALL INTERFERENCE COMPUTATIONS

5.3.3.1 INTRODUCTION

The development of present and future flight systems is placing stringent demands on wind-tunnel facilities to provide high-quality data at transonic speeds. Wall interference can significantly compromise the quality of transonic wind-tunnel data (Whorric and Hobbs [183]). While the perforated walls of AEDC transonic wind tunnels minimise wall-interference effects, significant wall interference can occur at high-subsonic and low-supersonic flow conditions even for models below one-percent solid-blockage ratio (Kraft, *et al.* [109]). In order to use wind-tunnel data to predict a flight vehicle's performance with confidence, the data must be assessed and/or corrected for wall effects. Wall interference is more pronounced and more difficult to correct at high-subsonic conditions where the sonic regions extend to

the walls. Such flows have been classified as Group 2 flows in Hornung [86] and Erickson [51], whereas Group 1 flows have lower Mach numbers with subcritical flows at the walls.

Model sizing is becoming a critical issue in testing. Users want larger models to achieve maximum possible Reynolds number. In the past, models for aerodynamic testing were sized to span less than sixty percent of the tunnel width and to be less than one-percent solid-blockage ratio. Although wall interference can compromise data at certain conditions for these size models, wall interference was not considered to significantly affect the data quality, and corrections for wall interference were not routinely applied. With more stringent data-quality requirements and the desire to test larger models, this assumption is no longer the case. At present no capability exists to routinely correct transonic data for wall interference. As will be shown, corrections are performed only for limited programs and only for limited flow conditions using computationally-intensive CFD techniques.

Several wall-interference assessment/correction (WIAC) techniques have been developed for three-dimensional non-linear flows and are summarised in Kraft, *et al.* [109]. A WIAC technique uses boundary data measured at an interface which is on or near the wind tunnel walls and consists of two components: (1) a flow solver that adequately represents the tunnel and free-air flows, and (2) a procedure for using the measured boundary data and the flow solver to determine wall interference. Although these techniques have been demonstrated numerically for Group 2 flows, there is a considerable need to validate them with experimental data (Kraft, *et al.* [109]). The examples in this contribution address that need.

Wall-interference corrections can also be obtained by pretest-predictive techniques. Application of these techniques requires a representation of the wall behaviour instead of measured boundary data. Classical global descriptions of the ventilated-wall boundary characteristics have proved to be inadequate. AEDC has developed a local semi-empirical description of the perforated-wall characteristic (Sec. 5.2.3.2). Provided that an adequate model of the ventilated walls can be achieved, the pretest procedure is an attractive alternative because it does not require the installation of a measurement system.

Application of WIAC and pretest-predictive techniques to experimental three-dimensional subsonic and transonic data were evaluated in Sickles and Erickson [167],[168]. Use of inviscid flow solvers gave accurate wall-interference corrections for subsonic and mildly supercritical Group 1 flows ($M \leq 0.8$). However, erroneous corrections were obtained for strongly supercritical Group 2 flows ($M \geq 0.9$). In most cases, the sign and magnitude of the lift increment were in error. The cause of the inaccuracies was attributed to the inability of the inviscid flow solvers to simulate the viscous effects on the model. Viscous effects become important for strongly supercritical flow, namely proper shock characterisation and trailing-edge behaviour, and must be represented in order to determine accurate corrections.

5.3.3.2 WALL INTERFERENCE PROCEDURE

Wall-interference effects are predicted by taking the difference between two CFD analyses. The first is a free-air flow-field calculation, while the second is a tunnel flow-field calculation which includes either a perforated-wall boundary condition for the pretest-predictive approach or a boundary condition where the measured pressure is specified for the WIAC approach. Thus, a pair of calculations must be performed for each test condition under investigation. The difference in calculated local pressures can then be used to correct the experimental pressure measurements. Also, the experimentally measured force and moment can be corrected by appropriately integrating the computed pressure differences and adding the integrated values to the measured data.

This procedure is an incremental approach that looks at the difference between two calculations. Therefore, exact replication of the experimental results with computations is not necessary, but rather the increments must be accurately simulated. However, previous investigation has shown that to obtain accurate increments certain attributes of the flow, such as shock position and strength, must be replicated with some degree of certainty. The sections that follow illustrate the AEDC approach and give results for research configurations as well as realistic test articles.

5.3.3.3 WALL INTERFERENCE RESULTS

Wall-interference assessment and corrections are given for four models. All models were tested in AEDC wind tunnels which employ perforated walls with sixty-degree inclined holes. The database for each model, except for the Space Shuttle Launch Vehicle (SSLV), consists of data obtained on the same model in a larger tunnel where conditions are assumed to be interference-free. For the SSLV, data exists for a smaller scale model in the same tunnel and in a different tunnel. All models are pressure-instrumented to make detailed comparisons of pressure distributions between data with and without interference. Details of these configurations as well as the wall-interference computations can be found in Martin, *et al.*, [126] and Sickles, *et al.* [167], [168], [169].

5.3.3.4 MODEL DESCRIPTIONS

The first two models are similar. They are generic wing/body/tail vertically-symmetric configurations with constant chord, 30-degree swept lifting surfaces. The first model is shown in Figure 5.37. The lifting surfaces have NACA 0012 cross sections. The model was tested in AEDC Aerodynamic Wind Tunnel (4T), in which the blockage ratio is 0.16 percent, to obtain reference data assumed to be interference-free. Data with varying amounts of wall interference were measured in the adaptive-wall test section of AEDC Aerodynamic Wind Tunnel (1T) (Erickson [51]; Martin, *et al.* [126]; and, Sickles and Sinclair [169]), in which the blockage ratio is 2.5 percent. This model will be referred to as the WIM1T (wall interference model for 1T). The pressure distribution was measured near the tunnel walls with a system of rotated static pipes shown in Fig. 5.38. The second generic configuration, to be referred to as WIM4T, is shown in Fig. 5.39. This model was tested in Tunnel 4T with a blockage ratio of 1.33 %, and in Aeropulsion Wind Tunnel (16T) for reference data assumed to be interference-free, since the blockage ratio is 0.08%. The lifting surfaces have NACA 0010.4 sections.

The third model is a three-percent model of the Space Shuttle Launch Vehicle (SSLV) which is shown in Fig. 5.40. This model was tested twice in 16T. The blockage of this model at angle of attack $\alpha = -5^\circ$, is 0.7 %. The second entry involved a refurbished, modified

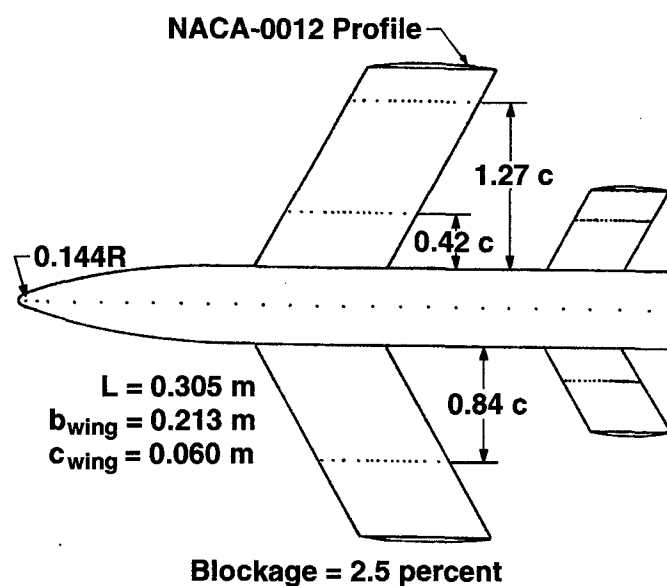


Figure 5.37 : Wall interference model for tunnel 1T (WIM1T)

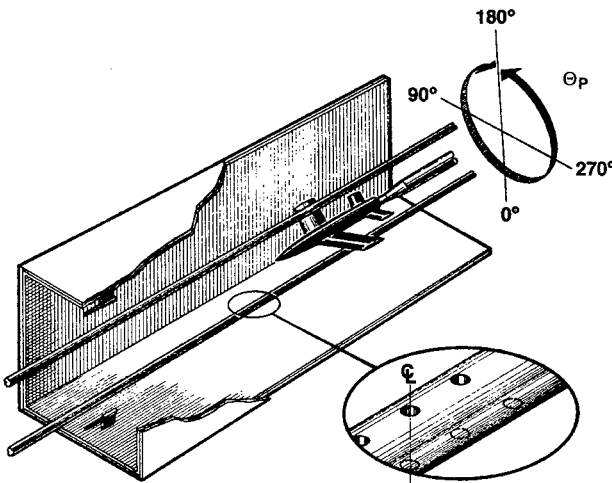


Figure 5.38 : Tunnel 1T interface measuring system

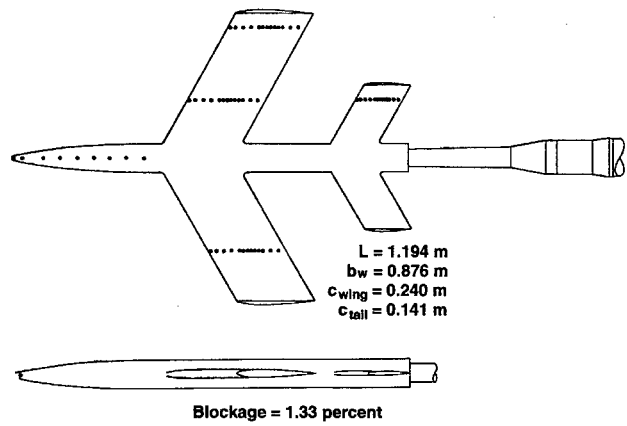


Figure 5.39 : Wall interference model for Tunnel 4T (WIM4T)

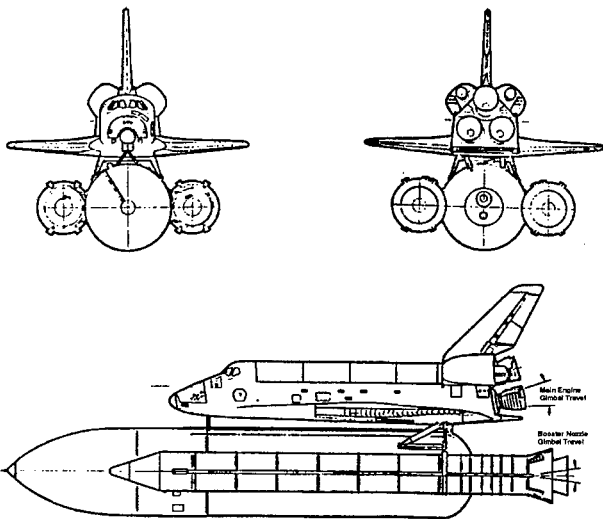


Figure 5.40 : Space shuttle launch vehicle model

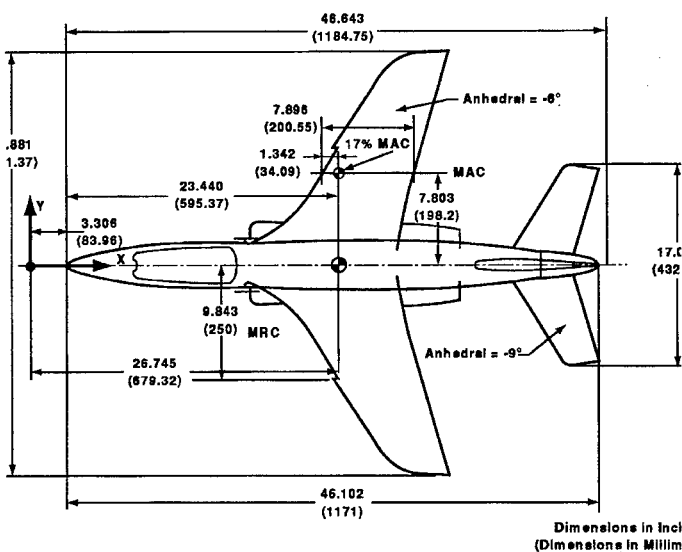


Figure 5.41 TST model schematic

configuration of the first model. A smaller scale model (two-percent scale with a different support system) was also tested and will be used as reference data. The blockage of this model is 0.3% at $\alpha = -5^\circ$.

The fourth model is the TST model, a 1/10-scale model of the Dornier Alpha Jet configured with a transonic technology wing, and is shown in Fig. 5.41. Tests were conducted in 1992 in Tunnels 4T and 16T as part of a co-operative effort between the United States Air Force (USAF) and the German Ministry of Education and Science, Research and Technology (BMBF). Additional tests were conducted in the DLR Kryo Kanal Köln (KKK) and the NASA Langley National Transonic Facility (NTF). Data were obtained over a wide range of chord Reynolds numbers that included conditions from conventional wind tunnels to flight. The objective of the test program was to develop a quality database for studying the interaction of tunnel-environment, wall-interference, and Reynolds-number effects that prevent wind tunnel data from being totally representative of flight, and to confirm the Viscous Simulation Methodology developed by AGARD Working Group 09. The primary objective of the 4T test was to study wall interference and to evaluate the AEDC correction procedures.

The TST model is large for 4T (solid blockage ratio of 1.8%) and significant wall interference was anticipated, particularly at the higher subsonic freestream Mach numbers. Although the TST model is a large model for an aerodynamics test, it is considered a typical size model for Captive Trajectory Support (CTS) testing. To determine the effects of wall interference, the 4T data are compared to the 16T data. The TST model is an extremely small model in 16T (0.1% blockage), and the data from 16T is considered interference-free.

Flow-field pressure measurements were made in 4T during the testing of the TST model to aid in understanding the data and to assist in the validation of the wall interference correction techniques. These pressure measurements were made on a circular interface near the tunnel walls with a series of two-component static pipes that ran nearly the entire length of the test section. Figure 5.42 shows the cross sectional view of the twelve pipe system. The diameter of the interface is 20.5 inches. Six pipes were instrumented with pressure orifices. The other six were dummy pipes that were installed to maintain flow symmetry. Each metric pipe was instrumented with 46 diametrically opposed orifice pairs, except the lower wall metric pipe which had 44 pairs, and two upstream unpaired orifices on the model side of the pipe. The orifices are aligned in the radial direction.

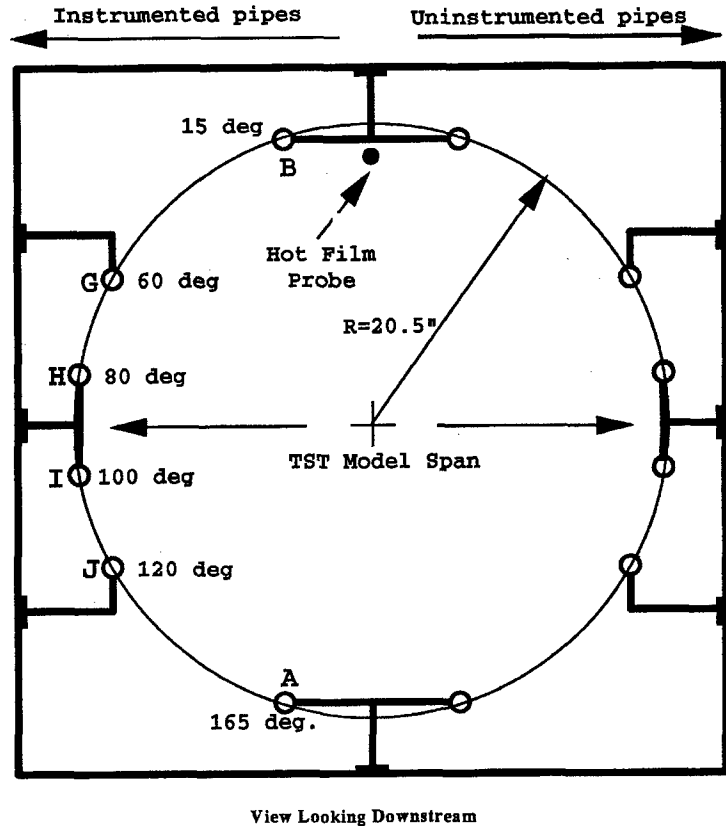


Figure 5.42 : Tunnel 4T static pipe layout for TST test

5.3.3.5 WIM1T AND WIM4T WALL-INTERFERENCE COMPUTATIONS

All flow computations for the WIM1T and WIM4T were performed with the chimera overset-grid code, XAIR (Benek, *et al.* [23]). The near-field about the wings was solved with the thin-layer Navier-Stokes (TNS) equations using a Baldwin-Lomax turbulence model. The fuselage, tail, and far field regions were all solved using the Euler equations. Previous results from Sickles and Erickson [167] showed that the viscous effects must be simulated at high subsonic freestream conditions to achieve accurate wall interference estimates. Both the AEDC perforated-wall boundary condition and a pressure boundary condition were incorporated into the flow solver to perform pretest-predictive and WIAC approaches, respectively.

Comparisons of the WIM1T calculated and measured wing-pressure distributions are given in Figure 5.43 for the WIAC approach and in Figure 5.44 for the pretest approach. The results were obtained for a $M = 0.9$. The Tunnel 1T wall porosity τ was set to three percent open area. Excellent fidelity exists between the calculated free-air and the 4T reference data as well as the calculated tunnel and the 1T

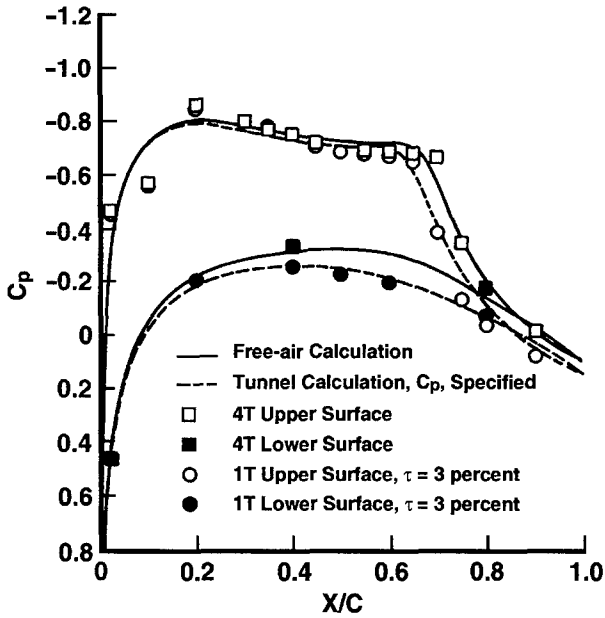


Figure 5.43 : WIM1T model pressures measured and calculated using the WIAC-TNS code at 40% wing semispan, $M = 0,9$, $\alpha = 4$ deg, $\tau = 3$ percent

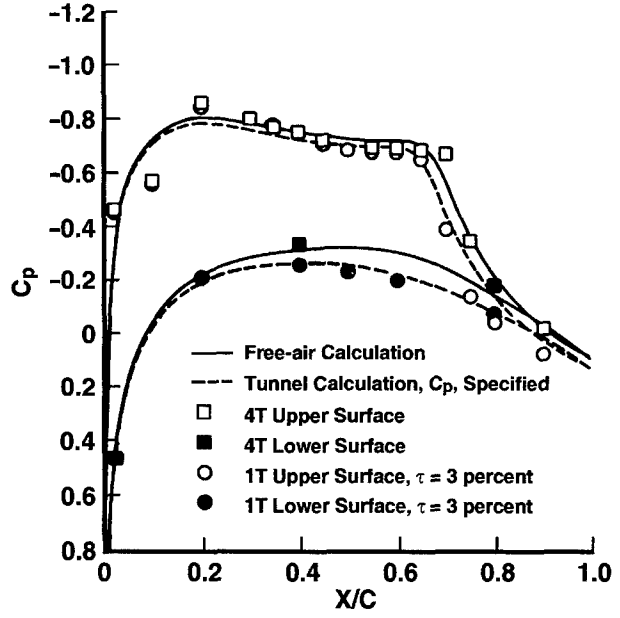


Figure 5.44 : WIM1T model pressures measured and calculated using the Pretest-TNS code at 40% wing semispan, $M = 0,9$, $\alpha = 4$ deg, $\tau = 3$ percent

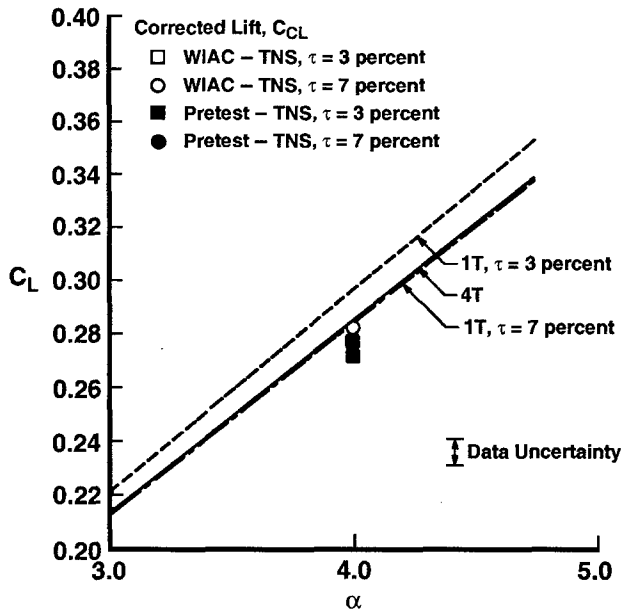


Figure 5.45 : WIM1T corrected lift coefficients using the WIAC-TNS and Pretest-TNS codes, $M = 0,9$, $\alpha = 4$ deg

data in the sense that the tunnel calculations with AEDC boundary condition are comparable to the tunnel calculation with measured pressure data prescribed as the boundary conditions. However, the shock is located farther aft on the wing in the tunnel calculations using the AEDC boundary conditions. The difference in shock location tends to amplify in the outboard wing direction (not shown). A comparison between the corrected lift coefficients for the WIAC and pretest codes is shown in Figure 5.45 for the three-percent porosity case and seven-percent case. The pretest corrections for both the $\tau = 3\%$ and the $\tau = 7\%$ cases are larger in magnitude than the WIAC by 0.0057. The larger correction is approximately two percent of the experimental lift, which is smaller than the uncertainty, and is attributable to the aforementioned shock location difference in the calculated pretest wing-pressure distributions. The small differences shown are consistent with the corrections discussed later in

Section 5.4.7 and the studies depicted in Figure 5.67. This can be related to the extended validity of slender body theory at transonic Mach numbers when “not-so-slender shapes” look “slender” because of the dominant effect of lateral disturbances along the Mach lines that are almost normal to the freestream, an observation that has been validated by Adams and Sears [1] and others.

The AEDC wall-boundary condition can be evaluated by comparing the calculated and measured distributions at the interface. For most azimuthal locations Θ_p , the calculations using the AEDC

boundary condition does remarkably well at duplicating the measured pressure distributions. A representative comparison is shown in Fig. 5.46 for $\tau = 3\%$ at the azimuthal location $\Theta_p = 85^\circ$ (to the side and below the wing tip). However, the calculated pressure distributions slightly underpredict the measured distribution in the vicinity of the wing. The underprediction is likely caused by the inability of the AEDC boundary condition to represent the behaviour of the walls in the region of strong gradients produced by the close proximity of the wingtip. Also, the underprediction could explain the wing shock location difference and its amplification at the outboard wing station in the pretest calculations. The interface pressures at $\Theta_p = 95^\circ$ indicate that the sonic region extends through the interface near the side wall. Thus, this case can be classified as a Group 2 flow.

The pretest approach has been applied to obtain corrections for the WIM4T data at $M = 0.95$ and $\tau = 5\%$ for three angles of attack. Pressures measured near the wall indicate that these cases are clearly Group 2 flows. The sonic region is larger than the WIM1T cases presented and extends to the upper as well as the side walls. Drag corrections for these cases are shown in Figure 5.47. Applying corrections to the Tunnel 4T data gives results that are in very good agreement with the Tunnel 16T reference data. Similar results have been determined for the corrected lift and pitching moment. The drag, lift, and pitching moment errors attributable to wall interference at $\alpha = 4^\circ$ are 11, 4 and 33% of their reference values, respectively, and are all corrected accurately. The uncertainties in the force measurements are approximately the size of the symbol in the graphs.

From another perspective, the results in Figure 5.47 show that the interference is practically constant with angle of attack α to within the data uncertainties. The figure suggests that this interference is simply the zero-lift blockage. This is consistent with the insensitivity of $C_{L\alpha}$ to small, but practical, changes in α , tunnel size and porosity, shown earlier in connection with the WIM1T in Figure 5.45 as well the TsAGI T-128 experiments described in Malmuth, Neyland and Neyland [124] and Section 5.4.9. It can simplify estimating interference effects on drag polars with approximations such as

$$\frac{\Delta C_D}{C_L^2} \sim 1/C_{L\alpha}$$

$$\Delta C_D \cong C_D - D_{D_0}$$

For these cases, the major interference effect is the change in zero-lift wave drag which alters C_{D_0} . This can be calculated for many practical shapes such as compact drag-rise fighters and blended wing-bodies from the Transonic Area

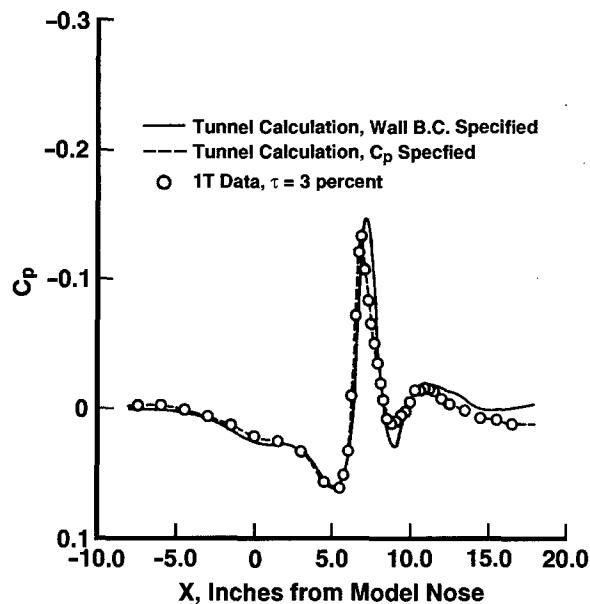


Figure 5.46 : WIM1T interface pressures measured and calculated, $M = 0.9$, $\tau = 3$ percent.

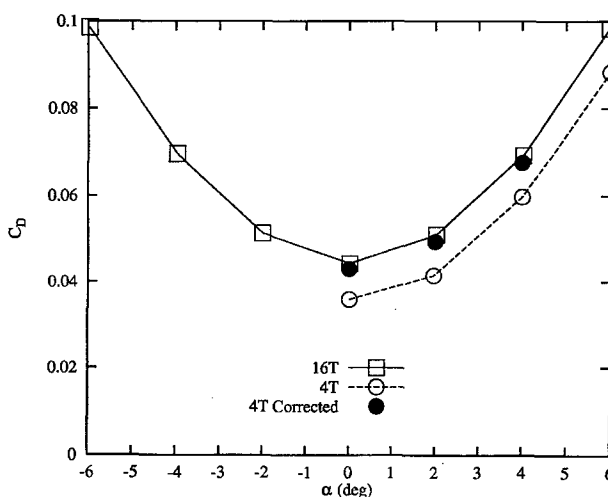


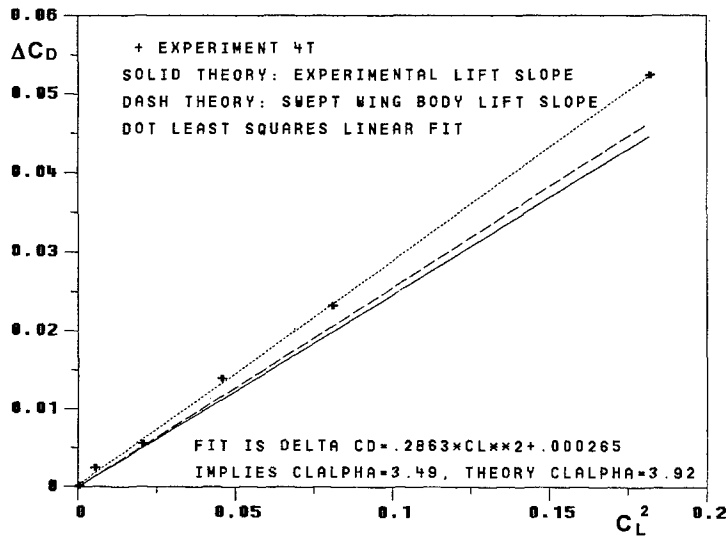
Figure 5.47 : WIM4T corrected drag coefficients using the Pretest-TNS code. $M = 0.95$, $\tau = 5$ percent

Rule for Wall Interference (TARWI) discussed in Section 5.4.8 and 5.4.9 in which the zero-lift wave drag blockage interference of the full-up three-dimensional configuration is identical to that of its equivalent body of revolution.

Fig. 5.48 tests applicability of the above approximation for the data of Figure 5.47. The solid curve uses the experimental value of $C_{L\alpha}$ from Figure 5.45.

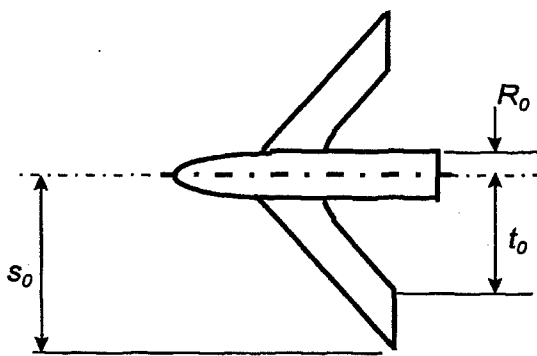
The dash curve uses the classical theoretical estimate of $C_{L\alpha}$ described in Heaslet and Lomax¹ (1954) for a swept trailing edge wing body approximating WIM4T

$$C_{L\alpha} = \frac{\pi}{2} AR \left[1 + \left(\frac{R_0}{s_0} \right)^4 - \left(\frac{t_0}{s_0} \right)^2 - \frac{R_0^2}{s_0^2 t_0^2} + \left(\frac{R_0}{s_0} \right)^2 \right]$$



where AR is the aspect ratio of the wing, R_0 is the body radius, and the other quantities are shown in Figure 5.49. Although a small discrepancy exists, the approximating equation for $\Delta C_D/C_L^2$ matches the trend of the data quite well, in view of the liberties taken in the approximation of WIM4T or WIM1T by the idealised configuration (IC) of Figure 5.49. It has the tips perpendicular to the flow as contrasted to that of WIM4T or WIM1T which are streamwise. Furthermore, the IC trailing edge is curved, to simplify the calculation by eliminating the upstream influence and coupling of the trailing edge vortex sheet. This effect has only received limited theoretical attention in the literature but is a pervasive issue.

Figure 5.48 : Comparison of WIM4T drag rise due to lift data from AEDC experiments with slender body theory for swept trailing edge wing bodies.



Additionally, boundary layer separation and transition effects have been ignored. The basic model is the previously-mentioned Adams-Sears transonic not-so-slender body theory which idealises the slender body flow as incompressible. To validate the linearity of the curve of ΔC_D against C_L^2 the dotted empirical linear fit is also shown. (For low aspect shapes, nonlinearities at higher incidence are associated with leading edge separation.) Summarising, the wall interference is roughly independent of incidence, and can be obtained by solving only **one** problem for zero lift, i.e. the shift in C_{D_0} from the free field to confined flow. This problem

Figure 5.49 : Swept slender body used to estimate $C_{L\alpha}$ for drag due to lift in the Heaslet and Lomax equation

¹Heaslet, M.A. and Lomax, H. 1954, "Supersonic and Transonic Small Perturbation Theory," High Speed Aerodynamics and Jet Propulsion VI, General Theory of High Speed Aerodynamics, Princeton Series, pp.122-344

can be further simplified by reducing it from a 3-D to 2-D desktop calculation by the TARWI. The robustness of the latter for not-so-slender swept trailing edge wing bodies such as the WIM1T needs to be assessed.

5.3.3.6 SSLV WALL-INTERFERENCE COMPUTATIONS

Computations of the Tunnel 16T wall interference were part of an effort to study the difference between existing wind-tunnel database and flight-measured, transonic aerodynamic loads experienced by the SSLV during ascent. The AEDC wall boundary condition was incorporated into the NASA/ARC OVERFLOW code (Buning, *et al.* [31]). The computations were all performed with the OVERFLOW code which was used to solve the TNS equation with a Baldwin-Lomax turbulence model in all regions except the far field. All tunnel computations were performed with the AEDC wall boundary condition. Wall interference computations were performed at one high subsonic freestream Mach number and at two low supersonic freestream Mach numbers, $M = 1.05$ and 1.25 . The former Mach number led to Group 3 flow.

A comparison of free-air and tunnel Mach number contours is shown in Figure 5.50 for $M = 1.05$ and $\alpha = -4.66^\circ$. The contours are shown for the lateral plane of symmetry with subsonic flow shown in grey, while supersonic flow is shown in colour. The launch vehicle profile is shown in white along with supersonic flow that exceeds $M = 1.1$. The bow shock and downstream Mach contours are seen to obliquely cross the line where the wind-tunnel walls would be located.

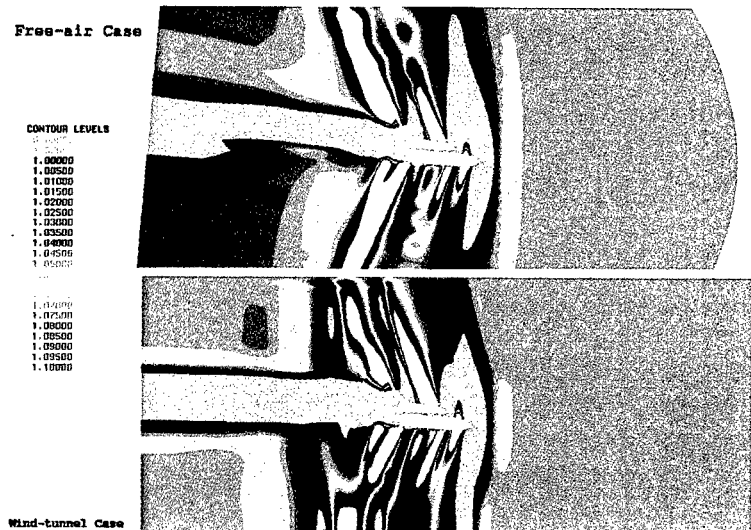


Figure 5.50 : Computed Mach number contours on the plane of symmetry, $M = 1.05$, $\alpha = -4.7$ deg.

A comparison of the Orbiter forebody (all surfaces except the base and top of the body flap) normal force and pitching moment for three 16T wind-tunnel tests is shown in Figure 5.51 along with the numerical results. The three wind-tunnel tests show very interesting trends. At $M = 0.95$ and $M = 1.25$, the data from IA-156 and IA-105A, which were conducted in 1977, agree very well thus indicating the lack of wall-interference effects at these Mach numbers. The data at $M = 1.05$ for the two-percent model (IA-156, blockage ratio = 0.3 percent) show a negative increment in forebody normal force, and a positive increment in forebody pitching moment, relative to the three-percent model (IA-105A, blockage ratio = 0.7%). These increments are attributed to wall interference effects in the data from the three-percent model.

In addition to the wall-interference effect, the bias between the recent IA-613A data and the two older tests is also very interesting. The difference between the test results could be due to the improved fidelity of the blockage between the Orbiter and ET at the aft attach station for the IA-613A test. Regardless of the cause, the data have moved closer to the Orbiter flight data.

The computed normal force and pitching moment from the free-air and wind-tunnel CFD solutions at $M = 1.25$ are in very good agreement with each other and the IA-613A data, indicating the absence of

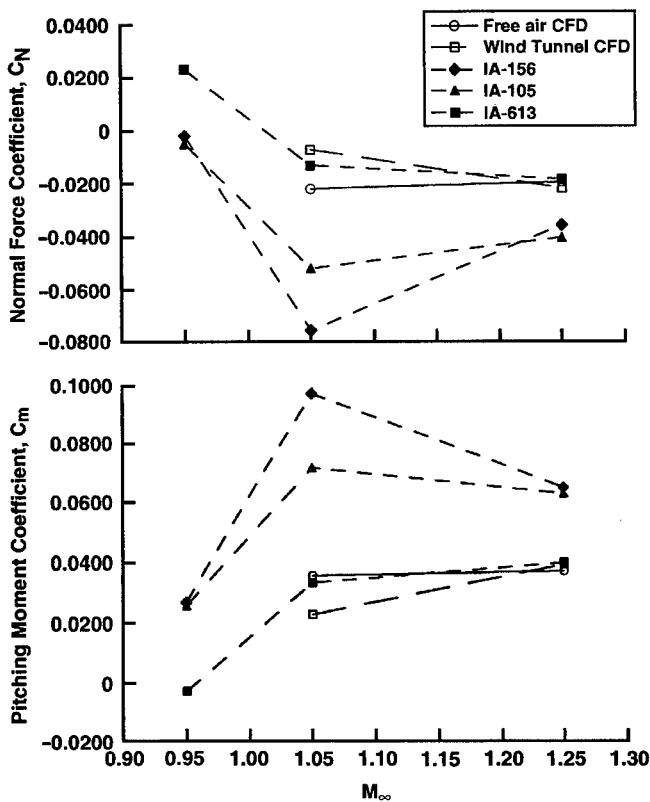


Figure 5.51 : Computed and experimental Orbiter forebody integrated loads

tunnel data. Agreement between the calculated wind-tunnel and the Tunnel 16T pressure distributions improved, particularly on the mid section of the vehicle where the interference effects are greatest. Increments between computed free-air and wind-tunnel normal force and pitching moment coefficients compared favourably with incremental data between models of two different scales.

wall interference effects at this Mach number as do the data from the IA-156 and IA-105A tests. At $M = 1.05$, the numerical results are near the IA-613A data, with the wind-tunnel CFD results showing a positive normal force and a negative pitching moment increment. The increment magnitude is approximately 70 percent of the difference between the IA-156 and IA-105A data. Absolute fidelity between the IA-613A data and the computed tunnel values is not achieved in the $M = 1.05$ case as in the $M = 1.25$ case. However, the increments are shown to be in the right direction and could be used to correct 70 percent of the wall interference at a near sonic condition.

By comparing the tunnel flow-field calculations with corresponding free-air flow-field calculations, an assessment of the wall interference was made. Significant wall interference effects were demonstrated at $M = 1.05$ while results at $M = 1.25$ showed no interference. Inclusion of the tunnel wall boundary condition in the CFD model improved the correlation of the numerical results with the

5.3.3.7 TST WALL-INTERFERENCE COMPUTATIONS

The difficulty of computing transonic wall interference in perforated-wall wind tunnels is demonstrated with this database as well as the need for additional technology development in this area. Wall interference computations for Tunnel 4T were performed on the TST model using the WIAC approach and the pretest-predictive approach. The computations involved computing the flow field with the Euler equations everywhere except in the vicinity of the wing. The near-field wing solutions were obtained by solving the thin-layer Navier-Stokes for fully turbulent flow. A Baldwin-Lomax turbulence model was used. The pretest approach involved imposing the tested wall configuration, 5% uniform porosity on all walls. The WIAC approach involved interpolating the measured pressure distribution onto the computational grid and prescribing it as the boundary condition.

Figure 5.52a shows a comparison of 16T reference and 4T drag variation with Mach number (drag rise) at a fixed lift coefficient $C_L = 0.3$ for natural transition at a chord Reynolds number (Re_c) of 2.7×10^6 . At $M = 0.6$, the drag measured in 4T is 22 counts (1 count = 0.0001) higher than measured in 16T while at $M = 0.9$ the 4T drag is 104 counts lower than 16T drag. The drag rise is delayed in 4T. A crossover point, where the drag difference is zero, occurs at $M = 0.835$. Figure 5.52b shows the drag rise

comparison for the same conditions while forward tripping the boundary layer at approximately 10% of wing chord. The drag levels for the tripped and untripped configurations are different, but the differences between 16T and 4T are almost identical indicating that wing transition is not a significant factor between 16T and 4T for this model at these conditions. This figure also illustrates how much the sign and magnitude of wall interference vary over the transonic regime.

At $M = 0.6$, the flow is subcritical and offers the opportunity to look at the data and computational comparison without shocks. Figure 5.53 shows the force and moment data comparisons between 16T and 4T for natural transition at $Re_c = 2.7 \times 10^6$. The normal-force coefficient comparison when plotted against angle of attack shows no slope difference and only a small variation at the larger angles. However, pitching-moment coefficient does show a slope variation. The slope of the 4T pitching-moment curve is much smaller than 16T. The drag-coefficient difference between the two tunnels remains fairly constant with angle of attack at approximately 22 counts.

The corresponding model pressures at the five wing spanwise arrays and on the canopy are shown in Fig. 5.54 for $\alpha = 3^\circ$. Also shown in Fig. 5.53 is a comparison of balance-cavity and average duct-exit pressures. The experimental model pressures indicate virtually no difference in the flow over the forward fuselage or the wings. Wall interference does not appear to be a factor on the local flow over these areas of the model. However, model pressures from the cavity and duct pressures (located at approximately the same model station) show a difference between the tunnels. Both show a slightly lower pressure in Tunnel 4T indicating a slight gradient in the pressure difference between the tunnels over the aft portion of the model. Figure 5.55 shows the pressures measured with the pipes corresponding to the model pressures in Fig. 5.54. These pressures indicate an acceleration of the flow above the centreline and starting at tunnel station 130. The end of the model was at tunnel station 130.7. The downstream pressure variation produces a buoyancy effect where the lower pressure in this region causes a higher drag coefficient in 4T. The lower pitching-moment coefficient slope is also attributed to the downstream variations. The flow accelerates over the tail and generates more lift and nose down pitching moment. Because most of the model lift is generated by the wings, it follows that an aft model

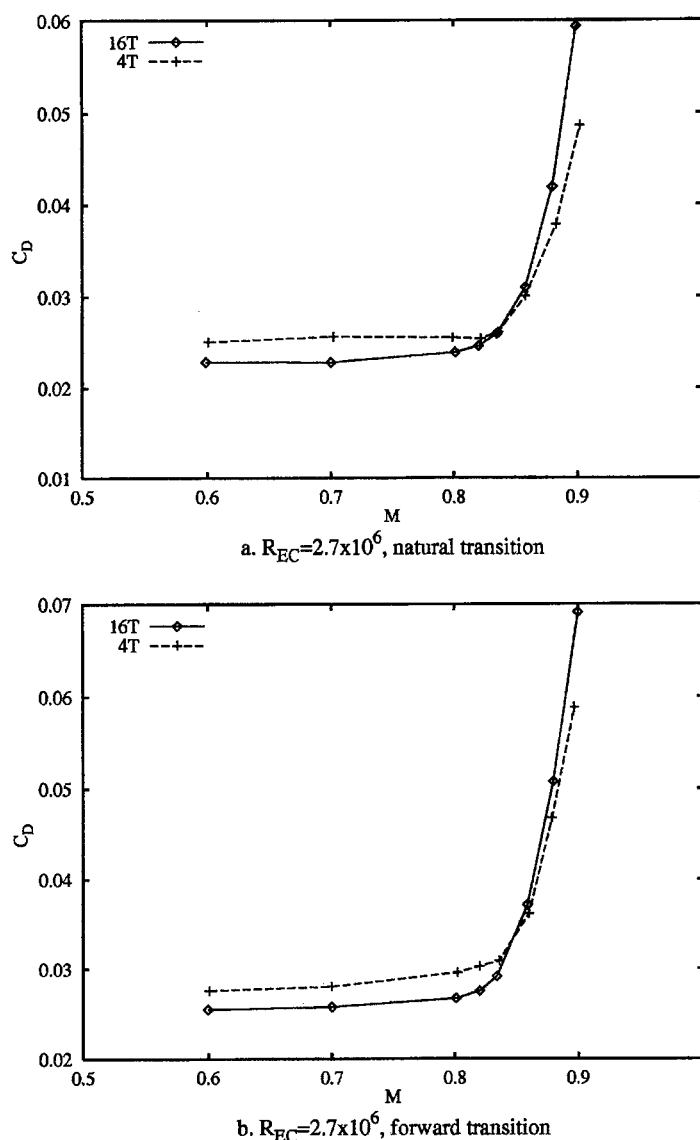


Figure 5.52 : 16T/4T drag-coefficient vs. Mach-number comparison, $C_L = 0.3$

gradient would not significantly affect the lift slope in 4T, which the data support. Since the pressure coefficient at the upstream pipe location is approximately zero, the blockage of the model did not affect the tunnel Mach number at these conditions.

Also, Figs. 5.54 - 5.55 show the computed model and measurement-surface pressure distributions for the free-air boundary condition, the AEDC boundary condition and the measured pressure distribution imposed. Good agreement is shown between the computed results and the corresponding data. The model-pressure increment between the free-air and AEDC boundary condition is larger than the experimental data show. These computational results indicate the AEDC perforated wall boundary condition prescribes a wall behaviour that is slightly too open. In addition, the AEDC boundary condition does not duplicate the downstream behaviour of the pressure distribution at the measurement surface. Imposing the measured pipe pressures yields model pressures that are in better agreement with the free-air computations than the wall boundary results. Specifying the pressures boundary condition does not seem to have any effect on the aft fuselage pressure distribution. To see an effect, the fuselage region must be computed by solving the Navier-Stokes equations. The pressure increments between the in-tunnel solutions and the free-air solutions have not been integrated to determine the force and moment corrections to the 4T data from these calculations.

The flow at $M = 0.835$ is supercritical. The force and moment data comparison between 16T and 4T are shown in Fig. 5.56, and the model pressure distribution for $\alpha = 3^\circ$ is shown in Fig. 5.57. The wing and canopy pressures distributions show significant differences between 16T and 4T. All but the first few canopy pressures in 4T are higher, the 4T shock position is upstream of 16T, and the 4T wing pressures are generally higher forward of the shocks. These model-pressure differences indicate that the 4T walls at a uniform porosity (τ) of five percent are too open for this flow condition. The 4T normal-force coefficient agreement is in good agreement with 16T and the drag coefficient difference is small. The 4T pitching-moment coefficient is more negative resulting from the drop in forward wing loading. The average duct-exit and balance-cavity pressures now show a higher pressure in 4T than 16T (reversed from the $M = 0.6$ trend). The pipe pressures in Figure 5.58 also show a trend reversal from the $M = 0.6$ data. The flow at the end of the test section is now decelerating (increasing pressure). The cavity pressures are sensing this increase while the duct-exit pressures are sensing the wall openness and the change in the duct flow due to local flow changes. Although the drag difference between the facilities is small, neither the local effects of wall interference nor the buoyancy effects from the downstream pressure are small. At this flow condition the effects tend to cancel each other. The downstream pipe measurements as well as the 4T balance-cavity and duct-exit pressures show an increase in the base pressure which decreases the drag. The much higher forebody and wing pressures indicate that the 4T walls are too open. These higher local pressures increase the drag. The openness of the wall reduces the shock strength and tends to alter the aft wing pressure recovery at $\alpha = 4^\circ$. Again, the upstream pipe pressure coefficients and the upstream canopy pressures appear to indicate tunnel Mach number is $M = 0.835$.

Figures 5.57 - 5.58 show the model and measurement-surface pressure distributions at $M = 0.835$ for the three computations. The model-pressure agreement between the AEDC tunnel wall boundary condition specified and with the interface pressure specified is good. The calculations also reproduce the corresponding measured model pressure including the difference in shock location and strength. In addition, the wall boundary condition reproduced the wall pressure signature everywhere except at the downstream end of the test section. Again, specifying the pressure boundary condition does not seem to have any effect on the aft fuselage pressure distribution. The pressure increments between the in-tunnel solutions and the free-air solution have not been integrated to determine the force and moment corrections for these calculations.

Goethert [71] shows the acceleration or deceleration of the downstream flow is caused by providing the wrong mass flow through the perforated walls. Excessive outflow causes the flow to decelerate, and insufficient outflow causes the flow to accelerate. From the pipe pressure measurements, it is evident that this is exactly the situation that occurred during this test. Because of the length and position of TST model, the downstream pressure distribution has a strong buoyancy effect. However, calculations to date, have not shown the buoyancy effect. Additional investigation is needed to integrate force on different areas of the test article, to model and compute the fuselage region using Navier-Stokes equations, and to investigate the use of different downstream boundary conditions.

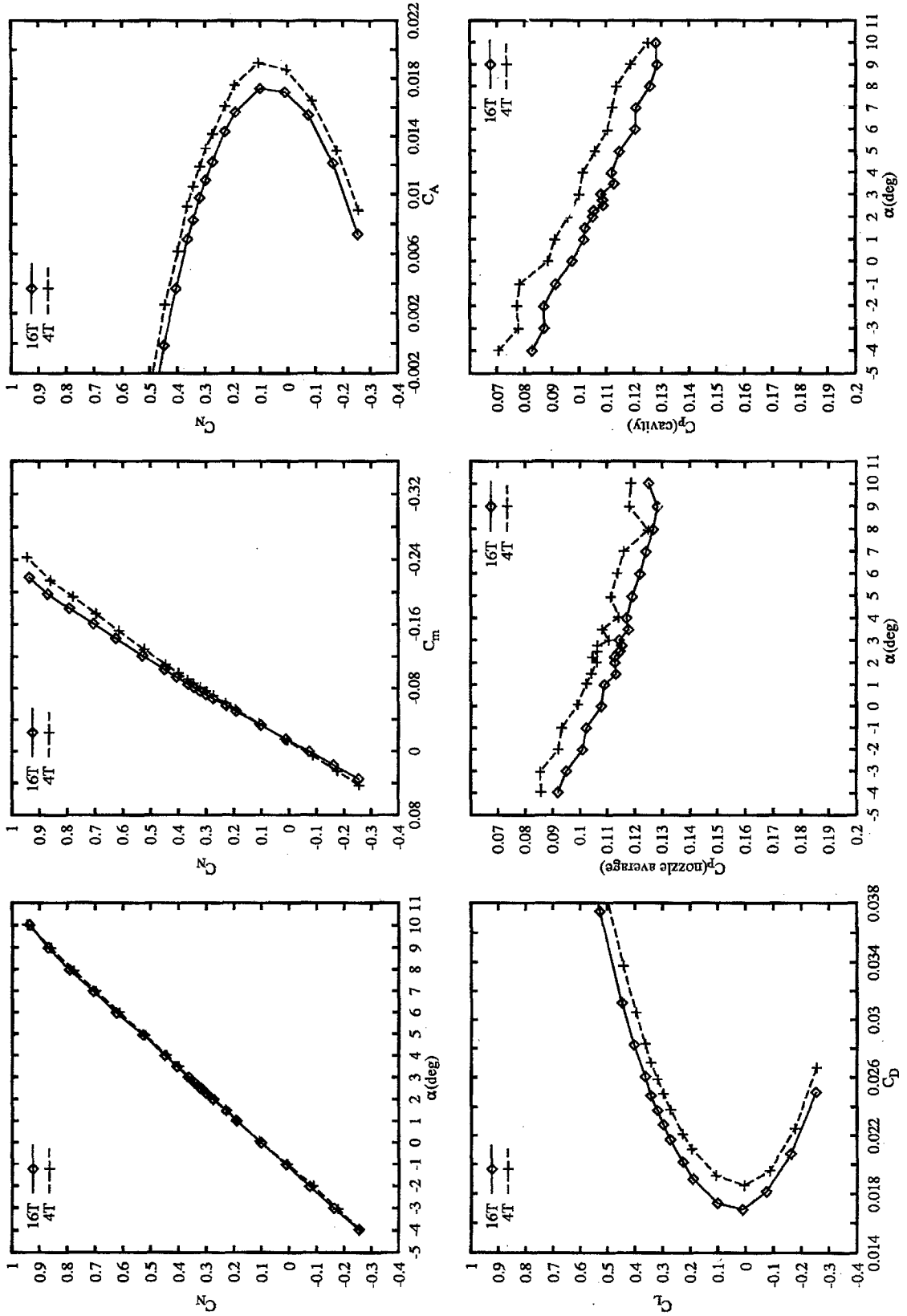


Figure 5.53 : 16T/4T force and moment, duct exit and balance cavity comparisons, $M=0.6$, $Re_c=2,7 \times 10^6$, natural transition

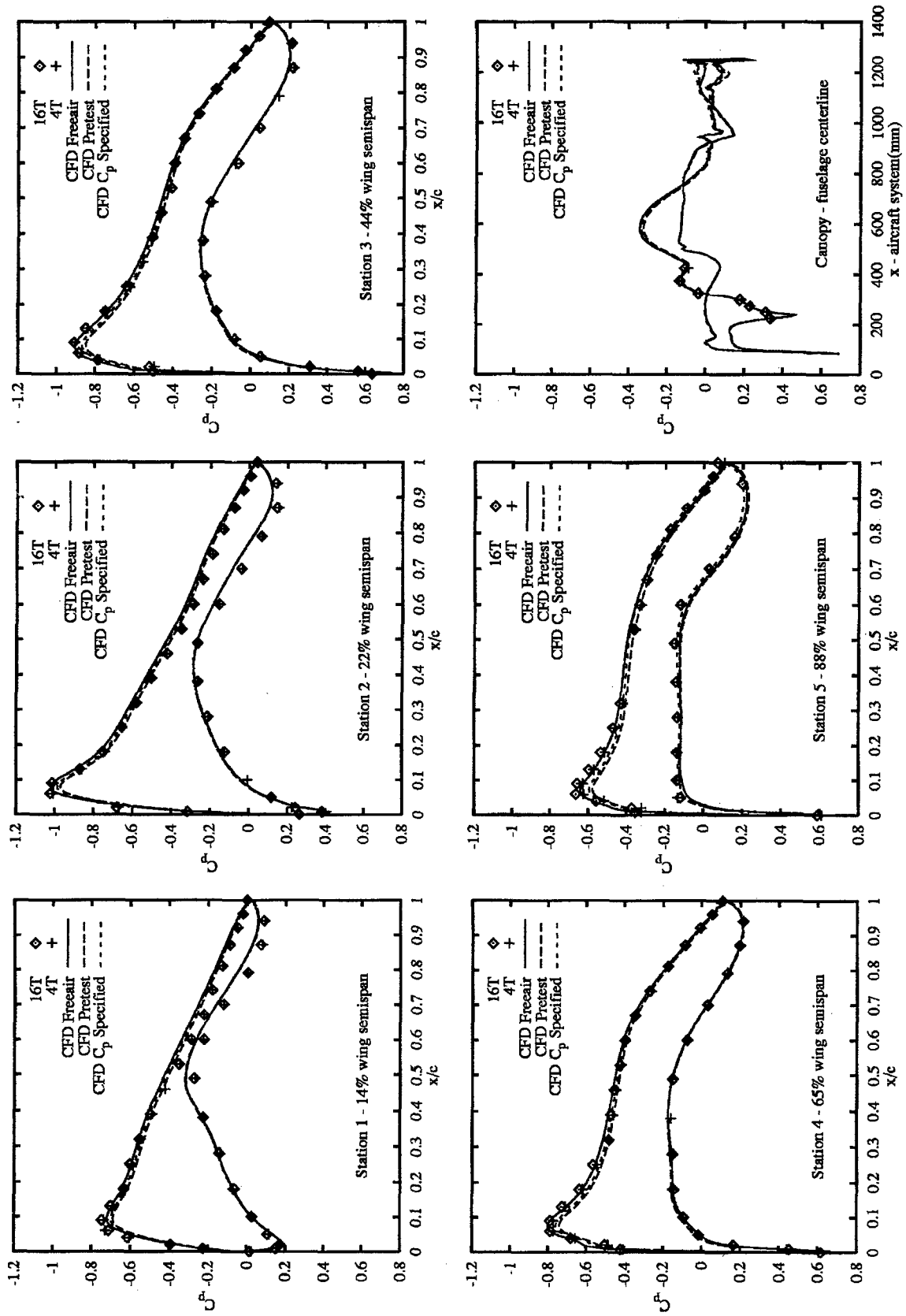


Figure 5.54 : Measured and computed model pressures, $M=0.6$, $\alpha=0.3$ deg, $R_{EC}=2.7 \times 10^6$

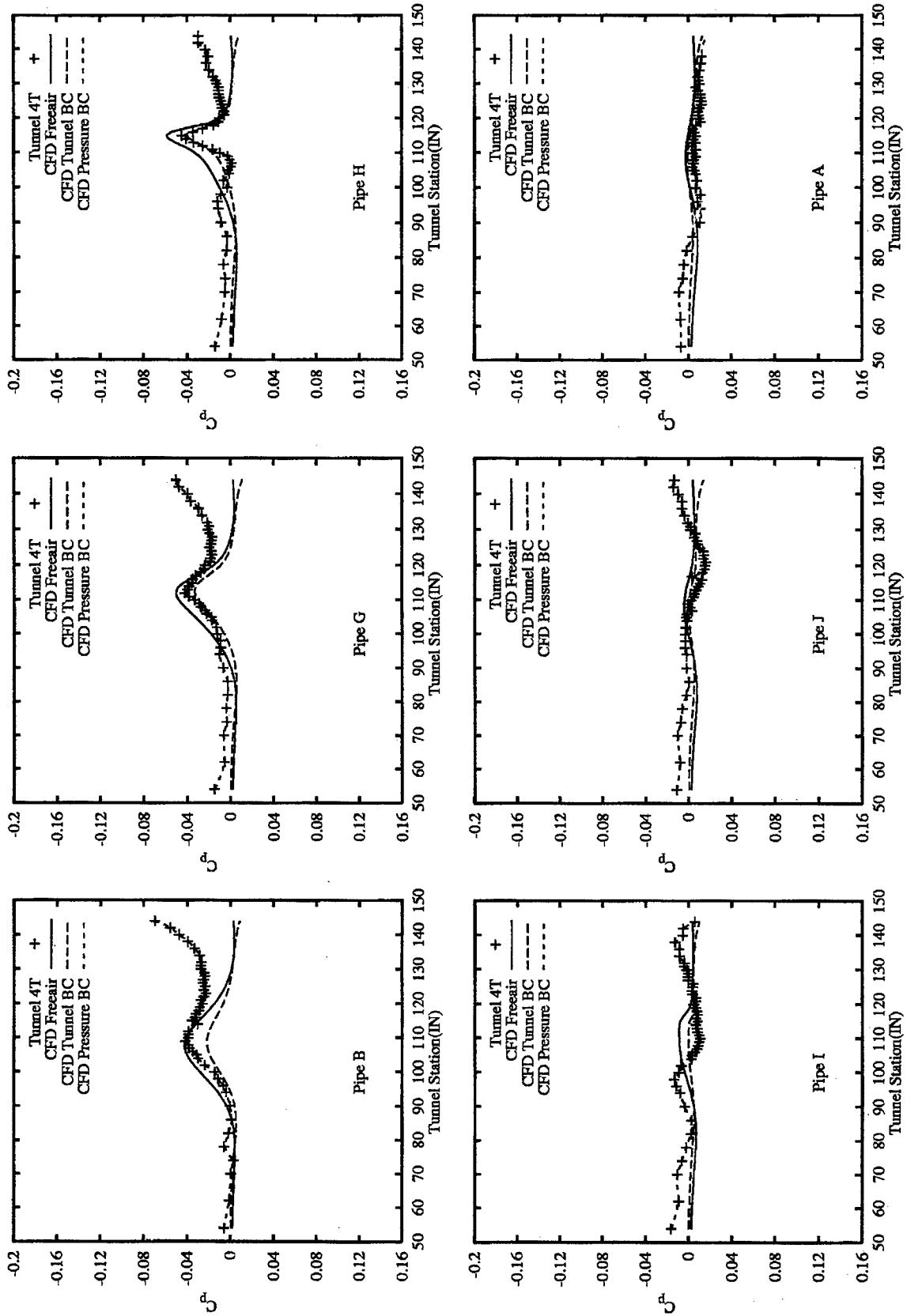


Figure 5.55 : Computational and measured interface-pressure comparison, $M = 0.6$, $\alpha = 3$ deg, $R_{EC} = 2.7 \times 10^6$, natural transition

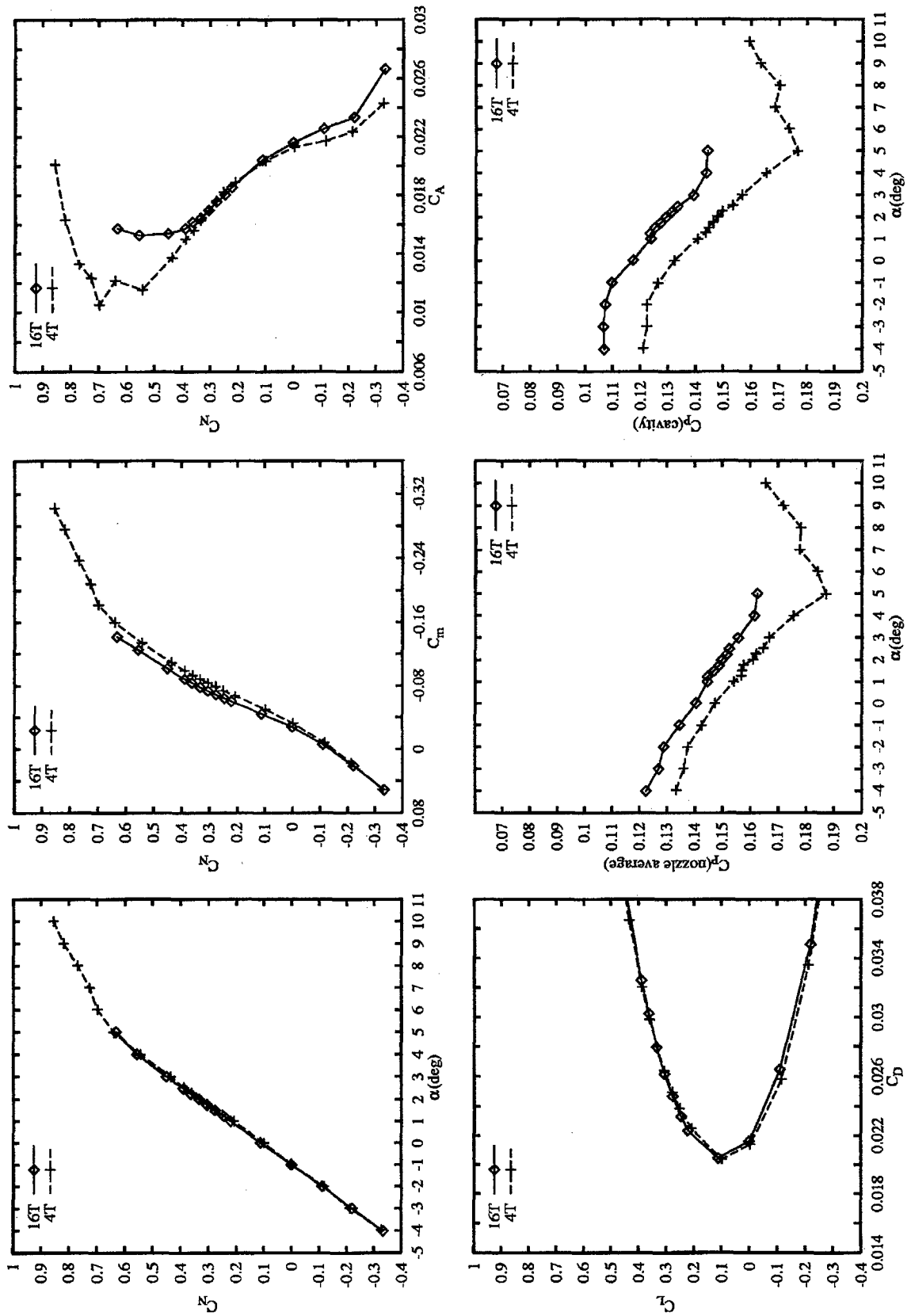


Figure 5.56 : 16T/4T force and moment, duct-exit and balance-cavity comparisons, $M = 0.835$, $R_{EC} = 2.7 \times 10^6$, natural transition

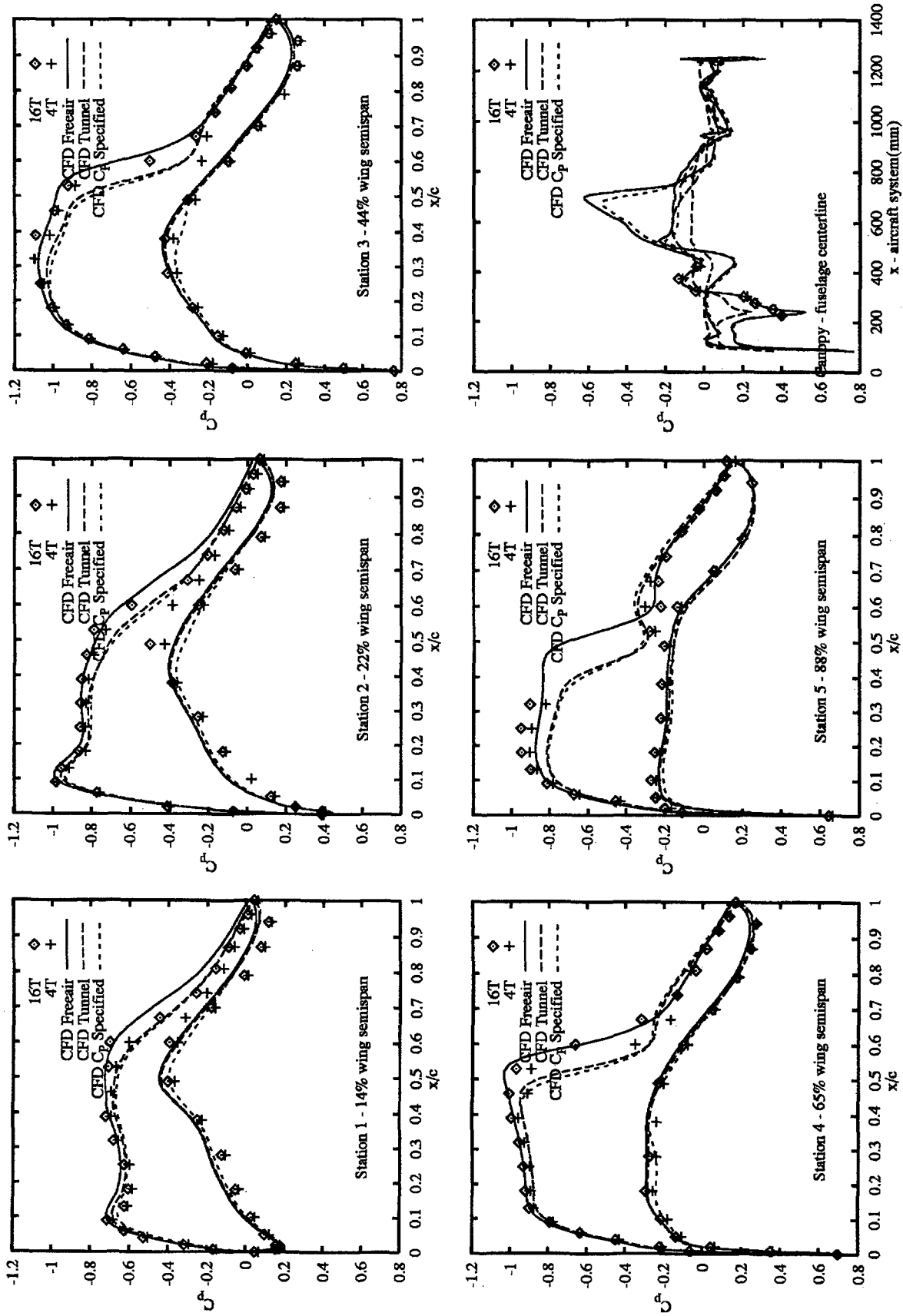


Figure 5.57 : Measured and computed model pressures, $M = 0,835$, $\alpha = 3$ deg,
 $R_{EC} = 2.7 \times 10^6$, natural transition

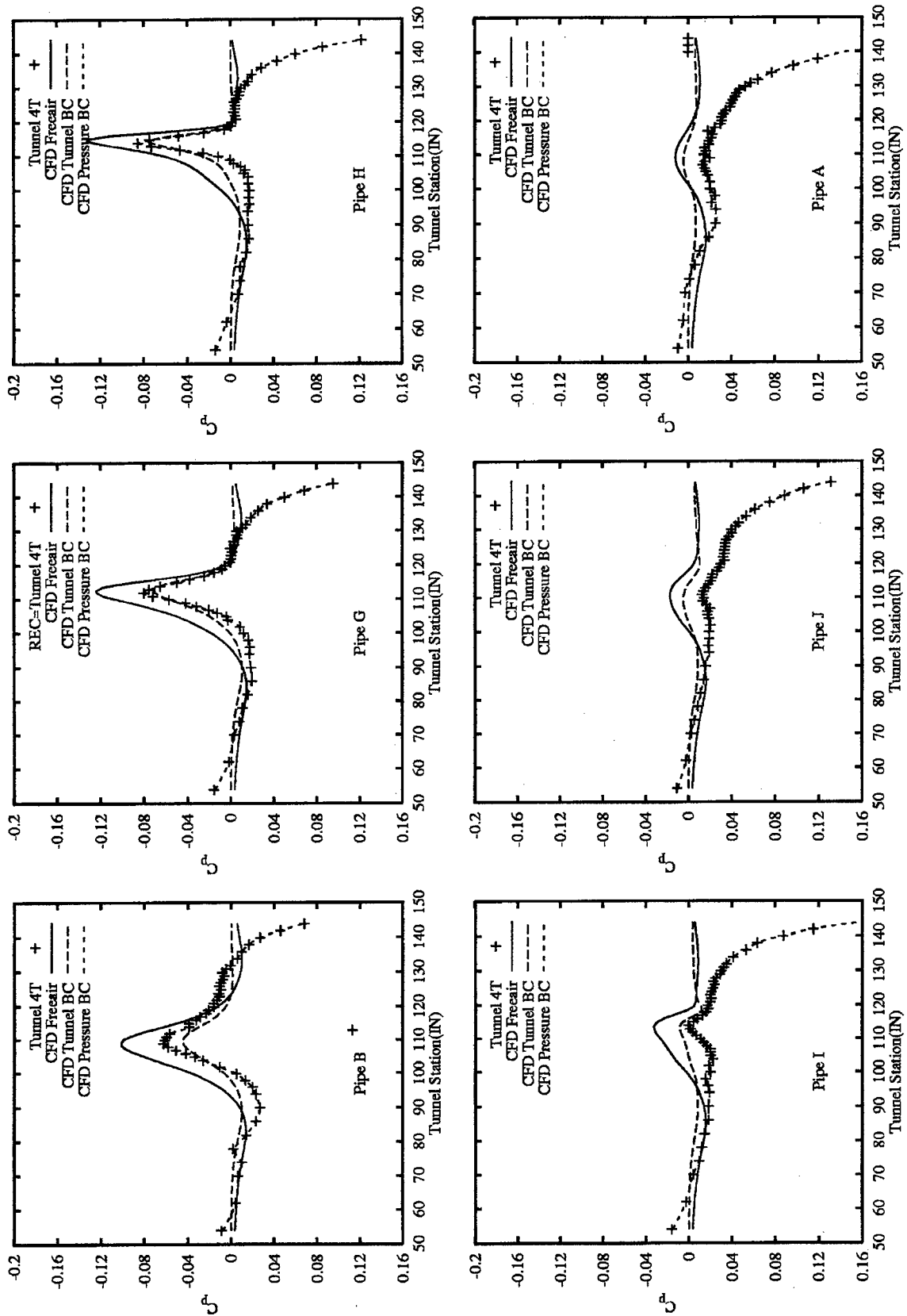


Figure 5.58 : Computational and measured interface-pressure comparison, $M = 0.835$, $\alpha = 3$ deg, $R_{EC} = 2.7 \times 10^6$, natural transition

5.3.3.8 CONCLUSION

Accurate wall interference corrections were demonstrated for high subsonic flow and low supersonic flow using the pretest-predictive approach where the AEDC perforated wall boundary condition is specified and using the WIAC approach where the pressure distribution is specified near the wall. The specification of the AEDC perforated wall boundary condition reproduced the pressure signature near the wall to a high degree of accuracy and yielded model pressures in good agreement with the pressure specified results. The TST database is an excellent database to evaluate wall interference strategies and should be exploited for these purposes.

5.3.4 NASA LANGLEY WIAC METHODS

The research interest in transonic wall interference correction techniques and methods at NASA Langley Research Center was prompted by the decision to build the National Transonic Facility (NTF) there in the mid 1970's. Since the NTF would be a variable speed, pressure, and temperature (cryogenic) facility, then one could simultaneously match flight Mach number, Reynolds number, and dynamic pressure, thereby ideally, leaving tunnel interference (wall and support) as the major source of uncertainty in its data. A summary of the resulting wind-tunnel-wall interference assessment and correction (WIAC) research from the mid 1970's through about 1990 is given in Newman, *et al.* [142], [143]. Many references giving the approaches used, details, and results are cited in these two papers.

The development of several sequences of WIAC codes occurred, more or less, in parallel. The non-linear transonic WIAC procedures were to be studied using a 2-D TSDE approximation in conjunction with an extensive airfoil database being generated in the 0.3-m Transonic Cryogenic Tunnel (TCT). Both linear (fast) and non-linear 3-D procedures were envisioned for eventual use in the NTF and sequences of WIAC codes were developed for both. Initial 3-D studies and codes were developed under NASA Contract by Flow Research Company with later development, implementation, and testing done in-house. The following two subsections will briefly discuss the 2-D and 3-D developments separately, with that for the non-linear airfoil WIAC first. Some of the important lessons learned there have not yet been incorporated in any 3-D procedure. However, a few remarks regarding the relationship of the present WIAC philosophies and procedures to those already discussed in 5.3.2 and 5.3.3 are needed first.

The WIAC procedures discussed in all three sections (5.3.2, 5.3.3, and the present section, 5.3.4) utilise differences between two CFD solutions, one in tunnel and one in free-air, to determine interference corrections and use measured wall or near-wall pressures to formulate the "wall" boundary condition for the in-tunnel simulation. However, for the WIAC procedures previously described in 5.3.2 and 5.3.3, corrections are made to determine a pressure difference on the model and, when integrated, corrections for the forces and moments result. This assumption is that the tunnel Mach number (M) and angle-of-attack (α) are correct. The present philosophy is that there are corrections to M and α , just as in the classical low-speed flow, because the tunnel has imposed an incorrect far field on the model flow. It is not known what the correct far-field conditions are, and the present non-linear procedures search for a far field M and α for which the computed surface pressure (not pressure coefficients) distribution best matches that measured (or computed) in the tunnel. This philosophy intends to preserve the sensitive transonic flow and its shock-wave/boundary-layer interactions which occurred in the tunnel flow on the model. In addition to the corrections for M and α , there also result corrections to the forces and moments due to normalising stream properties and incidence corrections. The present procedures are, therefore, variants of the initial or first point of view as discussed in 5.3.2.3. In any case, from whatever point of

view, one can determine corrections only by holding some property or properties invariant; perhaps it is not yet clear what the physical invariant(s) should be.

5.3.4.1 NON-LINEAR AIRFOIL TUNNEL WIAC CODES

The sequence of codes leading to TWNTN4A were developed from about 1977 to 1988. These codes are based on the (non-linear) TSDE CFD approximation and 1-D measured pressure data arrays on the top and bottom tunnel walls (outer boundary) and upper and lower airfoil model surfaces (inner boundary) are used as boundary conditions for the in-tunnel simulation. That is, this is a two-measured data array WIAC procedure. This inverse (pressure prescribed) boundary condition is essentially applied along the airfoil, a two-sided slit along the $y=0$ line of length equal to the chord, and allows an effective inviscid shape to be determined which approximates many of the viscous layer responses, including those associated with shock interactions and flow separations. It is then this effective inviscid shape which is used as the inner boundary condition for the free-air CFD calculation which is done on a Cartesian grid which is simply an extension of the in-tunnel grid. That is, the in-tunnel grid is a proper subset of the free-air grid, allowing cancellation of computational truncation errors in the flow field around the model.

The basic ideas and initial code, TWINTAN, were developed by Kemp [99], [100] and it was soon realised that the sidewall boundary-layer approximate models discussed in 5.2.2 due to Barnwell and Sewall [19] needed to be included for correction of the 0.3-m TCT airfoil data taken in the 8- X 24-inch slotted wall test section (see Kemp and Adcock [102] and Kemp [101]). Incorporation of this 4-wall code, TWINTN4, into an automated procedure for use with 0.3-m TCT airfoil data was accomplished by Gumbert, *et al.* [80], Gumbert and Newman [79], and Gumbert [78]. This procedure included a capability for multi-pass corrections, using the airfoil leading edge as a flow angularity probe, to iteratively determine the unmeasured far-upstream flow angularity. Use of this procedure by Gumbert, *et al.* [81] also uncovered limitations due to the subsonic origins of the SWBL approximations as mentioned in 5.2.2. Inclusion of the wall shapes appropriate to an adapted wall as the outer boundary upon which the measured far-field pressures are imposed on the in-tunnel flow simulation, produced the tool TWNTN4A, capable of also assessing and correcting residual interference in adapted-wall airfoil tunnels. The procedure and results have been reported by Green and Newman [75], [76], Green and Mineck [74], and Green, *et al.* [77].

The general premise is that transonic airfoil data contain wall interference; it is just a matter of how much. The TWNTN4A WIAC procedure is a post-test means for trying to quantify the severity of wall effects. Incorporation of the TWNTN4A code as part of the 0.3-m TCT data reduction is contemplated in the current re-engineering of NASA tunnels and is possible with present-technology high-end workstations. Space here does not permit showing the many WIAC results from the papers cited above, and showing only a few results would not be representative of all the studies. The major conclusions from these 2-D WIAC studies are:

- (a) Both upstream flow angle assessment and a non-linear SWBL approximation are required in transonic airfoil WIAC procedure.
- (b) Both the linear CAE-NAI interference potential and the non-linear NASA TSDE WIAC procedures make nearly the same and reasonably good corrections for M and α into the transonic flow regime if both items in (a) above are included.
- (c) The model shock interacting with the SWBL generally destroys the 2-D symmetry before this shock reaches the top or bottom tunnel walls.

- (d) Valid correction of transonic data that are subject to unsteady and even moderate 3-D SWBL effects may require an unsteady, 3-D, Navier-Stokes WIAC procedure.

5.3.4.2 LINEAR AND NON-LINEAR 3D WIAC CODES

Initial NASA Langley 3-D WIAC studies were done and codes developed under a contract to Flow Research Company. Linear, slender lifting-body, and non-linear TSDE potential theory based WIAC codes and procedures were formulated, developed, and tested, code-on-code. These results were reported by Rizk and Smithmeyer [156] and Rizk, *et al.* [157], [158]. Elements of the linear code LINCOR, written by Rizk and Smithmeyer [156], were used by Kemp [98], [95] in the STIPAN analysis and PANCOR WIAC codes, developed for the slotted-wall NTF, as discussed in 5.3.1.1. The non-linear TSDE WIAC code TUNCOR, originally developed by Rizk *et al.* [157], and later enhanced by Rizk [155], has been tested at NASA Langley and AEDC on transonic tunnel data. The NASA Langley results for several applications are given in Newman, *et al.* [142], [143]; results from the linear code PANCOR are also included. Both of these procedures are one-measured data array schemes; that is, 2-D pressure data arrays measured on or near the walls are used in the outer boundary condition for the in-tunnel flow simulation.

As pointed out by Sickles and Erickson [167], [168] and discussed here in 5.3.3.1, application of the TUNCOR and other inviscid flow solvers gave accurate corrections for subcritical and mildly supercritical flows (Group 1) but were inadequate, giving wrong corrections, for strongly supercritical flows (Group 2). This behaviour was associated with the inviscid codes' inability to properly simulate the viscous flow, particularly for strongly shocked and separated flows. As a consequence, NASA Langley began implementing the correction procedure of TUNCOR into another TSDE code in which a number of approximation improvements, including an interacted boundary layer (IBL) were being incorporated. This new code, WIACX (see Garriz and Haigler [68], has been used by Garriz, *et al.* [69] and Green, *et al.* [77] to correct semi-span wing data which falls into the Group 1 category. Since the IBL procedure has not been incorporated into the WIACX code, it has not been tried on Group 2 flows. However, the IBL procedure gives remarkable results for shocked and separated transonic flows when used in the CAP-TSD analysis code upon which WIACX is based.

As noted in 5.4.4.1, the TWNTN4A airfoil WIAC code makes use of two 1-D measured pressure arrays: the far-field array; generally taken above and below the airfoil and an airfoil surface array. Extensions of this concept to 3-D were made assuming that model surface pressure measurements would never be detailed enough to provide an adequate inner boundary condition for an inverse problem reconstruction of the effective test article shape. In addition, for many tests, pressure measurements are not made. Consequently, the 3-D implementations of Kemp's [99], [100] original concept were with 2-D measured far-field pressure arrays and a geometric model description as the inner boundary condition for a direct problem. Using this latter boundary condition, the flow code is required to produce the viscous effects, including shock interactions and separations, in order to obtain the effective shape that is present in the tunnel test and also the free-air simulation, both of which are required in a non-linear WIAC procedure. Successful application of pressure sensitive paint, predicted by some to be a routine technique soon, would provide the 2-D measured surface pressure arrays needed for a 3-D, two-measured variable array WIAC procedure, not requiring measured flow angularity arrays. Details of the envisioned procedure would involve using an unstructured grid Euler flow solver (to easily mesh the configuration and tunnel test section geometry) on a rather coarse grid (by current CFD standards) to solve the inverse in-tunnel problem very efficiently. The resulting "effective inviscid shape" (which contains viscous effect

contributions) is then used in the free-air simulation (unstructured-grid Euler flow solver with in-tunnel grid augmented to reach the required free-air far-field boundary) to obtain the Mach number and angle of attack which minimise an equivalence condition for determining wall interference. In this procedure, it is assumed that the pressures measured on the model are correct (valid) but that the tunnel has imposed the wrong far-field flow. The WIAC procedure deduces effectively averaged corrections to the magnitude and direction of the far-field flow subject to an equivalence condition. Experimental data are then re-reduced at the corrected flow conditions.

5.4 ASYMPTOTIC METHODS FOR TRANSONIC TUNNEL WALL INTERFERENCE*

5.4.1 BACKGROUND

As previously discussed, procedures to treat subsonic wall interference have received considerable attention. A view of existing wall correction technology for this regime can be obtained from Garner *et al.* [67], Pindzola and Lo [151], and Mokry *et al.* [133], other chapters in this AGARDograph and previous sections in this chapter. By contrast and as has been previously indicated in this chapter, the methodology for the transonic case is much less developed since it gives rise to a particularly difficult non-linear, mixed-flow environment. Current approaches are exemplified by Kraft *et al.* [109], Donegan *et al.* [47], and Newman *et al.* [142] and in Section 5.3. In addition to the utility of large-scale computationally intensive methods for transonic wall correction prediction, approaches that can reduce the number of input parameters necessary to compute the correction, shed light on the physics of the wall interference phenomena, simplify the necessary computations, and apply to three dimensions as well as unsteady flows are needed. Asymptotic as well as combined asymptotic and numerical (CAN) procedures such as those described in Lifshitz and Fonarev [115], Chan [34], Blynskaya and Lifshitz [29], Cole [39], Berndt [24], Malmuth and Cole [122], Malmuth *et al.* [125], Malmuth [121], [125], provide such advantages. Furthermore, such techniques can stimulate valuable interactions with the other methods previously mentioned to suggest possible improvements, as well as derive beneficial features from them. This section summarises CAN methods for predicting wall interference. Theories for slender aeroplane configurations and high aspect ratio wings will be outlined as well as computational methods to determine the interference flows for these limiting cases. Other approaches in which the asymptotics can be integrated with experimental measurements to improve WIAC procedures such as those in Sickles and Erickson [167], are summarised in Malmuth *et al.* [125], and Malmuth *et al.* [123].

5.4.2 OVERVIEW OF ASYMPTOTIC PROCEDURES FOR SMALL SLENDER AND LARGE ASPECT RATIO CONFIGURATIONS

For both the slender body and high aspect ratio cases, the wall interference is obtained by a systematic asymptotic expansion procedure. Each is represented by a secondary approximation within a Karman-Guderley (KG) Transonic Small Disturbance Theory framework. In what follows, the asymptotic structure for the two limits and the formulation of the boundary value problems for the interference perturbation potential are outlined.

* Portions of this effort were sponsored by the Air Force Office of Scientific Research, Air Force Materials Command, USAF under Contract No. F49620-96-C-0004, as well as Arnold Engineering Development Center, Air Force Systems Command, under Contracts F40600-82-C-0005 and F40600-84-C-0010. The U.S. government is authorized to reproduce and distribute reprints for government purposes notwithstanding any copyright notation thereon. The views and conclusions herein are those of the authors and should not be interpreted as necessarily representing the official policies or endorsements, either expressed or implied, of the Air Force Office of Scientific Research or the U.S. Government.

5.4.3 SMALL SLENDER CONFIGURATIONS

Figure 5.59 shows a schematic of a slender aeroplane of characteristic thickness ratio δ and incidence α within a circular wind tunnel. The quantities h and h' respectively represent radii of "pressure-specified interface" and wall cylinders. The h interface surface has been introduced to provide experimental pressure data to bypass difficult simulation of ventilated wall boundary conditions. A double limit consisting of the transonic small disturbance slender body theory (TSDST) described in Cole and Cook [37], and large tunnel radius in units of the body length h in Malmuth [121], [125], and Malmuth [120], give the three-deck structure shown. In the horizontally shaded "axis" region, cross-flow gradients dominate and the flow is nearly harmonic in cross flow planes. In the slant-shaded "central" zone, relaxation to an axisymmetric non-linear TSDST environment has occurred. This leads to the Equivalence Rule given in Oswatitsch and Keune [147], and elsewhere for the free field (no walls present) flow. TSDST in the central region is formulated within a distinguished asymptotic limit involving δ, α , and the freestream Mach number M_∞ and leads to the axisymmetric KG equation for the perturbation potential ϕ . For $H \equiv h\delta \rightarrow \infty$ as $\delta \rightarrow 0$ the walls linearly and weakly perturb the central region flow. Treatment of the case $H = O(1)$ is given in Section 5.4.8. **If the walls are axially symmetric,* then Malmuth [122], [121], [125], demonstrate that an "area rule for wall interference" holds in which the interaction of an asymmetric body with walls is the same as its equivalent body of revolution.** This interaction is computed from solution of a boundary value problem of the wall

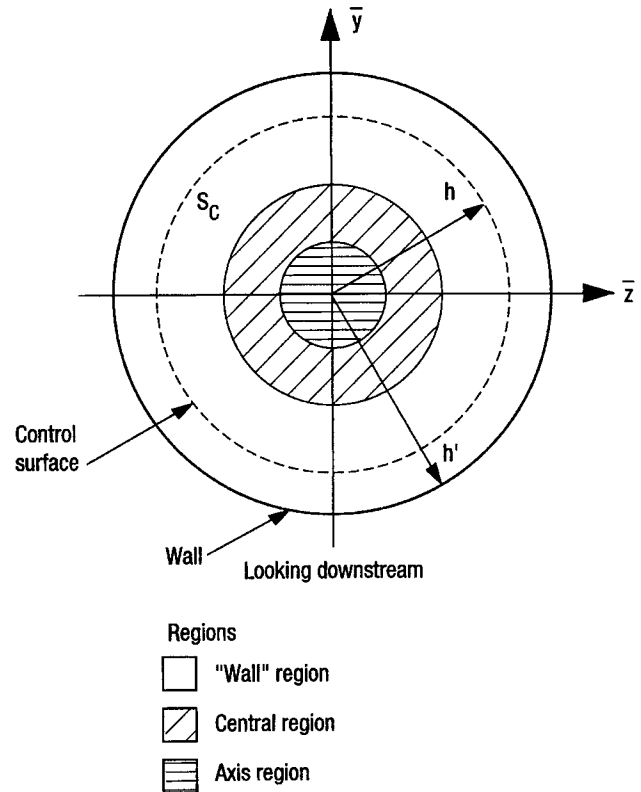


Figure 5.59 : Slender body within control surface in tunnel for $H^{-1} = O(1)$

correction ϕ_1 to the basic free field flow perturbation potential ϕ_0 whose equation of motion is linear and of mixed type with variable discontinuous coefficients. It is similar to an equation to be shown for the high aspect ratio problem. For slender bodies, boundary conditions for this "variational" equation are obtained from matching with the axis region and a wall region (unshaded zone in Figure 5.59) where the approximation of small perturbations of the central region becomes nonuniform due to the $O(1)$ wall boundary conditions. This wall region is governed by the Prandtl-Glauert equation and the body appears as an imaged multipole for free jet and solid walls. An inner limit of the wall region provides far field boundary conditions for the variational equation of the central region interference flow. More general pressure-specified wall boundary conditions introduce Fourier transforms and averages of the wall pressure distribution into the far field boundary conditions. Involved matching procedures to establish this result are detailed in Malmuth [125] Numerical procedures and associated issues in solving boundary value problems of this type have been also discussed for the high aspect ratio theory in Malmuth [121], [125], [123].

* As will be seen in subsequent sections, this condition as well as $H = O(1)$ can be relaxed.

5.4.4 HIGH ASPECT RATIO THEORY

A high aspect ratio wing is shown schematically in Figure 5.60 as confined within a cylindrical-pressure-specified interface. In contrast to the slender body case, the effect of the lift interference is more significant. Moreover, only two decks are in the flow. One of these is the classical "strip theory" inner (near field) region of lifting line theory in which each span station of the wing is in a two-dimensional flow independent of the others.

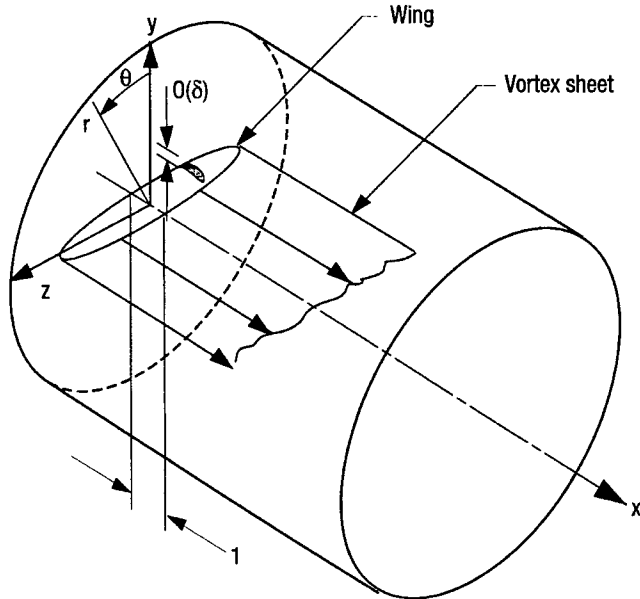


Figure 5.60 : Confined high aspect ratio wing

As in the slender case, the basic flow is assumed to be given by a KG model, which differentiates it from the classical Prandtl lifting line theory for incompressible flow. For slightly subsonic freestream conditions, the outer (far field) region structure is that of a lifting line with a trailing vortex sheet in the Prandtl-Glauert (PG) subsonic linear regime. Downwash from this vortex assemblage changes the "geometric" wing incidence. Cook and Cole [40], obtained this correction by matching for the free field problem. Small [171], computed the solution of this problem for the case of "similar wing sections" in which all airfoil sections are affinely related along the span. Proper matching conditions for the interference case considered here were obtained from an integral equation based on Green's theorem using a special kernel involving a

source reflected in a free jet cylindrical boundary. Further information on these developments is given in Malmuth [125], [123]. Pressure boundary conditions are incorporated into the model by a superposition procedure detailed in Malmuth [125]. For the latter, only the first few angular harmonics of Fourier means are important as well as the streamwise variations near the wing, in an asymptotic limit of span and wall height tending to infinity at the same rate. Matching, using the asymptotic solution of the non-linear integral equation, gives the induced downwash on the loaded line. The reflection effect arises naturally with use of the Green's function and can be interpreted to be phenomenologically the same as that for incompressible flow, *i.e.*, **inversion of the vortex system projection in the Trefftz plane into the wall/interface projection**. Non-linear corrections can be obtained systematically using this method. On implementing these ideas, the variational equation for the wall interference potential ϕ_1 is similar to that for slender bodies. This is a linear variational equation of mixed type whose variable discontinuous coefficients depend on the KG basic free field flow disturbance potential ϕ_0 . Asymptotic developments leading to this structure are detailed in Malmuth [125] and lead to the following boundary value problem for the wall correction potential ϕ_1 for "classical" free jet and solid wall boundary conditions

$$L[\phi_1] = (K - (\gamma + 1)\phi_{0,x})\phi_{1,xx} - (\gamma + 1)\phi_{0,x}\phi_{1,x} + \phi_{1,yy} = 0$$

$$\phi_{1,y}(x,0) = 0; \quad \phi_1 \rightarrow -\tilde{y}[d(z) + w(z)] - [\Gamma_1(z)/2\pi]\theta + \dots \text{ as } r \rightarrow \infty$$

$$[\phi_1]_{\text{wake}} = \Gamma_1(z) \equiv [\phi_1]_{\text{te}}.$$

Here, $d(z)$ and $w(z)$ are crucial functions controlling the size of the aspect ratio and wind tunnel corrections, respectively. They are given by the integrals

$$d(z) = \frac{1}{4\pi} \text{P.V.} \int_{-1}^1 \frac{\Gamma'_0(\xi)}{x - \xi} d\xi$$

$$w(z) = \pm \frac{\mu^2}{4\pi} \text{P.V.} \int_{-1}^1 \frac{\Gamma_0(\xi)}{(z\xi - \mu^2)^2} d\xi,$$

where P.V. signifies that the principal value of the integral is to be taken. The function $\Gamma_0(z)$ is the spanwise circulation distribution along the wing in the free field basic flow. The quantity $w(z)$ was obtained from the previously indicated integral equation far field analysis detailed in Malmuth [125], the (+) and (-) apply to free jet and closed wall test sections, respectively, and μ is the test section width in units of the wing span. A derivation using Green's theorem and a Green's function for the geometry shown in Figure 5.61 is given for free jet wall boundary conditions in Malmuth [125], [123].

Details of the special numerical methods needed to solve the preceding boundary value problem and its analogue for the slender body wall interference case are contained in Malmuth [125], [123], which are generalisations of methods used by Small [171]. As a practical outgrowth of this theory procedures in which asymptotics can be integrated with pressure and wake measurements to correct for viscous effects in interference estimates are discussed in Malmuth [125], [123].

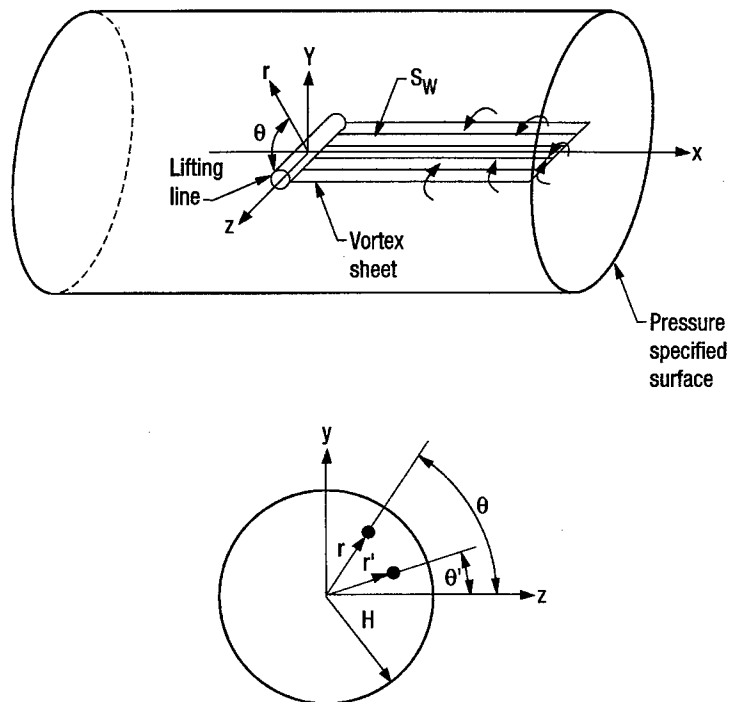


Figure 5.61 : Far field flow configuration showing lifting line and vortex sheet

5.4.5 RESULTS - SMALL SLENDER BODIES

Calculations for confined slender bodies for which $H^{-1} = o(1)$ discussed in Malmuth, [121], [123], [125], show a spikelike interference pressure field as well as a change of interference drag to thrust as the Mach number approaches unity and show the intrinsic similitudes of the asymptotic theory which is consistent with those obtained by Goethert [71] using non-asymptotic procedures. The spikelike detail which diffuses with decreasing Mach number is also obtained for high aspect ratios since it is due to the translation of the shock from its free field position. **Since the boundary conditions (obtained from asymptotic matching) depend only on the streamwise area progression rather than the cross sectional shape of the body, an equivalence rule holds that states that the interference flow for asymmetric bodies is identical to those for their equivalent bodies of revolution in TSDST.** Although this argument is made here for the $H^{-1} = o(1)$ case, a more detailed analysis given in Section 5.4.8 shows that it holds for $H = O(1)$. Also indicated in Malmuth [121], [123], [125], is the resemblance of the pressure distribution away from the spike with that obtained by Malmuth [119], for incompressible flow. Another outgrowth of our analyses of these

slender body flows is the shock position invariance law reported in Wu [186], Cole and Malmuth [38], Malmuth [120].

5.4.6 RESULTS - LARGE ASPECT RATIO WINGS

For high aspect ratio wings, free jet boundary conditions as well as pressure interface conditions such as

$$C_{pI} = \varepsilon_2 e^{-|x|} (1 + \varepsilon_1 \cos\theta), \quad -\infty \leq x \leq \infty$$

having certain qualitative features of near-wall pressure distributions were considered, where C_{pI} = the

interfacial pressure distribution, ε_1 and ε_2 are constants set to the value .2 for the calculations and $\text{sgn}(x) = 1$ for $x > 0$ and -1 for $x < 0$. In Figure 5.62, results for an aspect ratio 8 elliptic planform having a

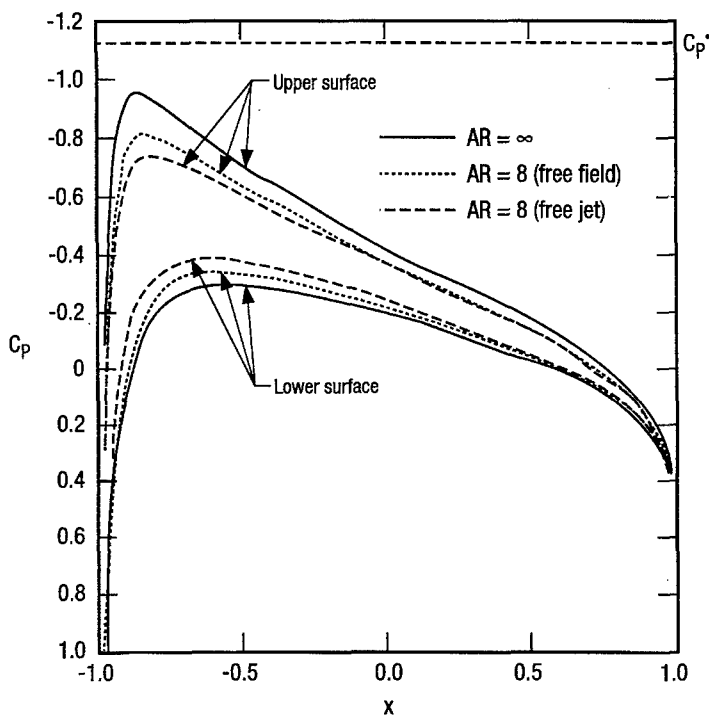


Figure 5.62 : Chordwise pressures on NACA 0012 wing, $M = .63$

NACA 0012 airfoil section are presented. The freestream Mach number M_∞ is .63 and the incidence $\alpha = 2^\circ$ for this subcritical case. If the three-dimensional wing has the same airfoil section along its span, (similar airfoil sections), the problem can be reduced to a two-dimensional one as shown in Malmuth, [125]. Effects of finite span and free jet wall interference on the chordwise pressures show the reduction of lift from both phenomena. Corresponding supercritical results for $M_\infty = .75$ at the same

angle of attack are shown in Figure 5.63. The upstream movement of the shock is associated with the loss of lift

that also occurs at this higher Mach number. Such behaviour is consistent with qualitative arguments concerning the fact that for proper imaging in the free jet boundary, the image vortex system outboard of a wingtip has the same sense as that around the wingtip. This therefore adds to the increased downwash associated with finite aspect ratio and reduces the angle of attack further. The assumed interface pressure gives the same effect in this example. Figure 5.63 shows an increase in the rate of re-expansion immediately downstream of the shock when the latter is weakened. This somewhat counterintuitive behaviour can be understood in terms of the singularity of Transonic Small Disturbance Theory discussed in Cole and Cook [37], and Gadd [65]. The trends in Figure 5.61 are supported by experiments and other calculations and are discussed more fully in Malmuth [125], [120]. The relevance of the experiments is that if the Reynolds number is sufficiently high, the post-shock expansion resembles that obtained from the inviscid predictions described in this review. (Smaller Reynolds numbers will result in post-shock boundary layer separation and are not germane to this discussion.)

In addition to the high aspect ratio cases shown, non-similar wings have been analysed. A normalising transformation that simplifies the computational problem has been discovered. Details of this transformation are discussed in Malmuth [125]. **An important result of the analysis is that with the renormalisations, the calculation can be reduced to the similar section calculation with the exception that the term $\phi_{0,x}, \phi_{1,xx}$ in (1a) is no longer computed at $z = 0$.** In addition, the quantities d and w are used parametrically at each span station from a knowledge of $\Gamma_0(z)$, the spanwise loading of the zeroth order problem. This corresponds to a kind of strip theory. In order to obtain Γ_0 , the semispan wing is divided into n span stations, and the zeroth order (KG) problem detailed in Malmuth [125] is solved at each. For the results to be presented, n was selected to be 5. Depending on the planform, some investigation is required to determine if this value provides a good enough approximation of the spanwise loading to obtain the ϕ_i variational solution accurately. Chordwise pressure distributions on the swept wing (wing A) configuration of Hinson and Burdges (1980), [84], were computed at various angles of attack α , and Mach number M_∞ . To achieve rapid convergence, the streamwise grid was clustered near the blunt leading edge.

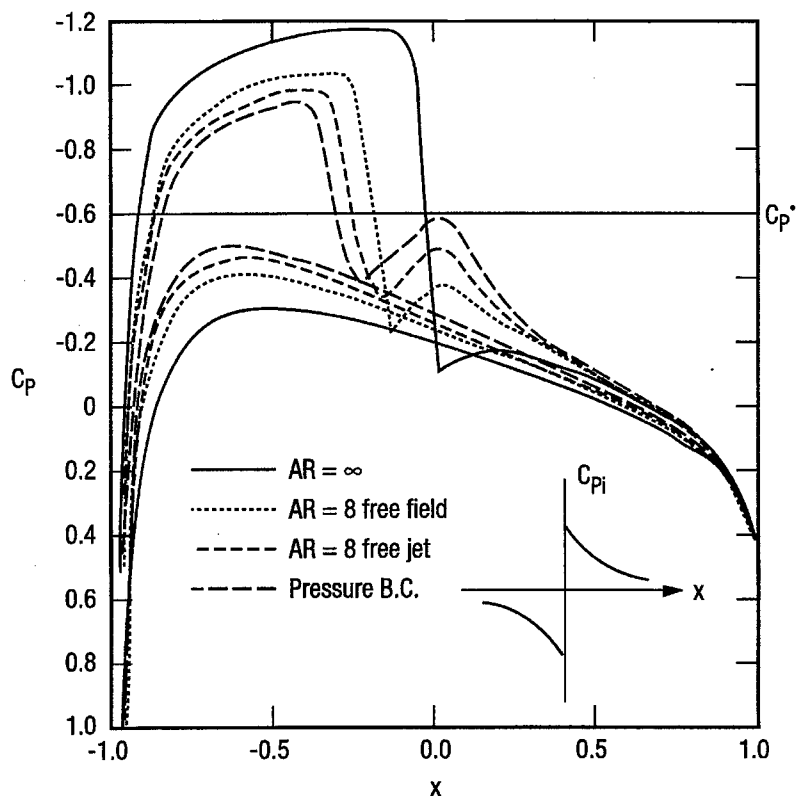


Figure 5.63 : Chordwise pressures on NACA 0012 wing,
 $M_\infty = .75, \epsilon_1 = \epsilon_2 = .2$

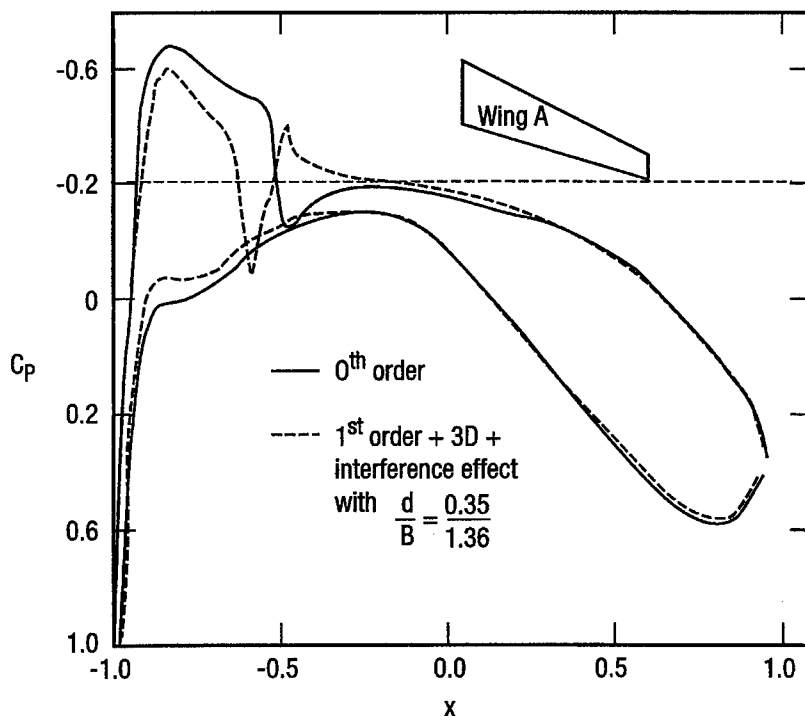


Figure 5.64 : Zeroth and first order chordwise pressure distributions on wing A, $\eta = .45, M_\infty = .76, \alpha = 0^\circ$

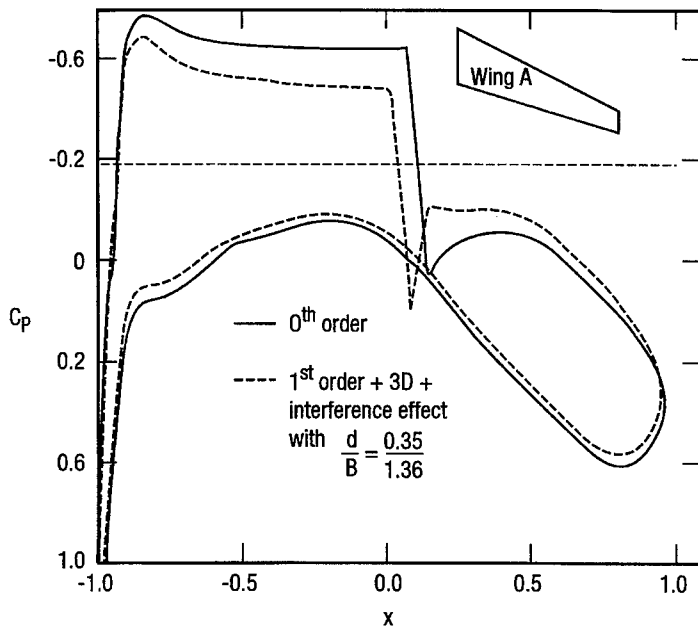


Figure 5.65 : Zeroth and first order chordwise pressure distributions on wing A, $\eta = .5$, $M_\infty = .76$, $\alpha = 1^\circ$

To demonstrate a typical calculation, Figure 5.64 and Figure 5.65 show the effect of wall interference and finite span corrections on the chordwise pressures of wing A at nearly midspan, and at two angles of attack. The largest corrections appear to be near the shock at $\alpha = 0^\circ$. By contrast, the more supercritical case corresponding to $\alpha = 1^\circ$ shows a greater extent of the corrections. For both incidences, they are most pronounced on the upper wing surface. In Cole and Cook [37], [40], modifications to the zeroth order KG boundary value problem are discussed for a yawed wing. The analysis shows that these changes occur in the far field for the three-dimensional first order perturbation flow and in both the far field and equations of motion for the second order flow. The high aspect ratio code is

based on a theory not designed for swept wings. This is because the dominant approximation of the inner flow assumes that all spanwise stations are approximately two-dimensional. If a discontinuity occurs in the slope of the leading edge, a local three-dimensional flow occurs, nullifying this assumption. Such discontinuities occur at the root apex and tips of swept and other kinds of planforms. More general cases are cranked shapes. Asymptotic procedures are under consideration to treat these corner flows and involve "canonical" numerical problems for the non-linear flow near the corner. These canonical problems remain

the same for planform changes away from the corner. In spite of this limitation, it was of interest to assess the correctness of the wing A results using the zeroth order code. Figure 5.66 and Figure 5.67 indicate chordwise pressure comparisons of our zeroth order code with data from Hinson and Burdges [84]. In both figures, the effective tunnel Mach number and angle of attack were modified to match the data. The similarity of the pressure distributions suggests the correctness of the test data. The sweep effect delaying supercriticality is evident and is not reflected in the unswept lifting line forming the basis of the present analysis. In Figure 5.66, the influence of shock-boundary layer interaction is not as great as in Figure 5.67. Results showing effective treatment of viscous effects are reported in Malmuth [125]. These

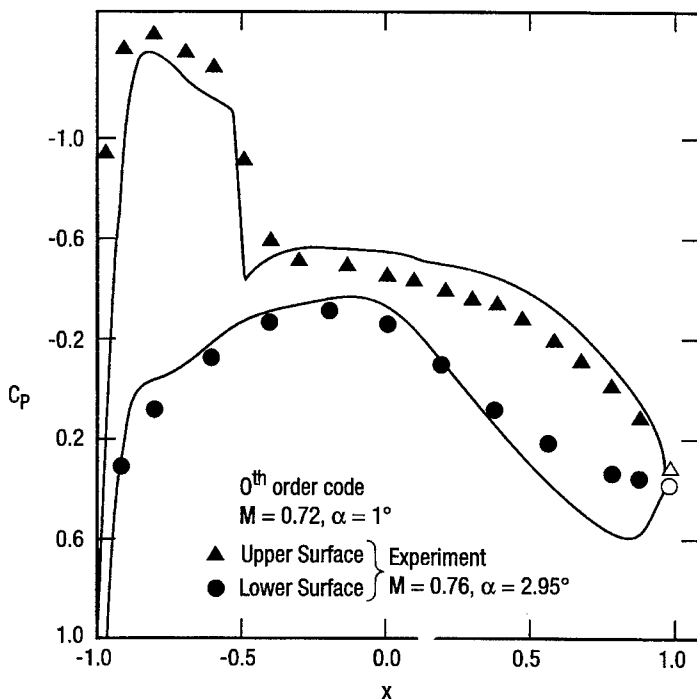


Figure 5.66 : Comparison of theoretical and experimental chordwise pressures for wing A, $\eta = .5$, tested at $M_\infty = .76$, $\alpha = 2.95^\circ$

calculations which use an interactive boundary layer model based on Green's lag entrainment method suggest that the effective increment in K associated with the combined Mach, angle of attack corrections used in Figure 5.66 and Figure 5.67 can be reduced if viscous interaction effects are systematically incorporated. In comparisons such as Figure 5.66 and Figure 5.67, what needs to be analysed are the combined effects of sweepback and viscous interactions on the interference. In Malmuth [125], the similarity parameter K was allowed to vary from the zeroth order flow to the first order wall interference flow. This flexibility should be investigated with the aim of systemising the corrections that can be obtained through studies of the type associated with Figure 5.66 and Figure 5.67. The variation of K is expressed in a perturbation form related to the asymptotic expansion of the perturbation potential ϕ . This perturbation gives the flexibility of varying the tunnel Mach number and geometric angle of attack to correct or simulate free field conditions.

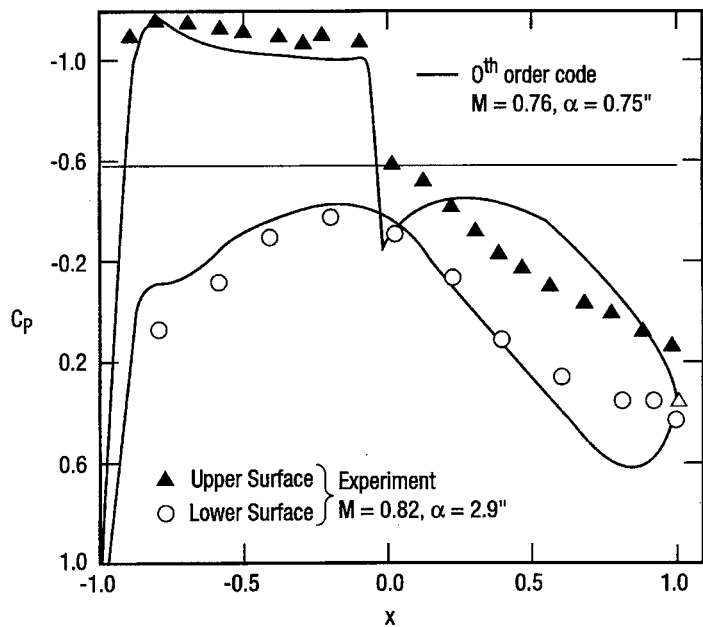


Figure 5.67 : Comparison of theoretical and experimental chordwise pressures for wing A, $\eta = .5$, tested at $M_\infty = .82$, $\alpha = 2.9^\circ$

5.4.7 LIFT INTERFERENCE AND POROUS WALL EFFECTS ON SLENDER WINGS

A current thrust of the CAN methodology is to develop a systematic asymptotic framework for computation of lift corrections due to the interaction of a slender model with walls. Strong theoretical evidence exists that the restrictions of slenderness are elastic so that lift corrections for slender shapes can be applied to not-so-slender-shapes. Because of the resemblance of the asymptotic developments to those for transonic flow, the subsonic case was considered for convenience. As indicated later, this approach actually seemed to provide good comparison with experiment at near-sonic speeds.

Initial developments are described in Malmuth, Neyland and Neyland [124]. There, the free field and wind tunnel problem of the incompressible flow over a flat wing of arbitrary planform in a circular wind tunnel test section was outlined. An in-depth continuation of that introductory treatment will be summarised in what follows: Malmuth and Cole [118] used expansions of limit process type to study the matching process in greater detail than in the preliminary analysis of Malmuth, Neyland and Neyland [124], as well as to derive a second order inner approximation.

Letting Φ be the velocity potential, limits involving the semispan of the wing b and the angle attack α have been considered. Near the wing, a limit process in which $b \rightarrow 0$ is used. Referring to Figure 5.68, an inner limit is defined as

$$\frac{\Phi_{\text{inner}}}{U} = x + ab\varphi_1(x, y^*, z^*) + ab^3 \log \frac{1}{b} \varphi_{21}(x, y^*, z^*) + ab^3 \varphi_2 + \dots \quad (5-20)$$

where the inner limit is

$$a = \tan \alpha, A = \alpha / b, y^* \equiv y / b, z^* \equiv z / b, \text{ fixed as } a, b \rightarrow 0 \quad (5-21)$$

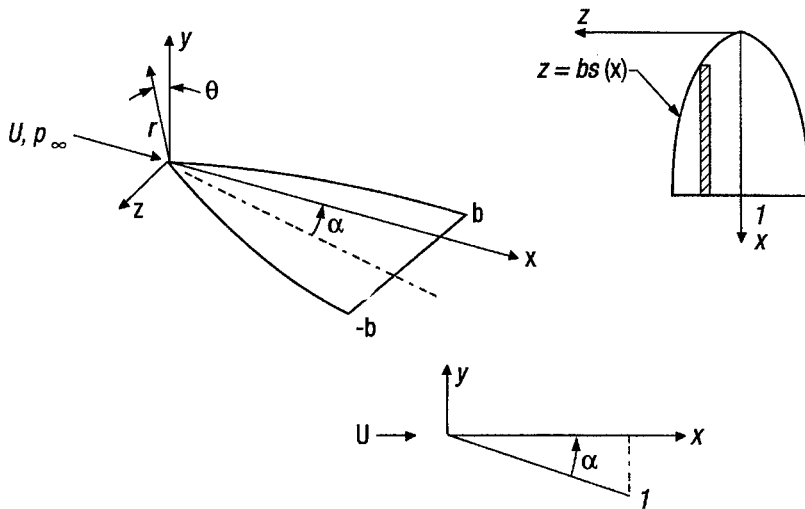


Figure 5.68 : Schematic of slender wing

In (5-21), the characteristic wing chord is fixed while the semispan b and angle of attack α tend to zero at the same rate. Near the wing, cross flow gradients dominate and these parameters give the characteristic lateral scale of the flow which is b . Equation (5-20) is an inner expansion for the velocity potential Φ in terms of approximating perturbation potentials ϕ_v , (v = order of the approximation). It contains the "switchback" term ϕ_{21} and the indicated gauge functions in anticipation of matching.

As detailed in Malmuth and Cole [122], the problems for the ϕ_v are obtained by substituting the asymptotic developments into the exact problem for Φ . The dominant orders in (5-20) solve harmonic boundary value problems in the cross plane perpendicular to the freestream and the higher orders solve Poisson problems.

The dominant inner approximation provides a first estimate for the flow and pressure field of the wing. The leading edge square root singularities dominate this flow field which is the stagnating flow on a finite flat plate. From a Joukowski mapping to the circle plane or the Circle Theorem, the solution of the dominant problem is

$$\phi_1 = -i \operatorname{Re} \left\{ \left[\sigma^2 - s^2 \right]^{1/2} - \sigma \right\} \quad \sigma \equiv z^* + i(y^* + Ax) \quad (5-22)$$

in which the freestream velocity has been normalised to unity through the non-dimensionalisations in (5-20). This solution has the proper far field (downwash at infinity) related to matching with outer solution.

A similar procedure gives

$$\phi_{21} = -\operatorname{Re} \frac{i}{2} (ss')' \sqrt{\sigma^2 - s^2} \quad (5-23)$$

Refinements of the unconfined flow field and wall interactions come from coupling with the far field. An outer expansion involving an $O(1)$ transverse length scale as $b \rightarrow 0$ gives a semi-infinite line doublet for this part of the flow. In particular, for an outer limit

$$x, y, z, A \text{ fixed as } a, b \rightarrow 0,$$

the appropriate outer expansion is

$$\frac{\Phi_{\text{outer}}}{U} = x + ab^2 \phi_1(x, y, z) + \dots \quad (5-24)$$

The solution ϕ_1 can be written as

$$\phi_1 = -\frac{1}{4\pi} \frac{\partial}{\partial y} \int_0^\infty \frac{D(\xi) d\xi}{\sqrt{(x-\xi)^2 + r^2}} + \text{wall correction function} \quad (5-25)$$

where the first term is a line doublet distribution of strength $D(\xi)$ that satisfies an approximation of the classical Darcy law boundary condition. The wall correction function is needed to satisfy Darcy's law. In (5-25), the Kutta condition at the effective trailing edge provides the appropriate continuation of the line doublet to downstream infinity and its convergent integral representation. Furthermore, (5-25) gives upstream influence not present in the inner solutions.

The inner expansion of (5-25) can be obtained from the $r \rightarrow 0$ expansion of its Fourier transform. This gives

$$\phi_1 \cong \frac{D(x) \cos\theta}{2\pi r} - \frac{D''(x)}{2\pi} \left\{ \frac{r}{2} \log r - \frac{r}{4} \right\} \cos\theta - G''(x) \frac{r}{2} \cos\theta + my + \dots \text{ as } r \rightarrow 0$$

where

$$my \equiv \cos\theta \left\{ \frac{D(x_r) r}{2h^2} \lambda - \frac{r}{2\pi h^2} \int_0^{x_r} D'(\xi) d\xi \int_0^\infty q \left[\frac{\beta^2 (K_0 q + K_1)(I_1 - qI_0) + q^2 I_1 K_1}{\beta^2 (qI_0 - I_1)^2 + q^2 I_1^2} \right] \sin \frac{q(x-\xi)}{h} dq \right\}$$

$$- \cos\theta \left\{ \frac{\beta r}{2\pi h^2} \int_0^{x_r} D'(\xi) d\xi \int_0^\infty \frac{q^2}{\beta^2 (qI_0 - I_1)^2 + q^2 I_1^2} \cos \frac{q(x-\xi)}{h} dq \right\}$$

$\lambda = 1$ for $\beta \neq 1$, (includes porous and closed walls)

$= -1$ for $\beta = 0$, (free jet), (degenerate limit $\beta \rightarrow 0$) (5-26)

$$G(x) \equiv -\frac{1}{4\pi} \int_0^1 D'(\xi) \text{sgn}(x-\xi) \log 2|x-\xi| d\xi$$

$$D(x) \equiv \frac{s^2(x)}{2} \alpha$$

where h is the wall height in units of the body length, β is the Darcy constant, $s(x)$ is the local semispan and the term my in (5-26) is the wall interaction effect due to the imaging of the doublet in the walls. As an alternate approach for the first term of (5-25), the integral can be directly expanded for $r \rightarrow 0$. This delicate procedure is described in Kevorkian and Cole [105]. In the Fourier integral method used, the solution naturally decomposes into a free field (no walls present part) and a wall interaction portion as indicated in (5-26). Special limiting processes of the singular integrals were developed to handle zero and infinite porosity, corresponding to solid wall and free jet cases respectively. Equation (5-26) agrees with the results from Pindzola and Lo [151], Goodman [72], and Baldwin [16], in the limit of vanishing chord to tunnel radius ratio. Extensions of our asymptotic procedure can be used to compute the **camber effect** associated with non-vanishing chord. To our knowledge, this study has not been made and we believe it is an important factor entering the comparison of our results with experiment to be discussed.

The inner and outer solutions match directly as shown in Malmuth and Cole [118], to the orders in (5-20). This can be shown by expressing each in terms of an intermediate variable r_η . For this purpose, an intermediate limit

$$r_\eta \equiv \frac{r}{\eta(b)} \text{ fixed as } b \rightarrow 0, \quad (5-27)$$

is used to compare the inner and outer representations in an "overlap domain" $r_\eta = O(1)$ in which both expansions are mutually valid. Note in the intermediate limit

$$r^* = \frac{\eta r_\eta}{b} \rightarrow \infty, \quad r = \eta r_\eta \rightarrow 0, \quad \frac{\eta(b)}{b} \rightarrow \infty, \quad \eta(b) \rightarrow 0.$$

The matching process consists of writing inner and outer expansions in terms of the intermediate variable r_η and comparing similar terms to determine unknown elements as detailed in Malmuth and Cole [118].

The essential wall interference effect is the additive term m from (5-26) affecting the matching. Another viewpoint is that the solution of which consists of a superposition of its homogenous solution (response to homogenous equation of motion and boundary conditions) and the effects of the forcing terms in the equation of motion and boundary conditions. The homogeneous solution is non-trivial because of the downwash far field associated with the line doublet imaging in the porous walls. Another interesting point is the surprising appearance of switchback terms. These normally are associated with transonic flow. They arise in this subsonic flow from logarithmic elements in the expansions.

Integration of the pressures on the wing gives the following expressions for the lift L . For the free field,

$$\frac{L}{\rho U^2} = b^2 \tan \alpha \ell_1 + b^4 \log \frac{1}{b} \tan \alpha \ell_{12} + b^4 \tan \alpha \ell_2 + \dots \quad (5-28)$$

where

$$\begin{aligned} \ell_1 &= \int_{-1}^1 [\varphi_1] dz^* = \pi \\ \ell_{12} &= \int_{-1}^1 [\varphi_{12}] dz^* = \frac{\pi}{2} (ss')'_{x=1} \\ \ell_2 &= \int_{-1}^1 [\varphi_{21}] dz^* = (\ell_{12} / 2)(1 + \log 2) - \frac{\pi}{2} (G''_{TE} + s'^2_{TE} + A^2) \end{aligned} \quad (5-29)$$

where G is an integral that involves the span function $s(x)$ and its derivatives and $_{TE}$ signifies the trailing edge. The dominant term for the lift ℓ_1 and pressure distribution agrees with Jones' (1946), [89], theory and a detailed analysis of Wang [181] who did not study wall interference.

As an experimental validation of the lift interference theory, Figure 5.69 compares lift versus angle of attack predicted by our asymptotic theory with transonic tests of a wing-body combination at TsAGI in Moscow and reported in Malmuth, Neyland and Neyland [124]. It is striking that the incompressible theory agrees so well with the experiment for the high transonic Mach numbers $M = .99$ and 1.02 tested. Plausibility of this finding is related to the elasticity of slender wing theory to not-so-slender planforms as $M \rightarrow 1$ as discussed in Cole and Cook [37], and Adams and Sears [1].

Approximations of wall interaction integrals give the porous wall corrections for wall openness factors $f = 2$ and 10% indicated in the figure. It shows that the experimental trend with increasing f is captured by the lift interference theory for vanishing chord to tunnel radius ratio. However, the comparison with the data shows an increasing slope with incidence not captured by the first order theory. Preliminary indications are that the free field second order effect shows a reduction in lift slope that is counter to experimental evidence. It is likely that the reverse trend is due to leading edge viscous separation and vortex formation as well the need to account for the finite chord of the wing. A refinement accomplished is an estimate of the effect of a vortex at the wing-fuselage juncture occurring at higher angles of attack.

An oil flow visualisation of this phenomenon from our Russian TsAGI experiment reported in Neyland and Neyland [144], is shown in Figure 5.70. Results from a preliminary model based on conical invariance of the vortex field is shown in Figure 5.71. The improvement in agreement is striking and suggestive of the importance of modelling discrete vortex effects. In spite of these, the wall interaction theory shows promise of modelling **relative** trends. As in the blockage theory work for wall height of the order of the body length to be discussed, estimation of the **absolute** levels can be improved independently of the interference estimations using vortex dynamic and leading edge separation approaches such as those just mentioned.

The main point of the previously discussed subsonic asymptotic framework is that it provides a natural launching pad for extension of the theory to non-linear transonic flow, accounting for higher approximations, thickness, viscous interactions and finite chord to tunnel height as well as systematic higher order refinement. With the exception of switchback terms and gauge functions, the inner problems for the transonic case are expected to resemble those associated with the incompressible asymptotic theory. However, the outer expansions will solve the three-dimensional Karman-Guderley instead of Laplace equation in the dominant approximation, and forced versions in the higher orders. However, a major simplifi-

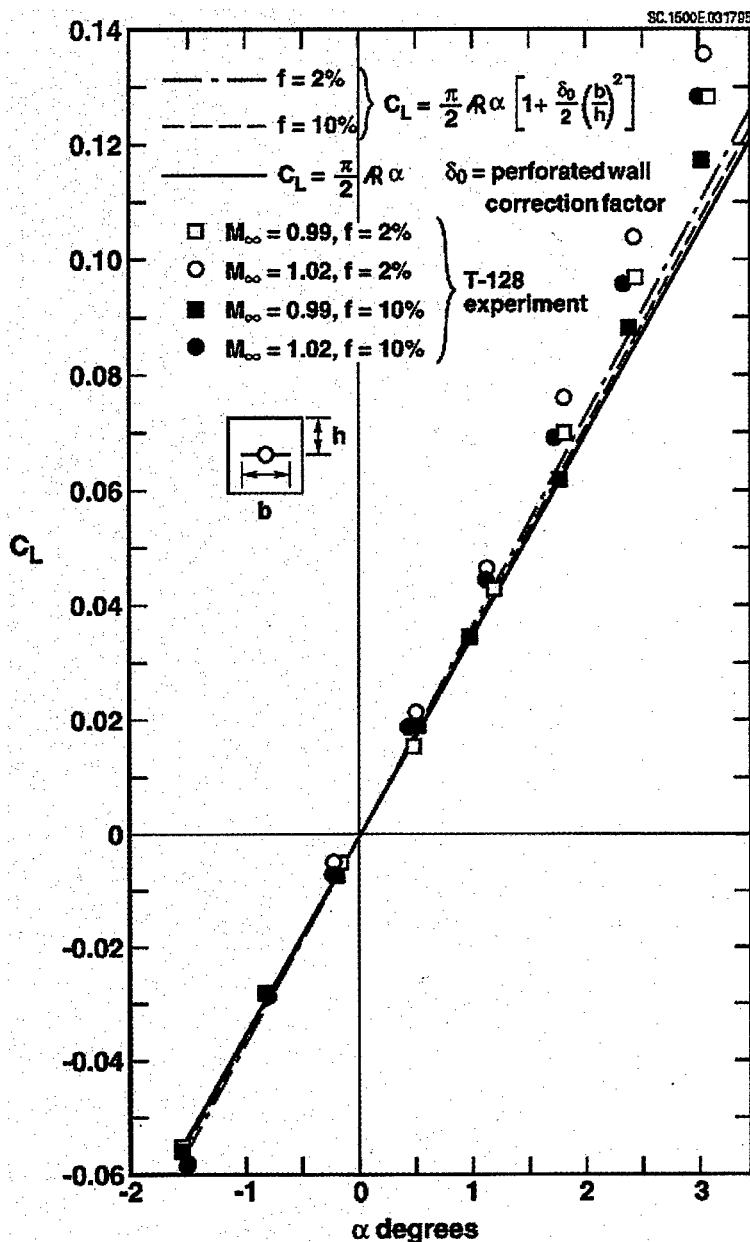


Figure 5.69 : Comparison of lift interference theory with TsAGI experiment

cation of the usual lifting surface (transonic small disturbance theory) numerical problem is anticipated since the angular variation can be separated out by matching with the inner multipole structure.

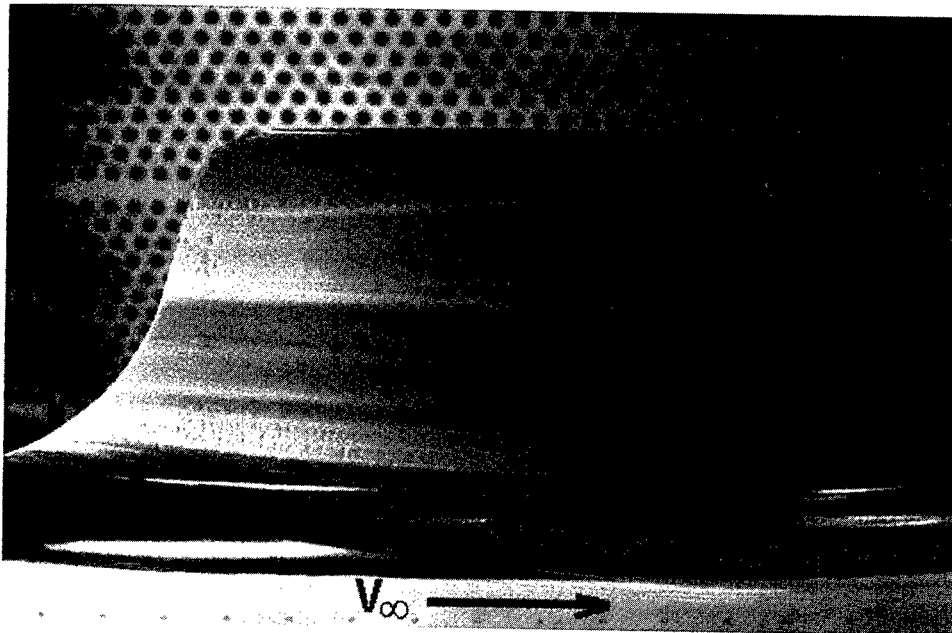


Figure 5.70 : Wing-body-juncture vortex formation in TsAGI wind tunnel

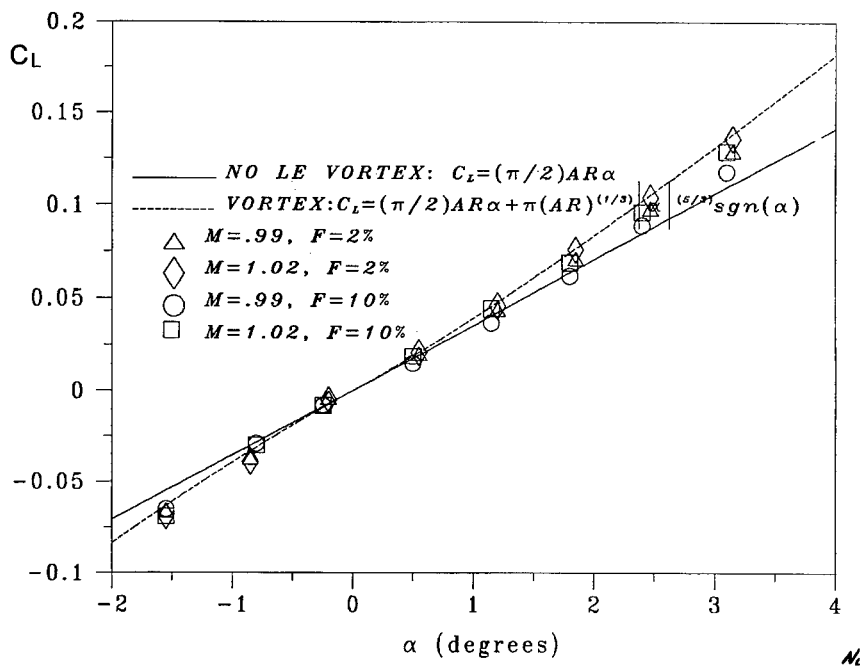


Figure 5.71 : Comparison of vortex improved theory with experiment

5.4.8 EXTENSION OF LARGE WALL-HEIGHT BLOCKAGE INTERFERENCE THEORY TO MODERATE WALL HEIGHT CASE

This section will deal with

1. Validating a transonic small disturbance baseline model for the flow in a wind tunnel against experimental data
2. Validating the equivalence rule for transonic wall interference

Referring to Figure 5.72, the walls or pressure interface boundary where pressures are assumed to be specified from experiment are at $r = h$, where h is assumed constant for convenience herein (circular test section).^{*} Defining $H = \delta h$, the case (i) $H = O(1)$ was considered, in contrast to the less practical situation (ii) described previously where $H \rightarrow \infty$. As indicated in Malmuth and Cole [118], the asymptotic solution of the Full Potential formula-

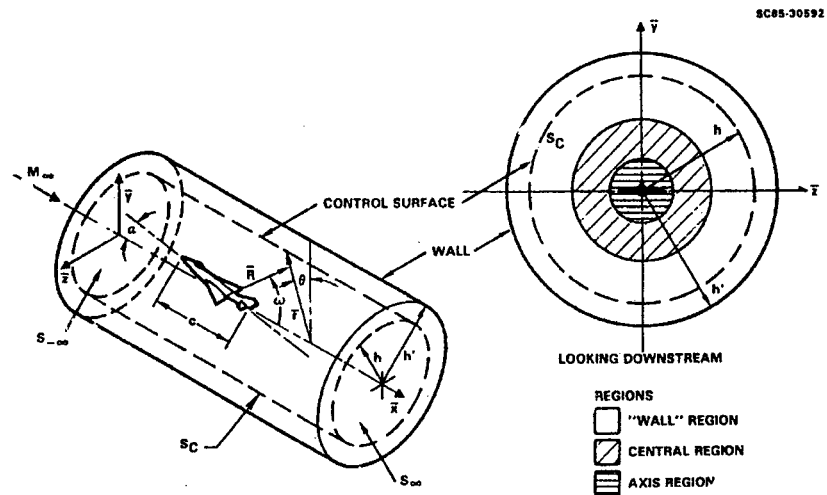


Figure 5.72 : Schematic of confined slender aeroplane

tion, for Case (i) leads to two, rather than three decks associated with (ii), i.e., no wall layer is required, the confined flow consisting only of a nearly axisymmetric "outer" region and a cross flow gradient-dominated inner core which is the near field of the body. In an inner limit in which

$$r^* \equiv r/\delta, \quad K \equiv (1 - M_\infty^2)/\delta^2, \quad A \equiv \alpha/\delta \text{ fixed as } \delta \rightarrow 0, \quad (5-30)$$

where α is the angle of attack, δ is the maximum thickness ratio of the equivalent of body of revolution and M_∞ is the freestream or tunnel Mach number which will correspond for convenience to the flight Mach number. The inner expansion (near field) of the slender aeroplane model $B = r - \delta F(x, \theta) = 0$ is

$$\frac{\Phi_{\text{inner}}(x, r, \theta; M_\infty, \delta, \alpha)}{U} = x + (2\delta^2 \log \delta) S_1(x) + \delta^2 \phi_1(r^*, \theta; x) + \dots \quad (5-31)$$

where $S_1(x)$ is a source strength determined by matching with the outer solution.

The outer limit is

$$\tilde{r} \equiv \delta r, \quad K \equiv (1 - M_\infty^2)/\delta^2, \quad A \equiv \alpha/\delta \text{ fixed as } \delta \rightarrow 0. \quad (5-32)$$

For (5-32), the appropriate outer expansion is

$$\frac{\Phi_{\text{outer}}(x, r, \theta; M_\infty, \delta, \alpha)}{U} = x + \delta^2 \phi_1(x, \tilde{r}, \theta, K, A) + \dots \quad (5-33)$$

^{*}All lengths are in units of the body length.

Malmuth and Cole [118] use these expansion procedures to obtain to the extension of our transonic area rule for wall interference (TARWI) from $H \rightarrow \infty^*$ to $H = O(1)$. From this generalisation, more practical situations than those for $H \rightarrow \infty$ can be considered in which the model distance from the walls is of the order of its length. These are typical of transonic testing. It should be noted that angle of attack effects are higher order for this $A = O(1)$ case as contrasted to $A \rightarrow \infty$ cases where they will interact with the near field in the dominant orders through line doublet-wall-imaging/reflection-induced downwash.

5.4.9 VALIDATIONS OF THEORETICAL AND COMPUTATIONAL SIMULATIONS FOR MODERATE WALL HEIGHT CASE

Experiments in TsAGI's T-128 wind tunnel in Moscow, Russia, described in Malmuth, Neyland and Neyland [124], have been performed to validate the previous theoretical developments. Figure 5.73 and Figure 5.74 show one of the wing-body configurations tested. Results for pressures over the equivalent

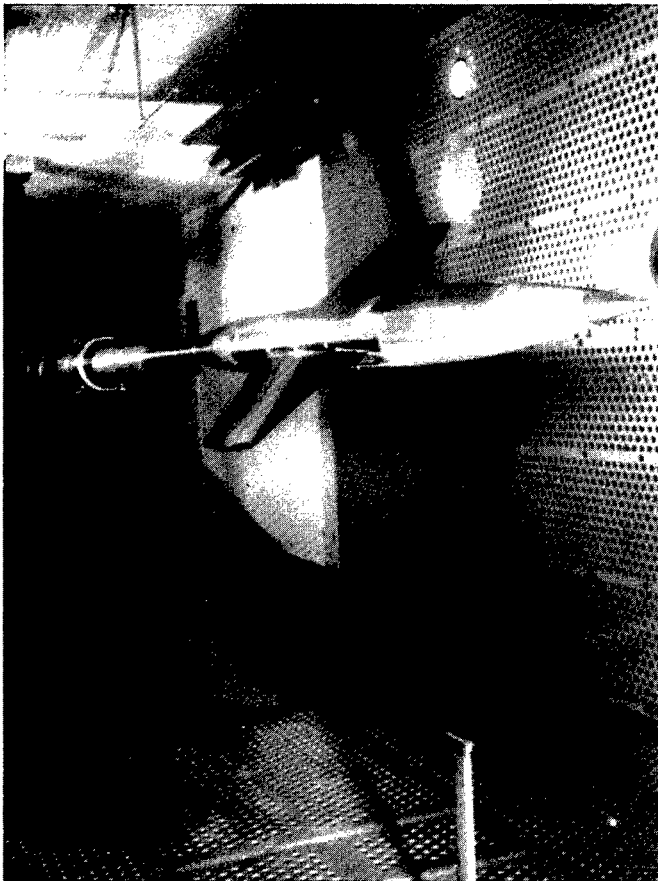


Figure 5.73 : Wing-body WB1 tested in TsAGI T-128 wind tunnel

body of revolution (EBR) for this wing body are shown in Figure 5.75 which compares the combined asymptotic and numerical method exemplified by Malmuth *et al.* [123], [125], and Malmuth and Cole [118], with the TsAGI experiments for the $H = O(1)$ case discussed in the previous section.

The code is quite efficient, requiring only a minute of execution time on a VAX 3100 work station and only 100 iterations to obtain the 2000 iteration fully converged solution. Figure 5.75 shows excellent agreement between the theory and experiment. To achieve this fidelity, it was important to accurately simulate the sting model support. This element was necessary to capture the proper recompression process to ambient levels. Additional validations discussed in Malmuth, Neyland and Neyland [124] are that the shock position estimates from Wu [186], Cole and Malmuth [38], and Malmuth [120], agree well with the TsAGI measurements. Work continues on specially designed experiments to adjust the level of interference by altering the wall porosity. This will provide a useful database for comparison with the $H = O(1)$ theory.

* Enunciated in [125]

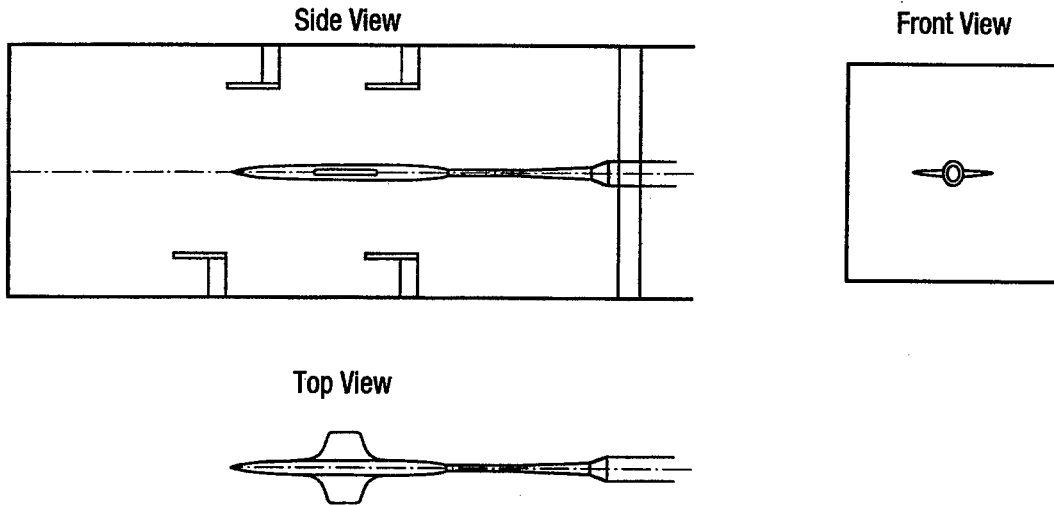


Figure 5.74 : WB1 three-view

A comparison of the larger aspect ratio wing-body with a smaller version is shown in Figure 5.76. Figure 5.77 and Figure 5.78 compare the drag rise of the smaller and larger aspect ratio wing body WB1 and WB2 respectively with their equivalent bodies EB1 and EB2 for two different wall porosities. These are

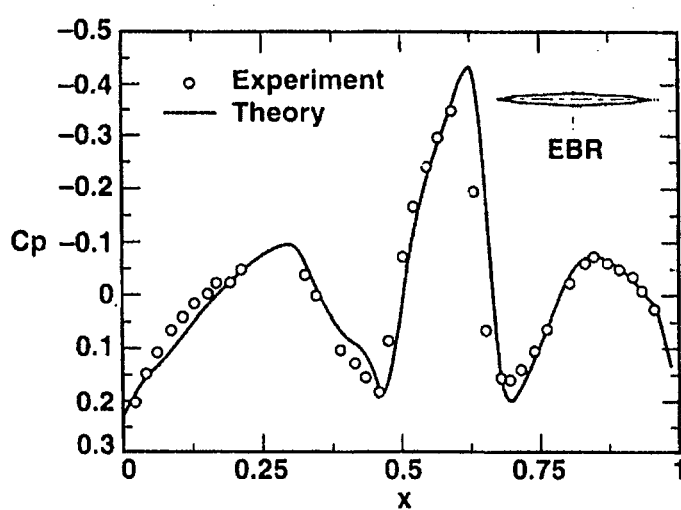


Figure 5.75 : Comparison of present theory with TsAGI experiment

expressed in terms of the wall openness area ratio, f , which is the area of the wall perforations as a percentage of the test section cross section area. Values of f were 2 and 10% for this study. Figure 5.77 and Figure 5.78 are, to our knowledge, the first experimental confirmation of the transonic area rule for wall interference (TARWI) previously discussed, *i.e.*, if

$$\Delta C_D \equiv C_D|_{f=10\%} - C_D|_{f=2\%}, \quad \text{then}$$

$$\Delta C_D|_{WB} = \Delta C_D|_{EBR} \quad (5-34)$$

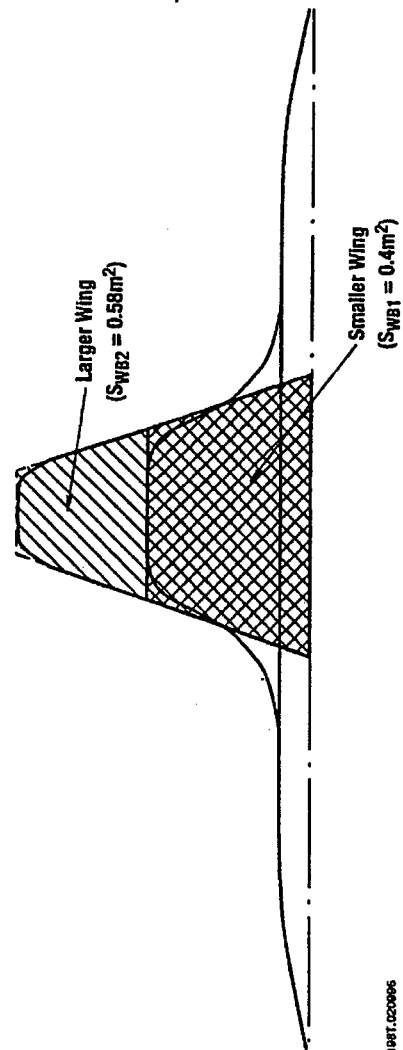


Fig. 5.76: Wing-body configurations tested

where C_D is the drag coefficient, subscripts WB and EBR denote the wing-body and its equivalent body respectively. Figure 5.78 shows the TARWI (5-34) has surprising robustness, *i.e.*, although the aspect ratio of WB2 is considerably larger than WB2, the TARWI (5-34) still holds near $M_\infty = 1$. This is related to the elasticity of slender body theory to not-so-slender shapes near sonic speeds. It is associated with the coefficient of the x derivative terms in the KG equation (28) being proportional to M_{local}^{-1} as $M_\infty \rightarrow 1$, where M_{local} is the local Mach number. Thus, although the cross flow gradients are no longer $O(1/\delta)$ but $O(1)$ for not-so-slender shapes such as WB2, the x derivative terms are still higher order. Accordingly, the near field remains harmonic in cross flow planes as in the classical slender body theory. Other robustness of (5-34) should also be noted. Although (5-34) is applicable to $H = O(1)$, the *nominal* H is closer to 0.1 for the Figure 5.77 and Figure 5.78 cases. This is related to the larger length body associated with inclusion of the sting in its definition for the computational modelling. However, if a large part of the sting is at nearly ambient conditions, $H = O(1)$ rather than the nominal $H = o(1)$.

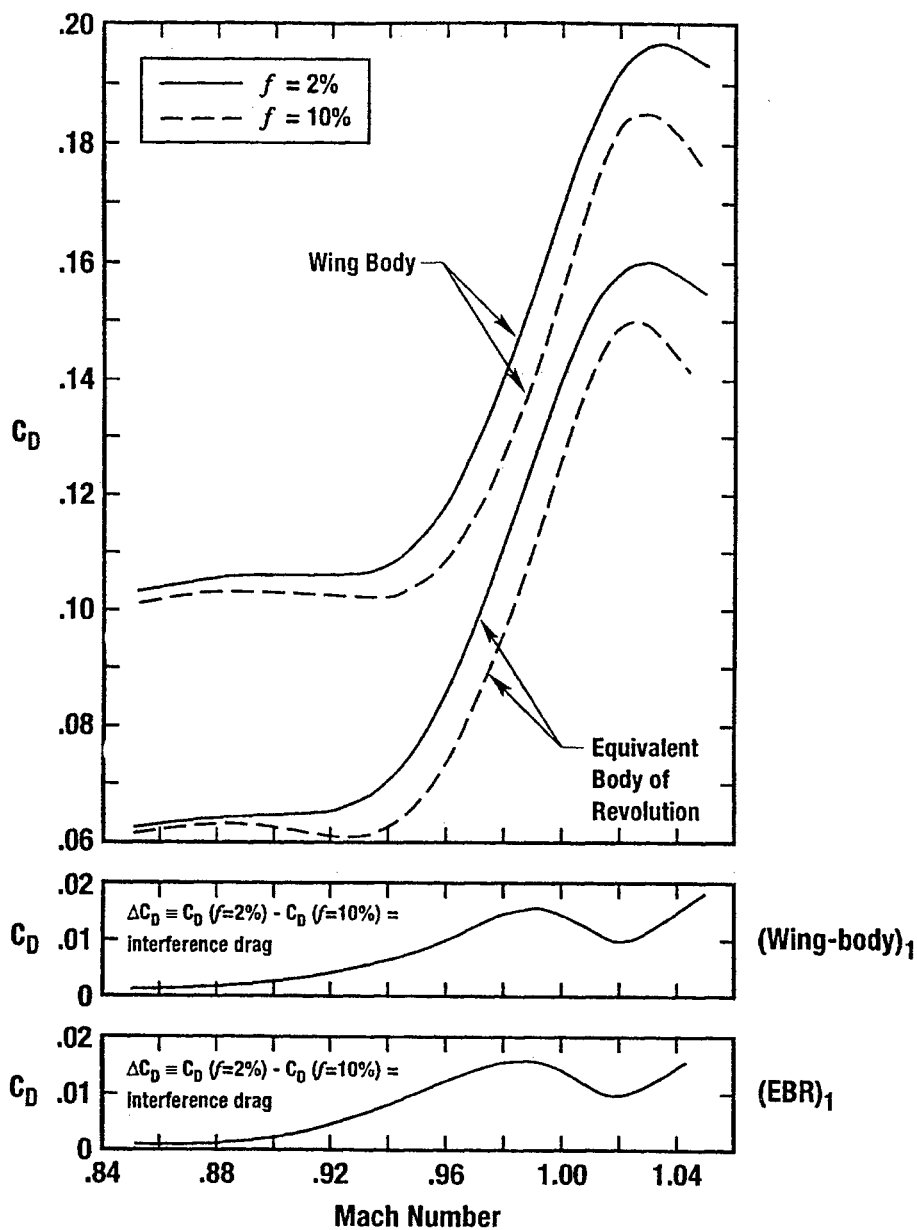


Figure 5-77 : Comparison of wave drag for wing-body WB1 and its equivalent body EBR1

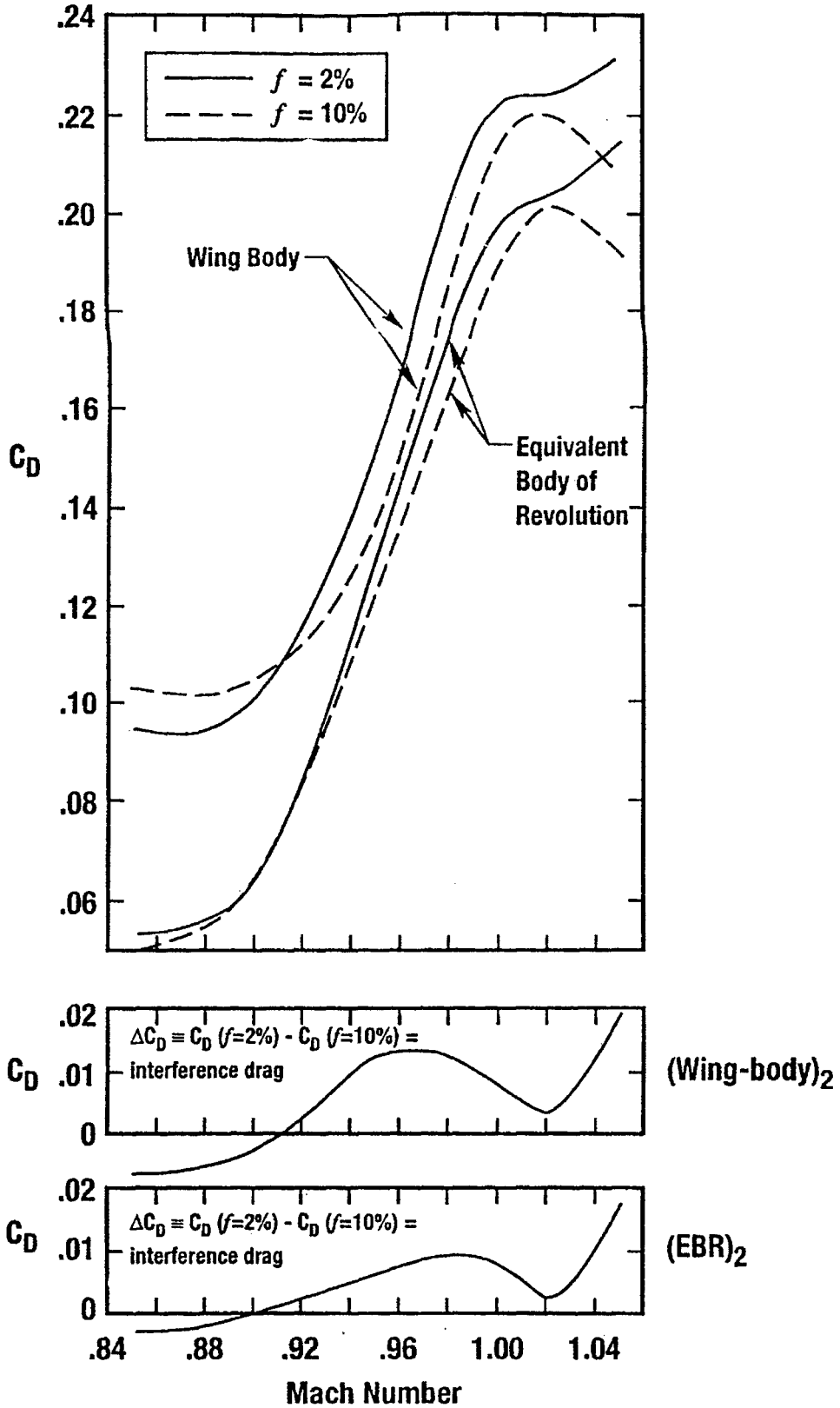
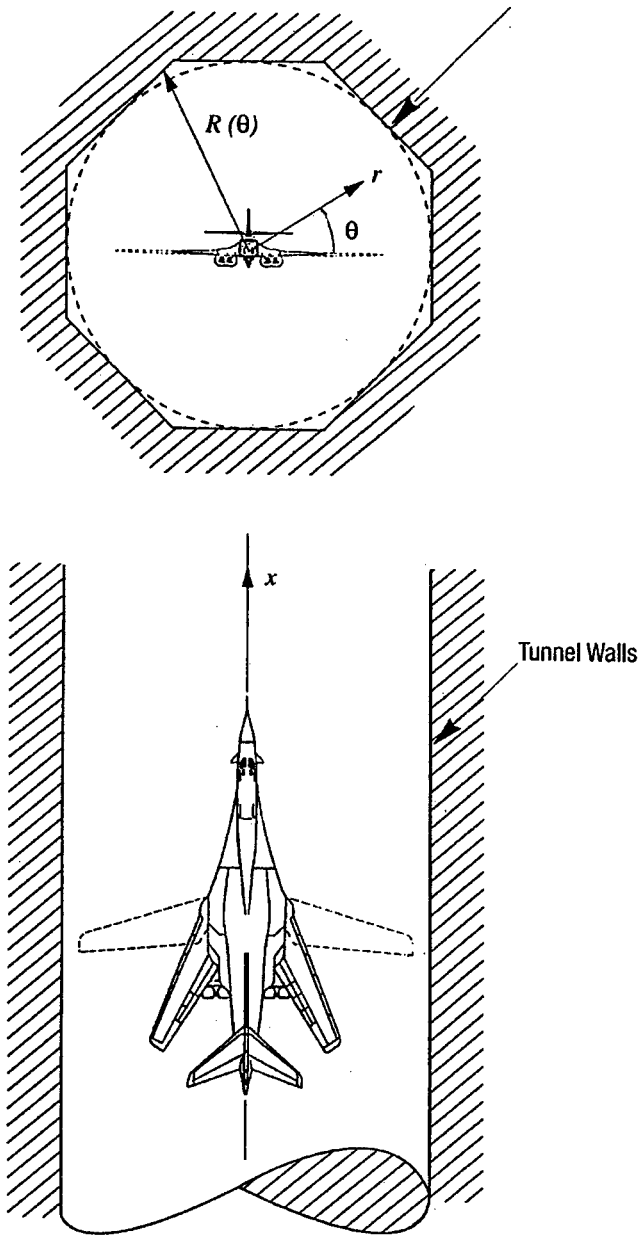


Figure 5-78 : Comparison of wave drag for wing-body WB2 and its equivalent body EBR2

5.4.10 NON-CIRCULAR WIND TUNNEL SECTIONS

Many wind tunnel test sections are non-circular. Typical U.S. installations have octagonal and rectangular test sections. Our testing in the T-128 wind tunnel strongly suggests that these non-circular cross sections have only a mild influence on the axisymmetric far field of a slender model tested at transonic Mach numbers. This observation motivated the theory to be described.



If the flow near the walls is subsonic, which is the case in transonic flow with a subsonic freestream, it is reasonable to expect rapid elliptic decay of the disturbances inward toward the centreline of the wind tunnel. This contrasts to Group 2 and 3 cases such as slightly supersonic freestreams, near choking and supersonic bubbles of the unconfined flows penetrating the walls. To explore this hypothesis, the flow inside a test section that is a slight perturbation of circular section will be treated. Figure 5.79 shows an example of such a perturbation which is an octagon. For generality, the following wall shape,

$$R = h + \epsilon g(\theta) \tag{5-35}$$

in which $\epsilon \ll 1$ and h is a constant. For specific shapes, it is possible to get an approximate numerical order of magnitude for ϵ which can be written as

$$\epsilon = \frac{g_{\max} - g_{\min}}{h} \tag{5-36}$$

Values of ϵ for square, hexagonal and octagonal test sections are given in Table 1.

Table 1

Section	n	ϵ
square	4	.414
hexagon	6	.155
octagon	8	.082

Figure 5-79 : Schematic of model in non-circular test section

These are based on the following relations for an n -sided polygon:

$$\frac{g}{h} = \frac{\sec\left(\theta - \frac{2k\pi}{n}\right) - 1}{\sec\left(\frac{\pi}{n}\right) - 1}, \quad k \frac{\pi}{4} \leq \theta \leq (k+1) \frac{\pi}{4}, \quad k = 1, 2, 3, \dots, n, \quad (5-37)$$

$$\varepsilon = \sec\left(\frac{\pi}{n}\right) - 1. \quad (5-38)$$

In the first quadrant,

$$k = 0, 1, 2, 3, \dots, n/4, \quad 0 \leq \theta \leq \pi/2.$$

Using the polar co-ordinates previously introduced and referring to Figure 5.79, as well as the outer limit (5-32) and expansion (5-33) as well dropping the subscript unity notation in ϕ_1 , the equation for the perturbation potential in the outer region is

$$\left(K - (\gamma + 1)\phi_x\right)\phi_{xx} + \tilde{r}^{-1}\left(\tilde{r}\phi_{\tilde{r}}\right)_{\tilde{r}} + \tilde{r}^{-2}\phi_{\theta\theta} = 0. \quad (5-39)$$

For convenience, a free jet boundary condition is considered. Accordingly, the exact boundary condition

$$C_p(x, R(\theta)) = 0$$

implies

$$\phi_x(x, R, \theta) = 0.$$

Since R is independent of x ,

$$\phi(x, R, \theta) = \text{constant}. \quad (5-40)$$

The constant can be assumed to be zero without loss of generality. Corresponding to (5-35), the perturbation potential ϕ can be decomposed into the axially symmetric outer part corresponding to $\varepsilon = 0$ and the secondary perturbation associated with the deviation of the walls from a circular cross section. Thus,

$$\phi(x, \tilde{r}, \theta) = \phi_0(x, \tilde{r}) + \varepsilon\phi_1(x, \tilde{r}, \theta) + \dots \quad (5-41)$$

A Fourier decomposition to reduce the three-dimensional Transonic Small Disturbance (TSD) problem for a wall perturbation from cylindrical to one in two dimensions is

$$\phi_1 = \sum_{n=0}^{\infty} \phi_{1n}(x, \tilde{r}) \cos n\theta. \quad (5-42)$$

This decomposition exploits the fact that the only way that asymmetry is introduced into the perturbation problem is through the multiplicative factor $g(\theta)$ in (5-35). Note also that the assumption of small perturbations allows the boundary conditions to be transferred from the perturbed surface to the simpler cylindrical test section's. This is essential to the reduction of the dimensionality of the problem. Equation (5-42) is a **factorisation** that reduces the problem P1 to the form

$$\left\{K - (\gamma + 1)\phi_{0x}\right\}\phi_{1nxx} - (\gamma + 1)\phi_{1nx}\phi_{0xx} + \frac{1}{\tilde{r}}\left(\tilde{r}\phi_{1n\tilde{r}}\right)_{\tilde{r}} - \frac{n^2}{\tilde{r}^2}\phi_{1n} = 0 \quad (5-43)$$

$$\lim_{\tilde{r} \rightarrow 0} \tilde{r}\phi_{1n\tilde{r}} = 0 \quad (5-44)$$

$$\phi_{1n}(x, H) = \phi_{0\tilde{r}}(x, H)A_n \quad (5-45)$$

$$A_n \equiv \frac{4}{\pi} \int_0^{\frac{\pi}{2}} g(\theta) \cos n\theta d\theta, (n > 0) \quad (5-46)$$

$$A_0 \equiv \frac{2}{\pi} \int_0^{\frac{\pi}{2}} g(\theta) \cos n\theta d\theta \quad (5-47)$$

By Malmuth and Cole [118], the function $g(x)$ which controls the drag and pressure distribution is the only part of the dominant near field that interacts with the dominant outer solution. Since there is no θ dependence in this portion, the only solution of interest is that corresponding to $n=0$. Thus the effect of the higher harmonics A_n for $n > 0$ are negligible to this order. Effectively, the angular dependence is "averaged out". **This is another kind of area rule for the effect of slightly asymmetric wall sections.**

To quantify this effect, the mild transonic case corresponding to large K in (5-43) was considered. To simplify the analysis, the problem is reduced to a harmonic (incompressible) one by scaling out K by an x transformation and noting that the second and third terms in (5-43) are negligible. The x transformation is

$$\tilde{x} = x / \sqrt{K}. \quad (5-48)$$

This is equivalent to another procedure that relates the KG to the Prandtl-Glauert (PG) equation from the definition of K in (5-32) and the fact that the appropriate outer variable for subsonic flow is r rather than \tilde{r} in the KG regime. This gives the reduced PG equation

$$\phi_{ln XX} + \frac{1}{r} (r\phi_{ln r})_r - \frac{n^2}{r^2} \phi_{ln} = 0. \quad (5-49)$$

where with some redundancy in notation used in a previous section, the transformation

$$X = x / \beta$$

in which

$$\beta \equiv \sqrt{1 - M_\infty^2}$$

is used.

The boundary conditions (5-44) and (5-45) are unaffected by the large K approximation. These relations and (5-49) constitute the problem P1' which can be solved by the exponential Fourier transform pair using the procedure detailed in Malmuth and Cole [118], to give the difference of the non-circular and circular cross section wind tunnel pressures on a body as

$$\Delta C_p \equiv C_p|_{\epsilon \neq 0} - C_p|_{\epsilon = 0}, \quad (5-50)$$

where

$$\Delta C_p = \frac{\delta \epsilon}{\beta \pi^2 h} A_0 \int_0^{\beta^{-1}} A'(\xi) d\xi \int_0^\infty \frac{\sin k(X - \xi)}{I_0^2(kh)} dk. \quad (5-51)$$

To illustrate (5-51), a parabolic arc body of revolution inside a square cross section tunnel is considered.

For this case

$$r_b(x) = \delta x(1-x), 0 \leq x \leq 1,$$

where r_b is the body radius. Accordingly,

$$A = \pi r_b^2 = \pi \delta^2 (x^2 - 2x^3 + x^4) \quad (5-52)$$

and

$$A_0 = \frac{2^{-1/2}}{(\sqrt{2}-1)\pi} \left\{ \log \left(\frac{\tan \frac{3\pi}{8}}{\tan \frac{\pi}{8}} \right) + \frac{\pi}{2} \right\} = 1.81. \quad (5-53)$$

Figure 5.80 shows the effect of increasing Mach number on the normalised correction of the pressures from a circular to a square test section, $\Delta \tilde{C}_p$, where,

$$\Delta \tilde{C}_p \equiv - \frac{\Delta C_p}{\frac{\delta \varepsilon}{\beta \pi^2 h} A_0}, \quad (5-54)$$

when $h=1$ for a parabolic arc body, *i.e.*, the tunnel average radius is equal to the body length. Note that although the body is in the interval $0 \leq x \leq 1$, wall asymmetry influences the flow considerably upstream

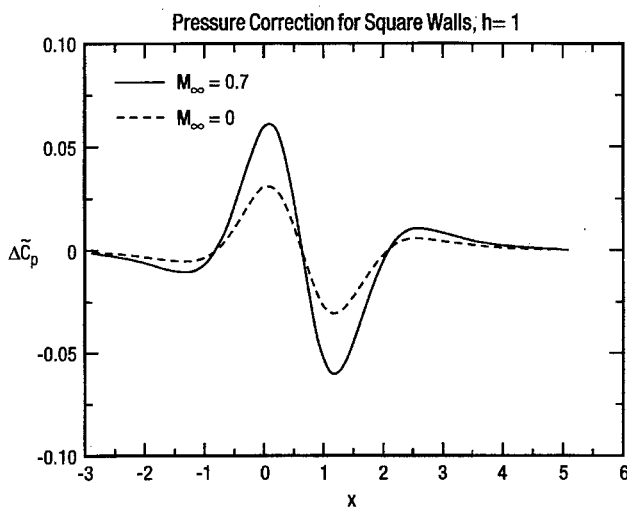


Figure 5-80 : Pressure corrections from circular to square test sections, parabolic body, $h = 1$

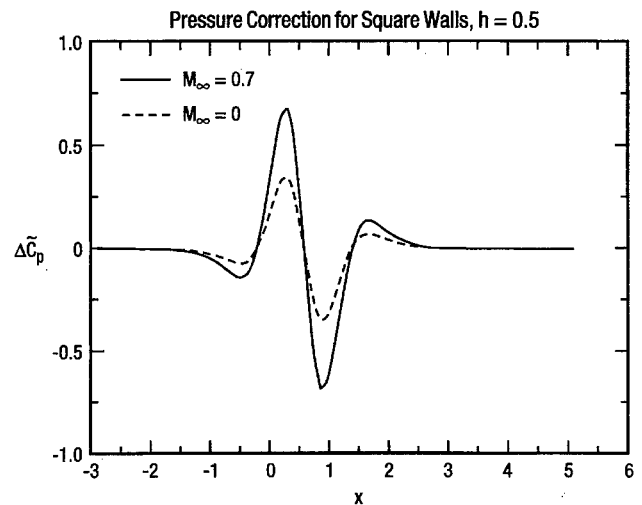


Figure 5-81 : Pressure corrections from circular to square test sections, parabolic body, $h = 0,5$

of the body nose. Moreover, the largest effects appear at the nose and tail of the body and the correction increases with Mach number as expected. Another observation is the rapid upstream and downstream decay of the effect. This is consistent with the flow ellipticity. Lastly and most important is the smallness of the effect which is in sharp contrast with the results for $h=.5$ which shows a dramatic ten-fold increase with merely halving the wall height. This effect is brought out in Figure 5.81 and Figure 5.82. for $M_\infty = 0$ and .7 respectively. In accord with expectations, Figure 5.83 shows that compressibility increases the change in pressure associated with wall asymmetry.

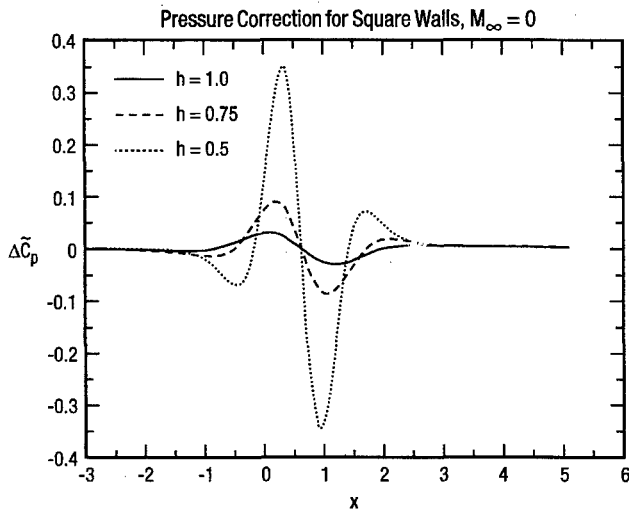


Figure 5-82 : Pressure corrections from circular to square test sections, parabolic body, effect of h for $M_\infty = 0$

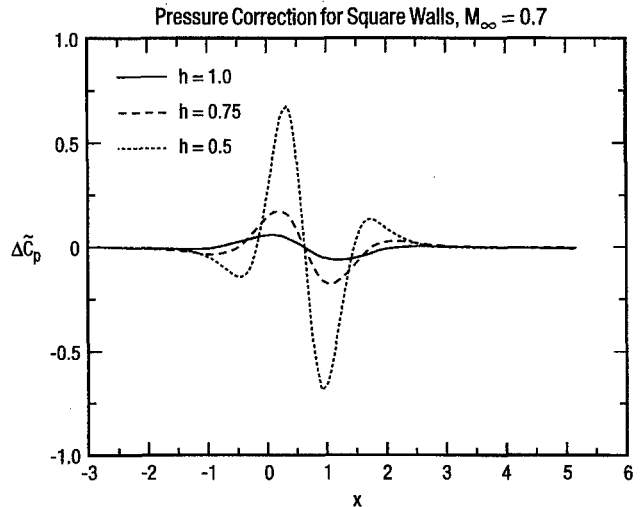


Figure 5-83 : Pressure corrections from circular to square test sections, parabolic body, effect of h for $M_\infty = 0,7$

5.4.11 SUMMARY, CONCLUSIONS AND RECOMMENDATIONS

The CAN methodology described in the previous sections provides a number of unique and useful tools to the wind tunnel test engineer. These are:

1. An area rule for blockage interference for wall heights of the order of the body length.
2. A systematic asymptotic theory for lift interference.
3. Simplified corrections for asymmetric deviations of circular wind tunnel sections.
4. Emerging database for transonic wall interference theories from Russian tests. Items 1 and 2 apply to porous wind tunnels. Item 3 can be readily extended to such sections.

The ultimate impact of this work is to

- Reduce computational intensity of transonic wall interference estimation.
- Help optimise model sizing to maximise test Reynolds number while minimising wall interference.
- Provide a quick means of extrapolating ground tests to free flight.

To enhance the utility of these tools the following further effort is recommended:

- Apply Items 1 and 2 to corrections to drag polars as in Section 5.3.3.5 .
- Extend Item 2 to transonic flow, moderate chords, and thickness
- Extend Item 3 to the moderate K case.
 - Strong evidence exists that the $n=0$ solution of (5-43) is appropriate to the strongly non-linear transonic case. The argument is similar to that following (5-50).
 - It is envisioned that $\delta'(x)$ "spiky" behaviour of the variational solution near shocks will be the principal modification of the solutions previously discussed for the high subsonic large K case.
 - Validation of the subsonic solutions against the exact eigenfunction and elliptic function Green's functions should be performed.

5.5 ASSESSMENT OF STATE OF THE ART

The previous sections gave a perspective of various aspects of transonic wind tunnel wall interference. Obviously, many topics could not be covered in this brief discussion. Nevertheless, some indication will be made where further improvement is needed. Some key issues in this connection are:

- Wall boundary conditions (wall boundary layer interactions; effects of geometry, viscosity, Reynolds number; acoustics, etc.)
- Identification of non-physical flow conditions (correctable vs. uncorrectable)
- Interaction with support interference
- Fast turn-around wall interference predictions/assessments
- Multibody problems
- Boundary layer transition considerations
- Turbulence modelling-direct simulation
- Transition
- Separation
- Coupling of separation and transition
- Reynolds number scaling to flight
- Unsteady effects

Since these topics strongly interact with each other, no attempt will be made to deal with them separately in this short overview.

In Section 5.2, current wall boundary condition technology was reviewed. In spite of progress involving the pressure pipe method and other boundary-measurement techniques, more work is required to enable accurate non-invasive static pressure measurements in the vicinity of ventilated walls. Detailed experiments which examine viscous interactions within the tunnel close-wall flow field are required for all types of wall geometries, particularly for conditions where flow is into the test section and where large model-induced gradients significantly interact with the wall boundary layers. Relatively minor changes in wall geometry can make significant changes in the close-wall flow field (or boundary condition) and, thereby, induce great changes in the wall-induced interference distribution in the vicinity of the model. Because of this, research directed at tailoring the wall flow via small modifications to wall geometry may enable inexpensive quasi-adaptive techniques for ventilated tunnels, i.e. the correctable-interference tunnel. Reynolds number scaling to flight issues will require transonic tunnels with quiet walls, and studies which examine the acoustic properties of various wall geometries are needed for both assessment of effects on model aerodynamic data and quiet wall/tunnel design. Very little has been done to quantify the upstream and downstream (test section end) effects on the corrections, and this should be addressed.

Computational methods were presented in section 5.3. Section 5.3.2.2.6 shows good progress in our ability to compute transonic wall interference over a complex configuration such as the fully-mated Space Shuttle launch configuration (SSLV). Reynolds-Averaged Navier Stokes (RANS) computational modelling has improved substantially since the last AGARD review. Modern unstructured grid methods as well as parallel computing have made simulation of complex configurations in wind tunnels more practical.

However, in addition to turbulence modelling, issues in computing such a shape are many. At transonic speeds, the interaction of the support structure in the wind tunnel is an artifact not seen in the free flight environment. Simulation of plumes and their interaction with walls and stings can be a source of concern in ground test-to-flight extrapolation. This effect is highly Reynolds number-dependent and solid wall simulation may be unrealistic, even for single plumes, to say nothing of multiple ones such as those from the Solid Rocket Boosters, External Tank and Orbiter. More work is required to deal with the very special questions associated with this topic such as interaction of the wakes and shear layers with each other and the walls.

Similar issues relate to wall corrections for transonic characteristics of HSCT's. Recent internally reported work by Malmuth, Neyland, and Neyland in 1995 [124] for TsAGI T-128 tunnel tests has studied the interaction of nacelle flows with wall interference and transonic wave drag rise simulations.* More effort will be required in dealing with the trade-off of model size needed for proper unit Reynolds number simulation at the expense of large wall corrections, or in the extreme, uncorrectability. For the unsteady ascent trajectory of vehicles such as SSLV and reusable launch vehicles (RLV), the adequacy of the pseudo-steady approximation especially at the maximum q (dynamic pressure) trajectory point needs further attention.

These questions also arise in assessment of wall interference associated with store carriage and separation. Currently, the Captive Trajectory Support System (CTS) is the workhorse of experimental databases for store certification. Complex store configurations such as the F-15, F-16 and F-22 involve multiple interfering bodies such as bombs, missiles, pylons, racks with parent bodies. The CTS method intrinsically assumes pseudo-steady conditions. Effort such as free drops in the wind tunnel is needed to validate this approximation. This becomes particularly important for simulating store separation from weapons-bay cavities. Here, as above, the interaction of the support and wall interference is critical. Also key is the coupling of the shear layer with the body dynamics and the store's steep wave system impinging on the walls. These are complexities that arise in the correlation of wind tunnel results and flight experiments as well as predictions.

Large-scale and CAN mid-range simulations such as those discussed in this chapter should be used to study the various time scales in the weapons-release problem. Unit problems that relate the wind tunnel simulation to the free flight environment should be tackled. They should evaluate sting mounted arrangements and their relationship to unsupported ones in and out of cavities. More work should be done with research configurations rather than complex ones to isolate the basic effects. Physical mechanisms that should be studied are unsteady shock and vortex evolution and convection effects. The data coming from such computational and experimental models could stimulate theoretical development and enhance our understanding of the various processes.

In the previous sections, the issue of correctability was mentioned. At transonic speeds, shock-induced transition plays strongly into this problem. Since a strong Reynolds number dependence is relevant, pre-test assessment of wall interference depends on accurate turbulence models. Although much effort has gone into developing such simulations, much more is required. As computer power increases into the next century, Direct Numerical Simulations (DNS) could provide dramatic new insights. This could flow to improved RANS and mid-range approaches that will improve our capability to make such pre-test assessments economically and rapidly

* This wave drag rise is vital in accurately assessing the "transonic pinch point" that affects noise-abatement, operational, payload and fuel considerations impacting HSCT and hypersonic vehicle mission viability and affordability.

In many cases, transitional separations are encountered. Treatment of interaction of separation and transition is a challenge in and out of the wind tunnel. It is so difficult that trips are used to provide a baseline for understanding the flow by making it fully turbulent over the model. However, many flight environments are really transitional and it is necessary to improve our computational simulations by inclusion of suitable stability and transition prediction modules so they can relate to natural transition wind tunnel experiments. Unfortunately, current transition prediction modules are in a very early stage of being able to handle interaction of separation and transition, even in the rudimentary cases of a leading edge separation bubble over a two-dimensional airfoil and flap hinge moment prediction.

Improved techniques will have a strong impact on computational simulations as well as adaptive wall technology and our understanding of the complex flow processes that are needed for control and prediction of transonic wall interference.

5.6 REFERENCES FOR CHAPTER 5

- [1] Adams, M.C.; and Sears, W.R. 1953: Slender-Body Theory, Review and Extension. *J. Aero. Sci.*, pp. 85-98.
- [2] Adcock, J.B.; and Barnwell, Richard W. 1984: Effect of Boundary Layers on Solid Walls in Three-Dimensional Subsonic Wind Tunnels. *AIAA J.* vol. 22, no. 3, pp. 365-371.
- [3] AGARD 1982: Wall Interference in Wind Tunnels. 50th Fluid Dynamics Panel Specialists' Meeting, London, England, May 19-20, 1982, AGARD-CP-335.
- [4] AGARD 1990: Adaptive Wind Tunnel Walls - Technology and Application. Report of the AGARD Fluid Dynamics Panel Working Group 12 Hornung, H.G., Chairman. AGARD-AR-269.
- [5] AGARD 1993: Wall Interference, Support Interference, and Flow Field Measurements. 73rd Fluid Dynamics Panel Symposium, Brussels, Belgium, October 4-7, 1993, AGARD-CP-535.
- [6] Agrell, Nada 1994: Computational Simulations for Some Tests in Transonic Tunnels. Presented at the 82nd Meeting of the Supersonic Tunnel Association, Wright Laboratory Flight Dynamics Directorate, Wright-Patterson Air Force Base.
- [7] Agrell, Nada; Pettersson, Björn; and, Sedin, Yngve C-J. 1986: Numerical Design Parameter Study for Slotted Walls in Transonic Wind Tunnels. Paper No. ICAS-86-1.6.2, presented at the 15th ICAS Congress, London.
- [8] Al-Saadi, Jassim A. 1991: Wall Interference Calculation in a Transonic Wind Tunnel With Discrete Slots. Ph.D. Dissertation, North Carolina State Univ.
- [9] Al-Saadi, Jassim A. 1993: Wall Interference and Boundary Simulation in a Transonic Wind Tunnel With a Discretely Slotted Test Section. NASA TP 3334.
- [10] Al-Saadi, Jassim A.; and, DeJarnette, F.R. 1992: Wall Interference Calculation in a Transonic Test Section Including Simulation of Discrete Slots. AIAA Paper No. 92-0032 presented at 30th Aerospace Sciences Meeting & Exhibit, Reno, NV.
- [11] Ashill, P.R. 1983: Effects of Sidewall Boundary Layers on Aerofoils Mounted from Sidewalls of Wind Tunnels - Experimental Evidence and Developments of Theory. RAE TR 83065, August 1983.
- [12] Ashill, P.R. 1993: Boundary-Flow Measurement Methods for Wall Interference Assessment and Correction - Classification and Review. Pp. 12-1 to 12-21 in AGARD 1993.
- [13] Ashill, P.R.; and Weeks, D.J. 1982: A Method for Determining Interference in Solid Wall Tunnels from Measurements of Static Pressure at the Walls. Paper No. 1 in AGARD 1982.
- [14] Ashill, P.R.; Taylor, C.R.; and Simmons, M.J. 1994: Blockage Interference at High Subsonic Speeds in a Solid-Wall Tunnel.
- [15] Bailey, F.R. 1971: Numerical Calculation of Transonic Flow About Slender Bodies of Revolution. NASA TN D-6582.
- [16] Baldwin, B.S.; and Turner, J.B. 1954: Wall Interference in Wind Tunnels with Slotted and Porous Boundaries at Subsonic Speeds. NACA TN 3176.
- [17] Barnwell, R.W. 1974: Transonic Flow About Lifting Wing-Body Combinations. AIAA Paper 74-185.
- [18] Barnwell, R.W. 1980: Similarity Rule for Sidewall Boundary-Layer Effect in Two-Dimensional Wind Tunnels. *AIAA J.* vol 18, no 9, pp 1149-1151.
- [19] Barnwell, R.W.; and Sewall, W.G. 1982: Similarity Rules for Effects of Sidewall Boundary-Layers in Two-Dimensional Wind Tunnels. Paper No. 3 in AGARD 1982.

- [20] Barnwell, Richard W. 1976: Improvements in the Slotted-Wall Boundary Condition. Proceedings--AIAA Ninth Aerodynamic Testing Conference, pp. 21-30.
- [21] Barnwell, Richard W. 1978: Design and Performance Evaluation of Slotted Walls for Two-Dimensional Wind Tunnels. NASA Technical Memorandum 78648.
- [22] Baronti, P.; Ferri, A.; and Weeks, T. 1973: Analysis of Wall Modifications in a Transonic Wind Tunnel. Advanced Technology Laboratories TR-181.
- [23] Benek, J.A.; Steger, J.L.; Dougherty, F.C.; and Buning, P.G. 1986: "Chimera 1986: A Grid-Embedding Technique. AEDC-TR-85-64 AD-A167466. April.
- [24] Berndt, Sune B. 1977: Inviscid Theory of Wall Interference in Slotted Test Sections. AIAA J., Vol. 15, No. 9, pp. 1278-1287.
- [25] Berndt, Sune B. 1982: Flow Properties of Slotted-Wall Test Sections. AGARD Fluid Dynamics Panel Specialist Meeting on Wall Interference in Wind Tunnels, Paper No. 6.
- [26] Berndt, Sune B.; and Sørensen, Hans 1976: Flow Properties of Slotted Walls for Transonic Test Sections. Wind Tunnel Design and Testing Techniques, AGARD-CP-174, pp. 17-1—17-10.
- [27] Bhat, Maharaj Krishen 1988: On Transonic Flow Over Segmented Slotted Wind Tunnel Wall with Mass Transfer. Ph.D. Diss., The University of Tennessee.
- [28] Binion, T.W., Jr. 1975: An Experimental Study of Several Wind Tunnel Wall Configurations Using Two V/STOL Model Configurations. AEDC TR-75-36.
- [29] Blynskaya, A.A.; and Lifshitz, Y.B. 1981: Transonic Flows Around an Airfoil in Wind Tunnels. Fluid Dynamics, Vol. 15, pp. 711-718.
- [30] Boppe, C.W. 1987: Aerodynamic Analysis for Aircraft with Nacelles, Pylons, and Winglets at Transonic Speeds. NASA CR-4066, April.
- [31] Buning, P.G.; Chan, W.M.; Renze, K.J.; Sondak, D.; Chiu, I.T.; and Slotnick, J.P. 1991: OVERFLOW/F3D User's Manual, Version 1.6p, NASA Ames Research Center, Moffett Field, CA, December.
- [32] Catherall, D. 1975: The Computation of Transonic Flows Past Aerofoils in Solid, Porous, or Slotted Wind Tunnels. Paper 19, AGARD CP 174.
- [33] Chan, Y.Y. 1982: Wall Boundary-Layer Effects in Transonic Wind Tunnels. AGARD-CP-335, May, pp. 7-1 to 7-15.
- [34] Chan, Y.Y., 1980. A Singular Perturbation Analysis of Two-Dimensional Wind Tunnel Interferences. ZAMP, 31 pp. 605-619.
- [35] Chen, C.F.; and Mears, J.W. 1957: Experimental and Theoretical Study of Mean Boundary Conditions at Perforated and Longitudinally Slotted Wind Tunnel Walls. AEDC TR-57-20.
- [36] Chew, W.L. 1955: Cross-Flow Calibration at Transonic Speeds of Fourteen Perforated Plates with Round Holes and Airflow Parallel to the Plates. AEDC-TR-54-65, July.
- [37] Cole, J.D.; and Cook, L.P. 1986: Transonic Aerodynamics. North-Holland, New York.
- [38] Cole, J.D.; and Malmuth, N.D., 1989: Shock Wave Location on a Slender Transonic Body of Revolution. Mechanics Research Communications, Vol. 10, no. 6, November-December, pp. 353-335
- [39] Cole, J.D.; Malmuth, N.D.; and Ziegler, F. 1982: An Asymptotic Theory of Solid Tunnel Wall Interference. AIAA Paper 82-0933, AIAA/ASME 3rd Joint Thermophysics, Fluids, Plasma, and Heat Transfer Conference, St. Louis, Missouri, June 7-11.
- [40] Cook, L.P.; and Cole, J.D. 1978: Lifting Line Theory for Transonic Flow. SIAM J. Appl. Math., Vol. 35, no. 2, September , pp. 209-228.

- [41] Crites, R. C. 1987: Transonic Wind Tunnel Boundary Interference - A Correction Method. AGARD CP-429, Oct., pp. 15-1 to 15-16.
- [42] Crites, R.; and Rueger, M. 1992: Modelling the Ventilated Wind Tunnel Wall. AIAA Paper No. 92-0035, presented at the AIAA 30th Aerospace Sciences Meeting, Reno, NV, January 6-9.
- [43] Crites, R.; and Steinle, Frank W., Jr. 1995: Wall Interference Reduction Methods for Subsonic Wind Tunnels. AIAA Paper No 95-0107 presented at 33rd Aerospace Sciences Meeting and Exhibit, Reno, NV.
- [44] Daugherty, N.S., Jr.; and Steinle, Frank W., Jr. 1974: Transition Reynolds Number Comparisons in Several Major Transonic Tunnels. AIAA Paper No. 74-627.
- [45] Daugherty, N.S., Jr.; Anderson, C.S.; and Parker, R.L., Jr. 1988: An Experimental Investigation of Techniques to Suppress Edge Tones from Perforated Wind Tunnel Walls. AEDC-TR-75-88.
- [46] Davis, Don D., Jr.; and Moore, Dewey 1953: Analytical Studies of Blockage- and Lift-Interference Corrections for Slotted Tunnels Obtained by the Substitution of an Equivalent Homogeneous Boundary for the Discrete Slots. NACA RM-L53-E07b.
- [47] Donegan, T.L.; Benek, J. A.; and Erickson, J. C., Jr. 1987: Calculation of Transonic Wall Interference. AIAA Paper No. 87-1432, presented at the AIAA 19th Fluid Dynamics, Plasma Dynamics, and Laser Conference, Honolulu, HI, June 8-10.
- [48] Doria, M.L.; and South, J.C., Jr. 1982: Transonic Potential Flow and Coordinate Generation for Bodies in a Wind Tunnel. AIAA Paper 82-0223.
- [49] Elsenaar, A., editor 1983: Two-Dimensional Transonic Testing Methods - Final Report. NLR-TR-83086, GARTEUR/TP-011 work completed July, 1981.
- [50] Emmons, H. W. 1948: Flow of a Compressible Fluid Past a Symmetrical Airfoil in a Wind Tunnel and in Free Air. NACA TN 1746.
- [51] Erickson, J.C. Jr. 1990: Adaptive Wind Tunnel Walls - Compendium of Final Report - AGARD FDP Working Group 12. AIAA Paper No. 90-1405, presented at AIAA 16th Aerodynamic Ground Testing Conference, Seattle, WA, June 18-20.
- [52] Erickson, J.C., Jr.; and Homicz, G. F. 1982: Numerical Simulation of a Segmented Plenum, Perforated, Adaptive-Wall Wind Tunnel. AIAA J., Vol. 20, No. 5, May, pp. 612-623.
- [53] Everhart, Joel L. 1987: Theoretical and Experimental Analysis of the Slotted-Wall Flow Field in a Transonic Wind Tunnel. SAE Tech. Paper Ser. 871757.
- [54] Everhart, Joel L.; and Barnwell, Richard W. 1978: A Parametric Experimental Study of the Interference Effects and the Boundary-Condition Coefficient Slotted Wind-Tunnel Walls. AIAA Paper No 78-805 presented at the AIAA 10th Aerodynamic Testing Conference, San Diego, CA.
- [55] Everhart, Joel L.; and Bobbitt, Percy J. 1994: Experimental Studies of Transonic Flow Field Near a Longitudinally Slotted Wind Tunnel Wall. NASA TP 3392.
- [56] Everhart, Joel L.; and Goradia, Suresh H. 1991: Mass Flux Similarity for Slotted Transonic-Wind-Tunnel Walls. NASA TM 4281.
- [57] Everhart, Joel L.; Igoe, William B.; and Flechner, Stuart G. 1991: Slotted-Wall Flow-Field Measurements in a Transonic Wind Tunnel. NASA TM-4280.
- [58] Everhart, Joel Lee 1988: Theoretical and Experimental Studies of the Transonic Flow Field and Associated Boundary Conditions Near a Longitudinally-Slotted Wind-Tunnel Wall. D.Sc. Diss., The George Washington Univ. Available as NASA TM-103381.
- [59] Ferri, A., and Baronti, P. 1973: A Method for Transonic Wind-Tunnel Corrections. AIAA J., Vol. 11, No. 1, pp. 63-66.
- [60] Foster, Jean M.; and Adcock, Jerry B. 1996: User's Guide for the National Transonic Facility Research Data System. NASA Technical Memorandum 110242.

- [61] Freestone, M.M.; and, Henington, P. 1981: Incorporation of Viscous Effects of Perforated Wind Tunnel Walls in Two-Dimensional Flow Calculations. City University (London) Res. Memo Aero 81/1.
- [62] Freestone, M.M.; and, Mohan, S.R. 1993: Interference Determination for Wind Tunnels with Slotted Walls. Paper No. 16 presented at AGARD Fluid Dynamics Panel Symposium on "Wall Interference, Support Interference, and Flow Field Measurements," AGARD CP 535, pp. 19-1 to 19-12, Brussels, Belgium.
- [63] Freestone, M.M.; Gascoigne, A.; and, Lock, R.C. 1984: Determination of Interference in a Transonic Wind Tunnel having Perforated Liners. Paper presented at Euromech Colloquium 187, Goettingen, West Germany.
- [64] Freestone, M.M.; Mohan, S.R.; and, Lock, R.C. 1992: Interference Corrections in Wind Tunnels with Slotted Walls. Paper 16, Proceedings of the Royal Aeronautical Society conference on "Wind Tunnels and Wind Tunnel Test Techniques."
- [65] Gadd, G.E., 1960. The Possibility of Normal Shock Waves On a Body With Convex Surfaces in Inviscid Transonic Flow," *Zeit. Ang. Math. and Phys.*, 11 pp. 51-55.
- [66] Gaffney, R.L., Jr.; Salas, M.D.; and Hassan, H.A. 1985: Assessment of Wind Tunnel Corrections for Multielement Airfoils at Transonic Speeds. 3rd Symposium on Numerical and Physical Aspects of Aerodynamic Flows, Jan. 20-24, Long Beach, CA.
- [67] Garner, H.C.; Rogers, E.W.E.; Acum, W.E.A.; and Maskell, E.E. 1966: Subsonic Wind Tunnel Wall Corrections. AGARDograph 109.
- [68] Garriz, J. A.; and Haigler, K. J. 1992: User Guide for WIACX: A Transonic Wind-Tunnel Wall Interference Assessment and Correction Procedure for the NTF. NASA TM-104168.
- [69] Garriz, J. A.; Newman, P. A.; Vatsa, V. N.; Haigler, K. J.; and Burdges, K. P. 1990: Evaluation of Transonic Wall Interference Assessment and Corrections for Semi-Span Wing Data. AIAA Paper 90-1433.
- [70] Gentry, Carl L.; Igoe, William B.; and Fuller, Dennis E. 1981: Description of 0.186-Scale Model of High-Speed Duct of National Transonic Facility. NASA TM 81949.
- [71] Goethert, Bernhard H. 1961: Transonic Wind Tunnel Testing. AGARDograph No. 49 Pergamon Press.
- [72] Goodman, T.R., 1951. The Porous Wind Tunnel, Part IV, Subsonic Interference Problems in a Circular Tunnel," Cornell Aeronautical Laboratory Report AD-706-A-2.
- [73] Goodyer, M. J. 1975: The Self-Streamlining Wind Tunnel. NASA TM X-72699.
- [74] Green, L. L.; and Mineck, R. E. 1991: Wall Interference Assessment/Correction for Transonic Airfoil Data. *J. of Aircraft*, Vol. 28, No. 11, pp. 774-780, also AIAA 90-1406.
- [75] Green, L. L.; and Newman, P. A. 1987: Transonic Wall Interference Assessment and Corrections for Airfoil Data from the 0.3-m TCT Adaptive Wall Test Section. AIAA Paper 87-1431.
- [76] Green, L. L.; and Newman, P. A. 1991: Wall Interference Assessment and Corrections for Transonic NACA 0012 Airfoil Data from Various Windtunnels. NASA TP 3070.
- [77] Green, L.; Zhang, Q.; Garriz, J.; Wang, S.; Vatsa, V.; Haigler, K.; and Newman, P. 1991: NASA/CAE Wind Tunnel Interference Cooperative Program-- Status and Sample Results, January 1991. ICAW 1991 Paper - W1, in He (1991).
- [78] Gumbert, C. R. 1985: User Manual for 0.3-m TCT Wall-Interference Assessment/Correction Procedure: 8- by 24-Inch Airfoil Test Section. NASA TM-87582.
- [79] Gumbert, C. R.; and Newman, P. A. 1984: Validation of a Wall Interference Assessment/Correction Procedure for Airfoil Tests in the Langley 0.3-m Transonic Cryogenic Tunnel. AIAA Paper 84-2151.

- [80] Gumbert, C. R.; Newman, P. A.; Kemp, W. B., Jr.; and Adcock, J. B. 1984: Adaptation of a Four-Wall Interference Assessment/Correction Procedure for Airfoil Tests in the 0.3-m TCT, pp. 393-414 in Newman and Barnwell (1984).
- [81] Gumbert, C.R.; Green, L.L.; and Newman, P.A. 1989: Nonlinear Transonic Wall- Interference Assessment / Correction (WIAC) Procedures and Application to CAST 10 Airfoil Results from the 0.3-m TCT 8- x 24-inch Slotted Wall Test Section. NASA CP 3052, pp 9-35.
- [82] Harris, C. D.; Harvey, W. D.; Brooks, C. W., Jr. 1988: The NASA Langley Laminar-Flow Control Experiment on a Swept, Supercritical Airfoil. NASA TP 2809.
- [83] He, J.J., editor 1991: Proceedings of International Conference on Adaptive Wall Wind Tunnel Research and Wall Interference Correction ICAW. June 10-14,1991, Chinese Aeronautical and Astronautics Establishment, Northwestern Polytechnical University, Xian, China.
- [84] Hinson, B.L.; and Burdges, K.P., 1980: Acquisition and Application of Transonic Wing and Far Field Test Data for Three-Dimensional Computational Method Evaluation," AFOSR Report 80-0421.
- [85] Hornung, H.; and Stanewsky, E., editors 1984: Adaptive Wall Wind Tunnels and Wall Interference Correction Methods. Oct. 15-17, 1984, DFVLR-IB-222-84-A-37.
- [86] Hornung, H.G., editor 1990: Adaptive Wind Tunnel Walls - Technology and Applications. Report of the Fluid Dynamics Panel Working Group 12, AGARD-AR-269.
- [87] Inger, G.R. 1967: Laminar Boundary-Layer Solutions with Strong Blowing. AIAA J., 5 9, Sept., pp. 1677-1679.
- [88] Jacocks, J.L. 1977: Aerodynamic Characteristics of Perforated Walls for Transonic Wind Tunnels. AEDC-TR-77-61.
- [89] Jones, R.T., 1946: Properties of Low-Aspect Ratio Pointed Wings at Speeds Below and Above the Speed of Sound. NACA Report 835.
- [90] Kacprzynski, J.J. 1975: Transonic Flow Field Past 2-D Airfoils Between Porous Wind Tunnel Walls With Nonlinear Characteristics. AIAA Paper 75-81.
- [91] Karlsson, K.R.; and Sedin, Y.C.-J. 1979: Axisymmetric Calculations of Transonic Wind Tunnel Interference in Slotted Test Sections. AIAA J. Vol. 17, No. 8, pp. 917-919.
- [92] Karlsson, K.R.; and Sedin, Y.C.-J. 1980: Numerical Design and Analysis of Optimal Slot Shapes for Transonic Test Sections - Axisymmetric Flows. AIAA Paper 80-0155, Jan.
- [93] Keller, James D. 1972: Numerical Calculation of Boundary-Induced Interference in Slotted or Perforated Wind Tunnels Including Viscous Effects in Slots. NASA TN D-6871.
- [94] Keller, James D.; and Wright, Ray, H. 1971: A Numerical Method of Calculating the Boundary-Induced Interference in Slotted or Perforated Wind Tunnels of Rectangular Cross Section. NASA TR R-379.
- [95] Kemp W.B., Jr 190: User's Guide to PANCOR: A Panel Method Program for Interference Assessment in Slotted-Wall Wind Tunnels. NASA CR-187479.
- [96] Kemp W.B., Jr 1986a: Computer Simulation of a Wind Tunnel Test Section with Discrete Finite-Length Wall Slots. NASA CR-3948.
- [97] Kemp W.B., Jr 1986b: User's Guide to STIPPAN: A Panel Method Program for Slotted Tunnel Interference Prediction. NASA CR-178003.
- [98] Kemp W.B., Jr 1988: A Panel Method Procedure for Interference Assessment in Slotted-Wall Wind Tunnels. AIAA Paper 88-2537.
- [99] Kemp, W. B. 1978: Transonic Assessment of Two-Dimensional Wind Tunnel Wall Interference Using Measured Wall Pressures. NASA CP-2045, pp. 473-486.

- [100] Kemp, W. B., Jr. 1980: TWINTAN: A Program for Transonic Wall Interference Assessment in Two-Dimensional Wind Tunnels. NASA TM-81819.
- [101] Kemp, W. B., Jr. 1984: TWINTN4: A Program for Transonic Four-Wall Interference Assessment in Two-Dimensional Wind Tunnels. NASA CR-3777.
- [102] Kemp, W. B., Jr.; and Adcock, J. B. 1983: Combined Four-Wall Interference Assessment in Two-Dimensional Airfoil Tests. AIAA J., Vol. 21, pp. 1353-1359, also AIAA Paper 82-0586.
- [103] Kemp, W.B., Jr 1985: A Slotted Test Section Numerical Model for Interference Assessment. J. Aircraft, Vol. 22, No. 3, pp. 216-222 also AIAA Paper 84-0627
- [104] Kemp, W.B., Jr. 1976: Toward the Correctable-Interference Transonic Wind Tunnel. Proceedings, AIAA Ninth Aerodynamic Testing Conference, June, pp. 31-38.
- [105] Kevorkian, J.; and Cole, J., 1980: Perturbation Methods in Applied Mathematics. Springer-Verlag, New York.
- [106] Kordulla, Wilhelm (Ed.) 1988: Numerical Simulation of the Transonic DFVLR-F5 Wing Experiment. Volume 22, Notes on Numerical Fluid Mechanics, Vieweg Verlag, Braunschweig.
- [107] Kraft, E.M. 1983: An Overview of Approaches and Issues for Wall Interference Assessment/Correction. NASA CP-2319, Jan.
- [108] Kraft, E.M.; and, Lo, C.F. 1973: A General Solution for Lift Interference in Rectangular Ventilated Wind Tunnels. AIAA Paper No. 73-209 presented at the 11th Aerospace Sciences Meeting, Washington, DC.
- [109] Kraft, E.M.; Ritter, A.; and Laster, M. 1986: Advances at AEDC in Treating Transonic Wind Tunnel Wall Interference. ICAS Paper 86-1.6.1.
- [110] Kraft, E.M.; Ritter, A.; and Laster, M.L.: Advances at AEDC in Treating Transonic Wind Tunnel Wall Interference. Proceedings, 15th Congress of the International Council of the Aeronautical Sciences, London, UK, September 1986, pp. 748-769.
- [111] Kuenstner, Rudi; Deutenbach, Klaus-Rainer; and, Vagt Jorg-Dieter 1992: Measurement of Reference Dynamic Pressure in Open-Jet Automotive Wind Tunnels. SAE Paper 920233.
- [112] Ladson, Charles L. 1973: Description and Calibration of the Langley 6- by 19-Inch Transonic Tunnel. NASA TN D-7182.
- [113] Laster, M. L., editor 1988: Boundary Layer Simulation and Control in Wind Tunnels. Report of the Fluid Dynamics Panel Working Group 09, AGARD-AR-224.
- [114] Lee, K.D. 1980: Numerical Simulation of the Wind Tunnel Environment by a Panel Method. AIAA Paper 80-0419.
- [115] Lifshitz, Y.B.; and Fonarev, A.S., 1978: Effect of Flow Boundaries on Parameters of Transonic Flows Around Bodies of Revolution. Fluid Dynamics, Vol. 13, pp. 393-399.
- [116] Lockman, William K.; and Seegmiller, H. Lee 1983: Experimental Investigation of the Subcritical and Supercritical Flow About a Swept Semispan Wing. NASA TM 84367.
- [117] Lynch, F.T.; Crites, R.C.; and Spaid, F.W. 1993: The Crucial Role of Wall Interference, Support Interference, and Flow Field Measurements in the Development of Advanced Aircraft Configurations. pp. 1-1 to 1-38 in AGARD CP 535.
- [118] Malmuth, N.; and Cole, J. 1996: Asymptotic Theory of Slender Configurations in and Out of Wind Tunnels. AIAA Paper 96-2119 at the AIAA Theoretical Fluid Dynamics Meeting, June 17-20, New Orleans, LA.
- [119] Malmuth, N.D. 1987: An Asymptotic Theory of Wind Tunnel Wall Interference on Subsonic Slender Bodies. J. Fluid Mechanics, Vol. 177, 1987, pp. 19-35.

- [120] Malmuth, N.D. 1993: Some Applications of Combined Asymptotics and Numerics in Fluid Dynamics and Aerodynamics. Chapter in *Frontiers in Applied Mathematics* SIAM. And *Numerical Methods for Partial Differential Equations with Critical Parameters*, AGARD. Kluwer Press, H.G. Kaper and M. Garbey, ed., Dordrecht, Holland, pp. 53-79.
- [121] Malmuth, N.D., 1991a: Asymptotic Methods for Prediction of Transonic Wind Tunnel Wall Interference. International Conference on Adaptive Wall Wind Tunnel Research and Wall Interference Correction, Xian, Shaanxi, China, June 10-14.
- [122] Malmuth, N.D.; and Cole, J.D. 1984. Study of Asymptotic Theory of Transonic Wind Tunnel Interference. Final Report for Period May 30, 1982, through August 30, 1983, Contract No. F40600-82-C-0005, Arnold Engineering Development Center/DOS Report AEDC-TR-84-8, Tullahoma, Tennessee.
- [123] Malmuth, N.D.; Jafroudi, H.; Wu, C.; Mclachlan, R.; and Cole, J. 1993: Asymptotic Methods Applied to Transonic Wall Interference. *AIAA J.* 31 5, pp. 911-918.
- [124] Malmuth, N.D.; Neyland, V.M.; and Neyland, V. Ya. 1995: Wall Interference Over Small and Large Aspect Ratio Wings in Wind Tunnels. Second Pacific International Meeting in Aerospace Technology PICAST2-AAC6, in proceedings, Melbourne, Australia.
- [125] Malmuth, N.D.; Wu C.C.; Jafroudi, H.; Mclachlan, R.; Cole, J.D.; and Sahu, R., 1991b: Asymptotic Theory of Wind Tunnel Wall Interference. AEDC Final Report for Contract F40600-84-C-0010, AEDC-TR-91-24.
- [126] Martin, F.W., Jr.; Sickles, W. L.; and Stanley, S. A. 1993: Transonic Wind Tunnel Wall Interference Analysis for the Space Shuttle Launch Vehicle. AIAA Paper No. 93-0420, presented at the AIAA 31st Aerospace Sciences .
- [127] Matyk, Gerald E.; and Kobayashi, Yasunori 1977: An Experimental Investigation of Boundary Layer and Crossflow Characteristics of the Ames 2- by 2-Foot and 11- by 11-Foot Transonic Wind-Tunnel Walls. NASA TM 73257.
- [128] Mercer, J. E.; Geller, E.W.; Johnson, M.L.; and Jameson, A. 1980: A Computer Code to Model Swept Wings in an Adaptive Wall Transonic Wind Tunnel. AIAA Paper 80-0156.
- [129] Mercer, J.E.; and Murman, E.M. 1980: Application of Transonic Potential Calculations to Aircraft and Wind Tunnel Configurations. Presented at AGARD Fluid Dynamics Panel Symposium on Subsonic/Transonic Configuration Aerodynamics. AGARD-CP-285, May 5-7.
- [130] Milholen, W.E.; and Chokani, N. 1992: Numerical Modelling of Transonic Juncture Flow. AIAA Paper 92-4036.
- [131] Mohan, S.R.; and Freestone, M.M. 1994: Interference Determination for Three-Dimensional Flows in Slotted-Liner Wind Tunnels. ICAS paper no. 94-3.3.1 presented at the 19th ICAS Congress, Anaheim, CA.
- [132] Mohan, S.R.; Lock, R.C.; and, Freestone, M.M. 1991: Experimental and Theoretical Investigations of Wall Interference in Slotted Test Sections. Proceedings—International Conference on Adaptive Wall Wind Tunnel Research and Wall Interference Correction, Xian, People's Republic of China, pp. W10-1 to W10-13.
- [133] Mokry, M., Chan, Y.Y. and Jones, D.V. 1983: Two-Dimensional Wind Tunnel Wall Interference. AGARDograph 281, edited by L.H. Ohman, Nat. Aeronautical Establishment, Nat. Res. Council, Canada, November.
- [134] Murman, E.M.; Bailey, F.R.; and Johnson, M.L. 1975: TSFOIL - A Computer Code for Two-Dimensional Transonic Calculations, Including Wind-Tunnel Wall Effects and Wave-Drag Evaluation. NASA SP-347, Part II, pp. 769-788.
- [135] Murman, M. 1972: Computational of Wall Effects in Ventilated Transonic Wind Tunnels. AIAA Paper 72-1007.

- [136] Murman, M.; and Cole, J. D. 1971: Calculation of Plane Steady Transonic Flows. AIAA J., vol. 9, no. 1, pp. 114-121.
- [137] Murthy, A.V. 1986: Effect of Aspect Ratio on Sidewall Boundary Layer Influence in Two-Dimensional Airfoil Testing. NASA CR-4088.
- [138] Newman P.A.; Mineck, R.E.; Barnwell, R.W.; and Kemp, W.B., Jr. 1986: Wind Tunnel Wall Interference. Langley Symposium on Aerodynamics, Vol. I, NASA CP-2397, pp. 225-260.
- [139] Newman, P.A.; and Barnwell, R.W., editors 1984: Wind Tunnel Wall Interference Assessment/Correction - 1983. NASA Langley Research Center, Jan. 25-26, 1983, NASA CP-2319.
- [140] Newman, P.A.; and Klunker, E.B. 1975: Numerical Modelling of Tunnel-Wall and Body-Shape Effects on Transonic Flow over Finite Lifting Wings. NASA SP-347, Part II, pp. 1189-1212.
- [141] Newman, P.A.; Anderson, E.C.; Peterson, J.B., Jr. 1984: Aerodynamic Design of the Contoured Wind-Tunnel Liner for the NASA Supercritical Laminar-Flow Control, Swept-Wing Experiment. NASA TP 2335.
- [142] Newman, P.A.; Kemp, W.B., Jr; and Garriz, J.A. 1988: Emerging Technology for Transonic Wind-Tunnel Wall Interference Assessment and Corrections. SAE Technical Paper No. 881454.
- [143] Newman, P.A.; Kemp, W.B.; and Garriz, J.A. 1989: Wall Interference Assessment and Corrections. NASA CP-3020, Vol. 1, Part 2, pp. 817-851.
- [144] Neyland, V.M.; and Neyland V. Ya. 1994: Special Features of Transonic Flows Over Models RI-1 and RI-2 in a Wind Tunnel and Infinite Flow. Final Report for Rockwell Science Center, Contract B4563029.
- [145] Obayashi, S.; and Kuwahara, K. 1987: Navier-Stokes Simulation of Side Wall Effect of Two-Dimensional Transonic Wind Tunnel. AIAA Paper 87-37.
- [146] Osborne, J. 1973: A Selection of Measured Transonic Flow Pressure Distributions for the NACA 0012 Aerofoil: Provisional Data From Our NPL Transonic Tunnel. Received at the NASA Langley Library, Aug. 29.
- [147] Oswatitsch, K.; and Kuene, F. 1955: Ein Aquivalenzsatz für Nichtangestellte Flüge Kleiner Spannweite in Schallnaher Strömung. Zeitschrift für Flugwissenschaften, Vol. 3, No. 2, S. 29-46.
- [148] Percy, H.H.; Sinnott, C.S.; and, Osborne, J. 1959: Some Effects of Wind Tunnel Interference Observed in Tests on Two-Dimensional Aerofoils at High Subsonic And Transonic Speeds. AGARD Rep. 296.
- [149] Phillips, Pamela S.; and Waggoner, Edgar G. 1988: A Transonic Wind Tunnel Wall Interference Prediction Code. AIAA Paper 88-2538 presented at the 6th Applied Aerodynamics Conference, Williamsburg, VA.
- [150] Phillips, Pamela S.; and Waggoner, Edgar G. 1990: Transonic Wind-Tunnel Wall Interference Prediction Code. AIAA J. Aircraft, Vol. 27, No. 11, pp. 915-916.
- [151] Pindzola, M.; and, Lo, C.F. 1969: Boundary Interference at Subsonic Speeds in Wind Tunnels with Ventilated Walls. AEDC TR-69-47.
- [152] Pope, A. 1954: Wind-Tunnel Testing. Wiley & Sons, pp. 268-344.
- [153] Radespiel, R. 1989: Calculation of Wind Tunnel Sidewall Interference Using a Three Dimensional Multigrid Navier-Stokes Code. AIAA Paper 89-1790.
- [154] Ramaswamy, M.A.; and, Cornette, E.S. 1982: Supersonic Flow Development in Slotted Wind Tunnels. AIAA J., Vol. 20, No. 6, pp. 805-811.
- [155] Rizk, M. H. 1986: Improvements in Code TUNCOR for Calculating Wall Interference Corrections in the Transonic Regime. AEDC-TR-86-6.

- [156] Rizk, M. H.; and Smithmeyer, M. G. 1982: Wind Tunnel Wall Interference Corrections for Three-Dimensional Flows. *J. of Aircraft*, Vol. 19, pp. 465-472.
- [157] Rizk, M. H.; Hafez, M.; Murman, E. M.; and Lovell, D. 1982: Transonic Wind Tunnel Wall Interference Corrections for Three-Dimensional Models. AIAA Paper 82-0588.
- [158] Rizk, M. H.; Smithmeyer, M. G.; and Murman, E. M. 1984: Wind Tunnel Wall Interference Corrections for Aircraft Models, pp. 301-322 in Newman & Barnwell (1984).
- [159] Rizk, M.H.; and Murman, E.M. 1984: Wind Tunnel Wall Interference Corrections for Aircraft Models in the Transonic Regime. *AIAA J. of Aircraft*, Vol. 21, No. 1, Jan., pp. 54-61
- [160] Rueger, M.; and Crites, R. 1992: Wind Tunnel Boundary Interference Prediction and Correction. AIAA 92-0036.
- [161] Rueger, M.L.; Crites, R.C.; Weirich, R.F.; Creasman, F.; Agarwal, R.K.; and Deese, J.E. 1993: Transonic Wind Tunnel Boundary Interference Correction. Wall Interference, Support Interference and Flow Field Measurements, AGARD CP-535, pp. 21-1 to 21-14.
- [162] Sears, W. R. 1974: Self Correcting Wind Tunnels. *The Aeronautical Journal*, Vol. 78, No. 758/759, pp. 80-89.
- [163] Sedin, Y.C.-J.; Agrell, N.; and, Zhang, N. 1985: Computation of Transonic Wall-Interference in Slotted-Wall Test Sections of Wind Tunnels. Paper presented at the International Symposium on Computational Fluid Dynamics Tokyo, Japan.
- [164] Sedin, Y.C.-J.; and, Karlsson, K.R. 1982: Some Theoretical Wall-Interference Calculations in Slotted Transonic Test-Sections, Three-Dimensional Flows. Proceedings of the 13th Congress of the International Council of the Aeronautical Sciences/AIAA Aircraft Systems and Technology Conference. ICAS Paper No. 82-6.3.2.
- [165] Sedin, Y.C.-J.; and, Karlsson, K.R. 1986: Computed and Measured Wall Interference in a Slotted Transonic Test Section. *AIAA J.*, Vol. 24, No. 3, pp. 444-450.
- [166] Sewall, W.G. 1982: The Effects of Sidewall Boundary Layer in Two-Dimensional Subsonic and Transonic Wind Tunnels. *AIAA J.* vol 20, no 9, pp 1253-1256.
- [167] Sickles, W.L.; and Erickson, J.C., Jr. 1988: Evaluation of Wall Interference Assessment and Correction Techniques. AEDC-TR-87-45 AD-A195873, June.
- [168] Sickles, W.L.; and Erickson, J.C., Jr. 1990: Wall Interference Correction for Three-Dimensional Transonic Flows. AIAA Paper No. 90-1408, presented at the AIAA 16th Aerodynamics Ground Testing Conference, Seattle, WA, June 18-20.
- [169] Sickles, W.L.; and Sinclair, D.W. 1998: Transonic Wind Tunnel Data Correlation on the Transonic Technology Wing Demonstrator TST in AEDC Tunnel 4T, 16T and the NASA National Transonic Facility NTF. To be published as an AEDC technical report.
- [170] Sickles, W.L.; and Steinle, Frank W., Jr. 1996: NWTC Slotted Wall Design Effort: Computational Task. Letter report dated May 21 to National Wind Tunnel Program Office Distribution, NASA/LeRC.
- [171] Small, R.D. 1978: Studies in Transonic Flow VI, Calculation of a Transonic Lifting Line Theory. UCLA Report UCLA-ENG-7836,
- [172] South, J.C., Jr.; and Keller, J.D. 1975: Axisymmetric Transonic Flow Including Wind-Tunnel Wall Effects. NASA SP-347, Part II, pp. 1233-1268.
- [173] Stanewsky, E. and Thibert, J.A. 1979; Airfoil SKF 1.1 with Maneuver Flap. AGARD Report No. AR-138, Experimental Database for Computer Program Assessment. May.
- [174] Steinle, F. W. Jr. 1991: Unpublished Work, Feb..
- [175] Steinle, Frank W., Jr. 1996: Personal communication.

- [176] Steinle, Frank W., Jr.; and Pejack, Edwin R. 1980: Toward an Improved Transonic Wind-Tunnel-Wall Geometry — A Numerical Study. AIAA Paper 80-0442 presented at the 11th Aerodynamic Testing Conference, Colorado Springs, Co.
- [177] Swanson, R. C.; Radespiel, R.; and McCormick, V.E. 1989: Comparison of Two- and Three-Dimensional Navier-Stokes Solutions With NASA Experimental Data for CAST 10 Airfoil. NASA CP-3052, pp. 238-258.
- [178] Tuttle, M.H.; and Cole, K.L. 1988: Wind Tunnel Wall Interference Jan. 1980-May 1988 — A Selected, Annotated Bibliography. NASA TM-4061.
- [179] Vandromme, D.; and Haminh, H. 1988: Turbulence Modelling for Compressible Flows, pp 139-158 in Kordulla (1988).
- [180] Vatsa, V.N.; and Wedan, B. W. 1988: Navier-Stokes Solutions for Transonic Flow over a Wing Mounted in a Tunnel. AIAA Paper 88-1002.
- [181] Wang, K.C. 1968: A New Approach to Not-So-Slender-Wing Theory. Studies in Applied Math, Vol. 4, pp. 391-406.
- [182] Whitfield, D.L. 1976: Analytical, Numerical, and Experimental Results on Turbulent Boundary Layers. AEDC-TR-76-62 AD-A027588, July.
- [183] Whoric, J.M.; and Hobbs, R.W. 1987: Hierarchy of Uncertainty Sources in Transonic Wind Tunnel Testing. AGARD-CP-429, September-October.
- [184] Wilcox, D.C. 1993: Turbulence Modelling for CFD. DCW Industries, Inc., La Canada, CA
- [185] Wood, W.W. 1964: Tunnel Interference from Slotted Walls. The Quarterly Journal of Mechanics and Applied Mathematics, Vol. 17, pp. 125-140.
- [186] Wu, C.C. 1989: Shock wave location on slender bodies," unpublished E-mail communication to N. Malmuth.
- [187] Wu, J.M.; Collins, F.G.; and, Bhat, M.K. 1982: Three-Dimensional Flow Studies on a Slotted Transonic Wind Tunnel Wall. AIAA Paper 82-0230 presented at 20th Aerospace Sciences Meeting, Orlando, Fl.

6. BLUFF-BODY BLOCKAGE CORRECTIONS IN CLOSED- AND OPEN-TEST-SECTION WIND TUNNELS

AUTHOR : KEVIN COOPER

	PAGE
LIST OF SYMBOLS	6-3
6.1 INTRODUCTION	6-5
6.1.1 HISTORY AND STATUS	6-5
6.1.2 CLOSED AND OPEN TEST SECTIONS	6-6
6.1.3 IMPORTANT TEST SECTION BOUNDARIES	6-6
6.1.4 COMPARISON OF CLOSED AND OPEN TEST SECTIONS	6-6
6.2 METHODS FOR CLOSED TEST SECTIONS	6-8
6.2.1 MASKELL'S ANALYSIS	6-8
6.2.2 COWDREY'S DEVELOPMENT	6-11
6.2.3 HACKETT'S TWO-STEP VERSION OF MASKELL'S ANALYSIS	6-11
6.2.4 COMMENTARY ON MASKELL'S CORRECTION	6-13
6.2.5 WAKE BUOYANCY AND THE WAKE-INDUCED DRAG INCREMENT	6-13
6.2.6 MERCKER'S ANALYSIS	6-14
6.2.7 UPSTREAM AND DOWNSTREAM EFFECTS	6-16
6.3 METHODS FOR OPEN TEST SECTIONS	6-18
6.3.1 RECENT RESULTS FROM AUTOMOTIVE TESTING	6-18
6.3.2 THE PRIMARY EFFECTS	6-18
6.3.2.1 NOZZLE BLOCKAGE	
6.3.2.2 SOLID BLOCKAGE AND JET EXPANSION	
6.3.2.3 EMPTY-TUNNEL PRESSURE GRADIENTS	
6.3.2.4 COLLECTOR EFFECTS	
6.3.2.5 WAKE-INDUCED EFFECTS	
6.3.3 THE METHOD OF MERCKER AND WIEDEMANN	6-23
6.3.3.1 NOZZLE BLOCKAGE	
6.3.3.2 SOLID BLOCKAGE AND JET EXPANSION	
6.3.3.3 EMPTY-TUNNEL PRESSURE GRADIENTS	
6.3.3.4 COLLECTOR EFFECTS	
6.3.3.5 APPLICATION OF THE OPEN-JET CORRECTION FORMULAE	

	PAGE
6.4 APPLICATION TO CLOSED TEST SECTIONS	6-29
6.4.1 AIRCRAFT	6-29
6.4.2 SURFACE VEHICLES	6-29
6.4.3 MISCELLANEOUS	6-30
6.5 APPLICATION TO OPEN TEST SECTIONS	6-30
6.5.1 SURFACE VEHICLES	6-30
6.6 REFERENCES	6-32

LIST OF SYMBOLS

B	Single or duplex tunnel width. For model reflected about the ground plane (duplex), $B = 2H_t$
B_t	tunnel width
C	duplex test-section area, $2C_t$ or $2C_n$
C_c	open tunnel single or duplex collector area
C_t	closed tunnel test section area
C_n	open tunnel test section area
C_{Dc}	blockage-corrected, wind-axis drag coefficient
C_{DcM1}	wind-axis drag coefficient corrected by Maskell's method, eqn. (6.3)
C_{DcM2}	wind-axis drag coefficient corrected by Hackett's two-step version of Maskell, eqn. (6.14)
C_{Di}	induced-drag coefficient
C_{Do}	drag due to skin friction coefficient
C_{Dr}	support rig (strut) drag
C_{Du}	uncorrected, wind-axis drag coefficient
C_{Duo}	uncorrected, wind-axis drag coefficient at zero yaw angle
C_{Dus}	uncorrected, separated-flow drag
$C_{D\infty}$	drag coefficient corrected for blockage only, excluding wake constraint, eqn. (6.13)
$C_{Du,vis}$	viscous component of drag, $(C_{Do} + C_{Dus}) = (C_{Du} - C_{Di})$
C_L	lift coefficient
C_Y	side force coefficient
C_{pbc}	corrected base pressure coefficient
C_{pbu}	uncorrected base pressure coefficient
F	duplex model projected frontal area, $2(S_m \cos \psi + S_Y \sin \psi)$, eqn. (6.19)
H	single or duplex tunnel height. For model reflected about the ground plane (duplex), $H = B_t$
H_t	tunnel height
K	empirical solid blockage constant for automobiles determined by Mercker, 1.0
L_m	model length
L_p	projected length of model, $L_m \cos \psi + w_m \sin \psi $
L_{ts}	test section length
m	Cowdrey's empirical blockage constant, eqn. (6.7)
m'	Cowdrey's empirical blockage constant, eqn. (6.9)
Q_s	source strength used in an open-jet tunnel to calculate nozzle interference due to a model
r	radial co-ordinate
R_c	hydraulic diameter of single or duplex open tunnel collector
R_n	hydraulic diameter of single or duplex open tunnel nozzle
S	single or duplex model frontal area, as appropriate
S_m	model frontal area
S_Y	model side area
S_b	model base area (area of separated-flow area on base)
T	blockage constant = $\tau\sqrt{\pi}/2 = 0.36(B/H+H/B)$
U_o	measured, upstream reference velocity not influenced by blockage

U_c	blockage-corrected reference velocity
U_m	measured, upstream reference velocity influenced by blockage
U_n	open-jet reference velocity measured using a nozzle reference static pressure
\bar{U}_n	average velocity over the nozzle exit plane of an open-jet tunnel with a model present
U_p	open-jet reference velocity measured using a plenum chamber reference static pressure
U_{wa}	velocity including attached-flow wake blockage
U_{wc}	velocity including collector-plane wake blockage
U_{ws}	velocity including separated-flow wake blockage
$U_x(x,r)$	total velocity due to point source at location (x,r)
$u_x(x,r)$	incremental velocity due to source at (x,r)
V	single or duplex model volume, as appropriate
V_m	model volume
V_e	effective model volume, $1.75V_m$
V_t	variable portion of test section volume, $L_p C$
w_m	model width
x	longitudinal position, positive downstream from reference point
ΔC_D	incremental drag, $(C_{Du} - C_{Dc})$
ΔC_{DM}	drag increment due to separated-flow wake constraint
ΔC_{DHB}	buoyancy drag increment due to empty tunnel longitudinal pressure gradient
ΔC_{Dwb}	buoyancy drag increment due to wake constraint
ΔC_{Dwi}	drag increment due to the wake constraint
ΔU_{wa}	velocity increment due to attached-flow wake blockage, $(U_{wa} - U_o)$
ΔU_{ws}	velocity increment due to separated-flow wake blockage, $(U_{ws} - U_o)$
ϵ	total blockage factor at the model location, $(U_c - U_o)/U_o$
ϵ_c	collector blockage factor at the model location
ϵ_d	attenuated blockage factor downstream of model centre, eqn. (6.22)
ϵ_n	nozzle blockage factor at the model location
ϵ_{qn}	nozzle blockage factor at the nozzle plane
ϵ_p	plenum blockage factor at the model location
ϵ_{qp}	plenum blockage factor at the nozzle plane
ϵ_s	solid blockage factor at the model location, $(U_s - U_o)/U_o$
ϵ_u	attenuated blockage factor upstream of model centre, eqn. (6.21)
ϵ_w	wake blockage factor at the model location, $(U_w - U_o)/U_o$
ϵ_{wc}	wake-blockage factor at the collector plane, $(U_{wc} - U_o)/U_o$
ϵ_{wa}	attached-flow, wake blockage factor at the model location, $(U_{wa} - U_o)/U_o$
ϵ_{ws}	separated-flow, wake blockage factor at the model location, $(U_{ws} - U_o)/U_o$
η	Mercker's empirical wake blockage constant, 0.41; eqn. (6.19)
θ	Maskell's separated-flow wake-blockage constant
τ	solid blockage constant, $= 2T/\sqrt{\pi} = 0.41(B/H + H/B)$
ψ	yaw angle

6.1 INTRODUCTION

6.1.1 HISTORY AND STATUS

The effects of the constraints imposed by wind tunnel test section boundaries on the flows around bluff bodies - those bodies having leading-edge separation without re-attachment or having large regions of separated flow further aft on the body - are even now not fully understood. The physics of the interaction of the boundaries of a wind tunnel test section on these wake flows was explored by Maskell [1, 2], based on an analysis of measurements made on three-dimensional flat plates mounted normal to the flow. His results demonstrated that the wall constraint in closed test sections was five times greater than predicted by the classical derivations for bodies with thin wakes. It was clear that large separated flows from stalled wings and bluff bodies must be treated differently than the attached-flow cases.

The impetus for Maskell's development was the need to understand the differences between measurements made on slender delta wings in different wind tunnels. Using normal-flat-plate measurements to develop the flow physics, Maskell was able to generalise these results to the separated-wing case. His derivation was predicated on the principle that the pressure distribution was invariant under constraint, meaning that the pressure field was only scaled by a constant speed increase in the presence of the constraining solid test section walls.

Since this first development for wing flows, the families of separated-flow shapes that have come under common study in the wind tunnel have increased. In particular, the sciences of wind engineering and surface vehicle aerodynamics have advanced rapidly. The aerodynamic loading and stability of bridges and tall buildings is a governing factor in their design while the efficient aerodynamic development of surface vehicles is of major importance in the areas of energy conservation, handling and noise. It is now standard practice to use wind tunnel studies to demonstrate the stability of long-span, cable-supported bridges, to measure the mean and unsteady loads on tall buildings, and to measure and improve the aerodynamic characteristics of surface vehicles. In the latter case, large wind tunnels of open and closed test sections are used routinely for full-scale road vehicle development. An obvious benefit of the availability of proven blockage-correction methods is the ability to minimise the size of the full-scale facility. Another reason for needing an accurate test speed correction method is to provide accurate speed setting during measurement of the sound pressure levels of road vehicles, which vary with the fourth to the sixth power of velocity. This point is particularly pertinent at the time of writing, when approximately one-half of all full-scale passenger car wind tunnel testing is utilised for wind-noise assessment and improvement.

In recent years, the major developments in wall corrections for bluff shapes have come through the development of boundary-measurement-based methods. Here, the mathematical models that are used to represent the bodies in the test section are sufficiently general to extend to both bluff and streamlined shapes. These methods are demanding of instrumentation and computing time. In many cases, the methods are not available or are too demanding for routine use, so there remains a continuing need for simple, analytically-based approximations to the bluff-body blockage effect.

6.1.2 CLOSED AND OPEN TEST SECTIONS

Both closed and open test sections are commonly used for studies of all the geometries mentioned above. In general, the closed-wall test section predominates in North America and the United Kingdom for automotive and bluff-body testing, while open-jet test sections are prevalent in Europe. The closed test section requires a larger correction, but has the benefit of precisely defined boundaries and a long test section. The open test section has a solid blockage effect of opposite sign to, and of smaller magnitude than, that of the closed test section. There is no velocity increment at the model due to the constrained wake for the open test section although there is a wake effect that changes the drag.

It has been recognised [3] that additional interference effects may occur on a bluff body in the short test section typical of open tunnels. These effects are not accounted for in the classical theories. The physics of corrections in closed test sections are the better developed because the need was evident - the corrections were known to be large, especially for bluff shapes. The development of open-test-section corrections has lagged, in part because they were small, or thought to be small. However, this assumption has been shown to be incorrect for bluff automotive shapes and has led to increased activity in the European automotive wind tunnels to understand the effects and to derive appropriate corrections for them [4].

6.1.3 IMPORTANT TEST SECTION BOUNDARIES

In the classical aeronautical derivations discussed in the earlier chapters, the important test section boundaries were the lateral boundaries - the side walls, floor and ceiling of the closed tunnel or the free-jet shear layer of the open tunnel. When a body under study has a large separated wake, the proximity of the end of the test section to the base of the model has an effect that reduces the measured drag. Further, high-drag bluff bodies have larger upstream flow-displacement effects in the test section than streamlined bodies have. These effects can interact with the pressure taps used to measure the static reference pressure at the entrance to the test section in open and closed tunnels, and can distort the flow leaving the nozzle of an open tunnel.

6.1.4 COMPARISON OF CLOSED AND OPEN TEST SECTIONS

As an introduction to the relative distortions produced in the two major test-section types, it is useful to compare the influences of solid-wall and free-jet boundaries on measurements on simple bluff bodies.

A typical comparison is presented in Figures 6.1 and 6.2, utilising data [5, 6, 7, 8] measured for normal flat plates and for various rectangular blocks, both wall-mounted and centrally-mounted in the test section. Figure 6.1 shows typical drag coefficient variations with model size and type. As expected, the closed test sections show a drag increase with model area while the open test sections show a drag reduction. The blockage effect in the open test section is less than in the closed test section, but the difference between open and closed is not as large as would be found for streamlined models. The slopes of the drag-blockage curves in the closed test sections are greater for the model families having higher drag. The drag data for the block model in the closed tunnel fall into a family of nearly parallel curves with yaw angle as the parameter, as seen in Figure 6.1.

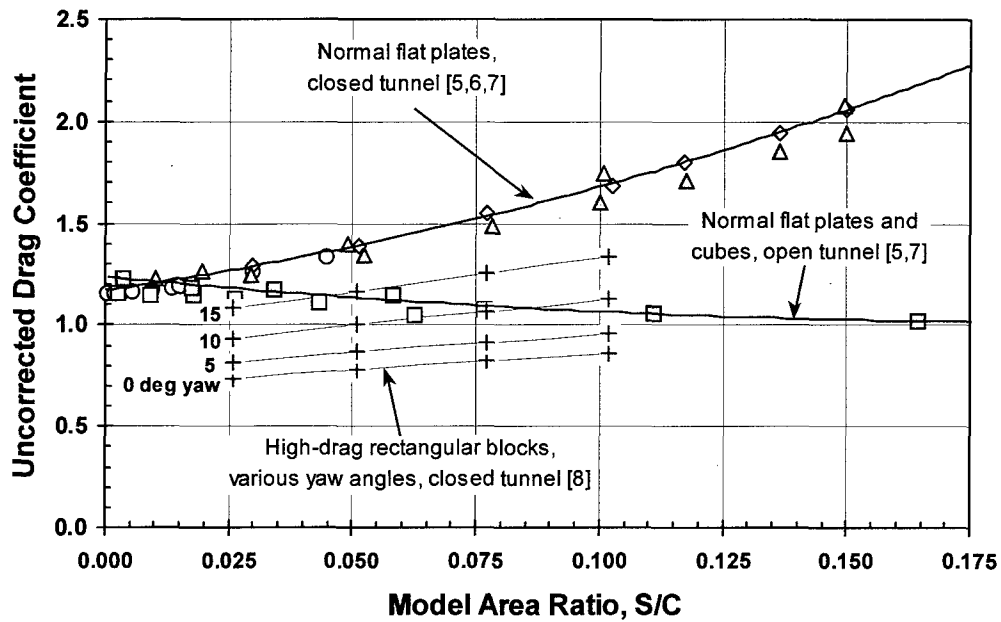


Fig. 6.1: Bluff-Body Blockage Effects on Measured Drag in Closed and Open Test Sections [5, 6, 7, 8]

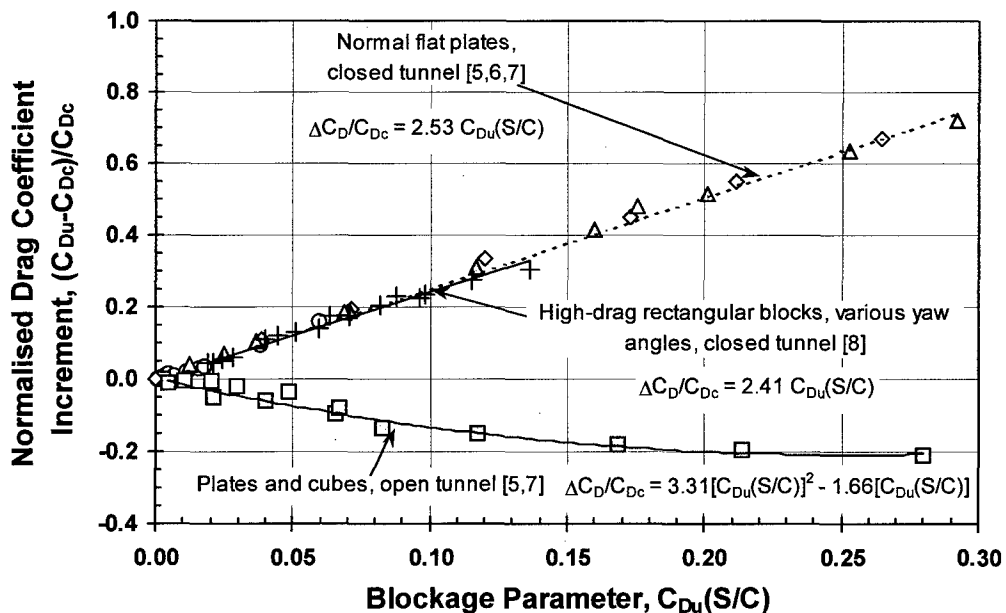


Fig. 6.2: Collapse of Normalised Drag Increments Due to Blockage in Closed and Open Test Sections [5, 6, 7, 8]

Figure 6.2 re-plots the data from Figure 6.1, presenting the normalised incremental drag change due to blockage, $(\Delta C_D / C_{Dc}) = (C_{Du} - C_{Dc}) / C_{Dc}$, as a function of the drag in the test section, given by the blockage parameter $C_{Du}(S/C)$. The corrected flat plate drag coefficients were determined by fitting the measured data with least squares, second-order polynomials. The rectangular block data were fitted with second-order polynomials having zero slopes at the origin. The data are now grouped primarily by wind tunnel test section type, with little difference due to model type. The dependence on yaw angle of the data for the block model in the closed test section has disappeared. The blockage effect on the plates in

the open test section, in the linear region at smaller blockage, is about 65% of that in the closed test section. It would appear that the boundary effects in the open test section are significantly larger than would be predicted from classical aerodynamic theory. The expression "boundary effects", rather than "blockage effects" was purposefully chosen because the observed drag distortion is strongly influenced by the finite length of the free jet.

6.2 METHODS FOR CLOSED TEST SECTIONS

The early classical boundary-correction theories were small-disturbance analyses. These theories assumed that the models were small in the test section, that the drag coefficients were small and primarily due to skin friction, that wakes were thin and that no flow separations existed. Growing requirements for bluff-body testing necessitated an extension of the classical theories to cater for these cases, examples of which were the stalled wing and the defining case, the flat plate normal to the flow. A summary of blockage corrections for bluff bodies can be found in [9].

6.2.1 MASKELL'S ANALYSIS

The founding approach to the estimation of the wake blockage of bluff models in closed test sections was that of Maskell [1]. He applied conservation of momentum and physical arguments supported by wind tunnel measurements on normal flat plates [10] to formulate a theory for the wake blockage produced by separated flows. The assumptions made by Maskell were:

1. that the pressure distribution was invariant under wall constraint,
2. that separated flows from three-dimensional bodies tended to become axially symmetric far downstream,
3. that the base pressure was constant over the separated region and was equal to the static pressure on the wake boundary,

After application of these assumptions, momentum theory led to a dynamic pressure correction of the form,

$$\left(\frac{q_c}{q_u} \right) = \left(\frac{C_{Du}}{C_{D\infty}} \right) = 1 + \theta C_{D\infty} (S/C) \quad (6.1)$$

where:

$$\theta = -1/C_{pbc} \quad (6.2)$$

C_{pbc} is the corrected base pressure coefficient and $C_{D\infty}$ is the drag coefficient corrected for blockage but not corrected for wake distortion due to the test section walls. Equation (6.1), requires iteration since the magnitude of the correction depends on the corrected drag coefficient. Maskell made a fourth assumption to include the effect of the walls on the shape of the wake boundary. He assumed

4. that the constraining effect of the test section walls reduced the expansion of the wake and that this reduction was in proportion to the contraction of the external stream around the wake.

The final form of the separated-flow component of the wake-blockage correction equation then became,

$$\left(\frac{q_c}{q_u}\right) = \left(\frac{C_{Du}}{C_{DcM1}}\right) = 1 + \theta C_{Du}(S/C) \quad (6.3)$$

Equation (6.3) contains the full blockage/wake-constraint correction and can be solved directly. The blockage constant remained as before, with $C_{D\infty}$ in the right hand side now replaced by the uncorrected, wind-axis drag coefficient, C_{Du} , increasing the correction magnitude. The correction is due to the separated-flow component of drag that, in the case of a normal flat plate, is almost the total drag. For other geometries, this may not be the case, and the separated drag component must be estimated for use in equation (6.3). The remaining drag components are treated in the standard fashion. The fully corrected drag coefficient, containing both flow speed increase and drag change due to wake constraint, is denoted by C_{DcM1} . The subscript 1 indicates a single-step correction and separates Maskell's original version from a later, two-step interpretation that will be presented in Section 6.2.3.

When the wake-blockage correction is applied to bodies that have drag contributions from other sources than flow separation, then the drag components must be estimated so that Maskell's correction can be applied only to the drag resulting from flow separation. Induced drag and skin friction are excluded. When the wake-blockage correction is to be applied to an aircraft model, for example, it is done as follows,

$$\begin{aligned} \left(\frac{q_c}{q_u}\right) &= [1 + 2\varepsilon_{wa} + 2\varepsilon_{ws}] \\ &= \left[1 + \left(\frac{1}{2}\right)\left(\frac{S}{C}\right)(C_{Dr} + C_{Do}) + \theta\left(\frac{S}{C}\right)(C_{Du} - C_{Di} - C_{Do})\right] \end{aligned} \quad (6.4)$$

$\varepsilon_{wa} = (U_{wa} - U_o)/U_o = \Delta U_{wa}/U_o$ is the blockage factor due to the thin, attached-flow wake (classical component) and $\varepsilon_{ws} = \Delta U_{ws}/U_o$ is the velocity increment due to the separated wake (Maskell component). U_o is the upstream reference velocity measurement that is assumed to be unaffected by blockage, C_{Dr} is the support rig drag, C_{Do} is the drag due to skin friction, C_{Du} is the total drag coefficient, and C_{Di} is the induced drag. The last term in parentheses of the right hand side of the equation, $(C_{Du} - C_{Di} - C_{Do})$, is the uncorrected, separated-flow drag, C_{Dus} . In the aircraft case, the drag breakdown can be done readily, with due care in accounting for separated flow on flaps. In other applications, such as to automobiles, the drag breakdown is less certain. As a result, the uncorrected drag coefficient is used often instead of C_{Dus} because no other choice is available and because most of the drag is pressure drag due to flow separation.

As will be seen, the correction due to wake constraint should be in the form of a drag increment, rather than a dynamic pressure change. When the correction is recast into this form, an improved correction to drag and to the other aerodynamic forces and moments results. The details of this derivation are presented in Section 6.2.3. Strictly speaking, equations (6.3) and (6.4) are drag coefficient corrections only.

Equation (6.2) can be used to calculate the value of the blockage constant θ , using the corrected, average base pressures measured over the separated region of the model under test or from generic measurements on bluff bodies with similar separated flows.

Maskell obtained θ as a function of aspect ratio from measurements on normal flat plates and argued that these data could be generalised to other, similar, bubble-type separations. The blockage constant

was found to be within ten percent of $\theta=2.5$ for plates (square plate $C_{pbc} \approx -0.4$) having aspect ratios between 1 and 10.

When base pressure measurements are made, the corrected base pressure coefficient is obtained by iterating the following equation,

$$(1-C_{pbc})_i = \frac{(1-C_{pbu})}{1+(-1/C_{pbc})_{i-1}(C_{Dus}S/C)} \quad (6.5)$$

The measured base pressure is used as the starting point for the iteration. Gould [6] pointed out that the required pressure is the separation pressure coefficient, which is the base pressure coefficient for a flat plate.

The fundamental assumption made by Maskell was that the pressure field was invariant under constraint. Thus, blockage only scales the flow speed. The implication is that flow-separation and flow-reattachment locations must not be changed by wall constraint. Maskell provides evidence of this for the flat plates that were used to determine the empirical constants.

In addition, Farrell et. al. [11] have provided further insight into the effect of constraint on the invariance of the pressure field based on the behaviour of two-dimensional circular cylinders. These authors showed that the pressure rise between the point of maximum suction on the side of a circular cylinder and the base of the cylinder was independent of blockage up to $S/C=0.21$. This finding suggests that wall constraint has little effect on flow separation on bluff bodies up to this blockage level.

While the derivation of Maskell's correction formula, and the commonly-used values of the blockage constant θ , were based on data from normal flat plates, these values of θ have been applied to wings with flow separation. The constant for two- and three-dimensional normal flat plates is a function of plate aspect ratio and is fitted by,

$$\theta = 0.96 + 1.94 \exp(-0.06 AR) \quad (6.6)$$

The variation of equation (6.6) with aspect ratio is compared to Maskell's estimates in Figure 6.3.

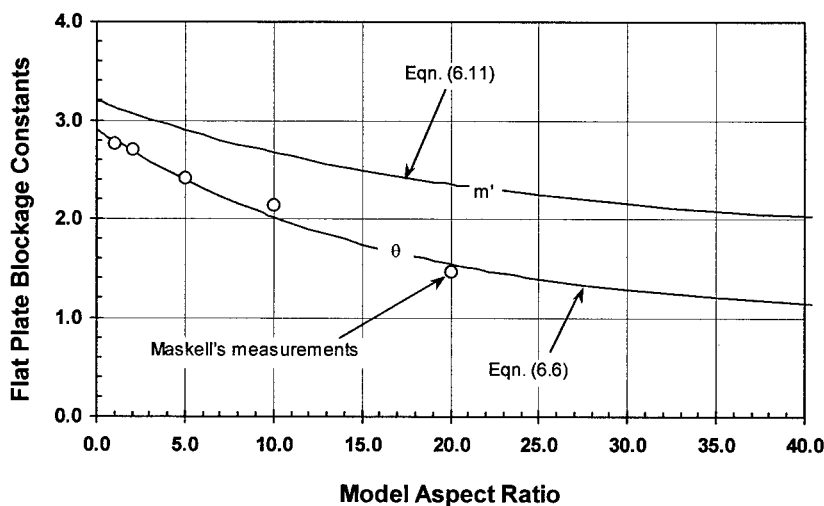


Fig. 6.3: Flat Plate Blockage Constants

The functional relationship implied in the data correlation of Figure 6.2 is that of equation (6.3), with the slope of the curve being θ . The flat-plate data from the closed test sections, Figures 6.1 and 6.2, were measured for aspect ratios between 1 and 3. Maskell's blockage constant takes on values in the range $2.5 \leq \theta \leq 2.8$ for these aspect ratios, which are close to the slopes of 2.53 for the flat-plates and 2.41 for the rectangular blocks in Figure 6.2.

Gould [6] showed that the correction was also valid for floor-mounted plates if the plate was considered as a plate of twice the height reflected about the floor as a plane of symmetry (duplex test section). As a result, the correction should apply equally well to two-dimensional testing, three-dimensional testing, and reflection-plane testing.

Although the correction is expressed as a dynamic pressure adjustment, it is more properly a correction to drag because of its momentum-based derivation. The inclusion of the wake distortion due to boundary constraint has effectively combined the incremental drag correction due to this effect with the dynamic pressure correction. Thus, while drag should be properly corrected, the other forces and moments will be over-corrected because the dynamic pressure correction has too large a value.

6.2.2 COWDREY'S DEVELOPMENT

Cowdrey [12] re-derived Maskell's method without the wake distortion effect for three-dimensional bodies that lie in their own wakes (leading-edge separation) and showed that the constant-base-pressure assumption was not required. He produced a correction that did not depend on the measured drag, although it still required an empirical constant that was a function of body geometry. His version of the correction had the form,

$$\left(\frac{q_c}{q_u}\right) = \left(\frac{C_{Du}}{C_{D\infty}}\right) = \frac{1}{1 - m(S/C)} \quad (6.7)$$

m is a semi-empirical constant that must be determined by experiment. If equations (6.1) and (6.7) are equated, then it can be seen that,

$$m = -(C_{D\infty}/C_{pbc}) \quad (6.8)$$

Equation (6.7) can also be written as,

$$\left(\frac{q_c}{q_u}\right) = \left(\frac{C_{Du}}{C_{DcMI}}\right) = 1 + m'(S/C) \quad (6.9)$$

When equation (6.9) is compared to equation (6.3), which contains the wake constraint effect, then the blockage factor, m' , can be represented by,

$$m' = -(C_{Du}/C_{pbc}) = \theta C_{Du} \quad (6.10)$$

An equation for m' for normal flat plates that is equivalent to equation (6.6) previously quoted for θ can now be written. It is,

$$m' = 1.85 + 1.35 \exp(-0.05 AR) \quad (6.11)$$

Equation (6.11) is shown in Figure 6.3 also.

6.2.3 HACKETT'S TWO-STEP VERSION OF MASKELL'S ANALYSIS

Maskell's momentum analysis combined the dynamic pressure and the incremental drag blockage components into a single dynamic pressure adjustment, making it a correction to drag only. Hackett [13, 14] realised this and separated Maskell's correction into its two constituent components, based on the difference between equation (6.3) and equation (6.1). This difference should be an increment in drag,

not a change in dynamic pressure. Hackett defined the drag increment to be $\Delta C_{DM} = C_{D_{cM1}} - C_{D_{\infty}}$, which is the difference between the corrected drag coefficients with and without the effect of wake constraint included.

The resulting 'two-step' version of Maskell's analysis should provide a superior adjustment to drag and to the other forces and moments, since the correction is separated into its correct components.

Maskell's correction for separated-flow blockage alone, equation (6.1), was restated by Hackett as,

$$C_{D_{\infty}} = (C_{D_{cM1}} - \Delta C_{DM}) = \frac{C_{Du}}{(q_c/q_u)_1} = \frac{C_{Du}}{1 + \theta(C_{D_{cM1}} - \Delta C_{DM})(S/C)} \quad (6.13)$$

Hackett then re-wrote the blockage correction in terms of a blockage-induced incremental velocity and a drag increment, to produce the following two-step (dynamic pressure and incremental drag) correction,

$$C_{D_{cM2}} = \frac{(C_{Du} + \Delta C_{DM})}{(q_c/q_u)_1} = \frac{(C_{Du} + \Delta C_{DM})}{1 + \theta(C_{D_{cM1}} - \Delta C_{DM})(S/C)} \quad (6.14)$$

$C_{D_{cM2}}$ is the drag coefficient corrected by Hackett's two-step version of Maskell's method. The dynamic pressure correction in the two-step approach, $(q_c/q_u)_1$, now *does not include* the wake distortion effect, which resides in ΔC_{DM} . ΔC_{DM} is obtained from the solution of the following quadratic equation, derived by equating C_{Du} in equations (6.3) and (6.13).

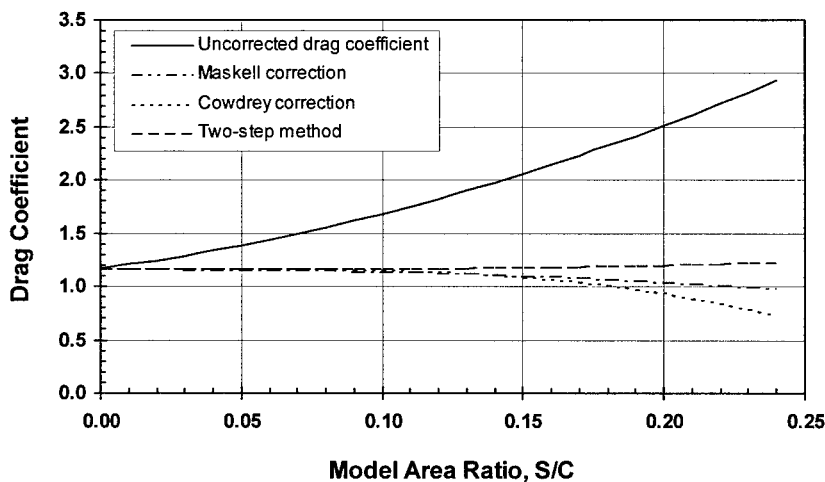
$$\Delta C_{DM}^2 - \left(\frac{1}{\theta(S/C)} + 2C_{D_{cM1}} \right) \Delta C_{DM} - C_{D_{cM1}}(C_{Du} - C_{D_{cM1}}) = 0 \quad (6.15a)$$

Only the negative solution to equation (5.15a) is physically valid since $C_{D_{cM1}}$ must be smaller than $C_{D_{\infty}}$.

It is important to note that the expressions presented in [13] and [14] differ, and that the results from [14] are used here. The linear approximation presented in [13] for ΔC_{DM} is incorrect due to a typographical error in the transactions paper. Further, the correct expression was applicable only for small values of $\epsilon C_{Du}(S/C)$. These issues are summarised in a discussions presented in the AIAA Journal [15]. In this discussion, Hackett presents the closed-form solution to equation (6.15a) as,

$$\Delta C_{DM} = \frac{C_{Du}}{(1 + \theta C_{Du}(S/C))} + \left[\frac{C_{Du}}{2\theta C_{Du}(S/C)} \right] \left[1 - \sqrt{1 + 4\theta C_{Du}(S/C)} \right] \quad (6.15b)$$

A comparison of Maskell's method [1], Hackett's two-step version [14] and Cowdrey's analysis [12] is provided



by applying them to the average fit line through the flat-plate drag coefficients in Figure 6.1. Equations (6.3), (6.7), and (6.14), along with their ancillary relations, were applied as corrections to these data. The results are collected in Figure 6.4. It can be seen that the tendency to over-correction in Maskell's method is removed by use of the two-step derivation of Hackett.

Fig. 6.4: Comparison of Separated-Flow Corrections For Three-Dimensional, Normal Flat Plates [6]

6.2.4 COMMENTARY ON MASKELL'S CORRECTION

Maskell's method has been found to over-correct at large area ratios when applied to many two-dimensional and three-dimensional bluff bodies, as demonstrated for two-dimensional rectangular cylinders in [16] and as seen for three-dimensional normal plates in Figure 6.4 [6]. The two-step development of Hackett should remedy this situation, and it would be beneficial to revisit many data sets to verify that this is the case. It would also be expected that the two-step version might be more accurate for aircraft with separated flows.

6.2.5 WAKE BUOYANCY AND THE WAKE-INDUCED DRAG INCREMENT

Controversy has arisen over the correct form of the drag increment at the body due to the constraint of the wake of the body by the tunnel walls. The classical adjustment [2], ascribed to buoyancy resulting from a wake-induced pressure gradient (excluding compressibility), is,

$$\Delta C_{Dwb} = -\varepsilon_s C_{Du,vis} = -T \left(\frac{V}{C^{3/2}} \right) C_{Du,vis} \quad (6.16)$$

where $T = (\sqrt{\pi}/2)\tau = 0.36(B/H + H/B)$ and $C_{Du,vis} = C_{Do} + C_{Dus}$ is the viscous component of the drag coefficient.

An alternative to this form has been derived recently by Taylor [17] as,

$$\Delta C_{Dwb} = -(\varepsilon_s + \varepsilon_w) C_{Du,vis} \quad (6.17)$$

It involves both the model volume and the wake blockage. Equations (6.16) and (6.17) express a buoyancy force on the model due to the pressure gradient at the model caused by the wake images. Thus, this form of wake-induced correction is referred to as 'wake buoyancy'.

Hackett [13, 14] has argued that both expressions are wrong because they do not include the cross terms acting between the full set of sources and sinks that approximate the body. The cross-terms cancel the buoyancy-based expression, leaving a new term that is not gradient related. Since Hackett's derivation is not limited to bluff flows, it should be more generally valid.

The new term, which had its origins in Hackett's and Wilsden's pressure-signature correction method [18], has the form,

$$\Delta C_{Dwi} = -C_{Du,vis}^2 \left(\frac{S}{4C} \right) \quad (6.18)$$

This equation does not contain volume either implicitly or explicitly, and is a function of the square of drag, whereas equations (6.16) and (6.17) are proportional to drag. The term 'wake-induced drag increment' is used to differentiate Hackett's version from the volume-based, buoyancy form. No direct experimental evidence exists to assist in clarifying this issue although one indirect experimental result can be found that supports the use of equation (6.18).

The relevant item is the flat-plate drag coefficient curve in Figure 6.4, which is a fit of the measured drag coefficients from [6] that are presented in Figure 6.1 as open diamonds. The flat plate is a geometry for which the classical buoyancy-based correction would be zero. Equation (6.15b) was applied to the fitted

curve to calculate the wake-induced drag increments for the plate as a function of area ratio. These drag increments are compared with those estimated from Hackett's expression, equation (6.18), in Figure 6.5 and are seen to be in reasonable agreement.

The issues raised above are not yet settled. Further discussion of them can be found in [15].

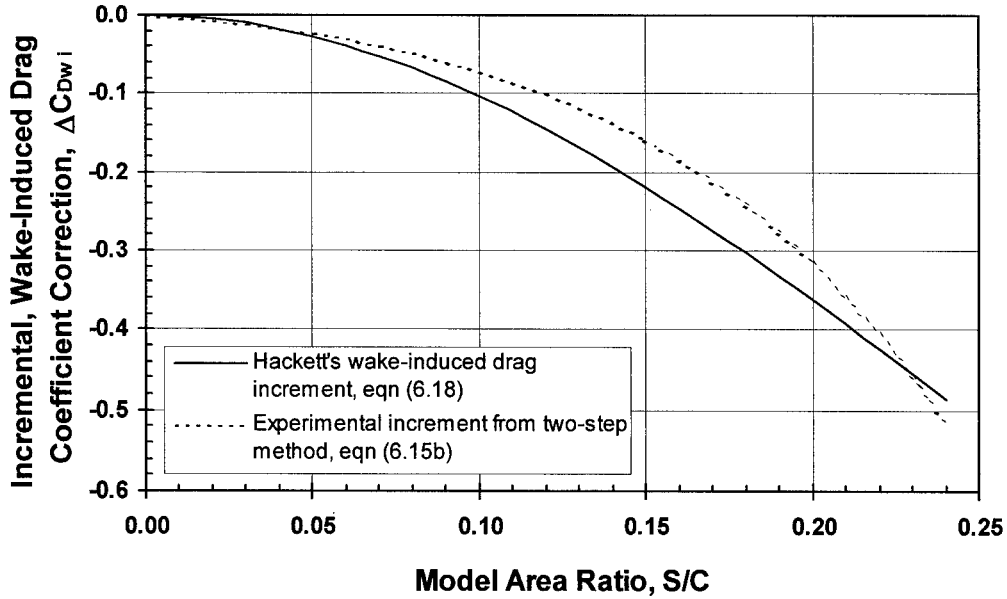


Fig. 6.5: Experimental Verification of Hackett's Wake-Induced Drag Increment For a Flat Plate Perpendicular to the Flow

6.2.6 Mercker's Analysis

A blockage correction has been developed by Mercker [19] for application to automotive shapes typified by rear-end flow separation, rather than the front-end separation of sharp-edged bodies. Maskell's constants will not apply to these shapes, although the base-pressure-dependent analysis should still be valid. Mercker's development was based on the solid-blockage analysis of Lock [20] and on the wake-blockage analyses of Maskell [1], Thom [21], and Glauert [22]. The following notation and constants differ from the derivation of [19] only because the correction has been re-written using the duplex test section and duplex model geometries for consistency. The blockage correction has the form,

$$\begin{aligned}
 \left(\frac{q_c}{q} \right) &= [1 + \varepsilon_s + \varepsilon_w]^2 \\
 &= \left[1 + K_\tau \left[\frac{L_p}{\sqrt{F}} \right] \left[\frac{V}{V_t} \right]^{3/2} \left[\frac{F^{3/2}}{V} \right] + \left\{ \left(\frac{S}{C} \right) \left[\frac{1}{4} C_{D_{uo}} + \eta \left(\frac{F}{S} \right) + \frac{5}{4} (C_{Du} - C_{Di} - C_{D_{uo}}) \right] \right\} \right]^2 \\
 &= \left[1 + K_\tau \left[\frac{F}{\sqrt{L_p V}} \right] \left[\frac{V}{C^{3/2}} \right] + \left\{ \left(\frac{S}{C} \right) \left[\frac{1}{4} C_{D_{uo}} + \eta \left(\frac{F}{S} \right) + \frac{5}{4} C_{D_{us}} \right] \right\} \right]^2 \quad (6.19)
 \end{aligned}$$

where:

C_{Du}	=	uncorrected, wind-axis drag coefficient at yaw angle ψ
C_{Dus}	=	uncorrected, separated-flow drag coefficient
C_{Du0}	=	uncorrected, wind-axis drag coefficient at zero yaw angle
C_{Di}	=	induced drag coefficient at yaw angle ψ
C	=	duplex test-section area = $2C_t$
L_p	=	projected length of model = $L_m \cos \psi + w_m \sin \psi $
L_m	=	model length
w_m	=	model width
ψ	=	yaw angle
S	=	duplex model frontal area = $2S_m$
F	=	duplex model projected frontal area = $2(S_m \cos \psi + S_Y \sin \psi)$
S_m	=	model frontal area
S_Y	=	model side area
τ	=	solid blockage constant = $2T/\sqrt{\pi} = 0.41(B/H + H/B)$
V	=	duplex model volume = $2V_m$
V_t	=	variable portion of test section volume = $L_p C$
η	=	empirical wake blockage constant determined by Mercker = 0.41
K	=	empirical solid blockage constant determined by Mercker = 1.0

The term $(S/C)[1/4C_{Du0} + \eta(F/S)] = [1/4C_{Du0}(S/C) + \eta(F/C)]$ effectively contains the wake blockage correction due to both skin friction and flow separation from the base of the bluff shape at zero yaw and small yaw angles. The third term in the curly bracket of equation (6.19) contains the additional separated-flow drag component that occurs at larger yaw angles. This additional separation drag is identified as the portion of the drag coefficient above the linear correlation of C_D versus $(c_L^2 + c_Y^2)$. Here, an analogy is made to the aircraft drag polar, except that the induced drag is now a function of both lift, C_L , and side force, C_Y .

The constant value $\eta=0.41$ differs from the value $\eta=0.43$ given in [19] because Mercker re-formulated his method to include the newly-proposed wake-induced-drag increment, equation (6.18). The term in the second line of equation (6.19), pre-multiplying $(V/V_t)^{3/2}$, also differs from that in Mercker's paper due to an improvement made by Mercker. This modification leads to the constant K changing from $(1/\sqrt{\pi})$ in [19] to the value of 1.0 used here.

The correction is applied to drag as,

$$C_{Dc} = \left[\frac{(C_{Du} + \Delta C_{Dwi})}{(q_c/q)} \right] \quad (6.20)$$

where ΔC_{Dwi} is given by equation (6.18).

6.2.7 UPSTREAM AND DOWNSTREAM EFFECTS

Boundary effects upstream and downstream of the model are important also. With more than one model in the test section, the blockage correction at each model will be a combination of the upstream and downstream effects caused by each model. Further, the model's blockage field may distort the reference measurement at the entrance to the test section and the model's flow field may be distorted when the model is too near the end of the test section. These position-in-test-section effects have been studied by Gould [6] and by Garry, Cooper, Fediw, Wallis, and Wilsden [23].

Gould's interest was the blockage interference effects between several axially separated bluff models. He measured the upstream and the downstream variations of the blockage of flat plates in a closed test section. His results showed that the downstream effect was the larger and persisted further. The downstream blockage effect collapsed on distance non-dimensionalised by the mean plate size, expressed as (x_d/\sqrt{S}) , because the downstream behaviour depends on the size and the development of the viscous wake. The upstream effect was found to collapse on (x_u/\sqrt{C}) . This behaviour can be ascribed to a potential flow effect, where the mirror image sets of singularities that can be used to describe the blockage have the image separation - the tunnel height and width - as the characteristic dimensions. A reasonable average of these lengths is \sqrt{C} .

The blockage variations with longitudinal position relative to the location of the generating body, as a fraction of the value at the body, are adequately fitted by,

$$\text{upstream effect : } (\varepsilon_u/\varepsilon) = \exp\left\{-\left[\frac{\pi}{2}\left(\frac{x}{\sqrt{C}}\right)\right]^2\right\} \quad (6.21)$$

$$\text{downstream effect : } (\varepsilon_d/\varepsilon) = 0.3 + 0.7 \exp\left\{-0.1\left(\frac{x}{\sqrt{S}}\right)^{1.7}\right\} \quad (6.22)$$

This pair of equations provides the multiplying factor on the blockage induced by a model at a position upstream or downstream of the model. The composite blockage at any location due to several models is

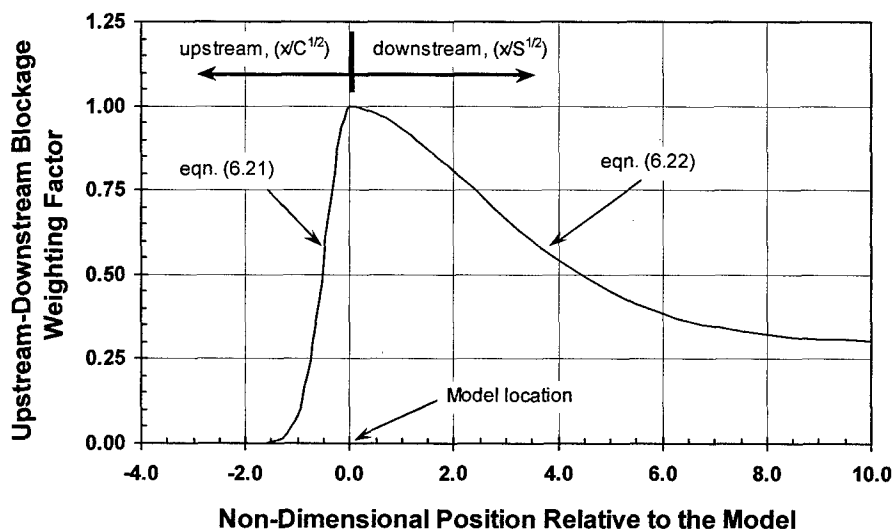


Fig. 6.6: Variation of Blockage Upstream and Downstream of the Model Location [6]

the sum of the individual effects. The blockage variations of equations (6.21) and (6.22) are shown in Figure 6.6.

Equation (6.21) indicates that a model should be positioned no closer than $1.5\sqrt{C}$ to the reference static pressure taps to keep the effect of blockage at the taps below one-half percent of the value at the model or no closer than \sqrt{C} to keep the

effect at five percent. Conversely, if the model location is fixed, and if the model blockage can be estimated, then equation (6.21) can be used to determine the error in the reference static pressure measurement.

The authors of [23] were interested in the effect of the proximity of an automobile model to the end of the test section. Here, the end of the test section was defined by the start of the diffuser or the end of a ground board used for improved ground-boundary simulation. Their measurements in three wind tunnels showed a large effect on the drag coefficient due to proximity to the end of the test section. The results suggested that the wake formation region was affected by the diffuser pressure field or by the flow discontinuity at the end of a ground board. In either case, the results were similar - drag was reduced by approximately ten percent. It was found that the drag distortions collapsed on distance from the end of the test section normalised by the square root of the base area, $\sqrt{S_b}$. This area is taken to be the area of the separated region on the base of the model.

Typical base-pressure behaviour as a bluff model approaches the diffuser is seen in Figure 6.7. A large effect on base pressure, and on drag, is seen when the model is too close to the diffuser. Based on these and similar measurements, the authors recommended that models not be positioned closer to the end of a test section than $2\sqrt{S_b}$ and, that whenever possible, models should be at least $4\sqrt{S_b}$ from the end of a test section. These limits should also apply to open-jet tunnels.

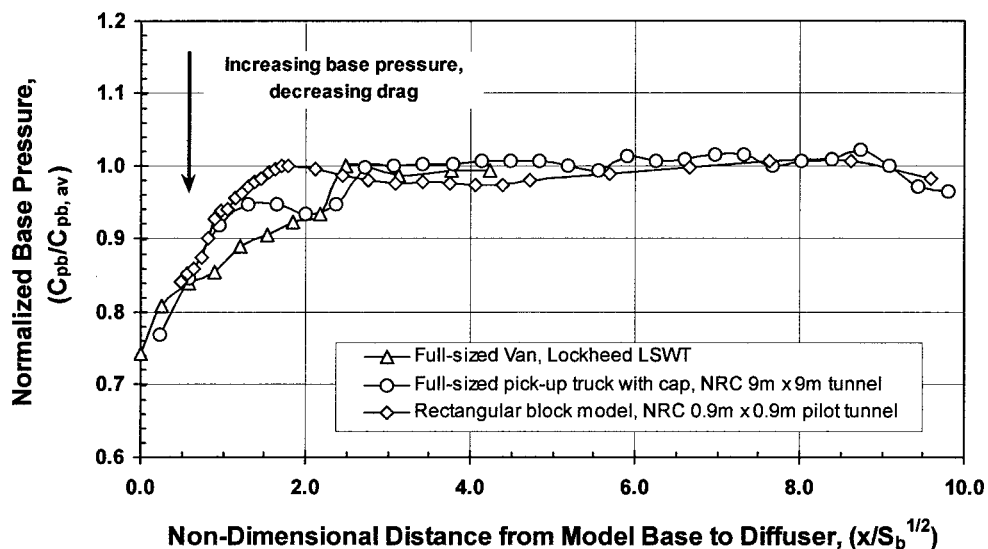


Fig. 6.7: Effect of Proximity of Model Base to Closed-Tunnel Diffuser [23]

6.3 METHODS FOR OPEN TEST SECTIONS

The open-jet wind tunnel has classical boundary corrections that are smaller and of opposite sign to those found for closed tunnels [1]. From the classical perspective, the major effect arises from the velocity reduction caused by solid blockage. Here, the jet over-expands, reducing the velocity at the model compared to the upstream measurement. There is no blockage velocity component due to wake blockage because the array of images that provide the free-jet boundary condition are of alternating sign. A correction should be made to drag for this wake constraint. Commonly, these corrections were ignored, as they were considered too small to be of concern.

6.3.1 RECENT RESULTS FROM AUTOMOTIVE TESTING

A working group was formed under the auspices of the Society of Automotive Engineers to prepare an Information Report on the boundary corrections used for automotive models in open tunnels [4]. The impetus for this work came from the automotive industry, rather than the aeronautical industry, because many of the world's large open-jet wind tunnels had been designed for the development of automobiles. Correlation studies on identical models in many closed and open full-scale wind tunnels [24] had shown significant differences amongst them.

It was realised that boundary effects for bluff shapes in open tunnels were not negligible, and that the observed behaviour was complex and was not explained by classical theory [4]. For example, comparisons of measurements made on the same full-sized passenger cars [24] and on a family of truck models [25] in open and closed wind tunnels had shown that the closed tunnels consistently measured higher drag coefficients than the open tunnels, even when blockage corrections had been applied. Furthermore, the open tunnel results were not self-consistent.

The classical theories that utilise reflected singularity sets to represent the model and its wake produce an infinitely long free jet. This is not the case in practice, where the jet length is typically 1.5 to 3.0 nozzle hydraulic diameters - limits posed by utility at the lower end and jet stability at the higher end. The finite jet length, not accounted for in the classical theories, is the source of the majority of the important boundary-produced distortions in an open-jet wind tunnel, especially for bluff bodies.

Much of the following discussion is based on the SAE Information Report [4] and on two SAE papers [26,27] written to address the open-jet issues.

6.3.2 THE PRIMARY EFFECTS

The situation under consideration is defined in the open-jet test-section schematic of Figure 6.8. A bluff object can create large distortions of the jet that lead to force changes at the body. The majority of these effects result from upstream/downstream constraints imposed by the finite-length jet. The classical representation of the free jet by mirror-image singularities produces an infinite jet and excludes important effects due to the solid wall boundaries at the nozzle and the collector. Mercker and Wiedemann were the first to identify and name the nozzle and the collector effects, and have derived a correction to account for them [26,27]. They grouped the interference effects into four categories. These are:

1. *Nozzle Blockage* – The interference of a model on the nozzle changes the calibration of the dynamic-pressure measuring system from the empty-tunnel value. The distortion is different when using either the nozzle or the plenum reference

- pressures. Both reference methods should produce the same result, independent of the model position.
2. *Solid Blockage and Jet Expansion* - A free-jet flow over-expands at the model, reducing the velocity at the model to a value below that measured during the empty-tunnel calibration. Proximity of the model to the nozzle increases this effect.
 3. *Empty-Tunnel Pressure Gradients* - Drag changes are caused at the model due to the empty tunnel pressure gradient.
 4. *Collector Blockage Effects* - The flow-speed at the model location is changed from the free-air condition due to the constraints on the wake imposed by the collector.

An additional effect due to the wake constraint, similar to the incremental drag correction in closed tunnels, may also exist.

5. *Wake-Induced Effects* - The solid-wall constraints on the wake as it enters the collector may produce a drag increment at the model.

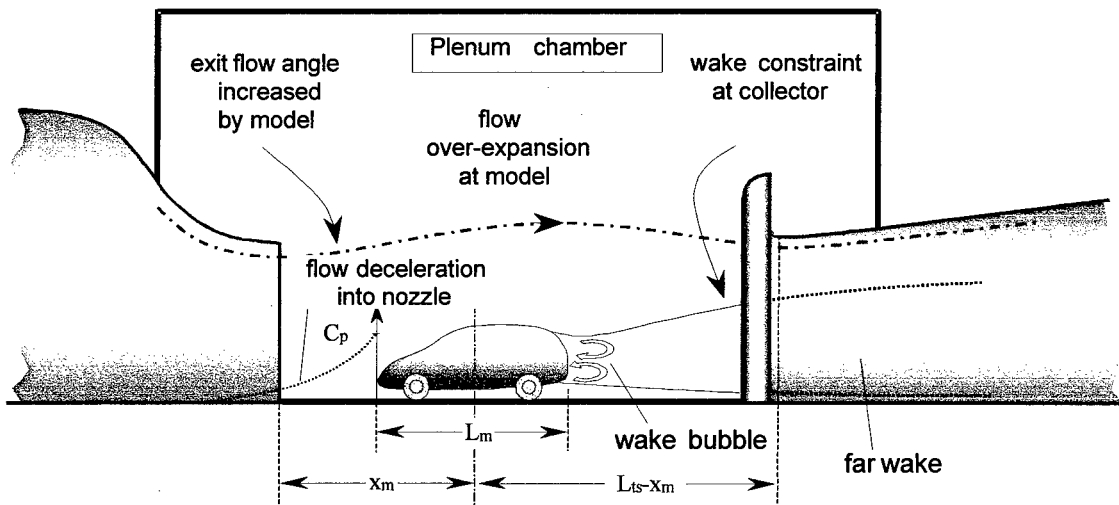


Fig. 6.8: Schematic View of the Open-Jet Wind Tunnel

6.3.2.1 NOZZLE BLOCKAGE

The most fundamental blockage effect is Item 1 in the preceding section - the influence of model proximity to the exit plane of the nozzle on the wind tunnel dynamic pressure calibration. The dynamic pressure in an open tunnel is usually measured in one of two ways; using the pressure drop between the settling chamber and the plenum surrounding the jet - the plenum method - or using the pressure drop between the settling chamber and the nozzle - the nozzle method. The nozzle-based measurement is denoted by q_n and the plenum-based measurement is denoted by q_p .

When using the nozzle pressure drop, the reference pressure taps in the nozzle should be positioned sufficiently far upstream into the nozzle that they are unaffected by the model. Both pressure drops are calibrated against a reference probe in the empty jet and give an equally good empty-tunnel calibration. The two calibrations change, however, when a model is present in the test section, so that each method provides a different dynamic pressure measurement for the same test condition. The difference between

the two measurements is usually a function of the axial position of a model relative to the nozzle exit plane and of the drag of the model.

Figure 6.9 shows an example of this behaviour through the drag coefficient changes measured by Kuhn [28] on a flat plate as a result of moving the plate upstream toward the nozzle. The drag coefficient based on the nozzle calibration is increasingly higher than that based on the plenum calibration, which is nearly constant with position. This behaviour is caused by model interference on the nozzle flow.

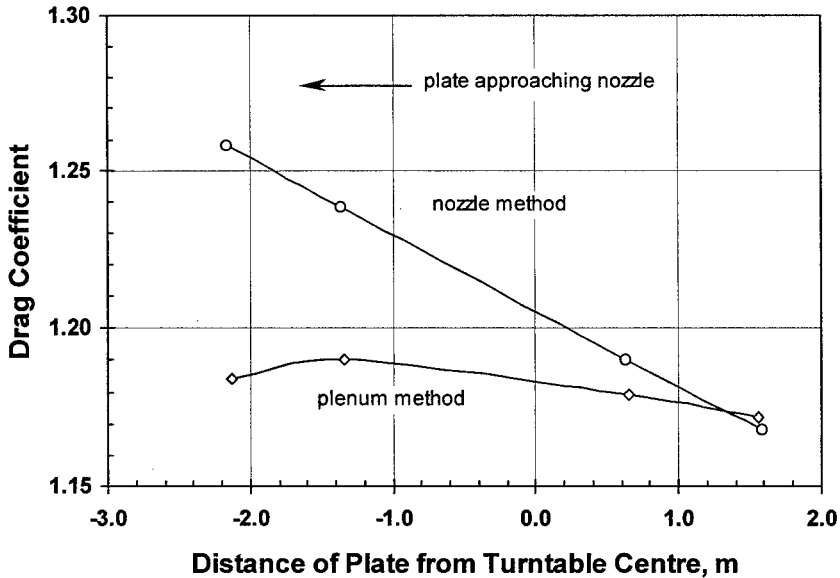


Fig. 6.9: Variation with Axial Position of the Drag Coefficient of a Flat Plate Based on Both the Plenum and the Nozzle Dynamic Pressure Measurements [28]

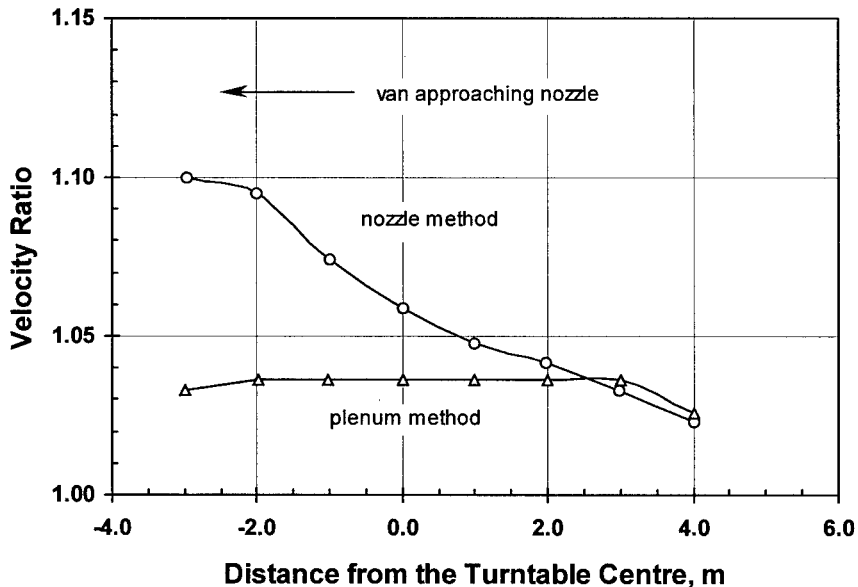


Fig. 6.10: Variation with Axial Position of the Ratio of the Velocity Measured Beside a Van to the Nozzle- and the Plenum-Method Velocities [28]

An explanation of this behaviour is contained in the jet velocity measurements of Figure 6.10 [28]. Here, the velocity beside a van having an area blockage of $S/C=0.118$ was measured near the edge of the jet by an anemometer and was compared to the plenum-based and the nozzle-based velocity measurements as the van was moved along the test section. The resulting velocity ratios were almost identical when the van was furthest from the nozzle. As the van was moved toward the nozzle, the anemometer velocity measurement increased compared to the nozzle calibration but remained nearly the same as the plenum calibration. Thus, the drag coefficient of a body would increase if based on the nozzle dynamic pressure measurement and would remain approximately constant if based on the plenum measurement, as the model approached the nozzle. This is the behaviour observed for the flat plate.

Figure 6.11 [28] shows that the cause of these velocity variations with van position lies in the effect of the model on the velocity distribution at the nozzle exit plane. The figure presents measurements of the

flow field over the exit plane of the nozzle with a van present in the test section. They are presented as contours of constant velocity ratio, where the measured, nozzle-plane velocities are normalised by the reference velocity obtained using the nozzle method.

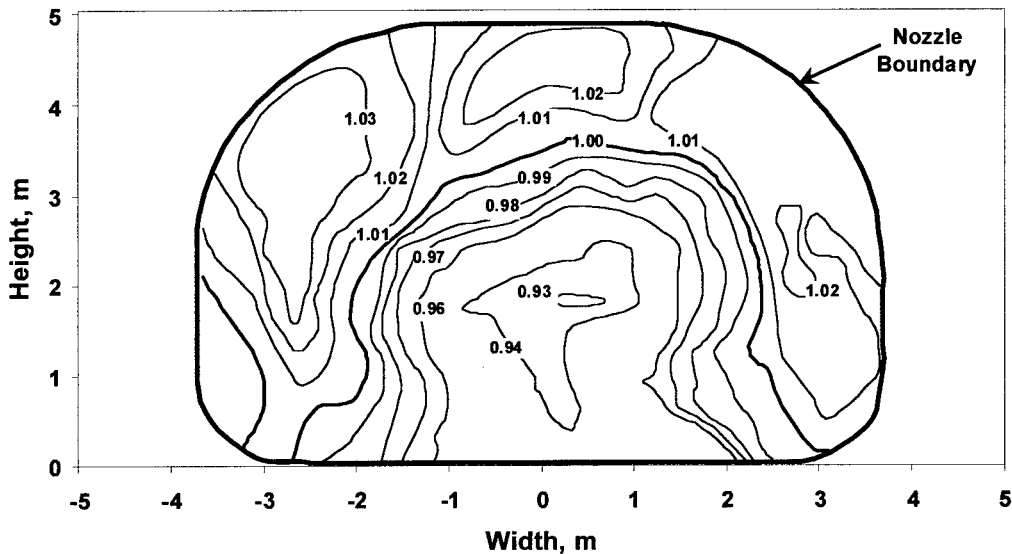


Fig 6.11: Ratio of the Velocity Measured over the Nozzle Exit Plane to the Nozzle-Method Reference Velocity with a Transit Van in the Test Section [28]

The flow deceleration upstream of the van can be seen to extend into the nozzle, producing a non-uniform velocity distribution. The flow velocities near the lower centre of the jet are retarded while the flow velocities around the periphery are accelerated, to satisfy continuity. The same deceleration would occur in free air, minus the closed-wall blockage effect due to the nozzle walls. Effectively, the open jet wind tunnel flow may be subjected to a speed increase similar to that normally associated with a closed tunnel and the reverse of that normally assumed for an open tunnel. The magnitude of this effect would depend on model size and proximity to the nozzle. The closer the model was to the nozzle exit plane, the larger the central speed reductions and the peripheral speed increases would be. The average velocity ratio over the nozzle area in Figure 6.11 is 1.0 because the nozzle method measures the average velocity at the nozzle.

The velocity in the jet periphery is higher than that measured using the nozzle method, by 2 percent to 3 percent, in this case. This increase is similar to the change in velocity ratio between the furthest downstream position of the van and the position of the van during the velocity survey, $x = -0.2$ m in Figure 6.10. As the van is moved closer to the nozzle, the gradients in velocity over the nozzle would be expected to increase further, leading to the increasing anemometer/nozzle velocity ratio seen in Figure 6.10.

The plenum-based velocity ratio remains nearly fixed because the plenum pressure is equal to the static pressure at the jet boundary and so the plenum-based velocity measurement tracks the velocity increase. As will be shown, neither measurement provides the effective free-stream approach velocity in the plane of the nozzle.

6.3.2.2 SOLID BLOCKAGE AND JET EXPANSION

The classical correction for blockage in an open tunnel [2] is a velocity *reduction* induced by over-expansion of the free-jet flow around the model, compared to the free-air flow. Additionally, as a bluff shape approaches a nozzle, the flow angle is increased by model proximity, further increasing the jet expansion. This effect is characterised in the free-streamline analyses for flat plate models in jet flows presented in Birkhoff, Plesset and Simmons [29], in which the emergent flow angle from a nozzle upstream of a flat plate is shown to increase with the approach of the plate to the nozzle. This expansion effect is not included in the classical, infinite-jet analysis and is more likely to be important for the flows associated with automobiles or trucks than for streamlined aircraft shapes.

6.3.2.3 EMPTY-TUNNEL PRESSURE GRADIENTS

The largest interference effect results from the pressure distribution that exists in the free jet (measured with the model absent) as it flows between nozzle and collector. Changes in the pressure distribution with the model present are dealt with separately, usually as a blockage effect that appears as an increment in drag at the model.

Typical empty-tunnel, axial static pressure distributions show a concave-upward characteristic [4]. The static pressure drops as the jet exits the nozzle, becoming nearly constant over the central region of the jet, generally not at zero pressure coefficient, before rising again as the flow decelerates on approaching the collector. The pressure gradients that occur are large compared to closed tunnels, and extend over the region usually occupied by models. The gradients are not constant over the model, necessitating some form of integration of the pressure distribution over the model for an adequate correction.

6.3.2.4 Collector Effects

There will be additional effects on a bluff model as its large wake enters the collector, going from an open-jet boundary condition to a closed-wall boundary condition. The entry of the bluff-body wake into the collector may result in a closed-wall, wake-induced velocity increment at the model due to the changed constraint on the wake. This effect is a result of the finite jet length and the fact that the model frequently terminates close to the entrance to the collector.

6.3.2.5 WAKE-INDUCED EFFECTS

The wake-induced drag increment for an open tunnel is small. However, as in the previous case, Section 6.3.2.4, wake constraint on entry into the collector may induce a base pressure change at the model in a fashion similar to that for a closed tunnel, Section 6.2.4. No adjustment for such an effect is yet available.

6.3.3 THE METHOD OF MERCKER AND WIEDEMANN

Mercker and Wiedemann [26, 27] have identified the major open-jet blockage elements and have developed procedures to correct for their effects. Their first paper [26] clarified the interactions between the model and the nozzle and the model and the diffuser. It corrected the dynamic pressure based on the nozzle-measurement method only. A second paper, by Mercker, Wickern and Wiedemann [27], extended the analysis to include dynamic pressure measurements using either nozzle or plenum measurements. The correction procedure offered a first attempt at analysing the major boundary-induced effects discussed in Section 6.3.2. and provides a framework for further development.

The correction methodology follows standard practice by breaking the boundary-induced effects into a series of components that are combined to provide the full adjustment to dynamic pressure. Following Section 2, the correction to dynamic pressure is written as,

$$\left(\frac{q_c}{q_u}\right) = (1 + \varepsilon)^2 = (1 + \varepsilon_s + \varepsilon_n + \varepsilon_c)^2 \quad (6.23)$$

The total blockage factor, $\varepsilon = (U_c / U_m) - 1$ is made up of the solid blockage factor ε_s , which is negative, the nozzle blockage factor ε_n , which is positive, and the collector blockage factor, ε_c , which is also positive. U_c is the velocity corrected for blockage and U_m is the velocity measured using either of the two reference methods - u_n or u_p . Unlike the classical approach to blockage for the infinitely-long open jet, which reduces dynamic pressure, the new correction terms that arise because of finite jet length - the nozzle and the collector effects - are positive and increase the velocity at the model.

It should be noted that the definition of ε used here is different than that used in either [26] or [27] and so will result in a different equation for the nozzle blockage, although the correction magnitudes that result are virtually identical.

6.3.3.1 NOZZLE BLOCKAGE

The flow velocity at the periphery of the jet, in the nozzle exit plane, has been found to increase as a model approaches the nozzle [28]. This behaviour results from a solid-wall blockage effect caused by the flow deceleration upstream of the model extending into the nozzle. It is the reverse of the effect usually ascribed to open tunnels.

This model influence at the nozzle is fixed, irrespective of the dynamic-pressure-measuring technique. However, the two measuring techniques commonly employed in open tunnels see this phenomenon differently, requiring two adjustment procedures to give correct and identical reference dynamic pressure measurements. The situation is as sketched in Figure 6.12, which shows the velocity field upstream of a body, in the plane of the nozzle.

Assuming that the approach velocity profile at the nozzle exit plane in the tunnel is similar to that in free air, it can be seen that the 'effective' undisturbed approach velocity, U_o , is higher than the velocity measured by either reference method. The difference between the velocity measured at the nozzle, either U_n or U_p , and the effective free-stream asymptote, U_o , provides the nozzle blockage factors.

The nozzle method measures the average velocity across the nozzle. This value must be increased by a velocity increment equal to $(\varepsilon_{qn}U_n)$ to equal the free stream asymptote. Because the plenum method

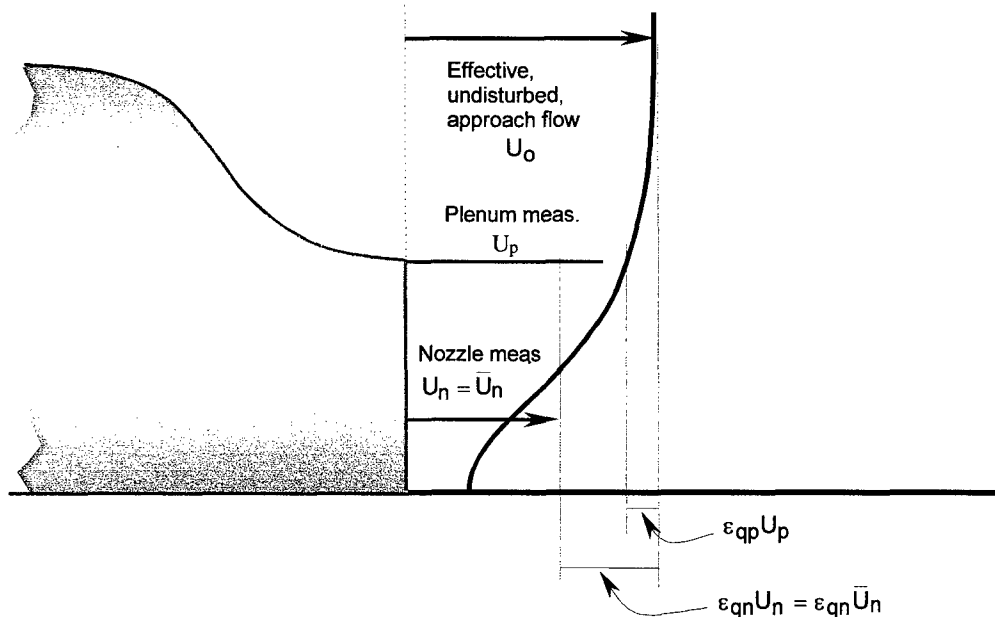


Fig. 6.12: Relationship Between Nozzle and Plenum Measurements and the Equivalent Undisturbed Free-Air Approach Flow

provides the velocity at the jet boundary, a smaller velocity increment is required to raise it to the same free-stream approach flow. This increment is $(\epsilon_{qp} U_p)$.

The derivation of the corrections for flow constraint in the nozzle proceeds through a representation of the upstream effects of the model at the nozzle plane by a simple point source. This source is sized to provide an area of the resulting body of revolution at downstream infinity that is equal to the frontal area of the model. The source is positioned so that the stagnation point on the semi-infinite body of revolution produced by it is located at the leading edge of the vehicle model that it represents.

The source strength is,

$$\left(\frac{Q_s}{U_o} \right) = S \quad (6.24)$$

S is the frontal area of the model for a centrally mounted model, or is twice the frontal area, the duplex model area, for a floor-mounted model such as an automobile. The nozzle area, C , is utilised in the single or the duplex fashion, as appropriate. The distance from the source to the nozzle, measuring positively downstream from the source location (thereby making this distance negative), is,

$$x_s = -x_m + \left(\frac{L_m}{2} \right) - \left(\frac{S}{2\pi} \right)^{1/2} \quad (6.25)$$

where x_m is the distance from the centre of the model to the nozzle (thus the negative sign) and L_m is the length of the model. The location of the stagnation point relative to the source is the last term on the right-hand side of equation (6.25).

Nozzle Method - Considering the nozzle-method measurement first, the correction proceeds by computing the average of the horizontal velocity component over the nozzle location, in the presence of the source, as a fraction of the effective approach free-stream velocity at infinity in the plane of the

nozzle, U_o . The magnitude of the horizontal velocity component, in cylindrical co-ordinates, with origin at the source location and measuring x positively downstream, is,

$$\left[\frac{U_x(x,r)}{U_o} \right] = \left[\frac{U_o + u_x(x,r)}{U_o} \right] = \left[1 + \left(\frac{Q_s}{4\pi U_o} \right) \left(\frac{x}{(x^2 + r^2)^{3/2}} \right) \right] \quad (6.26)$$

where the source strength is given by equation (6.24).

Taking continuity into account, the mean nozzle velocity, \bar{U}_n , from which the perturbation velocity at the nozzle can be determined, is obtained by integration of equation (6.26). This integration returns a velocity that is equal to the reference velocity measured by the nozzle method. The mean velocity at the nozzle plane was found to be [26],

$$\left[\frac{\bar{U}_n}{U_o} \right] = \left[1 - \left(\frac{S}{2C} \right) \left(1 + \frac{x_s}{(x_s^2 + R_n^2)^{1/2}} \right) \right] \quad (6.27)$$

The perturbation velocity at the nozzle plane due to nozzle blockage, when using the nozzle method, is,

$$\varepsilon_{qn} = \left[\frac{U_o}{\bar{U}_n} - 1 \right] = \frac{\left(\frac{S}{2C} \right) \left(1 + \frac{x_s}{(x_s^2 + R_n^2)^{1/2}} \right)}{\left[1 - \left(\frac{S}{2C} \right) \left(1 + \frac{x_s}{(x_s^2 + R_n^2)^{1/2}} \right) \right]} \quad (6.28)$$

where $R_n = \sqrt{2C_n/\pi} = \sqrt{C/\pi}$ is the hydraulic radius of the duplex nozzle.

A vortex ring positioned at the nozzle exit plane was used to project the blockage factor from the nozzle plane to the model location. The velocity reduction at the model location accounts for the flow relaxation once the solid-walled nozzle constraint is removed as the jet emerges from the nozzle. The circulation of the vortex ring is set to equate the velocity induced by the vortex ring at the centre of the nozzle to the velocity at the same point produced by the upstream effect of the model. The complete expression for the blockage factor at the model due to nozzle blockage becomes,

$$\varepsilon_n = \varepsilon_{qn} \left[\frac{R_n^3}{(x_m^2 + R_n^2)^{3/2}} \right] \quad (6.29)$$

Plenum Method – The plenum-method analysis proceeds in a similar fashion, with a blockage correction that is derived from the singularity-based velocity profile. This time, the ratio of the velocity at the edge of the jet to that far away, (U_p/U_o) , is required, recognising that the plenum method provides the wind speed at the jet periphery. Using equation (6.26), the ratio of the horizontal component of velocity at the edge of the jet to that far away in an unconstrained flow is,

$$\begin{aligned}
\left[\frac{U_p}{U_o} \right] &= \left[\frac{u_x(x_s, R_n)}{U_o} \right] \\
&= \left[1 + \left(\frac{Q_s}{4\pi U_o} \right) \left(\frac{x_s}{(x_s^2 + R_n^2)^{3/2}} \right) \right]^{1/2} \\
&= \left[1 + \left(\frac{S}{4\pi} \right) \left(\frac{x_s}{(x_s^2 + R_n^2)^{3/2}} \right) \right]^{1/2} \tag{6.30}
\end{aligned}$$

Thus, the blockage factor due to nozzle blockage at the nozzle exit plane, when using the plenum method, is,

$$\epsilon_{qp} = \left[\frac{U_o}{U_p} - 1 \right] = \frac{- \left(\frac{S}{4\pi} \right) \left(\frac{x_s}{(x_s^2 + R_n^2)^{3/2}} \right)}{\left[1 + \left(\frac{S}{4\pi} \right) \left(\frac{x_s}{(x_s^2 + R_n^2)^{3/2}} \right) \right]} \tag{6.31}$$

The perturbation velocity obtained from equation (6.30) is smaller than that obtained when using the nozzle method, equation (6.28), although the two flows are identical. Based on momentum considerations, the authors converted the plenum velocity to the average nozzle velocity through the assumed upstream profile to ensure that both measuring methods, and their corrections, produced the same velocity at the model. For small ϵ , this results in,

$$\epsilon_p = \epsilon_{qp} + \epsilon_n - \epsilon_{qn} \tag{6.32}$$

6.3.3.2 SOLID BLOCKAGE AND JET EXPANSION

The solid blockage term utilised is the classical form, modified to include an additional jet expansion due to model proximity re-directing the flow from the nozzle, causing the exit flow angle to increase. It has the form,

$$\epsilon_s = \tau \left(\frac{V}{L} \right)^{1/2} \left(\frac{S}{C_e^{3/2}} \right) \tag{6.33}$$

where V is the model volume, L is the model length, S is the reference area, and C_e is the 'effective' nozzle area that contains the additional jet expansion (jet deflection) effect due to proximity of the model to the nozzle. τ is the appropriate constant from [2]. The reduced nozzle effective area approximates the

additional velocity reduction at the model due to jet deflection caused by model proximity to the nozzle. The area reduction was related to the nozzle blockage, and was calculated from,

$$C_e = C / (1 + \varepsilon_{qn}) \quad (6.34)$$

where ε_{qn} is the nozzle blockage defined in equation (6.28). ε_s is negative, due to the sign of τ , reducing the velocity at the model.

6.3.3.3 EMPTY-TUNNEL PRESSURE GRADIENTS

The pressure distributions in an open-jet tunnel are often non-uniform over the model location. Thus, it is necessary to integrate the pressure gradient over the body under test to achieve an adequate correction for the pressure distribution present. The horizontal buoyancy force acting on a body in a pressure gradient is given by,

$$F_H = \int p da = \int (\partial p / \partial x) dV \quad (6.35)$$

A simplification to the full integration that was suggested by Mercker and Wiedemann [26] was the replacement of the volume integral by a linear approximation applied separately over the front and the rear halves of the model. The following horizontal-buoyancy correction to drag due to the empty-tunnel pressure distribution resulted,

$$\Delta C_{D_{HB}} = \left[\frac{(V_e / 2)}{S} \right] \left[\left(\frac{dC_p}{dx} \right)_n + \left(\frac{dC_p}{dx} \right)_c \right] \quad (6.36)$$

The subscripts n and c refer to the pressure gradients over the front and the rear halves (nozzle and collector ends) of the model, respectively. The use of an effective volume follows the classical works of Munk [30] and Glauert [22], which suggested that the effective volume was greater than the true model volume. The multiplying factor was found to be 1.5 for a sphere and 2.0 for an axial cylinder. A reasonable mid-range value of $V_e = 1.75V$ was chosen for automotive applications. The volume and the area are the single or duplex values for central or wall-mounted models, respectively.

6.3.3.4 COLLECTOR EFFECTS

Another solid-wall blockage effect was postulated to occur at the end of the test section, as the wake of the model flowed into the collector. The wake is then subject to a solid-wall blockage effect that is felt in a diminished fashion at the model. The blockage effect to which the wake was subject was taken as that derived for an automotive wake based on the analysis of Mercker [19] that was presented for solid wall tunnels in Section 6.2.6. The far-field effect was achieved by projecting the effect at the collector to the model location using the ring vortex model previously employed, with the ring vortex now positioned at the collector.

The wake-blockage factor in the collector throat is given by the small-yaw-angle component of the wake blockage from equation (6.19), which is,

$$\varepsilon_{wc} = \frac{C_{Duo}}{4} \left(\frac{S}{C_c} \right) + 0.41 \left(\frac{F}{C_c} \right) \quad (6.37)$$

C_c is the single or duplex collector throat area, F is the single or duplex projected frontal area and the empirical constant 0.41 is that given in Section 6.2.6 for bodies with rear-end separations, like automobiles. Bodies with increased separation at yaw angles greater than 15 degrees would require the full wake blockage correction, equation (6.19).

When the wake separation bubble is small, as for some fast-back cars, the wake-bubble term, 0.41, can be neglected, leaving only the first term in parentheses in equation (6.37).

The collector blockage at the model, using the ring-vortex model, is found to be,

$$\varepsilon_c = \varepsilon_{wc} \left[\frac{R_c^3}{[(L_{ts} - x_m)^2 + R_c^2]^{3/2}} \right] \quad (6.38)$$

where R_c is the hydraulic radius of the single or duplex collector throat, L_{ts} is the length of the test section, and $(L_{ts} - x_m)$ is the distance from the model centre to the collector throat.

6.3.3.5 APPLICATION OF THE OPEN-JET CORRECTION FORMULAE

The corrections to dynamic pressure and drag for all the effects discussed for the open tunnel are:

Nozzle measurement –

1. Dynamic pressure, $(q_c / q_n) = (1 + \varepsilon_s + \varepsilon_c + \varepsilon_n)^2$ (6.39)

2. Wind-axis drag coefficient, $C_{Dc} = \frac{[D / (q_n S_m)] + \Delta C_{DHB}}{(q_c / q_n)}$ (6.40)

The remaining forces and moments are corrected using equation (6.39).

Plenum Method –

1. Dynamic pressure, $(q_c / q_p) = (1 + \varepsilon_s + \varepsilon_c + \varepsilon_p)^2 \approx (1 + \varepsilon_s + \varepsilon_c + \varepsilon_n + \varepsilon_{qp} - \varepsilon_{qn})^2$ (6.41)

2. Wind-axis drag coefficient, $C_{Dc} = \frac{[D / (q_p S_m)] + \Delta C_{DHB}}{(q_c / q_p)}$ (6.42)

6.4 APPLICATION TO CLOSED TEST SECTIONS

6.4.1 AIRCRAFT

An example of the application of Hackett's two-step version of Maskell's correction procedure through the stall is presented in Figure 6.13. The measurements were made by Shindo [31] to support the simplified correction method that he had proposed using models of 0.016 and 0.16 area ratio. Only the two-step correction is shown because it and Maskell produced nearly identical corrections. For example, at the highest drag level for the larger model where $C_{Du} = 0.7072$, Maskell provided a dynamic-pressure

correction factor of 1.232 while Hackett's two-step method gave a dynamic-pressure correction factor of 1.212 and a drag increment of $\Delta C_{DM} = -0.0126$. Both corrections gave corrected drag coefficients within one count of each other. The lift coefficient corrections were different by the ratios of the dynamic-pressure correction factors.

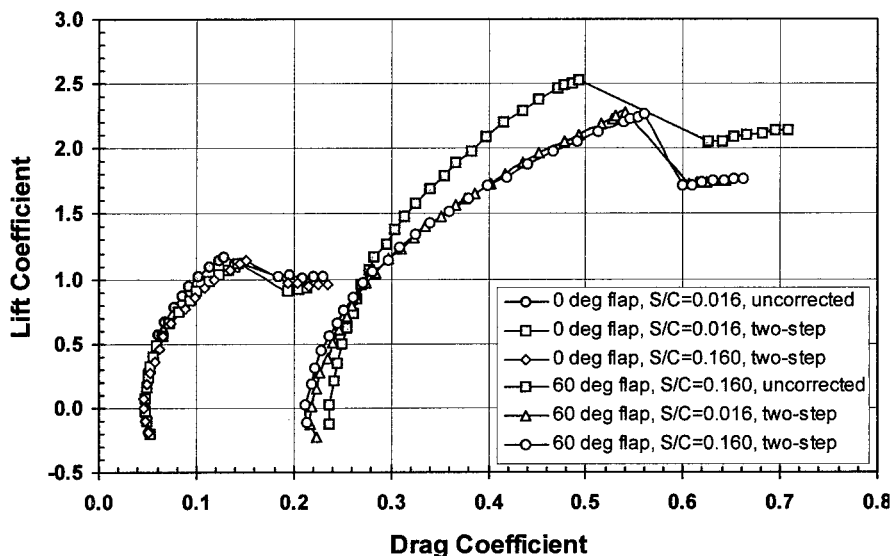


Fig. 6.13: Application of Hackett's Two-Step Version of Maskell's Method to Lift and Drag Measurements on a Rectangular Wing [31]

6.4.2 SURFACE VEHICLES

An example of the application of Mercker's method to a simple, rectangular-block automotive shape [8] near the ground is presented in Figure 6.14. Data from two versions of the model are shown - the low-drag model having rounded leading edges and attached front-end flow and the high-drag model having slightly bevelled front edges and a front-edge separation. It can be seen that the correction is not perfect, but that this method agrees well with a correction based on ceiling pressure measurements developed by Hackett, Wilsden and Lilley [18]. The residual error with increasing blockage may have resulted from non-blockage differences in the models or their test installation.

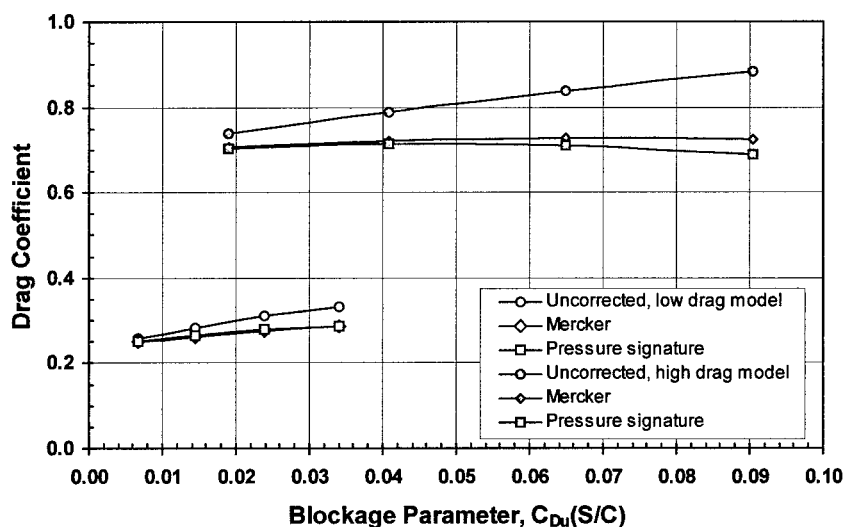


Fig. 6.14: Application of Mercker's Solid-Wall Correction to Bluff Automotive Shapes Near the Ground at Zero Yaw Angle [8]

6.4.3 MISCELLANEOUS

A final example is provided by measurements on parachutes made by Macha and Buffington [32] in six different wind tunnels. The authors found that Maskell's empirical blockage constant of $\theta=2.5$ was too large, overcorrecting the measurements. A more appropriate value of $\theta=1.85$ was found by fitting the data. The use of the two-step method returned nearly the same result as the adjusted constant, improving the correction, as seen in Figure 6.15.

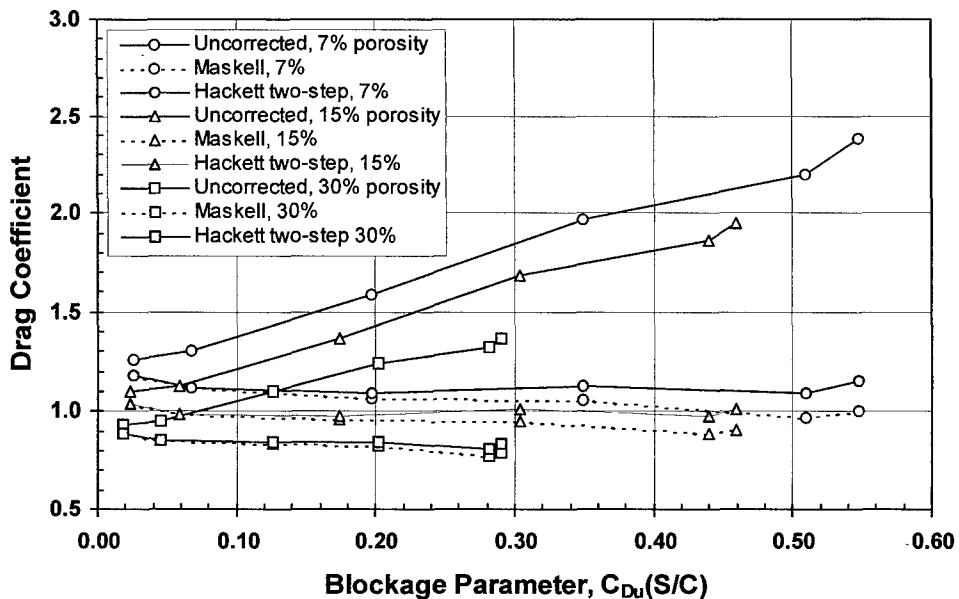


Fig. 6.15: Comparison of Maskell's Method and Hackett's Two-Step Version Using Measurements on Parachutes [32]

6.5 APPLICATION TO OPEN TEST SECTIONS

6.5.1 SURFACE VEHICLES

The open tunnel correction has been recently developed. It is supported by the data presented by Mercker and Wiedemann [26,27] based on measurements on a full-scale automobile in a series of open and closed wind tunnels. These measurements had initially shown different drag coefficients in the various open wind tunnels. Further, the drag coefficients measured in the open wind tunnels were lower than the measurements from the closed tunnels, even when the closed tunnel results were corrected for blockage. The application of the open-tunnel correction procedure reduced the differences between the open tunnels and brought the results from the open and the closed tunnels into close agreement.

Another example is provided through measurements of the variation with longitudinal position of the aerodynamic drag of a passenger car and a van, made by Mercedes-Benz in their 32.6 m² open-jet wind tunnel [33]. The sedan and van had area ratios of 0.065 and 0.116, respectively. The reference dynamic pressure was measured using both the nozzle and the plenum methods. Each method resulted in significantly different drag coefficients and both methods produced drag coefficient curves that had large slopes with longitudinal position. These trends can be seen in Figure 6.16. The bumpers of the vehicles were at the exit plane of the nozzle at the furthest upstream positions.

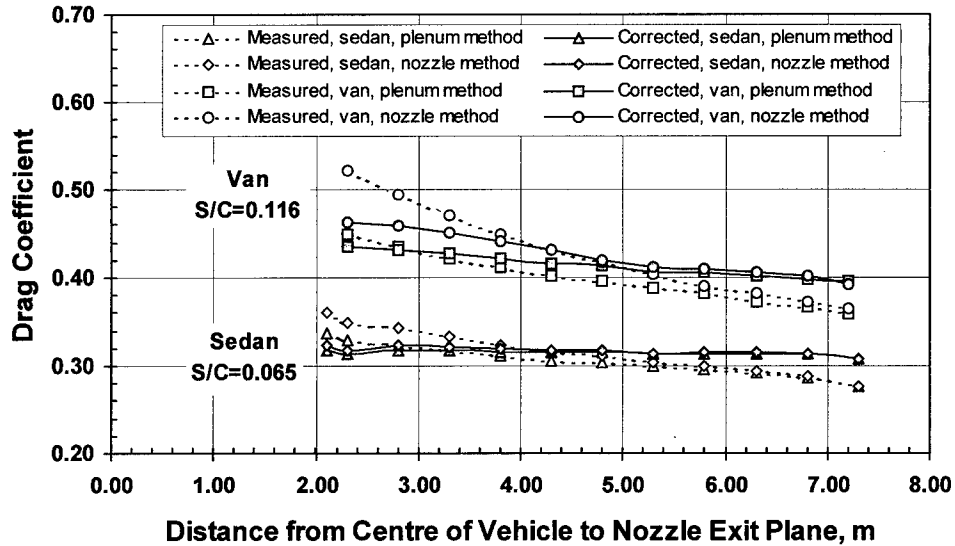


Fig. 6.16: Capability of Mercker's and Wiedemann's Open-Jet Correction [27] For Automotive Models

The application of Mercker and Wiedemann's correction produced almost horizontal drag coefficient curves with changing position for the sedan that were nearly identical for both dynamic-pressure-measuring methods. The correction was not as successful with the higher-blockage van where the corrected drag coefficient curves had residual gradients with position and the curves for the two dynamic-pressure-measuring methods were different. These differences were smaller after correction, however, at the normal 4.8 m measuring location, demonstrating that the method produced a significant improvement in the data. It was possible, that the large, high drag van interfered with the reference static taps.

6.6 REFERENCES

- [1] E.C. Maskell; A Theory of the Blockage Effects on Bluff Bodies and Stalled Wings in a Closed Wind Tunnel. ARC R&M No. 3400, HMSO, London, Nov. 1965.
- [2] H. C. Garner, E. W. E. Rogers, W. E. A. Acum and E. C. Maskell; Subsonic Wind Tunnel Wall Corrections. AGARDograph 109, Paris, France, Oct. 1966.
- [3] F. K. v. Schulz-Hausmann, J.-D. Vagt; Influence of Test Section Length and Collector Area on Measurements in $\frac{3}{4}$ -Open-Jet Wind Tunnels. SAE 880251, Society of Automotive Engineers, Detroit, MI, USA, Feb. 1988.
- [4] Aerodynamic Testing of Road Vehicles – Open Throat Wind Tunnel Adjustment. SAE Surface Vehicle Information Report J2071, Society of Automotive Engineers, Warrendale, PA, USA, 1994.
- [5] T.B. Owen; Measured Blockage Effects on Bluff Bodies in Closed and Open Wind Tunnels. RAE Technical Report 78151, HMSO, London, UK, Dec. 1978.
- [6] R.W.F. Gould; Wake Blockage Corrections in a Closed Wind Tunnel for One or Two Wall-Mounted Models Subject to Separated Flow. Aeronautical Research Council R.&M. No. 3649, HMSO, London, UK, 1970.
- [7] C. Kramer, H. J. Gerhardt, B. Regenscheit; Wind Tunnels in Industrial Aerodynamics. Journal of Wind Engineering and Industrial Aerodynamics, 16 (1984) 225-264, Elsevier Science Publishers B.V., Amsterdam, the Netherlands.
- [8] Closed-Test-Section Wind Tunnel Blockage Corrections for Road Vehicles. SAE SP-1176, Society of Automotive Engineers, Warrendale, PA, USA, Jan. 1996.
- [9] Blockage Corrections for Bluff Bodies in Confined Flows. Engineering Sciences Data Item No. 80024, ESDU, London, UK, Nov. 1980.
- [10] R. Fail, J.A. Lawford, R.C.W. Eyre Low Speed Experiments on the Wake Characteristics of Flat Plates Normal to an Airstream. ARC R.&M. 3120, June 1957.
- [11] C. Farrell, O. Guven, S. Carrasquel and V.C. Patel; Effect of Wind-Tunnel Walls on the Flow Past Circular Cylinders and Cooling Tower Models. The American Society of Mechanical Engineers. 1977.
- [12] F. Cowdrey; Two Topics of Interest in Experimental Industrial Aerodynamics – Part 1: Application of Maskell's Theory of Wind-Tunnel Blockage to Some Large Models. Part 2: Design of Velocity-Profile Grids. NPL Aero Report 1268, April 1968. Presented at the Symposium on Wind Effects on Buildings and Structures, Loughborough University of Technology, Loughborough, UK, April 1968.
- [13] J. E. Hackett; Tunnel-Induced Gradients and Their Effect on Drag. Paper 96-0562, AIAA 34th Aerospace Sciences Meeting, Reno, NV, Jan. 1996. AIAA Transactions, Vol. 34, No. 12, December 1996.
- [14] J. E. Hackett; Tunnel-Induced Gradients and Their Effect on Drag. Lockheed Corporation, LG83ER0108, Smyrna, GA, USA, Sept. 1994.
- [15] AIAA Journal, Feb., 1998.
- [16] J. Courchesne, A. Laneville; A Comparison of Correction Methods in the Evaluation of Drag Coefficient Measurements for Two-Dimensional Rectangular Cylinders. Journal of Fluids Engineering 79-WA/FE-3, 1979.
- [17] R. Taylor; Some Fundamental Concepts in the Theory of Wind-Tunnel Wall Constraint and its Applications. Defence Research Agency, DRA/AS/HWA/TR96055/1, Farnborough, UK, June 1996.
- [18] J. E. Hackett, D. J. Wilsden, and D. E. Lilley; Estimation of Tunnel Blockage from Wall Pressure Signatures: A Review and Data Correlation. NASA CR-152,241, March 1979.

- [19] E. Mercker; A Blockage Correction for Automotive Testing in a Wind Tunnel with Closed Test Section. *Journal of Wind Engineering & Industrial Aerodynamics*. 1986.
- [20] N. H. Lock; The Interference of a Wind Tunnel on a Symmetrical Body. *ARC R&M 1275*, 1929.
- [21] A. Thom; Blockage Corrections in a Closed High Speed Wind Tunnel. *ARC R&M 2033*, 1943.
- [22] H. Glauert; Wind Tunnel Interference on Wings, Bodies and Airscrews. *ARC R&M 1566*, 1933.
- [23] K. P. Garry, K. R. Cooper, A. Fediw, S. B. Wallis, and D. J. Wilsden; The Effect on Aerodynamic Drag of the Longitudinal Position of a Road Vehicle Model in a Wind Tunnel Test Section. *SAE 940414*, Society of Automotive Engineers, Detroit, MI, USA, Feb. 1994.
- [24] R. Buchheim, R. Unger, P. Jousserandot, E. Mercker, Y. Nishimura, F. K. Schenkel, D. J. Wilsden; Comparison Tests Between Major European and North American Automotive Wind Tunnels. *SAE 830301*, Society of Automotive Engineers, Detroit, MI, USA, Feb. 1983.
- [25] K. R. Cooper, H. J. Gerhardt, R. Whitbread, K. P. Garry, G. W. Carr; A Comparison of Aerodynamic Drag Measurements on Model Trucks in Closed-Jet and Open-Jet Wind Tunnels. *Journal of Wind Engineering and Industrial Aerodynamics*, 22 (1986) 299-316, Elsevier Science Publishers B.V., Amsterdam, The Netherlands.
- [26] E. Mercker, J. Wiedemann; On the Correction of Interference Effects in Open Jet Wind Tunnels. *SAE 96061*, Society of Automotive Engineers, Detroit, MI, USA, Feb. 1996.
- [27] E. Mercker, G. Wickern and J. Wiedemann; Views on Nozzle Interference Effects in Open Jet Wind Tunnels. *SAE 970136*, Society of Automotive Engineers, Detroit, MI, USA, Feb. 1997.
- [28] A. Kuhn; Ermittlung der Anströmgeschwindigkeit und der effektiven Windgeschwindigkeit in $\frac{3}{4}$ -offen Fahrzeugwindkanälen. *ATZ Automobiltechnische Zeitschrift* 97 (1995) 2, Germany.
- [29] G. Birkhoff, M. Plesset, and N. Simmons; Wall Effects in Cavity Flow - I. *Q. Appl. Math.*, 8, 2, 1950.
- [30] M. Munk; Some New Aerodynamic Relations. *NACA Report 114*, 1921.
- [31] S. Shindo; Simplified Tunnel Correction Method. *Journal of Aircraft*, Vol. 32, No. 1. January 1994.
- [32] J. M. Macha, R. J. Buffington; An Experimental Investigation of Wall-Interference Effects for Parachutes in Closed Wind Tunnels. *Sandia Report SAND89-1485*, Sandia National Laboratories, Albuquerque, NM, USA, Dec. 1985.
- [33] B. Schwartekopp; Private communication. Daimler-Benz wind tunnel data presented at SAE Subcommittee No. 9, Stuttgart Germany, April 1997.

7. WALL CORRECTION METHODS FOR POWERED MODELS OF CONVENTIONAL TAKE OFF AND LANDING AIRCRAFT

AUTHORS : J.E. HACKETT (CHAPTERS 7.1, 7.2, 7.4.2 - 7.4.4)
 P. R. ASHILL (CHAPTER 7.3)
 M. MOKRY (CHAPTERS 7.4.1, APPENDIX)

	PAGE
LIST OF SYMBOLS FOR CHAPTER 7	7-3
7.1 INTRODUCTION	7-4
7.2 DETERMINATION OF MODEL POWER SETTINGS	7-4
7.3 WALL CORRECTIONS FOR JET-POWERED MODELS	7-5
7.3.1 THE TEST ENVIRONMENT	7-5
7.3.2 ENTRAINMENT EFFECTS FOR JET-POWERED MODELS	7-7
7.4 WALL CORRECTIONS FOR PROPELLER-POWERED MODELS	7-10
7.4.1 CONVENTIONAL CORRECTION METHODS	7-10
7.4.1.1 GLAUERT'S METHOD	
7.4.1.2 REPRESENTATION OF A PROPELLER BY A SINK	
7.4.1.3 CORRECTIONS FOR A WINDMILL IN A WIND TUNNEL	
7.4.2 PRESSURE SIGNATURE-BASED CORRECTION METHODS: PROPELLER CALIBRATION	7-14
7.4.2.1 PROPELLER CALIBRATION: DIRECT TUNNEL EFFECTS	
7.4.2.2 AXIAL GRADIENT EFFECTS	
7.4.2.3 INTERACTION WITH TUNNEL-INDUCED VELOCITIES	
7.4.3 SEPARATION OF PROPELLER AND AIRFRAME FORCES AND MOMENTS	7-19
7.4.3.1 INTRODUCTION	
7.4.3.2 STEP-BY-STEP PROCEDURE	
7.4.3.3 APPLICATION TO A SINGLE-ENGINE TEST MODEL	
7.4.3.4 DISCUSSION	
7.4.4 APPLICATION OF TUNNEL CONSTRAINT CORRECTIONS	7-24
7.4.4.1 AIRFRAME FORCE AND MOMENT CORRECTIONS	
7.4.4.2 PROPELLER FORCE AND MOMENT CORRECTIONS	
REFERENCES FOR CHAPTER 7	7-26
APPENDIX: GLAUERT.C	7-27

7 WALL CORRECTION METHODS FOR POWERED MODELS OF CONVENTIONAL TAKE OFF AND LANDING AIRCRAFT

LIST OF SYMBOLS FOR CHAPTER 7 (ADDITIONAL SYMBOLS ARE DEFINED IN CHAPTER 7.4)

A_j	overall cross-sectional area of nacelle nozzle
B	working-section width
C	working-section cross-sectional area
C_{Du}, C_{Lu}	uncorrected drag and lift coefficients
C_{Dtc}, C_{Ltc}	thrust-corrected drag and lift coefficients
C_{Dwb}	drag increment due to wake interference (Figure 7.20)
C_p	pressure coefficient
C_s	spacing between solid blockage source and sink
C_T	net thrust coefficient = $2(\rho_j V_j / \rho_\infty U_\infty)(V_j / U_\infty - 1)$ (Section 7.3)
C_T	thrust coefficient = $T / (\rho n^2 D^4)$ (Section 7.4)
D	propeller diameter
H	working section height
J	propeller advance ratio, V/nD
n	propeller rotational speed, revolutions per second.
Q_{prop}, Q_{model}	in-tunnel dynamic pressure at propeller plane and model reference point. (Figure 7.23)
Q_s	magnitude of solid blockage source or sink
Q_w	wake blockage source strength
R	propeller radius
T	propeller thrust
T_C	propeller thrust coefficient, $T / (\rho V^2 D^2)$
U	stream speed
V_j	mean jet velocity (Section 7.3)
x	axial distance downstream of the calculated position of the origin of the potential core of the jet. (Section 7.3)
α	(Alpha) model angle of attack
ε	blockage factor (generic $\Delta u / U_\infty$)
ρ	air density
Ω	propeller rotational speed, radians/sec

Suffixes

j	jet or efflux
$0, \infty$	conditions far upstream of model

7.1 INTRODUCTION

When considering wind tunnel corrections for powered models, a distinction should be drawn between configurations that rely mainly on direct lift or directed thrust and those that obtain most of their lift aerodynamically. We shall see in Chapter 8 that powered flows dominate the interference for VTOL and some STOL configurations and tunnel effects can be large. However, we shall deal in this chapter with cases for which the thrust vector is horizontal or nearly horizontal, including cruise configurations. Airframe aerodynamics and the thrust-drag balance considerations predominate so the effects of the tunnel on airframe aerodynamics are just as important as the effects on the power unit or units.

Wind tunnel corrections can be applied with some confidence to an isolated power unit under calibration or to an unpowered model test, but significant tunnel/flight matching problems can arise when the two are combined. The principle difficulty occurs when a propeller or simulated jet engine is situated some distance away from the model reference point and axial gradient effects are significant. The problem becomes particularly acute for propeller powered models, because of the need to set rotational speed appropriately. However, a similar problem also arises in setting the thrust coefficient for jet-powered models. The subject of power unit settings will be discussed in Section 7.2.

Features peculiar to jet powered models include inlet effects, mass injection effects, vortical structures in powered streams and entrainment effects for high-energy jets. The tunnel interference implications of these effects will be reviewed in Section 7.3.

The special needs of propeller-powered model testing are described in Section 7.4. Classical corrections are described in Section 7.4.1. The remainder of Section 7.4 concerns tests on a generic, propeller-powered model. Section 7.4.2 describes the propeller calibration process and the application of wall pressure signature corrections procedures to it. The problem of separating propeller from model forces in the presence of a tunnel-induced gradient is described in Section 7.4.3. Having extracted the in-tunnel forces and moments on the propeller, the corrections to the residual airframe measurements are described in Section 7.4.4.

7.2 DETERMINATION OF MODEL POWER SETTINGS.

Whether propeller or jet, power units are often located some distance forward or aft of the aircraft c.g. and differences between tunnel interference at the engine location and that at the model reference point become significant. Vertical or lateral interference gradients may also have to be considered.

As an example, consider a conventional single-engine, propeller-driven aircraft model under test in a closed-test section wind tunnel. Depending on the net axial force on the model, blockage may cause either a velocity increase or a decrease along the tunnel axis. A positive axial velocity gradient induced by the tunnel walls will cause the velocity at the plane of a forward-mounted propeller to be less than that at the model reference point. The advance ratio will be lower than in free air and the thrust will be higher. A possible real-time adjustment would be to reduce the propeller RPM as needed to achieve the desired advance ratio. The swirl angles and flow geometry would then be correct, as would the local interactions with the airframe. However, the thrust and the local surface scrubbing would be too low, because of the reduction in velocity over the propeller blades. Another approach would be to retain the original RPM and reduce the blade angle as needed to achieve the required thrust level. The mean blade angle-of attack and CL would then be consistent with the in-tunnel conditions at the model reference point, though the

twist distribution and swirl would be compromised slightly. Rae and Pope [12] discuss the use of thrust and torque balances to select the best blade setting and give a number of other compromises that can be considered. An example of one of the simpler correction procedures will be given in Sections 7.4.3 and 7.4.4.

Except for the rotational aspects, the situation is similar for jet-powered models. Tunnel effects on thrust-drag matching are again an issue, particularly for aft-mounted engines. There is also the question of corrections for mass flow addition when external air is supplied for direct thrust or when using ejector or air-turbine powered engine simulators (see Section 7.3.1). Because of the higher jet speeds, entrainment into the jet, drawing from a finite tunnel mass flow, is a further consideration (see Section 7.3.2).

7.3 Wall Corrections for Jet-Powered Models

7.3.1 THE TEST ENVIRONMENT

Powered wind-tunnel models suitable for conventional take off and landing aircraft can be divided into two groups:

1. Models representing isolated powerplants, intakes or exhausts to assess the effects of forward speed and angle of incidence or yaw on the characteristics of the powerplant or the component parts of the powerplant.
2. Complete models including simulation of powerplants to assess installation effects.

In both cases the model may inject air into or remove air from the working section. In addition, the effects on wall interference of an exhaust of higher total energy than that of the main flow has to be represented or acknowledged in the method. These flows may be distinguished from the flows over Vertical or Short Take Off and Landing (V/STOL) models considered in Chapter 8 in that the velocity perturbations at the walls are small compared with free-stream speed.

It may be considered that the advent of methods of determining wall interference using measured wall velocities or pressures makes the problem of representing power effects academic. However, when applying these methods, a number of points need to be borne in mind, first, for model-representation methods.

1. A high energy exhaust entrains air from the main flow. Thus to represent a powered model for the calculation of wall interference, a distribution of sinks is required along the axis of the exhaust, as shown schematically in Figure 7.1, together with a source of appropriate strength far downstream to ensure that the static pressure far upstream is not affected by the presence of the model. This effect is likely to be the most serious for high jet velocity ratios, as are found for tests with jet-powered models at low speed, high thrust conditions. The strength of these sinks can be inferred from measurements of static pressure at a number of positions along the walls downstream of the model for solid-wall wind tunnels. For example, provided that the perturbations associated with the model at the wall are 'small', an average of pressures measured at the same streamwise position along the streamwise lines at A and B or C and D could be used in a method such as developed by Hackett et al [6] to determine sink strength for a model at zero lift on the tunnel axis (see Figure 7.1, which illustrates the more general lifting case). For other types of wind-tunnel wall, singularity strength cannot be inferred directly from wall-pressure measurement. Therefore, in this case,

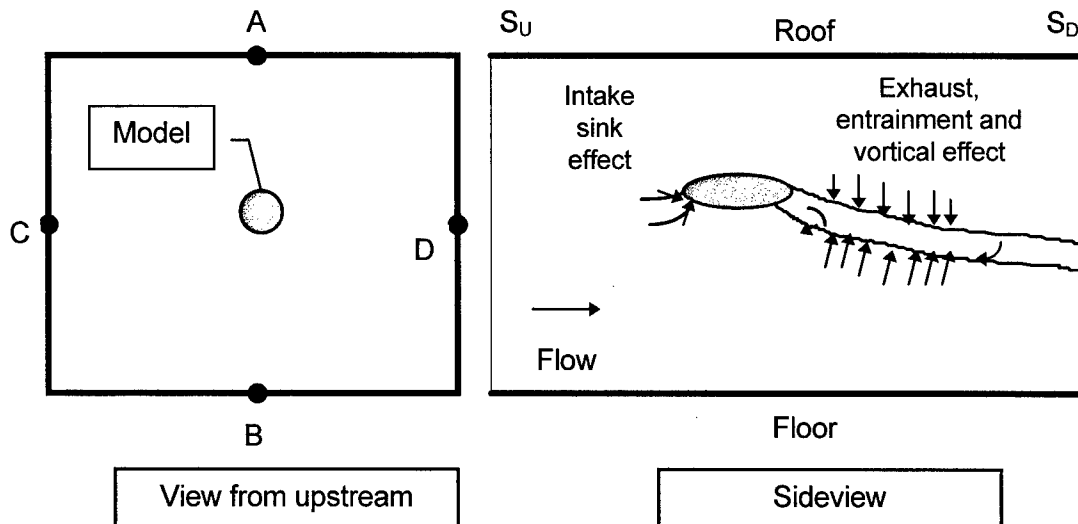


Fig 7.1 A jet-powered, lifting model in a wind tunnel

careful thought needs to be given to the model representation because there could be large errors resulting from the failure to model the direct effect of the model at the walls. This could, in turn, have serious consequences for the estimation of the interference velocity potential at the walls and consequently in the working section.

2. As shown in Figure 7.1, the flow into the intake of a ducted fan or jet engine needs to be represented by either a point sink or a distribution of point sinks on the engine face, the strength of which can be readily estimated knowing the mass-flow characteristics of the powerplant simulator or, if not, by wall pressure measurements made just upstream and downstream of the intake.
3. When the jet axis is inclined relative to the working-section axis, the exhaust is deflected and allowance needs to be made for the antisymmetric effect of the jet. This may be achieved by the use of horseshoe vortices or vortex doublets with axes parallel to the local jet direction. For a solid wall wind tunnel and provided the velocity perturbations at the walls are small compared with the free-stream velocity, the strength of these vortices can be inferred from the difference between the wall static pressures at A and B and for a yawed model from the difference in pressures between C and D (Figure 1).

For two-variable methods the problem of model and jet representation does not arise. However, consideration needs to be given to the conditions at the part of the surface bounding the model far downstream, S_D , as defined in chapter 4.1 and illustrated in Figure 7.1. For a model with a high-energy exhaust, wall pressures can continue to rise some considerable distance downstream of the model. Thus it may not be adequate to use the most downstream pressure measurement as the far-downstream value. A simple expression for the wall pressure coefficient far downstream for powered models has been derived by Ashill and Keating [2].

7.3.2 ENTRAINMENT EFFECTS FOR JET-POWERED MODELS

To illustrate the effects of the intake sink and jet entrainment, results are presented here of wall-pressure measurements made with a jet-powered model in the 13ft x 9ft Low Speed Wind Tunnel at DERA Bedford. This wind tunnel has solid walls. The model comprised an injector-powered nacelle which could either be tested in isolation (Figure 7.2) or in combination with a half model of a wing-body configuration (Figures 7.3 and 7.4). The wing was unswept and cylindrical with a leading-edge slat and a trailing-edge flap. The nacelle could be mounted either 'under' or 'over' the wing as shown in Figures 7.3 and 7.4.

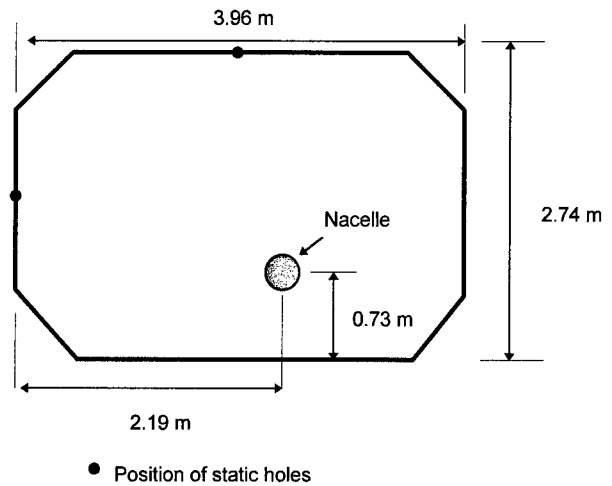


Figure 7.2 View of working section looking downstream, illustrating position of isolated nacelle

Incremental pressures at the roof station due to the effect of power for the isolated nacelle are shown in Figure 7.5. Here the axial distance x is measured downstream of a point about one fan nozzle diameter upstream of the 'hot-jet' nozzle, which corresponds to the calculated position of the origin of the potential core of the jet. The angle of incidence or inclination of the nacelle, α , was obtained by rotating the nacelle about a vertical axis. This axis was offset from the nacelle axis and this explains why the axial positions of the measurement points differ between the three nacelle inclinations. The thrust of the jet is defined by the net-thrust coefficient, C_T , based on the overall area of the nozzle, $A_j = 0.02559 \text{ m}^2$. Thus, since the cross sectional area of the wind tunnel is 10.33 m^2 , this implies that $A_j/C = 0.00248$.

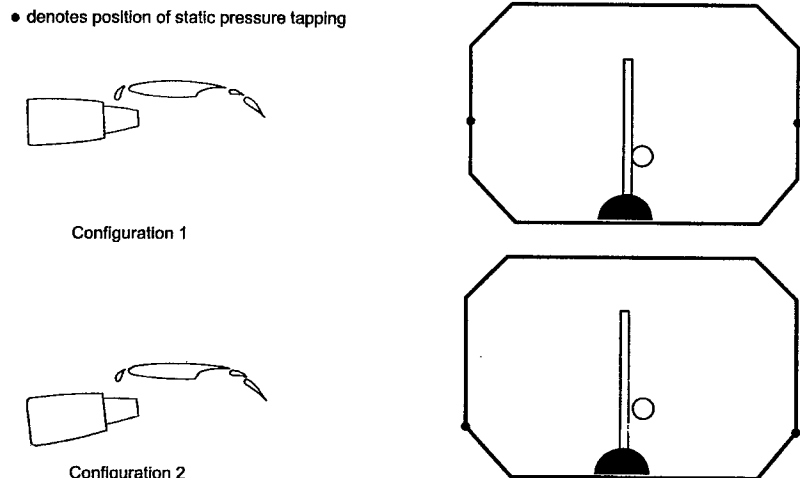


Figure 7.3 Geometry and layout of under-wing nacelle configurations in test section

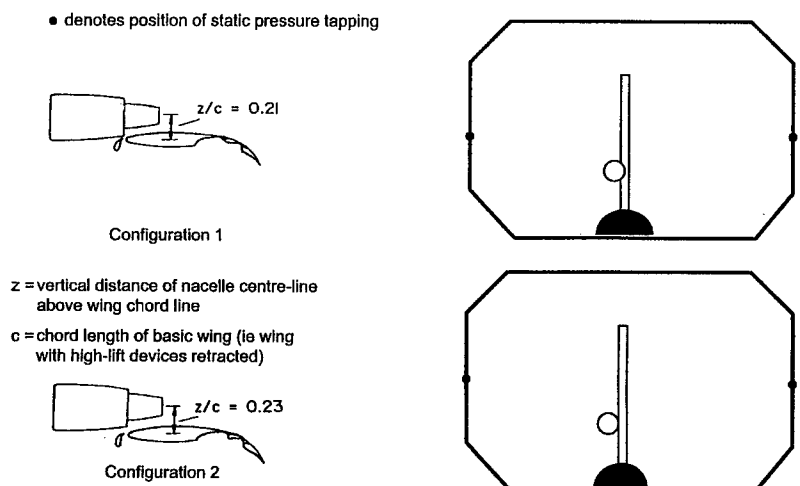


Figure 7.4 Geometry and layout of over-wing nacelle configurations in test section

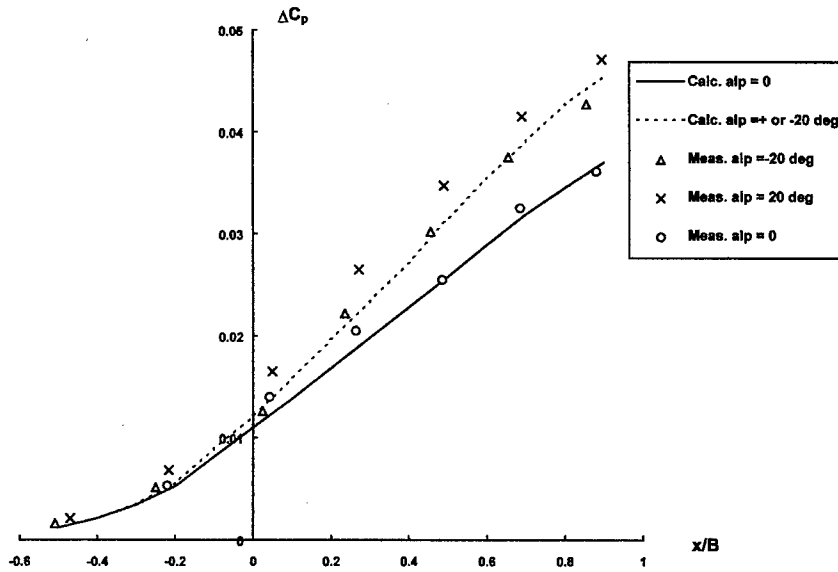


Figure 7.5 Distributions along tunnel axis of incremental pressure coefficient due to thrust at roof station for various nacelle inclinations, isolated nacelle (Fig 7.2), $C_T \approx 33$.

Figure 7.5 shows that the pressure increment increases with axial distance, consistent with the existence of the sink effect of the intake and the jet entrainment. Also shown on the figure are results of calculations made using a model representation method. In this method the intake effect is represented by a sink and the entrainment effect is simulated by an axial distribution of sinks along the jet efflux. The strength of the singularities simulating jet entrainment was determined using the model for jet flows proposed by Bradbury [3] with an empirical modification to allow for jet inclination proposed by Küchemann and Weber [10]. Wall interference was

determined by using the method of images. The agreement between calculation and measurement is fairly good, indicating that the main physical features are represented. This suggests that the wall-induced velocities predicted by this method are reliable. Calculations of the wall-induced blockage have been made for similar flows using a two-variable method (Ashill and Keating [2]) and the results of these are also in good agreement with those of the model representation method.

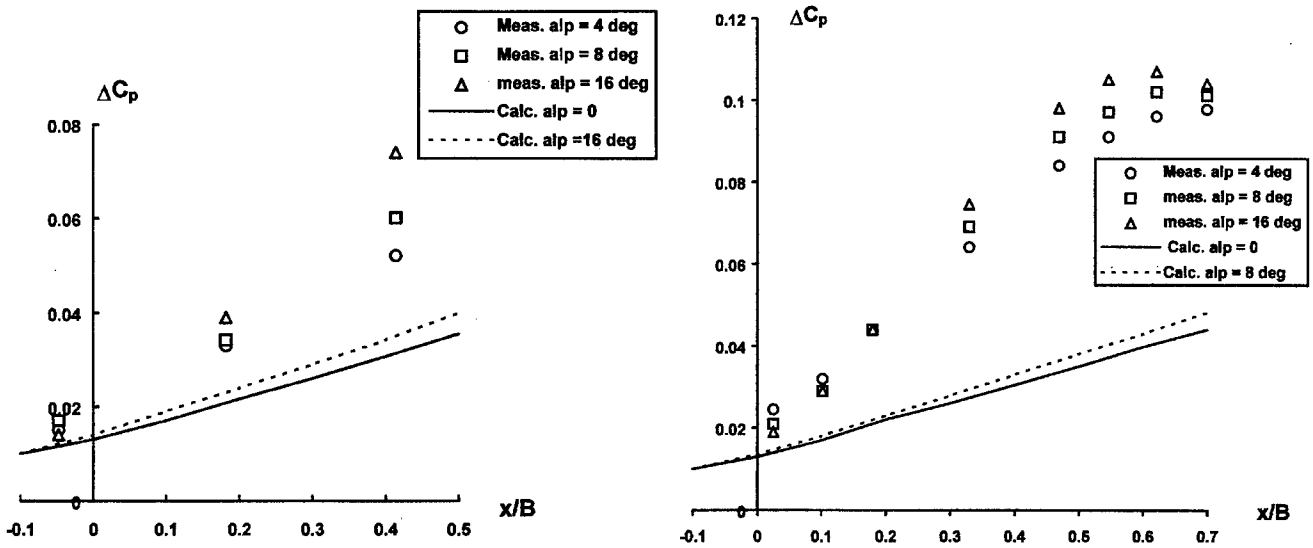


Figure 7.6 Distributions along tunnel axis of mean incremental pressure coefficient due to thrust, under wing configuration Figure 7.3, $C_T = 47.5$

It may be expected that model representation methods are less reliable for more complex flows. Examples of such flows are given in Figure 7.6. The cases shown are for the nacelle mounted under the wing (Figure 7.3), and in these flows the efflux impinges on the lower surface of the flap, providing some lift augmentation by the jet flap effect. To isolate the blockage effect from the lifting (antisymmetric) effect, results are shown for $\overline{\Delta C_p}$ the arithmetic mean of pressure-coefficient increments due to thrust

on opposite walls (see Figure 7.3). In contrast to the isolated nacelle, the model representation method does not give an accurate prediction of the axial variation of the wall pressure increment. However, this method does not allow for the expected large increase in entrainment following the impingement of the efflux on the flap lower surface, with the consequent rapid lateral spreading of the jet. For complex flows of this type wall-pressure signature or two-variable methods are probably the only satisfactory methods available to determine wall interference.

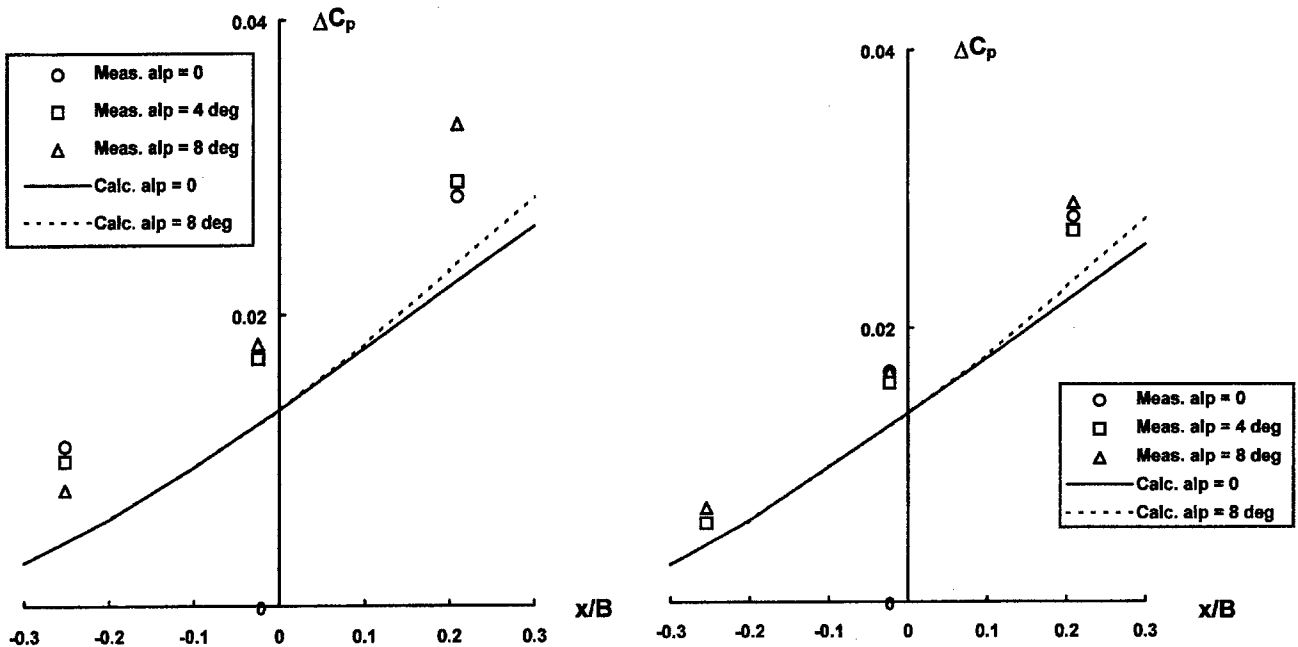


Figure 7.7 Distributions along tunnel axis of mean incremental pressure coefficient due to thrust, over-wing configuration, Figure 7.4, $C_T = 47.5$

Results for the mean pressure coefficient for a flow of somewhat less complexity is shown in Figure 7.7. In these cases the nacelle is 'over' the wing. Consequently, the efflux does not impinge on the flap. Therefore, there is probably little lateral spreading of the efflux and not much increase in the entrainment effect compared with that for the isolated nacelle. This is reflected in the comparatively good agreement between prediction and measurement in relation to the cases with the nacelle mounted under the wing. However, the agreement between prediction and measurement is not as good as for the isolated nacelle. In summary, these results show the importance of the entrainment effect and indicate the need for wall-signature methods to model the sink effect associated with entrainment.

7.4 WALL CORRECTIONS FOR PROPELLER-POWERED MODELS.

7.4.1 CONVENTIONAL CORRECTION METHODS

ADDITIONAL SYMBOLS for Section 7.4.1

A	streamtube cross-sectional area
C_T	thrust coefficient, Eq.(7.21)
f	auxiliary quantity, Eq.(7.5)
m	sink strength
r	distance from propeller centre
V	axial velocity
X	auxiliary quantity, Eq.(7.6)
α	blockage ratio, Eq.(7.2)
ϵ_T	thrust blockage factor
Φ	perturbation potential
η	ideal efficiency, Eq.(7.17)
λ	uncorrected to corrected stream velocity, Eq.(7.1)
σ	propeller disk area to slipstream cross-section far downstream, Eq.(7.4)
τ	Glauert's thrust coefficient, Eq.(7.3)

Suffixes

c	corrected
p	propeller (actuator disc)
T	associated with thrust
0	far upstream
1	far downstream

7.4.1.1 GLAUERT'S METHOD

Using the axial momentum theory, the problem of wall interference on a powered propeller tested in a solid-wall wind tunnel at low subsonic speeds has been solved in the 1930's by Glauert and is described in detail in his monograph (Glauert [5]). The corrected wind-tunnel stream velocity is defined as the free-stream velocity which for a given value of thrust provides the same axial velocity at the propeller as that observed in a wind tunnel. Combined with the appropriate laws of conservation, this condition determines the ratio of the uncorrected and corrected stream velocities,

$$\lambda = \frac{V}{V_c} \quad (7.1)$$

as a function of the blockage ratio

$$\alpha = \frac{A_p}{C} \quad (7.2)$$

and thrust coefficient

$$\tau = \frac{T}{\rho A_p V^2} \quad (7.3)$$

The pertinent geometrical parameters of a slipstream (propulsive streamtube) inside a wind tunnel are shown in Figure 7.8 a. Introducing

$$\sigma = \frac{A_l}{A_p} \quad (7.4)$$

the interdependence is described by the system of 4 non-linear equations

$$f = \frac{(1 - \sigma)(1 - \alpha\sigma)}{\sigma(1 - \alpha\sigma^2)^2} \quad (7.5)$$

$$x = \frac{1 + f}{1 - f} \quad (7.6)$$

$$\lambda = 1 + (x - 1)\alpha\sigma^2 - \frac{(2\sigma - 1)x - 1}{2\sigma} \quad (7.7)$$

$$\tau = \frac{(x + 1)(x - 1)}{2\lambda^2} \quad (7.8)$$

in 4 unknowns: σ , f , x , and λ .

To evaluate λ for the given α and τ , Glauert makes successive sweeps through Eqns. (7.5-7.8), adjusting σ until the prescribed value of τ is obtained. For a small blockage ratio α a suitable initial guess is the value of σ in free air:

$$\sigma = \frac{1 + \sqrt{1 + 2\tau}}{2\sqrt{1 + 2\tau}} \quad (7.9)$$

as may be derived from the subsequently introduced Eqns.(7.10), (7.11) and (7.15).

Although Glauert's method does not result in a simple correction formula, the procedure can easily be coded for a personal computer, producing corrections in a matter of seconds. The Appendix to this section contains the listing of a C-language code which updates σ by targeting on τ by the method of secants. The results, which were found to satisfactorily duplicate the original correction data produced by Glauert [5], are plotted by solid lines in Figure 7.9.

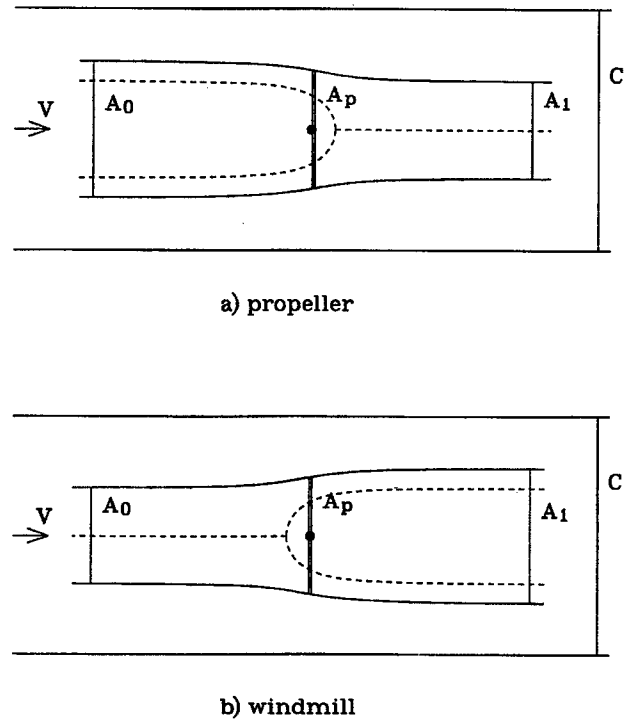


Figure 7.8 Cross-sections of a slipstream and wind tunnel

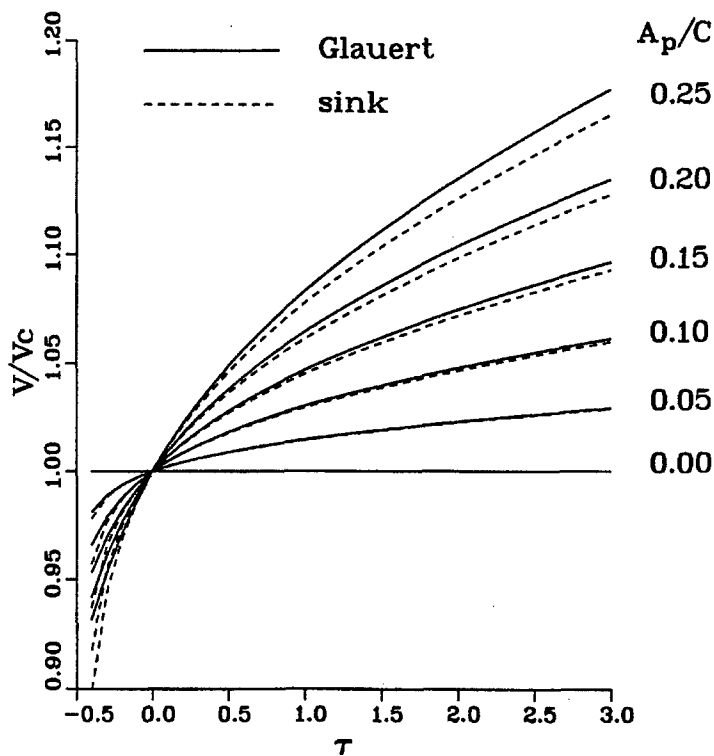


Figure 7.9 Ratio of uncorrected and corrected stream velocities in a solid wall wind tunnel

Glauert's method has successfully stood the test of time and became a standard method for correcting low-speed propeller tests in solid-wall wind tunnels (AGARD [1]). The limitations of the method are that it does not account for the actual shape of the test section and that axial momentum analysis is impossible to extend to ventilated-wall test sections if flow through the walls is not exactly known. Since until recently no alternative method of correction in ventilated wind tunnels has been devised, a large number of propeller tests in the past have been intentionally conducted in solid-wall test sections.

7.4.1.2 REPRESENTATION OF A PROPELLER BY A SINK.¹

As already discussed in chapter 7.4.1.1, the contraction or expansion of the wakes of propellers or windmills can be represented by sinks or sources respectively. This approach opens the doors to the conventional techniques of accounting for wall interference (images, one-variable method, etc.), which are also applicable to test sections of arbitrary geometry or ventilation.

Conservation of mass for incompressible flow inside the propeller streamtube, Figure 7.8a, implies

$$A_0 V_0 = A_p V_p = A_1 V_1 \quad (7.10)$$

From the Rankine-Froude theory it further follows that the axial velocity at the propeller is the average of the upstream and downstream axial velocities

$$V_p = \frac{1}{2}(V_0 + V_1) \quad (7.11)$$

The perturbation observed in the far field (near the walls) can be represented by the potential of a sink

$$\phi = \frac{m}{4\pi r} \quad (7.12)$$

where r is the distance from the propeller centre. The strength m , given by the contraction of the stream, is from Eqns.(7.10) and (7.11)

¹Note that, in this section, source strength has units of length-squared.

$$m = A_0 - A_1 = A_p \left(\frac{V_p}{V_0} - \frac{V_p}{V_1} \right) = \frac{1}{2} A_p \left(\frac{V_1}{V_0} - \frac{V_0}{V_1} \right) \quad (7.13)$$

Equation (7.13) can be derived more rigorously using the Stokes' stream function for a sink in uniform stream (Mokry [11]). It can also be shown that if the slipstream boundary is represented by a stream surface passing through the propeller disk circumference, the location of the sink is slightly upstream of the propeller disk. However, for typical test conditions this distance is negligible compared to the dimensions of the working section.

By the Rankine-Froude theory the thrust is given by

$$T = \frac{1}{2} \rho (V_1^2 - V_0^2) A_p \quad (7.14)$$

and, using Eqn.(7.3) thus

$$\frac{V_1}{V_0} = \sqrt{1 + \frac{V_1^2 - V_0^2}{V_0^2}} = \sqrt{1 + \frac{2T}{\rho A_p V_0^2}} = \sqrt{1 + 2\tau} \quad (7.15)$$

Substituting in Eqn.(7.13) it follows (Mokry [11])

$$m = \frac{1}{2} A_p \left(\sqrt{1 + 2\tau} - \frac{1}{\sqrt{1 + 2\tau}} \right) \quad (7.16)$$

The sink strength can also be related to the efficiency of the propeller. The ideal (Froude) efficiency is

$$\eta = \frac{2V_0}{V_0 + V_1} = \frac{2}{1 + \sqrt{1 + 2\tau}} \quad (7.17)$$

Evidently, $\eta \rightarrow 1$ as $V_1 \rightarrow V_0$ or $\tau \rightarrow 0$, in which case $m \rightarrow 0$. Conversely, $\eta \rightarrow 0$ as $V_1 \rightarrow \infty$ or $\tau \rightarrow \infty$, whereby $m \rightarrow \infty$. From these limits it is apparent that for a given propeller disk area, A_p the sink representing a more efficient propeller is smaller than that representing a less efficient propeller. This is of no surprise, since the efficiency of propulsion, defined as the ratio of the useful work to the total work, is higher if the propeller produces less thrust per unit propeller area.

We shall now discuss how the sink approach compares with Glauert's correction method. Towards this end, consider an infinitely long wind tunnel having a circular cross-section of area C and place a sink of strength m on its axis. Interpreting the corresponding wall interference effect as a negative wake blockage, the correction to the stream velocity at the sink is (Wright [14])

$$\Delta V = -\frac{Vm}{2C} \quad (7.18)$$

The ratio of uncorrected and corrected velocities is thus

$$\frac{V}{V_c} = \frac{V}{V + \Delta V} = \left(1 - \frac{m}{2C} \right)^{-1} \quad (7.19)$$

The sink strength is calculated from Eqn.(7.16) and the evaluated velocity ratio compared with that obtained by Glauert's method, chapter 7.4.1. The results shown in Figure 7.9 indicate that for blockage ratios $A_p/C < 0.10$ there is a close agreement of both methods. The discrepancy at larger blockage ratios is due to the fact that Glauert's correction technique utilises conservation of the axial momentum. To enforce agreement with Glauert, the sink strength would have to be adjusted (increased) as the blockage

ratio grows. This confirms some more recent observations (Hackett [7]) that singularities representing a model in the wind tunnel should be considered wind-tunnel dependent. For propeller-wing-body combinations, it is more convenient to work with the thrust blockage factor, which for a solid-wall test section is given by

$$\varepsilon_T = \frac{V_c}{V} - 1 = \frac{\Delta V}{V} = -\frac{m}{2C} \quad (7.20)$$

The thrust blockage factor is additive with the solid and wake blockage factors representing the other components of the model and their wakes. Substituting for m from Eqn.(7.16) and introducing an alternative form of the thrust coefficient

$$C_T = 2\tau \quad (7.21)$$

we obtain the thrust blockage factor for a solid-wall test section (Kupper [9]) :

$$\varepsilon_T = -\frac{A_p}{4C} \frac{C_T}{\sqrt{1 + C_T}} \quad (7.22)$$

Although the sink method is less rigorous than that by Glauert, its advantage lies in the fact that it is also applicable to working sections having ventilated walls. The extension of Eqn.(7.18) to ideal porous-slotted wall is obtained by using the theoretical result derived for a source by Wright [14]. The discussion of methods appropriate to ventilated working sections in general is given in Sections 3 and 4.3.

The evaluation of the sink strength for a compressible-flow slipstream is considerably more involved, since the axial velocity is discontinuous across the propeller disk and power is not uniquely determined by thrust. However, for highly efficient propellers at Mach numbers up to about 0.8, the value of m obtained from Eqn.(7.16) is adequate for the practical evaluation of blockage (Mokry [11]).

7.4.1.3 CORRECTIONS FOR A WINDMILL IN A WIND TUNNEL.

The axial momentum theory can also be applied to wall interference on a windmill tested in a wind tunnel. Since the windmill is designed to take power from the wind tunnel stream, it will experience a negative thrust or drag. The fluid is decelerated in the streamwise direction as the cross section of the slipstream increases, see Figure 7.8 b. Assuming $0 < V_1/V_0 < 1$, it follows from Eqn. (7.15) that for a windmill the thrust coefficient is restricted to the interval $-0.5 < \tau < 0$. To our knowledge, Glauert [5] has not considered applying his method to the windmill problem, but as the reader may have already noticed in Figure 7.9, the method produces results even for the negative values of thrust. The only difficulty is experienced when approaching the lower limit $\tau = -0.5$, where the slopes of the V/V_0 vs τ curves become very large and the method of successive approximations fails.

The far field effect of the windmill can also be represented by Eqns.(7.12-7.13). Since $A_1 > A_0$, we obtain $m < 0$, indicating that the singularity described by Eqn.(7.12) is a source. A practical evaluation of the velocity correction can be done as for the wake blockage, see for example Section 2.2.2.3. Another reference is made to windmill testing in chapter 7.4.2.1 .

7.4.2 PRESSURE SIGNATURE-BASED CORRECTION METHODS: PROPELLER CALIBRATION

This sub-section and the next will describe the application of the wall pressure signature method to a generic single-engined trainer model with a tractor propeller. The propeller was small compared to the

tunnel cross section, having a disk area only 2.02% of the test section area. Nonetheless, the data obtained were of good quality and the limited model size did not impede the present demonstration of correction methods. We shall consider first the application of the method to the propeller calibration process. Application in a whole-model test will be described in sections 7.4.3 and 7.4.4.

7.4.2.1 PROPELLER CALIBRATION: DIRECT TUNNEL EFFECTS.

The propeller was mounted on the tunnel centreline at the front of a long body that could be yawed. Pitch capability was unnecessary because the rig was axisymmetric. The propeller and drive motor were metric and forces and moments on them were transmitted to a below-floor tunnel balance. The cylindrical shielding around the motor and drive was non-metric and pressure taps were provided behind the spinner and at other locations on the metric/non metric interface. These were used to estimate pressure tares. Body tares and baseline roof pressures were measured with the propeller removed.

Figure 7.10(a) shows pressures measured on the wind tunnel roof during propeller calibration. Baseline pressures have been removed and the reference levels reset from an upstream to a downstream datum. Increasing pressures and decreasing velocities (Figure 7.10(b)) may be seen as the slipstream contracts. The lowest T_C value (filled circles) had no power input to the motor and the windmilling propeller produced a small drag.

The source-source-sink version of the pressure signature program is appropriate for analysing data of the present type. However, the standard program does not work properly for the propeller tested alone, because of the absence of a solid blockage 'hump' in the pressure signature (see Figure 7.10(a)). As an

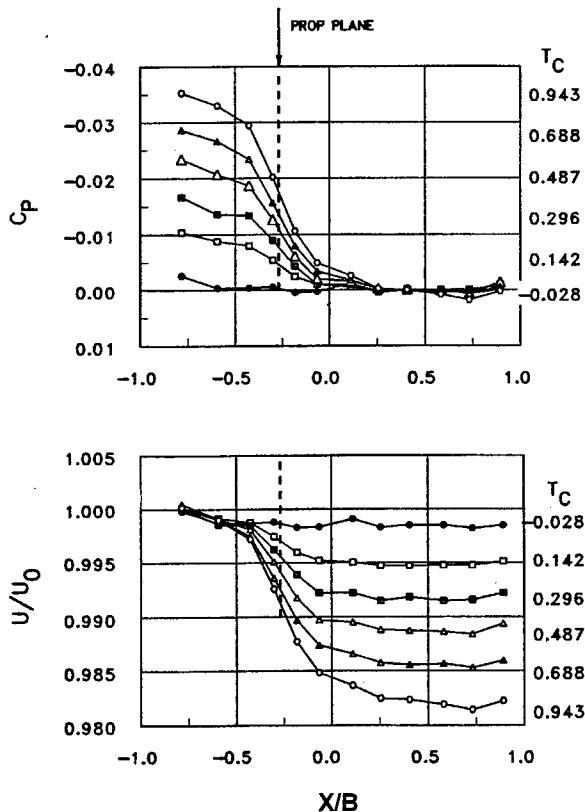


Figure 7.10 Typical data from propeller calibration test
(a) Measured tunnel roof cps
(b) Derived surface velocities

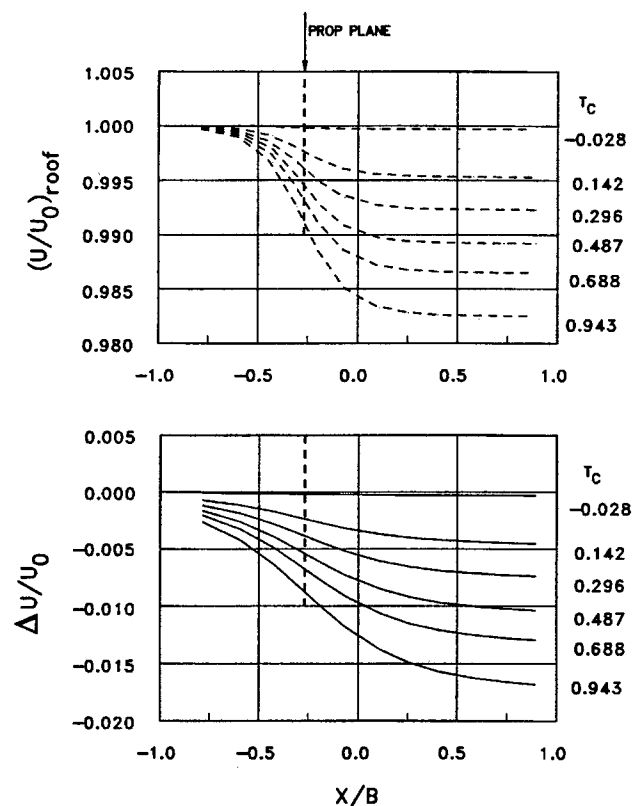


Figure 7.11 Tunnel conditions derived from wall pressures
(a) Velocities at the tunnel roof
(b) Centreline interference velocities

alternative, it was found that a single sink placed at the centre of the propeller represents it very well for estimating blockage. Figure 7.11(a) shows calculated roof velocities based on a single sink, and its wind tunnel images, whose strength was chosen by matching the measured asymptotes of Figure 7.10(b). Overlaying these two figures showed that the single sink represents the propeller well. Differencing the two data sets revealed only small random variations, with no discernible trends. Figure 7.11(b) shows the corresponding centreline interference that represents a decrease in velocity from the set value.

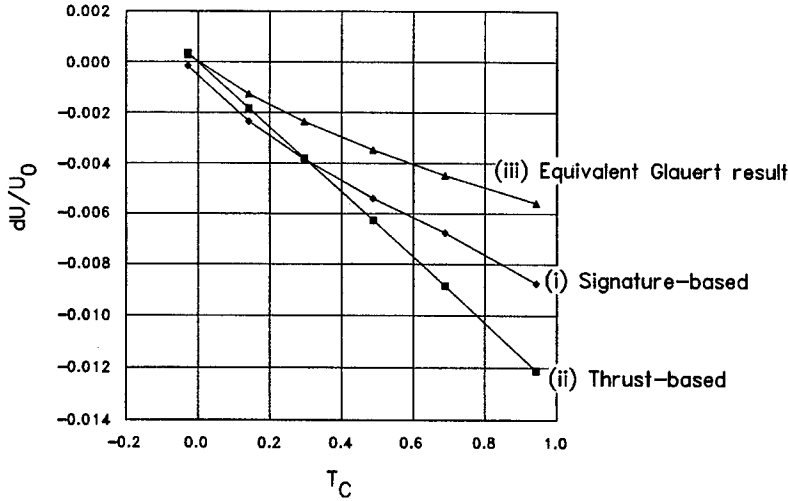


Figure 7.12 Changes in tunnel speed due to image effects

The interference velocities at the propeller plane, shown in curves (i) and (ii) of Figure 7.12, are used to estimate both the q-correction at the propeller and the change in thrust that occurs due to the change in advance ratio. Curve (i), which is a cross-plot of Figure 7.11(b), shows pressure signature results. Curve (ii), based on measured thrust, represents the classical result. The signature-derived interference velocities are about 75% of the force-derived ones. The difference between these curves is attributed to

increased scrubbing drag on the centrebody and possible changes in tunnel-wall skin friction caused by propeller-induced pressure gradients. Both increase the positive blockage, compared with the thrust-derived result.

Curve (iii) of Figure 7.12 is the Glauert result of the previous section, expressed as an increment. This result is solely thrust-based so it is surprising, at first, that the interference increment is only about half of that of curve (ii), which is also thrust-based. However curves (i) and (ii) reflect only the effects of velocity changes whereas the Glauert analysis gives an equivalent velocity that includes other effects.

Figure 7.13 shows the result of applying the corrections of Figure 7.12 to the propeller characteristic curve. Figure 7.14 gives the same information in a more visible, incremental form. It is emphasised that only corrections to thrust coefficient and advance ratio, as they occur in the tunnel, are involved at this point. Interactive effects, which will be discussed later, affect the measured thrust but are not involved directly in the tunnel corrections.

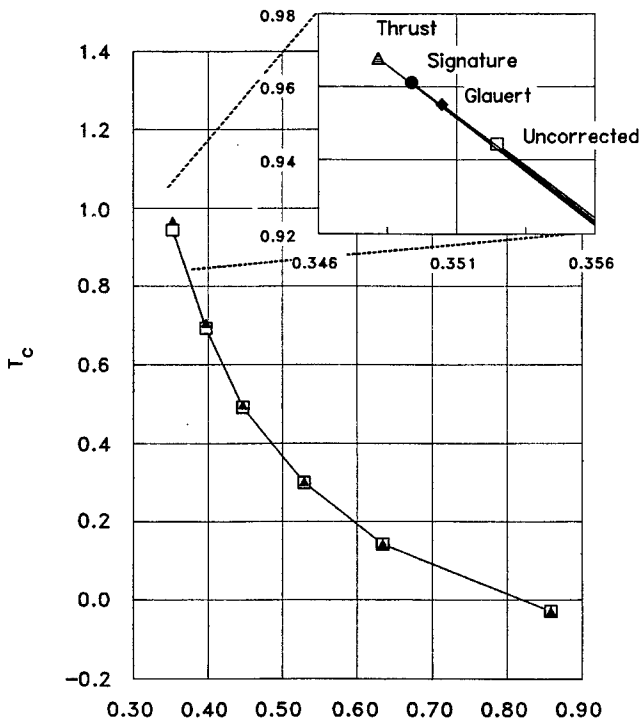


Figure 7.13 Uncorrected and corrected propeller characteristics

As already mentioned, the present model and its interference increments are small. The characteristics of the various correction procedures are illustrated by the top point of the propeller characteristic, shown inset in Figure 7.13. As already noted, the blockage is negative for a thrusting propeller. The thrust-based procedure, which parallels one of the standard methods used for drag (the 'quarter S/C' method), gives the greatest correction. Viscous effects in the tunnel test section are the most probable cause of the reduction in signature-based interference compared with the thrust-based value.

Both the Glauert and the pressure signature procedures recognise the higher total pressure of the slipstream. This is explicit for Glauert's analysis but occurs in the pressure signature method because real flow measurements are used. However, the downstream condition employed by Glauert differs from the other two methods when changes at the model are calculated. At this stage, neither the thrust-based and signature methods recognise the dual-stream condition but Glauert's momentum analysis does. It is not clear whether this is the reason for the lower interference given by the Glauert correction.

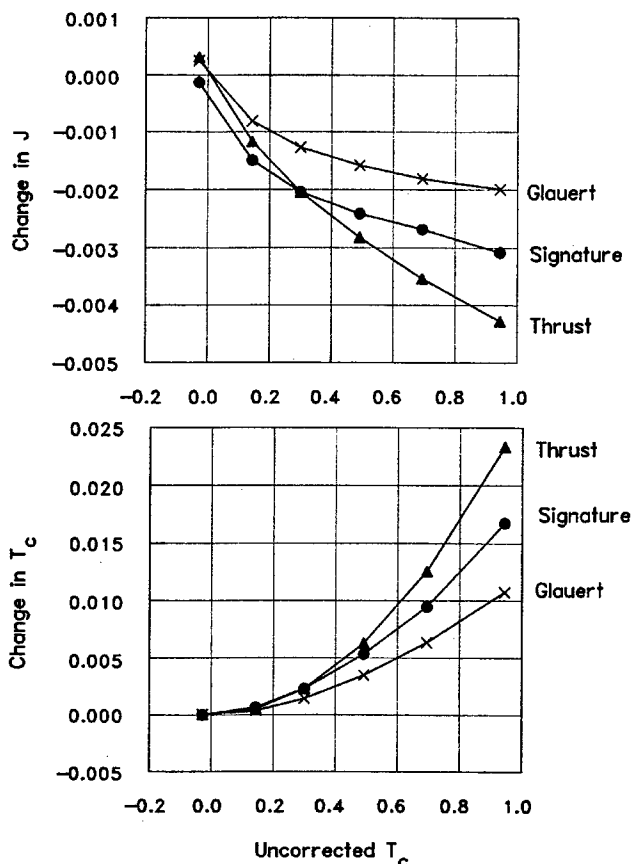


Figure 7.14 Changes in propeller parameters due to blockage (a) advance ratio (b) thrust coefficient

7.4.2.2 AXIAL GRADIENT EFFECTS

Hackett [7] describes the effect of an axial gradient on a separation bubble behind a normal flat plate (see also Chapter 6 of this document). A drag increment is derived, proportional to source-strength squared, that represents an in-tunnel drag increase. Similar principles apply for propeller testing except that the senses of the gradients and the resulting drag increments are reversed. It is suggested that

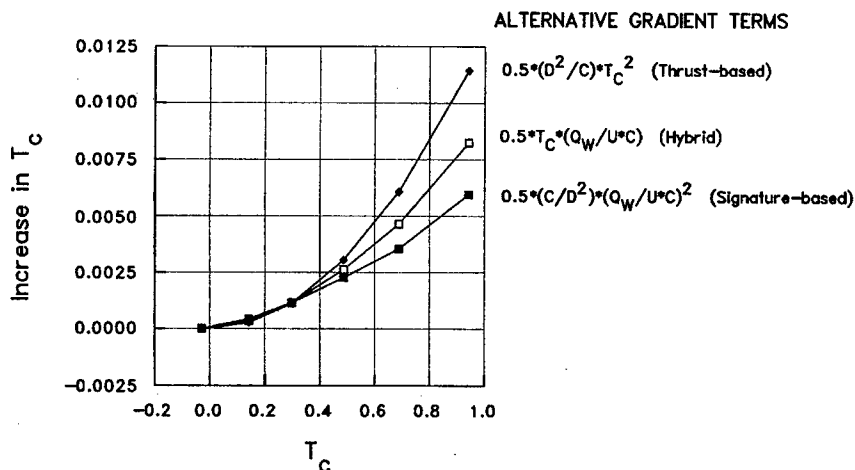


Figure 7.15 Gradient induced thrust increases on a propeller during calibration

adverse pressure gradients (e.g., Figure 7.10(a)) shorten the slipstream contraction and cause an increase in thrust that would not occur in free air. This effect is quite distinct from the effect of changes in velocity itself. The result just discussed is hypothetical because the appropriate experimental verifications have not been done for propellers². Figure 7.15, which shows the gradient corrections for the present model, is therefore presented here for information only.

The gradient corrections shown in Figure 7.15 have the same magnitude as the velocity corrections of Figure 7.14. Three versions of the gradient correction procedure are shown. These parallel those discussed by Cooper et al [4] for drag corrections, but are expressed here in terms of the thrust coefficient, T_C . The upper curve in Figure 7.15 is completely thrust-based and would be the only option if wall pressures were unavailable. The lower curve is totally wall-signature based. The curve marked 'hybrid' includes both and is the result of choice. This curve employs measured thrust to determine the source strength and the pressure signature to find the velocity increment applied to it.

7.4.2.3 INTERACTION WITH TUNNEL-INDUCED VELOCITIES.

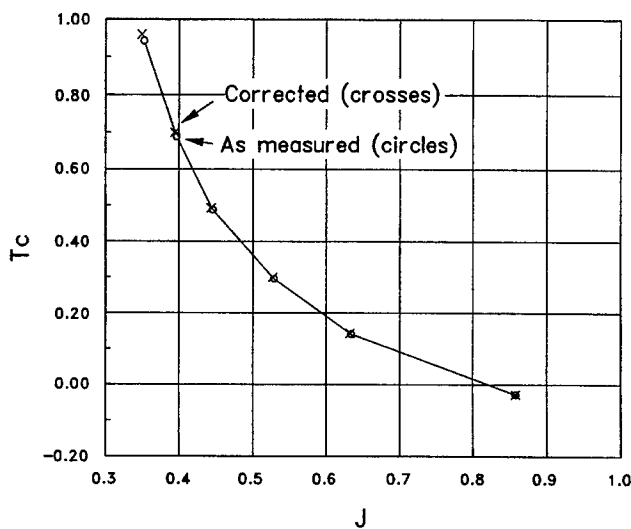


Figure 7.16 Effect of tunnel induced reduction in advance ratio

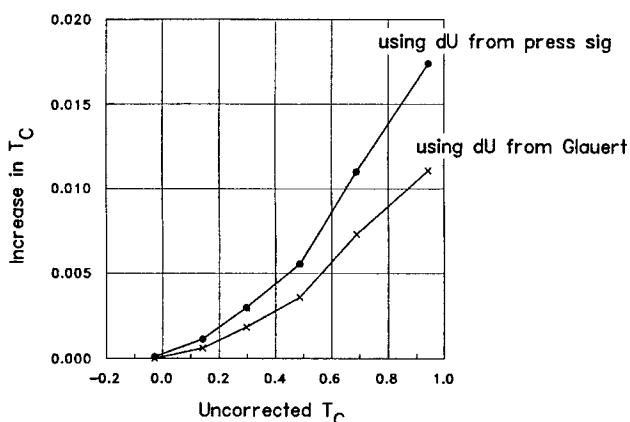


Figure 7.17 Increases in T_C due to tunnel induced reduction in J

The tunnel-induced reduction in velocity at the propeller plane causes the advance ratio to fall below the nominal value at the model reference point (see Figure 7.14(a)). This causes an increase in thrust that would not occur in free air. Figure 7.16 shows this on the propeller characteristic curve. The effect is quite distinct from the tunnel correction procedures just described which, in two of the three cases, involve only velocity renormalisation.

The apparent similarity between Figures 7.13 and 7.16 is deceptive. The shifts in Figure 7.13 are caused by renormalisation on both axes but those in Figure 7.16 reflect thrust increments that are caused by tunnel-induced changes in advance ratio. The advance ratios for the circles in Figure 7.16 are based on the uncorrected tunnel speed. The crosses are placed on the existing curve at the corrected J , using data from Figure 7.14(a). Thrust increments are then read from the curve. The results are summarised in Figure 7.17 for the Glauert and the pressure signature analyses.

Comparing Figure 7.17 with Figure 7.14(b), it is seen that the in-tunnel increase in thrust due to reduced advance ratio and the change due to velocity renormalisation are of similar size. Both the interactive and the direct increments are higher for the pressure signature approach than for the Glauert treatment.

² The experimental verification has, however been done for windmills (see He Dexin (1986))

7.4.3 SEPARATION OF PROPELLER AND AIRFRAME FORCES AND MOMENTS.

7.4.3.1 INTRODUCTION

This section concerns the resolution of whole-model forces and moments into airframe and propeller contributions. There are two motivations. From a project point of view, resolved airframe-only data can be combined, without further testing, with propeller data for a different blade angle or blade design. The implicit assumption is that propeller-airframe interactions at a given thrust level are not significantly different from the baseline. From a test point of view, it is essential to remove propeller forces and moments before applying tunnel constraint corrections to the rest of the airframe. This is because of the peculiarities of propellers, particularly their sensitivity to forward speed. The appropriate tunnel corrections are applied separately to prop and airframe data. Corrected forces and moments can then be recombined as needed.

The preferred way of separating propeller and model forces is to use a propeller balance. This gives not only a direct measurement of thrust and other forces but also propeller torque, which is of great interest in its own right. However such balances increase test complexity and cost significantly and a procedure using an extended propeller calibration (see Section 7.4.2) is frequently used instead. A procedure for using such a calibration will be described below.

Either the prop-balance or the calibration approach gives a set of uncorrected airframe forces and moments and a corresponding set of uncorrected propeller forces and moments. With certain exceptions that will be described in Section 7.4.4, conventional tunnel corrections may be applied to the airframe data. Tunnel effects are recognised as a part of the propeller-force removal process, below, but this does not address the conversion of propeller forces to the free air condition. This will be described in Section 7.4.4

The discussions below start with a step-by-step review of the thrust-removal process, followed by a test example that illustrates some major features. The step-by-step procedure covers combined pitch and yaw conditions but the test examples will be for zero-yaw only.

7.4.3.2 STEP-BY-STEP PROCEDURE

If prop-balance data are unavailable, propeller force and moment calibrations (see 7.4.2) may be employed. These calibrations include off-axis angles and are corrected to the free-air condition. The following procedure is used to remove the forces and moments acting directly on the propeller from the measured whole-model values:

- (1) Calculate the total in-tunnel velocity and dynamic pressure at the propeller hub. Adjustments for tunnel blockage effects must be included. Tunnel-induced upwash effects may need to be considered but lateral constraint effects are generally found to be insignificant.
- (2) Starting with aircraft pitch and yaw angles, determine the total inflow angle between the mainstream velocity vector and the propeller axis and the roll angle around the prop axis at which this occurs. The off-axis angle is equivalent to the yaw angle in the calibration described above.
- (3) Calculate the propeller advance ratio using the total velocity found in (1).
- (4) Using the propeller calibration at the off-axis angle and advance ratio calculated in (2) and (3), determine the thrust coefficient and the other five force and moment coefficients acting on the propeller. The calibration gives these in the off-axis/roll angle co-ordinates. These forces and moments are normalised using the dynamic pressure at the propeller hub.

- (5) Resolve the forces and moments just found to aircraft wind-axis co-ordinates and transfer them to the model reference point. Adjust for any alignment differences and offsets between the propeller and model axes.
- (6) Re-normalise the propeller force and moment coefficients found in (5) by multiplying by the ratio of 'q' at the propeller to 'q' at the model reference position or by applying an equivalent incremental correction.
- (7) Subtract the propeller force and moment coefficients generated in (6) from the corresponding whole-model values.

The in-tunnel forces and moments on the propeller have now been removed from the measured data leaving the airframe loads, which include slipstream-induced loads. The main tunnel corrections remain to be done.

7.4.3.3 APPLICATION TO A SINGLE-ENGINED TEST MODEL

The single-engined model had a tractor-propeller with a disc area of 2.02% of the tunnel cross section. The wing span was 57.3% of the tunnel width and the wing area was 7.09% of the tunnel cross section. The model was mounted on the centreline of the tunnel. Mid-height sidewall pressures were measured

for blockage estimation.

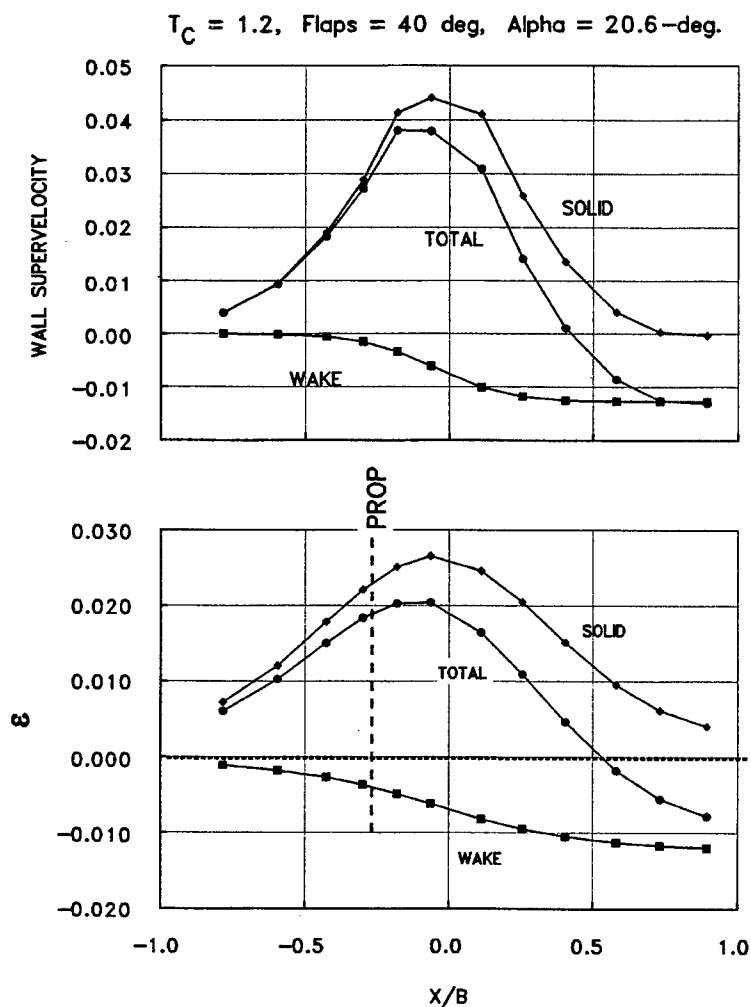


Figure 7.18 shows a typical set of sidewall data (upper plot) resolved into solid and wake-related components. At a thrust coefficient, T_C , of 1.2 and 40-deg flap there is excess thrust and a descending profile is seen for the wake component of the signature. The lower plot shows interference velocities derived from the measurements. The most noticeable feature of the total interference curve is the strong negative interference gradient aft of the model. The difference in total ε between the model reference point, at $X=0$, and the propeller plane is very small for this particular case.

Figure 7.18 Wall signature analysis and resulting interference distribution

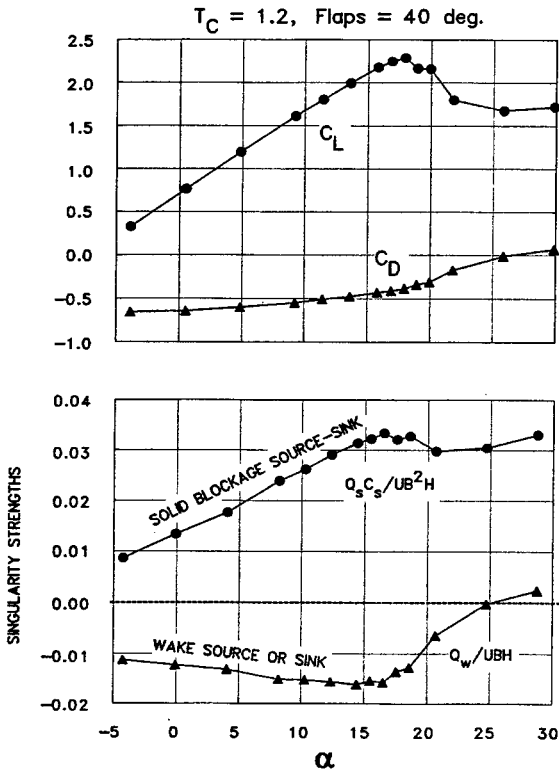


Figure 7.19 Measured force and flow model characteristics

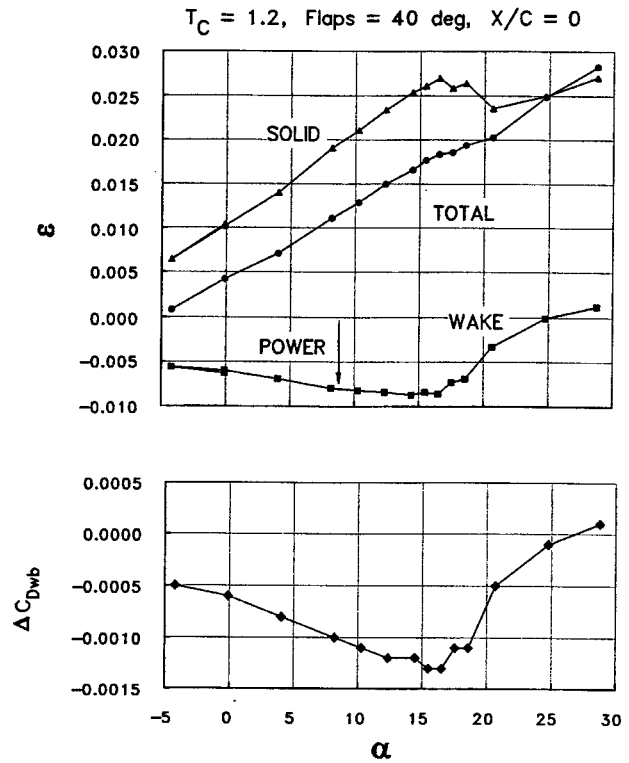


Figure 7.20 Interference break down as a function of angle-of-attack

Figure 7.19 (upper plot) shows the lift and drag characteristics of the model for $T_C = 1.2$ and 40-deg flap, together with solid and wake singularity strengths (lower plot) derived from pressure signatures. At this thrust level, the propeller thrust dominates the wake source strength until well into the stall. The product $Q_s C_s$ represents the effective doublet strength of the model and follows the same trend as the C_L curve. Figure 7.20 (upper) shows blockage velocities generated using the solid and wake blockage singularities of the previous figure. The total interference increases continuously with angle-of-attack: the post-stall reduction in solid blockage is offset by an increase in wake blockage. The lower plot, which shows the wake-induced blockage increment, follows the trends of the wake source strength itself.

The variation of blockage with power and angle-of-attack may be seen in Figure 7.21. At zero- T_C (upper plot), all the blockage velocities are positive and a rapid increase in blockage at stall is clearly evident. Adding power, with

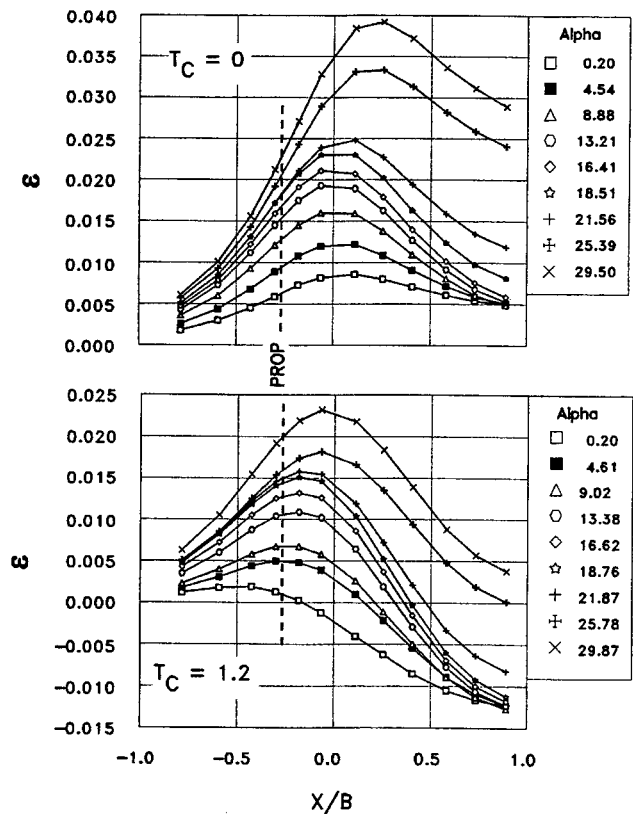


Figure 7.21 Interference at various angles-of-attack, and thrust coefficients of zero and 1.2, (no flap)

zero flap (lower plot), reduces the blockage velocities markedly and increases the negative gradient aft of the model. The increment in between the propeller and model reference locations can be either positive or negative, depending on angle-of-attack. This increment determines the adjustment that must be made to the nominal J-value before reading propeller thrust from the propeller calibration curves in Step (4), above.

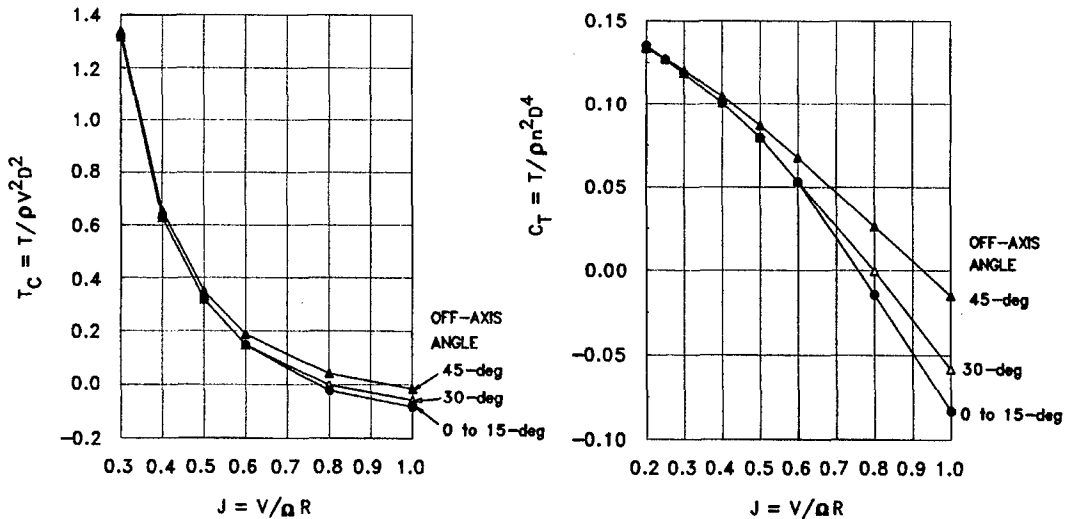


Figure 7.22 Effects of off-axis angle on propeller calibration. a) as T_C , b) as C_T

The propeller characteristics are presented in terms of T_C in the left plot of Figure 7.22. Curves are shown for off-axis angles ranging from zero to 45-degrees. In the examples shown here, which are for zero-yaw, the off-axis angle equals the angle-of-attack³ and the resolution process is very straightforward. At combined yaw and angle-of-attack, the resultant off-axis angle must be used when accessing the relevant propeller curves.

Expressed in terms of T_C , the off-axis angle effect appears weak. However it becomes more noticeable when the characteristic is expressed as C_T (right plot in Figure 7.22). Advantages of using C_T include the fact that the divisor does not include forward velocity (and so is unchanged by tunnel interference) and the fact that the characteristics are less curved. Either form may be used in Step (4), however.

A similar look-up approach is employed for other forces and moments.

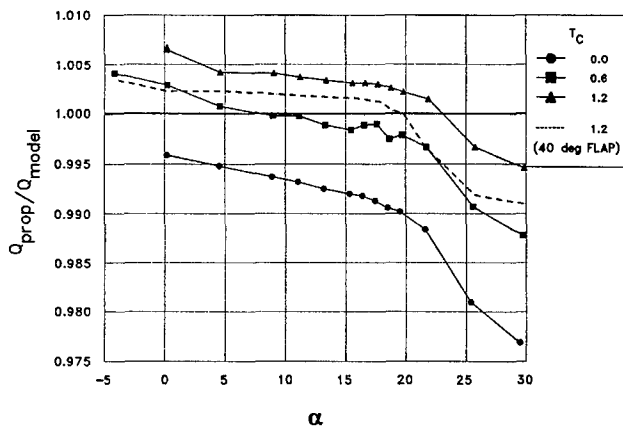


Figure 7.23 Ratio of dynamic pressures for propeller and model positions

Most propeller aerodynamic parameters are normalised on dynamic pressure at the propeller. They must therefore be re-normalised to conditions at $X = 0$ before subtracting them from whole-model values. Figure 7.23 shows the dynamic pressure ratio, used in Step (6), between propeller and model reference locations. This ratio can be greater or less than unity, depending on thrust, angle-of-attack and flap setting.

³Tunnel induced upwash was small and the propeller calibration was not very sensitive to angle so no tunnel correction was made to angle of attack in step 1. Tunnel induced upwash effects may need to be included in this step for larger, multi engined configurations.

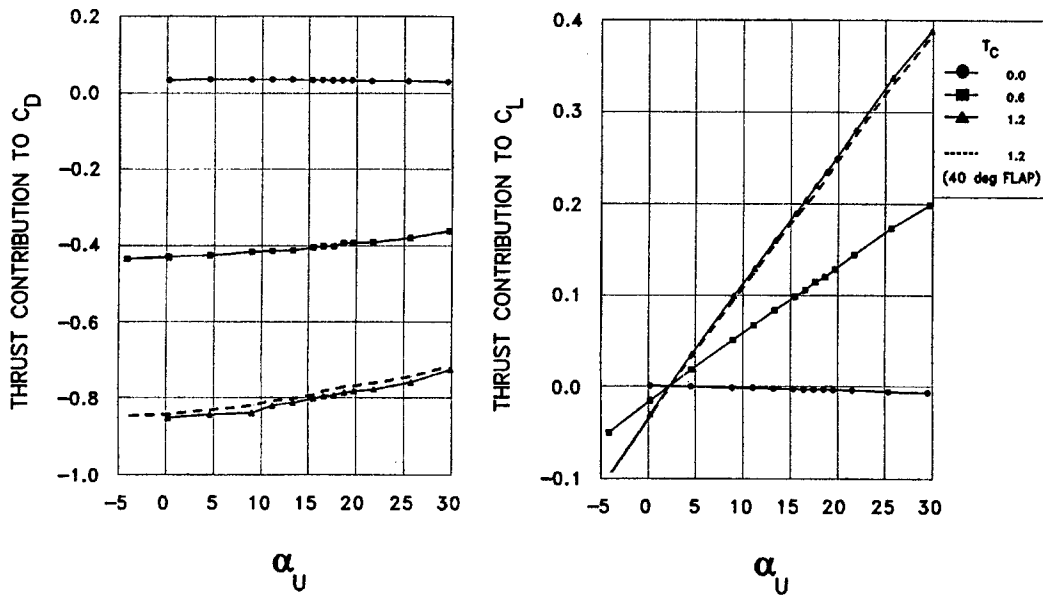


Figure 7.24 Thrust components to be removed from C_L and C_D

In the present zero-yaw cases the propeller-axis force is resolved into lift and drag using only angle-of-attack (Step (5)). Figure 7.24 shows re-normalised propeller thrust resolved into lift and drag components for all the cases considered. A loss in thrust component may be seen when high power is combined with high angle-of-attack (left plot, lowest curve). This reflects the loss of thrust seen under high- α , high thrust conditions in Figure 7.22. Finally, we see in Figure 7.25 the effect of removing the propeller forces from the measured values in Step (7). The left plot shows as-measured data; the right plot shows data with thrust components removed. No tunnel corrections have been applied. Neither the lift nor the drag curves in Figure 7.25 collapse to a single line. There is residual lift, increasing with thrust coefficient, that is probably slipstream-induced on the inner wing. There is also increased drag at high thrust settings. This

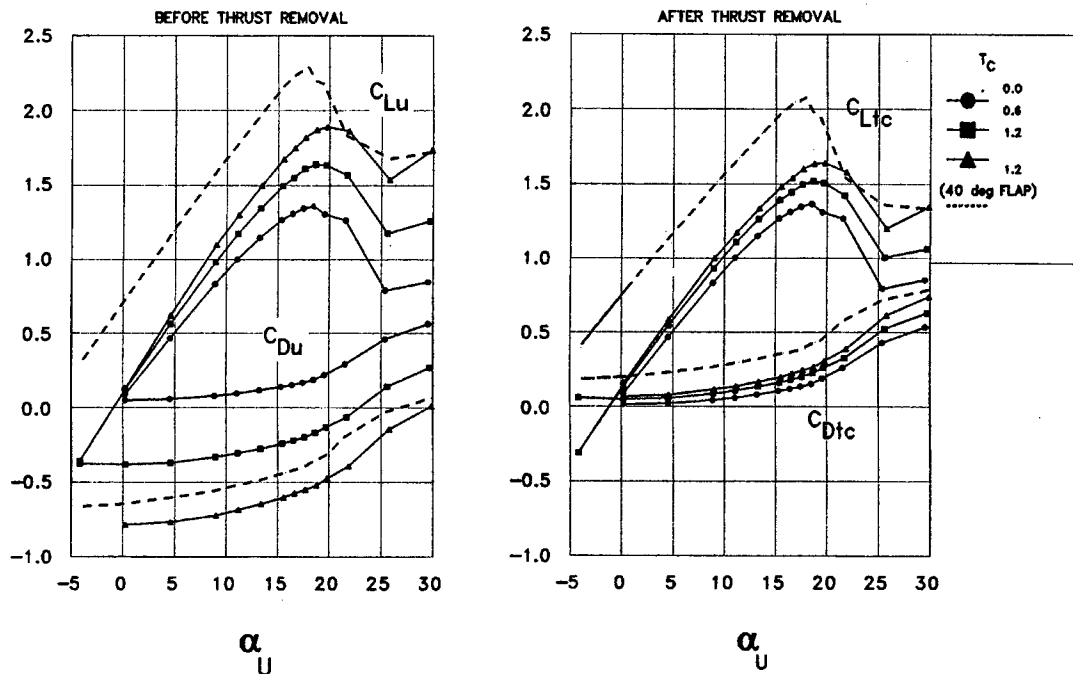


Figure 7.25 Effect of removing thrust components from measured C_L and C_D

certainly includes increased fuselage scrubbing drag and there is probably a vortex drag contribution, associated with slipstream-induced lift. We shall comment on this further in Section 7.4.4.

7.4.3.4 DISCUSSION

The above procedure is one of the simplest possible and so has some shortcomings. Since all data are referred to the model reference point, gradients in tunnel blockage and induced upwash result in conditions at the propeller (advance ratio, off-axis angle) that do not match those that would occur in free air. Consequently, the forces and moments on the propeller are also mismatched, which is why the propeller forces and moments are accounted separately. The mismatched propeller forces and moments are removed properly by the above procedure but the thrust level experienced by the propeller will be different from that in free flight. Consequently, the velocities within the slipstream, the scrubbing drag and any slipstream-induced lift will be slightly in error. These effects are usually secondary and errors in them are not likely to be important. Possible exceptions include situations in which slipstream-generated lift is used to enhance STOL capability, for example. More complicated test equipment and procedures (prop balances, near real-time blade angle tuning, etc.) may be needed in such cases.

7.4.4. APPLICATION OF TUNNEL CONSTRAINT CORRECTIONS

7.4.4.1 AIRFRAME FORCE AND MOMENT CORRECTIONS.

The principal feature that is observed with a propeller operating is the slipstream-induced loads (e.g., Figure 7.25). These will be of particular concern in cases where strong, slipstream-generated lift is present, as on some STOL aircraft. Shevell [13] gives the following description:

"...the total lift consists of the lift from the wing without engine operation, the lift due to deflecting the exhaust stream downward and the additional circulation lift created by the action of the slipstream on the wing and flap system. The additional lift is called powered circulation lift. The physical basis of the latter can be the increased velocity over the wing and/or a larger effective flap chord created by the high-speed exhaust flow roughly parallel to and in the same plane as the flap chord."

The powered circulation lift, described above, is equivalent to a horseshoe vortex, spanning the slipstream at the appropriate chordwise position and carrying the appropriate lift. A further horseshoe vortex may be required to carry slipstream-induced lift on a flap. There is also an increase in wing/flap skin friction that can be represented by introducing a line source across the span involved.

When calculating bound vortex or source strengths for standard constraint corrections, it is usually assumed that a given load is generated at mainstream velocity. However, the flow is accelerated within a slipstream and has higher than mainstream total pressure. The standard procedure will overestimate the singularity strengths in this situation and the tunnel interference will be overestimated. Two alternative procedures will be described that address this.

Kupper [9] gives an analysis of slipstream effects and their correction for a twin engine configuration with wing-mounted nacelles. His analysis is very detailed and slipstream-on-tail effects, for example, are included⁴. Kupper starts by estimating the area of the wing wetted by the slipstream and the local dynamic pressure there. He then determines the power-dependent force and moment coefficient

⁴Kupper does not indicate, however, how the slipstream trajectory and its intersection with the tail is determined

increments and re-scales them by the ratio of mainstream-to-slipstream dynamic pressure. These increments are used to form new power-on coefficients of reduced magnitude, to which tunnel corrections are applied. The principal effect of Kupper's procedure appears to be a reduced correction to angle-of-attack.

The second treatment of slipstream-induced forces parallels the kinematic description of the flow given above. Pressure signature-based corrections to airframe loads are obtained as follows:

- (1) Estimate the slipstream-induced forces, using the modelling techniques described above or those given by Kupper.
- (2) Estimate the corresponding (short-span) singularity strengths, recognising the increased velocity, within the slipstream, that acts on them.
- (3) Calculate the velocities at the tunnel-wall orifice locations induced by the singularities found in (2), with their images. Subtract these velocities from the measured signatures.
- (4) Calculate the effects at the model of the images of the singularities found in (2). This is the interference at the model associated with powered circulation and slipstream scrubbing drag.
- (5) Process the adjusted pressure signatures, from (3), using standard procedures to obtain 'rest-of-model' interference at the model sensing points.
- (6) Combine the interference velocities found in (4) and (5) and apply them as needed.

The relationship between the above approach and that of Kupper is not clear. The factoring of singularity strength is explicit in the treatment above and the use of short-span singularities to represent the slipstream-induced forces has some appeal. It is not obvious that this level of resolution is present in Kupper's approach.

7.4.4.2 PROPELLER FORCE AND MOMENT CORRECTIONS

Free-air propeller calibration data can, in principle, be combined directly with airframe-only data, obtained using the procedures of Section 7.4.3 and corrected as described above. It could therefore be argued that there is no need to retain propeller forces extracted from whole-model tests. Whether this is true depends on whether there are any significant "feed-forward" effects from the wing. For a wing-mounted tractor propeller, for example, bound vortex effects may increase the advance ratio above the wing and decrease the advance ratio below it. The propeller then experiences wing-induced pitching moment and other components. These may be evaluated by comparing propeller balance data with interference-free data obtained from a full, angle-dependent calibration (Section 7.4.2) using the procedure described below. This procedure may also be used to estimate propeller loads, without the need for a propeller balance, if feed-forward is small.

The 'ideal' (no feed-forward) loads on the propeller are found from the propeller calibration in Step (5) of the procedure of Section 7.4.3. This includes the effects of non-zero off-axis angles. The loads are already normalised on local, in-tunnel dynamic pressure and the moment centre is the model reference point. The steps still to be performed concern the reduced-J interaction effect, described at the end of Section 7.4.2, and conventional tunnel blockage and upwash corrections. A further possible correction, for streamwise tunnel gradient, is also described in Section 7.4.2. Whole-model gradients (e.g., Figure 7.21) should be employed when using this correction.

When correcting propeller forces to the free-air condition, it should be recalled that, by definition, the mainstream dynamic pressure at the propeller in free air equals that at the model reference point. It is not

modified by tunnel effects. It follows that, having corrected for the effect of incorrect advance ratio, the position error correction to dynamic pressure (Figure 7.23 and Step (6), above) should not be applied when calculating free-air force and moment coefficients⁵. However, conventional corrections for tunnel blockage and tunnel-induced upwash at the propeller location still apply. Whole-model blockage data (Figure 7.21) and the corresponding upwash data should be used for these corrections.

The above procedure may be summarised as follows :

- (1) Find the 'ideal' (no feed-forward) loads on the propeller using the calibration at the in-tunnel advance ratio and inflow angle. (Step (5) of Section 7.4.3).
- (2) Using the full propeller calibration, determine the loads corresponding to the tunnel-induced change in advance ratio, relative to the model reference position. Subtract these loads from those found in (1).
- (3) Apply standard blockage and angle-of-attack corrections to the loads just obtained using blockage and upwash interference velocities at the propeller location.

A gradient correction may be applied to the propeller loads after Step (2), above (see Section 7.4.2, last paragraph). The u-gradient at the propeller location should be used.

REFERENCES FOR CHAPTER 7

- [1] AGARD, 1984, "Aerodynamics and Acoustics of Propellers" AGARD-CP-366.
- [2] Ashill, P.R. and Keating, R.F.A., 1988, "Calculation of tunnel wall interference from wall-pressure measurements" *Aeronautical Journal*, Vol. 92, No.911, pp.36-53.
- [3] Bradbury, L. J. S., 1967, "Simple expressions for the spread of turbulent jets" *Aero. Quart.* 18, 2, 133-142.
- [4] Cooper, K.R., Hackett, J.E., Wilsden, D.J., 1995, "Closed test section wind tunnel blockage corrections for road vehicles" SAE SP 1176, May 1995.
- [5] Glauert, H., 1947, "The Elements of Aerofoil and Airscrew Theory" Cambridge University Press, 2nd ed., pp.199-207.
- [6] Hackett, J. E., Wilsden, D. J., and Stevens, W. A., 1981, "A review of the wall pressure signature and other tunnel constraint correction methods for high angle of attack tests" AGARD-R-692.
- [7] Hackett, J.E., 1996, " Tunnel Induced Gradients and Their Effect on Drag", *AIAA Journal*, Dec. 1996, pp 2575-2581
- [8] He Dexin, Jiang Giuqing, 1986, "An investigation of wall effect corrections for wind turbine tests in CARDC low speed wind tunnel" China Aerodynamic Research and Development Center Report CARDC-86-1020. (Presented at European Wind Energy Association Conference and Exhibition, Rome, Italy, Oct., 1986)
- [9] Kupper, A., 1992, "Wall Correction Method for Models with Propeller Induced Slipstream" Programme of Wind Tunnels and Wind Tunnel Test Techniques, European Forum, Southampton University.
- [10] Kuchemann, D., and Weber, J., 1953, "Aerodynamics of Propulsion" London, McGraw-Hill.

⁵This applies to data from a propeller balance as well as to calibration based data. The ensuing tunnel corrections are the same in both cases.

- [11] Mokry, M., 1995, "Evaluation of Blockage Interference on Propellers in a Perforated-Wall Wind Tunnel" Journal of Aircraft, Vol.32, No.5, pp.1079-1087.
- [12] Rae, William H., and Pope, Alan, 1984, "Low-Speed Wind Tunnel Testing" New York, p 290
- [13] Shevell, Richard S., 1980, "Fundamentals of Flight" Prentice-Hall, 1980, p 224.
- [14] Wright, R.H., 1959, "The Effectiveness of the Transonic Wind Tunnel as a Device for Minimizing Tunnel-Boundary Interference for Model Tests at Transonic Speeds" AGARD Rept.294.

Appendix: glauert.c

```
/* Ratio of Uncorrected and Corrected Stream Velocities
for a Propeller in a Solid-Wall Wind Tunnel (Glauert's Method) */
```

```
#include <stdio.h>
#include <stdlib.h>
#include <math.h>
```

```
double glauert(double alpha, double tau);
```

```
void main(void)
{
    double alpha, tau=0.0;
    printf("\nEnter Ap/C (blockage ratio): ");
    scanf("%lf", &alpha);
    while(tau > -0.5)
    {
        printf("\nEnter tau (thrust parameter): ");
        scanf("%lf", &tau);
        printf("\n V/Vc = %f\n", glauert(alpha,tau));
    }
}
```

```
double glauert(double alpha, double tau)
{
    int iter;
    double lambda, x, sigma, sigma1, ds, f, tau1, dt, dt1=0.0;
```

```
/* test of input parameters */
if(alpha < 0.0 || alpha >= 1.0) return(0.0);
if(tau <= -0.5 || tau > 10.0) return(0.0);
if(fabs(tau) < 1.0E-6) return(1.0);
```

```
/* free air condition */
x = sqrt(1. +2.*tau);
sigma = (x +1.)/(2.*x);
sigma1 = sigma;
```

```
/* iteration cycle */
for(iter=1; iter<=100; iter++)
{
```

```
f = (1. -sigma)*(1. -alpha*sigma)/(sigma*pow((1. -alpha*sigma*sigma),2.));
x = (1. +f)/(1. -f);
lambda = 1. +(x -1.)*alpha*sigma*sigma -((2.*sigma -1.)*x -1.)/(2.*sigma);
tau1 = (x +1.)*(x -1.)/(2.*lambda*lambda);
dt = tau -tau1;
if(fabs(dt) < 1.0E-6) return(lambda);
if(iter == 1) ds = 0.01*sigma1;
else ds = 0.20*dt1*(sigma -sigma1)/(dt -dt1);
sigma1 = sigma;
sigma = sigma -ds;
dt1 = dt;
}
return(0.0);
}
```

```
/* Example
```

```
Enter Ap/C (blockage ratio): 0.15
```

```
Enter tau (thrust parameter): 2.0
```

```
V/Vc = 1.074788
```

```
*/
```

8. WALL CORRECTION METHODS FOR V/STOL CONFIGURATIONS, HELICOPTERS, PROPELLERS AND WINDMILLS

AUTHOR: J.E. HACKETT

	PAGE
NOTATION	8-3
8.1 INTRODUCTION	8-5
8.1.1 POSSIBLE APPROACHES FOR POWERED FLOWS	8-5
8.1.2 THE V/STOL TESTING ENVIRONMENT	8-6
8.1.2.1 TUNNEL FLOW BREAKDOWN CRITERIA	
8.1.2.2 USE OF FLOOR-BLOWING	
8.1.2.3 FREE-AIR INTERPRETATION	
8.1.2.4 GROUND-EFFECT INTERPRETATION	
8.1.2.5 'TRUE-Q' TESTING	
8.1.2.6 TUNNEL INDUCED GRADIENTS	
8.1.2.7 'STIFFNESS' OF POWERED FLOWS	
8.1.2.8 OTHER CONFIGURATIONS	
8.2 FLOW MODELLING-BASED METHODS	8-11
8.2.1 HEYSON'S METHOD	8-11
8.2.1.1 INTRODUCTION	
8.2.1.2 HELICOPTER ROTORS	
8.2.1.3 DUCTED FLOW	
8.2.1.4 EXAMPLES OF ROTOR INTERFERENCE FLOW FIELDS, ACCORDING TO HEYSON	
8.2.1.5 LARGE ROTORS	
8.2.1.6 DETERMINATION OF WAKE SKEW ANGLE, χ	
8.2.1.7 EFFECTS OF REPLACING χ BY χ_E	
8.2.1.8 GENERATION OF INTERFERENCE COEFFICIENTS	
8.2.1.9 APPLICATION OF INTERFERENCE COEFFICIENTS	
8.2.1.10 ALTERNATIVE INTERPRETATION OF THE SOLUTION PROCESS	
8.2.1.11 SAMPLE RESULTS FOR V/STOL CONFIGURATIONS	
8.2.2 PANEL METHODS	8-20
8.3 THE WALL PRESSURE SIGNATURE METHOD	8-22
8.3.1 THEORETICAL OVERVIEW	8-22
8.3.1.1 THE THREE DIMENSIONAL INVERSE PROBLEM	
8.3.1.2 NON-LINEAR SOLUTIONS	
8.3.1.3 LINEAR SOLUTIONS	
8.3.1.4 QUASI-LINEAR SOLUTIONS	
8.3.1.5 THE WAKE-INDUCED DRAG INCREMENT	

	PAGE
8.3.2 EXPERIMENTAL ASPECTS	8-26
8.3.2.1 TESTING AND PRE-ANALYSIS	
8.3.2.2 SPECIAL INSTRUMENTATION CONFIGURATIONS	
8.3.3 ANALYSIS FOR THE "SOURCE-SOURCE-SINK" VERSION OF THE METHOD	8-27
8.3.3.1 BLOCKAGE SIGNATURE ANALYSIS	
8.3.3.2 CONSTRUCTION OF THE SOURCE-SOURCE-SINK THEORETICAL MODEL	
8.3.3.3 APPLICATION OF THE SOURCE-SOURCE-SINK MODEL	
8.3.4 ANALYSIS FOR THE "MATRIX" VERSION OF THE METHOD	8-31
8.3.4.1 LIFT-BLOCKAGE COUPLING	
8.3.4.2 ANGLE-OF-ATTACK CORRECTIONS	
8.3.4.3 POWERED APPLICATIONS AT VERY HIGH LIFT	
8.3.5 DISCUSSION	8-35
8.4 TUNNEL INTERFERENCE FOR A JET-IN-CROSSFLOW	8-35
8.4.1 INTRODUCTION	8-35
8.4.2 THEORETICAL FLOW MODEL	8-36
8.4.2.1 TUNNEL INTERFERENCE FOR A ROUND JET-IN- CROSSFLOW	
8.4.2.2 TUNNEL INTERFERENCE FOR OTHER CONFIGURATIONS	
REFERENCES FOR CHAPTER 8	8-41

8 WALL CORRECTION METHODS FOR V/STOL CONFIGURATIONS, HELICOPTERS, PROPELLERS AND WINDMILLS

Notation

A_m	momentum area of lifting system. (Equation 8.5)
A_{TUN}	tunnel cross sectional area. Usually B times H
B	total tunnel width
b	effective span of powered lifting system (in Souths criterion, Section 8.1.2)
b_S	span of line source used for wake modeling (Section 8.3)
c_S	X-spacing between solid blockage source and sink (Section 8.3)
C_L	lift coefficient, $L / q S$
C_D	drag coefficient, $D / q S$
$C_{D_{vis}}$	viscous part of model drag coefficient (Section 8.3).
ΔC_D	wake-induced drag increment (see Section 8.3.1).
C_{Lhb}	lift coefficient based on Reference area h times b (Souths criterion, chapter 1.2)
C_T	thrust coefficient, Thrust / $q S$
C_μ	jet momentum coefficient, (Jet mass flow times V_j) / $q S$
\bar{c}	mean chord (Figure 8.12)
D	total drag
D_i	induced drag
H	total tunnel height
h	model height above tunnel floor (in Souths criterion, Section 8.1.2)
J	advance ratio of rotor or propeller. $V / \Omega R$
L	lift
L_h	lift at hover
M_Y	pitching moment (Figure 8.12)
n	the ratio of final induced velocities in the far wake to initial induced velocities at the model (Chapter 8.2.1.9)
q	dynamic pressure = $\frac{1}{2} \rho V^2$
Q	generic total 3D source strength. (= span times strength/unit length)
$\pm Q_S$	total 3D source and sink strengths for line elements representing a model's solid blockage (Section 8.3)
Q_W	total 3D source strength for line source element representing a model's viscous wake (Section 8.3)
R	rotor or propeller radius (in definition of J , above)
S	reference area
T_S	static thrust (Figure 8.12)
u	generic streamwise velocity increment, relative to U . Positive rearward. (Section 8.3)

u_{ASYMP}	asymptotic streamwise velocity increment, at the downstream end of the u-signature, relative to U . (Section 8.3).
u_{SYM}	height of the symmetric part of the u-component signature, relative to U (Section 8.3).
u_{WALL}	increment of streamwise velocity at a tunnel surface, relative to U . (Section 8.3).
u_0	mean or momentum-theory value of absolute longitudinal induced velocity at model, positive rearward. (Section 8.2).
U	mainstream velocity.
V_R	wind tunnel velocity
V_J	jet efflux velocity (in definition of C_{μ} , above)
V	resultant velocity (Equation 8.2)
w_0	mean or momentum-theory value of vertical induced velocity at model, positive upward.
w_h	reference velocity, positive upward (Equation 8.5)
x, y, z	tunnel co-ordinates: axial, along right wing and upward
X_2	
X_3	locations of source elements in pressure signature flow model (Section 8.3)
X_4	
ΔX	half-width of solid blockage signature at half-height (see Figure 8.21).
α	angle of attack.
$\Delta\alpha$	tunnel-induced angle of attack.
Γ	strength of horseshoe vortex in flow model for matrix version of the pressure signature method (Section 8.3.4).
$\delta_{u,L}$	Interference factor for longitudinal interference velocity due to lift
$\delta_{u,D}$	Interference factor for longitudinal interference velocity due to drag
$\delta_{w,L}$	Interference factor for vertical interference velocity due to lift
$\delta_{w,D}$	Interference factor for vertical interference velocity due to drag
δ_{US}	Upper surface flap angle, to wing chord line (Figure 8.5).
θ	wake deflection angle from the horizontal, positive downward (Figure 8.9).
χ	wake skew angle from the downward vertical to the wake momentum centerline, positive rearward (Figure 8.9).
χ_e	effective wake skew angle from the downward vertical to the wake vorticity centerline. Determined from $\chi_e = \frac{1}{2}(\chi + 90)$. (Section 8.2)
ρ	mass density of tunnel air
σ	ratio of wind tunnel height to width. (Section 8.2)
Ω	angular velocity of rotor or propeller (in definition of J, above)

8.1 INTRODUCTION

8.1.1 POSSIBLE APPROACHES FOR POWERED FLOWS

The spectrum of V/STOL configurations that has appeared over the years is very extensive (see Figures 8.1 and 8.2). VTOL configurations may include direct-lift jets, lifting fans, tilt-propellers, tilt-rotors and helicopters. STOL configurations may include wings with highly-deflected flaps or some form of jet-flap, possibly in combination with direct lift. V/STOL systems are thus very diverse and each has its own peculiarities and needs.

The requirements of powered lift testing at low speed are different from those of cruise flight. In the eventual data analyses, the primary interest in tunnel speed corrections is likely to arise from intake momentum drag, for jets or ducted rotors, or advance ratio for open rotors and propellers. Aircraft control is critical in low speed transitional flight and tunnel-induced gradients can be high under these conditions. The gradients, rather than the magnitude, of a correction may determine the correctability of a particular data point. Free stream speed is usually used in normalising powered-flow coefficients such as advance ratio, J , for a rotor; momentum coefficient, C_{μ} , for a jet flap or thrust coefficient, C_T , for a direct thrust device. On-line blockage correction is desirable so that constant corrected speed can be maintained at the model reference point. The power coefficient or advance ratio can then be held constant as angle-of-attack, for example, is varied. Provision of on-line blockage corrections is a challenge because of the complexity of the corrections involved.

For the configurations then in vogue, early work showed that classical tunnel correction methods would suffice provided the test model was aerodynamically small, i.e. on the basis of C_D or C_L times reference area, for example, as opposed to reference area itself. Recognition of this in the fifties and sixties spawned a generation of large V/STOL tunnels and explicit powered flow modelling became an essential part of the correction process. This approach presents significant difficulties because powered, lifting flows generate complex flow structures that change with forward speed. At low speed, impingement on tunnel surfaces is not uncommon. One of the earliest attempts at modelling (Heyson [22]) involved a simple representation of a lifting plume using an inclined line of doublets extending from a jet

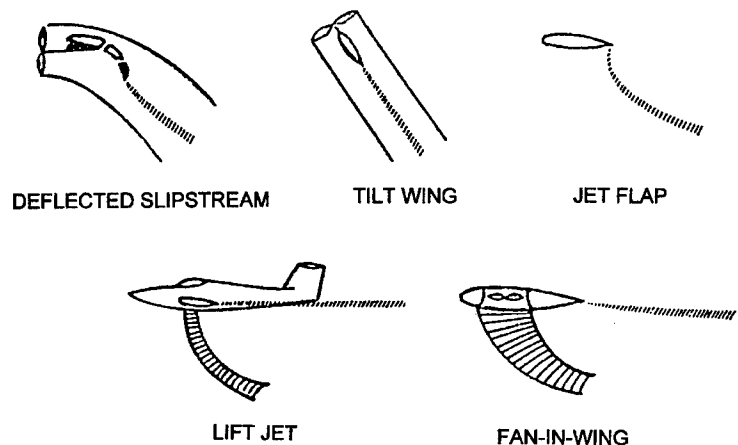


Figure 8.1 Sketches of various V/STOL configurations

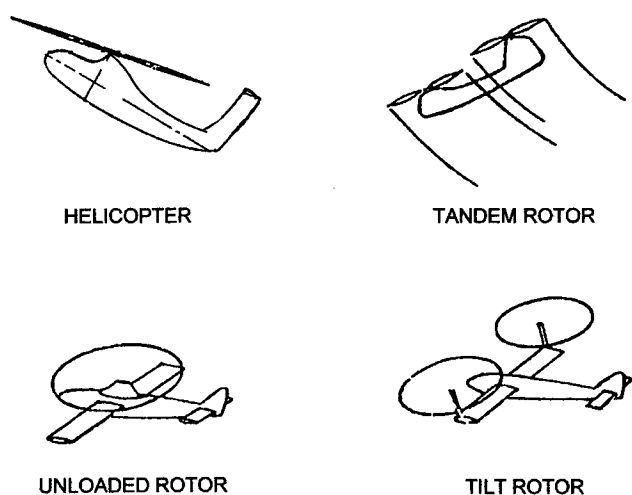


Figure 8.2 Sketches of various open-rotor VSTOL configurations

exit or the centre of a rotor (see Section 8.2). Later, the wall-pressure signature method was developed (See Hackett et al [5], [6] and Section 8.3) and applied with some success to jet flapped wings at very high lift levels ($C_L > 20$) and to round lifting jets. The tangential velocities, deduced from measured wall pressures at the centrelines of tunnel surfaces, were applied as boundary conditions in the theoretical flow model. The zero normal flow condition was imposed for the entire solid tunnel surface. Using tunnel wall measurements thus took some of the guesswork out of modelling V/STOL flows. The approach was augmented by the use of local flow control when a jet or a slipstream impinged upon the tunnel floor. This delayed the onset of tunnel flow breakdown significantly. Despite these advances, simple modelling was still required when using the pressure signature method and the numerics could be troublesome. With the recently available two-variable pressure-based correction method (Section 4), it is theoretically possible to avoid explicit modelling for non-impinging flows. However, only explicit modelling can reconstruct the "missing" extension of a powered wake that impacts a tunnel floor.

Methods currently in use cover the spectrum just described. Classical methods, Heyson's model, pressure signature and two-variable methods, and various empirically-based methods are all still in use. There is understandable reluctance to move from familiar methods with a substantial data base to more recent approaches that may require more tunnel time, more instrumentation or both. However, economic pressures are likely to reduce the size of new tunnels and the importance of good correction methods is increasing.

8.1.2 THE V/STOL TESTING ENVIRONMENT

A wide variety of installed power systems distinguishes V/STOL models from their conventional counterparts. As indicated in Figures 8.1 and 8.2, these range from shaft-driven rotors to air-powered fans, to jets and various powered wings. Despite this diversity, the test problems of these systems tend to be remarkably similar. Figure 8.3, taken from Tyler et al [41], [42], sketches the flow that arises when a jet impinges on a wind tunnel floor. There is forward flow ahead of the impingement point and, as this flow loses energy, it separates and forms a standing vortex at the tunnel centreplane. This wraps around the impingement region, forming what is sometimes called a "scarf" vortex as its ends trail downstream. The trailing vortices diverge under the influence of their images in the tunnel floor and may progress up the tunnel walls if the conditions are suitable. A similar flow pattern, differing in scale but with the same topology, may be generated by the slipstream from a rotor, a ducted fan or a jet-flapped wing. The term "tunnel flow breakdown" is applied to situations in which data become uncorrectable because of this phenomenon.

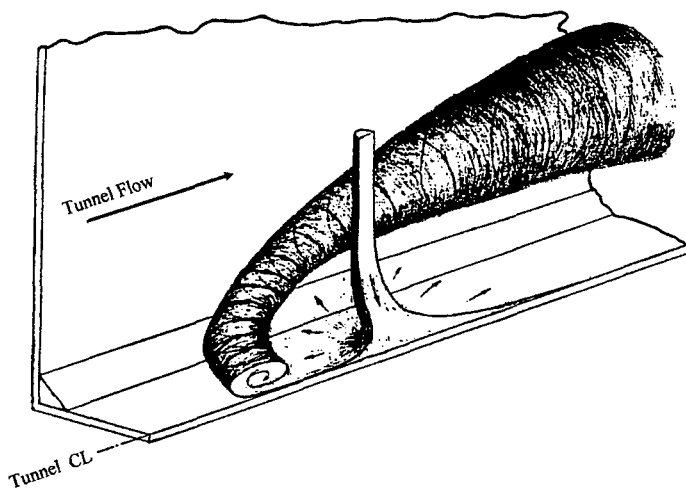


Figure 8.3 Tunnel Flow Breakdown for an Impinging Jet

topology, may be generated by the slipstream from a rotor, a ducted fan or a jet-flapped wing. The term "tunnel flow breakdown" is applied to situations in which data become uncorrectable because of this phenomenon.

The tunnel flow breakdown phenomenon is a distinguishing feature of powered flow testing; it rarely occurs with conventional models. It restricts the available test range at low speed and possibly under transitional conditions. For this reason, we shall review the phenomenon in some detail and suggest ways to extend the test envelope by floor blowing.

8.1.2.1 TUNNEL FLOW BREAKDOWN CRITERIA

South [40] describes experiments that determine limiting conditions for tunnel flow breakdown. Figure 8.4 shows the resulting criterion and compares it with similar work by Heyson [32]. The ordinate, C_{Lhb} , is a lift coefficient based on the likely tunnel area blocked by the impinging flow, usually expressed as the product of the powered span and the model height. The abscissa is drag-to-lift ratio. It will be observed that South's criterion is more restrictive than Heyson's under thrust conditions.

It is obviously important to monitor the tunnel floor flow in any powered lift test in which South's C_{Lhb} criterion might be exceeded. The use of floor tufts or, better yet, measurement of floor pressures is recommended. Once tunnel flow breakdown occurs in a conventional tunnel the results should be disregarded or at least viewed sceptically. However, the possibility of removing the ground vortex, or at least controlling it, should also be considered. This possibility was investigated, with some success, by Hackett et al [15]. They describe 'worst-case' experiments that employ ground-blowing to delay tunnel flow breakdown.

8.1.2.2 USE OF FLOOR-BLOWING

Figure 8.5(a), taken from Hackett et al [15], shows laser velocimeter measurements at the centre plane of a finite-span knee-blown flapped wing at a high blowing level. The combined model attitude and flap angle gave a near-vertical jet and a large ground vortex developed which grew as angle-of-attack was increased. Flow beneath the model was effectively blocked, resulting in a loss of lift. Ground blowing was applied to suppress the vortex, using floor pressure measurements to determine the blowing level. The injection point is shown in the figure. With ground blowing set "correctly" (see below), the flow pattern of Figure 8.5(b) was obtained. A ground vortex was still present but its size had been reduced substantially. Inspection of the wing flow reveals increased upper surface velocities, suggesting reduced lift loss.

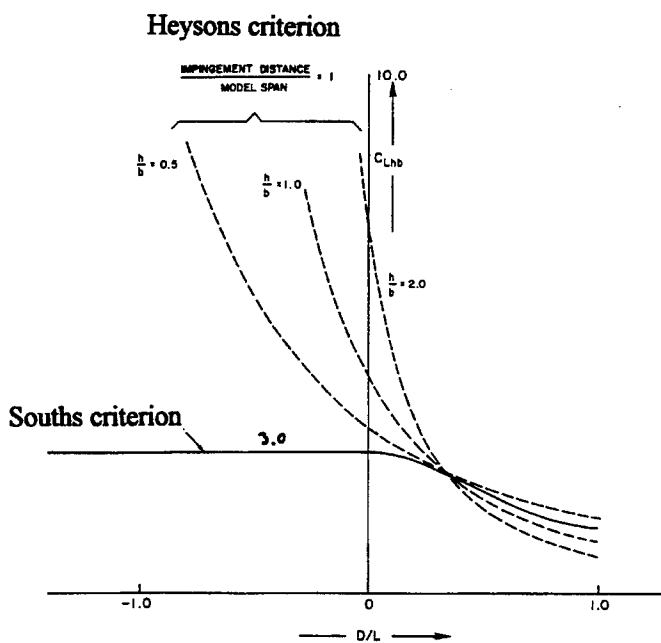


Figure 8.4 Criteria for Tunnel Flow Breakdown

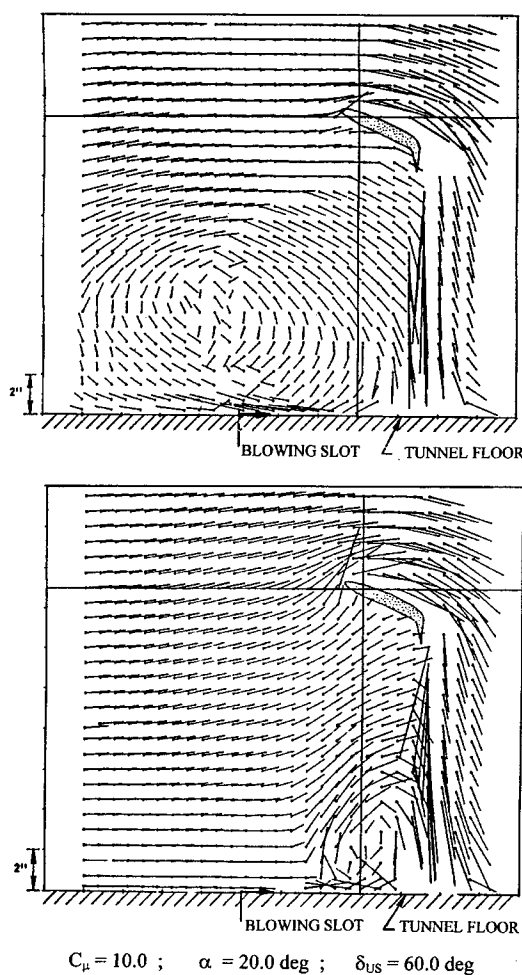


Figure 8.5 Velocity Field at the Centre Plane of a Kneeblowing Flap Model, (a) Fixed Ground (Upper Plot), (b) Blown Ground (Lower Plot)

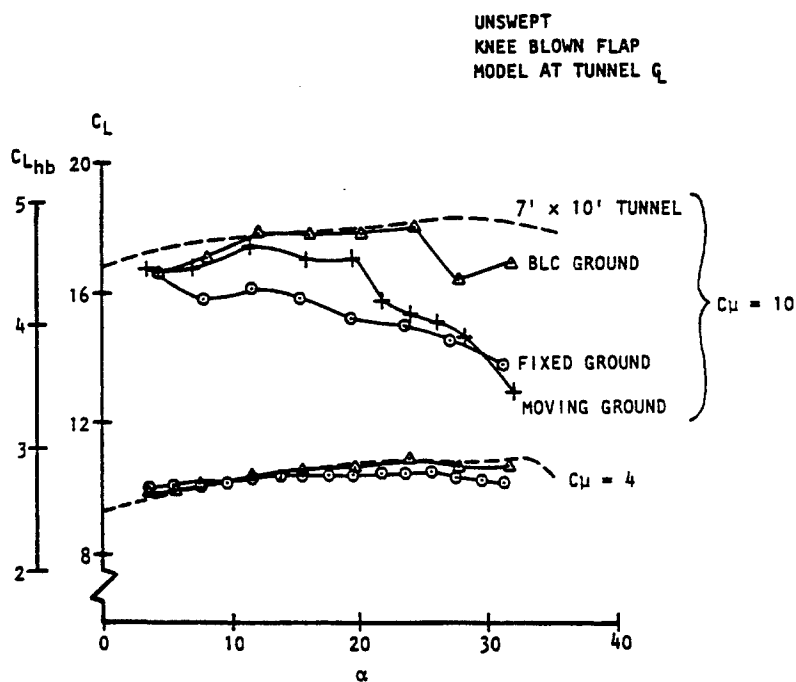


Figure 8.6 Demonstration of Lift-Loss due to Tunnel Flow Breakdown

Figure 8.6, from the same reference, shows the effects of ground flow control on lift. The test was run at "true-q" using the pressure signature method (see Section 8.3) in an on-line mode. A second scale has been added to the y-axis, showing South's tunnel flow breakdown parameter, C_{Lhb} . It is evident that the test values for $C_{\mu} = 10$ lie well above South's flow breakdown limit. Severe lift loss is apparent for the fixed ground case (circles) relative to the large-tunnel baseline (dashed lines). The loss increases with angle-of-attack. Use of a moving ground (plus-signs) removed most of the deficit but ground blowing (triangles) was more effective at angles of attack below 20-degrees, where the limit of the air supply was reached.

The difference between the moving and the blown-ground results draws attention to the distinction between model-in-ground and free-air interpretation of similar data. We shall now consider these individually.

8.1.2.3 FREE-AIR INTERPRETATION

If free-air data are required, more ground flow control may be needed than for the ground effect cases because the ground vortex must be removed as completely as possible. It has already been noted that the moving ground gave less lift recovery than the blown ground. Tunnel constraint corrections for the free-air case must include a four-wall blockage correction, a four-wall angle-of-attack correction and further corrections to both that compensate for the truncation of the powered wake at the tunnel floor.

8.1.2.4 GROUND-EFFECT INTERPRETATION

A moving ground is clearly appropriate for ground effect testing. The ground vortex is then smaller than with a fixed ground but larger than for the (free-air) blown ground case. Ground blowing may also be used for ground effect testing but the criterion for setting blowing level is different. For the free air case blowing was increased as needed to remove the suction peak under the ground vortex. However, it is necessary to monitor skin friction at the ground when doing ground-effect testing (see Hackett et al [7]). Preston tubes are installed at the ground surface and the condition is applied that the flow immediately above the ground must be going in the 'right' direction, i.e., the skin friction must be positive. This approximates the moving ground condition.

Three-wall blockage and three-wall angle-of-attack constraint corrections are required when reducing ground-effects data. The three-wall corrections will, of course, be smaller than the corresponding four-wall corrections: the floor images are "supposed" to be there for the ground-effect case. Replacement of the 'missing' plume extension, below the tunnel floor, is not required for in-ground cases.

8.1.2.5 'TRUE-Q' TESTING

To illustrate the importance of on-line blockage correction, effective "uncorrected" lift data have been backed out of the Figure 8.6 data. Figure 8.7 shows the result. The blockage corrections are very large and are much more important than those for angle-of-attack. The changes in C_L are almost completely blockage-driven and similar changes can be expected in C_{μ} . Each uncorrected point (cross) therefore corresponds to a different C_{μ} . If testing had been conducted at a nominal C_{μ} rather than using on-line blockage correction, cross-plotting would have been needed to obtain lines of constant corrected C_{μ} . Data quality would have suffered and there would probably have been difficulties in deciding on the proper test ranges for the blowing parameters.

8.1.2.6 TUNNEL INDUCED GRADIENTS.

The presence of very large interference effects implies correspondingly large tunnel-induced gradients. These are of concern, particularly with regard to control surfaces. The topic will be revisited as part of the discussion of correction procedures in the following sections.

8.1.2.7 'STIFFNESS' OF POWERED FLOWS.

An obvious concern when tunnel interference is large, or when a powered flow intersects a surface, is that the powered wake will distort. This is clearly the case when a jet or rotor wake hits the floor and some correction procedures recognise this by providing a theoretical extension as part of the correction process. However, the question remains whether the wake is distorted nearer to the model. This issue was investigated by Hackett et al [16] who showed that, for round jets at least, the jet trajectory is

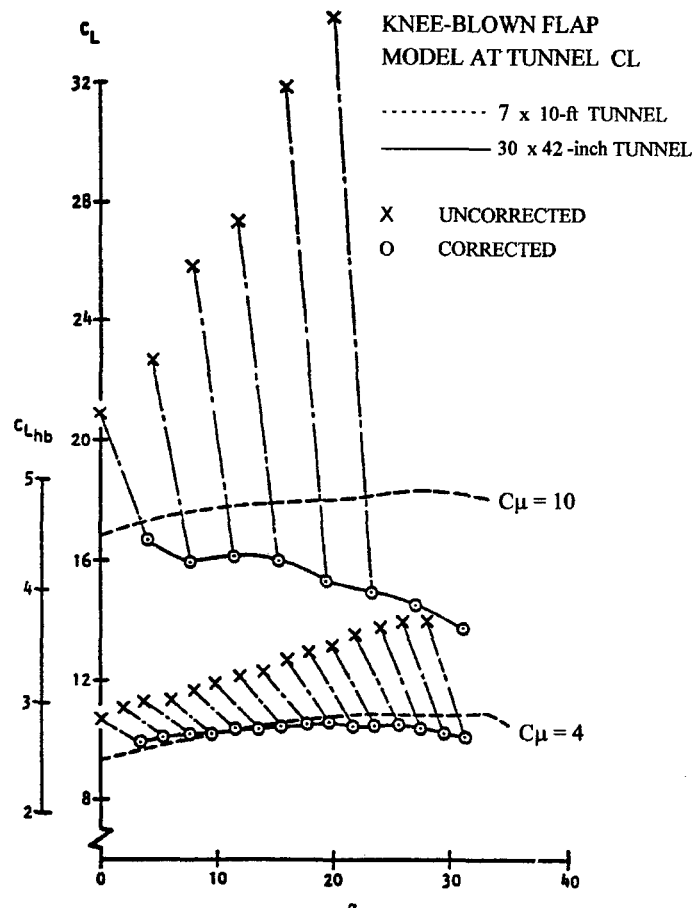


Figure 8.7 Constraint Corrections under Very High Blockage Conditions

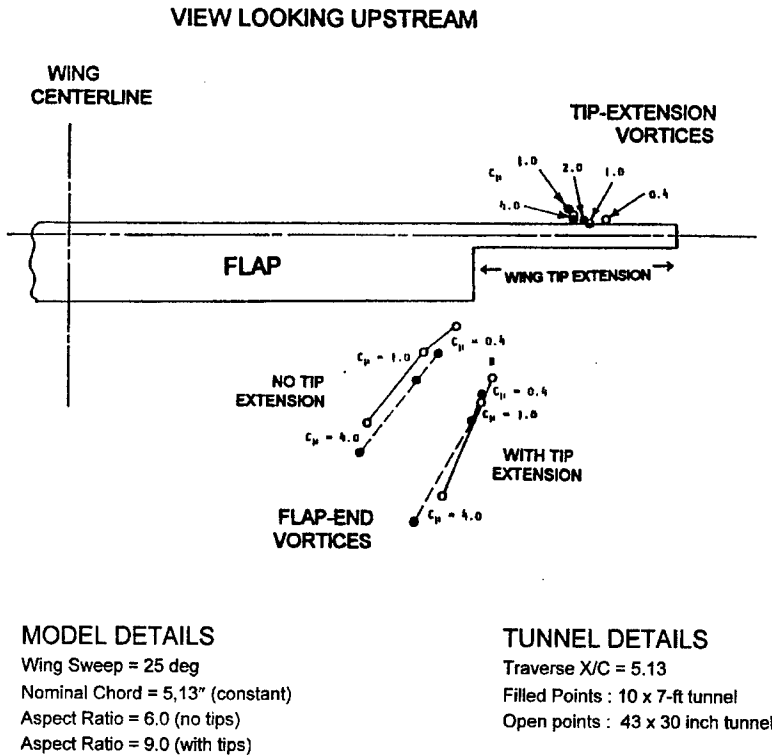


Figure 8.8 Measured Vortex Positions Behind a Knee-Blown Flap Model at Various Power Settings, in Small and Large Wind Tunnels

into the large tunnel flow as corrected C_{μ} was increased. On rotating the co-ordinate system by the tunnel-induced angle-of -attack, however, it was found that the vortex positions were essentially the same for both large and small tunnels. Wake yielding due to tunnel-imposed velocities was thus found to be insignificant for this configuration, provided flow rather than tunnel axes were used.

8.1.2.8 OTHER CONFIGURATIONS

A specific, blown-flap configuration has been used in the example above to illustrate some of the principles involved in powered lift testing. The range of possible V/STOL configurations is too large for individual treatment to be practical here. Multiple jet, multiple fan or multiple rotor configurations present special difficulties in this regard. Specialised instrumentation, data handling and constraint corrections may be needed in these cases. However, it can probably be assumed that the flow physics of each power unit will be similar to a unit acting alone and a similar approach can be applied. Closely spaced units should probably be treated as one.

changed only within one or two jet diameters of the impact point. This is reassuring for jet-powered configurations but it remains of concern for rotor testing.

Figure 8.8, taken from Hackett et al [7], shows small and large tunnel trailing vortex positions for a swept-wing version of the knee-blown flap model mentioned previously. The vortex positions were determined using a rotating vorticity meter. The model was tested at several flap blowing levels with and without wing tips. Neither flap blowing level nor tunnel size had much effect on the positions of the vortices springing from the extended tips, when these were fitted. However, the flap-end vortices penetrated the flow increasingly as blowing level was increased, whether or not the extended tips were present. As might be anticipated, the flap-end vortices penetrated more deeply

8.2 FLOW MODELLING-BASED METHODS.

8.2.1 HEYSON'S METHOD

8.2.1.1 INTRODUCTION

One of the earliest schemes for modelling V/STOL flows is given in Heyson [22]. His tunnel correction method was developed originally for single-rotor helicopters and was extended over a period of several years to include additional V/STOL configurations, several of which were checked out in the wind tunnel. The extensive collection of literature concerning Heyson's methods includes NACA and NASA reports, tech notes, memos and special publications, many of which are employed in this chapter as definitive references (see Heyson [22] through Heyson [34]). The mathematical developments and code listings are voluminous and no attempt will be made to reproduce them here. Rather, we shall try to highlight the physics and methods involved in Heyson's method, point out known limitations and errors and make appropriate references to the source material. Examples of its application to selected V/STOL examples will be included. Other reviews may be found in Rae and Pope [37] and in a review report by Olcott [36], which is more comprehensive.

It is important to note, at the outset, that Heyson's method models only the non-viscous flow. Drag input to the method, for example, thus includes only induced drag, which may be difficult to estimate for many powered flows. Blockage due to viscous drag must be estimated separately.

8.2.1.2 HELICOPTER ROTORS

The flow beneath a helicopter rotor in still air can be represented by a vortex tube built of vortex rings that lie parallel to the rotor disc. Vortex ring strength is defined by rotor lift and slipstream contraction is neglected. As the helicopter moves forward, or the tunnel is turned on, the vortex cylinder is sheared in the downstream direction and the intersection with the ground or the tunnel floor moves aft. If free-air results are the objective, there is a minimum forward speed below which flow reversal along the tunnel floor invalidates the data. If in-ground effects are required, the situation is more complicated because some forward flow is possible in flight cases (see Section 8.1).

In the theoretical development of Heyson [22], each vortex ring is first replaced by a circular sheet of doublets. The sheet is then condensed to a point. The original sheared vortex cylinder becomes an inclined line of doublets extending from the rotor centre to

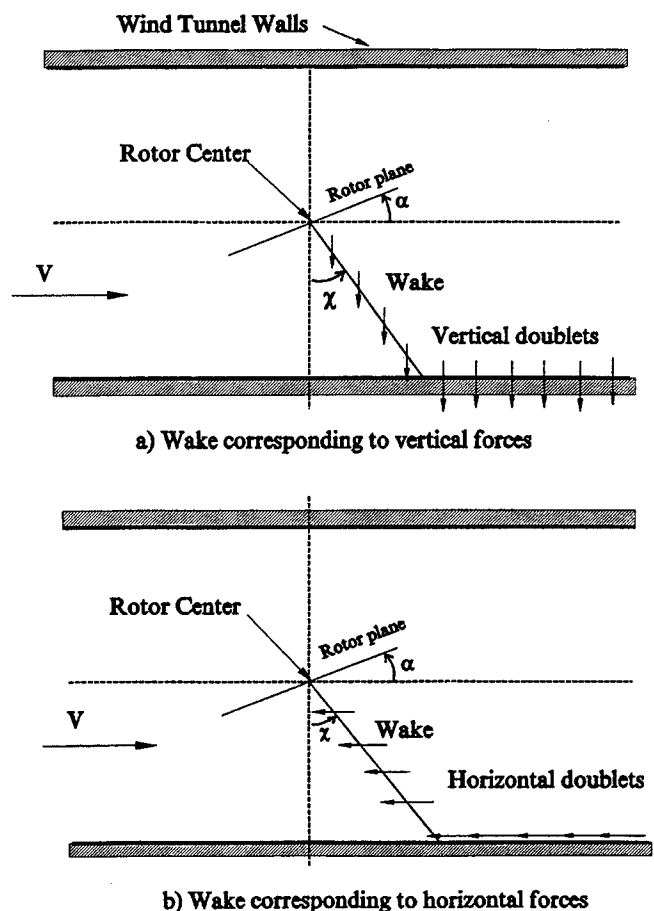


Figure 8.9 Rotor wake model used by Heyson

the floor as illustrated in Figure 8.9(a). The wake deflection angle is determined primarily by the lift-to-drag ratio for the particular data point concerned; the full analysis will be described below. Figure 8.9(b) shows horizontal doublets that also populate the wake. These were introduced to accommodate cases for which the jet axis is inclined at angle χ to the vertical. The vertical and horizontal doublet strengths are proportional to cosine χ and sine χ respectively.

On reaching the tunnel floor, the doublet line trails downstream. Each vertical doublet is cancelled by its image in the ground or tunnel floor, but the horizontal doublet vectors are additive. Tunnel effects due to the images of the system in Figure 8.9 are calculated using classical imaging techniques. Heyson's method reconstructs the "missing" part of the jet plume that has been cut off by the tunnel floor. (see also "*Generation of interference coefficients*" later in this chapter). A similar procedure is employed when applying the wall pressure signature treatment to jet-plumes, described in Section 8.3.

Tunnel interference for a finite wing can be determined as a special case of the system just described in which the line of vertical doublets trails aft and never intersects the floor. Because of differing definitions, there is a factor of minus four between Heyson's boundary correction factor and the classical value (see page 12 of Heyson [22]). Table 5 of the same reference demonstrates close agreement between Heyson's formulation and the classical values for wings in closed and in three-quarters-open wind tunnels.

8.2.1.3 DUCTED FLOW

The flow within a jet emerging from a duct at right angles to a mainstream can be thought of as being generated by a doubly infinite vortex tube with strength equal to the velocity jump across the jet boundary. The vorticity tube comprises boundary layer fluid on the duct walls, then a cylindrical shear layer when the fluid leaves the duct. A point at the centre of the jet exit plane 'sees' the full jet velocity because the vorticity tube is doubly-infinite. The Heyson model is *semi*-infinite, however, because the vorticity is generated at the rotor tips and does not extend above the rotor plane. Consequently, the velocity at the rotor centre is only half of that for the doubly-infinite system. For this reason the original interference factors must be multiplied by a factor of two ('n', in equations 8.3 to 8.5, below) for jet-powered cases (see also Appendix A of Heyson [31]). Options are provided in the Heyson algorithm for rotors, wings and jets.

An idealised V/STOL lifting jet or a control jet emergent from an aircraft surface may include a long approach region upstream of its exit plane. The doubly-infinite doublet line is usually a reasonable far-field approximation in such cases. However, the duct length ahead of the exit plane for realistic V/STOL configurations is finite and a factor of two will overpredict the interference. Engineering judgement is required to terminate the doublet line appropriately at its upstream end. Further details concerning the relationships between the corrections for rotors, wings and jets may be found in Heyson [31], Appendix A.

8.2.1.4 EXAMPLES OF ROTOR INTERFERENCE FLOW FIELDS, ACCORDING TO HEYSON

Figure 8.10 shows interference fields in a square tunnel, taken from Heyson [31]. The rotor spans 60% of the tunnel width and is positioned 15% of the tunnel height above the centreplane. The upper two plots depict upwash and axial interference velocity for a skew angle of 10-degrees, a near-hover condition. A downwash interference of approximately 1.0 is observed near to the tunnel floor (upper plot) where the rotor wake impacts the floor. The u- component interference is near zero at this point (second plot from

top). At higher forward speed (lower two plots), the impact region moves downstream and a streamwise downwash gradient appears in the plane of the rotor. At both forward speeds the u-component interference in the wake region is much greater than that in the rotor plane.

8.2.1.5 LARGE ROTORS

In cases for which the small-rotor assumption is invalid, Heyson uses multiple doublet lines, distributed through the rotor wake cylinder as shown in Figure 8.11. The enclosing cylinder in the sketch is the true vorticity cylinder. Heyson (1970) points out that there are difficulties associated with 'lumpiness' that affect both the rotor plane and the floor impact region. As he explains, these difficulties are also present in Heyson (1969 a) and Heyson (1969 b).

Even at low forward speed the assumption of uniform disc loading may be in question for large rotor diameters because the blade tips are highly loaded. The representation of triangular blade loading, using concentric vortex cylinders, is discussed in Appendix B of Heyson [31], and in Heyson [21].

At intermediate forward speeds, the load distributions on advancing and retreating rotor blades may differ significantly even though the total lift is centred (zero rolling moment). This further invalidates the assumption of uniform disc loading. Under these conditions the correct interference flow field for a large rotor would be expected to be asymmetric about the tunnel centre plane. No method appears to be available that deals with this situation. In counterpoint, it should be noted that a helicopter wake at high forward speed becomes very wing-like at an advance ratio of 0.095, for example (See Figure 46 of Heyson [21] or Figure 8 of Heyson [32]). It is also found that tunnel corrections for a finite wing of aspect ratio $4/\pi$ (i.e. the aspect ratio of a disc) work well when applied to a helicopter rotor at high values of advance ratio (see Heyson et al [21]).

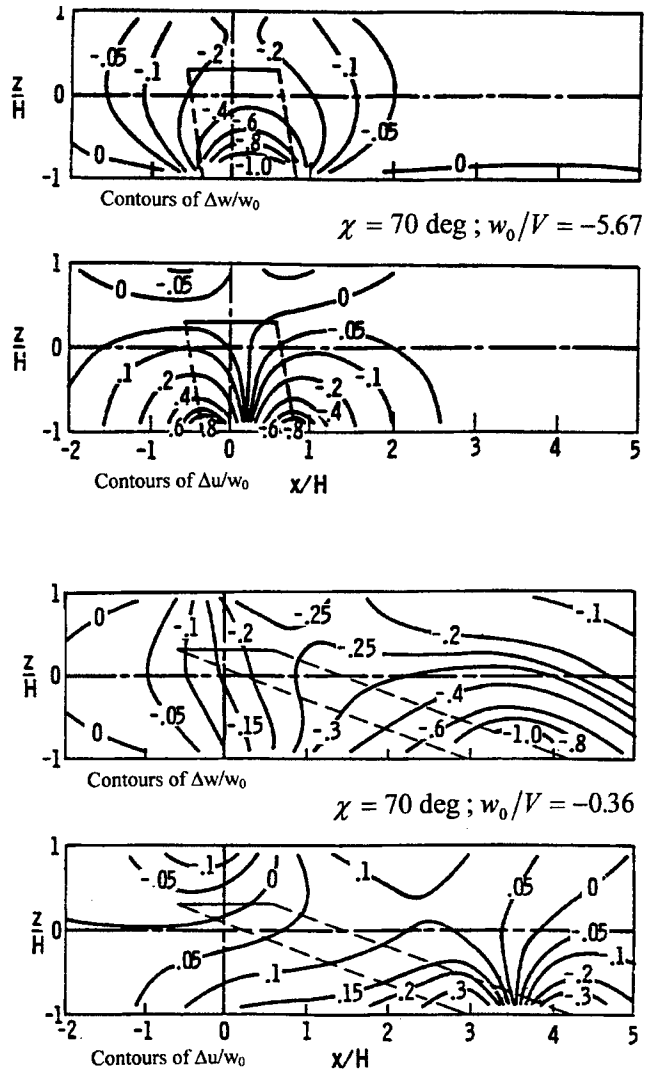


Figure 8.10 Wall induced interference velocities for a uniform loaded rotor mounted 30% of a semiheight above the centreline of a square, closed wind tunnel. $\sigma = 0.6$

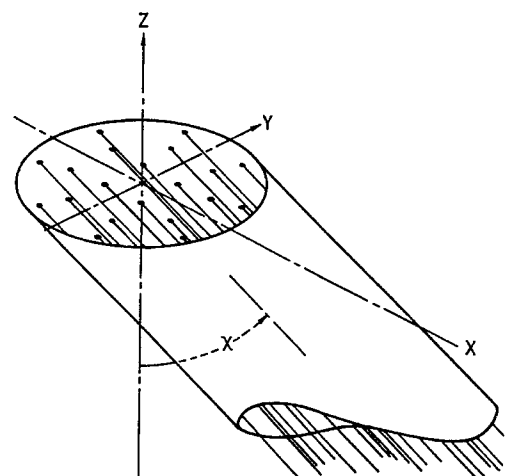


Figure 8.11 Sketch of a skewed cylinder of vorticity and the doublet-line system used to represent it.

8.2.1.6 DETERMINATION OF WAKE SKEW ANGLE, χ

The wake skew angle, (χ in Figure 8.9), is a major parameter in determining the tunnel corrections for powered lift models when using Heyson's method. To some approximation, it represents the trajectory of the wake. The measurement of χ from the vertical reflects its helicopter origins. However θ , the complement of χ , defines the deflection of the wake from the horizontal.

As originally defined for rotors (e.g. Heyson [24]) χ was based strictly on momentum theory (see below). The wake was assumed to be infinitely stiff and its initial slope at the rotor plane was assumed to persist until the wake impinged upon the tunnel floor. In Heyson et al [26], and subsequently, the fact was recognised that wake penetration is reduced by the action of the mainstream. To accommodate this, the momentum-based deflection angle, θ , was reduced to $\frac{1}{2} \theta$. This is equivalent to replacing χ by an effective value $\chi_e = \frac{1}{2} (\chi + 90)$ deg. This is implausible near to hover because χ_e becomes 45-degrees. However, Heyson et al [27] argue that "there are limitations on the minimum speed at which tests can be made in a meaningful fashion in wind tunnels, and it is believed that these limitations will generally be encountered before the failure of (the above approximation)". Recognising the difficulty, Heyson [30] states that "Even though experimental studies indicate remarkably improved agreement between comparative tests when the above relations are used, it is obvious that there is a limit to their applicability". Figure 3 of the same reference suggests other, more plausible definitions. However, most of Heyson's results use the $\frac{1}{2} \theta$ assumption.

It is important to note that the χ value determined from Equations 8.1 through 8.8, below, is momentum-based. χ_e represents only the vortical part of the wake and applies only to the tunnel interference part of the calculation. There is some justification for this in the flow physics since the trailing vorticity peels away from the sides of the powered jet, which then tends to maintain its original direction. Only far downstream (if ever) does the jet fluid become fully entrained into the vortex system. The half-angle assumption is also consistent with the situation in the wake of a finite wing, for example, for which the deflection of the trailing vortices from the horizontal is half of that for the central wake. The symbol χ_e is not used by Heyson but is introduced here, and also in Rae et al [37], for clarity.

8.2.1.7 EFFECTS OF REPLACING χ BY χ_e

One of the main motivations for revising the definition of skew angle concerned pitching moments. In a particular fan-in-wing study (Heyson et al [27]) tunnel corrections based on χ were of approximately the right magnitude, but of the wrong sign. It is apparent from Figure 8.12 (a) that the use of χ_e , rather than χ , shifted the peak downwash due to lift from a wing location to the tailplane. Figure 8.12 (b) shows that χ -based pitching moment corrections had the wrong sign, whereas χ_e -based corrections (Figure 8.12 (c)) worked well. It is understood (Margason [35]) that these benefits were obtained without seriously compromising the lift and drag correlations.

8.2.1.8 GENERATION OF INTERFERENCE COEFFICIENTS

Having established the theoretical jet trajectory, now at angle χ_e to the vertical rather than χ as in Figure 8.9, and knowing that the doublet vector is aligned with it, the tunnel interference may be calculated. This is achieved by determining the effects of a classical, doubly-infinite set of images in the tunnel walls. The basic formulation is given in Heyson [22] as Equations 18 and 19. The inclined line doublet and its image

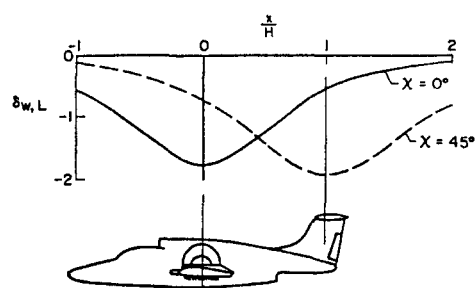
in the tunnel floor are considered as a unit that comprises four inclined semi-infinite doublet lines. Line 1 extends from the model centre at angle χ_e and continues downward through the tunnel floor to infinity. Line 2, which is applied negatively, overlays the lower part of Line 1 and cancels the part below the floor. Lines 1 and 2 therefore describe just the (inclined) in-tunnel line doublet. Lines 3 and 4 are used similarly to create the corresponding finite length ground image doublet. This completes the central tunnel-plus-ground-image unit.

The effects of the entire image set, excluding the central unit, are double-summed in the usual way to determine the tunnel interference. Since the basic unit includes the ground image, this means that, in leaving out the central unit, the ground image is excluded as well as the in-tunnel line doublet. The summation over the tunnel image set therefore gives the tunnel correction for the ground effect case. To obtain the tunnel correction for the free air case, the effects of Lines 2, 3 and 4 are added back, with due regard for their sense. These are the three trailing terms in Equation 19b of Heyson [22]. Additional details may be found on page 13 of Heyson [25].

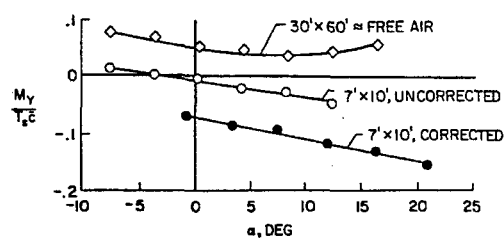
The interpretation of the added-back terms, Lines 2, 3 and 4, is important. As already indicated, Lines 3 and 4 are conventional images that represent the ground image of the in-tunnel wake. However, Line 2 is *not* the image of anything but is, rather, the below-floor extension of the inclined, in-tunnel line doublet downward to infinity. Its effect is subtracted from the value of δ which is, itself, a subtracted quantity. Line 2 therefore *adds* the effects of the wake extension to the solution. This means that the Heyson solution adds back the effects of the wake extension below the tunnel floor that would have been present in free air: it reconstructs the 'missing' part of the wake as well as providing image effects.

8.2.1.9 APPLICATION OF INTERFERENCE COEFFICIENTS.

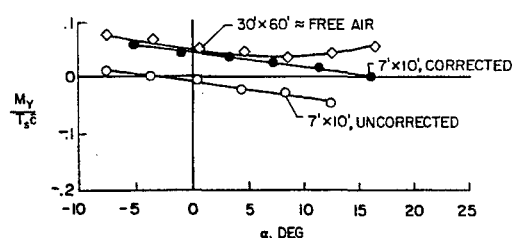
The interference factors, $\delta_{w,L}$, $\delta_{u,L}$, are used to determine tunnel-induced vertical and horizontal velocity associated with lift. $\delta_{w,D}$ and $\delta_{u,D}$ are the corresponding factors associated with drag. They are plotted typically as a function of χ , the momentum-based skew angle, with tunnel width-to-height ratio, σ , as a parameter. Numerous plots of this type may be found in Heyson [25], for example. Figure 8.13, adapted from Heyson [23], shows the variation of the four interference factors with x/H for various skew angles.



(a) Effect on downwash distribution



(b) Pitching moment correlation for original definition of χ



(c) Pitching moment correlation for revised definition of χ

Figure 8.12 Changes in downwash distribution and pitching moment due to redefined wake skew angle.

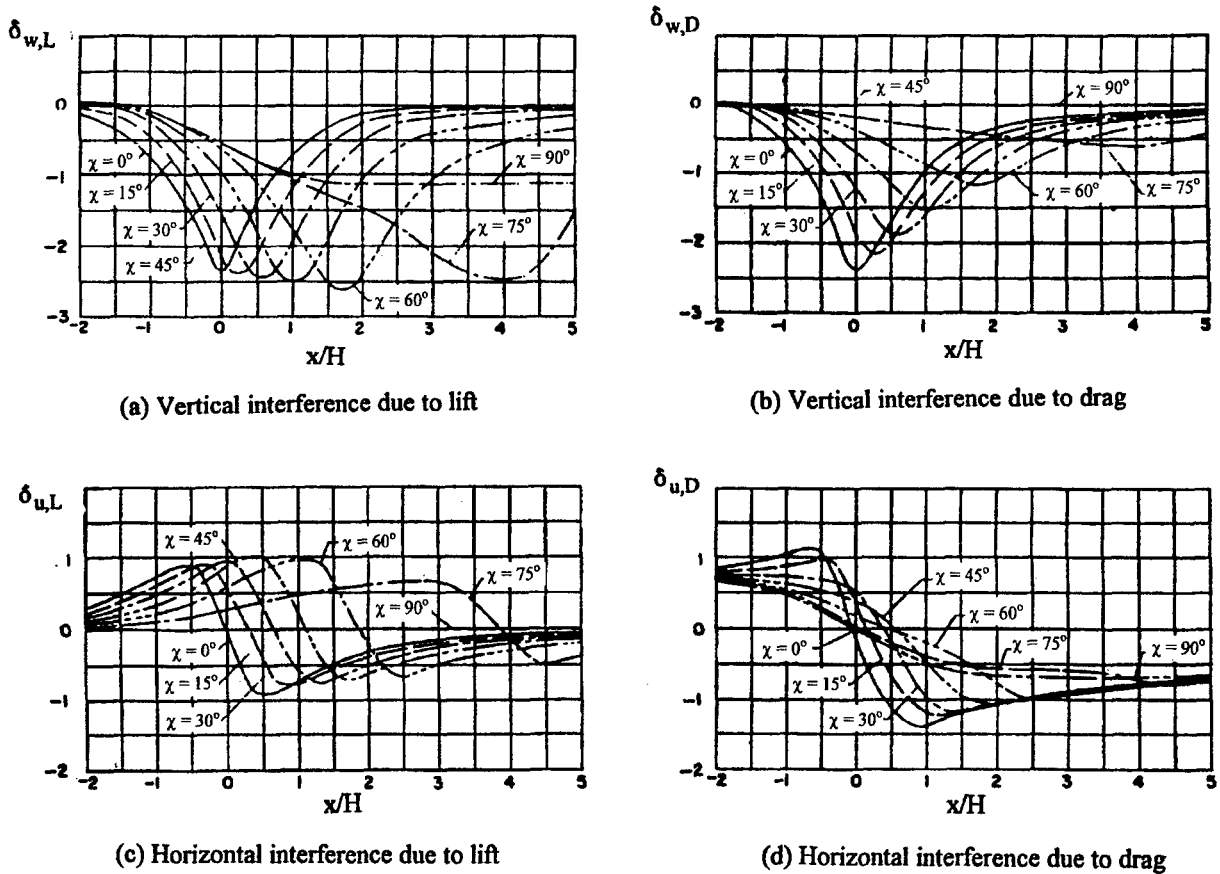


Figure 8.13 Examples of Interference coefficients

$\delta_{w,L}$, $\delta_{u,L}$, $\delta_{w,D}$ and $\delta_{u,D}$, are normalised on u_0 or w_0 . The parameter w_0 is defined in Heyson [24] as "the vertical induced velocity, at the force-generating system, required to produce a given vertical force, positive upward". u_0 is defined similarly for horizontal force. For a helicopter, "at the force generating system" means at the rotor hub. The wake skew angle (Figure 8.9) is then given by

$$\tan \chi = \frac{V + u_0}{-w_0} \quad (8.1)$$

where V is the mainstream velocity. The resultant velocity V_R is given by

$$V_R = \sqrt{(V + u_0)^2 + (-w_0)^2} \quad (8.2)$$

If the characteristic velocities in the far wake are nw_0 and nu_0 the lift and induced drag are given by

$$L = \rho A_m V_R (-nw_0) \quad (8.3)$$

$$D_i = \rho A_m V_R (-nu_0) \quad (8.4)$$

Now define a reference velocity w_h as the value of w_0 that would be required to hover with zero speed and induced drag and the same values of n and A_M that pertain to forward flight (see Heyson [31] for a more comprehensive development). Thus:

$$w_h = -\sqrt{\frac{L_h}{n\rho A_m}} \quad (8.5)$$

where the negative sign is required because positive lift requires negative induced velocity. The value of n is 2 for a rotor or wing and 1 for a ducted jet. A_m is the momentum area of the aerodynamic force generating system; the rotor disc area for a helicopter or the exit area for a jet. The momentum area for a wing is $(\pi/4)$ times span-squared. The parameter n expresses the change in effective velocity w_0 between the rotor plane, for example, and a location far downstream where slipstream contraction is complete.

Substituting equations 8.3 and 8.4 into 8.2 and normalising on w_h yields, (see Heyson [24]):

$$\left(\frac{w_0}{w_h}\right)^4 = -\frac{1}{\sqrt{1 + \left(\frac{V}{w_0} + \frac{D_i}{L}\right)^2}} \quad (8.6)$$

In equation 8.6, V is the mainstream velocity, D_i is estimated from measured drag, L is measured lift and w_h is determined from equation 8.5. Equation 8.6 is implicit in w_0 . Figure 2 of Heyson [24] is a nomographic procedure used to determine V/w_h (see also Figure 6 of Heyson [25]). (V/w_0) is then determined using $(V/w_0) = (V/w_h)/(w_0/w_h)$. One more chart look-up is then performed to determine χ , which is a unique function of (w_0/w_h) . There is now sufficient information to construct the flow model and determine the four interference δ 's. The subsequent procedure is described in Appendix C of Heyson [25], which details the entire twenty-eight step process.

8.2.1.10 ALTERNATIVE INTERPRETATION OF THE SOLUTION PROCESS

Equation 8.6 may be expanded to give

$$\left(1 + \left(\frac{D_i}{L}\right)^2\right)\left(\frac{w_0}{w_h}\right)^8 + 2\left(\frac{V}{w_h}\right)\left(\frac{D_i}{L}\right)\left(\frac{w_0}{w_h}\right)^7 + \left(\frac{V}{w_h}\right)^2\left(\frac{w_0}{w_h}\right)^6 - 1 = 0 \quad (8.7)$$

Equation 8.7 is an octic in (w_0/w_h) in which all of the coefficients and w_h are known. In effect, the nomographic approach of Heyson [24] solves this equation and selects the appropriate root.

We obtain u_0 using the auxiliary equation

$$u_0 = w_0\left(\frac{D_i}{L}\right) \quad (8.8)$$

which is obtained by dividing equation 8.3 by equation 8.4.

Finally, we substitute u_0 and w_0 into equation 8.1 to obtain χ . Construction of the in-tunnel flow model is completed by converting the momentum-based value of χ to the effective value, χ_e , as described previously.

Chart look-up or equivalent computer code is used to determine $\delta_{w,L}$, $\delta_{u,L}$, $\delta_{w,D}$ and $\delta_{u,D}$. These interference coefficients are then re-normalised on mainstream velocity using:

$$\begin{aligned}\frac{\Delta w_L}{V} &= \delta_{w,L} \left(\frac{A_m \rho_0 w_0}{A_T \rho V} \right) \\ \frac{\Delta u_L}{V} &= \delta_{u,L} \left(\frac{A_m \rho_0 w_0}{A_T \rho V} \right) \\ \frac{\Delta w_D}{V} &= \delta_{w,D} \left(\frac{A_m \rho_0 u_0}{A_T \rho V} \right) \\ \frac{\Delta u_D}{V} &= \delta_{u,D} \left(\frac{A_m \rho_0 u_0}{A_T \rho V} \right)\end{aligned}\tag{8.9}$$

where A_T is the tunnel cross sectional area, ρ_0 is the density of the powered flow and the remaining symbols are as defined previously.

8.2.1.11 SAMPLE RESULTS FOR V/STOL CONFIGURATIONS

Heyson [25], [26] and [33] give examples of the application of his correction procedures to V/STOL configurations. A summary is given in Heyson [32]. Somewhat surprisingly, in view of the method's origins and current use, it is difficult to find a good example for a pure helicopter. This is partly due to the fact that reliable small/large-tunnel helicopter test comparisons are very difficult to do but also because Mr Heyson's assignments within NASA were out of phase with the helicopter testing of that time (see Margason [35]).

Limited V/STOL examples will be given here that compare corrected data from models in a 7- by 10-foot test section with results measured in a 17-ft test section. All the present examples were taken from Heyson [25], which includes ground-effect cases and other V/STOL configurations.

Figure 8.14(a) shows lift and drag data for a 3.36-ft semi-span jet-flapped model prior to applying corrections. The flap angle was 60-degrees. A significant difference in stall angle may be seen. On applying first-level corrections (not shown), the stall angle difference was largely resolved, but a significant C_L discrepancy of about 1.0 arose, the small tunnel value being greater. This was consistent with the fact that corrected C_{μ} values differed by 0.62. Figure 8.14(b) shows good correlations after correcting the results to a common C_{μ} value of 6.75.

Figures 8.15(a) and (b) show data for a tilt-wing VTOL configuration before and after correction. In this case correction to a common C_T was not possible. Heyson [25] points out that the corrections are significant even for the large tunnel in this example. The fact that corrections to drag in the small tunnel move the upper part of the polar from drag to a thrusting condition has obvious performance implications.

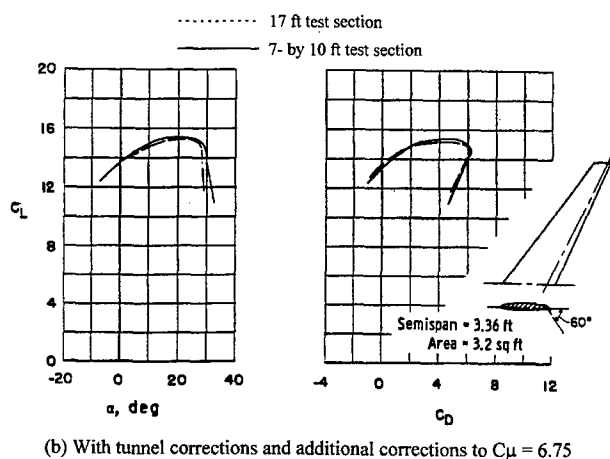
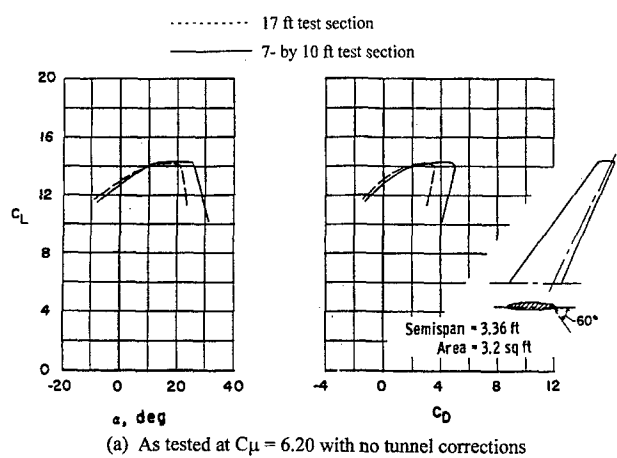


Figure 8.14 Application of Heyson's corrections to a swept-wing jet flapped model at very high lift

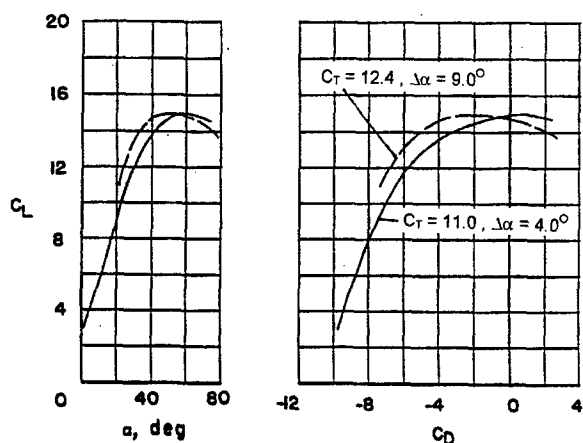
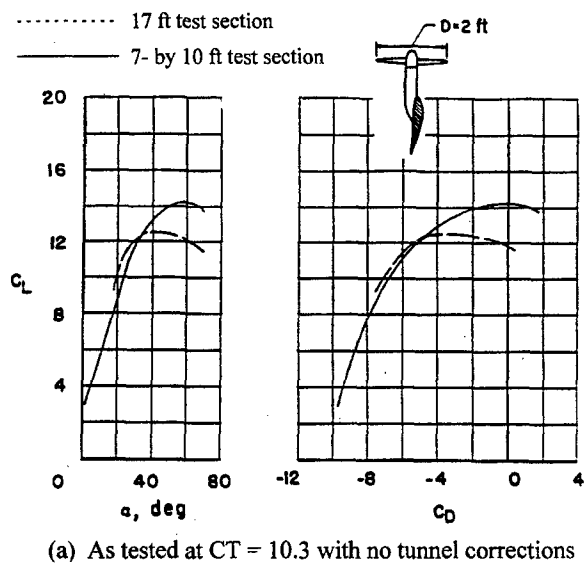


Figure 8.15 Application of Heyson's Correction to a tilt-wing VTOL configuration

The ducted fan, in the example of Figure 8.16, has an area of only 2% of the 7- by 10-foot tunnel area but nonetheless the correction is noticeable (Figure 8.16(b)). In this case the C_T discrepancy is only a few percent and the curves correlate quite well without further adjustment.

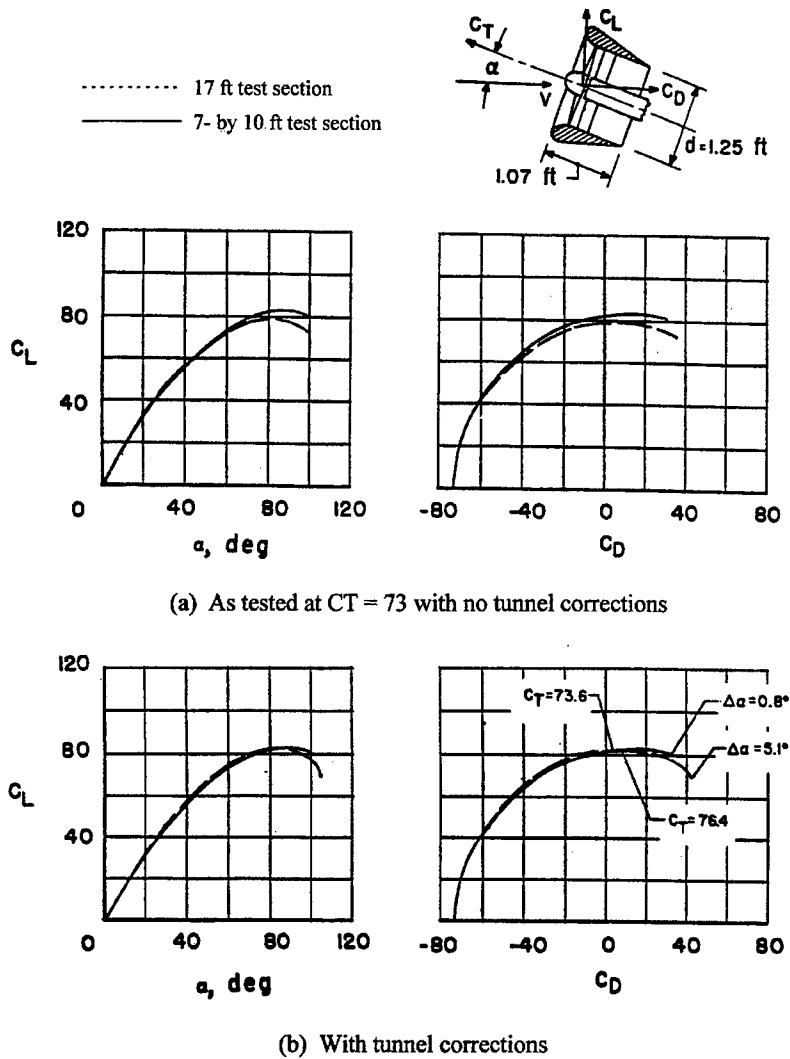


Figure 8.16 Application of Heyson's correction to a ducted fan configuration

8.2.2 PANEL METHODS.

Panel methods may be thought of as a bridge between the classical potential flow methods and more recent approaches based on wall pressure measurements (see Section 8.3). They permit larger model size and give more geometric flexibility; considerable detail is possible. However they do not automatically accommodate viscous effects or power effects which, if used, have to be added explicitly. The discussion in this section will be limited to the special needs of V/STOL flow representation. A more general description of panel methods may be found in chapter 2.3.

A principle difficulty in modelling V/STOL powered flows concerns the fact that the jet trajectory and cross sectional shape are usually unknown and cannot be measured readily. This was circumvented in the Heyson approach, above, by assuming a straight-line jet trajectory at an empirically determined angle. Other approaches employ more sophisticated empirical shapes based on experimental trajectories, as in Section 8.4, for example. The jet cross sectional shape is usually of secondary importance for far field calculations, such as wind tunnel effects, provided that the local turning forces are represented.

A second difficulty concerns the representation of bi-energy flows. We saw in Section 8.2.1 that a vortex ring cylinder, or its equivalent, is needed to represent a large helicopter wake properly. In the examples quoted in the previous section, Heyson shrinks the ring cylinder to a line, thereby preserving the thrust but eliminating the high energy part of the real flow. If a semi-infinite, constant-strength vortex tube is employed, an actuator disc is implied at the rotor plane that provides a uniformly distributed jump in velocity potential (total pressure). Strictly, the wake of an open rotor should be relaxed to allow slipstream contraction to occur, as for propellers (see previous chapter), but this is not usually done in tunnel effects applications. In a ducted flow, a semi-infinite vortex ring cylinder may be placed in the duct, to provide the energy jump, and radial equilibrium may be achieved by specifying a Neumann boundary condition (zero normal flow) at the duct wall.

Panel methods can be used to address both of the above difficulties. An early example (Figure 8.17) concerns the Boeing fan-in-wing program (See Rubbert et al [38]). This application was designed for free air performance estimation. However with the computing power now available, the method could also be used for estimating tunnel effects, by adding panelled tunnel walls, for example. In Figure 8.17, a panelled cylinder is wrapped around an empirically determined plume trajectory. Doublet panels were employed and the Neumann boundary condition was imposed at the centre of each. The boundary condition is specified all the way around the periphery of the cylinder so the effects of the exterior flow around the jet body are included.

The fan face is also represented by doublet panels but a finite, rather than a zero normal velocity is imposed there. No attempt is made to simulate the fan's geometry or its pressure rise characteristic. Directly specifying the velocity through the fan defines the jump in potential (and total pressure) across it. Since, at forward speed, there would be a finite velocity through the fan plane in free flow (i.e with the fan-face boundary condition unspecified), the actual jump in potential is determined by the difference between this free flow and the imposed velocity. This makes it very difficult to estimate the boundary condition that would provide a constant total pressure rise across the fan, for example. A poor choice of imposed velocity could even lead to pressure *loss* through the fan plane. Assumptions concerning this boundary condition therefore need to be made with considerable care and the use of experimental measurements at the fan inlet may be appropriate. Rubbert [38] shows significant flow changes as the imposed inlet velocity distribution is changed.

Viscous effects are simulated in Rubbert [38] using simplified strip methods: the same approach could be applied to the wind tunnel walls, including the effects of model-imposed pressures. While this might account for most of the viscous effects, wall pressure based methods are needed to capture the full interaction.

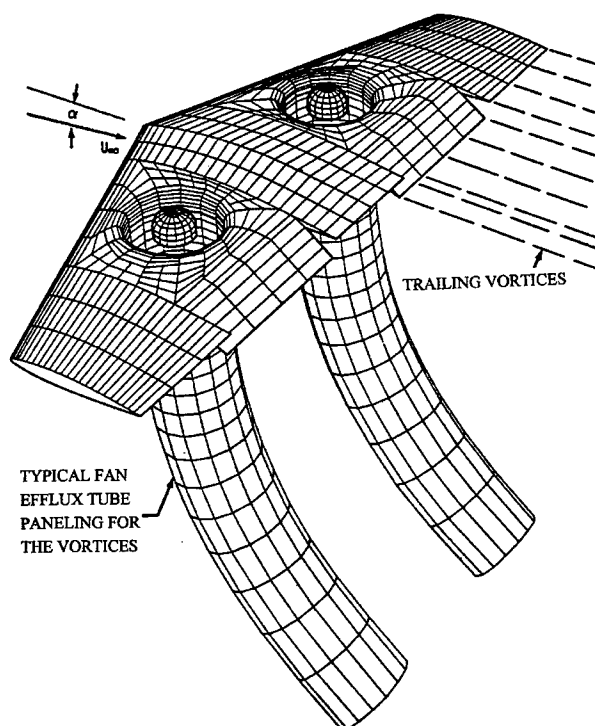


Figure 8.17 Application of a panel method to a fan-in-wing configuration

8.3 THE WALL PRESSURE SIGNATURE METHOD

8.3.1 THEORETICAL OVERVIEW

The pressure signature method uses pressure measurements ("signatures") along the tunnel wall, roof and floor centreline to determine the tunnel interference at locations on the test model. The pressure data, interpreted as streamwise velocities, are used to determine the strengths and locations of line sources and horseshoe vortices that constitute a simplified theoretical model of the object being tested. The underlying theory is developed in Section 4.1.3. This contrasts with the two-variable method (Section 4.1.4), which requires full area coverage of all four tunnel surfaces but requires no representation of the model. The pressure signature method has been employed for powered flows for about twenty years. There is much less powered flow experience with the two-variable method (see Ashill and Keating [1]).

The discussion that follows deals with practical aspects of applying the pressure signature method in its various forms. The underlying mathematical development is given in Section 4.1.

8.3.1.1 THE THREE DIMENSIONAL INVERSE PROBLEM.

The first task when using the pressure signature approach is to determine a theoretical flow model of the object under test in the wind tunnel using limited geometric information. This flow model includes a classical set of wall images. The output from the first task comprises the strengths and locations of the model elements; sources, sinks and horseshoe vortices. With these established, the second task - finding the interference at the model - is straightforward. This is accomplished by calculating the velocities induced at the model location by the tunnel image system. The effects of the tunnel-induced flow on model forces and pressures can then be determined.

The crux of any pressure signature method lies in determining the theoretical model. This particular three dimensional inverse problem is unusual because the boundary condition is specified at locations that are remote from the generating elements. The element locations are unknown and the expressions for induced velocity at the walls, due to model elements, are non-linear in X, Y and Z, the space coordinates. The problem to be solved is therefore algebraically non-linear. The fact that the theoretical model includes an infinite array of tunnel-surface images leads to very complicated equations with little prospect for a closed-form solution (see Hackett et al [12]), Appendix IV). Several different solution methods have been employed.

8.3.1.2 NON-LINEAR SOLUTIONS

Figure 8.18 (upper) shows the original theoretical flow model used for blockage solutions by Hackett et al [8] and subsequently (e.g. Hackett et al [12]). The lower plot shows how the solid and wake blockage contributions combine to give the total tunnel wall signature. The theoretical model comprises a solid-blockage line source and line sink, total strengths $+Q_s$ and $-Q_s$, located on the tunnel centreline at X_3 and X_4 (Figure 8.18), and a wake line source, total strength Q_w , at station X_2 . The solid blockage source-sink spans b_3 and b_4 are equal but different from b_2 . There are thus three unknown locations, two unknown spans and two unknown strengths, for a total of seven variables. The five geometric variables are non-linear; the two strengths are linear. Hackett et al [8] found non-linear solutions for a 9.53% normal flat plate using seven points selected from a measured wall signature. Multiple solutions are possible because the problem is non-linear: the particular root obtained depends upon the initial estimate given to the solver. Complex-number solutions have no meaning in the present context and can be

discarded. Three non-linear solutions were compared with results obtained using the chart look-up approach that eventually became standard for many applications (see Section 8.3.3). This showed that all of the calculated interference distributions lay within a narrow band, even though the geometry and element strengths varied significantly among the several solutions.

The full non-linear, seven variable approach is impractical for real-time use so additional assumptions were made to make the logistics more manageable. The source spans, which were found to be weak variables, are now estimated from the model geometry and it is assumed that all the spans are equal and that the wake source is positioned midway between the solid blockage source and sink. This approach, which has become known as the "source-source-sink method", leaves four quantities to be determined, Q_w , Q_s , X_2 and c_s (see Figure 8.18). The problem remains non-linear, however, and iteration is needed to find the solution. Results using this approach fall within the same band as for the seven-variable approach just described. (See Hackett et al [8]). Section 8.3.3 will describe the production implementation of the "source-source-sink" approach. Conventional angle of attack corrections are used in conjunction with this version.

It is possible in principle to consider an analogous non-linear approach for tunnel-induced upwash, using horseshoe vortices instead of line sources. However, in the context of the high lift situations for which the method was developed, interactions between lifting and blockage flows might make it necessary to couple the two solutions. For example, vortex-generated upwash, at the sidewalls, can be sufficient at very high lift to affect the sidewall blockage signatures. It was therefore decided to adopt a linear approach for combined lift and blockage interference (see below and Section 8.3.4)

8.3.1.3 LINEAR SOLUTIONS

During the early development of the pressure signature method, there was interest in applying it on-line so as to test at "true-q". Though the source-source-sink approach is reasonably efficient, the computers of the day were marginal for this task and a faster code was required. This provided additional incentive to develop the "matrix" version of the pressure signature method.

Fixed-span, fixed-location elements are used under the matrix method, thereby removing the non-linear geometric variables from the problem and leaving only element strengths as unknowns. An influence matrix is calculated for the measurement locations at the tunnel walls, including the effects of the full tunnel image system, as before. Typically, a source array might now include ten elements of unknown strength distributed uniformly from the model nose to a location in the wake.

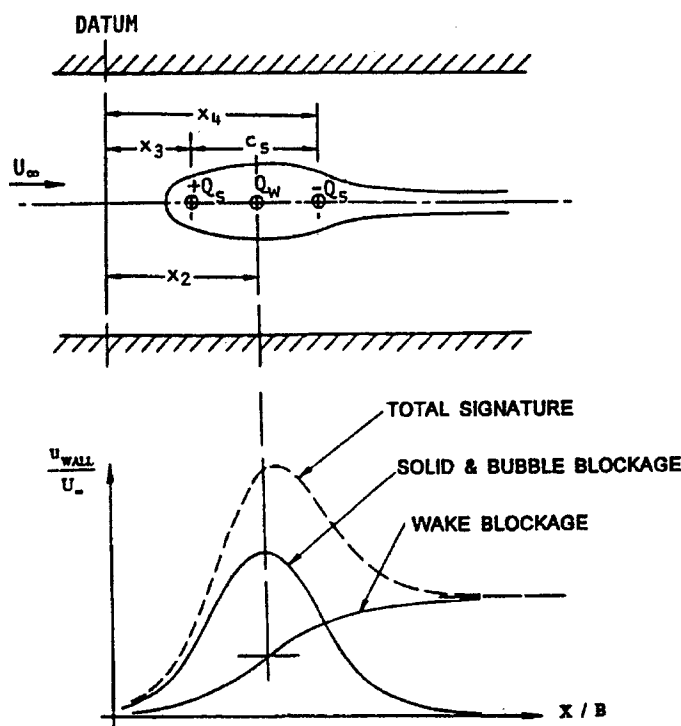


Figure 8.18 Flow model for the "Source-Source-Sink" version of the pressure signature method

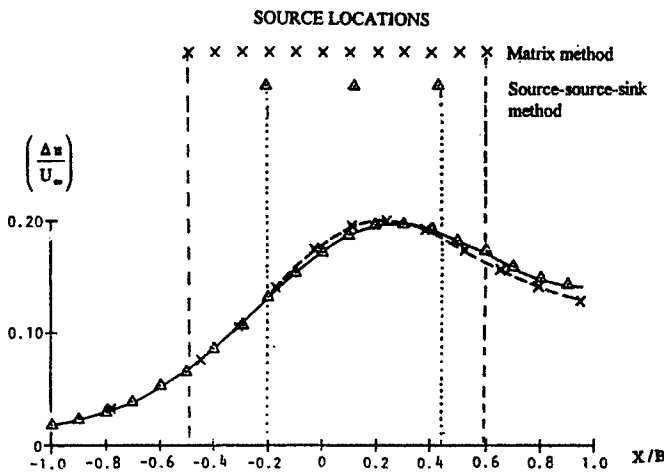


Figure 8.19 Centreline blockage distribution for a 9.53 % normal flat plate

In a practical installation, designed to accommodate a variety of models and test conditions, the number of wall pressure measurements may be several times the number of elements used in the theoretical model, so a least-squares solution is required. Figure 8.19, which uses the same 9.53% normal plate pressure signature as the example quoted above, shows results for the source-source-sink and matrix solutions as triangles and crosses respectively. It is apparent that the solutions are very similar, despite the fact that the element distributions differ significantly.

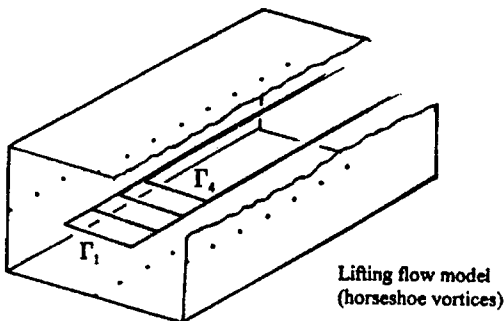
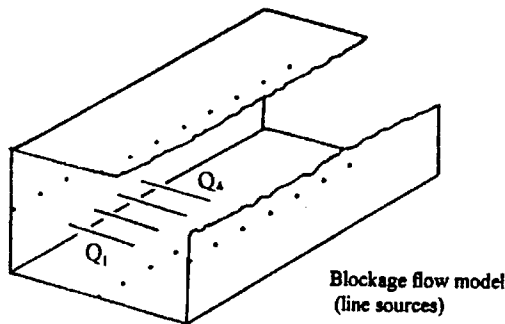


Figure 8.20 Flow model for the "Matrix" version of the pressure signature method

Influence coefficients for horseshoe elements add further columns to the influence matrix, which is solved using least-squares as before. Figure 8.20 shows the arrangement of four line sources and four horseshoe vortices in the wind tunnel. More elements than this are usually employed. Section 8.3.4 describes the implementation of the matrix method. A description is included of how the blockage/lift interaction, mentioned above, is handled.

8.3.1.4 QUASI-LINEAR SOLUTIONS

Hackett et al [14] and, more recently, Rueger, Crites et al [39] mention the proclivity of the matrix version of the pressure signature method to produce oscillating-strength solutions. In neither of the instances quoted was this harmful to the resulting interference distribution. These examples reflect the ill-conditioning that is common in influence matrices of the present type (see also Section 4.1.3). Ill-conditioning is also found in more conventional three dimensional inverse solutions. The problem has been handled, in pressure signature solutions to date, by increasing the element pitch and/or reducing the number of elements when the amplitude of the oscillations becomes too large.

A serious instability problem surfaced recently (1995) in an unpublished study of a non-planar, unpowered system that was located above the tunnel centreline. Having generated synthetic signatures using a theoretical vortex-source model with twenty elements at ten locations, it was found to be impossible to recover the original element strengths from the signatures because of extreme oscillations. In some instances, these oscillations propagated to the interference solution. This prompted the development of a solver that detects columns in the influence matrix that are "nearly-dependent" and

eliminates the redundant ones. Row reduction is also possible. With a suitably chosen "near-dependency" parameter, the element distribution is thinned and the matrix ill conditioning (solution oscillation) is reduced to an acceptable level. After applying this procedure, the interference distributions closely matched the theoretical ones generated by the original elements. This new approach could be called 'quasi-linear' because it edits out redundant elements from the original set. The overall effect is to select optimum element locations on a piecewise basis rather than the continuous basis of a true non-linear solution.

Further comments on the construction of the theoretical model are given in Section 4.2.6.

8.3.1.5 THE WAKE-INDUCED DRAG INCREMENT

The tunnel-induced drag on the source-source-sink model of Figure 8.18 was analysed first by Hackett et al [12] and later by Cooper, Hackett, Wilsden et al [2] and by Hackett [18], [19], who showed that the in-tunnel wind-axis drag coefficient exceeds the free air value by

$$DC_{D_{vis}} = \frac{1}{2} \left(\frac{Q_W}{U_\infty A_{TUN}} \right) C_{D_{vis}}$$

where $C_{D_{vis}}$ is the viscous part of the model drag coefficient and the symbols inside the brackets are as defined previously. $\Delta C_{D_{vis}}$ is subtracted from the measured drag coefficient prior to applying the dynamic pressure correction.

The $\frac{1}{2}(\)$ term is the tunnel-induced interference velocity at the wake source location, due to wake source interference, which is proportional to Q_W . This acts on a source that represents the model viscous drag. The two source values are different because Q_W , which is obtained from the wall signature, includes wall boundary layer effects whereas the source representing model drag does not. If $C_{D_{vis}}$ is not readily available, Cooper et al [2] suggest that a value derived from Q_W should be used instead. Conversely, a $C_{D_{vis}}$ based source strength is suggested if Q_W is unavailable. An example of the latter type is given in Section 8.2.3 of this report. The $C_{D_{vis}}$ based approximation will underestimate the correction while the Q_W based approximation will overestimate it. If the wall boundary layers are disturbed significantly by the model, as in car testing for example, the differences between these alternatives can be substantial.

Hackett [18], [19] discusses the flow physics implied by the above correction for a normal flat plate. He suggests, with some experimental support, that the added drag in the wind tunnel reflects a change in separation bubble shape caused by tunnel-induced velocity gradients. Both these references and Cooper et al [2] show, however, that this is *not* horizontal buoyancy as usually calculated from the product of static pressure gradient and model volume. Rather, it is shown by kinematic arguments that, when a full analysis of the system is conducted, the gradient-volume term cancels with another.

8.3.2 EXPERIMENTAL ASPECTS

8.3.2.1 TESTING AND PRE-ANALYSIS

Pressure instrumentation is installed along the centrelines of the tunnel roof, floor and walls with sufficient length to capture the upstream and downstream asymptotes (Figure 8.18) and sufficient resolution in the vicinity of the model to define the suction and pressure peaks properly. For aeronautical applications, this usually means that the full test section length must be covered, with about twenty orifices for each of the four signatures. The subject of orifice distribution within the test section length is discussed in Section 4.2.5. Hackett et al [11] give details of the layout used for the knee-blown flapped wing tests quoted in Section 8.1.

It is not unusual for a test section to be too short and special procedures may be needed to estimate the upstream and downstream asymptotes. Cooper, Hackett, Wilsden et al [2] describe an iterative procedure that is used to estimate the downstream asymptote and make appropriate adjustments. Situations with too-short an upstream test length should be avoided because the tunnel reference system may be compromised. However, it is demonstrated in Wilsden [43] that, with careful pressure signature analysis, even this situation is recoverable. A source of suitable strength is placed far upstream to shift the signature vertically and thereby correct the front asymptote. Good asymptotes will be assumed in the discussion below.

Real wind tunnel walls and pressure orifices may, in practice, be imperfect. For this reason, and because of the sensitivity of the method to measurement errors, it is important to acquire a reference set of pressures with the model removed from the test section ("empty tunnel signature"). These reference data, converted to velocities, are subtracted from the corresponding model-present data. In certain cases 'empty' tunnel data may be taken with model mounts or a sting installed. Flow calibration at the model position must, of course, be carried out with the same equipment in place. Furthermore, if the presence of the model imposes a significant supervelocity at the wall, the 'empty' reference velocities must themselves be corrected before subtraction. Thus the simple superposition equation:

$$\left[\frac{u}{U} \right]_{CORR} = \left(1 + \left[\frac{u}{U} \right]_{MEAS} \right) - \left(1 + \left[\frac{u}{U} \right]_{EMPTY} \right)$$

becomes, on correcting the empty tunnel data:

$$\left[\frac{u}{U} \right]_{CORR} = \left(1 + \left[\frac{u}{U} \right]_{MEAS} \right) - \left(1 + \left[\frac{u}{U} \right]_{EMPTY} \left(1 + \left[\frac{u}{U} \right]_{MEAS} \right) \right)$$

Only sidewall pressures are needed to determine the blockage for a centrally-mounted, vertically-lifting model. The lifting system generates mainly upwash at the sidewalls and this affects the pressures only at very high lift (see Section 8.3.4). In principle, a blockage signature can be obtained for a lifting model by calculating the mean of the roof and floor velocity signatures, thereby eliminating the lifting circulation. However there is no strong reason to do this (and there are often good reasons not to) so the necessary working charts (see below) have never been prepared.

8.3.2.2 SPECIAL INSTRUMENTATION CONFIGURATIONS.

A reduction from the full, four-wall pressure instrumentation is possible in some situations. As already indicated, only sidewall pressures are needed if the model is centred in the tunnel and conventional angle-of-attack corrections are to be used. Both sidewalls should be instrumented a) to accommodate yawed cases, b) as insurance against small tunnel/model asymmetries in nominally symmetric cases and c) to allow comparison between walls as an aid to troubleshooting.

Only ceiling pressures are needed to determine blockage when testing cars or floor-mounted half-models. The number of orifices can be tailored to approximately a dozen if it is known that model variations will be small. Three-surface instrumentation is sometimes used when tunnel operations preclude floor orifices or under conditions with heavy jet impact at the floor. Pressure signature-based angle-of-attack corrections are possible with this configuration, but lift corrections calculated without the floor signature may be less reliable.

A long test section is beneficial when testing models that are aerodynamically large, mainly to ensure that a good estimate can be made of the downstream asymptote (see below). A good example of this is the fact that, prior to the knee-blown flap model tests described earlier, it was determined that the test section length should be increased from 1.04 B to about 2.0 B. This was, in fact, done (see Hackett et al [11]). The model was situated at a station 0.55 B from the front of the test section. This test section length is not unusual. However, the model is placed further aft in most tunnels, between 0.75 and 1.00 B.

8.3.3 ANALYSIS FOR THE "SOURCE-SOURCE-SINK" VERSION OF THE METHOD.

8.3.3.1 BLOCKAGE SIGNATURE ANALYSIS

The object of the initial analysis is to resolve the measured signature into symmetric (solid blockage) and antisymmetric (wake blockage) parts (Figure 8.18). For a simple signature with well defined asymptotes the procedure starts by determining the normalised wake source strength from the asymptotic velocity, u_{ASYMP} (Figure 8.21) using

$$\left(\frac{Q_W}{U_\infty A_{TUN}} \right) = \left(\frac{u_{ASYMP}}{U_\infty} \right)$$

which is obtained from considerations of continuity. An initial estimate is then made for X_2 , the position of the wake source: the model position is usually selected. The wall signature is then calculated for the wake source acting alone in the wind tunnel, with its tunnel images included. This signature is

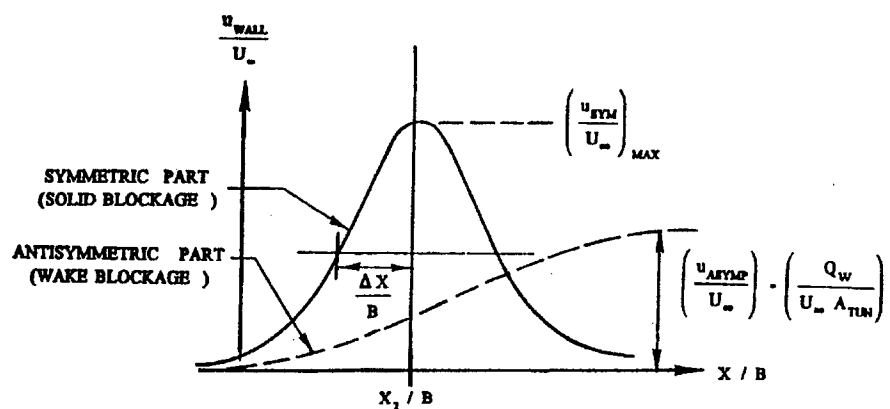


Figure 8.21 Wall pressure signature analysis for the „Source-Source-Sink“ version of the pressure signature method

subtracted from the measured data to yield a trial symmetric (solid blockage) signature. Next, the peak of this symmetric part is fitted using a parabola and the location of its apex is determined. If the X-value for the peak coincides with the position selected for Q_w , within a chosen tolerance, then this part of the signature analysis is complete and the flow model can be constructed. If the peak position lies forward or aft of Q_w , then the wake source is moved towards it and the process is repeated until the two coincide. The computer code includes the necessary logic to ensure convergence. This establishes X_2 (Figure 8.21). The signature analysis phase is completed by determining the height, $(u_{SYM}/U_\infty)_{MAX}$, of the symmetric part of the signature and then DX , the half-width at half-height.

8.3.3.2 CONSTRUCTION OF THE SOURCE-SOURCE-SINK THEORETICAL MODEL

Figure 8.22 shows the procedure for constructing the source-source-sink flow model. The quantities found from the analysis given above appear in the second row of the chart. The wake source analysis, which is already done, appears as the right hand column. The remainder of the chart shows how Q_s and c_s , the remaining components of the blockage model (Figure 8.18), are determined.

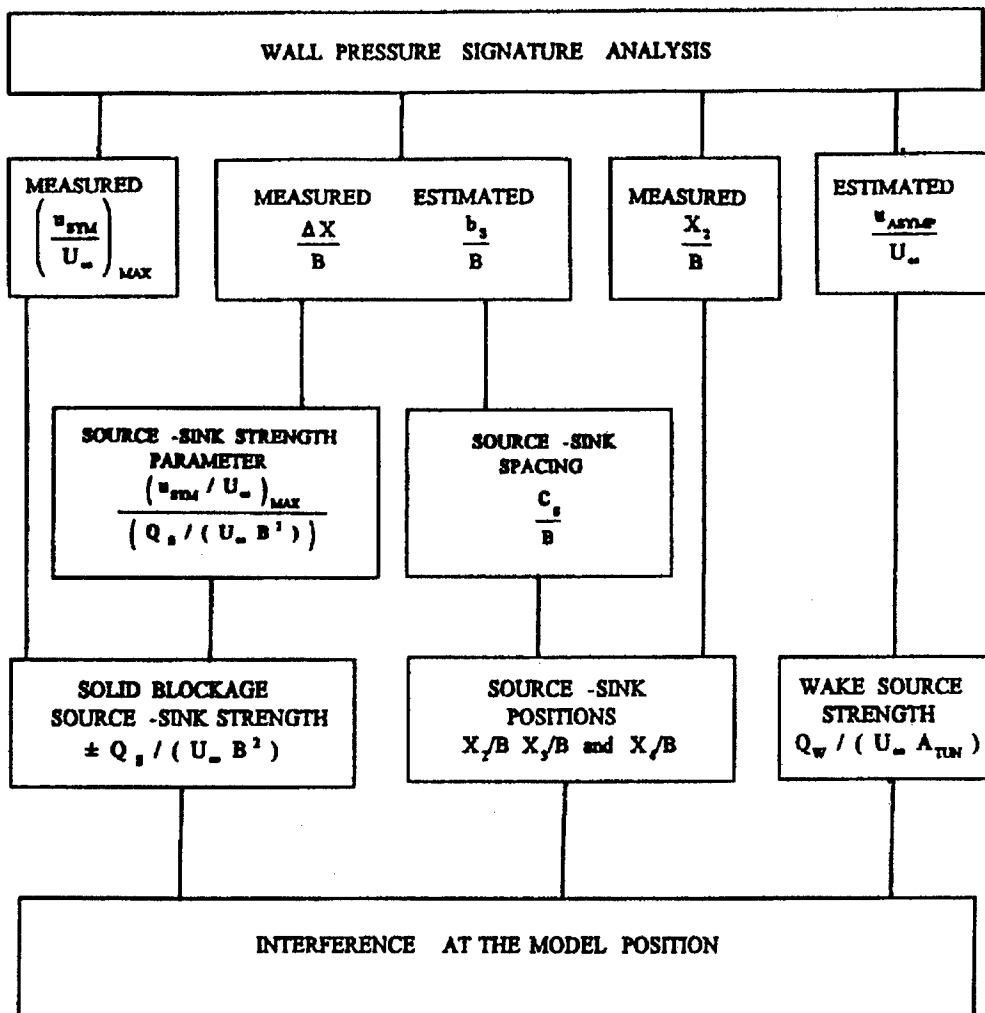


Figure 8.22 Flow Chart for the „Source-Source-Sink“ version of the pressure signature method

Figure 8.23 shows the source-sink strength parameter as a function of the peak semi-width $\Delta X / B$ for a range of source span b_s / B . The value of $(u_{SYM} / U_\infty) / (Q_S / U_\infty B^2)$, obtained from this plot, is divided into the measured value of (u_{SYM} / U_∞) to yield the normalised source-sink strength $(Q_S / U_\infty B^2)$.

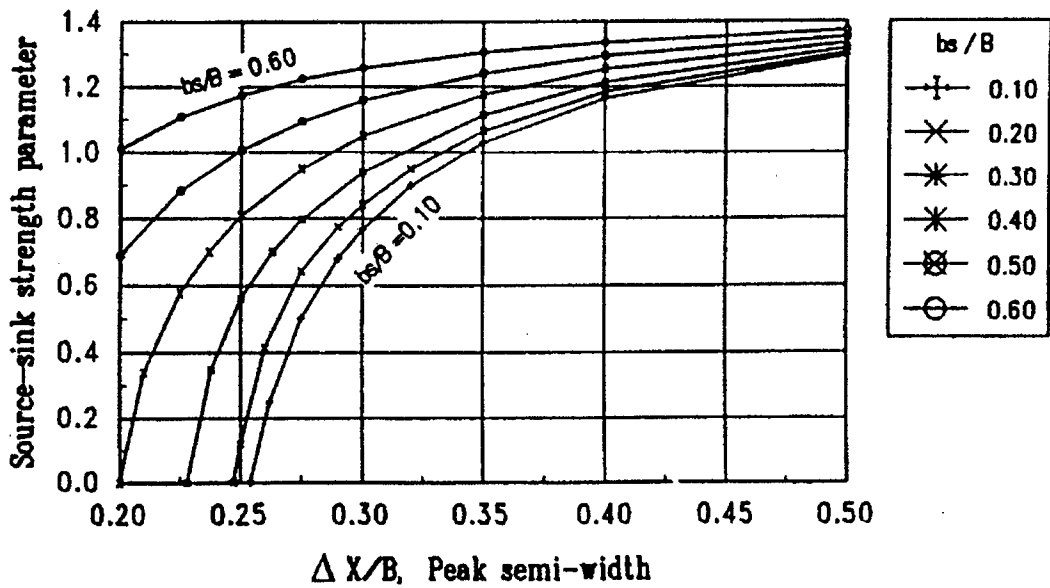


Figure 8.23 Source-sink strength parameter $[(u_{SYM}/U_\infty)/(Q_S/U_\infty B^2)]_{MAX}$ as a function of source-sink span and peak semi-width for $H/B = 0.707$

Figure 8.24, which has the same general layout as Figure 8.23, is used to determine the source-sink spacing c_s / B . X_3 / B and X_4 / B are then determined as $(X_2 / B) \pm \frac{1}{2} (c_s / B)$. This completes the definition of the source-sink model.

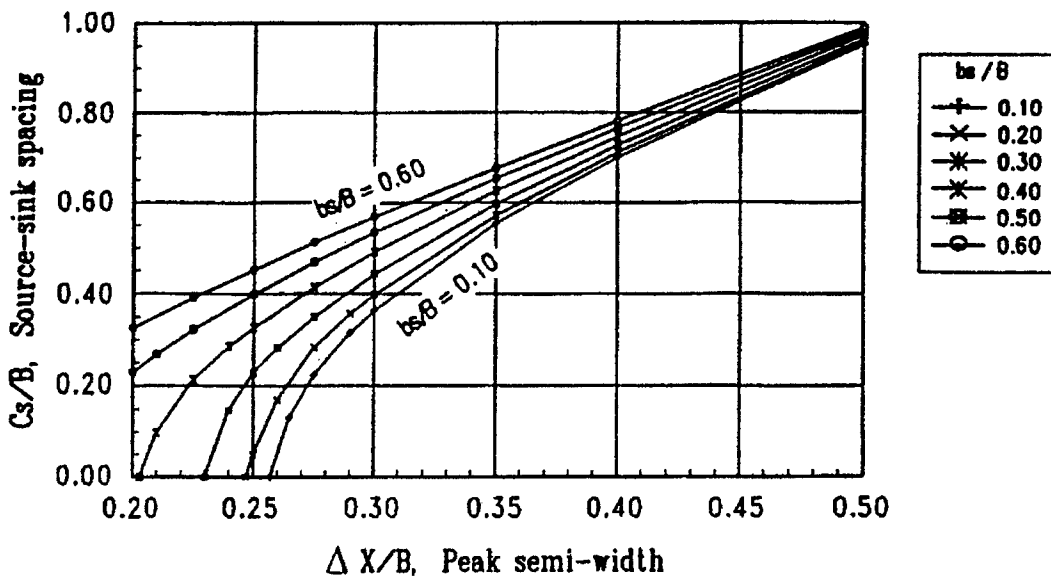


Figure 8.24 Source-sink spacing as a function of source-sink span b_s / B and peak semi-width for tunnel $H/B = 0.707$

8.3.3.3 APPLICATION OF THE SOURCE-SOURCE-SINK MODEL.

With the strengths, spans and locations of two sources and a sink now known, tunnel blockage is determined by superposing the image effects of each of these, using the generic interference curve of Figure 8.25. It will be noticed that the curve is essentially independent of b_s / B . The fact that the curve asymptotes to 1.414 ($= B / H$), rather than 1.00, is a consequence of employing B^2 in the normalisation, rather than BH . This is a carry-over from early versions of the method. Finally, the contributions of the three singularities, with suitable X-shifts, are summed to give the blockage velocity distribution along the tunnel centreline. This is now available for tunnel-q correction at the model reference point or at other significant points along a model such as for C_p corrections distributed along the model length. Figure 8.26, taken from Hackett [17], shows drag correlations for a family of four aspect-ratio 3.0 flat plate wings. Their sizes range from 1.6% to 16.7% of the test section area. Broken lines show the uncorrected C_D 's. Despite the very large corrections for the 16.7% plate, these data collapse well. Numerous additional examples may be found in Hackett [17] and earlier publications. Hackett, Wilsden and Lilley [12] provide FORTRAN code for this method, including iteration to allow for truncation of the forward and aft asymptotes. A methodology for preparing the charts (or their table equivalents) is also given.

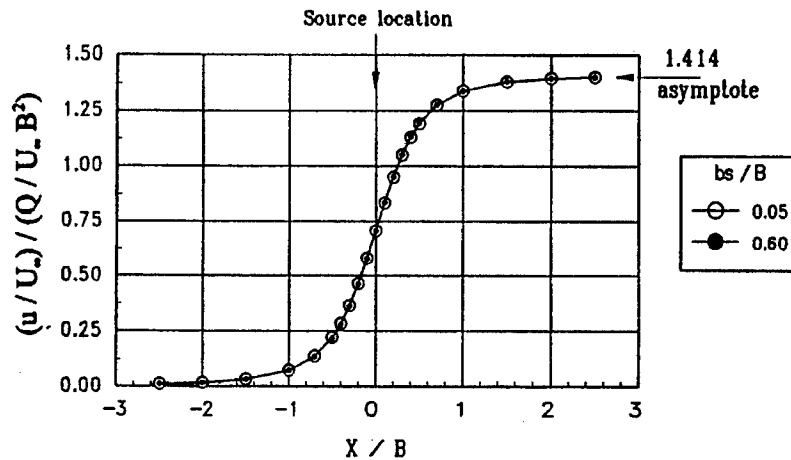


Figure 8.25 Generic curve for determining axial flow interference velocity for a source in a tunnel with $H/B = 0.707$

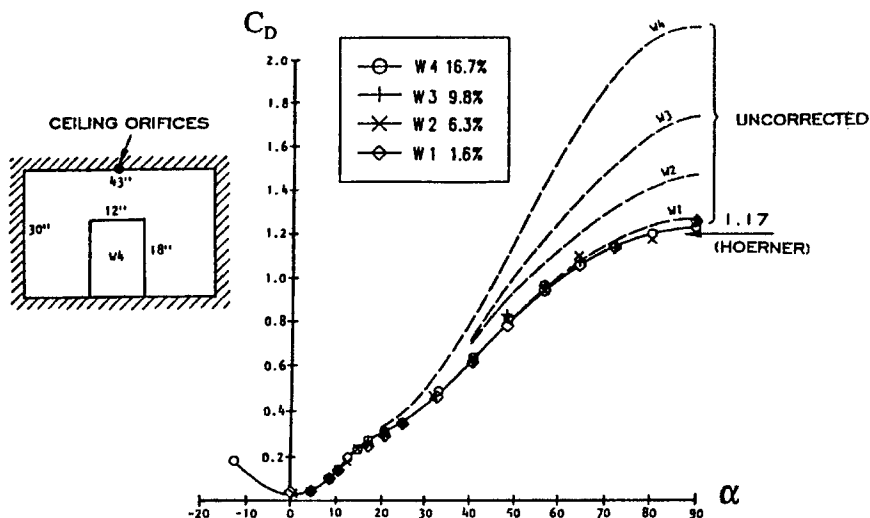


Figure 8.26 Drag correlation for a family of aspect-ratio three flat-plate wings

8.3.4 ANALYSIS FOR THE "MATRIX" VERSION OF THE METHOD.

As explained previously, the need for a matrix procedure arises for three main reasons. First, it is faster and more direct than the source-source-sink approach, just described. Second, it has greater geometric flexibility for unusual model shapes. Third, it is better suited to handle the "cross" effects between lift constraint and blockage, discussed in Section 8.3.1 and described in detail below.

8.3.4.1 LIFT-BLOCKAGE COUPLING

The effects of tunnel blockage are felt more or less equally on all four tunnel surfaces. The effects of vertical lift, being antisymmetric, are felt mainly at the floor and roof, particularly for unswept wing models. It follows that, as a first approximation, lift effects may be captured by finding the difference between the roof and floor signatures and blockage effects are characterised mainly by the wall signatures. However, these approximations start to break down for swept wings at angle of attack and in very high lift situations in which vortex-induced upwash, at the tunnel walls, is sufficient to influence the pressure measurements there. This is examined in detail in Hackett et al [15]. Nonetheless the above approximations provide a useful basis for a correction procedure.

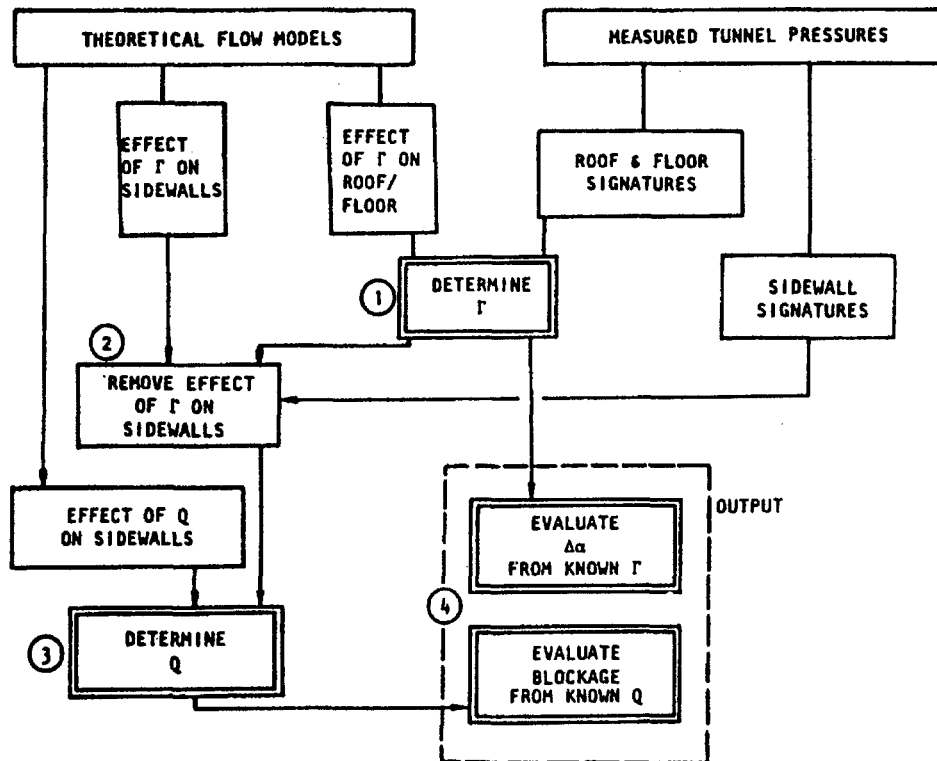


Figure 8.27 Flow chart for the „Matrix“ version of the pressure signature method

Figure 8.27, taken from Hackett [17], shows the flow diagram for the matrix version of the pressure signature method. The theoretical part of the procedure involves setting up influence matrices for the effects, at the tunnel walls, floor and roof of the source and vortex arrays that represent the model (see Figure 8.20). Examples of these matrices are given in Hackett et al [14]. The lifting signatures are analysed first (① in Figure 8.27) from which angle of attack corrections may be immediately calculated. The upwash is then calculated at the sidewalls, assuming the trailing vortices to be horizontal, and appropriate corrections are made to the sidewall pressures (see ②). The sidewall data are now ready for

use, and the blockage influence matrix is used to determine the source strength distribution (see ③). Finally, the blockage due to the source images is determined, at ④. A single pass through the procedure is usually sufficient for all but the most extreme cases. Hackett et al [15] describe a corresponding multi-pass procedure and include the necessary FORTRAN code.

8.3.4.2 ANGLE-OF-ATTACK CORRECTIONS

It is shown in Hackett [15] that, when applied to simple wings, the angle of attack corrections obtained using the above method agree well with those using conventional methods (e.g. Glauert [3]). The cross-effect corrections were negligible in these cases. For powered models lifting more strongly, the Williams and Butler [44] approach, derived for jet-flapped wings, has been preferred in the past. In this method, the classical Glauert result is divided by $(1 + (2 C_{\mu} / \pi AR))$. Figure 8.28 shows angle of attack corrections for a swept wing with a knee-blown flap that was tested to very high lift by Hackett et al [15]. Glauert corrections are given by the straight line through the origin; the Williams and Butler corrections are given by the short, inclined lines. These are located appropriately for the C_{μ} value concerned. Angle of attack corrections derived from wall pressures are denoted by lines with cross symbols. Successive crosses on a given line represent increasing angle of attack. Both the Glauert and Williams and Butler methods overestimate the low-alpha corrections but severely underestimate the rate of increase with C_L , particularly at high- C_{μ} . This suggests that the corrected lift curve slopes will be lower for pressure signature corrected data than when other correction formulations are used.

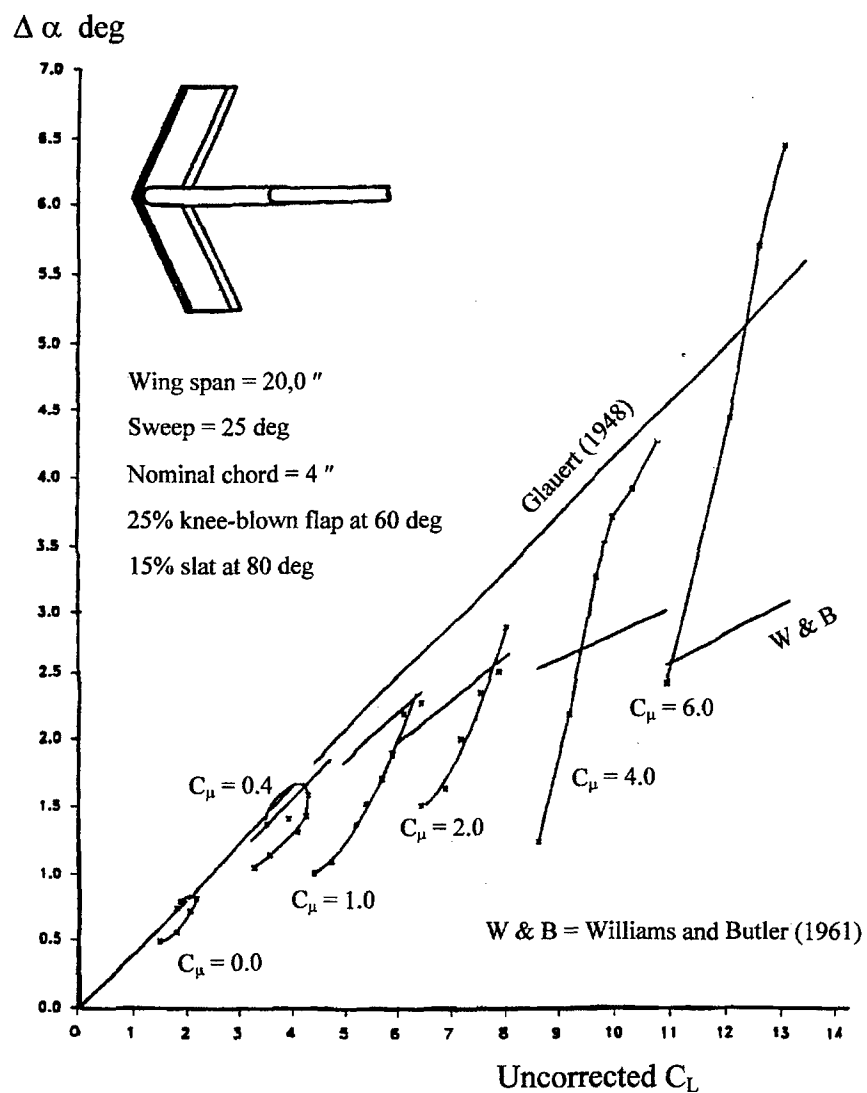


Figure 8.28 Angle of attack corrections for a jet-flapped wing determined by pressure signature and other methods.

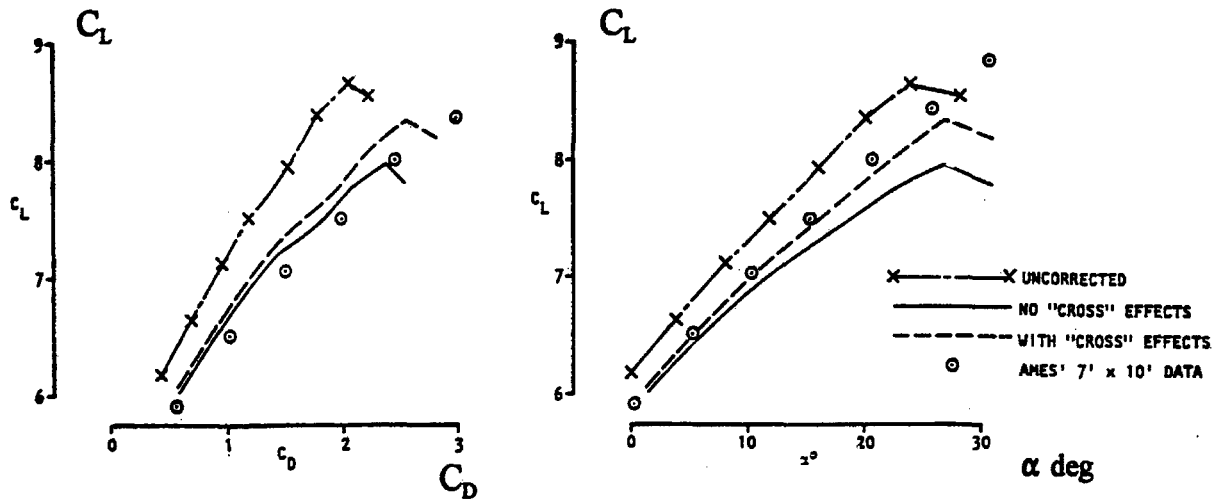


Figure 8.29 Sensitivity of corrections to upwash at the sidewall measuring points.
(Swept, knee-blown flap model at $C_{\mu} = 2.0$)

Figure 8.29 shows the effects of the lift-related sidewall pressure corrections for the $C_{\mu} = 2.0$ case of the previous figure. Uncorrected data are shown by crosses. Corrected data without wall cross flow effects are denoted by full lines and fully-corrected data have broken lines. These are compared with large-tunnel measurements on the same model, shown by circle-points. Both blockage and angle of attack effects are included. It is apparent that the lift curve is seriously over corrected if the wall cross flow effects are not included. The wall cross flow effects on drag are small, but they shift the curve in the wrong direction relative to the large-tunnel data.

The point is made, in Hackett et al [15], that the present wall cross flow terms can be in error because the vortex trajectory is "frozen" i.e., increases in vortex deflection, with increasing lift, are not accounted for. This is important because the upwash distribution on the wall opposite to a nearby vortex is peaky. This results in underestimation of the wall cross flow effects at low C_{μ} and overestimation at high C_{μ} . A wake relaxation procedure would remove this difficulty.

8.3.4.3 POWERED APPLICATIONS AT VERY HIGH LIFT

Extensive two-tunnel comparisons were made in the late 1970's for a range of knee-blown flap configurations. Two basic models were tested in the (then) Lockheed-Georgia 30 x 42-inch tunnel and the NASA/AAMRDL 7 x 10-foot tunnel. Both models had flapped spans of 20 inches with a nominal chord of 4.0 inches. The flap upper surface angles were 76-degrees and 60.0-degrees for the straight and swept models respectively. Slats were fitted to both models routinely, but these could be removed. 5.0-inch chord tip extensions could be added to both models, bringing their spans to 30-inches. Further details of the unswept and swept models are shown in Figures 8.8 and 8.28.

Sample results will be presented here for the swept-wing configuration with tips and slats fitted. The source references for this and other configurations are:

NASA CR 114,496 (Hackett et al [6])	Straight winged model section design.
NASA CR 137,857 (Hackett et al [9])	Straight winged model test.
NASA CR 152,032 (Hackett et al [13])	Straight and swept model tests.
NASA CR 166,186 (Hackett et al [15])	Straight and swept model tests.

The above references include a number of configuration variations and various developmental versions of the pressure signature method. Of these, the last reference should be considered definitive because it employs the matrix method, which is better suited to "difficult" pressure signatures.

Figure 8.30 shows the lift and drag characteristics for the swept knee-blown flap model, tested in small and large tunnels, with the tips fitted. Ground blowing was employed as needed. The broken lines show data from the NASA/AAMRDL 7 x10-foot tunnel, the full lines with points are corrected 30 x 43-inch tunnel data. The tunnel corrections were of similar magnitude to those shown in Figure 8.7, for the straight wing. Heavy ground impingement for the upper three curves (C_{μ} 's of 4.0, 6.0 and 10.0) rendered the floor pressure signatures unusable and the lifting solutions were obtained using a 'roof-only' program option. The sidewall lift-on-blockage corrections were found to be excessive in these cases and were omitted. These analysis difficulties could probably have been alleviated by a wake relaxation procedure, as mentioned earlier. Such a procedure would deflect the trailing vortices downward in these cases, away from the sidewall pressure orifices.

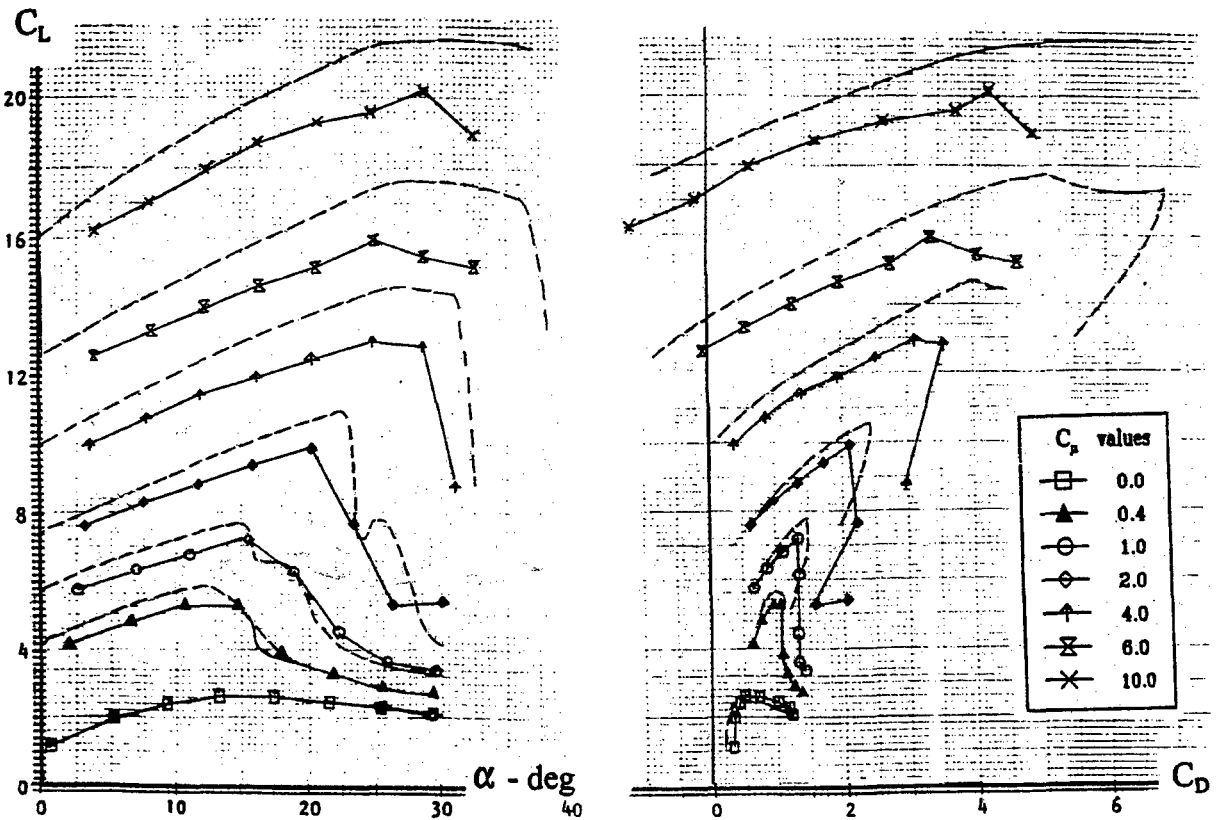


Figure 8.30 Large tunnel and corrected small tunnel lift and drag characteristics for a swept-wing, knee-blown flap model (Large tunnel : broken lines. Small tunnel : symbols)

Figure 8.30 demonstrates tendencies towards overcorrection and slightly early stall in the small tunnel that increase at the higher C_{μ} 's. Pitching moment characteristics, versus angle-of-attack, were well reproduced in the small tunnel with slightly reduced slopes at the highest C_{μ} 's (see Hackett et al [15]). By design, the lift range of Figure 8.30 and for the other configurations quoted above, is probably twice that which is likely to be used in practice. Even with moderate jet impact at the ground and despite the need for large boundary corrections to the small tunnel data, the use of ground blowing and "matrix" pressure signature corrections yields results in the one-to-ten C_L range that reproduce large tunnel data well.

8.3.5 DISCUSSION

The source-source-sink and matrix versions of the pressure signature method each have their own advantages and disadvantages. If pressure signature-based angle-of-attack corrections are required, the matrix method must be used because no code has been written for vortex elements comparable to the source-source-sink approach. Other reasons for using the matrix method include its greater geometric flexibility, the fact that an upstream source can be used to deal with asymptote problems at the front of a measured pressure signature and the fact that the method is better suited to batch processing. Balanced against these is the fact that, with too-close element spacing or noisy signature data, the matrix method can generate oscillations in singularity strength that may propagate into the interference distribution. The net wake source strength, used to estimate the wake-induced drag increment (Section 8.3.1), is much less accurate for the matrix method because it is the net of distributed values that may be oscillating. Both methods are susceptible to data scatter in the body of the signature and particular care is needed with the forward and aft asymptotes in both cases. A continued commitment is needed to make wall pressure signature software more self-tending in this regard, including intelligent system health monitoring. The design of the singularity model for the matrix method is still somewhat of an art and a certain amount of cut-and-try is needed to counter excessive oscillations when these are encountered. Work is in progress (Winter 1996) that addresses the latter problem.

8.4 TUNNEL INTERFERENCE FOR A JET-IN-CROSSFLOW

8.4.1 INTRODUCTION

Whether jet, fan or rotor powered, the defining flow for VTOL aircraft is a round jet directed at right angles to the mainstream. Figure 8.31, taken from Hackett et al [4], shows how a jet emergent from a tunnel floor, for example, is bent by the mainstream towards the streamwise direction. A trailing vortex pair forms and the jet fluid splits into two parts. An equivalent theoretical model, used for estimating tunnel interference effects, will be described below.

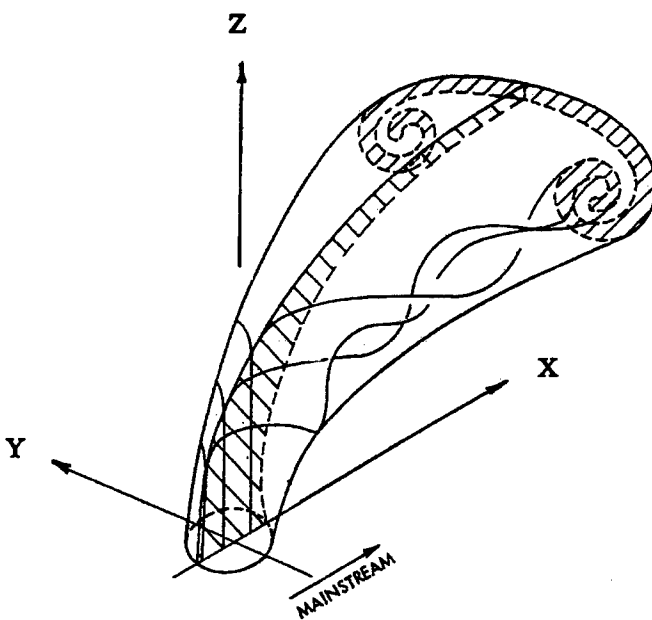


Figure 8.31 Sketch of jet deformation by a crossflow

There is little hope of solving for the details of a jet-in-crossflow theoretical flow model using the methods of Section 8.3: the details are too complex and the three-dimensional inverse process is too fragile. The procedure adopted therefore starts by modelling just the jet and finding its tunnel effects when acting alone. Next, the jet-in-crossflow wall signatures are removed from the measured signatures using the appropriate velocity superpositions. The resulting 'rest-of-model' signatures are then processed using standard pressure signature methods to find *that* part of the tunnel interference. The jet-in-crossflow and 'rest-of-model' interference effects are then added together to give the total tunnel interference.

8.4.2 THEORETICAL FLOW MODEL

Figure 8.32 shows the 'skeleton' of vortex, source and doublet lines that comprise the theoretical flow model developed by Hackett et al in 1981. The x-dimension has been foreshortened in this figure. The model recognises the possibility that, in a tunnel test situation, the jet will impinge on the opposite surface of the tunnel - the tunnel roof in the case shown.

The model details were derived using a combination of empirical fits to jet shape with simple jet mixing concepts. Three singularity types are employed in the theoretical model, each with its own specific task. These comprised vortex, source and doublet lines and the result was named the "VSD" flow model. The trajectory and strengths of the vortex model reproduce experimental measurements. The path of the source and doublet lines models the trajectory of the maximum total pressure point in measured jets; this penetrates more deeply into the flow than do the vortices. Source strength is derived from considerations of jet width, combined with simple mixing concepts to accommodate jet growth. The doublet lines provide the appropriate level of wake closure. The trajectory equations, derived in Hackett et al [15] are:

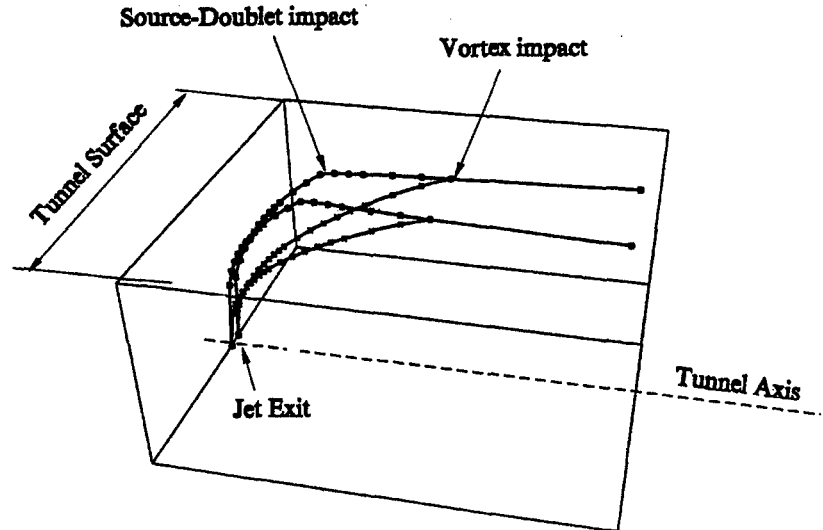


Figure 8.32 Geometry of the jet-in-crossflow theoretical model

Source strength is derived from considerations of jet width, combined with simple mixing concepts to accommodate jet growth. The doublet lines provide the appropriate level of wake closure. The trajectory equations, derived in Hackett et al [15] are:

$$\frac{Z}{D} = 0.352 \left[\frac{X}{D} \right]^{0.429} R^{1.122}, \text{ for the vortex pair}$$

$$\frac{Z}{D} = 0.758 \left[\frac{X}{D} \right]^{0.333} R^{1.000}, \text{ for the source and doublet lines}$$

$$\frac{Y}{D} = 0.0769 \left[\frac{X}{D} \right]^{0.440} R^{1.000}, \text{ for all of the trajectories}$$

The corresponding singularity strengths are given by:

$$\frac{G_{12}}{U_{\infty} D} = 0.600 \frac{R^2}{X_{12}/D} \left(1 - e^{-0.035(X_{12}/D)^2} \right) + 0.0865 R^2 \tanh(X_{12}/D) \quad (\text{vortex strength})$$

$$\frac{s_{12}}{U_{\infty} D} = \frac{(Z_2 - Z_1)}{D s_{12}} \sqrt{1 + 0.23 X_{12}/D} \quad (\text{source strength /unit length})$$

$$\frac{m_{12}}{U_{\infty} D^2} = -\frac{P}{2} \sqrt{(1 + 0.23 X_{12} / D)} \quad (\text{doublet strength})$$

where X_{12} is the mean X-position of a link 1:2, for example, Ds_{12} is its total length and R is the jet-to-mainstream velocity ratio¹. Density-corrected velocities are used for hot or cold jets. Only the x-wise component of the doublet vector is used.

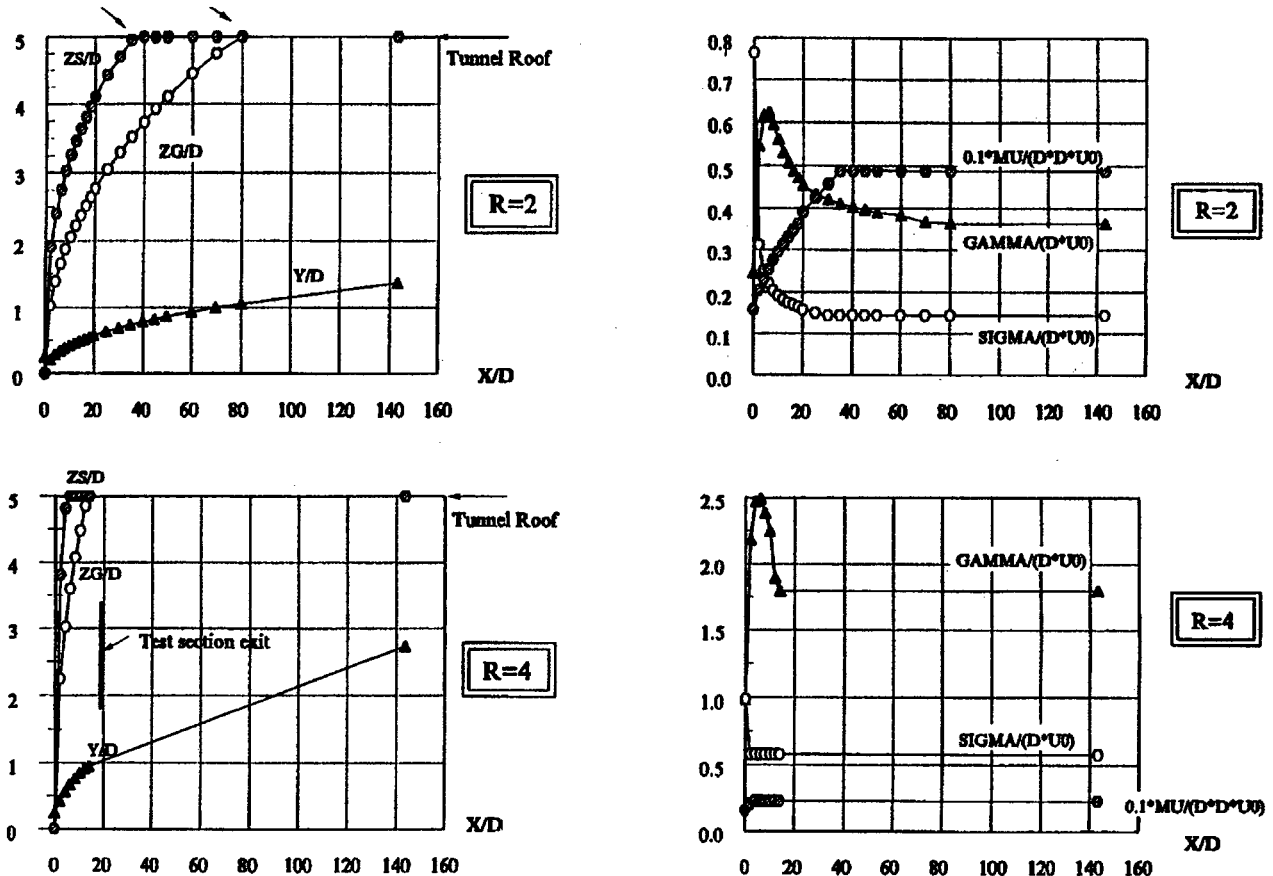


Figure 8.33 Geometry and element strengths for the 3-inch jet at $R = 2$ and $R = 4$

Figure 8.33 shows examples of applying the above equations to a 3-inch diameter jet tested in a 30-inch high tunnel. The jet was directed vertically upwards from a pipe whose exit was at mid-height i.e., the jet exit was five jet diameters from the roof and the floor. The test section extended approximately 20-diameters downstream of the jet exit. Data are shown for velocity ratios, R , of two and four. The roof impact occurred downstream of the test section exit for $R=2$ (left two plots) but fell within the test section at $R=4$ (right two plots). As already indicated in Figure 8.32, source and doublet impingement occurs before that for the vortex pair. When impact occurs, the vertical motion ceases, horizontal spreading continues and, in the absence of the relevant experimental data, the singularity strengths are 'frozen' at their impact values. The abrupt change in the theoretical plume trajectory at impact raises the issue of whether the real plume bends 'in anticipation' of contact. It was shown experimentally, however, that the jet remains essentially 'stiff' until it is about $1\frac{1}{2}$ diameters from the impingement point.

¹ It should be noted that the final term was omitted from the vortex strength equation of Hackett et al (1981). It was, however, included in the code listing in that document.

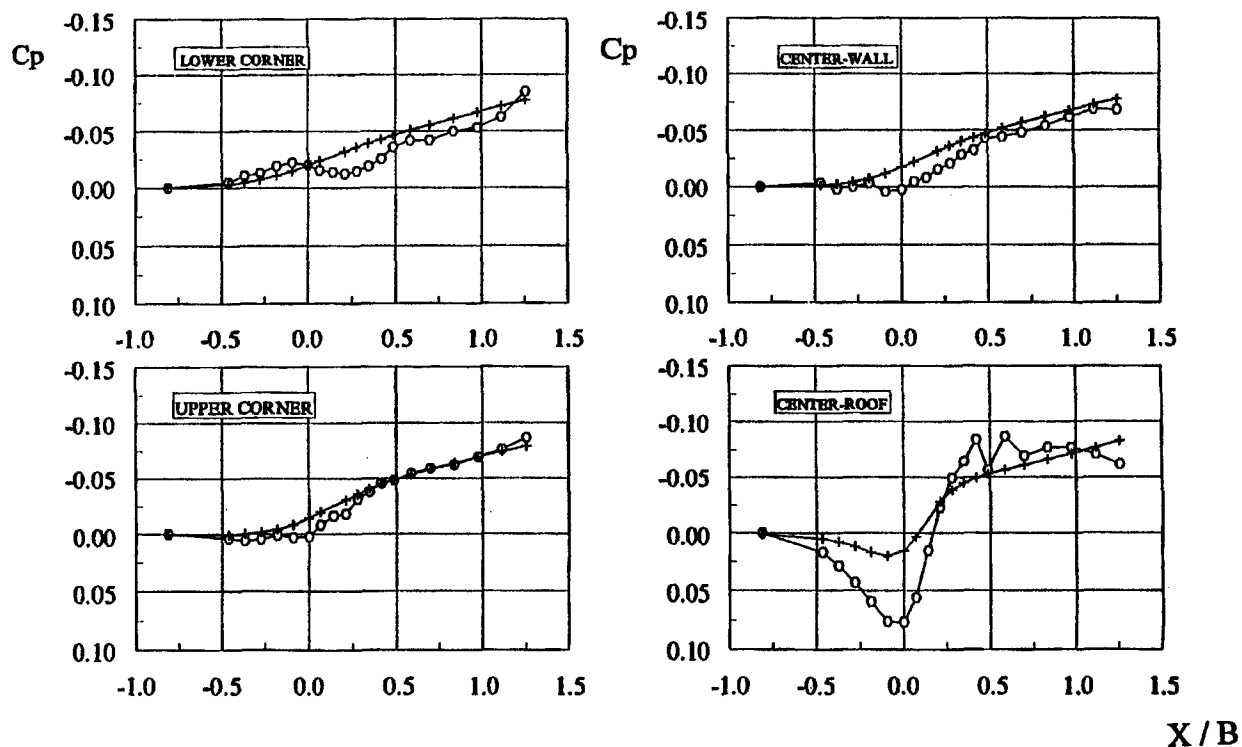


Figure 8.34 Comparison of VSD-model wall pressure preconditions (+) with measurements (o) (3-inch jet at $R = 2$)

An acid test of any model simulation of the present type concerns its ability to predict wall pressures. The walls are twice as close to the test model as the first tunnel image, so if the wall pressures can be predicted correctly then it is reasonable to assume that the interference predictions are also good. Figure 8.34 shows predicted and measured wall pressures for the $R=2$ case just described. 'Empty'-tunnel pressures, measured with the jet supply pipe installed, have been removed from the jet-on data using an appropriate superposition procedure. The theoretical model predicts the wall pressures quite well for the tunnel corners and the mid-wall (upper plots and lower left plot in Figure 8.34). However, the positive pressure on the roof ahead of the jet is under-predicted. The reasons are not immediately obvious for the $R=2$ case. However, for the impinging, $R=4$ case pressure coefficients greater than plus three were measured on the roof. This reflects higher-than-mainstream total pressures in the jet plume.² Upstream propagation of these pressures can be anticipated and it is hypothesised that a similar effect may have been present at $R=2$, despite the absence of impingement within the test section.

The comparisons quoted above involve a re-implementation of the original code, the electronic version having been lost as a result of various system upgrades. The opportunity was taken to improve the flow model by paying greater attention to detail in the impingement region. The original results show a levelling-out of the predicted pressures towards the end of the test section, rather than the continuously rising characteristics of Figure 8.34. This has been traced to premature plume truncation in the earlier model. The correlations are now significantly better than before for the three-inch jet and somewhat worse for the one-inch jet. However the pressures are much smaller for the one-inch jet (C_p 's of order 0.00 to 0.02) and are correspondingly more prone to experimental error when removing the empty tunnel datum pressures. Wall pressures, and by implication the tunnel interference effects, are much greater for the three-inch jet.

² Simulation of higher-than-mainstream total pressure is beyond the capability of the present theoretical model. A ring-vortex tube model would be required to simulate this condition.

8.4.2.1 TUNNEL INTERFERENCE FOR A ROUND JET-IN-CROSSFLOW

As for conventional models, the tunnel interference for jets at low velocity ratio, R , may be calculated using a standard wall image system. However at higher R values, when impingement occurs within the test section length, there is the additional issue of the changed jet shape. Instead of continuing on, the jet is bent suddenly as it hits the tunnel surface and is forced towards the streamwise direction. Changes in the flow field associated with this redirection are part of wind tunnel constraint.

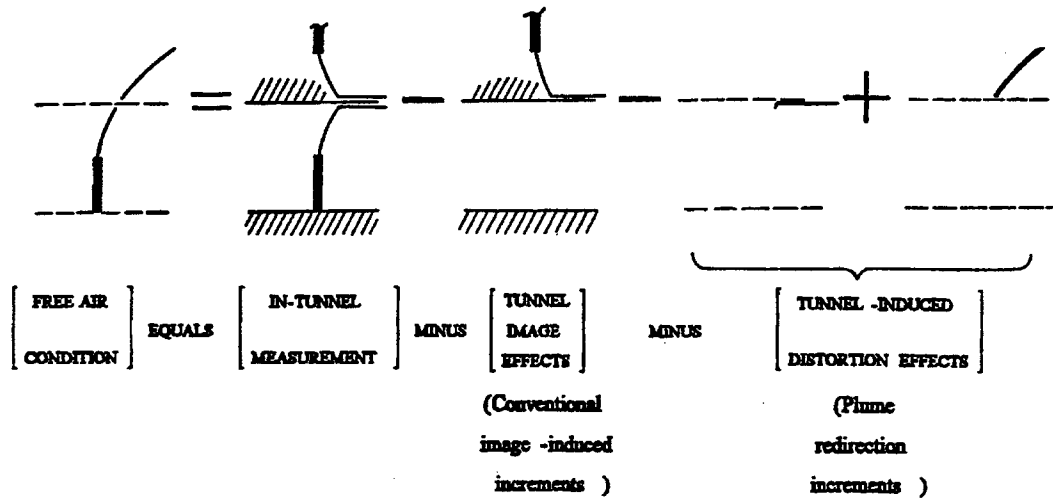


Figure 8.35 Derivation of free air condition from conventional tunnel interference and plume redirection effects

Figure 8.35 shows how this is handled for the present flow model. The desired free air condition, with the plume streaming freely, is built up from three major parts: the in-tunnel measurement; the classical image effect and a plume redirection effect, which has two parts. The first part of redirection removes the deflected part of the plume, within the tunnel, which runs along the tunnel surface. The second part of redirection replaces this by the free-flowing plume extension that would have been present in free air.

Figure 8.36 shows how this works out in practice. The example selected is the $R=4$ case for the three-inch jet quoted previously. The upper plot shows interference velocities in the mainstream direction. It is found that, at $X=0$, redirection adds almost 20% to the image-induced interference. The deflected plume at the tunnel surface (lowest curve) provides mainly aft-located source effects that slow the flow at the model location. Removing the roof elements therefore adds to the tunnel induced superevelocity. Adding the extended plume reduces this effect slightly.

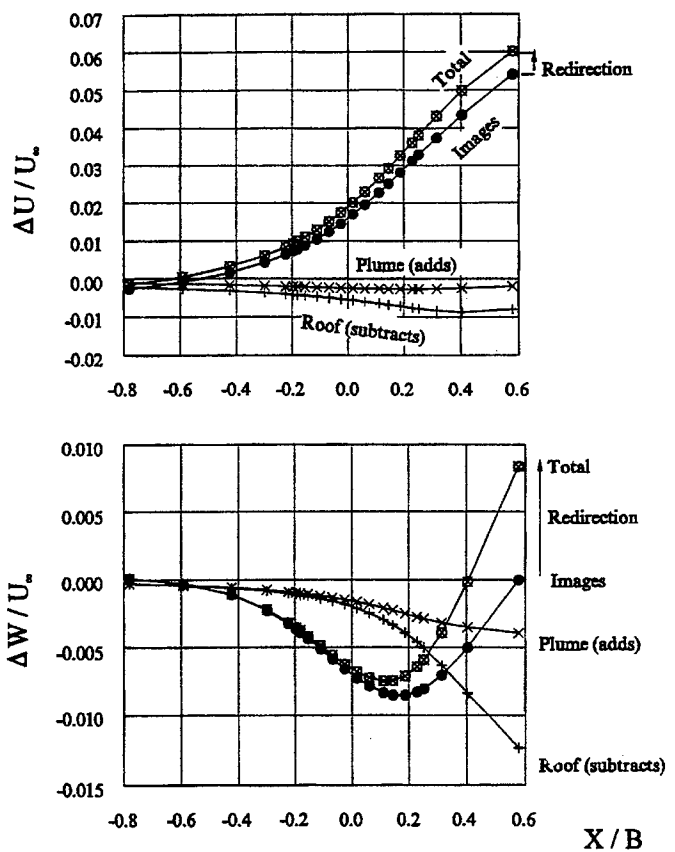


Figure 8.36 Jet plume interference due to image and plume redirection effects. (3-inch jet at $R = 4$)

The lower plot in Figure 8.36 shows the corresponding effects on upwash interference. The results shown are, of course, for an inverted jet. In this case, redirection *reduces* the interference at $X=0$ by about 6½%. The redirection effect increases rapidly on proceeding aft, however, so there may be pitching moment implications. Once again the flow mechanism centres around the source links at the roof, which provide significant downwash in the present case (upwash for a downward-directed jet). Removing this adds to the image effect. The extended plume reduces it.

The blockage curves given by Hackett et al [15] flattened out at about $X/B = 0.25$ whereas the present trend continues upward (upper plot, Figure 8.36). This is attributed to the extension of the present flow model in the impingement region and parallels a similar observation for the pressure signature predictions, discussed earlier. The upwash predictions differ for similar reasons. The present trends now resemble more closely those quoted for other methods.

8.4.2.2 TUNNEL INTERFERENCE FOR OTHER CONFIGURATIONS

The extension to multiple normal jets is straightforward, since the induced velocities are superposable. However, this covers only one angle of attack/jet deflection angle. The 1981 work was terminated before non-normal jet injection models could be formulated. However, corresponding experiments *were* done for jets directed 30-degrees forward and 30-degrees aft of the vertical. The corresponding flow maps and wall pressure signatures are available in the 1981 reference. These parallel those used to develop the theoretical model described above. It should be possible to model at least these configurations using a similar approach and interpolation for intermediate angles should be straightforward. The fact that the original code required no modification once the basic VSD model was established attests to the soundness of the fluid mechanics that underlie the jet-in-crossflow theoretical model.

For cases with the model in ground effect, no redirection is required, the ground image becomes part of the model and the tunnel image system is modified accordingly. However this option has not been coded into the programme. This approach assumes, of course, that the model is at the appropriate height above the tunnel floor. Ground blowing should be applied at the level for in-ground testing, rather than the level for free air simulation (see Section 8.1.2).

REFERENCES for CHAPTER 8

- [1] Ashill, P.R., Keating, R.F.A., 1988, "Calculation of tunnel wall interference from wall-pressure measurements" *The Aeronautical Journal of the Royal Aeronautical Society*, January 1988.
- [2] Cooper, K.R., Hackett, J.E., Wilsden, D.J. et al, 1995 "Closed test section wind tunnel blockage corrections for road vehicles." SAE Special Publication 1176, May 1995
- [3] Glauert, H., 1948, "The elements of airfoil and airscrew theory." Second Edition. Cambridge University Press, 1948.
- [4] Hackett, J.E., Miller, H.R., 1971, "A Theoretical investigation of a circular lifting jet in a cross-flowing mainstream." AFFDL-TR-70-170, January 1971.
- [5] Hackett, J.E., Praytor, E.B., 1972a, "Ground effect for V/STOL aircraft configurations and its simulation in the wind tunnel: Part I, Introduction and theoretical studies." NASA CR 114, 495. November 1972.
- [6] Hackett, J.E., Praytor, E.B., Boles, R.A., 1972b, "Ground effect for V/STOL aircraft configurations and its simulation in the wind tunnel: Part II, Experimental studies" NASA CR 114, 496. November 1972.
- [7] Hackett, J.E., Praytor, E.B., Caldwell, E.O., 1972c, "Ground effect for V/STOL aircraft configurations and its simulation in the wind tunnel: Part III, The tangentially-blown ground as an alternative to a moving ground : Application to the NASA-Ames 40- by 80-foot wind tunnel" NASA CR 114, 497, November 1972.
- [8] Hackett, J.E., Wilsden, D.J., 1975, "Determination of low speed wake blockage corrections via tunnel wall static pressure measurements." Proceedings of the AGARD Symposium on Wind Tunnel Design and Testing Techniques, Paper 22. See AGARD CP174, October 1975.
- [9] Hackett, J.E., Boles, R.A., 1976, "Wake blockage corrections and ground effect testing in closed wind tunnels." *Journal of Aircraft*, August 1976.
- [10] Hackett, J.E., Boles, R.A., Lilley, D.E., 1976 "Ground simulation and tunnel blockage for a jet-flapped, basic STOL model tested to very high lift coefficients." NASA CR 137,857, March 1976.
- [11] Hackett, J.E., Boles, R.A., 1977 "Ground simulation and tunnel blockage for a swept, jet-flapped wing tested to very high lift coefficients." NASA CR 152,032. June 1977. (also AIAA 74-641).
- [12] Hackett, J.E., Wilsden, Lilley, D.E., 1979, "Estimation of tunnel blockage from wall pressure signatures: a review and data correlation." NASA CR 152, 241, March 1979.
- [13] Hackett, J.E., Boles, R.A., 1979c, "Moving ground simulation by tangential blowing." *Journal of Aircraft*, December 1979 (see also NASA CR 152, 032 and AIAA Paper No.78-814).
- [14] Hackett, J.E., Wilsden, D.J., Stevens, W.A., 1980, "A review of the "Wall Pressure Signature" and other constraint correction methods for high angle-of-attack tests." Paper presented to the AGARD Fluid Dynamics Panel, see AGARD Report 692, May 1980.
- [15] Hackett, J.E., Sampath, S., Phillips, C.G., 1981a, "Determination of wind tunnel constraint effects by a unified wall pressure signature method: Part I, Applications to winged configurations." NASA CR 166, 186, June 1981.
- [16] Hackett, J.E., Sampath, S., Phillips, C.G., White R.B., 1981b, "Determination of wind tunnel constraint effects by a unified wall pressure signature method: Part II Application to jet-in-crossflow cases." NASA CR 166, 187, November 1981.
- [17] Hackett, J.E., 1982, "Living with solid-walled wind tunnels." AIAA Paper No. 82-0583, March 1982.
- [18] Hackett, J.E., 1994, "Tunnel-induced gradients and their effect upon drag." Lockheed Engineering Report LG83ER0108, September 1994 (Revised from June 1983).
- [19] Hackett, J.E., 1996, "Tunnel-induced gradients and their effect upon drag." AIAA paper
- [20] No 96-0562, January 1996 (Shortened version of Hackett (1994)).
- [21] Heyson, Harry H., and Katzoff, S, 1957, "Induced Velocities near a Lifting Rotor with Non-Uniform Disk Loading." NACA Report 1319, 1957.

- [22] Heyson, Harry H., 1960, "Jet-Boundary Corrections for Lifting Rotors Centered in Rectangular Wind Tunnels.", NASA TR R-71, 1960.
- [23] Heyson, Harry.H, 1961a, "Wind-Tunnel Wall Interference and Ground Effect for VTOL-STOL Aircraft.", J. Amer. Helicopter Soc., vol. 6, no. 1, Jan. 1961, pp. 1-9.
- [24] Heyson, Harry H., 1961b, "Nomographic Solution of the Momentum Equation for VTOL-STOL Aircraft." NASA TN D-814, 1961. (Also available as: "V/STOL Momentum Equation", Space/Aeronaut, vol. 38, no. 2, July 1962, pp. B-18 to B-20.)
- [25] Heyson, Harry H., 1962, "Linearized Theory of Wind-Tunnel Jet-Boundary Corrections and Ground Effect for VTOL-STOL Aircraft." NASA TR R-124, 1962.
- [26] Heyson, Harry H., 1966, "Equations for the Application of Wind-Tunnel Wall Corrections to Pitching Moments Caused by the Tail of an Aircraft Model." NASA TN D-3738, 1966.
- [27] Heyson, Harry H., Grunwald, K.J., 1966, "Wind Tunnel Boundary Interference for V/STOL Testing." In NASA SP 116, April 1966, p 409.
- [28] Heyson, Harry H., 1969a, "Use of Superposition in Digital Computers to Obtain Wind-Tunnel Interference Factors for Arbitrary Configurations, with Particular Reference to V/STOL Models." NASA TR R-302, 1969.
- [29] Heyson, Harry H., 1969b, "Fortran Programs for Calculating Wind-Tunnel Boundary Interference." NASA T X-1740, 1969.
- [30] Heyson, Harry H., 1969c, "The Flow throughout a Wind Tunnel containing a Rotor with a Sharply Deflected Wake." Paper presented at the Third CAL/AVLABS Symposium, Buffalo, NY., June 1969.
- [31] Heyson, Harry H., 1970, "Theoretical Study of Conditions Limiting V/STOL Testing in Wind Tunnels With Solid Floor." NASA TN D-5819, 1970.
- [32] Heyson, Harry H., 1971a, "General Theory of Wall Interference for Static Stability Tests in Closed Rectangular Test Sections and in Ground Effect." NASA TR R-364, 1971.
- [33] Heyson, Harry H., 1974, "The Effect of Wind Tunnel Wall Interference on the Performance of a Fan-in-Wing Model." NASA TN D-7518. February 1974.
- [34] Heyson, Harry H., 1994, Personal Communication, July 19, 1994.
- [35] Margason, Richard J., 1995, Personal Communications, April-July 1995.
- [36] Olcott, 1965, "A Survey of V/STOL Wind Tunnel Wall Correction and Test Techniques." Princeton University Report PU 725. (also AD 629 004), December 1965.
- [37] Rae, William H., Pope, Alan., 1984, "Low-speed wind tunnel testing", second edition, p 408. Wiley-Interscience, 1984.
- [38] Rubbert, P.E., Saaris, G.R., et al, 1967, "A general method for determining the aerodynamic characteristics of fan-in-wing configurations. Volume 1: Theory and application", USAAVLABS Technical Report 67-61A
- [39] Rueger, M., Crites, R., Weirich, R., 1995, "Comparison of conventional and emerging ("Measured Variable") wall correction techniques for tactical aircraft in subsonic wind tunnels". AIAA Paper 95-0108, January 1995.
- [40] South, P., 1968, "Measurements of flow breakdown in rectangular wind tunnel working sections" NRC Aeronautical Report LR-513. November 1968.
- [41] Tyler, R.A., Williamson, R.G., 1970, "Observations of tunnel flow separation induced by an impinging jet" NRC Aeronautical Report LR-537, April 1970.
- [42] Tyler, R.A., Williamson, R.G., 1971, "Tunnel flow breakdown from inclined jets", NRC Aeronautical Report LR-545, March 1971.
- [43] Wildsen, D.J., 1978, "A low speed wind tunnel test utilizing simple automotive shape (S.A.S.) models at 0.375, 0.475, and full scale in the 16.25 x 23.25 foot test section", Lockheed-Georgia Company Report No LSWT 303, December 1978.
- [44] Williams, J. and Butler, S.F.J., 1961, "Experimental Methods for Testing High Lift BLC and Circulation Control Models". See "Boundary Layer and Flow Control.", Volume I, p 390. Lachmann (Ed) Pergamon Press, 1961.

9. WALL CORRECTION METHODS FOR DYNAMIC TESTS

AUTHOR R. VOß

	PAGE
9.1 INTRODUCTION	9-3
9.2 PHYSICAL BASICS OF UNSTEADY WIND TUNNEL INTERFERENCE	9-5
9.2.1 CHARACTERISTICS OF MOTION-INDUCED UNSTEADY FLOW FIELDS	9-5
9.2.2 WIND TUNNEL INTERFERENCE EFFECTS IN UNSTEADY FLOW	9-7
9.2.3 UNSTEADY WIND TUNNEL WALL BOUNDARY CONDITIONS	9-9
9.2.4 ACOUSTIC INTERFERENCE AND TUNNEL RESONANCE	9-10
9.3 WALL ADAPTATION FOR DYNAMIC TESTS	9-13
9.3.1 STEADY WALL ADAPTATION	9-13
9.3.2 PASSIVE ADAPTIVE UNSTEADY WALLS	9-14
9.3.3 ACTIVE ADAPTIVE UNSTEADY WALLS	9-15
9.4 MODELLING OF UNSTEADY WALL INTERFERENCES AS A BASIC FOR CORRECTION METHODS	9-16
9.5 REDUCTION AND CORRECTION OF UNSTEADY WIND TUNNEL WALL INTERFERENCES	9-23
9.5.1 UNSTEADY WIND TUNNEL WALL CORRECTIONS BY ANALYTICAL METHODS	9-23
9.5.2 UNSTEADY WIND TUNNEL WALL CORRECTIONS USING MEASURED TUNNEL WALL PRESSURE VALUES AND NUMERICAL METHODS	9-24
9.5.2.1 DIRECT COMPUTATION OF THE TUNNEL WALL PROBLEM BY PANEL METHODS	
9.5.2.2 SOLUTION FOR THE CORRECTION POTENTIAL BY PANEL METHODS	
REFERENCES	9-27

9. WALL CORRECTION METHODS FOR DYNAMIC TESTS

9.1 INTRODUCTION

Wind tunnel wall interference in unsteady flow has not been as thoroughly investigated as it has been in steady flow. In the case of unsteady flow, the problem of wind tunnel wall interference is complicated even more by additional parameters describing the time dependent variation of the unsteady flow field. Moreover, other sources of interference such as tunnel wall reflections in the form of acoustic waves, and, as a consequence, wind tunnel resonance, play an important role as well.

Most investigations on unsteady wind tunnel wall interference known so far have concentrated on (harmonically) oscillating lifting systems and bodies undergoing small amplitudes of motion in closed and ventilated wind tunnel test sections. For the case of such motion-induced unsteady flow, a general outline of the problem from a theoretical point of view is given in Ref. [28]. [3] reports on investigations in a small wind tunnel test section with slotted walls and with closed walls. In cases with no different steady pressure distribution between the tests with the different walls, the unsteady results were in a good agreement as well, while for higher transonic Mach numbers both the steady and unsteady results were affected significantly by difference in tunnel walls. Experimental results from systematic wind tunnel interference measurements are reported in [29]. Lambourne [21] reports results of oscillatory wing tests in 4 European wind tunnels. Unsteady interference effects in the smaller tunnels (DRA Bedford, DLR Göttingen) were bigger and led to a suppression of unsteady pressure peaks (due to shock motions) that were clearly present in the larger tunnels (ONERA S2 Modane, NLR HST Amsterdam). The ratios of model span-to-tunnel width were 0.45 and 0.25 for the smaller and bigger tunnels, respectively (see Figure 1). Nevertheless, most unsteady aerodynamic tests are not even performed in tunnels with

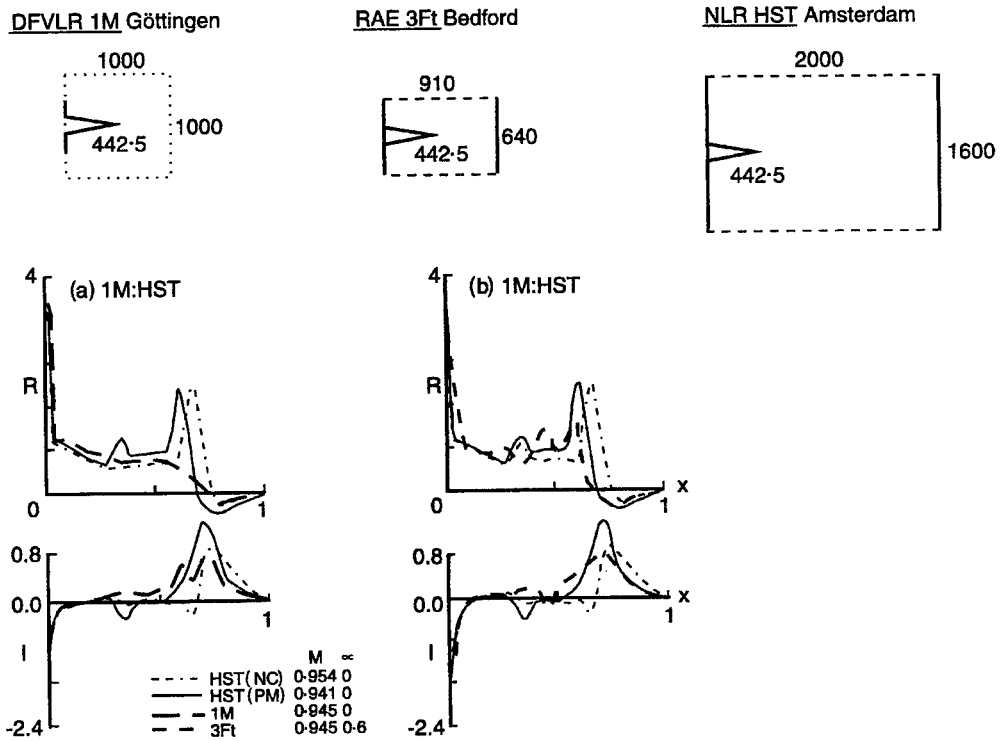


Figure 1 : Results of unsteady measurements in different wind tunnels (AGARD Tests on the NORA Wing).

stationary adaptation. Unsteady tunnel interferences are neglected, only the vicinity of tunnel resonance is avoided, and the largest ratio of tunnel-to-model size is chosen. But such results become questionable, especially when they are expected to serve for the validation of CFD codes. Meanwhile, these have reached a maturity that demands from validation experiments accuracies of a few percent for unsteady lift and moment coefficients.

Of course, tunnel interference may also affect flutter tests because the critical flutter index (speed or tunnel pressure) is strongly governed by unsteady motion-induced airloads. Lu [25] reports flutter tests with 3 flutter models of a Delta wing of different size but having structural dynamical similarity. Tests in the same wind tunnel have shown significant influence of the model-to-tunnel size ratio on the flutter boundary.

Additional complexity in wind tunnel wall interference arises for rotary balance tests and for oscillatory tests with large support systems. Model support structures have to be massive in order to provide the necessary stiffness while forcing the desired model motion. Large support structures lead to additional strong interferences between the model, support and tunnel walls. While interference between model and tunnel walls is characterised by one lag time for the convection of unsteady waves between the model and tunnel walls, model-support-wall interference (often including separated flow regions) will involve more characteristic time lags. While there is hardly a chance to correct these complicated interference effects, unsteady tunnel interferences for oscillatory 2D and 3D clean wing model tests in sub- and transonic flows have been investigated, modelled and also corrected for during the last years.

With the recent developments of adaptive wind tunnel walls, by which steady wall effects are eliminated or significantly reduced by actively controlling flow near the walls, new possibilities for the correction of wind tunnel wall interference have also emerged for unsteady flow. In the following, the prospects and concepts of experimental and analytical techniques for the correction of unsteady wind tunnel wall effects, appearing with aerodynamic and aeroelastic measurements of oscillating lifting systems and bodies, are presented. First, some fundamental relations of motion-induced unsteady flow fields, basic for a physical understanding and analytical treatment of unsteady flow phenomena, are explained. Then the principal causes of unsteady wind tunnel interference are described and the practicability of adaptive wind tunnel walls to eliminate unsteady aerodynamic wall interference effects in unsteady aerodynamic and aeroelastic wind tunnel model measurements is discussed. Finally, prospective wind tunnel wall corrections for motion-induced unsteady flow, applying steady flow wall adaptation and CFD techniques, are outlined.

9.2 PHYSICAL BASICS OF UNSTEADY WIND TUNNEL INTERFERENCE

9.2.1 CHARACTERISTICS OF MOTION-INDUCED UNSTEADY FLOW FIELDS

The differential equation which governs the inviscid unsteady flow due to small oscillatory perturbations imposed on a steady, uniform flow field is a wave equation. In reference to rectangular co-ordinates, see **Figure 2**, this equation for two-dimensional unsteady compressible flow, generated by an oscillating airfoil, reads as (see [23]):

$$(1 - M_\infty^2) \phi_{xx} + \phi_{yy} - 2 \frac{M_\infty^2}{U_\infty} \phi_{xt} - \frac{1}{a_\infty^2} \phi_{tt} = 0 \quad (9.1)$$

Here $\phi = \phi(x, y, t)$ is the time-dependent perturbation velocity potential, U_∞ the velocity of the undisturbed flow, M_∞ the corresponding Mach number and a_∞ the velocity of sound. When the steady free stream Mach number is close to unity, the governing equation for 2D transonic flow in its simplest form reads as:

$$(1 - M_\infty^2) \phi_{xx} - (\gamma + 1) \frac{M_\infty^2}{U_\infty} [\phi_x^0 \phi_x] + \phi_{yy} - 2 \frac{M_\infty^2}{U_\infty} \phi_{xt} - \frac{1}{a_\infty^2} \phi_{tt} = 0 \quad (9.2)$$

where γ denotes the ratio of specific heats. Eq. (9.2) is the time-linearised transonic small perturbation (TSP) equation, where we recognise a non-linear term associated with the steady flow potential ϕ^0 independent of time t . The corresponding 3D equation includes an additional term ϕ_{zz} . In the case of harmonic motion of the airfoil,

$$\phi(x, y, t) = \phi(x, y) e^{i\omega t} \quad (9.3)$$

with the co-ordinate transformations
(L = reference length)

$$\bar{x} = \frac{x}{L}, \bar{y} = \beta \frac{y}{L}, T = \frac{U_\infty}{L}, \beta = \sqrt{1 - M_\infty^2} \quad (9.4)$$

and upon introduction of a reduced velocity potential φ , Eq. (9.1) can be transformed into the well-known Helmholtz wave equation:

$$\phi = \varphi^{iex} \Rightarrow \varphi_{\bar{x}\bar{x}} + \varphi_{\bar{y}\bar{y}} + \lambda^2 \varphi = 0 \quad (9.5)$$

A fundamental solution is:

$$\phi \sim H_0^{(2)}(\lambda r) \quad (9.6)$$

with H denoting the Hankel function of a second kind and order zero, satisfying the Sommerfeld radiation condition and ω = circular frequency, k = reduced frequency, λ = reduced wave number; r denotes the hyperbolic distance between the transmitting point (ξ, n) and control point (x, y) of the flow field.

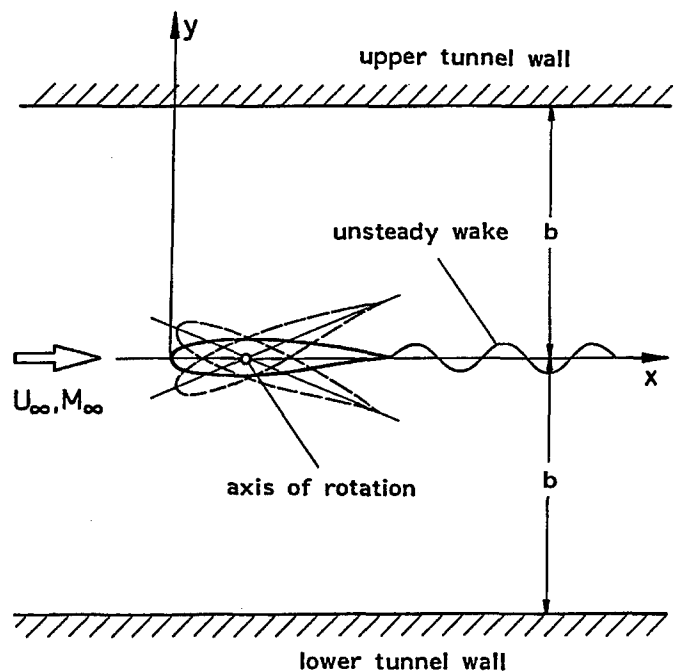


Figure 2 : Oscillating airfoil in a wind tunnel

$$k = \frac{\omega L}{U_\infty}, \lambda = \frac{k M_\infty}{\beta^2}, \varepsilon = \lambda M_\infty \quad \left(r = \sqrt{(\bar{x} - \bar{\zeta})^2 + (\bar{y} - \bar{\eta})^2} \right) \quad (9.7)$$

Hence, the unsteady part of the flow field of a harmonically oscillating airfoil may be represented by a superposition of perturbation sources which move with the basic flow velocity U_∞ and propagate in the form of waves with the velocity of sound a_∞ , thus exhibiting a waviness in the flow field dependent on the parameter λ and on the mode of oscillation as well. As a typical example, **Figure 3** illustrates the motion-induced unsteady flow field of an oscillating airfoil in 2D compressible flow, where φ' denotes the real part (in phase with the oscillating airfoil) and φ'' the imaginary part (90 degrees out of phase) of the unsteady velocity potential. It can be seen that this unsteady flow field is by far more complicated than the steady flow field of an airfoil at rest.

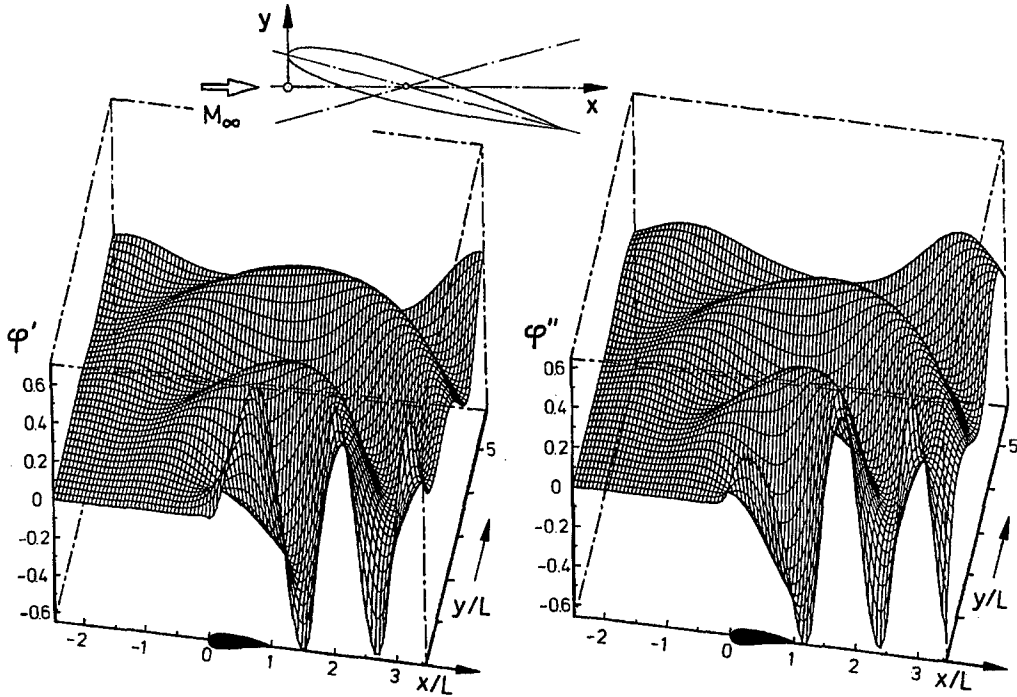


Figure 3 : Motion-induced unsteady flow field (complex unsteady potential) of an airfoil in harmonic pitch oscillation around 42.5% chord axis (φ' = real , φ'' = imaginary part)

For transonic flows, the oscillatory behaviour of motion-induced unsteady 2D and 3D flow fields was thoroughly investigated in [38]. Unsteady flow fields induced by small amplitudes may be modelled by singularity distributions, whose disturbances propagate as nearly plane waves through a non-homogeneous steady flow field. This propagation is described by a nonhomogeneous Helmholtz equation, which is derived from Eq. (9.2).

$$\varphi_{xx} + \varphi_{yy} + \lambda^2 \varphi = \left(\frac{\partial}{\partial \bar{x}} + i\varepsilon \right) \left(\frac{(\gamma+1) M_\infty^2}{\beta^2} \phi^0_{\bar{x}} (\varphi_{\bar{x}} + i\varepsilon \varphi) \right) \quad (9.8)$$

The right-hand side of (9.8) models the effects of nonuniform steady transonic flow on the propagation of disturbances. Of main importance are the curvature and density of acoustic rays, which are properties directly related to the transonic influence and to the density of disturbance energy. **Fig. 4** shows a typical result of propagation in a 2D transonic flow field. Only in the near field of the airfoil, transonic effects

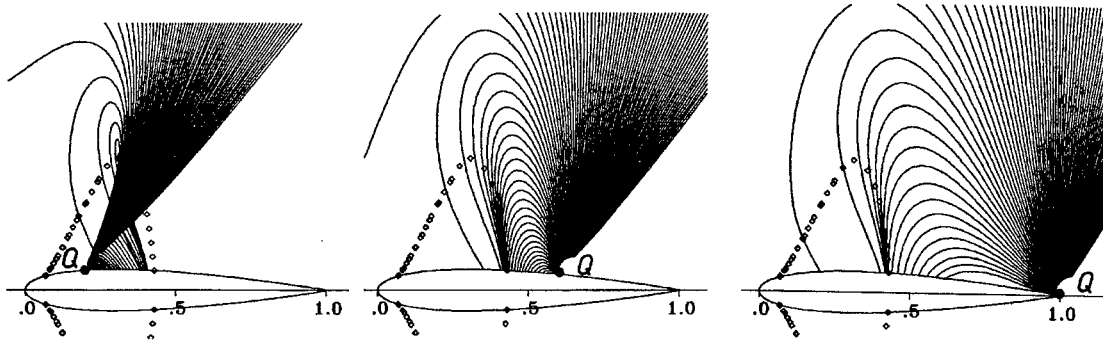


Figure 4 : Propagation of acoustic disturbances (rays) in a transonic flow field (NACA 0012, $Ma_\infty = 0.79$) $\diamond\diamond\diamond\diamond$: boundary of local supersonic bubbles

significantly change the ray curvature and ray density compared to the behaviour in a homogeneous flow (straight rays with uniform density). Note that upstream disturbances propagate themselves in such a manner that they are bent around the shock, which forms the downstream boundary of the local supersonic region. The ray density is very large near the shock and very small in the supersonic region. This corresponds to large and small values of disturbance energy. Rays reaching the tunnel walls are not significantly affected by the transonic effects as long as local supersonic regions do not extend close to the walls. Then the flow near the walls may be fully described by the linear theory because all disturbances from the airfoil reaching the walls propagate themselves, nearly unaffected by the local supersonic bubble.

9.2.2 WIND TUNNEL INTERFERENCE EFFECTS IN UNSTEADY FLOW

From the practical point of view, the most important types of motion-induced unsteady flow fields in a wind tunnel arise from forced or self-excited (flutter) oscillations of the model. In such wind tunnel investigations the unsteady aerodynamic data of main interest are the magnitude and phase of the motion-induced unsteady pressures. For instance, for an airfoil performing pitching oscillation of amplitude $\Delta\alpha$ about a mean incidence α_0 , the wall interference effects on magnitude and phase of the unsteady pressures can be considered under the following headings :

- steady effects on the flow for the mean incidence α_0 ,
- quasi-steady effects in context with the time-dependent kinematic flow conditions for all changes of incidence within the range $(\alpha_0 - \Delta\alpha) < \alpha < (\alpha_0 + \Delta\alpha)$,
- unsteady effects on the manner in which the magnitude and phase of the motion-induced unsteady pressure vary with frequency in context with the unsteady wake.
- unsteady effects in compressible flow from acoustic interference

Hence, the requirements for the avoidance of wind tunnel wall interference effects in unsteady tests are:

- correct (undisturbed) base flow and correct steady perturbations,
- absence of any additional unsteady effects,

i.e., an unsteady process may be directly affected by steady flow wall interference as well as by the purely unsteady sources of interference, as demonstratively shown in [22]. The principal causes of unsteady tunnel interference - in addition to the well known steady interference effects, such as wall constraint, shock wave reflection in transonic flow and wall boundary layers - are (see Figure 5) :

- unsteady effects of wall constraint,
- reflection by the walls of model generated acoustic disturbances, and - as a consequence -
- acoustic wind tunnel resonance,
- distortion of the oscillatory wake of the model by other tunnel deficiencies,
- inherent tunnel flow fluctuations,
- wing support interference.

In [7], wall effects on a transient motion of an airfoil in incompressible flow (stepwise change in angle of attack) is theoretically investigated. This is of importance for tests in response to control deflections. The unsteady development of lift strongly depends on the relative model size, as well as on the type of tunnel walls. Lift is built up faster for open walls than for closed ones and the influence of the relative model

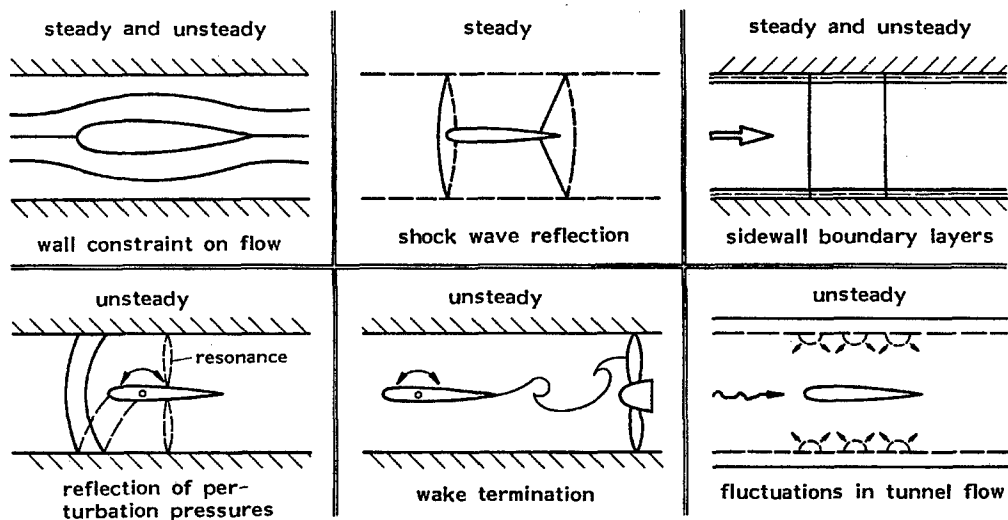


Figure 5 : Principal causes of wind tunnel interference

size is more significant for open walls.

Since a clear understanding of these unsteady wind tunnel interference effects is a basic concern for the application of adaptive wall concepts and the development of correction methods, they will be discussed in more detail in the following. Corrections for unsteady effects of wall constraint - excluding transonic flow- in tunnels having well-defined wall boundary conditions can readily be obtained from theoretical investigations. The corresponding boundary conditions for open and closed (solid) wind tunnel walls can easily be established, see [28], but it is difficult to obtain estimations for ventilated wind tunnel walls because of mathematical uncertainties about the boundaries. For two dimensional airfoils oscillating in sub- and supersonic flow several of such analytical unsteady wall correction techniques have already been elaborated.

In a free atmosphere an oscillating model would leave behind an oscillating wake, the vorticity distribution of which is consistent with the unsteady flow at the model. If this wake is affected by a tunnel shock wave in a tunnel, driving fan, a near tunnel corner, or a support system, the unsteady aerodynamic loading at the model may be notably influenced. There are reasons to suggest that this source of unsteady interference is of considerable importance in certain special cases of flow speed and less important in transonic flow.

Finally, various types of flow fluctuations, often collectively described as tunnel noise, can have several unwanted effects, particularly in aeroelastic model investigations. One of the principal sources of noise in

transonic tunnels is the flow over ventilated walls. It is possible to reduce the noise from these walls by covering the perforations with gauze cloth and to apply sound-absorbing material to the tunnel walls, as shown in [26].

9.2.3 UNSTEADY WIND TUNNEL WALL BOUNDARY CONDITIONS

Pressure in a flow field with small unsteady perturbations of an undisturbed homogeneous mean flow fulfils the following equation

$$c_p = -\frac{2}{u_\infty} \frac{d\phi}{dt} = -\frac{2}{u_\infty} \left(\frac{\partial}{\partial t} + u_\infty \frac{\partial}{\partial \bar{x}} \right) \phi \quad (9.9)$$

with the pressure coefficient

$$c_p = \frac{(p - p_\infty)}{0.5 \rho u_\infty^2} \quad (9.10)$$

In the following, the disturbance normal velocity component v with respect to the walls is important

$$\frac{v}{u_\infty} = \frac{\partial \phi}{\partial n} = \pm \frac{\partial \phi}{\partial y} \quad \text{with } n = \pm y \text{ for upper or lower wall} \quad (9.11)$$

In the following, it is assumed that the flow field may be modelled by a mean steady flow and an unsteady harmonic perturbation

$$\phi(x, y, t) = \phi^0(x, y) + \phi(x, y) e^{i\omega t} \quad (9.12)$$

While numerical computations of unsteady flow fields assume nonreflecting far field boundary conditions at outer boundaries (Sommerfelds radiation condition), tunnel walls have to be taken into account by special conditions.

Closed (solid) walls: vanishing normal velocity component at the walls for both steady and unsteady flow component

$$v = 0 \Rightarrow \frac{\partial \phi}{\partial n} = \phi_n = 0 \quad (9.13)$$

Open walls (free jet): vanishing pressure disturbances ($p = p_\infty$) at the walls

$$(c_p = (\phi_x + ik\phi) = 0 \Rightarrow \phi(x) = \phi(-\infty) e^{-ik(x-\infty)} \Rightarrow \phi = 0) \quad (9.14)$$

taking into account that the unsteady disturbance potential vanishes for infinite upstream position.

Ventilated walls: The two extreme conditions of closed and open walls yield opposite interference effects. While closed walls increase lift, open walls decrease the free air value of lift coefficient. The ventilated walls yield values between the two extreme wall types. In the following, the model is located at $z = 0$ midway between two (upper and lower) tunnel walls ($z = \pm b$)

Porous (perforated) walls:

$$\text{viscous effect } Zv = \frac{c_p}{2} \Rightarrow \phi_x + ik\phi + Z\phi_n = 0 \tag{9.15}$$

$$\left(\frac{\partial}{\partial x} + ik\right) c_p(x, \pm b) \pm Z \frac{\partial}{\partial y} c_p(x, \pm b) = 0 \tag{9.16}$$

with a complex porosity factor: $Z = R + iS$, $R = 1/P$ (resistance) and S reactance

Slotted walls: normal flow with velocity v through the walls is described by momentum equation

$$\rho_\infty \frac{dv}{dt} = \nabla p = \frac{(p - p_\infty)}{K} \tag{9.17}$$

with a slot parameter K (dimension length). This approach yields

$$\begin{aligned} \phi + K\phi_n &= 0 \\ c_p(x, \pm b) \pm K \frac{\partial}{\partial y} c_p(x, \pm b) &= 0 \end{aligned} \tag{9.18}$$

Here the limiting cases of $K = 0$ and $K = \infty$ describe the open jet and solid walls, respectively.

9.2.4 ACOUSTIC INTERFERENCE AND TUNNEL RESONANCE

In compressible flow, the reflection of acoustic disturbances from wind tunnel walls and their return to the model is a crucial unsteady interference problem. As shown in the previous section, an oscillating model generates unsteady pressure disturbances in the form of travelling acoustic waves which propagate outwards in the tunnel. After being reflected from the walls, these disturbances return to the model,

causing additional pressure changes there. This is in contrast to the Sommerfeld far field radiation condition, which requires a reflection-free propagation of disturbances to infinity in free atmosphere.

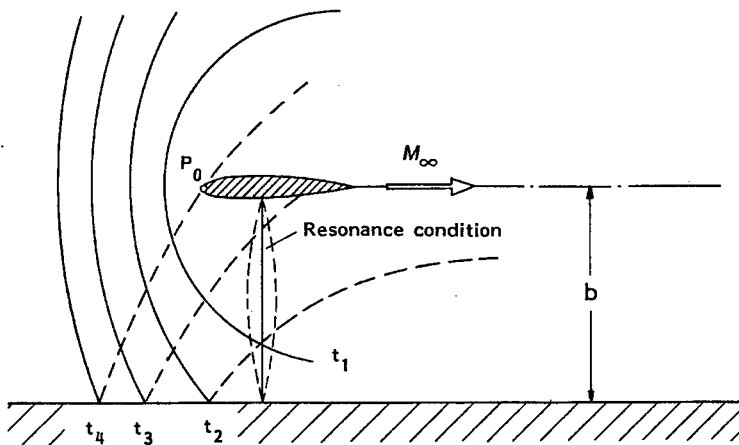


Figure 6 : Positions of wave front from a disturbance at P_0 and reflection of acoustic waves from a wall

the disturbance to be reflected by the wall and return to P_0 is :

$$\Delta t = 2 \frac{b}{\sqrt{a_\infty^2 - U_\infty^2}} = 2 \frac{b}{\beta a_\infty} \tag{9.19}$$

Figure 6 shows an airfoil in 2D subsonic flow and the wave fronts from an acoustic disturbance in a uniform flow. It is seen that the velocity of propagation of the pressure disturbance from a point P_0 in the direction normal to the walls is $a_\infty^2 - U_\infty^2$, and the time needed for

where b is the distance to the wall. The attenuation of the disturbance by the time it returns to the source will depend on the distance travelled in the moving air which is

$$a_{\infty} \Delta t = 2 \frac{b}{\beta} \quad (9.20)$$

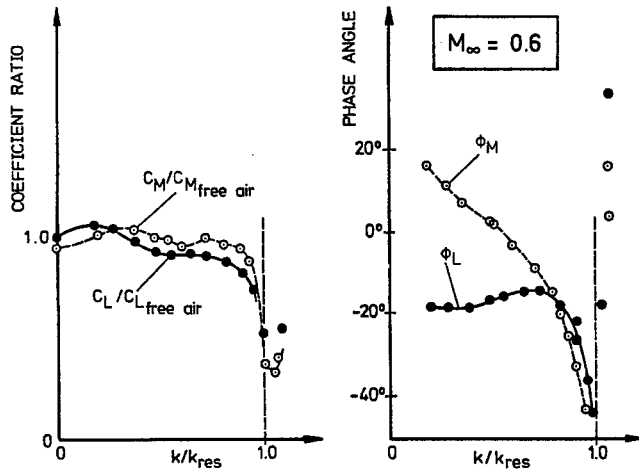


Figure 7 : Resonance in a solid wall test section (adapted from Fromme)

Thus the reflected wave when it returns will be weaker (by natural damping), the higher the Mach number. When a disturbance from the oscillating airfoil is reflected from the tunnel wall back to the wing with such a phase relationship that it reinforces or cancels out a succeeding disturbance and, hence, the pressure changes currently occurring on the model, the most severe unsteady wall interference problem happens, as first described in [33], [1], [14] and experimentally verified in [33], see **Figure 7**. At this resonance condition, the disturbances emitted from an oscillating wing and reflected by the walls form a standing wave pattern. For solid walls, that do not change the phase of the wave on reflection, the resonance circular frequency is :

$$\omega_n = (2n-1)\pi U_{\infty} \frac{\beta}{M_{\infty}} \frac{1}{2b} \quad n = 1, 2, \dots \quad (9.21)$$

For open jet boundaries the phase change on reflection is π , so that

$$\omega_n = 2n\pi U_{\infty} \frac{\beta}{M_{\infty}} \frac{1}{2b} \quad n = 1, 2, \dots \quad (9.22)$$

For a tunnel with ventilated walls, theoretical expressions for resonance frequencies depending on wall porosity, depth of plenum chamber and Mach number are given in [26]. In the case of resonance, where the disturbances form a standing wave pattern, the normal velocity has a maximum amplitude and the pressure has a node, i.e. is of zero amplitude at the position of the oscillating airfoil. Accordingly, the unsteady airloads on the oscillating airfoil will vanish at resonance. Whereas for incompressible flow ($M_{\infty} \rightarrow 0$) there is no tunnel resonance - the resonance frequency decreases with increasing Mach number - and since it tends to zero as ($M_{\infty} \rightarrow 1$), the predicted resonance frequency must coincide with a test frequency for some intermediate Mach number which causes dramatic changes in the magnitude and phase of the unsteady lift on the oscillating model.

The same expressions derived here for 2D tunnels are valid for tunnels with quadratic test sections.

The lowest value for resonance frequency for a quadratic test section are :

$$\omega_n = n_1 2\pi U_{\infty} \frac{\beta}{M_{\infty}} \frac{1}{2b} \quad (9.23)$$

The value of the parameter n_1 equals 0.5 or 1.0, for closed walls ($n_1 = 0.5$), and open walls ($n_1 = 1.0$), respectively.

For cylindrical test sections with closed walls the value of the lowest resonance frequency was derived in [33]:

$$\omega_n = n_2 U_\infty \frac{\beta}{M_\infty} \frac{1}{R} \quad (9.24)$$

with ($n_2 = 1.84$), R = radius of test section.

For ventilated walls the resonance frequencies are given by

$$\omega_n = 2\lambda_n b U_\infty \frac{\beta}{M_\infty} \frac{1}{2b} \quad (9.25)$$

Their values depend on Mach number, tunnel size, wall opening ratio and plenum depth. They are derived from the tunnel wall boundary conditions in chapter 2.3 by decomposition of the unsteady disturbance pressure field into plane waves propagating in the mean flow direction and the transverse direction. Reduced frequency values of resonance conditions depend on Mach number and eigenvalues λ_n of the tunnel section. For detailed derivation see [28].

For slotted walls the eigenvalues depend on the slot parameter K via a transcendental equation: The eigenvalues satisfy the inequalities

$$\lambda_n K + \tan(\lambda_n b) = 0 \quad (9.26)$$

The eigenvalues satisfy the inequalities

$$\left(n - \frac{1}{2}\right)\pi \leq \lambda_n b < n\pi \quad (9.27)$$

Again, the limiting lower and upper bounds represent values for closed and open walls, respectively.

For porous walls expressions for resonance frequencies were derived by Mabey [1980], (also see [28]) using the corresponding boundary condition for porous walls of chapter 2.3, but neglecting the reactance, thus approximating $Z = iS$. This yields

$$\lambda_n b = \text{atan}(-S\beta M_\infty) + n\pi \quad (9.28)$$

with the limiting cases $S = \infty$ and $S = 0$ for closed walls and open jet walls respectively.

Fortunately, at higher Mach numbers, there are influences to reduce these effects. Even for strong reflections from solid walls, the effective air distance increases with Mach number and the reflections thus become more attenuated. Also, the reflected disturbances travel more with the flow than across it, see **Figure 6**. Furthermore, for transonic conditions, when resonance frequencies are low enough, the (adapted) walls in typical transonic wind tunnels are perforated or slotted and the reflections are thus more diffuse and attenuated. Thus the strong phenomenon of tunnel resonance is milder in transonic flows.

9.3 WALL ADAPTATION FOR DYNAMIC TESTS

From the preceding explanations we have seen that the following wind tunnel interference effects, due to an unsatisfactory test environment, are of main concern in unsteady aerodynamic and aeroelastic experiments with oscillating models:

1. interference of the steady base flow field by steady wall constraints, including shock wave reflections in transonic flow,
2. interference of the (superimposed) motion-induced unsteady flow field by wall constraints,
3. reflection of the model-generated acoustic disturbances by the walls,
4. acoustic tunnel resonance in the test section.

With regard to the application of adaptive wind tunnel wall concepts to eliminate or significantly reduce these wall interference effects in unsteady flow measurements, the following statements can be made :

9.3.1 STEADY WALL ADAPTATION

The practicability and feasibility of wall adaptation for steady flow have already been successfully demonstrated.

The elimination or at least reduction of unsteady wind tunnel wall interference by means of adaptive walls seems to be extremely difficult to realise. The feasibility of unsteady wall adaptation has not yet been demonstrated. However, since unsteady aerodynamic processes are also affected by steady wall interferences, particularly in the transonic flow regime, the avoidance of steady flow wall effects by the application of steady flow wall adaptation will also significantly improve the results of unsteady wind tunnel measurements, as demonstrated by Kuczka [18] for the "Standard Dynamics Model" (SDM) shown in **Figure 8**. He obtained some satisfactory agreements between results from a tunnel with steady adapted closed walls and with results from tunnels with perforated walls for the in-phase component of unsteady lift and moment coefficients. However, the corresponding out-of-phase components disagree, even for low reduced frequencies. They are especially affected by reflections of model-generated disturbances from the walls, because they are, e.g., smaller than the in-phase components. In addition, the wall reflected disturbances are phase-shifted to the model oscillations.

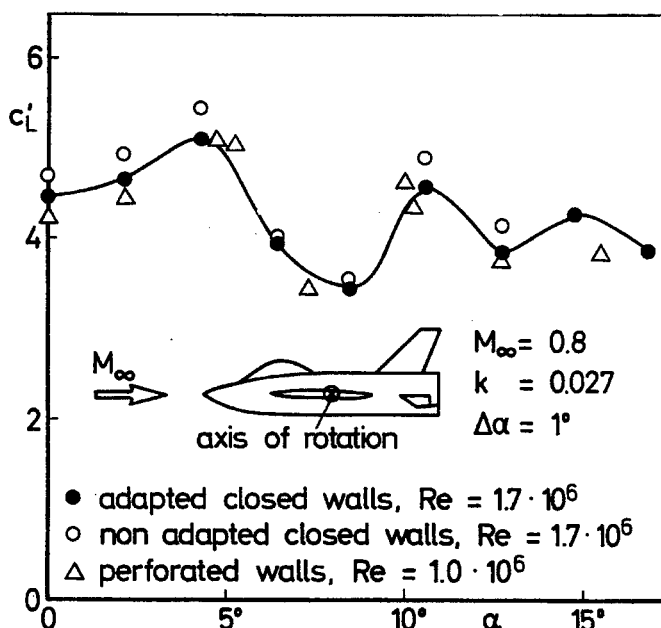


Figure 8 : In-phase component c_L' of unsteady lift coefficient of the oscillating SMD model with and without tunnel wall adaptation (adapted from Kuczka)

9.3.2 PASSIVE ADAPTIVE UNSTEADY WALLS

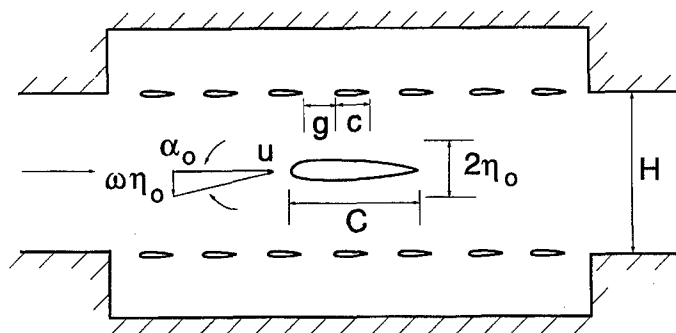


Figure 9 : Principle of airfoil slatted wind tunnel section (adapted from Kong)

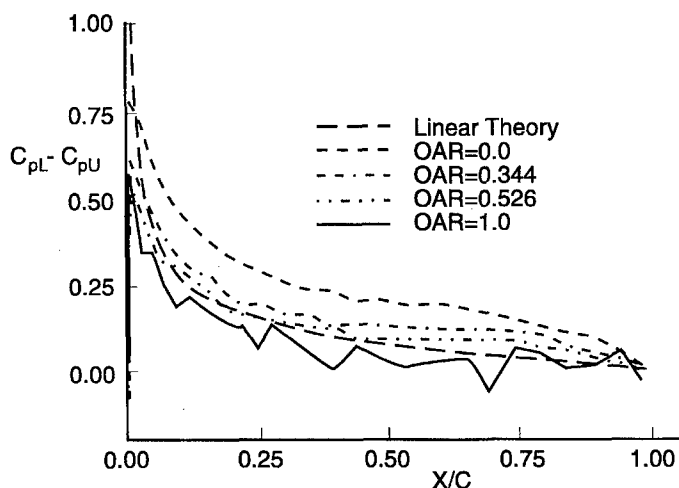


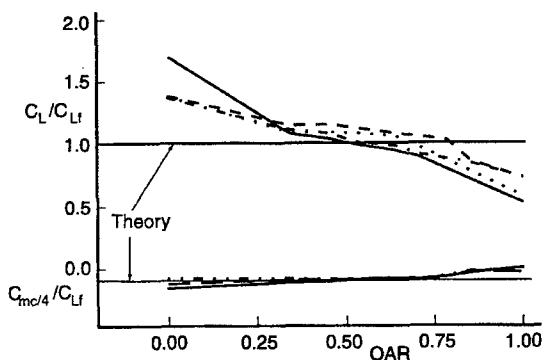
Figure 10 : Measured unsteady pressure distribution for different wall opening area ratios. (adapted from Kong)

In addition to steady adaptation, another promising procedure has shown to be the use of special partly open walls, namely airfoil-slatted tunnel walls. Kong [19] shows that this type of walls avoids the disadvantages of flow separation often appearing with slotted walls.

An opening area ratio parameter, $OAR = g/(c+g)$, see Figure 9, with a value of 0.6, has shown to be most successful in eliminating unsteady wall interference.

Figure 10 shows that this OAR provides the best agreement of measured unsteady pressure distributions with free air results.

Figure 11 compares the ratio of measured and analytical free air results for unsteady lift and moment coefficients. The results of tests with different ratios of model- to-tunnel size $C/H = 0.333$ and 0.667 and of different reduced frequencies for a subsonic oscillating airfoil in plunge motion show that the optimum desired value 1 is achieved with $OAR = 0.6$ again, for all parameter combinations, thus providing a calibrated value for all tests in this tunnel. This promising method has yet still to be validated for transonic tests as well.



Symbol	C/H	k	$\bar{\alpha}_0$	Re · (10 ⁻⁵)
---	0.333	0.52	0.62	2.5
---	0.333	0.52	0.31	2.5
---	0.333	0.37	0.44	2.5
---	0.333	0.37	0.22	2.5
---	0.667	0.48	2.16	7.3
---	0.667	0.48	1.44	8.0
---	0.667	0.28	0.82	8.0

k = reduced frequency
 Re = Reynolds number
 $\bar{\alpha}_0$ = amplitude of α_0

Figure 11 : Measured unsteady lift and moment coefficients for different wall opening area ratios and different reduced frequencies

9.3.3 ACTIVE ADAPTIVE UNSTEADY WALLS

It is clear that steady adaptation can remove a significant amount of interference effects on unsteady results (see point 1 in chapter 2.2). The effects mentioned in points 2 and 3 may be only cancelled by adaptive walls if a time-dependent adaptation is applied. This has not been done yet. So only the practicability of such a method may be studied theoretically or numerically.

Unsteady wall adaptation can be realised, at least theoretically, in the same way as with steady flow conditions. However, enormous technical effort is mandatory even for 2D measurements. Unsteady wall adaptation would require oscillatory moving flexible walls, where an unsteady motion of the wall contours would depend on the frequency and the vibration mode of the model, on the model amplitude of oscillation and on certain phase relationships with respect to the motion of the model. Streamlining algorithms for such a nonstationary wall adaptation, even for the simplest case of non-flexible (rigid body) oscillations of the model, would be very difficult to establish. They demand unsteady pumping tunnel walls governed by the unsteady varying stream surface contour. For imposed prescribed unsteady motions this might be feasible by pre-tests computing the wall contours in advance. It seems unlikely that point 4 (tunnel resonance) may be cancelled at all. Unsteady wall adaptation may be best realised for low-frequency flow fields because then acoustic interference is small and the speed of the wall contour changes is low.

In [6] a study on unsteady wall adaptation is carried out for 2D low-frequency oscillating airfoils in transonic flow. A CFD code based on the unsteady Euler equations is used to compute the unsteady airloads on the oscillating model in the presence of solid tunnel walls. The exact time dependent wall contours like the airfoil contour are precisely modelled by the computational grids. The parameter ratios of model-to-tunnel size, reduced frequency and Mach number are varied. Three different tunnel wall adaptation concepts (all based on the streamlining of the wall contours) with increasing degree of complexity are tested, namely:

- 1) steady wall adaptation for the mean flow field,
- 2) quasisteady synchronisation of wall adaptation (e.g. harmonically deforming walls between steady adapted wall contours obtained for maximum and minimum motion amplitude,
- 3) unsteady synchronisation by choosing wall contours compatible with streamlines for a time dependent vortex at the position of the model and compatible with the measured unsteady lift of the model.

Results for unsteady airloads obtained with these different wall adaptation procedures are presented in **Figure 12**, showing that the quasisteady adaptation for subsonic flow is sufficient while transonic flow

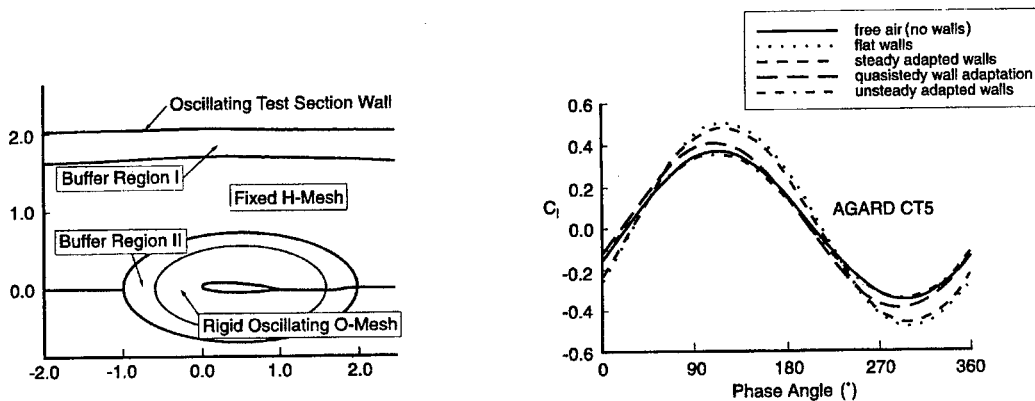


Figure 12 : Numerical simulation of unsteady wall adaptation strategies (adapted from Chang)

demands at least an unsteady synchronisation of the wall contours. There is still the question if the unsteady lift dependent synchronisation is sufficient for higher frequencies since significant time lags between streamline contour at the wall positions and the instantaneous lift will arise.

Summarising, steady wall adaptation is a necessary prerequisite for obtaining interference-free unsteady results. But this is not sufficient at least for transonic flows and higher frequencies, and one somehow has to correct the residual unsteady interference effects. An unsteady wall adaptation procedure working for different Mach numbers, frequencies and model motions seems difficult to realise. Sophisticated correction methods based on mathematical models and CFD computations offer a more promising approach instead. In order to model unsteady wall boundary conditions with such methods, unsteady pressure data should also be measured at the walls. Indeed, the application of adaptive walls to minimise interference from steady flow wall constraints, together with the application of CFD-techniques which take into account the unsteady wall pressure data from experiments to describe precise wall boundary conditions, is most promising in deriving corrections for wind tunnel wall interferences in unsteady flow. Prospects and concepts for such hybrid wind tunnel wall correction techniques are outlined in the following.

9.4. MODELLING OF UNSTEADY WALL INTERFERENCES AS A BASIC FOR CORRECTION METHODS

Analytical predictions of wall effects on unsteady pressures and airloads require the precise knowledge of the wall boundary conditions. Only three types of boundary conditions are well defined, namely those of solid (closed) walls, free jet and of prescribed unsteady wall pressure distributions (known from experiments). Porous and slotted walls can be simulated only approximately by mixed boundary conditions including free parameters. As wind tunnel tests with oscillating models are primarily performed for aeroelastic purposes, wind tunnel interference effects have to be studied within a wide range of Mach numbers, oscillation modes and reduced frequencies. For 2D subsonic flow in one of the first systematic analytical investigations on wind tunnel wall effects, Bland [5] derived an integral equation relating the downwash w (prescribed by the harmonic motion of the airfoil) to the induced unsteady pressure jump δp at the airfoil :

$$w(x) = \int_0^1 K(\bar{x} - \bar{\zeta}, M_\infty, k) \delta p(\bar{\zeta}) d\bar{\zeta} \quad (9.29)$$

This is an extension of Possio's integral equation [31], [13], which is valid for unbounded free air conditions. Bland derived a rather complicated corresponding kernel K , including tunnel wall boundary conditions to be automatically fulfilled on infinitely extended walls in the general form:

$$p \pm c_w \frac{\partial p}{\partial y} = 0 \text{ at } y = \pm b \left\{ \begin{array}{l} \text{upper} \\ \text{lower} \end{array} \right\} \text{ walls} \quad (9.30)$$

where c_w denotes a specific wall parameter. The limiting cases of solid walls and free jet condition are included:

$$c_w = 0 \rightarrow p = 0 \rightarrow \varphi = 0 \text{ (free jet)} \quad (9.31)$$

$$c_w = \infty \rightarrow \frac{\partial p}{\partial y} = 0 \rightarrow \frac{\partial \varphi}{\partial y} = 0 \text{ (closed wall)}$$

Thus the effects of ventilated walls are described by certain values of C_w , but its dependence on the type of walls, their opening ratio and perhaps Mach number and reduced frequency is unclear and would have to be systematically studied by comparing computations and experiments. Bland's method was completed by Fromme and Golberg [11], [13], who improved the numerical performance of the solution method and extended it to general oscillation modes, including control surfaces. They obtained results clearly showing the unsteady wall effects, especially the sharp drops in magnitude of the loads and their phase jumps in the case of tunnel resonance, see **Figure 13**. Wall effects are significant in the whole frequency regime and wall-influenced loads are bigger/smaller than the corresponding free air value for closed/open walls, which is well known for steady or quasisteady flow. In particular, the strong changes in phase deserve special attention. This analytical method provides exact reference results, but it is restricted to 2D flows and to the regime of linear compressibility, i.e. constant Mach number in the whole flow field, and thus subsonic flow. It hardly appears possible to extend it to 3D or transonic flow.

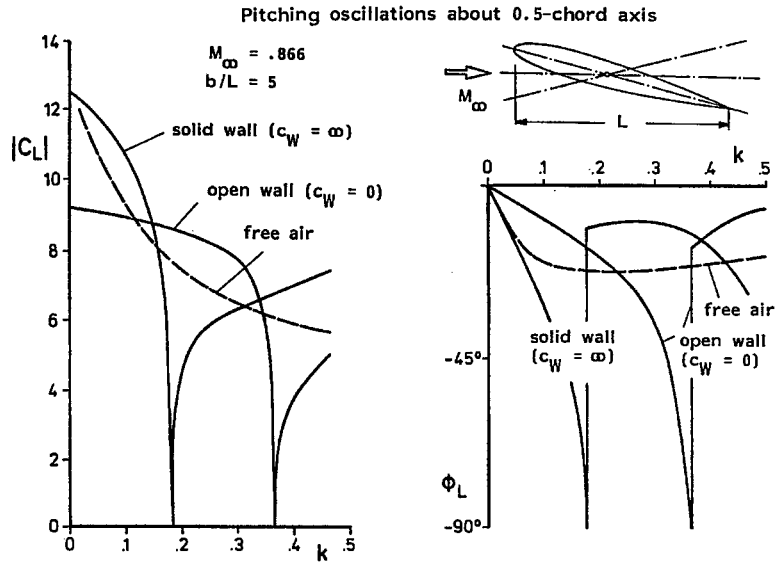


Figure 13 : Lift coefficient (magnitude and phase) of an airfoil performing harmonic pitch oscillations around a 50% chord axis (adapted from Fromme)

Another method of indirectly modelling the walls is the method of images. In an integral equation for the solution of the boundary value problem of an oscillating model the influence of solid tunnel walls is taken into account by an image of the model located on the other side of the wall, the wall being a mirror plane. This single image is sufficient in the presence of only one wall.

In the presence of upper and lower walls, images mirrored by both walls have to be taken into account, each of which has to then be mirrored again by the other wall as well, a procedure yielding an infinite series of images with increasing distances across all walls. This method has been thoroughly elaborated by Mabey [27] for ventilated walls as well. The rather complicated procedure of summing up contributions of the infinite series, each element of which is representing a model either by vortices or by more precise panel distributions, may be simplified, because often a small finite number of images is sufficient. This is demonstrated in

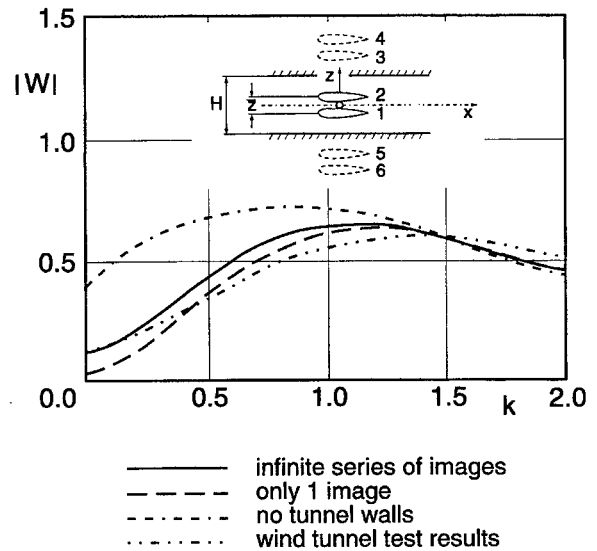


Figure 14 : Results of modelling unsteady tunnel wall effects by methods of images (adapted from Laschka). Induced unsteady downwash velocity behind an oscillating airfoil system in a wind tunnel ($H = 6.5$, $\bar{z} = 3.5$, $k =$ reduced frequency)

Figure 14, adapted from [24]. For a gust generator with two oscillating airfoils the induced normal velocity component w at the tunnel centre line $z = 0$ at a position downstream of the gust generator ($x = 5$) is shown. $|w|$ denotes the magnitude of the downwash velocity w , normalised by the amplitude of the airfoil oscillation. With respect to the measured results, the wall interference effects are modelled with sufficient accuracy by just one image. Note that, for reduced frequency $k = 0$ (quasisteady condition), $|w|$ is not zero because $w(k=0)$ is defined as the difference between the steady w values at the maximum and minimum incidence of the airfoils (normalised by $\Delta\alpha$).

The advantage of these two methods, namely the reformulation of integral equation kernels and method of images, lies in the fact that tunnel walls are taken precisely into account, being infinitely extended upstream and downstream. Thus, the walls do not have to be directly modelled by singularities (like the model).

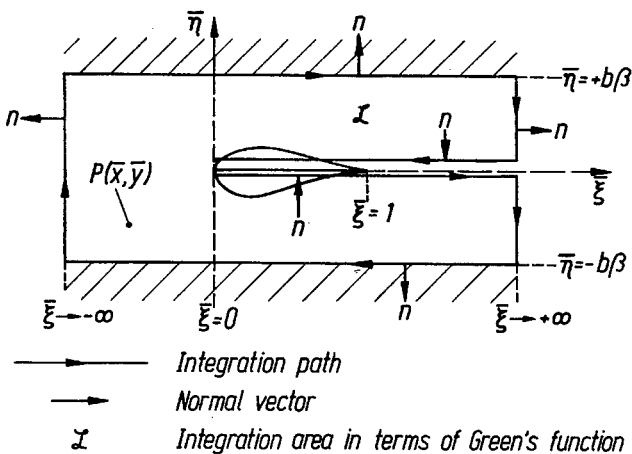
However, these methods will hardly be able to predict details of the wall affected pressure distribution at the model, because a derivation of modified 3D kernels seems very complicated, while the complexity of infinite series of images can be evaluated numerically only with a rough representation of the wing and its images, like simple horseshoe vortices.

The following numerical approach, see [36] and [39], is more flexible. It is also based on the 2D linear equation, but may be extended straightforward to 3D and transonic flows. Within the framework of unsteady linearised theory (small oscillation amplitudes) the position of the airfoil, its wake and the walls (even if curved for steady adaptation) may be assumed to be approximately parallel to the x -axis (freestream direction of the wind tunnel). The airfoil is located midway between the tunnel walls, a distance b away from them. Then this 2D boundary value problem can be solved by application of Green's theorem:

$$\varphi(\bar{x}, \bar{y}) = \oint_C \left(\psi \frac{\partial \varphi}{\partial n} - \varphi \frac{\partial \psi}{\partial n} \right) ds = 0 \quad \text{with} \quad \psi = \frac{1}{4i} H_0^{(2)}(\lambda r) \quad (9.32)$$

Green's function ψ satisfies the 2D Helmholtz-equation together with Sommerfeld's far field radiation condition for free air. For 3D problems Green's corresponding function reads as $\psi = \frac{e^{i\lambda r}}{r}$. The integration contour C and the integration path s run along the boundaries of the control volume and along those boundaries where φ is discontinuous, see **Figure 15**.

$$\varphi = \int_0^\infty \left(\delta\varphi_{\bar{y}} + \delta\varphi_{\bar{y}} \psi \right)_{profile} d\zeta - \int_{-\infty}^\infty \left(\left(\psi \varphi_{\bar{y}} + \varphi \psi_{\bar{y}} \right)_{lo} \right) d\zeta + \int_{-\infty}^\infty \left(\left(\psi \varphi_{\bar{y}} - \varphi \psi_{\bar{y}} \right)_{up} \right) d\zeta \quad (9.33)$$



For free air conditions, the infinite boundaries give vanishing contributions; only airfoils and wake contour lines have to be taken into account. For wind tunnel flows the integration path also runs along the tunnel walls. As a final result, one obtains an analytical relationship between the downwash w at the airfoil, which is prescribed by the airfoil's oscillatory motion, and the unsteady potential function value f and the normal unsteady velocity component g , both at the walls :

Figure 15 : Integration path and area for the unsteady flow problem of an oscillating airfoil in a wind tunnel

$$w = \frac{\partial \phi}{\partial y} \quad (\text{profile}), \quad f = \phi \quad (\text{walls}), \quad g = \frac{\partial \phi}{\partial y} \quad (\text{walls}) \quad (9.34)$$

For f and g indices "up" and "lo" denote values at the upper or lower tunnel wall, respectively. The downwash in the presence of tunnel walls is governed by the following relation

$$\begin{aligned} w(x) = & - \int_0^{\infty} \delta \phi(\zeta) \psi_{\bar{\eta}\bar{\eta}}(x - \zeta, 0) d\zeta \\ & - \int_{-\infty}^{\infty} (g^{up}(\zeta) \psi_{\bar{\eta}}(x - \zeta, b) - g^{lo}(\zeta) \psi_{\bar{\eta}}(x - \zeta, b)) \\ & - \int_{-\infty}^{\infty} (f^{up}(\zeta) \psi_{\bar{\eta}\bar{\eta}}(x - \zeta, b) - f^{lo}(\zeta) \psi_{\bar{\eta}\bar{\eta}}(x - \zeta, b)) \end{aligned} \quad (9.35)$$

Similar relations are derived for f and g on the walls, see [39]. If the integral operators are expressed by aerodynamic influence coefficients A , B , C etc., the final system reads :

$$\begin{aligned} w &= A \delta \phi + A_1 f + A_2 g \\ f &= (B_0)^{(-1)} (B \delta \phi + B_1 g) \\ g &= (C_0)^{(-1)} (C \delta \phi + C_1 f) \end{aligned} \quad (9.36)$$

These equations relate the downwash distribution w to an unknown dipole distribution $\delta \phi$, which provides the unknown pressure jump at the airfoil by taking the unsteady flow values f and g at the wind tunnel walls into account. For the numerical solution the wing profile and the walls are divided into line elements (panels) on which w , $\delta \phi$, f , g are approximated as constants. The dipole strength in the wake is approximated by the values near the trailing edge and by use of the Kutta condition. Since the unsteady potential function, especially downstream of the airfoil, decreases only slowly, see **Figure 3**, the control volume of the integral equation has to be extended far up- and downstream (to approximate infinity), as at least 10 airfoil chords as numerical tests have shown.

Applying this panel technique to the above equation yields a corresponding system of linear algebraic equations, where now the above aerodynamic influence functions are expressed by aerodynamic influence coefficient matrices (results of integration along one panel), and where w , $\delta \phi$, f , g are now column vectors of the corresponding values at the airfoil and at the tunnel walls. For the special cases of solid and open walls, the equations simplify to a closed form from which the (wall-affected) dipole strength, and hence the related unsteady pressures, can be calculated for a prescribed downwash w , i.e. oscillatory motion of the model.

$$\begin{aligned} \text{solid walls } g = 0 & \rightarrow w = (A + A_1 B_0^{(-1)} B) \delta \phi \\ \text{open walls } f = 0 & \rightarrow w = (A + A_2 C_0^{(-1)} C) \delta \phi \end{aligned} \quad (9.37)$$

For ventilated walls the boundary conditions outlined in chapter 2.3 have to be applied. Their implementation combines f , g , and $\partial f / \partial x$. If pressures on the walls are measured, f can be obtained by integrating (9.9) - see also (9.39) below - and then directly used in (9.36). In **Figures 16, 17** some typical results obtained from the described numerical method are illustrated. **Figure 16** shows the wall-influenced and the free-air unsteady pressure jumps in terms of the non-dimensional complex pressure coefficient $c_p = (p_{upper} - p_{lower}) / (q \Delta \alpha)$, with q = freestream dynamic pressure and $\Delta \alpha$ = amplitude, on a 2D plate performing pitching oscillations about a 42.5% chord axis, Mach number = 0.866, reduced frequency $k = 0.050$ and a wall distance $b/L = 5$. Solid walls increase the loads, while open walls produce the opposite effect. The results of **Figure 17** are obtained for the same conditions, except that the

reduced frequency has been changed to $k = 0.182$, which is close to the first solid wall resonance frequency. Now both the real and imaginary part are nearly zero.

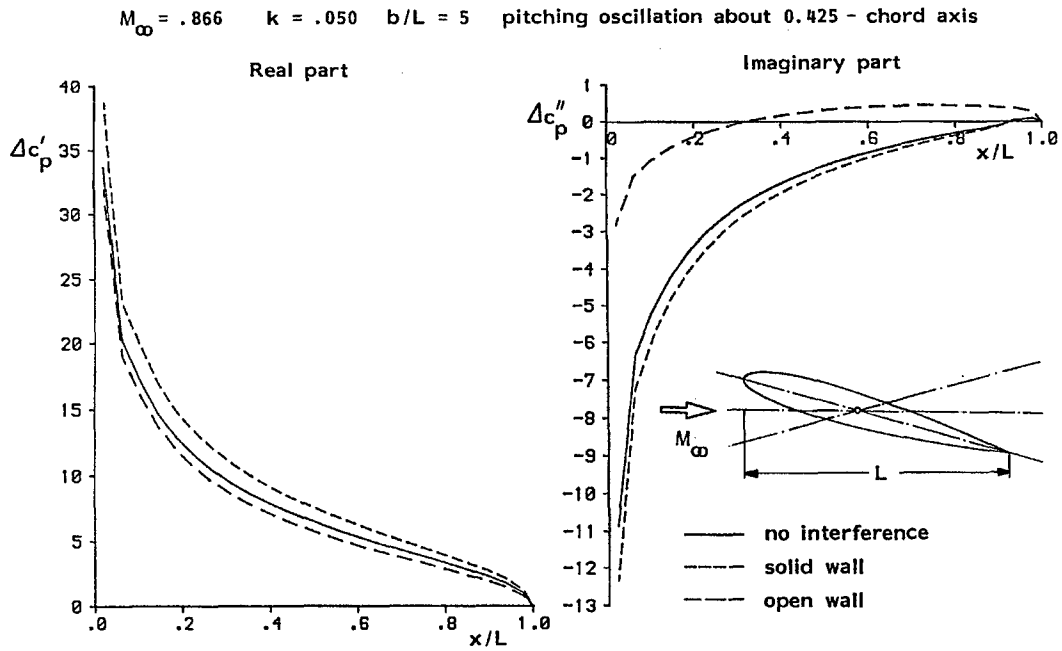


Figure 16 : Unsteady pressure around an oscillating airfoil with different tunnel wall conditions, far from tunnel resonance condition

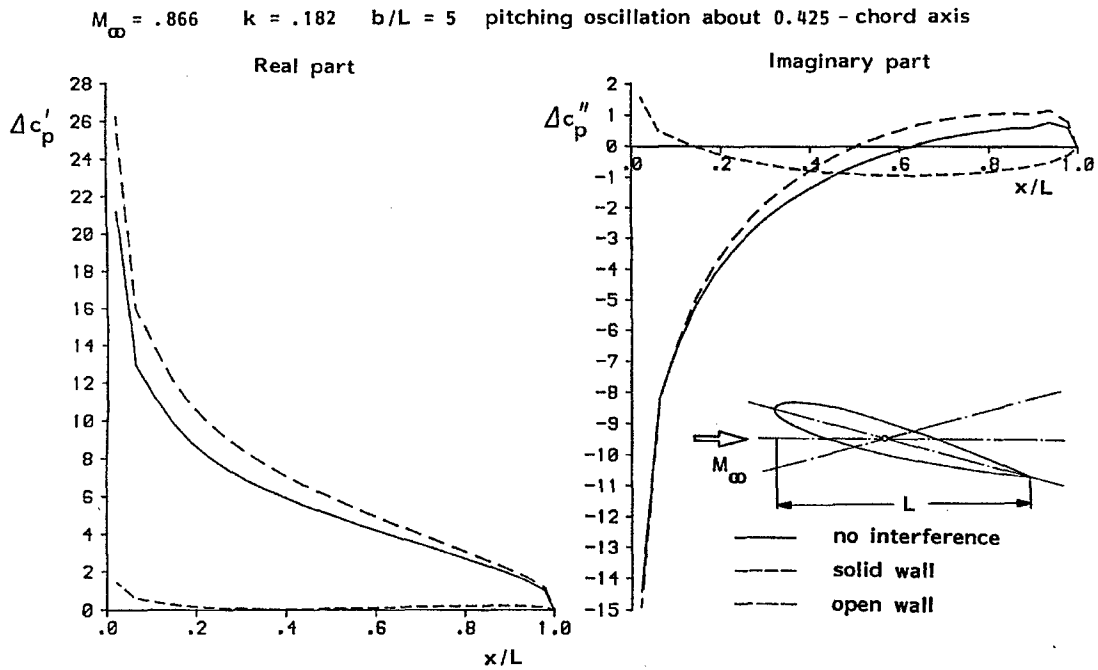


Figure 17 : Unsteady pressure around an oscillating airfoil with different tunnel wall conditions, close to tunnel resonance

The corresponding integrated unsteady lift values are shown in **Figure 18**. The overall agreement of the results with those of the analytical method of Fromme and Golberg, see **Figure 13** is good. The main discrepancy appears near the resonance frequencies, where the numerical panel method does not precisely predict the drop of magnitude to zero and produces oscillatory behaviour. The reason for this lies in the sensitivity of the numerical method with respect to modelling of the tunnel walls. These are modelled to be infinitely extended in the analytical method, while the panel method models only a finite extension (typically 10 - 100 chords).

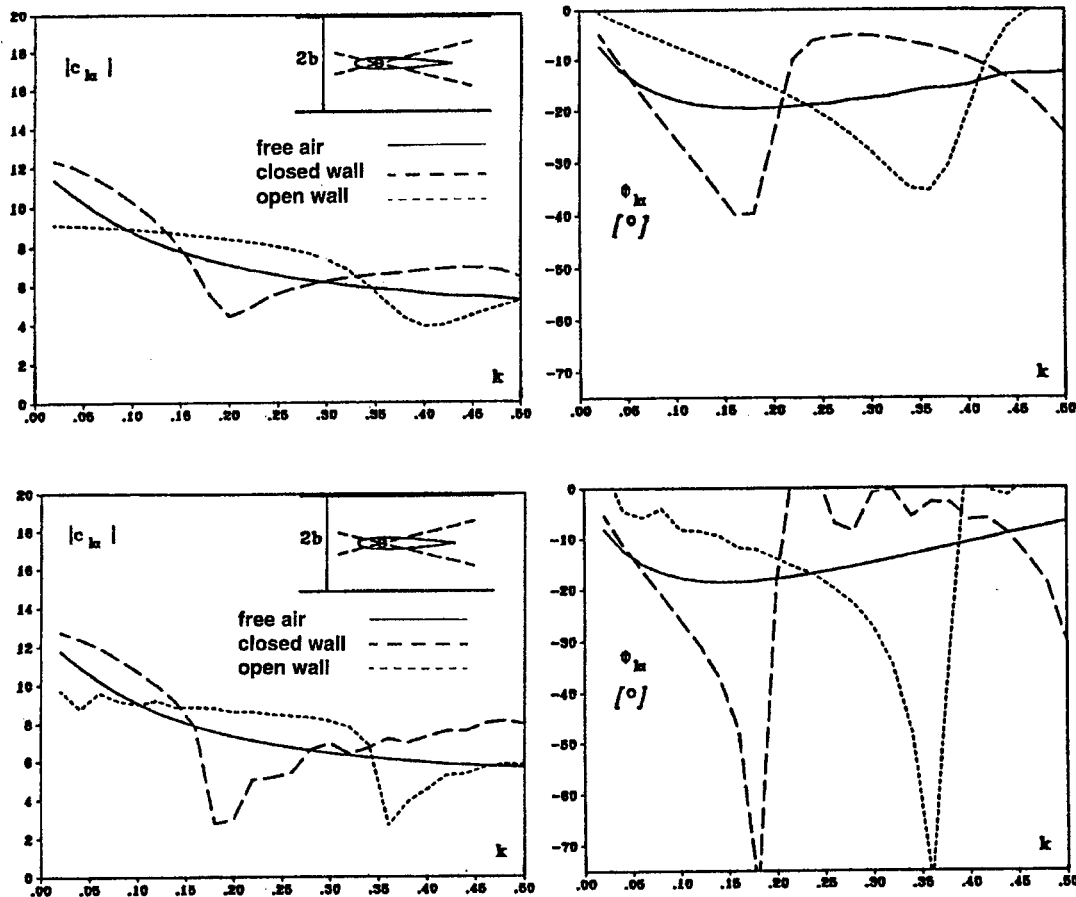


Figure 18 : Magnitude and phase of unsteady lift coefficient obtained by the linear panel method (same parameters as in Fig. 13)

Of course, unsteady aerodynamic predictions with wind tunnel wall effects can be obtained by other numerical methods as well. Today, the more sophisticated CFD-methods, which model the whole flow field and are based on non-linear equations, have also become a reliable tool in unsteady aerodynamics and they are easily applicable for the whole flow speed regime. **Figure 19** presents results for the test case of **Figure 17**, which have been obtained by one of the simplest CFD methods, based on the non-linear Transonic Small Perturbation (TSP) equation in the time domain, see [Voß 1990].

The unsteady results are obtained by solving the non-linear 2D TSP equations

$$\frac{\partial}{\partial x} \left(\beta^2 \phi_x - \frac{(\gamma+1)}{2} M_\infty^2 \phi_x^2 \right) + \frac{\partial}{\partial y} (\phi_y) - \frac{\partial}{\partial t} (M_\infty^2 (2\phi_x + \phi_t)) = 0 \quad (9.38)$$

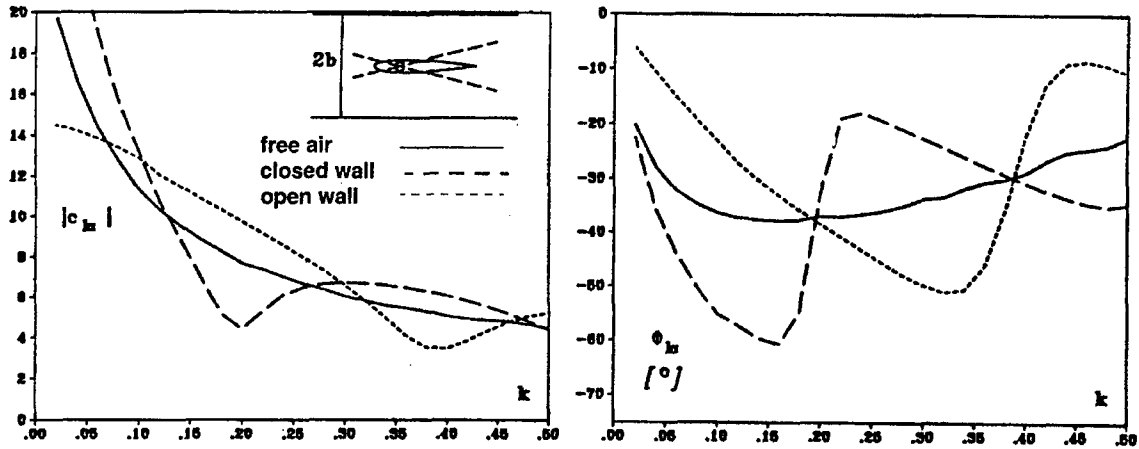


Figure 19 : Magnitude and phase of unsteady lift coefficient obtained by the TSP method (same parameters as in Figs. 13 and 18, $Ma_\infty = 0.866$, $b = 5$, pitching around a 50% chord, NACA 0006 airfoil).
 upper : linear simulation lower : non-linear transonic simulation

The unsteady results are obtained by Fourier analysis from the complete time-dependent flow field simulation. In its upper part, **Figure 19** presents linear results, which are directly compatible with those of the panel method. Linear theory was simulated by neglecting the non-linear term in the above equation. An overall agreement with the results of the panel method and the exact analytical method appears, but the strong jumps of magnitude and phase values at resonance frequencies are smeared, and the values of the corresponding sharp peaks (magnitude: zero, phase angle: -90 degrees) are not captured very well. Outside of the resonance frequencies the agreement is very good, and there are no oscillations. The corresponding transonic results in the lower part show that the effects of unsteady tunnel interference are very similar to the linear behaviour. The underlying acoustic effects are only altered in transonic flow. Resonance appears for the same frequencies, the wall effects on phase angles are even stronger for transonic than for subsonic flow. The increased values of magnitude are due to the transonic effects.

A similar behaviour has been investigated for 3D transonic flows, see [35]. In 3D flows the same tendencies appear as in 2D, especially the resonance frequencies are observed for the same values. These investigations were carried out for rectangular wings in transonic flows. The unsteady interference effects for the rectangular wing are as big as those for the 2D airfoil. **Figure 20** shows results for a rectangular wing oscillating in pitch, with an extremely large value of the ratio between tunnel width and wing chord of 21.2. In general, one should expect that unsteady interference effects for 3D flows are smaller than for 2D flows. A general investigation of swept wings has not been done yet.

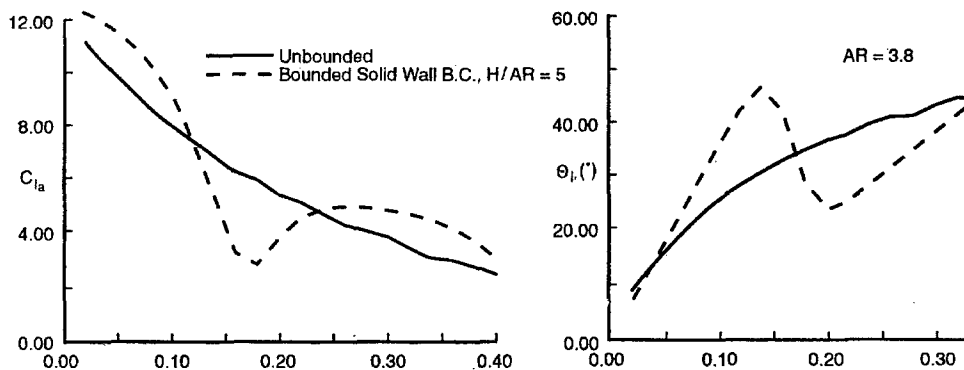


Figure 20 : Magnitude and phase of unsteady lift coefficient obtained by non-linear 3D TSP computation for a rectangular wing in a wind tunnel. (adapted from Seebass)

9.5 REDUCTION AND CORRECTION OF UNSTEADY WIND TUNNEL WALL INTERFERENCES.

9.5.1 UNSTEADY WIND TUNNEL WALL CORRECTIONS BY ANALYTICAL METHODS

In an early attempt, Jones [17] formulated a 2D correction technique, using an infinite series of image singularity distributions to model the tunnel wall effects. Similarly, Garner et al [14] developed a 3D correction method for ventilated tunnel walls by describing the wall influences through an infinite series of images of vortex distributions representing the model. This method has been modified by Kuczka, [18], for closed walls. Details can be found in the references. The applicability was demonstrated by computing unsteady tunnel wall pressure distributions by this analytical model and comparing them with corresponding test results. The agreements are very satisfying, even in transonic 3D flows at high incidences of the model. But the method is restricted to models of low aspect ratio and to low reduced frequencies (nearly quasi steady behaviour). The method was applied for the SDM model in wind tunnels with both a quadratic ventilated test section and a circular closed but stationary adaptive section. Due to the low frequencies, both the steady adapted closed walls and the ventilated walls provided results for the real part of unsteady lift and moment coefficients at the model with only a small remaining difference. This remaining unsteady interference can be corrected by Kuczka's method. **Figure 21a** shows that the correction method for unsteady interferences yields a slight shift of the real part of lift in a way that the corrected results of the different tunnels agree very well. The correction of the imaginary part is not as satisfactory. The corrected final results of both tunnels agree well only for low incidences; see **Figure 21b**. Nevertheless, this method should be further improved because it is simple and has the advantage that no precise knowledge about the model geometry and its motion are necessary - the measured wall-affected lift and moment coefficients are sufficient. General unsteady wall correction methods without restrictions with respect to model geometry and frequency need to take into account unsteady results measured at the tunnel walls.

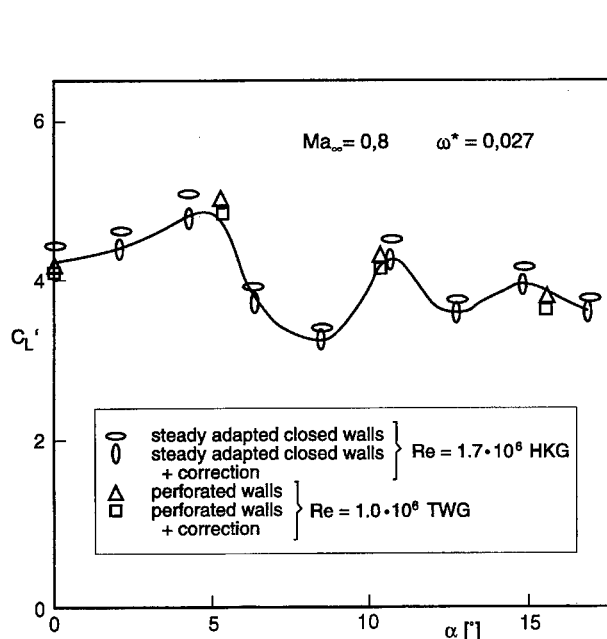


Figure 21a

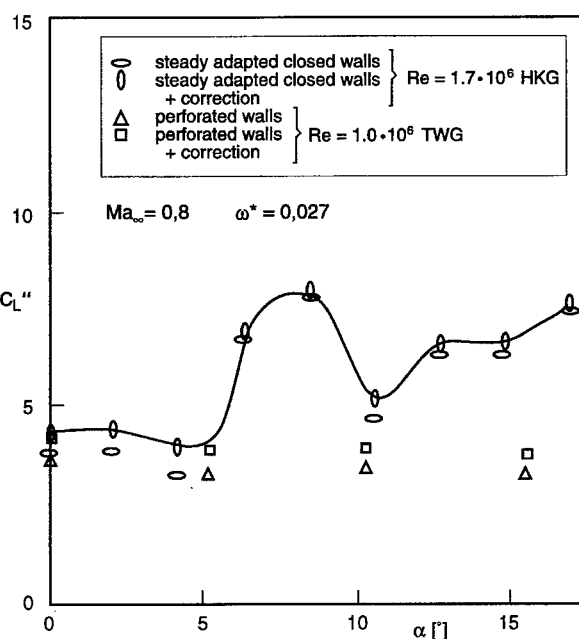


Figure 21b :

Unsteady in-phase and out-of-phase lift coefficients CL' and CL'' versus incidence for the SMD model tested in 2 wind tunnels and corrected for tunnel interference (adapted from Kuczka)

9.5.2 UNSTEADY WIND TUNNEL WALL CORRECTIONS USING MEASURED TUNNEL WALL PRESSURE VALUES AND NUMERICAL METHODS

9.5.2.1 DIRECT COMPUTATION OF THE TUNNEL WALL PROBLEM BY PANEL METHODS

If it is possible to measure the unsteady wall pressure distributions during the test, they can be used to correct the wall-influenced unsteady pressure data at the model to corresponding free air results. Such wall pressure measurements are a basic feature for steady flow adaptive wall concepts. For unsteady corrections both magnitude and phase of unsteady pressure have to be measured at a sufficient number of tunnel wall control points. These may serve for tunnel wall correction methods based on numerical unsteady aerodynamic methods. In [39] such methods for small amplitude oscillating models, based on the above panel method, are described and outlined in the following. As outlined in formula (9.9), the corresponding values of the velocity potential can be obtained from a measured unsteady (harmonic) tunnel wall pressure distribution C_p^w by the integration

$$c_p^w = -2 \left\{ \varphi_{\bar{x}}^w + i \frac{k}{\beta^2} \varphi^w \right\} e^{i k \bar{x}} \rightarrow \varphi^w = -\frac{1}{2} \int_{-\infty}^{\bar{x}} c_p^w(\bar{\zeta}) \exp \left[i \left(k \bar{\zeta} - \frac{k}{\beta^2} \bar{x} \right) \right] d\bar{\zeta} \quad (9.39)$$

The wall pressures have to be measured at a sufficient number of control points distributed on the tunnel walls, including the regions upstream and downstream of the model. Then one obtains an integral equation for the wall-affected dipole distribution on the model by application of Green's method to the wind tunnel wall bounded flow control volume. The final equation reads as:

$$\left(A + A_2 C_0^{(-1)} C \right) \delta \tilde{\varphi} = w - \left(A_1 + A_2 C_0^{(-1)} C_1 \right) \varphi^w \quad (9.40)$$

Here $\delta \varphi$ denotes the dipole strength for the wall-affected pressure on the airfoil. It can be seen that the wall interference effects change both the downwash and the kernel of the integral equation, compared to the free air equation $w = A \delta \varphi$. Substitution finally yields the following equation :

$$\tilde{A}_1 \delta \tilde{\varphi} = \left(w - \tilde{A}_2 \varphi^w \right) \quad \text{with} \quad A \delta \varphi = w \quad \text{follows} \quad \tilde{A}_1 \delta \tilde{\varphi} = A \delta \varphi - \tilde{A}_2 \varphi^w \quad (9.41)$$

Here the kernels (influence coefficient matrices) are known from theory and depend on model geometry, Mach number and reduced frequency. An extension to 3D problems is straightforward. For 3D cases Green's function is an exponential function instead of the Hankel function for 2D cases, and integration's have to be performed along the contour surfaces of tunnel walls, model and wake surface instead of lines. In the framework of the small disturbance approach, 3D models may be represented by panelling the projection area in the plane of streamwise and spanwise co-ordinate axes (parallel to upper and lower tunnel walls). With this method, no further information on the type of tunnel walls or model motion is needed, but the model geometry has to be represented by panels.

The 2D correction method of Sawada [34] uses Green's theorem as well, and is similar to the above approach. The advantage of his approach is that that pressure distributions appear directly in the integral equations, but integral kernels are rather complicated functions and extension to 3D will be very complicated. The results he obtained are encouraging for low frequencies and less satisfactory in the vicinity of resonance frequencies.

Extension of the described correction methods to transonic flows demands the reformulation of the integral equations based on an inhomogeneous Helmholtz equation, which can be derived from Eq. (9.2). Direct integral equation methods for the solution of 2D and 3D unsteady transonic flows under free air conditions and based on this approach are described in [16] and in [37]. The methods require the

computation of several additional kernel functions in order to model the transonic effects of the steady base flow field and for the inclusion of field sources in those parts of the flow field near local supersonic regions. **Figure 22** shows the control volume for these so-called field panel methods. These additional operators thus depend on the Mach number, reduced frequency, model geometry and steady flow, which would significantly complicate the procedure.

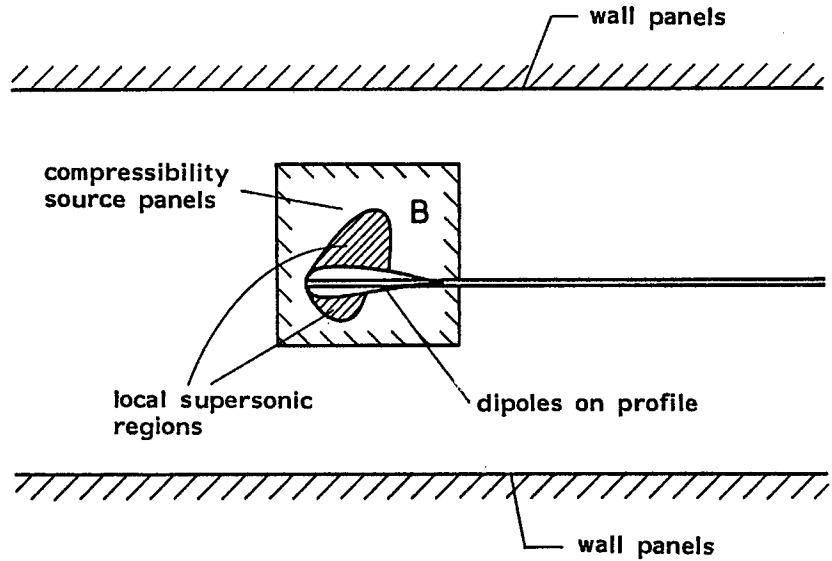


Figure 22 : Region of integration for the solution of transonic boundary value problem including the additional transonic near-field control area B

The corresponding integral equation for the correction

values $\delta\varphi^c$ and φ^c of the dipole strength on the airfoil and of the potential values in the field

$$\delta\varphi^c = \delta\tilde{\varphi} - \delta\varphi \quad \text{and} \quad \varphi^c = \tilde{\varphi} - \varphi \quad (9.42)$$

involving the right-hand-side S of the basic nonhomogeneous Helmholtz equation and the potential values φ^w on the tunnel walls reads:

$$\int_0^{\infty} \delta\varphi^c \psi_{\bar{\eta}\bar{\eta}} d\zeta - \int_B S(\varphi^c) \psi_{\bar{\eta}} dF - \int_{-\infty}^{\infty} \varphi^w \psi_{\bar{\eta}\bar{\eta}} d\zeta = 0 \quad \text{airfoil} \quad (9.43)$$

$$\int_0^{\infty} \delta\varphi^c \psi_{\bar{\eta}} d\zeta - \int_B S(\varphi^c) \psi dF - \int_{-\infty}^{\infty} \varphi^w \psi_{\bar{\eta}} d\zeta = -\varphi^c \quad \text{in the field}$$

9.5.2.2 SOLUTION FOR THE CORRECTION POTENTIAL BY PANEL METHODS

A slightly different approach is more promising. The method assumes closed adaptive tunnel walls which are adapted for the steady flow. Thus only the unsteady acoustic interferences will be corrected. A further assumption is that the component of the flow field which is caused by wall interference may be described by the linear theory. This is justified by the discussions in chapter 2.1. Thus the difference between velocity potential of the wall-affected tunnel flow and the desired value of the corresponding free air conditions fulfils the Helmholtz equation, and the correction value of the dipole strength and thus the airfoil pressure distribution is directly computed.

$$\varphi_{xx}^c + \varphi_{yy}^c + \lambda^2 \varphi^c = 0 \quad (9.44)$$

$$\varphi^c = \tilde{\varphi} - \varphi$$

The corresponding boundary conditions are obtained by subtracting those of the wind tunnel flow (vanishing normal flow velocity on both the model surface and on the tunnel walls) from the free air conditions (nonreflecting far field conditions at the locations of the tunnel walls). The model surface conditions are prescribed by the oscillatory motion and are the same with and without tunnel walls, thus yielding

$$\varphi_{\bar{y}}^c = 0 \text{ (profile)} \tag{9.45}$$

Nonreflecting far field conditions have been derived by different authors, see for example [20], or [9], for unsteady CFD methods, and they are applied here in their harmonic, time-dependent complex form, for the upper and lower walls, respectively

$$\left(\phi_x \pm \frac{M_\infty}{\sqrt{1-M_\infty^2}} \phi_t \right) = 0 \tag{9.46}$$

Application at the tunnel wall locations, together with the potential transformation and subtracting from this the condition for solid tunnel walls (vanishing y-components of disturbance velocity) yields

$$\varphi_{\bar{y}}^c \pm \chi \varphi^c = \chi f^w \tag{9.47}$$

for the upper and lower walls, respectively with f denoting the value of the potential on the upper or lower wall and with

$$\chi = \frac{ik M_\infty}{(1-M_\infty^2)} \tag{9.48}$$

The value of the velocity potential at the walls may be obtained from the measured wall pressures by integration as described above. Applying the notation of the preceding chapter yields

$$w^c = 0 \quad g^c \pm \chi f^c = \pm \chi f^w \tag{9.49}$$

and, finally, after some rearrangements, an integral equation for an unknown dipole distribution from which the pressure correction of the wall interference is obtained in the usual way, for details see [39]

$$(A + A_3 B) \delta \varphi^c = -(A_3 \tilde{B}_1 \pm \tilde{A}_2) \chi f^w \tag{9.50}$$

for the upper and lower walls respectively. **Figure 23** shows a result of this correction method for an unsteady transonic flow also including shock waves. Due to the non-existence of detailed unsteady transonic flow pressure measurements at the tunnel walls, this demonstration did not apply wind tunnel data,

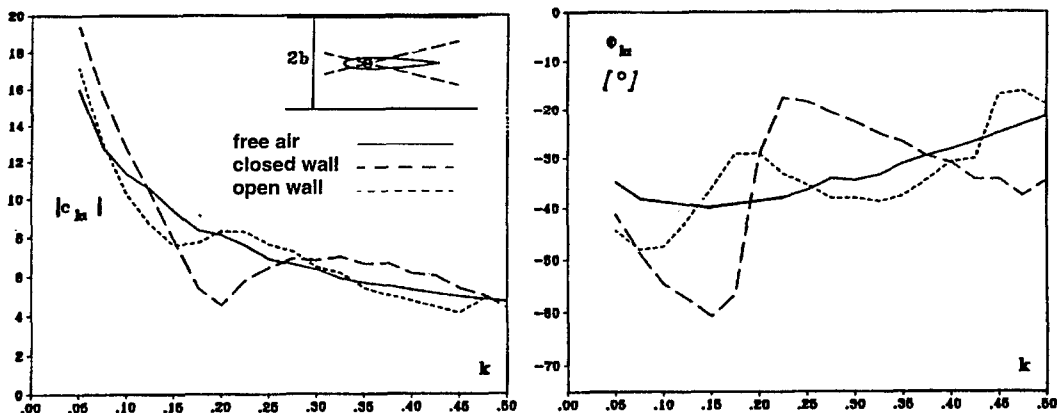


Figure 23 : Correction of unsteady tunnel wall interference in transonic flow (NACA 0006, $Ma_w = 0.866$, $b = 5$, pitching around a 25% chord).

but CFD results were computed by the above-mentioned TSP method for the wind tunnel flow with closed walls and for free air condition. Both the results on the airfoil and at the walls were used as "experimental" results and were corrected in the described manner. The correction shows significant improvements of the wind tunnel simulation results towards free air simulated results, although the agreement of corrected and free air methods is still unsatisfactory - not only near the tunnel resonance. Especially phase angles should be accurate within a range of ± 5 degrees. But one has to keep in mind that the correction procedure is based on a linear formulation, while both the wind tunnel flow and the free flow include large non-linear effects.

References

- [1] Acum, W.E.A., A Simplified Approach to the Phenomenon of Wind Tunnel resonance. ARC R&M 3371 (1962)
- [2] Ashill, P.R., Keating, R.F.A., Calculation of Tunnel Wall Interference from Wall Pressure Measurements. RAE TR 85086 (1985).
- [3] Bergh, H., Zwaan, R., Present Status of Unsteady Aerodynamics for Lifting Surfaces. AGARD CP 46 (1970)
- [4] Beyers, M.E., Unsteady Wind-Tunnel Interference in Aircraft Dynamic Experiments. J. Aircraft, Vol. 29 (1992), pp. 1122-1129.
- [5] Bland, S.R., The Two-Dimensional Oscillating Airfoil in a Wind Tunnel in Subsonic Flow. SIAM J. Appl. Math., Vol. 18, (1970), pp.830-848.
- [6] Chang, Byeong-Hee, Sung, Bongzoo, Chang, Keun-Shik., Unsteady Adaptive Wall Models for Wind Tunnel Testing. AIAA J., Vol. 33 (1995), pp. 1536-1538.
- [7] Cheung, C.W., Hancock, G.J. Wind Tunnel interference on Unsteady Two-Dimensional Airfoil Motions in Low Speed Flows. Aeronautical Journal, March 1988, pp.115-121.
- [8] Davis, J.A., Transonic Interference effects in Testing of Oscillating Airfoils, Dissertation Ohio State University (1982)
- [9] Engquist, B., Majda, A. Radiation Boundary condition for Acoustic and Elastic Wave Calculations. Comm. Pure and Appl. Math., Vol. 32 (1979) pp. 313-357.
- [10] Försching, H., Voß, R., Adaption for Unsteady Flow, in "Adaptive Wind Tunnel Walls : Technology and Application", AGARD AR 269 (1990)
- [11] Fromme, J.A., Golberg, M.A., Unsteady Two-Dimensional Airloads Acting on Oscillating Thin Airfoils in Subsonic Ventilated Wind Tunnels. NASA CR 2967 (1978)
- [12] Fromme, J.A., Golberg, M.A., Aerodynamic Interference Effects on Oscillating Airfoils with Controls in Ventilated Wind Tunnels. AIAA J., Vol. 18 (1980), pp.417-426.
- [13] Fromme, J.A., Golberg, M.A., Reformulation of Possio's kernel with Application to Unsteady Wind Tunnel Interference. AIAA J., Vol. 18 (1980), pp.951-957.
- [14] Garner, H.C., The Theory of Interference Effects on Dynamic Measurements in Slotted-Wall Tunnels at Subsonic Speeds and Comparisons with Experiment. ARC R&M 3500 (1968).
- [15] Garner, H.C., Theoretical Use of variable Porosity in Slotted Tunnels for Minimizing Wall Interference on Dynamic Measurements. ARC R&M 3706 (1971).

- [16] Geißler, W., Voß, R., Investigations of the Unsteady Airloads with Oscillating Control in Sub- and Transonic Flows, in Proc. 1st Int. Symp. on Aeroelasticity, DGLR Report 82-01 (1982).
- [17] Jones, M.A., Wind Tunnel Wall Interference Effects on Oscillating Airfoils in Subsonic Flow. ARC R&M 2943 (1953).
- [18] Kuczka, D., Hybridverfahren für instationäre Messungen in transsonischen Windkanälen am Beispiel der harmonischen Nickschwingung. DFVLR-FB 88-19 (1988).
- [19] Kong, L., Parkinson, G.V., Unsteady Flow testing in a Passive Low-Correction Wind Tunnel. In Wall Interference, Support Interference and Flow Field Measurements, AGARD CP 535 (1994), pp. 22-1-22-7.
- [20] Kwak, D., Non-Reflective Far Field Boundary Conditions for Unsteady transonic Flow Computation. AIAA J., Vol. 19 (1981), pp.1401-1407.
- [21] Lambourne, N., Destuynder, R., Kienappel, K., Roos, R., Comparative Measurements in Four European Wind Tunnels of the Unsteady Pressures on an Oscillating Model (The NORA Experiments). AGARD Report No. 673 (1980)
- [22] Lambourne, N., Wind Tunnel Wall Interference in Unsteady Transonic Testing. AGARD VKI Lecture Series 1981-4 (1981)
- [23] Landahl, M.T., Unsteady Transonic Flow. Pergamon Press (1969)
- [24] Laschka, B., Wegner, W., Theoretische Behandlung der Böensimulation im Windkanal, ZFW 10 (1986), pp.168-173.
- [25] Lu, Qizheng, Li, Qing, Lu, Bo., Experimental Investigation on the Interference effect of FL-23 Wind Tunnel Wall on Transonic Flutter. Acta Aerodynamica Sinica, Vol. 7 (1989), pp. 351-357.
- [26] Mabey, D.G., The Reduction of Dynamic Interference by Sound-Absorbing Walls in the RAE 3 ft. Wind Tunnel. RAE TR 77120 (1977).
- [27] Mabey, D.G., Resonance Frequencies of Ventilated Wind Tunnels. AIAA J., Vol. 18 (1980), pp.7-8.
- [28] Mokry, M., Chan, Y.Y., Jones, D.J., Two-Dimensional Wind Tunnel Wall Interference. Chapter 8. Unsteady Wall Interferences. AGARDograph No. 281 (1983), pp.131-158.
- [29] Moore, A.W., Wight, K.C., An Experimental Investigation of Wind Tunnel Wall Conditions for Interference-Free Dynamic Measurements. ARC R&M 3715 (1969).
- [30] Platzer, M.F., Wind Tunnel Interference on Oscillating Airfoils in Low Supersonic Flow. Acta Mechanica, Vol. 16 (1973), pp.115-126.
- [31] Possio, C., L'azione aerodinamica sul profilo oscillante in un fluido compressibile a velocità iposonara. L'Aerotecnica, Vol 18 (1938), pp. 441-458.
- [32] Runyan, H.L., Watkins, C.E., Consideration on the Effect of Wind Tunnel Walls on Oscillating Air Forces for Two-Dimensional Subsonic Compressible Flows. NACA Report 1150 (1951).
- [33] Runyan, H.L., Woolston, D.S., Rainey, A.G. Theoretical and Experimental Investigations of the Effect of Tunnel Walls on the Forces on an Oscillating Airfoil in Two-Dimensional Subsonic Compressible Flow. NACA Report 1262 (1955).
- [34] Sawada, H., A New Method of Estimating Wind Tunnel Wall Interference in Unsteady Two-Dimensional Flow. NRC No. 21274 (1983).
- [35] Seebass, A.R., Fung, K.Y., Przybytkowski, S.M., Advances in the Understanding and Computation of Unsteady Transonic Flow, in "Recent Advances in Aerodynamics", Springer (1983)

- [36] Vogt, U., Computation of Unsteady Wind Tunnel Wall Influences on Pressure Distributions of Oscillating Airfoils, DFVLR IB 232-85 J15 (in German) (1985)
- [37] Voß, R., Calculation of Unsteady transonic Flow about Oscillating Wings by a Field Panel Method, in Panel Method in Fluid Mechanics with Emphasis on Aerodynamics, Notes on Numerical Fluid Mechanics, Vol. 21 (1988), pp. 232-242.
- [38] Voß, R., Über die Ausbreitung akustischer Störungen in transsonischen Strömungsfeldern von Tragflügeln, DFVLR-FB 88-13 (1988).
- [39] Voß, R., Instationäre Windkanalwand-Interferenzen bei sub- und transsonischer Stömung, in Festschrift on the 60th birthday of Prof. H.W. Försching, DLR Institute of Aeroelasticity (1990), pp. 169-185.

10. ADAPTIVE WALL TECHNIQUES

**AUTHORS : DR. ERICH WEDEMEYER
DR. NIGEL J. TAYLOR
DR. HARTMUT HOLST**

	PAGE
LISTS OF SYMBOLS	10-3
10.1 INTRODUCTION	10-4
10.2 THE RUDIMENTS OF ADAPTIVE WALL TECHNIQUES	10-5
10.2.1 THE AIMS OF WALL ADAPTATION	10-5
10.2.2 THE FORMS OF WALL ADAPTATION	10-6
10.2.3 THE PROCESS OF WALL ADAPTATION	10-8
10.2.3.1 WALL INTERFERENCE ASSESSMENT	
10.2.3.2 WALL ADJUSTMENT STRATEGY	
10.2.3.3 COMPLETION CRITERIA	
10.2.4 FURTHER POINTS OF CLASSIFICATION	10-11
10.2.4.1 THE TYPE OF FLOWFIELD BEING SIMULATED	
10.2.4.2 THE NATURE OF THE FLOW AT THE CONTROL SURFACES	
10.3 TWO-DIMENSIONAL TESTING	10-12
10.3.1 WALL ADAPTATION BY ITERATION	10-13
10.3.2 ONE STEP METHODS OF WALL ADAPTATION FOR GROUP 1 FLOWS	10-13
10.3.3 WALL ADAPTATION IN SUPERSONIC FLOW (GROUP 5)	10-15
10.3.4 WALL ADAPTATION IN TRANSONIC FLOWS (GROUPS 2-4)	10-16
10.4 THREE-DIMENSIONAL TESTING	10-17
10.4.1 WALL ADAPTATION BY INTERFACE MATCHING	10-17
10.4.2 TARGET LINE METHODS: TWO-DIMENSIONAL WALL ADAPTATION FOR THREE-DIMENSIONAL FLOWS	10-18
10.4.2.1 ASSESSMENT OF THE WALL INTERFERENCE	
10.4.2.2 WALL ADAPTATION ALGORITHM	
10.4.2.3 COMPLETION CRITERIA	
10.4.2.4 EXPERIMENTAL RESULTS FOR GROUP 1 FLOWS	
10.4.2.5 WALL ADAPTATION FOR NON-LINEAR AND SUPERSONIC FLOWS (GROUPS 2-4)	
10.4.2.6 LIMITATIONS AND OPEN QUESTIONS	
10.4.3 EFFECTS OF THE SIDEWALL BOUNDARY LAYER	10-25

	PAGE
10.5 MANIPULATIVE ALGORITHMS	10-26
10.6 PRIORITIES FOR THE FUTURE	10-28
10.6.1 DATA QUALITY	10-28
10.6.2 RATE OF DATA ACQUISITION	10-28
10.6.3 COMPLEXITY AND COST	10-29
TABLES	10-31
FIGURES	10-31
10.7 REFERENCES	10-42
APPENDIX A	10-45
APPENDIX B	10-45

10. ADAPTIVE WALL TECHNIQUES

LIST OF SYMBOLS

AR	aspect ratio
b	width of test section
c	model chord
c_L	lift coefficient
c_p	pressure coefficient
d_t, d_b	wall displacement of top and bottom wall, positive when directed outwards
d_s, d_a	symmetric and anti-symmetric part of the wall displacement
h	height of test section
M	Mach number of free stream flow
p_e	wall pressure distribution of the (fictitious) exterior flow, Figure 10.5
p_i	wall pressure distribution of the interior flow, Figure 10.5
s	semi-span of wing
U_∞	free stream velocity
u, v	in two-dimensional flows: disturbance velocity components in flow direction (u) and upwards (v)
u_t, u_b	disturbance velocity at top and bottom wall
u_s, u_a	symmetric and anti-symmetric parts of wall velocity induced by the model, Equations 10.5a&b
u_{ws}, u_{wa}	symmetric and anti-symmetric parts of wall velocity induced by wall deflection
w	$= u - iv/\beta$, complex flow velocity
u, v, w	in three-dimensional flows: velocity components streamwise (u), spanwise (v), upwards (w)
u_{int}	in two-dimensional flows: interference velocity component in flow direction
v_{int}	in two-dimensional flows: interference velocity component upwards
w_{int}	$= u_{int} - iv_{int}/\beta$
x, y	in two-dimensional flows: co-ordinates streamwise (x) and upwards (y), Figure 10.5
z	$= x + iy\beta$ co-ordinate in the complex plane
x, y, z	in three-dimensional flows: co-ordinates streamwise (x), spanwise (y), upwards (z)
α	model incidence
β	$= \sqrt{1-M^2}$ Prandtl-Glauert compressibility factor
θ	wall angle
Θ	$= \cos^{-1}(1-2x/c)$, non-dimensional co-ordinate
δ	wall displacement, positive when directed outwards
δ^*	boundary layer displacement thickness
$\delta\alpha$	correction to model incidence
δy	wall displacement for two-dimensional wall adaptation, Equation 10.4
Δ_{upw}	normalised upwash variation
ϕ	disturbance potential, Equation 10.1
Ω, Γ	influence functions defined in Equations 10.6 a&b
X, M, Λ, N	influence functions defined in Equations 10.7 a&b

10.1 INTRODUCTION

In the context of wind tunnel wall corrections, adaptive wall techniques may be described as procedures which contrive to manipulate and control the levels and gradients of wall interference present in the test section by making appropriate adjustments to the wall boundary conditions. In so doing, they provide a measure of control over the nature of any primary corrections and residual variations that would not otherwise be available. As the adjustments to the walls are usually made in response to the information provided by conventional wall interference assessment procedures, adaptive wall techniques may be considered as extensions to many of the algorithms described elsewhere in this document.

The origins of these techniques can be traced back to the mid 1930's, when the activities of a group of engineers and scientists at the National Physical Laboratory (NPL) in England led to the use of two flexible walls being advocated as a means for alleviating wall-induced blockage effects in the high speed testing of two-dimensional models. Subsequently, the test section of a closed wind tunnel was converted for adaptive use by the installation of a flexible roof and floor and techniques enabling three-dimensional models to be tested at high subsonic reference Mach numbers were eventually developed. One of the adaptive wall tunnels at NPL was used extensively for over a decade, providing, amongst other things, valuable information to support the British war effort. However, its use fell into decline in the early 1950's, when it was realised that ventilated test sections offered a simpler means of testing through the speed of sound.

By this time, a number of other agencies had become involved in adaptive wall activities. Nevertheless, the advent and rapid development of transonic ventilated test sections marked the demise of the first era of adaptive wall research. Aside from the fact that the new ventilated facilities appeared to provide more effective mechanisms for preventing test section choking and alleviating the intensity of the reflections of shock or expansion waves from the tunnel walls, the principal reasons for interest being transferred away from adaptive wall techniques were as follows:

- i. The computational power required to conduct rigorous assessments of the wall interference on-line was not available. The methods used to adapt the walls at NPL were based on empirical correlations derived from potential flow analyses and required little or no on-line computation: the validity of this approach became increasingly uncertain as the reference Mach number was raised towards unity.
- ii. The operation of flexible-walled tunnels was cumbersome: wall profiles were adjusted manually via systems of screw-jacks and the static pressure distributions along each liner were monitored (by eye) on arrays of U-tube manometers. The lack of sophisticated analytical adaptation algorithms made the process of adapting the walls even more laborious: adjustments were made primarily on the basis of past experience and, even with the most experienced tunnel operators, it could, on occasion, take several minutes to derive the final wall settings.

Coinciding with the substantial advances that had been made in the fields of automation and computational technology by the end of the 1960's, adaptive wall techniques re-emerged as a potential means for alleviating a number of the concerns about contemporary wind tunnel testing practice that, with the ever-increasing demands placed on the quality of test data, were being scrutinised with renewed vigour. One of the principal motivations behind this development was the desire to reduce the uncertainties associated with the effects attributed to wall interference in transonic wind tunnel test data. Thus, unaware of the previous activities at NPL, researchers at various establishments set about the task of developing techniques that would minimise the effects of wall interference.

Considerable progress has been made towards achieving this goal in two- and three-dimensional testing. However, to date the vast majority of adaptive wall research has been conducted at the "proof-of-concept" level. Relatively little effort has been directed towards resolving the issues of more practical concern that will ultimately determine the cost of wall adaptation. Consequently, while adaptive wall techniques have been utilised productively and with some confidence in research environments for many years, they have yet to make a major impact on the procedures used for project-based production testing in large industrial wind tunnels.

Rather than attempting to present a comprehensive review of the principal developments that have occurred in recent years, or to offer explanations for the limited extent of their current utilisation, the purpose of this Chapter is to describe the most powerful and widely used adaptive wall techniques, explain their limits of applicability and provide a perspective on the priorities for future development. To this end, the underlying principles of wall adaptation for steady flows are reviewed briefly in Section 10.2, their application to the reduction of wall interference in two- and three-dimensional testing is described in Sections 10.3 and 10.4, further capabilities are reviewed in Section 10.5 and an outlook on the future is provided in Section 10.6. Sufficient information is also provided to enable potential users to construct techniques suitable for use in the subsonic testing of two- and three-dimensional models.

For further information, the interested reader is directed to the following works of reference: NASA Technical Memorandum 87639 (Tuttle and Mineck [39]), the latest edition of a bibliography on adaptive wall wind tunnels, AGARD Advisory Report 269 (Hornung, ed., [16]), which provides a catalogue of the activities surrounding adaptive wall technique development prior to 1990 and the "Proceedings of the International Conference on Adaptive Wall Wind Tunnel Research and Wall Interference Correction" held in June 1991 in Xian, China. The Adaptive Wall Newsletter (Wolf, ed., [44]) is a valuable additional source of otherwise unpublished information. The most recent attempts to review the state-of-the-art have been produced by Taylor and Goodyer [35], [36] and Taylor [37]. These publications provide a more comprehensive coverage of the results of experimental tests and more extensive citations of the original documents than those provided here.

10.2 THE RUDIMENTS OF ADAPTIVE WALL TECHNIQUES

10.2.1 THE AIMS OF WALL ADAPTATION

As the technology has matured, two different approaches to wall adaptation have evolved. These are distinguished by the nature of the objectives of wall adaptation and the manner in which its success is measured.

The first contrives to control components of the wall-induced perturbations to the flow throughout the test section in such a way as to enable the success of wall adaptation to be gauged purely from assessments of the admissibility of the adapted wall boundary conditions. Thus, if the wall boundary conditions can be shown to exhibit a direct correspondence with those of a streamtube in an equivalent unconfined flow, it may be inferred that wall adaptation has eliminated the effects of wall interference from the test section. The achievement of this goal over a suitably broad range of test conditions in practice is, of course, extremely unlikely. Nevertheless, the basic principle - often referred to as the principle of wall streamlining - has proved to be remarkably useful, particularly in the development of two-dimensional testing techniques. For the reasons described in Section 10.2.3.1, below, procedures which invoke this principle are referred to as interface matching techniques.

The second and more recently devised approach to wall adaptation contrives to control components of the wall-induced perturbations to the flow in more localised regions of the test section. The success of wall adaptation in these circumstances is gauged primarily from the extent to which the desired conditions have been attained in these targeted regions - although the admissibility of the adapted wall boundary conditions must also be verified. No attempt is made to control the flow away from these regions: it is merely hoped that by controlling the flow there, the magnitude of any unwanted residual perturbations in the immediate vicinity of each region will also have been reduced to acceptable levels. Procedures which adopt this approach to wall adaptation usually contrive to control the flow along lines passing through the test section. These are referred to as target line techniques.

In principle, the control of the test section flowfield afforded by wall adaptation may take any form the tunnel operator wishes. To date, it has been used primarily to minimise the effects of wall interference identified by established interference assessment procedures and thereby reduce the uncertainties associated with these features of wind tunnel testing. However, by intentionally manipulating the flow in the test section - imposing global velocity gradients or some other controlled form of wall-induced perturbation - wall adaptation may be put to a number of other uses. This subject is discussed further in Section 10.2.4.1, below.

10.2.2 THE FORMS OF WALL ADAPTATION

Of the various mechanisms that have been devised for providing adjustments to the wall boundary conditions, the most widely used may be grouped into two broad categories:

- i. those which modify the profiles of impervious flexible liners so as to manipulate the conditions at a surface - the displacement surface - within the adjacent boundary layers; and
- ii. those which contrive to manipulate the flow at a fixed surface near each wall by providing appropriate modifications to the test section ventilation.

The surfaces at which the flow conditions are manipulated are referred to as control surfaces. The principal differences between the control surfaces adjacent to impervious and ventilated test section walls are illustrated in Figure 10.1.

In flexible-walled test sections, the profile of each flexible liner is adjusted via a system of jacks. In ventilated test sections, the wall boundary conditions are modified by providing spatial adjustments to the wall geometry or the plenum pressure: these adjustments may be made in isolation or they may be combined in some way. The wall geometry is most often adjusted by modifying the open area ratio. In perforated test sections, this is most commonly achieved by employing sliding cover plates behind the perforations, while individually adjustable slats have been used in slotted facilities. Localised adjustments to the plenum pressure are made by segmenting the plenum chamber surrounding the test section and plumbing each sub-plenum independently.

The degree of control afforded by these forms of wall adjustment will be determined by the following factors:

- i. the precision with which each control surface may be defined;
- ii. the accuracy with which the conditions at each control surface may be monitored;
- iii. the nature of the relationship between the conditions at the control surfaces and the parameter used to adjust them; and
- iv. the extent of the practical constraints imposed on the nature of these adjustments.

In flexible-walled test sections, the control surfaces are reasonably well defined and measurement of the appropriate boundary conditions is usually relatively straightforward: the magnitude and direction of the local velocity vector may be derived directly from a knowledge of the wall geometry, static pressure measurements and computations of the boundary layer thickness. (The principal exception to this occurs when shock waves impinge on the control surfaces, in which case more detailed flowfield measurements in the immediate vicinity of the interactions may be required to provide adequate descriptions of the local boundary conditions.) Moreover, in circumstances where the wall boundary layer displacement thicknesses may be computed to an acceptable degree of accuracy, there is a direct correlation between the wall jack settings and the profiles of the control surfaces.

In contrast, considerable problems have consistently been encountered in procuring reliable measures of the conditions at the control surfaces adjacent to ventilated test section boundaries, particularly the normal (cross-flow) velocity. These are, of course, not unique to the adaptive forms of ventilated wall facility - see, for example, Section 4.3. However, the attendant uncertainties in any subsequent assessments of wall interference clearly have severe implications for the prospects of prescribing appropriate adjustments to the wall settings. Furthermore, even assuming that accurate measures of the residuals may be derived, the relationships between them and the parameters utilised to adjust the ventilation are ill-defined and non-linear.

Thus, it may be seen that the control afforded by adjusting the profiles of flexible liners is substantially more powerful than that provided by spatial modifications to the test section ventilation. However, the extent to which this control may be exploited in practice will be determined by the constraints imposed on their design. For instance, a practical mechanism capable of providing fully three-dimensional adjustments to the profiles of flexible liners has yet to be devised. Instead the walls are usually profiled in single curvature, affording two-dimensional or quasi-three-dimensional control, depending on the number and orientation of the walls being adjusted. Aside from making the complete elimination of wall interference a practical impossibility, this makes it necessary to ensure that, when prescribing the loci of target lines, each has a streamwise component throughout its length.

Flexible wall adjustments are further constrained by the use of a finite number of jacks to modify the wall shapes, leaving the profiles of the liners between the jacks to be determined by factors such as their structural properties and the local wind-on pressure loading. The manner in which the jacks are distributed along each liner, together with the limits of their travel, may also constrain the extent to which the wall shapes may be manipulated. These factors will dictate the range of test conditions for which the walls are operating optimally - a potentially important consideration given that the requirements for wall displacement will inevitably be functions of the reference conditions (Mach number and model attitude) and model geometry: two- and three-dimensional (full- and half-span) models may need to be accommodated.

Yet another important constraint is the requirement to ensure that the walls blend smoothly with the contraction and the diffuser. The impact of this constraint - which is closely related to the limits placed on the length of the test section - is likely to be most apparent in high-lift testing, when the upwash ahead of large two-dimensional models and the downwash aft of two- and three-dimensional models will be most pronounced. If the flow about the model is separated, there may also be substantial amounts of blockage present in these circumstances.

There are a number of other factors that may need to be addressed when designing flexible liners - providing for optical access to the test section, the housing of model strut mountings and the co-ordination of the adjustments to the wall contours and the model attitude, for instance. However, not all of these apply only to the design of adaptive flexible-walled test sections. Furthermore, few of these issues have yet been addressed by research activities. Therefore, to avoid cluttering the text with undue speculation or details

pertaining to the mechanical construction and operation of practical jacking systems, the emphasis of the remainder of this Chapter will be placed on describing the utility of closed test sections with two flexible walls. Despite the apparent limitations associated with the simplicity of their design, these facilities have proved to exhibit capabilities that surpass those of the alternative forms of adaptive wall test section in virtually all measures of quality and performance. A photograph of a typical research facility and a schematic illustration of its test section are presented in Figure 10.2.

10.2.3 THE PROCESS OF WALL ADAPTATION

The standard procedure for adapting the walls may be broken down into three stages, as follows.

- i. The wall interference at the control surface(s) or along the target lines (as appropriate) is assessed with the flexible walls set to pre-determined contours - such as those which may have been derived at a previous data point.
- ii. If, at any point at which it was assessed in (i), the indicated interference exceeds what are deemed to be acceptable limits, an appropriate algorithm is employed to prescribe improved wall contours.
- iii. The wall boundary conditions are then adjusted accordingly and the procedure repeated until the residual interference satisfies established acceptance criteria.

It is intuitive to expect that the process of *minimising* the effects of wall interference will be iterative, its iterative nature being most pronounced when the consequences of wall adaptation are particularly difficult to predict - as may be the case when the flow about the model is transonic or separated. Thus, the sequence of events beginning with an assessment of the wall interference and concluding with adjusting the wall boundary conditions is considered to be an adaptation iteration. The process of minimising or otherwise controlling the effects of wall interference is referred to as an adaptation cycle.

However, as wall adaptation should not reduce the rate at which data is acquired if it is ever to be used routinely in large industrial wind tunnels, a reliance on iteration is unlikely to be acceptable in production testing. This will require the necessary adjustments to the wall settings to be derived and applied rapidly and in one step - although the option to refine the data further by additional adaptation should always be available assuming practicalities allow it. In turn, this implies that a degree of anticipation or prediction will be required in deriving the adjustments - although it is also conceivable that the walls will not always need to be adjusted between successive data points and that a given wall setting may be acceptable for use over a range of test conditions.

Regardless of its potential application, an adaptive wall technique will always possess the following components: a wall interference assessment procedure, a wall adjustment strategy and a set of completion criteria. Subsequent treatments of the test data, including the application of post-test corrections, are not usually viewed as being part of the adaptive wall technique - although for the reasons outlined in Sections 10.2.3.3 and 10.2.4.1, this position may change in the future.

10.2.3.1 WALL INTERFERENCE ASSESSMENT

The ease with which accurate measures of the wall boundary conditions may be acquired in closed test sections means that the use of two-variable interference assessment methods, as described in Section 4.1.4, is favoured in flexible-walled facilities. This allows wall adaptation to be completed without invoking any

assumptions about the geometry or aerodynamic behaviour of the model under test. As is the case in conventional test sections, this is an important attribute as any errors in the assessment of interference will have a direct impact on the quality of the test data. It should also be noted that deficiencies in the assessment arising from random or systematic experimental error will influence the prescribed adjustments to the wall contours. Thus, the occurrence of such errors may often be identified by monitoring the admissibility of the control surface boundary conditions (flexible wall contours and pressure distributions) throughout the adaptation process. With experience, this information may allow appropriate corrective action to be devised.

To avoid the quality of wall adaptation being impaired by imperfections in the empty test section environment, the boundary conditions input to the wall interference assessment code are usually specified as perturbations from their empty test section or "aerodynamically straight" values: aerodynamically straight wall pressure distributions are nominally uniform and equal to the test section reference pressure; correspondingly, aerodynamically straight wall contours are monotonically divergent, in accordance with the requirement to accommodate the streamwise development of all four wall boundary layers.

The scope of the assessment conducted while adapting the walls is justifiably confined to addressing those components of interference that are controlled directly by wall adaptation. More rigorous analytical treatments - covering features such as sidewall interference - need only be completed post test. Thus, the principle of wall streamlining permits the quality of wall adaptation to be provisionally assessed purely in terms of the indicated mismatch between the "real" and "fictitious" flows: in two-dimensional testing, all that is required to minimise the effects of top and bottom wall interference is to match the flows at their interface - or to unload the control surfaces. As noted in Section 4.1.4, the fictitious flows need not be computed when their perturbation potentials are harmonic. In these circumstances, the relevant components of wall interference may be deduced directly from the measured boundary conditions. Examples of the methods currently used to assess wall interference in two- and three-dimensional testing are provided in Sections 10.3 and 10.4.

10.2.3.2 WALL ADJUSTMENT STRATEGY

The algorithm employed to prescribe improved wall settings is known as the wall adjustment strategy. In order to maximise productivity, this should allow the test programme to be completed with the minimum number of adjustments to the wall contours. Consequently, the formulation of a suitable strategy, together with its subsequent refinement, are amongst the most important tasks in the development of any adaptive wall technique - although it should be noted that, when contriving to minimise the effects of wall interference, deficiencies in their formulation only appear to impede the rate at which the walls converge to their optimum settings: they have no impact on the ultimate quality of the test data.

The effectiveness of a wall adjustment strategy will be determined by the extent to which the consequences of wall adaptation may be predicted. Thus, efficient strategies require the relevant components of wall interference to be related directly to parameters describing the wall setting and should also accommodate any aerodynamic coupling that may occur as a result of adapting the walls. When the flow in the test section is purely subsonic, linear theory has proved to be a powerful tool in predicting appropriate adjustments to the wall contours.

However, when the wall-induced perturbations cease to be harmonic, the consequences of wall adaptation become increasingly difficult to predict. As a result, the process of adapting the walls may be relatively inefficient. Nevertheless, the use of reasonably simple procedures - relaxation (adapting to a weighted mean contour somewhere between the current setting and an approximate prediction of an improved setting) or influence coefficient methods (which utilise theoretically derived quantities relating unit changes in wall setting

to the resulting flow perturbations at a particular location in the test section), for example - has often proved to be effective in ensuring that the prescribed adjustments to the wall settings become progressively smaller as the adaptation process progresses.

Thus, recognising that wall adaptation usually follows a law of diminishing returns and by paying careful attention to the order in which tests are conducted (by ensuring that the changes in wall contour between successive data points are relatively small, for instance), it is conceivable that, with experience, highly productive wall adjustment strategies may be developed. Several schemes have been proposed. However, relatively little effort has yet been directed towards their evaluation in practice. Perspectives on the demonstrated capabilities of current wall adjustment strategies are provided in Sections 10.3 and 10.4.

10.2.3.3 COMPLETION CRITERIA

While the principle of wall streamlining constitutes a mechanism for eliminating or otherwise controlling wall interference, factors such as those outlined in Section 10.2.2 make the attainment of interference-free flow a practical impossibility. Consequently, in seeking to minimise the effects of wall interference in two-dimensional testing, the practice has developed of terminating adaptation cycles at the stage when experience has shown that further adjustments to the wall settings are unlikely to produce detectable modifications to the model performance. However, it is possible that similar levels of refinement will not be required in production testing since there is probably little to be gained from adapting the walls beyond the point at which the test data become amenable to reliable post-test (or on-line) analyses in these circumstances.

Strictly speaking, the flow over a model is currently only deemed to be fully "correctable" if there is a free-air flow about the same shape that corresponds exactly to that in the wind tunnel. As the wall-induced velocity components will always vary by a certain amount in the vicinity of the model, this raises interesting - and as yet unresolved - questions as to the acceptability of these variations. This comment applies to the quality of the data obtained in conventional as well as adaptive wall test sections (although the variations present in adapted test sections will usually be appreciably smaller than those likely to be found in conventional test sections).

The current absence of clear guidance on this matter has impeded the development of highly productive adaptive wall techniques, particularly in three-dimensional testing, where the residual variations appear to be most pronounced. However, by allowing perturbations to the flow to be introduced in a controlled manner, wall adaptation enables the effects of localised variations in the wall-induced velocity to be studied systematically. Thus, it would appear that adaptive flexible-walled test sections constitute suitable platforms for investigating the rationale of the application of wind tunnel corrections in more detail. This subject is discussed further in Section 10.5.

10.2.4 FURTHER POINTS OF CLASSIFICATION

Before moving on to describe the features of several two- and three-dimensional testing techniques in more detail, it is convenient to introduce two additional factors that are used to distinguish between the different types of adaptive wall technique.

10.2.4.1 THE TYPE OF FLOWFIELD BEING SIMULATED

In principle, the ability to control the flow at the test section boundaries allows a diverse range of flowfields to be simulated within flexible-walled test sections. For example, in addition to facilitating the simulation of free-air boundaries, the principle of wall streamlining allows the conditions in an open-jet test section to be simulated simply by setting the walls to contours exhibiting uniform static pressure distributions. Those simulations already found to be practical in two-dimensional testing are illustrated in Figure 10.3.

It may be seen that the introduction of controlled levels of wall interference may be used to some advantage. However, the utility of wall adaptation in these circumstances may be viewed in several ways. For instance, instead of regarding the scenario depicted in Figure 10.3f as simulating steady pitching motion, it may also be considered as simulating the steady-state conditions about a model of modified camber. Therefore, in order to reflect the different ways in which wall adaptation may be exploited, it is convenient to distinguish between techniques which merely contrive to minimise the effects of wall interference - or, more precisely, reduce them to acceptable levels - and those which intentionally introduce controlled perturbations to the flow. This is achieved in the following sections by describing the adaptation algorithms as being either reductive or manipulative. The most powerful reductive techniques are described in Sections 10.3 and 10.4, while the use of manipulative algorithms is reviewed in Section 10.5.

10.2.4.2 THE NATURE OF THE FLOW AT THE CONTROL SURFACES

As the principle of wall streamlining allows the wall adaptation process to be driven purely by information gathered at the flexible walls, it is convenient to classify the various types of interface matching technique by the nature of the flow at the control surfaces. The groupings adopted to describe the range of test conditions currently straddled in two-dimensional testing are illustrated in Figure 10.4.

Group 1 Flows : the range of test section environments for which the reference Mach number is subsonic and regions of supercritical flow near the model, if they exist, do not extend to the control surfaces. The flow at the control surfaces and throughout the fictitious flowfields is purely subsonic in these circumstances and may be modelled using potential flow theory or the linearised compressible flow equations.

Group 2 Flows : the range of test section environments for which the reference Mach number is subsonic and at least one supercritical tongue emanating from the model extends beyond a control surface. The flow along this control surface is transonic in these circumstances and the region of supercritical flow in the fictitious flowfield is usually terminated by a near-normal shock. The ability of passive solid-walled tunnels to simulate these flows is limited by test section choking.

Group 3 Flows : the range of test section environments for which the reference Mach number is subsonic and the model is almost completely immersed in supercritical flow. This extends far into

both fictitious flowfields and may be (i) terminated by systems of oblique and normal shocks (when simulating subsonic freestream Mach numbers) or (ii) turned through oblique shocks before returning to its undisturbed state (when simulating sonic and very low supersonic freestream Mach numbers). Problems associated with test section choking, establishing appropriate reference conditions ahead of the model and starting the tunnel prevent passive solid-walled tunnels being used to simulate these flows.

Group 4 Flows : the range of test section environments for which the reference Mach number is supersonic and the strength of the bow shock is such that it precedes a region of subsonic flow which protrudes into one or both of the imaginary flowfields. The flow at the control surfaces and in the fictitious flowfields is, again, transonic in these circumstances. Difficulties in establishing appropriate reference conditions ahead of the model and starting the tunnel prevent passive solid-walled tunnels being used to simulate these flows.

Group 5 Flows : the range of test section environments for which the reference Mach number is supersonic and regions of subcritical flow between the bow shock and the model do not extend to the control surfaces. The flow at the control surfaces and throughout the fictitious flowfields is purely supersonic in these circumstances. Testing may proceed in passive solid-walled tunnels provided the model is safely within its test diamond.

The requirement to control the flow away from the control surfaces blurs the distinction between the different forms of target line technique. The nature of the flow at the control surfaces will, however, still play an important role in determining the most appropriate wall interference assessment procedure, wall adjustment strategy and completion criteria to employ.

10.3 TWO-DIMENSIONAL TESTING

A test section with flexible walls at top and bottom offers itself and appears to be ideal for the testing of two-dimensional models using the interface matching technique. Strictly speaking, when implemented in facilities with two flexible walls the (two-dimensional) interface matching technique can only eliminate the top and bottom wall interference. The influence of the sidewall boundary layers, being a three-dimensional effect, is not controlled and cannot be eliminated. A procedure, by which two-dimensional wall adaptation may alleviate the sidewall boundary layer effects is reviewed in Section 10.4.3 of this Chapter. Presently we assume that the flow past a two-dimensional wing, spanning the test section, is nearly two-dimensional.

In seeking to eliminate the effects of top and bottom wall interference, the aim of two-dimensional interface matching is to shape the flexible walls in such a way that the distribution of pressure and flow angle measured at the walls match those of a fictitious exterior flow resulting from computation. When this is achieved, within practical limits, the walls conform with the streamlines of the unconfined flow. The fictitious exterior flow is then the analytical continuation of the flow in the test section.

10.3.1 WALL ADAPTATION BY ITERATION

An iterative procedure for the wall adaptation may be contrived for example, in the following way:

Initially the walls may be straight or have any shape approximating the streamlines of the unconfined flow. During a test run, the wall pressures are measured along lines of pressure taps, usually the centrelines of the top and bottom walls. Next, a fictitious "external" flow is computed that is bounded by the test section walls and attains the conditions of undisturbed parallel flow at infinity (Figure 10.5). It should be noted that the "external" flow may be considered as an inviscid potential flow - in contrast to the flowfield adjacent to the model - and can be computed on the basis of inviscid or even linearised theory simply and fast with modern computers. The computed wall pressures of the external flow, p_e , are compared with the measured pressure distribution of the test flow, p_i . If p_e and p_i agree within prescribed error bounds, the external flow is the analytical continuation of the interior flow and the wall shape conforms with the streamlines of the unconfined flow. Otherwise, the difference $p_e - p_i$ is considered as remaining wall interference and the wall shape must be corrected in a second iteration cycle and so on.

This iterative procedure, as it was described in early publications (see, for example, Erickson & Nenni, [7]; Goodyer, [10]; Legendre, [22]; and Sears, [32]), is quite intuitive. It has, however, caused much confusion, leading to the widespread belief that the wall adaptation must necessarily be iterative. It will be shown in the following that for Group 1 Flows an explicit computation of the fictitious external flow is not required and that full wall adaptation can be attained within one iteration step.

10.3.2 ONE STEP METHODS OF WALL ADAPTATION FOR GROUP 1 FLOWS.

The principles of one step methods are equally valid for two- and three-dimensional flows, for interface matching and target line methods. In all cases the procedure requires an assessment of the wall interferences by a two-variable method and a subsequent computation of the wall movement required to eliminate the interferences. In the case of interface matching, the component of the interference velocity normal to the wall is evaluated which gives immediately the flow angle to which the wall must be adjusted in order to extinguish the interference velocity. The assessment of wall interferences using Green's formula is discussed in Chapter 4. In the case of two-dimensional flows, Green's formula reduces to the Cauchy integral formula which is discussed in the following.

The Cauchy Integral

It is assumed that the flow near the test section walls deviates from parallel subsonic flow by small disturbances. The two-dimensional disturbance potential fulfils the equation:

$$\beta^2 \phi_{xx} + \phi_{yy} = 0 \quad \text{with } \beta^2 = 1 - M^2 \quad (10.1)$$

(x, y) are the co-ordinates in the flow direction (x) and upwards (y) as shown in Figure 10.5.

The wall interference in two-dimensional tunnel flow is then computed by a Cauchy type integral :

$$w_{\text{int}}(z) = \frac{1}{2\pi i} \int_C \frac{w(\zeta)}{\zeta - z} d\zeta \quad (10.2)$$

where the complex variable z is defined by $z = x + i\beta y$ and ζ by $\zeta = \xi + i\beta\eta$ with (ξ, η) as the running co-ordinates in the x - and y - directions. While introducing the variables z and ζ use is made of the Prandtl-Glauert transformation.

The complex integral is taken along a counter-clockwise oriented closed path (C) around the model - suitably along the lower wall from the upstream to the downstream end of the test section, from there across the test section to the upper wall and along the upper wall upstream and back across the test section to the starting point (Figure 10.6).

$w(\zeta) = \beta u(\xi, \eta) - i v(\xi, \eta)$ is the disturbance velocity in complex notation at a point (ξ, η) and

$w_{int}(z) = \beta u_{int}(x, y) - i v_{int}(x, y)$ is the interference velocity at a point with co-ordinates (x, y) .

To evaluate the integral of Equation 10.2, the disturbance velocities (u, v) must be known along the closed path C. At the upper and lower wall of the test section the values of u and v are simply evaluated by measuring the wall pressure and the wall angle, which is the derivative of the wall displacement. Assuming that the linearised Bernoulli's equation may be applied to describe the disturbance velocity at the walls, then:

$$u/U_{\infty} = -c_p/2 \quad \text{and} \quad v/U_{\infty} = \theta$$

where θ is the wall angle and c_p the pressure coefficient measured at the walls.

The evaluation of u and v along those parts of the closed curve C that cross the test section at the upstream and downstream end is not as simple. However, if the test section is sufficiently long - a requirement for full wall adaptation - the disturbance velocities at the upstream and downstream ends are small and may safely be neglected.

Equation 10.2 is the wall correction formula of Smith (1982). A derivation of Equation 10.2 was given by Mokry [29]. The formula is the two-dimensional equivalent of Green's formula, introduced by Ashill & Weeks [2] for the computation of wall interferences in general three-dimensional flows (Equation 4.14 of Chapter 4). Because of the importance of Equation 10.2 both for the wall interference assessment and a wall adaptation strategy a brief derivation is reviewed in Appendix A.

Equation 10.2 may be used either to compute the wall interference velocity at the model or at any other point within the test section. When the Cauchy integral is evaluated for z -values on the wall, it must be regarded that the integrand is singular at $\zeta = z$. The proper integration is performed by taking the limit-value of the integral for z -values approaching the wall. For z -values at the wall, Equation 10.2 takes the form:

$$w_{int}(z) = \frac{1}{2} w(z) + \frac{1}{2\pi i} \int_C \frac{w(\zeta)}{\zeta - z} d\zeta, \quad z \in C \quad (10.3)$$

where the Cauchy principal value is to be taken for the integral.

Equation (10.3) leads immediately to a one step formula for the wall adaptation. The normal velocity at the walls for interference-free flow must be: $(v - v_{int})$. The wall angle is $\theta = (v - v_{int})/U$ and the wall displacement δy is:

$$\delta(y) = \int \theta dx = \int (v - v_{int})/U_{\infty} dx \quad (10.4)$$

where v_{int} is the negative imaginary part of w_{int} , evaluated at the wall according to Equation (10.3).

Equation (10.4), as a one step formula for the wall adaptation, was first described by Kraft & Dahm [17]. The discovery that wall adaptation for group 1 flows in two dimensions need not be iterative is attributed to Lo [26].

A final remark is due regarding the notion of one step methods. As mentioned above, the one step formula is limited to cases where linearised flow theory is applicable at least in a region near the wall (or the control surface about which the integral (Equation 10.2) is taken). In extreme cases a second iteration may be required even for the linearised flow. After adapting the wall to the computed wall shape the flow about the model will change by some small amount. The changed flow will produce slightly different wall interference. We may imagine that the singularities representing the model and consequently the images representing the wall interference are slightly modified by the wall adaptation. This second order effect is negligible in most cases. It may become significant e.g. when wind tunnel choking occurs at near sonic speeds. An initial adaptation step may bring the flow at the wall to subsonic conditions so that - in a second iteration step - the linearised flow assumption holds.

In wind tunnel practice, the test condition - angle of attack and freestream Mach number - will be changed in small steps so that at each step only small changes of the flow are encountered and, therefore, only small corrections to the wall displacements are required that can be done within a single iteration step. The wall adaptation procedure may not even slow down the model testing if wall pressure assessment and wall adjustments do not take more time than changes of the test condition (angle of attack or Mach number). The adapted wall shape for the succeeding configuration may be extrapolated from the previous values. During the test the wall pressure distributions will be measured and used to compute the proper wall shape that can be used for extrapolation to the next test configuration and so on. In this way a continuously self-correcting wind tunnel may be realised.

10.3.3 WALL ADAPTATION IN SUPERSONIC FLOW (GROUP 5)

In contrast with the situation for Group 1 Flows, the experience of adapting the walls in Group 5 Flows is rather limited. As a result, the testing techniques are far less refined. The most notable investigations were conducted on large aerofoils generating modest lift at Mach numbers up to 1.35. (Taylor, [37])

As the bow shock generated by the model was not attached at any of the conditions straddled during these tests, there was no obvious and immediately available means of procuring reliable estimates of the wall interference. Therefore, in the absence of suitable reference model data, it was necessary to rely entirely on the principle of wall streamlining to define the desired data quality: a Transonic Small Perturbation code was used to compute the fictitious external flows and the walls adapted until the mismatch between the real and fictitious flows, evaluated along the centrelines of the control surfaces, appeared to have been reduced to levels deemed to be acceptable in Group 1 Flows. A lag-entrainment method was used to compute the displacement thickness contours in the flexible wall boundary layers.

The wall adjustment strategy used differed from those employed in Group 1 Flows in several important respects. Aside from its lack of refinement, it reflected the fundamental differences between the elliptical and hyperbolic natures of subsonic and supersonic flow. For instance, recognising that supersonic disturbances cannot be propagated upstream, it was not used to adjust the full-length of the profiles of the flexible walls:

- i. In the early stages of the adaptation process, its use was confined to adjusting the slope of the upstream portion of each control surface. It was only applied further downstream once the local mismatch between the real and fictitious flows had been reduced to an acceptable level.
- ii. Adapting the walls ahead of the bow shock and beyond the point at which any reflected disturbances would pass downstream of the model and the subsonic portion of its wake was unnecessary.

Furthermore, as any wall-induced blockage adjacent to the model or the near-portion of its wake could force the bow shock stand-off distance to be appreciably larger than that in free-air, it was found that wall

streamlines could only be approached from one direction: adjustments to the wall contours should, in general, be directed towards the tunnel centreline. Thus, without the freedom to iterate via progressively smaller overshoots, it seems that, for practical purposes, wall adaptation in supersonic flows will exhibit a one-sided asymptotic convergence to free-air streamlines. Aside from making it more difficult to ascertain the stage at which the walls have attained their optimum settings, this indicates that errors in estimating the modifications to the control surface profiles associated with shock - boundary layer interactions or the provision of insufficient local control over the wall contours may prevent the adaptation process from ever reaching free-air streamlines.

Consequently, although these investigations demonstrated that wall adaptation yielded substantial alleviations in the intensity of any reflected disturbances, it was not possible to quantify the extent to which top and bottom wall interference had been reduced. No direct attempts were made to address the alleviation of sidewall interference, or to investigate the issues associated with shock - wall boundary layer interactions in any detail. Moreover, although attempts were made to assess the sensitivity of the model data to any (aerodynamically) undesirable waviness in the flexible walls, as the test section was not designed for supersonic testing, the results of these studies were not conclusive.

It may be seen that two-dimensional Group 5 interface matching techniques are still in the preliminary stages of development. Much is to be done before they may be utilised competitively beyond the research environment.

10.3.4 WALL ADAPTATION IN TRANSONIC FLOWS (GROUPS 2- 4)

Again, the experience of wall adaptation in circumstances where the flow at the walls is transonic is rather limited. Lewis [23] conducted the most systematic evaluation of the prospects for simulating Group 2 Flows while the most experience of testing in Group 3 and 4 Flows has been accumulated by Taylor [37].

Faced with difficulties in obtaining accurate measures of the residual wall interference or reliable independent sources of reference model data, these activities adopted similar approaches to wall adaptation as that described in Section 10.3.3 above. The principal distinctions between the techniques occurred in the wall adjustment strategy.

As the maximum attainable Mach number ahead of the model with the walls set in their aerodynamically straight positions was approximately 0.75 in these tests, it was not always possible to initiate wall adaptation at the desired reference Mach number. Therefore, a policy of adapting the walls at a speed below that ultimately required and relying on the attendant blockage relief to provide the necessary increase in choking Mach number was adopted for Group 2 simulations.

The process of initiating wall adaptation from a Group 1 Flow condition meant that subsonic wall adjustment strategies could be employed at much higher reference Mach numbers than would otherwise have been possible. However, once the point had been reached where the supercritical patches of flow at the walls could not be removed by wall adaptation, local adjustments to the wall contours were not so easily prescribed and the process of minimising the local wall loading became more iterative. Although the supercritical wall loading could not be reduced to the desired levels within one or two iterations, the residual wall loading elsewhere in the test section was very low and the supercritical patches in the real and fictitious flows were well matched - see Figure 10.7. Moreover, the model data - most noticeably, the upper surface shock location - and the wall loading exhibited a double convergence. The test data therefore appeared to be of a reasonably high quality. Nevertheless, with the effects of sidewall interference unaddressed, further experience is required to assess

the extent to which the technique must be refined if the most demanding contemporary standards for residual interference are to be guaranteed in production testing.

When simulating Group 3 Flows, wall streamlines derived from Euler free-air computations were initially used as the starting point in each adaptation cycle. As with Group 2 Flow simulations, subsequent wall adaptation proved to be relatively ad-hoc and was occasionally prolonged by difficulties in establishing appropriate reference conditions ahead of the model whilst simultaneously unloading the portions of the control surfaces adjacent to it.

However, once generated, the adapted wall contours for a given model incidence appeared to be valid for a wide range of freestream Mach numbers - a direct consequence of the Mach freeze phenomenon. Thus, once the walls had been adapted for a range of model incidences when simulating one freestream Mach number, it appeared that data for a range of neighbouring freestream Mach numbers (extending from about 0.96 to 1.15 in this case) could be obtained on a one-shot basis - although, as the flow in the adapted portion of the test section was remarkably insensitive to the freestream Mach number, there would have been little point in completing a detailed test matrix in these circumstances. With the influence of the sidewall boundary layers likely to be appreciably less important than in Group 2 Flows, this was a particularly refreshing discovery. Nevertheless, further experimental evidence and technique refinements - including reductions in the time required to compute the fictitious flowfields - will probably be required before this radically different approach towards near-sonic testing may be employed with confidence in production testing.

Initial experiences of adapting the walls to simulate Group 4 Flows also proved to be laborious. Following the general pattern established for Group 5 simulations, the first iterations were dedicated to improving the location of the bow shock - as judged by the progressive confluence of its positions in the real and fictitious flowfields. Effort was then focused on relieving the mismatch in the region of subsonic flow aft of the shock before moving on to address the supersonic flow further downstream. However, unlike the situation in Group 5 simulations, these phases of the adaptation cycle were not distinct as the region of subsonic flow on each control surface provided a path by which disturbances could be propagated upstream.

Thus, in many respects, the procedure for simulating Group 4 Flows currently appears to be the least refined of all two-dimensional interface matching techniques. Nevertheless, a measure of encouragement for future development was gained from the observation that the quality of the adapted test data appeared to be remarkably insensitive to model incidence. It remains to be seen whether the wall contours derived for a particular model incidence will be capable of producing data of an acceptable quality over a range of model incidences in Group 4 Flows.

10.4 THREE-DIMENSIONAL TESTING

10.4.1 WALL ADAPTATION BY INTERFACE MATCHING

Interface matching in ventilated test sections

Shaping the walls into a three-dimensionally curved surface meets, obviously, extreme technical difficulties. In an early study at AEDC Kraft et al. [18] restrained from using solid walls for three-dimensional wall adaptation, but rather investigated the capability of adaptable ventilated walls. The configurations investigated featured variable porosity in conjunction with suction through the walls. In this way significant reduction of wall interference could be obtained. Nevertheless, the method has not found much spread for the reasons outlined in Section 10.2.2. (See also Chapter 4.3 for more details).

Interface matching in test sections with impervious flexible walls

A configuration using eight flexible walls formed to an octagonal test section was investigated by Ganzer et al. [8] at the University of Berlin. Each of the walls was deflected by a set of jacks to accomplish a nearly continuous three-dimensional wall adaptation. Special attention was given to the sealing of the gaps between the flexible plates by lamellas manufactured from spring steel.

A cylindrical test section constructed from a thick walled rubber tube of 80 cm diameter was used at the DFVLR Göttingen by Wedemeyer et al. [42]. Full three-dimensional wall adaptation was achieved by deformation of the rubber wall with a set of 64 jacks, 8 jacks each at 8 cross sections. In conjunction with the rubber tube test section a one-step adaptation algorithm for three-dimensional flows was developed that takes advantage of the cylindrical geometry of the test section. A universal algorithm based on the two variable method of Ashill & Weeks [2] and capable of computing interference-free wall contours for arbitrary test section shapes as well as residual wall interferences in three-dimensional flows was developed by Holst [15]. The latter is particularly useful when the wall adaptation is imperfect as in the case of two-dimensional adaptation for three-dimensional flows, which is discussed in section 10.4.2.

It was demonstrated that interference-free flow can be achieved in the octagonal test section in Berlin as well as in the rubber tube test section of the DFVLR Göttingen. In spite of this success, the full three-dimensional wall adaptation methods were no longer pursued when it was shown that wall adaptation for three-dimensional flows can be accomplished within acceptable approximations in test sections with two flexible walls that had so far found prevailing use in two-dimensional testing. Since this two-dimensional wall adaptation for three-dimensional flows has become a standard method, a detailed description will be given in the following section.

10.4.2 TARGET LINE METHODS: TWO-DIMENSIONAL WALL ADAPTATION FOR THREE-DIMENSIONAL FLOWS

Interface matching by means of two flexible walls is, of course, not conceivable when the flow is three-dimensional. It is, however, appealing to use test sections with two flexible walls to relieve wall interferences in three-dimensional testing because of their relatively simple construction and their convenience. It was shown by Wedemeyer [41] that blockage and upwash interferences can be eliminated at the centreline of the test section by suitable adaptation of the flexible walls of a two-dimensional adaptive wall test section. An algorithm for the two-dimensional wall adaptation for three-dimensional flows was developed at the VKI by Wedemeyer [41] and Lamarche & Wedemeyer [20]. Similar methods have also considered to eliminate the interferences along some well defined "target line" that need not be the centreline of the test section. (In principle, target line methods are not limited to test sections having two flexible walls, although, for practical reasons, only these have been used so far).

Presently we consider the case where the model is mounted in a test section with two flexible walls so that its axis coincides with the centreline of the test section. It is supposed that the model is symmetrical or nearly so to the vertical plane of symmetry of the test section, i.e. a symmetrical model at zero or small yaw angle is assumed. The lateral extensions of the model are supposed to be not a large fraction of the lateral extensions of the wind tunnel so that the model is exposed only to the flow near the centreline. Although the wall interferences are eliminated strictly only along the target line, it is expected and was proven by numerical simulations (see Section 10.4.2.6) that the residual interferences are relatively small throughout the remainder of the test section. If the centreline is used as the target line, the residual interferences are of second order small in terms of the distance from the centreline. In half-model testing

the model is usually mounted with its axis along the centreline of a sidewall. Such an arrangement may be conceived of as a model mounted at the centreline of a duplex test section. For wall adaptation a line of pressure taps should be provided near the reflection plane on top and bottom wall.

For a symmetrical model at zero yaw angle the interference velocity along the centreline has a longitudinal component $u_{int}(x)$ and a vertical component $w_{int}(x)$. The walls are adapted now in such a way that the interference velocities ($u_{int}(x)$, $w_{int}(x)$) are extinguished at the centreline. By deflecting the upper and lower wall in a suitable symmetrical way (Figure 10.8a) a distribution of longitudinal velocity $u(x) = -u_{int}(x)$ is induced. Similarly, by deflecting the upper and lower walls anti-symmetrically (Figure 10.8b), a distribution of vertical velocity $w(x) = -w_{int}(x)$ can be induced. Combining symmetrical and anti-symmetrical wall deflections any wall interference can be extinguished along the centreline. The wall interference velocities at the tunnel centreline may be computed by the two variable method of Ashill & Weeks (see Chapter 4) which requires a detailed pressure measurement at all test section walls. The method of Lamarche & Wedemeyer [20] rests upon pressure measurements at the centrelines of top and bottom walls only. The wall interferences at the tunnel centreline can be inferred from the top and bottom wall pressure distributions under the supposition of symmetrical models with small lateral extensions (precisely, under the condition that the model can be represented approximately by singularities distributed along the tunnel centreline). With these assumptions the wall interference assessment and the wall adaptation algorithm are largely simplified to the evaluation of one-dimensional integrals.

10.4.2.1 ASSESSMENT OF THE WALL INTERFERENCES

The u -component of the disturbance velocity at the walls is evaluated via measurement of the pressure coefficient in the usual way: $u / U_\infty = -c_p / 2$. The w -component (normal to the wall) is inferred from the wall angle θ or, alternatively, the derivative of the wall displacement $d\delta/dx = \theta = w/U_\infty$.

Let us assume, at first, that the walls are aerodynamically straight, i.e. $\theta = 0$ at the top and bottom walls. Defining the symmetrical part u_s and the anti-symmetrical part u_a of the disturbance velocity at the walls:

$$u_s = (u_t + u_b) / 2 \quad (10.5a)$$

$$u_a = (u_t - u_b) / 2 \quad (10.5b)$$

where u_t and u_b are the velocities at the top and bottom walls, the interference velocities u_{int} , w_{int} at the centreline are related to the wall velocities by linear integral operators:

$$u_{int}(x) = \int u_s(\xi) \Omega(\xi - x) d\xi / \beta h \quad (10.6a)$$

$$w_{int}(x) = \int u_a(\xi) \Gamma(\xi - x) d\xi / h \quad (10.6b)$$

where the integration is, nominally, from $-\infty < \xi < +\infty$. As the wall velocities die out quickly with increasing distance from the model location the integrals encompass, in practice, only a finite path. Ω and Γ are functions of the normalised variables ($\xi - x$), with $x = x/\beta h$, $\xi = \xi/\beta h$, and the aspect ratio b/h of the test section.

Equations 10.6a and 10.6b are similar to (the real and imaginary parts of) the Cauchy-integral (Equation 10.2), but the influence functions Ω and Γ are, of course, more complicated. They are computed once for a given test section geometry b/h . The form of the influence functions and their computation is discussed in Appendix B.

10.4.2.2 WALL ADAPTATION ALGORITHM

As mentioned above, the wall adaptation strategy aims at eliminating the wall interferences along the centreline of the test section by displacing the flexible top and bottom wall so as to generate velocity distributions $u_c = -u_{int}$, $w_c = -w_{int}$ that counteract the interference velocities. The wall displacements are again divided into a symmetrical part $d_s = (d_t + d_b) / 2$ and an anti-symmetrical part $d_a = (d_t - d_b) / 2$ where d_t and d_b are the displacements of the top and bottom wall, positive in the outward direction. In the following the notation u_s and u_a will be used for the non-dimensional velocities $u_s = u_s / U_\infty$, $u_a = u_a / U_\infty$ and d_s , d_a for the non-dimensional wall displacements $d_s = d_s / h$, $d_a = d_a / h$ where U_∞ is the freestream velocity and h the test section height.

The wall displacements d_s and d_a required to eliminate the interference velocities in this way are related to the wall signatures, $u_s(\xi)$, $d_{s0}(\xi)$, $u_a(\xi)$, $d_{a0}(\xi)$ by linear integral operators:

$$d_s(x) = \int \beta^2 u_s(\xi) X(\xi - x) + d_{s0}(\xi) M(\xi - x) d\xi / \beta h \quad (10.7a)$$

$$d_a(x) = \int \beta^2 u_a(\xi) \Lambda(\xi - x) + d_{a0}(\xi) N(\xi - x) d\xi / \beta h \quad (10.7b)$$

d_{s0} and d_{a0} denote the pre-set wall displacements, usually the wall setting of a previous test condition. The influence functions X , M , Λ , N depend only on the normalised variable $(\xi - x) = (\xi - x) / \beta h$ and the aspect ratio b/h of the test section. A method for computing the functions X , Λ , M , N is discussed in Appendix B. An algorithm based on Equations 10.7a&b for the wall adaptation is used routinely in adaptive wall tunnels at ONERA/CERT Archambaud & Mignosi, [1] and at DLR (Holst & Raman, [14]).

It is important to note that the time required to perform the calculation of the adapted wall contours need not be an obstacle to fast wall adaptation procedures in production testing. A computational code used at the DLR Göttingen requires about 0.1 second on a 133 MHz Pentium computer to compute the wall contours from Equations 10.7a&b. In comparison, the algorithm employed by Holst [15] using full boundary measurements requires about 3 seconds for the calculation of wall contours in three-dimensional flow.

The method described above has been extended by Rebstock and Lee [31] who considered the more general case, that the model is not necessarily mounted at the centreline of the test section. The wall interferences are then computed from flow measurements at the full boundary of the test section and can be eliminated on a given target line that is, for example, the model axis. The generalised adaptation algorithm was used in the TCT wind tunnel at NASA Langley to verify the method. A distinct advantage of pressure measurements at the full boundary is, that residual interferences can be computed at once. The full wall interference assessment requires more testing time and, of course, a sufficient number of pressure taps distributed over the whole of the test section walls. The quality of the wall adaptation can, however, hardly be improved by using wall signature information on the full boundary because the elimination of the wall interferences is still limited to the target line.

Several approaches have been developed independently of these activities. Lewis and Goodyer [24] combined the two-variable method of Ashill & Weeks [2] with the influence coefficient method of Goodyer [11] and have employed various target lines, for example, a straight target line for blockage interferences following the fuselage and a target line for upwash interferences following the forebody of a model and subsequently a swept line following the wing geometry.

Another approach due to Le Sant and Bouvier [21] is used in the S3Ch adaptive wall wind tunnel at ONERA Chatillon. The ONERA S3Ch method may be seen as an improved version of the VKI method, using the same principles and ideas:

- i. A model representation is identified according to pressure measurements on the top and bottom wall.
- ii. Wall interferences are assessed on a target line.
- iii. A wall shape is predicted so as to cancel the wall interferences on the target line.

The application of these principles is, however, different in a two-fold respect:

- i. The location of the model is user defined, i.e. it is not necessarily aligned with the centreline. The singularities representing the model are set at the model location, including the model support sting. The model attitude is taken into account as well as the model support.
- ii. The target line on which wall interferences are assessed is not necessarily straight but it may follow the fuselage and continue along the 3/4-cord line of the wing.

The ONERA method is more complicated than the VKI method. Its use is less easy as information about the model is required. On the other hand the user may control model representation and target line. Large models may be used and support interferences may be taken into account.

It should be noted that severe restrictions exist on the extent to which a target line may be swept if wall interferences are to be eliminated along it. These arise because the perturbations to the flowfield introduced by wall adaptation are - for subsonic flows - analytic throughout the test section implying similar constraints on the form of the target line and the wall interferences to be eliminated. However, it should also be noted that elimination of wall interferences along a target line is not necessarily the best approach to take when adapting the walls. This point is discussed in Section 10.4.2.4.

10.4.2.3 COMPLETION CRITERIA

The importance of completion criteria, particularly in three-dimensional testing has been outlined in section 10.2.3.3. In the case of Group 1 Flows the wall adaptation may - as a rule - be completed by a one-step iteration. If in exceptional cases (or Group 2-5 Flows) more than one iteration is required, the iteration procedure may be terminated if further iterations do not produce detectable modifications to the adapted wall contour. In all cases an assessment of residual interferences may be desirable after completion of the wall adaptation. If wall pressure measurements on the full boundary are available residual interferences may be calculated by the method of Ashill & Weeks [2]. If pressure measurements at the full boundary are not available, residual interferences may still be calculated by conventional wall interference assessment methods (see Chapter 2). An example of the numerical assessment of residual upwash variations for various wingspan ratios is given in section 10.4.2.6.

10.4.2.4 EXPERIMENTAL RESULTS FOR GROUP 1 FLOWS

Since two-dimensional wall adaptation for three-dimensional flows can only be approximate, it is desirable to verify the methods experimentally. To this end a number of wind tunnel tests have been performed in wind tunnels at NASA Langley, ONERA/CERT, DLR Göttingen, the University of Southampton and at the Northwestern Polytechnical University (NPU) in Xian, China. Representative results of experimental tests are presented in Chapter 4 of AGARD Advisory Report 269 (Hornung, ed., [16] and original publications (citations of which are also found in AGARD-AR-269). In all cases where experimental results have been compared with interference free data from larger wind tunnels good agreement was found, even in cases where the ratio of wingspan to test section width and the blockage ratio were not small.

Figures 10.9 a&b show experimental results obtained in the T2 tunnel at ONERA/CERT for an axis-symmetric body (Figure 10.9a) and an aeroplane half model (Figure 10.9b). The results at $M=0.84$ show convincingly that wall adaptation is achieved within one iteration step since no significant changes are obtained for further iterations. Comparison with results for not adapted walls and with interference-free results from a large wind tunnel (NASA Ames 11 ft X 11 ft) gives an impression of the quality of the wall adaptation. The results for the half model, spanning 80% of the test section, show that wall interferences are largely reduced although spanwise variations of the wall induced upwash could not completely be eliminated.

As another example of the quality of wall adaptation in an extreme case, results obtained in the high speed wind tunnel of the DLR Göttingen for an aeroplane model spanning 75% of the test section width are given in Figure 10.10. Figure 10.10a shows a plan view of the model in the test section and Figure 10.10b the pressure distributions at two wing sections (the most outboard section $y/s=0.925$ could accommodate only three pressure taps because of its limited thickness). The Figure shows the improvement of the test data after wall adaptation and the agreement with interference free results at the wing section $y/s=0.6$. A small deviation is apparent for the wing section $y/s=0.925$ and this deviation agrees well with the predicted residual interferences.

By referring to the data presented in these Figures, it is possible to describe some more general observations that have been made about the capabilities of two-dimensional wall adaptation for three-dimensional Group 1 Flows :

- i. As, prior to adapting the walls, the distribution of wall-induced blockage in the plane of the model is remarkably one-dimensional (Figure 10.9b), two-dimensional wall adaptation is effective in reducing it throughout the test section, not merely in the vicinity of the target line: the residual variations in Figure 10.9b really are rather small. This situation appears to prevail at high reference Mach numbers, even for relatively large models.
- ii. In contrast, the wall-induced upwash is not distributed so evenly across the test section prior to adapting the walls, especially in regions aft of a lifting surface. Thus, while wall adaptation may be effective in eliminating it along its target line, the residual variations over the remainder of the model are much larger. When a target line that does not deviate far from the streamwise direction is employed during tests on models of high aspect ratio, the dominant residual usually takes the form of velocity gradients in the spanwise direction over the wing - in effect, wall-induced wing twist. This is evident in both Figure 10.9b (where, while wall adaptation has clearly reduced the overall levels of upwash - and hence the magnitude of any primary correction to incidence - it has actually increased the effective wing twist, for which there is currently no

correction) and in Figure 10.10 (where the differences in the residual interferences calculated at the two spanwise stations may be interpreted as evidence of wall-induced twist).

Three ways of reducing wall-induced wing twist have so far been identified: (i) reducing the overall model size, (ii) changing the cross sectional proportions of the test section (this way is discussed in section 10.4.2.6), and (iii) sweeping the upwash target line adjacent to the wing, foreplane or tailplane.

An example of the effects of employing a swept target line is provided in Figure 10.11. As mentioned above, target lines on which wall interferences are to be eliminated are subject to certain restrictions. In lack of definite rules a tentative line was assumed as depicted in Figure 10.11 and wall adaptation was aiming at the best possible reduction of the wall induced upwash along this line. Figure 10.11 and Table 10.1 show that wall induced wing twist could be reduced in this way to comply with the criteria proposed by Steinle & Stanewski [34] although at the expense of residual camber. Moreover, as a result of directing the target line along the root chord before sweeping it outwards towards the wing tip, and then aligning it with the tip chord, the penalties associated with sweeping the target line - the production of residual camber at the wing root and tip - have also been kept small. Consequently, the residual variations over the wing, the principal components of which are summarised in Table 10.1, are sufficiently small as to comply with the criteria proposed by Steinle and Stanewsky [34]. Having said this, the benefits of employing swept target lines will need to be balanced against the costs - the additional expense associated with acquiring wall pressure data at the full boundary and solving Equation 4.14 (as opposed to Equations 10.6 and 10.7), for instance - if they are to be used in routine production testing.

10.4.2.5 WALL ADAPTATION FOR NON-LINEAR AND SUPERSONIC FLOWS (GROUPS 2-4)

In the case of two-dimensional flow and generally in cases using interface matching techniques, the strategy of streamlining the walls could easily be extended to non-linear flows as discussed in Section 10.2.4.2, the main difference being that a computation of the fictitious external flow is required for non-linear flows. An extension of the target line technique to non-linear flows is not as straightforward because the described method depends on the assumption that the effects of the wall constraints and the wall displacements can be superimposed. The superposition principle is, however, not applicable for non-linear flows. It is difficult to define a strategy of two-dimensional wall adaptation for three-dimensional flow, if the superposition principle does not hold. A way that was investigated by Lamarche [19] depends on the "transonic area rule". To alleviate the blockage effect the two flexible walls were shaped in such a way that the area distribution of the test section equals the area distribution of a corresponding streamtube around the model in free-flight. The streamtube was computed for an "equivalent body of revolution". The equivalent body of revolution is an imaginary model that generates a wall pressure signature equal to that of the real model. The equivalent body was determined, more or less, by a method of trial and error, which is laborious and time consuming. It was shown, however, that nearly interference-free flow could be achieved in this way. For a lifting model only the symmetrical part of the wall pressure distribution was used to define the equivalent body of revolution. For the anti-symmetrical part of the wall pressure, which is related to lift, it was shown that the linear algorithm is still valid.

Theoretical and experimental investigations of the possibility of two-dimensional wall adaptation for three-dimensional supersonic flows have been performed at the DLR by Heddergott & Wedemeyer [13] and at NPU by He et al. [12].

10.4.2.6 LIMITATIONS AND OPEN QUESTIONS

Two-dimensional wall adaptation for three-dimensional flow is necessarily imperfect. The strategy in which the wall interferences are eliminated at the centreline of the test section is subject to the following assumptions:

- i. The lateral extension of the model is not a large fraction of the test section width.
- ii. The asymmetry of the flow with respect to the vertical centre plane of the test section is small.

In the following, we address the limitations imposed by these assumptions.

Limitations due to model size

It is common to all target line methods that wall interferences are eliminated only along the target line. It is expected, however, that the remaining residual interferences are small although they increase with distance from the target line. If the target line coincides with the centreline of the test section the residual interferences near the target line remain small to second order in terms of the distance from the target line. As a consequence the limitations due to model size are far less restrictive than might otherwise be anticipated. In order to have an estimate about the residual interferences to be expected, numerical studies have been performed for blockage and upwash interferences.

Blockage interferences - concerning the u-component - are caused mainly by the large volume of the fuselage of an aeroplane model. Residual blockage interferences on the fuselage are small just because the target line is chosen to run near the fuselage. This does, however, not imply that they are small elsewhere in the test section. It has been shown by numerical simulations that residual blockage interferences remain extremely small throughout the test section so that they are negligible even for large blockage ratios (for example Verte [40]). Unfortunately this is not the case for upwash interferences.

Upwash interferences - concerning the w-component - are caused by lifting bodies i.e. mainly by the wing of an aeroplane model. As the wing spans a large portion of the test section width, spanwise variations of the wall-induced upwash are to be expected while only a constant level of upwash can be eliminated at any streamwise position.

It was noted by Wedemeyer and Lamarche [43] that test sections with aspect ratios other than square can be advantageous as the spanwise upwash variations are reduced or even become negligibly small. Depending somewhat on the wingspan ratio, the ideal test section should be rectangular with a width to height ratio of about $b/h=1.4$. The upwash level at the tunnel centreline may also be reduced as was noted already by Glauert [9] in the context of wall interference corrections. An extensive numerical analysis by Lewis & Goodyer [24] has generalised these findings to cover a wide range of model spans and test section proportions. The results are summarised in Figure 10.12. The contour lines show the root-to-tip variation of the normalised upwash: $\Delta_{upw} = AR/(8c_L) (w_{int(max)} - w_{int(min)})/U_\infty$ (in degrees). For a wing with a typical aspect ratio $AR=8$ and lift coefficient of $c_L=1$ the factor $AR/8c_L$ becomes 1 and the upwash variation is shown directly on contour lines in a plane $2s/\sqrt{bh}$ versus b/h where $2s/\sqrt{bh}$ is the wing span ratio and b/h the width to height ratio of the test section. For a square test section ($b/h=1$) and a wing span ratio $2s/\sqrt{bh} = 0.7$ the normalised upwash variation is about 0.15° . More favourable conditions are found for a test section ratio of $b/h \approx 1.4$ where the upwash variations are less than 0.025° . It appears that residual upwash interferences remain relatively small if the wing span does not exceed 70% of the test section width for square test sections.

Another limitation due to model size concerns the capability of the flexible walls to be adjusted to the computed wall contour in that relatively large wall displacements are required to accommodate the downwash field. The flow downstream of a three-dimensional lifting model follows about a constant downwash angle that may be as large as 2 or 3 degrees for high-lift configurations. Consequently, the flexible walls have to be displaced significantly downstream of the model. As the tunnel flow must be directed back to the collector, significant deflections of the flexible walls are required that may set limits to the model size or maximum angle of incidence. These circumstances may be relieved using a rotated system of co-ordinates, i.e. the wall setting is rotated by about half the downwash angle. The model angle of incidence is then corrected by this amount.

Limitations in asymmetric flow

Obviously, two-dimensional wall adaptation cannot cancel sidewash interferences. This is a serious limitation of the method whenever sidewash interferences are significant. Such situations are, however, very rare. Objects tested in wind tunnels are, with few exceptions, designed to produce only small side force per unit yaw angle, while the opposite is true of the normal force. Interferences are proportional to the forces experienced by the model. Hence the relative sidewash interferences are usually very much smaller than the upwash interferences and may be neglected in most circumstances. Exceptions may arise in cases where model yaw is accomplished by rotation of the model about the support sting because in these cases the requirement of nearly symmetric flow (point ii above) is eventually violated. In cases where sidewash interferences are significant they may be corrected by classical correction formulas (see Section 2.2).

10.4.3 EFFECTS OF THE SIDEWALL BOUNDARY LAYER

In two-dimensional testing, the sidewall boundary layers are affected by the model and may cause serious interferences. These are not wall interferences in the classical sense, but it is appropriate to discuss these boundary layer effects in the context of target line techniques for three-dimensional flows. A method to reduce sidewall boundary layer interferences is presently developed at the DLR Göttingen in co-operation with ONERA/CERT (Michonneau [28]). The idea is briefly as follows.

Based on potential flow calculations about the wing section, the pressure distributions and subsequently the sidewall boundary layers are computed. The displacement thickness of the boundary layers induces interference velocities at the model which are computed either by linear flow theory or, in transonic flows, by means of a three-dimensional potential flow solver. Finally, the flexible top and bottom walls are adapted so that the interference velocities are eliminated along the central section of the model where pressure measurements are performed.

The wall adaptation is superior to global correction methods in cases where boundary layer interferences vary along the chord of the model. In this way models of larger chord length may be used.

10.5 MANIPULATIVE ALGORITHMS

The control of the test section flowfield afforded by wall adaptation may be exploited for purposes other than reducing the effects of wall interference in free-air simulations. For instance, the principle of wall streamlining allows the conditions at several different types of flowfield boundary to be simulated via interface matching techniques merely by imposing appropriate constraints in the fictitious flows. The range of two-dimensional Group 1 Flowfields already simulated in this way within flexible-walled test sections (Goodyer, [10]; Benvenuto and Pittaluga, [5]) is illustrated in Figure 10.3.

Moreover, the facts that the wall boundary conditions are well defined and may readily be adjusted mean that the effects of introducing a variety of controlled perturbations to the flow may also be studied systematically in flexible-walled test sections. However, while the ability to actively manipulate rather than simply reduce the wall-induced perturbations to the flow may be expected to yield a number of novel freedoms to the practice of adaptive wall wind tunnel testing (Taylor and Goodyer, [35], [36]), relatively little effort has yet been directed towards exploiting this interesting feature of wall adaptation.

The most notable attempts to exploit the manipulative nature of wall adaptation were made during a recent series of investigations by Lewis and Goodyer [24], [25]). Here, streamwise gradients of wall-induced blockage and upwash were intentionally introduced in order to gain an improved understanding of the effects of residual variations on wind tunnel test data and, wherever possible, to establish appropriate methods for correcting the data for these variations.

The scope of these studies was confined to the manipulation of two-dimensional Group 1 Flows. Although the effects of residual variations in blockage were investigated (by providing appropriate collective displacements of the flexible liners), efforts were focused on studying the seemingly more important effects of residual upwash gradients. This was accomplished by super-imposing displacements in the form of circular arcs onto wall contours that had been derived to minimise the effects of top and bottom wall interference. In this way, reasonably linear variations in upwash were generated over the model. The linearity of the gradient was, on occasion, refined by subsequent wall adaptation. Wall-induced blockage was kept to a practical minimum throughout.

The influence of linear variations in upwash along the tunnel centreline was studied by manipulating its gradient (via the radius of curvature of the circular arcs) and the point on the model chord at which the upwash was zero (via the streamwise location of the centre of wall curvature). The desired modifications to wall curvature were deduced using linear theory. A sample of the results is presented in Figure 10.13. This shows the sensitivity of the model lift coefficient at fixed geometric incidence. A clear pattern in the data is evident, namely that the lift coefficient is insensitive to the magnitude of the wall-induced camber provided it is centred at or near the three-quarter chord point. Therefore, this data provides evidence to support the validity of Pistoletti's three-quarter chord theorem (Thwaites, [38]), a widely used method for deducing corrections to model incidence for the effects of streamwise linear residual variations in upwash.

This theorem was subsequently invoked to construct portions of the lift-curve, the values of upwash at the three-quarter chord point being used to derive conventional corrections to the model incidence. In this way, the systematic manipulation of wall-induced upwash described above enabled the effective incidence of the model to be varied without adjusting its geometric attitude. The agreement between the resulting lift-curve and various independent sources of reference data provided further experimental corroboration of Pistoletti's theorem. The theory was then extended by Ashill et al. [3] to encompass the general case of non-linearity in the residual upwash variation as follows:

$$\delta\alpha = w(x_p)/U = (1/\pi) \int_0^\pi (w/U)(1 - \cos\Theta) d\Theta \quad (10.8)$$

where $\Theta = \cos^{-1}(1-2x/c)$ and x_p is the point on the model chord at which the residual upwash is used to produce the incidence correction, $\delta\alpha$. Note that linear variations in upwash yield $x_p=3c/4$. When the integral in this equation (rather than the upwash at point x_p) was used to construct the lift-curve, the agreement between the lift-curve and the reference data was improved.

During these experiments, it was found that the model's pitching moment coefficient appeared to exhibit similar trends in its sensitivity to wall-induced upwash as those illustrated in Figure 10.13 - although, in this case, the curves appeared to converge on a point towards the model's trailing edge. This observation suggested that a similar correction to incidence could be deduced from the residual wall-induced upwash. Subsequent analysis (Ashill et al., [3]) yielded:

$$\delta\alpha = w(x_p)/U = (1/\pi) \int_0^\pi (w/U)(1 - 2\cos\Theta + \cos 2\Theta) d\Theta \quad (10.9)$$

an equation applicable to linear and non-linear residual variations. It may be verified that $x_p=c$ for a wall-induced upwash that varies linearly with chordwise position. In other words, for linear residual variations of wall-induced upwash, the appropriate point for making a correction to incidence on plots of pitching moment against incidence is the trailing edge.

Although derived in flexible-walled test sections, the conclusions of these investigations may be exploited in all wind tunnels where the assessment of wall interference is reasonably detailed. It is also interesting to note that the data presented in Figure 10.13 was obtained at conditions where a portion of the flow on the upper surface of the model was supercritical. This implies that the wall interference assessment procedure used throughout these investigations - a two-variable method based on Equation 4.14 - may be used with some confidence in the analysis of non-linear flows. Although further experimental evidence is required to substantiate this claim, it would appear that similar comments might also apply to the use of Equations 10.8 and 10.9.

The fact that the residual variations in wall-induced blockage and upwash about three-dimensional models may not be eliminated by two-dimensional wall adaptation would appear to make similar studies of their effects in three-dimensional testing extremely attractive. Aside from supporting the development of correction procedures that could be used in conventional, unadapted test sections (as reviewed in Section 1.3.2), these types of investigation would yield valuable guidance on the balance that will need to be made between data quality, its rate of acquisition and the mechanical complexity of the test section in designing adaptive wall facilities for production testing. They would also enable the extent to which some of the more novel potential uses for wall adaptation may be exploited in practice to be established. The limited data to hand (Lewis et al., [25]) suggest that the use of swept target lines may enable wall-induced camber and twist to be controlled almost independently about wings of high aspect ratio.

10.6 PRIORITIES FOR THE FUTURE

Even though more than two decades have elapsed since the dawn of the modern era of adaptive wall research, the pace of technique development continues to be rapid. With the range of potential applications also continuing to expand, there are many ways in which the technology could develop. For convenience, these are reviewed under three broad headings: data quality, rate of data acquisition, and complexity and cost. With the walls of the test section being adapted, these factors are clearly interrelated. Each exerts an important influence on wind tunnel productivity.

10.6.1 DATA QUALITY

There is now considerable evidence to suggest that with the walls of the test section adapted to minimise the effects of top and bottom wall interference in Group 1 free-air simulations, the quality of the test data produced in facilities with two flexible walls is superior to that obtained in any other type of wind tunnel. This appears to be true of two-dimensional (Elsenaar, ed., [6]; McCroskey, [27]) and three-dimensional (Lewis et al., [25]) testing. However, further work is required to establish whether flexible wall adaptation can yield similarly tangible benefits in Group 2-5 flows. If these cannot be established, there may be no alternative but to persist with a reliance on test section ventilation in these simulations - although, for the reasons outlined in Section 10.2.2, it should be noted that ventilated wall adaptation is not always successful in removing uncertainty from the test data (Neyland, [30]).

In view of the fact that in production testing, there is probably little to be gained from adapting the walls beyond the point at which the test data become amenable to reliable analyses, there is also a need to establish appropriate completion criteria, particularly for three-dimensional testing where residual variations are inevitable. The ability to study controlled perturbations to the flow in a systematic manner would appear to make flexible-walled test sections suitable platforms for developing these. Aside from supporting the development of correction procedures that could be used in conventional wind tunnels, these types of study would provide valuable guidance towards resolving important test section design issues (number and distribution of wall jacks, etc.). They would also enable the extent to which active manipulation of the flow may enable novel forms of wind tunnel wall correction to be devised. For instance, Taylor and Goodyer [35], [36] have suggested that the wall-induced wing twist present in three-dimensional testing might be tailored to simulate the aeroelastic deformations that occur during flight or to compensate for the distortion of the model under load. If proven, the latter feature would provide an alternative means for separating the effects of Mach number, Reynolds number and dynamic pressure in pressurised wind tunnels - a capability that is currently only available in cryogenic facilities.

10.6.2 RATE OF DATA ACQUISITION

Once suitable completion criteria have been established, it will be possible to determine the degree of wall adaptation required to provide acceptable levels of residual variation. The rate at which correctable test data may then be produced will be determined by the number of adaptation iterations required to produce acceptable data and the time required to complete each iteration.

Procedures capable of reducing residual variations to very low levels in one step have already been developed for simulations of two- and three-dimensional Group 1 free-air flows. It is also conceivable that a single wall setting may, on occasion, be acceptable for use over a range of test conditions. Several schemes

have been proposed (Taylor and Goodyer, [35]) which seem likely to ensure that the rate of data acquisition is unlikely to be impeded by iteration, at least when simulating Group 1 Flows. Furthermore, recognising that future requirements for wind tunnel testing may be modified to accommodate the increasingly important role of CFD in the aerodynamic design process, there may be greater demand for some of the more novel uses of wall adaptation: it is possible to conceive of tests being conducted in twist (or camber) sweeps in addition to the more conventional longitudinal and lateral polars, for instance. There is clearly plenty of scope for research in developing highly productive wall adjustment strategies.

However, even if a reliance on iteration can be overcome, the requirements for rapid and accurate on-line assessments of wall interference and adjustments of the wall settings will need to be addressed if wall adaptation is ever to be used routinely in large industrial wind tunnels. These topics raise a number of test section design issues - such as the capabilities of the data acquisition system, the mechanical design and operation of the wall jacks and details of the overheads associated with the control logic required to safeguard against undesirable wall adjustments - that are beyond the scope of this AGARDograph. The following observations provide perspectives on the prospects for synchronising wall adaptation with changes to the test conditions (reference conditions and/or model attitude):

- i. Methods have been devised which reduce the computational overheads associated with wall interference assessment and the prescription of improved wall settings in Group 1 free-air flow simulations to reasonably low levels. For instance, in test sections with twenty jacks on both the top and bottom walls, Equations 10.3 and 10.4 may be solved to govern the adaptation required in two-dimensional testing in fractions of a second on a modern personal computer. Equations 10.7a and 10.7b may be solved at similar expense in three-dimensional model tests - although the time required to assess the wall interference will rise if swept target lines are required (see Section 10.4.2.2).
- ii. Mechanisms have been devised which allow reasonably rapid adjustment of the flexible walls. For example, in the test section of the pressurised and cryogenic T2 wind tunnel of ONERA/CERT, controlled adjustments to the wall contours are usually completed in under 0.5 seconds (Archambaud and Mignosi, [1]). It remains to be seen how far this type of timescale will be protracted in larger facilities. (The test section in T2 is 1.32m long, 0.39m wide and 0.37m deep.)

10.6.3 COMPLEXITY AND COST

It stands to reason that an adaptive flexible-walled test section will be more complex and costly to design, commission and operate than a conventional closed test section. Unfortunately, suitable measures of the value of these additional costs (and therefore acceptable limits for test section complexity) have proved rather difficult to establish. The reasons for this are reviewed briefly alongside suggestions by which the vagaries of the current situation may be resolved in Chapter 12. The additional complexity also implies additional risk - of system malfunction or failure to maintain acceptable levels of data repeatability, for instance. However, by appealing to the admissibility of the measured flow conditions at the control surfaces, schemes that may alleviate these concerns have been proposed (Taylor and Goodyer [36]).

The relative complexity of the techniques themselves (wall interference assessment and wall adjustments are required on-line), coupled with the fact that there is no one way of adapting the walls (the operator actually has a choice as to how the flow should be controlled) may also be viewed as sources of uncertainty and confusion amongst those unfamiliar with the technology. Therefore, once techniques have been developed to the point at which they may be used in production testing, effort in the forms of education and the development of robust, user-friendly operating sequences, will be required to install confidence in the user's mind that wall

adaptation is actually removing important sources of uncertainty from the test data and providing additional capabilities that would not otherwise be available. In this respect, it may be helpful to note that several direct parallels may be drawn between the utilisation of aerodynamic control surfaces on aircraft and in flexible-walled test sections. Both are mechanically complex and costly to install and maintain and both provide improvements in aerodynamic performance that would not otherwise be available.

Paradoxically, precedent suggests (Barnwell et al., [4]) that concerns about the relative costs and benefits of wall adaptation will only be fully resolved when it is utilised in large-scale industrial facilities. With this in mind, it is interesting to note that most industrial tunnels actually already utilise some form of wall adaptation - while calibrating the test section (wall divergence), controlling the reference Mach number (second throat) or generating supersonic reference conditions (flexible nozzle), for instance. In these circumstances, its use is justified, presumably, on the basis that (i) the majority of the cost associated with determining the optimum wall settings is only incurred once, (ii) the walls are not usually adapted during a typical production test, they are merely adjusted to pre-determined settings and (iii) adjustments are not made very often during a typical test programme.

Wall induced upwash parameter	Straight walls	Adapted Walls		
		Root	Tip	Swept
Root camber	0.38	0.00	0.12	0.03
Mid-span camber	0.28	0.01	0.05	0.07
Tip camber	0.09	0.00	0.00	0.00
Mean twist	- 0.22	0.13	0.11	0.02
Max. to min. spread	0.50	0.13	0.18	0.07

Table 10.1 Summary of residual upwash variations for test case presented in Figure 1.11.
(Straight walls v. three upwash target lines. All values quoted in degrees)

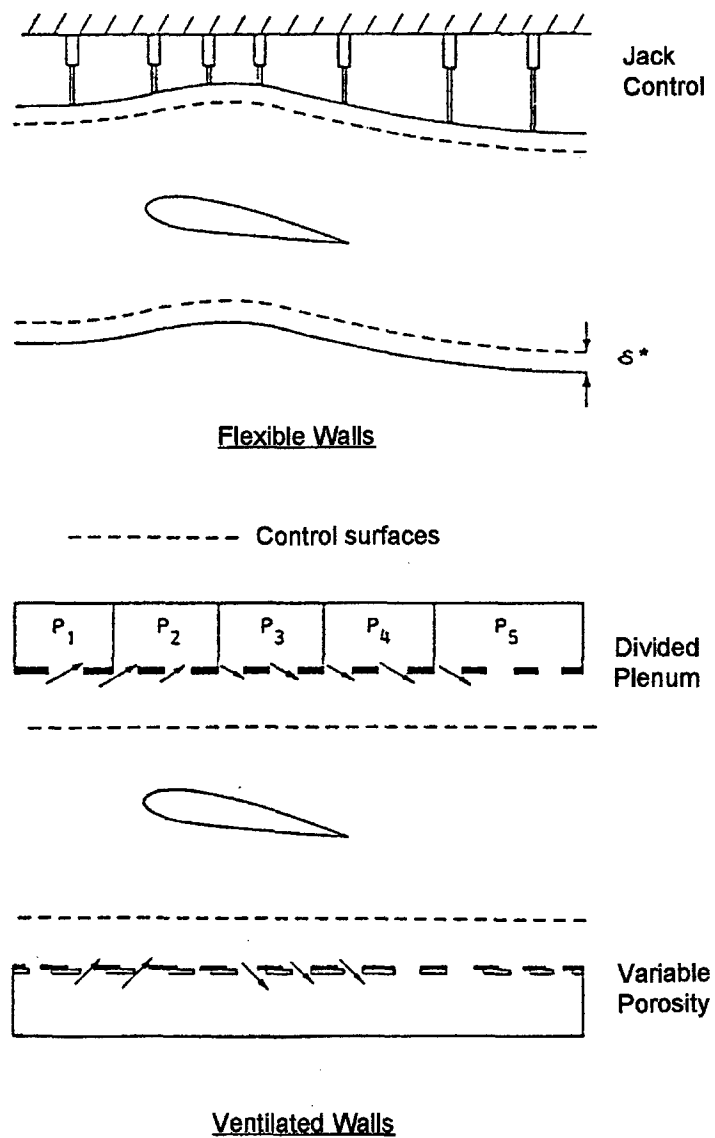
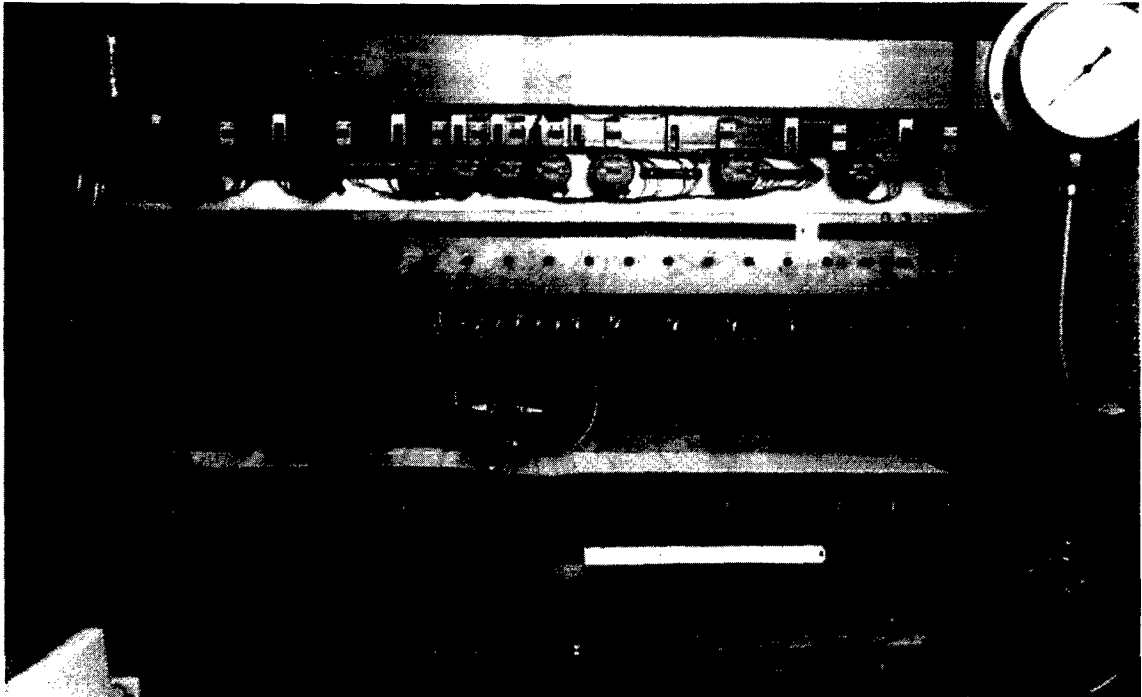
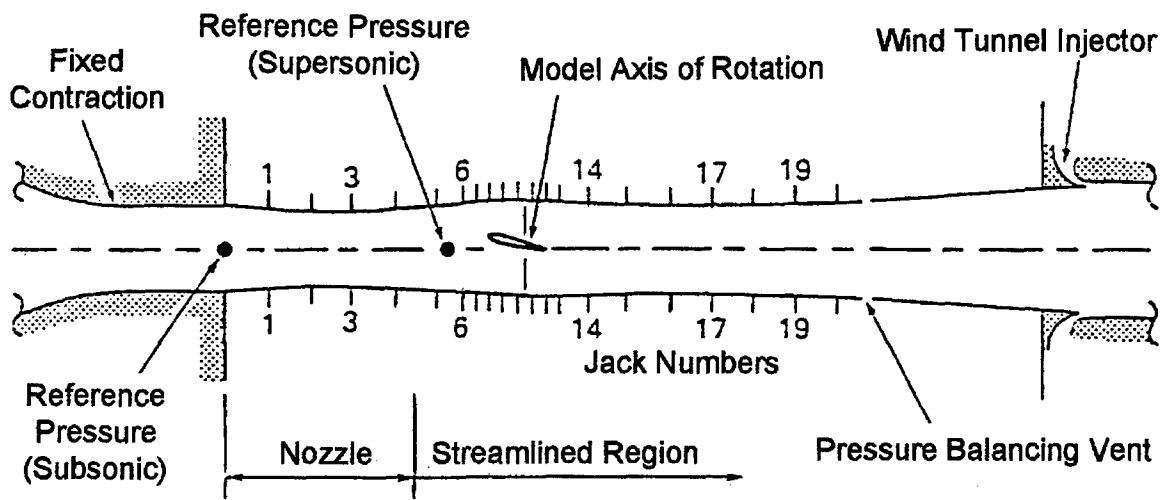


Figure 10.1 Two types of adaptive wall test section

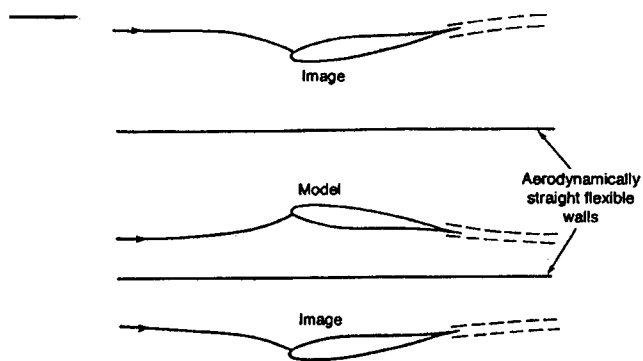


a. Photograph of the two-dimensional testing arrangement, near sidewall removed.

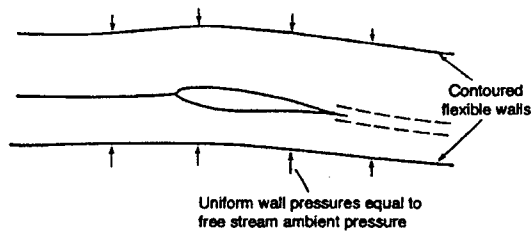


b. Schematic layout of the test section

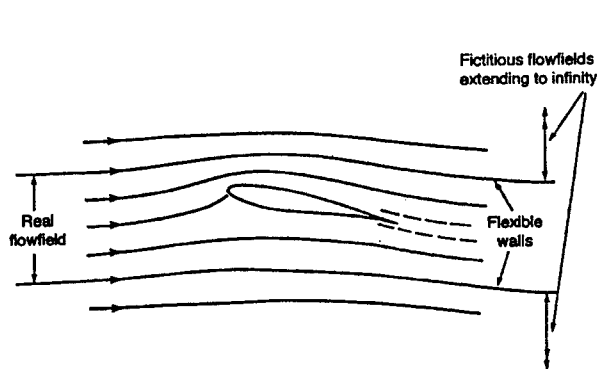
Figure 10.2 The adaptive flexible-walled test section of the Transonic Self-Streamlining Wind Tunnel of the University of Southampton



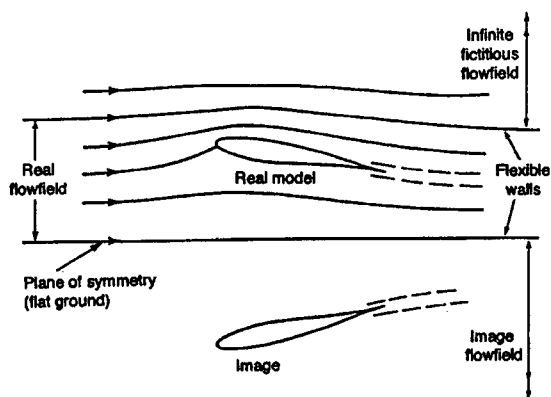
a) Closed test section simulation



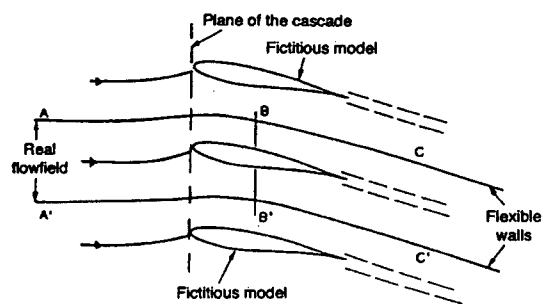
b) Open-jet test section simulation



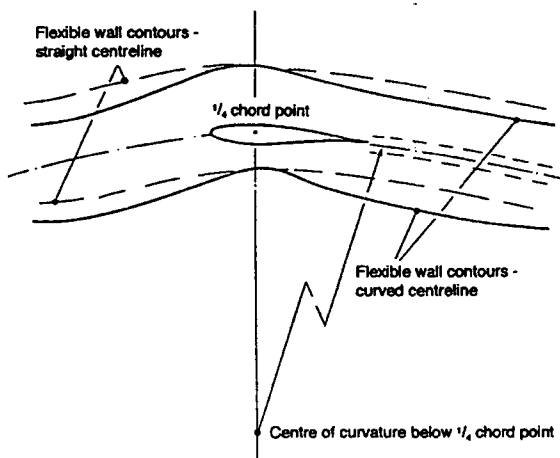
c) Free-air simulation



d) Ground effect simulation



e) Cascade flow simulation
 $(P_A = P_{A'} ; P_B = P_{B'} ; P_C = P_{C'})$



f) Steady pitching simulation

Figure 10.3 Examples of the ways in which the boundary conditions may be prescribed for two-dimensional testing in flexible-walled test sections.

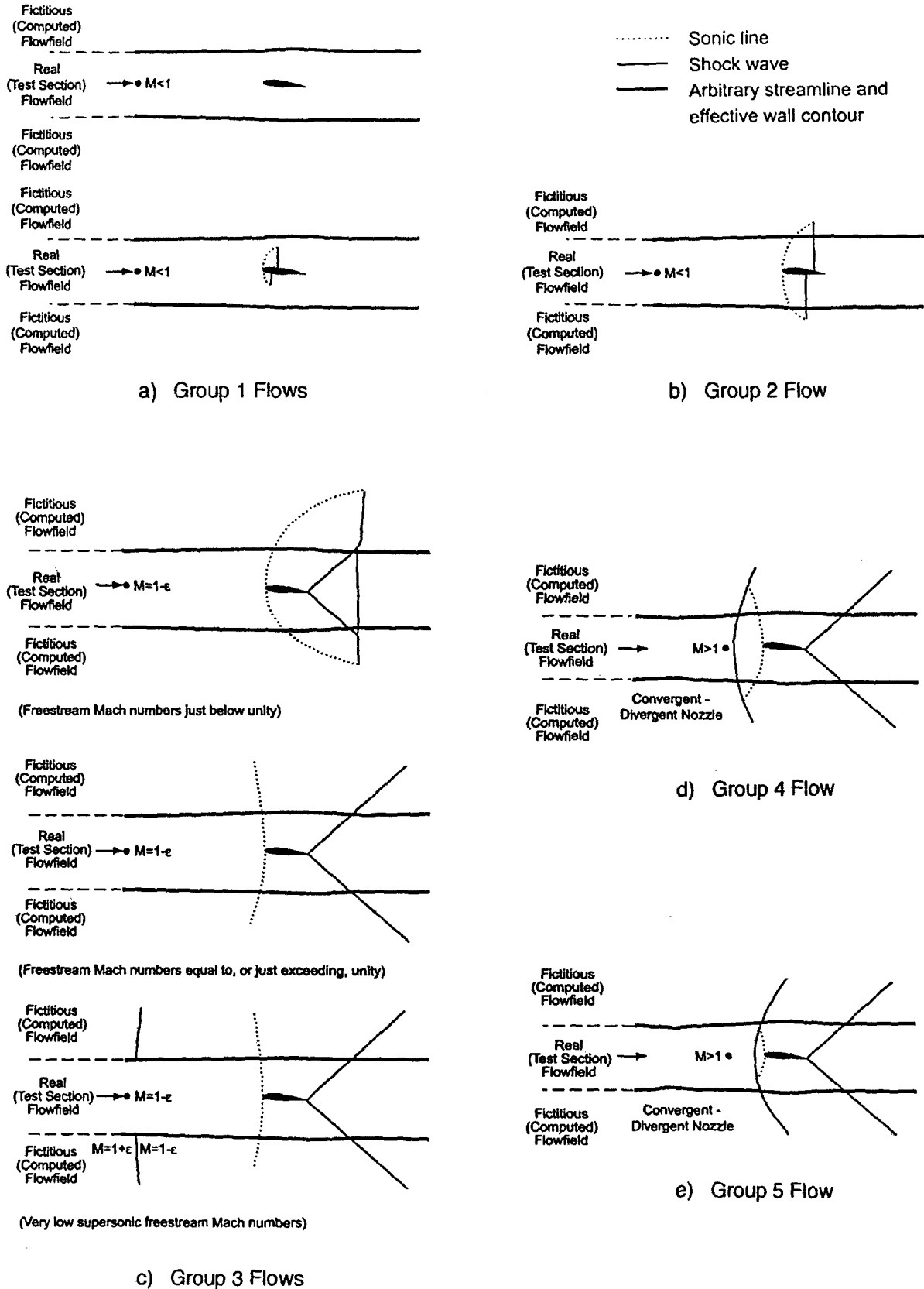


Figure 10.4 Ways in which the free air flowfield may be partitioned for two-dimensional interface matching in flexible-walled test sections

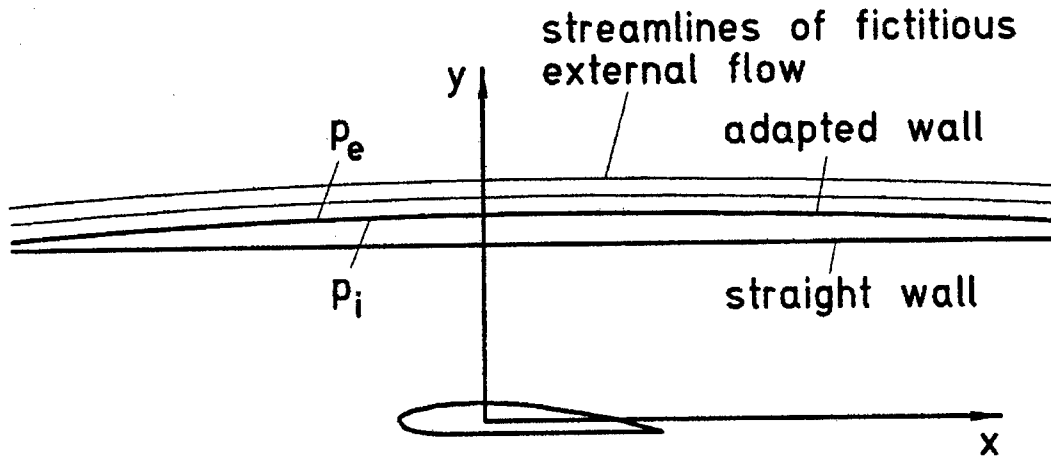


Figure 10.5 Internal and fictitious external flowfield

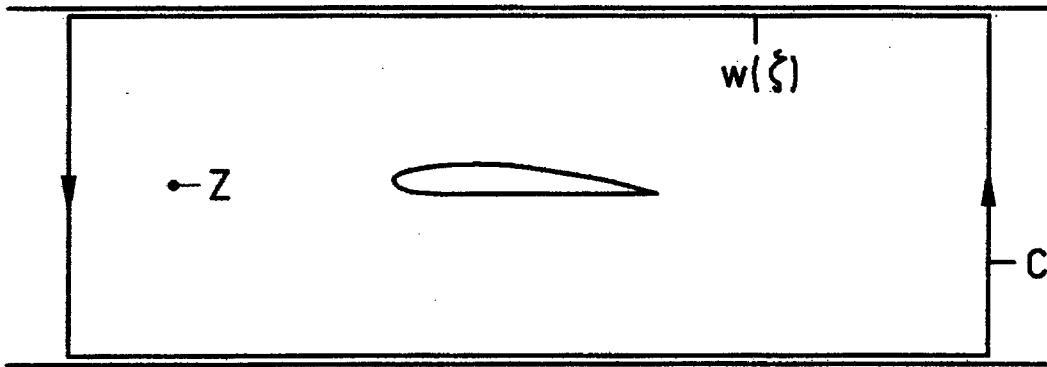


Figure 10.6 Path of Integration (Equation 10.2)

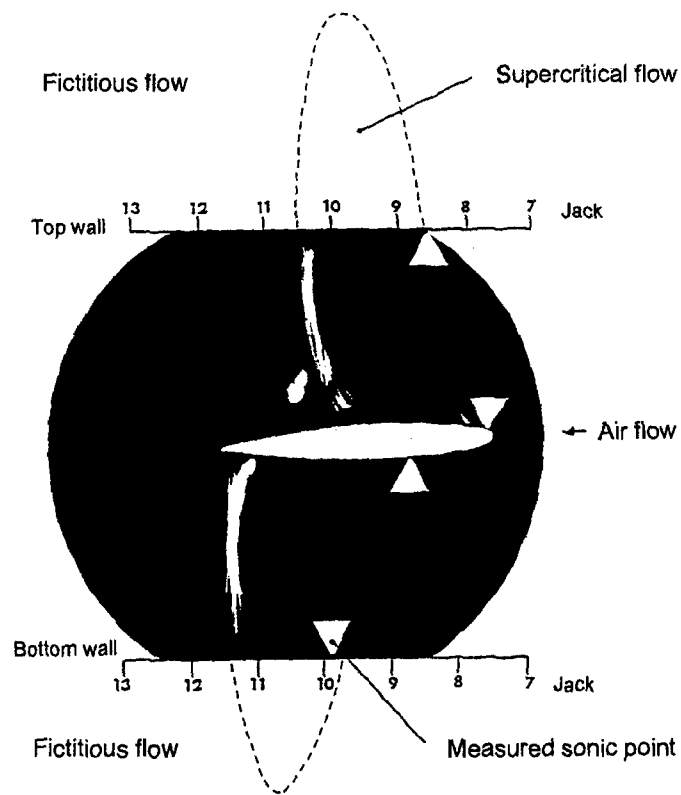


Figure 10.7 Montage of real and fictitious portions of a group 2 Flow after adapting the walls.
 NACA 0012-64 Section, $M = 0.87$, $\alpha = 4.0^\circ$ (Real flow : schlieren photograph;
 fictitious flow : TSP computation)

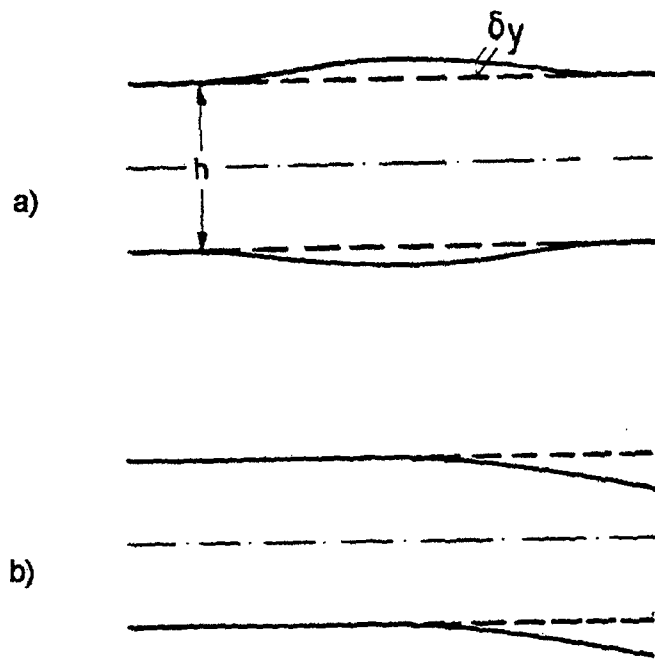
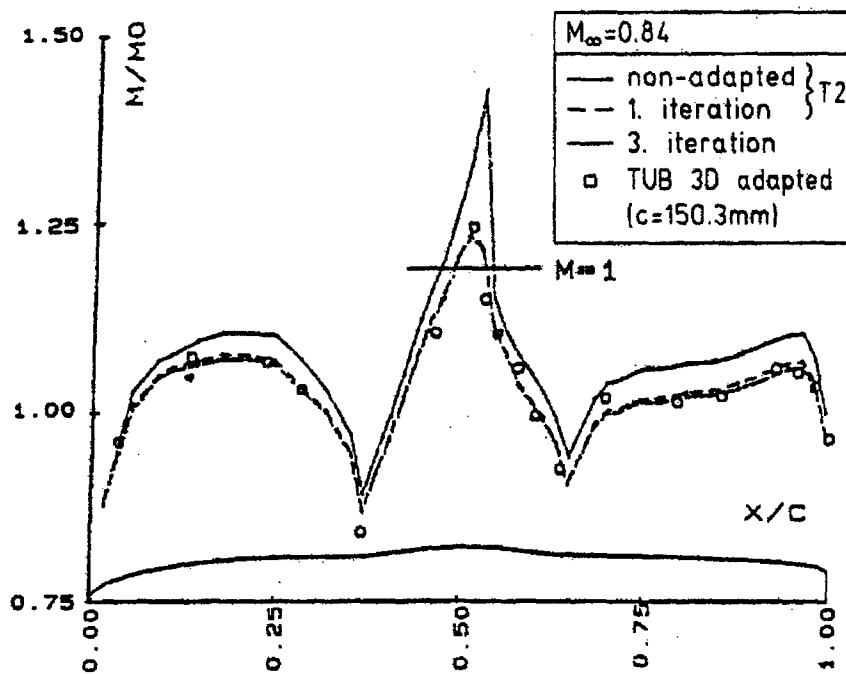


Figure 10.8 a) symmetrical and b) anti-symmetrical wall displacement

-C5 Model Mach Number $M=0.84$



-C5 Model Mach Number $M=0.90$

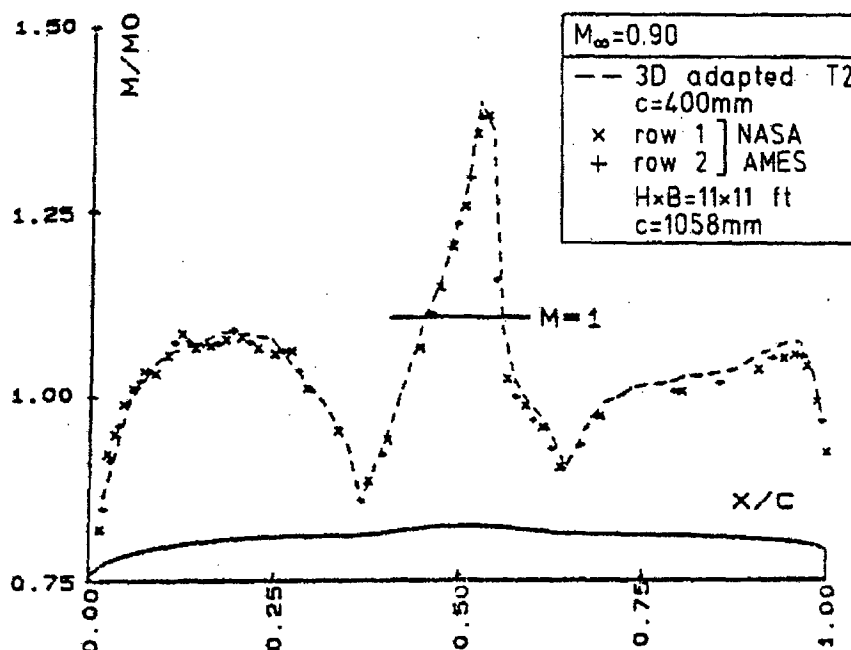
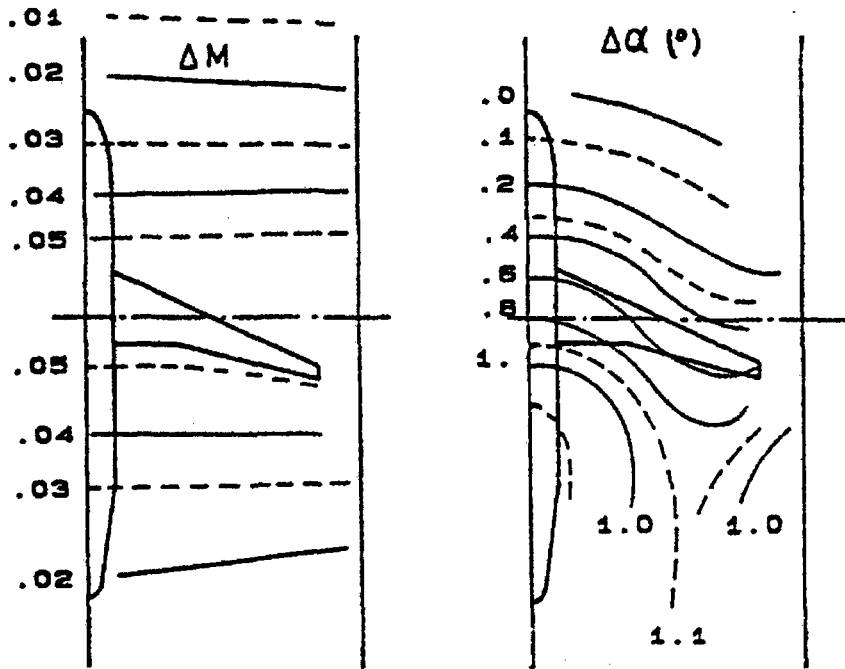


Figure 10.9a Pressure distribution on an axisymmetric body with 2% blockage in the ONERA T2 adaptive wall wind tunnel. Comparison with interference free results.

Straight Walls



Blockage

Upwash

Adapted Walls

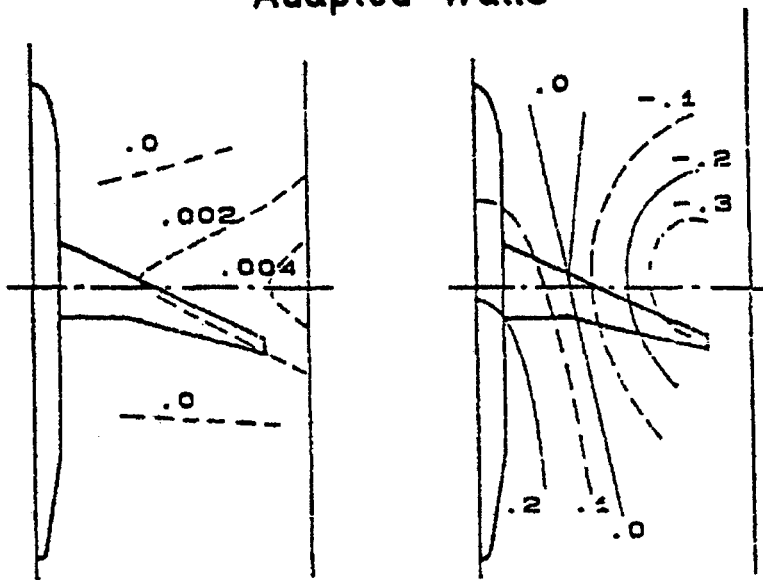


Figure 10.9b T2 half model. $M = 0.78$, $\alpha = 3.25^\circ$. Contour map of wall induced blockage and upwash in the plane of the model.

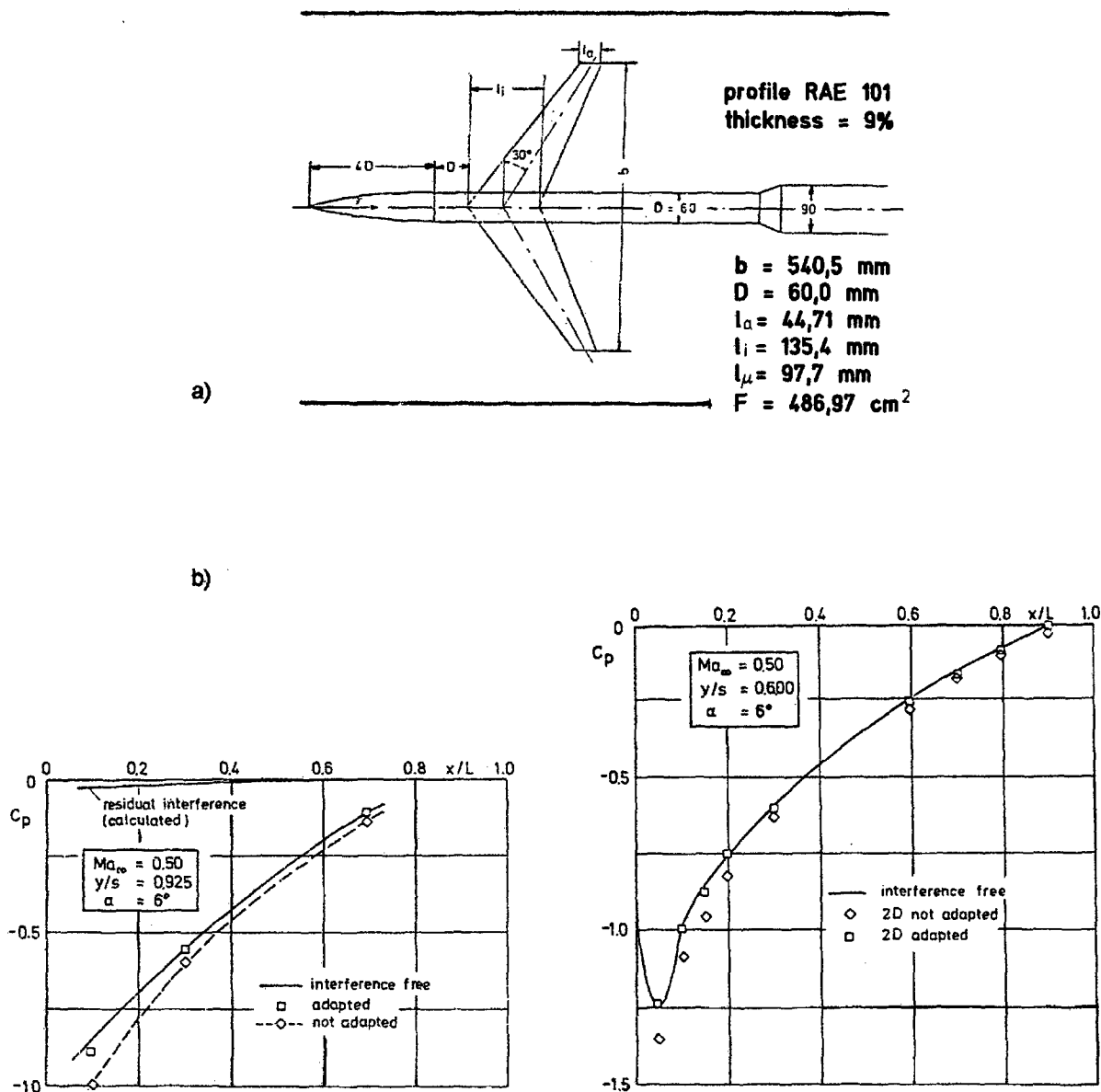


Figure 10.10 a) Planview of a model spanning 75% of the 0,75m x 0,75m adaptive wall test section of the HGK wind tunnel at DLR Göttingen.
 b) Pressure distribution at wing sections $y/s = 0,6$ and $y/s = 0,925$ for the models shown in a)

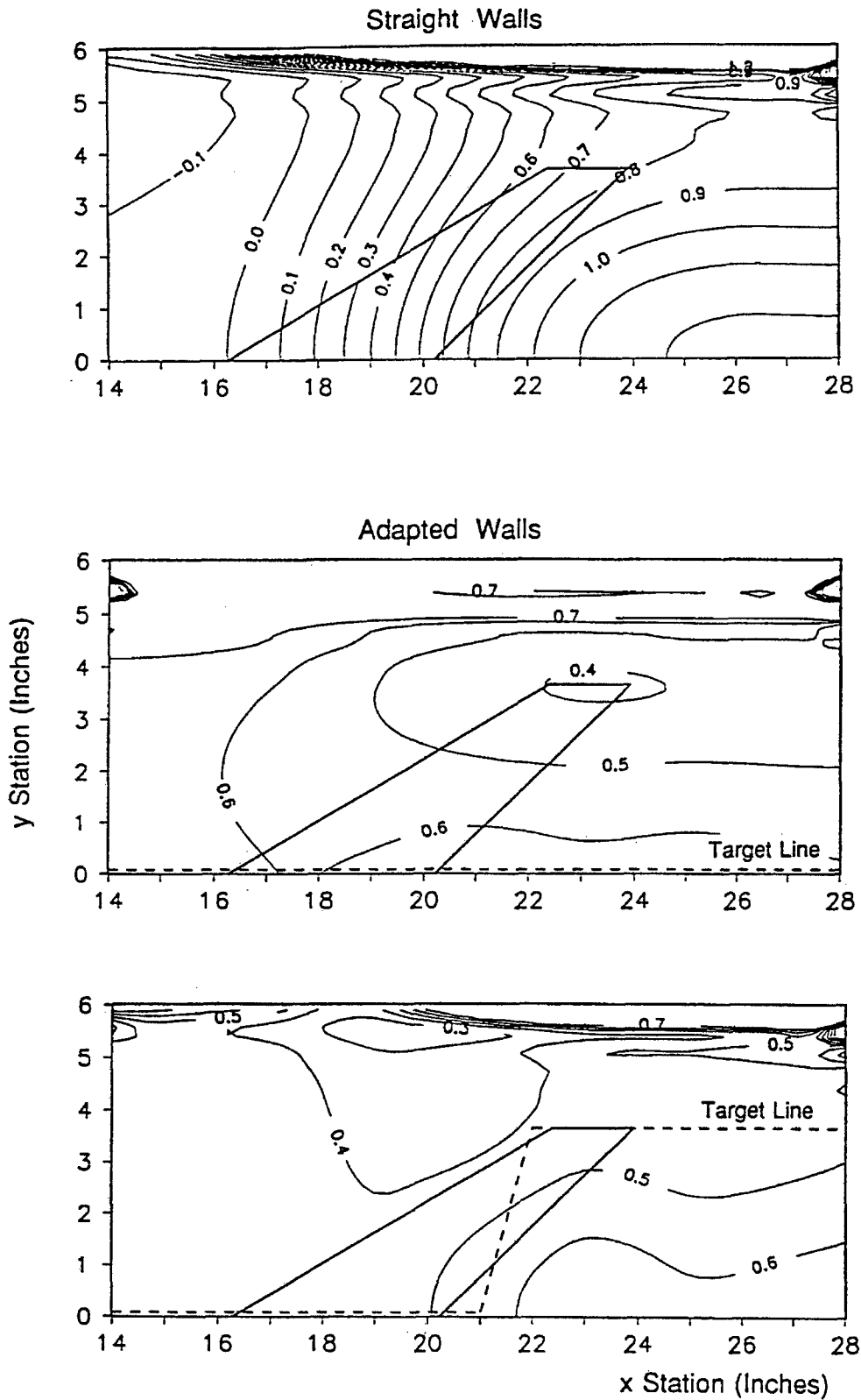


Figure 10.11 The effect of adapting the walls and sweeping the target line on the levels and distribution of wall-induced upwash in the plane of a simple half model ($M = 0.7$, $\alpha = 4^\circ$, $b/h = 1.0$, contours of w/U , %)

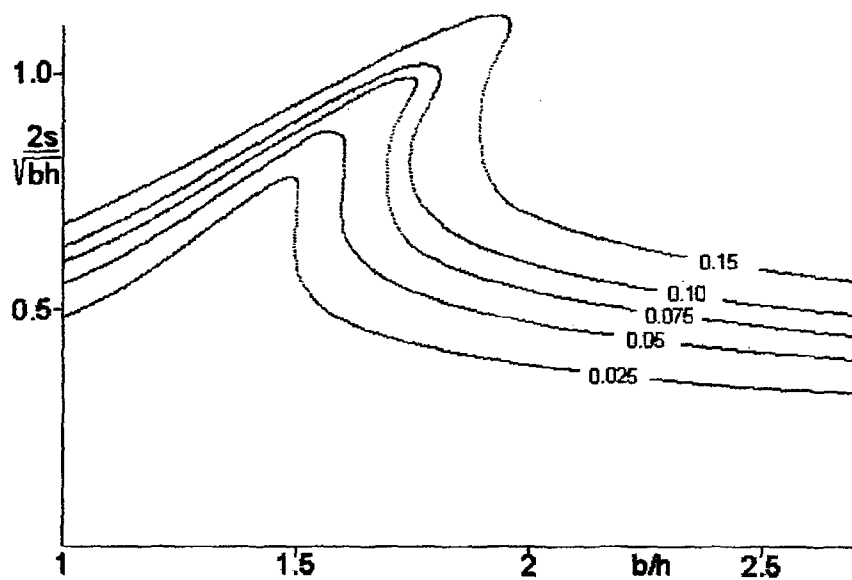


Figure 10.12 Contour lines of constant upwash variation in solid wall test sections of width to height ratio b/h

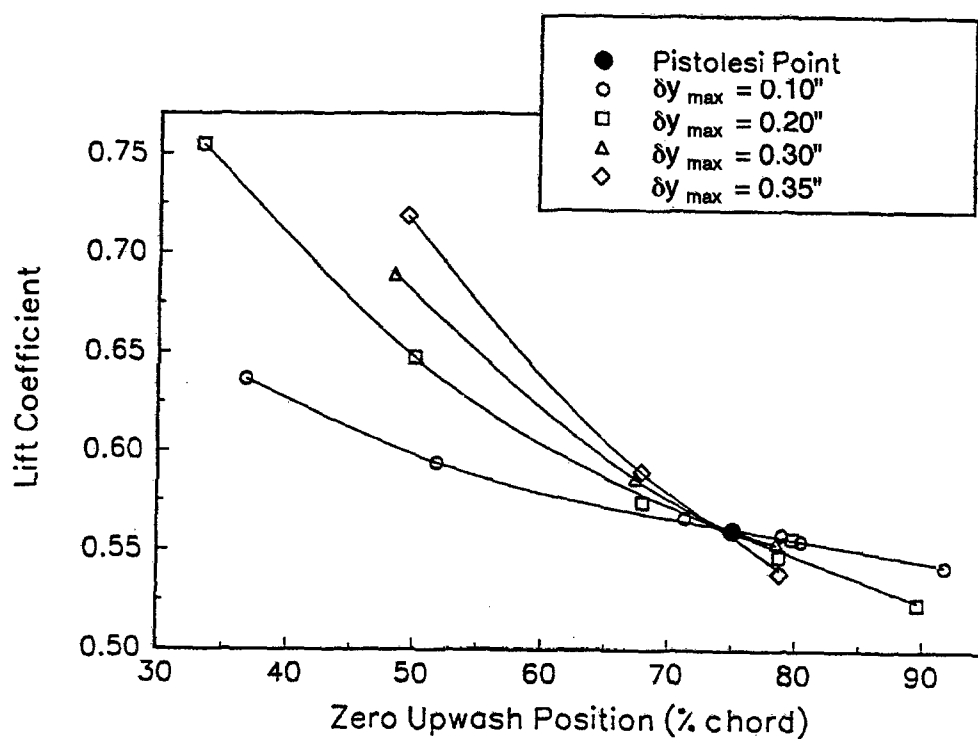


Figure 10.13 The influence of the magnitude and streamwise location of a linear gradient of wall-induced upwash on the lift coefficient of a two dimensional model (NPL 9510, $M = 0.7$, $\alpha \approx 2^\circ$)

10.7 REFERENCES

- [1] Archambaud, J.P. and Mignosi, A., 1988, "Two-dimensional and three-dimensional adaptation at the T2 Transonic Wind Tunnel of ONERA/CERT", AIAA 88-2038.
- [2] Ashill, P.R. and Weeks, D.J., 1982, "A method for determining wall-interference corrections in solid-wall tunnels from measurements of static pressure at the walls", Paper 1 in AGARD-CP-335.
- [3] Ashill, P.R., Goodyer, M.J. and Lewis, M.C., 1996, "An experimental investigation into the rationale of the application of wind tunnel wall corrections", ICAS 96-3.4.1.
- [4] Barnwell, R.W., Edwards, C.L.W., Kilgore, R.A. and Dress, D.A., 1986, "Optimum transonic wind tunnel", AIAA 86-0755.
- [5] Benvenuto, G. and Pittaluga, F., 1985, "Experimental investigation on the performance of a transonic turbine blade cascade for varying incidence angles", pp179-191 in 'Measurement techniques in heat and mass transfer', Hemisphere Publishing Corp.
- [6] Elsenaar, A. (Editor), 1981, "Two-dimensional transonic testing methods: final report by the GARTEur Action Group AD(AG-02)", NLR TR 83086 L (GARTEur/TP-011).
- [7] Erickson, J.C. and Nenni, J.P., 1973, "A numerical demonstration of the establishment of unconfined-flow conditions in a self-correcting wind tunnel", CALSPAN-RK-5070-A-1.
- [8] Ganzer, U., Igeta, Y. and Ziemann, J., 1984, "Design and operation of TU-Berlin wind tunnel with adaptable walls", ICAS 84-2.1.1.
- [9] Glauert, H., 1933, "Wind tunnel corrections for wings, bodies and airscrews", ARC R&M 1566.
- [10] Goodyer, M.J., 1975, "The self-streamlining wind tunnel", NASA TM-X-72699.
- [11] Goodyer, M.J., 1985, "Derivation of jack movement influence coefficients as a basis for selecting wall contours giving reduced levels of interference in flexible walled test sections", NASA CR-177992.
- [12] He, J.J., Zuo, P.C., Li, H.X. and Xu, M., 1992, "The research of reducing 3-D low supersonic shock wave reflection in a 2-D transonic flexible walls adaptive wind tunnel", AIAA 92-3924.
- [13] Heddergott, A. and Wedemeyer, E., 1991, "2-D Wall Adaptation for 3-D Models in Supersonic Flow", Paper A10 in "Proceedings of the International Conference on Adaptive Wall Wind Tunnel Research and Wall Interference Correction, June 10-14 1991, Xian, China".
- [14] Holst, H. and Raman, K.S., 1988, "2-D adaptation for 3-D testing", DFVLR IB 29112-88 A 03.
- [15] Holst, H., 1991, "Procedure for determination of three-dimensional wind tunnel wall interferences and wall adaptation in compressible subsonic flow using measured wall pressures", DLR FB 91-09.
- [16] Hornung, H. (Editor), 1990, "Adaptive wind tunnel walls: technology & applications", AGARD-AR-269.
- [17] Kraft, E.M. and Dahm, W.J.A., 1982, "Direct assessment of wall interference in a two-dimensional subsonic wind tunnel". AIAA-82-0187.
- [18] Kraft, E.M., Ritter, A. and Laster, M.L., 1986, "Advances at AEDC in treating wind tunnel wall interference", ICAS 86-1.6.1.
- [19] Lamarche, L., 1986, "Reduction of wall interference for three-dimensional models with two-dimensional wall adaptation", Dissertation, Université Libre de Bruxelles.

- [20] Lamarche, L. and Wedemeyer, E., 1984, "Minimization of wall interference for three-dimensional models with two-dimensional wall adaptation", VKI-TN-149.
- [21] Le Sant, Y. and Bouvier, F., 1992, "A new adaptive test section at ONERA Chalais-Meudon", Paper 41 in the Proceedings of the RAeS European Forum on Wind Tunnels and Wind Tunnel Test Techniques, University of Southampton (UK), September 14-17, 1992.
- [22] Legendre, R.G., 1974, "Self-correcting transonic wind tunnels", ONERA TP 1975-33 (in French).
- [23] Lewis, M.C., 1988, "Aerofoil testing in a self-streamlining flexible-walled wind tunnel", NASA CR-4128.
- [24] Lewis, M.C. and Goodyer, M.J., 1991, "Two-dimensional wall adaptation for three-dimensional flows", Paper A2 in "Proceedings of the International Conference on Adaptive Wall Wind Tunnel Research and Wall Interference Correction, June 10-14 1991, Xian, China".
- [25] Lewis, M.C., Taylor, N.J. and Goodyer, M.J., 1992, "Adaptive wall technology for three-dimensional models at subsonic speeds and aerofoil testing through the speed of sound", Paper 42 in the Proceedings of the RAeS European Forum on Wind Tunnels and Wind Tunnel Test Techniques, University of Southampton (UK), September 14-17, 1992.
- [26] Lo, C.F. and Kraft, E.M., 1978, "Convergence of the adaptive wall wind tunnel", AIAA Journal, vol.16, pp67-72.
- [27] McCroskey, W.J., 1988, "A critical assessment of the wind tunnel results for the NACA 0012 airfoil", Paper 1 in AGARD-CP-429.
- [28] Michonneau, J.F., 1993, "Analyse des perturbations induites par les couches limites des parois latérales d'une soufflerie sur un profil en régime transsonique", Thesis, École National Supérieure de l'aéronautique et de l'espace, Toulouse.
- [29] Mokry, M., 1990, "Limits of adaptation, residual interferences", Chapter 6 in AGARD-AR-269 (see Hornung, ed., 1990).
- [30] Neyland, V.M., 1993, "The traditional and new methods of accounting for the factors distorting the flow over a model in large transonic wind tunnels", Paper 25 in AGARD-CP-535.
- [31] Rebstock, R. and Lee, E.E., 1989, "Capabilities of wind tunnels with two adaptive walls to minimize boundary interference in 3-D model testing", NASA CP-3020, vol.1, pt.2, pp891-910.
- [32] Sears, W.R., 1973, "Self-correcting wind tunnels", CALSPAN-RK-5070-A-2.
- [33] Smith, J., 1982, "Measured boundary conditions methods for 2D flows", Paper 9 in AGARD-CP-335.
- [34] Steinle, F. and Stanewsky, E., 1982, "Wind tunnel flow quality and data accuracy requirements", AGARD-AR-184.
- [35] Taylor, N.J. and Goodyer, M.J., 1994a, "Towards the exploitation of adaptive wall technology in production testing environments", AIAA 94-2614 or DRA/AS/LBA/TR94021/1.
- [36] Taylor, N.J. and Goodyer, M.J., 1994b, "An insight into the unique affinities that characterise the relationship between adaptive flexible-walled test sections and CFD", AIAA 94-1934 or DRA/AS/LBA/TR94022/1.
- [37] Taylor, N.J., 1995, "Adaptive wall technology for two-dimensional wind tunnel testing at high-subsonic through to low supersonic speeds", Ph.D. Thesis, University of Southampton.

- [38] Thwaites, B., 1960, "Incompressible aerodynamics. An account of the theory and observation of the steady flow of incompressible fluid past aerofoils, wings and other bodies", pp341-8, Oxford University Press.
- [39] Tuttle, M.H. and Mineck, R.E., 1988, "Adaptive wall wind tunnels: a selected, annotated bibliography", NASA TM 87639 (corrected copy).
- [40] Verte, D., 1982, "Interférence résiduelle dans une soufflerie transsonique à parois adaptées à un écoulement bidimensionnel dans l'étude de l'écoulement autour d'un corps axisymétrique", Travail de fin d'études, Université Libre de Bruxelles, Institut de Mécanique Appliquée.
- [41] Wedemeyer, E., 1982, "Wind tunnel testing of three-dimensional models in wind tunnels with two adaptive walls", VKI-TN-147.
- [42] Wedemeyer, E., Heddergott, A. and Kuczka, D., 1985, "Deformable adaptive wall test section for three-dimensional wind tunnel testing", Journal of Aircraft, vol.22, pp1085-1091.
- [43] Wedemeyer, E. and Lamarche, L., 1988, "The use of 2-D adaptive wall test sections for 3-D flows", AIAA 88-2041.
- [44] Wolf, S.W.D. (Editor), 1986-92, "Adaptive wall newsletter", Issues 1-16, Informal Publication.

Appendix A

Cauchy's integral formula states that the integral $\int f(\zeta) / (\zeta-z) d\zeta$ taken about a positive oriented closed path in the complex plane containing z in the interior has the value $2\pi i f(z)$ if $f(z)$ is analytic in the interior, while the integral is zero if $f(z)$ is analytic in the exterior and zero at infinity.

In accordance with the assumption of linear flow theory, the flow within the test section may be decomposed into one part w_m due to the model in free air and one part w_{int} which is due to the wall interference. Thus $w = w_m + w_{int}$. The part w_{int} may be viewed as being generated by the images of the model reflected at the test section walls. This part has singularities only in the "exterior" flowfield while it is analytic in the interior flow (within the test section). The part w_m , however, has singularities only within the interior, while it is analytic in the exterior part and zero at infinity.

Applying Cauchy's integral formula to an interior point z and choosing $f(\zeta) = w_{int}(\zeta)$ the result is:

$$w_{int}(z) = \frac{1}{2\pi i} \int_C \frac{w_{int}(\zeta)}{\zeta - z} d\zeta$$

while :

$$0 = \int_C \frac{w_m(\zeta)}{\zeta - z} d\zeta$$

Adding the integrals and recognising that $w = w_m + w_{int}$, Equation 10.2 is obtained.

Appendix B

Computation of the influence functions

If u_s and u_{int} are known functions in a special case, Equation 10.6a may be considered as an integral equation for the unknown function Ω and, equally, Equation 10.6b as an integral equation for the function Γ . As an example, the computation of the influence function Ω is discussed in the following.

Writing $(\xi - x) = \eta$ Equation 10.6a reads:

$$u_{int}(x) = \int u_s(\eta+x) \Omega(\eta) d\eta \quad (A1)$$

Discretisation and approximation of the integral by a sum leads to:

$$u_{int}(i) = \sum_k u_s(k+i) \Omega(k) \Delta\eta \quad (A2)$$

which is a system of equations for $\Omega(k)$ at discrete points $\eta = k$. When solving Equation A2 numerically, care must be taken that the matrix $u_{s,i,k} = u_s(k+i)$ is not singular. For the present, the influence function Ω

is determined so as to solve Equation A1 for a special choice of functions u_{int} and u_s . The general validity of Equation A1 will be shown in the following.

Proof of the general validity of Equation A1

The functions u_{int} and u_s must be computed in a special case. They may be derived from the velocity field generated by a source doublet and its images (see for example Equation 2.60). Let $u_s^0(x-\xi)$ be the velocity at the wall and $u_{int}^0(x-\xi)$ the interference velocity generated by a source doublet at the location ξ and its reflections. The influence function Ω is determined so as to solve the equation:

$$u_{int}^0(x) = \int u_s^0(\eta+x) \Omega(\eta) d\eta . \quad (A3)$$

The most general symmetric flow can be generated by a distribution of doublets of strength $q(\xi) d\xi$. With this the wall velocity and interference velocity at a point $\eta+x$ become:

$$1) u_s(\eta+x) = \int q(\xi) u_s^0(\eta+x-\xi) d\xi \quad 2) u_{int}(x) = \int q(\xi) u_{int}^0(x-\xi) d\xi \quad (A4)$$

Multiplying the first Equation A4 by $\Omega(\eta)$, integrating by η and using Equation A3 yields:

$$\int u_s(\eta+x) \Omega(\eta) d\eta = \int q(\xi) \int u_s^0(\eta+x-\xi) \Omega(\eta) d\eta d\xi = \int q(\xi) u_{int}^0(x-\xi) d\xi = u_{int}(x) \quad \text{q.e.d.}$$

Computation of the wall displacement

The wall adaptation strategy aims at eliminating the wall interferences along the target line by displacing the walls so as to generate velocity distributions $u_c(x) = -u_{int}(x)$ and $w_c(x) = -w_{int}(x)$. In the following, the target line is assumed to be the centreline of the test section. $u_c(x)$ is generated by a symmetric wall displacement $d_s(x)$ as shown in Figure 10.8a and $w_c(x)$ by an anti-symmetric wall displacement $d_a(x)$ (Figure 10.8b). In order to derive a relation between $u_s(x)$ and $d_s(x)$ the disturbance potential generated by displacing the wall symmetrically may be expanded in a power series:

$$\Phi(x,z) = a_0(x) + a_2(x) z^2 + a_4(x) z^4 + \dots \quad (A5)$$

Considering that Φ must be a solution of the disturbance equation $\beta^2 \Phi_{xx} + \Phi_{zz} = 0$ it is found that: $a_2 = -\beta^2 a_0''/2$ and $a_4 = \beta^4 a_0''''/48$, where a_0'' and a_0'''' are the second and fourth derivatives.

The axial velocity at the centreline is (using non-dimensional quantities $u_s = u_s/U_\infty$, $d_s = d_s/h$ etc.):

$$(\partial\Phi/\partial x)_{z=0} = a_0'(x) = u_c(x) = -u_{int}(x) \quad (A6)$$

The normal velocity at the wall position $z=h/2$ is:

$$(\partial\Phi/\partial z)_{z=h/2} = -\beta^2 h a_0''/2 + \beta^4 h^3 a_0''''/48 + \dots = w_c(x) . \quad (A7)$$

As $a_0' = u_c = -u_{int}$ is a slowly varying function of x , the higher derivatives in the power series of Equation A7 may be neglected. The wall displacement is then: $d_s(x)/h = \mathbf{d}_s(x) = \int w_c(x) dx = -\beta^2 a_0'/2 + \beta^4 h^2 a_0''/48$, or, with Equation A6:

$$d_s(x) = \beta^2/2(u_{int} - (1/24)u_{int}''') \quad (A8)$$

where $'''$ is used to denote the second derivative with respect to the normalised variable $\underline{x}=x/\beta h$.

Equation A8 may be used immediately to compute the required wall displacement when $u_{int}(x)$ is known by evaluation of Equation 10.6a. Computing the second derivative of $u_{int}(x)$ numerically is, however, intrinsically inaccurate if u_{int} is given at discrete points. Higher accuracy and more convenience is attained by taking the second derivative of Equation 10.6a:

$$u_{int}''(x) = \int u_s(\xi) \Omega''(\xi-x) d\xi/\beta h \quad (A9)$$

Inserting Equation A8 into Equation A7 gives:

$$d_s(x) = \int \beta^2 u_{s0}(\xi) X(\xi-x) d\xi/\beta h \quad \text{with: } X = 0.5(\Omega - \Omega''/24) \quad (A10)$$

Equation A10 is the wall adaptation formula (Equation 10.7a) for the case that the walls are initially straight ($d_{s0}=0$).

If the wall adaptation is performed from a state of pre-adapted walls ($d_{s0} \neq 0$, $d_{a0} \neq 0$), the influence functions M and N must be known (Equations 10.7). M and N may be computed in the following way:

We consider the flow in an empty test section (test section without model). In this case the adapted walls will be straight, i.e. $d_s = d_a = 0$. We further assume that the walls are pre-adapted, but so that $d_{s0}(\xi)=X(\xi)$ and $d_{a0}(\xi) = \Lambda(\xi)$. With these assumptions Equation 10.7a becomes:

$$0 = \int \beta^2 u_s(\xi) X(\xi-x) + X(\xi) M(\xi-x) d\xi/\beta h. \quad (A11)$$

Using the transformation $\xi \rightarrow -\xi + x$ on the second part of the integral and considering that $X(-\xi)=X(\xi)$ and $M(-\xi)=M(\xi)$ we obtain:

$$0 = \int \beta^2 u_s(\xi) X(\xi-x) + M(\xi) X(\xi-x) d\xi/\beta h \quad (A12)$$

Equation (A12) suggests that $M(\xi) = -\beta^2 u_s(\xi)$. Thus, by computing the flowfield in an empty pre-adapted test section with $d_{s0}(\xi) = X(\xi)$, the wall velocity $u_s(\xi)$ is generating the function $M(\xi)$. The computation of $N(\xi)$ is analogous.

For the case of a square test section ($b/h = 1$) the functions Ω , Γ , X and Λ were computed numerically and tabulated by Lamarche & Wedemeyer [20]. Plots of these functions and functions M and N are shown in Figures 10.B1 to 10.B3. The symbols indicate computed values, the lines are analytic interpolations fitted to the numerical curves. For fast computations of wall interferences and wall deflections it is advantageous to use analytic functions rather than tables of the influence functions. (Using tabulated values necessitates time consuming interpolations). The use of algebraic functions approximating the numerical curves have reduced the computing time by orders of magnitude. The approximating formulas are shown within the figure captions. They are derived with consideration of global conditions as the correct value of the integral and asymptotic behaviour at infinity. The parametric constants have been adjusted to yield the best fit.

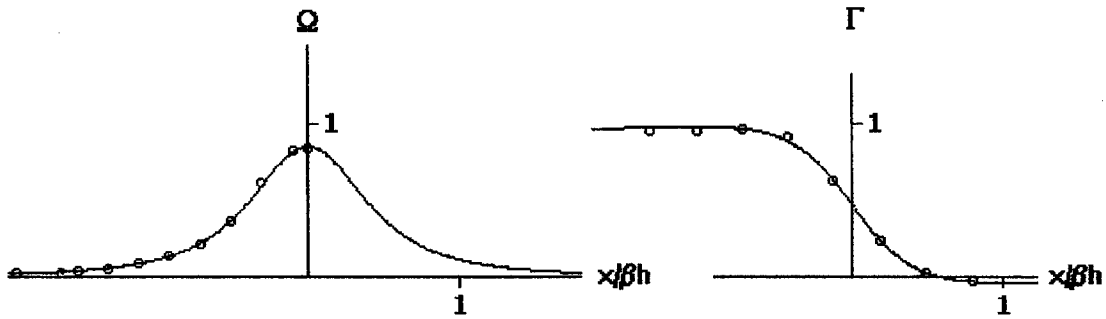


Fig.10.B1 Influence functions Ω and Γ . Symbols: numerical values, lines: interpolation formulas:
 $\Omega = e/2/(e+x^2)^{3/2}$, with: $e=0.346$; $\Gamma = e_1 + e_4 x/(e_3+x^2)^{1/2} - (e_1+e_4) x/(e_2+x^2)^{1/2}$ with: $e_1=0.47$,
 $e_2=0.40$, $e_3=0.60$, $e_4=2.0$. $x = x/\beta h$.

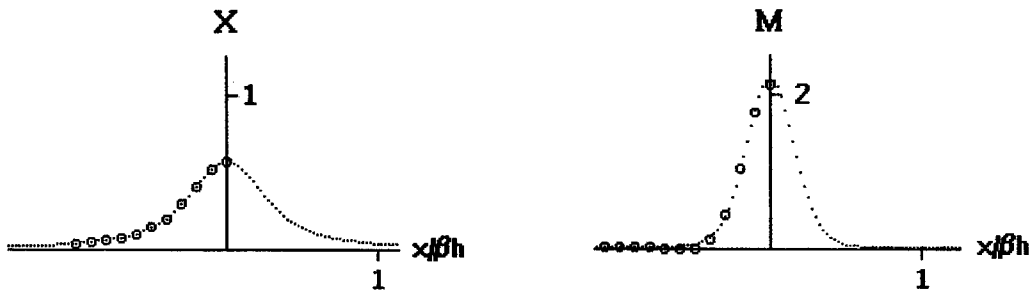


Fig.10.B2 Influence functions X and M . Symbols: numerical values, lines: interpolation formulas:
 $X = e/4/(e+x^2)^{3/2} + e(e-4x^2)/32/(e+x^2)^{7/2}$ with $e=0.346$, $M = e_1/2/(e_1+x^2)^{3/2} + e_3(e_2-4x^2)/(e_2+x^2)^{7/2}$
with $e_1=0.22$, $e_2=0.22$, $e_3=0.026$. $x = x/\beta h$.

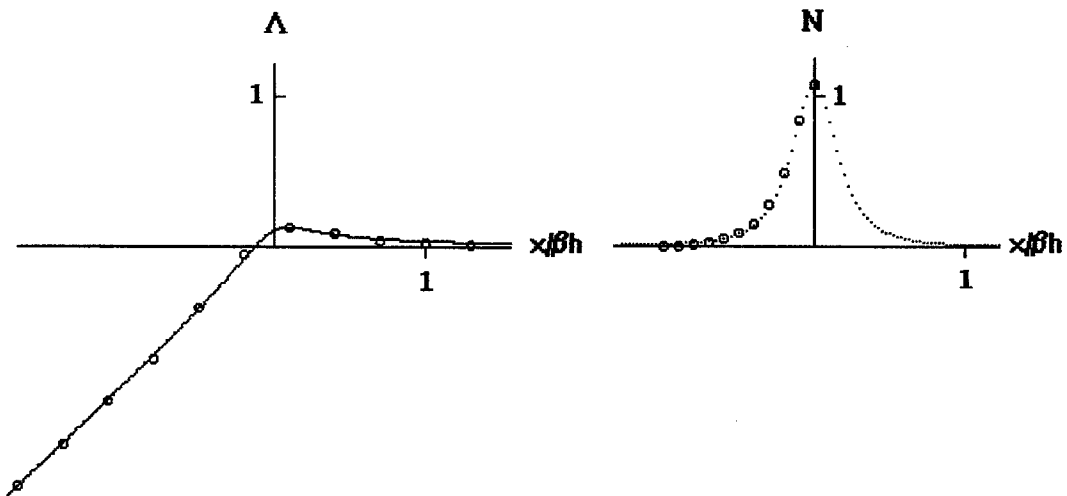


Fig.10.B3 Influence functions Λ and N . Symbols: numerical values, lines: interpolation formulas:
 $\Lambda = c_1 x + c_4(c_3+x^2)^{1/2} - (c_1+c_4)(c_2+x^2)^{1/2}$, with: $c_1 = 0.47$, $c_2 = 0.03$, $c_3 = 0.09$, $c_4 = 1.5$.
 $N = e_1/4/(e_1+x^2)^{3/2}$, with $e_1 = 0.055$. $x = x/\beta h$.

11. ADDRESSING UNCERTAINTIES IN WALL CORRECTIONS

11.1 INTRODUCTION

The previous ten chapters of this report have served to indicate the progress in wind tunnel wall correction technology during the thirty years since the publication of AGARDograph 109 by Garner, et al. [14]. Although significant progress has been made, much of it due to the emergence of enhanced computational capabilities which have been used in conjunction with the wind tunnel and its data, the present status of the wall interference technology has certainly not yet matured for the high-speed, or high-blockage, or high-lift, or powered-lift, or time-dependent flows. These flows, discussed in Chapters 5-9, typically exhibit large gradients, may be particularly sensitive to small perturbations due to the critical non-linear transonic and/or viscous effects that are present, and perhaps are not even amenable to correction in conventional wind tunnels. On the other hand, the adaptive wall technology, developed during these intervening thirty years and discussed in Chapter 10, may provide a means for providing correctable data; but it has not yet become a "production-testing" capability. However, at its present level of development, this latter technology should prove to be an extremely valuable test bed for understanding and evaluating wall interference phenomena, concepts, procedures, and limitations, as indicated in sections 1.3.2 and 10.5, for example.

Chapters 2 through 10 have outlined models for estimating wall-induced interference effects for different types of aerodynamic tests and test section wall types; each chapter has most adequately presented associated model-specific limitations and constraints. Chapter 1 of this report addresses the major assumptions; many of the general limitations of wall corrections have necessarily been discussed there as prerequisite to selecting an appropriate correction methodology. Chapter 12 discusses limitations from the standpoint of "Future Necessary Work" required to eliminate them as constraints on current testing techniques and correction capabilities.

Customers are requiring better quality wind tunnel data; that is, data with its uncertainty quantified and reduced to acceptable levels. As already pointed out, current and continuing customer requirements for these data at higher Reynolds number, yet obtained faster and cheaper, places even greater demands on wall (and tunnel) interference corrections and the uncertainties in them. Understanding the limitations of wall corrections is relevant not only to the corrections themselves, but also to their range of applicability and their uncertainties. The present chapter focuses on understanding the sources of uncertainties and approaches to resolving those uncertainties associated with wall corrections and methodologies. These aspects will arbitrarily be divided into three groups, with a major section for each: the fundamental aspects, the experimental aspects, and the computational aspects, respectively.

The limitations discussion herein will be for a broad interpretation of the word. That is, one will not find quantitative information such as

Method A, based on pressure signatures measured at 25 stations along top and bottom wall centrelines in Wind Tunnel B, produces wake blockage corrections accurate to ± 0.001 for solid model blockage ratios between 0.3 and 0.6 at Mach numbers between 0.1 and 0.4 and chord Reynolds numbers around 3 million, adding \$20 K to the cost and two days to the tunnel test time. However, Method B

Ultimately, such quantitative information will be required for characterising both correction methods and facilities so that customers can make informed technical and economic decisions about wind tunnel testing options. As already seen in the previous chapters, such quantitative information is generally not available and it depends not only on the wall correction method, but also on the facility and its testing

procedures, staff, instrumentation, data reduction, quality control, costing algorithms, ... ; i.e., aspects governed by institutional and customer commitments and resources. In the broader sense, limitations follow from assumptions, model sophistication, and physical or economic constraints.

11.2 FUNDAMENTAL ASPECTS

While Whorric and Hobbs [25] have cited wall interference effects as a significant source of uncertainty in wind tunnel data, in the past frequent discussions have occurred over whether or not to apply wall interference corrections. These discussions centred around the belief that no correction (a quantity of zero magnitude and unknown uncertainty) is better than a correction of known magnitude and unknown uncertainty, particularly when the experiments were conducted at transonic conditions where any verifiable correction was obtained with difficulty. Many times corrections were accepted based on whether they moved the test results in the perceived right direction; otherwise, they were rejected. It is now known that this perception can be false due to non-linear effects caused by compressibility and/or viscous interactions (see Chapter 5). Furthermore, a correction could overshoot the free-air solution (or the “*true value*”) even if the sign is correct. Classical and conventional wall correction ideas and procedures generally work well for most subcritical flows and do provide guidance in the higher speed flow regimes. However, uncertainties have not been established for most of these latter correction procedures by a formal error propagation technique.

11.2.1 CONSEQUENCES OF THE FUNDAMENTAL ASSUMPTION

As pointed out in section 1.1, the fundamental assumption underlying the theory and practice of most wind tunnel testing is that

there exists an “equivalent” free-air or unconstrained flow to or with which the aerodynamic quantities measured under strictly controlled and defined conditions can be associated or applied.

The goal of wind tunnel wall corrections is to find or deduce this association.

11.2.1.1 REGARDING “ ‘EQUIVALENT’ FREE-AIR FLOW”

What must be recognised is that the equivalent free-air flow (i.e. the “*true value*” or the “*truth*”) can never be determined with exactness, whether this determination is made via experimental or theoretical means. Rabinovich [22] presents the following postulates of the theory of measurements:

- (1) the true value of the measurable quantity exists;
- (2) the true value of the measurable quantity is constant; and,
- (3) the true value cannot be found.

The basis for these postulates is that the modelling or measurement of any physical system is an imperfect act and that the randomness in the result will cause it to scatter about the true value.

Analytical knowledge about or realistic assessment of this equivalent free-air flow (i.e., the “*true value*”) remains elusive for all but perhaps streamlined flow about some simple shapes in physical flow regimes adequately described and approximated by linearised equations. Knowledge of this “*truth*” for realistic

configurations is the desired goal of wind tunnel testing and CFD analysis. Both schools of endeavour have means for approximating the truth as discussed in the next two sections and Chapter 12. Not knowing this truth, for little more than some simple flows, is a fundamental limitation in assessing the practical limits of validity and uncertainty in wall correction methods. In fact, as noted in Chapters 1 and 5, rigorous definition of just what property (or properties) should be constrained or matched (the equivalence condition) in order to establish this correspondence between wind tunnel and equivalent free-air flows is open to discussion.

Experimentally, aerodynamic quantities measured on very small models tested in large tunnels are generally deemed to be interference free and to represent "truth". Testing relatively small models at low speeds is deemed to produce a small (linear) perturbation from free-air flow with primary corrections for the freestream magnitude and direction. As the relative model size increases, gradients and other nonuniformities in the wall interference show up on the model; these residual variations in interference lead to residual corrections as discussed in Chapter 1. However, nonlinearities due to compressible and viscous effects can also occur and produce flow nonuniformities that are not readily separable from the residual wall interference determined by conventional correction methods. When viscous nonuniformities become more severe and begin to predominate, their effects must be modelled or accounted for in the correction procedure.

In addition, the decomposition of corrections into primary and residual is also influenced by the choice of equivalence condition. Concepts and ideas derived from linear flow and theory must be re-examined to find their limitations in correction methods for other flow regimes.

11.2.1.2 REGARDING "MEASURED AERODYNAMIC QUANTITIES"

Increasing demands on the accurate measurement of aerodynamic quantities of direct interest to the customer generally requires more accurate measurement of many other parameters and quantities such as those related to reference conditions, tunnel control, instrument limits, safety, model control, wall data, support data, statistical correlations and assessments, flow quality, etc. One must quantify the uncertainties with every measurement and procedure, formally propagating these errors in order to establish, via continued accumulation, a statistical estimate of accuracy of the measured aerodynamic quantities. In many processes, this uncertainty quantification may be achieved by end-to-end replication thereby capturing and accounting for variations in all environmental variables, which may not be included in the data reduction equations. Measurement calibrations must be done via fixed procedure in order to establish the repeatability and its credibility at strictly controlled conditions. In particular, use of boundary measurement correction methods, as introduced and discussed in Chapter 4 and in all those chapters that follow it, requires accurate data measurements near the test section walls.

11.2.1.3 REGARDING "STRICTLY CONTROLLED AND DEFINED CONDITIONS"

Strictly controlled and defined (flow) conditions means more than just producing repeatability; it implies a continuing statistical assessment and configuration control of the experimental techniques, procedures, and all related processes for both software and hardware. One does not produce accurate aerodynamic data without the strict control required to define the conditions and quantify the measurement uncertainties (Belanger [3]; Croarkin [13]).

11.2.1.4 REGARDING "CAN BE ASSOCIATED OR APPLIED"

The task of wall interference correction is to find or deduce the association between the aerodynamic quantities measured under strictly controlled and defined conditions and a corresponding equivalent free-air flow, if one exists! There is uncertainty (hopefully quantified) in the measured data, there is uncertainty (generally not quantifiable) in approximating the "truth" (equivalent free-air flow, however it is assumed to be known or represented), and there is uncertainty in satisfying the equivalence or matching condition. All of these uncertainties contribute to the absolute uncertainty in the wall correction. If one accepts the approximation of truth as the absolute truth, then some quantitative measure of the uncertainty in satisfying the equivalence condition must also be propagated with the measurement uncertainties through the correction procedure to get the uncertainty of the wall corrections. If this latter uncertainty is small, relative to the corrections themselves, then the measured flow could be considered correctable; i.e., the association can be made. If not, then one must be prepared to modify the fidelity of the correction procedure, adapt or shape the tunnel walls (see chapter 10), or perhaps even adapt the model itself and then try again or else quit! Criteria for assessing what flows are not correctable within a given facility's capabilities must be established and readily available on line during testing.

11.2.2 COMPATIBILITY OF HARDWARE, SOFTWARE, AND PROCEDURES

Conventional or classical wall correction methods, as discussed in Chapters 2 and 3, can be applied to measured wind tunnel aerodynamic data knowing only a few characteristic tunnel and model dimensions and flow conditions. These parameters size and locate the linearised flow singularities and their images, allowing one to calculate and superimpose flow solutions to obtain the interference field. Questions and concerns about the compatibility of the tunnel (hardware) and its procedures with the correction method (software) and its procedures were of little concern. However, with the advent of boundary measurement (Chapter 4) and adaptive wall (Chapter 10) methods for wall corrections, many compatibility issues appear and must be resolved. These run the gamut from the basic calibration and bookkeeping of corrections (discussed in section 1.2) through the automated, integrated control of adaptive wall tunnels. If the correctable-interference tunnel concept of Kemp [16], discussed in section 5.1.4, is to become a production reality, then the hardware, software, and procedures associated with tunnel operation, data acquisition, data processing, wall interference assessment, limited wall control, and wall corrections must not only be made compatible, but also integrated and automated. In view of the rate at which computer capabilities improve, modularization will be highly desirable. If one is to have a hierarchy of potential correction methods, each requiring different measured data, then optional hardware and procedures will also be needed.

Hardware, software, and procedural compatibilities are also required in regard to obtaining, quantifying, and maintaining the customer-specified uncertainties in the measured aerodynamic data and wall or tunnel corrections. Sloppy tolerances at only one point in the chain, whether due to hardware, software, or procedural uncertainties, lead to inaccurate results. Limitations in the wall corrections can result from incompatibilities in the hardware, software, or procedures. For example, if some required input data for a correction method is not measured, then it must be estimated, deduced, or effectively neglected. Solution of boundary value problems generally require boundary data on all the boundaries; and wall corrections are attempting to account for the wind tunnel's imposition of the constraining (wrong) far-field boundary values on the measured aerodynamic data.

11.2.3 CONSEQUENCES OF PHYSICAL AND ECONOMIC CONSTRAINTS

Trade-offs and compromises have and will continue to be made with respect to our modelling the required physical phenomena and the cost in time and money for modelling. When it becomes important to meet a specified small uncertainty in a simulation, then both physical and economic constraints become even more contradictory. The more accurate data at higher Reynolds number obtained faster and cheaper places severe demands on tunnel testing and corrections. This scenario will be accomplished by producing less data, but of much better quality. More time and effort will be put into customising (or should we say "customerising") the wind tunnel tests for obtaining the required results from among readily available testing options at a facility. Both institutional and customer commitment and resources will be required; lack of either, seriously cripples what can be done to obtain accurate aerodynamic data.

As pointed out elsewhere (Chapter 12, in particular) much can be done with regard to implementing those wall correction methodologies (hardware and software) presented in the previous chapters herein. However, such implementation involves a commitment of people and money, both of which seem to be dwindling in the wind tunnel and CFD disciplines recently. This situation is a limitation and will remain so until such time as the stakeholders and/or customers can be convinced otherwise.

11.3 EXPERIMENTAL ASPECTS

This section presents experimental aspects for establishing uncertainty limits on wall interference corrections. While some of the topics are not usually grouped with wall interference discussions, they are required in the larger scheme to address the issue of obtaining valid uncertainty limits. For instance, discrepancies in wind tunnel data caused by flow nonuniformities or stream turbulence have many times been attributed to tunnel wall effects, so tunnel flow field surveys are briefly discussed. The first section (11.3.1) presents traditional approaches to determining interference. This section includes caveats that restrict their sole use for establishing uncertainty limits. Also presented is a recent, promising technique which may alleviate many of these restrictions under certain circumstances. Next, the requirement to establish data credibility is discussed in section 11.3.2. Here, use of modern methods of statistical quality control (SQC) typical of those advocated by national standards laboratories are suggested to enable the consistent achievement of the required level of measurement accuracy. Having presented the requirement for SQC, section 11.3.3 discusses how a measure of the true value of the wall interference correction may be realised. The subject of "truth" is, also, discussed in Chapter 12, "Future Necessary Work". The approach taken there is slightly different from that presented here; however, they are complimentary and the subject matter emphasises the perceived needs and approaches as viewed by the different authors. Finally, section 11.3.4 presents the characterisation of the National Transonic Facility as a case study in addressing these aspects of establishing uncertainty limits.

11.3.1 TRADITIONAL APPROACHES TO DETERMINING INTERFERENCE

Traditional experimental approaches to assessing wall interference effects have included (1) a single model tested in multiple test section geometries (i.e., solid and ventilated walls in the same tunnel), (2) multiple sizes of geometrically similar models tested in the same tunnel, and (3) a single model tested in multiple size tunnels.

The rationale for the first method is that solid wall boundary conditions are known with greater confidence than ventilated wall boundary conditions; therefore, more accurate corrections of solid wall data to free-air conditions can be determined for subsonic Mach numbers. Corrections to ventilated wall data are, then, empirically obtained by indexing these data to the corrected solid wall results. Unknown coefficients in ventilated-wall boundary conditions are obtained by tuning the numerical models to match the data at low Mach numbers. These boundary condition coefficients are assumed invariant with Mach number changes, and, subsequently, are used to extrapolate the computations to high Mach numbers. The approach is limited by non-linear, closed-wall model blockage at high speeds; numerical and physical modelling of the wind tunnel, test model and support system; and the formulation of the boundary condition and its performance across the facility test envelope. A representative example of this method is the procedure used by Steinle to establish the porous slot boundary condition for the Ames 11-Foot Transonic Tunnel (see section 5.2.5).

The second approach assumes that results from multiple size models can be extrapolated to zero model-span-to-tunnel-width ratio to yield interference free flow and that incremental corrections may be determined as a function of model size and test conditions. The method assumes that models may be fabricated with sufficient accuracy to assure geometric similitude (to negligible uncertainty), that deformation under load is the same for all models, and that model Reynolds number effects are negligible. In this method, extreme care must be exercised to insure the proper accounting of model mounting and support system effects because base effects are critical for drag computations and moment matching which is dependent on stream curvature over the model aft region. Wall Reynolds numbers may be significantly different for matched model Reynolds numbers; an implicit assumption is that the wall boundary conditions are insensitive to these changes. This fact alone can mask aerodynamic interactions and make proper comparisons difficult. Empirical interference corrections established by Crites and Rueger for the Boeing (formerly McDonnell Douglas) Polysonic and Transonic Wind Tunnels incorporate many of these ideas (see section 5.3.2.2). Additionally, the combined experimental and numerical approaches of Crites and Rueger (see section 5.3.2) and Sickles, et al. (see section 5.3.3) use this method.

The third approach assumes that large-tunnel aerodynamic tests of relatively small models may be assumed nearly interference free and, as such, may be used as the baseline from which to index smaller tunnel results obtained with the same model (see section 5.3.2 and 5.3.3). Besides being highly dependent on the Mach number, this approach is probably the most difficult to assess because it generally encapsulates any reference facility bias within the resulting corrections. However, this third approach is a subset to a process which will be proposed later in section 11.3.3.

Each of these approaches allow the determination of a wall correction; but, none of them allow a direct assessment of the associated uncertainty (or limitations). For example, in the first approach, mathematical and physical limitations preclude establishing uncertainty limits; in the second approach, multiple models imply multiple mounting systems and probable differences resulting from Reynolds number effects; and, in the third approach, the large facility may impose a bias different from that of the smaller facility. Reported attempts to assess the uncertainty limits on wall corrections are few.

One promising approach to directly addressing the issue of allowable or acceptable variations in wall induced interference is that recently presented by Ashill, Goodyer, and Lewis [2] and Lewis and Goodyer [19], [20]. They used the two-dimensional adaptive wall tunnel at the University of Southampton in conjunction with Ashill's correction method (see Chapter 4). In this approach, the tunnel walls are iterated to convergence for flow about an airfoil. Then, known levels of blockage, blockage gradient, upwash, and stream curvature are experimentally introduced into the tunnel flow via appropriate incremental

positioning of the top and bottom walls. The recorded data are used in Ashill's correction method to assess the theory's ability to properly recover the converged-wall solution. An important distinction is made that proper interference assessment doesn't necessarily imply the ability to correct wind tunnel data, but only the possibility that the data may be correctable. It should also be noted that, while they specifically address issues of the correction methodology, their focus is not the issue of establishing interference free flow. Uncertainties due to tunnel bias such as tunnel flow angularity and blockage due to sidewall boundary layers and tunnel calibration coefficients are ignored.

11.3.2 ESTABLISHING DATA CREDIBILITY

Wind tunnel customers are presently demanding absolute transonic cruise drag accuracies of 1 count ($\Delta C_d = 0.0001$) or less, which may only be obtained if proper accounting of all dominant error sources is realised. To place this number in economic perspective, for aircraft such as the proposed High Speed Civil Transport, 1 drag count equates to 8 passengers or 60 miles of range. To place this number in technical perspective, experimentally resolving 1 drag count requires measuring angle of attack to 0.01 degree or Mach number to 0.001 (see Table 1 in Chapter 1). Note the use of "or" in the preceding sentence for if all uncertainty is assumed to reside in one variable, then the contributions of all other possible uncertainty sources must be negligibly small. Therefore, the actual resolution of the angle of attack and Mach number must be less than the cited values. A root-mean-square analysis shows that "minor" uncertainties must be the order of one half the value of the "major" (or dominant) uncertainty to contribute to the total uncertainty. Any experimentalist who has measured back-to-back polars recognises the achievement of this level of measurement precision as a particularly daunting task, requiring much care and adherence to standardised testing procedures. The task is further complicated when comparing data obtained in different tests of the same model in the same tunnel. Even the smallest of changes in the tunnel circuit (such as contamination on or a tear in a turbulence screen), modifications made in the tunnel plenum, or something as simple as changing the data sampling period and/or rate may yield results which can bias test results and generate greater than the allowable differences between the repeat tests.

Achieving this required high level of test-to-test consistency mandates the implementation of statistical quality control (SQC) methods to establish "data credibility" (Belanger [3]; Croarkin [13]; Taylor and Oppermann [24]). Implementation of SQC methods are atypical of past practices generally applied in aerodynamic laboratories, but implementation of SQC methods are now being addressed (Anon. [1]). SQC in a given wind tunnel implies that the mean values of aerodynamic measurements made on the same model over widely separated repeat tests will compare to within the required accuracy at a specified level of confidence (typically 95 percent). Credibility of test results implies ongoing statistical assessment and configuration control of the experimental techniques, procedures, and all related processes. It is important to note that even though they are part of the same rigorous treatment, measurement corrections such as those due to tunnel calibrations and those due to wall interference effects have not yet been explicitly considered in this discussion. If SQC has been achieved, and if the bias uncertainty effects of the walls are approximately constant for small configuration changes to the model, then traditional methods of incremental testing may confidently be pursued with only minimal impact of the walls on the test results.

11.3.3 DETERMINING THE TRUE VALUE OR "TRUTH"

Assuming that statistical quality control (SQC) has been achieved in the wind tunnel environment, the aerodynamicist may begin to rationally consider tunnel-to-tunnel, tunnel-to-computation, and tunnel-to-flight comparisons at the required accuracy levels. At this point, each data set must be referenced to an absolute baseline; therefore, each data set will require an assessment of and correction for the bias imposed by the tunnel walls and other tunnel specific effects such as differences in mounting systems, dynamic loads, stream turbulence, and flow angularity. The obvious question is "How good are the corrections?" In actuality what is being asked is "How much uncertainty is attached to the corrections?" or "What are the limitations?" This is a most difficult question to resolve because it requires the true value and it implicitly poses the question "How is truth determined?"

The subject of truth can be directly approached in at least three ways, each of which has limitations. First, truth can be approached via direct analytical or numerical computational fluid dynamic (CFD) solutions of the Navier Stokes equations or approximations to them. While valuable for establishing model problems and for looking at gross effects on very simple geometries, the analytical approach is extremely limited because of present day mathematical capabilities. Truth from a numerical perspective via CFD solutions of the Navier Stokes equations is limited by grid resolution, computational algorithms, computer power, and a fundamental lack of understanding in fluid physics areas such as transition, turbulence, shock wave/boundary layer interactions, and separated flow.

The second approach to attaining truth is via experimental simulations in the wind tunnel. While attractive on the surface, experimental methods are probably the most difficult of the approaches to execute. Proper experiment design must consider the facility and its ability to accurately simulate the flight environment, including setting and maintaining test conditions, stream steadiness and turbulence, acoustic environment, and flow uniformity. Instrumentation types, accuracies, and locations are critical, particularly in three-dimensions where obtaining the required amount of data may be prohibitively expensive or destructively intrusive to the flow. Test models for wind tunnel experiments designed to capture truth will be very expensive due to any special fabrication materials, the required machining accuracies, surface finish specifications, and the required onboard instrumentation. As an example, it is not unusual for models designed for the cryogenic high-Reynolds number environment of the National Transonic Facility at NASA Langley Research Center to cost on the order of a million dollars. The actual ability to simulate the flow as desired may be an issue. For example, it is known that the wall boundary conditions for ventilated wall tunnels are sensitive to Reynolds number (see Binion [5]); in fact, in section 5.2.3.2 it can be seen that the wall Reynolds number is explicit in the boundary condition. Ventilated-wall interference studies which test, for instance, geometrically similar full-size and half-size models must consider that the wall Reynolds number for the half-size model is double that of the full-size model at matched model Reynolds numbers. Additionally, consideration must be given to different dynamic loads at matched test conditions resulting in different model deflections and different force balance uncertainties.

The third approach to truth is also experimental via actual flight demonstration tests. The cost of the flight program may be prohibitively expensive because of availability and operational costs associated with the aircraft, its required support staff, and the instrumentation requirements. Additionally, the required measurement accuracy may be unobtainable due to an inability to adequately resolve flight conditions such as dynamic pressure and aircraft attitude. As another flight test example, drag on a single "representative" vehicle selected from the fleet is determined by measuring fuel flow and consumption in the engine. In multi-engine aircraft, the single engine fuel-consumption results are assumed to hold for all engines. Currently, drag in flight can only be measured to within a few percent (ex., Paterson [21]).

The previously cited and limitation-filled ways of establishing truth in actuality point to a fourth approach which is not intuitively obvious; that is, to set a standard or to simply *declare truth*. In this approach, a consortium of test facilities/organisations (for example, those which conduct transonic performance testing on transports, or those which test fighters) would establish representative test conditions where a common check-standards model(s) would be tested. Each organisation would then analyse and correct their data using the techniques and the boundary conditions (empirical, analytical, or measured) which best describes their facility. All participants would be required to document their data, test procedures, correction methodology, and results for scrupulous examination by the consortium members. Strict adherence to SQC standards would necessarily be required to ensure data credibility. Upon acceptance by the standards committee, the results from all participants would be averaged and declared as truth. The variation about this *truth standard* would be used to establish associated uncertainty limits. Significant deviations from the mean could, then, be used as a measure of goodness and used to allow the critical assessment of where correction methods breakdown and where further research is warranted. The most significant limitations associated with this approach are institutional. This approach requires long-term management support and commitment in terms of funding, and, most importantly, the investment in knowledgeable personnel who will develop, implement, and maintain both SQC and wall interference correction methods. Additionally, technical limitations such as the installation of sufficient instrumentation and standardised data reduction techniques must be addressed. As a side note, results from these studies could be used to establish an advocacy position for facility funding and further investment in testing techniques.

11.3.4 CHARACTERISATION OF THE NATIONAL TRANSONIC FACILITY

After the occurrence of any significant change to a wind tunnel circuit, facility calibrations are in order to verify/establish the tunnel performance envelope and fan map. At the time of this writing (January 1998), the National Transonic Facility (NTF) is coming on line after a major upgrade which included the installation of a new drive system. This section presents an overview of the action plan which is currently underway in the NTF for defining the operational envelope, evaluating the system and aerodynamic uncertainties, and ensuring data quality. Ensuring data quality requires that all identifiable uncertainties be quantified, including those introduced by the presence of the wind tunnel walls. Obtaining the desired outcome of fewer data of higher quality at a higher rate (see section 11.2.3) emphasises the establishment of this approach. The previous section presented a procedure for establishing the true value of an interference free flow; this section discusses the activity which initiates that procedure in the NTF as an example of the process which must be undertaken to ensure the acquisition of high quality aerodynamic data.

11.3.4.1 THE TEAM

A team was formed prior to the 1997 facility upgrades to calibrate the NTF when it returned to active status; the team ultimately expanded to 13 full members and 5 consulting/specialist members as requirements were developed. NTF customers were invited to participate fully in all phases of the process, including planning, review, testing, and analysis. Weekly team meetings were held to formulate goals, to establish realistic objectives, and to define areas of responsibility. Most importantly, these weekly meetings were necessary to build a cohesive working relationship from a diverse range of technical backgrounds, to obtain individual buy-in to the process, and to establish working-level

communications. A wide range of disciplines was included early in the planning to ensure that as many issues as possible would be addressed and to minimise surprises which typically occur in this type of activity. Included were managers, test engineers, research engineers, scientists, technicians, and data systems personnel; the areas of expertise covered were statistical quality control and measurement uncertainty, wall interference, tunnel calibration, tunnel flow quality measurement, models, instrumentation, tunnel simulation and scheduling, and dynamics. Team communications and getting everyone understanding the same technical language is extremely important to success; for example, in this project, each discipline had a different unique definition of *tunnel empty* and this greatly affected test planning.

11.3.4.2 THE APPROACH

The approach of the team was to create a virtual future by defining the desired outcome, then to build backwards to determine how the outcome was achieved. This simple approach focused the team on actual requirements in test planning, priorities, and implementation. Data accuracy requirements for performance testing were established in partnership with the customers; these requirements are given in the following table.

TYPE OF TEST	INCREMENTAL	ABSOLUTE
High lift	0.2% C_L and C_D	0.4% C_L and C_D
Transonic cruise	1/2 count C_D	1 count C_D

The team was forced to recast its mission in the light of data quality upon recognition that a traditional wind tunnel calibration combined with wall interference corrections was insufficient to meet these requirements and to produce certifiable world-class results on a continuing basis.

In reality, a *characterisation of the facility* was required to achieve the overall goals. This characterisation was composed of many individual tests grouped in four general categories, or thrusts. These thrusts, which are distinguished in the next section, are (1) the standard, centreline calibration, (2) flow quality, (3) measurement uncertainty assessment, and (4) tunnel wall interference corrections. Implementation of statistical quality control methods was recognised as the only viable approach to achieving and maintaining the goal of certifiable data quality. By its very nature SQC is an ongoing, periodic process; it, therefore, allows and mandates continuous improvement. Recognising this distinction allowed a very success oriented approach to be assumed since problem areas which will occur can be re-addressed by the ongoing commitment to periodic testing.

11.3.4.3 CHARACTERISATION

As previously stated, the tunnel characterisation is divided into four categories or thrusts which are described in this section. Activities and tests in each of these thrusts are to be repeated on a continuing basis, some more frequently than others. It is recognised that many of these activities are not traditionally related to either wall interference or wind tunnel calibration; however, in order to establish uncertainty limits on corrections, it is necessary that each of the areas be considered in the process. Additionally, if

statistical quality control is to be achieved, all of these aspects of the facility must be documented, and improvements and changes must be made in the light of their impact on data quality.

11.3.4.3.1 Thrust I – Tunnel Calibration.

The objective of this thrust is to perform a traditional calibration of the tunnel over the test envelope. This is accomplished by measuring the static pressure distribution over the length of the test section using a centreline pipe and along the tunnel walls using pressure orifices. Measurements of total temperature and total pressure from which flow conditions are established will be made in the settling chamber, as will static pressure in the plenum. The results will be used to obtain the longitudinal Mach number distribution. In the future, this activity is anticipated to occur every three to four years, or as significant changes to the tunnel mandate.

11.3.4.3.2 Thrust II – Flow Quality.

Thrust II is a multi-test series of experiments designed to assess the uniformity and steadiness of the flow at the tunnel cross section corresponding to the model centre-of-rotation. In the first test, a rotary rake will be used to determine distributions of temperature, pitot pressure, and flow angularity. While this is an important first step for quantifying any flow nonuniformities, the complete numerical modelling of the test section will ultimately require both upstream and downstream surveys to be performed for use as farfield boundary conditions. Performing these types of surveys is most difficult, particularly in a cryogenic nitrogen environment, and it is hoped that future advances in non-intrusive flow diagnostics will progress at a rate sufficient to aid this task.

In the second test, turbulence and flow unsteadiness will be measured via hot wire and fluctuating pitot pressure sensors in the settling chamber and test section. When scaling high-Reynolds number tunnel data to flight, a mismatch between shock locations can occur if the facility Mach number is incorrect due to wall-induced blockage or an inappropriate choice of reference pressure. Shock location may also be erroneous if the turbulence level is too high, resulting in premature transition to turbulence, thereby changing effective body shape. These measurements provide quantitative data upon which an assessment can be made.

Finally, in the third test, the tunnel wall boundary layers will be obtained using pitot pressure boundary layer rakes. These measurements will be made ahead of the test section in the contraction and on a solid sidewall and on a slotted wall in the test section. Additional future experiments are anticipated such as the development of a check standard model which is sensitive to variations in stream turbulence.

11.3.4.3.3 Thrust III – Measurement Uncertainty Assessment

Measurement uncertainty will be regularly evaluated two to four times each year by testing two different check standard models. The data generated by a single test of the check standard models will be combined with data from previous test entries to generate control charts for statistical assessment of data quality. The first check standard model is a pitot-static probe used to provide a single-point measurement of total, static, and dynamic pressures at the model centre-of-rotation. Measurements made during this test and during frequent, periodic re-tests will be used to determine the stability of the tunnel calibration and to establish its reproducibility (variation over time), thereby characterising uncertainty limits on the dynamic pressure. When the NTF was built, two geometrically similar models (60-inch and 30-inch wing spans) of a generic transport configuration known as the Pathfinder I (PFI) were built to evaluate tunnel wall interference effects. The larger model, which is instrumented with pressure orifices on the wing, is

being removed from inventory as a general test bed for aerodynamic studies and is being reserved as the second check standard model. Frequent periodic testing of this model will be used to create an aerodynamic database to monitor all processes and subsystems associated with wind tunnel testing; including model installation, tunnel processes, instrumentation, data acquisition and reduction software, integrated tunnel flow angularity, pressure and aero-data repeatability.

11.3.4.3.4 Thrust IV – Wall Interference

The wall interference thrust is divided into several continuous improvement phases which, initially, are application and implementation of current technologies, followed by phases which concentrate on quantifying uncertainties and extending assessment techniques. The objective of the first phase is to tune the tunnel systems to enable on-line, post-point wind tunnel wall interference assessment and correction (WIAC) of standard performance aerodynamic tests. Typically, wall pressure measurements have been second tier measurements which were acquired if available and only if their acquisition did not inhibit the rapid acquisition of first tier data such as tunnel parameters and model forces and pressures. Because of their lower status, little attention was given to the quality of the measurement. Orifices were not protected and instrument calibrations were not monitored. With the implementation of boundary measurement methods for determining the interference effects of the walls, wall pressures must be elevated in importance to obtain wall corrections of the required accuracy. A significant effort is being expended to bring the NTF wall pressure system to first tier instrument status. This system includes an electronically-scanned pressure measurement system, temperature-controlled containers for the pressure scanner modules, and over 500 wall pressure orifices on 16 rows around the test section periphery. Raising this system to first tier status includes properly identifying, cleaning, and repairing all orifices, performing a leak-check verification, and continually monitoring the instrumentation calibrations. Empty tunnel pressure signatures will be obtained to ensure proper symmetry exists in the wall data, and to establish a pressure-signature baseline from which to assess orifice bias effects and generate tares. The model support system will be exercised over the angle of attack range to evaluate its effects on the tunnel-empty pressure field and to enable proper separation of these effects from those generated by the model.

In the second phase, preliminary data with the large PFI model installed will be obtained to assess model-plenum interaction effects on the tunnel calibration. These data will allow the proper specification of the tunnel reference pressure, whether the plenum pressure is sufficient or whether a more stable upstream value on the tunnel wall must be used (see section 5.2.4.3.5). All these data are required to rationally implement the PANCOR code (Kemp [17], [18]); see, also, section 5.3.1.1) in an on-line, post-point computational mode. Preliminary data to assess the effects of compressibility on wall pressure and drag rise in the NTF for a body of revolution will be generated by removing the wings from the PFI model and testing only the fuselage through Mach 1.

A third-phase series of experiments is being planned to advance the state of the art to the point where uncertainty limits can be placed on the interference corrections. This third phase will include tests of both the full-scale and the half-scale PFI models with the test section in both solid-wall and slotted-wall configurations.

11.4 COMPUTATIONAL ASPECTS

A number of fundamental aspects related to limitations in computation of wall corrections have already been discussed in section 11.2 and will not be repeated here. The major computational thrusts related to wind tunnel wall interference correction technology will be summarised in the first sub-section. Much has been said throughout this text about the importance of and need to define uncertainty in measured aerodynamic data for the customer. Since, at high Reynolds number, this desired data may well be subject to significant wall corrections, then their uncertainties must be assessed. The second sub-section discusses sources of uncertainty in CFD based interference correction procedures. The third sub-section suggests how formal sensitivity analysis via automatic differentiation (AD) may be used to aid in assessing these correction method uncertainties quantitatively for the modern measured-boundary-data interference procedures which are frequently CFD based.

11.4.1 MAJOR COMPUTATIONAL THRUSTS

The rapid development and advancement in computational capabilities, with respect to both hardware and software, have certainly found application in the wind tunnel testing and interference correction communities. These capabilities have created the possibility for better pre-test wall interference prediction, rigorous post-test wall interference assessment and correction, and greatly reduced interference testing in adaptive wall wind tunnels. The major computational thrusts in wall interference since the time that AGARDograph 109 was published by Garner, et al. [14] have paralleled developments in CFD and those technologies supporting the adaptive wall concept. These thrusts have been to provide:

- (a) rapid calculation of conventional corrections;
- (b) more realistic analytical modelling of tunnel wall geometry and boundary conditions, test article geometry, and model support systems;
- (c) initial application of these more realistic analytical models in both numerical tunnel simulations and wall interference assessment/correction methods;
- (d) prediction and control of wall adaptation in adaptive wind tunnels;
- (e) design assessment of ventilated test section walls; and
- (f) research studies related to correctability and its limits.

All of these computational thrusts have been discussed throughout the previous ten chapters. The assumptions, approximations, and empirical or analytical models used in specific computational approaches have generally been concisely stated in the first section or so of each chapter. The various results presented have essentially served to illustrate a given computational capability and its status. For many of the traditional models (simple wall, support, and configuration representation) and linear or full potential CFD approximations, a number of these capabilities have been reasonably well investigated and applied to real tunnel data, as seen in Chapters 2, 3, and 4 and in a few examples given in later chapters. However, for more advanced CFD algorithms and complex flow regimes, few of these capabilities have been extensively exercised or verified using real tunnel data. Limitations with respect to range of application for reasonable corrections and uncertainty in these corrections, therefore are not known.

Most of these major computational thrusts involving advanced CFD algorithms have been exploratory applications and investigations which have emphasised the physical possibility of performing the computational task as opposed to reducing it to practical feasibility. As pointed out in Chapter 12, much of the stage is set for implementation of many of these major computational tasks into what is to be the production testing environment. As already seen in the previous chapters, the modern measured-boundary-data correction methods for 3-D flows have not been verified using extensive data; there are very few adequate data bases and more are needed. Experimental uncertainty in the measured-boundary-data must be assessed, as discussed in section 11.3, for example, and propagated through the entire correction procedure to obtain an uncertainty for the correction.

11.4.2 UNCERTAINTY SOURCES IN CFD BASED CORRECTION PROCEDURES

Analytical or numerical models, at one degree of complexity or another, are used in all wall correction methods. In those that employ CFD, the levels and interaction of models are compounded so that establishing sources of inadequacy or uncertainty may be very tedious and, if located, may also be difficult to assess, modify, or correct. Typically, models are constructed empirically or analytically, guided by first principles, basic conservation laws, or assumed basis functions. The parameters in these models are determined by approximately matching or reproducing basic experimental or observed data. Then these models, generally with the determined parameters fixed, are used to predict or analyse (i.e., interpolate or extrapolate) the "fitted", dependent, output data for varying independent input data. The model may be a solution procedure or algorithms, or contain an algorithm, or require one for computation. These latter models also require parameters and input for controlling the procedure (such as discretisation, convergence, etc.). The variety of models already included in a CFD flow analysis code of interest here, for example, might include those for boundary conditions (such as tunnel walls, far-field free-air, test article geometry, and support geometry), fluid-flow conservation laws, solution algorithms, turbulence modelling, and elastic response. A wall correction procedure, particularly a non-linear CFD-based one, will then link two or more numerical CFD solutions subject to an equivalence or matching condition in order to compute corrections.

For a numerical model, the sources of uncertainty or error can be ascribed to those in the input data and those of the model. Model uncertainties arise due to inadequacies in the model's approximations (i.e., assumptions, rules, conservation laws, basis functions, etc.) to mimic physical reality and the uncertainties in the parameters which characterise the model (for instance, size and location of singularity strengths, coefficients of basis functions, and observed data). Assessing the model prediction uncertainty due to the inadequacy of the model approximations is a validation exercise requiring a measure of the physical truth or reality. If one has the latter and the model predictions are deemed inadequate, then, either bounds are established for acceptable tolerances or another model is obtained. These bounds for basic models, are assumed established at their development; however, when many basic models are coupled together, verification or validation is more difficult to assess or obtain. A number of the computational thrusts referred to in section 11.4.1 have involved such studies. As indicated elsewhere herein, a given model (or a collection of models) may be defined as truth for assessing relative prediction effects and uncertainties in the context of wall corrections where the truth is elusive.

Quantifying the uncertainty in a model's input data, or its parameters, is assumed to be done experimentally, for example, in a characterisation of the facility and its instrumentation (as discussed in section 11.3), or reasonably estimated sufficiently well. Some spatial or temporal dependence or

functional form, or modelling, of the uncertainty may also be known and required in order to propagate the uncertainty. For a method which determines wall corrections, using input data and parameters for many models, one needs to understand and be able to numerically quantify uncertainties in these output wall corrections for given (known) uncertainties in the input data and model parameters. Conversely, perhaps, it is desirable to be able to estimate allowable input and parameter uncertainties required to obtain a desired wall correction uncertainty.

Assessing the model prediction uncertainties due to those in model input data or model parameters is very tedious if errors are formally propagated and may be computationally very expensive if done by numerical perturbation, whether finite difference or statistical based. Jitter programs, as discussed by Coleman and Steele [12] for example, have recently been used to generate finite difference approximations to the partial derivatives needed in uncertainty analysis of experiments. Essentially, the data reduction computer program (a model) is perturbed with respect to each of its input and parameters (by the uncertainties in each) in order to obtain the individual influence of each on the output result(s). For a wall correction procedure (a model) which is not too computationally complex nor expensive to execute, this jitter procedure, which is a finite difference sensitivity analysis, may be feasible.

When a number of numerical models, within a single computer code or several computer codes are sequentially linked or iteratively coupled (i.e., one model's output is another model's input and vice-versa), then assessing the uncertainty in the ultimate predicted output due to those of an intermediate model's input and parameters is extremely difficult. In addition, the linking and coupling algorithms will introduce more uncertainty through their input and parameters, for example the tolerance required to satisfy the matching or equivalence condition.

11.4.3 SENSITIVITY ANALYSIS FOR CORRECTION UNCERTAINTY ASSESSMENT

Sensitivity analysis is a method of assessing the sensitivity of a model's output with respect to its input data or internal parameters. It involves obtaining an estimate of the partial derivative of the output with respect to a given input or parameter and can be accomplished experimentally, analytically, numerically, or by some combination, depending on the nature and complexity of the model. If the model is in the form of a computer code (i.e., FORTRAN or C), then automatic differentiation (AD) or computational differentiation (Griewank and Corliss [15]; Berz, et al. [4]) is a practical, robust means for obtaining sensitivity derivative (SD) information. As can be seen from the papers included and references cited in these two SIAM conference proceedings, this mathematical/computational technology has a well established history (Rall, [23]) and is a continuing interdisciplinary activity with many varied current applications. Our interest here is in what has been done with realistic CFD models and how this information can be used in the wall correction methodologies, particularly in regard to the models and the uncertainty in their predicted output results.

The interest in multidisciplinary design optimisation of aerospace vehicles prompted the initial applications of AD to CFD codes by Bischof, et al. [6] using the emerging AD tool ADIFOR (Automatic Differentiation of FORtran) developed by Bischof, et al. [7], [8], [9]. In design optimisation, derivatives of CFD code output functions with respect to design variables are required. These design variables are generally parameters which specify boundary data or transformations to body-oriented co-ordinate systems. They become inputs to the CFD code through both inner boundary conditions such as geometric model shape and outer boundary conditions such as non-geometric flow variables. A brief summary of the early ADIFOR applications to a realistic, iterative CFD solver to obtain SD of lift, drag, and pitching moment with respect to non-geometric flow variables, CFD algorithm parameters, turbulence

modelling parameters, and geometric model shape parameters is presented by Carle, et al. [11]. Recent applications have extended these ideas and techniques to other complex CFD flow solvers used in the aerospace enterprise. To our knowledge, however, no one has yet applied AD to ventilated wall simulation models, wall interference prediction codes, or wall correction procedures to obtain the sensitivities of the interference field, corrections, etc. (i.e., the output) with respect to Reynolds number, porosity parameters, measured wall signatures, wall slope, etc. (i.e., the input). Such sensitivity analyses are essentially just different AD applications to CFD codes that have been demonstrated as being differentiable by ADIFOR; these computational sensitivity exercises should be done. However, with respect to the propagation of uncertainties in model input and parameters, a somewhat different approach is, also, suggested and outlined below.

AD has also been used to obtain error bounds or estimates for the function and its derivatives as can be seen from several papers included in Griewank and Corliss [15] and Berz, et al. [4]. This interest, although originating in rounding-error estimation, is of importance in the data assimilation for improved weather prediction models and also in beam physics stability and control. Typically, second derivative information has been utilised. However, an idea that should be of interest in propagating uncertainties for wall correction applications was demonstrated by Bischof, et al. [10] for an initial-value problem where they showed:

“By differentiating the output of a model with respect to its parameters, one can quantify how sensitive or robust the model’s predictions are relative to variations of that parameter, as well as gain insight into how to adjust parameters that are poorly known. Questions regarding the sensitivity of the model output to more abstract quantities involving many model variables can also often be rephrased in terms of derivatives, either directly or by embedding the problem of interest into a larger parameterised framework Our approach is an example of this latter approach: we obtain the TLM” (Tangent Linear Model) “evolution of a perturbation in the initial-value data by introducing a parameter that linearly interpolates between the unperturbed and perturbed initial states. We shall show that formal perturbation theory with respect to the parameter yields the TLM and can be shown to be equivalent to evaluation of the derivative with respect to the interpolating parameter.”

For the CFD boundary value problems in wall correction procedures, it is suggested that interpolating parameters, scaling the (known) uncertainties in model data input and model parameters, can be introduced and that differentiation of the model output with respect to these interpolating parameters would produce SD that directly provide a first-order estimate of the propagated uncertainty. That is, derivatives with respect to the model input and parameters provide the output sensitivity to those quantities at that solution; where as, derivatives with respect to the interpolating parameters, which scale the respective uncertainties in model input and parameters, can be related to the uncertainty propagated to the output at that solution.

11.5 CONCLUDING REMARKS

Traditionally, theoreticians/CFD code developers and wind tunnel test engineers have not always communicated well with each other. Wind tunnel corrections have typically resided in one camp or the other because they were either theoretical or empirical. However, a new paradigm is emerging wherein the determination of wall corrections is smearing the dividing line between these two different cultures. The analyst must now take the best from each, the theory and computational capabilities of the theoretician and the measurement techniques of the experimentalist, and combine them into a rational

methodology for reducing the wall-induced uncertainty in the test data. With this blending, the analyst must also recognise the limitations of each method and actively work to establish and refine the measure of truth. The increased demands for high accuracy data with well-defined uncertainty specifications and the push to scale wind tunnel data to flight Reynolds numbers require that CFD and SQC play definitive roles in wall correction methodology.

11.6 REFERENCES

- [1] Anon. 1995: Assessment of Wind Tunnel Data Uncertainty. AIAA Standard S-071-1995.
- [2] Ashill, P. R.; Goodyer, M. J.; and Lewis, M. C. 1996: An Experimental Investigation into the Application of Wind Tunnel Wall Corrections. ICAS-96-3.4.1.
- [3] Belanger, Brian 1984: Measurement Assurance Programs Part I: General Introduction. National Bureau of Standards (US) NBS SP 676-I.
- [4] Berz, M.; Bischof, C.; Corliss, G.; and Griewank, A., editors 1996: Computational Differentiation - Techniques, Applications, and Tools. SIAM, Philadelphia.
- [5] Binion, T. W., Jr. 1988: Potentials for Pseudo-Reynolds Number Effects. Chapter 2 in AGARDograph No. 303, Reynolds Number Effects in Transonic Flow.
- [6] Bischof, C.; Corliss, G.; Green, L.; Griewank, A.; Haigler, K.; and Newman, P. 1992a: Automatic Differentiation of Advanced CFD Codes for Multidisciplinary Design. *J. Comp. Sys. in Engr.* 3(6), pp. 625-638.
- [7] Bischof, C.; Carle, A.; Corliss, G.; Griewank, A.; and Hovland, P. 1992b: ADIFOR: Generating Derivative Codes from FORTRAN Programs. *Scientific Programming* 1(1), pp. 1-29.
- [8] Bischof, C.; Carle, A.; Corliss, G.; and Griewank, A. 1992c: Automatic Differentiation in a Source Translator Environment. in *International Symposium on Symbolic and Algebraic Computing 92*, Wang, P., editor, ACM, Washington, pp. 294-302.
- [9] Bischof, C.; and Griewank, A. 1992d: ADIFOR: A FORTRAN System for Portable Automatic Differentiation. *Fourth AIAA/USAF/NASA/OAI Symposium on Multidisciplinary Analysis and Optimization*, Cleveland, AIAA 92-4744-CP. pp. 433-441.
- [10] Bischof, C.; Pusch, G.; and Knoesel, R. 1995: Sensitivity Analysis of the MM5 Weather Model Using Automatic Differentiation. Preprint MCS-P532-0895, Mathematics and Computer Science Division, Argonne National Laboratory.
- [11] Carle, A.; Green, L.; Bischof, C.; and Newman, P. 1994: Applications of Automatic Differentiation in CFD. AIAA Paper 94-2197.
- [12] Coleman, H. W. and Steele, W. G., Jr. 1989: *Experimentation and Uncertainty Analysis for Engineers*, John Wiley and Sons, New York, pp. 158-160.
- [13] Croarkin, Carrol 1984: Measurement Assurance Programs Part II: Development and Implementation. NBS SP 676-II.
- [14] Garner, H. C.; Rogers, E. W. E.; Acum, W. E. A.; and Maskell, E. E. 1966: Subsonic Wind Tunnel Wall Corrections. AGARDograph 109.
- [15] Griewank, A.; and Corliss, G. 1991: *Automatic Differentiation of Algorithms: Theory, Implementation, and Application*. SIAM, Philadelphia.

- [16] Kemp, W. B., Jr. 1976: Toward the Correctable-Interference Transonic Wind Tunnel. Proceedings, AIAA Ninth Aerodynamic Testing Conference, June, pp. 31-38.
- [17] Kemp W. B., Jr. 1988: A Panel Method Procedure for Interference Assessment in Slotted-Wall Wind Tunnels. AIAA Paper 88-2537.
- [18] Kemp W. B., Jr. 1990: User's Guide to PANCOR: A Panel Method Program for Interference Assessment in Slotted-Wall Wind Tunnels. NASA CR-187479.
- [19] Lewis, M. C.; and Goodyer, M. J. 1995: Initial Results of an Experimental Investigation into General Applications of Transonic Wind Tunnel Wall Corrections. Second Pacific International Conference on Aerospace Science & Technology, Sixth Australian Aeronautical Conference, Melbourne. Vol. 1, pp. 71-80.
- [20] Lewis, M. C.; and Goodyer, M. J. 1996: Further Results of an Investigation into General Applications of Wind Tunnel Wall Corrections. AIAA Paper 96-0560.
- [21] Paterson, John H. 1981: Wind Tunnel/Flight-Drag Correlation. Wind-Tunnel/Flight Correlation—1981, NASA CP 2225
- [22] Rabinovich, Semyon 1995: Measurement Errors—Theory and Practice. American Institute of Physics Press, New York
- [23] Rall, L. B. 1981: Automatic Differentiation: Techniques and Applications, Vol. 120 of Lecture Notes in Computer Science, Springer Verlag, Berlin.
- [24] Taylor, John K.; and Oppermann, Henry V. 1986: Handbook for the Quality Assurance of Metrological Measurements. NBS Handbook 145.
- [25] Whoric, James M.; and Hobbs, Randy W. 1987: Hierarchy of Uncertainty Sources in Transonic Wind Tunnel Testing. AGARD-CP-429.

12. FUTURE NECESSARY WORK

F. STEINLE, R. CRITES, A. KRYNYTZKY, T. BINION

	PAGE
12.1 INTRODUCTION	12-3
12.1.1 NEAR TERM OBJECTIVES	12-3
12.1.2 FAR-TERM OBJECTIVES	12-6
12.2 AREAS FOR EMPHASIS, VERSUS EXPECTATIONS	12-7
12.2.1 BETTER UNDERSTANDING OF APPLICATION OF WALL INTERFERENCE	12-7
12.2.1.1 INCREMENTAL CORRECTION VS ABSOLUTE CORRECTIONS	
12.2.2 DEFINITION AND MEASUREMENT OF BOUNDARY CONDITIONS	12-11
12.2.2.1 FORM TO USE FOR WALL BOUNDARY CONDITION	
12.2.2.2 VISCOUS EFFECTS	
12.2.2.3 UPSTREAM BOUNDARY CONDITIONS	
12.2.2.4 DOWNSTREAM BOUNDARY CONDITIONS	
12.2.3 COMPUTATIONAL METHODOLOGY, ASSESSMENT AND VALIDATION	12-14
12.2.3.1 TEST CONDITION CORRECTION TO REFERENCE CONDITIONS	
12.2.3.2 HIGH LIFT	
12.2.3.3 PERFORMANCE TESTING	
12.2.3.4 STABILITY AND CONTROL TESTING	
12.2.3.5 BUFFET AND UNSTEADY AERODYNAMICS	
12.3 COUPLING OF WALL INTERFERENCE WITH OTHER PHENOMENA	12-19
12.3.1 COMPRESSIBILITY EFFECTS	12-19
12.3.2 VISCOUS EFFECTS FOR HIGH LIFT AND TRANSONIC INTERACTIONS	12-19
12.3.3 SUPPORT INTERFERENCE EFFECTS	12-19
12.3.4 TUNNEL NON-UNIFORM FLOW	12-20

	PAGE
12.4 REDUCTION OF WALL INTERFERENCE	12-20
12.4.1 PASSIVE WALL DESIGN	12-21
12.4.2 VARIABLE CHARACTERISTICS WALL DESIGN	12-21
12.4.3 ADAPTIVE WALLS	12-21
12.5 SUMMARY OF RECOMMENDATIONS	12-22
REFERENCES TO CHAPTER 12	12-24

12. FUTURE NECESSARY WORK

**„They're difficult things, wind tunnels, aren't they!"
Pat Ashill, 17 January, 1995**

12.1 INTRODUCTION

The subject of wall interference dates back over 75 years. Developments in understanding and in methodology of applying wall corrections have more or less kept pace with progress in developmental testing of aircraft to the point that wind tunnel test programs, in general, have not come to grief for want of a better method. The future is changing and, as competition heightens the need for higher quality data to reduce uncertainty (e.g., in predicted performance), we discover more and more that wind tunnels are indeed *difficult things*. This is particularly true when testing models of large size either at highly loaded conditions or high subsonic speeds. Assessing and correcting test results from these large models for wall interference effects to provide a data accuracy commensurate with the objectives of the test is particularly challenging. Validation of any method of correction to be used is always of consideration. Measurement accuracy, numerical accuracy and accuracy in capturing the essential physics of the flow are concerns. Linear-theory based corrections, although highly useful, are increasingly becoming insufficient as are Euler methods, even when coupled with integral boundary layer representations of viscous effects. Further, the need to include details of the tunnel empty flow field, the tunnel geometry (especially the down-stream features), and a representation of the wall boundary conditions that is sufficient to capture the essential viscous features is becoming more apparent. The foregoing chapters of this report have provided the reader with an excellent reference source concerning current wall interference technology as well as a systematic approach to selecting an application. The question as to What Next? naturally arises. The following discussion is an attempt to address some of the issues which have come to light in this regard.

12.1.1 NEAR TERM OBJECTIVES

Near term objectives are considered as those objectives that are achievable now with current capability and that provide a measurable improvement in wall interference prediction and control. Therefore, by definition, these objectives are the ones that should be worked now. The need to continue working wall correction issues is self-evident to those working this discipline. It is not always self-evident to others who should be aware (e.g., test engineers, managers, etc.). To help put the need to develop and use wall-corrections in proper focus for all affected parties, it is suggested that an activity be undertaken to develop a measure of benefits to be derived from wall interference technology. Such benefits should be presented in customer-important terms such as reduced uncertainty in global quantities (Mach number and angle of attack), distributed distortions (induced velocity vector), and a measure of impact on force coefficients (historical results for specific cases tested). Failure to properly appraise the potential customer has an impact of the ability of work the discipline of wall corrections. For instance, to develop wall correction technology requires a funding

source which either must come from some form of general overhead, or be a direct charge to each test in addition to the cost of utilisation of wall correction capability. Thus, in the case of direct charges, the customer who will be the recipient of the corrections will be presented with a range of cost choices depending on what corrections, if any, are utilised. Unless the customer becomes accustomed to supporting these costs and understands the accrued benefits, the services will be under-utilised. In consequence, the budget allocation for wall interference development work is jeopardised. These cost considerations argue for a method of demonstrating that the benefits of having and applying wall corrections outweigh their cost. Mounting economic pressures on institutional activities which seem to be globally typical within the testing community indicate that being able to show benefits against costs is an urgent near-term need.

The preceding chapters of this report serve to bring the reader up-to-date on the technology of wall corrections. They also indicate how complicated wall corrections can be. And, as detailed in Section 12.2, there can be unresolved issues, even in classical methods. A particular example concerns drag increments due to tunnel-induced gradients. A new formulation has been applied successfully to bluff bodies (see Hackett [15] and Chapter 6) yet it conflicts with the classical result of AGARDograph 109 and with the result given in Chapter 1. Since Hackett's derivation is general and produces similar results to the accepted treatment of Maskell, this creates an issue for resolution in the validation for use of the methods in question. The topic is discussed further in Section 12.2.

Testing and user organisations have very few people who have conversant knowledge of data corrections in general and wall corrections in particular. Consequently, there is a community need to instill expertise in wall correction methodology in new personnel. An advocacy position is needed as well as a structured approach to becoming conversant in the wall correction methodology. The preferred media would be some form of "expert system" that employs "computer-aided" techniques for one to become self-taught along with access to a collection of "user-friendly codes" and data bases for computing or estimating wall corrections. Further, such media should have a means for growth to rapidly and efficiently incorporate new information. A simple form of the implementation of this concept is an electronic version of this report utilising an appropriate introduction, including terminology and a summary of benefits indicated above. The references contained herein along with the general discussion can then direct the user to specific sources for further consideration.

Regarding correction methodology, economic considerations call for corrections that are fast to produce and cost-effective. The implication according to Lynch, et al, is "... a collection of methods and techniques with various amounts of empiricism specialised for certain types of tests and specific kinds of wind tunnel walls and testing ranges." Having such a "collection" implies a method for cataloguing as well as a means for adding to the collection. The view taken here is that such a collection would not just be a compendium of various schemes with an assessment for each scheme, but would also include either reference to a specific code or data base or access to the actual code and/or data base as well. It is proposed that in the near-term, a standard means of assessing the range of applicability (model and tunnel configuration, Mach number, attitude, Re , etc.) be developed for verifying wall correction methods and data bases and, where permissible, the originator of the method (including any code) and custodian of the data base make the information commercially available. Notification of the method or any data base information should be accomplished through appropriate media (AGARD, GARTEUR, STA, SATA, AIAA, ASME, etc.)

Global competition for new aircraft forces the designer to work all technology areas that could contribute to higher quality performance predictions. There are numerous error sources affecting high quality predictions.

Many of those error sources were discussed in AGARD AR-304 [1]. This document is focused on only one of those error sources, wall interference, which can be a major contributor to data uncertainty. A better understanding of wall interference is very desirable, particularly as model and model support sizes are increased to maximise Reynolds numbers for a given test facility and as testing speeds are increased toward sonic conditions. It is particularly important to be able to make a trade-off decision between model size for increased test Reynolds number and accompanying increased wall interference. Work is required in the near-term to quantify the gains in Reynolds number benefits versus the losses due to increased wall interference. The "indefinitely-postponed" US National Wind Tunnel Complex (NWTC) program is a recent example where emphasis was placed on maximum model size.

A key thrust of the NWTC program was to provide new test capacity for aircraft development that would include high Reynolds number, high data quality, high productivity at data costs consistent with today's costs and high through-put (tests per year). Originally, the NWTC program was to provide a complex of two wind tunnel facilities that would cover both low speed and transonic speeds up to Mach number 1.5. One of the NWTC constraints was to be able to test models up to 80% of the applicable test section dimension so as to maximise Reynolds number for a given stagnation pressure and temperature. Owing to the goal of high data quality, strong consideration was given to the design of the test section for minimising wall interference as well as correcting for wall effects. Cost and productivity considerations constrained the design to a passive slotted test section with segmented throttle segments for each slot as opposed to a fully adaptive configuration. Sickles and Steinle [30], using a linear porous wall boundary condition for a large MD-11 type model in the proposed NWTC test section sized to this criteria at Mach number 0.85 test conditions, showed that, depending on the method for correcting the test results and establishing the wall setting (porosity distribution and side-wall divergence angle), the lift, drag, and pitching moment corrections as well as global corrections to Mach number and angle of attack could be very small. This result, although promising, is not conclusive since an Euler method was involved. Viscous effects can significantly change the magnitude of corrections. To properly evaluate the net increase in quality of test results through higher test Reynolds numbers achieved by increased model size, the accompanying losses in quality associated with increased wall interference effects should be assessed with a method that includes viscous effects.

As the maximum size of the model and its support system grows with respect to the tunnel, the details of the flow-field between the model and the wall and both the upstream and downstream boundary conditions become more important for proper prediction of the wall corrections. Further, both wall geometry and tunnel operational mode affect the flow about the model. Prior work of modelling wall boundary conditions is a good start. However, there is opportunity for improvement in the near term as will be discussed in section 12.2.

Many facilities today are undergoing upgrades to improve flow quality; but, little is being done to reduce the magnitude of wall interference in those facilities. Considerable activity has been going on for over a decade aimed at developing adaptive wall capability that theoretically offers the best technical solution for reducing wall interference. However, issues of productivity and maintainability are detractors. Other forms of variable walls that are limited in adaptive capability such as global-adaptation and passive-adaptation (pre-settable or controllable cross-flow resistance) offer less complex solutions that are not technically as good as fully adaptive walls, but are superior economically (capitalisation and productivity-driven.) For any form of adaptive walls used, a simplified method of computing wall settings in advance of the test will greatly ameliorate productivity issues. Regardless, near-term improvements or developments aimed at these more modest

productivity issues. Regardless, near-term improvements or developments aimed at these more modest goals will lay the foundation for even the more ambitious far-term goals. Both computational and experimental work aimed at the next generation large-scale, highly-productive test section, is sorely needed.

12.1.2 FAR-TERM OBJECTIVES

No end is seen to the competitive forces that have provided the impetus for wall-correction work. Economic pressures for "cheaper, faster, and better" are fully expected to result in far term (say, 20 to 25 years from now) objectives closely resembling near-term objectives in most respects. However, in the far term we will see technological improvements that will enhance the testing process and data quality that can affect both adaptive and passive wall tunnels. The capability of the computational resources is expected to improve dramatically: grid generation - substantially; code efficiency - significantly; and fluid-mechanics models (e.g., turbulence model, shock/boundary-layer interaction model, shear layer mixing, boundary-layer separation criteria) somewhat. With sufficient increase in computing power, Euler solutions with coupled integral boundary layer solutions may well be done on a desk-top size computer in seconds. Navier-Stokes equations may be computed in minutes. Further, we will have the benefit of the work in the near-term in areas such as model geometry definition, in-tunnel measurements (model and flow field parameters), wall correction methodology, basic CFD, etc.

Assuming the above technological advances and probably a moving test data quality target that will only be stopped if computational capability is ever fast enough, accurate enough, and affordable enough to obviate the need for wind tunnel testing, what should we plan for the far-term? The general idea is to keep on with continuous improvement consistent with experimental and computational capability (as long as they are cost-effective) until such time that the residual data uncertainty after wall corrections is negligible. Whenever an improvement in a solver, or a computer system is realised, the wall correction methodology that is affected should be verified. Planning should be initiated for what changes would be made in methodology for, say, each order of magnitude improvement in computational capability and then move in that direction when it occurs.

The role of the wind tunnel is expected to change with time. One view is the wind tunnel will only be required for code validation. Another view is it will still be required for product development and basic research as well as code validation; but, there will be substantial changes to what is tested and what measurements are required. Regardless of the change, the desire for high quality test results points toward elimination of wall interference to the maximum extent practical and correction of any residual wall effects. There is no change here from what is desired today. However, to be able to achieve this goal in a highly productive fashion probably resides in the far term. The far-term goal that is suggested is to strive for the capability to either compute real-time wall corrections with confidence or to support highly-productive fully-adaptive wall capability (e.g., two seconds per data point). How much growth in computational capability might be required for this to happen? It seems like between three and four orders of magnitude increase in computing power may be required for this to be a reality by direct computational means. Can such growth be reached? Optimistically, yes. Even if the answer is no, highly-productive capability could still become a reality, depending on the ability to characterise and store wall settings versus gross details of the model, support system, and flow condition. With this approach, although the ability to perform CFD calculations may not measure up to real-

time productivity requirements, real-time productivity could still be achieved by accessing a pre-computed data base, real-time measurements of wall boundary conditions and model loading.

Emphasis should be placed on three paths: making efficient direct computations in real-time during a test, developing a pre-computational approach to couple with real-time test measurements, and developing highly productive fully adaptive capability. In so doing, improvements in productivity and quality of wall interference computations can also be realised.

12.2 AREAS FOR EMPHASIS, VERSUS EXPECTATIONS

There are three basic requirements for dealing with wind tunnel wall interference effects regardless of the type of test section or kind of model. They are: "Ability to accurately establish maximum allowable model size for a specific test. Ability to reduce, or correct wall effects in any test in which the maximum allowable model size is not exceeded. Ability to estimate the uncertainty or accuracy of the corrections applied", Lynch, et. al [22]. These abilities are required for a wide range of wind tunnel testing. Commercial and tactical aircraft, space vehicles, as well as the automotive and trucking industry all have their requirements for improved data accuracy. The following discussion will address some specific areas pertaining to these requirements that warrant emphasis, included expectations for outcome of future work.

12.2.1 BETTER UNDERSTANDING OF APPLICATION OF WALL INTERFERENCE

Accurate, practical, wall interference correction techniques are needed for a wide variety of wind tunnel testing scenarios. These include:

- Cruise performance in ventilated (perforated, slotted, and porous-slotted) test sections
- High lift in solid wall, ventilated wall, and open-jet test sections
- Sting & distortion or support tare & interference testing for all wall types
- Stability and control for all wall types
- Power effects (jets, turbine simulators, rotors, propellers)
- Buffet and unsteady aerodynamics - all wall types
- Incremental testing, all types
- Advanced airfoil development,
- Bluff body tests (including automobile and truck)

Understanding of limitations on the accuracy of methods is required. Chapter 11 addresses issues related to the sources of uncertainties in wall correction methodologies and approaches to resolving those uncertainties. The finer points of underlying assumptions in determining drag increments due to model-image induce effects that led to the conflict noted in section 12.1 is an atypical example of the problem of understanding of limitations on methods. This is atypical because we have methods producing conflicting results that have the same basic underlying small disturbance, incompressible flow assumptions.

Nevertheless, it is worthy of note because the conflict does serve to illustrate that any method should be called into question if we are to work toward a full understanding of limitations. Briefly, the expression for low speed, model-image induced drag increment, developed by Taylor as Equation 1.3 is $\delta C_D = -C_D \epsilon$, where ϵ is the normalised sum of solid and wake image-induced velocities, ϵ_s and ϵ_w . In Section 1.3, Taylor assumes ϵ_w to be small and obtains the classical result, $\delta C_D = -C_D \epsilon_s$, as in AGARDograph 109, pp 109 -111. However, the derivation of Hackett [15], gives, $\delta C_D = -C_D \epsilon_w$. This works well in application to normal flat plates and gives corrections that agree closely with those of Maskell. If this is true in general, then application of Equation 1.3 would overcorrect by an amount, $-C_D \epsilon_s$. As seen in Chapter 1.3, the difference between the two representations is small, but could be significant. Consequently, further theoretical and experimental work is required to resolve this issue. Perhaps a sufficient means of resolution could be achieved by a numerical experiment which captures the physics of the flow about a body with a large wake.

Little has been done toward establishing accuracy requirements for wall corrections, or providing for the systematic validation of various techniques. However, Steinle & Stanewsky [31] state that, wall "... correction methods should be able to assess (1) relative changes in the free-stream flow conditions and (2) changes in local flow conditions at the wing location and along the model axis caused by configuration changes..." to the model. Required accuracy was given in flow inclination and Mach number as 0.010 degrees and 0.001 respectively. These criteria were intended to apply for Mach numbers from 0.5 to 0.85 at transport cruise lift conditions. These accuracy requirements were based on the ability to resolve drag coefficient to 0.0001 (one drag count). Krenz [19] repeats the need for 1 drag count accuracy at high speed; but, notes that an equivalent accuracy for typical take-off and landing conditions (Airbus) would be 5 drag counts. The NWTC project's Customer Requirements and Operations team established wall interference magnitudes not to be exceeded prior to correction for a base-line transport configuration that would span 80% of the applicable test section dimension (CR&O Release 11.0, Vol. 1) . Those requirements are repeated herein:

	Mach Number 0.3	Mach Number 0.85
Delta Mach	$\pm .006$	$\pm .003$
Delta Alpha @ $C_N = 1.0$	$\pm .150$	$\pm .150$
Delta CN body	$\pm .01$	$\pm .005$
Delta CA body	$\pm .0006$	$\pm .0003$
Delta CM	$\pm .02$	$\pm .01$

These requirements for uncorrected magnitude of wall corrections were established with the hope that by the time the NWTC would have been operational, a verified wall correction methodology could provide corrections with sufficiently low uncertainty residual that with sufficient quality in the measurements (e.g., forces, angle-of attack, reference conditions), the target values established by Steinle & Stanewsky [31] could be attained. Euler code calculations by Sickles & Steinle [30] indicate, with suitable control over wall resistive properties and wall divergence, all of the above criteria could probably be achieved for the reference transport configuration. The most difficult target to achieve is for pitching moment since, without a fully adaptive wall to provide inflow or outflow when wall pressure coefficient would result in the opposite effect, flow curvature effects will tend to dominate. Reduction in axial force coefficient to the above target value does require some form of active wall control (real-time scheduling of side wall-divergence angle was planned for the NWTC) to minimise buoyancy.

The NWTC project did not develop requirements for other types of tests. Such requirements would be useful since applying cruise transport wall interference criteria to other types of tests (e.g. manoeuvring fighter aircraft) could be overly restrictive. For each type of test, careful consideration needs to be given to test requirements, and allowable error in performance factors should be translated into test data uncertainty requirements. Of course, wall corrections represent only one potential error source among many. Therefore, allocating error magnitudes to wall corrections should be done in conjunction with an overall assessment of error sources and their magnitudes. Even if precisely defined uncertainty requirements were available for each type of test, there would still be a serious deficiency in establishing the uncertainty of wall corrections themselves. Computing wall corrections is not like measuring pressure. There is no readily available calibration standard from which to define "truth". Tunnel-to-tunnel comparisons can be very helpful in indicating general validity. However, wall corrections are just one of many factors which enter into wind tunnel data correlation studies and it would be difficult, time consuming, and expensive to establish absolute uncertainty from such efforts. Analytical approaches to estimating wall interference uncertainty are even more difficult. Error propagation from measured data can be tracked, but the relative validity of explicit and implicit assumptions contained in all correction schemes are difficult to assess. Despite all of the difficulties, the need still exists to pursue development of methods to assess the uncertainty of wall corrections for typical applications. Chapter 11 addresses methodology for this assessment.

Two obvious approaches to arriving at a calibration standard ("truth") from which to form a basis for validating wall interference methodology are seen. One is experimental and the other is strictly numerical. Both are artificial definitions of "truth" since boundary conditions and flow uniformity contaminate the experimental "truth" and limitations in modelling of fundamental flow physics and model shape affect the numerical "truth".

Traditionally, an experimental definition of "truth" has been taken as either the results from a very low blockage model at conditions assumed to be essentially interference free, or the corrected results from a model tested in a tunnel whose boundary conditions were assumed known (closed wall). In the former, adjustment to free air conditions is accomplished by applying a wall correction assumed sufficiently certain. Of these two experimental approaches, the low blockage approach is to be preferred since the goal is to validate wall correction methods and use of the other approach involves a correction to validate a correction. However, to improve the process, the test section used to provide the reference data should have exceptional flow quality and its upstream, downstream, and wall boundary conditions measured to provide a basis for future adjustment of the low interference results. Here, an adaptive wall test section, with validated methodology, is expected to be superior. From this point, there are two experimental choices. The first is to test the same reference model in a tunnel that will produce typical magnitudes of wall interference, measure the boundary conditions, correct the test results by the method in question and validate against the defined "truth". The second approach is to build a large model to the "same" scaled dimensions as the low blockage model (within tolerances consistent with allowable variation in computed pressure coefficients) and test as before. For all experimental activities, identical test techniques (including instrumentation, if possible, and data reduction programs) should be employed and the results corrected for every identifiable error source. Consideration of matching Reynolds number and model distortion effects leads to testing the same model in a smaller tunnel with both tests conducted at the same total pressure. For a relatively low loading condition with a high-stiffness model (non-lifting body) testing with scaled models in variable density tunnels to match Reynolds number should not lead to any significant uncertainty due to model distortion. However, other error sources would be present and must be accounted.

The basis for a numerical definition of "truth" is simply a shape whose surface flow conditions in free air can be represented by a computational method to a low enough uncertainty as to serve as the free air reference for validation of a wall correction method. This definition of truth would include say, a body of revolution for which a Navier Stokes representation could be computed with confidence. Representation of the installation in the tunnel to the degree necessary to capture the fundamental physics and flow non-uniformity's is required. Test results would include measurement of those parameters necessary to validate the basic physics model. Variation of parameters to tune the computation to match the essential features of the measured flow-field is required. From this work, the influence of the entire installation can be studied (upstream and down-stream boundary conditions as well as wall boundary representation). Extension to a lifting case requires other considerations such as aero-elastic distortion and potential separation. Sensitivity studies concerning the choice of turbulence model in any CFD calculations may be required as well as uncertainties in model geometry. Technically, this process can be implemented now. The effect of improvements in computational methods and better representation of tunnel boundary conditions will lead to a newer version of truth for each calibration configuration. Use of this method should not end with testing of a model that can be computed. Extreme cases are the ultimate goal and those can't be computed with sufficient certainty. Hence, the goal for validation of wall correction methods should include the previously mentioned experimental definition of truth.

Both the experimental and computational approaches to the definition of truth warrant careful consideration. It is anticipated that results of greatest value will emerge from a dual approach that employs both. Experimentally, the most difficult part is the determination of the boundary conditions (upstream, down-stream, and equivalent inviscid wall boundary) and the sensing of the model shape and orientation. Numerically, the representation of the model wake (including model - support system interaction) is expected to create the most challenge. A collection of standardised approaches with an uncertainty assessment for each for validating wall correction methodology would benefit the entire testing community.

Development of a standardised validation methodology is in keeping with the charter of the AGARD FOP and it is recommended for consideration of sponsorship.

12.2.1.1 INCREMENTAL CORRECTIONS VS ABSOLUTE CORRECTIONS

Strictly speaking, all wall interference corrections are incremental since they are applied to an experimental result. However, one thinks of an absolute value of a wall correction as correcting an experimental result to a condition of free air. An absolute value of wall correction is always desirable, even when comparing the results for an incremental configuration change. On the other hand, it is suggested that in many cases an incremental assessment may be sufficient. Clearly, in linear theory would suffice for determining the pressure loading on a model, an incremental wall interference correction due to a change in model geometry and/or loading would be sufficient for correction of a comparison of the effects of the change. Further, if the comparison was made between two configurations at the same total loading, the required wall correction incremental corrections are further reduced (e.g., no net change to measured angle of attack) although not necessarily eliminated (e.g., pitching moment and buoyancy). When the description of the model loading requires more than linear theory, a test condition correction (as in global corrections to Mach number and angle-of-attack) may still be required.

When a test condition correction is insufficient, even when testing for the effects of incremental configuration changes, integrated corrections to the measured data must be applied to both the base-line and the increment to the base line configuration. Establishment of the limits for applying an incremental wall correction to incremental test results has not been demonstrated. Incremental corrections can also apply to the baseline configuration since a change in angle-of-attack is an incremental change as well. Thus, for conventional testing, an incremental approach may serve to bridge the gap between computed absolute corrections sufficiently well as to minimise the extent of computations required. Accordingly, since the range of usefulness and application of incremental wall corrections is not established, work in this area is needed.

12.2.2 DEFINITION AND MEASUREMENT OF BOUNDARY CONDITIONS

Regardless of the solver used to estimate wall corrections, the result will be influenced by the representation of the boundary condition. The need to characterise the boundary condition with an accuracy consistent with the accuracy of the wall correction method to be employed has been long recognised. There is more to be done to improve the characterisation. Troublesome areas include the upstream and downstream boundary conditions, treatment of wall-divergence, growth of the tunnel wall boundary layer, auxiliary suction and wall pressure effects on cross-flow, localised effects versus homogenous representation for ventilated walls, amplification of wall cross-flow due to boundary layer effects, and modelling of jet (downwash) impingement effects.

12.2.2.1 FORM TO USE FOR WALL BOUNDARY CONDITION

Classical work has, of necessity, used linear homogenous boundary conditions. This work is well known and is not cited herein (see Chapter 3). The advent of solid adaptable walls for 2-Dimensional testing led to the use of a viscous correction. As model size and loading has increased, the impact of the model imposed pressure gradient on the wall boundary layer has forced adjustments to solid wall boundary conditions to take in to account the effect of change in displacement thickness caused by strong pressure gradients. Further, measurement of mass flux normal to the wall of a ventilated tunnel has led to the recognition that the viscous interaction amplifies the effect of the normal mass flux resulting in a higher order adjustment to the boundary condition. Additionally, pressure drop of flow through porous walls becomes dominated by the second power of normal velocity as expansion and viscous losses through the porous channel increase. Walls with open slots also exhibit fairly strong localised flow curvature effects which has led to higher order representations. Practically speaking, one should always use as simple a form as possible, consistent with the flow physics and the uncertainty requirement for computing wall corrections. It is important to understand the contribution the wall model makes to the uncertainty of a wall correction. It would be highly beneficial to investigate wall models systematically for non-linear effects caused by strong gradients and substantial boundary layer thickness (typical of large models in major wind tunnels) and report the results in a standard format. This would aid the user in a choice of wall boundary condition form to use.

12.2.2.2 VISCOUS EFFECTS

Modification of solid wall boundary condition by a correction to account for changes in boundary-layer behaviour owing to model-imposed pressure gradients currently is done in an approximate sense. Ashill, Taylor, and Simmons [2], for example treat the normal velocity at the wall as being related to the rate of growth of the displacement thickness, including the effects of pressure gradient. Some approximations were done. With their approach, computed wall pressure distribution from testing of a research body (representative of a civil transport volume) show significantly improved agreement with experimental results at high subsonic speeds in the DRA 8ft. x 8ft. Wind Tunnel. Some improvements are possible and are probably required for bodies producing stronger pressure gradients.

An elemental analysis employing continuity shows that for zero velocity gradient, the flow angle at a height, δ , from the wall due to boundary layer growth equals the rate of growth in displacement thickness. Velocity gradient (independent of changes to the rate of displacement thickness growth) changes the flow angle. Favourable gradient reduces the flow angle in an amount approximately proportional to boundary layer thickness. Further, it is argued that the boundary condition at the wall could then be represented by an analytic extension of the flow angle. For small tunnels, where the boundary layer is thin, this disparity may not be of enough significance to even warrant consideration. However, for tunnels in which the boundary layer height is of the order of 5% of the test section height or width, (either because of size or low Re) this difference may be an important consideration.

For porous walls, mass and momentum flux through the walls complicate the picture. Some progress has been made with incorporating adjustments to wall characteristics for distributed porous walls to account for changes in boundary layer properties. Vidal & Erickson [36], Jacocks [16], Crites & Rueger [9] have reported results from tests of mass flow through porous walls and the amplification of flow angle by the boundary layer interaction. Vidal measured his results directly. Both Jacocks and Crites & Rueger determined their results indirectly. Jacocks determined his by matching computed pressures with an assumed boundary condition. Crites & Rueger determined theirs by measuring the change in displacement thickness with wall normal velocity and using an expression for effective normal velocity at the wall which was derived from continuity considerations, the definition of displacement thickness, and an assumption of a constant edge velocity extension of the boundary layer. Both Jacocks' and Crites & Rueger's results match for low values of wall mass flux, Since Jacocks' results were, in essence, empirically derived on the basis of matching a CFD solution, they are only as good as the CFD model allows for the test installation. The match with the results for Crites and Rueger indicates that the non-analytic extension (constant velocity) of the flow to the wall boundary they used is not a bad assumption for their case. The results of all of the foregoing were from small-scale tests with a thin boundary layer. Flow curvature effects associated with large models and high loading may make it advisable to have a further analytic refinement. Likewise, the effects of a thick boundary layer are expected to further contribute to the need for an analytic extension. Matyk and Kobayashi [25] investigated cross-flow resistance for two porous slotted wall samples where the displacement thickness of the boundary layer was much less than the width of the porous slot (one was a full-scale representation of the NASA Ames 11-Foot Tunnel wall). This experiment showed that cross-flow resistance was basically insensitive to Mach number as did the later work of Crites & Rueger for a porous wall. Unpublished work by Steinle [32] established empirically the effective cross-flow property of the 11-Foot Tunnel wall (displacement thickness of the order 80% of the porous-slot width) by utilising wing pressure distribution and tests with

closed walls and a closed floor and ceiling for a large semi-span model mounted off the floor of the tunnel. The theory by Kraft and Lo [17] was used to determine the stream correction angle along the span of the wing and the wing pressure coefficient sensitivity to angle of attack was used to determine the flow correction along the span for both wall configurations. A variation of slot and porosity parameters led to the extrapolated porosity result. The Kraft and Lo result (semi-empirical with boundary-layer displacement thickness of the order of the slot width) differed significantly from the cross flow measurements of Matyk and Kobayashi (direct measurement, boundary-layer small with respect to slot width) which indicates that boundary layer effects are significant for this type of wall as well. In general then, considerable opportunity remains to improve our understanding of the wall boundary conditions for both solid and ventilated walls to capture the effects of boundary layer, pressure gradient, and mass flux for application to large-scale tunnels. A systematic approach to determining the wall boundary conditions which utilises empiricism and CFD, as appropriate, is needed. An agreed upon format for reporting the results of such work, along with a means of making the results available to the technical community would benefit all. Any results that can be reported in the near term will be quite beneficial to those contemplating test section improvements.

12.2.2.3 UPSTREAM BOUNDARY CONDITIONS

Upstream boundary conditions are usually treated by extending the computational boundary sufficiently far upstream in a constant cross section and assuming a constant velocity and Mach number profile. Some work has been done to consider representation of the model effects at the upstream boundary in an asymptotic sense. Other work, concerning finite test section length has been done. However, work to include boundary layer growth and wall divergence effects on the upstream flow field is lacking. A further complication is non-uniformity of flow at the upstream boundary (e.g., swirl or some other horrible condition). These three effects are clearly not separable. Although upstream nonuniformity is not a wall interference concern, it should be included in any improved modelling of the tunnel flow to compute wall corrections since the effects can not be separated.

12.2.2.4 DOWNSTREAM BOUNDARY CONDITIONS

Downstream boundary conditions are generally not faithfully modelled. However, as models become larger, the need to increase the fidelity of the representation of the downstream conditions increases. More work is required to characterise the effects of downstream condition should be done to aid in the understanding of what modelling is required.

Notable areas include the interaction at the plenum flow re-entry region, if used, as well as the presence of the model support system. The model support system is also of importance for transonic tunnels. These systems are generally not removable. Consequently, tests of large semi-span tests model with the model in the plane of the support strut do occur (e.g., the NASA Ames 11-Foot Transonic Wind Tunnel). Although probably less important than the model support system the proper characterisation of the re-entry region also should be done. Here, empiricism is expected to be the only viable approach. Bui [7] modelled the discrete porous-slotted walls and both the model support system and the re-entry flow field for a large semispan model installed in the Ames 11-Foot Transonic Wind Tunnel using a panel code. Treating the mixing at the

end of the test section as a ramp gave a reasonable match with measured ceiling pressure data near the exit of the test section. Trial and error was required to obtain the best match. Thus, it appears that an empirical approach, aided by inviscid calculations is practical. More work is required to characterise these effects and should be done to aid in the understanding of what modelling is required.

12.2.3 COMPUTATIONAL METHODOLOGY, ASSESSMENT AND VALIDATION

The current collection of methods for determining wall corrections has not reached maturity. Methods for correcting results from dynamic tests have not received as much attention as for steady flow tests. All correction methods (classical, one-variable, two-variable, etc.) can produce an interference perturbation field at any point about the model. Assessment poses the problem of rating methods for utility (ease of application, cost, accuracy of results, limits of applicability). Validation is the process whereby uncertainty of results and limits of applicability are determined. A cursory assessment of some general application areas of computational methodology and challenges associated with developing validated methodology for those areas follows:

12.2.3.1 TEST CONDITION CORRECTION TO REFERENCE CONDITIONS

It is assumed that there is no universally best method for determining test condition corrections to reference conditions. The challenge is to evaluate and report the results of investigating any and all methods for accuracy and limitations.

With modern high lift designs, or advanced configurations such as the HSCT, it is by no means obvious how to use the wall interference perturbation field to obtain a test condition correction -- or sectional weighted correction for that matter. Taylor (Chapter 1.3) has used linear theory ideas in conjunction with the Reverse Flow Theorem to provide simple rules for applying global corrections. Since these rules are based on linear theory, they might not be expected to be valid for transonic flows and for high-lift conditions. Goodier and his colleagues at Southampton University have found that the $\frac{3}{4}$ chord point for the correction of angle of incidence applies for certain transonic airfoil applications. Lewis and Goodyer's work [21] utilised an adaptive-wall tunnel to impose various variations of wall-induced velocities along the chord of the airfoil. Additional work is reported by Ashill, Goodyer, and Lewis [21]. Experiments of this nature are quite useful and further work is welcome.

Sickles and Steinle in their studies in support of the NWTC project investigated the choice of correction approach as well as reference positions for arriving at a correction to Mach number and angle of attack by considering separate locations for each including matching wing lift coefficient. In this study, "truth" is the result of an Euler calculation that imposes free air conditions on the computational domain four body lengths upstream and downstream and six wing spans horizontally and vertically from the model. For the two cases investigated (25% semispan and mid-semispan), the mid-semispan wing position gave the best overall results for the wing (pressure distribution). Applying a correction to Mach number and angle of attack reduced the residual wall interference to low values. Since this was a numerical experiment, blockage and angle of attack corrections were determined from a stream-tube calculation which used the difference

between prior solutions in the tunnel with a prescribed wall model and free air to determine the boundary flow at the stream tube. The flow field caused by this interference stream-tube was then interrogated to determine angle of attack and Mach number increments at chosen positions. With these corrections to Mach number and angle-of attack, computed tunnel results were scaled for dynamic pressure changes and the free air solution was recomputed for the new angle of attack. This method employed is equivalent to either a two-variable measured approach in the tunnel or a direct method where flow conditions on the boundary would be computed and compared with measurement. It is just one approach to be considered in evaluating the collection of 3-D methods either available, or coming in to existence. It serves to illustrate that work needs to be done to verify the range and quality of all correction methods.

12.2.3.2 HIGH LIFT

The wind tunnel testing needs of the commercial aircraft community seem to be focused toward high lift development and cruise performance. High lift equates to large wall interference (lift and blockage.) Maximum lift capability is a primary factor determining wing area which in turn affects cruise drag, and thus fuel consumption, gross take-off weight, passenger capacity, etc. High lift is dominated by 3-D viscous flows with separation and is very sensitive to Reynolds number (e.g., Lynch, et. al.[22]) Although CFD is useful for providing guidance for attached flow conditions, it is not (and is not expected to be for some time) capable of providing the needed accuracy for high lift conditions. This mandates an experimental high Reynolds number approach to design and development which leads the industry toward testing very large semi-span models in large, pressurised (or cryogenic) facilities. The trend for high speed cruise performance wing development is also toward achieving higher Reynolds by employing large models, including semi-span (e.g. Goldhammer and Steinle [13])

High lift testing is commonly done in solid wall or open jet low speed wind tunnels. The model flow field, at conditions of maximum interest, is dominated by viscous flows with off-body separations. As a result, because current CFD can not be used to predict high-lift performance as well as desired and because wing separation can be significantly affected by wall induced gradients, wall corrections to test conditions will not be sufficient for achieving satisfactory free air results. Regardless of how the wall-induced flow field corrections are to be used, the numerical representation of the model only needs to be aerodynamically correct in a far-field sense. Therefore, although it may not be possible to satisfactorily predict high lift performance, it should be possible to simulate the model well enough for the purpose of calculating the wall induced flow field. Some trial and error adjustment of the simulation would probably be necessary to obtain agreement between measured and computed wall pressures -- a necessary condition for valid correction.

At high model loads (high Reynolds number) the user of the test results is faced with the prospect of accounting for aero-elastic distortions. Consequently, if the flow conditions are in the range of linear aerodynamics, the induced distribution of flow angle can be treated as a global correction plus a localised twist and camber modification of the wing shape. Thus, if the blockage induced velocity gradient over the wing is negligible, then wall corrections of this nature can be adequately performed. To apply a correction for other than test conditions to say, wing flow development, would require a CFD code wherein the boundary condition at the model surface can be altered to accommodate a modification of the surface flow velocity by amount of the local induced velocity. This approach is not known to have been tried, but does seem possible

as a means of extending the applicability of even a classical or panel method. Such an approach to extending test condition corrections to include streamwise induced velocity gradient should be investigated.

Care must be taken in sizing models for high lift testing (with and with-out engine simulation). Currently, flow field correction techniques do not capture the detailed effects of pressure gradients. When these gradients are the determining factor in sizing, a numerical simulation of the model is required that at least predicts correct increments to small changes. Unless suitable predictive methods, based on CFD simulation of the model can be developed and validated, sizing will remain a subjective procedure that must rely on experience and judgement. Consequently, work is needed in the process of evaluating methods to develop and report criteria which can be used to establish model size and correct the data once obtained.

12.2.3.3 PERFORMANCE TESTING

Performance testing for commercial transports is usually limited to Mach numbers less than 1.0. Tactical aircraft require force and moment data through the transonic range. Between Mach numbers 0.6 and .95, correction methods based on transonic small disturbance, full potential, or Euler methods have been shown to provide corrections with varying degrees of uncertainty depending upon the relative appropriateness of the assumptions and the flow field characteristics. Above a Mach number at which viscous forces influence shock position (Sickles and Erickson [29] suggest Mach 0.90) inviscid representation of the model flow field becomes questionable and Navier-Stokes or boundary layer interaction methods are indicated. The point at which one must transition from one method to another is model and interference field dependent. As the test Mach number approaches about 1.2 to 1.25, the strength of the wall interference effects in ventilated wall tunnels sharply decrease to a generally acceptable value (Rueger, et. al. [28] and Martin, et. al. [24])

As gradients in the interference field become larger, the wall effects become less and equivalent to a change in Mach number and angle-of-attack. As the severity of the gradients increase, flow field correction methods begin to yield corrections representative of an equivalent distorted geometry that do not correspond to any real flight condition. The wall effects for such a situation become "uncorrectable." However, this is not necessarily the case for the surface pressure correction methods. Such methods inherently account for gradients in the interference field. Ideally, within the limits of the flow solver and the treatment of the boundary conditions, there are no uncorrectable cases, providing the model shape is properly represented. Practically speaking though, there are always situations where the flow field distortions are so large that any methodology is incapable of computing valid corrections. The challenge is to establish the uncertainty envelope and limiting conditions for any correction method.

12.2.3.4 STABILITY AND CONTROL TESTING

The determination of longitudinal and lateral directional forces is carried out at all speeds and over a large range of model attitude settings. High-lift devices may be employed to a varying extent -- clean configuration at high speeds to full deployment at low speeds. The wing plane may not be aligned with any of the tunnel walls, and the model may be located a considerable distance from the tunnel centreline. Furthermore, some model positioning systems allow considerable vertical travel of the model during pitch sweeps. Angle-of-

attack can be very large so that massive separation on the wings and fuselage is common. From a wall correction point of view, this kind of testing combines many of the most difficult aspects of performance and high-lift testing. Fortunately, the uncertainty requirements are not as stringent as for performance testing. Nevertheless, wall corrections may be necessary, particularly if the model to tunnel size ratio is large. Here, the method of choice is clearly open to question. It seems as if the two-variable boundary value approach which avoids the necessity of simulating the model is to be preferred, followed by the generalised wall pressure signature method which generates an aerodynamically equivalent model (in a far-field sense). However, if the wall interference field is strong enough to influence the separation characteristics of the model, a more exact representation of the model and flow field will be required. Methods for the various installations against agreed criteria should be evaluated and reported.

12.2.3.5 BUFFET AND UNSTEADY AERODYNAMICS

Buffet boundaries obtained in the wind tunnel have not been noted for precisely matching flight experience. Furthermore, it is seriously doubtful that wall interference effects are the main cause of the discrepancy. Buffet is caused by unsteady separation phenomena. It is sensitive to Reynolds number and model fidelity, among other things. If proper viscous scaling can be achieved, the model is built to the deflected aircraft shape, and the wind tunnel background noise is low enough, then perhaps wall effects might be the limiting factor.

To avoid a numerical representation of the model, a two-variable boundary value approach would likely be selected. However, the problem of deciding maximum model size, or allowable gradients, is more difficult. Gradients in the interference field have the effect of modifying model geometry (camber, twist, and thickness, separation bubble size and shape.) If small, the effects may be acceptable if the regions of separation or attached flow are stable. However, for buffet, the three-dimensional unsteady partial separation effects may be very sensitive to wall induced flow gradients. The determination of a valid assessment of this sensitivity is a challenge to be met.

To avoid the gradient problem, adaptive walls are an attractive option. Use of an adaptive wall tunnel (Taylor and Goodyear, [34], [35]) offers the potential to improve buffet assessment by additively inducing the equivalent of wing twist in opposition to aero-elastic distortion. Further, since wall effects can be made variable, added value in assessing both wall effects and corrective methods is realised. Alternatively, a surface correction method might be used. This type of correction can preserve the effective shape integrity of the model in the presence of strong interference gradients. Only valid increments between in-tunnel and free-flight conditions are needed. Absolute accuracy is not required. There is, however, a problem of interpretation. The surface pressure correction methods produce corrections to the forces and moments. It is not clear how the increments in forces are related to increments in buffet intensity. Perhaps it would be possible to compute the extent of unsteady separation. Even so, this does not guarantee success since buffet is controlled not only by the extent of unsteady separation, but by the phase relation and spatial distribution. A CFD code that could accurately provide that kind of information (in useful time) for the model in free air and in the wind tunnel might give better results than the wind tunnel.

The problems associated with wall corrections for buffet boundary testing are severe. Additional research into the fundamental physics of buffet is needed. In the meantime, some form of empirical correction seems

to be the only option for meaningful wall correction in buffet studies. Such a validated method has not been developed and remains a challenge. An experimental investigation aimed at the establishment of scaling laws and the generation of semi-empirical predictive capability is essential to solve this problem.

Dynamic testing poses severe challenges. Acoustic disturbances in the flow can affect dynamic phenomena (e.g., Mabey [23]). Coupling between the model flow field, support system, and test section walls can pose problems. For rotary-balance and oscillatory testing, the model support structure must be massive to provide the necessary stiffness while forcing the desired model motions. These model support structures lead to strong unsteady coupling with wall effects. The model generated dynamic loads interact with model support unsteady loads and the reaction at the walls. Together, the interactions are characterised by different convective lag times. Therefore, at various discrete reduced frequencies of model motion, the coupled interference reactions can amplify or damp unsteady flows on the model.

The interference effect can be strong, even for small models in big tunnels. For example, it has been observed (Ericsson and Beyers [12]) in rotary-balance testing that unsteady interference effect on vortex breakdown becomes a strong function of reduced roll rate. When phase relations are right the unsteady interference can alter even the qualitative nature of the aircraft manoeuvre characteristics. Rotary balance testing of an advanced tactical aircraft model was conducted in two different tunnels at the same Reynolds number. The smaller tunnel was the 2.4 x 1.8 m ($b/w = 0.6$) Trisonic Wind Tunnel at DRA Farnborough. The larger tunnel was the 4 x 2.7 m Low Speed Wind Tunnel ($b/w = 0.4$) at DRA Bedford. Beyers reported that unsteady interference effects completely masked a known unstable yawing-moment characteristic of the model in the smaller facility, but not the larger one. This kind of problem is not unique (e.g., den Boer, et. al.). Oscillating wing studies were conducted with the NORA wing & oscillator (Lambourne, et. al.) at several facilities. It was found that unsteady interference in smaller tunnels (DRA 3 ft. - Bedford, and DLR 1m - Göttingen) suppressed oscillatory pressure spikes (shock motion) that were clearly present in larger tunnels (ONERA S2 - Modane, and NLR HST - Amsterdam). The approximate span to width ratios were 0.45 for small tunnels and 0.25 for large tunnels.

Currently, there are no validated wall correction methods available for these dynamic tests that are available for general use. It seems that empirical or semi-empirical methods hold the greater promise for early application. However, there is a growing interest in unsteady testing.

Improved wall correction methods are needed for all dynamic type testing. Chapter 9 (R. Voss) of this report provides an excellent overview of the current wall correction methodology for dynamic tests that is available. Voss indicates that validation experiments for CFD methods are needed. Further, the need exists to continue development of promising concepts in wall adaptation to minimise unsteady wall interference effects. Feasibility of unsteady wall adaptation has not yet been demonstrated. A form of wall adaptation that may be possible is the modification of the boundary-jet self-streamlining wall concept. In this concept, wall jets would be actively driven (phase locked) to model motion to create a dynamic oscillation in wall boundary "stiffness" and thereby reduce the unsteady wave structures at the wall.

12.3 COUPLING OF WALL INTERFERENCE WITH OTHER PHENOMENA

As long as the sought after corrections can be determined by a linear method, wall corrections can be uncoupled from other considerations (non-linear compressibility effects, viscous interactions, support interference, and tunnel flow non-uniformity's) with reasonable success. However, as the flow interactions become large (as Mach number and/or attitude increase), the coupling increasingly warrants a single integrated computation. If accomplishable with sufficient accuracy, such a computation is the recommended approach. Characterisation of the limits wherein it is best to perform an integrated computation remains to be accomplished and should be done.

12.3.1 COMPRESSIBILITY EFFECTS

It is suggested that the first degree of coupling is associated with compressibility effects in the determination of test condition corrections. Rizk [27], for example, proposed a scheme whereby corrections to Mach number and angle of attack are determined iteratively for 2-D flow by matching the pressure distribution in some least squares sense as opposed to a classical based approach of say, selecting the 1/4 chord location for the Mach number blockage correction and the 3/4 chord location for angle-of-attack. Sickles and Steinle [30] investigated two different wing span locations at Mach number .85 using this classical-based approach as well as using the 1/4 chord location at 50% semi-span for Mach number correction and then adjusting angle of attack to obtain the best match of wing lift between tunnel and free-air conditions, corrected for blockage. This latter approach gave an excellent match with wing pressure distribution, including shock location. Since the inviscid solution provided a close match with the wing pressure distribution, incremental differences due to viscous effects are expected to be minimal. Guidelines are needed as to how to determine the best location to use as a reference for computing test condition corrections. Beyond that, the issues are what method should be used and how should they be determined.

12.3.2 VISCOUS EFFECTS FOR HIGH LIFT AND TRANSONIC INTERACTIONS

The importance of viscous effects for high lift has been touched upon in section 12.2. Situations of incipient separation are expected to be quite critical in determining maximum lift as well as shock-induced separation. In these instances, nothing short of a Navier Stokes method is apt to approach a useful answer. In this case, the turbulence model is the limiting factor, just as it is for the free air case. The other obvious situations for strong viscous coupling occurs for vortex and jet interaction with wall boundary layers and the shape of trailing wakes. Here, empiricism may be sufficient. Work is needed to understand the limitations and to develop useful empirical data.

12.3.3 SUPPORT INTERFERENCE EFFECTS

It is quite convenient to determine wall corrections by computing the difference between a solution for a model in tunnel and in flight. Since the support sting, or strut, looks like model to the walls, the interference

free case is a model in free air without a support mechanism. Viscous wakes for vertical struts or blades complicate the computational problem. On the other hand, if flow physics are reasonably modelled, one can go from the model with support directly to a model in free air with proper closure. It is much more appealing to not have to expend the computer budget attempting to compute the effects separately. This approach of not separating support interference from wall corrections is seldom (if at all) done. Work to develop a technique to do this direct approach could be highly beneficial. There are formidable problems of empirically modelling viscous wake effects.

12.3.4 TUNNEL NON-UNIFORM FLOW

Some discussion of upstream boundary effects is in section 12.2. Presumably, if the flow field at the upstream boundary (velocity and temperature), the model, and the wall boundary characteristics were sufficiently well known, it would be possible for the computation to replicate the convection of the stream non-uniformity's and thus capture the effect of tunnel non-uniform flow directly. Otherwise, a tunnel survey of the flow field in the test volume is required. To apply this information linearly, the survey results are then added as a vector to the calculated wall interference flow field disturbances. This latter approach (tunnel empty survey) neglects the change in location of flow non-uniformity caused by the upstream influence of the model pressure field. If the flow quality of the tunnel is relatively good, the impact of not simulating the change in location is expected to be negligible. A systematic study to investigate the effects of flow non-uniformity, typical of today's facilities, at both low speeds and transonic conditions is yet to be done.

12.4 REDUCTION OF WALL INTERFERENCE

It is well known that it is possible to improve the design of current wind tunnels to reduce wall interference; however, to do so is costly and thus, the community has seen almost no improvements in existing tunnels. Historically, in the course of developing a facility or a major modification to a facility, costs generally escalate beyond reserves, forcing compromise of a portion of original objectives or planned sophistication. It is expected that future improvements to significantly reduce wall interference by a redesign of a test section to incorporate advanced technology will experience funding difficulties unless the economic benefits of the full technology can be clearly demonstrated. To achieve success in marketing any such improvement, a means of assessing payback to the ultimate source of funding is needed. Such an assessment will undoubtedly include a high degree of subjectivity. A working group to discuss and establish a method for determining benefits of any improvement seems worthwhile. A compelling reason for pursuit of reduced wall interference arises from discovery that increasing complexity of methodology is required to assess wall corrections to a desired accuracy. Barring interference-free conditions, the least objectionable state is to achieve either negligible interference or low enough interference such that rapid and simple correction methods can produce acceptable results. Any improvement effort is expected to involve a design cycle of redefining a model of the tunnel wall boundary conditions. Comments concerning wall types for reduction of wall interference follow:

12.4.1 PASSIVE WALL DESIGN

A passive wall is one that has fixed geometry. This includes a closed wall. Work has been done with the intent of capitalising on viscous effects for solid walls as a means of reducing choking for slightly supersonic operation and for reducing wall interference. Taylor [33], Petersohn [26], Berndt [4], [5] and more recently Crites [10] addressed some of the benefits and limitations of using viscous effects to advantage. The use of such a technique has not been explored to the point of being routinely employed and is an opportunity for further study. Other forms of passive walls (holes, slots, porous slots) were established on the basis of model to tunnel size ratios smaller than the current trend. It should be relatively inexpensive to introduce redesigned porous plates or slotted sections that are shaped to passively minimise wall interference for larger models in current test sections. Current technology should be capable of defining such improved sections.

12.4.2 VARIABLE CHARACTERISTICS WALL DESIGN

The next best wall toward a fully adaptive wall is one that has variable characteristics which can be used to segmentally throttle the mass flux through the walls either in real time, or pre-settable. Such a wall requires appropriate instrumentation and methodology to determine the proper wall settings. A globally adjustable wall such as the AEDC 4T tunnel (e.g. Kraft and Parker [18]) is the simplest form of variable characteristic wall. Mechanically speaking, either a globally or segmentally variable characteristic wall is practical (e.g., T-128 facility at Zhukovsky, Russia.)

The addition of the ventilated wall for low speed, high lift testing listed in section 12.2.1 is a departure from the accepted norm of today. However, in anticipation of gains in wall correction methodology, it is quite likely that a significant portion of future high-lift testing will be done in tunnels with ventilated walls (lower wall interference than solid walls.) The argument against this concept is that one does not know the boundary conditions well enough to obtain a satisfactory answer. The counter argument is, if the wall interference is reduced by a properly configured ventilated wall, then any error in assessing the boundary condition influence is less than the error generated by having the substantially larger closed-wall induced flow field effects on the model. Calculations performed by Sickles and Steinle [30] in support of the NWTC project confirmed that significant reductions in wall interference for high-lift testing are possible by utilising a properly ventilated wall if the boundary condition is known. This, among other considerations led to the selection of a porous-slotted wall with controllable segments (including closed wall conditions) for the NWTC. Consideration should be given as to the benefits of incorporating this capability as a future upgrade to current closed wall tunnels.

12.4.3 ADAPTIVE WALLS

It can be seen that the need for high Reynolds number capability is a mutual concern for the development of tactical and commercial transport aircraft, and both are tending toward the same solution -- big models in big tunnels. Current large pressurised (and cryogenic) facilities do not use wall streamlining, nor are any known to be planned. The NWTC project planned to use a form of passive-adaptive walls (Crites & Steinle [10]),

controllable in real time, to minimise the wall interference. However, that project has been postponed for an indefinite time. Even with that type of test section which would provide reduced wall interference, the emphasis is still on correction as opposed to elimination. This is not to say that adaptive wall technology is unimportant. On the contrary, it is crucial that it be developed to a mature, highly productive state and it may ultimately be shown that for the large models necessary in future testing, some streamlining must be done to reduce the magnitude of the wall effects to a correctable value. However, in the near future it appears that adaptive wall technology will not play a major role in aircraft development simply because the major wind tunnels that must be used do not provide this capability. It seems more likely that the near term contribution of adaptive wall tunnels will lie in research directed toward application of wall corrections (e.g., Lewis & Goodyer, [21]). Work of this nature is needed.

12.5 SUMMARY OF RECOMMENDATIONS

By following the prevailing thread in the above discussion, it should be obvious to the reader that the characterisation of wall interference for all types of testing and test conditions is a formidable problem. Its solution requires physical knowledge and numeric capability that are either non-existent or too costly to implement in today's market. The current trend is to maximise test Reynolds number by pushing the model to tunnel size ratio to its limit. That situation, coupled with high subsonic Mach numbers or high lift, undoubtedly causes wall interference to be a major contributor to data uncertainty. While there are wall interference correction methods available, their uncertainty and range of applicability are not well known. Nevertheless, if the data quality requirements demanded by competitive aircraft manufacturers are to be achieved, wall corrections must be applied at least to the critical performance parameters. The challenge to the testing community is to provide the required corrections with a validated, time and cost-effective methodology.

A systematic, co-ordinated program to improve wall interference assessment and correction methodology and to both understand the limitations of proposed methods and develop useful empirical data is needed to meet the challenge. An AGARD FDP sponsored working group would be appropriate to plan such a systematic, co-ordinated program. The program should include the following elements :

1. Standard approaches of assessing the range of applicability (model and tunnel configuration, test type, Mach Number, attitude, tunnel and model Reynolds number, etc.) and determining the uncertainty of wall correction methods and data bases. The first requirement in devising such a standard is to define the method to determine "truth" against which the various methods will be assessed.
2. A systematic approach to determining the upstream, wall, and downstream boundary conditions using modelling, empiricism and CFD, as appropriate. There are three primary concerns :
 - First, the correction scheme should include the effects of non-uniform upstream flow, wall boundary layer, and wall divergence in the wall interference assessment. Although these three elements are not, strictly speaking, a wall interference concern their effects can not be empirically separated from wall interference.

Second, it is important to understand the contribution the wall model makes to the uncertainty of a wall correction. It would be highly beneficial to investigate wall models systematically for non-linear effects caused by strong gradients typical of large models and report the results in a standard format. This would aid in the choice of which wall boundary condition model to use for a given wall configuration.

Third, the downstream boundary conditions must include the wakes, model support system, and the diffuser entry region (including plenum flow re-entry, if re-entry occurs at the end of the test section). More work is required to characterise the support and diffuser entry region effects to aid in the understanding of what modelling is required. The approach of including support interference with wall corrections is seldom (if at all) done. However, since each of these elements affects the flow gradients in the region of the model, their effects cannot be empirically separated from wall interference.

3. An approach that yields guidelines for determining the best reference location and captures the detailed effects of interference gradients in order to assess their effects on pitching moment when using a method that corrects test conditions.
4. An experimental investigation aimed at the establishment of scaling laws and the generation of a semi-empirical predictive capability for correcting dynamic and buffet boundary test results. The problems associated with wall corrections for dynamic and buffet boundary tests are difficult. Additional research into the fundamental physics is needed and is essential to solving this problem. In the meantime, some form of empirical correction seems to be the only mechanism for meaningful wall correction in dynamic or buffet studies. Such a validated method has not been developed and remains a challenge.
5. A mathematical formulation that properly poses the wall interference problem, especially for Reynolds Averaged Navier Stokes formulation.

In the final analysis, any correction method to improve data quality must be verified, its uncertainty quantified, and its application economically justified in order to be useful to the community of vehicle developers. Economic justification to the community of developers implies establishment of a close working relationship with the developers so as to trace correction benefits directly to the cost-benefit uncertainty trades of their product. This need for understanding both the uncertainty of a method and the benefits to the user should be foremost in the mind of researchers as they tackle this very difficult problem. The product of that research which is vital to the future of both the testing community and the users of the information must be in a form useful and understandable to both parties. Thus, it is imperative that representatives from both groups be involved in both the near and far term efforts. To that end, it is strongly recommended that the AGARD FDP charter a working group to plan, co-ordinate, and guide the needed improvements to wall interference correction methodology.


REFERENCES TO CHAPTER 12

- [1] AGARD-AR-304, Assessment of Wind Tunnel Data Uncertainty, Results of Working Group Keith Kushman, Editor, 1994.
- [2] Ashill, P.R., Taylor, C.R., and Simmons, M.J., "Blockage Interference at High Subsonic Speeds in a Solid-Wall Tunnel, Proceedings, ICAST2-AAC6. Melbourne 20-23, March, 1995.
- [3] Ashill, P.R., Goodyer, M.J., and Lewis, M.C., 1996, "An Experimental Investigation into the application of Wind Tunnel Wall Corrections," ICAS-96-3.4.1, Sorrento, Italy, Sept. 1996.
- [4] Berndt, S.B., "On the Influence of Wall Boundary Layers in Closed Transonic Test Sections" Aeronautical Research Institute of Sweden, FFA Report 71. 1957.
- [5] Berndt, S.B., "Theory of Wall Interference in Transonic Wind-Tunnels," Symposium Transonicum, Aachen, 3-7 September, 1962.
- [6] Beyers, M.E., "Unsteady Wind-Tunnel Interference in Dynamic Testing", AIAA 91-0682, Jan. 1991.
- [7] Bui, T., "Numerical Simulation of the NASA-Ames 11 -foot Transonic Wind Tunnel by a Panel Code," Master's Thesis, California Polytechnic State University, 1989.
- [8] CR & O Master Customer Multi-Purpose Transonic Tunnel Requirements Document, Volume 1, Table 6.2, Flow Quality Requirements, Release 11.0, May 3, 1996.
- [9] Crites, R. and Rueger, M. "Modelling the Ventilated Wind Tunnel Wall", AIAA 920035, 30th Aerospace Sciences Meeting & Exhibit, January 6-9, 1992, Reno, NV.
- [10] Crites, R.C. and Steinle, F.W., "Wall Interference Reduction Methods for Subsonic Wind Tunnels," AIAA 95-0107, January, 1995.
- [11] den Boer, R.G., Houwink, R., and Zwaan, R.J., "Requirements and Capabilities in Unsteady Wind Tunnel Testing," AGARD-CP-429, Oct., 1987.
- [12] Ericsson, L.E., and Beyers, M.E., "Ground Facility Interference on Aircraft Configurations With Separated Flow", AIAA 92-0682, Jan. 1992.
- [13] Goldhammer, M.I. and Steinle, F.W., "Design and Validation of Advanced Transonic Wings Using CFD and Very High Reynolds Number Wind Tunnel Testing," 17th ICAS Congress, Stockholm, Sweden, Sept. 1990.
- [14] Jacocks, J.L., "An Investigation of the Aerodynamic Characteristics of Ventilated Test Section Walls for Transonic Wind Tunnels," Dissertation for the Doctor of Philosophy Degree, The University of Tennessee, Knoxville, December, 1976.
- [15] Hackett, J.E., "Tunnel-Induced Gradients and Their Effect on Drag", AIAA Journal, Vol. 34, No. 12, December 1996
- [16] Jacocks, J.L., "Aerodynamic Characteristics of Perforated Walls for Transonic Wind Tunnels," AEDC-TR-77-61, June, 1977.
- [17] Kraft, E.M. and Lo, C.F. "A General Solution for Lift Interference in Rectangular Ventilated Wind Tunnels", AIAA 73-209, AIAA 11 th Aerospace Sciences Meeting, Washington, D.C., January 10-12, 1973.

- [18] Kraft, E.M., and Parker, R.L., Jr., "Experiments for the Reduction of Wind Tunnel Wall Interference by Adaptive-Wall Technology," AEDC-TR-79-51, October, 1979.
- [19] Krenz, G., Ewald, B., "Accuracy Problems in Wind Tunnels During Transport Aircraft Development," AGARD -CP-429, pp. 31.1 - 31.9, Oct. 1987.
- [20] Lambourne, N., Destuynder, R., Kienappel, K., Roos, R. "Comparative Measurements in Four European Wind Tunnels of the Unsteady Pressures on an Oscillating Model (The NORA Experiments). AGARD Report No. 673, 1980.
- [21] Lewis, M.C., and Goodyer, M.J., "Initial Results of an Experimental Investigation into the General Application of Transonic Wind Tunnel Wall Corrections," PICAST 2 – AAC6, Melbourne, Australia, 20 – 23 March, 1995, pp. 71 – 79.
- [22] Lynch, F.T., Crites, R.C., and Spaid, F.W., "The Crucial Role of Wall Interference, Support Interference, and Flow Field Measurements in the Development of Advanced Aircraft Configurations", AGARD-CP-535, pp. 1.1 - 1.38, July, 1994.
- [23] Mabey, D.G., "The Reduction of Dynamic Interference by Sound-Absorbing Walls in the RAE 3 ft. Wind Tunnel Wall on Transonic Flutter," Acta Aerodynamica Sinica, Vol. 7, 1989, pp. 351-357.
- [24] Martin, F.F., Jr., Sickles, W.L., and Stanley, S.A., "Transonic Wind Tunnel Wall Interference Analysis for the Space Shuttle Launch Vehicle," AIAA 93-0420, Jan., 1993.
- [25] Matyk, G., and Kobayashi, Y., "An Experimental Investigation of Boundary Layer and Crossflow Characteristics of the NASA 2- by 2- Foot Transonic Wind-Tunnel Walls, NASA TM 73257, Dec. 1977.
- [26] Petersohn, E.G.M., "Some Experimental Investigations on the Influence of Wall Boundary Layers upon Wind Tunnel Measurements at High Subsonic Speeds," Aeronautical Research Institute of Sweden, FFA Report 44, 1952.
- [27] Rizk, M. H. "Improvements in Code TUNCOR for Calculating Wall Interference Corrections in the Transonic Regime," AEDC-TR-86-6, March, 1986.
- [28] Rueger, M., et.al., "Transonic Wind Tunnel Wall Interference Corrections," AGARD Symposium on Wall Interference, Support Interference, and Flow Field Measurements, Oct., 1993, Paper 21
- [29] Sickles, W., and Erickson, J., "Wall Interference Correction for Three-dimensional Transonic Flows", AIAA 90-1408, June 1990.
- [30] Sickles, W.L., and Steinle, F.W. "Global Wall Interference Correction and Control for the NSTC Transonic Test Section", AIAA 97-0095, January 1997
- [31] Steinle, F.W. and Stanewsky, E., "Wind Tunnel Flow Quality and Data Accuracy Requirements," AGARD AR-1 84, Nov. 1982.
- [32] Steinle, F.W., Private Communication, June, 1996.
- [33] Taylor, H.D., "Progress of Transonic Wind Tunnel Studies at U.A.C.", UAC Report R-95434-8, 1951.
- [34] Taylor, N.J. and Goodyer, M.J., "An insight into the Unique Affinities that Characterise the Relationship Between adaptive flexible-walled Test Sections and CFD," AIAA 92-1934.
- [35] Taylor, N.J. and Goodyer, M.J., "Towards the Exploitation of Adaptive Wall Technology in Production Testing Environments," AIAA 94-2614.
- [36] Vidal, R.J., Erickson, J.C., and Catlin, P.A., "Experiments with Self-Correcting Wind Tunnel," AGARD CP-174, pp.11.1-11.13, 1975.

REPORT DOCUMENTATION PAGE

1. Recipient's Reference	2. Originator's Reference AGARD-AG-336	3. Further Reference ISBN 92-836-1076-8	4. Security Classification of Document UNCLASSIFIED/ UNLIMITED
5. Originator Advisory Group for Aerospace Research and Development North Atlantic Treaty Organization BP 25, 7 rue Ancelle, F-92201 Neuilly-sur-Seine Cedex, France			
6. Title Wind Tunnel Wall Corrections			
7. Presented at/sponsored by The Former Fluid Dynamics Panel of AGARD			
8. Author(s)/Editor(s) Multiple			9. Date October 1998
10. Author's/Editor's Address B.F.R. Ewald Darmstadt University of Technology Federal Republic of Germany			11. Pages 560
12. Distribution Statement There are no restrictions on the distribution of this document. Information about the availability of this and other AGARD unclassified publications is given on the back cover.			
13. Keywords/Descriptors			
Winds tunnels		Boundary layer	
Walls		Interference analyzers	
Accuracy		Aerodynamics	
Correction		Wakes	
Computational fluid dynamics		Aerodynamic configurations	
Two dimensional flow		Blunt bodies	
Three dimensional flow			
14. Abstract			
<p>This AGARDograph has been compiled by an international team of wind tunnel wall correction experts. The state of the art in wall corrections is presented with special emphasis given to the description of modern methods based on Computational Fluid Dynamics (CFD). Topics covered include:</p> <ul style="list-style-type: none"> • Open Test Sections • Closed Test Sections • Ventilated Test Sections • Boundary Measurement Methods • Transonic Wall Interference • Bluff Body Corrections • Adaptive Walls • Panel Methods • CFD Methods 			

NATO  OTAN
BP 25 • 7 RUE ANCELLE
F-92201 NEUILLY-SUR-SEINE CEDEX • FRANCE
Télécopie 0(1)55.61.22.99 • Téléc 610 176

DIFFUSION DES PUBLICATIONS
AGARD NON CLASSIFIEES

L'AGARD détient un stock limité de certaines de ses publications récentes. Celles-ci pourront éventuellement être obtenus sous forme de copie papier. Pour de plus amples renseignements concernant l'achat de ces ouvrages, adressez-vous à l'AGARD par lettre ou par télécopie à l'adresse indiquée ci-dessus. *Veillez ne pas téléphoner.*

Des exemplaires supplémentaires peuvent parfois être obtenus auprès des centres de diffusion nationaux indiqués ci-dessous. Si vous souhaitez recevoir toutes les publications de l'AGARD, ou simplement celles qui concernent certains Panels, vous pouvez demander d'être inclus sur la liste d'envoi de l'un de ces centres.

Les publications de l'AGARD sont en vente auprès des agences de vente indiquées ci-dessous, sous forme de photocopie ou de microfiche. Certains originaux peuvent également être obtenus auprès de CASI.

CENTRES DE DIFFUSION NATIONAUX

ALLEMAGNE

Fachinformationszentrum Karlsruhe
D-76344 Eggenstein-Leopoldshafen 2

BELGIQUE

Coordonnateur AGARD - VSL
Etat-major de la Force aérienne
Quartier Reine Elisabeth
Rue d'Evere, B-1140 Bruxelles

CANADA

Directeur - Gestion de l'information
(Recherche et développement) - DRDGI 3
Ministère de la Défense nationale
Ottawa, Ontario K1A 0K2

DANEMARK

Danish Defence Research Establishment
Ryvangs Allé 1
P.O. Box 2715
DK-2100 Copenhagen Ø

ESPAGNE

INTA (AGARD Publications)
Carretera de Torrejón a Ajalvir, Pk.4
28850 Torrejón de Ardoz - Madrid

ETATS-UNIS

NASA Center for AeroSpace Information (CASI)
Parkway Center, 7121 Standard Drive
Hanover, MD 21076

FRANCE

O.N.E.R.A. (Direction)
29, Avenue de la Division Leclerc
92322 Châtillon Cedex

GRECE

Hellenic Air Force
Air War College
Scientific and Technical Library
Dekelia Air Force Base
Dekelia, Athens TGA 1010

ISLANDE

Director of Aviation
c/o Flugrad
Reykjavik

ITALIE

Aeronautica Militare
Ufficio Stralcio AGARD
Aeroporto Pratica di Mare
00040 Pomezia (Roma)

LUXEMBOURG

Voir Belgique

NORVEGE

Norwegian Defence Research Establishment
Attn: Biblioteket
P.O. Box 25
N-2007 Kjeller

PAYS-BAS

Netherlands Delegation to AGARD
National Aerospace Laboratory NLR
P.O. Box 90502
1006 BM Amsterdam

PORTUGAL

Estado Maior da Força Aérea
SDFA - Centro de Documentação
Alfragide
P-2720 Amadora

ROYAUME-UNI

Defence Research Information Centre
Kentigern House
65 Brown Street
Glasgow G2 8EX

TURQUIE

Millî Savunma Başkanlığı (MSB)
ARGE Dairesi Başkanlığı (MSB)
06650 Bakanlıklar - Ankara

AGENCES DE VENTE

NASA Center for AeroSpace Information (CASI)
Parkway Center, 7121 Standard Drive
Hanover, MD 21076
Etats-Unis

The British Library Document Supply Division
Boston Spa, Wetherby
West Yorkshire LS23 7BQ
Royaume-Uni

Les demandes de microfiches ou de photocopies de documents AGARD (y compris les demandes faites auprès du CASI) doivent comporter la dénomination AGARD, ainsi que le numéro de série d'AGARD (par exemple AGARD-AG-315). Des informations analogues, telles que le titre et la date de publication sont souhaitables. Veuillez noter qu'il y a lieu de spécifier AGARD-R-*nnn* et AGARD-AR-*nnn* lors de la commande des rapports AGARD et des rapports consultatifs AGARD respectivement. Des références bibliographiques complètes ainsi que des résumés des publications AGARD figurent dans les journaux suivants:

Scientific and Technical Aerospace Reports (STAR)

STAR peut être consulté en ligne au localisateur de ressources uniformes (URL) suivant:

<http://www.sti.nasa.gov/Pubs/star/Star.html>

STAR est édité par CASI dans le cadre du programme

NASA d'information scientifique et technique (STI)

STI Program Office, MS 157A

NASA Langley Research Center

Hampton, Virginia 23681-0001

Etats-Unis

Government Reports Announcements & Index (GRA&I)

publié par le National Technical Information Service

Springfield

Virginia 2216

Etats-Unis

(accessible également en mode interactif dans la base de données bibliographiques en ligne du NTIS, et sur CD-ROM)



Imprimé par le Groupe Communication Canada Inc.
(membre de la Corporation St-Joseph)
45, boul. Sacré-Cœur, Hull (Québec), Canada K1A 0S7

AGARD holds limited quantities of some of its recent publications, and these may be available for purchase in hard copy form. For more information, write or send a telefax to the address given above. *Please do not telephone.*

Further copies are sometimes available from the National Distribution Centres listed below. If you wish to receive all AGARD publications, or just those relating to one or more specific AGARD Panels, they may be willing to include you (or your organisation) in their distribution.

AGARD publications may be purchased from the Sales Agencies listed below, in photocopy or microfiche form. Original copies of some publications may be available from CASI.

NATIONAL DISTRIBUTION CENTRES

BELGIUM

Coordonnateur AGARD - VSL
Etat-major de la Force aérienne
Quartier Reine Elisabeth
Rue d'Evere, B-1140 Bruxelles

CANADA

Director Research & Development
Information Management - DRDIM 3
Dept of National Defence
Ottawa, Ontario K1A 0K2

DENMARK

Danish Defence Research Establishment
Ryvangs Allé 1
P.O. Box 2715
DK-2100 Copenhagen Ø

FRANCE

O.N.E.R.A. (Direction)
29 Avenue de la Division Leclerc
92322 Châtillon Cedex

GERMANY

Fachinformationszentrum Karlsruhe
D-76344 Eggenstein-Leopoldshafen 2

GREECE

Hellenic Air Force
Air War College
Scientific and Technical Library
Dekelia Air Force Base
Dekelia, Athens TGA 1010

ICELAND

Director of Aviation
c/o Flugrad
Reykjavik

ITALY

Aeronautica Militare
Ufficio Stralcio AGARD
Aeroporto Pratica di Mare
00040 Pomezia (Roma)

LUXEMBOURG

See Belgium

NETHERLANDS

Netherlands Delegation to AGARD
National Aerospace Laboratory, NLR
P.O. Box 90502
1006 BM Amsterdam

NORWAY

Norwegian Defence Research Establishment
Attn: Biblioteket
P.O. Box 25
N-2007 Kjeller

PORTUGAL

Estado Maior da Força Aérea
SDFA - Centro de Documentação
Alfragide
P-2720 Amadora

SPAIN

INTA (AGARD Publications)
Carretera de Torrejón a Ajalvir, Pk.4
28850 Torrejón de Ardoz - Madrid

TURKEY

Millî Savunma Başkanlığı (MSB)
ARGE Dairesi Başkanlığı (MSB)
06650 Bakanlıklar - Ankara

UNITED KINGDOM

Defence Research Information Centre
Kentigern House
65 Brown Street
Glasgow G2 8EX

UNITED STATES

NASA Center for AeroSpace Information (CASI)
Parkway Center, 7121 Standard Drive
Hanover, MD 21076

SALES AGENCIES

NASA Center for AeroSpace Information (CASI)
Parkway Center, 7121 Standard Drive
Hanover, MD 21076
United States

The British Library Document Supply Centre
Boston Spa, Wetherby
West Yorkshire LS23 7BQ
United Kingdom

Requests for microfiches or photocopies of AGARD documents (including requests to CASI) should include the word 'AGARD' and the AGARD serial number (for example AGARD-AG-315). Collateral information such as title and publication date is desirable. Note that AGARD Reports and Advisory Reports should be specified as AGARD-R-*nnn* and AGARD-AR-*nnn*, respectively. Full bibliographical references and abstracts of AGARD publications are given in the following journals:

Scientific and Technical Aerospace Reports (STAR)

STAR is available on-line at the following uniform resource locator:

<http://www.sti.nasa.gov/Pubs/star/Star.html>

STAR is published by CASI for the NASA Scientific and Technical Information (STI) Program
STI Program Office, MS 157A
NASA Langley Research Center
Hampton, Virginia 23681-0001
United States

Government Reports Announcements & Index (GRA&I)

published by the National Technical Information Service
Springfield
Virginia 22161
United States
(also available online in the NTIS Bibliographic Database or on CD-ROM)

